

ORGANIC GEOCHEMISTRY: CHALLENGES FOR THE 21st CENTURY

VOL. 2

**Book of Abstracts of the Communications presented to the
22nd International Meeting on Organic Geochemistry
Seville – Spain. September 12 -16, 2005**

Editors:

F.J. González-Vila, J.A. González-Pérez and G. Almendros

Equipo de trabajo:

Rocío González Vázquez
Antonio Terán Rodríguez
José M^a de la Rosa Arranz

Maquetación:

Rocío González Vázquez

Fotomecánica e impresión:

Akron Gráfica, Sevilla

© 22nd IMOG, Sevilla 2005
Depósito legal: SE-61181-2005
I.S.B.N.: 84-689-3661-8

COMMITTEES INVOLVED IN THE ORGANIZATION OF THE 22 IMOGE 2005

Chairman: Francisco J. GONZÁLEZ-VILA
Vice-Chairman: José A. GONZÁLEZ-PÉREZ
Consejo Superior de Investigaciones Científicas (CSIC)
Instituto de Recursos Naturales y Agrobiología de Sevilla (IRNAS)

Scientific Committee

Francisco J. GONZÁLEZ-VILA (Chairman)
IRNAS-CSIC, Spain

Gonzalo ALMENDROS <i>CCMA-CSIC, Spain</i>	Claude LARGEAU <i>ENSC, France</i>
Pim van BERGEN <i>SHELL Global Solutions, The Netherlands</i>	José C. del RÍO <i>IRNAS-CSIC, Spain</i>
Jørgen A. BOJESEN-KOEFOED <i>GEUS, Denmark</i>	Jürgen RULLKÖTTER <i>ICBM, Germany</i>
Chris CORNFORD <i>IGI, UK</i>	Stefan SCHOUTEN <i>NIOZ, The Netherlands</i>
Gary ISAKSEN <i>EXXONMOBIL, USA</i>	Eugenio VAZ dos SANTOS NETO <i>PETROBRAS RD, Brazil</i>

Local Committee

José Ramón de ANDRÉS <i>IGME, Spain</i>	M ^a Carmen DORRONSORO <i>Universidad del País Vasco</i>
M ^a Enriqueta ARIAS <i>Universidad de Alcalá</i>	Antonio GUERRERO <i>Universidad de Sevilla</i>
Tomasz BOSKI <i>Universidade do Algarve, Faro, Portugal</i>	Juan LLAMAS <i>ETSI Minas de Madrid</i>
Ignacio BRISSON <i>Repsol YPF</i>	Albert PERMANYER <i>Universidad de Barcelona</i>
Juan COTA <i>Universidad de Sevilla</i>	

EAOG Board

Richard L. PATIENCE (Chairman)
Sylvie DERENNE (Secretary)
Ger W. van GRAAS (Treasurer)
Walter MICHAELIS (Awards)
Francisco J. GONZALEZ-VILA (Newsletter)
C. Anthony LEWIS (Membership and Website)
James MAXWELL – Co-opted (Editor-in-Chief of Organic Geochemistry)

22 IMOG SPONSORS

Ministerio de Educación y Ciencia (MEC)
Consejo Superior de Investigaciones Científicas (CSIC)
Instituto Geológico y Minero de España (IGME)
Universidad de Sevilla
Junta de Andalucía
Consejería de Innovación, Ciencia y Empresa
Instituto Andaluz de Investigación y Formación Agraria, Pesquera, Alimentaria
y de la Producción Ecológica (IFAPA)
Consejería de Turismo, Comercio y Deporte. Delegación Provincial de Cádiz
Consortio de Turismo de la Provincia de Sevilla. Turismo de Sevilla
Patronato del Real Alcázar de Sevilla

Repsol YPF
Chevron Texaco
Unocal 76
British Petroleum
Shell
Exxon Mobil
Statoil
Hydro

Integrated Geochemical Interpretation Ltd.
Humble Instruments & Services Inc.
Baseline Resolution Inc.
Vinci Technologies S.A.
Thermo Electron Corp.

Iberia
Renfe
Viajes el Corte Inglés
Anorsur S.L.
Cruzcampo

CONTENT**VOL-2****POSTER COMMUNICATIONS (Cont.)**

- BIOGEOCHEMISTRY (Cont.)** **645**
- ENVIRONMENTAL BIOGEOCHEMISTRY-1 (EB1)** **647**
- PEB1-1. Exposure of marine organisms to polycyclic aromatic hydrocarbons (PAHs): use of PAH metabolites to track the impact of oil spills in relation to their toxicity.** H. Budzinski, O. Mazéas, J. Tronczynski, Y. Desaunay, M. LeDu
- PEB1-2. Trace analysis of hydrocarbons in coral cores from Saudi Arabia.** K. Burns, J. Lough, D. Barnes, D. Brinkman, A. Poulsen, S. Delean
- PEB1-3. Organic chlorinate pesticides (OCPs) and polycyclic aromatic hydrocarbons (PAHs) in the Xijiang River, South China.** H. Deng, J. Song, P. Peng
- PEB1-4. Oil spill bioremediation in Brazilian marine environment – A mesocosm simulation.** E.S. de Souza, M.F. Coelho, J.A. Trigüis
- PEB1-5. Occurrence of polycyclic aromatic hydrocarbons (PAHs) and organochlorine compounds in Iloilo River, Philippines.** P. Gerrez, V. Tañeza, R.P. Philp
- PEB1-6. Environmental organic geochemistry of polycyclic aromatic hydrocarbons (PAHs) and its environmental impact in coal from Huaibei coal field.** L. Gui-Jian, X. Jian, Z. Hao-Yuan, W. Xinming
- PEB1-7. Monitoring river pollution by molecular characterization of the sedimentary organic matter using Gas Chromatography – Mass Spectrometry (GC-MS).** L. Jeanneau, P. Faure, M. Ramelli, L. Mansuy-Huault
- PEB1-8. Organic pollutants of Merseyside inferred by SPOT data.** S. Mukherjee, A. Mukherjee
- PEB1-9. Simultaneous photochemical abatement of hexavalent chromium and organic pollutants.** P. Mytych, Z. Stasicka
- PEB1-10. The environmental effects of oil exploration and production in the East Shetland basin: composition and concentration of hydrocarbons in sediment samples collected in 2002 using a stratified random sampling design.** M. Russell, L. Webster, P. Walsham, G. Packer, E.J. Dalgarno, A.D. McIntosh, C.F. Moffat
- PEB1-11. Research of oils biodegradation in soils and its intensification.** O.V. Serebrennikova, L.D. Stakhina, E.V. Barabanova, N.Y. Andreeva, N.V. Sizova
- PEB1-12. Is Acid Troubling You? Studies of the Synthesis, Characterisation, Biodegradation and Toxicity of Naphthenic Acids.** B.E. Smith, C.A. Lewis, S.J. Rowland
- PEB1-13. Characterization of dry deposition dusts on an urban balcony surface, Guangzhou.** J. Song, P. Peng
- PEB1-14. Distribution and sources of polycyclic aromatic hydrocarbons in surface sediments from New York/New Jersey Harbor complex.** J. Song, B. Yan, L. Benedict, R. Bopp, T. Abrajano, D. Chaky

PEB1-15. *¹³C of volatile organic compounds (VOC's) in air samples by thermal desorption GC-ir-MS.* N. Turner, K. Grice, M. Ioppolo-Armanios, M. Jones, D. Dawson

PEB1-16. *The effects of oil exploration and production in the East Shetland Basin: composition and concentration of hydrocarbons in sediment samples collected in 1986, 1988, 1989 and 1994 – An historical perspective.* P. Walsham, L. Webster, M. Russell, A.D. McIntosh, P.R. Mackie, C.F. Moffat

PEB1-17. *PAH spectrum in the Quaternary water sediments.* I. Bojakowska

PEB1-18. *The development and application of a statistical sampling regime to map hydrocarbon distributions in marine sediment.* A.S. Ahmed, L. Webster, I.M. Davies, M. Russell, P. Walsham, G. Parker, R.J. Fryer, C.F. Moffat, P. Pollard

ENVIRONMENTAL BIOGEOCHEMISTRY-2 (EB2)

681

PEB2-1. *Chlorinated pesticides in river sediments in Poland.* I. Bojakowska

PEB2-2. *Distribution and spatial trends of PCBs in urban soils from six European cities.* A. Cachada, L. Lopes, S. Rodrigues, A. Duarte

PEB2-3. *Bioremediation of a polluted hydrocarbons soil.* B. Ceccanti, C. Garcia, G. Masciandaro, C. Macci, A. Carmignani, A. Filareto

PEB2-4. *The Prestige oil spill. Enhanced biodegradation of a heavy fuel oil under simulated conditions.* S. Diez, J. Sabaté, M. Viñas, J.M. Bayona, A.M. Solanas, J. Albaigés

PEB2-5. *Fate of the spill of The Prestige oil tanker in the deep sea.* S. Elordui-Zapatarietxe, A. Rosell-Melé, P. Masqué, J. Albaigés

PEB2-6. *Photolytic and microbiological degradation of the organic pollutants that originating from the petrochemical industry.* N. Kuburovic, M. Todorovic, V. Raichevic, L. Jovanovic, O. Ecim, B. Lalevic, T. Sholevic

PEB2-7. *Compound-specific isotope analysis applied to MTBE biodegradation studies.* T. Kuder, P. Philp, J. Wilson, J. Allen

PEB2-8. *Distribution patterns of atmospheric pollutants (PAH/PCN) accumulated on pine needles in the Cologne conurbation (Germany).* E. Lehndorff, L. Schwark

PEB2-9. *Interaction modes between humic colloids and surfactant molecules as identified by octanol-water partitioning experiments with radiolabelled humic acid.* H. Lippold, H. Kupsch

PEB2-10. *Sources of Polycyclic Aromatic Hydrocarbons (PAHs) in mussel tissues: a forensic study of hydrocarbon sources and biological exposure in the near-shore coastal waters of Avila Bay, California.* R.I. Haddad

PEB2-11. *Potential sources of the polar fraction associated with groundwater TPH.* R. Haddad, S.-T. Lu

PEB2-12. *Geochemical investigation of an offshore sewage sludge deposit, Barcelona, Catalonia, Spain.* M.A. Krüge, A. Permanyer, J. Serra

PEB2-13. *Microbial biodegradation of potential PAH sources in sewage sludge.* A. Regier, L. Mansuy-Huault, P. Faure, C. Leyval, T. Béguéristain

PEB2-14. Source apportionment of PAH in sewage sludge. A. Regier, L. Mansuy-Huault, P. Faure, E. Jardé

PEB2-15. Organic composition of Seville aerosols. J. Reyes, B. Hermosín, C. Saiz-Jiménez

PEB2-16. Limited bioaccessibility of polycyclic aromatic hydrocarbons leading to background soil pollution. R. Posada-Baquero, J.J. Ortega-Calvo

PEB2-17. Aryl isoprenoids in oil fluid and underground waters from Minusinsk depression. Y.P. Turov, M.Y. Gooznjaeva, B.D. Vasiljev

PEB2-18. Transformation of oil composition under natural factors. Y.P. Turov, M.Y. Gooznjaeva

PEB2-19. Selecting aerobic bacteria from petroleum formation water of special biodegradation characteristics. S.P. Vasconcellos, V.M. Oliveira, K.C.M. Simioni, E.V. Santos Neto, A.J. Marsaioli

PEB2-20. Drilling wastes management: case study in Southern Tunisia. H. Mejri, M. Saidi

BIOMARKERS-1 (B1)

718

PB1-1. Tricyclic terpenoids from Paleozoic tasmanites: a question of evolution, site or taxa? S. Dutta, P. Greenwood, R. Brocke, C. Hartkopf-Fröder, R.G. Schaefer, H. Wilkes, U. Mann

PB1-2. Estimating the number of endospores by determination of dipicolinic acid in sediments from the backbarrier tidal flat of Spiekeroog island. J. Fichtel, J. Köster, J. Rullkötter, H. Sass

PB1-3. Organic matter composition of two discrete thin layers from the Eocene Messel oil shale (Germany). S. Gerisch, U. Mann, N. Micklich, R.G. Schaefer, N. Volkmann

PB1-4. D/H of water, lipids and carbohydrates from modern plants grown under controlled conditions (temperature light intensity, CO₂ concentration and water availability). K. Grice, Y. Zhou, H. Stuart-Williams, S. Chin Wong, S. Schouten, S.X. Wang, G.D. Farquhar

PB1-5. Biomarker distributions and their stable isotopes in marine Permian/Triassic sections from around the globe. K. Grice, R. Twitchett, R.E. Summons, C.B. Foster, C.J. Barber, D. Dawson, R. Alexander, P. Greenwood

PB1-6. Utilization of lipid markers to delineate sources of organic matter in recent core sediments from Victoria Harbour, Hong Kong. M. Hsieh, R.P. Philp, W.W.S. Yim

PB1-7. The sedimentary fate of ladderane lipids, characteristic membrane lipids of bacteria performing anaerobic ammonium oxidation. A. Jaeschke, S. Schouten, E.C. Hopmans, J.S. Sinninghe-Damsté

PB1-8. Phenyl derivatives of polyaromatic compounds and terphenyls as indicators of organic matter oxidation in the Intra-Mountain Podhale basin, Poland. L. Marynowski, M.J. Rospondek, M. Góra

PB1-9. Influence of oxic and anoxic depositional regimes on sedimentary lipid composition in Lake Bled (Slovenia). G. Muri, S.G. Wakeham

PB1-10. The origin of 24-norcholestanes and their use as age-diagnostic biomarkers. S.W. Rampen, S. Schouten, B. Abbas, F.E. Panoto, G. Muyzer, C.N. Campbell, J. Fehling, J.S. Sinninghe-Damsté

PB1-11. Sources and seasonal production of long-chain diols and mid-chain hydroxy methyl alkanolates. S.W. Rampen, S. Schouten, B. Abbas, K.R. Timmermans, G. Muyzer, S.G. Wakeham, J.S. Sinninghe-Damsté

PB1-12. Novel phenyl derivatives of aromatic sulphur compounds in sedimentary rocks from the Holy Cross Mountains (Devonian) and the Fore Sudetic Monocline (Permian), Poland. M.J. Rospondek, L. Marynowski, M. Góra

PB1-13. Organic matter nature of a turbidite recorded in the Zaire Canyon inferred from a study of n-alcohols. C. Treignier, S. Derenne, A. Saliot

PB1-14. Anaerobic bacteria biosynthesise membrane-spanning tetraether lipids. J.W.H. Weijers, S. Schouten, E.C. Hopmans, J.A.J. Geenevasen, O. R.P. David, R. Pancost, J. Oleman, J. S. Sinninghe Damsté

PB1-15. Riverine, estuarine and near-coastal transport and transformation of natural organic compounds (RENTT)- Case study Siak River, Riau province, Sumatra. R. Wöstmann, G. Liebezeit

PB1-16. Terpanoid alkanes as diagnostic markers for benthic red algae? Evidence from the Upper Proterozoic organic-rich shales and cake-shaped bitumens in Northern China. S. Zhang, B. Zhang, Y. Xiong, Z. Jin, L. Bian, D. Wang, F. Song

PB1-17. Characterisation of amino acids in marine sediments from the Benguela Upwelling System. C.M. Bickers, L. Handley, R.D. Pancost

PB1-18. Molecular markers of Mesozoic seep carbonates from a convergent margin setting, California. D. Birgel, V. Thiel, K.A. Campbell, M. Elvert, J.D. Farmer, K.-U. Hinrichs, J. Peckmann

PB1-19. Calibration of organic signal in sedimentary lacustrine records. Molecular comparison between actual producers, dissolved organic matter and sedimentary organic matter (Lac Pavin; Massif Central Français). M. Boussafir, S. Drouin, P. Albéric, J.L. Robert

PB1-20. The occurrence of branched alkanes with quaternary carbon atoms (BAQCs) in the sediments of two large freshwater lakes: Lake Malawi (East Africa) and Lake Superior (USA/Canada). I.S. Castañeda, J.P. Werne, K.D. Pearson, F. Kenig

PB1-21. Organic matter as markers to evidence geochemical evolution of highly alkaline plumes during seepage in sedimentary column. M. Elie, L. Martinez, I. Suárez-Luiz

PB1-22. Chemical stratigraphy of the type Barreirinha formation, (Upper Devonian), Amazon basin – Brazil. J.A. Trigüis, R. Rodrigues, E.S. Souza

BIOMARKERS-2 (B2)

762

PB2-1. Organosulfur compounds (OSCs) identified in modern lacustrine sediments: an extremely sulfur-rich sediment from A Maar, Kata-numa, Japan. K. Fukushima, M. Kato, S. Takamatsu, A. Yoda

PB2-2. Synthesis of novel isomers of phytanol and hydroxyarchaeol. Y. Hebling, R.E. Summons

PB2-3. Multidimensional GC-FID and GC-MS identification of cycloalkanes in Neoproterozoic sediments and crude oils from Oman. Y. Hebling, R. Nelson, C. Reddy, G. Frysinger, E. Grosjean, R. Summons

- PB2-4. Regular isoprenoid hydrocarbons C₁₃-C₂₀ in recent sediments of hypersaline Lake Karachi, West Siberia.** E.A. kurakolova, V.N. Burkova
- PB2-5. Cyclisation of PUFAs as a pathway to cyclic compounds in sedimentary organic matter.** D.A. Lang, B.G.K. van Aarssen, T.P. Bastow
- PB2-6. An original aromatisation pathway of higher plant triterpenoids in recent sediments.** C. Le Milbeau, P. Schaeffer, P. Adam, P. Albrecht
- PB2-7. LC-MSⁿ studies of defunctionalised chlorophyll derivatives in the Vena del Gesso basin.** D.H. Mawson, B.J. Keely
- PB2-8. Photoinhibition of the marine picoalgal niche: a control on C₃₀ sterane abundance in geological samples.** D. Rocher
- PB2-9. Distributions and sources of hopanoids in sediments from ODP Leg 190, Nankai Trough, Japan.** H. Saito, N. Suzuki, K. Sawada
- PB2-10. An overview of pigment oxidation reactions and the potential use of tetrapyrroles as indicators of oxygen availability.** J.S. Walker, B.J. Keely
- PB2-11. Plant-internal variation of lipid composition and compound-specific isotopes of various crops.** G.L.B. Wiesenberg, J. Schwarzbauer, L. Schwark
- PB2-12. Australian oil families: a comprehensive assessment using principal components analysis of terpane, hopane and sterane biomarkers.** M.B. Yunker, G.A. Logan, M.T. Bradshaw, C.J. Boreham, R.E. Summons, D.S. Edwards, J.E. Zumberge
- PB2-13. Humic acids and biomarker distribution in the Holocene sediments accumulated in Boina-Arade estuary, Algarve, S. Portugal.** T. Boski, O. Polvillo, J.A. Gonzalez-Perez, F.J. Gonzalez-Vila, H. Knicker
- PB2-14. A cornucopia of hopanoids: revisiting the Thornton quarry bitumen (Thornton, Illinois, USA).** F. Kenig, S.C. Brassell, R.K. Nelson, G.S. Frysinger, C.M. Reddy, R.B. Gaines
- PB2-15. One-year seasonal variations of pigments in sweetgum (*Liquidambar styraciflua*) leaves.** R. Ocampo
- PB2-16. Organic compounds in hot thermal waters of Szentes, Hungary.** C. Sajgó, Z. Kárpáti, I. Varsányi
- PB2-17. Lipid biomarkers of chief primary producers and sediments in coral reef, seagrass bed, and mangrove forest ecosystems.** S. Sakata, M. Yamamuro
- PB2-18. Diatom biomarkers across the Eocene-Oligocene boundary in the Northeast Kamchatka Peninsula.** H. Shiine, N. Suzuki, I. Motoyama, S. Hasegawa, A.Y. Gladenkov, Y.B. Gladenkov, K. Ogasawara
- PB2-19. Biomarker analysis of solvent extractable organic matter from the Late Neoproterozoic Kwagunt formation, Chuar group (~800-742 Ma), Grand Canyon.** G.T. Ventura, F. Kenig, E. Grosjean, R.E. Summons
- PB2-20. Sources of organic carbon to a river dominated coastal shelf: the use of chemical biomarkers to trace organic carbon inputs to sediments.** L.A. Wysocki, T.S. Bianchi, T.R. Filley

PB2-21. The stratigraphic distribution of gem-dialkylalkanes in the Plio-Pleistocene Rio Dell and Merced formations, Northern California: implications for the paleoecology of the (as yet unknown?) source organisms. D.A. Zinniker, G. Nylén, M. Nell, P. Denisevich, J.M. Moldowan, J. Michael

PB2-22. Lipid biomarkers in Spanish saline lake sediments: indicators of organic inputs and environmental change. E.J. Pearson, P. Farrimond, S. Juggins

PALEOCLIMATE-1 (PC1)

804

PPC1-1. Upper Jurassic/Lower Cretaceous anoxic event of Adriatic-Dinaridic domain. G. Baric, V. Tari

PPC1-2. Paired measurements of the Sr/Ca-ratio and the carbon isotopic composition of C₃₇ alkenones in particulate matter from Caribbean Sea surface waters. D. Brouwer, B. Schnetger, C. Rühlemann, J. Rullkötter, S. Schulte

PPC1-3. Vegetation change in tropical East Africa since the last Glacial maximum: the molecular record from Lake Malawi. I.S. Castañeda, J.P. Werne, T.C. Johnson, L.A. Powers, Y. Huang

PPC1-4. Evidence for photic zone Euxinia during the Permian-Triassic "Superanoxic Event". K. Grice, M.E. Böttcher, R.J. Twitchett, E. Grosjean, R.E. Summons, S.C. Turgeon, W. Dunning

PPC1-5. Lipid residues as paleo-environmental tracers? – An example from the Emsian of the Prüm Syncline (Eifel Mts., Germany). M. Havertz, U. Mann, R.G. Schaefer

PPC1-6. An improved method for C and N isotopic analyses of sedimentary porphyrins and its application to studies of past geological events. Y. Kashiyama, N.O. Ogawa, H. Suga, Y. Chikaraishi, R. Tada, K. Matsumoto, T. Sakamoto, J. Kuroda, H. Kitazato, N. Ohkouchi

PPC1-7. Biogeochemistry of Neoproterozoic cap carbonates – A speculative hypothesis. D.M. McKirdy, P.R. Gammon, H.D. Smith, H.R. Hayward, S. Sonter

PPC1-8. Sapropels in shallow Holocene coastal lakes of Southeastern Australia: an elemental and isotopic perspective. A.C. Mee, D.M. McKirdy, E.S. Krull, M.A.J. Williams

PPC1-9. Nitrogen fixation enhanced organic matter production in Demerara Rise mid-Cretaceous black shales. P.A. Meyers, S.M. Bernasconi, J.-G. Yum

PPC1-10. Origin and accumulation of organic matter in Albian to Santonian black shales on the Demerara Rise. P.A. Meyers, A. Forster

PPC1-11. East-West comparison of nitrogen and carbon stable isotope systematics in same-age Mediterranean sapropels. P. Meyers, M. Arnaboldi, S.M. Bernasconi

PPC1-12. Isotopic biogeochemistry of lipids in recent sediments of Lake Planina, a remote mountain lake in NW Slovenia. N. Ogrinc, G. Muri, I. Tolosa

PPC1-13. Palaeoenvironmental changes in Padul basin (Granada, Spain) over the last 235 ka b.p. based on n-Alkanes. J.E. Ortiz, T. Torres, A. Delgado, M. Lucini, J.F. LLamas, M. Valle

- PPC1-14. *Palaeoenvironment of the Eocene Eckfeld Maar lake (Germany): implications from geochemical analyses of the oil shale sequence.*** M. Sabel, A. Bechtel, W. Püttmann, S. Hoernes
- PPC1-15. *Paleoclimatic variations recorded by biomarkers of higher plant wax and terpenoid in the deep sea sediments of Northwestern Pacific off Central Japan.*** K. Sawada
- PPC1-16. *Evaluation of past sources and sinks for CO₂ in the South Atlantic Ocean.*** S. Schulte, D. Brouwer, A. Benthien
- PPC1-17. *Orbital-derived lacustrine geochemical signatures and their application to the paleolimnology of perennial lake systems.*** S.C. Teerman, A.G. Fischer, A. Grippio
- PPC1-18. *The Cretaceous oceanic anoxic event 1b as revealed by cm-scale TEX86-based SST and isotope records from the Eastern subtropical Atlantic (Mazagan Plateau off NW-Africa, DSDP 545).*** T. Wagner, I. Stüsser, S. Schouten, J. Sinninghe-Damsté, J. Herrle, P. Hofmann
- PPC1-19. *Reconstruction of terrestrial organic matter input in marine sediments off the coast of Western Africa.*** J.W.H. Weijers, S. Schouten, E.C. Hopmans, E. Schefuß, T. Wagner, J.S. Sinninghe-Damsté
- PPC1-20. *Organic geochemical analysis of deep sea sediments from the African continental margin (ODP LEG 175, Holes 1075A, 1079A and 1082A).*** C. Wenzel, U. Güntner, S. Gebhardt, J. Rullkötter
- PPC1-21. *An integrated molecular and isotopic approach to assess historical changes in organic carbon sources and preservation in the Arctic Ocean.*** L.L. Belicka, H.R. Harvey
- PPC1-22. *Lipid biomarkers in stalagmites as environmental proxies.*** A.J. Blyth, P. Farrimond, M.D. Jones, A. Baker
- PPC1-23. *Organic geochemical reconstruction of productivity cycles in the Benguela upwelling system during the final stages of the intensification of Northern hemisphere glaciation.*** C.S. Boot, M.M. Maslin, R.D. Pancost
- PPC1-24. *Simultaneous evolution of marine and terrestrial carbon isotope records in the Early Miocene.*** J. Briggs, D. Large, C. Snape, M. Cooper
- PPC1-25. *Sequential fatty acid analysis of a peat core covering the last two millennia (Tritrivakely lake, Madagascar): diagenesis appraisal and consequences for palaeoenvironmental reconstruction.*** J. Disnar, M. Stefanova, S. Bourdon, F. Laggoun-Défarge
- PPC1-26. *A high resolution vegetation record of Late Quaternary climate variability in tropical South America.*** N. Drenzek, K. Hughen, T. Eglinton, M. Bice
- PPC1-27. *Elemental and isotopic records of the Early Aptian oceanic anoxic event from Shatsky Rise.*** M. Dumitrescu, S. Brassell
- PPC1-28. *Reconstruction of Holocene paleotemperature in the Iberian Peninsula using lipid biomarkers.*** M. Escala, A. Rosell-Melé

PALEOCLIMATE-2 (PC2)

853

PPC2-1. Lignin-phenol and $\delta^{13}\text{C}$ evidence of Quaternary vegetation change in South America. K.J. Ficken, T.R. Filley, F.A. Street-Perrott

PPC2-2. Last glacial cycle vegetation change in Himalaya from bulk and molecular $\delta^{13}\text{C}$ analyses in Bengal Fan sediments. V. Galy, F. Palhol, P. Faure, C. France-Lanord

PPC2-3. Climate change and the carbon cycle of small, hard water lakes. H.L. Gibbons, J.D. Marshall, G.A. Wolff

PPC2-4. Tracing of variability in geological barriers by molecular organic geochemistry. Case of the Callovo-Oxfordian series in East of Paris Basin (France). Y. Hautevelle, R. Michels, F. Malartre, A. Trouiller, M. Elie

PPC2-5. Confined pyrolysis: an experimental method for the correlation of biomarkers in ancient sediments with extant land plants? Y. Hautevelle, R. Michels, F. Malartre, F. Lannuzel, A. Trouiller

PPC2-6. Paleohydrology of tropical South America since the Last Glacial Maximum. Insights from the δD of algal and terrestrial molecular markers in lake sediments. J. Jacob, Y. Huang, A.L. Spadano Albuquerque, A. Sifeddine, J.R. Disnar

PPC2-7. Rapid paleoenvironmental variations in NE Brazil during the Late Glacial. Insights from TpS_2 , S_3CO_2 and S_3CO Rock Eval parameters. J. Jacob, J.R. Disnar, M. Boussafir, D. Kéravis, A. Sifeddine, A. L. Spadano Albuquerque, B. Turcq.

PPC2-8. The Frasnian/Famennian faunal turnover: new insights from lipid compositions of the Kellwasser horizons and adjacent strata. M. Kloppisch, F. Kenig, U. Mann, H. Wilkes

PPC2-9. New insights into the climatic and vegetational history of the subtropical crater lake "Tswaing", South Africa, for the last ~300.000 years. I. Kristen, A. Fuhrmann, G. H. Haug, B. Horsfield, H. Oberhänsli, J. Thorpe, H. Wilkes

PPC2-10. Possible correlation of the Palaeocene Eocene Thermal Maximum in multiple Late Palaeocene peatland $\delta^{13}\text{C}$ records. D.J. Large, B. Spiro, M.C. Goringe, J. Briggs, T.F. Jones, J.H.S. Macquaker, C. Somerfield, B.P. Atkin

PPC2-11. Biogeochemical markers for palaeoenvironment assessment of the Oligocene of the Rhine Rift Valley (Alsace, France). P. Le Metayer, P. Schaeffer, P. Albrecht, S. Rousse, P. Düringer

PPC2-12. Oceanic environments in Japan Sea during the deposition of thinly laminated layers in the latest Pleistocene. K. Matsumoto, H. Kitazato, R. Ishiwatari, S. Tsukawaki, N. Ohkouchi

PPC2-13. Alkenone and coccolith records of the mid-Pleistocene in the South-east Atlantic: implications for the $U^K_{37'}$ index and South African climate. E.L. McClymont, A. Rosell-Melé, J. Giraudeau, C. Pierre, J.M. Lloyd

PPC2-14. Paleoenvironmental significance of n-alkane δD from Ganga - Brahmaputra ancient sediments. F. Palhol, V. Galy, P. Faure, C. France-Lanord

PPC2-15. Compound-specific hydrogen isotope ratios of sedimentary n-alkanes as a new palaeoclimate proxy. D. Sachse, J. Radke, G. Gleixner

PPC2-16. Land-Ocean Interaction and oceanic response in the Mid-Cretaceous western tropical Atlantic – first geochemical results from ODP Site 1261, Demerara Rise. C. Schmidt, T. Wagner, P. Hofmann, S. Schouten, J.S. Sinninghe-Damsté

PPC2-17. Molecular and isotopic characterization of biomarkers in the Frick Swiss Jura sediments: a palaeoenvironmental reconstruction on the northern Tethys margin. V. Schwab, J.E. Spangenberg

PPC2-18. Late Quaternary palaeoenvironmental reconstructions, Central Andes, Bolivia, from geochemical and petrographical compositions of sedimentary organic matter. A. Sifeddine, L. Martin, P. Meyers, E. Lallier-Vergès, D. Wirrmann, J.R. Disnar

PPC2-19 Reconstruction of the West Pacific El Niño history using the (isotopic) biomarker record of marine anoxic lakes, Palau. R.H. Smittenberg, C. Saenger, M.N. Dawson, J.P. Sachs

PPC2-20. Palaeoenvironment in the site of zinc and lead ore formation at Topla-Mežica, Slovenia: insight from biomarkers and stable isotopes. J.E. Spangenberg, U. Herlec

PPC2-21. Carbon and hydrogen isotopic variations in specific compounds of the Irati Formation: reconstruction of a Permian sea environment in Southern Brazil. E. Vaz dos Santos Neto, J.R. Cerqueira

PPC2-22. Alkane and PAH hydrocarbons in Arctic Ocean sediments: interpretation of distributions in the context of Holocene and Glacial climatic regimes. M.B. Yunker, R.W. Macdonald, L.R. Snowdon, B.R. Fowler, F.A. McLaughlin, J.N. Smith, B. Billeck, G. Ilyin

PPC2-23. Submillennial evolution of global wind regime in the Southern hemisphere during the last three climatic cycles. M. Ferrer, J.O. Grimalt

PPC2-24. High-resolution multi-molecular stratigraphic records from North Atlantic drift sediments (ODP Sites 980, 984) reflecting Holocene climate and ocean dynamics. J. Holtvoeth, T. Wagner, D. Montluçon, G. Mollenhauer, J. McManus, D. Oppo, T. Eglinton

PPC2-25. Biomarker record from the Upper Tisdale (2707 – 2705 Ma) and Porcupine Assemblage (2685 – 2673 Ma) of the late Archaean Abitibi subprovince, Timmins, Ontario, Canada. G.T. Ventura, F. Kenig, C. Reddy, R. Nelson, R.E. Summons

PPC2-26. Molecular and C-isotopic study on biotic and environmental changes across the P/Tr Boundary based on the GSSP at Meishan, China. C.-J. Wang, Y.-M. Liu, H.-X. Liu

PPC2-27. Earth's precession and obliquity influences on sea surface temperature, oceanic primary production and terrestrial vegetation in the mid-latitude Western North Pacific (Core MD01-2421) during the last 14.000 years. M. Yamamoto, T. Oba, J. Shimamune, Y. Ichikawa, T. Ueshima, R. Suemune, D. Isono

MICROBIAL PROCESSES (MP)

905

PMP-1. Fossil DNA as a species-specific recorder of alkenone-biosynthesizing haptophytes: implications for $U^{K'}_{37}$ -based palaeothermometry (P). A. Boere, B. Abbas, J.S. Sinninghe-Damsté, M.J.L. Coolen

PMP-2. Methane formation in eutrophic mountain lake (Jezero na Planini pri Jezeru, Slovenia). M. Žagar, N. Ogrinc, J. Faganeli, T. Kanduč, P. Vreča

- PMP-3. *The geochemical characteristics of pore water and methane in Late Quaternary sediments of the Ulleung basin, East Sea (Sea of Japan).*** J.-H. Kim, M.-H. Park, U. Tsunogai, B.-J. Ryu, Y.-J. Lee, H.-W. Chang
- PMP-4. *Lipid composition of some picophytoplanktonic Choricystis species from freshwater lakes.*** P. Metzger, K.P. Fawley, M.W. Fawley
- PMP-5. *An organic geochemical investigation of Cretaceous cold-seep carbonates accompanied with chemosynthetic community of Central Hokkaido, Northern Japan.*** S. Ogihara
- PMP-6. *Molecular analysis of intact phospholipids of bacteria from Mediterranean sapropels.*** M. Seidel, J. Süß, K. Herrmann, H. Sass, J. Rullkötter
- PMP-7. *The experiment on the biogenic gas generation of Spirulina in different salinity.*** Zangying, Lijian, Huguoyi, Lizhisheng
- PMP-8. *Intact microbial lipid distribution in Lake Baikal sediments – Life markers in a unique deep freshwater environment.*** K.-G. Zink
- PMP-9. *The influence of bacteria on microhabitat selection by benthic foraminifera.*** J. Brandsma, A.M. Langezaal, M. Schmid, S. Schouten, E.C. Hopmans, G.J. van der Zwaan, M. Jetten, J.S. Sinninghe-Damsté
- PMP-10. *Insights into patterns of carbon flow in natural ecosystems using stable isotope labelling.*** S. I. Bühring, M. Elvert, S. Sievert, U. Witte, Kai-Uwe Hinrichs
- PMP-11. *Using lipids and genetic markers to monitor in-situ microbial community growth in Arctic waters.*** R.Y. Dyda-Rearick, M. Suzuki, H.R. Harvey
- PMP-12. *Biogeochemistry of microbial mats in coastal ponds of the Antarctic dry valleys.*** M.M. Hage, M.E. Uhle
- PMP-13. *Search for deep microbial communities in the terrestrial sediments of the Waikato coal area, New Zealand (DEBITS).*** K. Mangelsdorf, K.-G. Zink, J. Kallmeyer, B. Cragg, B. Horsfield
- PMP-14. *Vertical distribution of lipid biomarkers and their stable carbon isotopic signature in marine cyanobacterial mats.*** T. Pape, A. Wieland, J.-H. Klock, W. Michaelis
- PMP-15. *The use of stable-isotope probing to study prokaryotic functional diversity in estuarine tidal sediments.*** J. Rinna, G. Webster, J.C. Fry, A. Weightman, R.P. Evershed, R.J. Parkes
- PMP-16. *Hydrogen and methane in hydrothermal fluids of the Logachev field, MAR.*** R. Seifert, S. Weber, M. Blumenberg, W. Michaelis
- PMP-17. *Biomarker evidence for aerobic and anaerobic oxidation of methane in diverse fluid venting environments in the Nile Deep-Sea Fan, Eastern Mediterranean.*** A. Stadnitskaia, J.S. Sinninghe-Damsté, NAUTINIL 2003 scientific party
- PMP-18. *Formation of iron sulfide nodules during anaerobic oxidation of methane.*** B.E. van Dongen, A.P. Roberts, R.D. Pancost
- PMP-19. *Biomarker analysis of microbial diversity in groundwater-related salt seep sediments of the Lancaster Salt basin, Nebraska.*** J. Fang, O. Chan, R.M. Joeckel, Y. Huang, Y. Wang, D.A. Bazylinski, T.B. Moorman

PMP-20. Exploration of lipid classes and their molecular composition of cultured marine bacteria: progresses and paradigms towards bacterial proxy improvements. M. Laurence, L. Pinturier, H. Agogué, P. Lebaron, M. Goutx

PMP-21. Polar isopranyl glycerol ether lipids as biomarkers of living archaea in near-surface sediments from Nankai Trough. M. Oba, S. Sakata, U. Tsunogai

PMP-22. Labile biochemical indicators and biophile element isotopic ratio related with microbial distribution in sub-surface of semi-permafrost environment. Y. Takano, K. Marumo

PMP-23. Evidence of sub-vent biosphere: enzymatic activities and chiral amino acids in deep-sea hydrothermal sub-vent. Y. Takano, Y. Edazawa, K. Kobayashi, T. Urabe, K. Marumo

MACROMOLECULES (M)

947

PM-1. Thermal alteration of polysulfide cross-linked polymers: structural and $\delta^{34}\text{S}$ changes. A. Amrani, W.S. Ahmad, E. Krein, Z. Aizenshtat

PM-2. Possible biases in interpreting TMAH pyrochemolysis of proteinaceous matter considering glycine and alanine derivatives. N. Gallois, J. Templier, S. Derenne, C. Largeau

PM-3. Haloalkanes in polar geomacromolecules: Myth or reality? V. Grossi, R. De Mesmay, A. Galtayries, D. Raphael, C. Largeau, S. Derenne

PM-4. Analysis of lignin phenols and alkanolic acids in lake and marine sediments by on-line TMAH/thermochemolysis GC-MS: comparison with alkaline CuO oxidation method. S. Yamamoto, R. Ishiwatari

PM-5. Lignin and fatty acid records in Lake Baikal sediments over the Last 130 kyr: comparison with pollen analysis. R. Ishiwatari, S. Yamamoto, S. Shinoyama

PM-6. Refractory organic matter from recent sediments: all melanoidins? A. Riboulleau, N. Tribouvillard, F. Baudin

PM-7. Organic matter fate in externally and internally buffered contact metamorphism processes in the Debnik Anticline, South Poland. A. Lewandowska, M.J. Rospondek, L. Marynowski

PM-8. Nitrogen functionality in various fractions of riverine dissolved organic matter. J. Templier, S. Derenne, F. Mercier, N. Barré, F. Miserque, C. Largeau

PM-9. Formation of alkylphenols during flash pyrolysis. L.R. Boyd, B.G.K. van Aarssen, T.P. Bastow

PM-10. Micromorphological and (bio)chemical organic matter changes in a formerly cutover peat bog: Le Russey, Jura Mountains, France. L. Comont, F. Laggoun-Défarage, J.R. Disnar

PM-11. Sorption of organic matter on clay minerals in aquatic system and influence on sedimentary organic preservation. An example of lacustrine environment (Lac Pavin, France). S. Drouin, M. Boussafir, J.L. Robert, P. Albéric

- PM-12. Source organisms and preservation pathways of the organic matter from Negev Phosphorite samples with contrasting quality (Israel, Upper Cretaceous).** I. Franquin, A. Riboulleau, L. Bodineau, N. Tribouvillard, E. Tannenbaum
- PM-13. Extraction of natural organic matter from marine waters - Fluorometric characterisation of the isolated fractions.** A. Huguet, S. Relexans, E. Parlanti
- PM-14. Analysis of kerogens from Jurassic-Cretaceous boundary in the Sierra de Aralar (Navarra, Spain) by Curie point pyrolysis-gas chromatography-mass spectrometry and pyrolysis Rock Eval.** M. Iriondo, C. Dorronsoro, A. Permanyer, B. Hermosín
- PM-15. Properties of natural dissolved organic matter in the Seine Estuary (France).** E. Parlanti, L. Vacher, C. Garnier, S. Mounier, D. Fevrier, S. Relexans, A. Ficht, M. Olivier
- PM-16. Ruthenium tetroxide oxidation of Orgueil and Murchison insoluble organic matter: assessment on aliphatic moieties.** L. Remusat, S. Derenne, F. Robert
- PM-17. Time dependent changes during the degradation of lignin by the white-rot fungus *Pleurotus ostreatus*: linking the biological and geochemical.** S.A. Robertson, E. Hack, S. Mason, G.D. Abbott
- PM-18. Syngeneity and biogenicity of organic matter in a 3.5 billion year old chert as revealed by Electron Paramagnetic Resonance and pyrolysis GCMS.** A. Skrzypczak, S. Derenne, L. Binet, D. Gourier, F. Robert
- PM-19. Catalytic hydrolysis of Neoproterozoic kerogens from the South Oman Salt Basin.** C. Stalvies, G.D. Love, E. Grosjean, W. Meredith, P. Farrimond, J.P. Grotzinger, C.E. Snape, R.E. Summons
- PM-20. Modifications of dissolved organic matter along the Gironde Estuary (France) - impact on binding properties.** L. Vacher, E. Parlanti, J. Schaefer, G. Blanc
- PM-21. Spore chemistry as a proxy for UV-B flux.** J.S. Watson, M.A. Sephton, S.V. Sephton, D.J. Beerling, S. Self, I. Gilmour, C.H. Wellman
- PM-22. Biogeochemical comparison of modern and fossil woods.** A.O. Baki, M.L. White, E. Lopez-Capel, D.A.C. Manning, G.D. Abbott
- PM-23. The chemical structure of cutan revisited: reinterpretation of the TMAH/thermochemolysis data.** J.C. del Río
- PM-24. Detection of protein remnants in different types of kerogens upon pyrolysis in the presence of TMAH.** J.C. del Río, F.J. González-Vila, A. Amblès, H. Knicker
- PM-25. Aliphatic biopolymers and lignin signatures in resilient humic materials from an estuarine sedimentary sequence (Guadiana Valley, SW Iberian Peninsula).** F.J. González-Vila, T. Boski, O. Polvillo, A. Teran, J.A. González-Pérez, M.E. Arias
- PM-26. Organic matter preservation patterns in marine sediments from Celtic Sea & NW Iberian Margin. A contribution from the adsorption study of hydrolysable amino acids on mineral surfaces.** P. Pedro, T. Boski, J.C. Pessoa, J. Thorez
- PM-27. Characterization of the organic constituents of aqueous and sediment phases of the Cébron reservoir.** M. Poulain, C. Rodier, J.-P. Croue, A. Ambles
- PM-28. On the macromolecular structure of algal cell walls, notably dinoflagellate walls.** G.J.M. Versteegh, P. Blokker

SOIL BIOGEOCHEMISTRY (SB)**1003**

PSB-1. *Complexation properties of esterificated soil humic acids.* T. Andjelkovic, J. Perovic, M. Purenovic, S. Blagojevic, D. Andjelkovic

PSB-2. *Physical-chemical characterization of humic acids isolated from Chilean Andisols.* J. Canales, M. de la Luz Mora, M.J. Aguirre, M. González-Ibarra, R. Gaviño, B. King-Díaz, B. Lotina-Hennsen

PSB-3. *Characterization of humic acid from Pahokee peat using Electrospray Ionization Tandem Mass Spectrometry.* R.-H. Feng, P.-A. Peng, J.-Z. Song, W.-B. Zhang

PSB-4. *Study of some structural features related to the humic nature of different organic materials through the complementary use of fluorescence and UV-Visible spectroscopy.* M. Fuentes-Ramírez, G. González-Gaitano, J.M^a García-Mina

PSB-5. *Stability, solubility and maximum metal binding capacity in metal-organic complexes formed by humic substances with different origins and physico-chemical properties.* J.M^a García-Mina

PSB-6. *Lignin in soils turns over faster than bulk carbon.* A. Heim, M.W.I. Schmidt

PSB-7. *Organic geochemical studies of soil from a temperate-zone marsh.* M. Hetényi, C. Sajgó, T. Nyilas, A. Brukner-Wein

PSB-8. *Characterization of sulphur species in oxic and anoxic soils and soil particles using spectromicroscopy.* N. Tyufekchieva, J. Prietzel, J. Thieme, I. Kögel-Knabner

PSB-9. *Vegetation changes in the Sheng-Guang area using $\delta^{13}\text{C}$ values of soil organic matter.* W. Wang, Y.N. Wang, M.K. Wang, P.N. Chiang, S.Y. Zhuang, S.T. Lin

PSB-10. *Impact of particulate organic matter (POM) biodegradation on selenium solid partition.* C. Chabrouillet, F. Coppin, A. Martin-Garin, J. Balesdent, J.P. Gaudet

PSB-11. *The role of lipids and other biogenic compounds in the development of soil water repellency.* S.H. Doerr, P. Douglas, C.P. Morley, C.T. Llewellyn, K.A. Mainwaring, J. Schabauer

PSB-12. *Composition of mineral associated soil organic matter in a Podzol profile.* K. Eusterhues, C. Rumpel, I. Kögel-Knabner

PSB-13. *Characterization of humic acids in Tropical Spodosols by ^{13}C NMR spectroscopy.* M. González Pérez, P. Vidal Torrado, L. Martin Neto, L.A. Colnago, D.M.P.B. Milori, F. Haenel Gomes

PSB-14. *Labelling of humic substances with ^{14}C and their use for sorption studies with different geomatrices.* A. Mansel, H. Kupsch

PSB-15. *Assessment of high affinity methane oxidising bacterial biomass and growth kinetics in upland and forest mineral soils by time-series $^{13}\text{CH}_4$ PLFA labelling.* P. Maxfield, E. Hornibrook, R. Evershed

PSB-16. *Characterisation of physically extracted soil fractions in the course of decomposition of ^{14}C -labelled maize straw.* F. Schnitzler, A. Gierschner, A. Berns, P. Burauel

PSB-17. *Is atmospheric Suess-effect reflected in arable soils of urban areas?* G.L.B. Wiesenberg, M.W.I. Schmidt, L. Schwark

PSB-18. Tentatively quantifying fire impact, organic carbon balance and thermal structural rearrangements by ^{13}C CPMAS NMR of whole soil samples from Continental Mediterranean forests. G. Almendros, F.J. González-Vila, J.A. González-Pérez, H. Knicker, M.C. Zancada, O. Polvillo.

PSB-19. Can $\delta^{13}\text{C}$ and ^{14}C from organic matter in soils complement records of Mid-Holocene palaeoclimate change in lacustrine sediments? D.M. McKirdy, E.S. Krull, A.C. Mee, A.J. Brenchley, B. Spiro

PSB-20. Stabilization of nitrogen during humification. Study by acid hydrolysis. M. Toribio, P. Rovira, M.M. Coûteaux, V.R. Vallejo

PSB-21. Distribution of C and N in fractions of cultivated volcanic soil. S. Covalada, S. Pajares, J.F. Gallardo, J.D. Etchevers

CARBON SEQUESTRATION (CS)

1042

PCS-1. Preliminary data on carbon sequestration in soils and biomass in some ecosystems of the Canary Islands. C.M. Armas, J.L. Mora, C.D. Arbelo, A. Rodríguez Rodríguez, J.S. Notario

PCS-2. Carbon sequestration in Swedish boreal forests. J. Routh, T.S. Bianchi, L. Wysocki

PCS-3. Stabilization and turnover of fatty acids in soils of long-term experiments. G. Jandl, P. Leinweber

PCS-4. Detection of differences between soil organic matter storage in topsoil and subsoil samples. I. Schöning, I. Kögel-Knabner

PCS-5. Incorporation of elevated radiocarbon from roots or litter into protected and unprotected soil organic matter: evidence for a root-dominated soil carbon cycle. C. Swanston, M. Torn, P.I. Hanson

PCS-6. Is Arctic climate warming causing remobilization of the huge reservoir of Tundra/Taiga soil carbon? B.E. van Dongen, L. Guo, I. Semiletov, Ö. Gustafsson

PCS-7. Sequestration of bulk carbon, lipids and lignin in arable soils. G.L.B. Wiesenberg, M.W.I. Schmidt, A. Heim, J. Schwarzbauer, L. Schwark

PCS-8. A dynamic model of the carbohydrates component of soil organic matter. D. Derrien, J. Balesdent, C. Marol

PCS-9. Organic matter structure in the A horizons of Andosols from the Canary Islands. J.A. González-Pérez, C.D. Arbelo, A. Rodríguez-Rodríguez, H. Knicker, C.M. Armas, O.P. Polvillo, T. Verdejo, F.J. González-Vila

PCS-10. Land use change and carbon storage in soils from Galicia (Spain). L. López-Sangil, M. Toribio, J. Torras, E. Bertran, P. Rovira, V. Ramón Vallejo

PCS-11. Decoupled mechanisms of C and N stabilization in soil: evidence from sequential density fractionation of three soils of contrasting mineralogy. P. Sollins, C. Swanston, S. Crow, B. Caldwell, T. Filley, K. Lajtha

PCS-12. Moving from conventional to ecological farming in Mediterranean countries: any effect on carbon sequestration in soil? J. Torras, M. Toribio, E. Bertran, P. Rovira, J. Romanyà, V. Ramón Vallejo

PCS-13. Organic carbon mineralization and CO₂ evolution of paddy topsoil and the temperature dependence. X. Zhang, G. Pan, L. Li

PCS-14. Is substrate availability a major limiting factor for the degradation of soil organic matter? B. Marschner, U. Hamer

BLACK CARBON (BC)

1067

PBC-1. Slash-and-burn in Neolithic agriculture - Conversion of biomass to charred organic carbon and its fate in soil. E. Eckmeier, R. Gerlach, M. Roesch, O. Ehrmann, W. Schier, M.W.I. Schmidt

PBC-2. Characterisation and evaluation of reference materials for black carbon analyses using elemental composition, $\delta^{13}\text{C}$ and ^{13}C NMR. K. Hammes, R. Smernik, M.W.I. Schmidt

PBC-3. Particulate organic matter (POM) as a means for transport of black carbon in fire-affected Arenosols. A. Hilscher, F.J. González-Vila, J.A. González-Pérez, T. Boski, H. Knicker

PBC-4. Characterisation and quantification of black carbon in the refractory organic macromolecular fraction of forest and cultivated sandy soils. K. Quénéa, S. Derenne, C. Largeau, C. Rumpel, J.-N. Rouzaud, O. Gustafsson, C. Carcaillet

PBC-5. Comparative analysis of reference materials for organic geochemical studies of black carbon – Results. M.W.I. Schmidt, J.O. Skjemstad, C. Masiello, W.P. Ball, L. Currie, D.M. Smith

PBC-6. Insight into the structural features of various forms of refractory organic matter from marine sediments. J.M. de la Rosa, F.J. González-Vila, H. Knicker, E. López-Capel, O. Polvillo, J.A. González-Pérez, M.E. Arias

PBC-7. Thermal characterisation of refractory organic matter from marine sediments. E. Lopez-Capel, J.M. de la Rosa, J.A. Gonzalez-Perez, F.J. Gonzalez-Vila, D.A.C. Manning

PBC-8. Characterisation of charred materials left after slash-and-burn practices in agricultural tropical soils. C. Rumpel, J.A. González-Pérez, C. Largeau, C. Valentin, A. Mariotti

PBC-9. Cultivation-induced alterations recognized in the structural characteristics of resilient humic acids from a sequence of Southern African Soils with different maturity degree. G. Almendros, F.J. González-Vila, M.C. Zancada, M.T. Pardo, J.M. de la Rosa, H. Knicker

PBC-10. The chemical structure of a polar fraction obtained from diesel soot. B. Hermosín, M. Gaviño, C. Saiz-Jiménez

PBC-11. Condensed aromatic ring structures in DOM detected with electrospray ionization and ultrahigh resolution MS: insight to the cycling of black carbon. W.C. Hockaday, A.M. Grannas, S. Kim, P.G. Hatcher

PBC-12. Soot/Graphitic black carbon in Mediterranean forest soils. P. Rovira, V.R. Vallejo

PBC-13. Biogeochemical characterization of sedimentary organic matter in marine sediments. Black carbon isolation discussion. L. Sánchez-García, J.R. de Andrés, J.A. Martín Rubí, A. Terán, J.M. de la Rosa, F.J. González-Vila

PBC-14. Molecular level descriptors of the effect of fire on soils under pine forest in continental Mediterranean soils. P. Tinoco, G. Almendros, J. Sanz, F.J. González-Vila

FORENSIC ARQUEOLOGY (FA)**1093**

PFA-1. Biomarkers in archaeology: the degradation of botanical remains and loss/preservation of chemical information. J. Kool, M. van den Berg, H. Huisman, H. van Haaster, R. van Heeringen, O. Brinkkemper, H. Kars, P. Buurman

PFA-2. Mumie - the 'Blood of Mountains': an analytical approach. B.M. Scholz-Böttcher, A. Nissenbaum, J. Rullkötter

PFA-3. A shallow grave: using lipid and stable isotopic evidence in a murder case. R. Berstan, I.D. Bull, A. Vass, R.P. Evershed

PFA-4. Detection, use and occurrence of petroleum bitumen in Egyptian embalming. K.A. Clark, R.P. Evershed

PFA-5. Asphalt in the Iron Age excavations (12th-7th century BC) of the Philistine Tel Mique-Ekron city: origin and trade routes. J. Connan, A. Nissenbaum, K. Imbus, J. Zumberge, S. Brown

PFA-6. Recognition and evaluation of alteration of antique vegetal resins by the use of biomarkers. A. Charrié-Duhaut, J. Connan, M. Girard, B.T. Mai, C. Lampert, P. Albrecht

PFA-7. Identification and origin of bitumen in the Neolithic artefacts (8100 BC) of Demirköy Höyük in Eastern Turkey. O. Kavak, J. Connan, E. Akin, M.N. Yalcin, K. Imbus, J. Zumberge, S. Brown

PFA-8. Molecular archaeology: geochemical analysis of balms from «Osiris Mummies». J. Maurer, A. Charrié-Duhaut, J. Connan, M. Etienne, P. Albrecht

PFA-9. Resin artefacts from a Bronze Age royal tomb in Syria. A.J. Mukherjee, M.A. James, P. Pfälzner, R.P. Evershed

METHODS & NEW TRENDS**1111****METHODS-NEW TRENDS-1 (MN1)****1113**

PMN1-1. Analysis of organic matter by Flash Pyrolysis - Gas Chromatography – Mass Spectrometry in the presence of Na-smectite: when clay minerals lead to identical molecular signature. P. Faure, L. Jeanneau, F. Lannuzel

PMN1-2. Enhancement of the capability of the laser micropyrolysis GC-MS technique. S.C. George, S. Barcikowski, C. McIntyre, D. Fuentes, R. Sattari, S. Sestak

PMN1-3. Analysis of ladderane lipids in cultures, water samples, and sediments using HPLC/MS/MS. E.C. Hopmans, M.V.M. Kienhuis, J.E. Rattray, A. Jaeschke, S. Schouten, J.S. Sinninghe-Damsté.

PMN1-4. Hydropyrolysis as a preparative method for the compound specific carbon isotope analysis of fatty acids. W. Meredith, C.E. Snape, M.A. Sephton, G.D. Love

PMN1-5. Removal of olefin based drilling fluids from geologic materials. R.K. Olson, H. Dembicki Jr., N. Hung

PMN1-6. An improved method for micro-separation of straight chain and branched/cyclic-alkanes: Urea Inclusion Paper Layer Chromatography. S. Xu, Y. Sun, X. Mo, P. Chai

PMN1-7. Development of thermal extraction and thermal extraction-GC instruments for analysis of hydrocarbon pollutants in environmental studies. M. Bjorøy, I.L. Ferriday, B.B. Olsen

PMN1-8. Analysis and characterisation of dissolved organic nitrogen in aquatic environment. H. Gallard, S. Ambonguilat, Y. Touchard, B. Parinet, J.P. Croué

PMN1-9. Total Scanning Fluorescence (TSF) as an effective screening tool for delineating oil families. K. Liu, S.C. George, S. Li, X. Pang, S. Fenton, H. Volk, M. Ahmed

PMN1-10. Monofluorinated polycyclic aromatic hydrocarbons and dibenzothiophenes as internal standards. Introduction of a new method of PAH analysis. G.M. Luthe, H. Liu, G. Reijerink, J.E. Johansen

PMN1-11. Enhanced SARA compositional analysis of whole oil. S.R. Palmer, P. Walker, B. Olson

METHODS-NEW TRENDS-2 (MN2)

1133

PMN2-1. Fluorescence indexes: new criteria for the characterisation of dissolved organic matter in aquatic environments. E. Parlanti, L. Vacher

PMN2-2. Nanogram-scale stable isotope analyses by "nano-EA-IRMS". P. Polissar, C.H. Turich, K.H. Freeman

PMN2-3. Comparative study of results in Mexican samples of rock using the Rockeval II and Rockeval 6. L. Ramírez G., R. Martínez A., N. Cañipa M.

PMN2-4. A novel method for the determination of the acidity of crude oils using ¹³C-labelled iodomethane. N. Rouquette, P. Schaeffer, I. Kowalewski, A. Fafet, D. Levache, P. Albrecht

PMN2-5. Systematic statistical effects of sample collection method on geochemistry of petroleum compounds. S.A. Baylis

PMN2-6. The optimization of amino acid derivatisation for GC-C-IRMS for biogeochemical applications. L.T. Corr, R.P. Evershed

PMN2-7. Use of thermogravimetric-isotope ratio mass spectrometry to investigate C isotopic homogenisation of wheatstraw during growth of the oyster mushroom (*Pleurotus ostreatus*). E. Lopez-Capel, G.D. Abbott, D.A.C. Manning

PMN2-8. Optimization of the programmable pyrolysis method in rock Eval 6. R. Martínez A., L. Ramírez G., N. Cañipa M.

PMN2-9. SARA Fractionation of poor bitumen extracts by solid phase extraction. J. Téllez, S. Capella, L. Castro, N.K. Cañipa, C.R. Aldana, C.A. Zuñiga

PMN2-10. Separation of methane from gas mixtures as a technique of preparation for hydrogen isotopic analysis. H. Yoshioka, S. Sakata

PMN2-11. Direct analysis of polar fractions of heavy crude oils using a Finnigan LTQ FT hybrid mass spectrometer. V. Zabrouskov, M. Senko, T. Moehring, H. Muenster

AUTHOR INDEX

1153

KEYWORDS

1167

BIOGEOCHEMISTRY (Cont.)

PEB1-1: Exposure of marine organisms to polycyclic aromatic hydrocarbons (PAHs): use of PAH metabolites to track the impact of oil spills in relation to their toxicity

H. Budzinski¹, O. Mazéas¹, J. Tronczynski², Y. Desaunay², M. LeDu¹

1) LPTC, UMR 5472CNRS, Université Bordeaux I, 33405 Talence, France

2) IFREMER, 44311 Nantes, France

Polycyclic Aromatic Hydrocarbons (PAHs) have been found in many modern and ancient environments such as soils, sediments and petroleum. They belong to the list of priority pollutants established by the EPA (Environmental Protection Agency, USA) due to mutagenic and carcinogenic properties some of them.

Their ubiquity in the environment results from a great diversity of sources. Pyrolytic processes represent the major source of PAHs into the environment, this includes anthropogenic sources (incomplete combustion of organic matter such as petroleum derivatives) and natural sources (forest fires). PAHs and alkylated PAHs are also naturally present in crude oils resulting from the diagenetic and catagenetic transformation of organic matter. Despite the relatively low contribution to the total quantity of aromatic hydrocarbons released into the marine environment, oil spills can represent an important local source of PAHs. To assess the significance of such a contamination on organisms, the quantification of PAHs in marine organism tissues is usually carried out. However depending on the ability of organisms to metabolize PAHs, measurement of the bioaccumulated part of PAHs can be restrictive and not representative of the environmental contamination due to their transformation into more toxic molecules than parent ones. In this way the study of PAHs fate in marine organisms appears to be more and more necessary in order to assess bioavailability and toxicity of those contaminants. The toxicity of a compound is related to its physico-chemical properties but also depends on the combination of various competitive processes such as absorption, distribution, transformation and excretion of the compound by the organisms. In the case of PAHs it has to be noted that they are reactive species that can be biotransformed quite rapidly. Metabolites of PAHs are important parameters in the understanding of PAH toxic impact.

In this work we have developed a combined approach based on PAH bioaccumulation determination and PAH metabolite analyses in order to study PAH exposure of aquatic organisms. Indeed a more systematic analysis of PAH metabolites in monitoring programs should allow a better understanding of PAH contamination impact on organisms and enable to establish a link between exposure and effects.

We have applied this approach to the study of the Erika oil spill that has contaminated the French Atlantic coast at the end of 1999. We have followed over three years the contamination of fish (*Solea solea*) sampled all along the Atlantic coast by measuring PAH content, bile and plasma PAH metabolites (Figure 1) and coupling this with EROD measurement. Researches have been also undertaken in order to study the exposure of aquatic marine organisms to PAHs via the determination of PAH metabolites. Microcosms have been followed in order to link PAH contamination of the medium to PAH bioaccumulation and PAH biotransformation by aquatic organisms such as *Solea solea*. PAH metabolites have proven to be an efficient tool of exposure diagnostic of fish to oil spill pollution (which is not the case of PAH tissue contents).

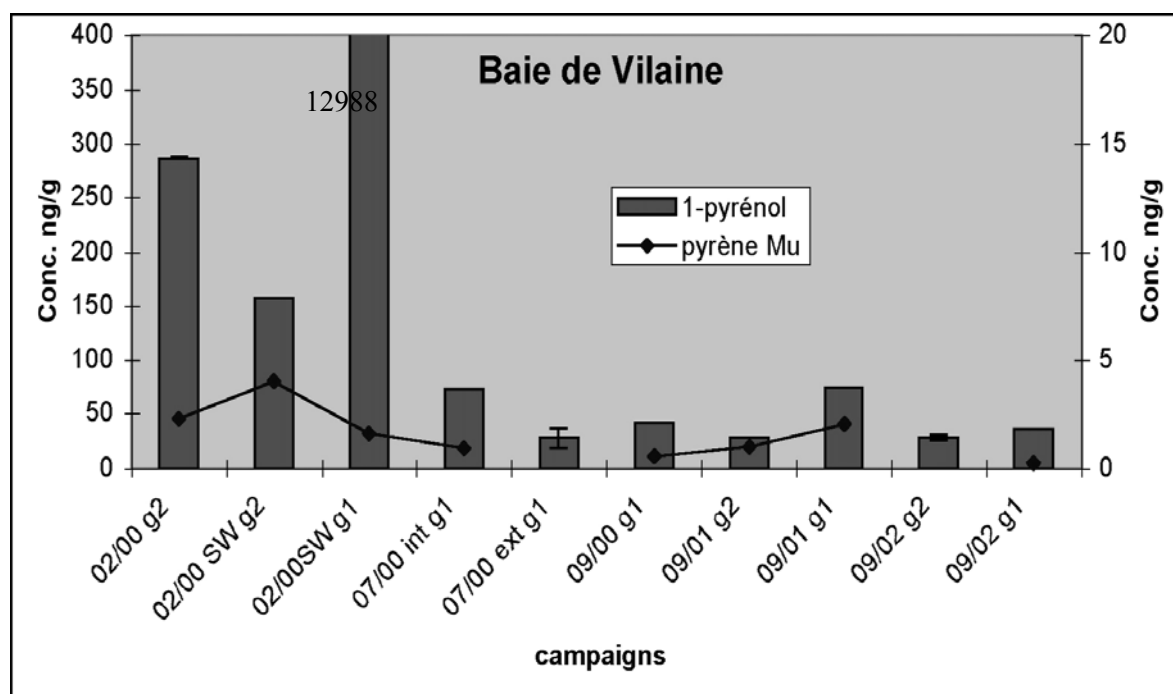


Fig.1. Pyrene content of sole muscle and pyrenol content of sole bile in the case of Vilaine Bay (Atlantic Coast of France) during the field monitoring (g2 = 2 year old sole, g1 = 1 year old sole, g0 = few month old sole)

Acknowledgements

This research was supported by the Région Aquitaine, The Erika program (Ministère Français de l'Écologie et du Développement Durable) and the BEEP European Project (n°EVK3-CT2000-00543).

PEB1-2: Trace analysis of hydrocarbons in coral cores from Saudi Arabia

K.A. Burns, J. Lough, D. Barnes, D. Brinkman, A. Poulsen, S. Delean

Australian Institute of Marine Science (AIMS), PMB 3 Townsville, Qld 4810 Australia
(e-mail: kburns@aims.gov.au)

As part of the long term environmental assessment of the 1991 Gulf War, AIMS conducted growth and chemistry studies on coral cores. We constructed specialized coring devices for the sampling of massive corals (*Porites lutea*) by SCUBA divers. The corer was 5 cm in diameter and 50 cm long. Twenty-eight cores were collected, ranging from 22 to 42 cm in total length, from four coral reefs located in the Arabian Gulf, offshore from Saudi Arabia. The cores were dried and sent to AIMS for analysis.

Sections of the cores from layers surrounding the 1991 oil spill were analysed in each core. Additionally, in cores that extended to the early 1980s, layers from 1980 to 1986 were analysed to find residues from the oil spill in 1983-4 after the Kargh oil terminal was damaged during the Iraq-Iran war. As very little is known about the mechanisms for incorporation of oil into coral skeletons or the stability time frames for occluded organics, both major spill events were targeted to provide additional confidence in relating oil concentrations to specific pollution events. Figure 1 shows statistical box plots of the sum of the triterpane plus sterane oil biomarkers. Two extreme samples (Karan 15, 1980 and Jana 6 2003) were excluded from this statistical plot. The highest and most consistent levels of hydrocarbons that may be related to the 1991 oil spill were observed in Jana cores 6 and 7. In both cores, the 1991 year-layers contained higher concentrations of hydrocarbons than the 1984 year-layer. The detection of both major oil spills confirms the success of detecting oil spills in coral skeletons using chemical analysis. However, residual oil remaining in these cores is altered over time and biomarker ratios differed from the Gulf crude oils. Thus it is difficult to relate composition to source oil and impossible to estimate the amount of oil to which the corals were exposed. High values of aromatic and biomarker hydrocarbons seen in 1980 samples (Karan 15) may relate to tanker bombings at the start of the Iraq-Iran war. Other apparently high values of hydrocarbons may relate to localized pollution incidents (Jana 6, 2003).

The concentrations of hydrocarbons in each core were compared with the growth parameters of the cores. The extremely high chemistry value for which growth data is available was the 1980 layer of Karan 15. (We would not be able to measure growth on the 2003 band, the year of collection.) The growth data for Karan 15 show a precipitous drop in extension rate between 1980 and 1981. Thus this is the only sample that may have recorded an "impact" of oil exposure. There was no other correspondence between slight changes in growth parameters between years and the trace chemistry. Therefore, chemical analysis

enables detection of the exposure incident, but provided no insight into the amount of oil to which the coral was exposed. The chemical data can only infer biological impact if growth was significantly decreased (Karen Core 15, 1980). If coral growth was significantly reduced in one year, then there would be no detectable growth band for that year, and the detection of an oiled layer may appear at an estimated year younger (eg. Jana Core 6 1985).

The average coral growth characteristics of *Porites* from the four sites in the Arabian Gulf fell within the average range for this species when assessed against the wide extent of reefs environments along the Great Barrier Reef, Australia. Average extension and calcification rates were normal, as predicted from the average water temperatures of the region. There was an indication of an overall decline in growth over time, which should be monitored in future. Statistically significant declines in calcification at specific year-layers later than 1986 were evident at: Karan (1988-1989), Jurayd and Jana (1990-1991), Karan and Gosp-4 (1991-1992), Jana and Gosp-4 (1995-1996) and Karan and Gosp-4 (2000-2001).

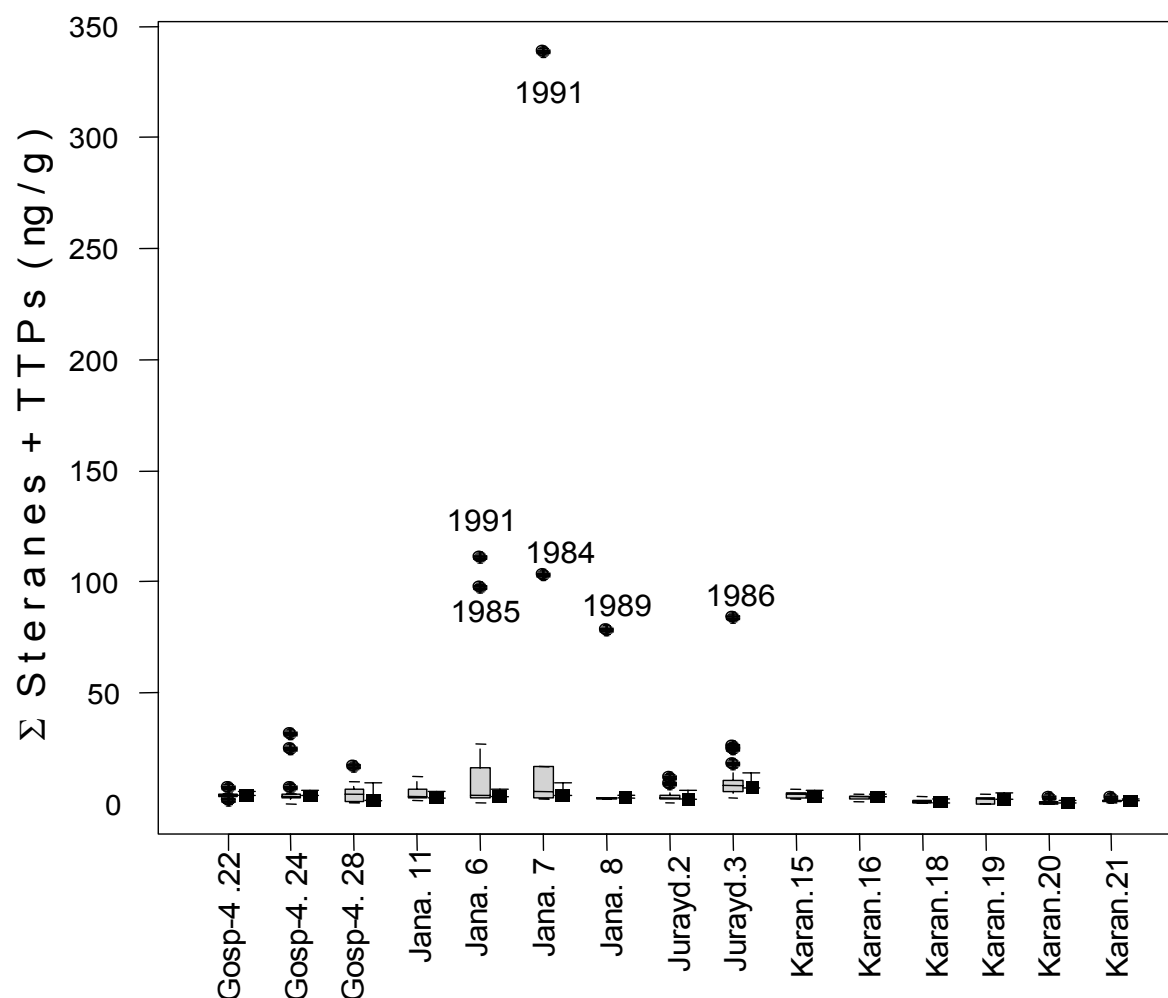


Fig.1. Statistical box diagram plus robust mean + 2 standard deviation for sum of steranes and triterpane oil biomarkers (ng g^{-1}) in coral cores, excluding two extreme samples (Karan 15, 1980 and Jana 6, 2003)

PEB1-3: Organic chlorinate pesticides (OCPs) and polycyclic aromatic hydrocarbons (PAHs) in the Xijiang River, South China

H. Deng^{1,2}, J. Song¹, P. Peng¹

1) State Key Laboratory of Organic Geochemistry, Guangzhou Institute of Geochemistry, Chinese Academy of Sciences, Guangzhou, P. R. China (e-mail: denghongmei51@126.com)

2) Graduate School of Chinese Academy of Sciences, Beijing 100039, China

Persistent organic pollutants (POPs), such as organic chlorinate pesticides (OCPs) and polycyclic aromatic hydrocarbons (PAHs), have received great concern due to their persistent occurrences in nature and possible transportation to remote areas by atmospheric circulation. Xijiang River is the major branch of the Pearl River, covering an area of 353,120 km², which takes 77.8% of area of the Pearl River. The rapidly developing in industry and agriculture and massive use of chemicals in last two decades had caused serious pollution problems, which have accordingly influenced the air and water quality in this area. It is important to quantify the flux and the particle-water distributions of OCPs and PAHs in Xijiang River that may help us to estimate the trend of pollution and thereby to provide the effective methods to control the POPs pollution in this area.

In this study we collected the upper, middle and lower part of water column samples at Gaoyao hydrological station of the Xijiang River in two seasons, May to August of 2003 representing the high river flow and November of 2003 to March of 2004 representing low river flow. Sterilized water was stored in a cleaned array of glass bottles. The Upper, middle and lower Samples were separated into particulate and dissolved phase using 0.7µm glass fiber filters. Particulate and dissolved phase were both analyzed for OCPs and PAHs. Black Carbon in the particulate phase was also quantified by a chem-thermal oxidation method.

Total OCPs concentration varies seasonally from 0.24 to 3.81 ng/l for particulate (Cp) phase, from 1.31 to 13.68 ng/l for dissolved (Cw) phase, while total PAHs concentration varies from 101.7 to 499.1 ng/l (Cp), from 3.74 to 110.3 ng/l (Cw). It is clear that the total OCPs concentration in high flow season was lower than in low flow, while the total PAHs concentration is opposite. The concentration of OCPs in particulate phase was lower than those in the dissolved phase mostly can be attributed to the volatility of OCP molecules, adsorption into particulate is the minor form. Otherwise, the PAHs concentration in the particle phase was higher than those in the dissolved phase can be explained by the fact that hydrophobic organic pollutants mainly occur in the particulate phase. Among HCHs (HCHs=α-HCH+β-HCH+γ-HCH+δ-HCH), the predominance of β-HCH of total HCHs was clearly observed both in the particle and dissolved phase. The ratios of DDT/(DDE+DDD) for

the Gaoyao water column samples demonstrate that such chemicals were polluted in this region in recent times. The predominant PAHs in the particle phase and dissolved phase are all 3-4 ring PAHs originate from combustion of fossil fuels. Take HCHs and DDTs as an example, the flux of these OCPs were 92.3 and 71.1kg/annual respectively. It showed the OCPs concentration was not high in comparison with other places in the world^[1,2]. However, the flux of anthracene (three ring of PAHs), benzo[a]pyrene (four ring of PAHs) and benzo[g,h,i]perylene (six ring of PAHs) were 4091.1, 5104.2, and 1390.4kg/annual respectively, it was much higher than it reported in the Mississippi River^[3].

References

1. Zhou J. L., Hong, H. Zhang Z., 2000. Multi-phase distribution of organic micropollutants in Xiamen Harbour, China. *Water researcher* 34, 2132~2140.
2. Mansingh A., Wilson A., 1995. Insecticide contamination of Jamaican environment III: Baselines studies on the status of insecticidal pollution of Kingston Harbour. *Marine Pollution Bulletin* 30, 640-645.
3. Mitra, S., Bianchi, T. S., 2003. A preliminary assessment of polycyclic aromatic hydrocarbon distributions in the lower Mississippi River and Gulf of Mexico. *Marine Chemistry* 8, 273~288.

PEB1-4: Oil spill bioremediation in Brazilian marine environment – A mesocosm simulation

E.S. de Souza, M.F. Coelho, J.A. Trigüis

Universidade Estadual do Norte Fluminense, Laboratório de Engenharia e Exploração de Petróleo, Rodovia Amaral Peixoto Km 163, Avenida Brennand s/n, Imboacica, Macaé, Rio de Janeiro, Brazil CEP: 27925-310 (e-mail: eliane@lenep.uenf.br)

The petroleum exploration, production and transportation activities along the Brazilian coast may impact the environment by releasing oil. The best response is to minimize the amount of oil that reaches the shoreline. This can be done using containment booms associated to a removal of the oil, by enhancing the naturally occurring biodegradation process just below the water line. Bioremediation is a technology that accelerates the natural biodegradation process in order to reduce the concentration and/or toxicity of various chemical substances, including petroleum ([6], [1]). Bioremediation is accomplished by the addition of microorganisms to the environment or, by promoting better conditions for their metabolic activities, such as incorporation of oxygen or nutrients rich in nitrogen and phosphorous compounds ([4], [5], [2]). Petroleum biodegradation process is influenced by indigenous oil-degrading microorganisms biodiversity and environmental parameters, mainly temperature, making tropical habitats, potential candidates for bioremediation ([2], [7]). This research includes a mesocosm simulation of an oil spill bioremediation in a tropical marine environment, using seawater, a light crude oil and an immobilized water-soluble NPK fertilizer, in substitution of an expensive slow release nutrient, over a period of 28 days. The extent of oil biodegradation was determined by whole oil gas chromatography and gas chromatography – mass spectrometry analyses. The results showed that the oil natural degradation, mostly due to evaporation process, was responsible for the loss of, approximately, 35 % of the light compounds by the end of the experiment. The residual oil mass, presented in bioremediation units, measured at the end of experiment was 83 % less than the original oil mass spilled, indicating that almost 50% of oil was bioremediated. The biodegradation of the *n*-alkanes and nutrient uptake was most effective between 4 and 7 days, as a result of bioremediation (Fig.1). The use of immobilized NPK promoted the biodegradation of approximately 70% of methyl-phenanthrenes and methyl-dibenzothiophenes after 28 days of the experiment (Fig.2). And according to GC/MS results, no changes were observed in the relative abundance of triterpanes during the oil spill bioremediation.

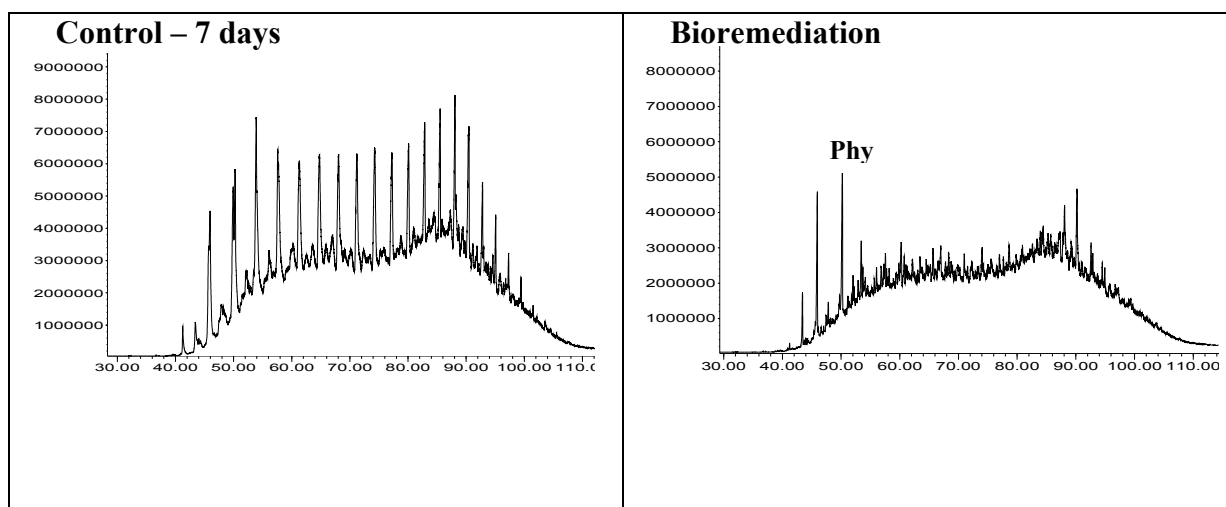


Fig.1. Chromatograms profiles of oil samples collected from Control and Bioremediation units at 7 days of the experiment

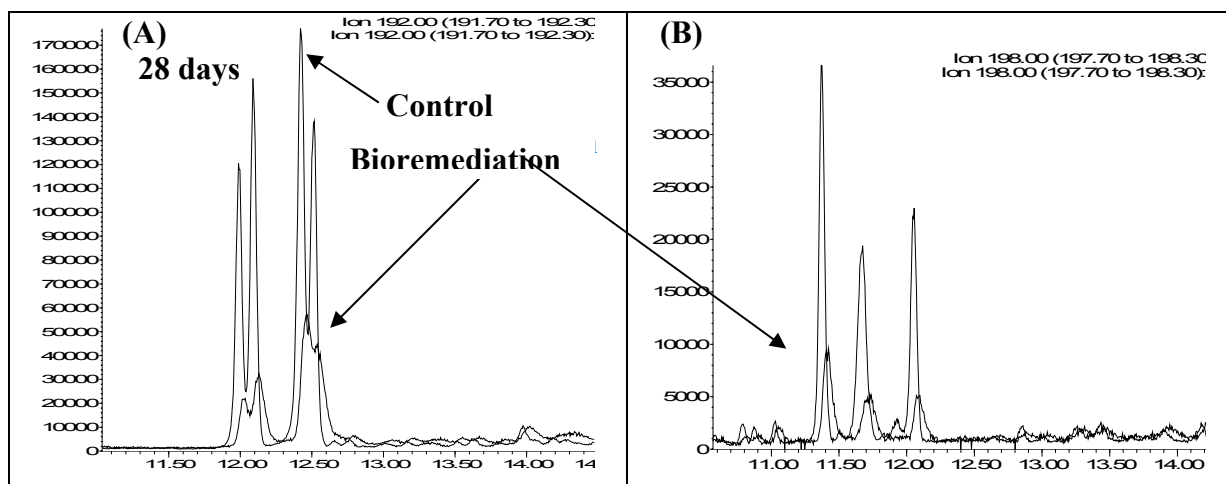


Fig.2. Mass chromatograms of methyl-phenantrenes (A) and methyl-dibenzothiophenes (B) of oil samples collected from Control and Bioremediation units at 28 days of the experiment

References

- [1] Atlas, R. M. 1995. Petroleum biodegradation and oil spill bioremediation. *Marine Pollution Bulletin* 31, (4). 178-182.
- [2] Foght, J., Semple, K., Gauthier, C., Westlake, D.W.S., Bleinkinsopp, S., Sergy, G., Wang, Z., Fingas, M. (1998b). Effect of nitrogen source on biodegradation of crude oil by a defined bacterial consortium incubated under cold, marine conditions. *Environmental Technology*, 20: 839-849.
- [3] Lee, K.. In situ bioremediation of oiled shoreline environments. 1999. Opportunities for Environmental Applications of Marine Biotechnology 45-60.
- [4] Prince, R.C. 1993. Petroleum spill bioremediation in marine environments, *Critical Reviews in Microbiology*, 19 (4). 217-242.
- [5] Rosenberg, E., Legmann, R., Kushmaro, A., Adler E., Abir H., Ron, Eliora Z. 1996. Oil bioremediation using insoluble nitrogen source, *Journal of Biotechnology*. 51. 273-278.
- [6] Rowland, S.J., Alexander, R., Kagi, R.I., Jones, D.M., Douglas, A.G. 1986. Microbial degradation of aromatic components of crude oils: A comparison of laboratory and field observations. *Org. Geochem.* 9 (4). 153-161.
- [7] Souza, E. S. 2003. Desenvolvimento de métodos de biorremediação aplicados a derrames de petróleo em água do mar – Testes laboratoriais. PhD Thesis, Universidade Estadual do Norte Fluminense, Brazil.

PEB1-5: Occurrence of polycyclic aromatic hydrocarbons (PAHs) and organochlorine compounds in Iloilo River, Philippines

P. Gerrez, V. Tañeza, R.P. Philp

School of Geology and Geophysics, The University of Oklahoma, Norman, Oklahoma 73069

Six sampling stations were established along the Iloilo River in the Philippines to investigate the spatial and temporal occurrence of polycyclic aromatic hydrocarbons (PAHs) and organochlorine compounds (polychlorinated biphenyls and chlorinated hydrocarbon pesticides). Studies on these persistent organic pollutants (POPs) are very limited in the tropical/subtropical countries in Asia, particularly in the Philippines. The Philippines is both an agricultural and industrial country that has used significant amounts of fertilizers and pesticides. It has also stockpiled probable toxic wastes due to the technical inability of the industries to safely dispose the generated persistent organic pollutants. In addition, the Clean Air Act (CAA) of the Philippines in 1999 prohibits any high temperature incinerations on POPs. These pollutants can be quickly dispersed into the atmosphere and into aquatic systems from point sources due to the tropical mild to high temperatures and heavy rainfall of the region.

The Iloilo River is a 10-km long tidal inlet utilized for navigation, recreation, and fish resources. However, it has also become the untreated sewage system, garbage disposal, and drainage outflow for several industrial, institutional, commercial, and informal settlers situated along the riverbank. The likely occurrence of POPs is of particular concern in assessing the biotic integrity and water quality of the river. The hydrophobic nature of PAHs and PCBs will typically yield low concentrations in rivers. But it is also the tendency of these contaminants to readily associate with organic matter in streambed sediments and bioaccumulate in the tissues of aquatic organisms that will allow for the detection of the organic compounds in the river. Moreover, they can adsorb to suspended particulate organic matter or in some cases, resuspension of the compounds from the bottom sediments to the surface water can also occur due to flooding and constant dredging of the river. Therefore, streambed sediments, surface water, and fish tissues were the different sample matrices that were collected for analysis. Lipids were isolated from three fish species gathered from the river. Two species were planktonic (Tarpon and Hawaiian ten pounder) and the third was benthic (Indian flathead). In order to assess the influence of precipitation on the concentration of organic compounds in the river, samples were collected in the wet season and the dry season.

The goal of this study is to use geochemical techniques in order to determine the occurrence, distribution, concentration, and potential sources of the POPs through the utilization of gas chromatography, gas chromatography-mass spectrometry, and gas chromatography-isotope ratio mass spectrometry. With the different techniques, identification and quantification of PAHs and organochlorine compounds were accomplished. Various methods were used to elucidate the potential sources of these contaminants. PAH compound ratios were calculated to evaluate the relative contribution between petrogenic and pyrogenic sources. In addition, sterane and hopane biomarker compounds and other hydrocarbons were utilized to aid in fingerprinting the sources of these persistent organic pollutants and their mode of entry into the river. Carbon isotopes of individual compounds further differentiated the degradation products of the parent compounds and between the different natural and anthropogenic sources of the pollutants. Results of this study will be discussed.

The results of the study will be discussed with particular emphasis being directed towards the distribution and origin of the POPs found in the sediments and various fish species.

PEB1:6: Environmental organic geochemistry of polycyclic aromatic hydrocarbons (PAHs) and its environmental impact in coal from Huaibei coal field

L. Gui-Jian^{1,2}, X. Jian¹, Z. Hao-Yuan¹, W. Xinming³

1) School Of Earth and Space Sciences, University of Science and Technology of China, Hefei 230026
(e-mail: lgj@ustc.edu.cn)

2) Key Laboratory of Loess and Quaternary Geology, Institute of Earth and Environment, CAS, Xi'an, 710075, Shanxi, China

3) State Key Lab. of Organic Geochemistry, Guangzhou Institute of Geochemistry, CAS, Guangzhou 510640

Polycyclic aromatic hydrocarbons (PAHs), which are mainly generated by fossil fuel's combustion, are a group of compounds that have no less than two benzene rings. Coal is formed by plants under long geologic process. In the process of coalification, high molecular-weight aromatic acids are formed by polymerization, which make increase the content of PAHs in coal. During coal combustion, the many the species, high content of polycyclic aromatic hydrocarbons will be formed because of organic composition in coal and combustion conditions. The relationship of the content, species and forming mechanism of polycyclic aromatic hydrocarbons in raw coal and the coal forming environment, coal rank and ingredient were studied. The species, rule of occurrence, change of distribution of polycyclic aromatic hydrocarbons and their relation to ingredient and combustion conditions were particular discussed. The conditions of combustion to the total amount of PAHs and its releasing characters were analyzed. The release of low ring PAHs and its environmental impact were discussed. On the basis of research, the problems of the research of PAHs in coal and directions of future research were analyzed.

The studied Sample were collected from the fresh raw coals in Huaibei coalfield. The samples were extracted by three different solvents, which are CS₂, CH₂Cl₂ and C₆H₁₄, with Soxhlet extracting method, separately. The extracted liquids were determined by GC-MS. And the species and concentration of 16 PAHs attented by EPA were analyzed. The impact on the species, concentration and distribution of PAHs extracted by different solvents from raw coal were studied. On the basis, It can be concluded that C₆H₁₄ has the weakest extraction ability, CS₂ is prefer to extract low-ring PAHs and CH₂Cl₂ is prefer to extract high-ring PAHs from raw coal. The five piror-PAHs and 17 none piror-PAHs were found in coal samples. And none piror-PAHs are main types of polycyclic aromatic hydrocarbons and there are two and three benzene rings of PAHs in the coals.

Acknowledgements

This work was supported by National Natural Science Foundation of China (No 40273035), Anhui Natural Science Foundation (04045064), Open foundation of State Key Lab. of Coal Conversion, Insyiyute of Coal Chemistry, CAS (04-904). The authors sincerely thank State Key Lab. of Organic Geochemistry, Guangzhou Institute of Geochemistry, CAS for their analytical assistance.

PEB1-7: Monitoring river pollution by molecular characterization of the sedimentary organic matter using Gas Chromatography – Mass Spectrometry (GC-MS)

L. Jeanneau, P. Faure, M. Ramelli, L. Mansuy-Huault

UMR 7566 CNRS G2R, Université Nancy I, BP 239, 54506 Vandoeuvre Lès Nancy Cedex, France (e-mail: Pierre.Faure@g2r.uhp-nancy.fr)

The aim of this project, part of a regional research program (ZAM: Zone atelier Moselle), is to assess the impact of a high-contaminated river draining an industrial area (The Fensch, watershed area = 83 km²) on a more important hydrologic system (The Moselle, watershed area = 10 761 km²). Our goal is to determine the sedimentary organic matter fingerprints and to check specific biomarkers in order to identify sources of the organic matter accumulated in sediments.

River sediment cores (60 cm) were sampled in the Fensch River near the confluence and in the Moselle River upstream and downstream the confluence (Figure 1) in winter 2004 and 2005, and summer 2004. Each core was divided into three parts in order to study the evolution of the organic fingerprints with depth. Each part was freeze-dried, then ground to a 500 µm particle size. The soluble organic matter was isolated from the mineral matter – insoluble organic matter matrix by extraction with dichloromethane at 130 °C under 100 bar during 16 minutes using an automatic extractor Dionex ASE 200. Extracts was fractionated by liquid chromatography in three families discriminated by their chemical nature: the aliphatic hydrocarbons, the aromatic hydrocarbons and the polar compounds. Each fraction was analysed by gas chromatography – mass spectrometry.

Aliphatic hydrocarbons from the upstream sediments are characterized by the occurrence of (i) n-alkanes with an odd over even carbon number predominance in the C₂₁ to C₃₃ range and (ii) degradation products of phytol both inherited from vegetal contributions (Bray and Evans, 1961). Fensch samples are marked by (i) a large UCM (Unresolved Complex Mixture) and (ii) the occurrence of mature pentacyclic triterpanes both inherited from fossil organic matter (petroleum and/or coal industries). The aliphatic hydrocarbons of the downstream sediments correspond to a mix of these two molecular signatures (figure 1).

The molecular distribution of the aromatic hydrocarbons is close for all the sampled, dominated by parents PAH (polycyclic aromatic hydrocarbons) typical of a pyrogenic organic matter (Yunker and *al.*, 2002).

The occurrence of long chains of alkanolic acids and alkanols and the predominance of stigmasterol and stigmastanol in the polar fraction (figure 1) reveal that upstream sediments of the Moselle river are dominated by higher plants inputs. On the contrary Fensch and downstream sediments are characterized by a high proportion of coprostanol inherited from human fecal matter revealing probably wastewater contributions (Leeming and *al.*, 1996).

The molecular analysis of each organic fractions (aliphatic and aromatic hydrocarbons as well as polar compounds) allow us to evaluate the influence of a high-contaminated river (Fensch) on the organic matter recorded in Moselle sediments downstream the confluence. Moreover comparison of (i) sediments sampled at different seasons (winter and summer) and (ii) suspended particulate matter sampled in the same location, allow us to better understand the spatial and temporal variation of the sedimentary organic matter.

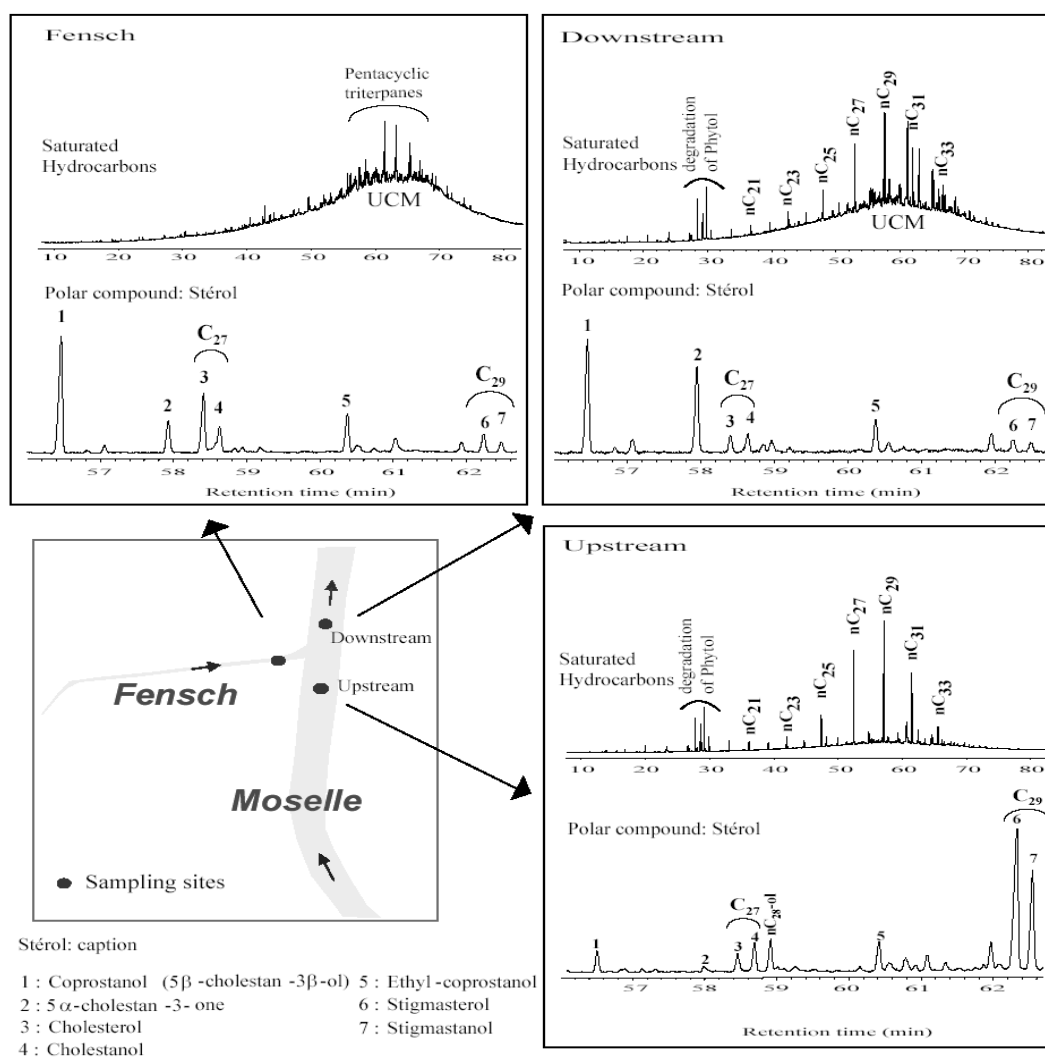


Fig.1. Typical aliphatic hydrocarbons and sterol chromatograms (fullscan) of Fensch River sediments and Moselle River sediments sampled upstream and downstream the confluence

References

- Bray E.E. & Evans E.D. (1961) Distribution of n-paraffins as a clue to recognition of source beds. *Geochim. Cosmochim. Acta*, **22**, 2-15.
- Leeming, R., Ball A., Asholt N. & Nichols P.D. (1996). "Using faecal sterols from humans and animals to distinguish faecal pollution in receiving waters." *Water Research* **30**, 2893-2900.
- Yunker, M.B., MacDonald, R.W., Vingarzan, R., Mitchell, R.H., Goyette, D. & Sylvestre, S. (2002) PAHs in the Fraser River basin: a critical appraisal of PAH ratios as indicators of PAH source and composition. *Org. Geochem.*, **33**, 489-515.

PEB1-8: Organic pollutants of Merseyside inferred by SPOT data

S. Mukherjee, A. Mukherjee

Department of Earth & Ocean Sciences The University of Liverpool 4, Brownlow Street, L693GP, Liverpool, UK (e-mail: Dr.saumitramukherjee@usa.net)

Liverpool was by far the largest urban centre within Merseyside, the development of a canal system throughout this period ensured better communications which allowed existing industries to expand and new ones to develop. The same period saw a rapid increase in the regions population; Liverpool grew from 77,500 in 1801 to nearly 437,740 in 1861 and 684,959 in 1901, and although natural increase accounted for some of this rise, the arrival of migrants from other regions of the country boosted the population figures considerably. Till date the population of Liverpool is increasing continuously. This increase in population provided the workforce for the expanding industries whilst at the same time stimulating the need for housing and other amenities and services. The industries were mainly Quarrying, Tobacco, Ship building, Soap making and Liverpool potteries. Along with the effluents of these industries sewage from the expanding population may have posed a threat to the aquifer system of Merseyside. River courses have changed in due course, which is inferred by the existence of series palaeochannels. These led to hidden organic pollutants in Liverpool. Vegetation anomalies were inferred along the specific landform features in Liverpool urban township. In the groundwater of Merseyside Liverpool, in some places groundwater is high in organic pollutants. The fingerprint of organic pollutants was inferred by using the SPOT satellite data. Palaeochannels of Alt river in the hinterland of Merseyside shows a sandwiched Sherwood sandstone aquifer. The hydraulic conductivity of this aquifer was arrested due to deposition of the clay of both the rivers in the fractures and interstices. Digitally enhanced and processed data has the potential to locate the relative variations of soil moisture rich or poor in organic pollutants. In places where soil moisture is rich in organic pollutant the spectral reflectance in near infrared spectrum is found relatively higher.

PEB1-9: Simultaneous photochemical abatement of hexavalent chromium and organic pollutants

P. Mytych, Z. Stasicka

Faculty of Chemistry, Jagiellonian University, Ingardena 3, 30-060 Kraków, Poland

Hexavalent chromium is accumulated in the environment together with a variety of organic pollutants in a number of contaminated sites including groundwater aquifers, lake and river sediments and soils [1]. As a class, phenolic substances and EDTA are among the most ubiquitous in the water and soil environment, both as natural products and as contaminants. Phenols, particularly chlorophenols, have a bad reputation not only due to their toxicity but also because of their persistence; thereby it has given rise to the development of different methods leading to their degradation [2-4]. Their presence in natural soils and waters is mainly due to intensive application of fungicides, insecticides or herbicides.

Two concurrent oxidation-reduction reactions between Cr(VI) and organic substances could be induced by sunlight, which lead to simultaneous abatement of pollutants. The results describe the behaviour of the two-component system containing Cr(VI) and phenolic compounds or detergents (e.g. EDTA, NTA) under nearly natural conditions. The photoredox reaction of either of components results in decreasing in concentration both of them. Moreover, the system demonstrates a synergistic effect: the Cr(VI) photoreduction is accompanied and enhanced by the phenols oxidation and vice versa, phenols photooxidation enhances the Cr(VI) reduction. Each reaction makes use of significantly different part of the solar spectrum that enables both photoreactions to progress concurrently of upon exposition to the sunlight. Furthermore, the photoreactions are inversely affected by the solution pH, so they are complementary to each other, leading to the same results by one of two alternative pH-controlled pathways [4]. This extends the abatement effectiveness to somewhat wider pH range within that characteristic for natural waters.

Effects of radiation wavelength, pH, temperature and presence of oxygen on the organic pollutants photodegradation were analyzed.

References

- [1] J. Kotaś, Z. Stasicka, *Environmental Pollution* 107 (2000) 263.
- [2] P. Kocot, P. Cieśła, P. Mytych, Z. Stasicka, *Journal of Molecular Catalysis A: Chemical* 224 (2004) 17.
- [3] P. Mytych, A. Karocki, Z. Stasicka, *Journal of Photochemistry and Photobiology: A Chemistry*, 160 (2003) 163.
- [4] P. Mytych, Z. Stasicka, *Applied Catalysis B: Environmental*, 52 (2004) 167.

PEB1-10: The environmental effects of oil exploration and production in the East Shetland basin: composition and concentration of hydrocarbons in sediment samples collected in 2002 using a stratified random sampling design

M. Russell, L. Webster, P. Walsham, G. Packer, E.J. Dalgarno, A.D. McIntosh, C.F. Moffat

Fisheries Research Services, Marine Laboratory, 375 Victoria Road, Aberdeen, AB11 9DB, Scotland (e-mail: M.Russell@marlab.ac.uk)

The North Sea has been the focus of offshore oil and gas production over the past 40 years. As a result of this activity, hydrocarbons have been discharged during drilling (*via* cuttings contaminated with oil-based drill muds), during production (*via* produced water (PW) discharges), and *via* incomplete combustion during flaring operations. Therefore it is known that oil exploration and production activity produces impacts in the marine environment – the real questions are how much, for how long and over what area?

Discharges of oil on cuttings during drilling have been by far the most important discharges and historically in the UK, most industry funded oil and gas monitoring has looked at the impacts of cuttings discharges and has been concentrated in what might be called the ‘near field’, *i.e.* close to installations or drill sites. All UK activity of this kind has been recently reviewed under the auspices of UKOOA (United Kingdom Offshore Operators Association)¹. This study concludes that most chemical contamination, and almost all observed benthos community effects, have been confined to the near field.

There are ways of improving our assessments of the changes in concentration of substances over time. One option is to conduct systematic, *i.e.* grid type, surveys covering large areas of the far field (defined here as >2 km from a single well or >5 km from a multiple well site). However, there are two disadvantages to the systematic surveys. First, they often require statistical analysis that is both complex and based on assumptions that are difficult to substantiate. Second, missing stations, arising because of *e.g.* bad weather at sea, can be difficult to accommodate in some analyses.

An alternative approach to systematic surveys would be to switch to a stratified random survey. Here, the area of interest is split into different zones, or strata, and samples taken at random within each stratum. The survey is repeated over several years, with new random stations selected each year. This approach allows a much simpler statistical analysis, requiring fewer assumptions, and is robust to a few missing stations. In particular, it allows time trends in hydrocarbon concentrations throughout areas to be assessed, and different time trends in different parts of the same area or in different areas to be considered.

The FRS ML has concentrated its assessment of the impact of oil and gas exploration and production activities on two areas of the North Sea; the Fladen Ground and the East Shetland Basin (ESB). Both areas have been the focus of offshore oil and gas production over the past 40 years and both areas are productive fishing areas dominated by pelagic and demersal catches. For these reasons, FRS has undertaken a number of sediment surveys in these areas, both systematic and random.

Several systematic grid surveys were carried out during 1986, 1988/89 and 1994 with the objective of assessing the impact of oil exploration and production in this potentially accumulative area of the North Sea (see contribution by Walsham *et al.*, this meeting). In addition, a random stratified survey of the far field ESB area was undertaken in 2002. The ESB area was divided into 21 areas and between 4 and 17 samples were taken at random positions, in the far field area only, from each area.

These samples were screened by ultraviolet fluorescence spectroscopy (UVF) and subsequently all were analysed for polycyclic aromatic hydrocarbons (PAHs) and aliphatic hydrocarbons including *n*-alkanes and biomarkers (steranes and triterpanes). The sediments are fine to medium sands with the TOC and the concentration of total PAH significantly correlated with the particle size (Pearson correlation, $p < 0.05$). All zones exhibit a predominantly pyrolytic input as shown by the preponderance of the 5- and 6-ring PAHs. There is some evidence of petrogenic input from minor UCMs in the aliphatic fraction.

References

¹Kingston P and Harries D. (2001) An analysis of UK offshore oil and gas environmental surveys 1975 – 1995. UKOOA

PEB1-11: Research of oils biodegradation in soils and its intensification

O.V. Serebrennikova, L.D. Stakhina, E.V. Barabanova, N.Y. Andreeva, N.V. Sizova

Institute of Petroleum Chemistry SB RAS Tomsk (e-mail: sl@ipc.tsc.ru)

The environmental pollution by crude oil or oil products results in serious ecological problems for oil and gas fields that is a characteristic feature of North regions similar to West Siberia. Emergencies at oil deposits and pipelines are known to cause considerable environmental pollution. But there is also a problem of natural shows of solid and liquid bitumens on the soil surface, as, e.g., Sokhochul oil show in Northern Khakassia, which was the subject of our study.

Oil, natural bitumens and oil products violate the environmental state of the topsoils and completely deform the biocenosis structure.

Elimination of impact on the environment by removing oil-polluted surface soil layer is a fairly labour intensive operation which leaves the problem of soil reclamation unsolved.

The study of the processes of oil biodegradation using different physicochemical methods to assess the mechanism and destruction degree is also urgent to solve some geochemical problems connected with the hypergenesis processes.

The work aimed at the examination of oil biodegradation in polluted soils and its natural shows on the surface. To intensify the process, we used the peat-mineral compositions (PMC).

The number of hydrocarbon oxidizing microorganisms (HOM) in native peat from West Siberia is 5-6 times more than the same index for mineral soil and it increases by 100-150 times after physical-chemical activation by PMC.

Oil degradation level was determined by the techniques of HPLC, GC, IR-spectroscopy and by microcalorimetry. Among the aliphatic alkanes, the amount of n-alkanes reduced in the highest degree, the isoprenoid Ki factor being increased by 3 times. The content of oxygen-bearing and other compounds possessing antioxidant activity increased.

The results of the work showed that in the process of oil biodegradation during the period from the 3-rd up to 6-th summer month the amount of aliphatic hydrocarbons reduced and there was an increase in the quantity of resins and asphaltenes. The study reveals that the efficiency of oil degradation ranges from 16 % to 53 % depending on oil sample and ambient conditions. One can observe an increase in a relative content of oxygen-containing structures.

The results of the study of the composition of the biodegraded oil samples are shown in the Table.

Table. The results of oil biodegradation

Sample	Level of oil destruction %	Content, %				Content C=O relative (D ₁₇₂₀ /D ₁₄₇₀)	Content antioxidants fn[InH] mol/kg
		Aliphatic hydrocarbons	Aromatic hydrocarbons	Resins	Asphaltenes		
Oil initial	-	74.1	12.9	12.0	1.0	-	0.36
Oil biodegraded (3 month)	16	65.2	13.8	15.9	5.1	0,15	0.39
Oil biodegraded + PMC (3 month)	24	52.8	21.1	21.7	4.4	0,27	0.44
Oil biodegraded + PMC (6 month)	53	42.7	20.3	28.9	8.1	0,47	0.57
Oil "Sohoshul"	-	71.9	6.0	17.4	4.7	0.40	0.35
Oil "Sohoshul" native biodegraded	-	57.5	5.7	20.1	16.7	0.75	0.40

The application of a complex of physicochemical methods for analysis allowed us to assess quantitatively and qualitatively the mechanism of the biodegradation process under the action of natural and technogenic factors.

The obtained results show that use of peat containing activated microorganisms appears to have considerable promise for reclaiming soil polluted with oil and oil products.

At the result of PMC influence the degradation of oil components reaches the same level as the degradation of oil components of natural oil show Sokhochu just in 6 months.

Under the PMC action during the biological destruction a level of the degradation of oil components similar to the destruction degree of oil components of natural oil show "I" occurring for a very long time is reached in 6 months.

PEB1-12: Is acid troubling you? Studies of the synthesis, characterisation, biodegradation and toxicity of naphthenic acids

B.E. Smith, C.A. Lewis, S.J. Rowland

Petroleum and Environmental Geochemistry Group, University of Plymouth, Drake Circus, Plymouth PL4 8AA, U.K. (e-mail:srowland@plym.ac.uk)

‘Naphthenic acid’ (NA) is a generic term used to describe the acidic but largely unidentified components of crude oils, found particularly in biodegraded crude oils and tar sands (e.g. [1], [2]).

Most previous attempts to identify NAs have been hampered by a lack of synthetic reference compounds (e.g. [3], [4], [5]). In the present study we have synthesised a series of monocyclic and polycyclic naphthenic acids *via* hydrogenation of the products of Haworth-type schemes (e.g. Figure 1). We characterised the purified products by spectroscopic methods (IR, NMR and GC-MS) and then used these reference acids to develop a generic LC-multistage MS (LC-MSⁿ) method for the characterisation of NAs from commercial sources and biodegraded crude oils. We discovered that LC-MSⁿ of derivatised acids was more sensitive and more informative than examination of the free acids and we developed a novel derivatisation procedure for this. The method allows an unprecedented resolution and characterisation of NAs.

NAs from tar sands and spilled biodegraded crude oils are also important environmental contaminants (e.g. [6]) and have been reported to be toxic to a variety of organisms ([7], [8]). We therefore determined the toxicity of the synthetic reference NAs by an oyster embryo bioassay. The toxicities compared closely to some natural NAs.

The NAs in tar sands and in-reservoir biodegraded oils are considered by some authors to have risen via anaerobic biodegradation ([1], [9]). Once spilled into the aerobic environment they may or may not be biodegraded further. We therefore studied the biodegradation of the synthetic NAs by various aerobic bacterial consortia to determine the likely persistence of the chemicals in the environment. Characterisation of the metabolites gave clues to the likely biodegradation pathways.

The results significantly advance our understanding of these industrially and environmentally important chemicals.

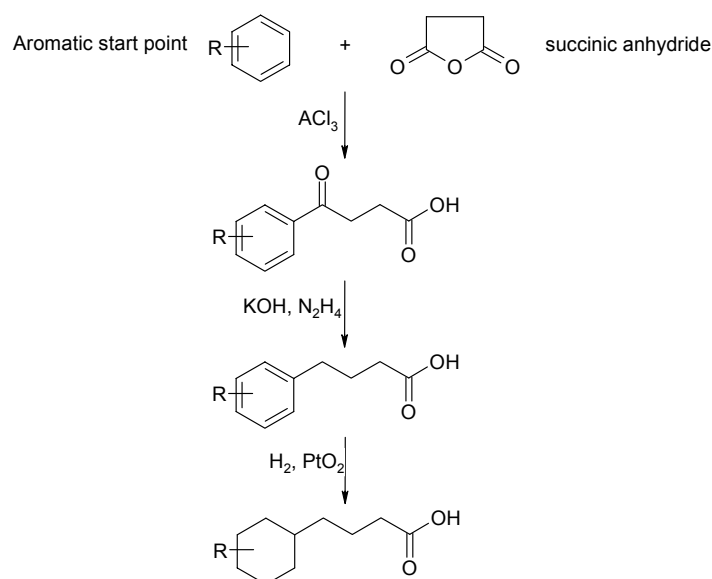


Fig.1. Typical synthetic scheme for model naphthenic acids. The aromatic synthon may contain one or two rings

References

- [1] Aitken, C.M., Jones, D.M., Larter, S.R., 2004. Anaerobic hydrocarbon biodegradation in deep subsurface oil reservoirs. *Nature* 431 (7006), 291-294.
- [2] Van Hamme, J.D., Singh, A., Ward, O.P., 2003. Recent advances in petroleum microbiology. *Microbiology and Molecular Biology Reviews* 67 (4), 503-549.
- [3] Lo, C.C., Brownlee, B.G., Bunce, N.J., 2003. Electrospray-mass spectrometry analysis of reference carboxylic acids and Athabasca oil sands naphthenic acids. *Analytical Chemistry* 75, 6394-6400.
- [4] Hao, C., Headley, J.V., Peru, K.M., Frank, R., Yang, P., Solomon, K.R., 2005. Characterisation and pattern recognition of oil-sand naphthenic acids using comprehensive two-dimensional gas chromatography/time-of-flight mass spectrometry. *Journal of Chromatography A* 1067 (1-2), 277-284.
- [5] Barrow, M.P., McDonnell, L.A., Feng, X., Walker, J., Derrick, P.J., 2003. Determination of the nature of naphthenic acids present in crude oils using nanospray fourier transform ion cyclotron resonance mass spectrometry: The continued battle against corrosion. *Analytical Chemistry* 75, 860-866.
- [6] Ritchie, W., O'Sullivan, M., 1994. *The Environmental Impact of The Wreck of The Braer*. The Scottish Office, Edinburgh.
- [7] Rogers, V.V., Wickstrom, M., Liber, K., MacKinnon, M.D., 2002. Acute and subchronic mammalian toxicity of naphthenic acids from oil sands tailings. *Toxicological Sciences* 66 (2), 347-355.
- [8] Herman, D.C., Fedorak, P.M., MacKinnon, M.D., Costerton, J.W., 1994. Biodegradation of Naphthenic Acids by Microbial-Populations Indigenous to Oil Sands Tailings. *Canadian Journal of Microbiology* 40 (6), 467-477.
- [9] Wilhelms, A., Larter, S.R., Head, I., Farrimond, P., di-Primo, R., Zwach, C., 2001. Biodegradation of oil in uplifted basins prevented by deep-burial sterilization. *Nature* 414 (6859), 85.

PEB1-13: Characterization of dry deposition dusts on an urban balcony surface, GuangzhouJ. Song, P. Peng

State Key Laboratory of Organic Geochemistry, Guangzhou Institute of Geochemistry, Chinese Academy of Sciences, Guangzhou, P. R. China (e-mail: songjzh@gig.ac.cn)

Dry deposition is the process by which atmospheric trace chemicals are transferred by air motions and the gravitational force to the surface of the Earth. It accounts for a large portion of the removal of trace chemicals from troposphere (Wesley and Hicks, 2000). Dry deposition has received increasing attention in recent years because it is believed to be an important pathway for transportation of air pollution materials in the urban environment. Dry deposition dust acts as a sink for vehicle exhaust, weathered material, and soil, and as a source of atmospheric particulate matter, house dust, and water run-off particulate matter.

Particulate dry deposition samples were collected from a residential building balcony in Guangzhou City, P. R. China. Twelve samples were monthly obtained over a period of 1 year (2003-2004). Every sample was subject to the elemental, particle size, flash pyrolysis-gas chromatography-mass spectrometry (Py-GC-MS) and thermodesorption GC-MS (Td-GC-MS) analysis.

The results show that average dry deposition flux varies from 406.4-1605.3 mg m⁻² month⁻². The dry season has a high dry deposition flux range from 932.2 – 1605.3 mg m⁻² month⁻², while rainy season has a low dry deposition flux range from 406.4-881.1 mg m⁻² month⁻². In general, the sizes of dry deposition particles range from about 0.3 to 100-200 μm with a medium of 21.0-25.6 μm. The relative contents of fine particle fraction (d < 2.5 μm) in the dry season samples higher than the rainy season samples, which may attributed to the fine particle can suspended a longer times in dry season.

Td-GC-MS of dry deposition detected a lot of volatile organic compounds, such as alkanes, fatty acids, PAHs, phenols, etc. A series of n-alkanes (C₁₆-C₃₄) were detected and the distribution pattern shows a strong odd-over-even carbon preference and the maximum carbon number varies from C₂₃ to C₃₁. These suggest a significant contribution of lipids from grass and wood plants. Ratios among PAHs have been widely used to detect combustion-derived PAHs (Luo et al., 2004). In the dry deposition particles, the An/178 ratio (0.07-0.12) approximated to be 0.1 and the Fl/202 (0.52-0.63) is above 0.5, which strongly suggest that vehicular emission and diesel exhaust emission.

Py-GC-MS of dry deposition dusts detected more than 100 pyrolysates at different abundances. These compounds were grouped into five major classes including polysaccharides (PS), proteins (PR), lignin-derived compounds (LG), alkenes/alkanes (AL), and fatty acids (FA). Although all dry deposition samples have similar types of pyrolysates, their relative contents are different. The relative content of aliphatic compounds varies from 20.47% to 27.59%. Comparing to others, the samples were collected in Oct-Dec 2003 and Jan 2004, have higher contents of protein-derived N-containing compounds and lower contents of polysaccharide-derived compounds. These suggest that the chemical composition of dry deposition particles are season variable, and the capacity of removed the trace chemicals from air by dry deposition is consequently season dependent.

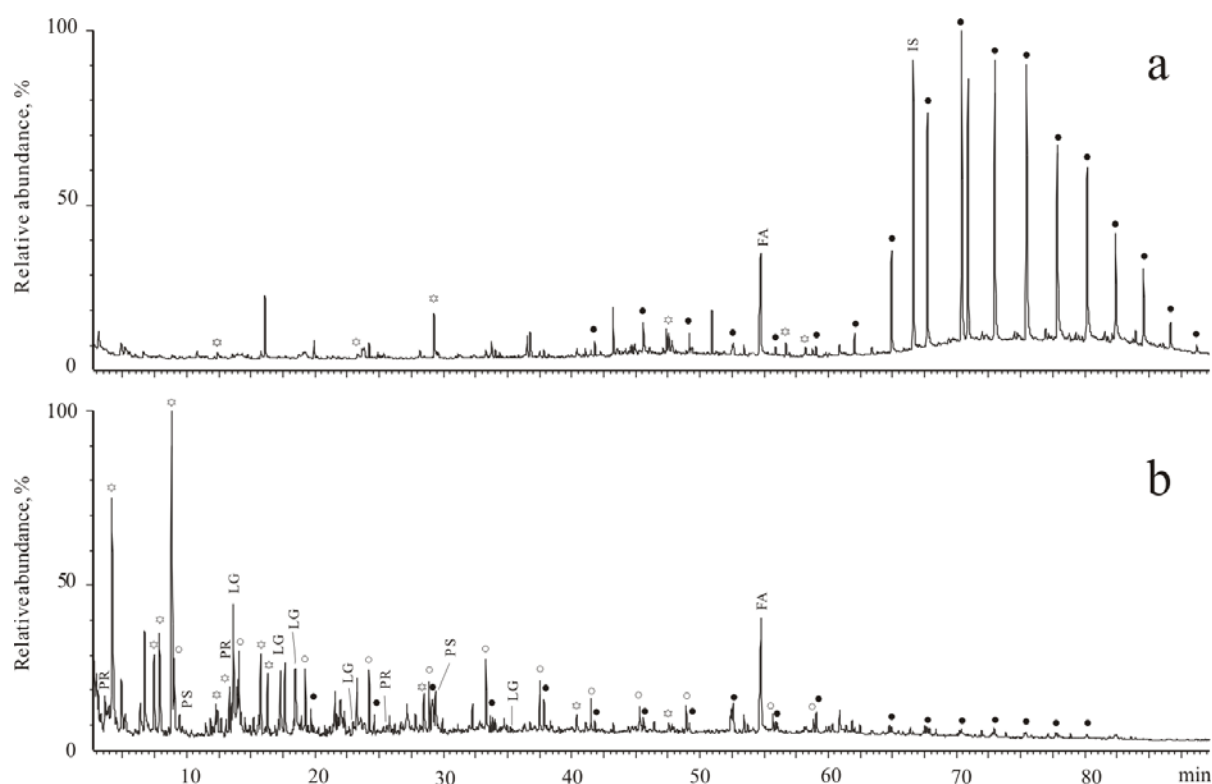


Fig.1. Thermogram (a) and pyrogram (b) of particulate dry deposition collected in January, 2004
 o: alkenes; ●: alkanes; ◻: aromatic hydrocarbons; PS: furan derivatives; PR: N-containing compounds; LG: phenolic compounds; FA: fatty acids

References

- Wesley, M.L., Hicks, B.B., 2000. A review of the current status of knowledge on dry deposition. *Atmos. Environ.* 34, 2261-2282.
- Luo, X., Mai, B., Yang, Q., Fu, J., Sheng, G., Wang, Z., 2004. Polycyclic aromatic hydrocarbons (PAHs) and organochlorine pesticides in water columns from the Pearl River and the Macao harbor in Pearl River Delta in South China. *Mar. Pollut. Bull.* 48, 1102-1115.

PEB1:14: Distribution and sources of polycyclic aromatic hydrocarbons in surface sediments from New York/New Jersey Harbor complexJ. Song¹, B. Yan¹, L. Benedict¹, R. Bopp¹, T. Abrajano¹, D. Chaky²

1) Department of Earth and Environmental Sciences, Rensselaer Polytechnic Institute, Troy, NY 12180 USA

2) Lamont-Doherty Earth Observatory, Columbia University, Palisades, NY, 10964, USA

INTRODUCTION: The New York /New Jersey (the NY/NJ) harbor complex have been heavily contaminated by organic chemical compounds and heavy metals (Bopp *et al.*, 1998; Bopp *et al.*, 1981; Crawford *et al.*, 1995; Wolfe *et al.*, 1996). Between 1990 and 1998, surface sediments were collected in the lower Hudson River Basin. Sample locations of the main stem of the Hudson River are reported in terms of statute miles upstream (positive) or downstream (negative) of the southern tip of Manhattan Island (milepoint 0) measured along the channel (Bopp *et al.*, 1981). For example, the 9.72W site has a channel distance of 9.72 miles from the tip, and it is taken near the west bank. Additional samples were collected near the mouth of Newtown Creek, Central Park Lake, Kill van Kull (KvK4) and Raritan Bay. The activities of the particle-associated radionuclides ⁷Be were analyzed to ascertain sedimentation within a year of sampling (Bopp *et al.*, 1998). PAH isolation and analyses follow procedures reported elsewhere (e.g., O'Malley *et al.*, 1994; Yan *et al.*, 2004a). Aliphatic and aromatic hydrocarbon compounds were identified using a Shimadzu GCMS-QP5050 with the help of standards and data from the Standard Reference Database of the National Institute of Standards and Technology (NIST).

RESULTS AND DISCUSSION: The Newtown Creek area has the highest concentrations (Σ PAH, 80,500 ng/g) among all the sites. It is almost two orders of magnitude greater than the concentrations in Raritan Bay (890 ng/g). The level in Central Park Lake (14,527 ng/g) was unexpectedly high, compared with that from the western harbor and the level in samples from the main stem of Hudson River (5,027 ng/g in 6.34W). It is likely that the higher levels in Central Park Lake are associated with the low deposition rate (~0.5 cm/year) in this environment (Chillrud *et al.*, 1999), in contrast to the much higher deposition rate (~10 cm/year) in the main stem. In the main stem Hudson, PAHs have a very localized distribution in contrast to similar levels observed for other contaminants (Bopp *et al.*, 1998). For example, even though 2.34E is only a few hundred meters away from 2.77 W, the concentrations at 2.34E are half that at 2.77W.

The ratio of 1,7-dimethylphenanthrene (DMP) to 2,6- dimethylphenanthrene is regarded as a very sensitive source indicator of softwood (e.g. pine) combustion (Benner *et al.*, 1995; Yunker *et al.*, 2002; Abrajano *et al.*, 2004). Samples from pine combustion have a value around 9, while fossil fuel combustion normally has a value of 0.74 or lower. In the

harbor surface samples, the ratios are all below 0.74 (Fig. 1), which suggest that wood combustion in the NY/NJ harbor area is not a major source at the present time.

In all of the sediment samples presented here, the value of $Fl/(Fl+Py)$ is higher than 0.4, indicating a predominantly combustion-derived contribution. Some sites, especially in those samples from western harbor area (KvK), have a signature from petroleum contribution. In these KvK, $Par/(Par+Alkyl)$ is 0.38, $Fl/(Fl+Py)$ is below 0.43, lower than 0.45, the cut-off ratio for motor vehicle burning (Yunker *et al.*, 2002). As mentioned above, the KvK waterway are important for petroleum transportation and oil-spills are known to have occurred (Gunster *et al.*, 1993a). Historically, because of the impact from petroleum spill in the Arthur Kill, Raritan Bay was dominated by petroleum-derived PAHs for a long time (Yan *et al.*, 2004a). In the 1990 surface sample from this core, PAH levels are low and prevalently combustion-derived. More studies are required to determine the relative influence of local petroleum and regional combustion sources at this location.

In Central Park Lake, the ratios of $Fl/(Fl+Py)$ and $Par/(Par+Alkyl)$ are 0.48 and 0.54 respectively, indicating a dominantly combustion-derived source. Newtown Creek has the highest ratio of $Fl/(Fl+Py)$ (0.51), and $Par/(Par+Alkyl)$ (0.65) compared to other sites except Raritan Bay. The combustion-derived elevated levels of PAHs in this area may have been introduced by the discharge of the nearby NC WWTP. On the other hand, natural gas-fired power plants could be another source for PAHs. Rogge *et al.* (1993) demonstrated that despite the low fine particle emission rate of gas-fired residential space heaters, PAH emission are quite high, and the ratio of $Fl/(Fl+Py)$ is around 0.51 (calculated from data presented in their paper). They also estimated that in 1982 in the Los Angeles area, the PAH contribution by natural gas was comparable with that from diesel vehicles, and about half as much as that released from catalyst-equipped automobiles (Rogge *et al.*, 1993b). At the current time, we are investigating the PAH distribution from natural gas- and oil-fired boilers.

PAH distributions in the harbor are site specific. For the sample from 9.72W, there is a relative higher contribution from petroleum than that in 6.4W, possibly due to the presence of petroleum terminals downstream. Sample 6.4W has the highest concentrations of PAH in the main stem and four ratios indicate the contribution from both petroleum and combustion sources. PAH at this site may originate from a nearby sewage plant and the petroleum terminal upstream. Four ratios in sample 2.77E all show an obvious petroleum contribution when compared with those in sample 2.34W. Sample -1.7C has similar ratios of these four indicators as 6.4W, indicating dominant contribution from combustion (Fig. 1).

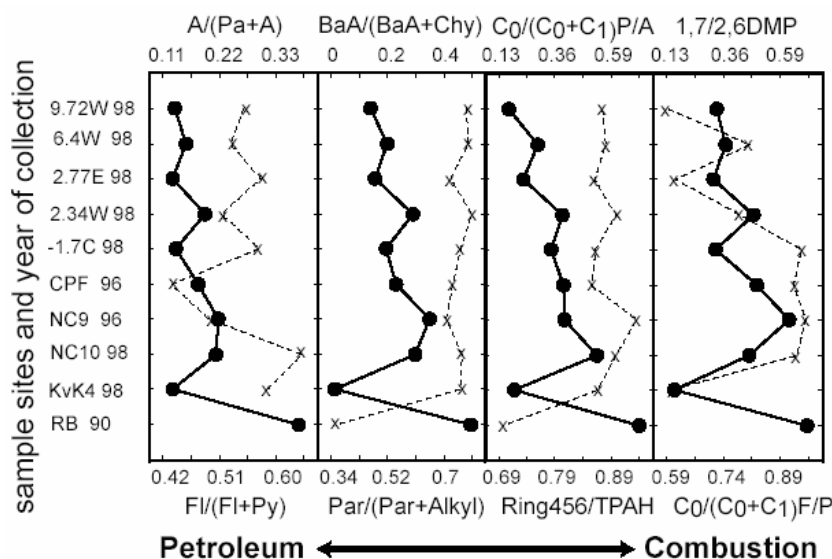


Fig.1. Spatial trends of various molecular indicators in samples from the New York/New Jersey harbor complex. Trends indicated by dashed lines follow the bottom scale; solid lines follow the top scale. Note that the ratios indicated by solid lines display a consistent pattern. For all indicators, a tendency towards the right suggests increasing contributions from combustion, while to the left, petroleum

CONCLUSIONS: Combined usage of the Fl/(Fl+Py), Par/(Par+Alkyl), Ring456/TPAH and $C_0/(C_0+C_1)F/P$ ratios suggest that in the New York/New Jersey Harbor area, localized PAH combustion sources dominate, but for the western segment of the harbor and some mainstem Hudson samples, contributions from petrogenic sources are demonstrably important.

References

- Abrajano, T.A., Yan, B., O'Malley, V.P., (2004) In: B.S. Lollar (Ed.), *Treatise on Geochemistry, Environmental Geochemistry* (Ed. by B.S. Lollar), Elsevier Publishing, NY pp. 475-510.
- Baek, S.O., Field, R.A., Goldstone, M.E., Kirk, P.W., Lester, J.N., Perry, R., (1991) *Water, Air, and Soil Pollution*, 60, 279-300.
- Benner, B.A., Wise, S.A., Currie, L.A., Klouda, G.A., Klinedinst, D.B., Zweidinger, R.B., Stevens, R.K., Lewis, C.W., (1995) *Environmental Science & Technology*, 29, 2382-2389.
- Bopp, R.F., Chillrud, S.N., Shuster, E.L., Simpson, H.J., Estabrooks, F.D., (1998) *Environmental Health Perspectives*, 106(suppl.4), 1075-1081.
- Bopp, R.F., Simpson, H.J., Olsen, C.R., Kostyk, N., (1981) *Environmental Science & Technology*, 15, 210-216.
- Chillrud, S.N., Bopp, R.F., Simpson, H.J., Ross, J.M., Shuster, E.L., Chaky, D.A., Walsh, D.C., Choy, C.C., Tolley, L.R., Yarme, A., (1999) *Environmental Science & Technology*, 33(5), 657-662.
- Crawford, D.W., Bonnevie, N.L., Wenning, R.J., (1995) *Ecotoxicology and Environmental Safety*, 30, 85-100.
- Gunster, D.G., Bonnevie, N.L., Gillis, C.A., Wenning, R.J., (1993a) *Ecotoxicology and Environmental Safety*, 25, 202-213.
- LaFlamme, R.E., Hites, R.A., (1978) *Geochimica et Cosmochimica Acta*, 42, 289-303.
- Mastral, A.M., Callen, M.S., C., M., Galban, J., (1995) *Fuel*, 74(12), 1762-1766.
- O'Malley, V.P., Abrajano, T.A., Hellou, J., (1994) *Organic Geochemistry*, 21(6/7), 809-822.
- Rogge, W.F., Hildemann, L.M., Mazurek, M.A., Cass, G.R., (1993b) *Environmental Science & Technology*, 27, 2736-2744.
- Rogge, W.F., Hildemann, L.M., Mazurek, M.A., Cass, G.R., (1998) *Environmental Science & Technology*, 32, 13-22.
- Wolfe, D.A., Long, E.R., Thursby, G.B., (1996) *Estuaries*, 19(4), 901-912.
- Yunker, M.B., Macdonald, R.W., Brewer, R., Mitchell, R.H., Goyette, D., Sylvestre, S., (2002) PAHs in the Fraser River basin: a critical appraisal of PAH ratios as indicators of PAH source and composting. *Organic Geochemistry*, 33(4), 489-515.

PEB1-15: $\delta^{13}\text{C}$ of volatile organic compounds (VOC's) in air samples by thermal desorption GC-ir-MSN. Turner¹, K. Grice¹, M. Ioppolo-Armanios², M. Jones², D. Dawson¹

1) Stable isotope and Biogeochemistry Group, Centre for Applied Organic Geochemistry, Kent Street, Bentley, Curtin University of Technology, Perth 6845, WA, Australia (e-mail: K.Grice@curtin.edu.au)

2) Alcoa World Alumina, Australia. Technology Delivery Group. PO Box 161, Kwinana WA 6167

Volatile organic compounds (VOC's) are hydrocarbons (except methane) with vapour pressures greater than 2 mm of mercury (0.27 kPa) at 25 °C and have boiling points in the range of 50-260°C and are thus present in a vapour or gas form at ambient temperature. Many toxic compounds including a range of VOC's from motor vehicles are emitted from the car exhaust. These include formaldehyde, acetone and benzene and other VOC's such as acetaldehyde and 1,3-butadiene, which form when fuel is not completely burnt during combustion.

The technique of thermal desorption-gas chromatography-mass spectrometry (TD-GC-MS) has been used in many studies to evaluate the molecular composition of emissions from different sources (e.g [1]). However a TD-GC unit has never been linked to an isotope ratio mass spectrometer enabling compound specific isotope analysis (CSIA) of VOC's in aerosol mixtures, although various methods for measuring the $\delta^{13}\text{C}$ composition of VOCs were recently reviewed ([2]). In this review the importance of such a technique to study atmospheric samples was emphasised. Solid-phase micro extraction has become routine for sampling VOC's in ambient air, but isotopic fractionation of the compounds can result from the extraction techniques. No studies to date have utilised the method of TD in conjunction with gas chromatography-isotope-ratio monitoring mass spectrometry (GC-ir-MS). Since the stable carbon isotopic compositions of VOC's in airborne samples remains a significant analytical challenge due to the complex and structurally diverse composition arising from many precursory inputs a routine compound specific isotope method for determining the $\delta^{13}\text{C}$ of individual VOC's in airborne emissions was developed.

During the method development, the following factors were tested- i) adsorbent resin choice, ii) tube conditioning time, iii) thermal desorption time, iv) reproducibility of the TD-GC-MS method and v) linearity of the TD-GC-MS method. Tenax TA was chosen as a suitable adsorbent resin, tubes were conditioned for 4 hours, a thermal desorption time of 5 minutes was chosen and the TD-GC-MS method employed was proven to be both reproducible and linear. $\delta^{13}\text{C}$ values of various standards were found to be consistent, within the error of analysis from both direct GC-ir-MS and TD-GC-ir-MS performed on an IsoPrime

isotope ratio mass spectrometer. It was proven that the novel TD-GC-ir-MS procedure developed caused negligible isotopic fractionation for benzene, toluene, chlorobenzene, ethylbenzene, *m*-xylene and propylbenzene and is therefore a viable method for $\delta^{13}\text{C}$ analysis of VOC's in airbourne samples (Figure 1).

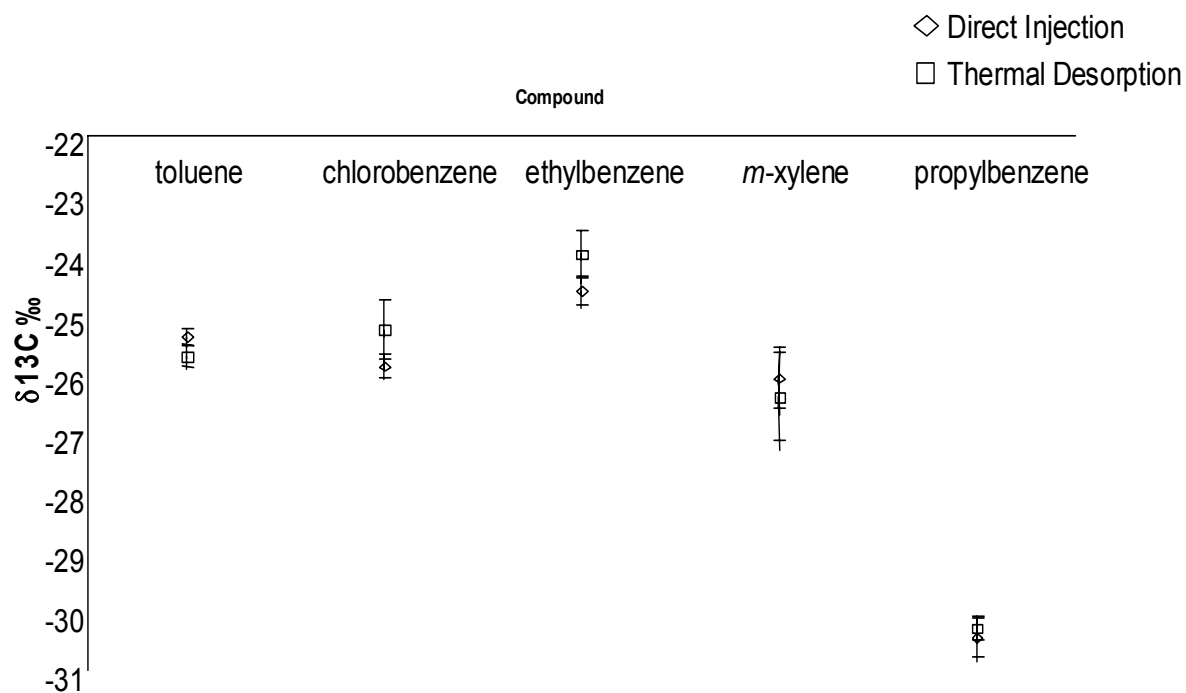


Fig.1. $\delta^{13}\text{C}$ of standard VOC's using direct injection by GC-ir-MS and by thermal desorption GC-ir-MS

References

- [1] Goldstein, A.H., and Shaw, S.L., 2003. Isotopes of volatile organic compounds: an emerging approach for studying atmospheric budgets and chemistry. *Chemical Reviews*, 103, 5025-5048.
- [2] Stefaniak, A.B., Breyse P.N., Murray, P.M., Rooney, B.C., and Schaefer, J., 2000. An evaluation of employee exposure to volatile organic compounds in three photocopy centre. *Environmental Science Research*, 83, 162-173.

PEB1-16: The effects of oil exploration and production in the East Shetland basin: composition and concentration of hydrocarbons in sediment samples collected in 1986, 1988, 1989 and 1994 – An historical perspective

P. Walsham, L. Webster, M. Russell, A.D. McIntosh, P.R. Mackie, C.F. Moffat

Fisheries Research Services, Marine Laboratory (FRS ML), 375 Victoria Road, Aberdeen, AB11 9DB, Scotland (e-mail: P.Walsham@marlab.ac.uk)

The North Sea has been the focus of offshore oil and gas production over the past 40 years. As a result of this oil production and exploration activity, hydrocarbons have been discharged during drilling, production and *via* incomplete combustion during flaring operations. Of these, discharges of oil on cuttings during drilling have been by far the most important. By 1985, discharges from this source over the whole of the UK North Sea had risen to ca 25,000 tonnes oil per annum¹. These discharges became the focus of increased regulatory control within OSPAR and in 1992, the Paris Commission Group on Oil Pollution set down maximum discharge limits of 10% mineral oil on cuttings with a further stipulation of a 1% threshold for all North Sea drilling from January 1997. Operations have continued to the present day and there is a clear need to continue to assess the impact of this industry on the maritime area. However, assessment of the current state requires an understanding of both the historical deposits and their impact on the sediments.

Over the years, FRS ML in Aberdeen has focussed its attention on two areas of the North Sea in order to assess the long-term impact of oil exploration and production activity on the marine environment; the Fladen Ground and the East Shetland Basin (ESB) (Fig. 1). Both areas have been the focus of offshore oil and gas production over the past 40 years and have the potential to accumulate hydrocarbons. In addition, both are productive fishing areas dominated by pelagic and demersal catches. For these reasons, FRS ML has undertaken a number of sediment surveys in both areas.

Of the total 2,703 million tonnes of crude oil produced in the UK sector between 1975 and 2003, 1,015 million tonnes was produced in the ESB². A systematic survey of the ESB was carried out in 1986, to assess the impact of oil exploration in this potentially accumulative area of the North Sea. In 1988, 1989 and 1994 further systematic sediment surveys were undertaken. Sediment samples were collected at approximately 10 km intervals along three legs. A further survey, using the random stratified sampling method (Russell *et al.*, this meeting) was carried out in 2002 by the FRS ML.

All sediment samples collected in 1986, 1988 and 1989 were screened using ultraviolet fluorescence spectroscopy (UVF) and selected samples were analysed for

polycyclic aromatic hydrocarbons (PAHs) and aliphatic hydrocarbons including *n*-alkanes. In 1986 diesel oil equivalent concentrations ranged from 10.1 to 28,202 $\mu\text{g g}^{-1}$ dry weight (DW), while Forties oil equivalent concentrations ranged from 6.2 to 14,744 $\mu\text{g g}^{-1}$ DW. Diesel oil equivalent concentrations in the 1988/89 samples ranged from 5.0 to 1,219 $\mu\text{g g}^{-1}$ DW, while Forties oil equivalent concentrations ranged from 3.9 to 737.0 $\mu\text{g g}^{-1}$ DW. PAH (2- to 6-ring, parent and branched) concentrations ranged from 59.9 to 1,084 $\mu\text{g kg}^{-1}$ DW in 1986 while in 1988/89 they ranged from 75.3 to 3,891 $\mu\text{g kg}^{-1}$ DW. *n*-Alkane ($n\text{C}_{12}$ - ranged from 370.7 to 2,098 $\mu\text{g kg}^{-1}$ DW in 1986 while in 1988/89 they ranged from 123.6 to 1,959 $\mu\text{g kg}^{-1}$ DW. In 1994 all samples were analysed by UVF for Forties oil equivalent concentrations only. Forties oil equivalent concentrations ranged from 6.7 to 254.5 $\mu\text{g g}^{-1}$ DW.



Fig.1. The Fladen Ground and the East Shetland Basin with the distribution of oil installations for both fields

The concentrations of Forties oil equivalents in sediments collected in 1994 showed a decrease compared to those collected in 1986, 1988/89. One possible explanation is the increased regulatory control on the discharge of oil on cuttings.

References

¹North Sea Task Force. 1993. North Sea Quality Status Report 1993. Oslo Paris Commission London. Olsen & Olsen, Fredensborg, Denmark. 132+vipp.

²Department of Trade and Industry Oil and Gas Information.

PEB1:17: PAH spectrum in the Quaternary water sedimentsI. Bojakowska

Polish Geological Institute, ul. Rakowiecka 4, 00-975 Warsaw, Poland (e-mail: izabela.bojakowska@pgi.gov.pl)

The concentrations of polycyclic aromatic hydrocarbons (PAHs) and of total organic carbon (TOC) in the Quaternary fossil and the Recent water sediments were determined. Samples were collected from varved clays and river sandy silts, as well as from the Recent lake and river sediments and they were taken far from the urban and industrial centres.

Table. Polycyclic aromatic hydrocarbon concentration in Quaternary sediments

Polycyclic aromatic hydrocarbon	Quaternary fossil sediments		Recent sediments	
	varved clays (n=17)	river sandy silts (n=5)	River sediments (n=25)	Lake sediments (n=81)
	ppm			
Acenaphthene	0,002-0,008*	<0,001-0,001	<0,001-0,009	0,001-0,201
Fluorene	0,003-0,01	0,002-0,008	<0,001-0,014	0,002-0,372
Phenanthrene	0,012-0,053	0,012-0,045	0,002-0,16	0,008-2,157
Anthracene	<0,001	<0,001	<0,001-0,041	0,003-0,611
Fluoranthene	0,002-0,005	0,001-0,004	0,002-0,419	0,009-6,041
Pyrene	0,002-0,005	<0,001-0,001	0,002-0,363	0,006-4,396
Benzo[a]anthracene	<0,001-0,001	<0,001	0,001-0,261	0,003-3,277
Chrysene	0,002-0,006	<0,001-0,002	<0,003-0,286	0,004-4,509
Benzo[b]fluoranthene	<0,003-0,004	<0,003	<0,003-0,294	0,006-4,93
Benzo[k]fluoranthene	<0,003	<0,003	<0,003-0,174	0,003-3,36
Benzo[e]pyrene	<0,003-0,005	<0,003	<0,003-0,229	0,003-3,616
Benzo[a]pyrene	<0,003	<0,003	<0,003-0,345	0,014-4,223
Perylene	0,039-0,119	<0,003	<0,003-0,086	0,006-1,133
Dibenzo[ah]anthracene	<0,005	<0,005	<0,005-0,052	0,021-3,934
Indeno[1,2,3-cd]piren)	<0,005	<0,005	<0,005-0,303	0,006-0,667
Benzo[ghi]perylene	<0,005	<0,005	<0,005-0,254	0,018-3,426

*Minimum-maximum

Contents of the total determined PAH range in varved clays from 0.079 to 0.202 ppm and in river silts – from 0.015 to 0.460 ppm, with the average values of 0.126 and 0.118 ppm respectively. The PAH spectrum of both types of Quaternary fossil sediments were similar and only fluorene, phenanthrene and fluoranthene were detected in all samples. Varved deposit differed from river silts with a low contents of acenaphthene, pyrene, chrysene and perylen, which average contents in varved clays was 0.082 ppm. TOC contents in varved

sediments range from 0.47 to 1.15% (average – 0.73%) and in river silts – from 0.16 to 0.30% (average – 0.44%). Average ratios of Σ PAHs to TOC concentrations in both sediment types were almost similar and they are up to 0.205 for varved sediments and to 0.206 – for river silts.

Contents of PAHs in Recent lake sediments were between 0.055 ppm and 25.289 ppm, and in river sediments – from 0.030 to 3.211 ppm; the average contents were respectively 3.18 ppm and 0.841 ppm. PAH spectra in Recent lake and river sediments are similar, but they are distinctly different from the PAH spectra observed in the Quaternary fossil sediments. In Recent sediments all discussed compounds were noticed and fluoranthene is dominant as well as high share of pyrene, benzo(b)fluoranthene and chrysene, which in the Quaternary fossil sediments are absent. TOC contents in Recent lake sediments (samples collected from deeps) were high and the average amount is 10.18% (from 2.4 to 34.43%). TOC contents in river sediments were considerably lower and it varies from 0.17 to 2.42% (average – 0.789%). The ratio Σ PAHs/TOC in Recent sediments were several times higher than in the fossil deposit and its ranges highly: in lake sediments it varies from 0.02 to 6.78 (average 1.71), and in river sediments – from 0.037 to 4.189 (average – 0.636).

A relatively poor “fingerprint” of PAHs in the Quaternary fossil sediments and a larger amount of high molecular weight PAH compounds in Recent sediments may suggest that most these hydrocarbons be linked to atmospheric fallout of PAHs derived from coal combustion.

PEB1-18: The development and application of a statistical sampling regime to map hydrocarbon distributions in marine sediment

A.S. Ahmed^{1,2}, L. Webster¹, I.M. Davies¹, M. Russell¹, P. Walsham¹, G. Parker¹, R.J. Fryer¹, C.F. Moffat¹, P. Pollard²

1) Fisheries Research Services (FRS) Marine Laboratory, Victoria Road, Aberdeen, Scotland.

2) School of Life Sciences, The Robert Gordon University, Aberdeen, Scotland

The input of polycyclic aromatic hydrocarbons (PAHs) to the Fladen area of the North Sea is one of the consequences of oil and gas production. The Fladen Ground sediments are predominantly fine muddy sediments (Fig. 1), and water current velocities are low. The area is one of the most heavily fished areas of the North Sea. A random stratified sampling design was developed for the sediments to assess any trends in hydrocarbon composition and concentration. Sixteen zones were constructed of equal size. The numbers of samples that were collected per zone were based upon the proportion of far field area (ie areas > 5km from multiple oil wells and/or >2km from a single well). Zones containing one or more oil platforms were classified as multiple oil zones, whilst zones with no oil platforms are single oil zones.

Two hundred and forty two (242) sediment samples were collected by Day Grab, from the FRV *Scotia*. The total organic carbon (TOC) and particle size (PSA) were determined on freeze-dried sediment. Ultraviolet (UV) fluorescence measurements were calibrated against Forties crude oil and diesel standards. The aliphatic hydrocarbons were determined by gas chromatography with flame ionization detection (GC-FID) and the aromatic hydrocarbons by gas chromatography-mass spectroscopy (GC-MS). The geochemical biomarker (steranes and triterpanes) composition of sediment was determined by GC-MS.

The mean values over the whole far field area were estimated as $\bar{y} = \frac{1}{A} \sum_{z=1}^{16} A_z \bar{y}_z$ and SE as $SE(\bar{y}) = \frac{1}{A} \sqrt{\sum_{z=1}^{16} (A_z SE(\bar{y}_z))^2}$, where \bar{y}_z is the mean value in the far field in zone z , A_z is the far-field area in zone z , and A is the total far-field area. The result showed that PAH concentrations were highest in zones with more oil installations and/or muddy sediments with a higher organic carbon content. PAH profiles were similar across the zones, and were dominated by the heavier, more persistent, 5- and 6- ring compounds. Concentration ratios were consistent with pyrolytic sources for the PAH in most of the Zones. The results also show significant differences in the spatial distributions of all the parameters (ANOVA; 0.05); there were also significant differences in the means of the all parameters. Significant

differences between the means for PAHs and Forties crude oil equivalents, especially between the multiple oil and single oil zones were explored using the *GT2* multiple comparison method of Gabriel (1978).

Table 1. Summary of TOC, PSA, UV fluorescence, *n*-alkane (nC_{13} - nC_{33}) and PAHs (2- to 6- ring, parent and branched) data. All concentrations are on a dry weight basis.

Zone numbers	Far field area (km ²)	Number of samples	TOC (%)		PSA (% <63μm)		Forties equivalents (μg g ⁻¹)		Diesel equivalents (μg g ⁻¹)		Total PAH (μg kg ⁻¹)		Total <i>n</i> -alkane (μg kg ⁻¹)	
			Mean	SE	Mean	SE	Mean	SE	Mean	SE	Mean	SE	Mean	SE
1	456.0	20	0.64	0.04	48.9	2.6	9.7	0.8	5.0	0.4	95.9	4.2	59.9	6.5
2	448.7	20	0.90	0.03	73.1	2.2	12.1	1.0	6.2	0.5	94.6	6.8	96.8	15.9
3	456.0	20	0.98	0.05	68.6	3.0	8.7	0.6	4.5	0.2	104.0	8.5	115.5	8.9
4	369.4	13	0.97	0.10	63.2	5.7	13.1	1.7	7.0	0.8	206.6	23.0	129.8	17.1
5	214.3	10	0.71	0.07	64.1	4.2	14.5	1.2	7.0	0.6	133.9	16.6	64.7	5.8
6	200.6	9	0.89	0.06	73.9	3.6	18.2	1.4	5.2	0.4	89.1	7.8	100.8	12.5
7	435.5	18	1.10	0.04	79.6	1.2	19.5	1.4	5.8	0.3	154.6	11.1	100.5	10.9
8	297.3	10	0.80	0.05	59.3	4.6	12.4	2.4	6.6	0.9	147.1	23.8	206.8	49.5
9	399.5	18	0.62	0.04	51.4	3.2	10.2	0.8	3.3	0.2	61.7	4.2	61.0	4.4
10	210.7	11	0.93	0.09	64.8	7.5	21.0	2.7	6.1	0.8	107.0	8.2	105.4	8.8
11	392.6	17	1.31	0.06	85.7	0.4	22.2	1.3	6.5	0.3	137.2	5.8	118.6	10.4
12	216.6	9	0.76	0.05	67.9	5.2	17.0	1.6	5.0	0.4	87.0	10.5	78.6	11.4
13	445.5	20	0.69	0.03	58.0	1.5	7.4	0.4	2.2	0.1	53.9	2.8	55.4	7.6
14	304.6	14	0.98	0.03	75.5	2.3	14.0	1.2	4.6	0.3	81.6	8.7	86.4	9.3
15	444.6	20	1.19	0.03	82.3	0.8	13.0	0.9	4.0	0.2	95.5	5.0	89.4	5.8
16	297.8	13	0.91	0.06	65.5	3.0	17.5	1.7	5.3	0.5	88.1	10.7	106.7	8.9
Total	5589.8	242	0.91	0.01	67.6	0.8	13.8	0.3	5.1	0.1	108.2	2.7	97.2	3.7

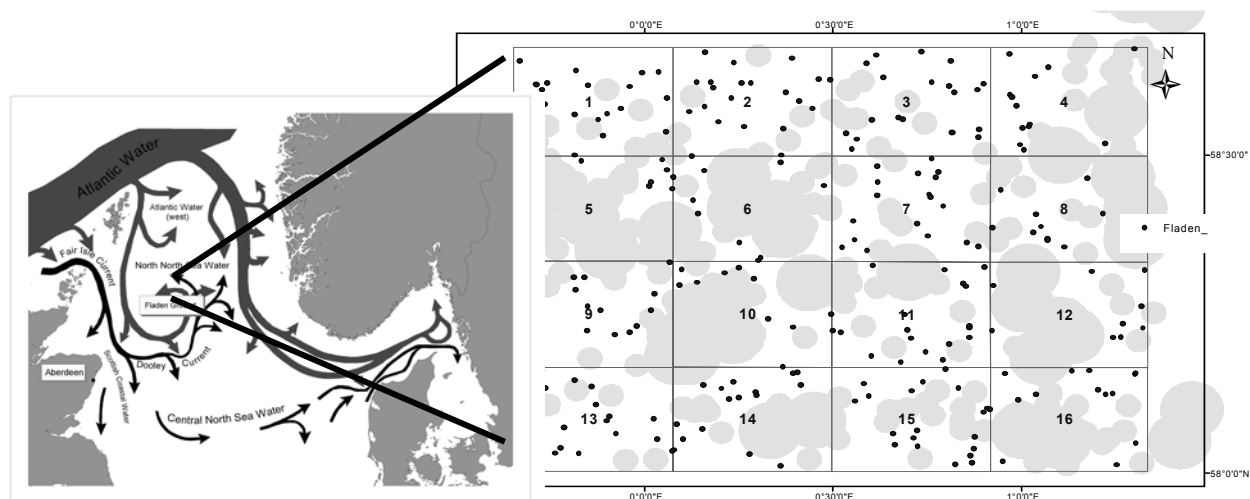


Fig.1. Location of the Fladen Ground and sampling design. Filled grey circles are near-field areas, and were not sampled

PEB2-1: Chlorinated pesticides in river sediments in PolandI. Bojakowska

Polish Geological Institute, ul. Rakowiecka 4, 00-975 Warsaw, Poland (e-mail: izabela.bojakowska@pgi.gov.pl)

Concentrations of chlorinated pesticides: α -HCH, β -HCH, γ -HCH, δ -HCH, Heptachlor, Heptachlor Epoxide, Aldrin, Dieldrin, p,p'-DDE., p,p'-DDD, p,p'-DDT, Methoxychlor, Endrin and Endrin Aldehyde were determined in 80 river sediment samples collected from the whole area of Poland. The sampled points were located at the mouths of rivers longer than 60 km, along course the major river channels and below the sewage discharges of major urban and industrial centres.

Table. Chlorinated pesticide concentration in river sediments of Poland

Pesticide	% samples above limit detection	Concentration (ppb)	
		Limit detection	Maximum
α -HCH	6.3	<0.5	11.0
β -HCH	2.5	<0.5	1.5
γ -HCH (Lindane)	95.0	<0.5	9.4
δ -HCH	2.5	<0.5	1.1
Aldrin	12.5	<0.1	2.5
Heptachlor Epoxide	6.3	<0.1	3.8
Endosulfan I	1.3	<0.5	8.2
Endosulfan II	5.0	<0.3	2.8
Dieldrin	18.8	<0.1	1.2
Endrin	12.5	<0.3	2.9
p,p'-DDE	97.7	<0.1	46
p,p'-DDD	86.3	<0.1	290
p,p'-DDT	87.5	<0.5	269
Methoxychlor	2.5	<5.00	69

Chlorinated pesticides were found in almost all samples. The most frequently detected pesticides were isomer γ -HCH (Lindane) and the DDT group compounds. The concentrations of Lindane exceeding the detection limit were recorded in 95% of samples and Lindane contents above the *PEL* value were noted in 32,5% of the analysed samples. The high Lindane contents were observed e. g. in sediments from the Vistula river at Oświęcim (9,4

ppb), from the Bug river at Kryłów (7,1 ppm) and the Biała river at Kaniów (6,7 ppm). The high pesticides contents in river sediments were detected mainly in the vicinity of urban-industrial centres except the sediments from the Bug river near the Ukraine-Poland border where this river flows across agricultural areas. Presence of p,p'-DDT and its metabolites were detected almost in all analysed samples (97,5%). Occurrence of p,p'-DDT were registered in 31 samples and its metabolite p,p'-DDE – in 78 samples and p,p'-DDD – in 69 samples. Concentration of p,p'-DDE above PEL value (6,75 ppb) were detected in nine samples, for p'-DDD (8,51 ppb) – in 9 samples, for p,p'-DDT – in 13 samples. The very high contents of DDTs were noticed in sediments from the Vistula river at Oświęcim (453 ppb) and at Tyniec (132 ppb), the Brda river at Bydgoszcz (340 ppb), the Bystrzyca river at Spiczyn (83 ppb) and from the Przemsza river at Chełmek (82 ppb). Among remaining pesticides the heptachlor epoxide concentrated above the detection limit was found in five sediment samples, Dieldrin – in 15 samples, Aldrin – in 10 samples, Endrin - in 10 samples, Endosulfan I only in one samples, Endosulfan II – in four samples and Methoxychlor – in two samples. Occurrence of Heptachlor epoxide with concentration higher than PEL value (2,74 ppb) was detected in one sample (1,3%).

PEB2-2: Distribution and spatial trends of PCBs in urban soils from six European cities

A.F.O. Cachada, L.V. Lopes, S.M. Rodrigues, A.C. Duarte

Department of Chemistry, University of Aveiro, 3810 Aveiro, Portugal (e-mail: acachada@dq.ua.pt)

Organic pollutants are persistent, bioaccumulative and several of them are carcinogenic and/or mutagenic. Anthropogenic activities such as traffic, industry, domestic heating and agriculture can be major sources of these compounds [1]. Soils constitute, even in the urban context, the main environmental compartment for accumulation of organic contaminants, such as polychlorinated biphenyl's (PCBs), as they are particle reactive chemicals and highly lipophilic [2]. Therefore, testing and validating methods for assessing the presence and the quantification of organic pollutants in soils is a useful and important tool for urban planning. In this context the PCBs content in soil samples from the following six European cities was determined: Aveiro (Portugal), Sevilla (Spain), Uppsala (Sweden), Glasgow (Scotland), Torino (Italy) and Ljubljana (Slovenia).

Determination was undertaken in soil surface (0-10 cm depth). Soil samples were air dried, sieved to <2 mm, homogenised and frozen involved in aluminium foil [3]. Ten grams of soil were extracted with a hexane/acetone mixture (2:1), using a Soxhlet apparatus. Extracts were then submitted to a neutral alumina clean-up and solvent changed to isooctane [4]. Internal standard (PCB congener 209), procedure blanks, duplicates and reference material were used in each extraction batch for quality control assessment.

Extracts were analysed using a Shimadzu Corporation GC/MS-QP5050A equipped with a DB-5 fused silica capillary column and helium as carrier gas. Column temperature was programmed as follows: 40 °C for 2 minutes, increased at a rate of 10 °C /min until 290°C and kept for 8 minutes. The column flow was 0.7 ml/min. The injector temperature was 280°C and 1µl of sample was injected in splitless mode. Interface temperature was 300 °C and the acquisition was programmed to monitor selected ion (SIM).

The average content of total PCBs was found to be high in Torino with a mean value of 34.7 µg kg⁻¹, and a range between 1.6 and 173.1 µg kg⁻¹, followed by Glasgow that shows a mean value of 31.5 µg kg⁻¹, ranging from 5.1 to 83.2 µg kg⁻¹. Ljubljana shows a mean value of 13.1 µg kg⁻¹ ranging from 2.6 to 48.2 µg kg⁻¹, very similar to Aveiro that has a mean value of 13.6 µg kg⁻¹, with range from 1.2 to 74.2 µg kg⁻¹. Uppsala and Sevilla showed the lowest mean values: 10.4 µg kg⁻¹ ranging from 2.6 to 76.6 µg kg⁻¹ and 6.6 µg kg⁻¹ ranging from 1.6 to 23.7 µg kg⁻¹, respectively.

PCBs are normally associated with industrial contamination [5], which may explain the differences obtained within cities. Therefore the highest concentrations of PCBs found in Torino and Glasgow it may be due to the industry, as this cities are known to be highly

industrialised. On the other hand, results found in Sevilla, the lowest mean value of all cities, show that contamination is due essentially to traffic. Differences between land uses within cities were found and all cities have shown the same trend, that is, higher values of PCBs associated to roadsides. This results obtained were found to be high but showing a similar trend as the ones found in previous studies ([6], [7]).

The median percentages of PCBs congeners in urban soils which can give some indications about the origin and the fate of these contaminants were calculated. In all cases the lower-chlorinated PCBs are in less percentage than the higher-chlorinated ones. Hexachlorinated congeners (Hexa-CBs) are predominant in soils from all cities, consistent with results in the literature ([6], [8]). The principal elimination pathway of PCBs from soil is volatilisation [5], with the air-soil system approaching a thermodynamic equilibrium. This process affects mainly the lightest congeners and may explain why these PCB congeners are normally below detection limit. It also may explain the low values found in Sevilla due to the climate in this region.

Acknowledgment

This work was developed under Project EVK4-CT-2001-00053: URBOSOIL. We would like to thank Professor Franco Ajmone Marsan, Professor Luis Madrid, Professor Franc Lobnik, Doctor Erasmus Otabbong, Doctor Andrew Hursthouse and Doctor Christine Davidson, who supplied us with the samples.

References

- [1] Singh, A. K., Spassova, D., White, T., 1998. Quantitative analysis of polychlorinated biphenyls, organochlorine insecticides, polycyclic aromatic hydrocarbons, polychlorinated hydrocarbons and polynitrohydrocarbons in spiked samples of soil, water and plasma by selected-ion monitoring gas chromatography–mass spectrometry. *Journal of Chromatography B* 706, 231-244.
- [2] Edgar, P. J., Davies, I. M., Hursthouse, A. S., Matthews, J. E., 1999. The biogeochemistry of polychlorinated biphenyls (PCBs) in the Clyde: Distribution and Source Evaluation. *Marine Pollution Bulletin* 38(6), 486-496.
- [3] Krauss, M., Wilcke, W., Zech, W., 2000. Availability of Polycyclic Aromatic Hydrocarbons (PAHs) and Polychlorinated Biphenyls (PCBs) to Earthworms in Urban Soils. *Environmental Science & Technology* 34(20), 4335-4340.
- [4] Folch, I., Vaquero, M. T., Comellas, L., Broto-Puig, F., 1996. Extraction and clean-up methods for improvement of the chromatographic determination of polychlorinated biphenyls in sewage sludge-amended soils: elimination of lipids and sulphur. *Journal of Chromatography A* 719, 121-13.
- [5] Montelay-Massei, A., Ollivon, D., Garban, B., Teil, M. J., Blanchard, M., Chevreuil, M., 2004. Distribution and spatial trends of PAHs and PCBs in soils in the Seine River basin, France. *Chemosphere* 55, 555-565.
- [6] Lead, W. A., Steinnes, E., Bacon, J. R. and Jones, K. C., 1997. Polychlorinated biphenyl's in UK and Norwegian soils: spatial and temporal trends. *The Science of the Total Environment* 193, 229-236.
- [7] Istituto Superiore di Sanita (ISS), 2003. Interpretazione del parametro "PCB" – D.M. 471/99. Italia.
- [8] Weiss, P., Lorbeer, G., Scharf, S., 2000. Regional aspects and statistical characterisation of the load with semivolatile organic compounds at remote Austrian forest sites. *Chemosphere* 40, 1159-1171.

PEB2-3: Bioremediation of a polluted hydrocarbon soil

B. Ceccanti¹, C. Garcia², G. Masciandaro¹, C. Macci¹, A. Carmignani¹, A. Filareto¹

1) CNR-Istituto per lo Studio degli Ecosistemi (ISE) – Sezione di Chimica del Suolo, Area della Ricerca, Via Moruzzi, 1 – 56124 Pisa (Italy) (e-mail: grazia.masciandaro@ise.cnr.it)

2) CSIC-Centro de Edafologia y Biologia Aplicada del Segura, Campus de Espinardo – Murcia (Spain)

Bioremediation is a biological strategy for the recovery of polluted environments ensuring the conservation of biophysical property of ecosystems; it is defined by the microbiology American academy like “The use of living organisms to reduce or eliminate environmental hazard resulting from accumulation of toxic chemicals and other hazardous wastes”. One of this technology involves the application of microorganisms with specific degradative abilities (bioaugmentation) e/o the stimulation of autochthonous microorganisms (biostimulation).

The present investigation is about the effects of some treatments on the bioremediation of a polluted soil and the selection of specific parameters useful to study the evolution of biochemical processes which take place in the decontamination.

The experiment was carried out, for three months, in laboratory microcosms under controlled temperature and humidity.

The bioremediation treatments were the following: 1) a mixture of microorganisms-enzymes-nutrients (MEN); 2) compost alone (C); 3) compost with earthworms (*Eisenia fetida*) (CL) like agents of bioremediation and 4) control soil (without treatment) (BN).

The earthworms (*Eisenia fetida*) has been selected because show the maximum efficiency in the soil with the presence of organic matter. The role of the earthworms is: 1) to ensure the continuous mixing of the soil and the proliferation of the autoctonous microorganisms in the soil; 2) the casting of the earthworms increases the microbiological and biochemical soil activity.

Chemical (total and water soluble carbon, anions, total and available forms of nitrogen and phosphorus), physico-chemical (pH, electrical conductivity), biological (ATP, CO₂) and biochemical (hydrolytic enzyme activity) parameters were determined to study the soil metabolic processes involved in the degradation of hydrocarbons. Total residue hydrocarbons (TPH) were carried out at the end of the experiment to assess the efficiency of the bioremediation process. The parameters have been determined monthly while the carbon dioxide every two days.

The study showed an intense microbiological activity expressed as CO₂ evolution (fig.1) during the time, with a tendency to stabilize at the end of the experiment. The highest CO₂ release was found in the compost treatments even in the presence of earthworms, showing the availability of organic substrate characterising the compost.

The C and N compounds, both in their total and available forms, showed a reduction during the time due to organic compound degradation and volatile form loss. The organic substrate reduction during the time caused a reduction of hydrolytic enzyme activities representative of C (β -glucosidase) and N (protease) cycles. However, the enzyme activities showed higher values in the treatments with compost. Highest reduction of hydrocarbons has been found in the treatments with compost, in particular with earthworms that have also contributed to regulate the biochemical equilibrium of the soil.

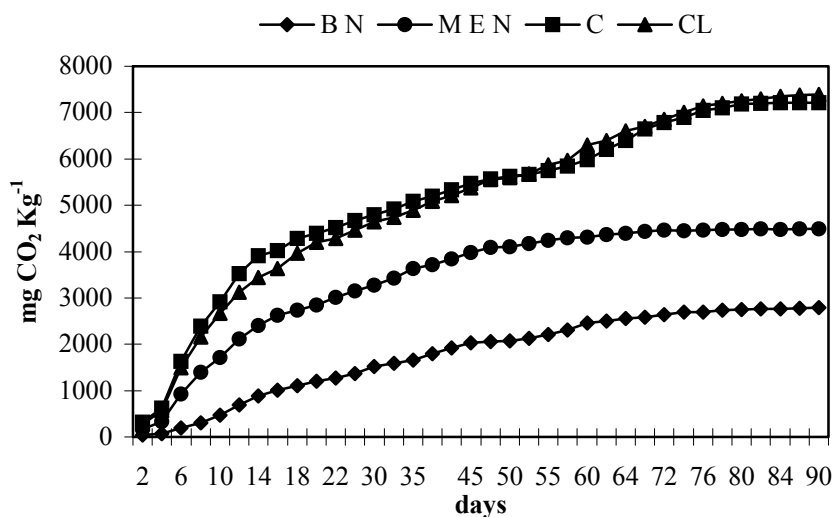


Fig.1. Production of CO₂ during the experimental period

PEB2-4: The Prestige oil spill. Enhanced biodegradation of a heavy fuel oil under simulated conditions

S. Diez¹, J. Sabaté², M. Viñas², J.M. Bayona¹, A.M. Solanas², J. Albaigés¹

1) Department of Environmental Chemistry. IIQAB-CSIC. Jordi Girona Salgado, 18-26. 08034-Barcelona, Spain (e-mail: albqam@cid.csic.es)

2) Department of Microbiology, University of Barcelona. Diagonal, 645. 08028-Barcelona, Spain

The *Prestige* oil spill involved 60000 tons of a Russian heavy fuel-oil (type M-100) that on November 2002 affected more than 800 km of the NW Spanish coast. A detailed understanding of weathering processes that oil is subjected to is required in order to foresee the environmental damage and to develop effective restoration strategies. An early assessment of the effects of biodegradation on the hydrocarbon composition will be useful not only for the feasibility studies regarding the application of these techniques but also for providing monitoring indicators of the natural evolution of the spill, which will be particularly valuable for the source recognition of oil samples collected a certain time after the incident.

Although numerous reports have covered various aspects of petroleum biodegradation and the environmental factors that influence the rate of this process, the case of heavy oils has been barely addressed. The presentation will show the results of a series of *in vitro* biodegradation experiments using two microbial consortia (TD and AM), obtained by enrichment procedures on selected fractions of different oil products. Different conditions such as incubation time (i.e. 20 and 40 days), oil weathering as well as the addition of an oleophilic fertilizer (S200) were evaluated. The evaluation of the biodegradation was performed on the basis of the changes observed in the different hydrocarbon profiles and, particularly, in the ratios of target hydrocarbon concentrations relative to the more recalcitrant components.

n-Alkanes, alkylcyclohexanes, alkylbenzenes and the 2-3 ring polycyclic aromatic hydrocarbons (PAHs) were degraded in 20-40 days of incubation of the original oil, whereas the biodegradation efficiency decreased for higher PAHs and with the increase of alkylation. Isomeric selectivity was also observed within the C₁ – C₃ naphthalenes, phenanthrenes, dibenzothiophenes, pyrenes and chrysenes.

Weathering slowed down the fuel oil degradation, probably due to the loss of lower and more labile components, but the addition of S200 enhanced significantly the biodegradation to the extent that acyclic isoprenoids, C₂₇-steranes and C₁ and C₂ naphthalenes, phenanthrenes and dibenzothiophenes were completely degraded. Molecular markers were degraded according to the following sequence: diasteranes > C₂₇-steranes > ββ-steranes > homohopanes > mono-aromatic steranes > tri-aromatic steranes, providing source correlation and weathering indices for the characterisation of the heavy oil spill.

The results are compared with the analysis of field samples collected along the coast during the last two years after the accident.

PEB3-5: Fate of the spill of The Prestige oil tanker in the deep sea

S. Elordui-Zapatarietxe¹, A. Rosell-Melé¹, P. Masqué¹, J. Albaigés²

1) Institute of Environmental Science and Technology, Autonomous University of Barcelona, Bellaterra 08193, Catalonia, Spain (e-mail: saioa.elordui@uab.es)

2) Department of Environmental Chemistry, CID-CSIC, Barcelona 08034, Catalonia, Spain

Introduction

On 13 November 2002 during severe weather the M/T *Prestige* suffered a hull fracture and started spilling crude oil into the north Atlantic off the coast of N.W. Spain. On the 19th the vessel broke in two (coordinates 42°15N and 12°08W) at about 130 nautical miles off the Spanish coast, west south-west of Cape Finisterre and sank through more than 3500 metres of water. It is estimated that 80 % of the 77.000 metric tons of the fuel oil in the tanker have been spilled, a significant part of which in the deep sea. The fate of this oil is unclear. Some of the fuel reached the coasts but the proportion that this represents of the total is not known.

There are no previous events in the region that can be used to evaluate the consequences of the accident from an environmental, social and economical standpoint.

As part of a project that investigates the fate of the oil spilled from the M/T *Prestige* wreck in the deep sea, we are assessing the dissolution potential of the fuel oil in the different water masses overlaying the wreck. This should help to understand which have been the main physical, biological and chemical processes involved in the distribution of the oil and its residual compounds in the water column and sediments in the area offshore affected by the accident.

Approach

The unmistakable correlation between the collected oil samples and the spilled product is essential to assess the impacted area. This task gets more difficult as the time goes by, due to the inputs of other anthropogenic sources of hydrocarbons to the marine environment, as well as from natural sources. We are carrying out a detailed characterization of the spill through the analysis of the remnants of fuel oil in the ship, using GCMS, HPLCMS and CSIA (Compounds Specific Isotope Analysis).

To assess the potential changes in the fuel composition undergone since the spill in the water column we are carrying out a suite of laboratory experiments to simulate the oceanographic conditions of the water masses surrounding the wreck. The first goal is to determine the water soluble fraction (WSF), by placing fuel oil samples in seawater tanks at different temperature and salinity conditions. All these experiments are being carried out in

darkness and stirring slowly to avoid water-in-oil emulsions. The monitoring of the solution is being carried out by means of two fixed interval techniques, a) measurement of the dissolved organic carbon and b) fluorescence. Deuterated standards are also used to control the losses at the end of the experiment. Water samples taken from the tanks at regular intervals are then extracted with organic solvents and the biomarkers in these extracts are characterized and quantified by means of GC and HPLC hyphenated techniques.

We are in the process of obtaining the first results. We expect to find changes in fuel composition, caused by dissolution according to changes in the physico-chemical properties of the fuel in the different experimental conditions. The data should then help to trace the chemical remains of the Prestige oil spill far from the tanker and understand which processes played a major role in dispersing and degrading the oil.

PEB2-6: Photolytic and microbiological degradation of the organic pollutants that originating from the petrochemical industry

N. Kuburovic¹, M. Todorovic², V. Raichevic², L. Jovanovic³, O. Ecim², B. Lalevic²,
T. Sholevic⁴

1) Univ. Belgrade Faculty of Technology and Metallurgy, YU 11001 Belgrade, Karnegijeva 4, Serbia and Montenegro (e-mail: natasa19@verat.net)

2) Univ. Belgrade Faculty of Agriculture, YU 11080 Belgrade - Zemun, Nemanjina 6, Serbia and Montenegro

3) Center for Multidisciplinary studies Univ. Belgrade, 11000 Belgrade, Kneza Visheslava 1A, Serbia and Montenegro

4) Center of Chemistry, IChTM, 11001 Belgrade, Njegosheva 12, Serbia and Montenegro

During the past decades many different technologies were used both for reducing the source of pollution and for improvements of the already contaminated areas. The most dangerous pollutants found in the waters and soils are different organic compounds originating from the petrochemical industries. For its remediation have been used different chemical and physical methods, mainly expensive ones and insufficiently efficient. New alternative methods, more efficient and economically feasible have been developing gradually.

In this study we are presenting the methods of photolytic and microbiological degradation of toxic organic compound that originated from petrochemical industry. We investigated the effects of concentrated solar radiation ([1], [3]), as well as different artificial lights (sodium, metal-halogen and UV lamps) on degradation of methyl-tertiary-butyl-ether (MTBE) [2], benzene and other gasoline compounds that are detected in wastewater and watercourse of petrochemical industry. Our result showed that bacteria *Pseudomonas* strain CY, isolated from the kerosene, added alone, was able to gradually degraded MTBE and benzene and so decreased its concentration for 93.6 % and 95.5 % respectively in twelve hours. However, when we used concentrated solar radiation and artificial light, the percentage of its degradation decrease for 99.2% and 91.1% respectively in only four hours. By adding *Pseudomonas* strain CY after four hours of light treatments the degradation was enhanced to 99.55% and 95.6% respectively, in five hour. Our experiments showed that combination of light and bacteria could be used as model system for another toxic organic substances that originated from another sources. The best result in degradation is obtained when we combine both methods, photolytic and microbiological degradation.

References

- [1] Ecim, O., Todorovic, M., 1999. Proceedings of the 30th International Congress of Air Conditioning, Heating and Refrigeration (KGH), Belgrade, pp. 112-117.
- [2] Kuburovic, N., Todorovic, M.S., Drmanic, S.Z., Raichevic, V.B., Jovanovic, Lj.B., 2005. Proceeding of the 2nd World Conference and Technology Exhibition on Biomass, Rome, (2005 - to be published).
- [3] Kuburovic, N.D., Valent, V.J., Todorovic M.S., 2003. Astronomical and astrophysical transaction, Vol. 22, No. 6, Taylor & Francis Ltd, Oxford, pp. 887-890.

PEB2-7: Compound-specific isotope analysis applied to MTBE biodegradation studiesT. Kuder¹, P. Philp¹, J. Wilson², J. Allen¹

1) University of Oklahoma, Norman, OK, 73019, USA

2) US EPA, Ada, OK, 74820, USA

Compound-specific isotope analysis (CSIA) is a technique gaining popularity in the studies of biodegradation of groundwater contaminants (such as BTEX, chlorinated ethenes and MTBE). In brief, biodegradation results in enrichment of “heavy” isotopes (e.g., ¹³C and D) in the remaining undegraded material, as a result of faster reaction rates of molecules substituted with the “lighter” isotopes (¹²C and H). The resulting isotopic enrichment can be identified by CSIA. In this presentation it is proposed to discuss the application of CSIA to the study of MTBE biodegradation.

The combined use of carbon and hydrogen isotopes allowed characterization of the MTBE degradation mechanism in methanogenic soil/groundwater microcosms. The magnitude of isotopic fractionation for carbon and hydrogen, and isotopic mass balance of the parent MTBE and its degradation product, *t*-butyl alcohol, show that MTBE degrades by cleavage of the methoxy group on the C_{methyl}-oxygen bond (similar conclusions were independently obtained by Zwank et al., 2005). The result of this cleavage is a characteristic pattern of isotope fractionation, easily distinguished from the isotope effect produced by aerobic biodegradation. Microcosm data from three other methanogenic cultures show carbon (Somsamak et al., 2005; Kuder et al., unpublished) and combined carbon and hydrogen (Kuder et al., unpublished) in the same numerical range as those reported in Table 1.

The two most significant conclusions of the microcosm experiments are: (i) it is practical to distinguish between the effects of aerobic and anaerobic MTBE biodegradation by combined carbon + hydrogen CSIA; and (ii) the magnitude of carbon isotopic fractionation in the anaerobic process is large and apparently consistent among different microbial cultures. The benefit for environmental studies lies in providing a tool for monitoring *in-situ* biodegradation, eliminating the need to verify biodegradation potential of a site by time consuming and indirect microcosm experiments. Definition of the enrichment factor (ϵ) for MTBE degradation in microcosm studies permits quantification of the extent of biodegradation based on the isotope ratios measured on field samples.

Field data presented herein are obtained from MTBE-contaminated sites in the USA. These results agree well with the anaerobic microcosm study, indicating that at a number of sites MTBE was extensively degraded by a process similar to that observed in the microcosm

experiment. Initial reports on the low biodegradation potential of MTBE implied that anaerobic biodegradation of MTBE is not environmentally significant. Several more recent studies show evidence of anaerobic MTBE biodegradation based on concentration trends and/or other “traditional” geochemical biodegradation indicators. CSIA data from multiple field sites suggest that anaerobic biodegradation of MTBE is not as unique as originally thought, and at a number of those sites near-complete MTBE attenuation was achieved by anaerobic biodegradation alone.

Table 1. Overview of isotope effects during MTBE biodegradation

Culture	ϵ (carbon) ‰ ^a	ϵ (hydrogen) ‰ ^a	reference
Aerobic microcosm enrichment	-1.64 ± 0.05	Not analyzed	Hunkeler et al. 2001
Aerobic cometabolic enrichment	-1.97 ± 0.05		
Aerobic microcosm; PM1	-2.0 ± 0.1 to -2.4 ± 0.3	-33 ± 5 to -36 ± 6	Gray et al., 2002
Aerobic microcosm; VAFB	-1.4 ± 0.1 to -1.8 ± 0.1	-29 ± 4 to -66 ± 3	
Methanogenic microcosm	-9.2 ± 5.0	Not analyzed	Kolhatkar et al., 2002
Methanogenic enrichment microcosm ^b	-13 ± 1.1	-16 ± 5	Kuder et al., 2005
Methanogenic enrichment microcosm	-15.6 ± 4.1	Not analyzed	Somsamak et al., 2005
	-14.6 ± 5.2		

^a Precision reported at 95 % confidence level on the regression

^b the same culture as in Kolhatkar et al., 2002

References

- Gray, J.R., G. Lacrampe-Couloume, D. Gandhi, K.M. Scow, R.D. Wilson, D.M. Mackay, and B. Sherwood Lollar, 2002, *Env. Sci. and Technology* 36: 1931-1938.
- Hunkeler, D., B.J. Butler, R. Aravena, and J.F. Barker, 2001, *Env. Sci. and Technology* 35: 676-681.
- Kolhatkar, R., T. Kuder, P. Philp, J. Allen, and J.T. Wilson, 2002, *Env. Sci. and Technology* 36: 5139-5146.
- Kuder, T., J.T. Wilson, P. Kaiser, R. Kolhatkar, P. Philp and J. Allen, 2005, *Env. Sci. and Technology* 39: 213-220.
- Somsamak, P., H. H. Richnow and M. Haggblom, 2005, *Environ. Sci. Technol.*, 39, 103-109.
- Zwank, L., M. Berg, M. Elsner, T. C. Schmidt, R. P. Schwarzenbach and S. B. Haderlein, 2005, *Env. Sci. Technol.*, ASAP online content.

PEB2-8: Distribution patterns of atmospheric pollutants (PAH/PCN) accumulated on pine needles in the Cologne conurbation (Germany)

E. Lehndorff, L. Schwark

Institute of Geology and Mineralogy, University of Cologne, Zulpicher Strasse 49a, 50674 Cologne, Germany
(e-mail: e.lehndorff@uni-koeln.de)

The overwhelming part of atmospheric pollutants in the Cologne Conurbation results from combustion processes, related to traffic, lignite fueled power plants and industrial emissions. Due to the high toxicity and carcinogenic potential of various PAH and PCN congeners these compounds are considered as primary pollutants. Although toxicity of PCNs and PCBs is almost identical, environmental studies of the former pollutants are limited. The passive biomonitoring approach chosen allowed acquisition of a time-integrated and spatially well resolved dataset impossible to obtain via direct and long term high volume air sampling. We here present results from a biomonitoring study conducted in a densely populated and highly industrialised region of Germany based on airborne PAH and PCN accumulated in/on *Pinus nigra* needles.

Pine is an evergreen conifer ubiquitous throughout the study area with needle generations representing a time range up to 5 years. Source characterisation can be applied on different scales, e.g. local traffic emissions or dispersed industrial emissions. Needles for this study were collected from 43 locations within a grid area of 20 x 30 km, comprising the inner city of Cologne and suburban residential areas as well industrial zones.

PAH-analysis of 43 locations in the Cologne Conurbation revealed concentrations of summed three to six-ring PAH ranging between 51 and 410 ng g⁻¹ (dry weight), averaging a median value of 124 ng g⁻¹ (Fig. 1), similar to concentrations observed in other urban studies. Amongst the PAH phenanthrene was the dominating analogue with median concentrations of 47 ng g⁻¹ followed by fluoranthene and pyrene at 22 and 13 ng g⁻¹, respectively. This indicates a preferentially gas-phase transport of 3- to 4-ring PAH. However, for the 4- to 6-ring PAH a good correlation with particle abundance on needles was observed. Particle loads on needles were examined by SEM-analysis and correlated with magnetic susceptibility [1] and iron concentrations.

The major proportion of PAH was attributed to traffic sources, with minor contribution from power plant, industrial, domestic heating, and vegetation burn emissions. Significant differences between major and minor roads were not observed indicating a thorough mixing of PAH-loaded air masses in the Cologne Conurbation. Needles taken in parks showed a differentiated airborne pollutant pattern. Needles from parks in the inner city

yielded much higher PAH concentrations than those from parks in suburban areas (Fig.1a). Identification of emission sources based on PAH ratios following Yunker et al. (2002) [2] and references given therein, proved to be difficult due to intensive mixing of air masses and associated loss of source specificity. However, discrimination diagrams employing the ratios of fluoranthene vs. pyrene and benzo[a]pyrene vs. benzo[ghi]perylene (Fig.1b) allowed identification of burning biomass, input associated with railway operations and gradients in road traffic influence.

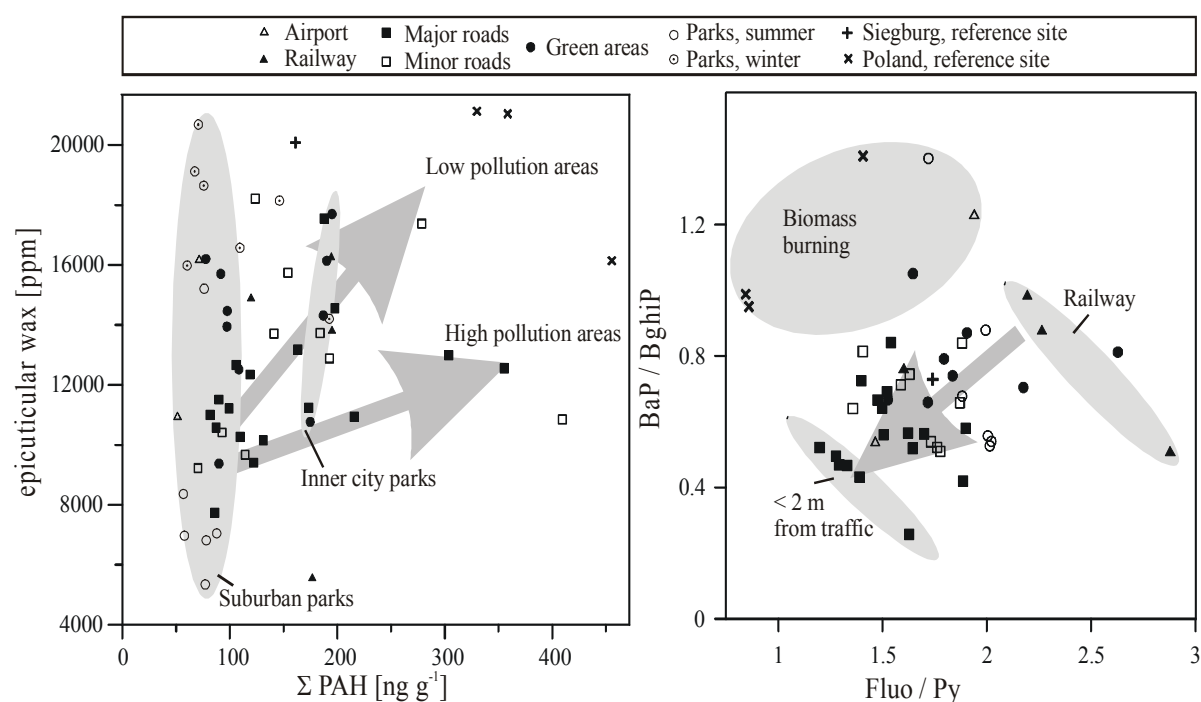


Fig.1. (a) Relation between epicuticular waxes and total PAH load. (b) Bivariance plot of BaP/BghiP-versus Fluo/Py-ratio. Fluoranthene and pyrene possess similar physicochemical properties, the ratio will thus primarily reflect source character. Low Fluo/Py-ratios indicate a dominant traffic source, high values power plant emissions. Samples taken near railway operations or affected by biomass burning bear a specific signature

PCN loadings of pine needles in the Cologne Conurbation show different distribution patterns. PCN may currently be released into the atmosphere via municipal waste incineration and industrial emissions. Alternatively, formerly emitted PCN (production ceased in the 70s in Germany) may be redistributed in environment due to revolatisation from landfill sites, contaminated soils and sediments. Although banned for about three decades now, the present atmospheric PCN concentrations do not show a significant decline. The degree of naphthalene chlorination in Cologne pine needles ranged from Cl_2 to Cl_6 . Several locations revealed a complete lack of hexa-chlorinated and very low abundance of penta-chlorinated congeners while others display the full PCN range. The dominance of tri- and tetra-chloronaphthalenes argues for preferentially gas-phase transportation of PCN in the Cologne Conurbation. Higher

chlorinated analogues occur predominantly particle-bound. The low absolute concentrations of hexa- and heptachlorinated congeners found may still pose a significant environmental risk as these congeners exhibit toxicity equivalence factors 100 times higher than their tri- to penta-chlorinated counterparts. The congener patterns are currently interpreted in terms of source allocation as the α -substituted congeners derive from industrial Halowax formulations, whereas the β -substituted analogues are formed upon combustion.

References

- [1] Urbat, M., Lehndorff, E., Schwark, L., 2004. Assessment of air quality in the Cologne conurbation using pine needles as a passive sampler Part I - magnetic properties. *Atmospheric Environment*, 38, 3783-3794
- [2] Yunker, M.B., MacDonald, R.W., Vingarzan, R., Mitchell, R.H., Goyette, D., Sylvestre, S., 2002. PAHs in the Fraser River basin: a critical appraisal of PAH ratios as indicators of PAH source and composition. *Organic Geochemistry* 33, 489-515.

PEB2-9: Interaction modes between humic colloids and surfactant molecules as identified by octanol-water partitioning experiments with radiolabelled humic acid

H. Lippold, H. Kupsch

Institut für Interdisziplinäre Isotopenforschung, Permoserstr. 15, 04318 Leipzig, Germany

The interaction of humic materials and anthropogenic organic compounds in soil and water has become a topic of interest in view of environmental risk assessments and remediation strategies. Owing to their polyfunctional and amphiphilic properties, humic substances (HS) are able to associate both with organic and inorganic pollutants. The possibility of a mobilization depends on the solid-liquid partitioning of HS under the given conditions. Besides geochemical factors, implications of anthropogenic inputs have to be considered as well. Surfactants constitute a major part of domestic and industrial organic waste. Due to the agricultural use of sewage sludge and pesticides or via waste waters, considerable amounts of surfactants get into the soil. Since biodegradation can be decelerated, there is opportunity to join in biological, physical and chemical processes [1, 2]. As amphiphilic compounds, surfactants possess a high potential of interaction with HS. Consequently, the question arises as to whether the association with pollutants is influenced by synergistic or antagonistic effects. Furthermore, it is essential to know how the transport properties of the colloids are modified.

In this study, radioanalytical measurements of octanol-water partitioning were successfully utilized as a tool to detect association processes between humic colloids and surfactant molecules. We present evidence of different interaction modes for anionic, non-ionic and cationic surfactants resulting in significant modifications of the hydrophilic / hydrophobic properties of the colloids. Implications on the adsorption behaviour and on metal-humate complexation were also investigated. Humic acid was radiolabelled by halogenation with ^{131}I using the iodogen method [3]. In addition, possible effects on the size distribution of the humic colloids were examined by means of size exclusion chromatography.

In Figure 1, the effects of sodium dodecylsulfate, dodecyl- β -D-glucopyranoside and dodecyltrimethylammoniumbromide on octanol-water partitioning of humic acid are demonstrated. Surfactant concentrations were below the critical micelle concentration in each case. The contact with the cationic surfactant causes a considerable shift in the overall partition ratio $P_{O/W}$ towards the octanol phase. Obviously, the organo-cations interact with dissociated acidic groups of the humic acid, and charge neutralization renders the colloids more hydrophobic. Contrary, for the anionic surfactant, $\log P_{O/W}$ values are shifted towards

the hydrophilic region. In this case, binding is only achieved by the hydrophobic groups, and the ionic head groups of the surfactant molecules are free of interaction. Consequently, the colloids are expelled from the organic phase. Interaction with the non-ionic surfactant does not influence the partitioning behaviour, presumably because its hydrophilic-lipophilic balance is comparable to that of the humic acid.

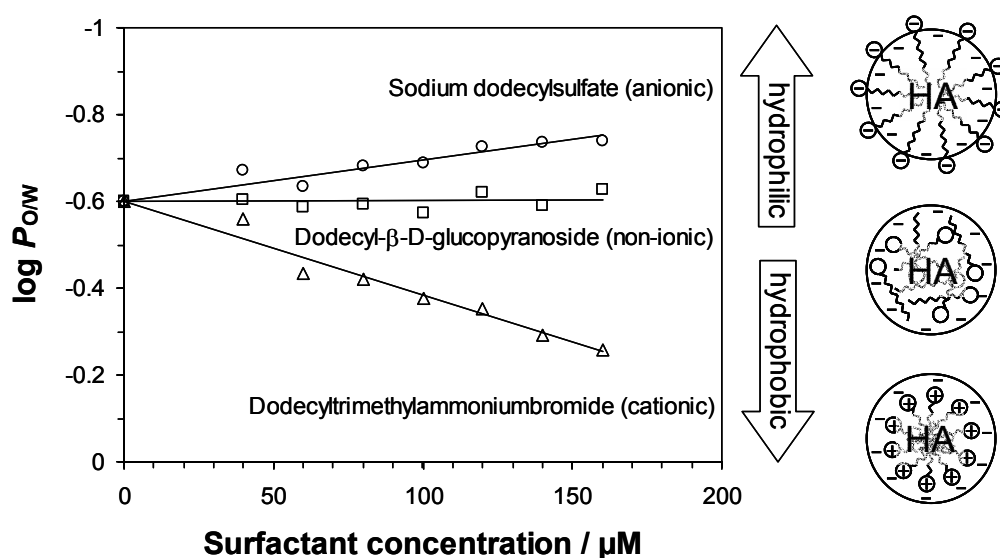


Fig.1. Effects of anionic, non-ionic and cationic surfactants on octanol-water partitioning of humic acid (5 mg L^{-1} , in 0.1 M NaCl , pH 4). Right: Schematic representations of different interaction modes as derived from the experiments

Adsorption of humic acid on kaolinite is increased in the presence of dodecyltrimethylammoniumbromide as a consequence of charge compensation, whereas a slight decrease is observed for sodium dodecylsulfate and dodecyl- β -D-glucopyranoside. Humate complexation of terbium(III), employed as an analogue of trivalent actinides, is not significantly influenced by the aggregation processes. Moreover, the size distribution of the humic colloids was found to be unaffected, indicating that there are no rearrangement processes among loose aggregates.

References

- [1] Klopper-Sams, P., Torfs, F., Fejtel, T., Gooch, J., *Sci. Total Environ.* **185** (1996) 171.
- [2] McAvoy, D.C., Eckhoff, W.S., Rapaport, R.A., *Environ. Toxicol. Chem.* **12** (1993) 977.
- [3] Fraker, P.J., Speck, J.C., *Biochem. Biophys. Res. Commun.* **80** (1978) 849.

**PEB2-10: Sources of polycyclic aromatic hydrocarbons (PAHs) in mussel tissues:
a forensic study of hydrocarbon sources and biological exposure in the
near-shore coastal waters of Avila Bay, California**

R.I. Haddad

Applied Geochemical Strategies, Inc., 2670 Appaloosa Way, Arroyo Grande, CA 93420, 805.474.9104
(e-mail: rhaddad@charter.net)

In an attempt to identify and assess the potential source(s) of hydrocarbons in the near-shore coastal waters of Avila Bay, CA, polycyclic aromatic hydrocarbons (PAHs) body burdens were measured in resident and transplanted populations of mussels associated with the Avila Pier. The objectives of this work were two fold: (1) to evaluate if there was evidence of PAH bioaccumulation in mussels (*mytilus edulis*) associated with the Avila Pier and Avila Beach (relative to mussel PAH body burdens associated with the regional background); and if so, (2) to assess the potential source(s) of these hydrocarbons. This work was undertaken in order to determine if a causal link could be established between the PAHs detected in resident and/or transplanted mussels and subsurface refined and unrefined petroleum contamination known to exist beneath part of the town and beach of Avila Beach.

For this study resident and transplanted mussels were collected from 4 locations on Avila Pier. Regional background mussels were also collected from a nearby working pier within Avila Bay (Harford Pier), a nearby pier outside Avila Bay (Pismo Pier), and a pristine area previously used as a station for the State Mussel Watch program (Montaña de Oro State Park). All samples were analyzed for lipid content and alkylated PAHs.

The results of both the resident and transplanted mussel studies showed elevated PAH concentrations at the Avila and Harford Piers (relative to the results from the Pismo Pier and Montaña de Oro). Further, the results suggest that mussel exposure to the source of the PAHs was most pronounced at the piers' seaward edge. Finally, the forensic assessment of the source of the mussel tissue PAHs showed that while there were likely several sources, the most prominent of these was characterized as having a pyrogenic signature. Analysis of potential PAH sources, including creosote associated with the wooden pier pilings and the refined and unrefined petroleum associated with the subsurface contamination, supports the hypothesis that the creosote associated with the wooden pier pilings are a substantial source of PAHs in this near-shore coastal environment.

PEB2-11: Potential Sources of the Polar Fraction Associated with Groundwater TPH

R. Haddad¹, S.-T. Lu²

1) Applied Geochemical Strategies, Inc., 2670 Appaloosa Way, Arroyo Grande, CA 93420, USA

(e-mail: rhaddad@charter.net)

2) ZymaX Forensics, 71 Zaca Ln, San Luis Obispo, CA 93401, USA

The precedent of using silica gel to differentiate between Total Oil and Grease (EPA Method 413) and Total Petroleum Hydrocarbons (TPH; EPA Method 418.1) has been cited as the basis for using a silica gel pre-treatment prior to quantifying sample extracts for TPH using newer gas chromatographic methods (e.g., 8015B). Despite this precedent, use of silica-gel to remove polar material in defining Total Petroleum Hydrocarbons (TPH) remains controversial.

Zemo and Foote (Ground Water Monitoring and Remediation, 2003) have presented a strong regulatory-based argument in favor of the use of silica-gel. However, this argument is not universally accepted. One assumes that at the heart of the controversy is the uncertainty associated with our lack of understanding of a molecular composition of TPH and the desire to err conservatively on the protection of human health and the environment. Clearly a resolution to this controversy requires an understanding of the sources of polar compounds derived from the release of petroleum into the environment. Silica gel effectively extracts “polar” compounds from the extract, allowing for a more sensitive analysis of the non-extracted non-polar hydrocarbons and often reducing the amount of material being identified as TPH in these samples.

In the first part of this study, we present our hypothesis that polar compounds associated with petroleum impacted groundwater can be derived directly from the separate-phase hydrocarbon (as nitrogen, sulfur, and/or oxygen-containing [NSO] compounds), from partial degradation of the hydrocarbons, from *in situ* organic material, and/or from bacterial biomass present as a result of the petroleum contamination. In testing this hypothesis, we present results from laboratory fuel/water partitioning experiments demonstrating that a series of Nitrogen, Sulfur, and Oxygen (NSO) containing polar compounds are partitioned from fresh petroleum fuels into water. These include benzamines, Indoles, quinolines, carbazoles, thiophenes, benzothiophenes, dibenzothiophenes, phenols, benzofurans, and dibenzofurans. For many of these compounds we are able to quantify alkylated homologues in addition to the parent compounds. These studies show that the quantified NSO polar compounds can comprise >25% of the dissolved TPH partitioning from the fresh fuels into water, thus

supporting the hypothesis that some fuel types can directly source polar compounds to petroleum-impacted groundwater.

In the second part of this study, results obtained from the laboratory partitioning studies are compared with groundwater analyses from a site containing separate phase hydrocarbons. The groundwater TPH concentrations from this site are generally low or absent with regards to saturates or aromatic compounds and, instead are supported by the polar content. The results of our studies show that much of the groundwater polar material is not attributable to the discrete types of NSO compounds identified in our laboratory partitioning experiments and suggest that direct partitioning from the separate phase petroleum mixture is not a significant source of the groundwater TPH.

**PEB2-12: Geochemical investigation of an offshore sewage sludge deposit,
Barcelona, Catalonia, Spain**

M.A. Kruger¹, A. Permanyer², J. Serra²

1) Department of Earth and Environmental Studies, Montclair State University, Montclair, New Jersey, USA
(e-mail: krugem@mail.montclair.edu)

2) Facultat de Geologia, University of Barcelona, Barcelona, Catalonia, Spain

For 20 years ending in the 1990's the city of Barcelona discharged the products from a large primary sewage treatment plant near the mouth of the Besòs River directly into the Mediterranean Sea via underwater conduits. The sewage sludge, rich in organic matter and heavy metals, now covers an area of over 3 km² with a volume of ca. 3 million m³, between 1 and 4 km offshore, at water depths between 30 and 55 m (Fig. 1A). The deposit is an elongated body perpendicular to the coast and formed due to successive underwater ruptures of the conduit with some resedimentation by marine currents. Following the adoption of improved environmental standards, the use of the discharge pipes ceased. The sludge deposit remains in place for the time being.

In an effort to understand the history and present state of the sludge deposit, a program of geophysical mapping (side scan sonar and seismic), sampling and analytical work was undertaken. Based on the mapping results, 10 coring sites were chosen and sampled by vibracorer (Fig. 1A). A total of 44 subsamples were taken from the cores for organic and inorganic geochemical analyses, including organic carbon determination, elemental analysis by atomic absorption, and molecular organic analysis by pyrolysis-gas chromatography/mass spectrometry (Py-GC/MS) of whole, dried sediment samples.

Sedimentary organic carbon (C_{org}) percentages range from 0.50 to 5.91, with the highest values in the upper 100 cm of sediment in cores taken on or near the sludge deposit (cores 2 and 5 in particular; Fig. 1A). Samples enriched in C_{org} also show high Ca concentrations (over 23 weight % in the upper portions of cores 2 and 5), likely derived from the flocculents applied during sewage treatment. Calcium is therefore a useful for mapping the sludge deposit (Fig 1A). The Ca plume to the southwest of the sludge deposit likely results from transport by marine currents. The concentrations of Na, P and Sr also strongly correlate with C_{org}. Among transition metals, Ag, Zn, Cu, Ni, Cd and Pb are all present in concentrations well above background levels, correlating positively with C_{org} concentrations. For example, Zn concentrations range up to 813 ppm in the upper portion of core 2.

The 41-42 cm interval of core 5 is representative of the sludge deposits. Its pyrogram (Fig. 1B) shows the common pyrolysis products of sedimentary organic matter such as

toluene, xylenes, styrene, naphthalene and phenol. Most striking, however, are the abundant C_{27} and C_{29} sterenes and steranes. Another remarkable feature is cluster of C_{11} - C_{13} linear alkylbenzenes. Anomalously high concentrations of C_{14} - C_{26} *n*-alkanes, indole, methylindole, and long-chain alkyl nitriles and alkylamides are also characteristic of the pyrolyzates of the organic-rich sludge.

The sterenes and steranes are likely produced from fecal and other steroids in the sewage sludge during pyrolysis. The steroids survived the primary sewage treatment process, as did the abundant linear alkylbenzenes, which are derived from detergent residues in the sludge. The indoles are likely the pyrolysis products of proteins, while the long-chain organonitrogen compounds in the pyrolyzate likely derive from bacterial biomass. These distinctive pyrolysis products and the trace elements would be useful geochemical markers to assess the effectiveness of a remediation program.

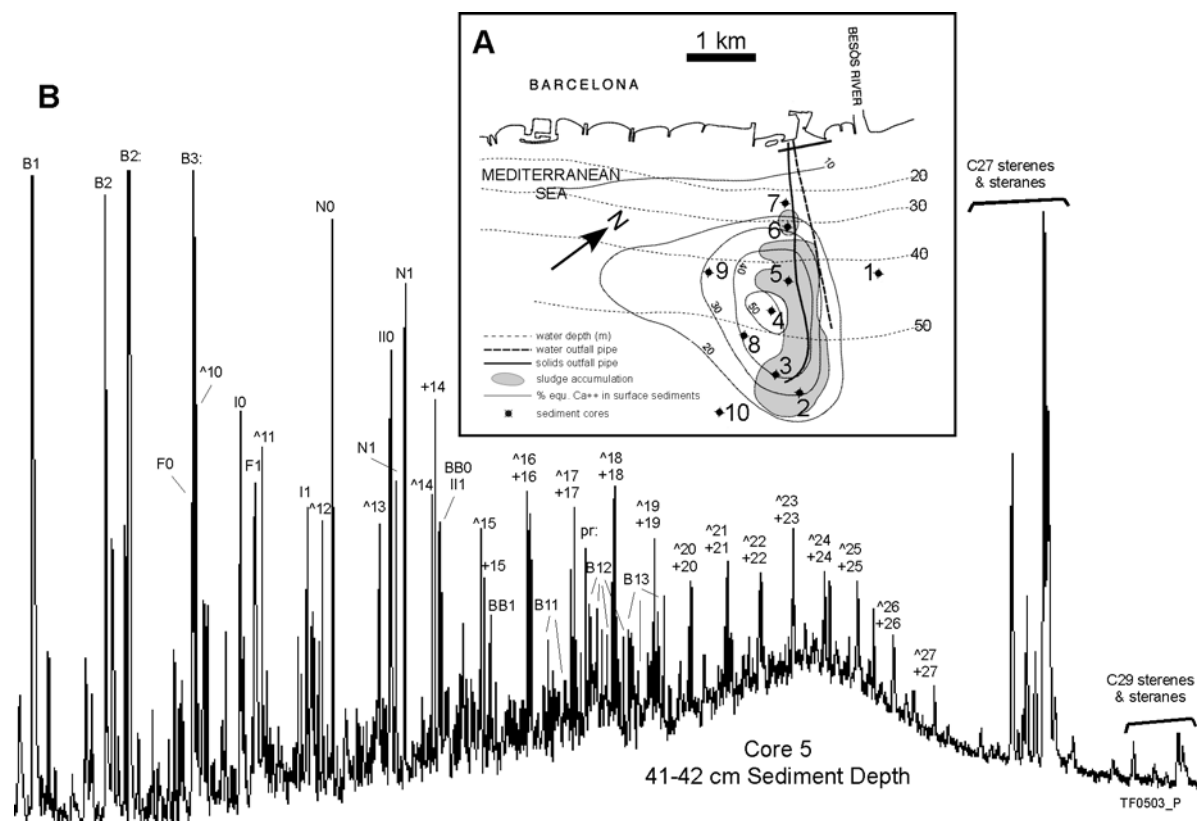


Fig.1. (A) Map showing the northwestern Mediterranean coast between Barcelona and the Besòs River, water depth, the sewage treatment plant submarine outfall pipes, the sludge accumulation, calcium concentrations in surface sediments, and core locations. (B) Total ion current pyrogram of the subsample at 41-42 cm sediment depth in core 5. Bn - alkylbenzenes, B2: - styrene, B3: - propylene benzene, Fn - phenols, In - indenenes, Nn - naphthalenes, Iln - indoles, BBn - biphenyls, ^n - n-alk-1-enes, +n - n-alkanes, pr: - prist-1-ene, where n is the extent of alkylation. (Py-GC/MS conditions: CDS 120 pyroprobe (600 °C, 20 sec.), HP 5890 GC, HP 5970 MSD, 50 m J&W Scientific DB-5MS column (0.2mm i.d., film thickness 0.33 mm). GC program: 5 min at 40 °C; 5 °C/min. to 300 °C and then isothermal for 30 min. The MS was operated in full scan (50-450 Da, 1.21 scans/sec., 70eV ionization voltage.)

PEB2-13: Microbial biodegradation of potential PAH sources in sewage sludge

A. Regier¹, L. Mansuy-Huault¹, P. Faure¹, C. Leyval², T. Béguéristain²

1) G2R UMR 7566, UHP Nancy, BP 239, 54506 Vandoeuvre-lès-Nancy
(e-mail: Laurence.mansuy-huault@g2r.uhp-nancy.fr)

2) LIMOS UMR 7137, UHP Nancy, BP 239, 54506 Vandoeuvre-lès-Nancy

Polycyclic aromatic hydrocarbons (PAH) are persistent organic pollutants frequently encountered in the environment. They originate mainly from combustion processes, fossil fuels or chemical products. To reduce PAH input it is necessary to know the PAH sources. For source apportionment of PAH the distribution pattern and various molecular ratios can be used to classify these PAH sources.

PAHs are often encountered in the sewer system and accumulate in sewage sludge. During their stay the PAHs are subdued to alteration processes, which change their distribution pattern and characteristic PAH ratios. We have been interested in changes of PAH fingerprints due to microbial biodegradation.

7 potential PAH sources (motor oil, diesel fuel, hard coal, coal tar, creosote, bitumen and heater soot) have been selected for biodegradation experiments. They were incubated at 28°C for 0, 6, 12 and 18 weeks. The inoculum used was a broad mixture of well adapted bacteria, extracted from a coal tar contaminated soil in Homécourt, France. The CO₂ evolution was monitored to follow the degradation process.

Samples were freeze dried, solvent extracted (pressurized solvent extraction or liquid-liquid extraction) and fractionated into compound classes: aliphatics, aromatics and polar compounds. All fractions were quantified by GC-MS.

All individual PAH as well as alkylated derivatives have been quantified to establish a detailed PAH distribution. Other associated compounds (aliphatics, NSO-compounds) complete the analysis.

The results show that PAH distribution changes during microbial biodegradation. Especially low molecular compounds are easily degradable, e.g. naphthalene, which disappears completely. Other compounds appear or their concentration increases during the experiment. They are formed or released from the matrix during microbial attack.

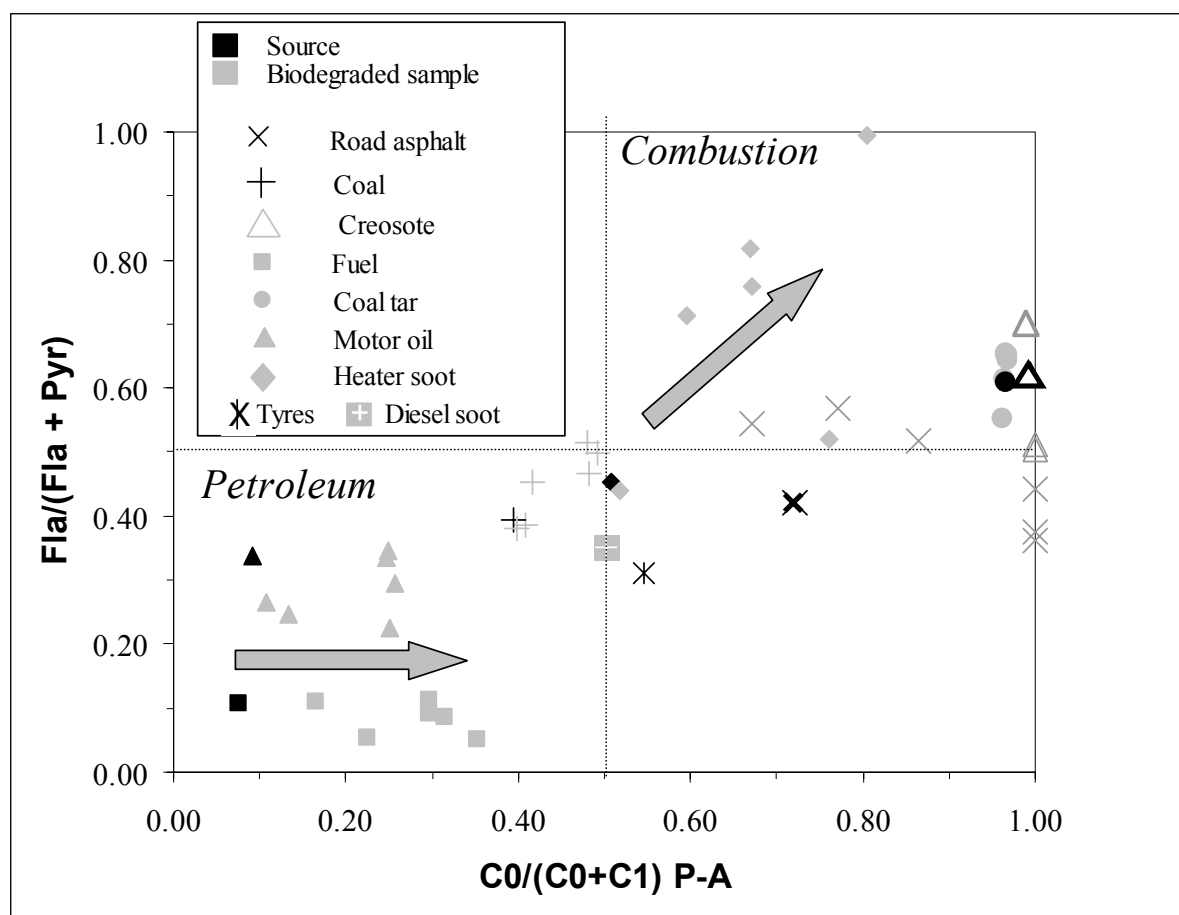


Fig.1. Evolution of PAH ratios (after Yunker et al. 2002¹) during microbial biodegradation

The degree of degradation of the potential PAH sources is mainly dependant on the global molecular composition. A high concentration of easily degradable aliphatic hydrocarbons increases CO₂ evolution (fuel, motor oil), but PAH composition changes most if PAH concentrations are high and aliphatic/aromatic ratios are low as for heater soot samples. As can be seen in figure 1 even isomeric ratios are not constant, but change during biodegradation and evolve towards the combustion area. These results questioned the validity of the PAH ratios for source apportionment in highly degraded samples such as sewage sludges.

References

¹Yunker et al. (2002): Organic chemistry, **33**, 489-515.

PEB2-14: Source apportionment of PAH in sewage sludge

A. Regier, L. Mansuy-Huault, P. Faure, E. Jardé

G2R UMR 7566, UHP Nancy, BP 239, 54506 Vandoeuvre-lès-Nancy
(e-mail: laurence.mansuy-huault@g2r.uhp-nancy.fr)

Polycyclic aromatic hydrocarbons (PAH) are persistent organic pollutants frequently encountered in the environment. Although the major path of introduction of these chemicals into the environment is the incomplete combustion of organic matter, PAHs have other sources, like fossil fuels or certain chemical products. They are often encountered in sewer systems and accumulate in the sewage sludge. According to their sources they can be introduced directly into the sewer or as surface runoff.

Since 1998 limiting values exist for 3 PAHs (fluoranthene, benzo[b]fluoranthene, benzo[a]pyrene) in sewage sludge for France. Sludge exceeding these limits cannot be applied to soils, but have to be subdued to further treatment or deposited in disposal sites. Even sludge from some small rural sewage treatment plants (STP) without obvious polluter, often exceed these limits. It is therefore a major interest of the operators of sewage treatment plants to know the sources of these PAHs.

In co-operation with the local water agency (Agence de l'eau Rhin-Meuse) a study of suitable STPs in Lorraine (France) has been launched to investigate PAHs' origin. Their input is traced back from the sludge via the sewer to a potential source.

In the sewer system preferentially the solid deposits are sampled to obtain a cumulative sample representative for a longer time window, not a "snapshot".

Samples are freeze dried, extracted by pressurized solvent extraction and fractionated into compound classes: aliphatics, aromatics and polar compounds. All fractions are quantified by GC-MS.

For PAH source apportionment it is necessary to quantify more than the major PAHs contained in most environmental legislation, but all PAHs as well as alkylated derivatives and other associated compounds (aliphatics, NSO-compounds). Individual compound concentrations, molecular patterns and molecular ratios of sludge and sewer are compared.

Figure 1 shows a cross plot of two molecular ratios for the sludge and waste water samples. Most samples are mainly influenced by pyrolytic sources, e.g. road run off. An exception are the samples from the industrially influenced STP in Aingeray, especially the associated waste water samples. The increased concentrations of PAH in small sewage

treatment plants is probably not due to a special source but the normal road run off and an insufficient cleaning performance.

This study also showed the importance of the characterization of the aliphatic fraction which allows to point out more precisely the type of pollution introduced in the sewer: motor oil, road asphalt, gasoline... Moreover, it appears that PAH source apportionment is more reliable when performed on a set of samples including waste waters collected in the sewer and sewage sludge. This allows to get moderately degraded samples with limited inputs when collected in sewer whereas sewage sludge is a mixture of numerous organic compounds with multiple sources sometimes highly biodegraded.

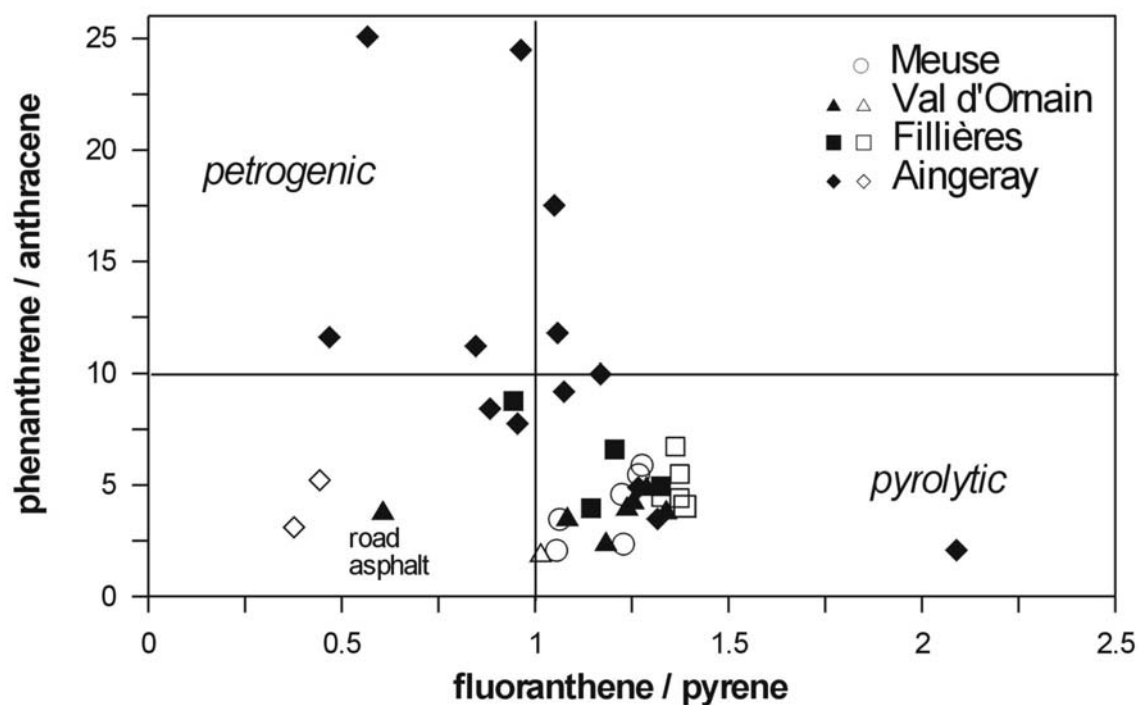


Fig.1. Source apportionment by PAH-ratio classification of sewage sludge (open symbols) and waste water (closed symbols) from four different sampling points (after Budzinski et al. 1997¹)

References

- [1] Budzinski et al. (1997): *Marine Chemistry*, **58**, 85-97.

PEB2-15: Organic composition of Seville aerosols

J. Reyes, B. Hermosin, C. Saiz-Jimenez

Instituto de Recursos Naturales y Agrobiología, CSIC, Apartado 1052, 41080 Sevilla, Spain
(e-mail: saiz@irnase.csic.es)

Residents and public officials in urban areas around the world are concerned about traffic congestion and air pollution. Traffic congestion and air pollution are exemplified in the city of Seville with a historic centre formed by very narrow streets. One of the streets conducting to the very centre of the city is Constitution Avenue, which is delimited in one of the sides by the cathedral. For more than five decades, exhaust emissions from gasoline- and diesel-powered vehicles contributed to the deterioration of the cathedral of Seville. The years 60-80 were particularly harmful for the cathedral, since the trams were substituted by diesel buses. Until the mid-90s the belt of narrow streets surrounding the cathedral was fully active, routing all the traffic of the city centre as well as serving the surrounding areas, with continuous traffic congestion. In addition, the squares facing the eastern and southeastern façades were used as parking lots. Today, the traffic has been partially restricted, but only under the northern, southern and eastern façades, while intense traffic continues on Constitution Avenue where the main façade and the Birth, Assumption and Baptism portals, with sculptures from the 15th and 19th centuries, are located. It is on this narrow street where the greatest concentrations of gases and aerosols are reached as it routed all downtown traffic. The particular situation of the western façade permits to investigate the impact of air pollution on the cathedral and with this aim an aerosol monitoring was carried out. This paper focuses on organic characterization of the sampled aerosols. A study on the chemical composition of aerosols sampled at different periods of the year under distinct traffic regimes is presented. The aerosol composition was compared with previously studied black crusts from the cathedral.

PEB2-16: Limited bioaccessibility of polycyclic aromatic hydrocarbons leading to background soil pollution

R. Posada-Baquero, J.J. Ortega-Calvo

Instituto de Recursos Naturales y Agrobiología, CSIC, Sevilla, Spain (e-mail: jjortega@irnase.csic.es)

Far from behaving as passive catalysts, microorganisms inhabiting polluted soils and sediments can solve a range of low-bioavailability situations by improving their modes of pollutant acquisition. However, there are a number of environmental situations, for example involving compounds aged in soils for long periods, or chemicals strongly sorbed to black carbon in sediments and soils, where the physical constraints for biodegradation are hardly modifiable by physiological means, leading to pollutant fractions that remain not bioaccessible. Recently, we have examined the accessibility to degrading microorganisms of native PAHs present in soils exhibiting different levels of pollution, i.e., from background levels ($\mu\text{g}/\text{kg}$), originated by atmospheric deposition, to acute concentrations (g/kg) corresponding to industrial spills. We developed an accelerated biodegradation assay, consisting in the incubation of the samples in aqueous suspensions with a sufficient number of PAH-degrading microorganisms (*Mycobacterium* sp. VM552). The addition of ^{14}C -labelled PAH to the samples, that were equilibrated during two days before adding the microorganisms, allowed the measurement of mineralization as a physiological indicator of biodegradation. In some experiences, we used solid-phase conditions and did not inoculate, relying on the activity of the autochthonous microbial populations to degrade the pollutants. During the whole experiments or after mineralization reached the plateau, the residual concentrations of the native compounds were determined by extraction and HPLC analysis in replicate samples that contained no ^{14}C and that had been maintained under the same conditions. In this way, we could identify situations involving different degrees of bioaccessibility: from heavily polluted soils containing highly bioaccessible (>95 %) compounds, to soils previously treated with bioremediation or containing background levels of pollution, showing a reduced bioaccessible fraction (< 30 %). An example of the results obtained with this assay is shown in figure 1. The soils studied were collected from the surroundings of an industrialized site in Southern Spain (Campo de Gibraltar, Cádiz). These five soils differed in their phenanthrene content (13-110 $\mu\text{g}/\text{kg}$) and organic matter (1.7-10.0%). The biodegradation assay showed that, after 100 days, the native phenanthrene remained highly persistent in all cases, in spite of being detected a significant percentage of

mineralization (30-40 %) of the labelled compound. The compound bioaccessibility was not related to the content in organic matter of the soils.

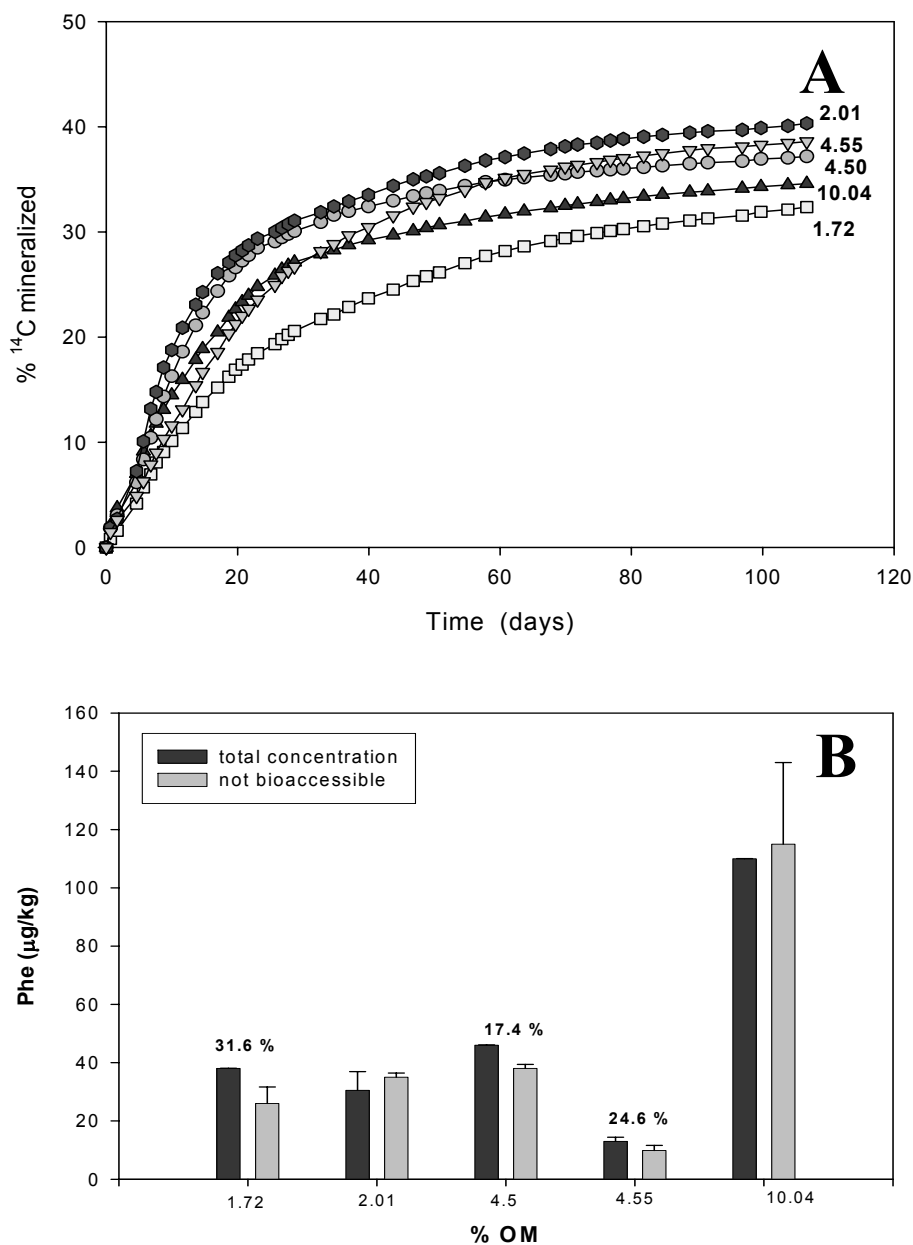


Fig.1. Bioaccessibility of native phenanthrene to the autochthonous microbial population in soils from Gibraltar area (Southern Spain). A, Mineralization of ^{14}C -phenanthrene added at a concentration of $11.8 \mu\text{g}/\text{kg}$. B, initial and final concentrations of native phenanthrene. Numbers in A and B indicate, respectively, the content in organic matter of the soils, and the percentage, when applicable, of reduction of the native compound after biodegradation.

PEB2-17: Aryl isoprenoids in oil fluid and underground waters from Minusinsk depression

Y.P. Turov¹, M.Y. Gooznjaeva¹, B.D. Vasiljev²

1) Ugra State University, 16 Chekhov Str., Khanty-Mansiysk, 628012 Russia (e-mail: yuri_tom@rambler.ru)

2) Tomsk Politechnical University, 30 Lenin Ave., Tomsk, 634050 Russia

Aromatic hydrocarbons in organic geochemistry have mainly been used as indicators of organic sources in ancient sediments and petroleum.

Alkylbenzenes in the range C₁₃-C₂₂ were investigated in oil fluid and *Solzavodskaja* petroleum of Minusinsk Depression as well in dissolved organic matter (DOM) of underground waters from this area.

The oil fluid was sampled in natural oil seepage on the Sohochul area (Khakasia, South Siberia, Russia). The organic matter composition of *Solzavodskaja* petroleum, oil fluid from seepage and CHCl₃-extractable DOM in water samples were investigated by column chromatography, TLC and GC/MS.

This study examines the geochemistry of alkylbenzenes in selected oil and oil fluid and their corresponding source rock. Sokhochul oil seepage is located in Lower Devonian within the conjunction zone of tectonic structures of the southern edge of North-Minusinsk Depression. The oil seepage is confined to the zone of layer-by-layer tectonic crush with slickensides in massive basalts. Oil occurrences in basalts are rather unique ones.

The most alkylbenzenes in oil fluid are presented by the 2-alkyl-1,3,4-trimethyl substitution pattern with a predominance of C₁₃-C₂₂ homologues series (Fig. 1). Alkyl chain has an isoprenoid structure and thus providing a potential link with carotenoid precursors. The principal compounds possess the 2-alkyl-1,3,4-trimethyl substitution pattern characteristic of diaromatic carotenoids precursors found in photosynthetic sulfur bacteria of the family *Chlorobiaceae*.

Tetra-alkylbenzenes series of unusual substitution pattern (aryl isoprenoids) is also presented in *Solzavodskaja* petroleum from South-Minusinsk Depression as well in dissolved organic matter of underground waters from these areas. Identification and the wide distribution of aryl isoprenoids from these areas (in oil fluid from seepage, in *Solzavodskaja* petroleum and in DOM of underground waters) show a similar origin of organic matter on the researched territory.

Previous studies reported that aryl isoprenoids in the range C₁₃-C₃₁ were identified in source rock bitumen and oils from several Paleozoic-age petroleum system, in Silurian oils and in Ordovician source rock.

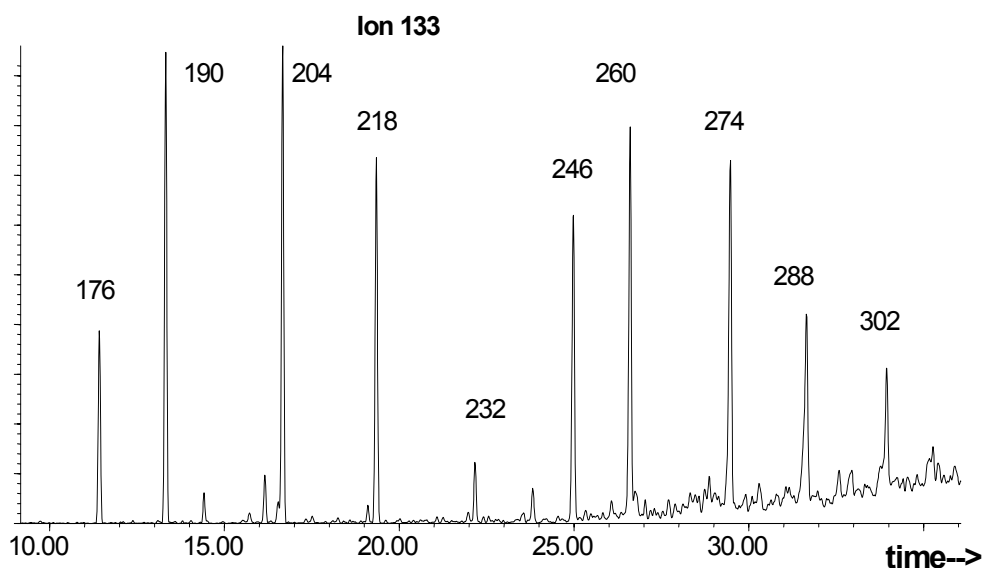


Fig.1. Mass chromatogram of m/z 133 depicting distribution alkylbenzenes in aromatic fraction from oil fluid. 176, 190, 204, ... - molecular mass of corresponding aryl isoprenoid

Several publications suggested that the occurrence of 2-alkyl-1,3,4-trimethyl benzenes are not associated exclusively with elevated salinity depositional regimes, but also with “normal” marine carbonate-rich environment containing intervals of condensed clastic or mixed clastic/carbonate sedimentation. Therefore, it has been proposed that the association of aryl isoprenoids with Paleozoic-age source rocks is more a function of depositional environment than of the specific ages of the source rocks.

Our results (the predominance of aryl isoprenoids in the tectonic crush basalts) don't agree with the previously published conclusions that an unusual abundance of alkylbenzenes (aryl isoprenoids) is exclusively a function of depositional environment.

PEB2-18: Transformation of oil composition under natural factors

Y.P. Turov, M.Y. Gooznjaeva

Ugra State University, 16 Chekhov Street, Khanty-Mansiysk, 628012 Russia (e-mail: yuri_tom@rambler.ru)

Oil composition change studies in the environment are essential both for forecasting of oil spill consequences and for comprehension of the nature of oil systems, as such. The distribution and spreading as well as dissipation processes of oil and others organic pollutants in natural waters, soils and other environmental constituents in some territories of the south-east of West Siberia were studied. The distribution among components of the environment, the change of concentration and molecular weight distribution (MWD) of paraffins, alkylbenzenes, polycyclic aromatic hydrocarbons and oxidized compounds in the dissipation processes were investigated.

The identification and quantification of oil spills, weathering and biodegradation products in the spilled areas of West Siberia were determined. The analyses of crude oil, degraded samples, natural water, soil, bottom sediments and peat samples were carried out by gravimetry, column chromatography, spectroscopy and GC/MS techniques.

The qualitative and quantitative changes of oil composition were investigated and compared during the laboratory biodegradation experiment and in field oil spills under natural factors. In model experiments the compounds, considered relatively recalcitrant to the effect of microorganisms, were found as the most degradable (resins and asphaltenes). Moreover, in some experiments we observed no detectable changes in n-alkane profile, while losses of total mass of crude oil sample reached about 60 %.

The relative amounts of the saturate, aromatic and residue fractions in the control sample from the column chromatography separation were 51.7, 10.4, 37.9 %, and after biodegradation 51.4, 15.1 and 33.5 %, respectively.

The biodegradability of the saturated fraction was lower than that of residual fraction which was presented by high molecular and low solubility compounds (resins and asphaltenes). Biodegradability of aromatic fraction was the lowest. Pr/n-C₁₇, Ph/n-C₁₈, and Pr/Ph ratios were not correlated to total crude oil mass losses.

In general, microbial attack on petroleum was shown to occur towards *n*- and branched alkanes or light aromatic compounds. High molecular aromatics, resins and asphaltenes exhibit very low rates of biodegradation. Nevertheless, some studies reported a significant alteration and extensive biodegradation of more resistant hydrocarbons prior to detectable

changes in *n*-alkane profile of the crude oil tested. Also extensive losses of resins (52 %) and asphaltenes (74 %) were observed during the biodegradation of all crude oil fractions [1].

We studied the hydrocarbon composition of original (oil fluid) and weathered OM (bitumen) samples which allow us to characterize the organic matter transformation processes under natural conditions.

The oil fluid and oil bitumen were sampled in natural oil seepage on the Sohochul area (Khakasia, South Siberia, Russia). The oil bitumen was derivated as result of oil fluid weathering in the point of its outcropping. All distinctions of oil fluid and oil bitumen composition exclusively caused by modern natural processes, occur without effect of high temperature and other extreme factors - high pressures, essential changes of composition of gas environment *etc.*

It is known, that aerobic biodegradation is the main contribution to weathering (oxidation) processes of oil hydrocarbons in soil layers. Isomeric and homologous composition of alkyl benzenes in bitumen is significantly varied as compared with that in oil fluid. The contents of *n*-paraffins are increased as a result of natural processes of oil system transformation. The absolute contents of alkyl benzenes are also increased, and their isomeric composition becomes more numerous.

These facts are inconsistent with the conventional submissions about relative stability and biodegradability of different parts of oil systems and, probably, testify about availability of non-conventional mechanism of formation at least the parts of oil paraffins and alkyl benzenes. The results of our work indicate that oil is subjected to degradation as an entire (whole) complex system both in environment and in model laboratory experiments.

Thus, from our investigation (although the obtained data are limited), it appears that biodegradation of petroleum as a whole is a "quasi-stepwise" process too, in which "more resistant" compound classes can be attacked prior to complete destruction of a "less resistant" class.

References

[1] Leahy, J.G., Colwell, R.R., 1990. Microbial degradations of hydrocarbons in the environment. *Microbiological Reviews* 54, 305-315.

PEB2-19: Selecting aerobic bacteria from petroleum formation water of special biodegradation characteristics

S.P. Vasconcellos¹, V.M. Oliveira², K.C.M. Simioni², E.V. Santos Neto³, A.J. Marsaioli¹

1) Chemistry Institute, State University of Campinas (UNICAMP), PO 6154, D-13084-971 Campinas, Brazil (e-mail: anita@iqm.unicamp.br)

2) Center of Chemical, Biological and Agr. Researches (CPQBA) – UNICAMP, D-13081-970 Paulínia, Brazil

3) Petrobras – CENPES, D-21949-900 Rio de Janeiro, Brazil

The aerobic and anaerobic microbiota present at the interface of petroleum and formation water in reservoirs are responsible for the petroleum biodegradation. However full understanding of these processes is hard to achieve and there are several unanswered questions like the origin of alkyl sterane and norhopanes. What microorganisms are the responsible for these reactions? Are they aerobic or anaerobic? Can we visualize microorganisms that selectively degrade the asphaltenes instead of the “good biomarkers “? Our goal is to search for such microorganisms.

In order to select and characterize the microbiota preference for petroleum biomarkers ,we are investigating the aerobic and anaerobic microbiota present in formation water and crude oil samples from Campos Basin, Brazil. We are now reporting the biotransformation preference of an isolated bacterial strain from formation water. This microorganism biodegradation ability was tested using pure compounds representing the main classes of biomarkers present in petroleum and it was demonstrated that this microbial culture had the preference for hydrocarbons, while the anaerobic consortium seemed to prefer the oxygenated biomarkers. Microscopic analysis of the aerobic microbiota demonstrated the presence of Gram-negative and Gram-positive rods, as well as Gram-positive coccus in the consortium. Identification based on 16S rDNA sequencing and phylogenetic analysis revealed the presence of bacteria belonging to the genera *Bacillus*, *Micrococcus*, *Microbacterium* and *Pseudomonas*. *Micrococcus* spp. was first evaluate because its abundant growth when cultivated as pure culture.

Thus *Micrococcus* spp biodegrading abilities were evaluated over a mixture of compounds (dihydrophenantrene, phytol, phytane, nonadecanoic acid and cholestane), in Zinder medium¹, at 28° C, 150 rpm, during 20 days. GC-MS monitoring using pentadecane (0,01 mg/mL) as an internal quantification standard (IQS) revealed a good degradation of the cholestane (Fig. 1) and of pentacyclic compounds. This preference was unexpected because pentacyclic and sterane are generally accepted as biodegradation resistant.

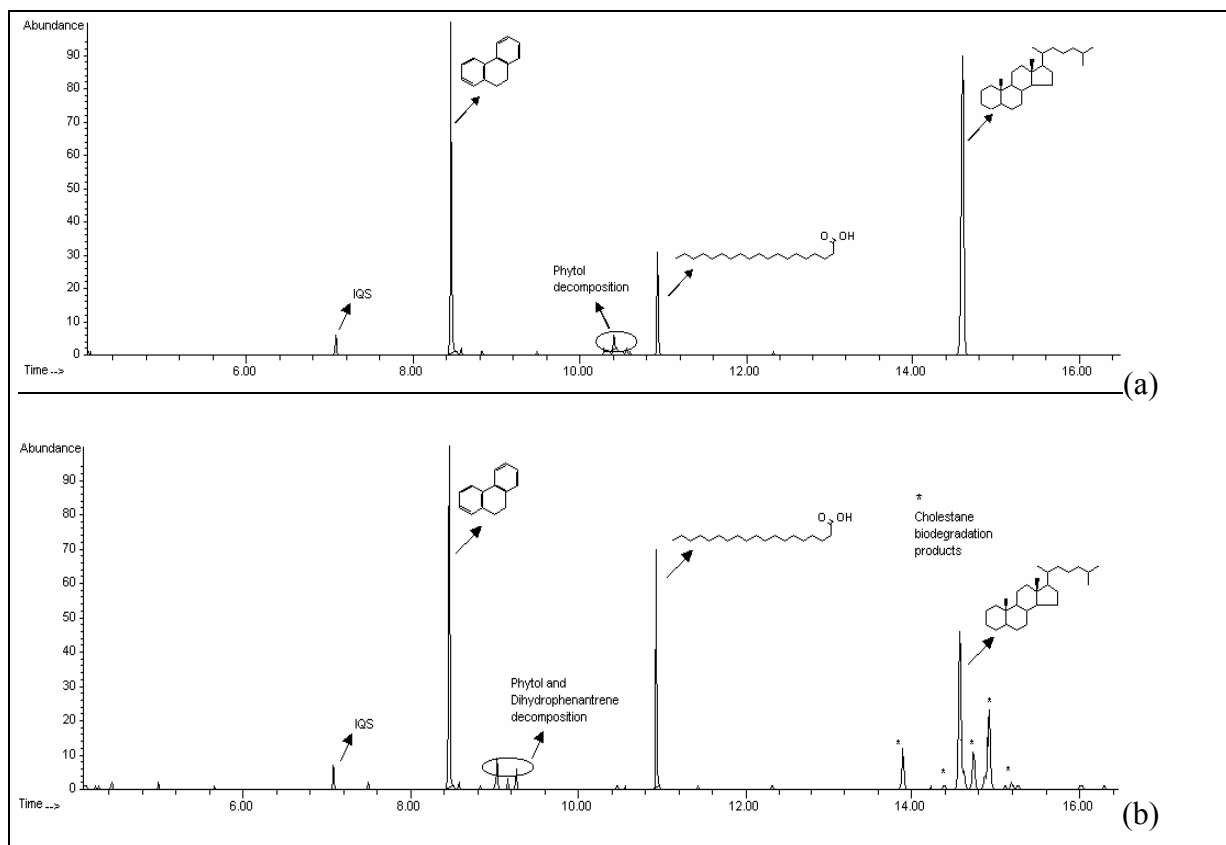


Fig.1. (a) Total ion chromatogram of mixture of compounds (initial time). (b) Total ion chromatogram of mixture of compounds after cholestane biodegradation (15 days)

We are now isolating the biodegradation products in order to fully characterize the obtained products. However these results clearly indicate the potential of these aerobic bacteria to petroleum biotechnology.

References

- ¹Zinder, S.H., Cardwell, S.C., Anguish, T., Lee, M., Koch, M., Applied Environmental Microbiology, 47, 1984, 796-807.
- ²Fang, J., Lovanh, N., Alvarez, P.J.J., Water Research, 38, 2004, 2529-2536.

PEB2-20: Drilling wastes management: case study in Southern Tunisia

H. Mejri, M. Saidi

Centre de Recherches et de Développement Pétroliers, Entreprise Tunisienne d'Activités Pétrolières, 27 Bis, Avenue Kheirddine Pacha, Bélvédère, 1002, Tunis, Tunisie (e-mail : houcine.mejri@etap.com.tn)

Hydrocarbon exploration/production activities generate, as well as the most industries, effluents that may contain traces of hydrocarbons and or chemical products. These products have to be eliminated according to some international regulations in order to safe environment.

This paper presents the results of the geochemical study (using pyrolysis and liquid and gas chromatography techniques) undertaken on drilling wastes (21 samples) from Sabria oil field in southern Tunisia. The main purposes are to evaluate quantitatively and qualitatively the hydrocarbon pollution within the wastes and to determine a most safety method (chemical extraction, thermal desorption) to eliminate or to reduce the pollutants.

The interpretation of the results was made through certain statistics (correlation between measured parameters, variations of hydrocarbon concentrations against depth and calculation of decontamination rates).

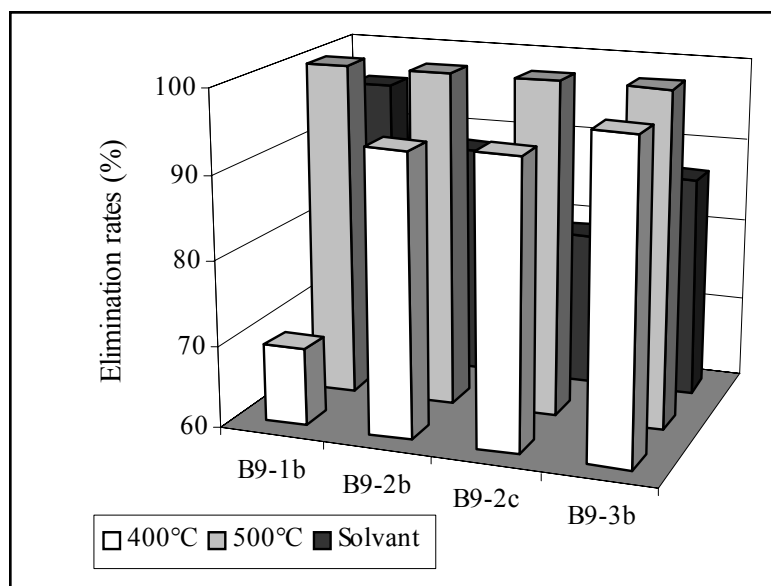
Obtained results (Table.1) show that almost all the samples are rich in hydrocarbons as indicated by the high values of total hydrocarbon compounds (TPH), high TOC and free (S₁) and “potential “ (S₂) hydrocarbons. These “potential “(S₂) hydrocarbons correspond to heavy hydrocarbon products as indicated by the shale of S₂ peak as well as by the low Tmax values (around 390 °C).

In order to remedy to this pollution phenomena, laboratory tests have been conducted for technique improvements. These tests show that thermal desorption at 500°C (Figure.1) can be considered as an economic and efficient technique (efficiency > 99.9% for all the studied samples).

Table.1: TOC and Rock Eval results

Reference	Depth (cm)	S1 (ppm)	S2 (ppm)	TPH (ppm)	TOC (%)
B9-1a	25	10710	17680	17300	2.40
B9-1b	40	22020	51950	63560	6.23
B9-1c	50	12940	25350	21130	3.22
B9-2a	25	24380	55760	38690	6.78
B9-2b	40	29480	134610	64390	13.87
B9-2c	50	31010	67350	46471	8.26
B9-3a	25	20310	21590	33220	3.53
B9-3b	40	48860	33760	77860	12.64
B9-3c	50	32960	70520	47180	10.07
B10-1a	60	520	630	1100	0.25
B10-1b	80	680	580	950	0.25
B10-1c	100	480	480	730	0.18
B10-2a	60	3670	3080	5740	0.62
B10-2b	80	830	950	1250	0.16
B10-2c	100	490	750	760	0.13
B10-3a	60	2530	1980	4740	0.47
B10-3b	80	2740	2720	4330	0.43
B10-3c	100	2470	2510	4090	0.39
B10-4a	60	4050	3560	6480	0.83
B10-4b	80	3500	2360	5440	0.49
B10-4c	100	1040	1370	2110	0.21

S₁, S₂: Rock Eval parameters, **TPH**: Total Petroleum Hydrocarbons, **TOC**: Total Organic Carbon

**Fig.1.** TOC Elimination rates

**PB1-1: Tricyclic terpenoids from Paleozoic tasmanites:
A question of evolution, site or taxa?**

S. Dutta¹, P.F. Greenwood², R. Brocke³, C. Hartkopf-Fröder⁴,
R.G. Schaefer¹, H. Wilkes⁵, U. Mann¹

1) Forschungszentrum Jülich, Institut Sedimentäre Systeme, D-52425 Jülich, Germany

(e-mail: s.dutta@fz-juelich.de)

2) Curtin University of Technology, Perth, GPO Box 1987, WA 6845, Australia

3) Forschungsinstitut Senckenberg, Paläobotanik, D-60325 Frankfurt, Germany

4) Geologischer Dienst Nordrhein-Westfalen, D-47803 Krefeld, Germany

5) GeoForschungsZentrum Potsdam, D-14473 Potsdam, Telegrafenberg, Germany

Tasmanites (green algae) are generally believed to be a biological source of tricyclic terpenoids ([1], [2]). However, extremely well preserved *Tasmanites* which have been recovered from sedimentary rocks of the Fetlika-1 borehole, SE Turkey [3], and which have suffered low-temperature conditions only [4], do not show any tricyclic terpenoids in pyrolysates. Thus, the *Tasmanites* association to tricyclic compounds, which has been previously queried ([5], [6]), might be a question of evolution, site or taxa.

In order to avoid any misinterpretations due to migrated soluble organic matter or compositional mixing by signals from other microfossils, for our study we have exclusively used handpicked palynomorphs, which have taxonomically been well assigned. Palynomorphs were separated from the sediments by using HF and HCl and water filtration. Organic residues were cleaned several times with dichloromethane to remove free hydrocarbons. Samples were pre-enriched mechanically by sieving, classified palynologically, photographed, handpicked and then subjected to Curie point pyrolysis-gas chromatography-mass spectrometry (Curie temperature = 650°C), some also to temperature programmed pyrolysis-gas chromatography (temperature range = 300-600°C).

The pyrolysates from both *Tasmanites* (thick-walled prasinophyte) and *Leiosphaeridia* (thin-walled prasinophyte) from SE Turkey are dominated by a series of *n*-C₆₋₂₂ alkene/alkane doublets which are typical of pyrolysis products of algaenan, the microbiological resistant algal biopolymer [7]. Aromatic hydrocarbons such as alkylbenzenes, alkyl-naphthalenes and alkylphenanthrenes occur in minor concentration.

No traces of tricyclic terpenoids have been detected from the pyrolysates of *Tasmanites* from SE-Turkey, but interestingly, the pyrolysates of *Leiosphaeridia* from the same stratigraphic horizon do show the presence of monounsaturated and diunsaturated tricyclic terpenes as well as monoaromatic tricyclic terpanes [8]. Thus, it is concluded that an inherent relationship between *Tasmanites* and tricyclic terpenoids may not always exist and that these biomarkers also have other source(s) (i.e., *Leiosphaeridia*) – as suggested by [5]

who pointed out that the occurrence of tricyclic terpenoids is not limited to areas of high *Tasmanites* content. The corresponding analysis of the *Tasmanites* from Tasmania (Australia) where we see a normal tricyclic terpenoid product distribution confirms the integrity of present chemical analysis.

The molecular compositions of the pyrolysates of prasinophytes from SE Turkey and Tasmania are compared to the corresponding data of predominantly Silurian to Devonian aged prasinophytes sourced from other locations e.g. the Rheinisches Schiefergebirge, Famennian, Germany; the Chattanooga Shale, Upper Devonian, Virginia, USA and the Arbuckle Mts., Upper Devonian, Oklahoma, USA.

References

- [1] Greenwood, P.F., Aroui, K.R., George, S.C., 2000. Tricyclic terpenoid composition of *Tasmanites* kerogen as determined by pyrolysis GC-MS. *Geochimica et Cosmochimica Acta* 64, 1249-1263.
- [2] Simoneit, B.R.T., McCaffrey, M.A., Schoell, M., 2005. Tasmanian tasmanite: II – compound specific isotope analyses of kerogen oxidation and Raney Ni reduction products. *Organic Geochemistry* 36, 399-404.
- [3] Brocke, R., Bozdogan, N., Mann, U., Wilde, V. (2004) Palynology of the Silurian/Devonian boundary interval at the northern margin of the Arabian Plate (Hazro area, SE Turkey). *Polen* 14, 164-165.
- [4] Kranendonck, O., 2004. Geo- and biodynamic evolution during Late Silurian to Early Devonian time (Hazro Area, SE Turkey). *Schriften des Forschungszentrum Jülich, Reihe Umwelt/Environment* 49, pp. 268.
- [5] Revill, A.T., Volkman, J.K., O'Leary, T., Summons, R.E., Boreham, C.J., Banks, M.R., Denwar, K., 1994. Hydrocarbon biomarkers, thermal maturity and depositional setting of tasmanite oil shales from Tasmania, Australia. *Geochimica et Cosmochimica Acta* 58, 3803-3822.
- [6] Talyzina, N.M., Moldowan, J.M., Johannisson, A., Fago, F.J., 2000. Affinities of Early Cambrian acritarchs studied by using microscopy, fluorescence flow cytometry and biomarkers. *Review of Paleobotany and Palynology* 108, 37-53.
- [7] Hatcher, P.G., Clifford, D.J., 1997. The organic geochemistry of coal: from plant materials to coal. *Organic Geochemistry* 27, 251-274.
- [8] Dutta, S., Greenwood, P.F., Brocke, R., Schaefer, R.G., Mann, U., (submitted). New Insights on the Relation between *Tasmanites* and Tricyclic Terpenoids. *Organic Geochemistry* 00, 000-000.

PB1-2: Estimating the number of endospores by determination of dipicolinic acid in sediments from the backbarrier tidal flat of Spiekeroog island

J. Fichtel¹, J. Köster¹, J. Rullkötter¹, H. Sass²

1) Institute of Chemistry and Biology of the Marine Environment (ICBM), Carl von Ossietzky University of Oldenburg, P.O. Box 2503, D-26111 Oldenburg, Germany (e-mail: joerg.fichtel@icbm.de)

2) School of Earth, Ocean and Planetary Sciences, Cardiff University, Cardiff, CF10 3YE, Wales, U.K.

In the last years it turned out that living organisms are present in sediment layers down to 800 m below the sea floor [1] and even deeper in subterrestrial granitic rocks [2]. The biosphere within these subsurface layers was estimated to harbour a quarter to a third of the global biomass [3]. However, very little is known about the metabolic state, the community composition and adaptation of these microorganisms. A main problem for the understanding of this so called “deep biosphere” is the fact that by epifluorescence microscopy, which is normally used for quantification of microorganisms, metabolically active and inactive cells cannot be distinguished. A special case of the latter are endospores which are formed by bacteria of the phylum *Firmicutes*. Endospores reveal no active metabolism but are viable and can survive for more than 25 million years [4]. It is therefore probable that their relative abundance within the microbial community increases with sediment burial. Up to now, the numbers of endospores can only be estimated by culture-dependent methods, and it is very likely that these methods highly underestimate the actual numbers *in situ*. Nevertheless, even by culture-based methods the presence of some 10^5 endospores per cm^3 sediment was proven.

The aim of this work was to develop an analytical method for the detection and quantification of bacterial spores in sediments. Therefore, a protocol for quantification of dipicolinic acid (DPA, pyridine-2,6-dicarboxylic acid) was developed. DPA is a universal and specific component of bacterial endospores [5] and was hence suggested to be a suitable biomarker for estimating the number of endospores in soils and sediments. A first approach involved quantification of the DPA content of cultivated spores of different species. For extraction of DPA from the spore protoplast the samples were suspended in a buffer solution and autoclaved. The released DPA was quantified by fluorimetric detection of its chelates with terbium. DPA contents of 10^{-16} to 10^{-15} mol were determined, showing a positive correlation with spore volume.

For determination of DPA in sediments only the fluorimetric method was suitable because of its high sensitivity, but quenching effects and other fluorescing organic matter components required further purification steps. Via extraction with ethylacetate DPA was enriched and could be determined in sediment samples from a backbarrier tidal flat of

Spiekeroog island. Fig. 1 shows the emission spectra of sediment samples from 40 cm depth. For quantification of the released DPA some of the samples were spiked with DPA standard solutions. By this method a DPA concentration was measured that related to an endospore number of $5 \cdot 10^6 \text{ g}^{-1}$ sediment (approximately 0.5% of the total cell count).

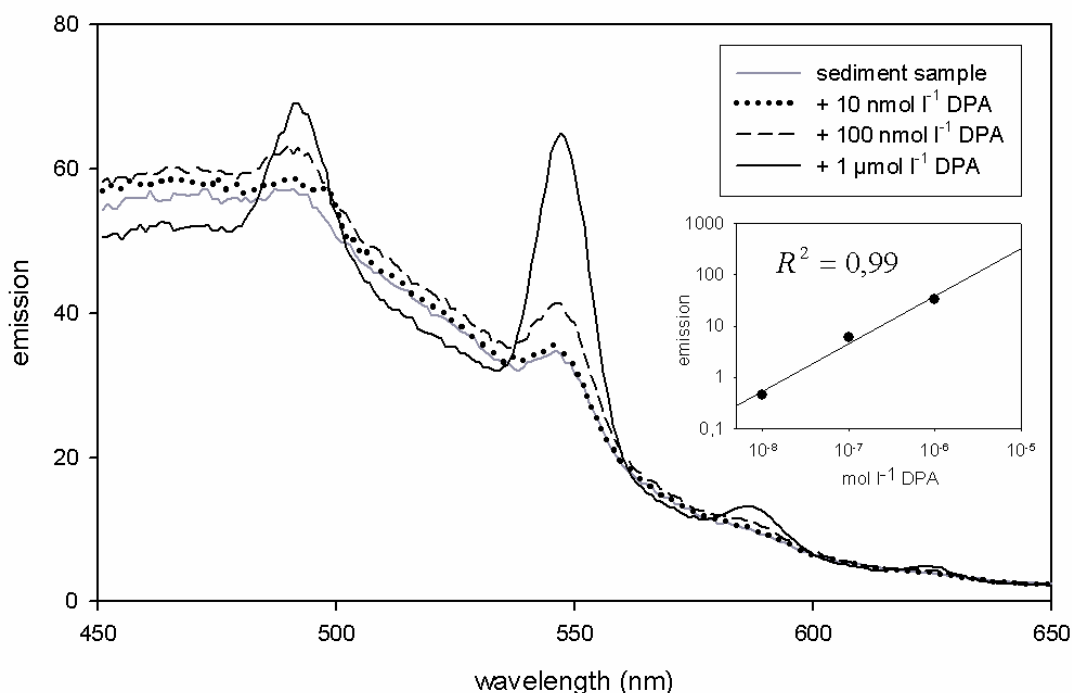


Fig.1. Emission spectra of extracts from autoclaved sediment samples after addition of terbium chloride. Three of the sediment samples were spiked with DPA standard solution.

References

- [1] Parkes, R.J., Cragg, B.A., Wellsbury, P., 2000. Recent studies on bacterial populations and processes in subseafloor sediments: A review. *Hydrogeology Journal* 8, 11-28.
- [2] Szewzyk, U., Szewzyk, R., Stenstrom, T., 1994. Thermophilic, anaerobic bacteria isolated from a deep borehole in granite in Sweden. *Proceedings of the National Academy of Science USA* 91, 1810-1813.
- [3] Whitman W.B., Coleman D.C. and Wiebe, W.J., 1998. Prokaryotes: The unseen majority. *Proceedings of the National Academy of Science USA* 95, 6578-6583.
- [4] Cano, R.J., Borucki, M.K., 1995. Revival and identification of bacterial spores in 25- to 40-million-year-old Dominican amber. *Science* 268, 1060-1064.
- [5] Powell, J.F., 1953. Isolation of dipicolinic acid (pyridine-2,6-dicarboxylic acid) from spores of *Bacillus megatherium*. *Biochemical Journal* 54, 210-211.

**PB1-3: Organic matter composition of two discrete thin layers
from the Eocene Messel oil shale (Germany)**

S. Gerisch^{1,3}, U. Mann¹, N. Micklich², R.G. Schaefer¹, Norbert Volkmann³

1) Forschungszentrum Jülich, Institut Sedimentäre Systeme, D-52425 Jülich, Germany
(e-mail: u.mann@fz-juelich.de)

2) Hessisches LandesMuseum Darmstadt, D-64283 Darmstadt, Germany

3) Technische Universität Bergakademie Freiberg, Institut für Geologie, D-09596 Freiberg, Germany

The Messel Pit fossil site near Darmstadt, Germany, is famous because of its numerous well-preserved mammal and other fossils, and therefore, in 1995 became a UNESCO-World Heritage (www.unesco-welterbe.de/en/). The respective host rock, the Messel oil shale [1], a dark, finely laminated organic rich mudstone, was deposited in a Maar lake about 47Ma ago (lower Middle Eocene). One subunit, the “Middle Messel Fm.“ can be subdivided by several specifically named marker beds (M, α , β and γ), but also by further characteristic layers. Two of them represent green-brown deposits with a maximum thickness of up to one millimetre only. They are encountered at a level of 35cm (L-A) and 100cm (L-B) below Marker Bed α . Typically, both layers are extremely ductile, and thus can easily be manually separated like individual paper-like book-sheets from their adjacent host rock. Because of their leather-like plasticity, they must be considered to be rich in organic material. Accordingly, it was the objective of this study to reveal the type of organic matter (OM) they consist of.

Our approach tested the lateral variation of OM of L-A and L-B by comparison of the molecular compositions exhibited by the analytical results of temperature programmed pyrolysis-gas chromatography and thermovaporisation-gas chromatography which need small sample amounts only. In addition, the molecular compositions of the C₁₅₊-soluble OM of the layers were compared to their adjacent host rocks.

All bulk parameters (TOC, S, HI) confirm higher contents and a better quality of OM for both layers, with stronger enrichments for layer L-B. L-B exhibits a surprising high sulphur content of 7%, which can not be explained so far. In respect to the molecular compositions, influences by migrated OM can be excluded due to a maturity stage below 0.5%Rr (mean T_{max} below 430°C and a strong predominance of the odd- to-even-numbered *n*-alkanes). Lipid compositions with predominance of the C₂₃ to C₃₁- region pointing to high proportions of terrestrial plant material are in contrast to HI values above 620mg HC/g TOC. Thus, high bacterial/microbial contributions have to be assumed which is confirmed by individual biomarker data. Both layers and the host rock have incorporated similar amounts of

bacterial/microbial OM. In contrast, layers L-A and L-B exhibit similar enrichments of algal and terrestrial plant organic matter compared to their host rock. Individual results of bulk parameters and for individual biomarker groups being typical for predominantly terrestrial, algal and bacterial/microbial OM are summarized in Table 1.

In respect to the deposition of layers L-A and L-B, we conclude that both do not include any other kind of specific OM in comparison to their host rocks. However, identical enrichments of both algal and terrestrial OM may be explained by increased bioproductivity, but much more probable seems a nearly to zero diminished sedimentary input. Accordingly, for the time of deposition of layers L-A and L-B, we favour a short period of a relative arid climate, with extremely small amounts of rain fall and therefore, more or less no erosion.

Table 1. Summary of organic geochemical bulk parameters and biomarkers of Marker Beds A and B of the Messel oil shale in comparison to their adjacent host rocks (*data by [2])

	Above	L-A	Below	Above	L-B	Below						
<div style="border: 1px solid black; padding: 5px; display: inline-block;"> +++ main component (+) traces ++ existent - insignificant + minor existent </div>												
Bulk Parameters												
TOC [%]	35	38	25	32	48	34						
S [%]	1.1	1.0	0.9	1.1	7.2	0.8						
HI [mg HC/g TOC]	535*	622	535*	535*	789	535*						
dominant <i>n</i> -alkanes	27,29,31	27,29,31	27,29,31	23,25,27	23,25,27	23,25,27						
Typical of Predominantly Terrestrial OM												
20S-diacholestene	(+)	+	-	-	+	-						
20R-diacholestene	(+)	+	-	-	+++	-						
20S-24-ethylidiacholestene	-	+	-	-	+	-						
20R-24-ethylidiacholestene	-	+	-	-	+	-						
20R-24-ethylidiacholestene	(+)	++	-	-	+++	-						
des-A-lupane	(+)	+	+	(+)	++	(+)						
Typical of Terrestrial and Algal OM												
20S-4-methylidiaster-13(17)-ene	-	++	-	-	++	-						
20R-4-methylidiaster-13(17)-ene	(+)	+++	-	-	+++	-						
20S-4,24-dimethylidiaster-13(17)-ene	-	+	-	-	+	-						
20S-4-methyl-24-ethylidiaster-13(17)-ene	-	++	-	-	+	-						
20R-4,24-dimethylidiaster-13(17)-ene	-	++	-	-	+++	-						
20R-4-methyl-24-ethylidiaster-13(17)-ene	-	+++	-	-	+++	-						
Typical of Predominantly Bacterial/Microbial OM												
des-A-arbor-9(11)-ene	+	+	+	+	+	+						
17β(H)-22,29,30-trinorhopane	-	-	(+)	-	-	-						
hop-17(21)-ene	+	(+)	(+)	+	-	+						
17β-norhopane	++	++	++	++	++	++						
17β-hopane	(+)	(+)	(+)	(+)	(+)	(+)						
17β-homohopane	++	++	++	++	++	++						

References

- [1] Franzen, J.L. and Michaelis, W., 1988. *Eocene Lake Messel*. Cour. Forsch. – Inst. Senckenberg, 107: 1-452
 [2] Hagedorn-Götz, I., 1983. Organisch-geochemische und organisch-petrographische Untersuchungen an Bohrproben des Messeler Ölschiefers. Diploma thesis, RWTH Aachen, 81 pages.

PB1-4: D/H of water, lipids and carbohydrates from modern plants grown under controlled conditions (temperature, light intensity, CO₂ concentration and water availability)

K. Grice¹, Y. Zhou², H. Stuart-Williams², S. Chin Wong², S. Schouten³, S.X. Wang¹, G. D Farquhar²

1) Stable isotope and biogeochemistry Group, Centre for Applied Organic Geochemistry, Curtin University of Technology, GPO Box U1987, Perth, 6845, Western Australia, Australia (e-mail: K.Grice@curtin.edu.au)

2) Environmental Biology Group, Research School of Biological Sciences, Australian National University, Canberra, ACT, 2601, Australia.

3) Department of Marine Biogeochemistry and Toxicology. Royal Netherlands Institute for Sea Research (NIOZ), PO Box 59, 1790 AB Den Burg, Texel, The Netherlands.

D/H of individual organic compounds shows great potential for the reconstruction of D/H of palaeoenvironmental water and climatic variation (e.g. [1], [2]). D/H and ¹⁸O/¹⁶O in precipitation are strongly influenced by changes in the environment making isotopic proxies of past precipitation valuable in palaeoclimatic reconstruction. For plants, water is the prime source of hydrogen; thus D/H of biomarkers in sediments derived from higher plants carries valuable information on past precipitation and changes in the isotopic composition of water within the global water cycle.

The stable hydrogen isotopic composition of a plant is determined by the isotopic composition of the source water, evapotranspiration effects and biochemical fractionations in biosynthesis (e.g.[3], [4], [5]). In a preliminary study ([6]) the stable hydrogen isotope composition of individual lipids, as well as bulk stable hydrogen isotopes of total biomass, total lipids and total residue (after lipid extraction) from 16 different terrestrial C₃ and C₄ plants grown under controlled conditions were investigated. δD and δ¹⁸O of (1) leaf water and soil water isolated cryogenically from each plant type (2) water vapour in the greenhouse and (3) irrigation water were measured. δD versus δ¹⁸O of the leaf water show a strong enrichment in D and ¹⁸O compared to irrigation H₂O due to evapotranspiration effects that result in the relatively greater loss of H₂¹⁶O (Figure 1). C₄ plants show a greater leaf water enrichment compared to C₃ plants related to differences in stomatal conductance. All plants show a greater variation in both δD and δ¹⁸O, attributed to differences in leaf morphology pending further work (Figure 1). The leaf water enrichment is also reflected in δD of individual leaf wax lipids. In addition the effects of temperature, humidity, light level, light quality, CO₂ concentration and water availability are under investigation.

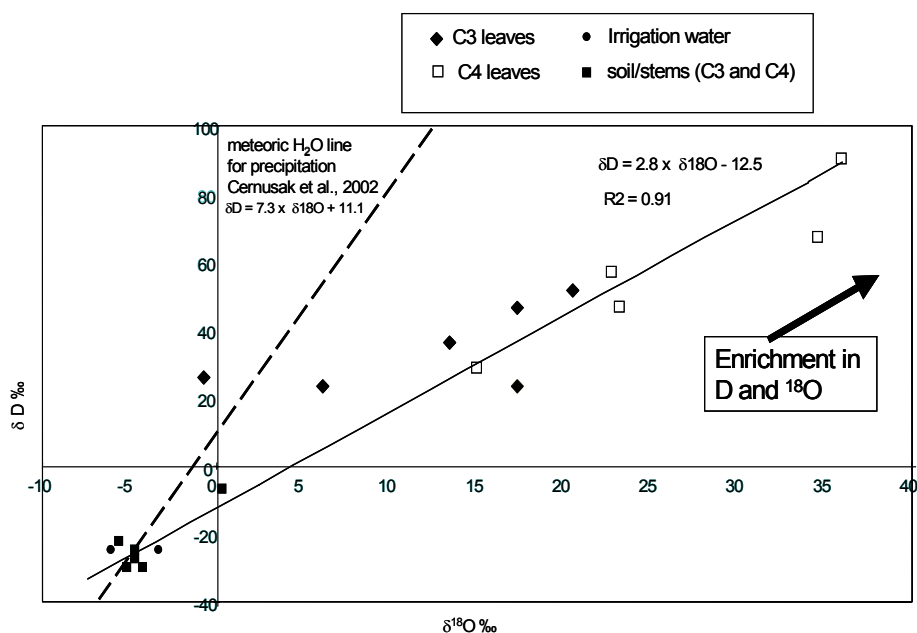


Figure 1 δD versus $\delta^{18}O$ (VSMOW) of H₂O in leaves, stems, soil and source

References

- [1] Dawson, D., Grice, K., Wang, S., Alexander, R., and Radke, J., (2003) *Organic Geochemistry* **35**, 189-197.
- [2] Sauer, P.E., Eglinton, T.I., Hayes, J.M., Schimmelmann, A., and Sessions, A.L., (2001) *Geochimica et Cosmochimica Acta* **65**, 213-222.
- [3] Dongmann, G., Nurnber, H.W., Forstel, H., and Wagner, K., (1974) *Radiation and Environmental Biophysics* **11**, 41-52.
- [4] Farquhar, G.D., and Gan K.S., (2003) *Plant, Cell and Environment* **26**, 1579-1597/
- [5] Gan, K.S., Wong, S.C., Yong, J.W.H., and Farquhar, G.D. (2003) *Plant, Cell and Environment* **26**, 1479-1495.
- [6] Grice, K., Schouten, S., Wong, S.C., Stuart-Williams, H., Farquhar, G.D. 2003. Compound specific D/H isotopes of lipids and carbohydrates from extant plants grown under controlled conditions. 21st International Meeting on Organic Geochemistry, Kraków. Book of Abstracts, Part I, 47-48.

PB1-5: Biomarker distributions and their stable isotopes in marine Permian/Triassic sections from around the globe

K. Grice¹, R. Twitchett², R.E. Summons³, C.B. Foster⁴, C.J. Barber¹, D. Dawson¹,
R. Alexander¹, P. Greenwood¹

- 1) Curtin University of Technology, Perth, Australia
- 2) Plymouth University, Plymouth, United Kingdom
- 3) Massachusetts Institute of Technology, Cambridge MA, USA
- 4) Geoscience Australia, Canberra, Australia

In many parts of the world marine and terrestrial life experienced the most severe ecological crisis in the Phanerozoic between the Permian (P) and Triassic (Tr) periods. Evidence for and the consequences of this catastrophic event can often be extracted from the analysis of sediments at the P-Tr boundary. The mechanisms leading to the mass extinction are still an ongoing matter of debate. Development of global anoxia, overturn of stagnant deep ocean waters and the melting of gas hydrates are the mechanisms that are continually invoked. More recently it has been suggested that sulfide toxicity in the oceans may have been an important driver of the extinction and may have also been a major factor in the protracted recovery (Grice et al., 2005a; Summons et al., these proceedings).

A compound specific isotope approach using biomarkers associated with the event from P-Tr sections from around the globe (Western Australia, Eastern Greenland and Kashmir-Tibet) is in progress. A unique biomarker - a C₃₃ alkylcyclohexane - that first appears within the extinction interval of the end-Permian ecological crisis is reported in a key high northern palaeolatitude P-Tr section from East Greenland (Grice et al., 2005b). This section preserves a complete, well-documented and very expanded P-Tr sequence of over 40 m and contains the Early Triassic, globally recognized index fossil *Hindeodus parvus*. Prior to this study, the C₃₃ alkylcyclohexane compound had only been reported from Early Triassic organic-rich marine rocks and oils from the northern Perth Basin, Western Australia. The organism from which this compound is derived appears to be associated with a unique marine ecosystem that bloomed during and after the extinction.

In addition an attempt to substantiate the notion of synchronous disturbance in oceanic and atmospheric conditions that occur at the P-Tr boundary will be presented using $\delta^{13}\text{C}/\delta\text{D}$ of biomarkers, $\delta^{13}\text{C}$ of carbonates and $\delta^{13}\text{C}/\delta\text{D}$ of kerogen. Certainly, gradual changes in $\delta^{13}\text{C}$ of dissolved inorganic carbon in the marine realm appeared to have occurred perhaps over several million years before the end of the Permian. It appears in many cases (but not all) that isotopic trends are not just simple records of changes in $\delta^{13}\text{C}$ of carbon reservoirs, since some trends are consistent with a palynofacies change from charcoal-wood to algal-amorphous

dominated organic matter, respectively (Foster et al., 1997). In contrast, $\delta^{13}\text{C}$ values of the molecular fossils such as pristane and phytane can represent robust proxies for the isotopic composition of phytoplanktonic organic matter inputs, and/or an increase in stratification towards the Triassic causing enhanced recycling of ^{13}C -depleted CO_2 . $\text{C}_{14}\text{-C}_{18}$ *n*-alkyl carbon chains have multiple inputs, comprising phytoplankton and heterotrophs. If derived from phytoplankton, the isoprenoids are depleted in ^{13}C compared to the co-occurring isoprenoids by *ca.* 1.5 ‰ (Hayes et al., 1993; Schouten et al., 1998). This pattern is observed in the Triassic for several P-Tr sections (e.g. Grice et al., 2005a). There is also independent evidence such as the abundance and $\delta^{13}\text{C}$ of porphyrins, the abundance and $\delta^{13}\text{C}$ of selected polycyclic aromatic hydrocarbons, for high algal productivity in the Triassic. $\delta^{13}\text{C}$ values of higher plant and phytoplankton biomarkers, and carbonates in the P-Tr section from Eastern Greenland show similar isotopic changes across the P-Tr transition indicating a global disruption to the carbon cycle. This data provides further evidence for a switch in the mode (or extent) of organic carbon remineralisation at the P-Tr transition.

References

- Foster, C.B., Logan, G.A., Logan, Summons, R.E., Gortler, J.D., and Edwards, D.S. (1997) *Journal of the Australian Petroleum Exploration Association*, **37**, 442-459.
- Grice, K., Cao, C., Love, G.D., Böttcher M.E., Twitchett R.J., Grosjean E., Summons, R.E., Turgeon, S.C., Dunning, W. and Jin, Y., (2005a) . *Science* 307, 706-709 (2005a).
- Grice, K., Twitchett, R.J., Alexander, R., Foster, C.B., and Looy, C., (2005b) *Earth and Planetary Science Letters*, in review.
- Hayes, J.M., (1993) *Marine Geology* **113**, 111-125.
- Schouten, S., Klein Breteler, W.C.M., Blokker, P., Schogt, N., Rijpstra, W.I.C., Grice, K., Baas M., and Sinninghe Damsté, J.S., (1998) *Geochimica et Cosmochimica Acta* **62**, 1397-1406.

PB1-6: Utilization of lipid markers to delineate sources of organic matter in recent core sediments from Victoria Harbour, Hong KongM. Hsieh¹, R.P. Philp¹, W.W.-S. Yim²

1) School of Geology & Geophysics, University of Oklahoma, Norman, OK 73019, USA

2) Department of Earth Sciences, The University of Hong Kong, Hong Kong SAR, China

Lipid markers are widely utilized for studying the origin and fate of sedimentary organic matter. A lipid marker approach has been used in this study to ascertain the sources of organic matter deposited in a 4m sediment core section from Victoria Harbour, Hong Kong. Various classes of lipids (*e.g.* free-, ester-bound, and amide-/ether-bound lipids) have been characterized to reconstruct past environmental conditions, assess impacts of anthropogenic activities, and to study remnants of bacteria responsible for reworking and degrading originally deposited organic material. Elemental and bulk stable isotope compositions of carbon and nitrogen in sedimentary organic matter have also been utilized to discriminate and quantify proportions of algal and terrigenous plant material, evaluate records of microbial activity, and to monitor raw sewage contributions (Gearing *et al.*, 1991; Meyers, 1994; Rogers, 2003). Compound specific carbon isotopes have also been used to differentiate more specific sources of lipid markers recorded in marine sediments.

Victoria Harbour is located within the southeast prodelta region of the Pearl River system (Fyfe *et al.*, 1999), and has undergone many changes over time (*e.g.* coastal reclamation, large-scale sewage discharge, resuspension and redistribution of sediments due to typhoons). The 4m sediment core section provides a historic record of organic matter deposited within two sedimentary units represented in Victoria Harbour – Holocene marine sediments and pre-Holocene marine sediments of the last-interglacial. Terrestrial sediments of the last glacial unit are absent in this core section (Yim *et al.*, 2002).

Free-, ester-bound, and amide-/ether-bound lipids have been extracted from sediment intervals within the 4m sediment core section and analyzed by gas chromatography, gas chromatography-mass spectrometry, and gas chromatography-isotope ratio mass spectrometry. Free lipid extracts are dominated by n-alkanoic acids ranging between C_{12:0} to C_{34:0}, with distinct even-over-odd predominance patterns. Short chain n-alkanoic acids (<C_{20:0}) are more abundant than long chain n-alkanoic acids (>C_{20:0}) in the upper 2.3m of the core section indicating a higher input from marine sources. At depths greater than 2.3m, an increase in abundance of long chain n-alkanoic acids suggests greater input of terrigenous plant material. n-Alkanols were detected in low abundance with carbon number distributions between C₁₄ and C₃₂, with even-over-odd predominance patterns. Long chain n-alkanols (C₂₂-

C₃₂) are more abundant than short chain n-alkanols (C₁₄-C₂₀) suggesting that terrigenous plant material are more important sources of n-alkanols. Sterols and stanols were also identified in the free lipid fraction, where stanols appear more abundant than their corresponding sterols. This reflects reducing conditions, where sterols are most likely hydrogenated to stanols. The occurrence of coprostanol in the upper 2m of the core reflects periods of high discharge of raw sewage.

Ester-bound and amide-/ether-bound lipids appear to primarily reflect remains of anaerobic and sulphate-reducing bacteria. Lipids in these fractions are comprised of n-alkanoic acids, branched alkanoic acids, β -hydroxy acids, and branched β -hydroxy acids. β -Hydroxy acids in the ester-bound and amide-/ether-bound lipid fractions are directly derived from cell membranes of bacteria. More detailed characterization of composition and distribution of bound lipids, and application of compound-specific carbon isotopes will enable us to evaluate changes in bacterial communities over time, and speculate on processes that have occurred with organic matter deposited in Victoria Harbour.

References

- Fyfe, J. A., Selby, I. C., Plater, A. J., Wright, M. R., 1999. Erosion and sedimentation associated with the last sea level rise offshore Hong Kong, South China Sea. *Quaternary International*, 55, 93-100.
- Gearing, P. J., Gearing, J. N., Maughan, J. T., Ovlatt, C. A., 1991. Isotopic distribution of carbon from sewage sludge and eutrophication in the sediments and food web of estuarine ecosystems. *Environmental Science and Technology*, 25, 295-301.
- Meyers, P. A., 1994. Preservation of elemental and isotopic source identification of sedimentary organic matter. *Chemical Geology*, 114, 289-302.
- Rogers, K. M., 2003. Stable carbon and nitrogen isotope signatures indicate recovery of marine biota from sewage pollution at Moa Point, New Zealand. *Marine Pollution Bulletin*, 46, 821-827.
- Yim, W. W. -S., Chan, L. S., Hsieh, M., Philp, R. P., Ridley Thomas, W. N., 2002. Carbon Flux during the last interglacial cycle in the inner continental shelf of the South China Sea off Hong Kong. *Global and Planetary Change*, 33, 29-45.

PB1-7: The sedimentary fate of ladderane lipids, characteristic membrane lipids of bacteria performing anaerobic ammonium oxidation

A. Jaeschke, S. Schouten, E.C. Hopmans, J.S. Sinninghe Damsté

Royal Netherlands Institute for Sea Research, Dep. Marine Biogeochemistry & Toxicology, 1790 AB Den Burg, Texel, The Netherlands (e-mail: jaeschke@nioz.nl)

As the availability of the nutrients Nitrogen (N) and Phosphorus (P) limits the production of phytoplankton in the ocean surface water, the marine nitrogen cycle has consequently a strong link with the marine carbon cycle. In contrast to P, fixed organic nitrogen is not only lost to the sediment but also to the atmosphere – in form of dinitrogen gas (N₂), which cannot be used directly by most phytoplankton. So far, denitrification was thought to be the only significant pathway for N₂ formation and, in turn, the main sink for nitrogen in the oceans. Denitrification occurs in anoxic environments where bacteria use nitrate or nitrite instead of oxygen as an oxidator for organic matter. Recently it has been shown that N is not only lost via denitrification but also via anaerobic ammonium oxidation (anammox) [1]. In this process ammonium and nitrite are directly combined to N₂. The microorganisms responsible for anammox were first discovered in a wastewater treatment system and belong to deeply branching members of the order Planctomycetales, one of the major, distinct divisions of the domain Bacteria [2]. These Bacteria have a specific compartment where the anammox reaction takes place, the so-called anammoxosome. It is surrounded by a dense and highly impermeable lipid membrane composed of chemotaxonomically unique lipids, so-called ladderane lipids [3], which is required to protect the cell from the toxic intermediates hydrazine and hydroxylamine as well as to maintain concentration gradients during the exceptionally slow metabolism of anammox bacteria [3]. The first direct evidence for activity of anammox bacteria in natural settings comes from the Black Sea, the world's largest anoxic basin [1]. Further evidence for anammox activity was also found in continental shelf sediments, estuarine systems as well as in arctic sea ice, and anammox was estimated to contribute up to 50 % to the global present day loss of N from the oceans [4]. This represents a large but presently unknown sink in the biogeochemical cycling of nitrogen in the ocean with also large consequences for the present marine carbon cycle. In the geological past, for example during Jurassic and Cretaceous oceanic anoxic events, anammox could have also made a large contribution to the loss of N from the oceans.

Ladderane lipids occur in a variety of different forms either ester or ether bound and contain up to five fused cyclobutane moieties which is unprecedented in nature. This makes them ideal biomarker to assess past anammox bacterial activity. However, so far, no fossil

remnants of ladderane lipids have been identified in marine sediments. This is likely due to the very strained conformation of the cyclobutane rings in the ladderane lipids, and their structures are probably modified by reactions during diagenesis. Additionally, very low concentrations as well as detection problems with normal GC-MS hampered their proper identification up to now. To investigate how ladderane lipids are transported from the water column to the sediment we are currently analyzing a set of sediment trap samples as well as surface sediments from different sites. To further assess the changes the lipids undergo during diagenesis and how these diagenetic products look like, we are performing thermal degradation experiments with anammox biomass. In this study we use a newly developed HPLC-MS method for the detection of specific ladderanes and their diagenetic products. These results will hopefully contribute to a better understanding of the functioning of the past oceanic nitrogen cycle.

References

- [1] Kuypers, M.M.M., Sliemers, A.O., Lavik, G., Schmid, M., Jørgensen, B.B., Kuenen, J.G., Sinninghe Damsté, J.S., Strous, M. and Jetten, M.S.M., 2003. Anaerobic ammonium oxidation by anammox bacteria in the Black Sea. *Nature*, 422, 608-611.
- [2] Strous, M., Fuerst, J.A., Kramer, E.H.M., Logemann, S., Muyzer, G., van de Pas-Schoonen, K.T., Webb, R., Kuenen, J.G. and Jetten, M.S.M., 1999. Missing lithotroph identified as new planctomycete. *Nature*, 400, 446-449.
- [3] Sinninghe Damsté, J.S., Strous, M., Rijpstra, W.I.C., Hopmans, E.C., Geenevasen, J.A.J., van Duin, A.C.T., van Niftrik, L.A. and Jetten, M.S.M., 2002. Linearly concatenated cyclobutane lipids form a dense bacterial membrane. *Nature*, 419, 708-712.
- [4] Devol, A.H., 2003. Solution to a marine mystery. *Nature*, 422, 575-576.

PB1-8: Phenyl derivatives of polyaromatic compounds and terphenyls as indicators of organic matter oxidation in the Intra-Mountain Podhale basin, PolandL. Marynowski¹, M.J. Rospondek², M. Góra²

1) Department of Earth Sciences, University of Silesia, 41-200 Sosnowie, Poland

(e-mail: marynows@wnoz.us.edu.pl)

2) Jagiellonian University, Kraków, Poland

Phenyl polyaromatic compounds (Ph-PAC) and polyphenyls distribution vary regularly with the increasing maturity showing their potential applicability for the assessment of organic matter maturity in the case of lack of other unambiguous maturity parameters [1]. This is the case in the Inner Carpathian Podhale Paleogene Flysch sedimentary rocks, where the vitrinite reflectance is misleading due to the presence of wide maturity spectrum of reworked vitrinite [2]. This work presents the preliminary results on distribution of phenyl derivatives of the polyaromatic compounds and polyphenyls in the sedimentary rocks from boreholes drilled in the Podhale Flysch, and its Mesozoic basement. The wells were drilled for the thermal water survey as an alternative source of energy for the towns in the Tatra National Park region. In the Inner Carpathian Podhale Paleogene Flysch sedimentary rocks the phenyl derivatives of polycyclic aromatic compounds (Ph-PAC) are important constituents in aromatic fractions of the organic matter extracts. The most common phenyl derivatives are phenylnaphthalenes, phenylphenanthrenes and terphenyls, which are sometimes accompanied by phenyldibenzothiophenes (Fig. 1) and phenyldibenzofurans. In all the samples analysed, except those from the shallowest depths, the phenyl derivatives are dominated by the thermally most stable isomers such as 2-phenylnaphthalene, 3-, 2-phenylphenanthrenes, *m*- and *p*-terphenyls (depth 3154 m - Fig. 1). In the Chochołów PIG-1 borehole, at the depth up to 2000 m, 1-phenylnaphthalene is present (depth 280 m, Fig. 1). This compound is replaced by 2-phenylnaphthalene below the depth of 2000 up to 2400 m, which corresponds to R_c ca. 0.7-0.8 %. In the all other wells, only thermally stable isomers of Ph-PAC and terphenyls are present. In the Mesozoic basement the presence of phenyldibenzothiophenes (PhDBT) is noteworthy. Perhaps this is a result of advanced diagenesis of more labile organic sulphur compounds originally produced in environments with operating bacterial sulphate reduction. These compounds are represented by all isomers, and dominated by most stable 2- and 3-PhDBT. The presence of all these aromatics reveal diagenetic oxidation of organic matter. It seems plausible to suggest that these compounds are generated due to hydrothermal water oxidative activity because the Ph-PAC amounts are relatively higher in the rocks serving as the water conduits. Interestingly, extremely high

concentrations of Ph-PAC are encountered in metal deposits like Kupferschiefer [1] formed due to oxidation of organic matter by migrating waters.

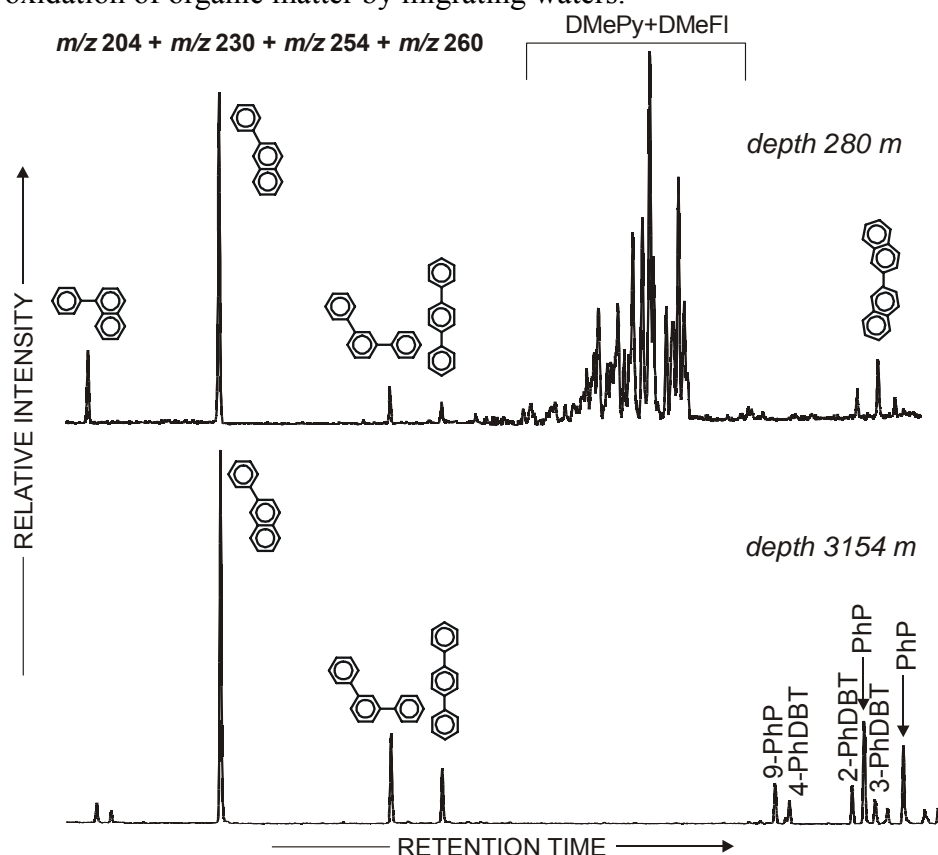


Fig.1. Partial mass chromatograms showing variation in distribution of phenylnaphthalenes (m/z 204), terphenyls (m/z 230), PhP – phenylphenanthrenes (m/z 254), PhDBT – phenyldibenzothiophenes (m/z 260) in the section of the Chochółów PIG-1 well with increasing depth (the other compound abbreviations: DMePy- dimethylpyrenes; DMeFl- dimethylfluorenes)

Ph-PAC isomer distribution pattern depends on the maturation, and to lower degree on the origin of sedimentary organic matter. The most regular variations are observed in the distribution of phenylnaphthalenes as exemplified the best by samples of the Chochółów PIG-1 borehole. Geographically, the maturation increases eastward in the basin, which observation agrees well with the results based on the measurements of diagenesis of clay minerals [2].

Acknowledgements

This study was partially supported by grant PB0354/P04/2003/25.

References

- [1] Marynowski, L., Rospondek, M., Mayer zu Reckendorf, R., Simoneit, B.R.T. 2002. Phenyldibenzofurans and phenyldibenzothiophenes in marine sedimentary rocks and hydrothermal petroleum. *Organic Geochemistry* **33**, 701-714.
- [2] Kotarba, M. 2004. Historia diagenety illitu/smektytu w skałach ilastych Karpat Zachodnich (przekrój Kraków-Zakopane), Ph.D. thesis, PAN Kraków.

PB1-9: Influence of oxic and anoxic depositional regimes on sedimentary lipid composition in Lake Bled (Slovenia)

G. Muri¹, S.G. Wakeham²

1) National Institute of Biology, Vecna pot 111, 1000 Ljubljana, Slovenia (e-mail: gregor.muri@nib.si)

2) Skidaway Institute of Oceanography, 10 Ocean Science Circle, Savannah, GA, 31411, USA

1. Introduction

Lipids comprise only a minor fraction of sedimentary organic matter. However, these molecular constituents can be used as reliable proxies for reconstructing the history of production, delivery, and preservation of organic matter in lakes [1].

2. Material and methods

A subalpine Lake Bled (46° 22' 30" N, 14° 07' 30" E) was selected as a study site, with co-occurring oxic and anoxic depositional environments and lipid compositions, i.e. aliphatic hydrocarbons, aliphatic alcohols, sterols and fatty acids were therefore analyzed in two sediment cores.

3. Results and discussion

Lipid concentrations were the highest at the surface sediments and decreased with depth. Nevertheless, total lipid concentrations in the anoxic sediment were almost one order of magnitude higher than in the oxic sediment (Figure 1). Composition of lipids also varied in the sediments. In the anoxic surface sediment layer, sterols and fatty acids predominated. In contrast, aliphatic hydrocarbons and aliphatic alcohols predominated in the oxic surface sediment layer. The latter two lipids were also more abundant in the deeper sections of both sediments, since aliphatic hydrocarbons and aliphatic alcohols are less susceptible to degradation. In addition, relative enrichment of longer chain vs. shorter chain lipids with depth was observed in the sediments. Shorter chain lipids were the most abundant in the anoxic surface sediment layer. These lipids are mostly of planktonic and bacterial origin [1]. In contrast, longer chain lipids of terrestrial origin were relatively enriched with depth, and thus prevailed in the deeper sediments. Since longer chain lipids are relatively more refractory than shorter chain homologues [2], the former also prevailed in the oxic surface sediment layer.

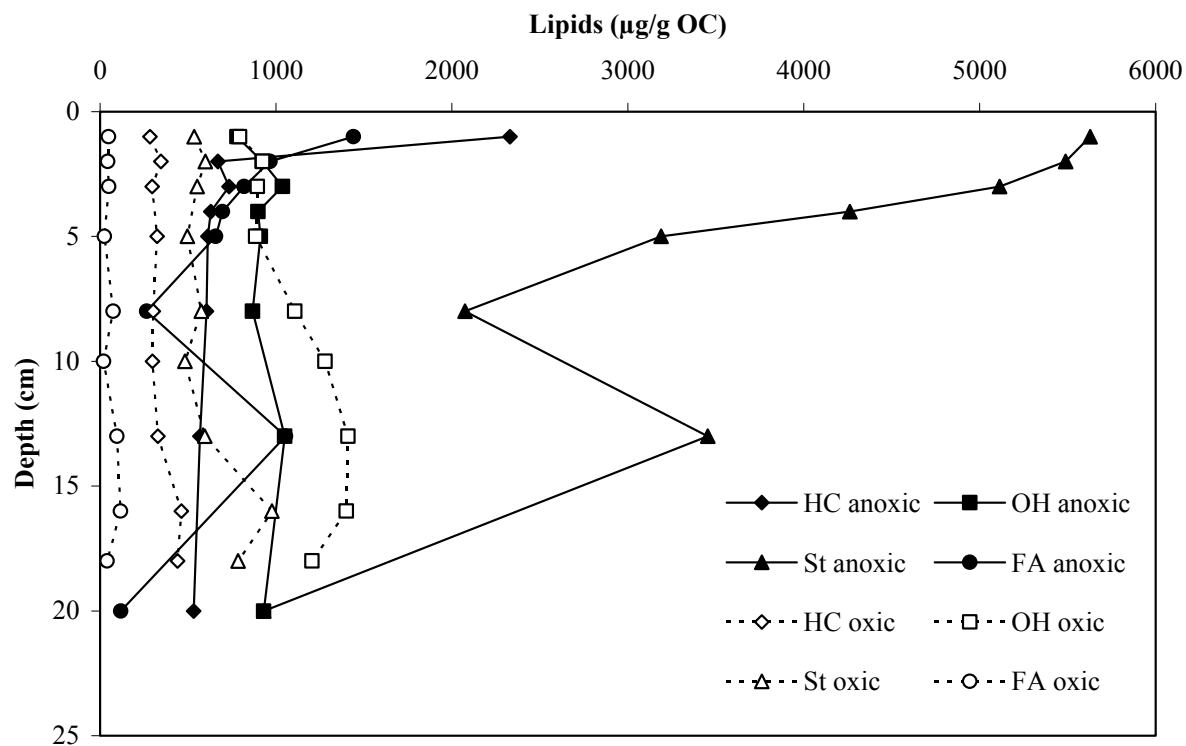


Fig.1. Depth profiles of the total aliphatic hydrocarbons (HC), aliphatic alcohols (OH), sterols (St) and fatty acids (FA) in anoxic and oxic sediments of Lake Bled

References

- [1] Meyers, P.A., 2003. Applications of organic geochemistry to paleolimnological reconstructions: a summary of examples from the Laurentian Great Lakes. *Organic Geochemistry* 34, 261-289.
- [2] McCaffrey, M.A., Farrington, J.W., Repeta, D.J., 1991. The organic geochemistry of Peru margin surface sediments: II. Paleoenvironmental implications of hydrocarbon and alcohol profiles. *Geochimica et Cosmochimica Acta* 55, 483-498.

PB1-10: The origin of 24-norcholestanes and their use as age-diagnostic biomarkers

S.W. Rampen¹, S. Schouten¹, B. Abbas¹, F.E. Panoto¹, G. Muyzer^{1,2}, C.N. Campbell³,
J. Fehling³, J.S. Sinninghe Damsté¹

1) Department of Marine Biogeochemistry and Toxicology, Royal Netherlands Institute for Sea Research (NIOZ), PO Box 59, 1790 AB Den Burg, Texel, The Netherlands (e-mail: rampen@nioz.nl);

2) Department of Biotechnology, Environmental Biotechnology Group, Delft University of Technology, Julianalaan 67, 2628 BC Delft, The Netherlands;

3) Scottish Association for Marine Science, Dunstaffnage Marine Laboratory, Dunbeg, OBAN, Argyll PA37, Scotland

24-Norcholestanes have been found in sediments and crude oils. Stepwise increases of the relative concentrations of this sterane in sediments and oils from the Jurassic, Cretaceous and the Oligocene/Miocene respectively, make these steranes useful age-diagnostic biomarkers (Holba et al., 1998). At present it is, however, not clear what the main biological source is for the 24-norcholestanes. There are some reports of trace amounts of C₂₆ sterols in cultures of dinoflagellates and red algae and 24-norsterols have been frequently found in a large variety of invertebrates. The identification of 24-norsterols and their derivatives in diatom blooms and diatomaceous sediments suggests that diatoms are an important source for nor-sterols. This is in line with their fossil record, which suggests a diatomaceous origin (Holba et al., 1998). However, so far these sterols have not been identified in diatoms from laboratory cultures.

We have analyzed the sterol composition of over 100 marine diatoms, covering the main groups of diatoms as indicated by their 18S rDNA phylogeny (Sinninghe Damsté et al., 2004). In one species of the planktonic centric diatoms, i.e., *Thalassiosira aff. antarctica*, the sterol 24-norcholesta-5,22-dien-3 β -ol comprised 10% of the total sterols. In contrast to previous tentative identifications, we unambiguously identified the carbon skeleton of this sterol by transforming it into a 24-norcholestane, using hydrogenation and HI/LiAlH₄ treatment and co-injection with an authentic standard. This also enabled us to unambiguously identify this sterol in a culture of the dinoflagellate *Gymnodinium simplex*, where it comprised 0.2% of the total sterols. These are the first unambiguous reports of 24-norcholesta-5,22-dien-3 β -ol in cultured algae and also the first report of a cultured alga, *Thalassiosira aff. antarctica*, that contains this sterol in such high concentrations.

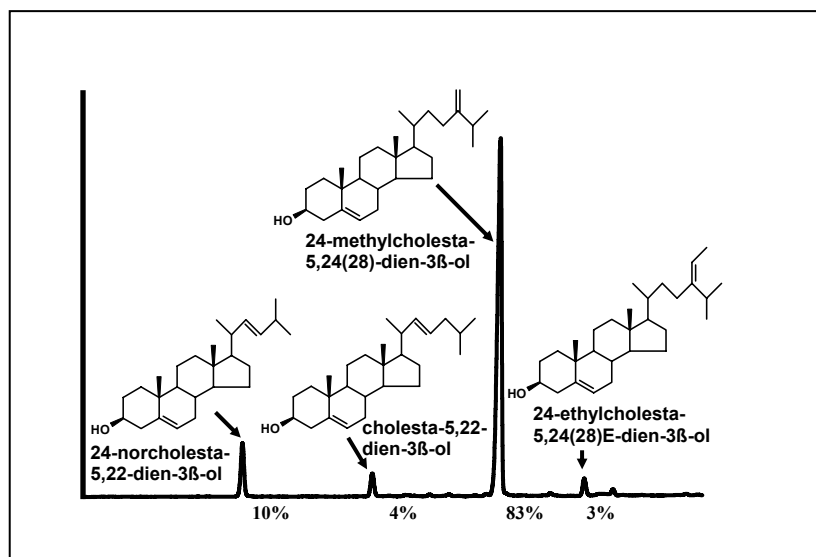


Fig.1. GC-chromatogram of the polar fraction of *Thalassiosira aff. antarctica* (CCAP 1085/9)

A possible function for the 24-norsterol is that this sterol is used as an adaptation to the environment (e.g. adaptation to different temperatures) in which the algae live. Therefore, 5 cultures of cold-water *Thalassiosira* species have been investigated, among them the culture *Thalassiosira antarctica borealis*. However, none of these cultures contained C₂₆ sterols. The question arises whether this means that *Thalassiosira aff. antarctica* is an exception in its ability to produce these 24-norsterols, or that the culture conditions for the other *Thalassiosira* species did not trigger the production of the unusual sterol.

Nevertheless, our results clearly show that there may be a relation between diatoms and the occurrence of 24-norcholestanes and this may provide a theoretical background for the application of 24-norcholestanes as an age diagnostic biomarker in petroleum geochemical studies. Based on this knowledge, the first increase of the 24-norcholestane ratio, in the Jurassic, might have a relation with expansion or origin of new species of dinoflagellates or red algae. The second increase, occurring in the Cretaceous, is likely associated with the origin of new diatom genera, e.g. the *Thalassiosira* genus. The third and last increase of the 24-norsterane ratio, during the Oligocene, could be related to the expansion of diatoms in this period.

References

- A.G. Holba *et al.*, *Org. Geochem.* **29**, 1269 (1998).
 J.S. Sinninghe Damsté *et al.*, *Science* **304**, 584 (2004).

PB1-11: Sources and seasonal production of long-chain diols and mid-chain hydroxy methyl alkanates

S.W. Rampen¹, S. Schouten¹, B. Abbas¹, K.R. Timmermans², G. Muyzer^{1,3}, S.G. Wakeham⁴, J.S. Sinninghe Damsté¹

1) Department of Marine Biogeochemistry and Toxicology, Royal Netherlands Institute for Sea Research (NIOZ), PO Box 59, 1790 AB Den Burg, Texel, The Netherlands (e-mail: rampen@nioz.nl)

2) Department of Marine Chemistry and Geology, Royal Netherlands Institute for Sea Research (NIOZ), PO Box 59, 1790 AB Den Burg, Texel, The Netherlands

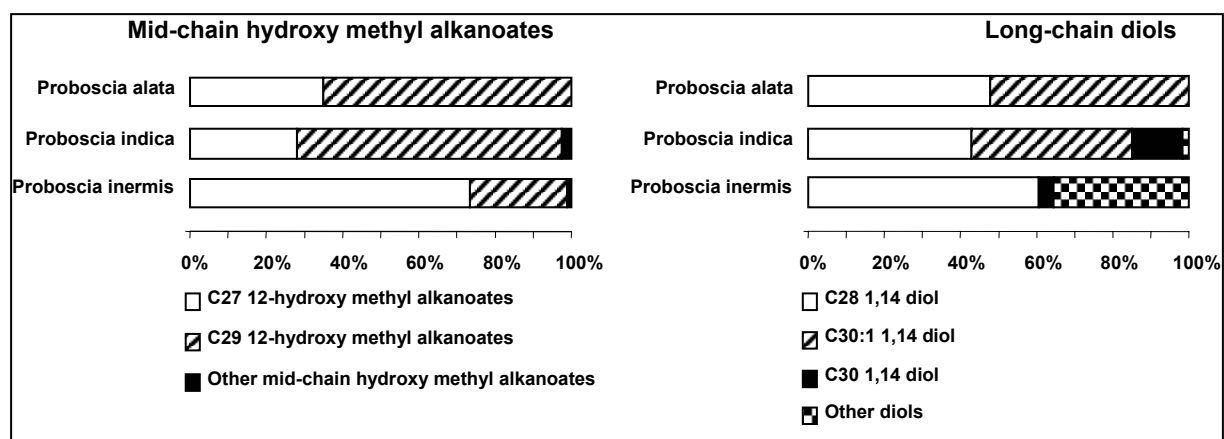
3) Department of Biotechnology, Environmental Biotechnology Group, Delft University of Technology, Julianalaan 67, 2628 BC Delft, The Netherlands

4) Skidaway Institute of Oceanography, 10 Ocean Science Circle, Savannah, GA 31411, U.S.A.

Long-chain diols and mid-chain hydroxy methyl alkanates occur widespread and abundant in marine particulate matter and sediments. Presently two sources are known for these compounds: Eustigmatophyceae algae, mainly of the genus *Nannochloropsis* (Gelin et al., 1999; Volkman et al., 1992; Volkman et al., 1999) and diatoms of the genus *Proboscia* (Sinninghe Damsté et al., 2003). Identification of these compounds and their derivatives in sediments and water columns provide information on their sources since *Proboscia* species mainly produce C₂₈ and C₃₀ 1,14 diols and C₂₇ and C₂₉ 12-hydroxy methyl alkanates (Sinninghe Damsté et al., 2003), whereas *Nannochloropsis* species mainly produce 1,13 and 1,15 diols containing 28-34 carbon atoms (Volkman et al., 1992; Volkman et al., 1999). Until now 16-,17- and 18-hydroxy methyl alkanates have only been found in *Nannochloropsis* (Gelin et al., 1997).

As *Proboscia* species often form a large part of the primary production during the start of the upwelling season in upwelling regions, their remnants may serve as biomarkers for high-nutrient conditions. Both culture experiments of different species and studies of sediments and water columns may reveal how we can use these specific lipids of *Proboscia* to reconstruct the palaeoenvironmental conditions.

We have analyzed cultures of different *Proboscia* species which showed different ratios between the various mid-chain hydroxyl methyl alkanates and the various long-chain diols (see figure). These differences do not seem to be a direct effect of temperature, as the relative distributions of compounds of *Proboscia indica* and *Proboscia alata* are very similar, while they were grown at resp. 18-22°C and 1-3°C, respectively. In contrast, *Proboscia inermis* has different distributions and contains additional long-chain diols, although this culture was grown at the same temperature as that of *Proboscia alata*. Future culture experiments may reveal what effect the nutrient conditions have on these distributions.



Wakeham et al. (2002) reported high concentrations of incompletely characterized C_{30} diols and their derivatives, C_{30} keto-ols, and C_{29} 12-hydroxy methyl alkanates, in sediment trap samples from the Arabian Sea. More detailed examination of these trap samples now show a shift from C_{30} 1,15-diols in the low-flux period to C_{30} 1,14-diols in the high-flux period. This is consistent with the rapid increase of the *Proboscia* species during upwelling. These results will help us to recognize the potential that these components have as biomarkers.

References

- F. Gelin *et al.* *Phytochem.* **45** (1997).
 F. Gelin *et al.* *Org. Geochem.* **30** (1999).
 J.S. Sinninghe Damsté *et al.* *Geochim. Cosmochim. Acta* **67** (2003).
 J.K. Volkman *et al.* *Org. Geochem.* **30** (1999).
 J.K. Volkman *et al.* *Org. Geochem.* **18** (1992).
 S.G. Wakeham *et al.* *Deep-Sea Res. II* **49** (2002).

PB1-12: Novel phenyl derivatives of aromatic sulphur compounds in sedimentary rocks from the Holy Cross Mountains (Devonian) and the Fore Sudetic Monocline (Permian), Poland

M.J. Rospondek¹, L. Marynowski², M. Góra³

1) Institute of Geological Sciences, Jagiellonian University, ul. Oleandry 2a, Kraków
(e-mail: ros@geos.ing.uj.edu.pl)

2) Department of Earth Sciences, University of Silesia, ul. Będzińska 60, Sosnowiec, Poland

3) Institute of Chemistry, Jagiellonian University, ul. Ingardena 3, Kraków, Poland

Dibenzothiophene (DBT) and its alkyl derivatives are by far the most common aromatic sulphur compounds in mature geological samples. The interest in these compounds stems from their application for oil and source rock maturity assessment. DBT has three asymmetric structural isomers: naphtho[*b*]thiophenes, which are rarely identified in geological samples. This is partly due to co-elution problems on apolar stationary phases [1]. One of the isomers, namely naphtho[1,2-*b*]thiophene co-elutes with DBT, and the other naphtho[2,1-*b*]thiophene with phenanthrene on DB-5. However, on more polar stationary phases, these compounds can be well separated [1]. GC-MS analysis of some sedimentary rocks from the Holy Cross Mountains (Devonian) and Fore Sudetic Monocline (Permian, Zechstein) revealed that the samples contain two naphtho[*b*]thiophenes, i.e. naphtho[1,2-*b*]thiophene and naphtho[2,1-*b*]thiophene, although in small quantities, in addition to the abundant DBT. Interestingly, the same samples contain a series of unidentified compounds having $M^{+} 260$ (Fig. 1) in addition to the abundant phenyldibenzothiophenes $M^{+} 260$ (PhDBTs). The additional compounds are the major group in relatively immature samples (Fig.1, Góra Łgawa). This novel series elute immediately after four isomers of PhDBTs (Fig.1), which have been recently identified by MS-spectral and chromatographic comparison with authentic standards [2]. They have very similar to the PhDBTs mass spectra, and to each other, suggesting that these are phenyl derivatives of the DBT structural isomers. Considering the presence of naphtho[1,2-*b*]thiophene and naphtho[2,1-*b*]thiophene in these samples, syntheses of two most probable isomers 2- and 3-phenylnaphtho[2,1-*b*]thiophene was performed. Comparisons of these synthetic standards and compounds in the samples analysed revealed that 2-phenylnaphtho[2,1-*b*]thiophene is the second eluting compound of the additional suite (Fig. 1), while the 3-phenylnaphtho[2,1-*b*]thiophene is present only in the trace amount. 2-Phenylnaphtho[2,1-*b*]thiophene is sometimes the most abundant compound of the novel series (Fig. 1, Piskrzyn sample). However, the usually dominating compound of this series, eluting as the first after PhDBTs (Fig. 1), still remains unidentified. It can only be speculated that this is either 2-phenylnaphtho[1,2-*b*]thiophenes (the 3- isomer was synthesised and it is minor) or one of phenylnaphtho[2,1-*b*]thiophene isomers with phenyl attached to the naphthalene rings. The presence of phenylnaphtho[2,3-*b*]thiophenes is less probable due to the fact that naphtho[2,3-*b*]thiophene is missing. At this stage of the study, it can not be excluded, however, that some of these unidentified compounds represent

naphthylbenzo[*b*]thiophenes ($M^{+} 260$). One of them, namely 3-(2-naphthyl)-benzo[*b*]thiophene was encountered in immature samples in small amounts. Synthesis of further dibenzothiophene structural isomers is being currently performed.

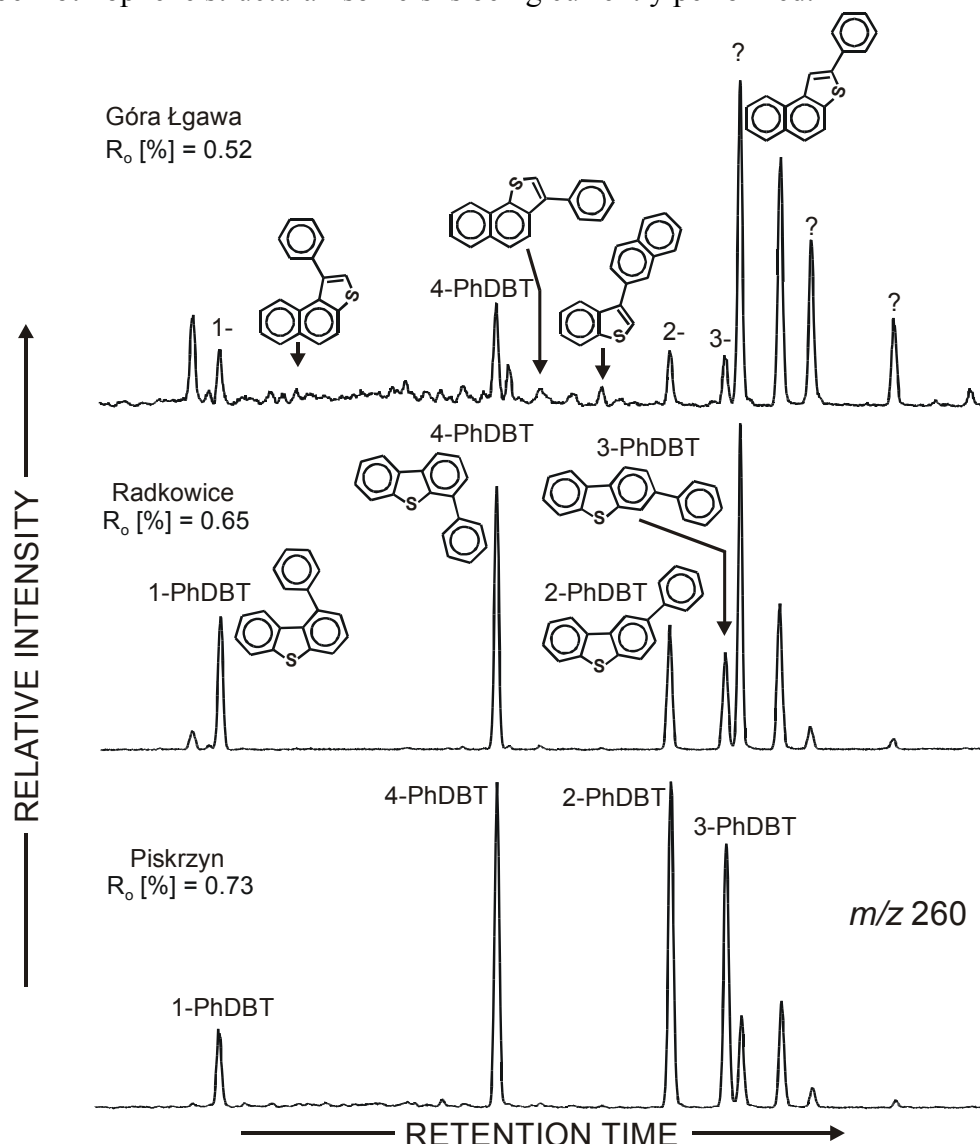


Fig.1. Partial mass chromatograms (m/z 260) showing so far unidentified series of phenylnaphtho[*b*]thiophenes in addition to phenyldibenzothiophenes (PhDBT) in samples of the different maturity (on the DB-35 column)

Acknowledgements

This study was partially supported by grant PB0354/P04/2003/25 and DS/V/ING/12/2004.

References

- [1] Marynowski, L., Rospondek, M., Mayer zu Reckendorf, R., Simoneit, B.R.T. 2002. Phenyldibenzofurans and phenyldibenzothiophenes in marine sedimentary rocks and hydrothermal petroleum. *Organic Geochemistry* 33, 701-714.
- [2] Mössner, S.G., Lopez de Alda, M.J., Sander, L.C., Lee, M.L., Wise, S.A. 1999. Gas chromatographic retention behavior of polycyclic aromatic sulfur heterocyclic compounds, dibenzothiophene, naphtho[*b*]thiophene, benzo[*b*]naphthothiophenes and alkyl-substituted derivatives on stationary phases of different selectivity. *J. Chromatography A* 841, 207-228.

PB1-13: Organic matter nature of a turbidite recorded in the Zaire Canyon inferred from a study of n-alcoholsC. Treignier¹, S. Derenne², A. Saliot¹

1) Laboratoire LOCEAN, IPSL/CNRS, UMR 7159, Université Pierre et Marie Curie, Case 134, 4 place Jussieu, 75252 Paris Cedex 05, France (e-mail: treignie@ccr.jussieu.fr)

2) Laboratoire de Chimie Bioorganique et Organique Physique, UMR CNRS 7573, École Nationale Supérieure de Chimie de Paris, 11 rue P. et M. Curie, 75231 Paris Cedex 05, France

Submarine canyons act as natural conduits for sediment transport from the continental margins down to the deep sea. Most of them are nowadays inactive due to the high sea level (e.g. Amazon). The Zaire canyon, one of the world's largest, is still very active (60 turbidites per century). It extends westward off the Congo-Angola margin (South-East Atlantic) for 760 km and connects directly the estuary to the abyssal plains (>4000 m). In the framework of the BIOZAIRE project we observed a turbiditic event in March 2001 (Khripounoff *et al.*, 2003). Simultaneously sediment traps moored on the channel levee collected huge amount of this material. It was a rare opportunity to study the organic nature of such a material, on which direct information is lacking. One aim of the BIOZAIRE program, developed by IFREMER in collaboration with TOTAL, is to study the benthic ecosystems (diversity and density) in relation to their sedimentary environment. The origin (marine vs terrigenous) of the sedimentary organic carbon (OC) and its degree of alteration might influence the fauna.

n-Alcohols are very useful biomarkers to address this question. Two criteria were used in the present study: the relative abundance of short (<C₂₀) and long (>C₂₂) *n*-alcohols (Eq. 1) derived from marine organisms and higher plants, respectively, and the ratio of odd to even carbon numbered <C₂₀ *n*-alcohols to assess the extent of alteration.

$$\text{Abundance of terrigenous material in OC} = \frac{[>C_{22}]}{[<C_{20}] + [>C_{22}]} \quad (\text{Equation 1})$$

The abundance of terrigenous material in the two samples collected at a Levee station by sediment traps moored at 400 and 30 m above the bottom (ab) as the turbidite occurred were firstly compared to a sediment trap sample, reference of the usual sinking particles at this site i.e. in absence of turbidite. Secondly, the influence of the turbidite on the sediment was studied by comparing the surficial sediments (0-0.5 cm) sampled 3 months before and 9 months after the event.

The trap material collected at 400 m ab while the turbidite occurred exhibits the same contribution of terrigenous material to the organic carbon (35% of OC) as the 400 m Levee sediment trap sample collected in absence of turbidite (Fig. 1). The similarity between both samples is confirmed by their close odd/even ratios (0.15 and 0.19). The stronger terrestrial signal (68% of OC) in the sample from the trap 30 m ab indicates that this lower trap did

collect turbidite material on the contrary to the 400 m one. Furthermore, the turbidite material is more degraded (0.26) than the previous samples. The influence of the turbidite is also displayed in the surface sediment of the levee. The terrigenous material constitutes 92% of OC in the surface sediment sampled after the turbidite (BZ2 cruise, Dec. 2001), while it only represented 45% of OC before it (BZ1 cruise, Dec. 2000). The BZ2 surface sediment exhibits a similar degree of alteration (0.23) to that of the 30 m turbidite trap. Assuming a first order degradation rate between the initial material (30 m turbidite trap) and the BZ2 surface sediment, it leads to degradation rate constants 2 orders of magnitude higher than the values so far reported. However, our degradation rate constants are not calculated from down-core profiles, which are probably underestimated as the initial concentration of deposited material is difficult to evaluate.

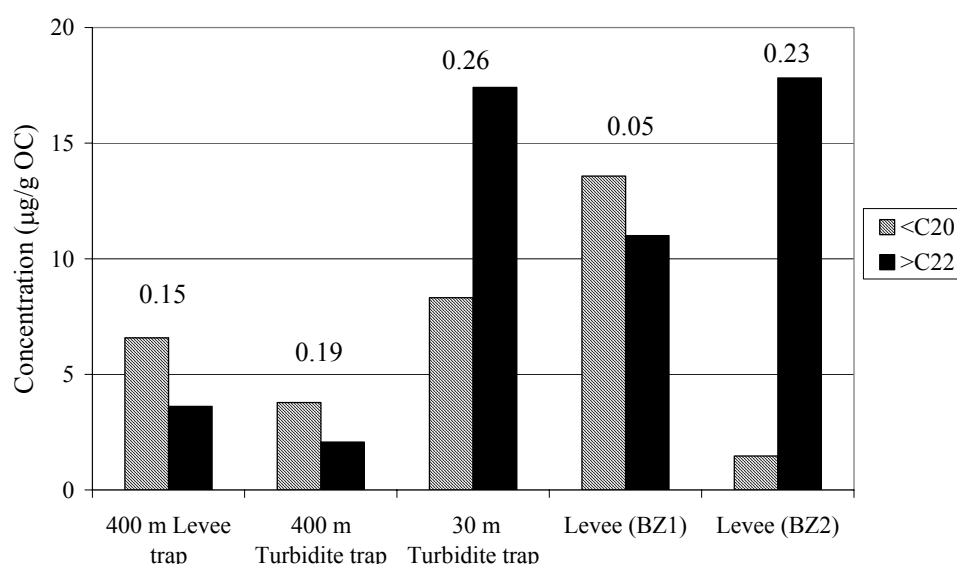


Fig.1. <C₂₀ and >C₂₂ *n*-alcohol concentrations (µg/g of OC) and odd/even ratio values indicated above the histogram

References

Khripounoff, A., Vangriesheim, A., Babonneau, N., Crassous, P., Dennielou, B., Savoye, B., 2003. Direct observation of intense turbidity current activity in the Zaire submarine valley at 4000 m water depth. *Marine Geology* 194, 151-158.

PB1-14: Anaerobic bacteria biosynthesis membrane-spanning tetraether lipids

J.W.H. Weijers¹, S. Schouten¹, E.C. Hopmans¹, J.A.J. Geenevasen²,
O.R.P. David², R. Pancost³, J. Coleman³, J.S. Sinninghe Damsté¹

1) Royal Netherlands Institute for Sea Research (NIOZ), PO Box 59, 1797 AB Den Burg – Texel, the Netherlands (e-mail: jweijers@nioz.nl)

2) University of Amsterdam, the Netherlands

3) University of Bristol, UK

Archaea were long considered to represent the ancestors of the Bacteria. Phylogenetic studies of 16S ribosomal DNA genes, however, revealed that Archaea and Bacteria do not share the same genetic fingerprint. This phylogenetic distinction is supported by distinct differences in the membrane lipid composition of Archaea and Bacteria; **a)** ether bonds in Archaea versus ester bonds in Bacteria; **b)** membrane spanning lipids in Archaea versus their absence in Bacteria; **c)** isoprenoid carbon chains in Archaea versus straight or branched carbon chains in Bacteria; **d)** the 2,3-di-O-alkyl-*sn*-glycerol stereoconfiguration of archaeal membrane lipids versus the 1,2-di-O-alkyl-*sn*-glycerol stereoconfiguration of bacterial membrane lipids. Some exceptions to these general classifications are known. Thermophilic, but also some non-thermophilic, Bacteria are known to produce non-isoprenoid dialkyl glycerol di-ether membrane lipids, instead of di-esters (e.g. Langworthy et al., 1983). Membrane spanning lipids containing 13,14-dimethyloctacosane, 15,16-dimethyltriacontane and 13,16-dimethyloctacosane carbon chains are reported in a few thermophilic Bacteria (e.g. Jung et al., 1994). Yet, to the best of our knowledge, no exceptions are reported to date regarding the nature of the carbon chains (isoprenoid versus branched or straight chain) and the stereoconfiguration.

A few years ago, a new group of branched glycerol dialkyl glycerol tetraethers (GDGTs) was discovered in peat bogs and soils (see figure). In contrast to known GDGTs, these branched GDGTs contain a mixture of archaeal and bacterial characteristics; a membrane-spanning tetraether structure and branched carbon chains respectively. A bacterial origin was proposed because of the presence of straight carbon chains and the fact that ether bonds and membrane spanning carbon chains have been found in Bacteria before. However, the combination of the ether bonds and the membrane spanning carbon chains, i.e. tetraether membrane lipids, is as yet unknown in the bacterial kingdom and casts doubt on the proposed bacterial origin.

¹⁹F-NMR spectroscopy was performed on a branched GDGT isolated from a peat and derivatised with S- and R-Mosher acids to elucidate the stereoconfiguration at the

glycerophosphate backbone of the lipid. Reaction products of the Mosher acids with the branched GDGTs gave chemical shifts for the CF_3 group comparable to reaction products of the Mosher acids with a commercially available 1,2-di-O-alkyl-*sn*-glycerol alcohol. This showed unambiguously that the glycerol backbone of this lipid has the bacterial 1,2-di-O-alkyl-*sn*-glycerol stereoconfiguration and hence, that these branched GDGT lipids are of a bacterial origin. As the branched GDGTs are abundant in the permanently water saturated part of peat bogs, anaerobic Bacteria are proposed to be the source of this compound. Concentrations of the branched GDGTs in two peat profiles from Sweden and England, are up to twice as high as those of the main isoprenoid GDGT produced by methanogens. Since methanogenesis is an important process in wetlands, the anaerobic Bacteria producing the branched GDGTs must be an ecologically significant part of the microbial population present as well. Moreover, as the profiles of the branched GDGTs and the isoprenoid GDGT from the methanogens strongly co-vary, a similar ecological niche for both groups of organisms is supposed.

Our current research focuses on the identification of the source bacteria of the branched GDGTs. Samples from a second Swedish peat core are currently analysed for their 16S rDNA content in order to see which bacteria are abundant and show a similar abundance pattern as the branched GDGT lipids. Furthermore, isolation followed by ^{13}C NMR spectroscopy is carried out on two similar kinds of branched GDGTs found, which seem to contain one or two cyclopentane moieties, another archaeal trait.

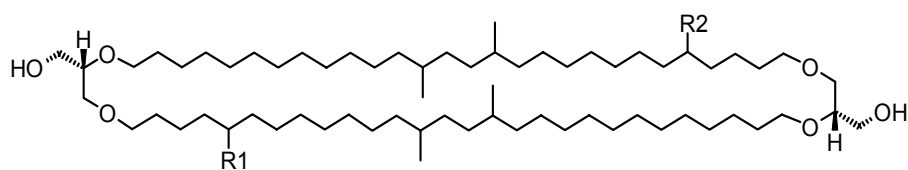


Fig.1. Structure of branched glycerol dialkyl glycerol tetraethers:

I) $\text{R}_1=\text{R}_2=\text{H}$; II) $\text{R}_1=\text{CH}_3$ $\text{R}_2=\text{H}$; III) $\text{R}_1=\text{R}_2=\text{CH}_3$

References

- Jung, S., Zeikus, J.G., Hollingsworth, R.I., 1994. A new family of very long chain α,ω -dicarboxylic acids is a major structural fatty acyl component of the membrane lipids of *Thermoanaerobacter ethanolicus* 39E. *Journal of Lipid Research* 35, 1057-1065.
- Langworthy, T.A., Holzer, G., Zeikus, J.G., Tornabene, T.G., 1983. Iso- and anteiso- branched glycerol diethers of the thermophilic anaerobe *Thermodesulfotobacterium commune*. *Systematic and Applied Microbiology* 4, 1-17.

PB1-15: Riverine, estuarine and near-coastal transport and transformation of natural organic compounds (RENTT)- Case study Siak River, Riau province, Sumatra

R. Wöstmann, G. Liebezeit

Centre for Research on Shallow Seas, Coastal Zones and the Marine Environment, Terramare, Schleusenstraße 1, D-26382 Wilhelmshaven

Coastal areas represent an important region of organic matter transport, recycling, degradation and accumulation. The organic material in coastal waters and sediments originates from both marine and terrestrial sources. The Indonesian-German project RENTT aims at characterising and quantifying these sources in the coastal sea of eastern Sumatra with emphasis on inputs from the Siak river and transformation processes occurring in its estuary. By including river drainage area, estuary and river-influenced coastal ocean in one sampling and analysis scheme a complete coverage of a large variety of processes and compounds is achieved. This approach may serve as a model for other tropical river systems and provides together with the results of the joint projects comprehensive information for political and administrative bodies to assess the environmental situation.

In order to characterise the natural organic matter from their place of origin to their final or temporary deposition location in a paleochemotaxonomical way recent plant material collected from the Siak River bank as well as different Siak river sediments and deposited peats were selected for biomarker investigation. The analysed plants were chosen according to botanical analysis, which revealed them as being main constituents of today's Siak River shoreland vegetation. The use of lipid biomarkers is well documented in the literature (e.g. Okhouchi et al., 1997; Volkman et al., 2000) although for many common recent tropical plants lipid data are still not available (e.g. water hyacinth, *Eichornia crassipes*).

The first data of the *n*-alkane distribution pattern of the Siak River shoreland vegetation show the strong predominance of odd over even carbon numbers in all samples typical for higher plant waxes (Eglinton and Hamilton, 1967). A significant variation in the maximum of the carbon number distribution was detected. The analysed plants showed an alternating *n*-alkane maximum in their distribution pattern at C₂₇, C₂₉, C₃₁ or C₃₃. There are, however, compared to samples from temperate regions species which have chain lengths exceeding C₃₅. This is probably an effect of the higher growth temperatures and might serve as a useful indicator for a plant specific input to river sediments.

In the selected river sediments the *n*-alkane distribution showed an odd over even carbon number predominance with maxima at C₂₉ or C₃₁, indicating an origin from different

plant types but also a significant content of C₃₅ and C₃₇ in some cases correlating with recent plant material in this area (Fig. 1).

In contrast to this *n*-alcohols, ω -hydroxy fatty acids, *n*-alkan-2-ones, mid-chain alcohols, steroid ketones and alcohols do not allow a distinction between different types of plants. However, pentacyclic triterpenoids are characteristic biomarkers of plant communities. Their distribution patterns and total amounts allow a clear distinction between different type of river shoreland vegetation.

The distributions of characteristic biomarkers shows that the molecular composition of Siak river shoreland vegetation corresponds to that of the lipid extracts from Siak river sediments.

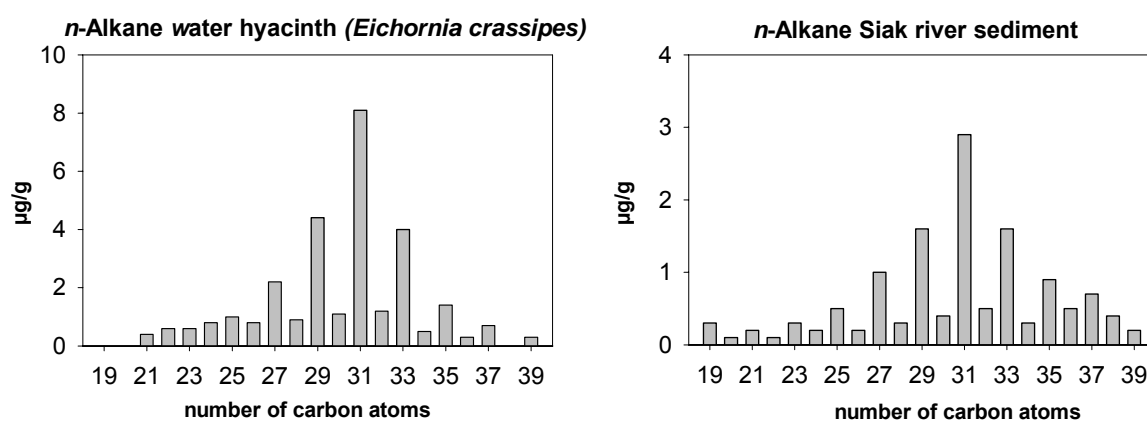


Fig.1. *n*-Alkane distribution pattern of water hyacinth (*Eichornia crassipes*) and a selected Siak river sediment

References

- Eglinton G. and Hamilton R.J., 1967. Leaf epicuticular waxes. *Science* 208, 1322-1335.
- Ohkouchi, N., Kawamura, K. and Taira, A., 1997. Fluctuations of terrestrial and marine biomarkers in the western tropical Pacific during the the last 23.300 years. *Paleoceanography* 12, 623-630.
- Volkman JK., Rohjans D., Rullkötter J., Scholz-Böttcher BM., Liebezeit G., 2000 Sources and diagenesis of organic matter in tidal flat sediments from the German Wadden Sea. *Cont. Shelf Res.* 20, 1139-1158.

PB1-16: Terpanoid alkanes as diagnostic markers for benthic red algae? Evidence from the Upper Proterozoic organic-rich shales and cake-shaped bitumens in Northern China

S. Zhang¹, B. Zhang¹, Y. Xiong¹, Z. Jin², L. Bian³,
D. Wang¹, F. Song¹

- 1) CNPC Key Laboratories for Petroleum Geochemistry, PetroChina Research Institute of Petroleum Exploration & Development, Beijing 100083, China (e-mail: sczhang@petrochina.com.cn)
2) SINOPEC Exploration & Production Research Institute, Beijing, China
3) Department of Earth Sciences, Nanjing University, Nanjing, China

This paper presents detailed organic petrographic and organic geochemical results obtained from a suite of Upper Proterozoic organic-rich black shales and associated bitumens in northern China, suggesting terpanoid alkanes as diagnostic benthic algal markers in Proterozoic to Phanerozoic sediments. The samples were collected from the third member (X₃) of the Xiamaling Formation within the Upper Proterozoic Qinbaikou Group (900-873 Ma). The X₃ member in the sampling area (Xiahuayuan, Hebei Province) consists of approximately 350 m of carbonaceous to siliceous rocks, with relatively low maturity level (ca. 0.6 - 0.7 %VRE), high TOC contents (10.83-24.26 wt%), and high extract yields (1731-8787 µg/g rock). The black mudstones and paper shales from the X₃ member generally display high oil saturation (3.71-10.57 wt%), and organic petrographic results indicate that organic matter in these shales includes mostly benthic red algae. Such high TOC and extract yields from macroalgae in Upper Proterozoic oil shales are rarely documented. Interestingly, the gray-green shales and siliceous rocks in the X₄ member that directly overly above the oil shales contain abundant cake-shaped bitumen nodules with varying size. Thin section observation illustrates that these bitumen nodules are either lithified red algae (similar to modern Rhodolith that flourishes under 200 m of water column) or red algae nodules with bitumen filling in pith-cavity and trichome. The oil distribution patterns in these algae are similar to those observed from the coelom of organism, suggesting the indigenous nature of the bitumens.

Biomarker distributions in these shale extracts are significantly different from those in other marine rocks from the surrounding area, with relatively low sterane but high terpane concentrations. The *m/z* 191 mass fragmentogram is characterized by (1) extremely high abundance of a C₁₉ unknown tricyclic, C₂₀ and C₂₁ tricyclic, and C₂₄ tetracyclic terpane, (2) the presence of a unknown C₃₀- pentacyclic triterpane eluted between the Ts and Tm, and (3) moderate 17α(H) C₂₉- and C₃₀-diahopanes. Similar biomarker assemblages are common in extracts of Mesozoic nonmarine source rocks and derived oils in petroliferous basins of western China, indicating possible contribution of benthic red algae to sedimentary organic

matter. The presence of a diagnostic series of C₁₈-C₂₉ long-chain 13 α -(H)-*n*-alkylated tricyclic terpanes in both the X₃ black shales and X₄ cake-shaped bitumen nodules suggests that both members contain similar benthic algae with subtle variation. While organic matter in the oil shales of the X₃ member consists mainly of compressed fossil red algae, the cake-shaped bitumens in the X₄ member are largely silicated nodules.

The results suggest that the high abundance of pentacyclic triterpanes, 17 α (H)-diahopane homologues, C₂₀ and C₂₁ tricyclic terpanes, and C₂₄ tetracyclic terpane in a rock extract or crude oil is not restricted to a terrigenous source, as proposed previously. An alternative to the hypothesized origin from clay-catalyzed transformation of bacterial hopanoid precursors under sub-oxic conditions is that these compounds are diagnostic of benthic algae. The occurrence of such compounds in a variety of rock extracts and oils from different ages implies that red algae and associated benthic organisms evolved very early in the history of the earth. These algae possess considerable hydrocarbon source potential and may have played a significant role in hydrocarbon generation in many sedimentary basins.

PB1-17: Characterisation of amino acids in marine sediments from the Benguela Upwelling System

C.M. Bickers, L. Handley, R.D. Pancost

Organic Geochemistry Unit, Bristol Biogeochemistry Research Centre, School of Chemistry, University of Bristol, Bristol UK (e-mail: claire.bickers@bristol.ac.uk)

Stable nitrogen isotopic analysis of bulk organic matter in sediments is a well-established method for tracing the sources and history of organic matter in the geosphere¹, but differential diagenesis of isotopically distinct compound classes can complicate interpretation of bulk sedimentary $\delta^{15}\text{N}$ values. Important diagenetic and organic source information is also contained within amino acids, the building blocks of proteins and the major form of nitrogen in most marine organisms. They make up a relatively labile fraction of the bulk organic matter and are generally only abundant in marine sediments at sites exhibiting good preservation. However, where present, they can facilitate interpretation of the sedimentary isotopic record – their carbon and nitrogen isotopic compositions can be used to reconstruct past environments, and by measuring stable isotope values of individual amino acids we can evaluate the reliability of bulk sedimentary $\delta^{15}\text{N}$ values. To explore how diagenetic alteration of organic matter influences the geochemical record, we have examined the influences on the preservation and degradation of N-bearing organic matter via the analysis of amino acids and bulk organic parameters.

We analysed sediments from the coastal Benguela Upwelling region (ODP Leg 175) near the edge of the continental shelf. These organic-rich sediments contain an excellent record of past productivity change and are well preserved. The samples comprise two sets, spanning 0.21 ky – 60.28 ky (covering the last glacial-interglacial cycle) and spanning 2.4 Ma – 2.5 Ma (covering glacial-interglacial cycles at the Intensification of Northern Hemisphere Glaciation). These sediments were analysed using GC, GC/MS, GC-CF-IRMS and GC-C-IRMS, after appropriate extraction, hydrolysis, clean-up and derivatisation. Specifically we determined %TOC and %TN, the total hydrolysable amino acid abundances, D/L enantiomers of THAAs, bulk sediment $\delta^{13}\text{C}$ and $\delta^{15}\text{N}$ values, and compound specific $\delta^{13}\text{C}$ and $\delta^{15}\text{N}$ values of THAAs.

The concentration of TOC (and to a lesser degree, TN) in both recent and older sediments is mainly influenced by the productivity changes associated with glacial-interglacial transitions. The TOC/TN ratios are comparatively high (up to 18) compared to those generally observed in marine sediments, and this can be attributed to preferential

mineralization of nitrogen-containing compounds over carbon-containing compounds. Total hydrolysable amino acids (THAAs) are present and diverse in all sediments, with both protein and non-protein amino acids observed. The relative concentration of the THAAs is likely to have been influenced by a number of factors including sources and magnitude of organic matter inputs and subsequent degradation of organic matter. The application of a protein based Degradation Index² (DI) based on the mole % of THAAs (Fig. 1C) shows that changes in amino acid composition occur with depth and can be linked to the altering degradation state of the organic matter. The DI reveals that these sediments are relatively fresh and become degraded with increasing depth. THAA enantiomer distributions have also been determined (Fig. 1A) allowing sedimentary profiles of specific amino acid D/L ratios (Fig.1B) to be developed. The D/L ratio of alanine increases downcore, as expected with progressing racemisation. However, unexpected variations in all parameters including the proportion of D-amino acids, indicates that the controls on amino acid abundances are complex and record a variety of processes.

Because the composition and abundances of THAAs are changing downcore, it is possible that the content and $\delta^{15}\text{N}$ values of bulk sediment are also changing. Bulk organic $\delta^{13}\text{C}$ and $\delta^{15}\text{N}$ measurements have been made on all sediments, and we evaluate the reliability of these bulk measurements by comparison with individual amino acid $\delta^{13}\text{C}$ and $\delta^{15}\text{N}$ values.

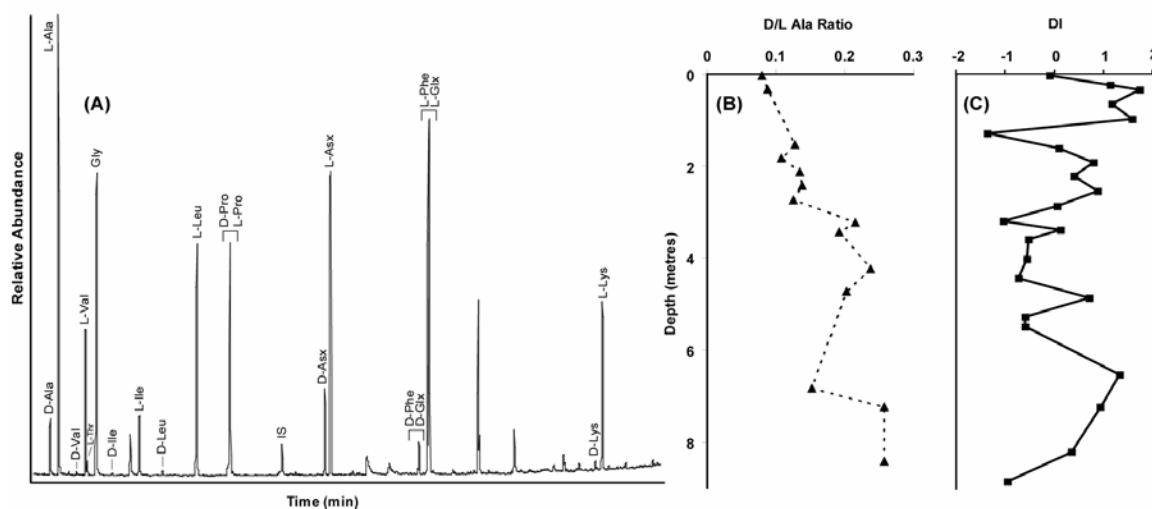


Fig.1. Total ion current of (A) amino acid enantiomers as trifluoroacetyl isopropyl esters (TFA/IP) in a sediment from Site 1083 of ODP Leg 175, (B) the depth profile of D/L enantiomers of alanine. (C) the DI depth profile depicting freshness of organic matter downcore based on amino acid mole%, (more positive numbers indicative fresher material)

References

- [1] Macko S.A., Uhle M.E., 1997. Stable Nitrogen Isotope Analysis of Amino Acid Enantiomers by Gas Chromatography/Combustion/Isotope Ratio Mass Spectrometry. *Analytical Chemistry* 69, 926-929.
- [2] Dauwe, B., Middelburg J.J., 1998. Amino Acids and Hexosamines as Indicators of Organic Matter Degradation State in North Sea Sediments. *Limnology and Oceanography* 43(5), 782-798.

PB1-18: Molecular markers of Mesozoic seep carbonates from a convergent margin setting, California

D. Birgel¹, V. Thiel², K.A. Campbell³, M. Elvert¹, J.D. Farmer⁴, K.-U. Hinrichs¹, J. Peckmann¹

1) Forschungszentrum Ozeanränder, Universität Bremen, Postfach 330 440, D-28334 Bremen, Germany (e-mail: dbirgel@uni-bremen.de)

2) Geowissenschaftliches Zentrum der Universität Göttingen, Goldschmidtstrasse 3, D-37077 Göttingen, Germany

3) Geology Department, University of Auckland, Private Bag 92019, Auckland 1020, New Zealand

4) Geology Department, Arizona State University, P.O. Box 871404, Tempe, AZ 85287, USA

Hydrocarbon-dominated cold-seeps occur at convergent plate boundaries as well as at passive continental margins. Such hydrocarbon-seep settings are dominated by chemosynthesis-based communities. The key reaction providing both energy and carbon substrates is the anaerobic oxidation of methane (AOM), which is carried out by consortia of methanotrophic archaea that oxidize methane to bicarbonate, and sulphate-reducing bacteria (SRB). To date, numerous cold-seep settings have been reported from modern and ancient environments, but for Mesozoic seeps supporting evidence from the analysis of molecular biomarkers is only available for one Late Jurassic seep deposit from southern France (Peckmann et al., 1999). Here we present lipid biomarker data from several hydrocarbon-seep carbonates embedded in Late Jurassic (Tithonian) to Early Cretaceous (Aptian/Albian) forearc and accretionary prism strata in western California. These carbonates accumulated in turbidite/fault-hosted or serpentinite diapir-related settings (Campbell et al., 2002).

Archaeal lipids in these seep carbonates exhibit extremely negative $\delta^{13}\text{C}$ values. Specific biomarkers comprise tail-to-tail linked acyclic isoprenoids such as crocetane ($\delta^{13}\text{C} \sim -80$ ‰) and PMI (~ -100 ‰). Isotopically-depleted crocetane found in one of the samples represents the first record of this compound in a Mesozoic seep deposit. Moreover, a sequence of head-to-tail linked acyclic isoprenoids (C_{21} to C_{24}) with strong ^{13}C -depletions (-70 to -110 ‰) suggests methane oxidizing archaea as possible source organisms. These compounds may represent fragments of former archaeal sesterterpanylglycerol diethers.

Isotopically-depleted $17\alpha,21\beta$ (H) and $17\beta,21\alpha$ (H) hopanes (C_{30} to C_{34}) with S- and R-isomer couplets are present in all samples indicating a low to moderate thermal maturity of the carbonate rocks investigated. The precursors of isotopically-depleted hopanoids at cold-seeps are still unknown. They may derive from aerobic bacteria, including methanotrophs, but could also originate from yet unknown anaerobic bacteria linked with AOM (cf., Pancost et al., 2000; Thiel et al., 2003). Notably, isotope ratios for the stereoisomers show a specific

pattern. S-isomers are relatively enriched in ^{13}C (–60 to –65 ‰) compared to the R-isomers (–64 to –74 ‰).

Our lipid biomarker results represent the first report of AOM at seeps in the Cretaceous. The manifestation of 70 myr of seepage activity and AOM along the Mesozoic margin of western California fills the gap between the earliest cold-seep biomarker record (Late Jurassic) and the more widely recognized Cenozoic examples (for a review see Peckmann and Thiel, 2004).

References

- Campbell, K. A., Farmer, J. D., Des Marais, D., 2002. Ancient hydrocarbon seeps from the Mesozoic convergent margin of California: carbonate geochemistry, fluids and palaeoenvironments. *Geofluids* 2, 63-94.
- Pancost, R. D., Sinninghe Damste, J. S., de Lint, S., van der Maarel, M. J. E. C., Gottschal, J. C., the Medinaut Shipboard Scientific Party, 2000. Biomarker evidence for widespread anaerobic methane oxidation in Mediterranean sediments by a consortium of methanogenic archaea and bacteria. *Applied and Environmental Microbiology* 66, 1126-1132.
- Peckmann, J., Thiel, V., Michaelis, W., Clari, P., Gaillard, C., Martire, L., Reitner, J., 1999. Cold seep deposits of Beauvoisin (Oxfordian; southeastern France) and Marmorito (Miocene; northern Italy): microbially induced authigenic carbonates. *International Journal of Earth Sciences* 88, 60-75.
- Peckmann, J., Thiel, V., 2004. Carbon cycling at ancient methane-seeps. *Chemical Geology* 205, 443-467.
- Thiel, V., Blumenberg, M., Pape, T., Michaelis, W., 2003. Unexpected occurrence of hopanoids at gas seeps in the Black Sea. *Organic Geochemistry* 34, 81-87.

**PB1-19: Calibration of organic signal in sedimentary lacustrine records.
Molecular comparison between actual producers, dissolved organic matter and
sedimentary organic matter (Lac Pavin; Massif Central Français)**

M. Boussafir, S. Drouin, P. Albéric, J.L. Robert

ISTO (UMR 6113, CNRS - Université d'Orléans), Bâtiment Géosciences, Rue de Saint Amand, BP. 6759, 45067 Orléans Cedex 2, France

Paleoenvironmental studies undertaken in the past few years on lacustrine sediments indicate highly complex organic records. Indeed, the organic sources in lacustrine environments are numerous and early diagenetic transformations further complicate the molecular signal. This diagenetic filter can sometimes mask environmental information (by degradation of organic source biomarkers) as well as revealing it by simplification of the signal (information on condition of sedimentary organic matter (SOM) incorporation). The preliminary calibration between primary producers and organic matter in sediments is essential to understand the processes prevailing in deposition and preservation of sedimentary organic material.

The main objective of this work is to study and compare the composition of lipid fractions contained in primary producers and those preserved in recent sediments. This work forms part of a project aimed at understanding the role of the minerals especially clays in the transfer and the preservation of hydrocarbon-rich SOM (S. Drouin *et al.*, this meeting).

Specific information obtained on molecular composition of the primary producers, dissolved organic matter, through to SOM compositions will aid elucidation of the evolution and fate of OM, and allow the determination of organic species susceptible to be adsorbed by clay minerals i.e. those likely to be protected from organic recycling.

GC/MS analysis was carried out on the extracted lipids of the following:

- Living lacustrine organisms. These are Macrophytes algae existing at the sediment-water column interface at 2-10m depths, and phytoplanktonic algae.
- 5 litre water aliquots, collected in various depths in the lake.
- Greenish surface sediments collected on the first 15 cm of a small sedimentary core
- Brownish sediment at a more advanced stage of diagenesis representing the oldest part (15-30 cm) of the previous sediment core.

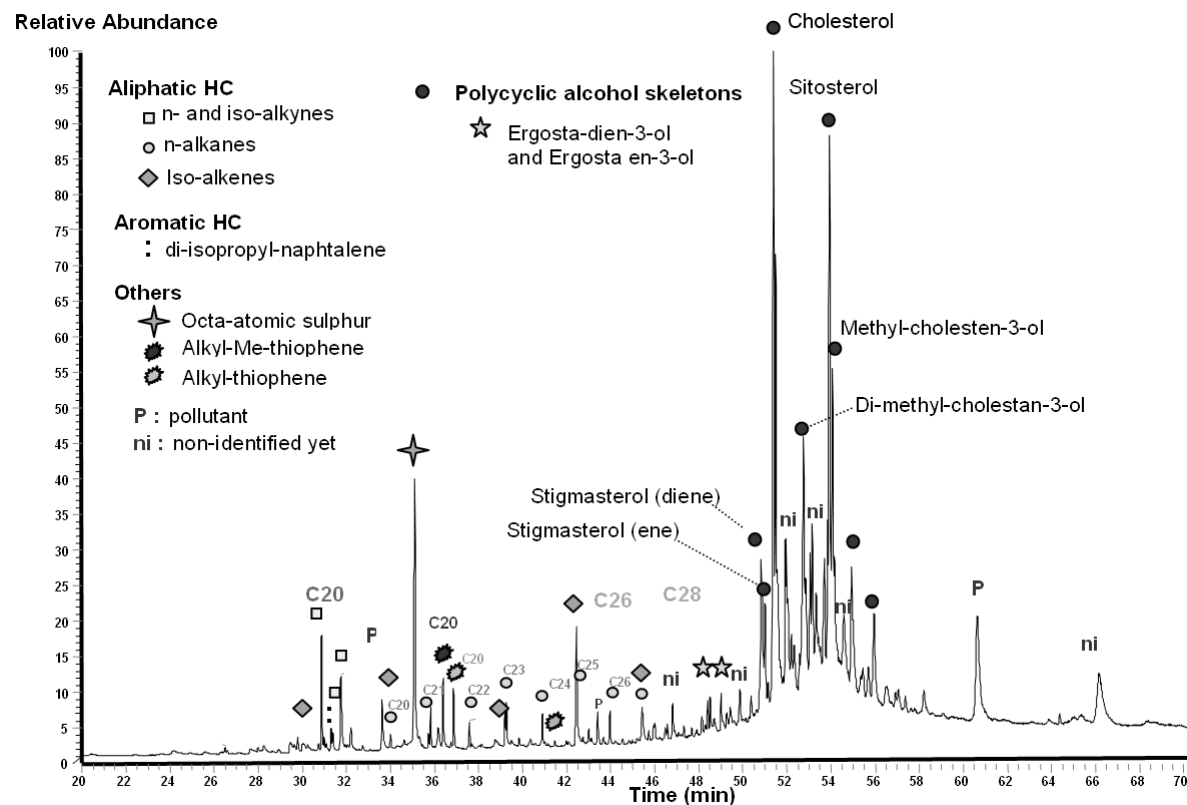


Fig.1. Total ion current of neutral lipid fraction of greenish surface sediment sample

Preliminary results show that the extractable lipids of these various studied fractions are dominated by a remarkable diversity of alcohols, particularly polycyclic moieties. The Macrophytes algae and phytoplanktonic algae present the same molecular signatures with different relative proportions. Some of these lipid fractions are found in the dissolved organic matter and in recent sediments bearing signs of oxidative deterioration witnessing the transfer of OM through the water column.

The lipid composition of dissolved organic matter in the anoxic water column is richer and better-preserved compared to lipids in the oxygenated water column. The molecular comparison of the green recent sediment (figure 1), and the brown older deeper sample one highlights the molecular transformations typifying this diagenetic sequence, with increasing amounts of some aliphatic compounds and the complete disappearance of few molecular families.

PB1-20: The occurrence of branched alkanes with quaternary carbon atoms (BAQCs) in the sediments of two large freshwater lakes: Lake Malawi (East Africa) and Lake Superior (USA/Canada)

I.S. Castañeda¹, J.P. Werne¹, K.D. Pearson¹, F. Kenig²

1) Large Lakes Observatory, Univ. of Minnesota Duluth, 10 University Dr., 109 RLB Duluth, MN 55812, USA

2) Dept. of Earth and Environmental Sciences, University of Illinois at Chicago, M/C 186 845 West Taylor, Chicago IL 60607-7059, USA

The presence of branched alkanes with quaternary carbon atoms (BAQCs) in the geological record is of interest as pseudohomologous series of these compounds exhibit solely odd or even carbon number predominance, suggesting a biological source (Kenig et al., 2005; 2003). At present, BAQCs have been reported from a range of environments including Cenomanian-Turonian shales (Kenig et al., 2005; Simons et al., 2003), Neoproterozoic sedimentary rocks associated with microbial mats (Greenwood et al., 2004), deep-sea hydrothermal waters (Kenig et al., 2003), hydrothermal sulfide deposits (Simoneit et al., 2004) and in modern and Holocene marine shelf sediments (Kenig et al., 2003). As BAQCs are well-preserved in the geologic record (Kenig et al., 2005), they have potential as paleoenvironmental biomarkers, however, at present the source organism(s) for BAQCs remain(s) unknown. Based on the geologic environments from which BAQCs have been reported, several studies have suggested that these compounds are produced by organisms associated with redox gradients (Kenig et al., 2005, 2003; Greenwood et al., 2004). Specifically, it has been suggested that BAQCs are produced at redox boundaries by non-photosynthetic, thermophilic bacteria or archaea, which may be sulfide oxidizers (Kenig et al., 2003). Here we report on the occurrence and paleoenvironmental significance of BAQCs identified in two large freshwater lake systems.

We have identified branched alkanes with quaternary carbon atoms (BAQCs) in sediment cores from Lake Malawi (East Africa, 22 kyrs) and Lake Superior (USA/Canada, 10 kyrs), dominated by C₁₇-C₄₁ 5,5-diethylalkanes and C₁₆-C₃₄ 2,2-dimethylalkanes but with several other series present as well. BAQCs are present in all Lake Superior sediment samples examined whereas in the Lake Malawi samples BAQCs are present only during distinct intervals, which appear to correlate with periods of drier climate in East Africa. In some samples, 5,5-diethylalkanes are similar in abundance to n-alkanes. The observation that BAQCs are present in the sediments of freshwater lakes provides important information on the environmental significance of these compounds. First, BAQCs are now known to be associated with both fresh and saline environments. Second, the fact that not all Lake Malawi

samples contained BAQCs indicates that these compounds are not ubiquitous in lakes. We also note that BAQCs are not present in Holocene samples analyzed in our laboratory from Elk Lake (Minnesota) or in modern samples from Lake Edward (East Africa).

References

- Greenwood, P.F., Arouri, K.R., Logan, G.A., Summons, R.E., (2004) Abundance and geochemical significance of C_{2n} dialkylalkanes and highly branched C_{3n} alkanes in diverse Meso- and Neoproterozoic sediments. *Organic Geochemistry*, 35, 331-346.
- Kenig, F., Simons, D.-J.H., Crich, D., Cowen, J.P., Ventura, G.T., and Rehbien-Khalily, T. (2005). Structure and distribution of branched aliphatic alkanes with quaternary atoms in Cenomanian and Turonian black shales of Pasquia Hills (Saskatchewan, Canada). *Organic Geochemistry* 36, 117-138.
- Kenig, F., Simons, D.-J.H., Crich, D., Cowen, J.P., Ventura, G.T., Rehbien-Khalily, T., Brown, T.C., Anderson, K.B., (2003) Branched aliphatic alkanes with quaternary substituted carbon atoms in modern and ancient geologic samples. *Proceedings of the National Academy of Sciences*, 100(22), 12554-12558.
- Simons, D.-J., Kenig, F., and Schroder-Adams, C. (2003) An organic geochemical study of the Cenomanian-Turonian sediments from the Western Interior Seaway, Canada. *Organic Geochemistry*, 34, 1177-1198.
- Simoneit, B.R.T., Lein, A.L., Peresykin V.I., and Osipov, G.A. (2004) Composition and origin of hydrothermal petroleum and associated lipids in the sulfide deposits of Rainbow Field (Mid-Atlantic Ridge at 36°N). *Geochimica et Cosmochimica Acta*, 68, 2275-2294.

PB1-21: Organic matter as markers to evidence geochemical evolution of highly alkaline plumes during seepage in sedimentary column

M. Elie¹, L. Martinez¹, I. Suárez-Luiz²

1) UMR CNRS 7566, Université H. Poincaré, 54506 Vandœuvre, France

2) Instituto Nacional del Carbon (CSIC), Ap. Co., 73, 33080 Oviedo, Spain

At Khushaym Matruck site in Central Jordan, spontaneous combustion of bituminous-rich marls (Upper Cretaceous – Upper Palaeocene), in sub-surface conditions, has produced 60 m of metamorphic units composed of marbles and specific mineral phases similar to those observed in industrial cements. After combustion phase, though interaction with meteoric and groundwaters, these marble/cement units would have produced hyper-alkaline plumes which have percolated in the underlying marls. Both thermal and alkaline plume effects were superimposed and the extent to which organic matter is affected by each of them can be blurred. The question arises as to whether these alteration processes can be discriminated, and the geochemical evolution of highly alkaline plumes during seepage through sedimentary column can be observed by studying organic matter.

Samples were collected in underlying marls as a function of increasing distance from metamorphosed zone. Isolated kerogens were analysed by Rock-Eval pyrolysis, optical microscopy, transmission infrared microspectroscopy. The whole rocks were extracted with dichloromethane and the extractable organic matter was fractionated on silica microcolumn in hydrocarbon and non hydrocarbon compounds. Aliphatic and aromatic hydrocarbons were analysed by gas chromatography-mass spectrometry.

Tissot's classification (HI-OI plot) of isolated kerogens points to a large contribution of strongly oxidized organic matter and identified as inertinite, which is known to derive from either wildfires or reworked woody materials. The high Rock-Eval T_{max} values ($> 480^{\circ}C$) along the profile suggest that organic matter has reached the wet-gas zone. The extractable organic matter profile increases towards the cement zone and maximises at 2.6 m from metamorphic contact. The mixed origin (marine + land-derived) of organic matter can explain the prominence of shorter *n*-alkanes and the observed slight odd-to-even preference in the C_{23} to C_{33} range. Hopanes (m/z 191) have been detected in low abundance and their distribution is dominated by the stable thermodynamically $\alpha\beta$ -isomers. The calculated R/S isomerisation ratios for the C_{32} hopanes are ranged between 0.50 and 0.54, close to values found in the oil-generative window.

On the contrary, other parameters reveal that organic matter in underlying marls is much more immature. The Methylphenanthrene Index values (MPI), deduced from GC-MS analyses of aromatic hydrocarbons and based on the relative abundances of phenanthrene (m/z 178) and its methyl homologues (m/z 192), coincide with immature zone. Petrographic analyses of the whole rock show that the vitrinite is present under the gel form and/or huminite, and is commonly accompanied of well-preserved lignocellulosic structures, which are typical of immature particles. The vitrinite reflectance is lower than 0.6. Some microalgae, type lamalginite with an important hydrogen content were identified under fluorescence suggesting an immature stage of organic matter (early diagenesis).

The uncertainty regarding the thermal influence of combustion process on organic components of the underlying marls provides that oxidising fluid circulation induces similar effects than thermal maturation. Oxidizing fluid percolation induced an “overmaturation” of organic matter in underlying marls. On the other hand, vitrinite reflectance is unaffected by oxidation, and the observed values indicate that thermal effect due to combustion process is not a major parameter in the observed changes in organic matter properties. μ -IRTF allows one to evidence the geochemical evolution of highly alkaline plumes during seepage through underlying marls. The spectral features of the lignocellulosic debris reveal that the relative abundance of polysaccharide bands decreases towards the metamorphosed zone, and polysaccharide/lignin ratio indicates a progressive pH neutralization of alkaline plumes.

Acknowledgments

The Centre National de la Recherche Scientifique (CNRS) and Agence Nationale pour la Gestion des Déchets Radioactives (ANDRA) are thanked for providing the financial support *via* GdRFORPRO (action FORPRO 2001.VII) for this research. Dr P. Verdoux is also gratefully acknowledged.

PB1-22: Chemical stratigraphy of the type Barreirinha formation, (Upper Devonian), Amazon basin - Brazil

J.A. Trigüis¹, R. Rodrigues², E.S. Souza³

1) LENEP/UENF, Rod. Amaral Peixoto, km.163, Av. Brenand SN - Macaé, Rio de Janeiro, CEP: 27925-310 (e-mail: triguis@lenep.uenf.br)

2) UERJ – Rua São Francisco Xavier, 524, Faculdade de Geologia – Maracanã, Rio de Janeiro, RJ CEP: 205550-900

3) LENEP/UENF, Rod. Amaral Peixoto, km. 163, Av. Brenand SN, Imboacica, Macaé, Rio de Janeiro, CEP: 27925-310

Introduction

This research represents the first organic geochemical study on the immature Barreirinha Formation, basal Curuá Group, (late Early Frasnian through Late Famennian), which is the source rock of the Amazon Basin. The pre-existent data belongs to studies realized on samples from Petrobras deep-drillings, (Rodrigues, 1982) where the Devonian section is thermally mature to overmature.

This present contribution is based on the unique detailed geochemical investigation of core samples of the entire Barreirinha Formation in its type locality, taken from the Caima PH-2 shallow borehole, 137 metres deep. The analysed section extends from the lower Curiri Formation (middle Curuá Group), down to the basal portion of the Barreirinha Formation, or the top of the underlying Ererê Formation, (Loboziak et al., 1997).

Results and discussion

The lithostratigraphic characteristics of the drilled section were presented in Loboziak et al., (1997). Total organic carbon results shows variations correlated to the lithological characteristics.

Pyrolysis Rock-Eval and optical data demonstrate that the kerogen composition and preservation vary throughout the studied section, according to the changes in lithology and TOC (Fig.2). The upper interval, correspondent to the Curiri Formation (7,80m to 45,22m) shows an average HI of 260 mg HC/g COT and a predominance of liptinitic organic matter, represented mainly by acritarchs and miospores and humic debris secondarily. The top unit of Barreirinha Formation (non radioactive interval between 45,22m and 99,85m) contains lower abundance of liptinitic organic matter and normally higher amounts of humic debris than the Curiri Formation. It also shows some variations in the contents of amorphous organic matter. These results are consistent with its lower values of HI (average values of 163mg HC/g COT). The lower Barreirinha interval (99,85m to 136,75m), with an average HI of 329mg HC/g COT shows amorphous marine microplankton as the predominant fraction, followed by

liptinitic organic matter, mainly acritarchs and *Tasmanites* algae, and lower percents of humic debris.

GC of aliphatic hydrocarbon fractions demonstrate some differences from the top to the bottom of the studied section: the increasing values of pristane/phytane and pristane/*n*-C₁₇ ratios is obvious, reflecting more favourable paleo conditions to the pristane antecessors in the Barreirinha radioactive unit, probably archaeobacterias, or even lower continental influence. The lower part of the Curiri Formation and the non radioactive interval of the Barreirinha Formation are characterized by the presence of higher molecular weight *n*-alkanes, which could be explained by the increased content of terrestrial derived organic matter.

Terpane and sterane biomarkers show distinct features through the analysed core samples. The Curiri Formation display high hopanes/steranes ratios (av. 12,90), decreasing values of tricyclics/hopanes to the bottom of this unit (from 0,43 to 0,12), and predominance of C₂₇ over C₂₈ and C₂₉ steranes. The values of hopanes/steranes and tricyclics/hopanes ratios may be mainly related to a greater input of terrestrial derived organic matter. The predominance of C₂₇ steranes, which normally indicates marine phytoplankton origin, could be related to acritarchs and algae in this interval. The upper unit of the Barreirinha Formation shows lower values of hopanes/steranes ratios (av. 6,13) and continuous decreasing values of tricyclics/hopanes (from 0,13 to 0,08), demonstrating lower bacterial and more abundant partially oxidized marine-derived organic matter. The predominance of C₂₉ over C₂₇ steranes could be attributed to increased humic debris as shown by organic petrography. The lower part of the Barreirinha Formation, the radioactive interval, is characterized by the lowest ratios of hopanes/steranes (av. 0,69), denoting higher marine organic matter input, and by the highest values of tricyclics/hopanes ratios (av. 0,74), indicating high percents of *Tasmanites* algae, (Aquino Neto et al., 1992). The variable predominance of C₂₇, and C₂₉ steranes could indicate some variations in the type of organic matter, from marine phytoplankton (C₂₇ steranes) to cyanobacterias (C₂₉ steranes).

References

- Loboziak, S.; Melo, J.H.G.; Matsuda, N.S. and Quadros, L.P. – 1997, Miospore Biostratigraphy of the Type Barreirinha Formation (Curuá Group, Upper Devonian) in the Tapajós River Area, Amazon Basin, North Brazil. *Bull. Centre Rech. Elf. Explor. Prod.*, **21**, 1, 187-205.
- Rodrigues, R. – 1982, Análise Geoquímica da Bacia do Amazonas: Integração Geoquímica das Bacias do Alto, Médio e Baixo Amazonas. PETROBRAS/CENPES, RJ, Relatório Interno.

PB2-1: Organosulfur compounds (OSCs) identified in modern lacustrine sediments: an extremely sulfur-rich sediment from A Maar, Kata-numa, Japan

K. Fukushima, M. Kato, S. Takamatsu, A. Yoda

Shinshu University, Matsumoto, Nagano 390-8621, Japan

Introduction

Sequestration of unsaturated fatty acids in surface sediments has been eventually ascribed to a selective degradation, because of less stability of unsaturated moieties against chemical (oxidation / reduction) and microbial attacks in the environments. Recent advances in the researches on organic sulfur compounds (OSCs: Sinninghe-Damsté and de Leuw, 1990; Urban *et al.*, 1999), however, have demonstrated a key role of sulfur in the early diagenesis of labile biological organic molecules. Possible reactions of sulfur are intra- and inter-molecular ones, the former of which will give simple OSCs, while the latter may result in a complex high-molecular weight kerogen-like material (Rullkötter, 2000). Simple OSCs hitherto identified in recent sediments are rather minor and limited. Lately, Russell *et al.* (2000) identified C₁₈ carboxylic acid isomers containing a thiophene in the carbon-chain, from the Neogene Tripoli Formation, Spain. Considering that sulfur tends to attack C=C double bonds, particularly dienes having structures facile to give thiophene (Sinninghe-Damsté *et al.*, 1989; De Graaf *et al.*, 1992; Fukushima *et al.*, 1992; Rowland *et al.*, 1993), the precursor of these thiophene carboxylic acids are thought to be octadeca-9,12-dienoic acids (linoleic acid, C_{18:2}).

In the present study, we detected trace amounts of some C₁₈ thiophene carboxylic acid isomers, as well as a series of alkylated thiophenes (Sinninghe-Damsté *et al.*, 1986) and C₃₅ hopanoid thiophenes in the surface sediment of an acidic and extremely sulfur-rich maar, Kata-numa, Japan. Among them, the formation of C₁₈ thiophenic carboxylic acids was confirmed by a simulation reaction of oleic acid (C_{18:2}) with H₂S in aqueous media.

Experimental

Kata-numa (surface area: 0.126 km², altitude: 306 m and maximum depth: 20 m) is a small maar located in the active geothermal field in Miyagi Prefecture. Evolution of hot spring water and fumaroles make the lake strongly acidic (pH \cong 2.2) and only some acid-tolerant benthic diatoms such as *Pinnularia braunii* var *amphicephala* and an insect *Chironomus* sp. are viable (Satake, 1980). The sediment taken from the center of the lake in Aug. 2000 is characterized by low (<0.6%) organic carbon and high free sulfur (up to 25%) concentrations. Freeze-dried sediment was extracted with benzene-methanol (6:4). The

extract was removed of sulfur (Blumer, 1975) and saponified. Aliphatic hydrocarbon fraction, separated from the neutral constituents was applied to an argentous silica gel column to concentrate those containing a thiophene ring. Fatty acids were methylated with BF_3 /methanol and purified according to the conventional procedure.

Free sulfur concentration in sediment was determined gravimetrically by extracting the dried sediment with carbon disulfide, supposed that the CS_2 -soluble organic matter is negligibly small in weight.

In order to confirm possible chemical reaction of linoleic acid with hydrogen sulfide, 100 μg linoleic acid was treated either with H_2S -saturated distilled water or the lake water in a sealed ampoule at 50 °C for more than 40 hrs (Fukushima et al., 1992). The reactants were extracted with n-hexane, removed of free S with activated Cu granules, dried, methylated on a silica gel column.

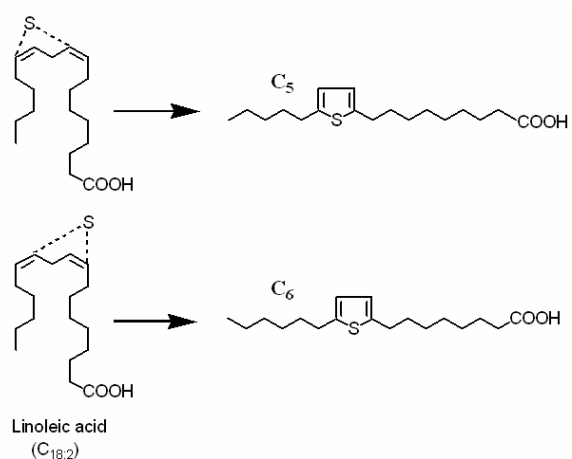
The lipid constituents were analyzed on a HP-5890 Series II gas chromatograph (GC) and an HP-6890 GC coupled with an HP-5973 MSD (GC-MS).

Results and Discussion

The OSCs identified in the hydrocarbon fraction from the lake sediment are series of 2-methyl-4-*n*-alkyl thiophenes (C_{13} - C_{20}), 2-ethyl-4-*n*-alkylthiophenes (the same carbon-number range), three C_{20} isoprenoid thiophenes and two C_{35} hopanoid thiophenes. The precursors of methyl- and ethylalkyl thiophenes are not known, while those of C_{35} hopanoid thiophenes should be functionalized hopanoids.

In the acid fraction, several isomers of C_{18} carboxylic acids with a thiophene ring are found, where C_5 and C_6 alkylated compounds were dominant. The simulation reaction of linoleic acid with H_2S in water evidently gave the two isomers, presumably *via* the mechanisms shown in the right Figure.

These findings prove sulfurization of unsaturated compounds occurring under the environments of sulfur-rich and slightly upraised temperature (50 °C) during the very early stage of diagenesis.



Possible Sulfurization Reaction of Linoleic Acid ($\text{C}_{18:2}$) to give two Major Thiophene Carboxylic Acid Isomers

PB2-2: Synthesis of novel isomers of phytanol and hydroxyarchaeol

Y. Hebting, R.E. Summons

Massachusetts Institute of Technology, Department of Earth, Atmospheric and Planetary Sciences, Cambridge, MA 02139, USA (e-mail: yhebting@mit.edu)

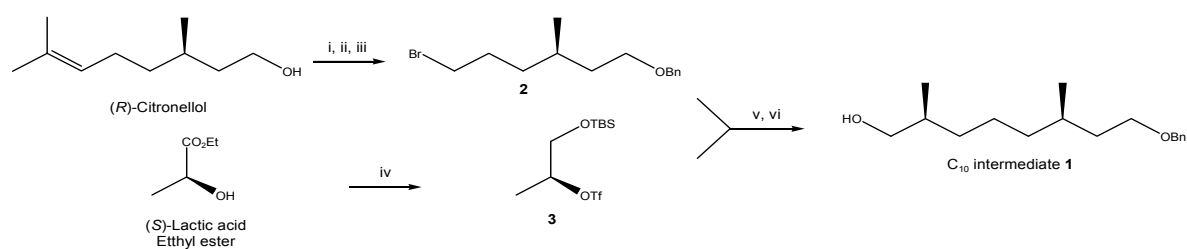
The main core lipids of archaea, and particularly methanogenic and methanotrophic archaea, comprise C₂₀ and C₄₀ isoprenoid chains linked through ether bonds to glycerol at the sn-2 or sn-3 positions. In some cases, the C₂₀ chains are hydroxylated at the C-3 position of the geranylgeraniol chains giving rise to hydroxyarchaeol. Additional structural diversity is encoded into the polar head groups attached to the glycerol ether cores. The structural diversity of methanogen polar lipids is most valuable when it can be directly correlated to 16S rRNA phylogeny [1].

Recently, structures of lipids from thermophilic methanogens (four *Methanococcus* species and *Methanopyrus kandleri*) have been systematically re-examined and many potential new biomarkers that have previously been overlooked have been identified. As well as archaeol, sn-2- and sn-3-hydroxyarchaeol, a dihydroxyarchaeol and isomers of the hydroxyarchaeols and caldarchaeols that are hydroxylated at 3 or 7 or 11 or 15 positions of both isoprenoid chains were tentatively identified [2]. Unambiguous structural assignments using conventional spectroscopic techniques are hampered given the amount available and the complexity of the mixtures studied. However, it is a relatively straightforward matter to compare the methanogen lipids with synthetic standards using liquid and gas chromatography as well as mass spectroscopy techniques. We therefore decided to undertake the total synthesis of the four different isomers of phytane hydroxylated on the methyl-bearing positions 3,7,11 or 15 respectively, as well as their dihydroxy homologues containing an additional hydroxyl function at C-1 for structural comparison purposes of individual C₂₀ isoprenoid alcohols and intact dihydroxyarchaeols.

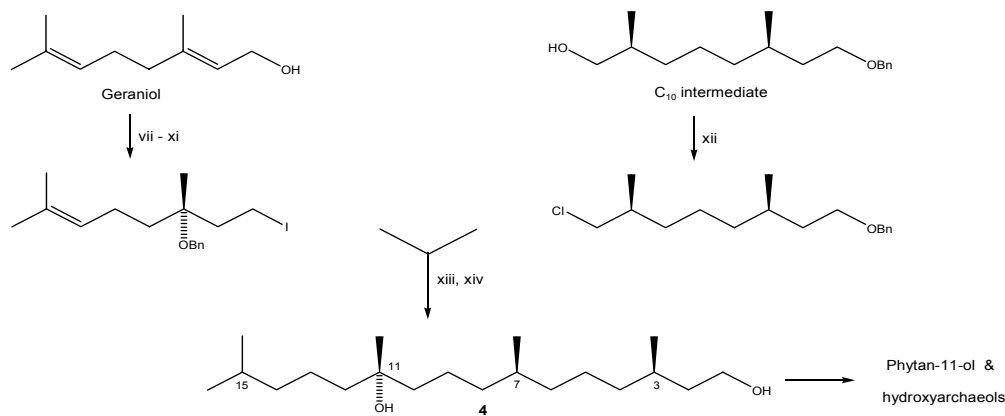
For the synthesis, we developed a shorter route to the previously described key intermediate C₁₀ compound 8-(benzyloxy)-2,6-dimethyloctan-1-ol **1** [3]. Its synthesis was accomplished by combining, through a challenging specific nucleophilic substitution on a secondary carbon, two natural products based synthons: a citronellol derived reagent **2**, namely (*R*)-6-(benzyloxy)-1-bromo-4-methylhexane and a C-3 substrate **3** derived from lactic acid, namely (*S*)-2-(trifluoromethanesulfonyloxy)-ethylpropanoate, using a Cu(I) catalyzed Grignard reaction [4] (Fig. 1, Scheme 1) without affecting the ester group. The synthetic approach of the most challenging isomer **4**, hydroxylated at positions 1 and 11, is depicted in

scheme 2 (Fig.1). The other three diol isomers were synthesized using similar methods, by coupling the intermediate C₁₀ compound to derivatives of citronellol and geraniol. In all cases, the hydroxyl group in C-1 was then selectively removed to yield the four isomers of phytanes hydroxylated at position 3, 7, 11 and 15. These were characterized by liquid and gas chromatography as well as mass and NMR spectrometry. Finally, structural assignments of methanogen phytanols were confirmed by comparison with the synthesized standards.

The four phytanediol compounds synthesized are projected to be coupled to glycerol to obtain isomers of dihydroxyarchaeols in order to provide standards for the structural elucidation of thermophilic methanogens and methanotrophs lipids isolated from naturally occurring extreme settings such as the Yellow Stone National Park and The Lost City Hydrothermal Field in the mid-Atlantic rift.



i) BuLi, BnBr; ii) O₃, NaBH₄; iii) CBr₄, PPh₃; iv) Tf₂O, 2,6-Lutidine; v) Mg, Cu(I); vi) DIBAL-H



vii) SAE; viii) Red-Al; ix) p-anisaldehyde dimethylacetal; x) DIBAL-H; xi) I₂, PPh₃; xii) TsCl, DMAP, TEA; xiii) t-BuLi; xiv) H₂, Pd/C

Fig.1. C₁₀ Intermediate and phytan-11-ol synthetic approaches

References

- [1] Hinrichs, K. U., Hayes, J. M., Sylva, S. P., Brewer, P. G. and DeLong, E. F., 1999. Methane-consuming archaeobacteria in marine sediments. *Nature*, 398, 6730, 802-805.
- [2] Summons R.E., Embaye T., Jahnke L.L. and Baumgartner M., 2002. New Ether Lipid Biomarkers from a Hyperthermophilic Methanogen, Abstracts with Program, 12th Annual VM Goldschmidt Conference, Davos Switzerland *Geochim. Cosmochim. Acta*, 66, A752.
- [3] Egushi T., Arakawa K., Terachi T. and Kakinuma K., 1997. Total synthesis of archaeal 36-membered Macrocyclic Diether Lipid. *J. Org. Chem.*, 62, 1924-1933.
- [4] Petit Y., Sanner C., and Larchevêque M., 1990. Stereoselective synthesis of optically active α -methyl esters. *Tetrahedron Lett.*, 15, 2149-2152.

PB2-3: Multidimensional GC-FID and GC-MS identification of cycloalkanes in Neoproterozoic sediments and crude oils from OmanY. Hebting¹, R. Nelson², C. Reddy², G. Frysinger³, E. Grosjean¹, R. Summons¹

1) Massachusetts Institute of Technology, Department of Earth, Atmospheric and Planetary Sciences, Cambridge MA 02139, USA (e-mail: yhebting@mit.edu)

2) Woods Hole Oceanographic Institution, Department of Marine Chemistry and Geochemistry, MS#4, Woods Hole MA 02543 USA

3) United States Coast Guard Academy, Department of Science, 27 Mohegan Ave., New London, CT 06320-8101, USA

Application of multidimensional GC-FID and GC-MS has enabled positive identification of two series of cyclic hydrocarbons in Precambrian oils and sediments from Oman: alkylcyclohexanes and alkylcyclopentanes (Fig.1). A clean separation of these cycloalkane series was afforded by their increased retention time, compared to co-occurring *n*-alkanes and isoalkanes, on the second, polarity based, chromatographic axis. The alkylcyclohexanes have slightly longer retention times compared to alkylcyclopentanes with a distinctive saw-tooth pattern revealing a novel even-over-odd predominance for the alkylcyclopentanes and an odd-over-even for the alkylcyclohexanes. A quantitative analysis revealed a maximum at total carbon numbers of C₁₇ and C₁₈.

Alkylcyclohexanes were identified by coinjecting commercially available standards. As the alkylcyclopentanes are not commercially available, their initial identification was based on mass spectra obtained in GC-MS using a Time-of-Flight mass analyser. The occurrence of alkylcyclopentanes has previously been reported in various sediments and oils but their structures have never been rigorously established [1]. Here we present the first unambiguous characterization of alkylcyclopentanes in oils and sediments by coinjection of synthetic standards.

A previously published organic synthesis of alkylcyclopentanes, using the Grignard and Wurtz reactions, with unsatisfying synthetic yields was devoid of any spectral information that could be used for comparative purposes [2], [3]. We therefore decided to develop a more efficient synthesis of alkylcyclopentanes of a series of representative homologues to establish unequivocally the structure of these compounds.

Our synthetic approach was initially based on the improvement of described procedures of the Grignard reaction. All possible combinations using cyclopentyl and alkyl reagents were unsuccessful in our hands, giving reduction reaction and other undesired side products of Wurtz coupling, despite modifications in reagents, solvents, complexing agents and temperature. We then attempted a phosphorus-based Wittig reaction on cyclopentanone. The reaction halted at the oxaphosphetane reaction intermediate. Finally, when the reverse strategy was used, with cyclopentanebromide and alkyl aldehyde, the reaction proceeded

smoothly. The first step produced alkylcyclopentenes in 85-90% yields which were then quantitatively hydrogenated over platinum oxide in refluxing ethyl acetate to yield the desired alkylcyclopentanes. Coinjections of the synthetic alkylcyclopentanes in multidimensional GC with the alkane fractions of Oman samples were successful and confirmed our initial identifications.

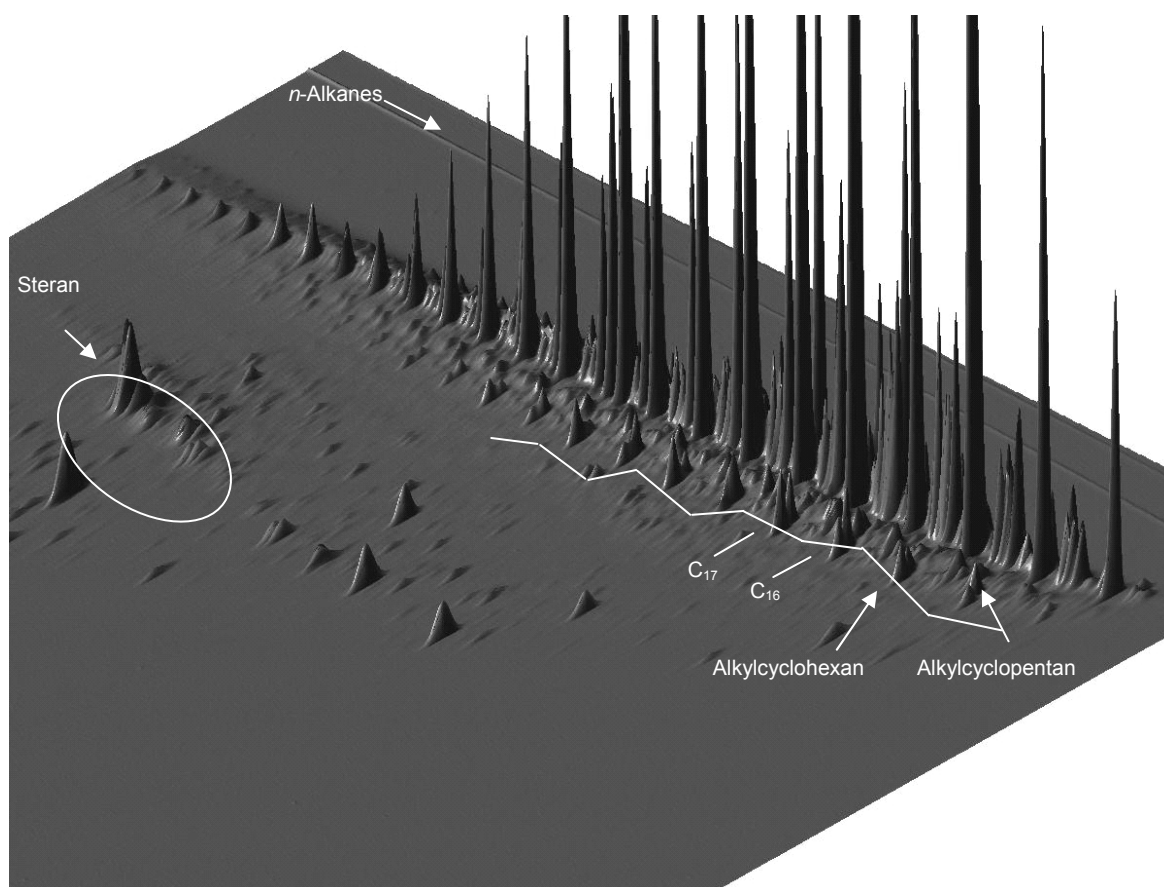


Fig.1. Multidimensional gas chromatographic data for saturated hydrocarbons from a sediment sample from the Thuleilat Shale depicts the oscillating relative abundances of cyclohexanes compared to cyclopentanes.

The origins of these alkylcyclopentanes and alkylcyclohexanes remain unknown. The pattern of carbon number predominance of alkylcyclopentanes compared to the cyclohexanes suggests a common origin from distinctive biotic precursors, possibly through cyclisation of linear compounds with specific loci of unsaturation.

References

- [1] Yamamoto, S., Ishiwatari, R., Machihara, T. and Morinaga, S., 1990. Characterization of hydrocarbons from sediments of the Panama Basin (ODP Hole 677A and 678B). *Res. Org. Geochem.* 7, 41-44.
- [2] Schmidt, A. W., 1940. Physical data on monoalkylcyclopentenes and cyclopentanes. *Ber.* 73B, 359-366.
- [3] Antheaume, J. and Guiochon G., 1965. Application de la chromatographie en phase gazeuse à l'étude de la composition des fractions moyennes d'un brut pétrolier. *Bull. Soc. Chim. Fr.* 2, 298-307.

PB2-4: Regular isoprenoid hydrocarbons C₁₃-C₂₀ in recent sediments of hypersaline Lake Karachi, West Siberia

E.A. Kurakolova, V.N. Burkova

Institute of Petroleum Chemistry SB RAS, 634021, Tomsk (Russia) (e-mail: ovs@ipc.tsc.ru)

According to Kissin (1993) regular low-molecular isoprenoid HCs (RLI) of crude oils ranging from C₉ to C₁₆ are formed by alteration of two predecessors, Pr and Ph. The chemical reactions are: extensive thermal cracking giving isoprenoids and branched olefins and the latter conversion into saturated analogues promoted by acidic clays. The only favourable factor to produce the lighter homologues of RLIs is prolonged thermolysis, which takes place during late catagenesis. As a result the equal distribution of isoprenoids, especially amongst C₁₄ - C₁₆, occurs in crude oils of the same maturity regardless of their geographical locations.

Basing on this finding and taking into account that Pr and Ph are originated from chlorophylls in early diagenesis we suppose that relative abundance of a RLI comparing to its predecessors can be used for distinguishing among geological samples of different maturity. In fact $i\text{-C}_{16}/\text{Pr}+\text{Ph}$ ratios for objects studied by Kissin seem to be satisfactory: 0-0.2 in oil shales, Green River including, about 0.5 in heavy naphthenic oils and up to 1.0 in low-gravity paraffin oils and in condensates. The results allow us to consider this ratio as a parameter of sedimentary OM maturity.

Whereas light HCs of immature sediments are considered as redeposited, information about sedimentary isoprenoids lighter than Pr and Ph is scanty (Barrick et al., 1980; Yunker et al., 1993; Peters and Moldowan, 1993). They are found to be ubiquitous, minor, equally distributed all along a sedimentary basin and lack in $i\text{-C}_{12}$ and $i\text{-C}_{17}$ homologues. From this viewpoint it was of interest to study RLIs, which occurred in recent sediments of hypersaline Lake Karachi (West Siberia). Sediments were taken out in a summer season.

In the sediments RLIs are represented by a series of homologues $i\text{-C}_{13-20}$. They occur as freely extracted HCs and as inclusions within both aluminium silicate and protokerogen matrixes. In the surface sediments by the eastern lakeside RLI homologue distributions are uniform with a gradual, rather linear, decrease in concentration along with diminution of their molecular masses contrary to exponential relations established by Kissin in mature samples. Nearly the same RLIs distributions are revealed in the sedimentary column extracted at depths up to 1 m except for the core of the 10-20 cm interval, which markedly differing by higher anoxity is enriched with Pr and Ph and contains little or no isoprenoids lighter than C₁₆.

The portions and homologue distributions of freely extracted RLIs occurring in bottom sediments which were mined across the lake westward gradually become much dissimilar to those in the eastern samples. Thus, the RLI portions in the whole HC fractions are about 3

times more in western samples than in the eastern ones. RLIs of western sediments are also clearly distinguishable by nonlinear C₁₃-C₂₀ homologues distributions that are far from exponential as well. Actually there are abundances of Pr and Ph together with the predominance of their lightest products, i.e. i-C₁₅ and i-C₁₄, in the surface sediments deposited by the western lakeside. It follows that i-C₁₆/Pr+Ph ratios vary in bottom sediment layer corresponding to figures of heavy oils to the east and of oil shales – to the west (Table).

Isoprenoid ratios	In bottom sediments				In 10-20 cm core; freely extracted; east
	Freely extracted		In protokerogen; east	In mineral; east	
	East	West			
i-C ₁₄ /Pr+Ph	0.06	0.40	0.15	0.10	-
i-C ₁₅ /Pr+Ph	0.29	0.64	0.35	0.36	0.07
i-C ₁₆ /Pr+Ph	0.58	0.20	0.47	0.50	0.11
i-C ₁₈ /Pr+Ph	0.65	0.35	0.59	0.63	0.40

The i-C₁₄₋₁₅/Pr+Ph ratios of the sediments obtained in the western area contradict to the conclusion though. We presume to come out with a suggestion in this respect.

Abundance and uneven distribution of RLIs all along the lake testify against their petrogenesis. Model simulation carried out under conditions close to natural has proved a possibility of RLI origin from immature OM through its intensive bacterial reworking; at that i-C₁₆/Pr+Ph parameter increased up to the figures of heavy oils.

Unlike eastern sediment HCs, which comprise mainly the inputs of planktonic organisms and higher terrestrial plants, HCs of the western sediments are characterized with abundance of both bacterially reworked components (UCM hump, steranes and hopanes of so called “biogenic oils”) and newly synthesized by photo- and non-specific bacteria (n-alkenes, phytanes, low-molecular n-alkanes of C₁₂ - C₂₂ range with prevalence of even members).

Despite the lake is about 700 m wide there is a noticeable difference in living organism distributions between two areas. Thus, one can observe no algal mats of *Microcystis sal.* but a great number of brine shrimps *Artemia sal.* occurring by the western lakeside as well as *Artemia* eggs ashore. Specific pigments, i.e. cantoxantine, myxoxantophylls, echinenone and chlorophylls distribution in these sediments confirms the observation. To saprophytes, a physiological group of the benthos microbiocoenosis, which are drawn towards cyanobacteria in eastern area, other groups of bacteria are gradually added: first denitrifying, then sulfur oxidizers and at last sulfur reducers as to coming near the western lakeside.

These facts are evidence of an anoxic environment in western area, which is likely to prevent chlorophyll degradation as it was seen in the 10-20 cm core. Besides the lack of cyanobacteria makes *Artemia* eat other photobacteria, and bacteriochlorophylls become the main source of RLIs. Isoprenoid releasing process might proceed via biotransformation with farnesane as the parent member of the RLI series.

PB2-5: Cyclisation of PUFAs as a pathway to cyclic compounds in sedimentary organic matterD.A. Lang¹, B.G.K. van Aarssen¹, T.P. Bastow^{1,2}

1) Centre for Applied Organic Geochemistry, Curtin Univ., GPO Box U1987, Perth 6845, Western Australia

2) CSIRO Land and Water, Private Bag No 5, PO Wembley, Perth WA 6913, Australia

Fatty acids (FAs) are an essential component of many lipids and are abundantly present in the natural environment. Algae and bacteria are particularly rich sources of polyunsaturated fatty acids (PUFAs). Although most fatty acids are readily mineralised, it is quite conceivable that a fraction can be preserved upon deposition, and either be incorporated into kerogen, or react to form other products. It can thus be envisaged that these compounds may eventually contribute to the formation of petroleum. In this paper we pursue the possibility that PUFAs may undergo cyclisation during diagenesis.

A series of off-line pyrolysis experiments were carried out to determine the extent of cyclisation experienced by PUFAs under elevated temperatures. These experiments were carried out in an inert atmosphere, as PUFAs are known to react easily with oxygen. Docosahexaenoic acid (DHA) and eicosapentaenoic acid (EPA), ethyl esters with six and five double bonds respectively, produced a suite of aromatic compounds when heated at 290°C with a Pt/C catalyst. The reaction mixtures were dominated by compounds containing one carbon less than the parent PUFA, reflecting cyclisation, aromatisation, hydrogenation and decarboxylation reactions.

In addition to *n*-alkanes, homologous series of alkylbenzenes, alkylbiphenyls and alkylnaphthalenes were formed as products of these reactions, with small amounts of phenanthrene formed as well. The series of alkylbenzenes and alkylbiphenyls all displayed an *ortho* configuration, reflecting the preferred cyclisation pathway of PUFAs. Interestingly, at lower reaction temperatures (180°C) significant amounts of cyclic compounds were produced, with most of these present as ethyl esters. This suggests that decarboxylation is not necessarily the first reaction that PUFAs undergo to start off the cyclisation process.

The addition of water induced a further degree of cyclisation. *o*-Terphenyl and *o*-methylterphenyl were formed in high relative abundances. It is still unclear how the presence of water aids in the cyclisation. It is possible that water limits hydrogenation occurring, thus enabling more double bonds in a molecule to partake in the cyclisation.

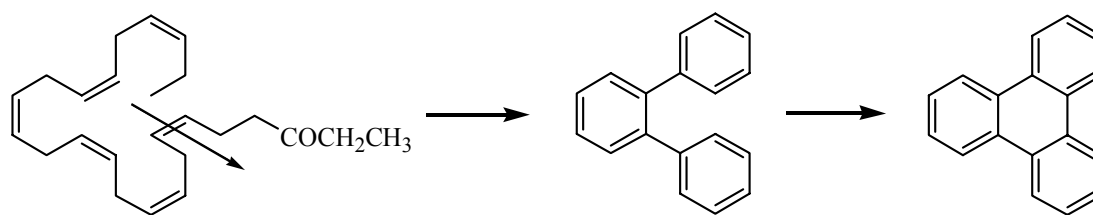


Fig.1. The formation of *o*-terphenyl and triphenylene through the cyclisation of DHA ethyl ester

These findings suggest that cyclic components of algal rich sediments may also demonstrate these characteristics. This may be shown by a high relative abundance of aromatic moieties, with one less carbon than common PUFAs. A dominance of compounds in an *ortho* configuration may also indicate a high algal input, although such characteristics are likely to wane upon maturation. Especially the presence of structurally specific PAHs such as *o*-terphenyl and triphenylene may prove to be a useful indicator of contributions of PUFAs to sedimentary organic matter.

References

Bastow, T. P., van Aarssen, B. G. K., Grice, K., Alexander, R. and Kagi, R. I. 2001, 'Origins of some alkylbiphenyls', in *20th International Meeting on Organic Geochemistry*, Nancy, France.

PB2-6: An original aromatisation pathway of higher plant triterpenoids in recent sediments

C. Le Milbeau, P. Schaeffer, P. Adam, P. Albrecht

Laboratoire de Géochimie Bio-organique, UMR 7509 du CNRS, Ecole de Chimie, Polymères et Matériaux, Université Louis Pasteur, 25 rue Becquerel, 67200 Strasbourg, France (e-mail: pschaeffer@chimie.u-strasbg.fr)

The hydrocarbon skeletons of higher plant triterpenoids undergo various transformations in recent sediments, and among these, aromatisation is one of the most important microbially-mediated process that occurs at the earliest stages of diagenesis [1-3]. This process can start with the loss of the ring A of the triterpenoid, followed by progressive aromatisation from the ring B to the ring D, leading to the formation of mono- and polyaromatic tetracyclic hydrocarbons. Alternatively, aromatisation may start directly in ring A, triggered by the loss of the oxygenated functionality at C-3, and proceeds from ring A to ring D, yielding mono- to tetraaromatic pentacyclic hydrocarbons.

In the course of a detailed molecular investigation of various freshwater recent sediments, the « usual » higher plant triterpenoids, including notably the aromatic triterpenoids described above, were observed, together with another series of unknown triterpenoids bearing a keto or an hydroxy functionality. On the basis of their molecular ions and mode of fragmentation in mass spectrometry, the compounds of the latter series were thought to correspond to novel aromatic derivatives. In particular, one compound having the polarity of ketones showed a mass spectrum with strong similarities with that of the ring B monoaromatic fernane derivative identified by Hauke et al. (1992) [4] and hence, this ketone was originally thought to be related to fernenes. Since the same compound was also observed among the triterpenoids of an organic residue collected from an archaeological oak wood piece in which it was present in sufficient amounts to allow its isolation, we carried out its structural identification by means of 1D and 2D NMR studies. Thus, we could determine that the hydrocarbon skeleton of the isolated compound was not related to fernene derivatives as initially expected, but to higher plant triterpenoids of the oleanene series (**1**, fig. 1). Furthermore, structural identification allowed to establish that aromatisation has occurred in ring D and that the keto group was located at the C-2 position instead of the usual C-3 position. By analogy with the fragmentation pattern observed for this compound in MS, di- and triaromatic ketones which possibly bear C, D and E aromatic rings were also tentatively identified (fig. 1) and may represent the possible intermediates between a functionalised precursor molecule such as maslinic acid (**2**, fig. 1) detected in the sediments investigated and

PB2-7: LC-MSⁿ studies of defunctionalised chlorophyll derivatives in the Vena del Gesso basin

D.H. Mawson, B.J. Keely

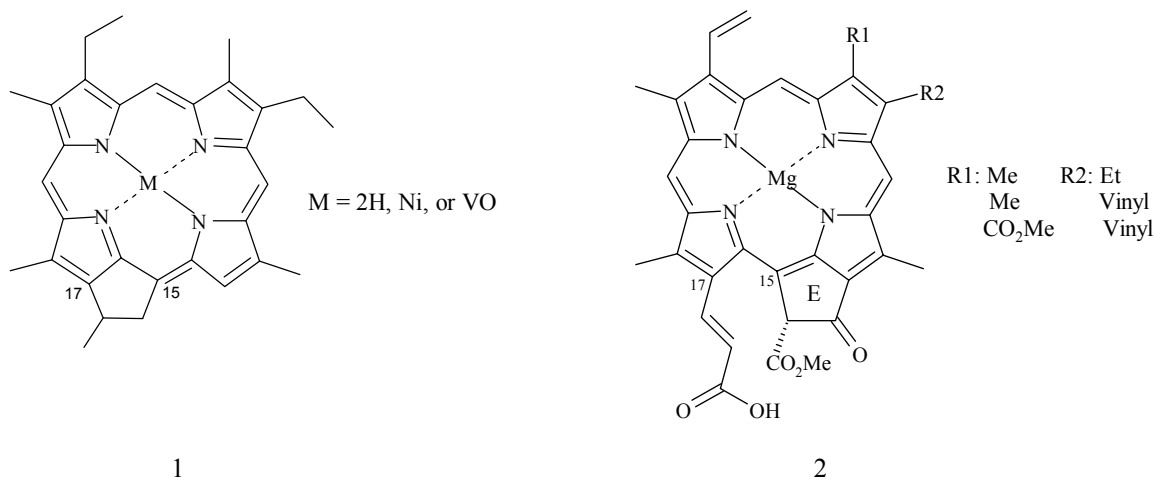
University of York, Dept of Chemistry, Heslington, York, YO10 5DD, UK (e-mail: dhm102@york.ac.uk)

Miocene sediments of the Vena del Gesso basin (Northern Italy) have been shown to contain free base alkyl porphyrins together with unidentified chlorins and the aromatic carotenoid isorenieratene (Keely et al., 1995). The co-occurrence of both classes of tetrapyrroles indicates that the conversion of chlorins to porphyrins, as proposed in the Treibs scheme (Treibs, 1936; Keely et al., 1990), has not proceeded to completion. Source specific porphyrin structures either bear a structural resemblance to their precursor pigments, such as extended alkylations at the C-8 or C-12 positions of their macrocycle (Ocampo et al., 1985), or arise from specific rearrangement of substituents during diagenesis. An example of the latter is the group of porphyrins exhibiting five-membered exocyclic rings between the C-15 and C-17 positions of their macrocycles (e.g. 1; Ocampo et al., 1984; Verne-Mismer et al., 1988), which have been proposed to arise from chlorophyll *c* (2) *via* a rearrangement involving ring E, and the C-17 acrylic acid chain. This reaction is known to occur under acidic conditions (Dougherty et al., 1970) and may have diagnostic implications.

Defunctionalised chlorophyll derivatives within a single horizon of the Vena del Gesso sediment have been examined using a reversed phase high performance liquid chromatography method (Airs et al., 2001). Separation of chlorin / porphyrin mixtures has been achieved, and the identities of the chlorophyll fossils present determined using liquid chromatography – multistage tandem mass spectrometry (LC-MSⁿ). Although separation of alkyl porphyrins typically relies upon normal phase chromatographic methods (Barwise et al., 1986), the resolution achieved using the reversed phase method is comparable to that accomplished using the normal phase solvent programme. The LC-MSⁿ approach for the identification of components has allowed the detection of a wider variety of tetrapyrroles in this sedimentary sequence than was possible previously (Keely et al., 1995). The components identified include a number of highly defunctionalised chlorophyll derivatives, representing the later stages of the Treibs transformation scheme, some of which represent previously unreported structures.

The abundances of key porphyrins and chlorins have been profiled throughout a 130 cm section of the Vena del Gesso core (marl IV; Keely et al., 1995) and reveal distinct variability in the distributions of the chlorin and porphyrins present. The stratigraphic studies

of the chlorin / alkyl porphyrin distributions facilitate the development of a better understanding of the environmental factors that influence transformation pathways and rearrangements of chlorophylls during diagenesis.



References

- Airs, R. L., Atkinson, J. E., Keely, B. J., 2001. Development of a high resolution liquid chromatographic method for the analysis of complex pigment distributions. *Journal of Chromatography A* 917, 167-177.
- Barwise, A.J.G., Evershed, R.P., Wolff, G.A., Eglinton, G., Maxwell, J.R., 1986. High Performance Liquid Chromatographic analysis of free base porphyrins I. An improved method. *Journal of Chromatography* 368, 1-9.
- Dougherty, R. C., Strain, H. H., Svec, W. A., Uphaus, R. A., Katz, J. J., 1970. Structure, properties, and distribution of chlorophyll *c*. *Journal of the American Chemical Society* 92, 2826-2833.
- Keely, B. J., Prowse, W. G., Maxwell, J. R., 1990. The Treibs hypothesis: An evaluation based on structural studies. *Energy and Fuels* 4, 628-634.
- Keely, B. J., Blake, S. R., Schaeffer, P., Maxwell, J. R., 1995. Distributions of pigments in the organic matter of marls from the Vena del Gesso evaporitic sequence. *Organic Geochemistry* 23, 527-539.
- Ocampo, R., Callot, H. J., Albrecht, P., Kinzinger, J. P., 1984. A novel chlorophyll-*c* related petroporphyrin in oil-shale. *Tetrahedron Letters* 25, 2589-2592.
- Ocampo, R., Callot, H. J., Albrecht, P., 1985. Occurrence of bacteriopetroporphyrins in oil shale. *Journal of the Chemical Society, Chemical Communications* 4, 200-201.
- Treibs, A., 1936. Chlorophyll and hemin derivatives in organic materials. *Angewandte Chemie International Edition* 49, 682-686.
- Verne-Mismer, J., Ocampo, R., Callot, H.J., Albrecht, P., 1988. Molecular fossils of chlorophyll-*c* of the 17-nor-DPEP series – structure determination, synthesis, geochemical significance. *Tetrahedron Letters* 29, 371-374.

PB2-8: Photoinhibition of the marine picoalgal niche: a control on C₃₀ sterane abundance in geological samples

D. Rocher

Baseline Resolution Inc., 8701 New Trails Drive, The Woodlands, Texas 77381 (e-mail: DRocher@brilabs.com)

The picoalgal niche hypothesis [1] is based upon the population dynamics of the contemporary picoplanktonic pelagophyte alga *Aureococcus anophagefferens*. Specific water column conditions allow *Aureococcus* to out-compete similar sized organisms - particularly the cyanobacterium *Synechococcus* - for position within the photic zone of shallow bays and estuaries. High water clarity and low nutrient levels favor the growth of *Synechococcus* while *Aureococcus* prefers turbid water containing high levels of organic carbon and nitrogen. *Aureococcus* is susceptible to photoinhibition because it synthesizes few photoprotective carotenoids [2]. Consequently, it must dwell in the shade of *Synechococcus* blooms for protection. As a *Synechococcus* bloom declines and decomposes, organic nutrients are released. When this is accompanied by wave-generated sediment resuspension, *Aureococcus* can bloom in the now turbid water and dominate the picoalgal niche.

Pelagophyte algae are the primary source of sedimentary propylcholesterols [3,4], precursors of the C₃₀ steranes that differentiate marine from non-marine depositional environments [5]. Propylcholesterols serve as defensive compounds against filter-feeding metazoans [6], although detection of their diagenetic derivatives in sediments deposited before the advent of predation [7] indicates that this was not their original function. Minor amounts of propylcholestane isolated from the hydrogenation products of a prasinophyte [8] suggest that green algae may have contributed to the low levels of C₃₀ steranes reported from Proterozoic and Lower Paleozoic sediments. During the Late Paleozoic, a dramatic increase of sedimentary propylcholesterols can be interpreted as a biosynthetic defensive response by pelagophyte algae to the filter-feeding metazoans that comprise Sepkoski's Marine Evolutionary Fauna #2. The mismatch between the low diversity of Late Paleozoic phytoplankton compared to the elevated diversity of benthic marine invertebrates [9] can be resolved – at least partially - by invoking a major radiation of pelagophyte algae. Their small size and nondescript features account for the lack of visual recognition of pelagophytes in the fossil record.

The switch from evolutionary development to deposition and diagenesis as the primary controls on the sedimentation of propylcholesterols was recorded in Lower Permian rocks wherein the range of abundance reached levels typical of younger rocks. Carbonate

rocks contain a lower percentage of C30 steranes compared to shales [10]. Such a finding is explained by equating *Synechococcus* domination of the picoalgal niche with carbonate deposition, and *Aureococcus* domination of the picoalgal niche with shale deposition. *Synechococcus* is included among contemporary microbial species capable of producing calcium carbonate minerals [11]. C30 sterane and C34 hopane concentrations are inversely correlated [10]. As predominance of C34 hopane within homohopane distributions is considered indicative of carbonate deposition, sediments containing this biomarker configuration were likely deposited when cyanobacteria occupied the picoalgal niche at the expense of pelagophyte algae.

References

1. Gobler CJ, Renaghan MJ, Buck NJ (2002) Impacts of nutrients and grazing mortality on the abundance of *Aureococcus anophagefferens* during a New York brown tide bloom. *Limnol. Oceanogr.* V.47/1, p.129-141
2. MacIntyre HL, Lomas MW, Cornwell J, Suggett DJ, Gobler CJ, Koch EW, Kana TM (2003) Mediation of benthic-pelagic coupling by microphytobenthos: an energy- and material-based model for initiation of blooms of *Aureococcus anophagefferens*. Abstract. 2nd Symposium on Harmful Marine Algae in the U.S. 8-13 Dec 2003, Marine Biological Laboratory, Woods Hole, Massachusetts
3. Giner JL, Boyer GL (1998) Sterols of the brown tide alga of *Aureococcus anophagefferens*. *Phytochemistry* V.48/3, p.475-477
4. Giner JL, Li X, Boyer GL (2001) Sterol composition of *Aureococcus lagunensis*, the Texas brown tide alga. *Phytochemistry* V.57/5, p.787-789
5. Moldowan JM, Seifert WK, Gallegos EJ (1985) Relationship between petroleum composition and depositional environment of petroleum source rocks. *AAPG Bulletin* V.69/8, p.1255-1268
6. Giner JL, Boyer GL, Faraldos JA, Li X, Zhao H (2001) Unusual sterols from harmful algae: more than biomarkers? Abstract. ASLO Aquatic Sciences Meeting, 12-16 Feb 2001, Albuquerque, New Mexico
7. Brocks JJ, Buick R, Summons RE, Logan G (2003) A reconstruction of Archean biological diversity based on molecular fossils from the 2.78 to 2.45 billion-year-old Mount Bruce Supergroup, Hamersley Basin, Western Australia. *Geochimica et Cosmochimica Acta*, V.67/22, p.4321-4335
8. Volkman JK, Barrett SM, Dunstan GA, Jeffrey SW (1994) Sterol biomarkers for microalgae from the green algal class Prasinophyceae. *Organic Geochemistry* V.21/12, p.1211-1218
9. Strother PK, MacRae RA, Fricker A, Fensome RA, Williams GL (1996) Phanerozoic phytoplankton diversity is decoupled from marine invertebrate diversity. Abstract. Ninth International Palynological Congress, 23-28 June 1996, Houston, Texas
10. Peters KE, Moldowan JM (1993) *The Biomarker Guide*. Prentice Hall, Englewood Cliffs, New Jersey
11. Yates KK, Robbins LL (1998) Production of carbonate sediments by a unicellular green alga. *American Mineralogist*, V.83, p.1503-1509

PB2-9: Distributions and sources of hopanoids in sediments from ODP Leg 190, Nankai Trough, Japan

H. Saito, N. Suzuki, K. Sawada

Division of Earth and Planetary Sciences, Graduate school of Science, Hokkaido University, N10 W8, Kita-ku, Sapporo 060-0810, Japan (e-mail: saito@ep.sci.hokudai.ac.jp)

The total amount of prokaryotic cellular carbon on the Earth is estimated to be 350-550 Gt of C, which is 60-100 % of the estimated total carbon in plants [1]. However, total biomass of prokaryotes in subsurface sediments is still uncertain. Our knowledge on microbes living in deep subsurface sediments is limited. Among various biomarkers of prokaryotes, hopanoids in sediments can provide useful information to estimate prokaryote biomass in deep sedimentary basin. Hopanoids in deep subsurface sediments, however, are generally thought to be fossil molecules of eubacteria which were living in the comparatively aerobic environment, since hopanoids have not yet been identified in obligately anaerobic bacteria [2]. Hopanes, hopanoic acids, hopanols, and other related compounds were investigated in the present study to understand the distributions and sources of hopanoid compounds in deep subsurface sediments from ODP Leg 190, Nankai Trough.

The Japanese Island arc system is flanked to the east by deep trenches which are subduction boundaries of the Pacific and Philippine Sea oceanic plate. Nankai Trough is located between plate boundaries of the Shikoku Basin and the southwest Japan arc. One of the objectives of ODP Leg 190, Nankai Trough was to clarify the interplay of various processes taking place in the Nankai Trough accretionary prism. Prokaryotes in sediments play an important role for material transformation and circulation during the diagenesis. Significant amount of bacteria have been detected in many of the samples based on the direct observation of microbes under the microscope on board ship during ODP Leg 190. The sediment samples from ODP Leg 190, Sites 1175, 1176 and 1178 in Nankai Trough were used for geochemical analyses in the present study.

The average TOC concentrations of the samples from Sites 1175, 1176 and 1178 were 0.58 %, 0.53 % and 0.78 %, respectively. The samples from 200 to 400 mbsf (Subunit IIA) at Site 1178 are characterized by high TOC concentrations, high C/N ratios, high concentrations of plant-derived long chain *n*-alkanes, *n*-alkanoic acids and *n*-alkanols, and their high terrigenous to aquatic (H/L) ratios, showing richness of terrigenous organic matter.

The concentrations of total hopanes and the diagenetic products of diploptene in the samples from Site 1178 were higher than those at Sites 1175 and 1176. This is attributed to that the diagenesis is more progressive at Site 1178 because of the older geologic age

compared to Sites 1175 and 1176. Although diploptene was commonly detected in all the samples from Sites 1175 and 1176, the concentration was not high to be 3.2 $\mu\text{g/g}$ TOC at most. Hop-17(21)-ene to diploptene ratios decrease with depth.

The major hopanoid in the acid fraction was 17 β (H), 21 β (H)-bishomohopanoic acid. The concentrations of total hopanoic acids tend to be higher in Subunit IIA at Site 1178 characterized by much contribution of terrigenous organic matter. It is suggested that hopanoic acids are mainly terrestrial organic compounds derived from oxidation products of bacteriohopanepolyols on land.

The C₃₁-C₃₃ series of 17 β (H), 21 β (H)-hopanols and hopanediols were detected in the alcohol fraction treated with BSTFA. In addition to hopanediols, hopanetriols and trace hopanetetrols were detected in the acetylated samples. Most of them have shorter side-chains. The 17 β (H), 21 β (H)- bishomohopanol was the most abundant. The concentrations of total hopanols in the samples from Sites 1175 and 1176 are nearly constant. The concentrations of total hopanols in sediments at Site 1178 are comparatively high and tend to decrease with depth. The variation of hopanol distribution can not be explained by diagenetic change with depth. Drastic increase of both concentrations and H/L ratios of *n*-alkanols in sediments from Subunit IIA at Site 1178 reflects significant variation of terrestrial organic matter contribution, whereas the concentration of total hopanols decreases with increasing depth.

Polyfunctionalised hopanoids with shortend side-chains have been detected in lacustrine sediments and cultured bacteria [3, 4]. They could be biomarkers directly obtained from living bacteria or intermediates of biohopanoids. The hopanepolyols were identified up to about 400 mbsf, and the presence of hopanepolyols in the comparatively old and mature sediments suggests their origin of living bacteria. These results suggest that the hopanols in deep subsurface sediments from Site 1178 were possibly originated from in situ living bacteria.

References

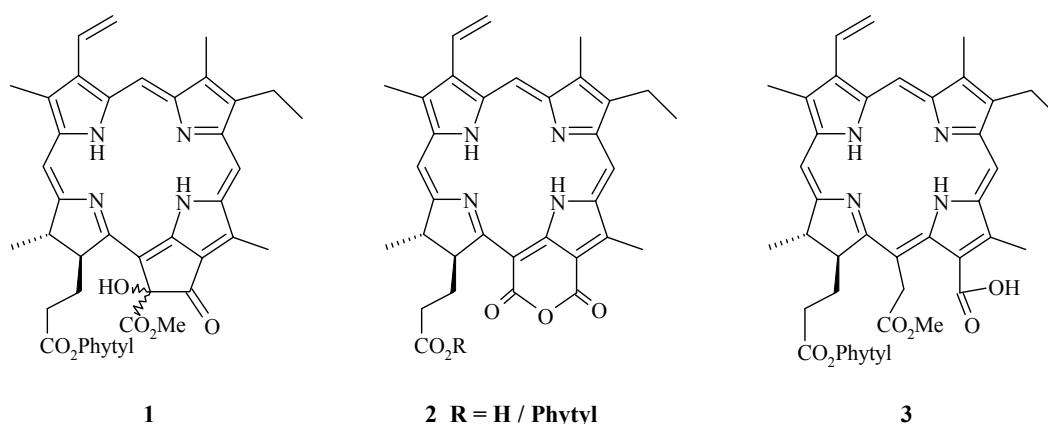
- [1] Whitman, W.B., Coleman, D.C., Wiebe, W.J., 1998. Prokaryotes: The unseen majority. Proceedings of the National Academy of Sciences of the United States of America 95, 6578-6583.
- [2] Rohmer, M., Bouvier, P., Ourisson, G., 1984. Distribution of hopanoids triterpenes in prokaryotes. Journal of Genetic Microbiology 130, 1137-1150.
- [3] Rodier, C., Llopiz, P., Neunlist, S., 1999. C₃₂ and C₃₄ hopanoids in recent sediments of European Lakes: novel intermediates in the early diagenesis of biohopanoids. Organic Geochemistry 30, 713-716.
- [4] Peiseler, B., Rohmer, M., 1991. Prokaryotic triterpenoids. (22R,32R)-34,35-dinorbacteriohopane-32,33-diols from *Acetobacter aceti* ssp. *Xylinum*: New bacteriohopane derivatives with shortened side chain. Journal of Chemical Society, Perkin Transaction 1 2449-2453.

PB2-10: An overview of pigment oxidation reactions and the potential use of tetrapyrroles as indicators of oxygen availability

J.S. Walker, B.J. Keely

Department of Chemistry, University of York, Heslington, York, YO10 5DD, UK

Functionalised chlorophyll derivatives that are products of oxidation reactions centred on ring E occur widely in sediments. Structures identified include hydroxyl- (**1**; Airs et al., 2000), anhydride (**2**; Naylor et al., 1998), and ring-opened derivatives (**3**; Airs et al., 2000). The same species also occur in extracts of senescent algal cells, indicating the facile nature of the oxidation reactions (Louda et al., 1998, 2002).



Chlorophyll oxidation occurs by two distinct mechanistic pathways, type 2 leading to destruction of the macrocycle and type 1 to structures in which the macrocycle remains intact. Detailed studies of the reaction products of type 1 chlorophyll oxidation reactions have been performed in the laboratory, employing isotopic labelling and detailed analysis including LC-MSⁿ. The work extends earlier studies of the mechanism (Woolley et al., 1998) and has allowed the formulation of a new mechanism that fully accounts for the range of structures formed in laboratory studies in solvent and also accounts for the analogous structures formed in the natural environment. Thus, autoxidation reactions are implicated in the production of the ring-opened derivatives and it is evident that they play an important role in the fate of chlorophyll in many environments.

Studies of water column particulates and sediments in Lake Baikal by liquid chromatography multistage tandem mass spectrometry (LC-MSⁿ) reveal a larger reservoir of chlorophyll oxidation products than has been observed previously in studies of natural waters and sediments. The greater relative abundance of oxidation products within this reservoir is consistent with type 1 oxidation reactions of chlorophyll occurring mainly in the water column. When interpreted in conjunction with the revised mechanistic pathway, the results

validate the use of sedimentary pigment ratios as indicators of changes in oxygen availability within the water column of lakes in times past (Walker et al., 2002). Thus, it appears likely that sedimentary pigment signatures have the potential for use in palaeoenvironmental studies to provide a proxy for oxygen availability within the water column. There are, however, several issues to be addressed before comparisons that reveal differences in relative levels of oxygenation can be superseded by more exact estimates of mean water column oxygenation.

References

- Airs R.L., Jie C., Keely B.J. (2000). A novel sedimentary chlorin: structural evidence for a chlorophyll origin for aetioporphyryns. *Organic Geochemistry*, 31, 1253-1256.
- Louda J.W., Li J., Liu L., Winfree M.N., Baker E.W. (1998). Chlorophyll *a* degradation during cellular senescence and death. *Organic Geochemistry*, 29, 1233-1251.
- Louda J.W., Liu L., Baker E.W. (2002). Senescence- and death-related alteration of chlorophylls and carotenoids in marine phytoplankton. *Organic Geochemistry* 33, 1635-1653.
- Naylor C.C. and Keely B.J. (1998). Sedimentary purpurins: oxidative transformation products of chlorophylls. *Organic Geochemistry* 28, 417-422.
- Walker J.S., Squier A.H., Hodgson D.A., Keely B.J. (2002). Origin and significance of 13²-hydroxychlorophyll derivatives in sediments. *Organic Geochemistry* 33, 1667-1674.
- Woolley P.S., Moir A.J., Hester R.E., Keely B.J. (1998). A comparative study of the allomerization reaction of chlorophyll *a* and bacteriochlorophyll *a*. *Journal of the Chemical Society Perkin Transactions 2*, 1833-1839.

PB2-11: Plant-internal variation of lipid composition and compound-specific isotopes of various cropsG.L.B. Wiesenberg¹, J. Schwarzbauer², L. Schwark¹

1) University of Cologne, Dep. of Geology and Mineralogy, Zulpicher Str. 49a, D-50674 Cologne, Germany (e-mail: lorenz.schwark@uni-koeln.de)

2) RWTH Aachen, LEK, Lochner Str. 4-20, D-52056, Germany

Seasonal and plant-internal variations of lipid composition and compound-specific isotopic signatures were previously described for various plant groups [1], [2]. So far, no observations were documented concerning lipid variations of annual and perennial crops. In this study, we simultaneously applied biomarker and isotopic analysis to obtain information on compartmentalization of plant lipid distributions.

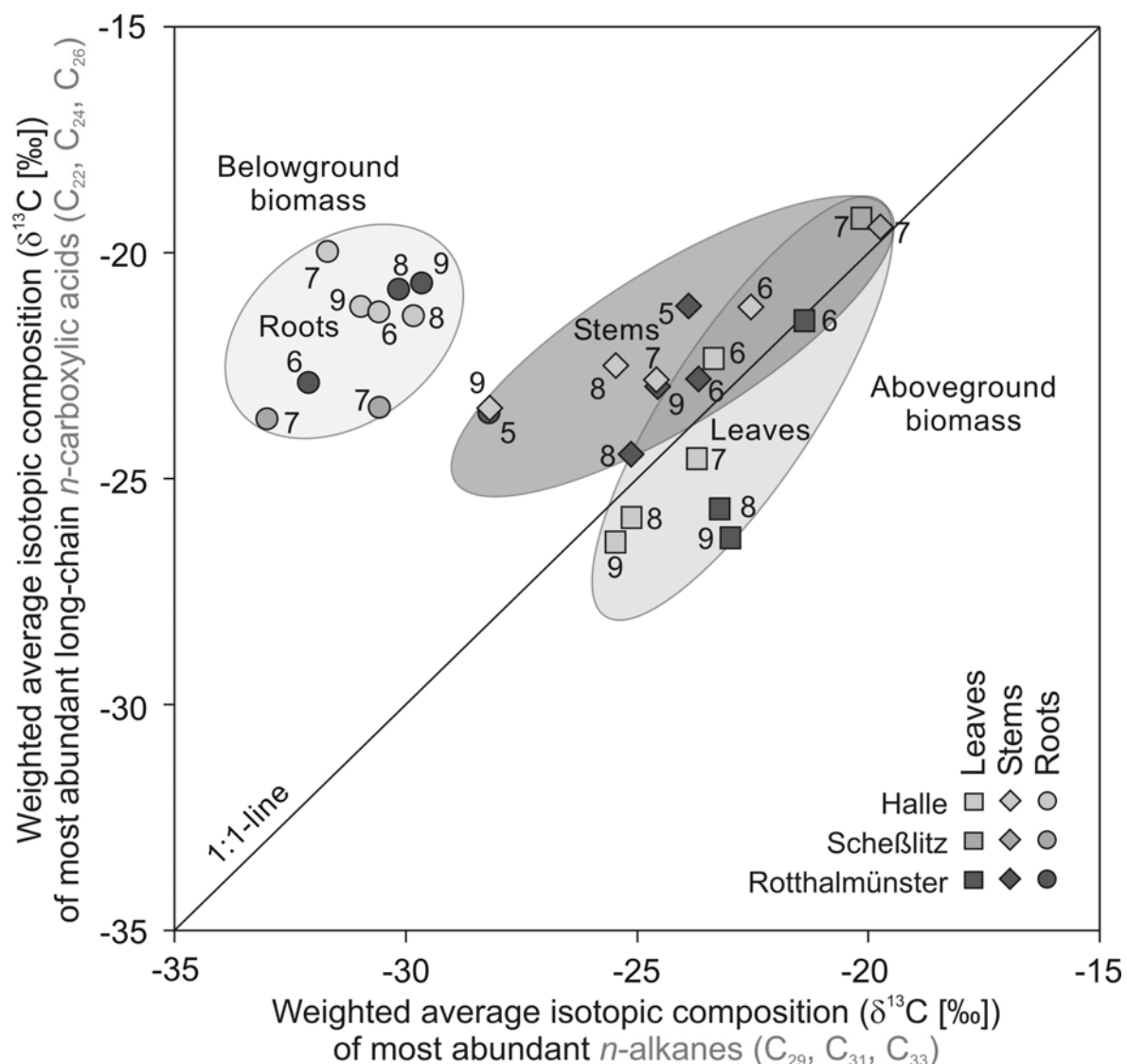
Plant samples were taken from several sites in Germany, where parallel cropping of C3-plants (rye, wheat) and C4-plants (maize) are practiced, whereby C3- and C4-crop plant samples were taken several times during the growing season. Plant samples were divided into leaf, stem and root biomass for each growth stage and analyzed separately, to obtain information on plant internal lipid and C-isotope variations. Extractable lipids of plant and soil samples were recovered by accelerated solvent extraction and separated into fractions of different polarity by automated liquid chromatography [3]. Fractions of aliphatic hydrocarbons and carboxylic acids were analyzed by GC-MS and GC-irmMS.

Within the total carboxylic acid fraction the short-chain (C₁₂₋₁₈) fatty acids, originating from various sources including bacteria, fungi, animalia, and crop plants, gave the highest concentrations. Amongst the crop lipid-derived *n*-carboxylic acids, however, the long-chain even carbon-numbered homologues (C₂₂₋₂₆) were most abundant. The aliphatic hydrocarbon fraction was dominated by long-chain (C₂₉₋₃₃) odd carbon-numbered *n*-alkanes. Compound-specific $\delta^{13}\text{C}$ -compositions were determined for the most abundant alkanes and carboxylic acids and weighted averages calculated. Aboveground biomass (stems and leaves) of maize showed similar isotopic compositions for alkanes and carboxylic acids (see figure). During the growing season the plant parts became isotopically depleted, most likely due to successive incorporation of light carbon isotopes during biosynthesis. This isotopic depletion was similar for stems and leaves.

In terms of isotopic composition belowground biomass significantly differed from aboveground biomass (see figure). $\delta^{13}\text{C}$ values of belowground carboxylic acids remained fairly constant during the growing season. Root *n*-alkanes, however, became isotopically depleted in comparison to aboveground *n*-alkanes. The difference in isotopic signature of roots versus aboveground biomass argues against an origin of alkanes and carboxylic acids in roots. Root lipids do not derive from photosynthates of aboveground biomass, which were

then plant-internally translocated towards the roots. These lipids must be biosynthesized *in situ* by either (a) direct assimilation of soil organic carbon by root tissues, or (b) interaction with soil microbes growing on or within the roots as proposed by [4]. Compound-specific $\delta^{13}\text{C}$ -signatures of long-chain carboxylic acids and alkanes are thus suitable for source apportionment of lipid production in different plant compartments.

Weighted averages of compound specific isotopic signatures of most abundant *n*-alkanes and *n*-carboxylic acids of maize plant parts taken at different sampling months during the growing season (numbers beneath symbols).



References

- [1] Lockheart, M.J., van Bergen, P.F., Evershed, R.P., 1997. Variations in the stable carbon isotope compositions of individual lipids from the leaves of modern angiosperms: implications for the study of higher land plant-derived sedimentary organic matter. *Organic Geochemistry* 26, 137-153.
- [2] Nguyen Tu, T.T., Derenne, S., Largeau, C., Bardoux, G., Mariotti, A., 2004. Diagenesis effects on specific carbon isotope composition of plant *n*-alkanes. *Organic Geochemistry* 35, 317-325.
- [3] Wiesenberg, G.L.B., Schwark, L., Schmidt, M.W.I., 2004. Improved automated extraction and separation procedure for soil lipids. *European Journal of Soil Science* 55, 349-356.
- [4] Bonkowski, M., 2004. Protozoa and plant growth: the microbial loop in soil revisited. *New Phytologist* 162, 617-631.

PB2-12: Australian oil families: a comprehensive assessment using principal components analysis of terpane, hopane and sterane biomarkers

M.B. Yunker¹, G.A. Logan², M.T. Bradshaw², C.J. Boreham², R.E. Summons³, D.S. Edwards², J.E. Zumberge⁴

1) 7137 Wallace Dr., Brentwood Bay, BC, Canada V8M 1G9 (e-mail: Mark-Yunker@telus.net)

2) Geoscience Australia, GPO Box 378, Canberra ACT 2601, Australia

3) Department of Earth, Atmospheric and Planetary Sciences, Massachusetts Institute of Technology, Cambridge, MA 02139, USA

4) GeoMark Research Inc., 9748 Whithorn Drive, Houston, Texas 77095, USA

Work over the past decade at Geoscience Australia has produced an Australia-wide coverage of data for paleogeography, petroleum systems, source rock distribution and oil geochemistry. To provide a framework for understanding hydrocarbon occurrence in Australia, previously this data has been used to formulate a classification scheme of petroleum supersystems. In this study we use Principal Components Analysis (PCA) of the concentrations of 50 terpane, hopane and sterane biomarkers in a data set of 451 Australian oil samples to obtain a consistent, continent-wide overview of known Australian oils. Most of these samples were analysed by GeoMark Research Inc. under the Oils of Western Australia and Oils of Eastern Australia (WOZ and EOZ, respectively) projects, but the data set also included 17 additional oils from the Cooper/Eromanga, Browse, Gippsland and Bass basins that were analysed by Geoscience Australia. This “top down” approach differs from the usual methodology of considering each petroleum basin as a separate entity. The resulting PCA model produces an unbiased comparison of oils from different parts of Australia based on their biomarker composition and provides a test of variability for the different oil families. Because the PCA results can be used to evaluate the suitability of the different oil families for classifying oils, they provide an independent test of the oil family approach and, by extension, the suitability of existing classifications.

The uniformity of PCA composition across basin boundaries for oils from the Larapintine (primarily Devonian to M. Carboniferous; tropical marine), Gondwanan (L. Carboniferous to M. Triassic; largely terrestrial with more marine input in the west) and Westralian (M. Triassic to Tertiary; marine with varying terrigenous inputs) supersystems supports the existing supersystem framework for Australian petroleum basins. There are not enough oil samples available to evaluate the Murta supersystem (E. Cretaceous; lacustrine). The Austral (Jurassic to Tertiary; non-marine deltaic with coals and lacustrine shales) supersystem works well between basins for Perth oils and many Gippsland oils, but proves inadequate for other Gippsland oils and oils from the Bass and Otway basins. In particular,

with the large variability in composition shown by the Otway basin samples in the PCA model, it is impossible to determine which samples are characteristic of the different reservoirs/depositional environments, and which are outliers, and the Otway basin evidently is very under-sampled. Overall the PCA results support a common source in the Austral supersystem for the Carnarvon and Perth basin oils, as well as for most oils from the Gippsland basin. However, oils from the Bass, Browse and Otway basins are very heterogeneous in composition, a result that is inconsistent with an origin in a single supersystem. Accordingly, for these basins new petroleum supersystems or further subdivisions within the supersystem approach are possible. Such subdivisions could be basin specific or could span basin boundaries where geochemical correlations can be established.

PB2-13: Humic acids and biomarker distribution in the Holocene sediments accumulated in Boina-Arade estuary, Algarve, S. Portugal

T. Boski¹, O. Polvillo², J.A. González-Perez², F.J. González-Vila², H. Knicker³

1) Centro de Investigação Marinha e Ambiental. Universidade do Algarve, 8000 FARO, Portugal
(e-mail: tboski@ualg.pt)

2) Instituto de Recursos Naturales y Agrobiología, IRNAS-CSIC., P.O. Box 1052, 41080-Seville, Spain

3) Lehrstuhl für Bodenkunde, Technische Universität München, 85350 Freising-Weihenstephan, Germany

Understanding the biogeochemical processes and environmental conditions that lead to the preservation of organic matter (OM) in marine sediments has been the subject of a wealth of studies in the last decades (1). Many of these studies have been carried out in fine sediments from estuarine zones, where they are rapidly deposited and sealed from bacterial remineralization. In such semi-enclosed environments the period of climatic warming and sea level rise that occurred since the last glacial maximum may be reflected in the characteristics of organic carbon supplied to and buried in their sediments.

The study of the lipid and macromolecular fractions at a molecular level of this sedimentary organic material, i.e. the so-called molecular geochemistry, has become an independent climatic proxy for low-resolution climate-reconstruction, offering complementary information to the classical climatic proxies, such as the study of pollen, macroscopic remains and organism assemblages, isotopic analyses, etc.

This communication is a part of a wider, paleoenvironmental survey of the estuarine zone in the area of Portimao (Algarve, South Portugal), where several Holocene sedimentary sequences were investigated. The actual estuary that occupies the Boina-Arade paleovalley received the Holocene sedimentary sequence whose thickness does not exceed 35 m in the deepest zones, as registered from destructive geotechnical borehole data. We present here geochemical data of two continuous cores (P5 and P6, Boina River) that crossed the Holocene sequence until the Pre-Quaternary substratum. In the P5 core, the sedimentary column, which spans 20 m accumulated during ca 8500 years, starts with a sequence of inter-bedded layers of sandy-pebbles and silty-clays that corresponds to a transitional period from fluvial to estuarine regime. It is followed by a period of silty-clay deposition during a regime of fast sea level rise. The top 6 meters of the sequence are mainly sandy and represent the progressive infilling of the estuary with material from the continental shelf after the sea level stabilization in the Upper Holocene.

The heavy minerals with a contribution of 10 to 19 % of total weight are very abundant. The iron oxide/hydroxides are predominant and their source lies probably in the

altered basic rocks from the volcano-sedimentary complex. Pyrite, which is also abundant in the heavy fraction, comes from the reaction between the already mentioned iron and the sulphur released during microbial mediated sulphate-reduction processes.

Lipids were solvent extracted using a dichloromethane-methanol (2:1) mixture during 48 hours from three sediment sections taken at different depth along the core P5 . Total extracts were concentrated at reduced pressure, derivatized with trimethylsilyldiazomethane and analyzed by GC-MS. Humic acids fractions (HA) were isolated by conventional methods from the same lipids-free sediment samples, and characterized by FT-IR, ¹³C-NMR spectroscopy and analytical pyrolysis (Py-GC-MS).

The main results obtained can be summarized as follows:

- i) A great variety of biomarkers compounds were identified throughout the core. In all the sections of the core it was possible to recognize the contribution of both terrigenous and aquatic organisms to the sediment column in variable concentrations. The observed downcore changes in the lipid assemblage within the Holocene suggest recent variations in the planktonic and terrigenous supply, which are attributed respectively to evolution of the fully estuarine pattern of circulation and to the changes of the vegetation cover within the Boina River drainage basin.
- ii) Spectroscopic data seems to indicate a close similarity between the structural characteristics of the HA isolated from samples irrespective to sampling depth. In addition, both FT-IR and solid state ¹³C-NMR spectra confirmed the large relative occurrence of alkyl moieties, as well as a lignin signature, in the sedimentary HA
- iii) All the HA fractions released by pyrolysis major series of substituted aromatic compounds in addition to typical alkyl series consisting of triplets of *n*-alkanes, *n*-alkenes, and α,ω -alkadienes dominated by a series of alkane/alkene pairs in the range C₁₂-C₂₈, typical pyrolysis products of recalcitrant aliphatic biopolymers. Trace amounts of carbohydrate and protein pyrolysis products points to an extensive rearrangement of the original constituents into a newly-formed condensed thermodynamically stable C-C random macro-molecular network.

References

- (1) Hedges, J.I. and Keil, R.G., 1999. Organic geochemical perspectives on estuarine processes: sorption reaction and consequences. *Marine Chemistry* 65, 55-65.

**PB2-14: A cornucopia of hopanoids: revisiting
the Thornton quarry bitumen (Thornton, Illinois, USA)**

F. Kenig¹, S.C. Brassell², R.K. Nelson³, G.S. Frysiner⁴,
C.M. Reddy³, R.B. Gaines⁴

1) Dept. of Earth and Environmental Sciences, University of Illinois at Chicago, M/C 186, 845 West Taylor Street, Chicago IL 60607-7059, USA (e-mail: fkenig@uic.edu)

2) Geology Dept., Indiana University, 1005 E. 10th Street, Bloomington, IN 47405, USA

3) Dept. of Marine Chemistry and Geochemistry, MS#4, Woods Hole Oceanographic Institution, Woods Hole MA 02543-1543, USA

4) Department of Science, U.S. Coast Guard Academy, New London, CT 06320-8101, USA

The high-purity dolomite of the Silurian reefs of the Chicago regions have been a source of lime during the nineteenth century and are currently quarried extensively for crushed stone. Reefs of the same age are petroleum reservoirs in the Michigan and Illinois basin. In the south western suburb of Chicago, the dolomite pinnacle reef exploited at the Thornton Quarry (Thornton, Illinois) contain, well distributed, black bitumen particles in its pores. Those bitumen were first analyzed by Ref [1] who noted the absence of *n*-alkanes, the presence of steranes and hopanes, as well as a high sulfur content (6.3 wt.%). Few years later, a distillation cut of this bitumen was analyzed and unusually abundant 17 α (H),21 β (H)-hopanes with extended side chains (C₃₁-C₄₀) as well as C₂₉-C₃₅ moretanes were observed [2]. However, hopanes with more than 40 carbon atoms could not be detected and it was suggested that this limit was the result of the experimental procedure used. The origin of the Thornton Quarry bitumen is unclear. In Michigan, it has been suggested that the oil found in the Silurian (Niagaran) reefs, distinct from other oils in the Michigan basin, were derived from intra-reef laminated carbonate sediments [3]. However, if the belt of pinnacle reef of the Michigan basin was buried enough to have reached the oil window, the Thornton Quarry reef is located on the Kankakee arch separating the Illinois and Michigan basins and might not have been buried so deeply.

In this report, we investigate the biomarker composition of the sulfur-rich, Thornton Quarry bitumen to find clues to its source and level of biodegradation as well as to test for the presence of extended hopanes with more than 40 carbon atoms. The distribution of biomarkers, largely dominated by hopanoids, was monitored by gas chromatography mass spectrometry (GC-MS) in the saturated/unsaturated hydrocarbon fraction, the aromatic fraction, the pyrolysate of the asphaltene fraction, and the hydrocarbon fraction released upon nickel boride desulfurization of the polar lipid fraction. The biomarker composition is reviewed to find clues on the environment of deposition of the bitumen source rock. Additionally the saturated/unsaturated fraction and the aromatic fraction were analyzed by

comprehensive two dimensional gas chromatography-FID (GC×GC-FID) and GC×GC-time of flight mass spectrometry. The increased resolution and compound-class separation provided by comprehensive two-dimensional gas chromatography (GC×GC) and GC×GC-time of flight mass spectrometry was used to resolve the complex mixture of compounds of the aromatic fraction. The very high sensitivity afforded by GC×GC instruments allowed detection of 17 α (H),21 β (H)-hopanes up to C₄₅ (Fig. 1) in the saturated/unsaturated hydrocarbon fraction (Fig. 1). 17 α (H),21 β (H)-hopanes and 17 β (H),21 α (H)-moretanes extended series, were only observed in moderately biodegraded crude oils and source rocks extracts of the Liaohe Basin (China) [4].

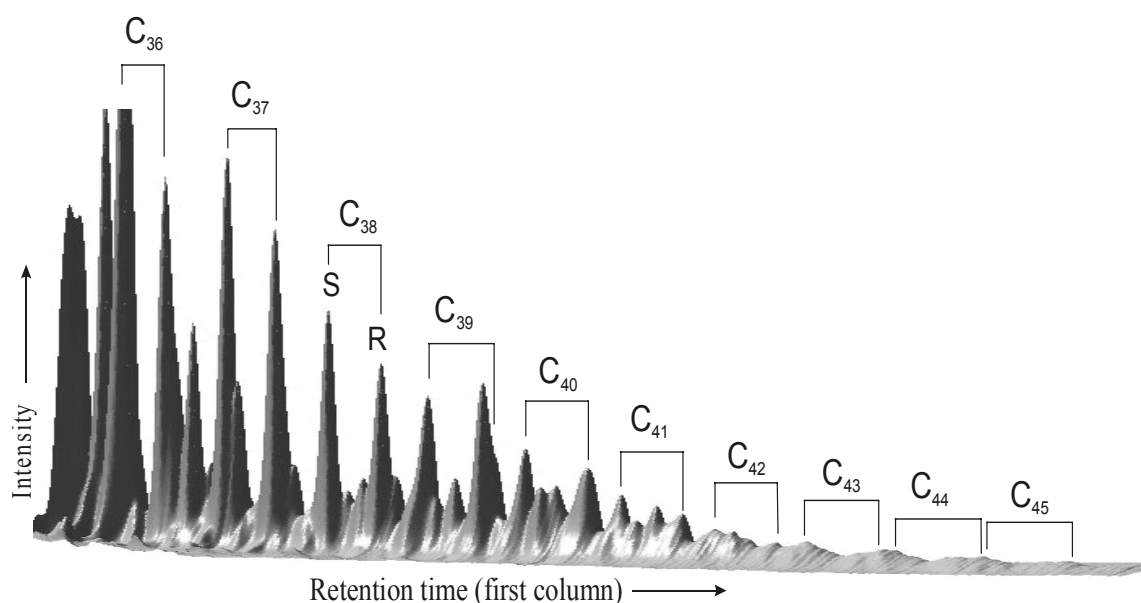


Fig.1. Matlab[®] 3D rendering of partial GC×GC-FID data showing the distribution of C₃₆-C₄₅ 17 α (H),21 β (H)-hopanes (20S and R) in the saturated/unsaturated hydrocarbon fraction of Thornton Quarry bitumen

References

- [1] Marschner R.F., Duffy L.J., Winters J.C. (1975) Bitumen from Thornton quarry. *Trans. Ill. State Acad. Sci.* 68, 3, 263-277.
- [2] Rullkötter J. and Philip P. (1981) Extended hopanes up to C₄₀ in Thornton bitumen. *Nature* 292, 616-618.
- [3] Gardner W.C. and Bray E.E. (1984) Oils and source rocks of Niagaran Reefs (Silurian) in the Michigan Basin. *AAPG Studies in Geology* 18, pp 33-44.
- [4] Wang P., Li M and Larter S.R. (1996) Extended hopanes beyond C₄₀ in crude oils and source rock extracts from Liaohe Basin, N.E. China. *Organic Geochemistry* 24, 547-551.

PB2-15: One-year seasonal variations of pigments in sweetgum (*Liquidambar styraciflua*) leaves

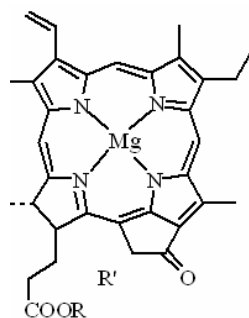
R. Ocampo

Laboratoire de Géochimie Bioorganique, UMR 7509 (CNRS-ULP), ECPMS, 25, rue Becquerel, 67200 Strasbourg, France (e-mail: ocampo@chimie.u-strasbg.fr)

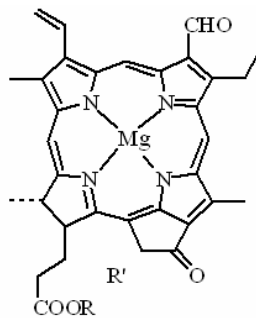
Seasonal disappearance of chlorophyll coinciding with partial retention of carotenoids and new synthesis of red anthocyanins leads to the emergence of the autumnal coloration of foliage in some deciduous trees. This is probably one of the most spectacular natural phenomena that we can enjoy every year.

Since the year 2000 we followed the one-year seasonal variations of chlorophyll, carotenoids and anthocyanins in leaves of several deciduous trees located in the Strasbourg area. In this work we will present the 2004 one-year results concerning the sweetgum tree.

Leaves of sweetgum (*Liquidambar styraciflua*) tree were collected monthly between May and November 2004. Leaves samples were always split into two. One part was extracted with methanol and the other one with acetone. Pigments were monitored by HPLC (RP-18,



Chlorophyll a
R = phytyl
R' = COOMe



Chlorophyll b
R = phytyl
R' = COOMe

photodiode array detector on line system). A special interest was devoted to the study, at the molecular level (HPLC, UV-Vis, MS, NMR) of chlorophyll degradation products in order to compare to chlorophyll degradation products related to senescence and death in marine phytoplankton or to those observed during the early diagenetic transformations occurring in sedimentary organic matter.

References

- Airs, R.L., Jie, C., and Keely, B.J. (2000) A novel sedimentary chlorin: structural evidence for a chlorophyll origin for aetioporphyrins. *Organic Geochemistry* **31**, 1253-1256
- Hendry, G.A., Houghton, J.D., and Brown, S.B. (1987). The degradation of chlorophyll. A biological enigma. *New Phytol.*, **107**, 255-302
- Hörtensteiner, S., and Kräutler, B. (2000). Chlorophyll breakdown in oilseed rape. *Photosynthesis Research*, **64**, 137-146
- Louda, J.W., Liu, L., and Baker E.W., (2002) Senescence-and death-related alteration of chlorophylls and carotenoids in marine phytoplankton. *Organic Geochemistry* **33**, 1635-1653
- Matile, P. (2000). Biochemistry of Indian summer: physiology of autumnal leaf coloration. *Experimental Gerontology*, **35**, 145-158
- Naylor, C.C., and Keely, B.J. (1998) Sedimentary purpurins: oxidative transformation products of chlorophylls. *Organic Geochemistry* **28**, 417-422
- Ocampo, R., and Repeta, D.J. (1999). Structural determination of purpurine-18 (as methyl ester) from sedimentary organic matter. *Organic Geochemistry* **30**, 189-193
- Ocampo, R., and Repeta, D.J. (2002). Isolation and structure determination of two novel C(13²)-OH bacteriopheophytin *a* allomers from a coastal salt pond sediment. *Organic Geochemistry* **33**, 849-854.

PB2-16: Organic compounds in hot thermal waters of Szentes, HungaryC. Sajgó¹, Z. Kárpáti², I. Varsányi³

1) Inst. for Geochemical Research, Hung. Acad. of Sci., H-1112 Budapest Budaörsi út 45, Hungary
(e-mail: sajgo@sparc.core.hu)

2) National Institute of Hygiene, Gyáli út 2-6, H-1097 Budapest Hungary

3) University of Szeged, H-6701 Szeged PO Box 651, Hungary

In Hungary over 500 organic compounds (mainly aromatic and heteroaromatic hydrocarbons; phenols; fatty acids) were identified (Sajgó et al., 1998; Kárpáti et al., 1999; Varsányi et al., 2002) in hot thermal waters. The order of the appearance of the different organic compounds is as follows i) humic acids during sedimentation; ii) hydrocarbon gases (in two steps: microbial and thermogenic light HCs); iii) pyrolytic like aromatic HCs; iiiii) phenols (over ~80°C outflow temperature) and iiiiii) finally fatty acids (in C₆-C₁₆ range). The carbon-chain shortening was observed in the homologues as a function of increasing temperature of waters.

The aim of this paper to study the distribution of pyrolytic like compounds in waters after the onset of aromatic HC genesis, on the basis of quantification of 3 homologue series: alkylbenzenes (15 compounds), PAHs (18 compounds) and phenols (13 compounds) in hot thermal waters from the Great Hungarian Plain (Szentes).

The study samples are located close to each other in the southeastern part of the Great Hungarian Plain, around Szentes (Fig. 1). The age of screened aquifer intervals is Pliocene. In the samples studied the aromatic HC and phenols generation has already taken place but the onset of fatty acids generation in C₆-C₁₆ range has not started yet. Some selected parameters of waters are summarised in Table I. The samples were ranked as a function of phenanthrene/anthracene ratio, because it can be considered as source indicator. Several authors suggested that pyrolytic like aromatic hydrocarbon yields of diagenetic processes are mainly inherited from their precursors' structure through oxidation or, more properly dehydrogenation reactions, particularly phenanthrene may be a quasi-end product of both steroids and di/triterpenoids, and probably of anthracene in the case of a rearrangement. The phenanthrene/anthracene ratio is about 50 in oils, and it is much lower in coals, where it might be <1. Both compounds can be the product of thermogenic decay of kerogen or humic acids.

The source of the studied thermal water samples are similar, except Kert.Kut.I. sample, which seems to be of different origin. The waters were also classified by other type of source parameters (organic, inorganic and isotopic) and according to level of maturity (e.g. condensation, alkyl chain shortening, mineralization).

Acknowledgement

This work was funded through grant: OTKA T 034579, T 037269 and T 048829 from the Hungarian National Science Foundation.

Table 1. The most important parameters of the thermal waters studied from Szentes

Well name	*Phen/Ant	¹ Perf. (m)	² T (°C)	Na ⁺ mmol/l	Cl ⁻ mmol/l	³ Σbenz. µg/L	⁴ ΣPAH µg/L	⁵ Σphen µg/L	⁵ Σcomp. µg/L	⁶ TOC mg/l	⁷ huma mg/l	⁸ δ ¹³ C ‰
Árpád I (II/1)	2.4	1896	99	23.2	0.21	1109.8	30.0	2957	4096	19.5	2.3	-5.27
Ilonapart IV	4.7	2255	96	15.0	0.29	259.8	17.1	6342	6619	7.5	0.7	-2.18
Árpád VII/3	5.0	1900	99	25.1	0.23	1464.5	23.7	852	2340	26.4	2.1	-2.94
Árpád VI/2	6.2	1842	97	25.0	0.24	964.1	12.6	681	1658	17.8	2	-3.73
Árpád V/2	8.7	1889	101	26.9	0.23	1524.7	16.3	1624	3165	25.5	2.7	-3.21
Árpád II (II/2)	9.7	1717	86	16.8	0.2	155.8	9.9	1836	2002	4.7	1.3	-3.21
Dónát I	13.0	1930	96	31.6	0.22	1565.9	12.8	13312	14891	39.3	3.2	-4.01
Ilonapart I	32.2	1901	86	19.5	0.21	332.8	9.3	550	893	6.4	1.1	-4.64
Berekhát	40.1	1875	86	17.9	0.65	226.9	3.8	8589	8820	4.2	1	n.m.
Kórház I	103.5	1677	87	21.0	0.32	593.2	10.0	10078	10681	5.6	0.7	-4.66
Kert.Kut.I	625.9	1665	78	17.3	0.4	197.8	12.1	11254	11464	7.7	0.7	-4.81

*Phen/Ant: ratio of phenanthrene and anthracene; ¹Perf.: mean depth of perforated interval; ²T: water temperature at surface; ³Σbenz.: summarised concentration of benzenes = benzene + 14 identified alkylbenzenes (C₁-C₄ range); ⁴ΣPAH: amount of 18 identified PAHs (in di-pentaaromatic range); ⁵Σphen: amount of phenol + 12 identified alkylphenols (C₁-C₄ range); ⁵Σcomp.: sum of all the identified organic compounds (46 items) = (³Σbenz.+ ⁴ΣPAH+⁵Σphen); ⁶TOC: Total organic carbon; ⁷huma: humic acids; ⁸δ¹³C: measured of bicarbonate ‰ vs. PDB; n.m.: not measured

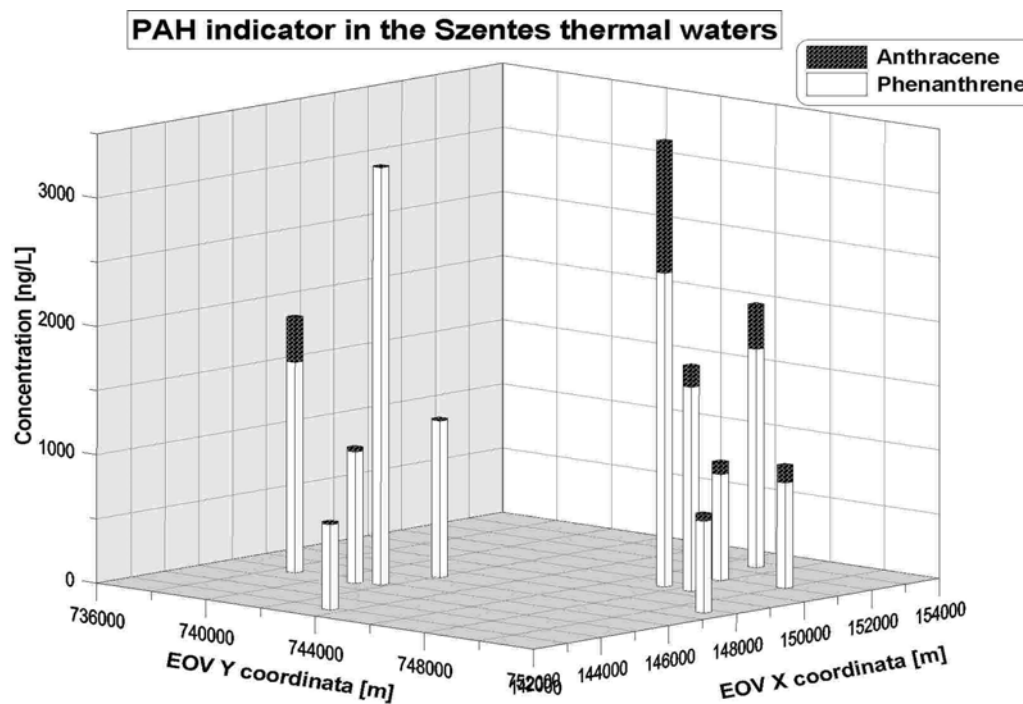


Fig.1. The concentrations of phenanthrene and anthracene from deep and hot Pliocene layers (~1700-2200 m; ~80-100°C) in neighbouring thermal water wells at Szentes (town of southeast Hungary) in Pannonian Basin. The locations of wells are shown as a function of N-S and W-E national coordinates

References

- Sajgó Cs., Kárpáti Z., Klopp G. and Vető I.: New Contributions to Organic compositions of Thermal Waters in *The water and the protection of aquatic environment in the Central Basin of the Danube* (eds. Pandi G. and Imecs Z.) IIIrd Hydrology Conference Cluj-Napoca 24-26. Sept. 1998. Conference Proceedings vol. II. pp. 241-249. Univ. Babeş-Bolyai, Facultatea de Geografie, Cluj-Napoca, 1998.
- Kárpáti Z., Sajgó Cs., Vető I., Klopp G. and Horváth I. : Organic matter in thermal waters of the Pannonian Basin - A preliminary report on aromatic compounds. *Organic Geochemistry* 30, 701-712. 1999.
- Varsányi I., Ó. Kovács L., Kárpáti Z. and Matray JM.: Carbon forms in formation waters from the Pannonian Basin, Hungary. *Chemical Geology* 189, 165-172. 2002.

PB2-17: Lipid biomarkers of chief primary producers and sediments in coral reef, seagrass bed, and mangrove forest ecosystems

S. Sakata, M. Yamamuro

Geological Survey of Japan, AIST, Tsukuba 305-8567, Japan (e-mail: su-sakata@aist.go.jp)

Coral reef, seagrass bed, and mangrove forest are characteristic ecosystems in tropical and subtropical coast, and they are often situated close to one another. Among them, coral reef is highly vulnerable against eutrophication, while seagrass bed may act as sink for nutrient and terrestrial organic matter as is often described in temperate beds. Mangrove forest may also act as sink for terrestrial organic matter and protect seagrass bed from excess accumulation of organic matter. To investigate how these ecosystems depend on one another from the viewpoint of organic geochemistry, we analyzed chief primary producers and sediment in each ecosystem for the distribution of lipid biomarkers and the ^{13}C content of total organic carbon.

Materials and methods

Samples of the primary producers, i.e., terrestrial higher plants, *Halophila* seagrass, *Enhalus* seagrass, and corals, were collected together with surface sediments at sites along the line of mangrove forest (upstream and downstream) - seagrass bed (*Halophila* and *Enhalus*) - coral reef in Ishigaki Island, Okinawa Prefecture, Japan. The samples were freeze-dried, homogenized/pulverized, and saponified with 0.5M KOH in 20:1 methanol/water. Neutral lipids were collected from the residue and from the solution by extraction with hexane/ethyl acetate (9:1). The extracts were combined and divided into fractions of different polarity by column chromatography on silica gel. The alcohol fraction was subjected to trimethylsilylation using BSTFA. Subsequent GC-MS/FID analysis employed a Hewlett-Packard 6890-5972 system with on-column injector, a CP-SIL 5CB-MS capillary column, and helium carrier gas. The ^{13}C content of TOC was determined with a system of elemental analyzer (Fisons Instruments EA1108) - isotope-ratio mass spectrometer (Finnigan Delta Plus) after treatment of the samples with drops of 1N HCl.

Results and discussion

Lipids in the terrestrial higher plants were characterized by the distribution of *n*-alkanes high at $\text{C}_{29}/\text{C}_{31}$, high contents of diterpenes (phylocladene, kaur-16-ene), high contents of triterpenones (β -amyrone, lupeone, friedelin), and the predominance of triterpenols (e.g., β -amyrin, lupeol, taraxerol) over sterols. Lipids in the seagrasses were characterized by the distribution of *n*-alkanes high at C_{21} , C_{23} , and C_{25} , low contents of

triterpenones, and the predominance of sterols (β -sitosterol, stigmasterol, campesterol) over triterpenols. Lipids in corals were characterized by the distribution of sterols predominated by campesterol and gorgosterol, and the absence of *n*-alkanes, triterpenones, and triterpenols.

Lipids in the sediments from mangrove forest were found to resemble those in the terrestrial higher plants. Lipids in the sediments from seagrass bed were characterized by high content of triterpenones, and the predominance of triterpenols over sterols, reflecting a major input of organic matter from mangrove forest. Lipids in the sediment from coral reef did not include triterpenones or triterpenols.

The data of ^{13}C content of TOC also suggested that the contribution of terrestrial organic matter was large to the sediments from seagrass bed, but little to the sediment from coral reef. We therefore conclude that seagrass bed works as a barrier against terrestrial input, and protects coral reef from eutrophication in the subtropical ecosystems in Ishigaki Island.

**PB2-18: Diatom biomarkers across the Eocene-Oligocene boundary
in the Northeast Kamchatka Peninsula**

H. Shiine¹, N. Suzuki¹, I. Motoyama², S. Hasegawa³, A.Y. Gladenkov⁴,
Yu.B. Gladenkov⁴, K. Ogasawara²

1) Division of Earth and Planetary Sciences, Graduate School of Science Hokkaido University N10 W8, Kita-ku, Sapporo, 060-0810, Japan (e-mail: shii@ep.sci.hokudai.ac.jp)

2) Institute of Geoscience, University of Tsukuba, Tsukuba, Ibaraki 305-8572, Japan

3) Graduate School of Science and Technology, Kumamoto University 40-1, Kurokami 2-chome, Kumamoto 860-8555, Japan

4) Geological Institute, Russian Academy of Sciences, Pyzhevskii per.7, Moscow 119017, Russia

The Eocene-Oligocene transition is one of the critical turning points in the Earth's history. The rapid global lowering of atmospheric and oceanic temperatures initiated the formation and expansion of Antarctic continental ice sheet during the Eocene-Oligocene transition. This interval was the most significant episode of climatic change and extinction in the Cenozoic. Among various biotic responses during the Eocene-Oligocene transition, the evolution of diatom in the high latitude of North Pacific is of great interest. Dramatic changes in the diatom communities and a large increase in diversity of diatom species took place in the Oligocene. However, we have few diatom fossil records during the Eocene-Oligocene transition. One reason is that the silica tests of diatoms are prone to dissolution during settling in the water column and early diagenesis. Highly branched isoprenoids (HBIs), typical diatom biomarkers, in sedimentary rocks from the Il'pinskii Peninsula, Northeast Kamchatka, were investigated to reveal the variation in diatom production during the Eocene-Oligocene transition.

The Il'pinskii Peninsula, Northeast Kamchatka, Russia is located to the northwest of Bering Sea. Diatom fossil preservation is extremely poor in mudstones and carbonate concretions exposed in the Il'pinskii section, which has the complete Eocene-Oligocene succession [1]. The Eocene-Oligocene boundary in the Il'pinskii section, estimated based on mollusk fossils, is unclear [2]. A total of 40 mudstones samples were collected from the Il'pinskii section. The SiO₂ and Al₂O₃ concentrations of mudstones range from 60 to 70% and from 13 to 15%, respectively. The total organic carbon concentration is in the range from 0.5 to 0.9%. The comparatively low C/N ratios, less than 10, suggest higher marine organic matter contribution. Sterane isomers ratios, 20S/(20S+20R)-C₂₉ steranes, are generally less than 0.1, showing low maturity levels of the samples.

Diatom biomarkers, such as the C₂₅ HBI alkane and C₂₅ HBI thiophenes, 2-(2'-methylbutyl)-3,5-di-(2'-16'-methylheptyl)thiophene and 2,3-dimethyl-5-[7'-(2',6',10',14-tetramethylpentadecyl)]thiophene, were commonly detected in mudstones from the Il'pinskii

section. Concentrations of these HBI diatom biomarkers ($>1.0\mu\text{g/gTOC}$) in Oligocene mudstones are clearly higher than those ($<0.1\mu\text{g/gTOC}$) in Eocene mudstones. Concentrations of C_{25} HBIs tend to increase drastically after the Eocene-Oligocene boundary. The earliest Oligocene is defined by occurrence of *Rhizosolenia oligocaenica* zone [3]. C_{25} HBI alkenes have been identified in the diatom genera *Rhizosolenia*, *Haslea*, *Navicula*, and *Pleurosigma* [4]. Drastic increase of C_{25} HBIs concentrations indicates the higher production of diatoms in high latitudes of North Pacific, in and after the Eocene-Oligocene transition.

Variations of SiO_2 and Al_2O_3 concentrations and some terrestrial biomarkers with stratigraphic depth in the Il'pinskii section are insignificant. Marked increase of C_{25} HBIs concentrations can be attributed to upwelling of deep oceanic water rich in dissolved silica. The climatic deterioration in the Eocene-Oligocene transition is hypothesized to be due to the opening of the Tasmanian gateway, which led to the growth of Antarctic continental ice sheets. Invasion of proto-Antarctic bottom water and its upwelling in high latitudes of North Pacific can be responsible for the abrupt increase of C_{25} HBIs during the Eocene-Oligocene transition. C_{25} HBIs can be useful diatom biomarkers applicable to biomarker stratigraphy in high latitudes of North Pacific. The new Eocene-Oligocene boundary in the Il'pinskii section, Northeast Kamchatka, is proposed based on C_{25} HBIs distributions in the present study.

References

- [1] Gladenkov, Y.B. and Shantser, A.E., 1993. Paleogene Geological Events in Kamchatka. Stratigraphy and Geological Correlation 1, 1, pp. 88-98.
- [2] Gladenkov, Y.B., Bagdasaryan, G.P., Beniamovskii, V.N., Vitukhin, D.I., Volobueva, V.I., Muzylev, N.G., Tariverdieva, T.I., Fregatova, N.A., 1988. Plankton from the Il'pinskii Peninsula (Koryak Upland), Izvestiya Akademiy Nauk SSSR, seriya Geologicheskaya 10, pp. 85-91. (in Russian)
- [3] Gladenkov, A.Y., 1999. A new lower Oligocene Zone for the North Pacific diatom scale. In: Mayama, s., Idei, M., Koizumi, I., the International Society for Diatom Research (Eds.) Proceedings of the 14th International Diatom Symposium: Tokyo, Japan, September 2-8, Koeltz Scientific Books, Germany, pp. 581-590.
- [4] Sinninghe Damsté, J.S., Muzzer, G., Abbas, B., Rampen, S.W., Massé, G., Guy Allard, W., Belt, S.T., Robert, J.-M., Rowland, S.J., Moldowan, J.M., Barbanti, S.M., Fago, F.J., Denisevich, P., Dahl, J., Trindade, L.A.F., Schouten, S., 2004. The Rise of the Rhizosolenid Diatoms. Science 304, 5670, pp. 584-587.

PB2-19: Biomarker analysis of solvent extractable organic matter from the Late Neoproterozoic Kwagunt formation, Chuar group (~800-742 Ma), Grand Canyon

G.T.Ventura¹, F. Kenig¹, E. Grosjean², R.E. Summons²

1) Earth and Environmental Sciences, University of Illinois at Chicago, 845 W. Taylor St, UIC, Chicago, IL 60607-7059 (e-mail: gventu1@uic.edu)

2) Earth, Atmospheric and Planetary Sciences, Massachusetts Institute of Technology, E34-546, 42-44 Carleton Street, Cambridge, MA 02139

Twenty-seven predominantly siliclastic sediment samples from the Awatubi and Walcott Members of the Neoproterozoic Kwagunt Formation were solvent extracted and analyzed for hydrocarbon biomarkers using metastable reaction monitoring gas chromatography-mass spectrometry (MRM-GCMS). These samples mark a nearly continuous record of Neoproterozoic deposition along an intracratonic rift basin located within 10°N and S of the equator that predates the breakup of Rodinia and the onset of the Sturtian snowball Earth event (750-700 Ma). Deposition occurred in a shallow, subtidal to intertidal-supertidal marine environment. The Kwagunt Formation records a large positive $\delta^{13}\text{C}_{\text{TOC}}$ excursion of up to 13‰ that is globally correlated (Fig. 1).

The aliphatic fraction of the extractable organic matter contained a diverse array of biomarkers including *n*-alkanes, monomethyl alkanes, acyclic isoprenoids, branched alkanes with quaternary carbon atoms and polycyclic terpanes (bi-, tri-, tetra-, penta-). The data indicate the extracted hydrocarbons are syngenetic and thermally mature. Three general stratigraphic trends are observed. i) Biomarker abundance and TOC is lower during the positive $\delta^{13}\text{C}_{\text{org}}$ isotopic excursions suggesting lower productivity. ii) Samples that are stratigraphically above the isotopic excursion, near the base of the Walcott, have highly variable biomarker abundances that suggest rapid changes in environmental conditions. Higher concentrations of gammacerane during this interval indicate restricted circulation and elevated salinity. iii) The abundance of organic matter gradually decreases at the top of the Walcott Member before the onset of the Sturtian snowball Earth episode. The diversity and abundance of hopanes, including a homologous series of C₃₀-C₃₅ diahopanes, and elevated abundances of rearranged C₂₇-C₂₉ steranes are indicative of clay-mediated diagenesis.

These results suggest that organic matter production varied greatly during shifting climate conditions associated with the isotopic anomaly. The variations in compound class abundances also suggest a fluctuating redox state and salinity in the water column.

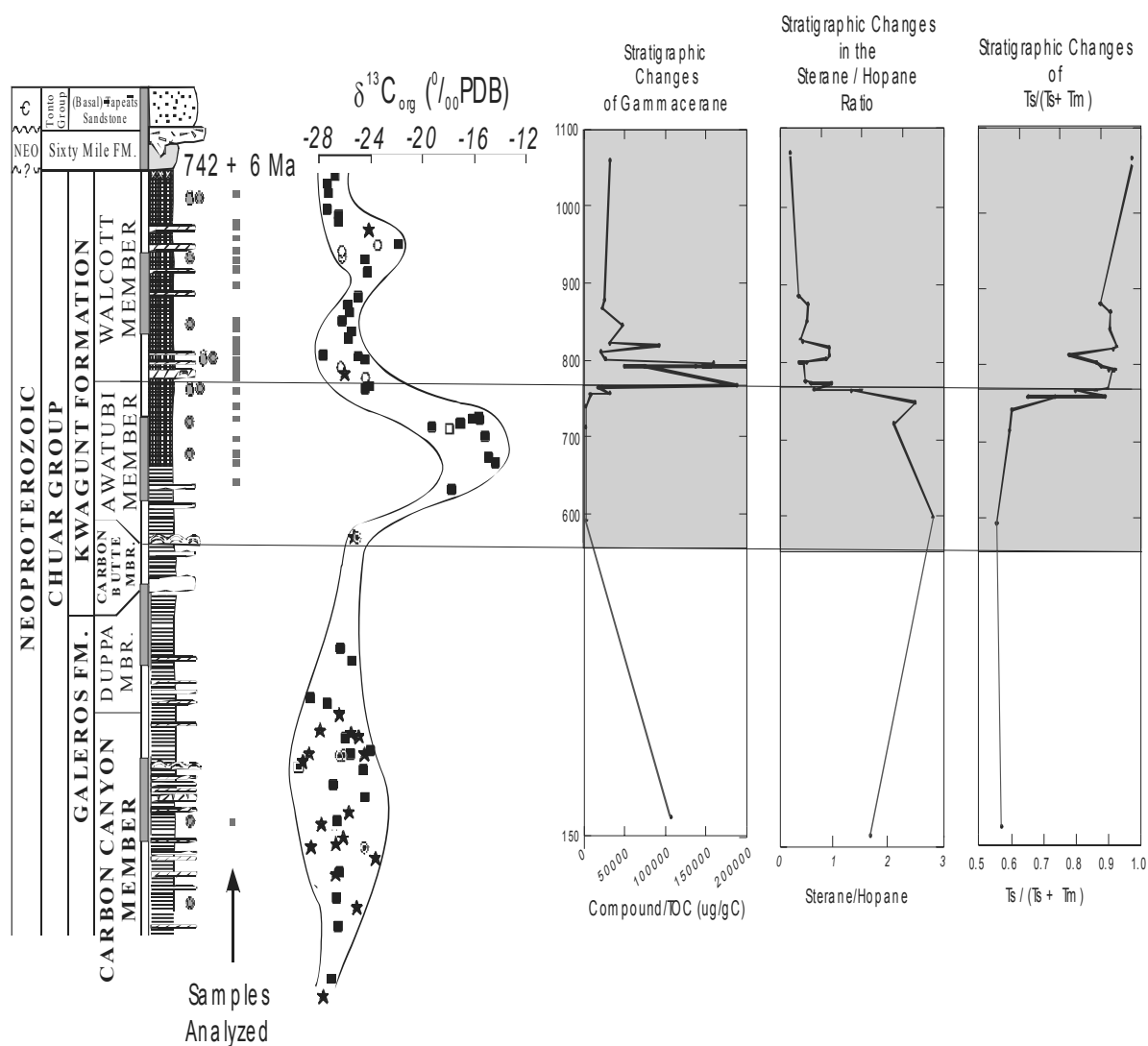


Fig.1. Stratigraphic profile of the Kwagunt Formation including the profiles of $\delta^{13}C_{org}$ [1], changes in the concentration of gammacerane, changes in the ratio of hopane to sterane concentrations, and stratigraphic changes in Ts and Tm

References

- [1] Karlstrom, K.E.; Bowring, S.A.; Dehler, C.M.; Knoll, A.H.; Porter, S.M.; Des Marais, D.J.; Weil, A.B.; Sharp, Z.D.; Geissman, H.W.; Elrick, M.B.; Timmons, M.J.; Crossey, L.J.; and Davidek, K.L. 2000. Chuar Group of the Grand Canyon: Record of breakup of Rodinia, associated with change in the global carbon cycle, and ecosystem expansion by 740 Ma. *Geology*. Vol. 28. Pg. 619-622.

PB2-20: Sources of organic carbon to a river dominated coastal shelf: the use of chemical biomarkers to trace organic carbon inputs to sediments

L.A. Wysocki, T.S. Bianchi, T.R. Filley

Department of Earth and Environmental Science, Tulane University, New Orleans, LA, 70118, USA
Department of Earth and Atmospheric Sciences, Purdue University, West Lafayette, IN, 47907, USA

The ability of the oceans to act as a global sink for excess carbon dioxide is considerable, not only from direct transfer of CO₂ from the atmosphere to the oceans via primary production, but also through sinking organic matter and burial (Hedges and Keil, 1995). Because of high sedimentation rates in the coastal ocean, particularly along river-dominated ocean margins, estuarine and coastal sediments can be important repositories for organic carbon derived from both allochthonous and autochthonous sources. Using molecular biomarker analyses (C/N, bulk isotopes, lignin, pigments, and compound-specific isotopes) this study examines the sources of organic carbon to the Louisiana shelf within the dispersive path of the Mississippi river.

Materials and Methods: two cruises were conducted in the Mississippi River plume and receiving waters of the Louisiana shelf. The cruises took place in April and October of 2000; the times were chosen to represent low- and high-flow periods of river discharge. Sediment samples were collected on a grid of 50 sampling sites that spanned the area of the plume and the surrounding waters. Surface sediment (0-2 cm) was oven-dried and acidified for bulk C, N, and stable isotope analyses. Freeze-dried sediment was analyzed for pigment biomarkers by HPLC (Bianchi et al., 1995) and for lignin by CuO (Hedges and Ertel, 1982). The $\delta^{13}\text{C}$ signature of specific lignin compounds are being analyzed by GC-IRMS.

Results and Discussion: organic carbon (%OC) in surface sediment ranged from 0.28 – 1.4 during high discharge and from 0.59 – 1.8 during low discharge. The $\delta^{13}\text{C}$ values ranged from -20.6 to -22.9‰, and from -14.9 to -21.8‰ during each discharge period, respectively. It is not possible, therefore, to precisely distinguish between marine and terrestrial inputs based on the bulk carbon and $\delta^{13}\text{C}$ values of TOC. Chlorophyll *a* in the sediment (0.1 – 8.9 $\mu\text{g/g}$) was used as an indicator of marine organic carbon inputs, while lignin oxidation products (Λ_8 , 0.3 to 4.7 mg/100 mg OC) were used as a biomarker for terrestrial organic carbon. A simple two end-member isotope mixing model incorporating the bulk $\delta^{13}\text{C}$ values of TOC and the biomarker concentrations suggests approximately 32-41% of the TOC in surface sediments is composed of terrestrial material during high discharge, while only 14-29% of the TOC is of terrestrial origin during the low discharge period. During the low flow period however, there were several stations whose isotope values indicate an almost

exclusively terrestrial signature, possibly from local salt marsh inputs. The acid/aldehyde ratios of the guaiacyl lignin compounds increased offshore (up to 0.7) while relatively fresher material (0.2-0.3) was observed within the regions of highest riverine deposition. Such deposition occurs further out from the river mouth with increased discharge, in agreement with previous studies which concluded that degraded material is preferentially transported further (Goni et al., 1997).

Conclusion: the relative proportion of allochthonous and autochthonous carbon deposition on the Louisiana shelf varies with river flow. The amount of terrestrial organic carbon is dependent not only on the river discharge, but upon the amount of *in situ* production. However, even with the high productivity during spring months there is still a substantial terrestrial contribution to the surface sediments. With compound specific isotope data on lignin biomarkers we will be able to further elucidate the composition and sources of the terrestrial organic carbon.

References

- Bianchi, T.S., Lambert, C., and Biggs, D.C., 1995. Bulletin of Marine Science. 56: 25-32.
Goni, M.A., Ruttenberg, K.C., and Eglinton, T.I., 1997. Nature. 389(6648):275-278.
Hedges, J.I. and Ertel, J.R., 1982. Analytical Chemistry. 54(2): 174-178.
Hedges, J.I. and Keil, R.G., 1995. Marine Chemistry. 49(2-3): 81-115.

PB2-21: The stratigraphic distribution of gem-dialkylalkanes in the Plio-Pleistocene Rio Dell and Merced formations, Northern California: implications for the paleoecology of the (as yet unknown?) source organisms

D.A. Zinniker, G. Nylén, M. Nell, P. Denisevich, J.M. Moldowan, J. Michael

Department of Geological and Environmental Sciences, Stanford Univ., Stanford California, 94305-2115, USA

Nine homologous series of unique *gem*-dialkylalkanes (GDAAs) (a.k.a. branched alkanes with quaternary carbon centers -- BAQCAs), have been identified and quantified in two Plio-Pleistocene sedimentary sequences exposed along the California coastline. While the source organisms of these compounds remain unknown, there is significant evidence that these compounds are derived from the membranes of colorless sulfur bacteria and/or other redox gradient dependent chemotrophic bacteria (Greenwood *et al.*, 2004; Kenig *et al.*, 2003).

While their abundance varies by two orders of magnitude through inferred glacial-interglacial cycles, GDAAs were found in all Merced and Rio Dell formation samples across diverse depositional environments: lacustrine, fresh water marsh, salt marsh, embayment, shoreface, shelf, and slope. Detailed analysis of sedimentary structures, ichnofossils, macrofossils, benthic foraminifera, the stable isotopic composition of foraminiferal carbonate, and a range of environmentally sensitive molecular fossils provides an invaluable context within which variations in GDAA abundance can be interpreted.

In both formations, the abundance of GDAAs appears to be negatively correlated with evidence of higher benthic oxygen concentrations and positively correlated with the occurrence of elemental sulfur in solvent extracts (Figure 1). In the Rio Dell Formation, dominant 2,2-dimethylalkanes and 5,5-diethylalkanes are inversely correlated with the abundance of neritic benthic foraminifera and both trace fossil and macrofossil assemblages indicative of higher benthic oxygen concentrations. In the Merced Formation the lowest concentrations of GDAAs are found in well oxygenated, high-energy nearshore and backshore environments, and C₂₁, C₂₃, and C₂₅ 5,5-diethylalkanes are highly correlated with normal marine, low energy, organic-rich shelf sediments.

Evidence compiled in this study supports a widespread chemotrophic or chemoorganotrophic source organism for GDAAs. More specifically, the source organism(s) may belong to bacterial consortiums oxidizing metal sulfides at redox boundaries within sediments. The abundance of such organisms would be a function of both the activity of sulfate reducing bacteria and the rate of bioturbative/diffusive penetration of electron acceptors (O₂, MnO₂, NO₃⁻, etc.). If true, GDAA source organisms may also thrive in certain deep subsurface environments where sedimentary, igneous, or metamorphic metal sulfides exist in the presence of appropriate electron acceptors.

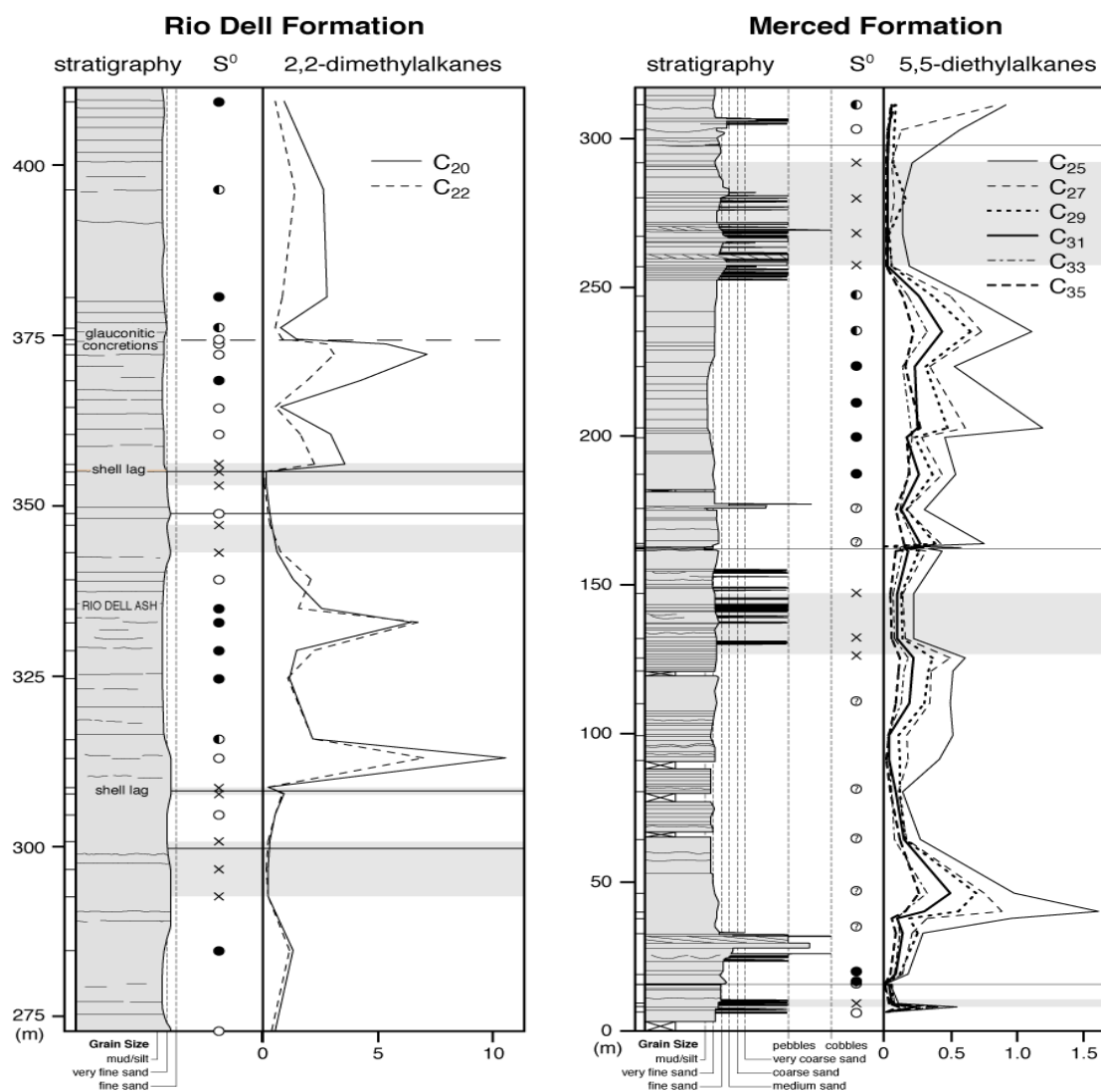


Figure 1. The relative abundance of 2,2-dimethylalkanes in the Rio Dell Formation and 5,5-diethylalkanes in the Merced Formation. Abundance is expressed as a simple ratio to C₂₀ *n*-alkane. Zones free of elemental sulfur (S⁰) are shown in grey. In the Rio Dell Formation, ferric-stained horizons are shown as solid tie lines, and zones with glauconite rich concretions are shown as dashed tie lines. In the Merced Formation, solid tie lines represent lignite horizons.

References

- Greenwood, P.F., Arouri, K.R., Logan, G.A., Summons, R.E., (2004) Abundance and geochemical significance of C_{2n} dialkylalkanes and highly branched C_{3n} alkanes in diverse Meso- and Neoproterozoic sediments. *Organic Geochemistry*, 35, 331-346.
- Kenig, F., Simons, D.-J.H., Crich, D., Cowen, J.P., Ventura, G.T., Rehbein-Khalily, T., Brown, T.C., Anderson, K.B., (2003) Branched aliphatic alkanes with quaternary substituted carbon atoms in modern and ancient geologic samples. *Proceedings of the National Academy of Sciences*, 100(22), 12554-12558.

PB2-22: Lipid biomarkers in Spanish saline lake sediments: indicators of organic inputs and environmental change

E.J. Pearson¹, P. Farrimond², S. Juggins¹

1) School of Geography, Politics & Sociology, University of Newcastle, Newcastle-upon-Tyne, NE1 7RU, UK
(email: e.j.pearson@ncl.ac.uk)

2) Integrated Geochemical Interpretation Ltd., Hallsannery, Bideford, Devon, EX39 5HE, UK

This presentation outlines the development and application of novel lipid-environment models for reconstructing past hydrological and hydrochemical change in Spanish saline lakes.

The approach involves the construction of a modern surface sediment dataset and uses relationships between organic source inputs, environmental conditions and lipid composition to construct lipid-environment models for application to sediment records. The surface sediment training set includes 54 lakes from a wide range of environments spanning both hydrochemical and hydrological gradients (fresh to hypersaline, ephemeral to permanent, shallow to deep) likely to have occurred in these environments in the past.

Multivariate statistical analysis of normalised lipid biomarker abundances in the surface sample dataset shows a clear distinction between dominant source inputs that can be generally characterised as being from bacterial, algal and higher plant material. Further statistical analysis enables dissection of the broad source input groups into smaller groups based on compound similarity for more detailed source input and environmental analysis. Although source input controls the largest variation in the data, within the broad source grouping there are also statistically significant influences from the major environmental parameters (salinity, water depth, degree of lake permanence).

Lipid-environment relationships are investigated for individual compounds and models are developed to relate lipid composition and lake type. These models are cross validated and give high predictive success for the surface sample dataset.

Down-core lipid-inferred changes in organic inputs and depositional environments and model reconstructions are compared and correlated with published data using other proxies. Results suggest good predictive abilities of these lipid-environment models for reconstructing past environmental change at these sites.

PPC1-1: Upper Jurassic/Lower Cretaceous anoxic event of Adriatic-Dinaridic domain

G. Baric, V. Tari

INA –NAFTAPLIN, Exploration and Development Department, 10000 Zagreb, Subiceva 29, Croatia
(e-mail: gertrud.baric@ina.hr)

Worldwide shallow epicontinental seas transgressing over platforms and depressions have occurred several times during geological history. Special significance has extensive sea level rises during Upper Jurassic/Cretaceous time, when the main world's source rocks were deposited.

The presence of organic rich Upper Jurassic and Lower Cretaceous strata was evidenced in Tethys domain, involving North Africa, Italy and Adriatic-Dinaridic realm [1]. The paper represents the results of geological and geochemical investigation and correlation study of Adriatic and Dinaridic carbonate platforms. Many factors control organic facies formation in this period, as well as preservation, maturity and hydrocarbon generation.

The Adriatic offshore and external Dinarides represent a part of the Apulian continental plate placed within the Tethys Ocean between Africa and Europe for the most of the Mesozoic age. Apulian plate, according geological and geophysical records, was composed of several platforms and basins created by rifting processes during Middle Triassic-Late Jurassic time [2]. The area was influenced by tectonics and rapid sea level rise causing anoxic conditions both in basinal and carbonate platform environments. Therefore two genetic sections are recognized: 1) facies with pelagic influence and 2) very shallow platform facies.

1) Dinaridic carbonate platform was intersected during Late Jurassic time (Oxfordian-Kimmeridgian) by considerably deep tectonic graben, which was filled, due to a global sea level rise, with organic rich laminated shaly limestone. These Upper Jurassic sediments contain high concentration (up to 26.6%) of amorphous organic matter, deposited in restricted deep marine environments. High hydrogen indices (400-700mgHC/gTOC) correspond to type II kerogen (oil prone). Petroleum potential (S1+S2) reaches a maximum of 153,1 mgHC/g rock. Stable carbon isotope and biomarker analyses varied in broad range. On some localities organic matter is characterized by carbon isotope values of $\delta^{13}\text{C}$ -23.3 to -24.7 ‰, but depletion of heavy isotope ^{13}C with high negative ratios ($\delta^{13}\text{C}$ -27.8 to -29.7 ‰) were recognized as well. The samples showed differences in regular sterane distributions also, and were detected predominance of C29 or C27 steranes. All analyses point to that organic matter originated from hydrogen rich algal or bacterial lipids.

2) Particularly interesting is the thick Late Jurassic-Lowermost Cretaceous sequence deposited in high reductive carbonate-evaporate environments in the central part of Adriatic carbonate platform. Source rocks intervals with organic carbon values from 0.30 to 4.72% were recognized in dark gray highly bituminous, laminated micritic limestone in wells at the depths from 600 to 4600 m. Pyrolysis, microscopy and isotopic analyses ($\delta^{13}\text{C}$ -22.7 to -23.9 ‰) indicated that the marine organic matter constituents are hydrogen and lipid rich components (kerogen Type II S) with good oil-generating capacities [3].

Maturation parameters for both source rock types indicate an immature to marginally mature stage of thermal transformation, resulting from low geothermal gradients of the study area. Despite the immaturity, bitumen concentrations in the source rocks of evaporite-carbonate complex are extremely high. This could be attributed to sulfur rich-kerogen, where weak S-C bonds require significantly lower activation energy during cracking; thus hydrocarbon generation occurs at lower maturity levels. The bitumen characterized large amount of resins and asphaltenes. All parameters lead to conclusion that the identified low maturity source rocks are sourcing heavy hydrocarbons of low migration capacity, which appear in noncommercial quantities.

Conclusion

Geochemical research of Upper Jurassic and Lower Cretaceous strata in Adriatic/Dinaridic carbonate platform area indicate the presence of good source rock sequences with high generative potential. Organic rich strata were developed by global anoxic events and tectonic disintegration of the area. The similarity of organic facies of these sequences was established by correlation studies. Organic matter consists of amorphous, hydrogen and sulfur rich components originated predominantly from algal and bacterial lipids. Source rock maturity varies between immature to early mature stage, depending on subsidence, thermal history and tectonic position and can be correlated with other source rocks of the same age in broader Mediterranean area.

References

- [1] Jenkyns, H.C., 1991. Impact of Cretaceous Sea Level Rise and Anoxic Events on the Mesozoic Carbonate Platform of Yugoslavia, American Association of Petroleum Geologists Bulletin, 75, 1007-1017
- [2] Barić, G. and Tari V., 2001. Petroleum Systems of the Adriatic Offshore, 63rd European Association of Geoscientists & Engineers 13. (EAGE) Conference, Amsterdam, Extended abstracts Vol. 2, P 504. (2001).
- [3] Sinninghe Damste, J.S. and de Leeuw, J.W., 1990. Analysis, structure and geochemical significance of organically-bound sulphur in the geosphere: State of the art and future research. Organic Geochemistry, 16 (4-6), 1077-1101.

PPC1-2: Paired measurements of the Sr/Ca-ratio and the carbon isotopic composition of C₃₇ alkenones in particulate matter from Caribbean Sea surface waters

D. Brouwer¹, B. Schnetger¹, C. Rühlemann², J. Rullkötter¹, S. Schulte¹

1) Institute of Chemistry and Biology of the Marine Environment, Carl von Ossietzky University of Oldenburg, P.O. Box 2503, D-26111 Oldenburg, Germany (e-mail: brouwer@icbm.de)

2) Federal Institute for Geosciences and Natural Resources (BGR), Hannover, Germany

Carbon dioxide is one of the greenhouse gases controlling the global heat budget, and there is growing evidence that the increase in the atmospheric CO₂ level observed since the 19th century contributes to global warming. However, predictions of future changes of climate on Earth are difficult since the relationship between atmospheric CO₂ and long-term climatic cycles is complex and poorly understood. To define better the mechanisms by which oceanic and atmospheric levels of CO₂ have changed over geological time scales, palaeoceanic sources and sinks of CO₂ must be delineated. This requires accurate palaeo-indicators (proxies) for past CO₂ concentrations in the surface oceans.

The carbon isotopic fractionation (ϵ_p ; expressed in ‰) of C₃₇-alkenones was used to reconstruct past atmospheric CO₂ concentrations [1]. ϵ_p is mainly a function of the growth rate, the factors influencing the growth rate (e.g. nutrients) and the ambient CO₂(aq) concentration. Consequently, precise reconstructions of CO₂(aq) based on ϵ_p of alkenones require a correction for the influence of growth rate and factors influencing the growth rate, respectively. Based on surface sediment studies Stoll and Schrag [2] suggested the Sr/Ca ratio in coccolithophorid calcite to be an independent proxy of coccolithophorid growth rate. Indeed, culture experiments confirmed the growth rate dependence of Sr incorporation during coccolith calcification. Thus, it was suggested to combine coccolith Sr/Ca ratios with the carbon isotopic fractionation of C₃₇ alkenones in order to improve palaeo-CO₂ estimates.

In the present study we determined, for the first time, paired data of the partition coefficient of strontium (D_{Sr}) into coccolith calcite and the isotopic fractionation (ϵ_p) of C₃₇ alkenones in particulate matter from oceanic surface waters of the Caribbean Sea. Consistent with sediment-based and culture studies, a positive relationship is observed between D_{Sr} and surface water phosphate concentration ($[PO_4^{3-}]$) suggesting a growth rate-depending control on D_{Sr} . In contrast to laboratory studies no temperature dependence of D_{Sr} was observed. The obtained relationships between ϵ_p and surface water concentrations of phosphate and carbon dioxide ($[CO_2(aq)]$) imply that ϵ_p is mainly influenced by two factors, the growth rate and the ambient CO₂(aq) concentration. Following the approach of Stoll and Schrag [2], in a further step we used the observed relation between $[PO_4^{3-}]$ and D_{Sr} to correct ϵ_p for the growth rate

influence. The resulting corrected values (ϵ_p -corrected) show a significant negative correlation ($R= 0.93$) with the inverse of the carbon dioxide concentration $[\text{CO}_2(\text{aq})]$ as expected from model calculations. Apparently, coccolith Sr/Ca ratios in combination with the carbon isotopic fractionation of C_{37} alkenones permits more reliable calculation of past dissolved CO_2 in the surface ocean.

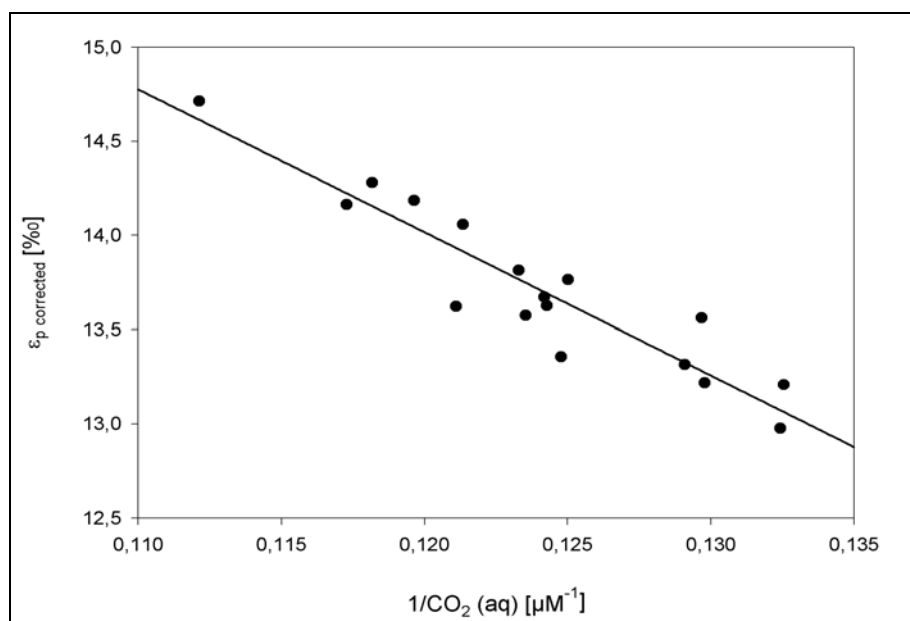


Fig.1. Corrected carbon isotopic fractionation (ϵ_p -corrected) of alkenones in relation to $1/[\text{CO}_2(\text{aq})]$ in particulate matter from Caribbean Sea surface waters

References

- [1] Jasper, J.P. and Hayes, J.M., 1990. A carbon isotope record of CO_2 levels during the late Quaternary. *Nature* 347, 462-464.
- [2] Stoll, H.M. and Schrag, D.P., 1999. Coccolith Sr/Ca as a new indicator of coccolithophorid calcification and growth rate. *Geochemistry, Geophysics, Geosystems* 1 (5), doi:10.1029/1999GC000015.

**PPC1-3: Vegetation change in tropical East Africa since the last Glacial maximum:
the molecular record from Lake Malawi**

I.S. Castañeda¹, J.P. Werne¹, T.C. Johnson¹, L.A. Powers¹, Y. Huang²

1) Large Lakes Observatory, 10 University Drive, 109 RLB, Duluth, MN 55812 USA

2) Brown University, Geological Sciences, 324 Brook Street, Providence, RI 02912 USA

Understanding the response of terrestrial vegetation to global climate change is important as vegetation strongly controls the partitioning of energy between latent and sensible heat fluxes at earth's surface and can impart important feedbacks on global carbon, water, and nutrient cycles (Ostendorf et al., 2001). It is well-known that major changes in the distribution of C₃ and C₄ plants have occurred on glacial-interglacial and longer timescales, and this has important implications for the global carbon cycle since woody vegetation is generally thought to store more carbon than grasslands (Jackson et al., 2002; Schimel et al., 2001; Scholes and Archer, 1997; Schlesinger et al., 1990). At present, the main forcing factors controlling the global distribution of C₃ and C₄ vegetation are debated (Schefuß et al., 2003). Temperature, aridity, and atmospheric CO₂ concentrations (*p*CO₂) are known to be important drivers of vegetation change (Huang et al., 2001; Pagani et al., 1999; Kuypers et al., 1999; Collatz et al., 1998; Cerling et al., 1993), however, the relative importance of each of these factors is not well understood (Zhang et al., 2003).

Lake Malawi, situated in low-latitude tropical Africa, provides an ideal location to examine the response of tropical terrestrial vegetation to global climate change. Lake Malawi contains a continuous and high-resolution sedimentary record of the past 25,000 years, is situated within a climatically important geographical location that is heavily influenced by the intertropical convergence zone (ITCZ) (Jury and Gwazantini, 2002), and is located in an ecologically sensitive location near the boundary of tree savannah (C₃ dominated) and grass savannah (C₄ dominated) vegetation zones. Here we use molecular biomarkers and compound-specific carbon isotopes to examine changes in the terrestrial vegetation of East Africa since the LGM. As detailed reconstructions of temperature (Powers et al., submitted) and aridity (lake level) (Gasse, 2002) exist for Lake Malawi, and since past *p*CO₂ is known from ice core records (Monnin et al., 2004), reconstructing terrestrial vegetation from this site allows for the examination of the relative influences of temperature, aridity, and *p*CO₂ on the distribution of C₃ vs. C₄ biomass. We have also refined the existing diatom based aridity (lake level) record from Lake Malawi (Gasse, 2002) through analysis of compound-specific deuterium isotopes.

Results of this study show that the terrestrial vegetation of tropical East Africa has undergone major and rapid changes over the past 23,000 cal BP (Figure 1). In particular, significant changes are noted at the LGM, during the Younger Dryas, at ~8 cal ka, and at 5 cal ka. Results of this study are also in agreement with previous studies of Lake Malawi that have provided evidence for variability in the position and strength of the ITCZ over the past 25,000 years, as we note a correlation between abundances of terrestrial plant biomarkers with periods of increased northerly winds over Lake Malawi (Johnson et al., 2002).

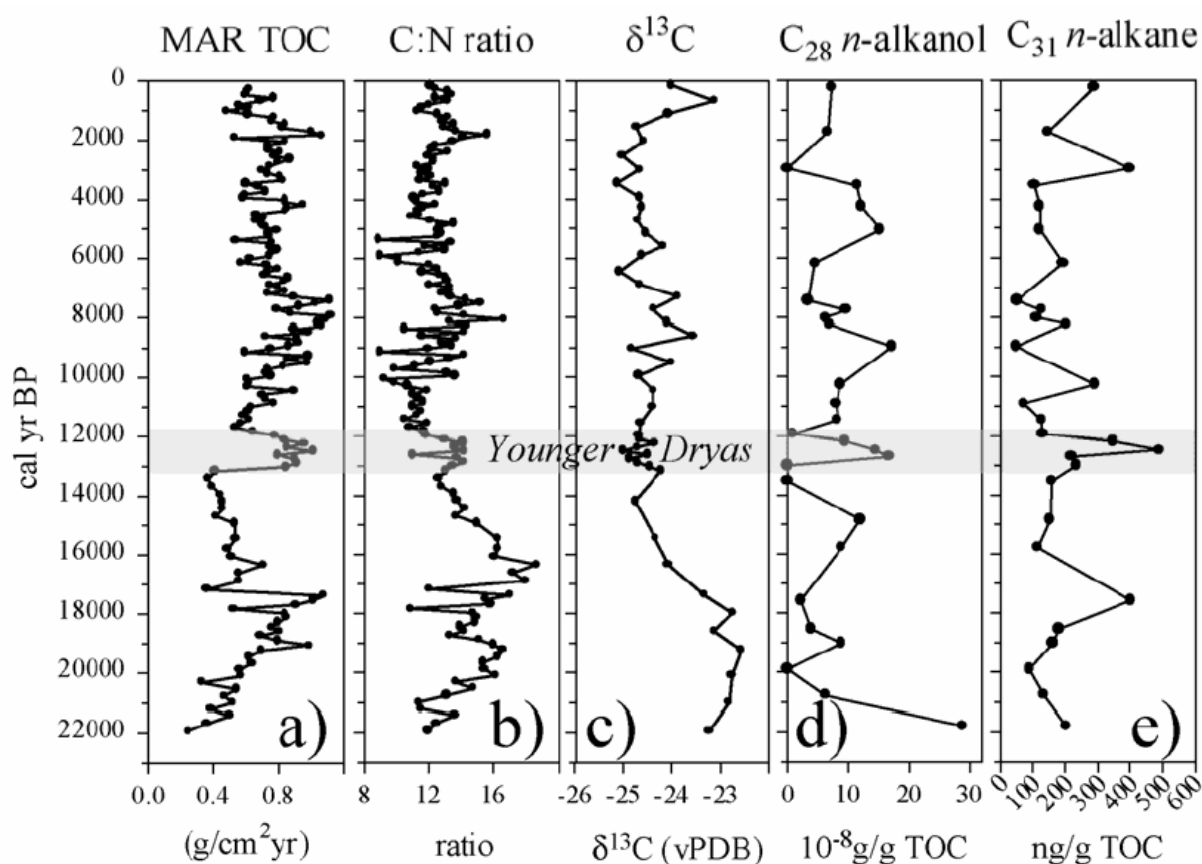


Fig. 1. Lake Malawi data. The Younger Dryas Cold Period, an interval of significant variability, is highlighted. a) Mass accumulation rate of total organic carbon (TOC). b) Carbon/nitrogen (C/N) ratio. c) Bulk carbon isotope data. d) Abundance of the C₂₈ n-alkanol. e) Abundance of the C₃₁ n-alkane.

PPC1-4: Evidence for photic zone Euxinia during the Permian-Triassic “Superanoxic Event”

K. Grice¹, M.E. Böttcher², R.J. Twitchett³, E. Grosjean⁴, R.E. Summons⁴, S.C. Turgeon⁵,
W. Dunning¹

1) Curtin University of Technology, Perth 6845 WA, Australia (e-mail: K.Grice@curtin.edu.au)

2) Max Planck Institute for Marine Microbiology, Germany

3) Plymouth University, United Kingdom

4) Massachusetts Institute of Technology, Cambridge MA, USA

5) Oak Ridge National Laboratory, USA

The most severe extinction of the past 500 million years occurred in the Latest Permian during a period of global warming (e.g. [1]). In the oceans, 49 % of invertebrate families became extinct, representing about 80-96 % species loss. It took almost 100 million years until global marine biodiversity to recover to pre-crisis levels. Many modern marine groups originated and radiated in the extinction aftermath. Anoxia has been proposed as having a crucial role in driving the mass extinction ([2], [3]). Surface outcropping of sulfidic waters, and emissions of hydrogen sulfide to the atmosphere provides a kill mechanism that probably accounts for the marine and terrestrial extinctions ([4]).

In the present study we have undertaken the first detailed geochemical study of the redox conditions that existed in the paleowater column during the P-Tr 'Superanoxic Event'. We have utilised carbon and sulfur isotopic data, biomarker (metalloporphyrins and green sulphur bacterial biomarkers) and redox sensitive metal abundances (dithionite-extractable iron- Fe_D + pyrite iron- Fe_P) / total Fe- Fe_T), of a proven petroleum source rock of a recently discovered marine Permian-Triassic (P-Tr) drill core (Hovea-3) from the onshore northern Perth Basin, Western Australia (Figure 1). Several biomarkers attributed ultimately to anoxygenic photosynthetic green sulfur bacteria (GSB) have been identified in the Early Triassic (Griesbachian) drill core. Summons et al. (these proceedings) report similar results from the P-Tr Global Stratotype section and Point in South China. Thus, waters of the southern Tethys Ocean were periodically euxinic in the photic zone during and after the mass extinction event and the pervasiveness and duration of sulfide in surface waters may have been a leading factor in the mass extinction and the protracted recovery ([4]).

Stable carbon isotopic data from the bulk kerogen fraction of Hovea-3 shows an abrupt 7.5 ‰ negative shift from the Upper Permian to Lower Triassic consistent with a localised palynofacies change from charcoal-wood dominated organic matter to algal-amorphous organic matter, respectively. However, $\delta^{13}C$ data on higher plant and phytoplankton biomarkers show similar isotopic changes across the P-Tr transition indicating

a global disruption to the carbon cycle. GSB biomarkers have also been identified in several Perth Basin crude oils ([5]). Photic zone euxinia (PZE) is usually associated with the widespread deposition of organic matter-rich sediments that constitute important source rocks for petroleum deposits that are being exploited today. With the exception of the Perth Basin, such organic matter-rich sediments are virtually absent from Upper Permian and Lower Triassic sediments globally. The onset of PZE in Hovea-3 coincides with a sharp facies change, reflecting rapid transgression. Localized surface ocean productivity must have played a key role in the deposition of a petroleum source rock at this location, although PZE was globally more widespread during the P-Tr' Superanoxic Event'.

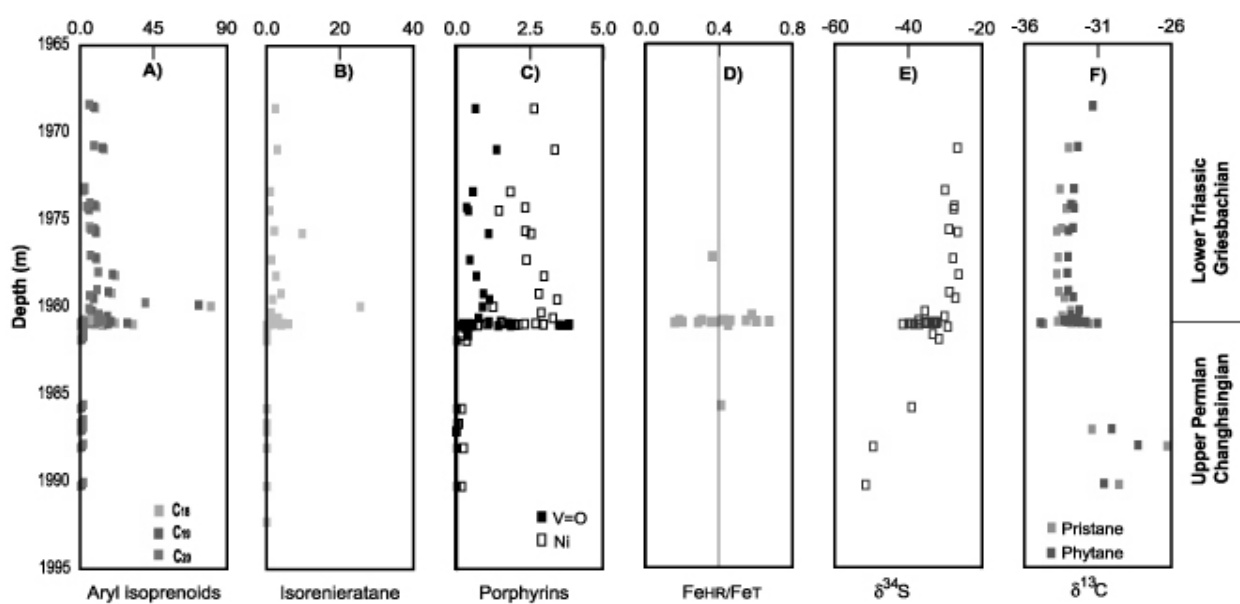


Fig.1. Organic and inorganic parameters from Hovea-3 borehole ([4])

References

- [1] Benton, M.J., Twitchett, R.J., 2003. How to kill (almost) all life: The end-Permian extinction event, *Trends in Ecology and Evolution* 7, 358-365.
- [2] Wignall P.B., Hallam, A., 1992. Griesbachian (Earliest Triassic) palaeoenvironmental changes in the Salt Range, Pakistan and southwest China and their bearing on the Permian-Triassic mass extinction event, *Palaeogeography, Palaeoclimatology, Palaeoecology* 93, 21-46.
- [3] Klump, L.R., Pavlov A., Arthur, M., Kato Y., Riccardi, A., 2003. Death by hydrogen sulfide: a kill mechanism. Abstracts of GSA Meeting, Paper 81.
- [4] Grice, K., Cao, C., Love, G.D., Böttcher, M.E., Twitchett R.J., Grosjean, E., Summons, R.E., Turgeon, S.C., Dunning, W., Jin, Y., 2005. Photic zone euxinia during the Permian-Triassic superanoxic event. *Science* 307, 706-709.
- [5] Grice, K., Summons, R.E., Grosjean, E., Twitchett, R.J., Wang, S.X., Dunning, W., Böttcher, M.E., 2005. Depositional conditions of the northern onshore Perth Basin (Basal Triassic). *Journal of the Australian Petroleum Exploration Association* (in press).

**PPC1-5: Lipid residues as paleo-environmental tracers? –
An example from the Emsian of the Prüm Syncline (Eifel Mts., Germany)**

M. Havertz, U. Mann, R.G. Schaefer

Forschungszentrum Jülich, Institut Sedimentäre Systeme, D-52425 Jülich, Germany
(e-mail: u.mann@fz-juelich.de)

In order to investigate the Emsian sedimentology and paleoecology (*ESPEC Research Programme*), a core sequence of 150m with proximal sediments were recovered from the Prüm syncline in the Eifel Mountains (Germany). Relevant geological information about the stratigraphic section is primarily based on [1].

The sedimentary sequence represents an overall regressive cycle part with quartzitic sandstones at the base (*“Emsquarzit”*), silt- and fine sandstones in the middle part, and alternations between silt- and claystones at the top. In total, all sediments have to be classified as being deposited at a strongly oxic sediment/water interface [2]. Accordingly, strongly degraded organic matter has to be assumed.

In order to examine if the molecular composition is still capable to monitor the changing environmental conditions in parallel to the lithofacies changes, the amounts of the residual organic matter and their lipid composition were analysed.

The approach is based on a screening of 169 samples for organic carbon, carbonate carbon and hydrogen index by Leco and Rock-Eval, respectively. Based on 30 selected samples, absolute yields of the C₁₅₊-soluble organic matter were determined as extracted by dichloromethane. After separation into saturated hydrocarbons, aromatic hydrocarbons and NSO-compounds, the molecular composition of the respective saturated fractions were analysed by gas chromatography.

Values for mean hydrogen index and extract yields of the total *n*-alkane fraction are extremely low with 15mgHC/g TOC and 10-40µg/g TOC, respectively. Nevertheless, three groups of samples exhibiting maxima of their C₁₅₊ envelope curve at C₁₅₋₁₇, at C₂₃ or at C₂₉ seem still to be able to carry information on variable contributions of algal, bacterial and terrestrial derived organic matter (Fig. 1).

If the residues of varying contributions of different types of organic are still able to monitor relative environmental changes correctly in spite of highly oxic depositional conditions, will be discussed.

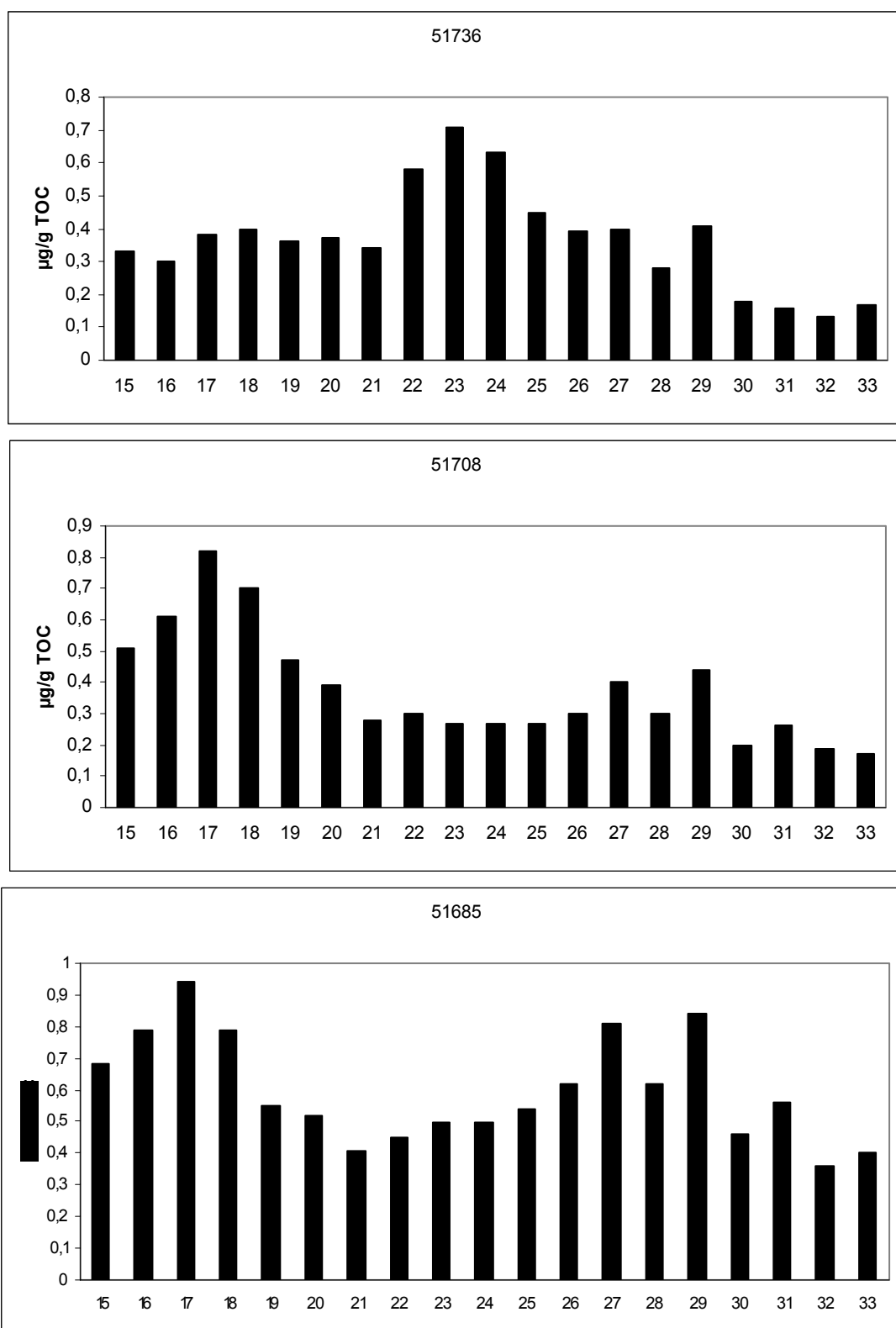


Fig.1. Molecular composition of the C_{15-33} *n*-alkanes of representative samples from 54.41m (sample 51708), 86.81m (sample 51685) and 126.27m depth (sample 51736)

References

- [1] Struve, W., Plodowski, G. and Weddige, K. (1997) Biostratigraphische Stufengrenzen und Events in der Prümer und Hillesheimer Mulde. *Terra Nostra* 97 (7), 3-51.
 [2] (Wonik, pers. comm.).

PPC1-6: An improved method for C and N isotopic analyses of sedimentary porphyrins and its application to studies of past geological events

Y. Kashiwama¹, N.O. Ogawa², H. Suga², Y. Chikaraishi², R. Tada¹
K. Matsumoto², T. Sakamoto², J. Kuroda³, H. Kitazato², N. Ohkouchi²

1) Department of Earth and Planetary Science, University of Tokyo, Tokyo 113-0033, Japan

2) Institute for Research on the Earth Evolution, Japan Agency for Marine-Earth Science and Technology, Yokosuka 237-0061, Japan

3) Ocean Research Institute, University of Tokyo, Tokyo 164-8639, Japan

The majority of porphyrin compounds found in sedimentary rocks have been known to be derived from tetrapyrrole structures of various chloropigments through structural studies. They should carry information of past phototrophic communities hence surface oceanic conditions. Significantly, porphyrins comprise both C and N and thus are potential biomarkers based on which C and N isotopic compositions of primary producers can be estimated. In conjunction with other geological information, it should allow, not only precursor-biomarker correlation by multi-dimensional isotopic analysis, estimations of ocean-atmospheric states of the past, including N-cycling. We have developed a high-throughput / high-sensitivity method for C and N isotopic analyses of sedimentary porphyrins, aiming for application to high resolution studies of palaeoenvironments. Extracts from organic-rich siliceous mudstones of the middle Miocene Onnagawa Formation are used in the methodological development. Over 20 varieties of alkyl-metalloporphyrins (as Ni-, VO-, and Cu-complexes) and metal-free porphyrins and several porphyrinic acids are baseline-separated and collected for purposes of isotopic analyses in semi-preparative HPLC. Carbon and N isotopic compositions are measured in EA-IRMS with an improved performance, in which, for instance, only ca. 40 micro grams of purified porphyrins are required for a satisfactory analysis for N isotope. We will also report structural and isotopic study of sedimentary porphyrins in the black shales of the mid-Cretaceous OAE intervals (Bonarelli and Selli, Italy) and discuss palaeoenvironmental conditions lead to such unusual world-wide depositions of organic-rich sediments and the biological turnovers.

PPC1-7: Biogeochemistry of Neoproterozoic cap carbonates – A speculative hypothesis

D.M. McKirdy¹, P.R. Gammon^{1,2}, H.D. Smith^{1,3}, H.R. Hayward¹, S. Sonter¹

1) Organic Geochemistry in Basin Analysis Group, School of Earth & Environmental Sciences, University of Adelaide, SA 5005, Australia (e-mail: david.mckirdy@adelaide.edu.au)

2) 177 Sydenham St., Gananoque, Ontario K7G 1C1, Canada

3) Roads & Traffic Authority, Newcastle, NSW 2300, Australia

Within the Neoproterozoic succession of the Adelaide Fold-Thrust Belt, South Australia, two of the most severe ice ages in Earth history are recorded in the glacial rocks at the base and top of the 4.5 km-thick Umberatana Group (McKirdy et al., 2001). These are the Sturtian (*ca* 710 Ma) and Marinoan (*ca* 635 Ma) glaciations, the latter being regarded by some as the product of a "Snowball Earth" (Hofmann and Schrag, 2002). Similar glacial deposits occur elsewhere in Australia and on every other continent but their supposed age equivalence, based in part by C- and Sr-isotope chemostratigraphy, is the subject of ongoing debate. Prominent among the characteristics that distinguish Sturtian (Riphean) and Marinoan (Vendian) glacial intervals worldwide are the amount of organic matter (OM) preserved as kerogen in their respective cap carbonates, and the slopes of the $\delta^{13}\text{C}$ profiles of the latter. Kennedy et al. (1998) noted that "dark, organic-rich cap carbonate" which becomes isotopically heavier up-section is typical of the older glacials, in stark contrast to the negative isotopic excursion recorded in the organically lean, younger cap rocks, but otherwise this important difference has gone largely unremarked. Following careful petrographic, elemental and isotopic analyses of the carbonate phases in the dark grey, dolomitic Tindelpina Shale (0.14–1.1% TOC) and the buff yellow Nuccaleena Formation (<0.01% TOC) from the Flinders Ranges and Stuart Shelf, we are now able to offer an explanation for the geochemical contrast between these two archetypical Neoproterozoic cap carbonates. Like their counterparts elsewhere, both are "cap dolomites" that pass the conventional tests for lack of post-depositional alteration. However, according to other petrographic and geochemical criteria (based on carbonate vein paragenesis) they in fact comprise early post-depositional "organogenic dolomite" (Mazzullo, 2000). This means that their $\delta^{13}\text{C}_{\text{carb}}$ profiles are artefacts of sub-seafloor bacterial oxidation of organic matter and in no way reflect the chemistry of the contemporary ocean.

The negative slope of the Nuccaleena $\delta^{13}\text{C}_{\text{carb}}$ profile (typically -1.5 to -3.5% over *ca* 1 m) is consistent with dolomitisation of primary micrite having taken place entirely within the zone of bacterial sulphate reduction in the upper 3 m or so of the sediment column (Gammon et al., 2005). Pore water sulphate is a well-known inhibitor of dolomite precipitation in modern oceanic sediments. The organic-leanness of the Nuccaleena cap dolostone suggests that the rate of supply of dead planktonic biomass (rich in protein) to the

Marinoan seafloor was insufficient for anaerobic heterotrophy to continue into the zone of methanogenesis. Thus, by the time sulphate was exhausted, so too was the dispersed OM. Meanwhile, the diagenetic bicarbonate contributed to the pore waters by the sulphate reducers ($\delta^{13}\text{C} \sim -25\text{‰}$) shifted the isotopic signature of the organogenic dolomite to values progressively more negative than the $-2 \pm 1\text{‰}$ starting point of most post-glacial $\delta^{13}\text{C}_{\text{carb}}$ profiles.

The elevated TOC contents of the dolomitic, pyritic Tindelpina Shale suggest that it was deposited while the oxic-anoxic boundary was located within the water column, well above the Sturtian seafloor. This in turn led to a higher rate of preservation of planktonic biomass, and enough labile OM to support methanogenic bacteria following the cessation of sulphate reduction. The bicarbonate produced by methanogens is isotopically heavy ($\delta^{13}\text{C} \sim +15\text{‰}$), ensuring that any organogenic dolomite would be enriched in ^{13}C relative to the contemporary ocean water carbonate. The observed positive excursion recorded by the Tindelpina's dolomite (-5 to $+1.5\text{‰}$) is thus explained. It is of interest that the co-existing kerogen (-29 to -26‰ over 79 m in the central Flinders Ranges; -34 to -31‰ over 13 m on the Stuart Shelf) records a much smaller excursion (albeit in the same direction). This is further evidence for the decoupling of the carbonate and organic carbon isotopic signals. Only the latter would seem to be a potentially reliable proxy (offset by $\sim 28.5\text{‰}$) for the C-isotopic composition of the photic zone in the post-glacial Sturtian ocean. But, even then, one has to take account of likely changes in the balance of pelagic (algal) versus benthic (bacterial) inputs to the kerogen that may accompany regional variations in water depth across the basin. Our hypothesis, if validated, has important implications for isotope chemostratigraphy and what it can (and cannot) tell us about Neoproterozoic carbon cycling, palaeoclimates and oceanic circulation.

References

- Kennedy, M.J., Runnegar, B., Prave, A.R., Hoffmann, K.H. & Arthur, M.R., 1998. Two or four Neoproterozoic glaciations? *Geology* **26**, 1059–1063.
- Gammon, P.R., McKirdy, D.M. & Smith, H.D., 2005. The timing and environment of tepee formation in a Marinoan cap carbonate. *Sedimentary Geology* (in press).
- Hoffman, P. F. & Schrag, D. P., 2002. The snowball earth hypothesis: testing the limits of global change. *Terra Nova* **14**, 129-155.
- McKirdy, D. M., Burgess, J.D., Lemon, N.M., Yu X., Cooper, A.M., Gostin, V.A., Jenkins, R.J.F. & Both, R.A., 2001. A chemostratigraphic overview of the late Cryogenian interglacial sequence in the Adelaide Fold-Thrust Belt, South Australia. *Precambrian Research* **106**, 149-186.
- Mazzullo, S. J., 2000. Organogenic dolomitization in peritidal to deep-sea sediments. *Journal of Sedimentary Research* **70**, 10-23.

PPC1-8: Sapropels in shallow Holocene coastal lakes of Southeastern Australia: an elemental and isotopic perspective

A.C. Mee¹, D.M. McKirdy¹, E.S. Krull², M.A.J. Williams³

1) CRC LEME and Organic Geochemistry in Basin Analysis Group, School of Earth and Environmental Sciences, University of Adelaide, SA, 5005 (e-mail: aija.mee@adelaide.edu.au)

2) CRC GA, CSIRO Land and Water, PMB 2, Glen Osmond, SA, 5064

3) CRC LEME, Geographical and Environmental Studies, University of Adelaide, SA, 5005

Many lakes along the Coorong coastal plain of southeastern Australia contain one or more discrete sapropels (0.01-1 m thick; TOC >2%; HI >300 mg hydrocarbons/g TOC) within their Holocene calcareous mudstone successions. Numerous studies have linked sapropel deposition in marine and deep-lake settings to abrupt palaeoenvironmental changes (e.g. Hassan et al., 1997; Tolun et al., 2002). The three shallow, alkaline lakes of the present investigation (North Stromatolite, Old Man and Amy) represent a distinctly different aquatic environment (water depth <4 m) yet also preserve organic matter (OM) in high concentrations (max. TOC = $18 \pm 2.6\%$). By identifying key geochemical and sedimentological triggers to sapropel formation in the coastal Coorong lakes, this study aims to throw further light on the environmental variations (fluctuating wet-dry phases) that affected Holocene SE Australia.

Radiocarbon ages of bulk OM isolated from uncompacted cores show that the aforementioned lakes have been accumulating sediment for the last 7000 years. Across SE Australia a shift from generally warmer and wetter to cooler and drier climatic conditions occurred at ca. 5 ka BP (Dodson and Ono 1997). Thus, sedimentation in these lakes spanned a period of regional climate change. The influence of this change on local lacustrine conditions should be reflected to some degree by variations in the elemental and isotopic composition of sedimentary OM. Knowledge of OM origin is fundamental to interpretation of the observed geochemical trends. For these lakes C/N ratios lie between the values typical of terrestrial ($C/N > 20$) and aquatic ($4 < C/N < 10$) organic inputs, but are skewed heavily toward the latter ($C/N_{\text{avg}} = 11.9 \pm 3.6$). Hayball *et al.* (1991) and McKirdy *et al.* (2002) also inferred a predominantly aquatic source for this lacustrine OM yet noted a significant terrestrial plant signature in its extractable *n*-alkanes. Clearly a multi-proxy approach is required to understand both the sedimentological processes acting in, and environmental conditions affecting these lakes.

In North Stromatolite Lake the basal unit ($C/N = 17.0$, $\delta^{13}\text{C} = -24.2\%$) has a higher terrestrial input than the overlying one metre thick sapropel ($C/N_{\text{avg}} = 13.2$, $\delta^{13}\text{C}_{\text{avg}} = -19.0\%$, $\delta^{15}\text{N}_{\text{avg}} = 4.8\%$). Sapropel deposition lasted for ca. 1200 years and halted remarkably

abruptly at 5120 ± 50 yrs BP (ANSTO code: OZH213). Within the sapropel $\delta^{13}\text{C}$ values increase steadily from -19.1 to -17.0 ‰. This range of $\delta^{13}\text{C}$ values suggests that the sapropel OM is principally derived from algae and cyanobacteria that were using HCO_3^- as their dissolved inorganic carbon (DIC) source. The increase in $\delta^{13}\text{C}$ over the sapropel thickness is evidence of photosynthesis in a closed, increasingly saline water body. A large negative shift in $\delta^{13}\text{C}$ since the end of sapropel deposition (to -22.3 ‰ at 7 cm depth) is attributed to a relative increase in the terrestrial component of the OM pool following an abrupt decrease in aquatic productivity at ca. 5 ka BP. With no fluvial input to this groundwater-fed lake the terrestrial contribution would most likely be aeolian soil-derived OM transported under the cooler, drier conditions thought to exist in the region since ca. 5 ka BP. Mee *et al.* (2004) demonstrated that aeolian material has contributed significantly to soils in SE South Australia during the Holocene.

In Old Man Lake and Lake Amy (100 km south of North Stromatolite) the deposition of comparable, albeit not as uniform, organic facies occurred from ca. 4 to 3 ka BP. The multiple sapropels of the two southern depocentres display similar $\delta^{13}\text{C}$ trends throughout their sedimentary successions but exhibit no strong internal correlation between $\delta^{13}\text{C}$ and C/N. If the majority of the observed isotopic variation were due solely to changes in OM source, such a relationship would be expected. Thus, the $\delta^{13}\text{C}$ values of these lacustrine sediments are interpreted as reflecting changes both in precursor biota and in local environmental conditions (water levels, nutrient status, pH, salinity). ^{13}C -NMR analysis of the lacustrine OM (pending) will help quantify the relative aquatic and terrestrial contributions to the individual sapropels and therefore assist in distinguishing the biotic and physicochemical drivers of the observed geochemical trends. The sedimentary successions of these three Coorong lakes may yet contribute to local Holocene environmental reconstruction.

References

- Dodson J.R., Ono Y., 1997. Timing of Late Quaternary vegetation response in the 30-50° latitude bands in southeastern Australia and northeastern Asia. *Quaternary International* 37, 89-104.
- Hassan, K.M., Swinehart J.B., Spalding R.F., 1997. Evidence for Holocene environmental change from C/N ratios, and $\delta^{13}\text{C}$ and $\delta^{15}\text{N}$ values in Swan Lake sediments, western Sand Hills, Nebraska. *Journal of Paleolimnology* 18, 121-130.
- Hayball A.J., McKirdy D.M., Warren J.K., von der Borch C.C., Padley D., 1991. Organic facies of Holocene carbonates in North Stromatolite Lake, Coorong region, South Australia. 15th International Meeting on Organic Geochemistry Abstracts, 19-20.
- McKirdy D.M., Brenchley A.J., Edwards S., 2002. Lacustrine sapropels as proxies for Late Quaternary environmental change in southeastern Australia. *Geological Society of Australia Abstracts* 67, 23.
- Mee A.C., Bestland E.A., Spooner N.A., 2004. Age and origin of Terra Rossa soils in the Coonawarra area of South Australia. *Geomorphology* 58, 1-25.
- Tolun, L., Catagay M.N., Carrigan W.J., 2002. Organic geochemistry and origin of Late Glacial-Holocene sapropelic layers and associated sediments in the Marmara Sea. *Marine Geology* 190, 47-60.

PCC1-9: Nitrogen fixation enhanced organic matter production in Demerara Rise mid-Cretaceous black shales

P.A. Meyers¹, S.M. Bernasconi², J.-G. Yum³

1) Marine Geology and Geochemistry Program, The University of Michigan, Ann Arbor, Michigan, U.S.A., 48109-1063

2) Geologisches Institut, Eidgenössische Technische Hochschule Zentrum, CH-8092 Zürich, Switzerland

3) Marine Geology and Geochemistry Program, The University of Michigan, Ann Arbor, Michigan, U.S.A., 48109-1063

The high concentrations of organic carbon that are common to Cretaceous black shales imply levels of sustained primary production that are unknown in the modern ocean. How organic matter productivity could be maintained for many millennia remains an open question. Cenomanian to Santonian black shale sequences in the five sites drilled by ODP Leg 207 on the Demerara Rise range in thickness from 56m to 93m. The finely laminated sequences contain between 1 and 28 percent organic carbon, and their organic geochemical properties reveal aspects of the exceptional conditions of organic matter production and preservation involved in their formation. The results of Rock-Eval pyrolysis show that the bulk of the organic matter originates from marine primary production. Improved preservation of the carbonaceous fraction organic matter relative to its nitrogenous fraction is implied by C/N ratios that increase to 40 as organic carbon concentrations increase. Land-plant organic matter appears to be important only in the lower Cenomanian black shales from Site 1260 in which C/N ratios sometimes reach 60. Nitrogen isotope compositions that become lighter as organic carbon concentrations increase indicate that organic matter production was enhanced by a consortium of primary producers that included nitrogen-fixing bacteria. Expansion of an intensified oxygen minimum zone into the photic zone probably permitted coexistence of algae and the photosynthetic bacteria that function best under dysaerobic and anaerobic conditions and that are not limited by nitrate availability.

PPC1-10: Origin and accumulation of organic matter in Albian to Santonian black shales on the Demerara Rise

P.A. Meyers¹, A. Forster²

1) Marine Geology and Geochemistry Program, The University of Michigan, Ann Arbor, Michigan, U.S.A., 48109-1063

2) Netherlands Institute for Sea Research (NIOZ), 1790 AB Den Burg, Texel, The Netherlands

Albian to Santonian black shale sequences were recovered at all five sites drilled by Ocean Drilling Program Leg 207 on the Demerara Rise in the western equatorial Atlantic Ocean. The finely laminated, dark-colored calcareous claystones typically contain between 2% and 15% organic carbon, and they range in thickness from 56m at Sites 1258 and 1259 to 93m at Site 1260. Organic geochemical properties of the black shales reveal aspects of the exceptional conditions of organic matter production and preservation involved in their formation. The results of Rock-Eval pyrolysis show that the bulk of the organic matter originates from heightened algal and microbial primary production. Organic matter is thermally immature, as evidenced by both the high Rock-Eval hydrogen index and low T_{max} values. In addition, depressed organic matter degradation is implied by $C_{organic}/N_{total}$ ratios that increase to ~40 as organic carbon concentrations increase. The C/N values that are elevated relative to algal organic matter and instead resemble those of land-derived organic matter are likely to result from retarded, selective alteration of the algal and microbial organic matter. A likely scenario is that nitrogen-rich components were degraded faster than other organic matter components during sinking of organic matter through a strongly developed oxygen minimum zone, thereby elevating the C/N ratio of the surviving organic matter.

PPC1-11: East-West comparison of nitrogen and carbon stable isotope systematics in same-age Mediterranean sapropels

P.A. Meyers¹, M. Arnaboldi², S.M. Bernasconi³

1) Marine Geology and Geochemistry Program, The University of Michigan, Ann Arbor, Michigan, U.S.A., 48109-1063

2) Marine Geology and Geochemistry Program, The University of Michigan, Ann Arbor, Michigan, U.S.A., 48109-1063

3) Geologisches Institut, Eidgenössische Technische Hochschule Zentrum, CH-8092 Zürich, Switzerland

The modern Mediterranean Sea is oligotrophic, yet its sediment record contains distinctive layers of organic-carbon-rich sapropels at 21 ky (precessional) spacing that imply past periods of elevated productivity that were equivalent to the high rates of modern upwelling systems. This apparent paradox may be resolved by lines of evidence suggesting that the mode of primary productivity changed from one dominated by algae to one dominated by photosynthetic bacteria during times of sapropel deposition. We have made a high-resolution comparison of the total nitrogen and organic carbon isotopic compositions of three sapropels and their background sediments in sequences that cover 1000 to 945 ka at two locations. ODP Site 967 is in the Levantine Basin of the eastern Mediterranean, whereas ODP Site 974 is in the Tyrrhenian Basin towards the west. Total $\delta^{15}\text{N}$ values systematically decrease at both locations from 5‰ to -1‰ as organic carbon mass accumulation rates increase. The decrease in nitrogen isotope values implies major contributions of nitrogen-fixing cyanobacteria to the total productivity. At Site 974, $\delta^{13}\text{C}$ values systematically increase from -25‰ to -22‰ and mirror the increase in marine productivity indicated by the increased organic carbon mass accumulation rates. In contrast, $\delta^{13}\text{C}$ values decrease in the sapropel layers at Site 967. The precessional minima with which sapropels coincide were times of wetter climate, which increased fluvial delivery of soil-derived phosphorus and diluted the surface Mediterranean Sea. Cyanobacteria function best under strongly stratified conditions when an amplified oxygen minimum zone extends into the photic zone, which also enhances recycling of phosphorus from detrital organic matter and thereby stimulates primary production. The east-west difference in response of the carbon isotope values to the increased organic matter production implies some combination of greater recycling of isotopically light organic matter and greater delivery of isotopically light continental carbon in the eastern parts than in the western parts of the Mediterranean Sea.

PC1-12: Isotopic biogeochemistry of lipids in recent sediments of Lake Planina, a remote mountain lake in NW SloveniaN. Ogrinc¹, G. Muri², I. Tolosa³

1) Dep. of Environmental Sciences, »J. Stefan« Institute, Jamova 39, 1000 Ljubljana, Slovenia

2) National Institute of Biology, Vecna pot 111, 1000 Ljubljana, Slovenia

3) IAEA – Marine Environmental Laboratory, 4, quai Antoine 1^{er}, Monte Carlo 98000, Monaco

The molecular distribution of lipids provides particularly useful information about the sources, diagenetic alteration, preservation and historical changes in organic matter. Isotopic composition on lipid biomarkers contains also important source information that can be used for understanding the carbon flow in complex ecosystems. Lipid biomarkers were analysed in sediments from Lake Planina, a remote mountain lake in NW Slovenia and the isotopic composition of aliphatic hydrocarbons, aliphatic alcohols and sterols are presented. Sterols were the most abundant lipids in the surface sediment layer and exhibited $\delta^{13}\text{C}$ values ranging from -40.5 to -44.4‰. These values indicated a freshwater planktonic source of the organic matter. It was noteworthy that the $\text{C}_{29}\Delta^5$ sterol (24-ethylcholest-5-en-3 β -ol) which has been commonly associated with terrestrial sources showed $\delta^{13}\text{C}$ values similar to the other planktonic sterols confirming their autochthonous component.

A bimodal distribution of *n*-alkanes maximizing at *n*-C₁₇ and *n*-C₂₉ was observed in the surface sediment layer. The isotopic composition of *n*-C₁₇ was -45.0‰ evidencing its origin from phytoplankton. The longer chain *n*-alkanes, *n*-C₂₅ to *n*-C₃₃, showed $\delta^{13}\text{C}$ values between -34.0 and -37.0‰ confirming their terrestrial origin. Similar to the *n*-alkanes, the longer chain *n*-alcohols exhibited $\delta^{13}\text{C}$ between -35.0 and -36.0‰, indicative of terrestrial sources. Diploptene, which is an unsaturated terpene, was also identified in the sediments and their isotopic composition of -67.5‰ inferred a methanotrophic bacterial source. These results point out that the combination of biomarker distributions and isotope measurements can enhance our ability to trace the inputs of organic material and help to clarify origins of allochthonous vs autochthonous sources.

**PPC1-13: Palaeoenvironmental changes in Padul basin (Granada, Spain)
over the last 235 ka b.p. based on *n*-Alkanes**

J.E. Ortiz¹, T. Torres¹, A. Delgado², M. Lucini³, J.F. Llamas¹, M. Valle⁴

1) L.E.B., E.T.S.I. Minas. Madrid, Spain (e-mail: jeortiz@dinge.upm.es)

2) Estación Experimental El Zaidín (C.S.I.C.). Granada, Spain

3) IZASA, S.A. Alcobendas, Spain

4) Facultad de Ciencias, Universidad de Salamanca, Spain

Padul Basin which is located in the southern part of Spain, has one of the best available records of Pleistocene sediments, with more than 100 metres thick, ranging from 1 Ma to 4.5 ka B.P. Previous papers based on its stratigraphy and palynology have been published ([1], [2], [3]) or biomarkers ([4]). In 1997, a new 107 m-deep borehole was drilled. Recently, two markedly different hydrogeological scenarios were observed in the Padul Basin ([5]) from the concentration of the organic carbon, the atomic H/C and C/N ratios, the $\delta^{13}\text{C}$ and CPI values: 1) from *ca.* 1 Ma B.P. (metre 107) to *ca.* 400 ka B.P. (metre 60), lacustrine conditions prevailed; and 2) from *ca.* 400 to 4.5 ka B.P., the Padul Basin became a peat bog. However, the global climatic changes occurring from *ca.* 170 to 25 ka B.P. (from metre 33.6 to 7) did not strongly affect these proxies, whose values vary little.

Nevertheless, the relative percentages of C₂₇, C₂₉ and C₃₁ *n*-alkanes do show important variations in the upper 40 m (last 235 ka B.P.), which are interpreted in terms of palaeoenvironmental changes. In fact, according to [6] and our own data, grasses and herbs have high concentrations of the C₃₁ *n*-alkane, while deciduous trees assemblages are dominated by the *n*-C₂₇-alkane. Four different palaeoenvironmental scenarios have been interpreted: cold-humid, cold-dry, warm-dry, and transitional phases (more humid). The 5th and 7th OIS are considered as warm and dry regimes in Padul Basin, while during the even OIS more humid conditions prevailed, except the time span from 30 to 15 ka B.P., which is interpreted as a cold and arid phase.

Percentage (%)

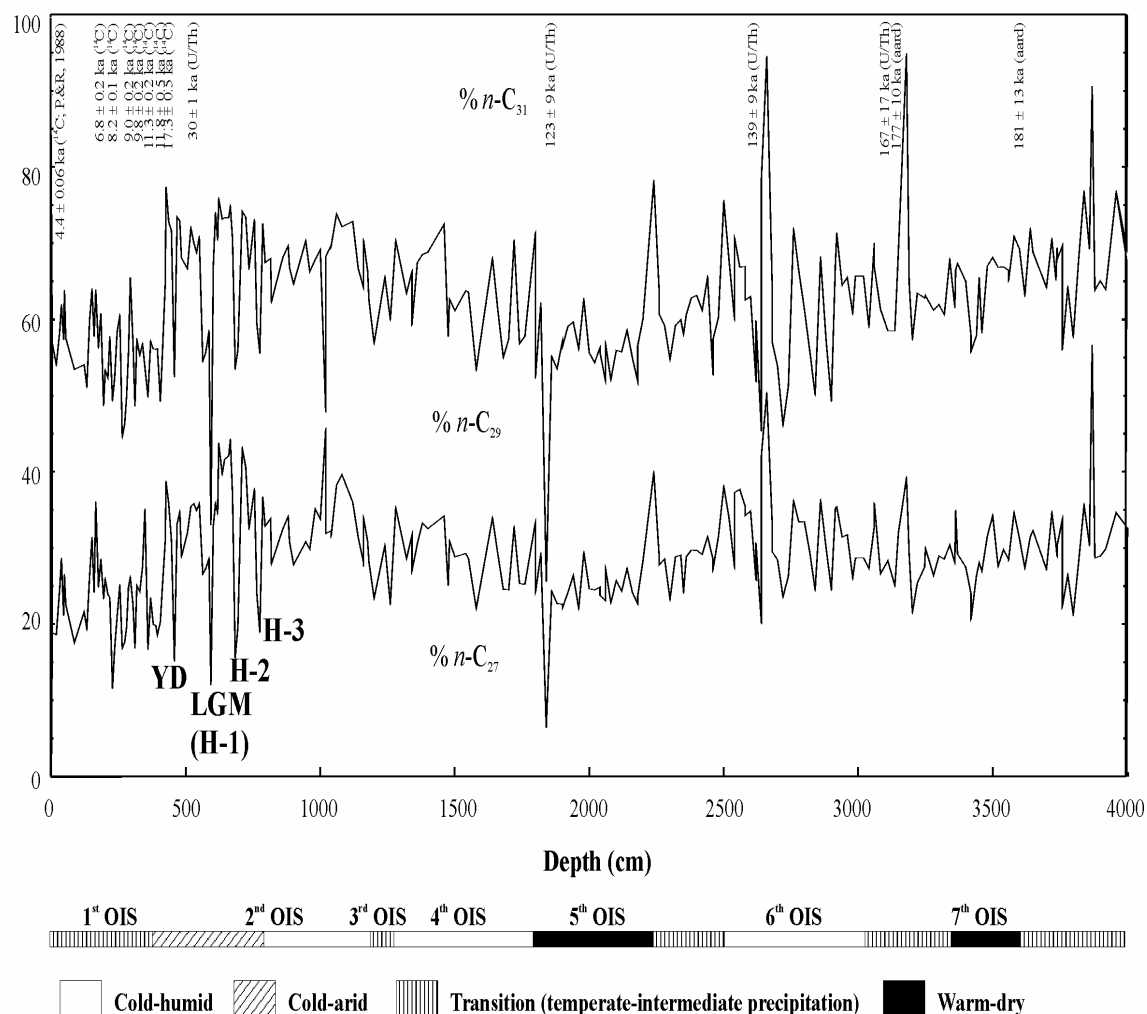


Fig.1. Percentages of C_{27} , C_{29} , and C_{31} isomers respect to the sum $C_{27} + C_{29} + C_{31}$ along the upper 40 metres of Padul borehole with the palaeoenvironmental interpretation

References

- [1] Menéndez Amor, J., Florschütz, F., 1964. Results of the preliminary palynological investigation of samples from a 50 m boring in southern Spain. *Bol. Real Soc. Esp. Hist. Nat. (Geol.)* 62: 251-255.
- [2] Florschütz, F., Menéndez Amor, J., Wijmstra, T.A., 1971. Palynology of a thick Quaternary succession in southern Spain. *Palaeogeogr., Palaeoclimatol., Palaeoecol.* 10, 233-264.
- [3] Pons, A., Reille, M., 1988. The Holocene and upper Pleistocene pollen record from Padul (Granada, Spain): a new study. *Palaeogeogr., Palaeoclimatol., Palaeoecol.* 66, 243-263.
- [4] del Río, J.C., González-Vila, F.J., Martín, F., 1992. Variation in the content and distribution of biomarkers in two closely situated peat and lignite deposits. *Organic Geochem.* 18(1), 67-78
- [5] Ortiz, J.E., Torres, T., Delgado, A., Julià, R., Lucini, M., Llamas, J.F., Reyes, E., Soler, V., Valle, M., 2005. The palaeoenvironmental and palaeohydrological evolution of Padul Peat Bog (Granada, Spain) over one million years, from elemental, isotopic, and molecular organic geochemical proxies. *Org. Geochem.* 35 (11-12), 1243-1260.
- [6] Schwark, L., Zink, K., Lechterbeck, J., 2002. Reconstruction of postglacial to early Holocene vegetation history in terrestrial Central Europe via cuticular lipid biomarkers and pollen records from lake sediments. *Geology* 30(5), 463-466.

**PPC1-14: Palaeoenvironment of the Eocene Eckfeld Maar lake (Germany):
implications from geochemical analyses of the oil shale sequence**

M. Sabel¹, A. Bechtel², W. Püttmann³, S. Hoernes¹

1) Mineralogisch-Petrologisches Institut, Universität Bonn, Poppelsdorfer Schloss, D-53115 Bonn, Germany

2) Angewandte Geowissenschaften und Geophysik, Prospektion und Angewandte Sedimentologie, Montanuniversität Leoben, Peter-Tunner-Str. 5, A-8700 Leoben, Austria
(e-mail: Achim.Bechtel@notes.unileoben.ac.at)

3) Institut für Mineralogie – Umweltanalytik, J. W. Goethe-Universität, Georg-Voigt-Str. 14, 60054 Frankfurt a.M., Germany

Drill core samples (depth interval between 19.4 and 32.0 m) of the laminated central lake facies of the Eocene Eckfeld Maar were investigated for biomarker and stable isotope composition. Bulk organic geochemical parameters (C/N, HI) and the molecular composition of the soluble organic matter indicate the dominance of particulate organic matter from land plants and microbial-derived lipids in the lower part of the sedimentary succession. An angiosperm-dominated vegetation is indicated based on the terpenoid biomarker composition. Enhanced Hydrogen Indices (HI) are at least partly caused by the supply of waxy, terrigenous organic matter (e.g. leaf waxes, resins, bark) to the lake, as indicated by a positive relationship between HI values and the sum of oleanane, ursane and lupane type triterpenoid concentrations. Slightly decreasing C/N ratios towards the top of the profile are interpreted as being the result of an increasing contribution of biomass from algae and microorganisms. Abundant 4-methylsteroids in the 25.6 to 30.8 m section of the oil shale sequence reflect the contribution of algal-derived biomass. Samples with high concentrations of methylsteroids are characterized by low amounts of triterpenoids related to the arborane skeleton, and *vice versa*. This pattern is interpreted as reflecting differences in autochthonous organic matter production versus microbial activity.

The observed depletion in ¹³C of the total organic matter of the sediments ($\delta^{13}\text{C}$ from –27.5 to –31.4 ‰), in comparison with the fossil wood (average $\delta^{13}\text{C}$ values of –24.9 ‰), is explained by the dominance of waxy, lipid-rich land plant material (e.g. leaf waxes, resins, bark) over wood in the terrigenous organic matter supplied to the lake. No systematic differences in $\delta^{13}\text{C}$ corresponding to different ratios of terrestrial, microbial, and algal organic matter, estimated on the basis of biomarker analyses of the total extracts, are obtained. The overall trend of the isotopic composition of organic carbon towards heavier values from depths around 26 m to the top of the sequence is consistent with generally decreasing C/N ratios in this depth range, indicating increasing autochthonous organic matter production. Carbon cycling during anoxic decomposition of organic matter is assumed to further affect

the $\delta^{13}\text{C}$ values of the sediments through the activity of anaerobic (e.g. methanogenic) bacteria, resulting in a depletion of the biomass in ^{13}C .

The isotopically heavy $\delta^{13}\text{C}$ values of siderite argue for the activity of methanogenic bacteria. The trend towards heavier $\delta^{18}\text{O}$ and $\delta^{13}\text{C}$ values of siderites in the lowest part of the profile, indicates an increasing extent of methanogenesis due to the evolution of meromictic conditions in the water column. The lighter $\delta^{18}\text{O}$ values of siderites from turbiditic layers are explained by temporary phases of increased precipitation, followed by landslides and an improved water circulation within the lake.

A high-productivity ecosystem with intense microbial activity under meromictic conditions in the Maar is indicated by the geochemistry of the oil shale succession. The results are consistent with paleontological data from the Eckfeld Maar, the Messel oil shale, and coal seams from the Geiseltal area, documenting a highly diverse terrestrial flora and fauna indicating a warm and humid climate during middle Eocene in central Germany.

PPC1-15: Paleoclimatic variations recorded by biomarkers of higher plant wax and terpenoid in the deep sea sediments of Northwestern Pacific off Central Japan

K. Sawada

Division of Earth and Planetary Sciences, Graduate School of Science, Hokkaido University, N10W8, Kita-ku, Sapporo 060-0810, Japan (e-mail: sawadak@ep.sci.hokudai.ac.jp)

Distributions and carbon isotope compositions ($\delta^{13}\text{C}$) of biomarkers derived from terrestrial higher plant wax and higher plant terpenoids (HPTs) were investigated in surface sediments and sediment cores of northwestern Pacific off central Japan. The objectives of this study are to evaluate the atmospheric transport of materials from land to ocean by mass accumulation rates (MARs) of the biomarkers and to reconstruct the millennial-scale variations of terrestrial climate by $\delta^{13}\text{C}$ of the biomarkers, in Japan Islands and eastern Asian areas of Eurasian Continent.

Surface sediments collected from Nishishichitou Ridge across a latitudinal transect at 138°35'E (LM-5P: 32°40'N, LM-4: 30°23'N, and LM-3: 29°45'N) were analyzed. Also, piston cores collected from the same sites (KT92-17 St. 14: 32°40'N and St. 20: 30°23'N; [1]) were used. Lipids were extracted and separated to acidic and neutral fractions. The neutral fractions were further fractionated to aliphatic and aromatic hydrocarbons, ketones and polar lipids as alcohols. HPTs were identified by GC/MS and quantified by GC/FID. $\delta^{13}\text{C}$ values of biomarkers were determined by GC-C/IRMS.

Long-chain ($\text{C}_{25} - \text{C}_{31}$) *n*-alkanes were commonly contained with strong odd carbon number predominance in all surface sediments. This result showed a significant terrestrial input as plant wax material in deep sea sediments of Nishishichitou Ridge. The HPTs derived from angiosperm could be identified, while no gymnospermous ones as a previous report [2]. Oleanoidal ketones as friedelin were mainly identified in all surface sediments. In sediment core samples, terpenoidal hydrocarbons as oleanenes, oleandienes and ursenes were detected. In general, the oleanenes and ursenes were formed from biological terpenoids by post-depositional diagenesis. Therefore, the detection of such HPT hydrocarbons indicated that the terrigenous materials which had been experienced significant diagenesis and attached to soils were transported from land, especially Chinese area of Eurasian Continent, to ocean through aeolian systems. $\delta^{13}\text{C}$ values of C_{29} and C_{31} *n*-alkanes were consistent with -30.5 to -30‰ and -31 to -30.5‰ in all surface sediments, respectively. These values were similar to those in surface sediment of Japan Sea (KH79-3 L-3) [3]. However, $\delta^{13}\text{C}$ values of friedelin varied between -32‰ (LM-5P) and -27‰ (LM-3) in surface sediments, which disagreed with those

of wax alkanes. The friedelin might be biological compound and mainly originated from tree bark [4], so that the differences of $\delta^{13}\text{C}$ values reflect the source organisms and/or source areas, and transport system of compounds.

MARs of long-chain *n*-alkanes and HPT in St. 14 and St. 20 tended to increase during the glacial period (oxygen isotope stage 2). Thus, the terrigenous materials might be efficiently supplied to the northwestern Pacific with aeolian transport during the glacial period. $\delta^{13}\text{C}$ values of long-chain *n*-alkanes (C_{29} and C_{31}) and friedelin were higher in glacial period than those of the present. According to Hanba and Wada [5], the carbon isotopic fractionation of organic matter in higher plant varied critically depending on climatic conditions as aridity and solar radiation. From the insight, it was speculated that the higher $\delta^{13}\text{C}$ values of the plant biomarkers might reflect the arid conditions in terrestrial areas of eastern Asia, especially Chinese continental area, during glacial period.

References

- [1] Sawada, K. and Handa, N., 1998. Variability of the path of the Kuroshio ocean current over the past 25,000 years. *Nature* 392, 592-595.
- [2] Sawada, K. 2003. Eolian transport of higher plant terpenoids (HPTs) in the northwestern Pacific off central Japan. *Geochimica et Cosmochimica Acta* 67/18S, A419.
- [3] Yamada, K. and Ishiwatari, R., 1999. Carbon isotope compositions of long-chain *n*-alkanes in the Japan Sea sediments: implications for paleoenvironmental changes over the past 85 kyr. *Organic Geochemistry* 30, 367-377.
- [4] Hanisch, S., Ariztegui, D. and Püttmann, W., 2003. The biomarker record of Lake Albano, central Italy-implications for Holocene aquatic system response to environmental change. *Organic Geochemistry* 34, 1223-1235.
- [5] Hanba, Y. and Wada, E., 1995. Factors controlling carbon isotope ratio of plant. *Kaiyou Monthly* 27, 512-516 (in Japanese)

PPC1-16: Evaluation of past sources and sinks for CO₂ in the South Atlantic OceanS. Schulte¹, D. Brouwer¹, A. Benthien²

1) Institute of Chemistry and Biology of the Marine Environment, Carl von Ossietzky University of Oldenburg, P.O. Box 2503, D-26111 Oldenburg, Germany (e-mail: schulte@icbm.de)

2) Alfred-Wegener Institute for Polar and Marine Research, P.O.Box 120161, D-27515 Bremerhaven

Atmospheric CO₂ levels depend on the balance of CO₂ between the world's oceans and terrestrial ecosystem. To a first approximation, equatorial regions of the modern ocean are supersaturated in CO₂ with respect to the atmosphere while sub-polar regions approach air-sea equilibrium and polar regions are undersaturated. In order to recognize better the mechanisms controlling atmospheric and oceanic levels of CO₂ over geological time scales paleoceanic sinks and sources of CO₂ must be defined. This requires reliable paleo-indicators (proxies) for past CO₂ concentrations in the surface oceans.

Stoll and Schrag [1] suggested using the carbon isotopic composition of alkenones in combination with the Sr/Ca-ratio of coccolith carbonate as a reliable proxy for surface water CO₂ levels. The use of these parameters as paleoceanographic proxies in marine sediments requires a sediment-based calibration. Therefore we determined in a suite of core-top sediments from different oceanic regimes of the South Atlantic the $\delta^{13}\text{C}$ -value of the C_{37:2}-alkenone and the Sr/Ca-ratio in the size fraction <10 μm , respectively. Since the Sr/Ca-ratio is related to surface water phosphate concentration it is used to correct the isotopic fractionation (ϵ_p) of C₃₇-alkenones for the known influence of growth rate. The corrected ϵ_p -values are calibrated against the surface water carbon dioxide concentration ([CO₂(aq)]). Following this approach we determine CO₂(aq) levels for the South Atlantic during the last glacial maximum and the marine isotopic stage 5.5. We further evaluate the surface water carbon dioxide concentration in core GeoB1722 (11°W/29°S) during the last 140 kyr.

References

[1]Stoll, H.M. and Schrag, D.P., 2000. Coccolith Sr/Ca as a new indicator of coccolithophorid calcification and growth rate. *Geochemistry, Geophysics, Geosystems* 1 (5), doi:10.1029/1999GC000015.

PPC1-17: Orbital-derived lacustrine geochemical signatures and their application to the paleolimnology of perennial lake systems

S.C. Teerman¹, A.G. Fischer², A. Grippo²

1) ChevronTexaco, Houston, Texas 77002

2) Department of Earth Science, University of Southern California, Los Angeles, CA 90089

In the spectrum of lacustrine facies that occur within the Eocene Green River Formation, Wyoming (USA), the Tipton Scheggs and Rife Beds represent freshwater, overfilled and brackish/saline, balanced-fill lake systems, respectively. This lithologically homogenous interval of oil shale represents highly dynamic yet repetitive lake conditions as defined from sonic and gamma log patterns, Fischer assay oil-yields, and geochemical signatures. Time-series analysis of oil-yields from the paleogeographic lake center of the Tipton Member defines Milankovitch cyclicality, which includes the eccentricity, precession, and obliquity cycles. This continuous, well-defined cyclicality documents that in addition to tectonic modification and regional paleoclimatic variations, the limnology of paleo-lake Gosiute was controlled by orbital-driven changes in insolation.

Tipton precessional cycles are 6-9 feet thick and consist of an organic-rich base with a reduced but variable organic content in the remainder of the cycle. The cycle base contains an algal-dominated, aliphatic-rich kerogen that is sometimes depleted in $\delta^{13}\text{C}$. The $\delta^{13}\text{C}$ of the matrix carbonate in the basal part of some cycles, is enriched ($> +4.0\%$) compared to the remainder of the cycle. In contrast, differences in the kerogen and bitumen in the middle and upper parts of these cycles reflect a greater proportion of bacterial input and subtle increase in degradation. Extracts display a decrease in the sterane/hopane, $\text{C}_{29}/\text{C}_{27}$ steranes, and gammacerane/ C_{30} hopane ratios along with other molecular changes. A positive correlation exists between extracts with a large $\Delta^{13}\text{C}$ [aromatic-saturate] and hopane abundance indicating an increased methanotrophic input into the soluble biomass in some cycles. These changes between the base, and the middle and upper parts of the cycle are consistent with a shift in the maceral composition from an algal-derived lamalginite-dominated kerogen to a mixed bituminite and lamalginite. Geochemical variations in the kerogen and bitumen throughout individual precessional cycles are independent of their narrow range of thermal maturity, and thus document environmental-driven changes, which are correlated to the Milankovitch cyclicality.

These precessional cycles record a perennial, two-stage cyclical lake with repetitive trends in net moisture availability. The cycle base was deposited during the "rainy" precessional phase when an expanded, nutrient-rich lake enhanced productivity and elevated

stratification. During the “dry” precessional phase, less inflow resulted in lower lake levels, and a reduced eutrophication, and stratification. Besides a decline in productivity, the amount and types of eukaryotic and prokaryotic precursors also changed. The orbital-derived climatic signal dictated lacustrine conditions that continuously imprinted these sediments. Yet, the evolving Tipton lake systems simultaneously modified, magnified or suppressed lacustrine processes, resulting in different cyclical expressions. The magnified geochemical expression of Rife cycles compared to the Scheggs results from the larger precessional fluctuation in the size and water column conditions of the balanced-fill lake, which optimized changes in productivity, precursors and preservation. The sensitive response of these lakes to environmental change provides geochemical signatures that help reconstruct the changing limnology, and define mechanisms by which orbital signals were transferred through different lake systems into the sedimentary record.

PPC1-18: The Cretaceous oceanic anoxic event 1b as revealed by cm-scale TEX₈₆-based SST and isotope records from the Eastern subtropical Atlantic (Mazagan Plateau off NW-Africa, DSDP 545)

T. Wagner¹, I. Stüsser³, S. Schouten², J. Sinninghe Damsté², J. Herrle⁴, P. Hofmann³

1) University Bremen, Geosciences, Bremen, Germany and University of Newcastle, School of Civil Engineering and Geosciences, Newcastle, UK

2) Royal Netherlands Institute for Sea Research, Den Burg, Texel, The Netherlands

3) University of Cologne, Geological Institute, Cologne, Germany

4) Southampton Oceanography Centre, School of Ocean & Earth Science, Southampton, UK

Oceanic anoxic events (OAEs) represent extraordinary and short-lived modes of the atmosphere-ocean when massive burial of marine organic carbon was accompanied by major perturbations in the global carbon budget and ocean chemistry. Controls and feedbacks discussed for OAEs range from global-scale submarine volcanic activity, paleogeographic configuration and ocean circulation to regional/local-scale hydrological and nutrient cycling, ocean productivity, microbial and plankton biomass communities, and ocean water chemistry. The OAE 1b is thought to be a regional phase of carbon burial that was mainly restricted to the North Atlantic and Western Tethys. The development of the OAE 1b also differs from the other OAEs of the Cretaceous with respect to mechanisms that determined water column stability and the organism groups adapted to these conditions.

We present a first continuous TEX₈₆-based SST record (Schouten et al., 2002) that covers the late Albian OAE 1b at Mazagan Plateau DSDP Site 545, eastern subtropical Atlantic at cm- (millennial-) scale. The TEX₈₆-SST record principally follows the concentration of total organic carbon (TOC) with regular modulations on the order of 2°C below the OAE, a rapid ~3.5 °C increase at the base of the event, high temperatures exceeding 32°C across the event, and a progressive but highly variable return to almost pre-OAE levels at the top of the section. The aliphatic fractions of the sediment extracts contain abundant *n*-alkanes from higher plant waxes, C₂₇-C₂₉ delta4 and delta5 sterenes and sterolethers from eukaryotic organisms, C₃₀-C₃₂ hopenes from prokaryotes, and minor amounts of 2,6,10,15,19-pentamethylcosane and lycopane. This suggests that the TOC is very immature and of dominant marine origin with a substantial contribution of terrestrial OM. Relative proportions of the biomarkers are fairly constant over the study section

The overall modulation in SST and TOC probably documents fluctuations in upwelling intensity as controlled by eccentricity forcing (Herrle et al., 2003). Notably, surface waters started to heat up a few thousand years before (equivalent to ~5 cm below) the initial TOC enrichment indicating that SST and OAE1b black shale deposition were partly

decoupled. To identify interactions with the global carbon budget and discuss possible cause-effect relationships between the atmosphere and the ocean, we compare the TEX₈₆-based SST record with stable carbon isotope profiles from both compound-specific marine and terrestrial compounds and bulk carbonate/organic carbon. The sudden increase in SST is paralleled by an abrupt ~2‰ negative shift in ¹³C of long-chain, terrestrial n-alkanes, supporting the conclusion that atmospheric and surface ocean properties pre-dated the onset of enhanced carbon burial by a few thousand years. The onset of enhanced carbon burial is accompanied by a distinct ~1.5‰ negative shift in bulk organic and inorganic carbon isotopes. The pattern in SST, compound-specific isotopes, and bulk isotopes resemble features and time relationships that suggest a short-term and massive injection of isotopically light carbon into the early Albian climate system. One plausible mechanism to explain the geochemical records at Mazagan Plateau is release of methane from marine gas hydrates, comparable to the succession of events associated with Paleocene Thermal Maximum.

References

- Herrle, J.O., Pross, J., Friedrich, O., Köbller, P., Hemleben, C., (2003) Forcing mechanisms for mid-Cretaceous black shale formation: evidence from the Upper Aptian and Lower Albian of the Vocontian Basin (SE France). *Palaeogeography, Palaeoclimatology, Palaeoecology*, 190, 399-426.
- Schouten, S., Hopmans, E.C., Schefuß, E., Damste, J.S.S., (2002) Distributional variations in marine crenarchaeotal membrane lipids: a new tool for reconstructing ancient sea water temperatures? *Earth and Planetary Science Letters*, 204, 265-274.

PPC1-19: Reconstruction of terrestrial organic matter input in marine sediments off the coast of Western Africa

J.W.H. Weijers¹, S. Schouten¹, E.C. Hopmans¹, E. Schefuß²,
T. Wagner³, J.S. Sinninghe-Damsté¹

1) Royal Netherlands Institute for Sea Research (NIOZ), PO Box 59, 1797 AB Den Burg – Texel, the Netherlands (e-mail: jweijers@nioz.nl);

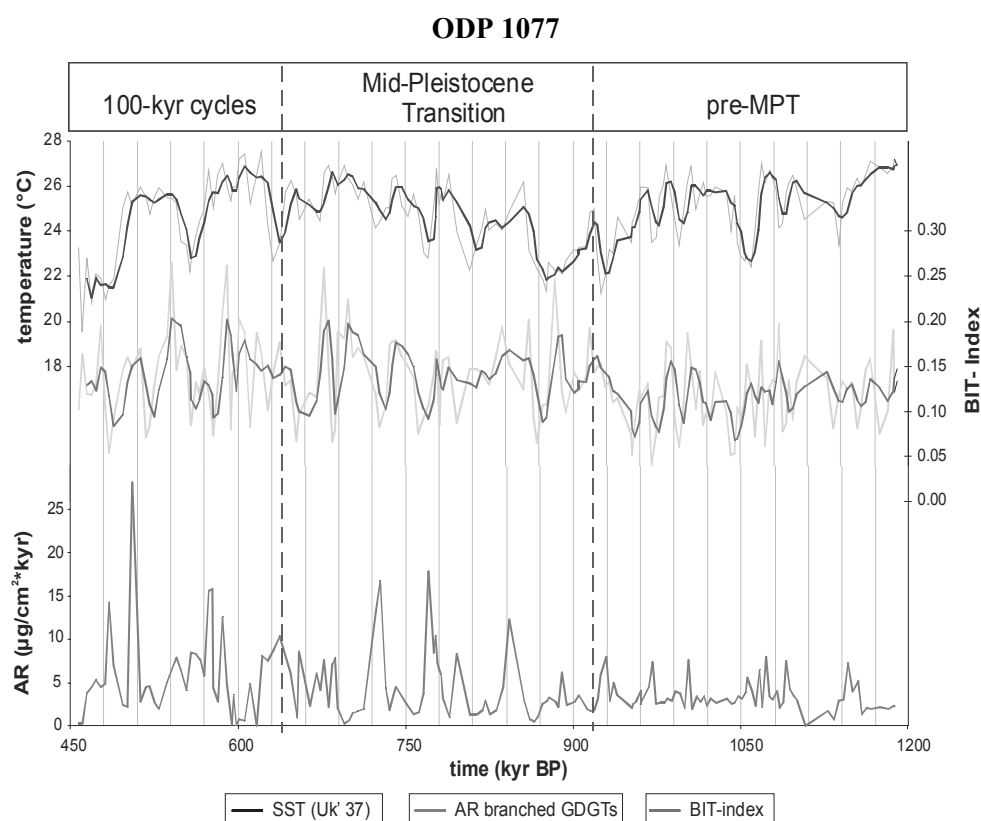
2) Woods Hole Oceanographic Institution, USA; ³University of Newcastle, UK

Branched glycerol dialkyl glycerol tetraethers (GDGTs) constitute the core membrane lipids of as yet unknown anaerobic Bacteria and are abundantly present in peat bogs and to a lesser extent in soils. They are fluvially transported to the marine environment where they are, amongst others, found together with crenarchaeol, the isoprenoid core membrane tetraether lipid of the ubiquitous pelagic Crenarchaeota. The Branched versus Isoprenoid Tetraether (BIT) index quantifies the amount of branched tetraethers present, relative to this marine derived crenarchaeol (Hopmans et al., 2004). The BIT-index acts as a semi-quantitative proxy for the input of Terrestrial Organic Matter (TOM) into the marine environment. Indices vary between 0 and 1, where indices near 0 are indicative for a relative low input of TOM (e.g. open marine) and values near 1 are indicative for a relatively high TOM input. Determining the BIT-index in marine cores can provide information about changes in the input of TOM from the adjacent continent into the marine environment relative to marine organic matter production over different time scales. Moreover, together with estimates of the accumulation rates of the branched GDGTs over time, the BIT-index can give insights into the different climate parameters controlling the fluvial input of TOM into the marine environment.

BIT-indices were determined in a core (ODP 1077) from the Congo river fan, off the coast of western Africa, over the time span 450-1200 ka BP, which covers the Mid-Pleistocene Transition (MPT) (see figure). The MPT is characterised by a change from obliquity to eccentricity dominated changes in polar ice volume. Although BIT-indices do show substantial variability over this time range (values between 0.05 and 0.25), they do not reflect the predominant Milankovitch cycles present around this MPT, which are visible in the Uk'37 sea surface temperature (SST) record. Frequency analysis reveals a significant cycle of about 71 ka, which cannot be assigned to any known astronomical cyclic variation. Accumulation rates of the branched GDGTs do not fluctuate much in the oldest part of the record (1 to 6 $\mu\text{g cm}^{-2} \text{ kyr}^{-1}$), whereas in the younger part large fluctuations are observed (up to 25 $\mu\text{g cm}^{-2} \text{ kyr}^{-1}$), suggesting large changes in the discharge of the Congo River and/or changes in the rate of release of the branched GDGTs stored in wetlands and soils. Some of

the peaks in branched GDGT accumulation rates seem to occur just after large drops in SST. A possible explanation is the lower atmospheric moisture content during lower SSTs, giving rise to dryer conditions on the adjacent continent accompanied with a lowered vegetation density, which results in a decreased soil stability and a higher rate of soil erosion. As soon as moisture content increased again with increasing SSTs, precipitation and river discharges will have increased, resulting in a higher flux of TOM to the ocean.

Results of analyses of two other deep sea cores off the coast of western Africa will also be presented: GeoB-6518 near the mouth of the Congo River, covering the time span 0-20 ka BP and GeoB-4901 near the mouth of the Niger River, covering the time span 0-250 ka BP. Results of frequency analyses will be presented to see to which extent orbital Milankovitch parameters could be detected in the records. Comparisons will be made with other proxies, like SST, and will be discussed in terms of climate parameters controlling the input of branched GDGTs and the flux of TOM into the marine environment over different time scales.



References

- Hopmans, E.C., Weijers, J.W.H., Schefuß, E., Herfort, L., Sinninghe Damste, J.S., Schouten, S., 2004. A novel proxy for terrestrial organic matter in sediments based on branched and isoprenoid tetraether lipids. *Earth and Planetary Science Letters* 224, 107-116.

PPC1-20: Organic geochemical analysis of deep sea sediments from the African continental margin (ODP LEG 175, Holes 1075A, 1079A and 1082A)

C. Wenzel, U. Güntner, S. Gebhardt, J. Rullkötter

Institute for Chemistry and Biology of the Marine Environment (ICBM), Carl von Ossietzky University of Oldenburg, P. O. Box 2503, D-26111 Oldenburg, Germany (e-mail: C.Wenzel@icbm.de)

Organic matter in deep sea sediments samples from three ODP sites (Ocean Drilling Program Leg 175) that form a North-South transect, was investigated to reconstruct the palaeoclimatic and palaeoceanographic conditions on the African continental margin.

Two main areas can be distinguished, which are separated by the Angola-Benguela Front (ABF). A persistent shallow thermocline (at 25 m) occurs north of the ABF, whereas surface waters are much less stratified south of the front [1]. The environmental conditions differ considerably on both sides of the front. Alkenone-derived palaeo-sea surface temperatures (calculated from the $U^{k'}_{37}$ index; [2]) are about 5°C lower south of the ABF in the Namibian permanent upwelling area.

A high downward flux of organic matter under areas of high productivity led to total organic carbon contents (TOC) up to 5% in the investigated sediment samples. Lipids characteristic of marine biota (e.g. alkenones and sterols) are abundant in the extracts, and the bulk organic matter (-18.9 to -23.5‰ V-PDB) and molecular stable carbon isotopic composition are also typical of material of marine origin.

In addition to the principally marine organic matter, the sediments at ODP Site 1075 in the lower Congo Basin contain considerable amounts of terrigenous lipids (e.g. taraxerol, long-chain *n*-alkanes and *n*-alkanols). The terrestrial supply in the northern Congo Fan is predominantly driven by the Congo River discharge. The samples from ODP Site 1079 on the Angola margin contain intermediate amounts of terrigenous lipids. A direct supply of river-transported terrigenous material is unlikely because of the absence of rivers draining into this area. The average contents of *n*-alkanes and *n*-alcohols in sediments at ODP Site 1082 in the Walvis Basin are low, and taraxerol is absent. The terrigenous lipids at this locations are predominantly wind-derived, a fluvial transport of terrestrial material can be neglected. Pentacyclic triterpenoids (e.g. taraxerol and β -amyrin) were only detected in sediments from sites north of the ABF. This is in agreement with the present restriction of mangrove swamps to humid, tropical environments north of the ABF and supports the hypothesis of fluvial rather than atmospheric transport of mangrove lipids [3]. The ABF in the North limits southward transport of terrigenous lipids.

At the northern sites (1075 and 1079), elevated concentrations of marine biomarkers (e.g. sterols) together with high TOC contents and a heavier stable carbon isotopic composition of the organic matter during glacial intervals indicate an increased marine productivity during those periods. Besides that high amounts of long-chain *n*-alkanes and *n*-alkanols point to an enhanced terrigenous supply of organic matter during cold, arid stages. In samples from ODP Site 1082A the organic carbon content as a function of depth closely follows the accumulation profiles of marine and terrigenous biomarkers. At the southern location, the lipid compositions indicate that the marine productivity may have fluctuated over time at a relatively high level due to changes in the upwelling intensity in the southeastern Atlantic Ocean. The fluctuations are not related to the glacial-interglacial cycles which exhibit increased productivity during glacials at the northern locations. The different lipid biomarker accumulation patterns and the variation in productivity at the investigated three sites along the southwestern African margin are generated in different ways, reflecting different oceanographic settings (off the Congo, near the Angola Dome and in the upwelling cell north of the Walvis Ridge).

References

- [1] Shannon L.V., Agenbag, J.J., Buys, M.E.L., 1987. Large and mesoscale feature of the Angola–Benguela front. *South African Journal of Marine Science* 5, 11-34.
- [2] Prahl, F.G., Muehlhausen, L.A., Zahnle, D.L., 1988. Further evaluation of long-chain alkenones as indicators of paleoceanographic conditions. *Geochimica et Cosmochimica Acta* 52, 2303-2310.
- [3] Schefuß, E., Versteegh, G.J.M., Jansen, J.H.F., Sinninghe Damsté, J.S., 2001. Marine and terrigenous lipids in South-East Atlantic sediments (Leg 175) as paleoenvironmental indicators: initial results. In: Wefer, G., Berger, W.H., Richter, C. (Eds.), *Proceedings of the Ocean Drilling Program, Scientific Results*, 175. Ocean Drilling Program, College Station, TX, 1-26 [CD-Rom].

PPC1-21: An integrated molecular and isotopic approach to assess historical changes in organic carbon sources and preservation in the Arctic Ocean

L.L. Belicka, H.R. Harvey

Chesapeake Biological Laboratory, University of Maryland Center for Environmental Science, 1 Williams Street, Solomons, Maryland, 20688, U.S.A.

In the modern Arctic Ocean, terrestrial carbon input from large rivers is estimated at 12 Mt/yr of POC. This is in addition to the 250 Mt/yr POC produced through marine photosynthesis. Although the marine carbon signal greatly exceeds that of terrestrial carbon, the utilization and preservation of each pool must be understood to define carbon cycling in the Arctic. Recent evidence suggests that marine carbon is quickly remineralized, while significant fractions of terrestrial carbon are preserved, especially in the central Arctic basin (Belicka et al., 2004; Stein and Macdonald, 2003). This project relies on an integrated approach to combine lipid biomarkers, carbon isotopic composition, and radiocarbon dating techniques to assess historical changes in the sources and preservation of organic carbon. The examination of multiple sites across the shelf boundary allows for us to estimate transport of organic carbon to the central Arctic basin and constrain the natural variability of carbon inputs over recent climatic changes.

A large suite of lipid biomarkers in particles and sediments from western Arctic shelves and basins were measured and combined with $\delta^{13}\text{C}$ composition and radiocarbon dating to evaluate historical changes in the sources and preservation of organic carbon and its exchange between shelf and basin environments. Offshore particles from the chlorophyll maximum contained abundant algal markers (e.g. 20:5 and 22:6 FAMES), low concentrations of terrestrial markers (amyrins and 24-ethylcholest-5-en-3 β -ol), and reflected modern ^{14}C values. In deeper waters in the halocline, particles also contained predominantly algal biomarkers, but ranged in age from 300-400 years indicating the presence of an older, recalcitrant carbon pool accompanying the sinking of the spring bloom. Basin sediments averaged 6000-9000 years old and contained low concentrations of algal biomarkers, suggesting that the high concentrations of marine carbon found in shelf and slope sediments is not transported offshore in substantial amounts. The fact that concentrations of a suite of terrestrial biomarkers in sediments showed little downcore variation and the fraction of terrestrial carbon increased in surface sediments offshore suggest that marine production provides the fuel for carbon cycling while more recalcitrant terrigenous carbon is slowly recycled and ultimately sequestered. The increasing fraction of terrestrial carbon with distance from land is opposite of that often observed in lower latitudes and reflects the

extensive ice coverage over much of the Arctic Ocean which limits primary production. Measurements of stable carbon isotopic composition, further radiocarbon dating, and analysis of redox reactive elements is currently underway to enhance biomarker evidence of the changes in historical carbon sources.

References

- Belicka, L.L., Macdonald, R.W., Yunker, M.B., and Harvey, H.R., 2004. The role of depositional regime on carbon transport and preservation in Arctic Ocean sediments. *Marine Chemistry* 86:65-88.
- Stein, R., and Macdonald, R.W., 2003. Organic carbon budget: Arctic Ocean versus global ocean. In: Stein, R., Macdonald, R.W. (Eds.), *The Organic Carbon Cycle in the Arctic Ocean* Springer-Verlag, Berlin, pp. 315-322.

PPC1-22: Lipid biomarkers in stalagmites as environmental proxies

A.J. Blyth¹, P. Farrimond¹, M.D. Jones¹, A. Baker²

1) School of Civil Engineering and Geosciences, Drummond Building, University of Newcastle upon Tyne, Newcastle Upon Tyne, NE1 7RU, United Kingdom (e-mail: A.J.Blyth@ncl.ac.uk)

2) School of Geography, Earth and Environmental Sciences, The University of Birmingham, Edgbaston, Birmingham, B15 2TT, United Kingdom.

Lipid biomarkers are widely recognised as useful proxies for environmental change, and are frequently used in studies of soil, peat and sediment cores. This work continues the development of novel biomarker time series, by investigating the biomarker signals present in stalagmites - layered cave deposits that are formed in mounds by the precipitation of CaCO₃ from drip waters. Stalagmites are particularly useful for constructing palaeoenvironmental time series as they form closed systems post-deposition, within which the proxies are trapped, and the relative stability of the cave environment means that the various records preserved in stalagmites are generally subject to less geochemical and taphonomic disturbance than those in sediments.

The work presented here focuses on the recovery of environmental information from the small concentrations of lipids extractable from stalagmites, in order to develop their use in palaeoclimatic records. A streamlined method for the routine analysis of lipids with minimal contamination is presented, together with results from suites of samples from two caves in Assynt, northwest Scotland. One cave (Lower Traligill) lies under uncultivated grassland, whilst the second (Uamh an Tartair) is overlain by peat deposits. Stalagmites, and overlying soil/peat were analysed from both caves. In addition, straw stalactites and cave sediments were analysed from Tartair. Lipid data from different layers within the stalagmites are compared with those from the other environmental deposits to identify the sources of the stalagmite biomarker signal.

Figure 1 shows example lipid biomarker chromatograms from an actively-growing stalagmite from Lower Traligill Cave. The lipids are dominated by *n*-fatty acids ranging from C₁₂ to C₃₂ with a clear even over odd predominance and a maximum at C₁₆ (0.158µg/g calcite). Significant concentrations of branched (*iso*- and *anteiso*-) C₁₆ and C₁₅ fatty acids demonstrate a marked bacterial input to the signal; from soil and/or cave microbes. The *n*-alcohols range from C₁₂ to C₃₀, with a strong even over odd predominance, and, as for the *n*-fatty acid distribution, a weakly bimodal plot, although with a maximum at C₁₈ (0.0046µg/g calcite) rather than C₁₆. In contrast, the *n*-alkane signal is dominated by long-chain compounds, ranging from C₂₃ to C₃₃, with a strong odd over even predominance and a

maximum at C₂₉ (0.0013 μg/g calcite), indicating an input from higher plants (presumably via soils). Two sterol compounds have also been identified in the sample; cholesterol (0.005 μg/g calcite) and a much weaker β-sitosterol signal (0.0008 μg/g calcite).

Our results show that excellent lipid data can be obtained from relatively small samples of stalagmite (5-50g, with the possibility of reducing sample size to <5g), and demonstrate the potential of the proxy for recording environmental and climatic change.

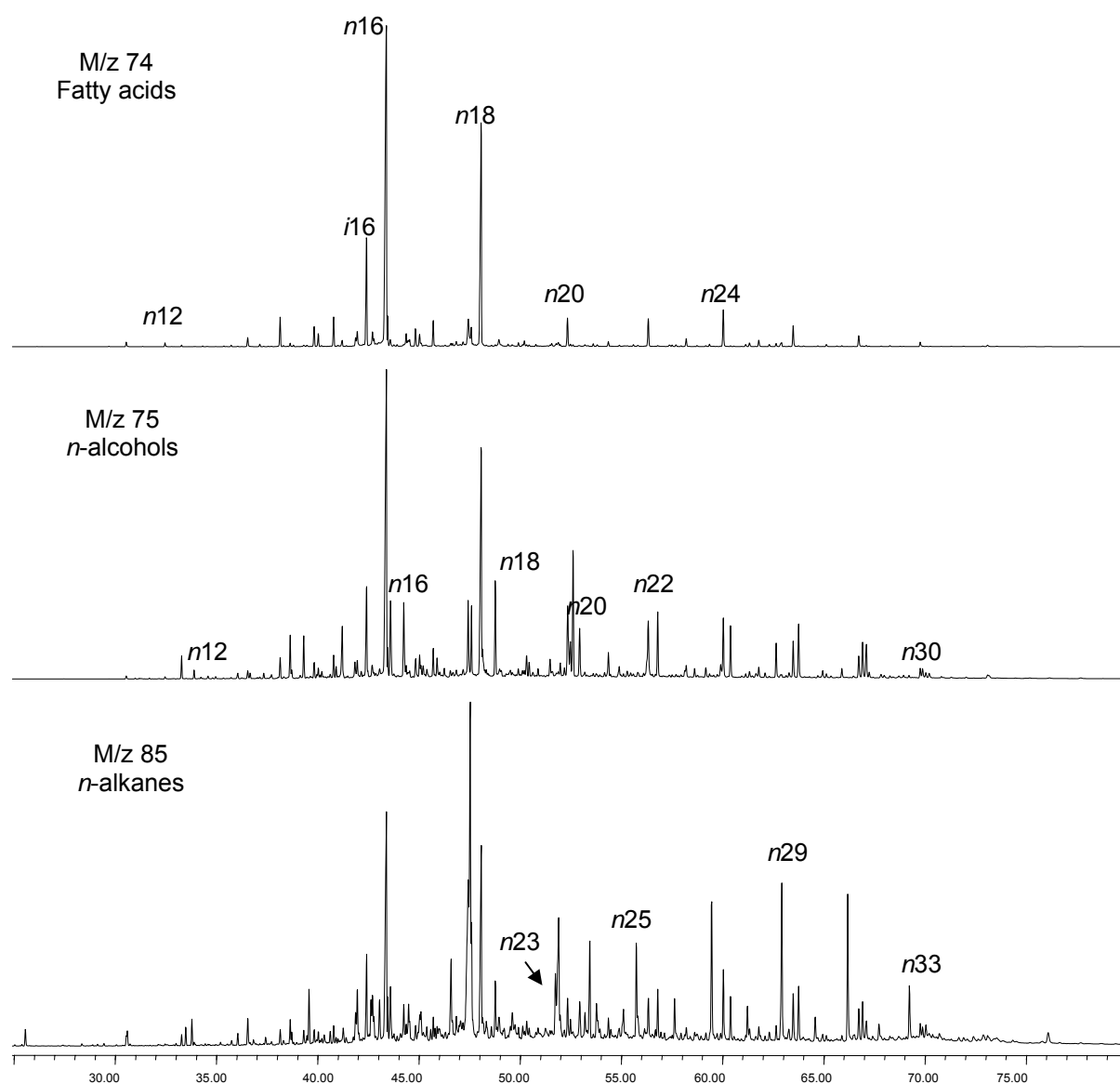


Fig.1. Selected ion chromatograms showing fatty acid, n-alcohol, and n-alkane distribution in an active Scottish stalagmite.

PPC1-23: Organic geochemical reconstruction of productivity cycles in the Benguela upwelling system during the final stages of the intensification of Northern hemisphere Glaciation

C.S. Boot¹, M.M. Maslin², R.D. Pancost¹

1) Organic Geochemistry Unit, Bristol Biogeochemistry Research Centre, School of Chemistry, University of Bristol, Bristol, UK (e-mail: C.S.Boot@bristol.ac.uk)

2) Environmental Change Research Centre, Department of Geography, University College London, London, UK

The productivity of major coastal upwelling systems has been demonstrated to increase during late Quaternary glacial periods, leading to the suggestion that these upwelling systems act as a CO₂ sink during glacial periods contributing to the lower atmospheric concentrations of CO₂. To examine further how this could have contributed to the development of the modern climate mode, we have examined the Intensification of Northern Hemisphere Glaciation (INHG), one of the most important climate events of the recent geological past and marking the transition into the system of intense and periodic glacial-interglacial cycles ca 2.5 my ago. Specifically, we examine changes in the photoautotroph populations and consequential sedimentary redox variations in the Benguela Upwelling system, one of the Earth's most productive regions, during the final stages of the INHG. Total organic carbon (TOC) contents and marine biomarker abundances indicate the onset of strong productivity cycles at the same time as the onset of high-amplitude glacial-interglacial cycles as indicated by U^K₃₇ derived sea surface temperatures and foraminiferal δ¹⁸O values. TOC cycles are not always in phase with changes in SST/δ¹⁸O values, with TOC contents maximising during glacial transitions and returning to interglacial levels for much of the glacial periods. Therefore the relationship between glacial/interglacial climate, upwelling and marine productivity in the Benguela system during the period studied seems different to that of the late Quaternary.

Biomarker assemblages in Benguela sediments are diverse, comprising compounds derived from higher plants (*n*-alkanes, *n*-alkanols, levoglucosan), phytoplankton (alkenones, dinostanol, alkyl diols, loliolide, hopanols) and microbes (biphytane diols, archaeol, non-isoprenoidal diethers). While all of these compound classes are present in all analysed sediments, there are significant variations in the biomarker assemblages among the three productivity maxima examined, suggesting a signal complicated by diagenetic influences and/or shifts in the photoautotroph assemblage. For example, the biomarker assemblage during the productivity maximum at 2.53 Ma is dominated by alkenones with little input from

other marine biomarkers, whereas during the maxima at 2.49 and 2.45 Ma there is also a large contribution from alkyl diols and biphytane diols.

These changes in the marine biomarker assemblage are associated with variations in the abundances of biomarkers originating from sedimentary organisms. Non-isoprenoidal glycerol diethers, thought to originate from sulphate-reducing bacteria, are highly abundant in some of the sediments analysed. Compound-specific carbon isotopic analysis of the non-isoprenoidal diethers indicates that the organisms producing these compounds are not primarily involved in methanotrophic processes. Therefore, they seem likely to have been produced by sulphate reducing bacteria carrying out sulphate reduction via the remineralisation of organic matter in near surface sediments. Similarly, relatively high $\delta^{13}\text{C}$ values suggest that archaeol in these sediments derives from methanogens rather than methanotrophs as observed elsewhere. Intriguingly, both archaeol and non-isoprenoidal diether abundances vary with the changing marine biomarker assemblage. This apparently reflects different redox conditions in the sediments in response to different productivity regimes.

In total, our data indicate that the transition to a climatic state characterized by intense glaciations was complex and involved not only an increase in primary productivity, but also reorganization of photoautotroph assemblages and changes in sedimentary redox conditions.

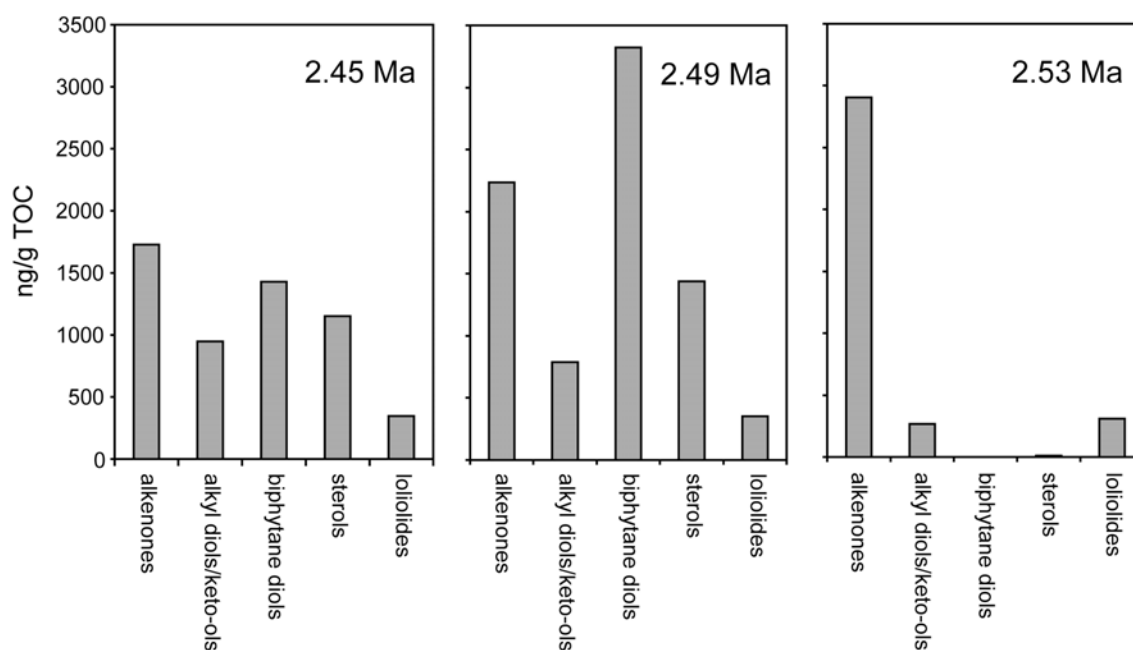


Fig.1. Abundances of various biomarker classes (normalised to TOC) during the three observed productivity maxima (at 2.53, 2.49 and 2.45 Ma), demonstrating the shifts in the marine biomarker assemblage.

PPC1-24: Simultaneous evolution of marine and terrestrial carbon isotope records in the Early Miocene

J. Briggs, D. Large, C. Snape, M. Cooper

School of Chemical, Environmental and Mining Engineering, University of Nottingham, University- Park, Nottingham NG7 2RD, UK

Peatland is an important terrestrial carbon reservoir that currently contains >25% of soil carbon. Both peat and its derivatives lignite and coal should have the potential to provide high resolution carbon isotope records and thereby help inform our understanding of this significant terrestrial component of the carbon cycle. To achieve this understanding it is essential that marine and terrestrial records can be correlated at high resolution. Here we present a high-resolution c.a. 1 m.y. $\delta^{13}\text{C}$ record from the Morwell 1B seam, an early Miocene lignite from the Latrobe Valley, Victoria, Australia, and consider its high resolution correlation with the marine record.

The bulk $\delta^{13}\text{C}$ was established for 80 m of the Morwell 1B seam, an early Miocene lignite. The mean $\delta^{13}\text{C}$ of the seam is -25.95‰, with a standard deviation range of 0.58 ‰. To compare with the marine record the Morwell 1B record was placed at 21.6 Ma the stratigraphic position determined using orbital tuning for the Morwell seam (Large et al 2004). The high-resolution bulk $\delta^{13}\text{C}$ record from the lignite displays similar long term trends and oscillations to the marine record. However, the long-term oscillations in the terrestrial record are amplified by a factor of 2-3 relative to the marine record (marine carbonate $\delta^{13}\text{C}$ standard deviation 0.259, mean 1.074). The similarity of the long term trends in $\delta^{13}\text{C}$ indicate that the marine and terrestrial records are coupled on time scales exceeding 10^5 years and that bulk $\delta^{13}\text{C}$ are useful for correlating terrestrial and marine records. Variation in the degree of amplification appears to reflect the combined influence of the sea temperature as recorded by marine oxygen isotopes and changes in the isotopic composition of the exogenic carbon reservoir. The influence of sea temperature is probably reflects the strong link between sea surface temperature, peatland hydrology and associated plant stress. The amplification may also result from the smaller size of the terrestrial and atmospheric carbon reservoirs. The exact cause of the amplification is being investigated.

References

Large, D.J., Jones, T.F., Briggs, J., Spiro, B., and Macquaker, J.H.S., 2004, Orbital tuning and correlation of 1.7 m.y. of continuous carbon storage in an early Miocene peatland.: *Geology*, v. 32, p. 873-876.

PPC1-25: Sequential fatty acid analysis of a peat core covering the last two millennia (Tritrivakely lake, Madagascar): diagenesis appraisal and consequences for palaeoenvironmental reconstruction

J.R. Disnar¹, M. Stefanova^{1,2}, S. Bourdon¹, F. Laggoun-Défarge¹

1) I.S.T.O., UMR CNRS 6113, bâtiment Géosciences, Université d'Orléans, BP 6759, 45067 Orléans Cedex 2, France (e-mail: Jean-Robert.Disnar@univ-orleans.fr)

2) Present address: Bulgarian Academy of Sciences, Institute of Organic Chemistry, Acad. G. Bonchev str., bld.9, 1113 Sofia, Bulgaria

When studying fatty acids (FAs) organic geochemists classically paid attention either to the "free" fraction or to "bound" compounds commonly released by saponification. However, it is now well established that more detailed information can be obtained by a study of the various pools of FAs that can be released successively by different chemical treatments (e.g. [1]). Following previous geochemical and petrographical work [2], we applied such an approach to the analysis of a peat core section to get additional information on the palaeoenvironment of the study area and its changes during the last 2300 yr. Thus, seven samples from the 1m long upper section of a core taken from the centre of the Tritrivakely maar lake (Madagascar), were successively submitted to solvent extraction, acid hydrolysis and saponification to release their "free", H⁺-labile and OH⁻-labile bound fatty acids, respectively. The main conclusions that can be drawn from this approach can be summarized as follows:

(1) High amounts of "free" and OH⁻-labile FAs (saturated and unsaturated n-FAs, plus i-C₁₆) at the surface of the peat sequence and low amounts in the immediately underlying level indicate rapid hydrolysis of lipid esters inherited from the primary production, followed by slightly slower consumption.

(2) A whole range of OH⁻-labile FAs (diacids, i- and ai-C₁₅, 3-OH-C₁₄) that are almost or even totally absent from the peat surface, but are abundant at the sub-surface before decreasing just below, denote *in situ* secondary production and subsequent decay. All the corresponding compounds are totally missing from the "free" fraction.

(3) Once past the upper levels where FA dynamics are very active in response to primary inputs, secondary production and active diagenesis, most of the H⁺-labile FAs attest to an important but late *in situ* microbial production that rather rapidly slows down with increasing depth. The latter can be considered as a third production.

(4) In contrast, compounds such as i-C₁₅ and ai-C₁₅ acids also released by acid hydrolysis and which are abundant at the sub-surface but vary very irregularly at depth, might be inherited from consumers acting as secondary producers. As a matter of fact, these

compounds maximize at depth at levels (ca. 30 cm and 60 cm) strongly depleted in "free" and OH-labile FAs normally inherited from the primary producers.

(5) High OM preservation conditions (e.g. at ca. 98 cm depth) are indicated by high relative amounts of nearly all compounds especially in the "free" and OH-labile fraction (i.e. inherited from the primary as well as from the secondary producers, consumers included).

(6) The comparison of compound concentration profiles permits recognition of whether compounds are related to each other or not, i.e. whether they have the same source (e.g. i- and ai-C₁₅), or be independent.

(7) Sequential FA extraction combined with comparison of depth-related compound concentration profiles constitutes what looks like a molecular stratigraphy approach.

(8) However, the previous statement must also take into account the fact that active molecular dynamics during diagenesis hardly allows the drawing of a reliable geochemical portrait for isolated recent geological samples (sediments or soils) after FA analysis. As formulated in a previous study on lake sediments [3], extensive diagenesis can provoke the disappearance of most fatty acids and thus nearly all give information on the contributing organisms except the latest consumers-producers, i.e. methanotrophs.

References

- [1] Barnes, M.A., Barnes, W.C., 1978. Organic compounds in Lake Sediments. In: Lerman A. (Ed.), Lakes. Chemistry Geology Physics, pp.127-152. Springer-Verlag.
- [2] Bourdon, S., Laggoun-Défarge, F., Disnar, J. R., Maman, O., Guillet, B., Derenne, S., Largeau, C., 2000. Organic matter sources and early diagenetic degradation in a tropical peaty marsh (Tritrivakely, Madagascar). Implications for environmental reconstruction during Sub-Atlantic. *Organic Geochemistry* 31, 421-438.
- [3] Stefanova, M., Disnar, J. R., 2000. Composition and early diagenesis of fatty acids in lacustrine sediments, lake Aydat (France). *Organic Geochemistry* 31, 41-55.

PPC1-27: A high resolution vegetation record of Late Quaternary climate variability in tropical South America

N. Drenzek, K. Huguen, T. Eglinton, M. Bice

Department of Marine Chemistry & Geochemistry, Woods Hole Oceanographic Institution, Woods Hole, MA 02543 USA

Assessing the exact timing and magnitude of millennial scale climate change in the tropics remains one of the key challenges in Late Quaternary paleoclimate research. Species modification of terrestrial vegetation in response to such variability can be recorded in proximal marine and lacustrine sediments, where the stable carbon isotopic compositions of their corresponding lipid biomarkers may be used as a sensitive indicator of relative C₃ and C₄ vascular plant abundance. When applied to high deposition rate sediments, such molecular records can provide paleoclimatic information on decadal timescales.

We exploit these characteristics in epicuticular leaf waxes extracted from Cariaco Basin (Caribbean Sea) sediment cores to construct a record of aridity over the past 60,000 years in northern South America. Preliminary results show large amplitude (up to 8 ‰) variations in the $\delta^{13}\text{C}$ values of fatty acids during MIS 3 that parallel Dansgaard/Oeschger variability in high latitude ice cores (Figure 1). Interestingly, large positive excursions possibly reflecting an increasing proportion of C₄ plants appear to be coincident with several North Atlantic Heinrich Events, suggesting that these periods of intense cold were accompanied by a significant southward deflection of the Intertropical Convergence Zone (ITCZ). After a more quiescent MIS 2 period, the events of Termination 1 are recorded as a rapid wetting over the Glacial-Bolling transition followed by a return to drier conditions during the Younger Dryas similar to observations by Huguen et al. (2004). Moreover, these high frequency fluctuations are superimposed upon a long-term precessional signal, highlighting the influence of local insolation on precipitation in this region. Taken together, these data indicate that the seasonal precipitation gradient associated with the meridional migration of the ITCZ can be modulated on longer timescales by both low and high latitude forcing mechanisms.

The molecular distributions of these wax homologues were also measured at high resolution (Figure 1). Although the average chain length (ACL) (Huguen et al., 2004) of several higher molecular weight homologues co-varies with their corresponding stable carbon isotopic compositions during the GL-B/A-YD-PB sequence, this correlation does not hold

over the long term record and suggests that the ACL index at this site may be sensitive to other climate parameters such as temperature (Rommerskirchen et al., 2003).

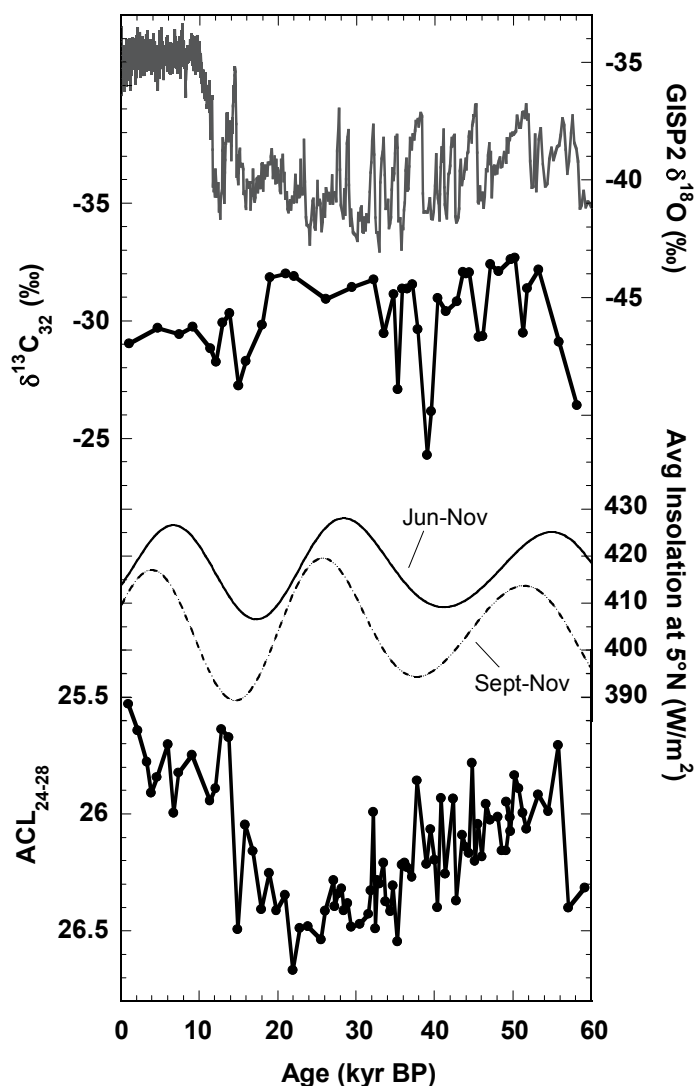


Fig.1. $\delta^{13}\text{C}$ variation of the $n\text{C}_{32}$ fatty acid homologue as well as the ACL index [$=\frac{\sum(iX_i)}{\sum X_i}$, where X = abundance and $i = 24, 26,$ and 28 carbon atoms] over the past 60 kyr along with the local insolation and GISP2 $\delta^{18}\text{O}$ records

Future D/H measurements of these same fatty acids should aid the interpretation of these signals and will be presented along with a supplemented $\delta^{13}\text{C}$ record at 500 year resolution.

References

Hughen, K.A., Eglinton, T.I., Xu, L., Makou, M. 2004. Abrupt tropical vegetation response to rapid climate changes. *Science* 304, 1955-1959.

Rommerskirchen, F., Eglinton, G., Dupont, L., Güntner, U., Wenzel, C., Rullkötter, J. 2003. A north to south transect of Holocene southeast Atlantic continental margin sediments: Relationship between aerosol transport and compound-specific $\delta^{13}\text{C}$ land plant biomarker and pollen records. *Geochemistry, Geophysics, Geosystems* 4(12).

PPC1-27: Elemental and isotopic records of the Early Aptian oceanic anoxic event from Shatsky Rise

M. Dumitrescu, S. Brassell

Biogeochemical Laboratories, Department of Geological Sciences, Indiana University, Bloomington, IN 47405, USA

The occurrence of intervals of enhanced sequestration of organic matter (OM) during the mid-Cretaceous – collectively termed ‘Oceanic Anoxic Events’ (OAE) – reflect abrupt changes in global carbon cycling. These episodes raise questions about the causes for such perturbations, and their linkages to fluctuations in climate, marine biota, and ocean geochemistry preserved in the sedimentary record. The limited recovery of these intervals in the Pacific has largely precluded detailed assessment of the stratigraphic profiles of the Early Aptian event (OAE1a), in contrast to the many records from the Tethyan realm. The recovery of pelagic sequences of organic-rich sediments from Shatsky Rise (ODP Leg 198) confirmed as the early Aptian OAE1a by biostratigraphy (nannofossil zone NC6; Bralower *et al.*, 2002), now makes feasible investigation of high-resolution temporal variations in the elemental and isotopic compositions of this event in the Pacific.

Elemental and isotopic composition of sub-samples from the organic-rich interval show significant temporal fluctuations that enable division of the core into sub-sections (I-IV) (Fig. 1b). The $\delta^{13}\text{C}$ composition of OM is lowest (-27.7‰) at the base of the recovered organic-rich interval (zone I in Fig. 1b), representing a negative $\delta^{13}\text{C}$ excursion, and is followed by a 2.4‰ shift to more positive values at the top of zone I (Fig. 1b). This profile is comparable to segments C3 and C4 of the Cismon record (Menegatti *et al.*, 1998), and parallels that observed for $\delta^{13}\text{C}_{\text{carb}}$ at nearby Resolution Guyot (Jenkyns, 1995). However, natural gamma and uranium logs (Robinson *et al.*, 2004) for Site 1207B show the organic-rich interval to be approximately 1.2m in thickness. This suggests that the continuous 45 cm interval recovered likely represents the initiation of OAE1a rather than a complete section (Fig. 1a). Exceedingly high organic carbon ($\text{C}_{\text{org}} > 20\%$) and total sulfur ($\text{TS} > 5\%$) contents (zone IV) - among the highest ever recorded for pelagic Cretaceous sequences - attest to the enhanced sequestration of OM during OAE1a. $\delta^{15}\text{N}$ values are lower ($< -1.5\text{‰}$) in zones II and III (Fig. 1b), consistent with the possibility of nitrogen fixation within this interval (Rau *et al.*, 1987) related to elevated cyanobacterial populations (Kuypers *et al.*, 2004). These temporal fluctuations likely reflect differences in productivity and plankton populations associated with environmental and climate changes.

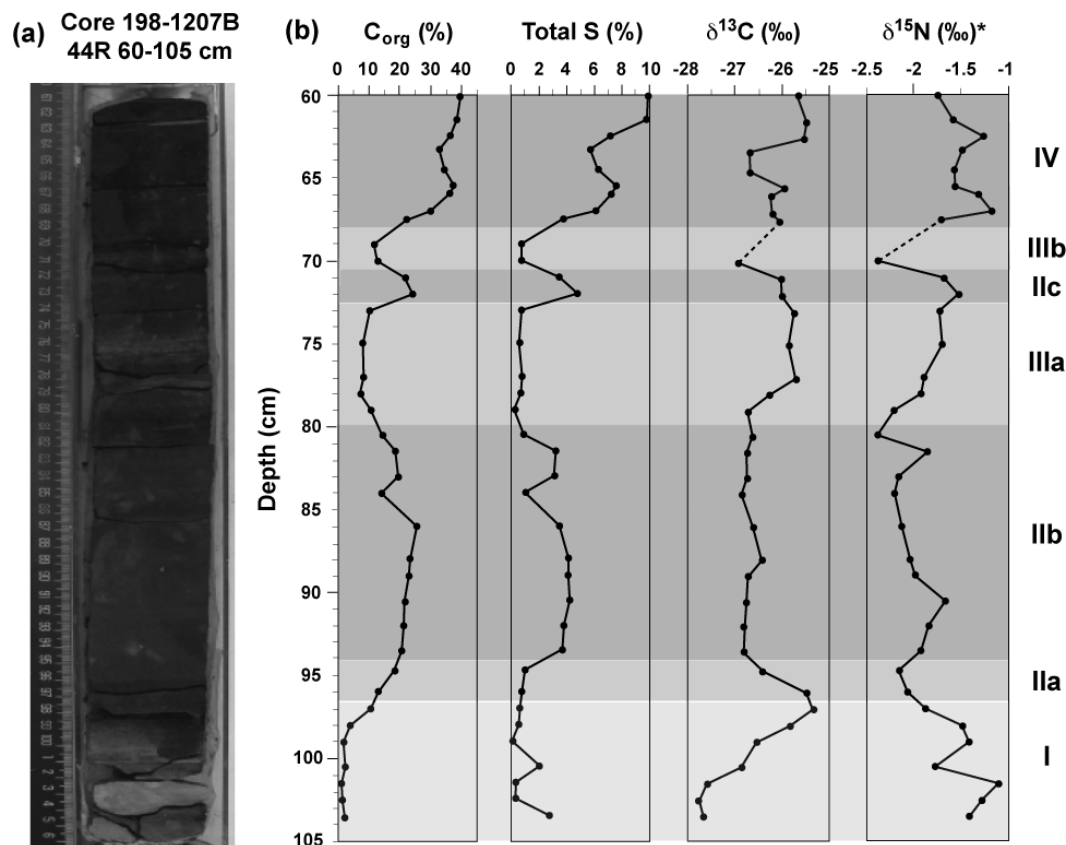


Fig.1. Stratigraphic trends in elemental and isotopic data for Lower Aptian organic-rich sediments from Shatsky Rise. **(a)** Photograph of a portion of ODP Core 198-1207B-44R-1. **(b)** Profiles of C_{org} contents, total S, δ¹³C of OM and δ¹⁵N for intervals obtained by sub-sampling the entire section (*δ¹⁵N values are uncalibrated; they represent raw data relative to N₂ tank gas)

References

- Bralower, T.J., *et al.*, 2002. *Proceedings of the Ocean Drilling Program, Initial Reports*, 198: [online]. (www-odp.tamu.edu/publications/198_IR/198ir.htm).
- Jenkyns, H.C., 1995. Carbon-isotope stratigraphy and paleoceanographic significance of the Lower Cretaceous shallow-water carbonates of Resolution Guyot, Mid-Pacific Mountains. *In Proceedings of ODP, Scientific Results*, 143: (Eds. Winterer, E.L., *et al.*), 99-104.
- Kuypers, M.M., *et al.*, 2004. N₂-fixing cyanobacteria supplied nutrient N for Cretaceous oceanic anoxic events. *Geology*, 32, 853-856.
- Menegatti, A.P., *et al.*, 1998. High-resolution δ¹³C stratigraphy through the early Aptian "Livello Selli" of the Alpine Tethys: *Paleoceanography*, 13, 530-545.
- Rau, G.H., *et al.*, 1987. 15N/14N variations in Cretaceous Atlantic sedimentary sequences: implications for past changes in marine nitrogen biogeochemistry. *Earth and Planetary Science Letters*, 82, 269-279.
- Robinson, S.A., *et al.*, 2004. Fluctuations in biosiliceous production and the generation of Early Cretaceous oceanic anoxic events in the Pacific Ocean (Shatsky Rise, Ocean Drilling Program Leg 198). *Paleoceanography*, 19, PA4024.

PPC1-28: Reconstruction of Holocene paleotemperature in the Iberian Peninsula using lipid biomarkers

M. Escala, A. Rosell-Melé

Institute of Environmental Science and Technology, Autonomous University of Barcelona, Bellaterra 08193, Catalonia, Spain (e-mail: marina.escala@campus.uab.es)

Introduction

At present, quantitative paleotemperature data in continental environments comes mostly from pollen reconstructions, but it is a proxy with limited spatial and temporal resolution. Biomarkers are proxies that can yield quantitative results and overcome the drawback in resolution. One of the most used biomarkers for reconstructing paleotemperature are alkenones, which were found in limnic systems as early as 1985 (Cranwell, 1985). Nevertheless, it has not yet been demonstrated if alkenone based indices, which have been widely applied to marine environment, are effective for reconstructing paleotemperatures in lakes, although some attempts have been carried out (e.g. Zink et al, 2001). Recently, a new paleotemperature proxy, TEX86, based on crenarchaeotal membrane lipids, has been proposed (Schouten et al., 2002). Initial results suggest that this could be an important quantitative paleoreconstruction tool, but few studies have been published to date and there are no temperature reconstructions from TEX86 comparable with other well-established proxies.

Approach

The aim of this study is to set a quantitative reconstruction of Holocene temperatures in the Iberian Peninsula, using lipid biomarkers, especially alkenones and crenarchaeotal lipids, which will be calibrated and compared in several limnic and also marine environments. We have started studying these two classes of biomarkers in the Iberian Peninsula, and have located some lakes in which they are present, especially in endorheic areas of the Peninsula where saline lakes occur (Pearson, 2003). The goal is to ascertain how these biomarkers reflect environmental conditions in the Iberian Peninsula, and use this relationship to elucidate temperature trends during Holocene.

Calibration is of fundamental importance for biomarkers being useful as paleoreconstruction tools. That is especially urgent for TEX86, as few attempts have been made in this direction. We are in the process of evaluating the robustness of this method by means of analyzing sediments and water samples from different latitudes and environments, both lacustrine and marine. Amongst these samples we have sediments from Baikal Lake, which offers a deep, oligotrophic and oxic environment; water samples from a South Africa -

Antarctica transect, where we expect to see the effect of the latitude gradient; and sediments from Spanish lakes, as Llac Banyoles in the north-west part of the Iberian Peninsula. The calibration process in this multi-site set of samples will assess the robustness of the TEX86 method thus allowing us to validate this paleotemperature proxy for continental reconstructions.

References

- Cranwell, P.A., Long-chain unsaturated ketones in recent lacustrine sediments. *Geochim. Cosmochim. Acta* 49, 1545-1551, 1985.
- Schouten, S., Hopmans, E.C., Schefub, E., Sinninghe Damsté, J.S., Distributional variations in marine crenarchaeotal membrane lipids: a new tool for reconstructing ancient sea water temperatures? *Earth and Planetary Science Letters* 204, 265-274, 2002.
- Zink K.G., Leythaeuser D., Melkonian M., Schwark L., Temperature dependency of long-chain alkenone distributions in recent to fossil limnic sediments and in lake waters. *Geochim. Cosmochim. Acta* 65, 253-265, 2001.
- Pearson, E.J., Lipid biomarkers in spanish saline lake sediments: indicators of organic inputs and environmental change. PhD Thesis, School of Geography, Politics and Sociology, University of Newcastle, UK, 2003.

PPC2-1: Lignin-phenol and $\delta^{13}\text{C}$ evidence of Quaternary vegetation change in South America

K.J. Ficken¹, T.R. Filley², F.A. Street-Perrott¹

1) Dept of Geography, University of Wales Swansea, Singleton Park, Swansea, SA2 8PP
(e-mail: K.J.Ficken@swansea.ac.uk)

2) Dept of Earth and Atmospheric Sciences, Purdue University, 550 Stadium Mall Drive, West Lafayette, IN 47907, USA

Previous work on the molecular $\delta^{13}\text{C}$ values of long-chain *n*-alkyl lipids from lake sediments situated along a palaeoclimatic transect from NE Chile (24°S) to Venezuela (8°N) has permitted the ecophysiological effects of glacial/interglacial variations in atmospheric $p\text{CO}_2$ (global) and monsoon precipitation (regional) to be differentiated. All the lake sites lie below the upper limit of C_4 graminoids in the Andes (ca. 4200 m a.s.l.) and therefore should have been sensitive to past increases in the proportion of C_4 biomass resulting from lower atmospheric $p\text{CO}_2$, higher temperatures or decreased precipitation. Past changes in the C_3/C_4 ratio of the sedimentary organic-matter input that are evident from the $\delta^{13}\text{C}$ record should also be reflected in the chemistry of vascular plant tissue stored in the sediments. Biopolymer analysis of lignin phenols allows this hypothesis to be tested.

Lignin-phenol concentrations extracted from the sediments of 6 lakes along the transect were determined by CuO oxidation (Hedges and Ertel, 1982; Goñi and Hedges, 1992). $\delta^{13}\text{C}$ values of the lignin phenols will be obtained shortly. Lignin-phenol concentrations ranged from 0.1 to 0.65 mg/100 mg OC in Laguna Casercocha near the southern end of the transect and 0.09 to 1.59 mg/100 mg OC in Laguna Los Lirios at the northern end. The acid/aldehyde (Ad/Al) ratios ranged from 0.43 to 0.93 and 0.37 to 0.8 for the vanillyl compounds, and from 0.28 to 0.81 and 0.29 to 0.66 for the syringyl compounds, in Casercocha and Los Lirios, respectively.

At the southern end of the transect, the lignin phenol vegetation index (LPVI) (Tareq *et al.*, 2004) indicates more woody vegetation during the glacial period (wet and cold) and more non-woody vegetation during the Holocene (dry and warm) (Figure 1). The two northernmost lakes show a reverse trend, with more non-woody vegetation during the glacial (dry and cold) and more woody vegetation during the wetter, warmer Holocene (Figure 1). The two intermediate sites exhibit no strong overall glacial/interglacial trend. Samples that contain lignin phenols indicative of a woody-plant origin are more oxidized than those dominated by non-woody material. This contrast may reflect either their different ecological sources or different degrees of degradation during transport.

The contrasting temporal patterns in lignin-phenol concentration agree well with the bulk isotope data (Figure 1). $\delta^{13}\text{C}_{\text{TOC}}$ values at the southern end of the transect suggest an increase in the C_3/C_4 biomass ratio during the glacial and a decrease during the Holocene, while $\delta^{13}\text{C}_{\text{TOC}}$ values for lakes at the northern end of the transect show an opposite temporal trend. The LPVI and bulk isotope results are supported by the molecular-isotope values of long-chain *n*-alkyl lipids, and by the available pollen and lake-level data.

If global changes in $p\text{CO}_2$ were the main factor driving glacial/interglacial variations in the C_3/C_4 biomass ratio, all the sites should have responded in parallel. The same applies for temperature. However, similar latitudinal contrasts are exhibited by both the lignin-phenol and ^{13}C data, confirming that precipitation was the dominant control on the glacial distribution of C_3 and C_4 plants rather than low $p\text{CO}_2$, which would have favoured the spread of C_4 plants or lower temperatures, which would have favoured C_3 plants.

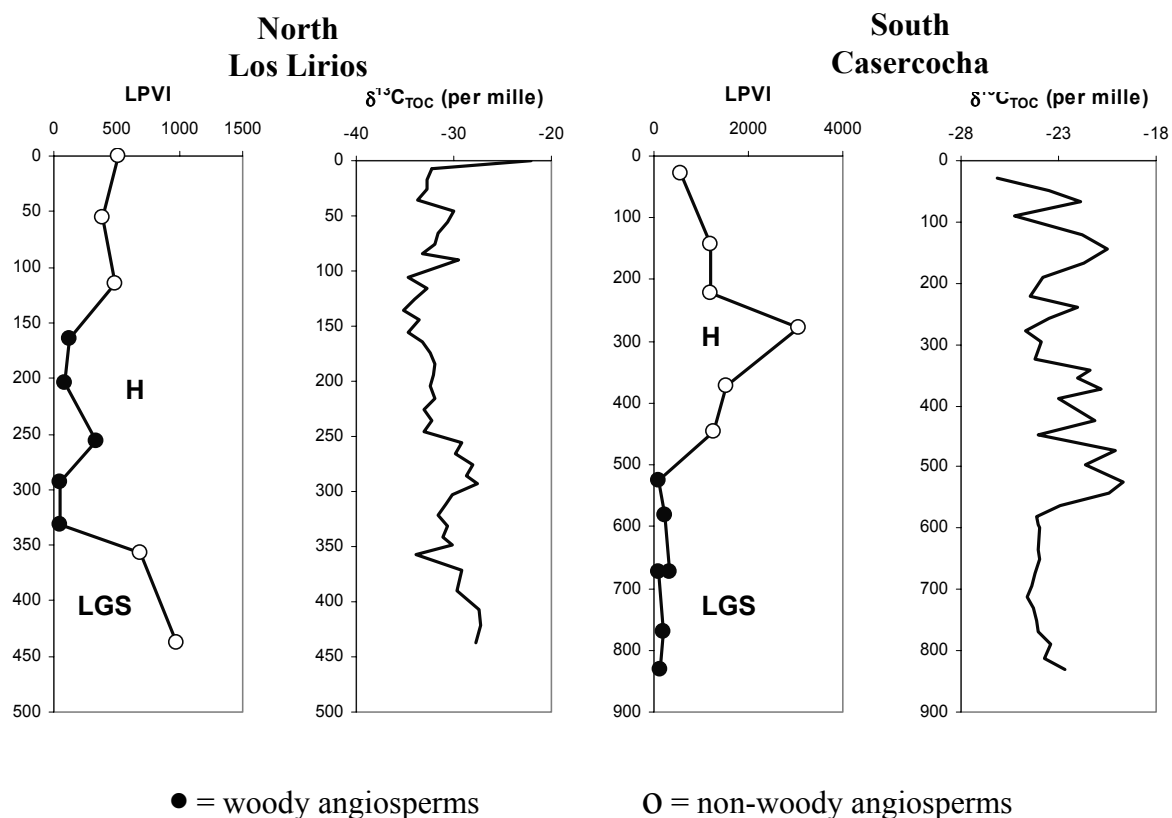


Fig.1. LPVI and $\delta^{13}\text{C}_{\text{TOC}}$ for Los Lirios (northern end of transect) and Casercocha (southern end of transect). Values on y axes represent depth in cm

References

- Goñi M.A. and Hedges J.I. (1992) *Geochim Cosmochim Acta* **59**, 2965-2981.
 Hedges J.I. and Ertel J.R. (1982) *Anal Chem* **54**, 174-178.
 Tareq S.M. *et al.* (2004) *Science of the Total Environment* **324**, 91-103.

PPC2-2: Last glacial cycle vegetation change in Himalaya from bulk and molecular $\delta^{13}\text{C}$ analyses in Bengal Fan sediments

V. Galy¹, F. Palhol¹, P. Faure², C. France-Lanord¹

1) Centre de Recherches Pétrographiques et Géochimiques - CNRS, BP 20, 54501 Vandoeuvre-les-Nancy, France (e-mail : vgaly@crpg.cnrs-nancy.fr)

2) UMR-CNRS 7566 G2R, Université Henri Poincaré, BP 239, 54506, Vandoeuvre-les-Nancy, France

The Bengal fan is the largest active sedimentary system of the Earth. Receiving the products of Himalayan erosion, it represents a record of past conditions in the Himalayan system over the last 20 million years. A few molecular analyses have demonstrated that the organic matter contained in the Bengal fan sediments is largely dominated by terrigenous organic matter (Poynter and Eglinton, 1990; Freeman and Colarusso, 2001). $\delta^{13}\text{C}$ of bulk organic matter in sediments from deep drillings in the distal Bengal fan shows a dramatic positive shift 7 million years ago (France-Lanord and Derry, 1994). This reflects the expansion of C4 plants in the Himalayan basin which is also documented by floodplain paleosoils (e.g. Quade and Cerling, 1987).

Samples used in this study belong to the modern channel-levee system located in the upper Bengal fan. This sedimentary system was sampled during cruise SO93 of the RV Sonne in February 1994 and provide a 16 kyear sedimentary record (Weber et al.1997). Bulk and molecular organic matter analyses have been performed in order 1) to precise the nature of the organic matter contained in these sediments and 2) to reconstruct the basin vegetation evolution during the last glacial cycle. The molecular composition of soluble organic matter was analysed using a GC-MS. Special attention has been paid to saturated and polar fractions. Bulk organic carbon isotopic composition was determined for 32 samples from 3 cores recording 16 kyear of sedimentation. Observed variations were confirmed by analysing molecular carbon isotopic composition of odd high-molecular-weight n-alkanes extracted from 4 selected samples.

Carbon Preference Index (CPI) values range from 4.5 to 5.2, characteristic of organic matter largely dominated by terrestrial higher plants. Compound distribution of saturated and polar fractions are highly similar throughout time. This lead to the conclusion that no major changes in organic matter input occurred during the last glacial cycle. Bulk organic matter $\delta^{13}\text{C}$ values range from -22.5 to -18.6 ‰, characteristic of mixed C3/C4 vegetation. These data show a dramatic negative 4 ‰ shift from 16 to 7 kyear, followed by a more stable period up to present. Molecular isotopic data on odd n-alkanes (C23 to C35) confirm this trend and allow to link it directly to higher plants changes in the basin. This reflects an evolution from

C4 dominated vegetation at LGM to C3 dominated vegetation since the Holocene hypsithermal. Considering our knowledge of the modern Ganga-Brahmaputra system, this evolution correspond to a change in the C3/C4 ratio from approximately 40/60 at LGM to 80/20 for the modern system.

This vegetation evolution may be related to environmental conditions changes such as monsoon intensity and seasonality. Although requiring further investigations, these data are consistent with more arid and seasonal conditions at LGM and are in good agreement with other paleoenvironmental proxies such as foraminifera $\delta^{18}\text{O}$ (Duplessy, 1982; Weber et al., 1997) or molecular δD (Palhol et al., this session).

References

- Duplessy J.C. (1982) Glacial to interglacial contrasts in the northern Indian Ocean. *Nature* **295**, 494-498.
- France-Lanord C. and Derry L. A. (1994) $\delta^{13}\text{C}$ of organic carbon in the Bengal Fan: source evolution of C3 and C4 plant carbon to marine sediments. *Geochimica et Cosmochimica Acta* **58**(21), 4809-4814.
- Freeman K. H. and Colarusso L. A. (2001) Molecular and isotopic records of C₄ grassland expansion in the late Miocene. *Geochimica et Cosmochimica Acta* **65**(9), 1439-1454.
- Palhol F., Galy V., Faure P., and France-Lanord C. (2005) Paleoenvironmental significance of n-alkane δD from Ganga - Brahmaputra ancient sediments. *22th IMOG*.
- Poynter J. and Eglinton G. (1990) Molecular composition of three sediments from Hole 717C: The Bengal Fan. *Proceedings of the Ocean Drilling Program, Scientific Results* **116**, 155-161.
- Quade J., Cerling T. E., and Bowman J. R. (1989) Development of Asian monsoon revealed by marked ecological shift during the latest Miocene in northern Pakistan. *Nature* **342**, 163-166.
- Weber M. E., Wiedicke M. H., Kudrass H. R., Hübscher C., and Erlenkeuser H. (1997) Active growth of the bengal Fan during sea-level rise and highstand. *Geology* **25**, 315-318.

PPC2-3: Climate change and the carbon cycle of small, hard water lakes

H.L. Gibbons, J.D. Marshall, G.A. Wolff

Department of Earth and Ocean Sciences, University of Liverpool, 4 Brownlow Street, Liverpool L69 3GP UK
(e-mail: hgibbons@liv.ac.uk)

A study of lake sediments has been carried out to determine the relationship between carbon cycling and climate change since the last glacial. This study uses a multiproxy approach, applying quantitative indicators that can be easily evaluated at tightly spaced stratigraphic intervals, including carbon preservation and isotopic, elemental and molecular approaches.

Sediment cores collected from Sunbiggin Tarn in Cumbria UK, were sampled at 1 cm intervals. Data from loss on ignition (LOI) and carbon and oxygen isotope analysis of carbonate were used to construct a composite core representing approximately 15,000 to 8,000 years BP (Fig. 1). TOC's and C/N ratios have been obtained and a study of detected biomarkers carried out. Chironomid and pollen data will provide independent evidence for faunal and floral variations.

The stratigraphy and pattern of environmental change is similar to that in other sites in northwest England (Marshall et al., 2002) with cold events reflected in high clay content and low carbonate oxygen isotope values (Fig 1a). Decreases in carbonate production suggest four cold periods during the post-Devensian warming phase and a longer cold period that correlated with the Younger Dryas stadial. Initial results show an increase of ~4.5 % TOC during the post-Devensian interstadial. There is also a negative shift of 3.3 ‰ in $\delta^{13}\text{C}$ of inorganic carbon; this reflects a decline in productivity, possibly due to reducing nutrient availability.

The LOI profile clearly shows that amount of carbonate differs between the 3 climate regimes of the post-Devensian interglacial, the Younger Dryas and the Holocene. Climatic changes are mirrored by changes in sedimentary OM composition. Table 1 shows mean C/N ratio, range of C/N ratios, and average MC# for n-alkanes. The C/N ratio increases up the profile (see Fig 1b), suggesting a change from a regime dominated by autochthonous production, to an allochthonous system (Meyers, 1997). The MC# ($>\text{C}_{21}$) shows that higher plant inputs were greater during warm periods than during the Younger Dryas. Values are commonly between 21 and 25, suggesting that much of the OM may originate from submerged and floating macrophytes (Ficken et al., 2000). During the post-Devensian interstadial, MC#'s increase with silicate concentration, as terrestrial material is delivered to

the lake via erosion. It can therefore be concluded that climate change has had a significant impact on the trophic status of the lake and that lake sediment records provide an important record of larger scale climate change.

Further work will involve characterisation of isotopic composition of OM and use of the membrane lipids of Crenarchaeota as a novel palaeotemperature proxy.

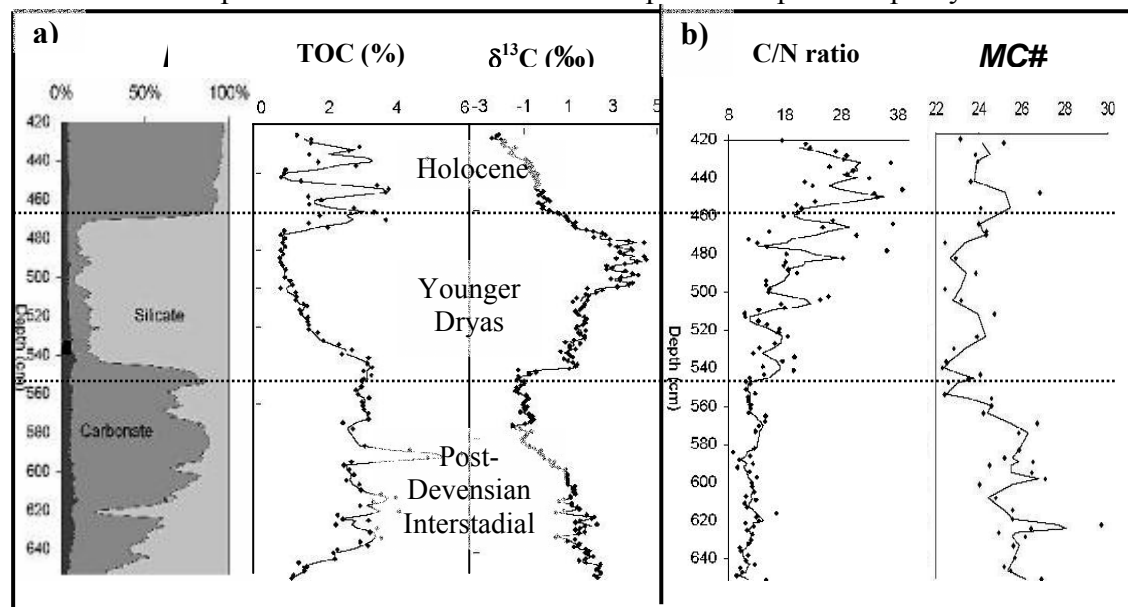


Fig.1. a) Comparison of LOI (black is OM); TOC; & $\delta^{13}\text{C}$ of carbonate, showing timing of Holocene, Younger Dryas & Post-Devisian Interglacial (b) Comparison of C/N ratio & MC# alkanes

Table 1. Mean C/N ratio, range C/N ratios & average MC# (>C₂₁ alkanes only). C/N ratios are highest in the Holocene & MC# higher during interstadials

	Post-Devisian Interglacial	Younger Dryas	Holocene
Mean C/N ratio	11.9	16.9	26.3
Range C/N ratios	8.8 to 16.4	10.8 to 30.7	17.5 to 38.8
Average MC#	25.8 ± 0.9	23.2 ± 0.8	24.1 ± 0.6

References

- Ficken, K.J., Li, B., Swain, D.L. & Eglington, G. (2000) An n-Alkane proxy for the sedimentary input of submerged/ floating freshwater aquatic macrophytes. *Organic Geochemistry*, **31**, 745-749.
- Marshall, J.D., Jones, R.T., Crowley, S.F., Oldfield, F., Nash & Bedford, A. (2002) A high resolution Late-Glacial isotopic record from Hawes Water, Northwest England - Climatic oscillations: calibration and comparison of palaeotemperature proxies. *Palaeogeography, Palaeoclimatology, Palaeoecology*, **185**, 25-40.
- Meyers, P.A. (1997) Organic geochemical proxies of paleoceanographic, paleolimnologic and paleoclimatic processes. *Organic Geochemistry*, **27**(5/6), 213-250.

PPC2-4: Tracing of variabilities in geological barriers by molecular organic geochemistry. Case of the Callovo-Oxfordian series in the East of the Paris Basin (France)

Y. Hautevelles^{1,2}, R. Michels¹, F. Malartre³, A. Trouiller², M. Elie¹

1) UMR 7566 CNRS G2R, Université Henri Poincaré, Nancy 1, BP 239, 54506 Vandoeuvre-lès-Nancy cedex, France (e-mail: Yann.Hautevelles@g2r.uhp-nancy.fr)

2) ANDRA, 1-7 rue Jean Monnet, 92268 Châtenay-Malabry, France

3) UMR 7566 CNRS G2R, Ecole Nationale Supérieure de Géologie, BP 40, 54501 Vandoeuvre-lès-Nancy cedex, France

In order to study the feasibility of a deep geological nuclear waste repository, the French government assigned Andra (the French National Radioactive Waste Management Agency) to evaluate the confinement properties of claystones located 500 meters deep in the East of France (Meuse/Haute Marne). In this objective, the physico-chemical variabilities of the geological barrier have to be studied. Variabilities of sedimentary series are inherited from their sedimentologic and diagenetic history. These 130 m thick claystones are dated from Callovian and Oxfordian (Jurassic) and are limited on base and top by limestones. Molecular organic geochemistry appears to be an adequate tool for tracing source variability because biomarkers distribution is well sensitive to the origin of the sedimentary input as well as the depositional and diagenetic conditions. Study of the lateral and vertical variability of the molecular composition of organic matter has been successfully used to characterize variabilities in the Silty Layer of Marcoule (Fleck et al., 2001). Five wells drilled by Andra distributed on two perpendicular transects were investigated in the East of the Paris Basin. The geological data including sequence stratigraphy, lithology, well-logs, geochemistry and mineralogy and were used as a framework for interpretation of our data.

Total yields. Maximum yields of soluble organic matter (0.15-0.20 mg/g of rock) are located in the middle Callovian then decrease to a minimum (≈ 0.05 mg/g of rock) when approaching the Dogger/Malm boundary. The values remain constant within the Oxfordian.

Aliphatic/Aromatic/Polar proportions. Weight proportions of aliphatic, aromatic and polar fractions are relatively similar in all samples (respectively 17, 13 and 70% in average).

n-alkanes. Aliphatic fractions contain n-alkanes ranging from n-C₁₃ to n-C₃₄ with a CPI = 1.5 to 3. The n-C₂₄⁺/n-C₂₄⁻ ratio, a marker of continental/marine contributions, shows significant evolutions (from 0 to 2) for the different wells.

Iso- and cyclo-alkanes. Aliphatic fractions sometimes show a UCM (Unresolved Complex Mixture) ranging between n-C₁₃ and n-C₂₀ due to a great diversity of iso- and cyclo-

alkanes. Pristane (Pr) and phytane (Ph) are abundant and Pr/Ph ratio range between 1 and 4.5. Values close to 1 are associated with limestones and values >3.5 are only found in EST 342.

Sesqui- and diterpenoids. These compounds are essentially land plants biomarkers. A major evolution induced by a climatic change indicates a modification of the nature of the continental organic contribution (Hautevelle et al., 2005).

Steroids. Aliphatic fractions show low proportions of steranes essentially ranging from C₂₇ to C₂₉ with a predominance of C₂₉. Their relative proportions do not change significantly. Low molecular weight steranes as pregnane and androstane are also present. Diasterenes are significantly more abundant than steranes in clays due to steroid rearrangement controlled by acid catalysis on clay minerals. Their relative abundance decreases drastically in limestones.

Hopanoids. Pentacyclic triterpenoids are represented by hopanes and benzohopanes. Hopanes distribution shows a great abundance of $\beta\beta$ hopanes and hopenes in claystones which decrease significantly in limestones. Benzohopanes are cyclised at C(16) and C(20).

The molecular distribution of the Callovo-Oxfordian deposits shows that the organic matter is a mixture of three main contributions, marine organisms, bacteria and land plants. The identified hydrocarbons families are always the same but their relative proportions change, notably through claystone/limestone transitions. The abundance of hopenes, hopanes in biological configuration ($\beta\beta$ hopanes) and benzohopanes cyclised at C(16) in claystones indicates well preserved biological markers and thus a very low thermal maturity. These observations are consistent with previous studies (Landais and Elie, 1997). Organic geochemical data indicate that sources and preservation conditions of organic matter were not significantly modified during the deposition of clays while some changes can be related to evolutions of the quantity and quality of land plant input. Thus, the overall organic content of the geological barrier can be considered as homogeneous at the sedimentary formation scale. However, this conclusion does not take into account possible variabilities at the microscopic scale, which could locally modify the nature of organic matter / mineral interactions within the geological barrier. Authors thank Andra for providing samples and financial support.

References

- Fleck S. et al. (2002). *Org. Geochem.*, **33**, 1533-1557.
Hautevelle Y. et al. (2005). Oral presentation at 22nd IMOG Meeting. 12-16 september 2005.
Landais P. and Elie M. (1997). *Acte des journées scientifiques CNRS/ANDRA*, 35-61.

PPC2-5: Confined pyrolysis: an experimental method for the correlation of biomarkers in ancient sediments with extant land plants?

Y. Hautevelle^{1,2}, R. Michels¹, F. Malartre³, F. Lannuzel¹, A. Trouiller²

1) UMR 7566 CNRS G2R, Université Henri Poincaré, Nancy 1, BP 239, 54506 Vandoeuvre-lès-Nancy cedex, France (e-mail: Yann.Hautevelle@g2r.uhp-nancy.fr).

2) ANDRA, 1-7 rue Jean Monnet, 92268 Châtenay-Malabry, France

3) UMR 7566 CNRS G2R, Ecole Nationale Supérieure de Géologie, BP 40, 54501 Vandoeuvre-lès-Nancy cedex, France

The nature and proportion of plant species in continental paleovegetation are excellent paleoclimatic markers. Paleobotany and palynology are classically used in the reconstruction of ancient vegetations and climates. However, these yet complementary approaches provide only partial information because of the rare occurrence of well preserved macrofossils and the difficulty to associate fossils, spores and pollen to precise taxa with certainty. The analysis of land plant biomarkers is routinely performed on whole rock and do not need to be collected in locations of exceptional preservation (e.g. Lagerstätten Formations). Also, some terpenoids have a good paleochemosystematic value and thus can be linked to specific taxa (e.g. cuparane-type sesquiterpenoids for Cupressaceae). Therefore, paleochemotaxonomy is an excellent tool to study land-plants paleobiodiversity. Most studies relating biomarkers of extant land-plants to fossil taxa rely on comparisons with well preserved macrofossils and ambers. Studies are commonly conducted by using hydrolysis and solvent extraction methods followed by molecular analysis. However, fossilization often modifies the original biochemical signatures (partial loss of labile functions), and direct comparison with extant plants is not easy. Furthermore, most taxa have not yet been investigated for (paleo)chemotaxonomic biomarker research. The catalogue of taxa related biomarkers needs still to be significantly expanded.

In order to improve the search for specific biomarkers in extant plants, we propose an alternative experimental method based on artificial maturation. Initially developed to study the maturation of kerogen, confined pyrolysis (Monthieux et al., 1985; Landais et al., 1989) was recently successfully applied to evidence the chemical genetic relationship between fossil and extant organisms (Stanckiewicz et al., 2000; Gupta et al., 2003). Several extant plant species were submitted to confined pyrolysis, some of them containing well known specific biomarkers (mainly conifers as Araucariaceae, Cupressaceae, Taxodiaceae, Pinaceae and also *Ginkgo biloba*) while others do not (Cycadales, Sphenophyta). Fresh leaves and sometimes branches, pure resins and fruits were fine-cut then dried. A few grams of plant samples were packed in gold capsules under argon atmosphere and sealed, then introduced in stainless steel

autoclaves and submitted to temperatures ranging from 250°C and 350°C during 24 hours under 700 bars pressure.

The plant samples as well as their pyrolysed counterparts were submitted to dichloromethane extraction. The extracts were fractionated then analysed by GC-MS.

Chromatograms of plants pyrolysates are used for identifying potential specific biomarkers. Those plants which produce well-known specific biomarkers are used for the validation of our method. The molecular signatures obtained on the non-pyrolysed samples are used for the search for biomarkers precursors. The confined pyrolysis of extant plant samples induces the partial conversion of biological configured molecules into their fossil counterparts. The results acquired on pyrolysed plants can therefore be compared to macrofossil or molecular signatures derived from macrofossil or sediment extracts.

Our results provide information, for instance, on the occurrence of cadalene. Cadalene is considered as an unspecific biomarker because cadinane-type biosesquiterpenoids are widely distributed in the plant kingdom. However, cadalene is not found in all pyrolysis products of extant plants (as Cycads for instance). However, it is significantly detected in all conifer and *Ginkgo* samples. The presence of cadalene in conifers and *Ginkgo* pyrolysis products is consistent with analysis of macrofossils. These results show that cadalene, despite its weak chemosystematic value, has a more restricted occurrence than expected and could potentially bring paleobotanical information. Confined pyrolysis is potentially a new method for foreseeing molecular composition of fossil plants having still living counterparts and for increasing our knowledge of biomarkers with chemotaxonomic value. This methodology is expected to increase possibilities to correlate geochemical signatures with plant taxa and to help in the study of biodiversity in ancient sediments.

References

- Gupta N. et al. (2003). 21st IMOG, Krakow, Poland, Book of Abstracts, p. 179.
Landais et al. (1989). J. Anal. Applied Pyrolysis, **16**, 103-115.
Monthieux et al. (1985). Org. Geochem., **8**, 275-292.
Stanckiewicz et al. (2000). Geology, **28**, 6, 559-562.

PPC2-6: Paleohydrology of tropical South America since the Last Glacial Maximum. Insights from the δD of algal and terrestrial molecular markers in lake sediments

J. Jacob^{1,2}, Y. Huang¹, A.L. Spadano Albuquerque³, A. Sifeddine⁴, J.-R. Disnar²

1) Dept. of Geological Sciences, Brown Univ. Providence, Rhode Island, USA

(e-mail: jeremy.jacob@univ-orleans.fr)

2) Laboratoire de Géochimie Organique, Institut des Sciences de la Terre d'Orléans, France

3) Dept. de Geoquímica, Univ. Federal Fluminense, Niteroi, RJ, Brazil

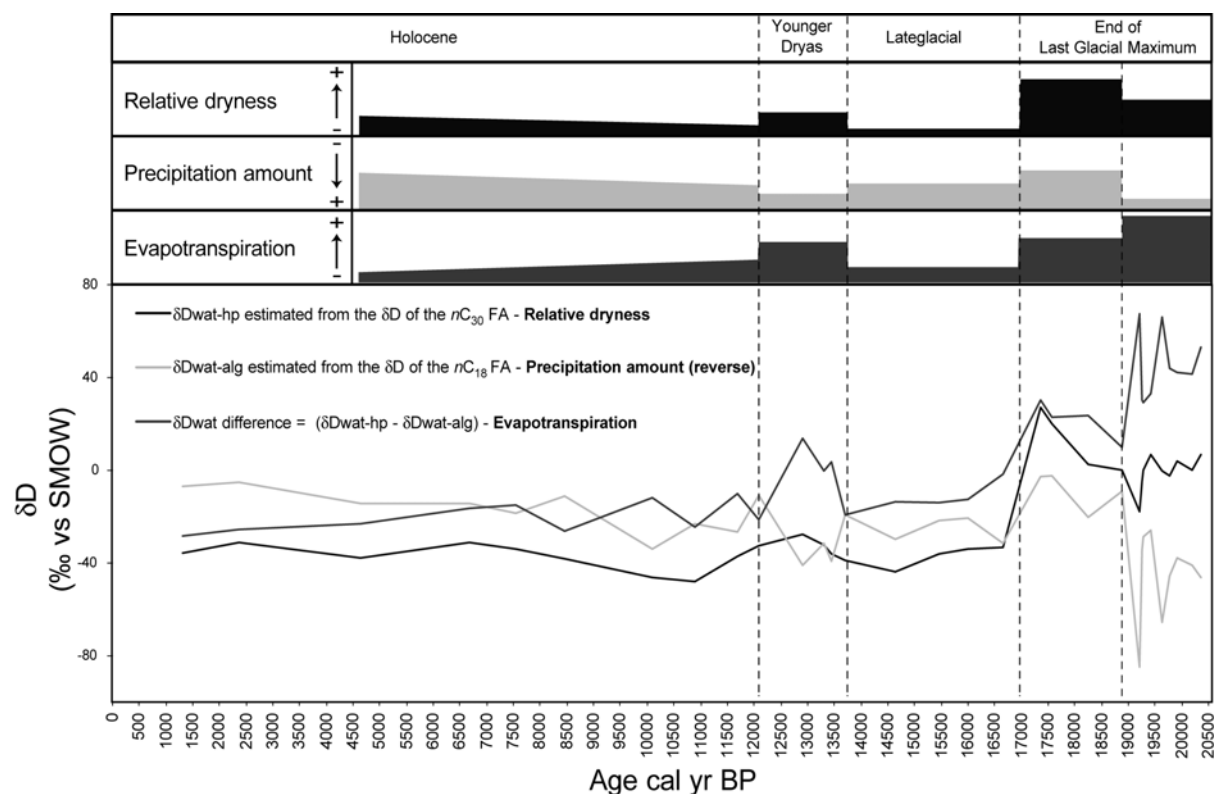
4) IRD/Bondy, 32 avenue Henry Varagnat, 93143 Bondy Cedex, France

There is renewing evidence that the Tropics might strongly influence climate dynamics on millennial time-scales. Part of this "tropical forcing" is related to changes in the water cycle that impacts atmospheric and oceanic processes on a broad scale. Past variations of the continental hydrology are poorly documented due to the few available records and the lack of quantitative data on climate parameters. The deuterium/hydrogen ratio (δD) of algal-derived biomarkers captures the isotopic composition of meteoric waters (Huang et al., 2002; Sachse et al., 2004). In turn, terrestrially-derived biomarkers captures the isotopic composition of meteoric waters through their δD but with a strong influence of the evapotranspiration. A combination of these two factors should thus allow the quantification of the variations in relative humidity (i.e. precipitation–evaporation; P-E). We applied such an approach to estimate hydrological changes in Northern Brazil during the last 20,000 yr. The δD of algal (*n*-C₁₈) and land plant (*n*-C₃₀) fatty acids (FA) have been measured on 30 samples selected on a 6 m long lacustrine sediment core.

In a first approximation, we considered a mean hydrogen isotope fractionation of -157 ‰ between the *n*-C₁₈ FA and water and between the *n*-C₃₀ FA and water of -128 ‰ (e.g. Sachse et al., 2004). Because the amount of precipitation is the major control on the isotopic composition of meteoric waters in tropical systems, we used the $\delta D_{\text{wat-alg}}$ (δD of the water used by algae for lipid synthesis, estimated from the δD of the *n*-C₁₈ FA) as a proxy of precipitation amount. The $\delta D_{\text{wat-hp}}$ (δD of the water used for land plant lipids synthesis) is measured from the δD of the *n*-C₃₀ FA and used to estimate relative moisture (P-E). The difference in isotope fractionation between land plants and phytoplankton ($\delta D_{\text{wat-hp}} - \delta D_{\text{wat-alg}}$) is used to quantify evapotranspiration (evaporation from soils and transpiration from plants).

These results allowed to distinguish five contrasted periods in our 20,000 yr record (see below). The 20-19 kyr period is characterized by high precipitation associated with high evapotranspiration, i.e. a semi-arid climate. By comparison, from 19 to 17 kyrs, both

precipitation and evapotranspiration are both reduced. The resulting climate is nevertheless dryer than during the previous stage. During the Lateglacial interval, i.e. from 17 up to 13.5 kyrs, evapotranspiration is reduced but the precipitation which remains at the same level than before entails a more humid climate. The Younger Dryas interval (YD) shows higher precipitation levels but stronger evapotranspiration, thus a dryer climate than during the Lateglacial but nevertheless more humid than at the end of the Last Glacial Maximum (LGM). Finally, the Holocene shows a decreasing trend in the amount precipitation and with few variations of the evapotranspiration that finally delineate a drying trend. These results are coherent with independent data produced by palynology and biomarker analysis (Ledru et al., 2001; Jacob et al., 2004) and give clue information on the variations in water cycling in the Tropics since the LGM.



References

- Huang, Y., Shuman, B., Wang, Y., and Thompson, Webb III, 2002. Hydrogen isotope ratios of palmitic acid in lacustrine sediments record late Quaternary climate variations. *Geology*, 30, 1103–1106.
- Huang, Y., Shuman, B., Wang, Y., Grimm, E.C., Boutton, T., Terwilliger, V., Jacobson, G.L. and T. Webb III, A 62,000 year record of environmental and climatic change inferred from carbon and hydrogen isotope stratigraphy of higher plant biomarkers at Lake Tulane, Florida. *EPSL*, submitted.
- Jacob, J., Disnar, J.R., Boussafir, M., Ledru, M.-P., Sifeddine, A., Albuquerque, A.L.S. and B. Turcq, 2004. Onocerane attests to dry climatic events during the Quaternary in the Tropics. *Org. Geochem.*, 35, 289-297.
- Ledru, M.P., Cordeiro, R.C., Dominguez, J.M.L., Martin, L., Mourguiart, P., Sifeddine, A. and B. Turcq, 2001. Late-glacial cooling in Amazonia as inferred from pollen at Lagoa do Caçó, Northern Brazil. *Quat. Res.*, 55, 47-56.
- Sachse, D., Radke, J. et Gleixner, G., 2004. Hydrogen isotope ratios of recent lacustrine sedimentary n-alkanes record modern climate variability. *Geochim. et Cosmochim. Acta*, 68, 4877-4889.

**PPC2-7: Rapid paleoenvironmental variations in NE Brazil during the Late Glacial.
Insights from TpS2, S3CO₂ and S3CO Rock Eval parameters**

J. Jacob¹, J.-R. Disnar¹, M. Boussafir¹, D. Kéravis¹, A. Sifeddine²,
A.L. Spadano Albuquerque³, B. Turcq³

1) Laboratoire de Géochimie Organique, Institut des Sciences de la Terre d'Orléans (ISTO) - UMR 6113 du CNRS, Bâtiment Géosciences, 45067 Orléans Cedex 2, France (e-mail : jeremy.jacob@univ-orleans.fr)

2) IRD/Bondy, 32 avenue Henry Varagnat, 93143 Bondy Cedex, France

3) Departamento de Geoquímica, Universidade Federal Fluminense, Morro do Valonguinho s/n, 24020-007 Niterói, RJ, Brazil

The Rock-Eval pyrolysis technique was first developed as a rapid mean for evaluating the petroleum potential of source rocks, via the measurement of bulk organic parameters such as Total Organic Carbon (TOC), Hydrogen Index (HI), Oxygen Index (OI) and the maximum pyrolysis temperature Tmax (Espitalié et al., 1985; Lafargue et al., 1998). This method was then used to rapidly estimate organic matter quality and quantity in sedimentary series for paleoenvironmental studies (Talbot and Livingston, 1989). Recently, it has been proposed that there could be more information gained from the Rock-Eval parameters (Disnar et al., 2003). When considering also the recent analytical developments available from the Turbo6 version of the apparatus, there is a large field of investigation that remains unexplored in paleoenvironmental studies.

Here we present results from the sedimentary infill of Lagoa do Caçó (Northern Brazil) that records paleoenvironmental changes since the Last Glacial Maximum (Jacob et al., 2004). The present study focuses on the Lateglacial interval (ca. 17,000 to 11,000 cal yrs BP), a time period where different Rock-Eval parameters such as TpS2 (Tmax equivalent), HI and OI produce controversial information. In order to better understand the meaning of these parameters, we propose an original mean of obtaining more pertinent information. S3CO₂/S3CO ratio and TpS2 surprisingly display similar trends over the considered period, in two different cores. Furthermore, the evolution of these parameters is comparable with that of $\delta^{18}\text{O}$ in the ice core record of Sajama (Bolivia) during the Lateglacial (Figure 1). Although the significance of these parameters and the origin of these variations remain to be cleared, our results confirm a pattern of rapid climate variability over the South American Tropics during the last deglaciation, as seen in the Northern Hemisphere.

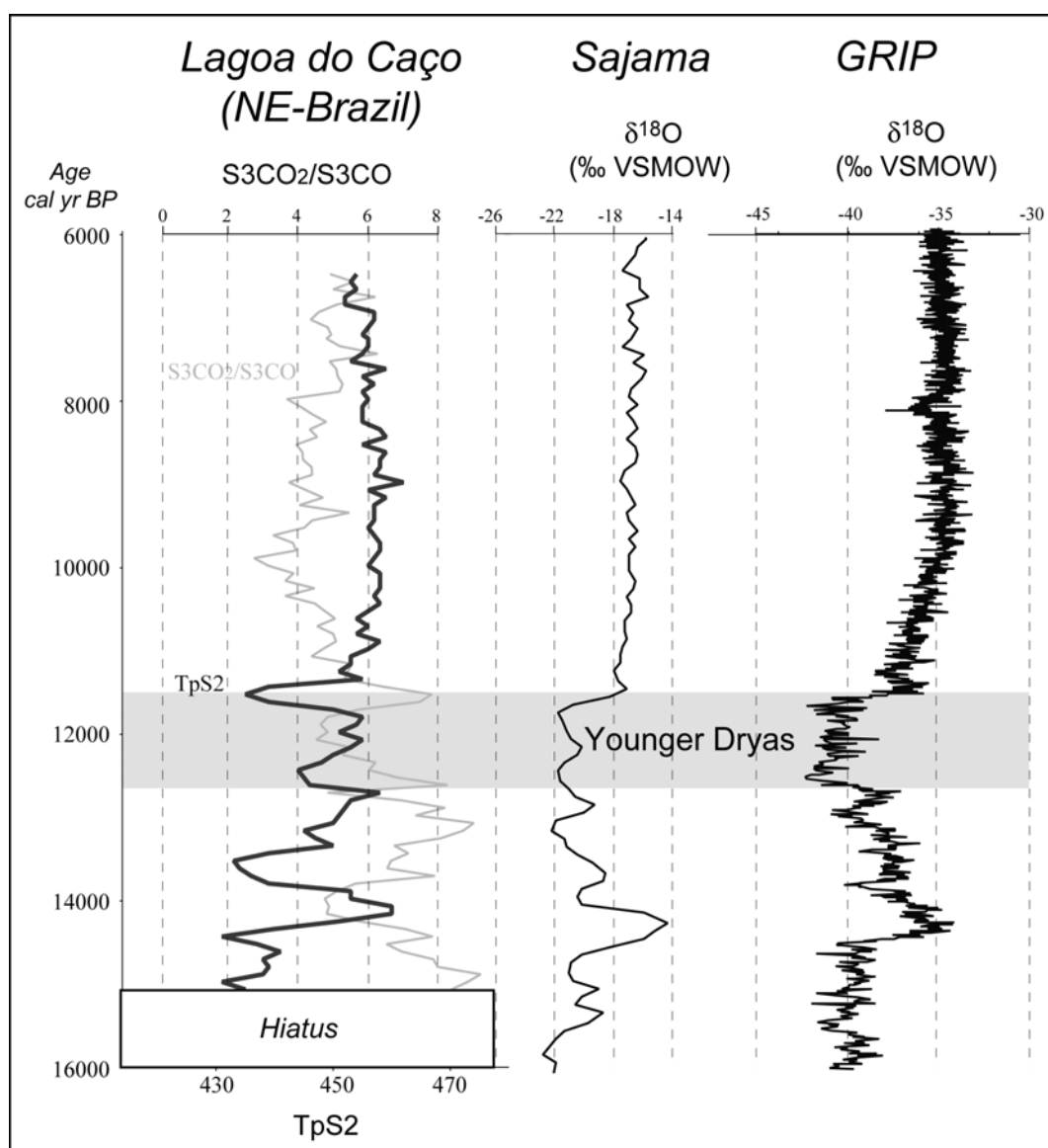


Fig.1. Comparison of S3CO₂/S3CO and TpS2 Rock Eval parameters variations in the Lateglacial interval of core 98-3 (Lagoa do Caço, NE Brazil) with South American (Sajama) and Greenland (GRIP) ice core δ¹⁸O records

References

- Disnar, J. R., Guillet, B., Kéravis, D., Di-Giovanni, C. and Sebag, D., 2003. Soil organic matter (SOM) characterisation by Rock-Eval pyrolysis: scope and limitations. *Org. Geochem.* 34, 327-343.
- Espitalié, J., Deroo, G. and Marquis, F., 1985. La pyrolyse Rock-Eval et ses applications; première partie. *Rev. Inst. Fr. Pét.* 40, 563-579.
- Jacob, J., Disnar, J.R., Boussafir, M., Sifeddine, A., Albuquerque, A.L.S. and Turcq, B. Major environmental changes recorded by lacustrine sedimentary organic matter since the Last Glacial Maximum under the tropics (Lagoa do Caço, NE Brazil). *Pal., Pal., Pal.* 205, 183-197.
- Lafargue, E., Marquis, F., Pillot, D., 1998. Rock-Eval 6 applications in hydrocarbon exploration, production, and soil contamination studies. *Rev. Inst. Fr. Pét.* 53/4, 421- 437.
- Talbot, M.R. and Livingstone, D.A., 1989. Hydrogen index and carbon isotopes of lacustrine organic matter as lake level indicators. *Pal., Pal., Pal.* 70, 121-137.

PPC2-8: The Frasnian/Famennian faunal turnover: new insights from lipid compositions of the Kellwasser horizons and adjacent strata

M. Kloppisch¹, F. Kenig², U. Mann¹, H. Wilkes³

1) Forschungszentrum Jülich, Institut Sedimentäre Systeme, D-52425 Jülich, Germany (e-mail: u.mann@fz-juelich.de)

2) University of Illinois at Chicago, Dept. of Earth and Environmental Sciences, Chicago, USA

3) GeoForschungsZentrum Potsdam, Telegrafenberg, D-14473 Potsdam, Germany

In order to reveal the significance of the phytoplankton-blackout at the Frasnian/Famennian (F/F) boundary of the Upper Devonian ("Kellwasser Horizons" KW), we have investigated sediment cores from the Rhenish, Michigan, and Appalachian Basins. The F/F boundary is known as one of the most striking world-wide catastrophic bio-events of the Phanerozoic [5]. Although the effects of this event on the invertebrate fauna are well known [4], information considering the phytoplankton is sparse. Here we compare Late Devonian sedimentary organic matter from Avalonia (Rhenish Basin) to that of Laurentia (Michigan and Appalachian Basin). The respective sedimentary rocks were analyzed for organic geochemical bulk parameters, selected trace metals as redox proxies, and extractable biomarkers.

Total organic carbon contents (TOC) show maxima around 5% for the Appalachian Basin and the Rhenish Basin, whereas the TOC values for the Michigan Basin are significantly higher (up to 18%). With 2% for the Rhenish Basin, maximal total sulphur contents do not reach half of the concentrations for the Michigan (5.5%) and the Appalachian Basin (5.7%). With respect to the bulk quality of organic matter, we found a consistent decrease of the peak values from the Michigan (699mg HC/g TOC) via the Rhenish (526) to the Appalachian Basin (312). Nevertheless, relatively low values for both TOC (0.1%) and HI (45mg HC/g TOC) have also been recorded. Thus, both type-II (algal-bacterial) and type-III (terrestrial) organic matter are present. For TOC and HI, maxima generally occur within the KW or shortly afterwards. Sulphur data show no specific relation to the Kellwasser Horizons.

With values of $431 \pm 5^\circ\text{C}$, $433 \pm 8^\circ\text{C}$ and $439 \pm 3^\circ\text{C}$ for the Rhenish, Michigan and Appalachian Basin, respectively, very similar temperatures for T_{max} were determined, indicating a low thermal maturation stage (approx. vitrinite reflectance 0.50-0.55% R_r). Therefore, a redistribution of soluble organic matter is very unlikely.

For the Rhenish Basin, trace metals suggest a clear dysoxic/anoxic stage in the lower Upper Devonian. Similar conditions prevail within the lower KW. Trace metal concentrations of the sections above indicate more or less oxic conditions. Sageman et al. [3] and Brown and

Kenig [1] proposed an alternation of euxinic, suboxic and oxic conditions for the Appalachian and Michigan basin, respectively. In the Michigan Basin, variation in the elevation of the oxycline controlled the black shale distribution [1]. The presence of aryl isoprenoids related to isorenieratene in the sediments from the Rhenish Basin indicates that photic zone anoxia played a role during the entire time represented by the profile. Profiles from the Michigan and Appalachian Basin were analysed for comparison to allow global conclusions.

Envelopes of the *n*-alkane distributions are generally more or less unimodal with highest concentrations of the C₁₅₋₁₉ *n*-alkanes and with a slight odd-carbon-number predominance. For the Rhenish Basin, LHCPI values are high in the sections between the KW, whereas all other samples exhibit low values. Only one sedimentary sequence from the Michigan Basin follows this trend. All other sedimentary sequences investigated from the Michigan and the Appalachian Basin show low variations and do not reveal any trend.

Reduced values for the sterane/hopane ratio for the interval in between the two KW in the Rhenish Basin profile indicate a high microbial activity and/or a high incorporation of bacterial biomass into the organic material. These variations in the relative amounts of bacteria and algae may be associated with changes of the depositional environment [2]. Thus, a regressional phase with less algal and more bacterial input should have started shortly after the lower KW. However, already the upper KW is part of a transgressional phase. Due to more or less identical values for the sterane/hopane ratio in the two KW and the sections above and below, the two KW seem not to represent a pronounced algal bloom. Therefore, the two KW appear to be characterized by specific depositional conditions rather than a variation in the type of OM.

References

- [1] Brown, T.C, Kenig, F, 2004. Water column structure during deposition of Middle Devonian-Lower Mississippian black and green/gray shales of the Illinois and Michigan Basins: a biomarker approach. *Palaeogeography, Palaeoclimatology, Palaeoecology* 215, 59-85.
- [2] Kranendonck, O., 2004. Geo- and biodynamic evolution during late Silurian/early Devonian time (Hazro Area, SE Turkey). *Schriften des Forschungszentrums Jülich, Reihe Umwelt / Environment, Band / Volume 49, 2004, 268pp.*
- [3] Sagemann, B.B., Murphy, A.E., Werne, J.P., Ver Straeten, C.A., Hollander, D.J, Lyons, T.W., 2003. A tale of shales: the relative role of production, decomposition, and dilution in the accumulation of organic-rich strata, Middle-Upper Devonian, Appalachian Basin. *Chemical Geology* 195, 229-273.
- [4] Schindler, E., 1990. Die Kellwasser-Krise (hohe Frasn-Stufe, Ober-Devon). *Göttinger Arb. Geol. Paläont.* 46, 115 pages
- [5] Walliser, O.H., 1996. Global events in the Devonian and Carboniferous. In: Walliser, O.H. (ed.): *Global events and event stratigraphy in the Phanerozoic.* 225-250

PPC2-9: New insights into the climatic and vegetational history of the subtropical crater lake “Tswaing”, South Africa, for the last ~300.000 years

I. Kristen¹, A. Fuhrmann¹, G.H. Haug¹, B. Horsfield¹, H. Oberhänsli¹, J. Thorpe², H. Wilkes¹

1) GeoForschungsZentrum Potsdam, Telegrafenberg, 14473 Potsdam, Germany
(e-mail: kristen@gfz-potsdam.de)

2) University College London, Department of Geography, 26 Bedford Way, London WC1H 0AP

Records for palaeoclimate reconstructions reaching far back in time are still rare on the continental southern hemisphere. Here we present results of biogeochemical investigations of a core recovered from the crater lake “Tswaing” (formerly “Pretoria saltpan”) in 2001 which opens a unique chance to get a more detailed view into climate variability of the subtropical region of South Africa on glacial/interglacial time scales. This study is performed in the framework of Inkaba yeAfrica, a joint research initiative of the German and South African earth science communities.

According to [2] the crater “Tswaing” was formed around 220 ± 52 kyr ago by a meteorite impact. However, ongoing investigations for improving the age model with U/Th analyses of autogenic carbonates provide preliminary evidence that the lake might be older than 300 kyr.

Today the basin contains a shallow (< 3 m), hypersaline (pH ~ 10) lake with a water budget governed by rainfall. The 90 m composite core profile investigated in this study consists of partly fine-laminated lake sediments intercalated with gravelly and sandy mudflow deposits. Former investigations (e.g. [1]) and preliminary results reveal a considerable variability of bulk geochemical proxies such as total inorganic carbon (TIC), total organic carbon (TOC) and the C/N ratio (Fig. 1). The upper half of the core is clearly dominated by fluctuations in TOC while TIC controls the variation in the lower half of the core. These data indicate substantial changes in the aquatic versus terrestrial influence on the lake system that might be ultimately driven by precessional forcing. The investigations focus on carbon and nitrogen isotopic compositions, maceral analysis and lipid biomarkers which may provide new insights into hydrological changes and the development of lacustrine biota as well as the surrounding vegetation in the catchment area.

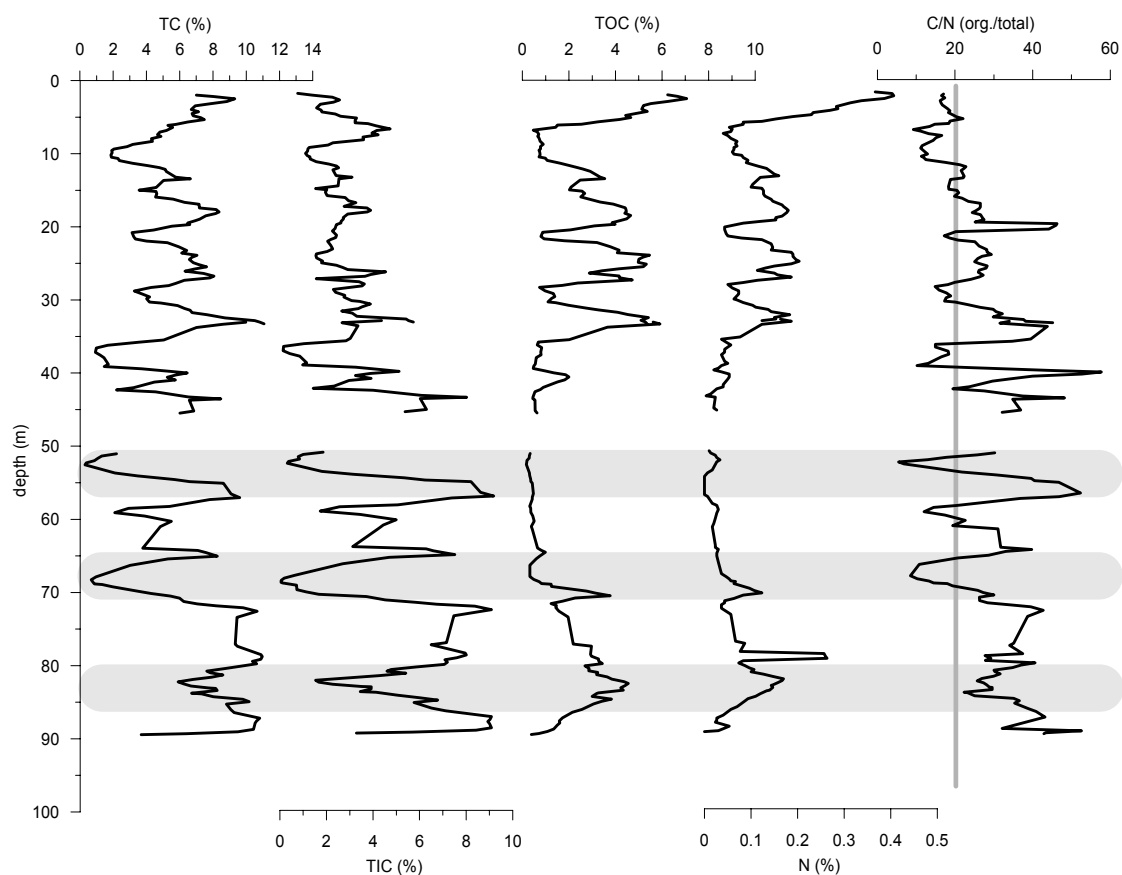


Fig.1. 3-point-running average of the percentages of Total Carbon (TC), Total Inorganic Carbon (TIC), Total Organic Carbon (TOC), Total Nitrogen (N) and C/N ratio for sediments from lake "Tswaing". Grey bars indicate laminated sequences

References

- [1] T.C. Partridge et al. (1999): Tswaing – investigation into the origin, age and palaeoenvironments of the Pretoria Saltpan. Memoir 85, Council for Geoscience, Pretoria, pp. 198.
- [2] D. Storzer, W.U. Reimold and C. Koeberl (1999): Fission-track age of the Saltpan impact crater. In T.C. Partridge (Ed.): Tswaing – investigation into the origin, age and palaeoenvironments of the Pretoria Saltpan. Memoir 85, 64-71.

PPC2-10: Possible correlation of the Palaeocene Eocene Thermal Maximum in multiple Late Palaeocene peatland $\delta^{13}\text{C}$ records

D.J. Large¹, B. Spiro², M.C. Gorringer¹, J. Briggs¹, T.F. Jones¹, J.H.S. Macquaker³,
C. Somerfield¹, B.P. Atkin¹

1) School of Chemical, Environmental and Mining Engineering, University of Nottingham, University Park, Nottingham, NG7 2RD, UK

2) The Natural History Museum, Cromwell Road, London, SW7 5BD

3) Department of Earth Sciences, University of Manchester, Oxford Road, Manchester, M13 9PL, UK

The late Paleocene was a period of global warming encompassing long-term and short-term changes in Earth's carbon cycle. The marine record for this period is excellent and has been orbitally tuned for at least 1.5 m.y. either side of the Palaeocene-Eocene boundary. To date the terrestrial record lacks a high-resolution internal time frame and correlation depends on widely separate age determinations and wiggle matching the carbon isotope excursion associated with Palaeocene Eocene Thermal Maximum. Here we present a 700 k.y., composite, $\delta^{13}\text{C}$ record derived from late Paleocene peatland deposits preserved as thick coal in the Powder River Basin, USA. The composite record was produced from three records each displaying a prominent negative isotope excursion of 2.5 to 3‰. Spectral analysis of the composite record reveals a highly significant oscillation at 0.6 cycles per metre. This oscillation is interpreted as obliquity and enables the record to be internally tuned. The tuned record is 700 k.y. long and experienced an average carbon accumulation rate of 28g/m²/yr. Comparison with the marine $\delta^{13}\text{C}$ record 1.5 m.y. either side of the PETM reveals that the only comparable carbon isotope excursion is the PETM. A negative isotope excursion, 400 k.y. before the PETM, at the base of the Upper Clarkforkian corresponds to a similar event recorded in the Bighorn Basin. There is no evidence of this earlier isotope excursion in the marine record. An extreme positive isotope excursion occurs in some of the peatland records during the inferred PETM interval. This event has a local expression and is interpreted as reflecting extreme ecological stress, probably hydrological stress, in the more raised parts of the peatland. The positive excursion also corresponds to a period of mammalian dwarfism associated with the PETM, which may reflect a response to the same ecological stress. If this correlation with the PETM is wrong then it is important to consider the self-similarity of the geological record and question what criteria should be used to identify the terrestrial expression of the PETM.

PPC2-11: Biogeochemical markers for palaeoenvironment assesment of the Oligocene of the Rhine Rift Valley (Alsace, France)

P. Le Métayer¹, P. Schaeffer¹, P. Albrecht¹, S. Roussé², P. Düringer²

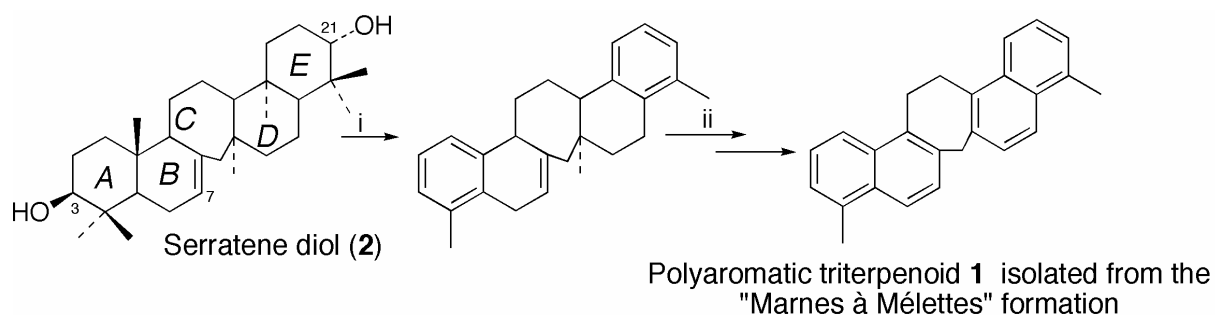
1) Laboratoire de Géochimie Bio-organique, UMR 7509 du CNRS, Ecole de Chimie, Polymères et Matériaux, Université Louis Pasteur, 25 rue Becquerel, 67200 Strasbourg, France (e-mail: pschaeffer@chimie.u-strasbg.fr)

2) Centre de Géochimie de la Surface, UMR 751 du CNRS, EOST, 1 rue Blessig, 67084 Strasbourg, France

In the frame of a joint collaboration involving sedimentologists and organic geochemists, a series of sediments from outcrops and from cores deposited during the Oligocene of the Rhine Valley has been investigated in order to reconstruct their palaeoenvironments of deposition. The Oligocene is a key period for the formation of the Rhine rift, which started at the Upper Eocene (-37 to -34 Myrs), initiated by tectonic constraints linked to the raising of the Alps. During the Oligocene, the subsidence of the rift valley and the uplift of the margins occurred at an irregular rate, and lead to the accumulation of more than 1600 meters of sediments deposited under various environmental conditions [1].

In a first stage, sedimentation occurred globally under an evaporitic context (“Zone salifère supérieure”), as confirmed by the mineralogy (deposition of halite) and by the presence of diagnostic biomarkers such as ring D monoaromatic oleanane [2] or abundant benzohopanes [3]. Following this period, the conditions turned rapidly to marine conditions (“Marnes à Foraminifères“ and “Schistes à Poissons“), the seawater flooding initially the Rhine valley from the North. However, the geological system was quite complex at this period, with temporary connections either with the North Sea (north of the basin) or with the Perialpine Sea (south of the basin). Analysis of the biological markers from these two formations indicates indeed that marine conditions were established. During deposition of the “Marnes à Foraminifères“, marine oxygenated conditions prevailed, whereas strongly anoxic conditions occurred during deposition of the “Schistes à Poissons“. The confinement of the environment is clearly indicated by the presence of a number of carotenoid derivatives originating from sulfur photosynthetic bacteria. Progressively, a marine regression occurred, leading to continental sedimentary deposits (“Marnes à Mélettes“ and “Marnes à Cyrènes“). Biomarker distributions are dominated by various higher plant terpenoids indicative of lacustrine and fluvial/deltaic conditions. However, locally, the presence of isorenieratene derivatives suggests that there were temporarily short episodes of marine anoxic conditions. Among the various higher plant terpenoids present in the sediments from the “Marnes à Mélettes“ formation, we have detected several unknown aromatic compounds. Some of them have been isolated for NMR structural identification. So far, we have identified one

pentacyclic tetraaromatic hydrocarbon **1** which bears a central seven-membered ring. This compound is structurally-related to higher plant triterpenoids of the serratane series and has been formed by diagenetic aromatisation of a functionalised molecule precursor such as serratene diol **2** (figure 1) reported to occur in various plant species like ferns, lycopodium or picea (e.g., [4], [5]). In the case of serratene diol **2**, aromatisation started in the rings A and E, triggered by the presence of functionalised groups at C-3 and C-21, and proceeded to rings B and D. The presence of a central seven-membered ring C has precluded further aromatisation to occur. Serratane derivatives are rather uncommon in the sediment record, and the presence of compound **1** among the predominant aromatic hydrocarbons of some of the sediments investigated is unclear. Its significance in terms of palaeoecology is unknown, but it may have implications for palaeoenvironmental and/or palaeoclimatic studies. Further work is currently underway to characterise the other unknown higher plant terpenoids which have been isolated and to determine their significance as proxies for palaeoenvironmental assessment.



- i : aromatisation of ring A and ring E triggered by the presence of functional groups at C-3 and C-21
 ii: progression of the aromatisation from ring A to ring B and from ring E to ring D

Fig.1. Diagenetic pathway leading to compound **1** from serratenediol **2**

References

- [1] Sissingh, W., 1998. *Tectonophysics* 300, 249-284.
 [2] Poinso, J., Adam, P., Trendel, J.M., Connan, J., Albrecht, P., 1995. *Geochimica et Cosmochimica Acta* 59, 4653-4661.
 [3] Hussler, G., Cesario, M., Guilhem, J., Pascard, C., Albrecht, P., Ourisson, G., 1984. *Tetrahedron Letters* 25, 1179-1182.
 [4] Ageta, H., Shiojima, K., Masuda, K., 1982. *Chemical and Pharmaceutical Bulletin* 30, 2272-2274.
 [5] Tanaka, R., Tsujimoto, K., Muraoka, O., Matsunaga, S., 1998. *Phytochemistry* 47, 839-843.
 [6] Inubushi, Y., Sano, T., Tsuda, Y., 1964. *Tetrahedron Letters*. 21, 1303-1310.

PPC2-12: Oceanic environments in Japan Sea during the deposition of thinly laminated layers in the latest Pleistocene

K. Matsumoto¹, H. Kitazato¹, R. Ishiwatari², S. Tsukawaki³, N. Ohkouchi¹

1) IFREE, JAMSTEC, 2-15, Natsushima-cho, Yokosuka, 237-0061 JAPAN (e-mail: kohei@jamstec.go.jp)

2) Faculty of Science, Tokyo Metropolitan University, 1-1, Minami-Osawa, Hachioji, 192-0397 JAPAN

3) General Education Hall, Kanazawa University, Kakuma-machi, Kanazawa, 920-1192 JAPAN

We present abundances and carbon isotopic compositions of bacterial biomarkers in the sediments from the southeastern Oki-Trough, Japan Sea (KT96-17, P-2 core). Our study focused on biogeochemical cycles and oceanic environment during the deposition of thinly laminated layers (TL) in the latest Pleistocene using biomarker approaches. The concentrations of bacterial biomarkers (*n*-C₁₅, *iso*-C₁₅, *anteiso*-C₁₅, *n*-C₁₇, *iso*-C₁₇ and *anteiso*-C₁₇ fatty acids and C₃₂ hopanoic acid) in the TL-1 (11-10 ka) are higher than those in the non-laminated layers (15-12 ka) and Holocene (Figure 1). However, the carbon isotopic compositions of these biomarkers from TL-1 are comparable with those from non-laminated layers. In addition, we did not find any biomarkers related to green sulfur bacteria such as farnesol and isorenieratene. Therefore, even at the time of TL-1 deposition, O₂-H₂S interface could have been located beneath the bottom of photic zone (~200 m).

On the other hand, isotopically large negative excursions of diploptene (from -74.0 to -63.6 ‰) and C₃₂ hopanoic acid (from -40.9 to -31.9 ‰) were observed in TL-2 sediments. These suggest that the negative isotopic excursions are the evidence for the methane emissions by methanogen at anoxic bottom waters in the period of TL-2 and for methanotrophic bacteria consuming methane with large isotopic fractionation. In comparison with KH-79-3, C-3 core and L-3 core, the northeastern Oki-Trough, and abundances and δ¹³C values of biomarker trends and timing do not agree with P-2 core. A potential explanation for this discrepancy is that the biogeochemical processes related to methane occur regionally around Oki-Trough. In addition, we will newly show the radiocarbon ages of individual fatty acids and will discuss the marine environment at TL-1.

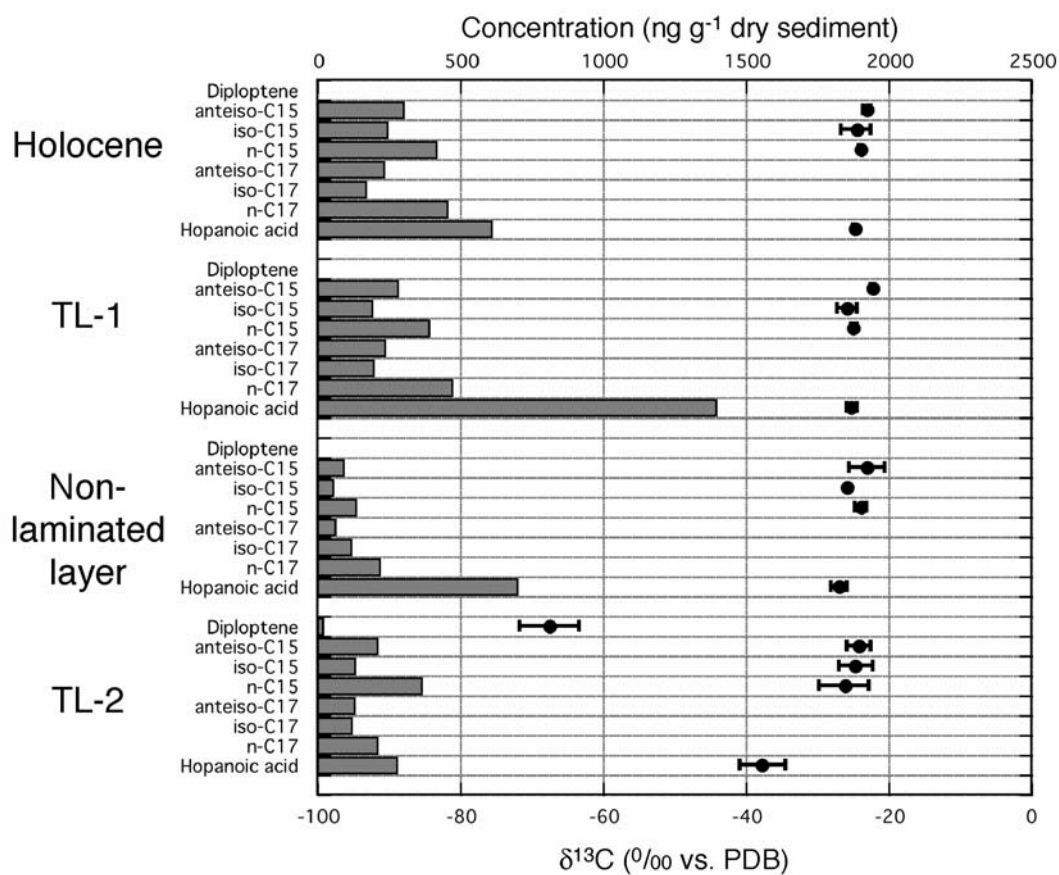


Fig.1. The abundances and carbon isotopic compositions of bacterial biomarkers in each event of the Japan Sea in the latest Pleistocene

PPC2-13: Alkenone and coccolith records of the mid-Pleistocene in the South-east Atlantic: Implications for the U_{37}^K index and South African climate

E.L. McClymont^{1,5}, A. Rosell-Melé², J. Giraudeau³, C. Pierre⁴, J.M. Lloyd¹

1) Department of Geography, University of Durham, Durham DH1 3LE, UK
(e-mail: erin.mcclymont@bristol.ac.uk)

2) ICREA and ICTA, Universitat Autònoma de Barcelona, 08193 Bellaterra, Catalonia

3) DGO, UMR 5805 EPOC, Université Bordeaux I, Avenue des Facultés, 33405 Talence, France

4) LODYC, UMR 7617 CNRS, Université Pierre et Marie Curie, 4 Place Jussieu, 75252 Paris, France

5) Organic Geochemistry Unit, School of Chemistry, University of Bristol, Cantock's Close, Bristol BS8 1TS, UK (erin.mcclymont@bris.ac.uk)

Successful application of the alkenone palaeothermometer, the U_{37}^K index, relies upon the assumption that fossil alkenone synthesisers responded to growth-temperature changes in a similar manner to the modern producers, chiefly the coccolithophores *Emiliania huxleyi* and *Gephyrocapsa oceanica*. During the early- and middle-Pleistocene, the final coccolithophore extinctions prior to the emergence of *E.huxleyi* occurred, but the impact of these evolutionary events on the U_{37}^K -SST relationship has not been tested. This period of time is also marked by a series of zones where the coccolithophore assemblage is dominated by a single species of coccolithophore ('acme zones', [1]). If during these events the nature of the U_{37}^K -SST relationship was altered, application of the modern U_{37}^K -SST calibration prior to the late Quaternary could be inappropriate.

Here, we test the application of the U_{37}^K index to sediments pre-dating the late Pleistocene by comparing the U_{37}^K record at ODP 1087 in the south-east Atlantic to records of coccolithophore assemblages and alkenone distributions between 1500 and 500 ka. Samples for alkenone analysis were selected with a 5-kyr resolution using a benthic foraminifera $\delta^{18}O$ age model. Coccolith analysis was undertaken at a lower resolution, and reveals both changes in the coccolithophore species assemblage correlating to the mid-Pleistocene acme zones, and the evolutionary events used to provide biostratigraphic age models.

We show that evolutionary events and changes in species dominance within the coccolithophore populations had little impact on the U_{37}^K record. A negative shift in average U_{37}^K values, representing a fall in average SSTs of 1.67°C, occurred at 1150 ka without significant change to the coccolithophore species distributions (Figure 1). Furthermore, the relative abundances of the C_{37} and C_{38} alkenones (expressed as the ratios K_{37}/K_{38} and $K_{37}/K_{38ethyl}$) fall within a restricted range and show no shifts to correlate with the U_{37}^K shift. Values of K_{37}/K_{38} and $K_{37}/K_{38ethyl}$ also closely resemble those found within modern

populations (e.g. [2], [3]) and late Pleistocene sediments [4] and suggest a similar temperature sensitivity of $U^{K}_{37'}$ during the early and mid-Pleistocene to that found at present.

A molecular response to coccolithophore species changes was identified by a negative shift in the $U^{K}_{37'}/U^{K}_{38}$ ratio at ca. 770 ka, which correlates to the shift away from small coccolithophore species (<5 μ m) to a population dominated by *Gephyrocapsa oceanica* and *Gephyrocapsa caribbeanica*. Despite this shift, values of $U^{K}_{37'}/U^{K}_{38}$ continue to plot within modern values for cultured species and surface sediments (e.g. [5],[6]). The results presented here thus continue to support the application of $U^{K}_{37'}$ to reconstruct sea-surface temperatures (SSTs) throughout the Quaternary.

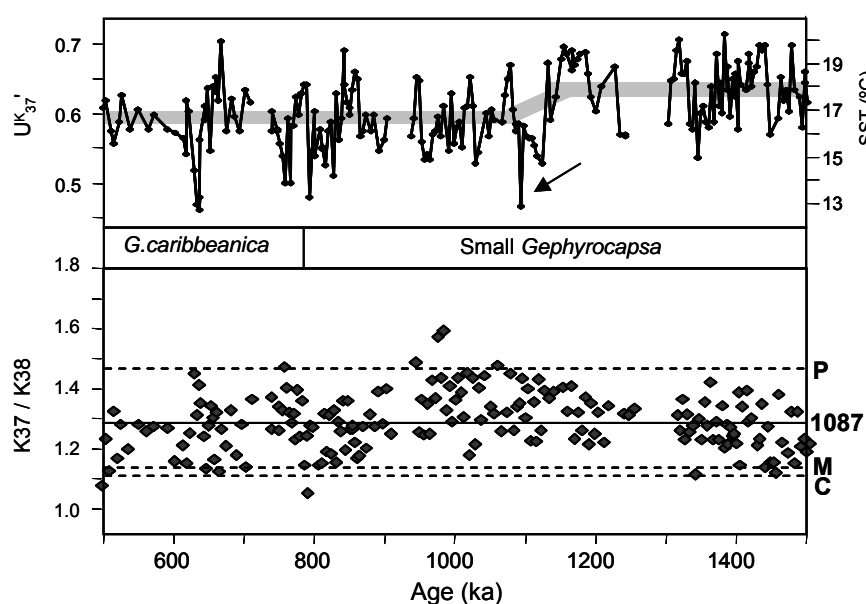


Fig.1. Comparison of mid-Pleistocene $U^{K}_{37'}$, dominant coccolith species and alkenone distributions at ODP Site 1087. Mean $U^{K}_{37'}$ values are shown by the grey shading, which highlights a negative shift in $U^{K}_{37'}$ at 1170 ka. This occurs with no major change in coccolithophore species, nor to the K37/K38 values. The latter fall within the range of published values for cultures of *Emiliana huxleyi* (dashed horizontal line and 'P': [3]), cultures of *E. huxleyi* and *G. oceanica* ('C': [2]) and late Quaternary sediments from the Walvis ridge ('M': [4]). The mean value at Site 1087 is marked by the solid horizontal line and '1087'

References

- [1] Weaver, P. P. E. (1993). High resolution stratigraphy of marine Quaternary sequences. In "High Resolution Stratigraphy." (E. A. Hailwood, and R. B. Kidd, Eds.), pp. 137-153. Geological Society Special Publication No 70.
- [2] Conte, M. H., Thompson, A., Lesley, D., and Harris, R. P. (1998). Genetic and physiological influences on the alkenone/alkenoate versus growth temperature relationship in *Emiliana huxleyi* and *Geophyrocapsa oceanica*. *Geochimica et Cosmochimica Acta* **62**, 51-68.
- [3] Prahl, F. G., Muehlhausen, L. A., and Zahnle, D. I. (1988). Further evaluation of long-chain alkenones as indicators of paleoceanographic conditions. *Geochimica et Cosmochimica Acta* **52**, 2303-2310.
- [4] Müller, P. J., Cepek, M., Ruhland, G., and Schnieder, R. R. (1997). Alkenone and coccolithophorid species changes in late Quaternary sediments from the Walvis Ridge: Implications for the alkenone paleotemperature record. *Palaeogeography, Palaeoclimatology, Palaeoecology* **135**, 71-96.
- [5] Rosell-Melé, A., Carter, J., and Eglinton, G. (1994). Distributions of long-chain alkenones and alkyl alkenoates in marine surface sediments from the North East Atlantic. *Organic Geochemistry* **22**, 501-509.
- [6] Conte, M. H., Weber, J. C., King, L. L., and Wakeham, S. G. (2001). The alkenone temperature signal in western North Atlantic surface waters. *Geochimica et Cosmochimica Acta* **65**, 4275-4287.

PPC2-14: Paleoenvironmental significance of *n*-alkane δD from Ganga - Brahmaputra ancient sedimentsF. Palhol¹, V. Galy¹, P. Faure², C. France-Lanord¹

1) Centre de Recherches Pétrographiques et Géochimiques - CNRS, BP 20, 54501 Vandoeuvre-les-Nancy, France (e-mail :fpalhol@crpg.cnrs-nancy.fr)

2) UMR-CNRS 7566 G2R, Université Henri Poincaré, BP 239, 54506, Vandoeuvre-les-Nancy, France

Large isotopic variations, combined with biosynthetic fractionation and temperature dependence made hydrogen an interesting isotopic proxy for paleoclimate studies. For example, past isotopic composition of precipitations can be estimated from ice cores, or tree cellulose. Recent developments in molecular analyses by Gas Chromatography-Pyrolysis-Isotope Ratio Mass Spectrometry (GC-Pyr-IRMS) and further improvements of this technique allow to analyse D/H ratios in geological samples with a precision convenient with paleoclimatic applications of molecular data. The δD value of organic compounds such as *n*-alkanes preserved in sediments are of great interest because they can reflect environmental conditions linked with hydrogen isotopic ratio of precipitations. This was used for modern or sub-actual environmental reconstructions (eg. Xie et al, 2000) and less often for ancient samples (Andersen et al., 2001; Yang and Huang, 2003).

In order to test the usefulness of *n*-alkanes δD for paleoenvironmental reconstruction, we analysed two types of samples: (1) river sediments of the Ganga river, and (2) marine sediments from cores in the upper and distal Bengal Fan, with Total Organic Carbon content as low as 0.1 %. Bengal fan represents a good laboratory for this purpose as organic matter has been demonstrated to be largely derived from continental source (Poynter and Eglinton, 1990; Freeman and Colarusso, 2001). Moreover, the basin configuration is relatively constant throughout geological timescale and reflects dominantly an input analogous to the modern Ganga-Brahmaputra river system (France-Lanord et al., 1993). The Bengal fan record represents also an important interrogation on the environmental changes that occurred during the expansion of C4 flora during the Miocene (France-Lanord et al, 1994; Cerling, 1997). ¹³C/¹²C isotopic signature of individual *n*-alkanes in Bengal fan sediments have proved that they are efficient and reliable proxies of this event and are well preserved in Bengal sediments (Freeman and Colarusso, 2001).

CPI values of high molecular weighted *n*-alkanes (between 2.5 and 5.4) extracted from our sediments clearly show a terrigenous origin for the organic matter. After Accelerated Solvent Extraction, molecular hydrogen isotopic ratios of odd HMW *n*-alkanes were measured by GC-Pyr-IRMS (gas chromatography-pyrolysis-isotope ratio mass spectrometry)

with a precision usually around 5 ‰. Results for modern river samples show a very good correlation with plants n-alkanes δD described in the literature (e.g. Chikaraishi et al., 2004) and clearly recorded precipitation δD . Moreover, the signal observed in Miocene and Pleistocene sediment argues in favour of the preservation of the original isotopic signal over geological timescale. δD values of analysed sediments allow us to distinguish several type of sediments which record contrasted isotopic compositions. The maximum difference is observed between Pleistocene distal sediments and one 14 kyr sample from the Upper Fan, corresponding to the end of the Last Glacial Maximum. These differences in δD of organic matter in our sediments likely record changes in environmental conditions which will be discussed.

References

- Andersen N., Paul H. A., Bernasconi S. M., McKenzie J. A., Behrens A., Schaeffer P., and Albrecht P. (2001) Large and rapid climate variability during the Messinian salinity crisis: Evidence from deuterium concentrations of individual biomarkers. *Geology* **29**(9), 799-802.
- Cerling T. E. (1997) Late Cenozoic vegetation change, atmospheric CO₂, and tectonics. In *Uplift and Climate Change* (ed. W. F. Ruddiman), pp. 313-327. Plenum Press.
- Chikaraishi Y., Naraoka H., and Poulson S. R. (2004) Hydrogen and carbon isotopic fractionations of lipid biosynthesis among terrestrial (C₃, C₄ and CAM) and aquatic plants. *Phytochemistry* **35**, 1369-1381.
- France-Lanord C., Derry L., and Michard A. (1993) Evolution of the Himalaya since Miocene time: isotopic and sedimentologic evidence from the Bengal Fan. In *Himalayan Tectonics*, Vol. 74 (ed. P. J. Treloar and M. Searle), pp. 603-621. Geol. Soc. Lond.
- France-Lanord C. and Derry L. A. (1994) $\delta^{13}C$ of organic carbon in the Bengal Fan: source evolution of C₃ and C₄ plant carbon to marine sediments. *Geochimica et Cosmochimica Acta* **58**(21), 4809-4814.
- Freeman K. H. and Colarusso L. A. (2001) Molecular and isotopic records of C₄ grassland expansion in the late Miocene. *Geochimica et Cosmochimica Acta* **65**(9), 1439-1454.
- Poynter J. and Eglinton G. (1990) Molecular composition of three sediments from Hole 717C: The Bengal Fan. *Proceedings of the Ocean Drilling Program, Scientific Results* **116**, 155-161.
- Xie S., Chen F., Wang Z., Wang H., Gu Y., and Huang Y. (2003) Lipid distributions in loess-paleosol sequences from northwest China. *Organic Geochemistry* **34**, 1071-1079.
- Yang H. and Huang Y. (2003) Preservation of lipid hydrogen isotope ratios in Miocene lacustrine sediments and plant fossils at Clarkia, northern Idaho, USA. *Organic Geochemistry* **34**, 413-423.

PPC2-15: Compound-specific hydrogen isotope ratios of sedimentary n-alkanes as a new palaeoclimate proxy

D. Sachse¹, J. Radke^{1,2}, G. Gleixner¹

1) Max-Planck-Institut für Biogeochemie Jena, Germany (email: dirk.sachse@bgc-jena.mpg.de)

2) ThermoElectron (GmbH) Bremen, Germany

Hydrogen isotope ratios (δD) of biomarkers are emerging as a new palaeoclimate proxy, since they are suggested to record the hydrogen isotope signal of the source water for the organisms and to preserve it over geological timescales. Since δD values of meteoric water are dependant on climatic parameters and atmospheric circulation patterns, δD values from biomarkers could track changes in the water cycle over the geologic past.

Here we present the first systematic approach calibrating recent sedimentary n-alkane (n-C₁₂ to n-C₃₁) δD values to modern meteoric water δD values. δD values from n-alkanes (n-C₁₇ to n-C₃₁) extracted from lake sediments along a N-S European climatic gradient from northern Finland to southern Italy are significantly correlated with δD values of meteoric water. This clearly demonstrates that sedimentary n-alkanes record the source water δD value (SACHSE et al., 2004). The isotopic fractionation during biosynthesis (ϵ) for the n-C₁₇ alkane of algal origin is constant at -158‰ over a wide range of different climates and lakes of different trophic states, indicating an environmental parameter independent biosynthetic fractionation for hydrogen and supporting laboratory experiments. The observed deuterium enrichment of ca. 30‰ in the terrestrial n-alkanes (n-C₂₅ to n-C₃₁) relative to the aquatic biomarkers is due to evapotranspiration processes in the plants leaves, where those substances originate. If evaporation is the dominant process controlling this enrichment, the difference between the δD values of aquatic n-alkanes and terrestrial n-alkanes could serve as a palaeo-evaporation marker for lake ecosystems.

To clarify, if seasonal variations in the δD values of leaf-wax n-alkanes exist, e.g. if those compounds are synthesised de-novo year-round, we have sampled 2 temperate forest sites (beech and maple trees) for leaves throughout 2004. Our results show, that the relative abundance of long-chain n-alkanes varies for maple, but not for beech leaves over the year. Both samples show seasonal variations in n-alkane δD values of up to 50‰ , suggesting a subsequent synthesis of leaf-wax n-alkanes throughout the year. The n-alkane δD values track the meteoric water signal, being modified by evapotranspiration. Consequently, the δD value preserved in the sedimentary archives, will carry the autumn signal.

Our results prove that δD values from sedimentary n-alkanes (n-C₁₇ to n-C₃₁) can be used to reconstruct the hydrogen isotope composition of meteoric water and may be applied to study palaeohydrology of lake systems, changes in atmospheric circulation and hence climate history.

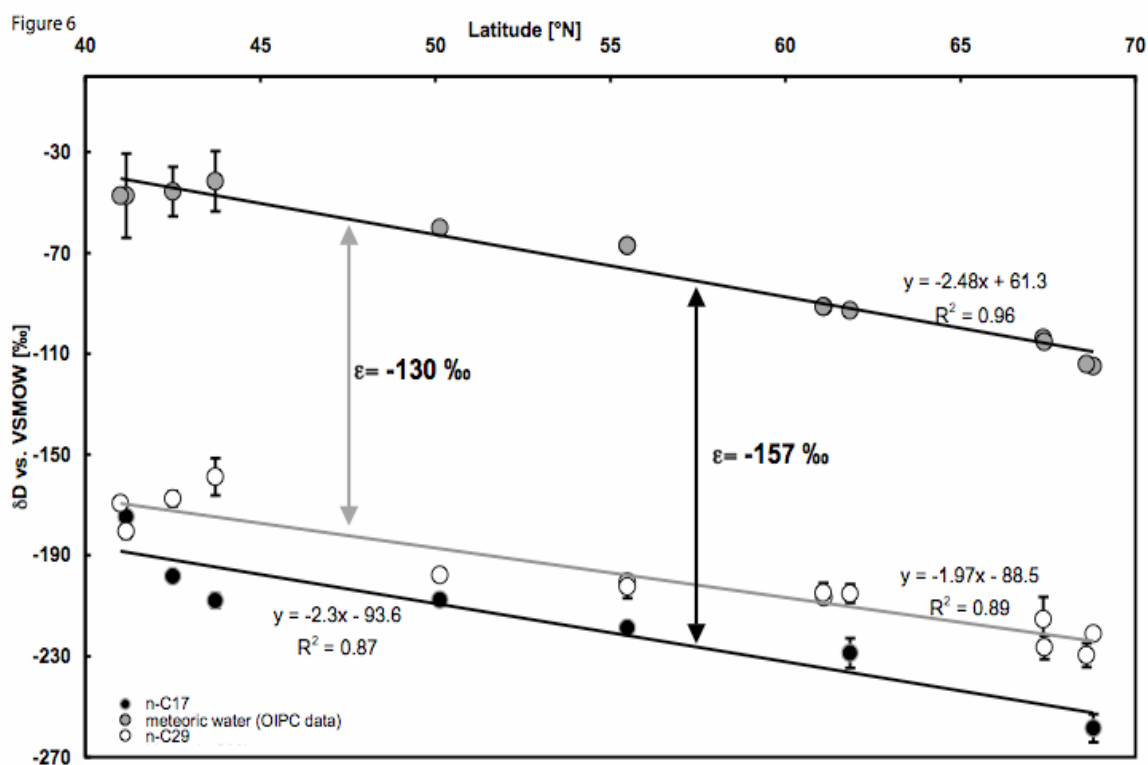


Fig.2. Comparison of δD values from sedimentary n-alkanes to meteoric water along a N-S european transect. The terrestrial n-alkane n-C₂₉ is about 30‰ heavier than the aquatic n-C₁₇, due to evaporative enrichment of leaf water in the plants leaves

References

Sachse D., Radke J., and Gleixner G. (2004) Hydrogen isotope ratios of recent lacustrine sedimentary n-alkanes record modern climate variability. *Geochimica et Cosmochimica Acta* **68**(23), 4877-4889.

PPC2-16: Land-Ocean Interaction and oceanic response in the Mid-Cretaceous western tropical Atlantic – first geochemical results from ODP Site 1261, Demerara Rise

C. Schmidt¹, T. Wagner¹, P. Hofmann², S. Schouten³, J.S. Sinninghe-Damasté³

1) Fachbereich Geowissenschaften, Universität Bremen, Postfach 330 440, D-28334 Bremen, Germany (e-mail: csrcom@uni-bremen.de)

2) Geological Department, University of Cologne, Züricher Str. 49a, 50674 Köln

3) Department of Marine Biogeochemistry and Toxicology, Royal Netherlands Institute for Sea Research (NIOZ), PO Box 59, 1790 AB Den Burg, Texel, The Netherlands

In this study we want to develop integrated, orbital-scale records of the Coniacian-Santonian Oceanic Anoxic Event 3 (OAE 3) for the western tropical Atlantic at Sites 1261 and 1259, (ODP Leg 207, Demerara Rise) combining inorganic and organic geochemistry. ODP Leg 207 was specifically designed to recover expanded Paleogene-Cretaceous sections to (1) evaluate paleoceanographic and paleoclimatic changes, with emphasis on major and abrupt events, (2) reconstruct the history of deep water circulation associated with the opening of the Equatorial Atlantic Gateway, and (3) to assess short- and long-term changes in greenhouse forcing. Previous studies and newly recovered sections from Demerara Rise document thick organic matter-rich sections covering the OAE2 and OAE3 bundled in sediment cycles that were tentatively linked to Milankovitch cycles (Erbacher et al., 2003). Up to now, none of these studies provide complementary biostratigraphical and geochemical records at a time resolution detailed enough to identify fluctuations in sediment chemistry and climate attributable to higher frequency orbital forcing.

To contribute to this central issue the goals of this study are (1) the development of an orbital-scale reference profile for Demerara Rise Sites 1261 and 1259 that consists of terrigenous and marine proxy records including TEX₈₆-based SST to reconstruct the evolution of black shale formation in the western tropical Atlantic in response to continental climate and run-off, marine productivity and the development of oceanic anoxia/euxinia, to (2) establish a high resolution cyclostratigraphic model for the OAE3, and (3) discuss east-west relationships in tropical climate development and black shale formation by correlation with records from the eastern Equatorial Atlantic at ODP Site 959 (Hofmann et al., 2003; Wagner et al., 2004). Black-shale sections covering the Turonian–early Santonian interval have been re-sampled at 1cm resolution. The sediments comprise two major lithologies, i.e. finely laminated claystone with organic matter and laminated clayey limestone and clayey chalk with nannofossils showing cyclic alternations and gradational contacts over a cm/dm scale.

First results from continuous, cm-scale bulk carbonate and organic carbon profiles at ODP Site 1261 not only reflect these general alternations in lithology but also reveal distinct cm-scale sedimentological features that support repetitive interruption/intercalation of the marine sedimentation. CaCO₃ ranges from 40–50% in the claystone and approaches up to

96% in various laminae (Fig. 1). TOC is in general negative correlated to carbonate content and ranges from below 2% in carbonate-enriched beds to more than 10% in laminated shales. Both records confirm persistent cyclicities at various frequencies below 2 m. Supplementary analysis on sediment extracts are in progress and will provide insights on the evolution of sea surface temperature using the novel biomarker-based TEX_{86} -SST index and the input of sedimentary organic matter.

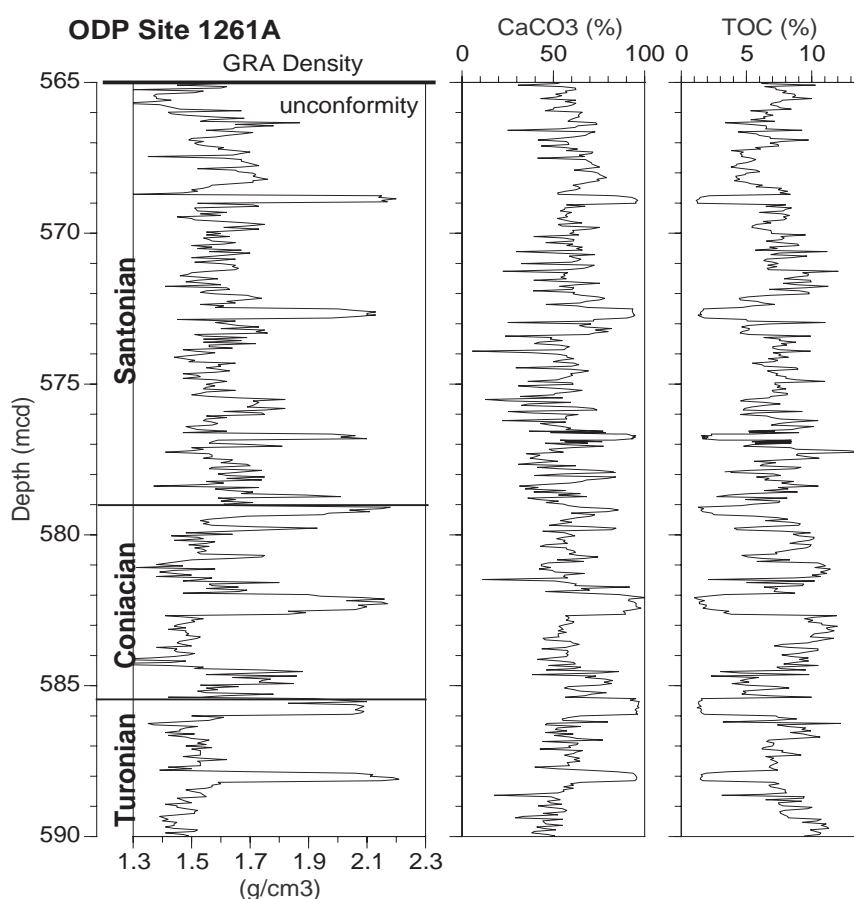


Fig.1. GRA Density-, CaCO_3 - and TOC-Plot

References

- Erbacher, J., Mosher, D.C., Malone, M.J., et al. (2004). Demerara Rise: Equatorial Cretaceous and Paleogene Paleooceanographic Transect, Western Atlantic, Sites 1257 – 1261, 11th January – 6th March 2003. Proceedings of the Ocean Drilling Program, Initial Reports. Vol. 207
- Hofmann, P., Beckmann, B., Wagner, T. (2003). A millennial- to centennial-scale record of African climate variability and organic carbon accumulation in the Coniacian-Santonian eastern tropical Atlantic (ODP Site 959, off Ivory Coast/Ghana). *Geology*, 31(2), 135-138.
- Wagner, T., Sinninghe Damsté, J., Beckmann, B. and Hofmann, P. (2004). Euxinia and primary production in Upper Cretaceous eastern equatorial Atlantic surface waters fostered orbital-driven formation of marine black shales. *Paleoceanography*, 19, PA4099, doi:10.1029/2003PA000898.

PPC2-17: Molecular and isotopic characterization of biomarkers in the Frick Swiss Jura sediments: a palaeoenvironmental reconstruction on the Northern Tethys marginV. Schwab, J.E. Spangenberg

Institute of Mineralogy and Geochemistry, University of Lausanne, BFSH-2, 1015 Lausanne, Switzerland
(e-mail: Valerie.Schwab@unil.ch)

Molecular and stable carbon isotope compositions of source-specific hydrocarbons have been used to reconstruct palaeoenvironmental changes during deposition of Middle Hettangian to Upper Sinemurian sediments on the northern epicontinental Tethys margin. The studied samples, outcropping in an excavation situated at Frick in the Swiss Jura, were deposited on the northern submarine sill of the Alemanic land - a southeastern extension of the Bohemian massif. They consist of a heterogeneous marly clay and dark grey limestones succession that records different depositional environments extended to the storm-wave base (about 20-50m) and marked by a synsedimentary subsidence (Wetzel et al., 2003). Middle Hettangian samples were deposited in a quiet and restricted anoxic lagoon (Jordan, 1983). Upsection, the presence of more diversified open-sea fauna indicates an increase in water depth and more favorable life environments (Jordan, 1983).

Throughout the Frick section, distribution and carbon isotope compositions of source-specific hydrocarbons indicate a complex organic matter mixture mainly derived from algae and cyanobacteria. The ^{13}C -depletion of pristane and phytane relative to the $n\text{-C}_{17}$ and $n\text{-C}_{18}$ indicates different precursors as algae and cyanobacteria for these isoprenoids. The correlation between the $\delta^{13}\text{C}$ values of $n\text{-C}_{17}$ and the mean $\delta^{13}\text{C}$ values of $\text{C}_{<19}$ acyclic isoprenoids suggests that the short chain isoprenoids mainly originate from thermal degradation of algal and/or cyanobacterial phytol. Traces of 7- and 8-methylheptadecane and the occurrence 2 β -methylhopanes indicate continuous cyanobacteria contribution. The large variations of the hopane $\delta^{13}\text{C}$ values (from -39.5 to -27.1‰) indicate different prokaryote precursors across the section. The hopanes with similar carbon isotopic composition as MMA (-31.0‰ to -28.8‰) are most likely related to a cyanobacterial origin. During Middle Hettangian sedimentation, contribution of anaerobic photosynthetic green sulphur bacteria (*Chlorobiaceae*) is supported by the occurrence of isorenieretene derivatives, including ^{13}C -enriched aryl isoprenoids ($\sim\delta^{13}\text{C} \approx -15\%$), tetramethylalkylbiphenyls, aromatized diaryl isoprenoids and isorenieretane (e.g., Summons and Powell, 1986; Koopmans et al., 1996.). The presence of *Chlorobiaceae* points to depositional environment with reduced water current, photic zone anoxia and H_2S in the deeper layers. This is consistent with geological

observations (e.g., scarcity of fossils, organic-rich sediments, absence of burrowing organisms) that suggest sedimentation in an anoxic and restricted lagoon. Considering evidences of photic anoxia, ^{13}C -depleted C_{29} hopanes (up to 11.8‰) in these samples are most likely derived from phototrophic purple sulfur bacteria utilizing isotopically light dissolved CO_2 at the base of the aerobic zone. In these sediments, ^{13}C -depleted pristane and phytane may be related to bacterial phytol contributions from purple photosynthetic bacteria. In Middle Hettangian samples, trace amounts of cadalene and significant concentration of perylene point to higher terrestrial organic matter inputs under largely anoxic and reducing depositional environments. During the Upper Sinemurian sedimentation, a relatively larger algal contribution is indicated by the occurrence of isotopically heavier $\text{C}_{>17}$ *n*-alkanes (with an average of 3‰) which display ^{13}C -enriched even carbon number homologues and a progressive ^{13}C -enrichment with chain length of even and odd carbon number homologues. This is associated with progressively more oxygenated marine depositional environment upsection related to the occurrence of methylsteranes and dinosteranes, and increasing $\text{C}_{27}/\text{C}_{29}$ sterane and hopane/sterane ratios. The presence in these sediments of significant amounts of pyrolytic-derived PAH indicates the occurrence of forest or peat fires suggesting climatic fluctuations with humid and dry periods.

References

- Jordan, von P., 1983. Zur Stratigraphie des Lias zwischen Unterem Hauenstein und Schinznach (Solothurner und Aargauer Faltenjura). *Eclogae Geologicae Helvetica* 76, 335-379.
- Koopmans, M. P., Köster, J., Van Kaam-Peters, H.M.E., Schouten, S., Hartgers, W.A., de Leeuw, J.W. and Sinninghe Damsté, J.S., 1996. Diagenetic and catagenetic products of isorenieratene: Molecular indicators for photic zone anoxia. *Geochimica et Cosmochimica Acta* 60, 4467-4496.
- Summons, R.E., Powell, T.G., 1986. Chlorobiaceae in Palaeozoic Seas revealed by biological markers, isotopes and geology. *Nature* 319, 763-765.
- Wetzel, A., Allenbach, R., Allia, V., 2003. Reactivated basement structures affecting the sedimentary facies in tectonically "quiescent" epicontinental basin: an example from the NW Switzerland. *Sedimentary Geology* 157, 153-172.

**PPC2-18: Late Quaternary palaeoenvironmental reconstructions,
Central Andes, Bolivia, from geochemical and petrographical
compositions of sedimentary organic matter**

A. Sifeddine¹, L. Martin¹, P. Meyers², E. Lallier-Vergès³, D. Wirmann⁴, J.-R. Disnar³

1) Paléotropique. UR 055. IRD: Institut de Recherche pour le Développement, 32, Av. Henri Varagnat, 93143, Bondy Cedex – France (e-mail: sifeddin@bondy.ird.fr)

2) Department of Geological Sciences. The University of Michigan, 425 East University Avenue, Ann Arbor, Michigan 48109-1063 USA

3) ISTO. UMR 6113 - CNRS/Université d'Orléans 1A, rue de la Férollerie 45071 Orléans Cedex2 – France

4) Paléotropique IRD BP A5 98848 cedex Noumea, New Caledonia

Geochemical and petrographical studies of a 755 cm long core collected in the middle of a marshy depression “Lake Siberia” (Central Andes, Bolivia; lat. 17°50'S, long. 64°43'W) surrounded by a cloud forest in the central Andes reveal that this site has recorded important late Quaternary environmental changes (Thérézien 1991; Sifeddine et al., 1998).. Three lithological units can be recognized: the basal unit below 430 cm composed of dark grey organic clay, the intermediate unit between 430 and 128 cm, made up of beige clay, and the uppermost 128 cm, made up of peat. Six radiocarbon ages show that this site has preserved an uninterrupted record of the last 30,000 years (Sifeddine et al. 1998). There are considerable fluctuations in the geochemical and petrographic parameters. In the basal unit, TOC values fluctuate around 5%, while the C/N and “Terrestrial/Planktonic” ratios average between 10 and 2, respectively. The $\delta^{13}\text{C}$ values are about -22 ‰. All these parameters show comparable values in the intermediate interval, except for TOC, which has negligible values. Some larger amplitude fluctuations in this intermediate unit also occur in the C/N and T/P ratios, which vary from 8 to 11 and 2 to 6, respectively. $\delta^{13}\text{C}$ values in the middle unit fluctuate between -20 and -24 ‰. The top peaty layer can be distinguished from the lower units by having high TOC values between 30 and 50%, C/N ratios between 20 and 30, T/P ratios between 2 and 20, and $\delta^{13}\text{C}$ values averaging -27 ‰.

The combination of C/N and $\delta^{13}\text{C}$ data enables a clear separation between two groups of points. One group, corresponding to sediments deposited during the glacial period, including the Last Glacial Maximum, is characterized by the predominance of organic matter having a planktonic origin. The poor preservation of organic matter in these LGM sediments is consistent with dry climatic conditions inferred also from pollen analyses (Mourguiart and Ledru 2002). The other group of points is chiefly attributable to organic material derived from C_3 terrestrial vegetation growing around the lake during the Holocene. These Holocene data are consistent with pollen evidence for establishment of cloud forest in the lake catchment,

attributed to increasingly humid climatic conditions. The high concentration of micro-charcoal content recorded between ca 8000 and 4500 14C yrs, likely from paleofires, underlines an intensification of dry conditions.

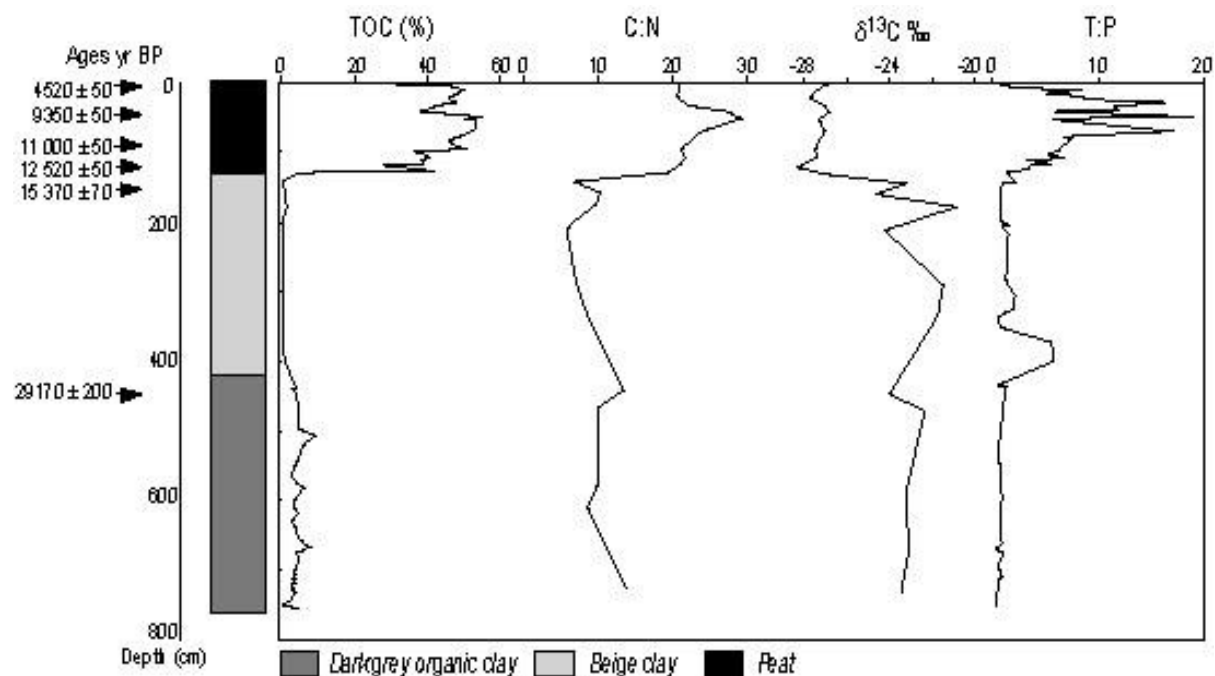


Fig.1. Core Si 93/1 (Lake Siberia, Bolivia). Simplified lithological log compared with profiles of TOC, C/N, $\delta^{13}C$ and T/P

References

- Mourguiart, Ph., Ledru, M.P., 2002. Last Glacial Maximum in an Andean cloud forest environment (Eastern Cordillera, Bolivia). *Geology*, 31, 195-198.
- Sifeddine, A., Bertaux, J., Mourguiart, Ph., Martin, L., Disnar, J.R., Laggoun-Défarge, F., 1998. Etude de la sédimentation lacustre d'un site de forêt d'altitude des Andes centrales (Bolivie). Implications Paléoclimatiques. *Bulletin de la Société Géologique de France*. 169, 3, 395-402.
- Thérézien, Y., 1991. Algues d'eau douce des mares de la "La Siberia" en Bolivie. *Bibliotheca Phycologica*, 88, 1-129.

PPC2-19: Reconstruction of the West Pacific El Niño history using the (isotopic) biomarker record of marine anoxic lakes, Palau

R.H. Smittenberg¹, C. Saenger¹, M.N. Dawson², J.P. Sachs¹

1) Dept. Earth, Atmospheric and Planetary Sciences, Massachusetts Institute for Technology. 77 Massachusetts Avenue, room E34-166, Cambridge, MA 02139, USA (e-mail: smitten@mit.edu)

2) School of Biological, Earth, and Environmental Sciences, University of New South Wales, Sydney, NSW 2052, Australia

El Niño-Southern Oscillation (ENSO) is the largest perturbation to global climate on inter-annual timescales, significantly shifting global precipitation patterns. The effect of anthropogenic climate change on ENSO intensity and frequency is currently unknown, and model predictions range from a significant strengthening of El Niño and/or an increase in its frequency ⁽¹⁾, to no effect or even weakening ⁽²⁾. Only a few and partially contradictory paleoclimate proxy data sets exist to evaluate these models. To remedy part of this deficiency, sediment cores were taken from several marine anoxic lakes situated on limestone islands in Palau. Radiocarbon dates on plant macrofossils indicate the cores span the last 10.2 kyr. Palau lies on the northwestern edge of the so-called west Pacific warm pool, which is a key region in the Pacific ocean-climate system, and the island group is significantly influenced by El Niño events when severe drought occurs.

The lakes receive seawater through cracks and fissures in the karstic rocks, while also plenty of meteoric water in the tropical wet climate of the region, resulting in permanent stratification of the lakes with a physically and biotically variable mixed layer (mixolimnion) atop euxinic bottom water. The hydrogen isotopic composition (δD value) of the mixolimnion is influenced by the balance between meteoric water ($\delta D = \sim -25\text{‰}$) and seawater ($\delta D = \sim -5\text{‰}$), and this is recorded within the biomass that is produced using the lake water: mangroves and other lake edge vegetation, algae, bacteria and archaea. During ENSO events the region receives much less rain than normal ⁽³⁾, resulting in a shift from meteoric mixolimnion δD values to oceanic values. Individual biomarkers from various organisms exhibit a constant hydrogen isotopic fractionation independent of the source water isotopic value ^(4,5), and downcore analyses of δD values of specific biomarkers (e.g. taraxerol for mangroves, dinosterol for dinoflagellates, C₁₆ fatty acid for bacteria), are used to reconstruct precipitation variations through time. Additionally, the terrestrial jungle vegetation around the lake suffers substantially during the droughts brought by El Niño, and the water stress of the plants bear their effect on the isotopic composition of terrigenous lipids produced during such

events ⁽⁶⁾. If not significantly diluted by material produced during normal wet conditions, this additional isotopic ENSO signal will also be recorded in the lake sediments.

In addition to the water isotopic composition, there is a clear relationship between the lake water temperatures and the ENSO stage ⁽⁷⁾, with lower than average lake temperatures during El Niño years (-0.5 to -1.0°C) and higher than average during La Nina years (+0.5 to +1.0°C). Lake water temperatures may be reconstructed using the recently developed Tex₈₆ proxy based on archaeal lipids ^(8,9), assuming a local calibration is successful in accounting for the dilution of terrigenous archaeal lipids.

A distinct feature of the lakes is their photic zone euxinia, resulting in a thick layer of photosynthetic sulfur bacteria just below the chemocline. ENSO perturbations of the physical-chemical properties of the lake systems may affect these bacteria on a species composition level (*Chlorobiaceae* vs. *Chromatiaceae*), their abundance, or even presence in case the water column becomes temporarily unstratified. Downcore analysis of the characteristic pigments, isorenieratene, okenone and chlorobactene may thus result in an additional proxy for ENSO activity or stage. Besides the biomarker record, additional sedimentological features and biogenic proxies (e.g. the $\delta^{18}\text{O}$ value of gastropods, the pollen record), analyzed by collaborators, may help resolve a decadal ENSO record of the West Pacific through most of the Holocene.

References

- 1) e.g. Collins (2000) *Geophys. Res. Letts.* 27 p3509.
- 2) e.g. Fedorov & Philander (2000) *Science* 288 p1997.
- 3) <http://lumahai.soest.hawaii.edu/Enso/enso/rain/palau.html>.
- 4) Zhaohui Zhang, pers. Comm.
- 5) Huang et al. (2002) *Geology* 30 p1103.
- 6) e.g. Roden & Ehleringer (1999) *Plant Physiology* 120 p1165.
- 7) Laura Martin, pers. comm.
- 8) Schouten et al (2002) *EPSL* 202 p265.
- 9) Powers et al (2004) *Geology* 32 p.613.

PPC2-20: Palaeoenvironment at the site of zinc and lead ore formation at Topla-Mežica, Slovenia: insight from biomarkers and stable isotopes

J.E. Spangenberg¹, U. Herlec²

1) Institute of Mineralogy and Geochemistry, University of Lausanne, BFSH-2, 1015 Lausanne, Switzerland (e-mail: Jorge.Spangenberg@unil.ch)

2) Department of Geology, University of Ljubljana, Aškerčeva 12, 1000 Ljubljana, Slovenia

The biomarker distributions (steranes, hopanes) and the bulk and molecular carbon isotopic compositions provide evidence for a diverse community of algal and bacterial organisms in the sedimentary organic matter from the carbonate host rocks of the Topla (250,150 tones ore of 10 wt % Zn and 3.3 wt % Pb; Drovenik et al., 1988) and Mežica (19 Mt ore of 5.3 wt % Pb and 2.7 wt % Zn) Zn-Pb deposits, Northern Karavanke/Drau Range, Slovenia. These data combined with sedimentological evidence provide insight into the palaeoenvironmental conditions at the site of ore formation. The Topla Anisian host dolostones and Mežica Ladinian host limestones have relatively high concentrations of redox sensitive trace elements (V, Mo, U) and a lack of Ce and Eu anomalies, indicating that sediments were formed in a reducing environment. Anoxic conditions enhanced the preservation of organic matter and resulted in a relatively higher total organic carbon content (up to 0.41 wt % TOC). The similar $\delta^{13}\text{C}$ values of the organic extracts and associated kerogens suggest indigeneity of the hydrocarbons extracted from the ore and host rocks. The maturity biomarker parameters (S/S + R C₃₁ hopane, S/S + R C₂₉ sterane, $\beta\beta/\beta\beta$ $\alpha\alpha$ C₂₉ steranes) do not indicate any significant thermal maturity differences between Topla and Mežica samples. Therefore, the differences in the hydrocarbons distribution (concentrations of methylalkanes, *n*-pentadecylcyclopentane, squalane, and 17 α (H),21 β (H)-C₃₀ hopane) observed in the bitumens from both deposits do not appear to result from maturity variations, and suggest that they were derived from different organic facies, but most possibly from the same source rock that generated the bitumens in Anisian and Ladinian barren carbonate rocks. The $\delta^{15}\text{N}$ values of kerogen around 0 per mil, ¹³C depleted kerogen, ¹³C enriched *n*-heptadecane, and high amount of short-chain (C_{<22}) monomethylalkanes in the bitumen of mineralized samples (> 1 wt% Pb + Zn) indicate the preservation of a high concentration of cyanobacterial remains at the site of ore formation. Furthermore, in Topla and Mežica bitumens, the lower $\delta^{13}\text{C}$ values of pristane and phytane suggest that these compounds were derived from sulfate reducing bacteria. These data are consistent with a supra-tidal hypersaline facies and fine laminated dolomite sedimentation at Topla. Laminated microbial mat ecosystems, dominated by cyanobacteria and other phototrophic microorganisms cover

most of the sediment surface in hypersaline and shallow marine environments, such as lagoons, upper intertidal and supratidal ponds (Herbert and Welsh, 1994). A large population of dissimilatory sulfate-reducing bacteria can be found at the bottom of the microbial mat, in the immediate vicinity of the cyanobacteria (e.g., Elshahed et al., 2003). The sulfate reducers feed on the cyanobacterial low-molecular fermentation products (e.g., Canfield and Des Marais, 1991). Further evidence regarding higher bacterial activity at the ore site is obtained from the hopane/steranes concentration ratios that reflect the input of eukaryotic (algae, higher plants) versus prokaryotic (bacteria) organisms to the source rock. These ratios ranging from 1.15 to 2.96 in Topla and 1.44 to 14.95 in Mežica are roughly correlated with the sum of Pb and Zn concentrations ($r = 0.75$ and 0.49 , respectively). This correlation is consistent with mixing of hydrothermal metal-rich fluids and locally derived biogenic H_2S . An early diagenetic near-surface bacterial reworking of organic matter explains the observed differences in the hydrocarbons distribution between barren and mineralized dolostones at Topla and Mežica. A cyanobacterial mat, sustaining the sulfate-reducing bacteria, was the motor of sulfate reduction, leading to accumulation of H_2S in the pore water of the sediments. Mixing of the incoming hydrothermal metal-rich fluids with the H_2S -rich pore waters caused the precipitation of the strongly ^{34}S depleted sulfides (average = -15.6% , $n = 74$, Drovenik et al., 1988).

A shallow depth ore formation seems more feasible as an explanation for the preservation of unperturbed layers with biogenic H_2S -rich pore waters in an anoxic environment.

References

- Canfield, D.E. and Des Marais, D.J., 1991. Aerobic sulfate reduction in microbial mats. *Science*, 251, 1471-1473.
- Drovenik, M., Pezdic, J. and Pungartnik, M., 1988. Sulfur isotope composition of sulfides in the zinc-lead deposit Topla. *Razprave IV, razreda SAZU, Ljubljana*, 29, 113-128 (in Slovene).
- Elshahed, M.S. et al., 2003. Bacterial diversity and sulfur cycling in a mesophilic sulfide-rich spring. *Applied and Environmental Microbiology*, 69, 5609-5621.
- Herbert, R.A. and Welsh, D.T., 1994. Establishment of phototrophic purple sulphur bacteria in microbial mat systems. In: L.J. Stal and P. Caumette (Editors), *Microbial Mats: structure, development and environmental significance*. NATO Advances Science Institute Series, Series G, Ecological Sciences. Springer, Berlin, pp. 51-60.

PPC2-21: Carbon and hydrogen isotopic variations in specific compounds of the Irati Formation: reconstruction of a Permian sea environment in Southern Brazil

E. Vaz dos Santos Neto, J.R. Cerqueira

PETROBRAS R&D Center, Av. Hum, Quadra 7, Cidade Universitária, 21949-900, Rio de Janeiro, RJ, Brazil
(e-mail: eugenioneto@petrobras.com.br)

The Irati Formation (Upper Permian) is represented by a wide lithologic variation that reflects the complexity of depositional conditions over an area of more than 1,500,000 km² in the Paraná Basin, mostly in Brazil. Geological, paleontological, and geochemical characteristics indicate that this formation was deposited under specific marine conditions, during a relatively warm climate with periods of higher and lower humidity.

Studied samples were collected in two organic rich layers in an open pit mine operated by PETROBRAS, in São Mateus do Sul city, state of Paraná. These samples were analyzed by organic carbon content and Rock-Eval pyrolysis. The organic extract was fractionated by MPLC in paraffins, aromatic hydrocarbons, and NSO compounds. The *n*-alkanes were segregated from isoprenoids and cyclic compounds using molecular sieve (5 Å). The carbon and hydrogen isotopic compositions of the specific compounds were analyzed, in separated instruments, *via* gas chromatography-combustion-ion ratio monitoring system. Results are the average of, at least, two measurements with repeatability better than 0.5‰ and 2‰ for $\delta^{13}\text{C}_{\text{PDB}}$ and $\delta\text{D}_{\text{SMOW}}$, respectively.

The $\delta^{13}\text{C}$ values of the isoprenoids, *e.g.*, farnesane, *iC*₁₆, norpristane, pristane and phytane, and *n*-alkanes (C₁₆-C₂₃) are remarkably similar, $-24.05\text{‰} < \delta^{13}\text{C}_{\text{isoprenoids}} < -22.32\text{‰}$, suggesting a common origin. The only sterane (C₂₇R) with acceptable analytical repeatability gives $\delta^{13}\text{C} = -22.92\text{‰}$ (layer 1) and $\delta^{13}\text{C} = -20.72\text{‰}$ (layer 2). The first result strengthening the origin from phytoplanktonic algae of the isoprenoids and *n*-alkanes. However, the ¹³C enrichment in this C₂₇ sterane from layer 2, suggests an additional control on ¹³C/¹²C.

In the hopanoids, *e.g.*, norhopane, C₃₀ hopane, and C₃₁ S and R homohopanes, the depletion in ¹³C comparatively to $\delta^{13}\text{C}_{\text{pristane}}$ can reach up to 15‰, suggesting that chemoautotrophs (HS⁻ oxidizers?) apparently was the source. Methane generation and consumption probably did not occur in the Irati sea because of the availability of sulfur in that paleoenvironment. And, no substantial contribution of cyanobacteria source is expected because $\delta^{13}\text{C}_{\text{hopanoids}}$ is significantly heavier than those $\delta^{13}\text{C}$ of phytoplanktonic derived compounds.

Gammacerane is isotopically the heaviest compound $\delta^{13}\text{C} = -19.32\text{‰}$ (layer 1) and $\delta^{13}\text{C} = -18.24\text{‰}$ (layer 2). At the moment, it is not possible to ascribe the food source for the ciliate protozoan (*Tetrahymena sp.*) that is the presumed source of this compound. The $\delta^{13}\text{C}$ values of β -carotane, -25.80‰ (layer 1) and -26.23‰ (layer 2), are depleted in ^{13}C by 2-3‰ compared to $\delta^{13}\text{C}_{\text{pristane}}$, suggesting that algae (Dunaliella-like?) would not be the only source, but some contribution of other source (bacteria?) would also be possible.

It was possible to analyze δD only in *n*-alkanes of the layer 2, that has shown a systematic enrichment in D from $n\text{C}_{15}$ ($\delta\text{D} = -229\text{‰}$) to $n\text{C}_{32}$ ($\delta\text{D} = -138\text{‰}$). Variations of δD in saturated hydrocarbons are related to the δD of the water in the depositional environment of source rocks, thus it can be used as a climate proxy. Although with few results, this depletion in D in *n*-alkanes may suggest a global process of ice cap melting that influenced oceanic water and, consequently, the meteoric water cycle. Regional processes that can cause D-depletion in meteoric waters, e.g., intensification of rains, increase of altitude and/or latitude, and continentality are unlikely in this case.

Similar carbon isotopic composition of isoprenoids, *n*-alkanes and C_{27} sterane suggests a common and homogeneous phytoplanktonic source during the evolution of the Irati Permian sea at the time when deposition of both layers occurred. The wider variations of $\delta^{13}\text{C}_{\text{hopanoids}}$ may indicate that the prokaryote community thriving in the anoxic zone changed over time, and suggests that chemoautotrophs were the most abundant group.

Low values of δD in *n*-alkanes can be related to an overall isotopic lightness throughout the global water cycle as consequence of global process of ice cap melting, that is likely to occur in interglacial periods, as it is the case of the Upper Permian.

Acknowledgements

To PETROBRAS for the authorization to publish this results, to CENPES lab personnel for the analyses, and to Luiz Carlos da Silva Freitas for the critical review.

PPC2-22: Alkane and PAH hydrocarbons in Arctic Ocean sediments: interpretation of distributions in the context of Holocene and Glacial climatic regimes

M.B. Yunker¹, R.W. Macdonald², L.R. Snowdon³, B.R. Fowler⁴,
F.A. McLaughlin², J.N. Smith⁵, B. Billeck⁶, G. Ilyin⁷

1) 7137 Wallace Dr., Brentwood Bay, BC, Canada (e-mail: Mark-Yunker@telus.net)

2) Institute of Ocean Sciences, Sidney, BC, Canada

3) Institute of Sedimentary and Petroleum Geology, Calgary, AB, Canada

4) Axy's Analytical Ltd., Sidney, BC, Canada

5) Bedford Institute of Oceanography, Dartmouth, NS, Canada

6) Freshwater Institute, Winnipeg, MB, Canada

7) Murmansk Marine Biological Institute, Murmansk, Russia

Parent and alkyl PAH, *n*-alkane, and terpane, hopane and sterane biomarker concentrations have been determined for sediment cores and grabs from the Beaufort, Barents, Chukchi and Laptev Seas and the principal Arctic Ocean basins. Concentrations generally decrease between the shelves and the basin margins and are lowest in the interior basins. The extremely low sedimentation rates and shallow mixed layers (2-4 cm, based on fallout ¹³⁷Cs and ^{239,240}Pu) at all basin locations and bulk ¹⁴C data for one core suggest that material deposited since the industrial revolution is all in the surface layer. The highest basin hydrocarbon concentrations are found in the Eurasian Basin and Greenland Sea; these locations receive substantial ice-rafted sediment from the Laptev and Kara Sea shelves by offshore transport in the Transpolar Drift. Much lower hydrocarbon concentrations are present in sediments from the Canadian Basin; these locations receive little ice-rafted sediment from the adjacent Beaufort or Chukchi Sea shelves by the Beaufort Gyre.

Arctic Ocean sediments contain very low amounts of anthracene, benz[*a*]anthracene and benzo[*a*]pyrene, suggesting that most reactive and small-ring combustion-derived PAHs have been degraded. Proportions of these PAHs are consistent with a petroleum source, likely in bitumens, shales or coals delivered by rivers or eroded from coastal margins. Accordingly, degradation-resistant compounds such as the high molecular weight PAHs and the petroleum-derived hopanes and steranes promise to provide the best tracers of combustion and petroleum processes in basin sediments.

PAH, *n*-alkane, hopane and sterane distributions indicate a natural origin for Arctic basin hydrocarbons. Significant amounts of diagenetic hopanes and C₁-C₄ alkyl substituted PAHs are present in surface sediments at all Arctic Ocean locations. Dimethylnaphthalene, monomethylphenanthrene and hopane profiles suggest that petrogenic material of the similar maturity is present in surface sediment on the shelves and in the basins. Ternary plots for the steranes and the principal *m/z* 276 and 278 PAHs suggest that sediment from the eastern

Russian shelves provides a major contribution to the basins, while sediment from the Mackenzie River/Beaufort Sea and Chukchi Sea makes only a negligible contribution. Samples from the Eurasian Basin contain significant amounts of the rearranged hopanes 17 α (H),18 α (H),21 β (H)-28,30-bisnorhopane (BNH) and 17 α (H),18 α (H),21 β (H)-25,28,30-trisnorhopane (TNH). These hopanes are minor components in the Canadian Basin and Chukchi Sea, are absent in the Beaufort Sea and appear to be specific to the western Russian shelves. Both TNH and BNH are present in Russian petroleum basins and in sediments from Russian shelves (particularly the Barents Sea). Hence, sediment deposited in the Eurasian Basin appears to primarily originate from Russian shelves.

Hydrocarbons such as the vascular plant *n*-alkanes and the higher molecular weight (primarily combustion derived) PAHs can be transported both on atmospheric aerosols and on water-borne and ice-associated particulate. These compounds are present at all basin stations and their proportions increase in core intervals that correspond to Glacial eras. In contrast, sediment-bound hydrocarbons such as the petroleum-derived alkyl naphthalenes and phenanthrenes or the vascular plant-sourced tetrahydrochrysenes and picones remain present in Glacial times at the basin margins but are largely absent in the central basins. A shift in parent PAH composition towards the thermodynamically less-stable combustion-derived PAHs (indeno[1,2,3-*cd*]pyrene, indeno[7,1,2,3-*cdef*]chrysene or dibenz[*a,j*]anthracene) is also observed in the pre-Holocene core sections of the basin samples.

Concentration profiles with depth in the basin cores imply a reduced transport of sediment to the central Arctic Ocean during Glacial times, but suggest that off-shelf transport was relatively unaffected by ice cover at the basin margins. Profiles also indicate that the atmospheric delivery of vascular plant alkanes and combustion PAHs to the central Arctic basins apparently continued uninterrupted when ice rafting and the supply of presumably sediment-borne alkyl PAHs (both petroleum and vascular plant-derived) were curtailed. A reduced flux of petrogenic material during glacial interval(s) is also supported by a decrease in 31 $\alpha\beta$ and 32 $\alpha\beta$ S/R hopane maturity (based on GC-MS-MS) in a deep core section at the North Pole station.

PPC2-23: Submillennial evolution of global wind regime in the Southern hemisphere during the last three climatic cycles

M. Ferrer, J.O. Grimalt

Institute of Chemical and Environmental Research (CSIC) 08034-Barcelona (e-mail: mfcqam@iiqab.csic.es)

Higher plant biomarkers such as C₂₅-C₃₃ n-alkanes and C₂₄-C₃₀ n-alkan-1-ols are constituents of the leaf wax of continental vegetation. These compounds are transported into the sea either by wind or by fluvial inputs. Records of the sedimentary fluxes of these molecules in marine areas, far away from potential land mass water inputs, can be used to estimate the intensities of wind regime.

This approach has been followed to study the changes in wind regime in the subantarctic Indian Ocean using core MD00-2374 (46°2'S, 96°29'E, 3250 m depth) over the last three climatic cycles at submillennial time scale. The changes observed in both continental markers show a general pattern dominated by the well defined glacial-interglacial oscillation in which eolian inputs were much stronger during the glacial periods. Strong wind decreases were observed at the onset of each deglaciation which is coincident with the glacial-to-interglacial $\delta^{18}\text{O}$ variation in benthic foraminifera recorded in the same core. These terrigenous input markers also exhibit significant variability at the submillennial scale.

The continental biomarker profiles in tropical Indian Ocean core MD 98-2165 (9°38'96 S, 118°20'31 E, 2100 m) reveals a similar glacial-interglacial pattern than MD00-2374 and, for some time periods, parallel changes at the submillennial level (Fig. 1). In both cases, higher inputs of higher plant markers were found during the glacial periods exhibiting a pattern which is also consistent with previous observations in sedimentary sites within the South China Sea. The parallelism between the two open Indian Ocean cores is surprising having in mind the large distance between the two core sites and, particularly, their strong latitudinal difference which belong to two different atmospheric cells.

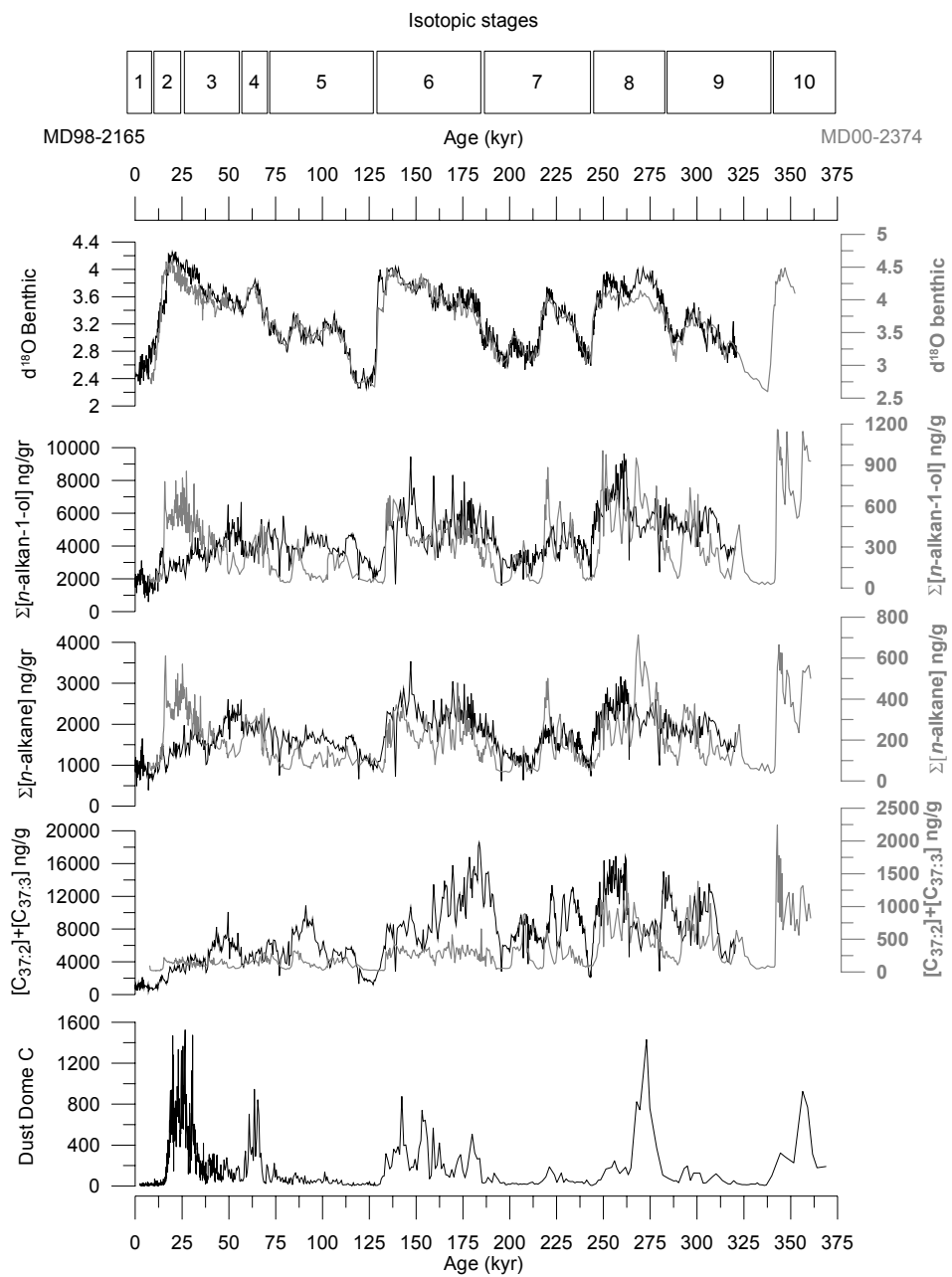


Fig.1. Biomarkers and benthic isotopes of cores MD98-2165 and MD00-2374 and dust from Dome C

PPC2-24: High-resolution multi-molecular stratigraphic records from North Atlantic drift sediments (ODP Sites 980, 984) reflecting Holocene climate and ocean dynamics

J. Holtvoeth¹, T. Wagner², D. Montluçon¹, G. Mollenhauer¹, J. McManus¹, D. Oppo¹,
T. Eglinton¹

1) Woods Hole Oceanographic Institution, Woods Hole, USA (e-mail: jholtvoeth@whoi.edu)

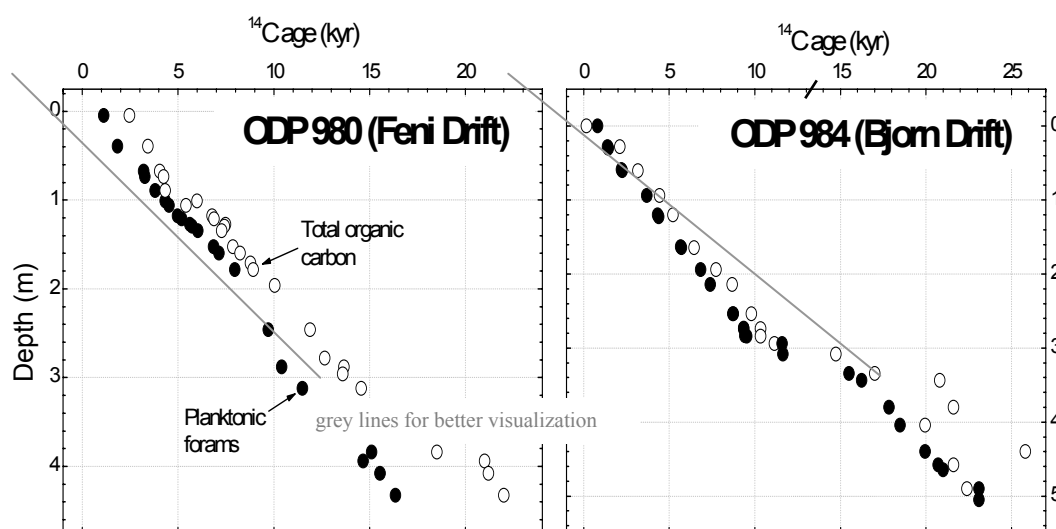
2) University of Newcastle, Newcastle upon Tyne, UK

The North Atlantic plays an important role as the source region for northern component waters of thermohaline circulation. The hydrological system (including e.g. NADW production) is highly sensitive to climatic changes. Underlying drift sediments record both, changes of the hydrological system (lateral advection) and of 'direct' material input from the water column (primary production and eolian supply), and therefore represent excellent archives for past ocean and regional climate variability. Two sediment cores from North Atlantic drift sediments were taken during ODP Leg 162 (ODP 980, Feni Drift, 55°N 15°W, water depth 2179 m, and ODP 984, Bjørn Drift, 61°N 24°W, water depth 1648 m). While both sites experience similar atmospheric forcing, the present-day Bjørn Drift is bathed by Iceland-Scotland Overflow Water, while the Feni Drift is influenced by more southern sourced waters. Both sites exhibit exceptionally high sedimentation rates and thus enable reconstruction of climate-related changes within the North Atlantic with high temporal resolution. The composition of the organic matter (OM) in these sediments is closely coupled to the dynamics of the environment. Key factors that control the quantity and quality of OM from marine and terrigenous sources in North Atlantic drift sediments are surface water temperatures and nutrient supply (marine primary productivity), wind speeds (eolian supply of terrigenous OM), and strength and direction of bottom water currents (lateral redistribution of OM, and export from continental margins). Down-core ¹⁴C data for planktonic foraminifera show distinct shifts in sedimentation rate between the deglacial and Holocene at each site. These sedimentation rate changes occur 3 to 4 kyr earlier at the Bjørn Drift than at the Feni Drift, implying a shift in depositional regimes resulting from changes in currents that focus sediments at these locations. Geochemical signatures in entrained sediments are thus anticipated to reveal information on past changes in the trajectory and vigor of currents at each site.

This study seeks evidence for rapid climate changes through development of high-resolution multi-molecular stratigraphic records of the sedimentary OM using Gas Chromatography/Time-Of-Flight Mass Spectrometry (GC-TOF-MS) analysis of total lipid extracts. We present continuous high-resolution (< 100 yr) molecular proxy records from both

ODP sites that indicate changes in heat transport, marine productivity, and terrigenous supply from the Last Glacial Maximum to the present. Alkenones, sterols, and other biomarkers characteristic for different phytoplankton groups (e.g., long-chain diols) as well as lipids derived from terrigenous plant waxes serve as the primary molecular tools. Marine biomarker fluxes document past variations in climate-controlled marine productivity. Variations in the degree of saturation of alkenones (U_{37}^K) are used to reconstruct varying sea surface temperatures (SST). Vascular plant lipids, transported and deposited over the oceans as aerosols or via bottom currents, are interpreted in terms of eolian or advective terrigenous fluxes. Each of these processes is linked to specific climate conditions.

We also compare ^{14}C AMS ages of bulk OM and selected marine (alkenones) and terrigenous (plant waxes) biomarkers to those of planktonic foraminifera in order to examine current-driven sediment redistribution and advective transport. Preliminary ^{14}C data indicate that bulk OM tends to be generally older (up to 6 kyr) than foraminiferal carbonate in both cores (see figure). These age offsets are more pronounced for the Feni Drift, however the offsets appear to be coupled to sedimentation rate changes at both sites. We investigate whether these age relationships reflect changes in current-driven redistribution of marine OM or supply of pre-aged terrigenous OM.



PPC2-25: Biomarker Record From the Upper Tisdale (2707 – 2705 Ma) and Porcupine Assemblage (2685 – 2673 Ma) of the late Archaean Abitibi subprovince, Timmins, Ontario, Canada

G.T. Ventura¹, F. Kenig¹, C. Reddy², R. Nelson², R.E. Summons³

1) Dept. of Earth and Environmental Sciences, University of Illinois at Chicago, M/C 186, 845 W. Taylor St., Chicago, IL. 60607-7059 (e-mail: gventu1@uic.edu)

2) Dept. of Marine Chemistry and Geochemistry, Woods Hole Oceanographic Institution, Woods Hole, MA

3) Dept. Of Earth, Atmospheric and Planetary Sciences, E34-44, 42-44 Carleton St., Massachusetts Institute of Technology, Cambridge MA, 02139

Biomarkers were analyzed from the saturated/unsaturated and aromatic hydrocarbon fractions extracted from metasedimentary greywackes, siltstones, and shales of the Viapond and Gold Center Formation of the upper Tisdale Assemblage (2707-2690 Ma) and the Krist and Hoyle Formation of the Porcupine Assemblage (2685-2673 Ma) from the Abitibi Subprovince, Ontario Canada. Core and hand samples were obtained from Porcupine Joint Ventures and the core library at the Ministry of Northern Development and Mines, Timmins, Ontario. Tisdale Assemblage sedimentary facies were previously interpreted as hydrothermal laminated massive sulfide and/or interflow sediments between subaqueous komatitic-tholeiitic flows associated with island arc collision. Porcupine Assemblage turbidite facies were interstratified by massive, brecciated alkaline lava flows and reworked volcanoclastic facies. All Porcupine Assemblage samples contained primary depositional fabric [1].

Hydrothermal alteration and mineralization of the Timmins host rock occurred between 2688 and 2691 Ma. [2]. Gold mineralization occurred late in the evolution of the hydrothermal system from focused fluid flow along lithostructural features. Metamorphism of Timmins area later proceeded to lower and upper greenschist facies leading to a second phase of hydrothermal activity from fluid producing reactions such as hydrogenation and decarbonation of the host rock. The last tectonic events to occur in the Abitibi Greenstone Belt were diabase (Matachewan) dyke swarms, which became emplaced during the Paleoproterozoic (2454 Ma). Since the Paleoproterozoic, the Canadian Craton has been tectonically inactive and no Proterozoic and Phanerozoic sedimentary rocks are known from this area.

Biomarker maturity calculations indicate the sediments are mature and either reached or surpassed oil generation. The origin of the extracted hydrocarbons will be discussed. However, some biomarker contributions are consistent with the depositional environment of their host rocks. The Viapond Formation display a mixed hydrocarbon source signal with hydrothermal components including branched alkanes with quaternary carbon atoms, alkyl-

cyclohexanes, alkyl-cyclopentanes, and alkyl-benzenes with either even or odd carbon number predominance, and biphytane. Steranes and hopanes (especially 3 β -methylhopanes) were likely detrital input from more shallow waters (aerobic) environments by deposition of interflow sediments. These samples have unresolved complex mixtures (UCM) spanning the entire range of compounds, total organic carbon (TOC) ranges from 0.06-3.0 Wt. %, and $\delta^{13}\text{C}_{\text{kerogen}}$ from -15.71 to -32.52 ‰.

Samples from the Porcupine Assemblage display a complex history. Biomarkers common to all samples include C₁₆-C₃₅, branched alkanes, C₁₆-C₂₉ alkyl-cyclohexanes and alkyl-cyclopentanes (with no carbon number preference) and C₂₇-C₃₅ hopanes. These samples have TOCs ranging from 0.39 – 5.11 and $\delta^{13}\text{C}_{\text{kerogen}}$ from -29.24 to -42.0 ‰ (ave. -33.27‰). Samples from the Hoyle Formation display two different hydrocarbon signatures. The first contains aryl-isoprenoids, low abundance of biphytanes, C₁₉-C₃₀ tricyclic terpanes, no UCMs, and TOCs ranging between 0.39-5.11 Wt. % suggesting deposition within a stratified water column. The second hydrocarbon signature contains high abundances of C₃₄-C₄₀ biphytanes, no aryl-isoprenoids, UCMs at late retention times and higher TOC values of 0.98-9.32 Wt. %.

Most samples contain varying abundance of C₃₄-C₄₀ acyclic and mono-, bi-, and tricyclic irregular isoprenoids consistent with cleaved products of glycerol dialkyl glycerol tetraethers (GDGTs) derived from archaea. High relative abundance of these lipids corresponds to samples with abundant hopanes, near absence of tricyclic terpanes, UCMs at late retention times and occasionally biodegradation of lower molecular weight compounds. Differences in archaeal lipid abundance between samples may reflect the intensity of hydrothermal circulation that promoted habitats favorable for archaea or the remains of interterrestrial prokaryotic communities that actively biodegraded the buried organic matter. Whether the archaeal lipids were syngenetic or later contributions, these samples provide direct evidence for the existence of archaea and the diversity of microbial life during the Late Archaean.

References

- [1] Brisbin, D.I. 1997. Geological setting of gold deposits in the Porcupine gold camp, Timmins, Ontario. Ph.D. Thesis.
- [2] Mason, R., Brisbin, D.I. and Aitken, S., 1988. The geological setting of gold deposits in the Porcupine mining camp. In Geoscience Research Grant Program, Summary of Research, 1987-1988. Ontario Geological Survey, Miscellaneous Paper 140. Pg. 133-145.

PPC2-26: Molecular and C-isotopic Study on Biotic and Environmental Changes Across the P/Tr Boundary Based on the GSSP at Meishan, China

C.-J. Wang, Y.-M. Liu, H.-X. Liu

Laboratory of Geochemistry and Environmental Sciences, Faculty of Geosciences, China University of Petroleum, Beijing, 102249 (e-mail: wchj333@126.com)

The GSSP of Permian-Triassic boundary at Meishan, Zhejiang province of China, has attracted more and more scientists to devote their attention to the related scientific questions about the end-Permian mass extinction. In view of the important potential of molecular organic geochemistry in revealing information of biotic and/or environmental events, we carried out the project “Molecular Organic Geochemical Records on the Biotic and Environmental Changes Across the Permian-Triassic Boundary” (funded by NSFC) from 2002. Here we first present one aspect of the results — Pristane spike and C-isotope negative excursion as the records of the abrupt mass extinction and marine anoxia at the end-Permian.

1. It has been revealed that a spike of pristane abundance occurs near the boundary, the beds 23~26 (In which bed 24e is regarded as the last appearance interval of most species of animals), where Pr/Ph and Pr/nC₁₇ value are averaged as high as 2.98 and 2.23, respectively. This is an abnormal distributions because these intervals are typical marine sediments deposited in reducing conditions, with OMs composed predominantly of marine amorphous organic matters. We propose that this abnormal distribution are most probably caused by the input of pristane from marine animal lipids and fecalites, by accumulating, migrating and preserving in some suitable depositing facies during the catastrophic death of animals and/or by developing of anoxic water column (during marine transgression). By most extensive investigations, we have also found that the situation of isoprenoid HCs enrichment and high Pr/Ph characters also occurs in other typical marine anoxic sediments during the most important geological periods with mass extinctions in different extent, such as late Ordovician, end of Devonian, early Jurassic and late Cretaceous, etc. These occurrences not only strongly support the above mechanism, but also give the first probable interpretation to high Pr/Ph characters of some typical marine anoxic sediments.

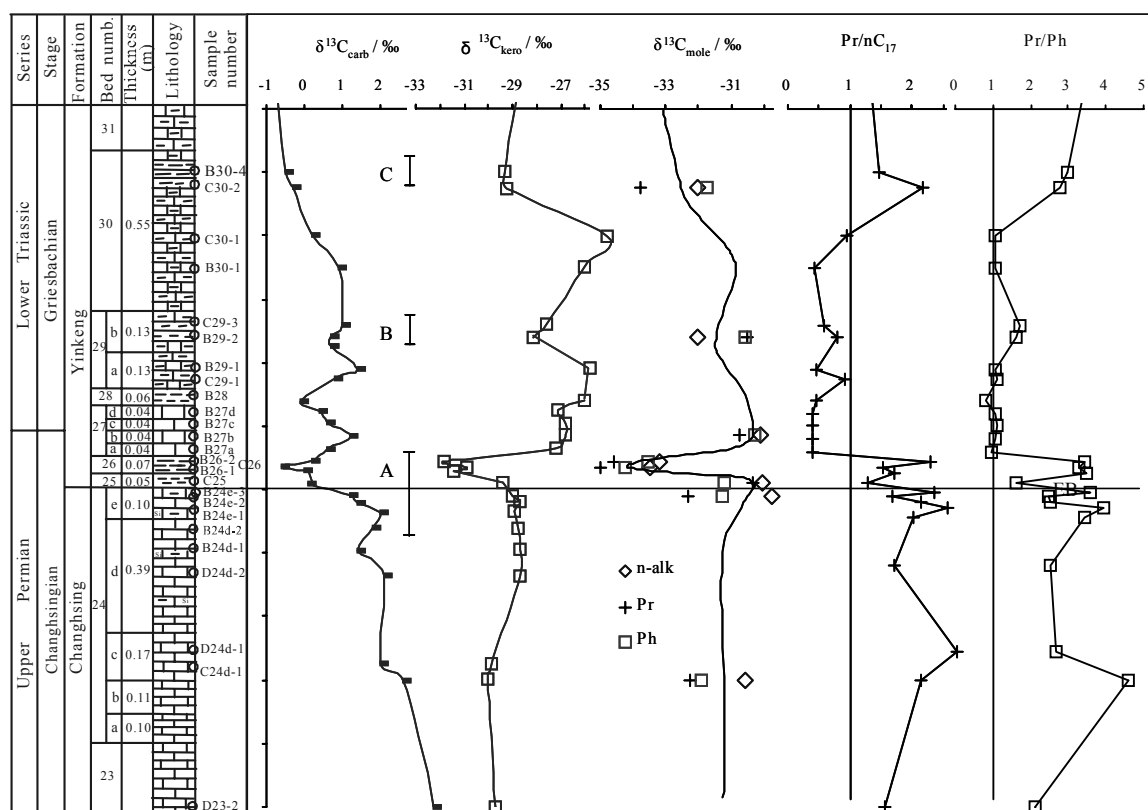


Fig. 1. Variation in Pr/nC₁₇, Pr/Ph, $\delta^{13}\text{C}_{\text{carb}}$, $\delta^{13}\text{C}_{\text{kero}}$ and $\delta^{13}\text{C}_{\text{mole}}$ across PTB at Meishan, China

2. C-isotopic geochemical study on PTB strata has revealed that $\delta^{13}\text{C}_{\text{kero}}$ variation is coincided with $\delta^{13}\text{C}_{\text{carb}}$, showing the strong negative excursions from bed 24 to bed 26, where $\delta^{13}\text{C}_{\text{kero}}$ ranges from -28.7‰ to -31.8‰. But the variation in $\delta^{13}\text{C}_{\text{mole}}$ should more accurately reflect the fast change of CO₂ source in ocean-atmosphere system, such as $\delta^{13}\text{C}_{\text{Pr}}$ ranges from -32.4‰ to -35.0‰, and $\delta^{13}\text{C}_{\text{n-alk}}$ from -29.8‰ to -33.3‰, respectively. The relative positive $\delta^{13}\text{C}_{\text{kero}}$ shift in bed 27 and in bed 29a or lower bed 30 are partly induced by the contribution of dinoflagellates OM (with as 4-methyl-steranes occurring in higher abundance as evidence) and by the most heavily biodegraded and oxidized. An integrated interpretation is suggested to the genesis relationships between the end-Permian environmental change — mass extinction — molecular/isotopic records: Methane release triggered by global warming caused by the Siberian Traps and by the ‘runaway greenhouse’ lead to ocean-atmosphere system rich in ¹²CO₂, marine anoxic, acidification and toxic, and then result in negative excursion in $\delta^{13}\text{C}$, mass extinction and pristane enrichment, respectively.

PPC2-27: Earth's precession and obliquity influences on sea surface temperature, oceanic primary production and terrestrial vegetation in the mid-latitude Western North Pacific (Core MD01-2421) during the last 145,000 years

M. Yamamoto, T. Oba, J. Shimamune, Y. Ichikawa, T. Ueshima, R. Suemune, D. Isono

Graduate School of Environmental Earth Science, Hokkaido University, Kita-10, Nishi-5, Kita-ku, Sapporo 060-0810, Japan. (e-mail: myama@ees.hokudai.ac.jp)

We have generated high-resolution records of alkenone sea surface temperature (SST), total organic carbon (TOC) and lignin composition during the last 145 kyrs from Core MD01-2421 off central Japan, in the northwestern Pacific.

The records of SST in the Japan and California margins showed orbital-scale anti-phase SST variations between the two margins during the last 145 ka. This east-west seesaw-like change agreed well with the long-term El Niño-Southern Oscillation (ENSO) behavior predicted by the Zebiak-Cane ENSO model (Clement et al., 1999) as regards both the timing and frequency during 0-60 ka and 120-145 ka, and is attributed to the precession-controlled change in tropical ENSO behavior. This anti-phase SST change was not clearly demonstrated during 60-120 ka. This finding suggests that the influence of tropical climatic dynamics on the mid-latitude North Pacific varied in response to glacial-interglacial cycles.

The variation of TOC was pronounced with a 41-kyr periodicity. High TOC corresponds to a high angle of the Earth's obliquity. The variation of TOC was delayed behind the variation of obliquity by ~1 kyr and preceded the variation of $\delta^{18}\text{O}$ of benthic foraminifera *Uvigerina* by ~6 kyrs. The TOC varied inversely with Polar Circulation Index (Mayewski et al., 1997). Since the primary production in the Kuroshio-Oyashio mixed zone is related to the intensity of the winter Aleutian Low, these correspondences imply that the intensity of the winter Aleutian Low has responded to the obliquity forcing by the atmospheric reorganization in the northern high latitudes. The winter Aleutian Low was stronger when the obliquity was large, implying that the lower insolation in winter presumably increased the temperature contrast between the land and the ocean, deepening the winter Aleutian Low.

Lignin composition was analyzed by TMAH-pyrolysis-GC/MS. The relative abundance of lignin was significantly low in early MIS-1 and MIS-5e and higher in MIS-5c to early MIS-4. This reflects glacial-interglacial changes in sea level and riverine runoff. The ratio of syringyl (S)- to vanillyl (V)-phenols (S/V ratio), which is a contribution index of angiosperms against gymnosperms, was lower in MIS-2, MIS-4 and MIS-6, reflecting the glacial-interglacial variation of air temperature. The ratio of cinnamyl (C)- to vanillyl (V)-phenols (C/V ratio), which indicates the contribution of grasses, was higher in late MIS-2, early-mid MIS-3 and MIS-6. The periods of higher C/V ratio correspond to the periods of lower SSTs, suggesting a dry and cold climate in late MIS-2, mid-MIS-3 and MIS-6.

PMP-1: Fossil DNA as a species-specific recorder of alkenone-biosynthesizing haptophytes: implications for $U_{37}^{K'}$ -based palaeothermometry (P)

A. Boere, B. Abbas, J.S. Sinninghe Damsté, M.J.L. Coolen

Netherlands Institute for Sea Research, Dept of Marine Biogeochemistry and Toxicology, PO Box 59, 1790 AB, Den Burg Texel, The Netherlands

Recently, preserved ribosomal DNA of ancient haptophytes was recovered from Holocene anoxic sediments of Ace Lake (Antarctica), and resulted in the identification of six phylotypes related to known alkenone and alkenoate-biosynthesizing haptophytes with the non-coccolithophorid *Isochrysis galbana* UIO 102 as their closest relative (Coolen et al., 2004). The similar concentration profiles of 18S rDNA of haptophytes and their alkenones and alkenoates revealed that fossil 18S rDNA also served as quantitative biomarkers in that environment. The relative abundance of these phylotypes changed as the lake chemistry, particularly salinity, evolved over time. Changes in the alkenone distributions reflected these population changes rather than a physiological response to salinity by a single haptophyte. Using this novel paleo-ecological approach of combining data from lipid biomarkers and preserved DNA, it was shown that the post-glacial development of Ace Lake from freshwater basin to marine inlet and the present-day lacustrine saline system caused major qualitative and quantitative changes in the biodiversity of alkenone and alkenoate biosynthesizing haptophytes over time (Coolen et al., 2004). The identification of ancient alkenone producing haptophytes is of importance to calibrate alkenone-unsaturation based sea surface temperature (SST) proxies (Brassell et al., 1986) since different species are known to have different alkenone distributions (e.g. Marlowe 1984).

The occurrence of distinct organic-rich intervals (sapropels) within Pliocene to Holocene eastern Mediterranean sediments, appear to be cyclic and astronomically associated. Various climate-proxies, including the $U_{37}^{K'}$ -based palaeothermometry, register a transition to a warmer climate at the onset of the formation of sapropels. This warming resulted in an increased intensity of freshwater and nutrient input in the eastern basin causing water column stratification with a lowering of the photic-zone salinity and severe bottom water anoxia. The reconstruction of SST before, during, and after sapropel deposition is primarily based on the $C_{37:2}$ and $C_{37:3}$ alkenone ratio (e.g. Menzel et al., 2003; Giunta et al., 2003). Since the alkenone-biosynthesizing coccolithophorid haptophyte *Emiliana huxleyi* is common in temperate oceans and their fossil calcareous skeletons were identified microscopically in Mediterranean sapropels (e.g. Giunta et al., 2003), this species is assumed to be the main

marine precursor of alkenones in the marine environment. The U_{37}^K -based SST proxy in these studies is therefore calibrated for *E. huxleyi*.

Similar as for Ace Lake, a varying salinity prior and during the formation of Quaternary sapropels might have caused shifts in the alkenone biosynthesising haptophyte community in the eastern Mediterranean Sea. We are currently employing our species-specific lipid and rDNA stratigraphy initially used for the Holocene sediments of Ace Lake, to identify ancient coccolithophorid as well as non-coccolithophorid alkenone biosynthesizing haptophyte species which colonized the eastern Mediterranean photic zone prior, during, and after the deposition of Quaternary sapropels. These results will prove whether U_{37}^K -based SST reconstructions should be (re)calibrated for the presence of alkenone-biosynthesizing non-coccolithophorid haptophytes.

References

- Brassell, S.C., Eglinton, G., Marlowe, I.T., Pflaumann, U., Sarnthein, M., 1986. Molecular stratigraphy: a new tool for climatic assessment. *Nature* 320, 129-133.
- Coolen, M.J.L., Muyzer, G., Rijpstra, W.I.C., Schouten, S., Volkman, J.K., Sinninghe Damsté, J.S., 2004. Combined DNA and lipid analyses of sediments reveal changes in Holocene haptophyte and diatom populations in an Antarctic lake. *Earth and Planetary Science Letters* 223, 225-239.
- Giunta, S., Negri, A., Morigi, C., Capotondi, L., Combourieu-Nebout, N., Emeis, K.C., Sangiorgi, F., Vigliotti, L., 2003. Coccolithophorid ecostratigraphy and multi-proxy paleoceanographic reconstruction in the Southern Adriatic Sea during the last deglacial time (Core AD91-17). *Palaeogeography Palaeoclimatology Palaeoecology* 190, 39-59.
- Marlowe I.T., Green, J.C., Neal, A.C., Brassell, S.C., Eglinton, G., Course, P.A., 1984. Long chain (n -C₃₇-C₃₉) alkenones in the Prymnesiophyceae. Distribution of alkenones and other lipids and their taxonomic significance. *Br. Phycol. J.* 19, 203-216.
- Menzel, D., Van Bergen, P.F., Schouten, S., Sinninghe Damsté, J.S., 2003. Reconstruction of changes in export productivity during Pliocene sapropel deposition: a biomarker approach. *Palaeogeography Palaeoclimatology Palaeoecology* 190, 273-287.

**PMP-2: Methane formation in eutrophic mountain lake
(Jezero na Planini pri Jezeru, Slovenia)**

M. Žagar¹, N. Ogrinc¹, J. Faganeli², T. Kanduč¹, P. Vreča¹

1) Dept. of Environ. Sci. "J. Stefan" Institute, Jamova 39, 1000 Ljubljana, Slovenia

2) Marine Biological Station, National Institute of Biology, Fornace 41, 6330 Piran, Slovenia

In this presentation, the results of an incubation experiment performed in sediment from the eutrophic mountain lake Jezero na Planini pri Jezeru are reported. Chemical and stable C and D isotope analyses were used in order to determine the processes of CH₄ formation during the experiment. Benthic fluxes were estimated from linear regressions of solute concentrations against incubation time and corrected for dilution. The isotopic composition of dissolved inorganic carbon, $\delta^{13}\text{C}_{\text{DIC}}$, indicates three different processes occurring during incubation. First, oxic degradation of organic matter where $\delta^{13}\text{C}_{\text{DIC}}$ values decreased from -7.9‰ to -13.5‰. During anoxic degradation the isotopic composition stayed stable at $-12.6 \pm 0.6\text{‰}$ and after 56 days the $\delta^{13}\text{C}_{\text{DIC}}$ value reached -7.6‰ and did not change much until the end of experiment. ¹³C enrichment coincided with the formation of CH₄ which started to increase at the same time. Methane produced had a measured average $\delta^{13}\text{C}$ value of $-70.1 \pm 1.1\text{‰}$ and δD value of -208‰ indicating, formation thought bacterial CO₂ reduction. The flux-weighted ¹³C/¹²C content of DIC and CH₄ is equivalent to the isotopic composition of the deposited metabolizable organic carbon and plankton. Thus, at least at the surface of the sediment, oxidized carbon reflects the reactivity of planktonic organic matter, since the $\delta^{13}\text{C}$ of remineralized carbon was estimated to be -40.3‰. The fraction of metabolized organic carbon during CH₄ formation was estimated to be 0.48, a value expected in the complete oxidation of sedimentary organic carbon by methanogenesis. A similar value of 0.47 was obtained when the major contribution of DIC derived from methanogenesis was estimated using the isotope mass balance. The fraction of sedimentary organic carbon degradation was calculated to be 0.22, while the fraction derived from the dissolution of calcite was estimated to be 0.31.

PMP-3: The geochemical characteristics of pore water and methane in Late Quaternary sediments of the Ulleung basin, East Sea (Sea of Japan)J.H. Kim¹, M.H. Park², U. Tsunogai³, B.J. Ryu¹, Y.J. Lee¹, H.W. Chang⁴

1) Petroleum and Marine Resources Research Division, Korea Institute of Geoscience and Mineral Resources, Daejeon, 305-350, Korea (e-mail: yjl@kigam.re.kr)

2) Research Institute of Basic Sciences, Chungnam National University, Daejeon, 305-764, Korea

3) Earth and Planetary Sciences, Graduate School of Science, Hokkaido University, N10W8, Kita-ku, Sapporo, 060-0810, Japan

4) School of Earth and Environmental Sciences, Seoul National University, Seoul, 151-742, Korea

There has been rarely researched on the pore water and methane gas in late Quaternary sediments of the Ulleung Basin, East Sea (Sea of Japan). Hence, this study is to elucidate the geochemical characteristics of pore water and methane in the core sediments. For the purpose, major anions and stable isotopes of pore water, and methane concentration and its $\delta^{13}\text{C}$ values were measured. Sulfate concentrations evidently show two depleted trends with a sediment depth. One is a linearly depleted type (cores 03GHP-01, 03GHP-02, 03GHP-03, and 03GHP-04), and the other is a concave down (core 03GHP-05). Methane concentration, pH, alkalinity and $\delta^{34}\text{S}$ also increase with a depth. By using the gradient of sulfate concentration, the SMI (Sulfate-Methane Interface) depth of cores 03GHP-01 and 03GHP-02 is situated at about 4 mbsf (meters below seafloor), while that of the other cores is deeper than 6 mbsf. This is a good agreement with the enrichment of methane concentration. Methane rapidly enriches below 4 mbsf at cores 03GHP-01 and 03GHP-02, and its concentration is relatively low and constant at the other cores. Accordingly, the reduction stage can be divided into two types. The first type is to reach the methanogenesis throughout AMO (Anaerobic Methane Oxidation), and the second type is to gradually change into the AMO and methanogenesis. The cores from the southern part of the Ulleung Basin (cores 03GHP-01 and 03GHP-02) belong to the first type, whereas the cores from the northern part of the Ulleung Basin (cores 03GHP-03, 03GHP-04, and 03GHP-05) show the characteristics of the second type. These results could be caused by the somewhat different post-depositional environment. The $\delta^{13}\text{C}$ values of DIC (dissolved inorganic carbon) provide an additional evidence for the reduction stage. In the cores, the $\delta^{13}\text{C}$ values of methane range from -86.5 ‰ to -69.5 ‰ and are relatively constant with a depth. It means that the methane has been derived from bacterial origin rather than thermogenic, and its origin has the same throughout the cores. The relationship between $\delta^{13}\text{C}$ values in methane and in DIC of pore water indicates that methane production occurred through CO_2 reduction.

PMP-4: Lipid composition of some picophytoplanktonic *Choricystis* species from freshwater lakes

P. Metzger¹, K.P. Fawley², M.W. Fawley²

1) LCBOP, UMR CNRS 7618, ENSCP, 11 Rue Pierre et Marie Curie, 75231 Paris cedex 05, France
(e-mail: pierre-metzger@enscp.fr)

2) Department of Biological Sciences, North Dakota State University, Fargo, ND 58105-5517, USA

Microalgae are an important source of lipids and biomarkers found in many recent and ancient sediments (Volkman et al., 1998). Although numerous microalgal sources have been identified, several classes and groups of these microorganisms have not been yet investigated in details for their lipids. This is the case of the freshwater picoplanktonic algae characterised by a cell size of less than 2 μm , and contributing significantly to the production of biomass as their marine homologues. While the wide diversity of marine picoalgae is well established since the last decade (Potter et al., 1997), investigations on the diversity of freshwater species were by comparison relatively rare. The morphology of freshwater picoalgae is often uniform, for instance as in coccoid green algae, that leads authors to refer these latter as "*Chlorella*-like" or "*Nannochloris*-like" algae, from which an apparent lack of diversity in freshwater picoalgae. However, some recent studies based on the determination and comparison of 18S rDNA sequences of numerous isolates have revealed high diversity in freshwater picophytoplankton just as in marine species (Krienitz et al., 1996; Hepperle and Schlegel 2002; Fawley et al., in press).

The genus *Choricystis* constitutes one of the major lineages identified in picoplanktonic algae, and numerous isolates have been characterised from freshwater lakes in Europe and North America. The aim of the present study is to compare the chemotaxonomic and phylogenetic relationships between some of these algae. Several cultures originally isolated from lakes in Itasca State Park, Minnesota, USA, were grown in the laboratory. Here, we report the analyses of lipid extracts from these isolates.

Fatty acid and sterol compositions appear rather uniform in the algal isolates, with respectively the predominance of palmitic and oleic acids, and cholesterol. Saturated series of C₂₂-C₂₈ α -hydroxy acids are present in all isolates. Frequently found in recent sediments, these biomarkers were rarely reported in microalgae (Volkman et al., 1999). A series of C₁₆-C₃₀ saturated *n*-alcohols with even carbon numbers predominating was also identified. The major fatty alcohol was 16:0; the occurrence of two monounsaturated alcohols, 28:1 and 30:1, appears to be strain dependent. In addition, C₁₅-C₂₉ straight chain hydrocarbons, with odd carbon numbers predominating, were also identified, essentially *n*-alkanes (mainly 17:0) and

(or) *n*-alkenes (mainly terminal olefins 19:1, 21:1 and 23:1); Fig.1. Although such compounds are relatively common in microalgae, their distribution in *Choricystis* could take on a taxonomic value.

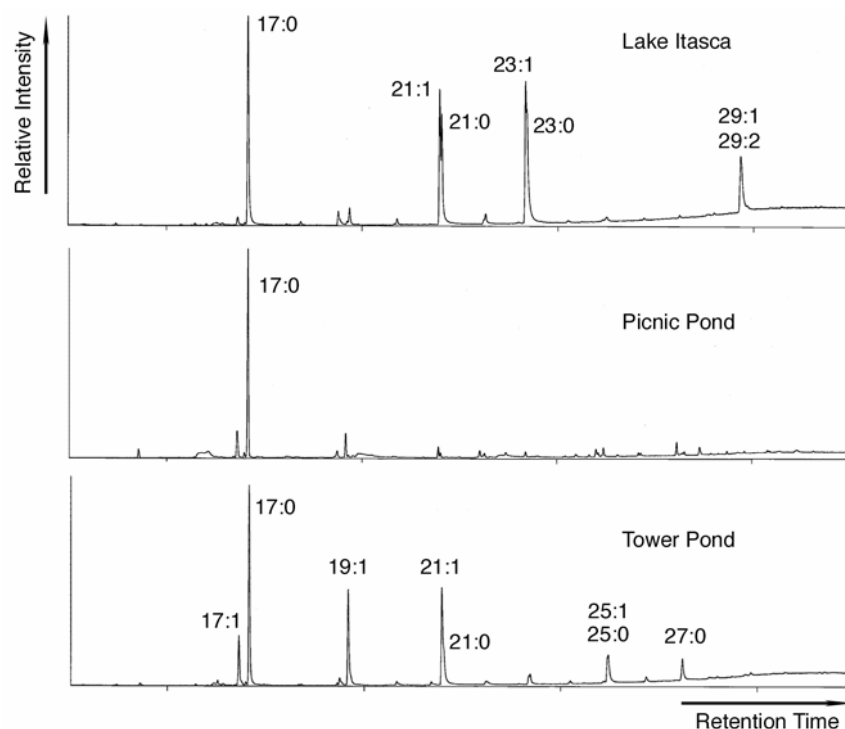


Fig.1. TIC chromatograms of the hydrocarbon fractions isolated from three *Choricystis* strains originating from lakes in Itasca State Park, Minnesota

References

- Fawley, M.W., Fawley, K.P., Owen, H.A. *Phycologia*, in press.
 Hepperle, D., Schlegel, I., 2002. *International Review of Hydrobiology* 87, 1-10.
 Krienitz, L., Huss, V.A.R., Hümmer, C., 1996. *Phycologia* 35, 332-341.
 Potter, D., LaJeunesse, T.C., Saunders, G.W., Anderson, R.A., 1997. *Biodiversity and Conservation* 6, 99-107.
 Volkman, J.K., Barrett, S.M., Blackburn, S.I., Mansour, M.P., Sikes, E.L., Gelin, F., 1998. *Organic Geochemistry* 29, 1163-1179.
 Volkman, J.K., Barrett, S.M., Blackburn, S.I., 1999. *Journal of Phycology* 35, 1005-1012.

PMP-5: An Organic Geochemical Investigation of Cretaceous Cold-seep Carbonates Accompanied with Chemosynthetic Community of Central Hokkaido, Northern Japan

S. Ogihara

Department of Earth and Planetary Science, Graduate School of Science, The University of Tokyo 7-3-1, Hongo, Bunkyo-ku, Tokyo, 113-0033 Japan (e-mail: ogi@eps.s.u-tokyo.ac.jp)

Anaerobic oxidation of methane (AOM) occurred in Cretaceous carbonate rocks associated with cold-seep biological fossil communities from Tappu-Kanajirizawa (TK) and Teshionakagawa-Abeshinaigawa (TA) in Hokkaido, northern Japan. Lipid distribution and $\delta^{13}\text{C}$ values of biomarkers for Archaea and bacteria associated with AOM in these cold-seep carbonates were investigated.

TK limestone is light-brown marly limestone including *Thrasia yezoensis* and *Miltha* sp. which correspond to a recent chemosynthetic community dominating the family of Lucinae. TA limestone is light-gray micritic tube-worm limestone containing *Thrasia* sp., *Nipponothracia* sp. and *Calyptogena* sp. The ^{13}C values of carbonate carbon of TK limestone range from -43.4‰ to -39.9‰ , and ^{18}O values range from -5.8‰ to -2.5‰ . The ^{13}C values of carbonate carbon of TA limestone range from -45.5‰ to -43.7‰ , and ^{18}O values range from -2.3‰ to $+1.7\text{‰}$. The carbonate carbon of both limestone is significantly ^{13}C depleted.

These samples contain the “tail to tail linked” irregular isoprenoid hydrocarbons, acyclic C_{20} -isoprenoid 2,6,11,15-tetramethylhexadecane (crocetane), its C_{25} -homologue 2,6,10,15,19-pentamethyleicosane (PME), and some unsaturated derivatives. Furthermore, C_{30} -homologue 2,6,10,15,19,23-hexamethyltetracosane (squalane), as well as specific acyclic and cyclic C_{40} isoprenoid hydrocarbon were detected. The $\delta^{13}\text{C}$ values of PME and crocetane were depleted between the range of -128.7‰ to -115.6‰ . The carbon isotopic compositions of biphytanes were strongly depleted in ^{13}C ranging between -120.9‰ to -96.1‰ .

The isotope data implies that biosynthesis of the archaeal isoprenoids involved the utilization of isotopically depleted carbon such as that derived from methane. The similar biomarker patterns obtained from Manji-Shikoroza and Yubari-Utagoezawa carbonates, which were absent from the cold-seep fossil community. These carbonates can be identified as cold-seep carbonates by biomarkers, and biomarkers are a useful tool for identifying cold-seep carbonates.

The newly discovered biomarkers in this study were C_{13} and C_{18} isoprenoid ketones which could potentially be identified as the methane oxidizing Archaea. They also had low

$\delta^{13}\text{C}$ values ranging from -114.5‰ to -103.5‰ which are similar values to that of crocetane and PME. A small amount of C_{14} and C_{19} isoprenoid ketones were also detected with the C_{13} and C_{18} isoprenoid ketones. The origin of isoprenoid ketones detected in this study are complicated. C_{18} and C_{13} isoprenoid ketones, which were extremely depleted in ^{13}C , could be derived from hydroxyarchaeol containing polar lipids of methane oxidizing Archaea such as *Methanosarcina*, but the origin of C_{14} and C_{19} isoprenoid ketones is unknown.

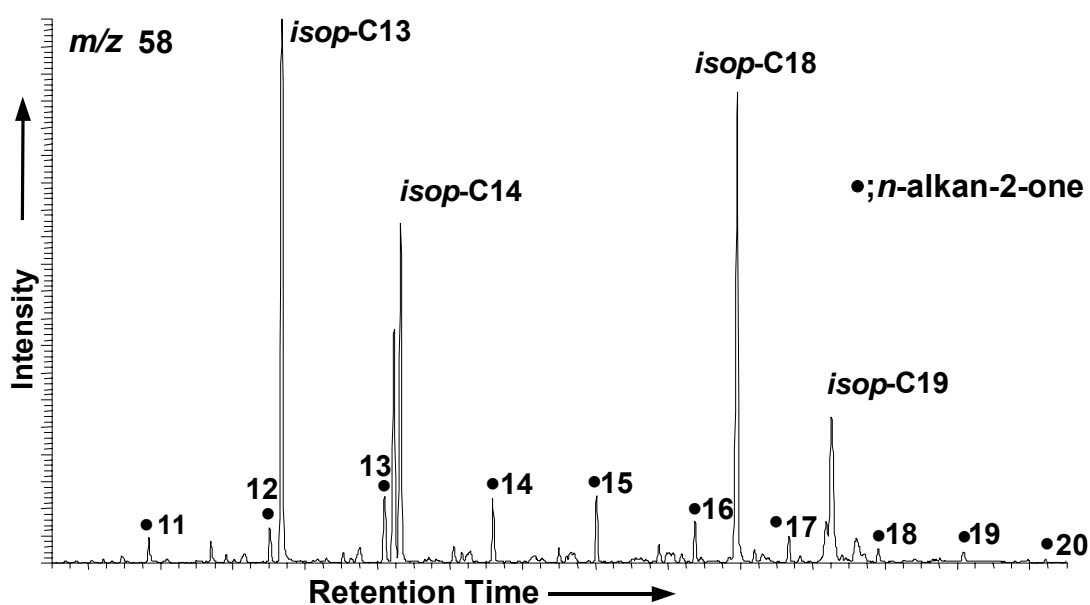


Fig.1. m/z 58 Mass chromatogram of ketone/ester fraction isolated from Tappu-Kanajirizawa limestone. The $\delta^{13}\text{C}$ values of C_{13} , C_{14} , C_{18} and C_{19} isoprenoid ketones were -113 , -108 , -103 , and -109‰ , respectively. *isop-C*₁₃ = C_{13} -isoprenoid ketone

PMP-6: Molecular analysis of intact phospholipids of bacteria from Mediterranean sapropels

M. Seidel¹, J. Süß¹, K. Herrmann¹, H. Sass², J. Rullkötter¹

1) Institute for Chemistry and Biology of the Marine Environment (ICBM), Carl von Ossietzky University of Oldenburg, P.O. Box 2503, D-26111 Oldenburg, Germany (e-mail: michael.seidel@icbm.de)

2) School of Earth, Ocean & Planetary Sciences, Cardiff University, Cardiff CF10 3YE, Wales, U.K.

Sediments of the eastern Mediterranean Sea are characterized by the consecutive appearance of dark sediment layers. These sapropels reveal high organic carbon contents up to over 30% TOC and are embedded in organic-carbon-lean calcareous sediments (<0.5% TOC). Sapropel formation is proposed to have occurred periodically approximately every 20 000 years due to Milankovich cycles. As a result of good preservation of organic matter high amounts of potentially metabolizable organic compounds may still provide an energy source for indigenous microorganisms [1]. However, the analysis of microorganisms in the environment with conventional molecular techniques, e.g. by measuring DNA, is still problematic because living and dead matter are not distinguished. In contrast, intact phospholipids (IPL) and polar lipid fatty acids (PLFA) are suitable biomarkers to trace vegetative bacteria taking into account that these diagnostic membrane lipids are rapidly degraded after cell lysis. Consequently, IPL and PLFA patterns of cultured bacteria can be used to determine structure and size of microbial communities in sapropels. Furthermore, phylogenetic and chemotaxonomic relationships can be determined.

This report presents a study of IPL and PLFA patterns of a variety of cultured bacteria isolated from sapropel samples obtained during cruise M51/3 of R/V Meteor in November 2001 from station 567 in the eastern Mediterranean Sea [2]. Anoxic isolates used in this study were closely related to *Photobacterium profundum* and isolated from sapropel layers S1 (Holocene) and S5 (Eemian). Considering the high cultivation success, this genus can be assumed to be a typical sapropel bacterium. Special emphasis was placed on the qualitative and quantitative analysis of IPL by a high-performance liquid chromatograph coupled *via* an electrospray interface to a hybrid quadrupole/time-of-flight (Q-TOF) mass spectrometer (HPLC-ESI-MS). Exact mass measurements of the TOF analyzer provides extensive structural information by applying precursor ion scans with tandem MS studies. For evaluation of this method, the phospholipid composition of *Desulfosporosinus* sp. A10, a sulphate reducing bacterium, was successfully determined (Fig. 1a). Investigations revealed that the bacterium contained four phospholipid classes substituted with different, characteristic fatty acids. Additionally, phospholipids substituted with straight-chain alkylethers were detected.

In further investigations, IPL fingerprints of the isolated *Photobacterium* strains (Fig. 1b) will be compared with patterns acquired from environmental sapropel samples. In conclusion, this technique can have a great impact on examining viable biomass in sapropels and hence help to understand the nature and activity of subsurface communities in the deep biosphere.

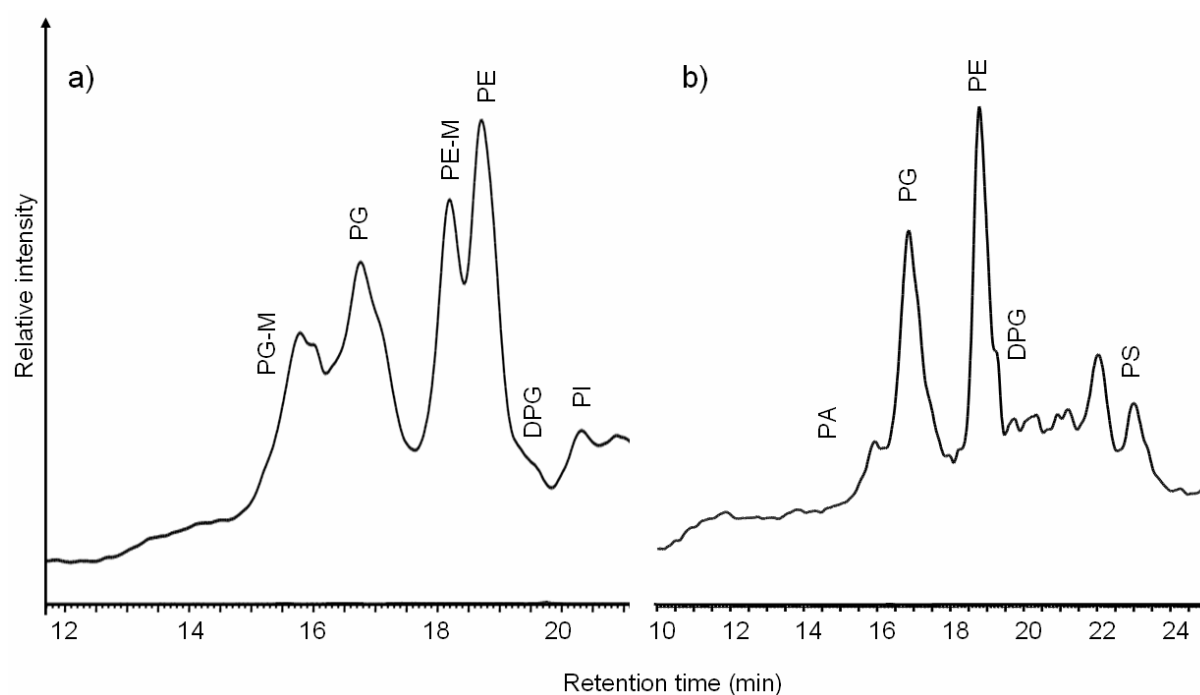


Fig.1. Total ion current chromatograms (negative ion mode) of phospholipid fractions of a) *Desulfosporosinus* sp. A10 and b) *Photobacterium* sp. J10. All sapropel strains contained mainly PE and PG with traces of PA, DPG and PS, but no alkylether side-chains. PE was the major phospholipid type in all investigated strains, whereas PG was found in minor amounts.

PA Diacyl phosphatidyl acids, *PG* diacyl phosphatidyl glycerols, *PE* diacyl phosphatidyl ethanolamines, *DPG* tetracyl diphosphatidylglycerol, *PI* diacyl phosphatidyl inositols, *PS* diacyl phosphatidyl serines.

PGM, *PEM* phospholipids with glycerol or ethanolamine head group, tentatively identified as occurring with mixed O-alkyl and acyl side chains

References

- [1] Coolen, M.J.L., Cypionka, H., Sass, A., Sass, H., Overmann, J., 2002. Ongoing modification of Mediterranean Pleistocene sapropels by green nonsulfur bacteria and crenarchaeota. *Science* 296, 2407-2410.
- [2] Süß, J., Engelen, B., Cypionka, H., Sass, H., 2004. Quantitative analysis of bacterial communities from Mediterranean sapropels based on cultivation-dependent methods. *FEMS Microbiology Ecology* 51, 109-121.

PMP-7: The experiment on the biogenic gas generation of *Spirulina* in different salinity

Zhangying^{1,2}, Lijian¹, Huguoyi¹, Lizhisheng¹

1) Langfang Branch research Institute of Petroleum Exploration and Development, Petrochina

2) China University of Geoscience, Beijing

Biogenic gas could be found in varied salinity environments. In this study, a series of experiment were designed to discover the amount of generated biogenic gas and the geochemical characteristics of the products in different salinity. The *Spirulina* samples were fermented in anaerobic conditions for 182 days at 35°. The salinity was set as 0, 3%, 6%, 9% and 12% NaCl.

There are two major products during the fermentation process: CH₄ and CO₂. CH₄ is the dominant composition in biogenic gas. In fresh water, 85% *Spirulina* was changed to biogenic gas: the production rate of CH₄ was 1213ml/gTOC (*Spirulina* sample); the production rate of CO₂ was 395ml/g (*Spirulina* sample). With the rising of salinity, the production rate of CH₄ and CO₂ is decreasing. Hypersaline environments inhibited the generation of biogenic gas. In 12% salinity condition, only 4% *Spirulina* was changed to biogenic gas: the production rate of CH₄ was 0.4ml/gTOC (*Spirulina* sample); the production rate of CO₂ was 82.1ml/gTOC (*Spirulina* sample).

The isotope composition of generated CH₄ and CO₂ was changed with salinity. The $\delta^{13}\text{C}_{\text{CH}_4}$, $\delta\text{D}_{\text{CH}_4}$ and $\delta^{13}\text{C}_{\text{CO}_2}$ of biogenic gas in low salinity environments were heavier than the results in high salinity environments. The distribution of $\delta^{13}\text{C}_{\text{CH}_4}$ was -50.5~ -66.1‰, the distribution of $\delta^{13}\text{C}_{\text{CO}_2}$ was 0~ -11.9‰. In fresh water, $\delta\text{D}_{\text{CH}_4} = -360\text{‰}$, in 6% salinity, $\delta\text{D}_{\text{CH}_4} = -385\text{‰}$.

It was suggested that the distribution of the isotope composition of generated CH₄ and CO₂ was controlled by the production rate of biogenic gas. The isotopic fractionation resulted from the organic matter (*Spirulina*) fermentation process.

PMP-8: Intact microbial lipid distribution in Lake Baikal sediments – Life markers in a unique deep freshwater environment

K.-G. Zink

GeoForschungsZentrum Potsdam, Section 4.3, Telegrafenberg, 14473 Potsdam, Germany
(e-mail: zink@gfz-potsdam.de)

The detection and characterization of microbial life in marine and terrestrial deep subsurface environments is still a challenging purpose. Although numerous studies have proven cell numbers reaching 10^5 to 10^6 cells/cm³ in several hundreds to 1000 metres depth (e.g. Parkes et al., 2000; Colwell et al., 2004), obtaining a deeper insight into the composition of these microbial communities and their activity is still highly desirable. However, the detection of viable biomass requires highly sensitive analytical methods. We use an HPLC-ESI(electrospray ionisation)-MS-MS approach (Zink et al., 2003; Zink & Mangelsdorf, 2004), which enables the chemical structure of intact microbial lipids (i.e. phospholipids) extracted from the sediment to be elucidated and their occurrence with depth to be quantified. Furthermore, potential adaptation to high pressure, temperature or substrate changes, reflected in the molecular composition of microbial chemical cell components, can be elucidated (see Mangelsdorf et al., this meeting). In this communication investigations on highly diverse intact phospholipid (PL) distribution patterns in a lacustrine sedimentary environment are presented reflecting predominant contribution of living bacterial biomass and its decay within the first metre of sediment. All cores were treated by inner coring to eliminate bacterial contamination from outside. These sediments give an excellent opportunity to study sedimentary PL occurrence and degradation in high resolution in contrast to marine settings where yields of intact microbial lipid compounds are often near the detection limit (ODP Legs 190, 199, 201, 204) except for surface sediments (Sturt et al., 2004). Lake Baikal (max. water depth 1630 m), an example of an unique biological setting, has high amounts of different PL groups in the first metre of sediment, particularly of acylphosphatidylglycerols which are known to occur in certain bacteria, e.g. *Corynebacterium* (Niepel et al., 1998), although with different fatty acyl side-chains (Zink & Mangelsdorf, 2004). High turnover rates for organic matter in the water column of Lake Baikal and in the first centimetre of sediment imply intensive decay also for phospholipids, consequently identified intact PL's reflect most probably constituents of living bacterial communities. The investigation of short cores from different locations demonstrates distinct differences in the degradation intensity of PL's with depth. Core 19 for instance, at a water depth of 450 m, show a PL decay of 90 % in 60 cm depth, whereas in sediments from the deepest part of the lake (1630 m) PL concentrations even increase slightly with depth (Fig. 1).

For a comprehensive characterization of living organic material the analysis of PLFA's (phospholipid fatty acids, using GC-MS) is in process. First results demonstrate the dominance of common bacterial fatty acyl side-chains: 16:0, 16:1, 14:0, 18:1, br15:0, br17:0.

In addition two groups of microbial lipids have been detected in Lake Baikal in high abundance which are also present in marine ODP Leg 201 sediments of different depths. Both compound series are to date interpreted as being ether lipids containing a high variety of side-chain lengths: the first compound group was identified as lysophosphatidylglycerol (LPG) ethers, the second tentatively identified as glycerophospholipid ethers. In contrast to ester-linked lipids, they seem to be less affected by degradation, in particular the LPG ethers, due to their presence in the deeper part of Baikal core 19, where ester-linked PL's are already heavily degraded (Fig. 1). In addition, their widespread and depth-independent occurrence in the marine deep subsurface – especially in ODP Leg 201 sediments - provide evidence for a increased stability against degradation.

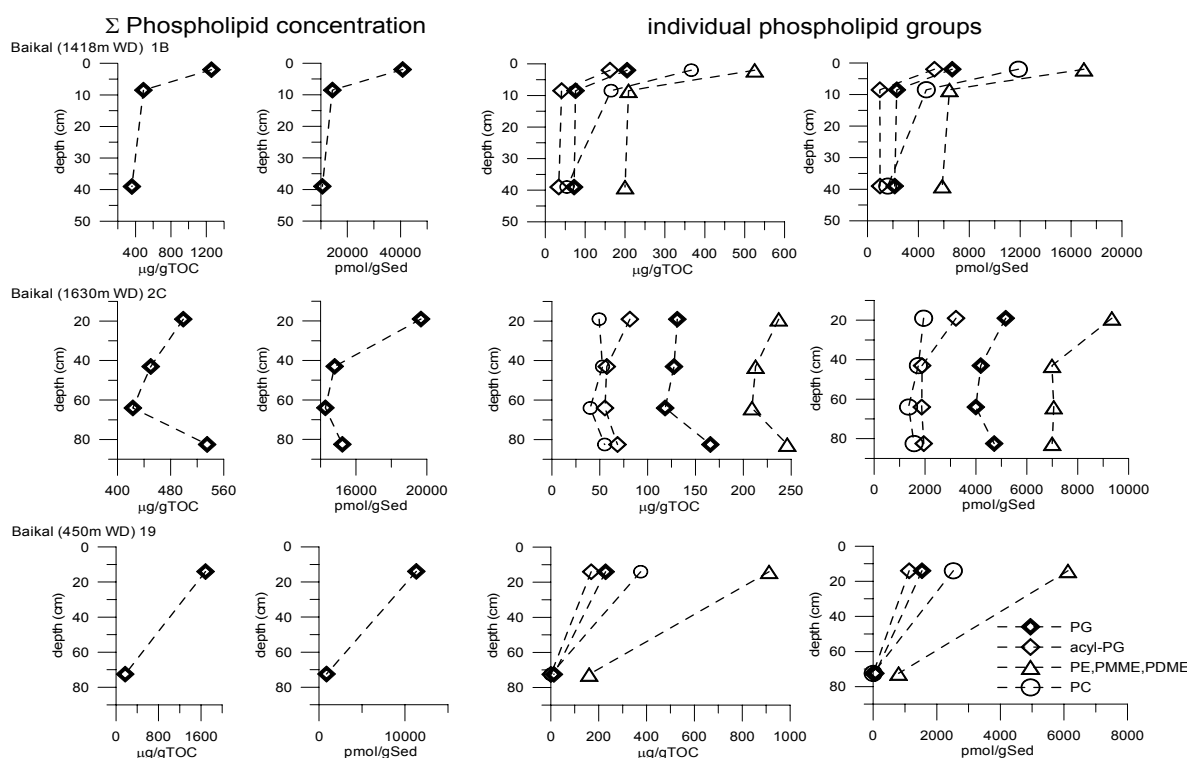


Fig.1. Sediment depth profiles of Lake Baikal bacterial phospholipids, plotted as sum and for main individual PL groups (in $\mu\text{g/gTOC}$ and pmol/g Sed)

References

- Colwell, F., Matsumoto, R., Reed, D., 2004. *Chem. Geol.* 205, 391-404.
 Niepel, T., Meyer, H., Wray, V., Abraham, W.-R., 1998. *J. Bact.* 180, 4650-4657.
 Parkes, R.J., Cragg, B.A., Wellsbury, P., 2000. *Hydrogeol. J.* 8, 11-28.
 Sturt, H.F., Summons, R.E., Smith, K., Elvert, M., Hinrichs, K.-U., 2004. *Rapid Commun. Mass Spectrom.* 18, 617-628.
 Zink, K.-G., Wilkes, H., Disko, U., Elvert, M., Horsfield, B., 2003. *Org. Geochem.* 34, 755-769.
 Zink, K.-G. & Mangelsdorf, K., 2004. *Anal. Bioanal. Chem.* 380, 798-812.

PMP-9: The influence of bacteria on microhabitat selection by benthic foraminifera

J. Brandsma¹, A.M. Langezaal², M. Schmid³, S. Schouten¹, E.C. Hopmans¹,
G.J. Van der Zwaan², M. Jetten³, J.S. Sinninghe-Damsté¹

1) Royal Netherlands Institute for Sea Research (NIOZ), Department of Marine Biogeochemistry and Toxicology, P.O. Box 59, 1790 AB Den Burg, The Netherlands (e-mail: brandsma@nioz.nl)

2) Utrecht University, Faculty of Earth Sciences; P.O. Box 80021, 3508 TA Utrecht, The Netherlands

3) Radboud University Nijmegen, Department of Microbiology; Toernooiveld 1, 6525 ED Nijmegen, The Netherlands

Foraminifera are a group of unicellular protozoa with calcareous shells that live in most marine environments, often in large quantities. Since foraminiferal shells reflect some of the geochemical parameters of their environment and have a good chance of being preserved in the fossil record, foraminifera are widely used as proxies in paleoenvironmental reconstructions. Specifically benthic foraminifera are believed to provide insight into the fluxes of oxygen and organic matter in marine sediments, as well as being indicators for basin depth. The validity of these proxy values however, depends strongly on the environmental behaviour of the individual foraminifera. Any (vertical) movement of the organism through the sediment column will influence the chemical composition of its shell, making for example the interpretation of isotope measurements more complex (*Van der Zwaan et al., 1999*).

To increase the proxy value of benthic foraminifera, a solid understanding of the environmental forcing on their behaviour is required. The vertical distribution and migration of benthic foraminifera in marine sediments is determined principally by the oxygen content, the flux of organic matter and the variability of the redox zonation. Additionally, recent research indicates that the presence and/or activity of bacteria may be important (*Langezaal, 2004*). Bacteria can for example provide an attractive food source, considering that the flux of organic material decreases downward through the sediment in both quantity and quality. Furthermore, bacterial activity determines the distribution and depth of the different redox zones, through processes such as nitrification and denitrification or sulphate reduction and may thereby influence foraminiferal depth distribution. Finally, bacteria may form a symbiotic relationship with benthic foraminifera, allowing the protozoa to thrive in anaerobic environments. In order to study the bacterial-foraminiferal relationship, it is therefore crucial to establish which bacterial groups or species are involved.

To this end, marine sediments taken from the Swedish Gullmarfjord are analyzed for their bacterial and foraminiferal content. The microbial community structure present is determined by molecular techniques, such as 16S rRNA combined with FISH. In addition, intact phospholipids, derived from the bacterial membranes, are extracted from sediment

samples, hand-picked foraminifera and bacterial cultures using a modified Bligh-Dyer extraction method and analyzed by HPLC-ESI/MS (following the method of *Sturt et al., 2004*). This allows for the attribution of specific lipids to selected bacterial groups or species that are most likely to influence foraminiferal behaviour. By focussing on intact phospholipids, any signals that are not derived from *in situ*, viable bacteria can be excluded.

Once the bacterial groups or species are identified, their spatial and temporal variations in distribution can be studied in experimental setups or *in situ* sediments. The possibilities of a geochemical, symbiotic or predatory interaction can hereby be addressed. Furthermore, the excellent preservation potential of both foraminiferal shells and bacterial lipids makes it possible to study the existence and evolution of this relationship in older sedimentary records.

References

- Van der Zwaan, G.J., Duijnste, I.A.P., Den Dulk, M., Ernst, S.R., Jannink, N.T., Kouwenhoven, T.J., 1999. Benthic foraminifers: proxies or problems? A review of paleocological concepts. *Earth-Science Reviews* 46, 213-236.
- Langezaal, A.M., Van Bergen, P.F., Van der Zwaan, G.J., 2004. The recovery of benthic foraminifera and bacteria after disturbance: experimental evidence. *Journal of Experimental Marine Biology and Ecology* 312, 137-170.
- Sturt, H.F., Summons, R.E., Smith, K., Elvert, M., Hinrichs, K.-U., 2004. Intact polar membrane lipids in prokaryotes and sediments deciphered by high-performance liquid chromatography/electrospray ionization multistage mass spectrometry – new biomarkers for biogeochemistry and microbial ecology. *Rapid Communications in Mass Spectrometry* 18, 617-628.

PMP-10: Insights into patterns of carbon flow in natural ecosystems using stable isotope labeling

S.I. Bühring^{1,4}, M. Elvert¹, S. Sievert^{2,3}, U. Witte⁴, K.-U. Hinrichs¹

1) Organic Geochemistry Group, DFG-Research Center Ocean Margins & Dept. of Geosciences, University of Bremen, P.O. Box 330 440, D-28334 Bremen, Germany

2) Biology Dept., Woods Hole Oceanographic Institution, Woods Hole, MA 02543, USA

3) Hanse Institute of Advanced Studies, 27753 Delmenhorst, Germany

4) Max Planck Institute for Marine Microbiology, Celsiusstrasse 1, 28359 Bremen, Germany

The use of stable isotope labeled substrates is a promising approach to get insights into carbon processing in natural environments. In combination with biomarker analysis it enables direct identification of microbes involved in specific biogeochemical processes and also allows incorporation of prokaryotes into food web studies. The great advantage of stable isotope labeling experiments is that they do not suffer from legal restrictions and health problems associated with radioisotopes and therefore can be used directly in the field (Boschker and Middelburg 2002). Studies in natural environments preserve the complexity of an ecosystem and minimize artifacts related to experimental conditions.

We will present the highlights from three studies that utilized the ¹³C-labeling approach. The first study aimed to elucidate the fate of a settling phytoplankton bloom in a fine sandy sediment in the German Bight (southern North Sea). A three-step time series of on-board incubations with 12h, 30h and 132h duration was performed. The study revealed a stepwise short-term processing of a settling phytoplankton bloom, with the bacteria reacting faster than the macrofauna.

In the second study in the highly oligotrophic deep Cretan Sea (1500 m water depth; Eastern Mediterranean), we determined the response pattern of a deep-sea benthic community to varying carbon inputs. *In situ* experiments with a chamber lander system were carried out using different amounts of ¹³C-labeled algal material to obtain insights into the relationship between amount, speed and amplitude of the benthic reaction. The partitioning of carbon within the benthic community differed between experimental setups. Preferential assimilation of label by bacteria combined with comparably low ¹³C-enrichment in CO₂ was observed for the experiment with low carbon load, while at high carbon load, the majority of the processed carbon was remineralized and only minor incorporation of label into bacterial fatty acids was detected.

The third investigation targeted the anoxic Zodletone sulfidic spring in Oklahoma/USA. ¹³C-labeled bicarbonate was used under light and dark conditions to elucidate the role of autotrophic processes in a prokaryotic community that builds up

extensive streaming structures in the emerging creek. Microscopic observations gave evidence for close associations of sulfur-oxidizing bacteria and cyanobacteria. In this consortium, most carbon is apparently fixed by phototrophic activity of cyanobacteria.

References

Boschker, H. T. S., and Middelburg, J. J. 2002. Stable isotopes and biomarkers in microbial ecology. *FEMS Microbiol Ecol*, 40, 85-95.

PMP-11: Using lipids and genetic markers to monitor microbial community growth in Arctic waters

R.Y. Dyda-Rearick, M. Suzuki, H.R. Harvey

Chesapeake Biological Laboratory, University of Maryland Center for Environmental Science, 1 Williams Street, Solomons, MD 20688 USA (e-mail: dyda@cbl.umces.edu)

Bacteria play critical roles in biogeochemical cycles, particularly in the uptake, transformation and release of organic matter. Standard culturing methods have been largely unsuccessful for natural bacterial communities, emphasizing the need for new approaches for their identification, quantification and the determination of bacterial contribution to organic matter cycling and formation. For this study, seawater culture experiments were conducted to monitor the response of naturally occurring bacterial communities to various sources of organic matter in the Arctic Ocean. These experiments consisted of carbon enrichments with diverse Arctic organic matter sources including ice algae, ice entrained debris and terrestrial peat as well as unamended controls. The phylogenetic response of the bacterial community to the organic matter enrichments was monitored by following changes in ribosomal RNA genes (rDNA) among different members of the bacterial community by length heterogeneity-polymerase chain reaction (LH-PCR). LH-PCR identifies PCR amplicons from differing organisms using the natural length variation found in the small subunit rDNA's. Samples for lipid analysis were collected to examine the relationship between lipids and bacterial community structure and the impact of differing sources of organic matter on the lipid distribution.

Results on bacterial community composition suggest that the community structure shifted in all of the treatments over time. rDNAs putatively identified as alpha and gamma-*Proteobacteria* contributed approximately equally to the bacterial community of the inoculum water. Over time, unamended controls showed a shift in community structure towards rDNAs putatively identified as beta and gamma-proteobacteria. Community composition was similar in the algal and ice rafted debris additions, with a dominance of LH-PCR fragments corresponding to members of the gamma *Proteobacteria* or *Flexibacter*, *Bacteroides* and *Cytophaga* phylum. Based on LH-PCR peak heights, gamma-*Proteobacteria* contributed to a substantial portion of the microbial community in all amended incubations. Peat enrichments with extended incubation times were dominated by LH-PCR fragments corresponding to the alpha-*Proteobacteria*. Clone library results for the peat enriched incubation show that approximately half of the clones are 99% related to the Arctic *Roseobacter* ARK10278 and

that at least 5 different phylotypes of *Roseobacter* contributed to the observed shift in community composition.

To link communities with organic carbon cycling, the distribution of fatty acids (GC and GC-MS) and intact polar lipids (LC-MS) in regrowth communities will be compared with rDNA to ascertain whether shifts in bacterial community structure over time were also reflected in bacterial lipids.

PMP-12: Biogeochemistry of microbial mats in coastal ponds of the Antarctic dry valleys

M.M. Hage, M.E. Uhle

The University of Tennessee, Department of Earth and Planetary Sciences, 1412 Circle Drive, 306 Earth and Planetary Sciences Bldg., Knoxville, TN 37996, USA (e-mail: mhage@utk.edu)

The McMurdo Dry Valleys of Antarctica are one of the driest, coldest, and windiest locations on earth, yet despite these extreme conditions, life exists. The Dry Valleys contain both recalcitrant paleo-carbon derived from ancient glacial till and modern carbon derived from photoautotrophic production (Burkins et al., 2000). One potentially important source of modern organic matter that has yet to be investigated is the numerous small ponds found throughout the dry valleys, but are concentrated near the coast, which contain photosynthetic benthic microbial and/or algal mat communities. The transient nature of these ponds results in the mat communities being exposed to prolonged periods of desiccation caused by the freezing temperatures and low vapor pressure typical of the polar desert ecosystem. The desiccated mats are then vulnerable to eolian and hydrologic transport, where upon rewetting, they may recover from complete desiccation in a new environment. The mat communities within the coastal pond ecosystem represent a significant source of highly labile organic carbon and understanding the biogeochemistry and transport of these mat communities may substantially affect currently-held views of nutrient cycling throughout the Dry Valleys ecosystem.

Microbial mat communities are complex, dynamic systems, typically dominated by only a few functional groups of microbes, with the driving force of the mat being photosynthesis by cyanobacteria and algae. Typically, microbial mats are no more than 5-10 mm thick with metabolically distinct groups co-existing, each in their own layer, with their activities resulting in steep physio-chemical microgradients (van den Ende and van Gemerden, 1994). It is believed that photosynthetic cyanobacteria are present near the surface of the Antarctic microbial mats, while sulfate-reducers inhabit the anoxic bottom layers. To understand microbial mat dynamics in the Dry Valleys specifically, different mat communities are being investigated at the individual layer, whole mat, pond, and ecosystem scales. Environmental factors such as water temperature, pH, salinity, conductivity, dissolved oxygen, dissolved inorganic carbon, and photosynthetically active radiation (PAR) have been measured for each pond. All microbial mat samples (bulk and individual layers) and pond water filters from different ponds are being analyzed for organic carbon, nitrogen and sulfur isotopic signatures, as well as for lipid (fatty acids and alkanes) presence and concentrations.

The coastal ponds have been found to be slightly basic freshwater and austral summer pond water temperature varies from pond to pond, typically between 5°-7°C. Preliminary data indicate that microbial mats are enriched in ^{13}C relative to other microbial mat communities found in lakes and streams elsewhere in the Dry Valleys. High growth rates in the ponds in conjunction with low CO_2 availability results in a CO_2 limited ecosystem, decreased C-fractionation, and bulk carbon isotopes enriched in ^{13}C . By examining the biogeochemistry of these communities at a variety of organismal and spatial scales, a better understanding of nutrient cycling in the Dry Valleys ecosystem may be developed.

PMP-13: Search for deep microbial communities in the terrestrial sediments of the Waikato coal area, New Zealand (DEBITS)

K. Mangelsdorf¹, K.-G. Zink¹, J. Kallmeyer², B. Cragg³, B. Horsfield¹

1) GeoForschungsZentrum Potsdam, Telegrafenberg, D-14473 Potsdam, Germany
(e-mail: Mangelsdorf@gfz-potsdam.de)

2) NASA Astrobiology Institute, Graduate School of Oceanography, University of Rhode Island, South Ferry Rd., Narragansett, RI, 02882, USA

3) School of Earth, Ocean and Planetary Sciences, University of Cardiff, PO Box 914, Cardiff, CF10 3YE, UK

In recent years the discovery of ubiquitous microbial life in deep subsurface successions (Parkes et al., 2000) has fundamentally changed our perception of how deep and under what conditions life can exist on Earth. Especially, how microbial life can survive in such deep and ancient formations, where free substrates should have been long ago consumed, is still unclear. It is hypothesized that nutrients for deep microbial life are continuously formed in the deep subsurface itself. It is known that not only fermentative alteration but also thermal maturation of the indigenous organic matter can release small substances, such as carbon dioxide, acetate and methanol, which can be used as substrates by deep microbial communities. Furthermore, molecular hydrogen produced by aromatization processes may enable autotrophic reaction such as methanogenesis and acetogenesis (see also Vu et al., this volume). Thus, these alteration and maturation processes are suggested to stimulate microbial activity in the deep subsurface.

During the DEBITS (Deep Biosphere in Terrestrial Systems) drilling campaign performed in Feb. and Mar. 2004 in the Waikato coal area (Taranaki basin, New Zealand) a 6 “ diameter core of 148 m Cenozoic sediments was drilled taking strict precautions to avoid any microbial surface contamination. Fluorescence microbeads have been used to estimate the penetration depth of the drill mud into the core material. To discard potentially contaminated outer core sections only the central part of the core was sampled under anaerobic conditions. The 148 m sedimentary section contains several organic rich layers of different maturity, ranking from peats to sub-bituminous coals, intercalated by claystones, siltstones and sandstones. The organic carbon rich layers represent potential “feeder” formations for deep microbial communities and the closely juxtaposed coarse grained sediments may act as a habitat for microorganisms. At ca. 76 m the core contains an unconformity. Sediments below this boundary have already been subsided to depth deeper than 2000 m and therefore have experienced significant higher temperatures.

To document the occurrence of viable deep microbial populations in the DEBITS core, the sample material is being investigated especially for intact phospholipids (PLs), which act as “life markers”, in that they are constituents of almost all organisms and degrade quickly after cell death (White et al., 1979). The detailed structural elucidation of the various PL head groups and the different acyl side-chains helps to characterize or to identify deep microbial communities. Adaptation mechanisms of deep microorganisms to increasing hostile environmental conditions with increasing depth appear to be reflected in the intact phospholipids geochemistry.

The occurrence and abundance of PLs have been and continue to be correlated with the organo- and lithofacies, therefore transects have been taken from the organic carbon rich “feeder” sediments into the adjacent coarser grained “carrier” sediments (silt- and sandstones). These profiles across the different lithological boundaries may reveal evidence for feeder-carrier pairs.

Sediments above and below the unconformity will be investigated with regard to their PL occurrence and distribution. It is of special interest, whether the sediments below the unconformity have experienced a paleopasteurisation during the process of subsidence and geothermal heating.

Other microbial biomarkers such as specific aliphatic hydrocarbons (crocetane, PMI, etc.) and hopanoids are also be investigated in great detail. Carbon isotope signals of individual compounds will be used to identify specific metabolic pathways.

The biomarker results will be compared with result from microbiological investigation done by our DEBITS project partners to demonstrate the occurrence of active microbial populations and to assign sedimentary PL distribution patterns to identified isolated bacterial species.

References

- Parkes, R.J., Cragg, B.A., Wellsbury, P., 2000. Recent studies on bacterial populations and processes in subseafloor sediments: A review. *Hydrogeology Journal* 8, 11-28.
- White, D.C., Davis, W.M., Nickels, J.S., King, J.D., Bobbie, R.J., 1979. Determination of the sedimentary microbial biomass by extractible liquid phosphate. *Oecologia* 40, 51-62.

PMP-14: Vertical distribution of lipid biomarkers and their stable carbon isotopic signature in marine cyanobacterial mats

T. Pape, A. Wieland, J.-H. Klock, W. Michaelis

Institute of Biogeochemistry and Marine Chemistry, University of Hamburg, Bundesstr. 55, 20146 Hamburg, Germany (e-mail: michaelis@geowiss.uni-hamburg.de)

Cyanobacterial mats are stratified microbial communities growing on illuminated surfaces thereby stabilizing sediments and thus contributing to coastal morphology. Cyanobacteria are principal primary producers and sulphate reduction is the dominant anaerobic mineralisation process. Close interactions between autotrophic and heterotrophic mat-building microorganisms in the upper most active layer of ~2-3 mm thickness lead to almost closed cycles of essential elements like C, O, and S ([1], [2]).

Distribution patterns and stable carbon isotopic ratios ($\delta^{13}\text{C}$) of lipid biomarkers, like hydrocarbons, fatty acids, alcohols, triterpenoids, and alkenones, were analyzed with depth to trace the origin and fate of organic matter in marine cyanobacterial mats. Highly resolved analyses at 1 mm depth intervals revealed significant microscale changes of the amount and distribution pattern of lipids attributed to specific mat-building bacterial groups, like cyanobacteria and sulfate-reducing bacteria, and to eukaryotes. The most active mat layer concerning C-cycling was identified and characterized by measurements of microgradients with microsensors for oxygen, pH, and hydrogen sulfide gas. Depth profiles for several lipids showed that beneath this surface layer lipid concentrations decreased and haptophyte-derived C₃₆-C₄₀ alkenones emerged. These data show that bulk analyses give only a general picture of lipid biomarker composition, ignoring stratification of some bacterial groups in response to physico-chemical gradients or temporary input of allochthonous organic matter in the form of algal or terrestrial material.

Significant changes with depth were also found for the $\delta^{13}\text{C}$ -values of lipid biomarkers diagnostic for specific microorganisms ([3]). These data suggest variations in the carbon isotopic composition of the substrates utilized or distinct modes of metabolism of a given bacterial group, like sulfate-reducing bacteria, in different depth horizons. Our data clearly show that biomarker and stable carbon isotope analysis at high spatial resolution reveal stratification patterns in modern microbial mats, as well as biogeochemical variations during decomposition of such microbially driven ecosystems. These observations could help to interpret the ancient counterparts of cyanobacterial mats preserved in the fossil record as stromatolites.

References

- [1] Wieland, A., Kühl, M., 2000. Short-term temperature effects on oxygen and sulfide cycling in a hypersaline cyanobacterial mat (Solar Lake, Egypt). *Marine Ecology Progress Series* 196, 87-102.
- [2] Wieland, A., Zopfi, J., Benthien, M., Kühl, M., 2005. Biogeochemistry of an iron-rich hypersaline microbial mat (Camargue, France). *Microbial Ecology*, in press (published online December 2004).
- [3] Blumenberg, M., Seifert, R., Reitner, J., Pape, T., Michaelis, W., 2004. Membrane lipid patterns typify distinct anaerobic methanotrophic consortia. *Proceedings of the National Academy of Sciences of the United States of America*, 101(30), 11111-11116.

PMP-15: The use of stable-isotope probing to study prokaryotic functional diversity in estuarine tidal sediments

J. Rinna¹, G. Webster^{1,2}, J.C. Fry³, A. Weightman³, R.P. Evershed³, R.J. Parkes¹

1) Cardiff School of Earth, Ocean and Planetary Sciences, Cardiff University, Main Building, Park Place, Cardiff, Wales, CF10 3YE, U.K.

2) Cardiff School of Biosciences, Cardiff University, Main Building, Park Place, Cardiff, Wales, CF10 3TL, U.K.

3) School of Chemistry, University of Bristol, Cantocks Close, Bristol, England, BS8 1TS, U.K.

A major challenge to microbial ecologists is to link the vast microbial diversity identified by culture-independent molecular techniques to the function of active prokaryotes within the environment. The technique of stable-isotope probing (SIP) has been used to link functional activity to microbial community structure by incubating environmental samples with ¹³C-labelled substrates and subsequently searching for specifically labelled biomarkers, such as either phospholipid derived fatty acids (PLFA), DNA and RNA (Boschker et al., 1998; Radajewski et al., 2000, 2002; Manefield et al., 2002).

Here we report results from a series of SIP experiments to investigate the functional prokaryotic diversity of an estuarine tidal flat from the Bristol Channel, Portishead, UK. Sediment samples were obtained from different biogeochemical zones based on the sediment sulphate/methane profile and presence of black FeS zones characteristic for active sulphate reduction. Sediment slurries (25% v/v) made up in artificial seawater were then set up and their composition adjusted to mimic different sedimentary zones. After an initial 12 h stabilisation period at 25°C, ¹³C-labelled substrates were added at a concentration of 100 µM. For slurries prepared with sediments taken from the aerobic and fermentative zone, ¹³C-labelled glucose was added whilst for slurries incubated under sulphate reducing (high sulphate) and under methanogenic conditions (low sulphate), ¹³C-labelled acetate was added. Addition of labelled substrate was repeated after 24, 48, 72, and 96 hours, respectively. Subsamples were taken at time zero and at regular time intervals thereafter. Selected samples were analysed for PLFAs including isotopic composition, and DNA using CsCl-EtBr density-gradient centrifugation, followed by amplification, DGGE and sequencing of dominant bands.

From CsCl density-gradient analyses the incorporation of ¹³C-labelled substrates was evident, and clearly demonstrated the potential of stable isotope probing with substrates in the sub-mM range. In addition, comparison of bacterial 16S rRNA gene PCR products from total community DNA with density-gradient fractionated DNA indicated that the changes observed in the total bacterial populations with time were due to organisms being able to utilise the labelled substrate. For example, DGGE analysis of DNA from the slurry incubated under

sulphate reducing conditions showed a clear change in the bacterial population after 24 hours. Afterwards community composition based on DGGE remained relatively stable with sequences from ^{13}C -DNA having a high sequence similarity to the Epsilonproteobacterium, *Arcobacter* sp. and two *Deltaproteobacteria*.

PLFA compositions showed a relative increase of unsaturated compounds and higher ^{13}C –incorporation with time in all experiments. This might be related to the general stimulation of activity in the slurry in comparison to sedimentary conditions, and thus a physiological response of the whole community. ^{13}C -incorporation resulted in a wide range of isotopic composition with values as high as 40-atomic% ^{13}C ($\approx 58,000\%$ vs V-PDB) for some compounds, underlining the high sensitivity of stable isotope probing and the potential to use of labelled substrates at much lower concentrations for future ecological studies. Also, with such high ^{13}C -enrichments of single compounds isotopic composition can be determined using GC/MS systems without combustion interface, thus making SIP PLFA analyses more widely applicable. Moreover, careful interpretation of molecular (and fragment) ions can give additional information with respect to pathways of phospholipid synthesis. For example, in the aerobic experiment mass spectra of hexadecanoic acid (and other compounds) clearly indicates the growth of a subpopulation almost exclusively using labelled glucose as substrate, in contrast anteiso branched fatty acids never showed a complete ^{13}C -labelling.

References

- Boschker H. T. S., Nold S. C., Wellsbury P., Bos D., de Graaf W., Pel R., Parkes R. J., and Cappenberg T. E. (1998) Direct linking of microbial populations to specific biogeochemical processes by ^{13}C -labelling of biomarkers. *Nature (London)* **392**, 801-805.
- Manefield M., Whiteley A. S., Griffiths R. I., and Bailey M. J. (2002) RNA stable isotope probing, a novel means of linking microbial community function to phylogeny. *Appl. Environ. Microbiol.* **68**(11), 5367-5373.
- Radajewski S., Ineson P., Parekh N. R., and Murrell J. C. (2000) Stable-isotope probing as a tool in microbial ecology. *Nature (London)* **403**, 646-649.
- Radajewski S., Webster G., Reay D. S., Morris S. A., Ineson P., Nedwell D. B., Prosser J. I., and Murrell J. C. (2002) Identification of active methylotroph populations in an acidic forest soil by stable-isotope probing. *Microbiology* **148**(8), 2331-2342.

PMP-16: Hydrogen and methane in hydrothermal fluids of the Logachev field, MAR

R. Seifert, S. Weber, M. Blumenberg, W. Michaelis

Institute of Biogeochemistry and Marine Chemistry, University of Hamburg, Bundesstrasse 55, 20146 Hamburg, Germany (e-mail: seifert@geowiss.uni-hamburg.de)

The priority program (SPP 1144) of the German research Foundation (DFG) is a multi-disciplinary approach to study hydrothermal systems at the Mid-Atlantic-Ridge (MAR) focussing on two areas (15°N and 4-11°S). A state-of-the-art remotely-operated vehicle (ROV) is used for precise well-located sampling and observation of the seafloor. Repeated investigations of the same areas over several years will elucidate temporal variations in the different processes at spreading axes (e.g. hydrothermal and biological activities).

Hydrothermal circulation cycles a volume of water equivalent to that of the total ocean through the oceanic crust once every million years. The chemical processes associated with these hydrothermal circulation systems have major influences on the composition of the oceanic lithosphere and seawater. The composition of the hydrothermal fluids is controlled by water/rock reactions over a wide range of temperatures and pressures, by microbial activity, by fluid phase separation and by mixing between hydrothermal fluids and cold seawater. Phase separation possibly plays an important role in many hydrothermal processes. Condensed vapour phases are gas-rich but metal-poor, making them uninteresting for mineral deposit formation but highly desirable for biological activity. The metal and salt-rich fluids on the other hand are not conducive to biological activity. Both fluid types can be vented at different times and at different locations within one vent field, the factors controlling when and how these different fluids are vented are unknown.

We here report concentrations and signatures of stable isotope of CH₄, H₂, and He in vent fluids and hydrothermal plumes. Samples were obtained during September 2004 at the Logachev hydrothermal field located at 15°N, MAR ([1]). This field belongs to the two so far known hydrothermal areas hosted by ultramafic rocks and which are influenced by serpentinization. The hydrothermal fluids are characterized by extremely high concentrations of dissolved hydrogen and methane and feed a massive vent fauna.

Comparison between the concentrations of CH₄, H₂ and He in the hydrothermal plume illustrates the relative stability of these gases. It shows that H₂ underlies much higher consumption rates compared to CH₄. Fluid samples obtained by ROV revealed up to 0.28 mmol L⁻¹ and 1.8 mmol L⁻¹ of CH₄ and H₂, respectively, with CH₄ / H₂ ratios mostly > 4. Calculated concentrations in the fluid endmembers are about 2.5 mmol L⁻¹ (CH₄) and

13.5 mmol L⁻¹ (H₂). Relatively ¹³C enriched signatures of methane (mean $\delta^{13}\text{C}$ of -12.2‰) are indicative of a methane source from abiotic CO₂ reduction.

A first calculation of fluid temperature at first intense mixing with seawater was done based on $\delta^2\text{H}$ of H₂. The obtained temperatures versus the respective H₂/CH₄ ratios (fig. 1) show a clear distinction between samples taken above a densely populated mussel field (38 ROV, low ratio and temp.) and those taken from active black smokers (64 and 53 ROV).

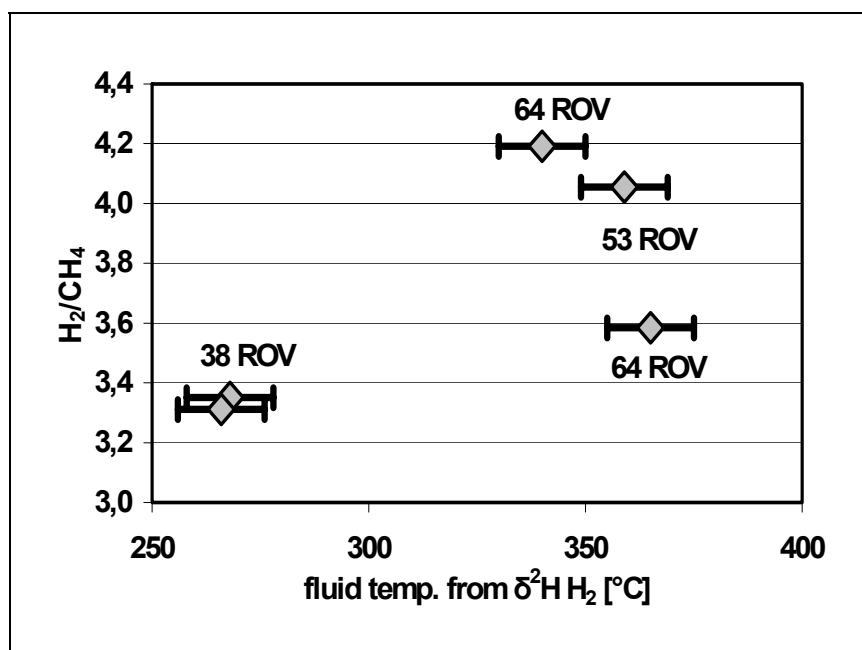


Fig.1. Fluid temperatures at first intense mixing with sea water (liquid), ROV samples M60/3, Logatchev hydrothermal field, MAR

References

- [1] Kuhn T., Alexander B., Augustin N., Birgel D., Borowski C., de Carvalho L.M., Engemann G., Ertl S., Franz L., Grech C., Herzig P.M., Hekinian R., Imhoff J.F., Jellinek T., Klar S., Koschinsky A., Kuever J., Kulescha F., Lackschewitz K., Petersen S., Ratmeyer V., Renken J., Ruhland, G., Scholten J., Schreiber K., Seifert R., Stiling J., Türkay M., Westernströer U., Zielinski F. (2004) The Logatchev hydrothermal field – revisited: preliminary results of the R/V METEOR Cruise HYDROMAR I (M60/3). *InterRidge News*, 13.

PMP-17: Biomarker evidence for aerobic and anaerobic oxidation of methane in diverse fluid venting environments in the Nile Deep-Sea Fan, Eastern Mediterranean

A. Stadnitskaia¹, J.S. Sinninghe-Damsté¹, NAUTINIL 2003 scientific party

1) Royal Netherlands Institute for Sea Research, P.O.Box 59, 1790 AB Den Burg, Texel, the Netherlands
(e-mail: alina@nioz.nl)

A comprehensive study of fluid seepage through the seabed has been performed during the NAUTINIL cruise (September-October 2003) in the Nile deep-sea fan (NDSF). Three mud volcanic provinces, the Eastern, Central and Western, were investigated with detailed observations and subsampling using the mini-submersible *Nautil*. These observations revealed various seepage environments, escaping-structure morphologies, associated carbonate precipitants and chemosynthetic symbionts. The venting activity within the study area can be grouped according to the geographical location of the explored seepage sites and mud volcanoes (MVs). Four MVs, Amon (Eastern province), North Alex (Central province), Chefren and Mikerinos (Mimes Caldera, Western province) were chosen for detailed biomarker examination. The main goal was to identify and compare the occurrence of specific archaeal and bacterial lipids in the sediments collected from different seepage environments with different emitted products (methane, wet gas, oil, sulfide, brines, etc.). Via biomarker study, we aim to characterize the environments and the microbial processes based on the oxidation of methane and its regional or sequential variability.

Archaeal biomarkers [pentamethylcosane, archaeol, hydroxyarchaeol, glycerol dibiphytanyl glycerol tetraethers(GDGTs)] were found in all investigated settings with different distribution patterns among the studied locations. The strongest signal for the anaerobic oxidation of methane (AOM) was detected in the North Alex MV (Central province) where free gas emanations were observed during dives with the submersible. Biomarkers such as diplopterol (aerobic methanotrophic bacteria), tetrahymanol (bacterial ciliates) mainly occur in MVs from the Western province (Caldera area). The Chefren MV is located within the Caldera area. It is characterized by the wide occurrence of brine fluids emitted together with methane and other hydrocarbons. Such fluid venting environments result in new ecosystems discovered during the cruise. The unexpected co-occurrence of specific sterols, previously found in cultures of aerobic methanotrophic bacteria *Methylococcus capsulatus* (Bird et al., 1971) and *Methylosphaera hansonii* (Schouten, et al., 2000), diplopterol, archaeol and hydroxyarchaeol was detected in these sediments. The $\delta^{13}\text{C}$ values of the sterols, diplopterol, archaeol and hydroxyarchaeol are all substantially depleted

(-60‰ to -90‰), indicating that carbon from methane is used for biomass production. The presence of these specific sterols signifies aerobic methanotrophy whereas archaeol, hydroxyarchaeol and specific GDGTs are characteristic for methane consumption in anaerobic environments. Therefore, this would imply local changes in the seepage environments reflected in consequent alteration of syntrophic associates which indicates that either archaeal lipids or the specific sterols are “relicts” from prior times when the redox zones in the sediment were differently positioned. It could also suggest a co-existence of contrasting ecological groups of microorganisms in the same environments, using methane as a carbon source. Both hypotheses have to be carefully checked with the results from on-going molecular ecology studies.

Composition of glycerol dibiphytanyl glycerol tetraethers (GDGTs), intact archaeal core membrane lipids, also demonstrate substantial variations among the MVs. GDGT patterns from the sediments and carbonates of North Alex MV (Central province) indicate active AOM. The composition of GDGTs in the Chefren MV (Western Province) is similar to that previously found in sediments from hydrothermally active site (30-65°C) in the Guaymas Basin with intense AOM (Schouten et al., 2003). Temperature measurements in the Chefren MV indicate that over 200 meters of warm brine the temperature is up to 57°C. It demonstrates that lipids biosynthesizing by archaea in the seepage from the Chefren MV (Western province) are different compare to these observed in the gas saturated sediments from the North Alex MV (Central province).

The study of fluid venting environments within the NDSF revealed diverse bacterial lipids and a variety of archaeal biomarkers. This signifies different syntrophic and symbiotic interactions among prokaryotes. The key factors determining the biogeochemical pathways and microbial mutual benefits in the various seepage environments are still not fully understood. This presentation will discuss newly found association of prokaryotic biomarkers and lipid signatures of AOM in relation to diverse fluid venting environments within the NDSF area.

References

- Schouten, S., S.G.Wakeham, E.C.Hopmans, J.S.Sinninghe Damsté. 2003. Applied and Environmental Microbiology 69: 1680-1686.
Bird C.W., J.M. Linch, F.J.Pirt, W.W.Reid. 1971. Nature 230: 473

PMP-18: Formation of iron sulfide nodules during anaerobic oxidation of methane

B.E. van Dongen¹, A.P. Roberts², R.D. Pancost¹

1) Organic Geochemistry Unit, Bristol Biogeochemistry Research Centre, School of Chemistry, University of Bristol, Bristol, UK

2) School of Ocean and Earth Science, University of Southampton, Southampton Oceanography Centre, Southampton, UK

Iron sulfide nodules (ISNs) are observed globally and in a range of sedimentary environments, where they can significantly complicate magnetostratigraphy due to the presence of ferromagnetic greigite (Fe₃S₄) (Roberts and Weaver in press). Remagnetisation of sediments is consistent with the secondary diagenetic origin of such nodules, but little is known about the processes leading to their formation and, in particular, late diagenetic growth of greigite. Thus, we examined three sulfide nodules to determine if they contained preserved lipid biomarkers and, if so, what the biomarker distributions revealed about (i) the origin of ISNs and (ii) the diagenetic growth of greigite that causes remagnetizations.

The ISNs were collected from the upper Pliocene Valle Rica section in a clay mine North East of Rome and analysed using GC, GC/MS and GC-IRMS. All three nodules contain a diverse group of compounds originating from sulfate reducing bacteria (SRB; fig.1). Such compounds include a variety of low-molecular-weight and branched alkanols and several non-isoprenoidal dialkyl glycerol diethers (DGDs). Also present is a tentatively identified unusual non-isoprenoidal macrocyclic DGD (I), which has been previously observed only New Zealand hydrothermal systems (Pancost et al. 2005). In addition, a variety of archaeal lipids are present and abundant, including archaeol and macrocyclic isoprenoidal DGDs containing one or two cyclopentane rings (II and III; Fig.1). Archaeol is found in a variety of settings but the abundances present here are comparable to those found in cold seep settings. The macrocyclic compounds are very uncommon and have so far only been found in a single cold seep setting (Stadnitskaia et al. 2003). The above indicates that a consortium of SRB and Archaea were present during the formation of ISNs and is suggestive of microbial communities currently found in cold seeps where methane is oxidized under anaerobic conditions (AOM) with sulfate serving as the terminal electron acceptor. Consistent with this, both SRB and archaeal lipid $\delta^{13}\text{C}$ values are depleted in ¹³C ($\delta^{13}\text{C}$ values typically less than -60‰). In addition to the microbial biomarkers, the presence of terrestrial biomarkers, predominantly *n*-alkanes and higher-molecular-weight (>C₂₀) *n*-alkanols, and lower abundances of marine biomarkers is consistent with formation of sulfide nodules in coastal marine sediments.

This is the first report that lipid biomarkers are present in association with ISNs, and thus, can be used to evaluate the microbial assemblage associated with their formation. Reduction of sulfate during AOM mediated by Archaea and SRB causes a late diagenetic increase in pore water sulphide concentrations. However, in many cold seep settings, while

significant authigenic carbonate crusts are formed, ISNs are not reported. Thus, the formation of ISNs, and particularly greigite, is probably contingent on the specific organisms present and their physiology, e.g. intracellular precipitation of sulfides, and environmental conditions, e.g. iron availability. Indeed, the role of very specific archaea and SRB that may not be ubiquitous in AOM sediments is suggested by the unusual occurrence of macrocyclic diethers. Moreover, our work indicates that upward migration of methane in marine sediments can have a profound impact on the paleomagnetic record and that the depositional environment should be considered when evaluating such records.

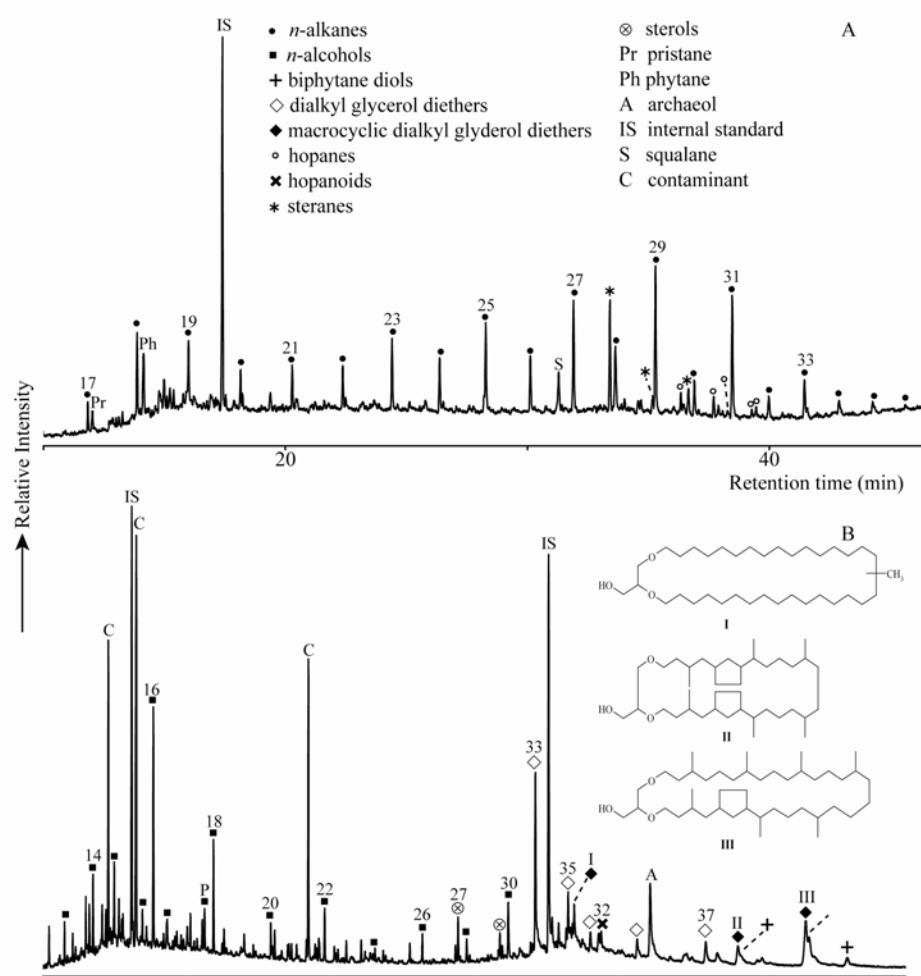


Fig.1. Total ion currents of (A) the unsaturated hydrocarbon fraction and (B) the polar fraction of an iron sulfide nodule. Numbers indicate carbon chain length. Contaminants are generally plasticizers and probably derive from storage of nodules.

References

- Roberts, A.P. and Weaver, R. *Earth Planet. Sci. Lett.* in press.
 Pancost, R. D.*, Pressley, S., Coleman, J. M., Benning, L. G., and Mountain, B. W. (2005) Lipid biomolecules in silica sinters: Indicators of microbial biodiversity. *Environmental Microbiology* 7, 66-77.
 Stadnitskaia, A., M. Baas, M. K. Ivanov, T. C. E. van Weering and J.S. Sinninghe Damsté (2003). *Archaea* 1(3): 165-174.

PMP-19: Biomarker analysis of microbial diversity in groundwater-related salt seep sediments of the Salt basin, NebraskaJ. Fang¹, O. Chan¹, R.M. Joeckel², Y. Huang³, Y. Wang³, D.A. Bazylinski⁴, T.B. Moorman⁵

1) Department of Geological and Atmospheric Sciences, Iowa State University, Ames, IA 50011
(e-mail: jsfang@iastate.edu)

2) School of Natural Resources, University of Nebraska, Lincoln, NE 68588

3) Department of Geological Sciences, Brown University, 324 Brook Street, Providence RI 02912

4) Department of Biochemistry, Biophysics, and Molecular Biology, Iowa State University, Ames, IA 50011

5) USDA/ARS National Soil Tilth Laboratory, 2150 Pammel Drive, Ames, IA 50011-4420

Lipids extracted from a saline seep in the Salt Basin of Lancaster County, Nebraska include alkanes, alkenes, alkanols, phytol, C₂₇₋₃₀ sterols, C₃₀₋₃₂ hopanoids, tetrahymanol, membrane glycolipid and phospholipid fatty acids, and lipopolysaccharide fatty acids. Biomarker profiles suggest that Salt Basin brine seeps support a unique microbial ecosystem adapted to high salt concentrations, sulfidic environment. The phospholipid fatty acid and lipopolysaccharide fatty acid profiles suggest the presence of abundant sulfate reducing bacteria (SRB) in the black sulfidic mud of the basin. The SRB probably mediated the reduction processes of phytol in the anaerobic zone, as indicated by the detection of a number of degradation intermediates (pristenes, phytene, and phytadiene). The detection of large amounts of glycolipid fatty acids suggests the presence of abundant photosynthetic microorganisms (cyanobacteria, phytoplankton, and purple sulfur bacteria). These organisms probably play an important role in the saline seep environment. The abundant phytol detected provides further evidence of the presence of photosynthetic organisms. The $\delta^{13}\text{C}$ of phytol shows that most of the phytol was probably contributed by microalgae/cyanobacteria/higher plants, with a fraction (18%) from phototrophic sulfur bacteria. The sterol profile and the detection of polyunsaturated alkenes (C_{12:6}, C_{21:7}, C_{30:4}, and C_{30:5}) suggests the contribution of organic matter from microalgae. The C₃₀₋₃₂ hopanols can be attributed to cyanobacteria and methanotrophs in oxic regions of the water column. The bacterivorous ciliates and phototrophic sulfur bacteria living at the chemocline are likely source of tetrahymanol. Carbon isotopic composition of individual fatty acids and neutral lipids help pinpoint the source organisms of the lipids. These microorganisms constitute a unique and integrated ecosystem prescribed by the geochemistry of the Salt Basin.

PMP-20: Exploration of lipid classes and their molecular composition of cultured marine bacteria: progresses and paradigms towards bacterial proxy improvements**M. Laurence¹, L. Pinturier², H. Agogu ³, P. Lebaron³, M. Goutx⁴**

1) Laboratoire de Biog ochimie et Chimie Marines – UMR CNRS 7034 - IPSL – Case 134, Universit  P. et M. Curie, 4 place Jussieu – 75252 Paris CEDEX 05-France

2) Total AS – Research and Development-PO Box 168- 4001 Stavanger – Norway-

3) Laboratoire Arago - Universit  P. et M. Curie- BP 44 -66651 Banyuls Sur Mer CEDEX–France

4) Laboratoire de Microbiologie, G ochimie et Environnement Marins UMR 6117 –Universit  Marseille II – Case 907-13288 Marseille CEDEX 9- France

Measuring bacterial biomass is not straightforward, and confidence is largely gained through agreement among various methods, for instance cell counting and so-called “direct methods”, quantifying specific biomolecules of living microorganisms. The use of phospholipids, major lipid of viable bacteria, to estimate their biomass was developed by the pioneer work of White and coworkers and implies the use of conversion factors derived from *Escherichia Coli* grown in cultures. Furthermore, the molecular composition of phospholipids gives insight in microorganism consortium structure. Recent years have witnessed an increased interest of geochemists for applying phospholipid ester-linked fatty acids to characterize bacteria of marine and deep biosphere ecosystems (R tters et al., 2002; Zink et al., 2003). While this technique is routinely used to estimate soil bacterial biomass, seldom studies combine lipid characterization and microorganism counts in the marine environment.

To contribute to the improvement of proxies for marine bacteria, fifteen monospecific bacterial strains were isolated from the sea-surface microlayer and identified to the specific level. Their lipid composition was screened by Thin Layer Chromatography coupled to FID detection (Iatroscan) and by adsorption chromatography followed by GC-MS characterization of purified lipid fractions. In most cases, polar lipids predominate over other lipid classes. Phosphatidylethanolamine and phosphatidylglycerides + diphosphatidylglycerides were the dominant phospholipids. Monogalactosyldiglycerides were the sole glycolipids identified and they were also dominant in some actinobacteria, firmicutes, cytophaga and α -proteobacteria. Glycolipids are seldom reported in bacteria, which is possibly related to analytical issues (extraction procedure, identification). The fatty acid moieties of phospholipids and glycolipids are dominated by short chain branched and aliphatic acids, the well-known bacterial markers *iso* and *anteiso* C15:0 and C17:0 acids occur in almost all strains under study. Fatty acid composition of polar lipids differed from one strain to another, for instance *iso* and *anteiso* C19:0 and C21:0 were particularly abundant in *Brevundimonas vesicularis* and *iso* and *anteiso* C13:0 in *Exigobacterium auranticum*. Further differences concerned the contribution

of branched saturated acids, branched monounsaturated acids and lactones. Phospholipid cellular content of the studied strains spans over two orders of magnitude, and agrees well with values including the whole free-living bacterial consortium.

Besides phospho and glycolipids, other lipid classes occur at important levels in a few strains. Hydrocarbons are relatively more abundant in *Arthrobacter agilis*, and *Staphylococcus warnerii* and the characterization of their molecular composition is in process. Free fatty acids, mono and di-acylglycerol esters are degradation products of phospho and glyco-lipids and accounted for a variable portion of total lipids, without reaching such high levels as lysophospholipids observed in deep subsurface sediments (Zink et al., 2003).

Cultures are a powerful tool for bridging microbiology to geochemical analysis requirements to refine biomass conversion factors and to explore the levels of specificity of biomarkers. However not all bacterial species are amenable to culture. Studies combining microbiological data to phospholipids on natural ecosystems or microcosms are scant and often incomplete, however a joined examination of both types of data will be carried out to tackle biomass conversion factors adapted to the marine environment, and to discuss their validity.

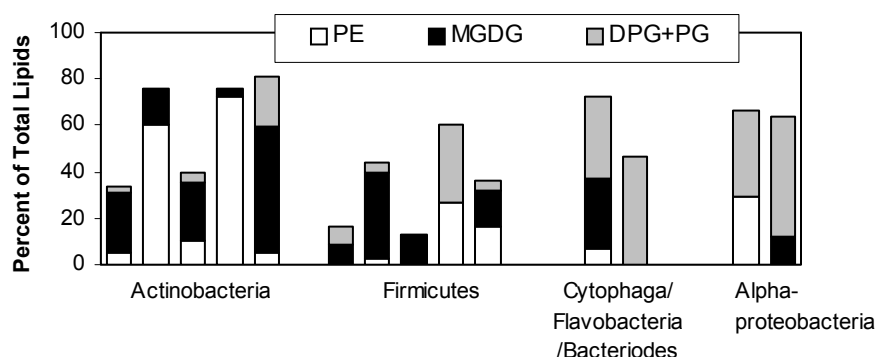


Fig.1. Major phospholipid classes (% of total lipids) in bacterial cultures

References

- Rütters H., Sass H., Cypionka H. and J. Rullkötter, 2002. J. Microb. Methods 48: 149-160.
 Zink K-G, Wilkes H., Disko U., Elvert M. And B. Horsfield, 2003. Org. Geochem. 34: 755-769.

PMP-21: Polar isopranyl glycerol ether lipids as biomarkers of living archaea in near-surface sediments from Nankai Trough

M. Oba¹, S. Sakata¹, U. Tsunogai²

1) Geological Survey of Japan, AIST, Tsukuba 305-8567, Japan (e-mail: m.oba@aist.go.jp)

2) Graduate School of Science, Hokkaido University, Kita-ku, Sapporo, 060-0810, Japan

Previous studies on microbial lipids have shown that methanogens and other archaea synthesize polar isopranyl glycerol ether lipids (PIELs) with polar head groups of organic phosphate ester and sugar residue as structural components of their biomembranes. By the analogy of phospholipids for living bacteria [1], PIELs can be considered biomarkers for living archaea, being hydrolyzed to lose the polar head groups immediately upon cell death or cell lysis. Based on this idea, we have undertaken to measure marine sediments for the concentrations and carbon isotopic compositions of PIELs in order to elucidate the biomass of living archaea.

Near-surface core samples were collected from Nankai Trough off Tokai, where occurrence of gas hydrates has been expected from previous seismic surveys and ocean drillings. Total lipid of sediments was extracted by the method of Bligh and Dyer modified to use trichloroacetic acid-acidified solvent [2]. The extracts were separated into apolar, less polar, and polar fractions using column chromatography on silica gel. PIELs in the polar fractions were hydrolyzed with HCl/methanol/chloroform (1:10:1, v/v/v) at 100°C for 2 h. Ether lipids in the less polar and polar fractions were trimethylsilylated with BSTFA and/or converted to hydrocarbons [3] to be analyzed with GC-MS, GC-FID and GC-C-IRMS for identification, quantification and compound-specific carbon isotopic analyses.

From sediment samples, we found high concentrations of PIELs with archaeol, *sn*-2-hydroxyarchaeol and glycerol dialkyl glycerol tetraethers as the core lipids. A similar set of ether lipids were detected from the less polar fraction, as expected to be generated from the hydrolysis of PIELs. PMI (2,6,10,15,19-pentamethylcosane), crocetane, and their unsaturated homologues were also detected from apolar fraction.

The concentrations of archaeol, *sn*-2-hydroxyarchaeol, PMIs and crocetanones tend to decrease with increasing depth, and anomalously high at the depth of 82 cm. Similar depth profiles suggest that these compounds have a common origin. Furthermore, the carbon isotopic compositions of these compounds at 82 cm were lower than -100‰ (vs. PDB). We thus consider that these compounds were derived mostly from methane-consuming archaea, such as ANME-2, whose lipids are characterized by high concentrations of *sn*-2-

hydroxyarchaeol, PMIs and crocetanones [4]. We should also mention that the process of anaerobic methane oxidation (AMO) in these samples has been inferred from the concentrations and $\delta^{13}\text{C}$ values of methane dissolved in porewaters.

In contrast, the concentrations of glycerol dialkyl glycerol tetraethers tend to increase with depth, and their $\delta^{13}\text{C}$ values were relatively high, ranging from -47‰ to -20‰. It is likely that these compounds were derived from non-methanotrophic archaea.

References

- [1] White, D.C., Davis, W.M., Nickels, J.S., King, J.D., Bobbie, R.J., 1979. Determination of the sedimentary microbial biomass by extractable lipid phosphate. *Oecologia* 40, 51-62.
- [2] Nishihara, M., Koga, Y., 1987. Extraction and composition of polar lipids from the archaeobacterium *Methanobacterium thermoautotrophicum*: effective extraction of tetraether lipids by an acidified solvent. *J. Biochem.* 101, 997-1005.
- [3] Schouten, S., Wakeham, S.G., Hopmans, E.C., Sinninghe Damste, J.S., 2003. Biogeochemical evidence that thermophilic archaea mediate the anaerobic oxidation of methane. *Appl. Environ. Microbiol.* 69, 1680-1686.
- [4] Blumenberg, M., Seifert, R., Reitner, J., Pape, T., Michaelis, W., 2004. Membrane lipid patterns typify distinct anaerobic methanotrophic consortia. *Proc. Natl. Acad. Sci.* 101, 11111-11116.

PMP-22: Labile biochemical indicators and biophile element isotopic ratio related with microbial distribution in sub-surface of semi-permafrost environment

Y. Takano^{1,2}, K. Marumo²

1) 21st Century COE on "Neo-Science of Natural History", Division of Earth & Planetary Sciences, Graduate School of Science, Hokkaido University, N8W10, Kita-ku, Sapporo 060-0810, Japan

(e-mail: takano@nature.sci.hokudai.ac.jp)

2) Institute of Geology & Geoinformation (IGG), National Institute of Advanced Industrial Science & Technology (AIST), AIST Central 7, 1-1-1 Higashi, Tsukuba, Ibaraki 305-8567, Japan

Permafrost- perennially frozen ground represents a unique stable, physical-chemical environment that has allowed the prolonged survival of microbial lineage at subzero temperatures incomparably longer than any other known habitats. Recently, the interest in the limit of life in low temperature environments has been growing [1]. It is known that permafrost contains a large number of a variety of ancient viable microorganisms. It is the only microbial community known to have retained viability over geological times and, upon thawing, to be able to renew their physiological activity. Microbial activities and biochemical indicators are correlatively interacted each other, hence systematical study of permafrost environment are required in terms of extremophilic biogeochemistry.

Here we present that core samples of semi-permafrost terrestrial sediments at Rikubetsu, Hokkaido, Japan were analyzed for the determination of product moment correlation coefficient (r) regarding amino acids, amino sugars, total organic carbon, total sulfur, enzymatic activities and microbial cell density. The $\delta^{13}\text{C}$ and $\delta^{15}\text{N}$ values of organic matter ranged from -24.7 permil to -28.1 permil and from $+2.0$ to $+6.5$ permil, respectively. These points plotted yield a straight line defined by a least-squares method and expressed by the following equation, $\delta^{13}\text{C} = 1.1^{15}\text{N} + 33.4$ ($r = 0.93$). The fluctuation of biophile isotope ratio is remarkable in the shallow depth, likewise viable microbial cell density. Abundance of sedimentary organic matters and the density of viable microorganisms were greatest at the surface and drastically decreased with the depth. D/L ratio of chiral amino acids and non-proteinous amino acids such as beta-alanine and gamma-aminobutyric acid showed negative correlation with the depth, which was evidence of processing refractory organic matter. The racemization reaction for labile organic matter on the surface could be markedly affected by the rapid hydrolysis: for examples, the initial racemization rate constant $k_{\text{ASX}1}$ was $1.1 \times 10^{-4} \text{ yr}^{-1}$ ($r = 0.98$) until about 2,200 yrBP. After the inflection point, the rate constant $k_{\text{ASX}2}$ was $2.4 \times 10^{-5} \text{ yr}^{-1}$ ($r = 0.93$) in the refractory organic matter. Vertical distributions of biomarkers are highly consistent with the subterranean microbial activities in the sediment. Consequently we clarified that biophile isotopic fluctuations in the labile

organic matter (LOM) phase are also more remarkable progress rather than refractory organic matter (ROM).

This research was partly funded by the Ministry of Education, Culture, Sports, Science and Technology of Japan through the Special Co-ordination Fund for the Archaean Park Project; an international research project on interaction between the sub-vent biosphere and the geo-environment.

PMP-23: Evidence of sub-vent biosphere: enzymatic activities and chiral amino acids in deep-sea hydrothermal sub-vent

Y. Takano^{1,2}, Y. Edazawa³, K. Kobayashi³, T. Urabe⁴, K. Marumo²

1) 21st Century COE on "Neo-Science of Natural History", Division of Earth & Planetary Sciences, Graduate School of Science, Hokkaido University, N8W10, Kita-ku, Sapporo 060-0810, Japan
(e-mail: takano@nature.sci.hokudai.ac.jp)

2) Institute of Geology & Geoinformation (IGG), National Institute of Advanced Industrial Science & Technology (AIST), AIST Central 7, 1-1-1 Higashi, Tsukuba, Ibaraki 305-8567, Japan

3) Department of Chemistry & Biotechnology, Yokohama National University, 79-5 Tokiwadai, Hodogaya-ku, Yokohama, Kanagawa 240-8501, Japan

4) *Department of Earth & Planetary Science, The University of Tokyo, 7-3-1 Hongo, Bunkyo-ku, Tokyo 113-0033, Japan*

Since the discovery of Galapagos submarine hot spring, deep-sea hydrothermal systems have been proposed to be plausible environments for chemical evolution and the origins of life on Earth. So far number of particular submarine ecological colonies have been recognized near black or clear smokers and its organic rich seafloor mat. Recently, ocean drilling experiments on submarine hydrothermal vents have made possible to clarify direct subjacent extreme environments [1].

Phosphatase is one of important enzymes for life on Earth, hence enzymatic activities is good evidence for microbial markers. Phosphatase activities were evaluated by using p-nitrophenyl phosphate as a substrate: Aliquot of pulverized sample was incubated with 0.1 ml of toluene, 2 ml of modified universal buffer (pH 8.0 or pH 6.5), 0.5 ml of 25 mM p-nitrophenyl phosphoric acid at for an hour, and then CaCl₂-NaOH was added for termination of the reaction. After filtration, absorbance at 410 nm was observed. Production rate of p-nitrophenol was calculated as phosphatase activity value. Here we present the vertical distribution of enzymatic activities under extreme condition up to 308°C and ca. 140 atm. Deep-sea hydrothermal sub-vent boring core samples were collected on Archaean Park Project Cruise for Suiyo seamount, Izu-Bonin Arc, Pacific Ocean (28° 33 N, 140° 39 E).

The vertical distribution of ACP and ALP presented here is essentially independent from the nature of the surface, with energy derived from chemical sources in the form of fluids discharging upward from deeper levels in the present study. It was demonstrated in the room experiment that enzymatic activities were not stable under simulated hydrothermal conditions. In the actual hydrothermal systems, however, large amounts of organic matter derived from microbial activities might be greater than that associated with thermal degradation in the sediment. Consequently, the apparent enzymatic activities of ACP and ALP would be determined on the base of biogenic organic matter and microbial activity in the sub-vent region.

This approach can make up a description of deep-sea subterranean chemistry and biology. Significant enzymatic activities were revealed in hydrothermal sub-vent systems, which is crucial evidence of vigorous microbial oasis. It is consistent with the fact that large enantiomeric excess of L-form biogenic amino acids were found in same core sequences [2] and water [3]. Hyperthermophiles and halophiles loving high pressure are likely widespread below hydrothermal vents, which extends the upper habitable zone.

This research was partly funded by the Ministry of Education, Culture, Sports, Science and Technology of Japan through the Special Co-ordination Fund for the Archaean Park Project; an international research project on interaction between the sub-vent biosphere and the geo-environment.

References

- [1] Urabe, T., Maruyama, A., Marumo, K., Seama, N., and Ishibashi, J. (2001) The Archaean Park project update. *Inter Ridge-Crest Res.*, **10**, 23-25.
- [2] Takano, Y., Kobayashi, K., Yamanaka, T., Marumo, K., and Urabe, T. (2004) Amino acids in the 308 °C deep-sea hydrothermal systems at Suiyo Seamount, Izu-Bonin Arc, Pacific Ocean. *Earth. Planet. Sci. Lett.*, **219**, 147-153.
- [3] Horiuchi, T., Y. Takano, K. Kobayashi, K. Marumo, J. Ishibashi, and T. Urabe. (2004) Amino acids in hydrothermal water samples obtained from deep-sea hydrothermal vents at Suiyo seamount, Izu-Bonin Arc, Pacific ocean. *Org. Geochem.*, **35**, 1121-1128.

**PM-1: Thermal alteration of polysulfide cross-linked polymers:
structural and $\delta^{34}\text{S}$ changes**

A. Amrani, W.S. Ahmad, E. Krein, Z. Aizenshtat

Casali Institute of Applied chemistry and Department of Organic chemistry. The Hebrew University of Jerusalem, 91904 Jerusalem, Israel

Most of the organically bound sulfur in immature Type IIS kerogen is transformed during maturation from polymeric S-S bonds in the source kerogen to aromatic sulfur (thiophene) in oil. Petroleum is usually ^{34}S enriched in comparison to its source kerogen. Based on column cuts (polarity) of the Dead Sea oils it has been suggested that aromatic sulfur is ^{34}S enriched compare with saturate fraction (Aizenshtat and Amrani, 2004). The present study focuses on the use of synthetically prepared analogues of Type IIS kerogens: polysulfide cross linked polymers (Krein and Aizenshtat, 1995; Amrani and Aizenshtat, 2004), their pyro-products and $\delta^{34}\text{S}$ changes during thermal alteration. The use of synthetically prepared polymers enables us to follow more easily the structural changes during these thermal changes. In order to elucidate the mechanistic controls on the various sulfur functionality due to thermal processes, we examined different fractions i.e. aliphatic, aromatic, polymeric. Well-defined (isotopically and structurally) sulfur cross-linked polymers were prepared and subjected to thermal alteration under different pyrolysis methods (dry, hydrous, continues-flow) and temperatures (130-300°C). The pyro-products were analyzed by GC (MS, FID, FPD), IRMS, NMR (^1H , ^{13}C) and elemental analysis. Hydrogen sulfide was trapped as Ag_2S and analyzed for $\delta^{34}\text{S}$. In general, we observed release of high amounts of H_2S and a sharp decrease in sulfur amount in the residual OM. During these processes a significant structural changes occurred in the pyro-products, mainly aromatization. The most dominant pyro-products were end-chain thiophenes. These reactions are accompanied by decrease in the H/C ratio in comparison to the unheated polymer. In all cases, we observed ^{34}S enrichment of the residual organic sulfur in comparison to the starting material. Pyrolyses conducted with elemental sulfur and non-containing sulfur compounds (such as $\text{C}_{14:1}$) produced variety of thiophens, thiols, and alkenes with different unsaturation positions than the original alkenes. In addition, sulfur cross-linked polymerization occurred as determined by Meli/MeI studies of the products. High amounts of hydrogen sulfide were released during these reactions, with significantly lighter $\delta^{34}\text{S}$ in comparison to the starting elemental sulfur and organic sulfur produced. The aromatization and thiophenes formation that observed during these experiments further support the extraction of hydrogen by active species of

sulfur (mainly $S_{x\cdot}$) through aromatization and isotopic discrimination to form organic sulfur (mainly thiophenes) and $H_2S_{(gas)}$. Detailed study of structural and isotopic ($\delta^{34}S$) changes in the different pyro-products produced will enhanced our understanding on the catagenetic mechanisms of Type IIS kerogens during maturation.

References

- Aizenshtat Z. and Amrani A.,(2004) Significance of $\delta^{34}S$ and evaluation of its imprint on sedimentary organic matter II. Thermal changes of Type II-S Kerogens Catagenetic stage controlled mechanisms. Study and conceptual overview. In Hill, R.J. et al. (Eds.)*Geochemical Investigations: A tribute to Isaac R. Kaplan*, The Geochemical Society, Special Publication No. 8, pp 35-50.
- Amrani, A. and Aizenshtat Z., (2004) Reaction of polysulfide anions with α,β unsaturated isoprenoid aldehydes in aquatic media: simulation of oceanic conditions. *Org. Geochem.* 35, 909-921.
- Krein E. B. and Aizenshtat Z. (1995) Proposed thermal pathways for sulfur transformation in organic simulation macromolecules: laboratory simulation experiments. In: Vairavamurthy, M. A., Schoonen, M. A. A. (Eds.)*Geochemical Transformation of Sedimentary Sulfur*. American Chemical Society Symposium Series 612, Washington, D.C. pp. 110-137.

PM-2: Possible biases in interpreting TMAH pyrochemolysis of proteinaceous matter considering glycine and alanine derivatives

N. Gallois, J. Templier, S. Derenne, C. Largeau

Laboratoire de Chimie Bioorganique et Organique Physique, CNRS UMR 7573, ENSCP 11 rue Pierre et Marie Curie, 75231 Paris Cedex 05, France

Nitrogen-containing organic compounds represent the second most abundant reservoir of nitrogen of the earth. Geochemical organic nitrogen occurs mainly in soil organic matter (SOM) in terrestrial pools and in dissolved or particulate organic matter (DOM, POM) in aquatic ones. Despite the important implication of these forms of nitrogen in environmental processes, their chemical structure and origin remain widely unknown likely due to the refractory nature of their source macromolecules (30 to 50% of total nitrogen in humic substances) (Schulten & Schnitzer, 1998). Recent studies (Knicker & Hatcher, 2001; del Rio *et al.*, 2004), using ^{15}N NMR spectroscopy, pointed to the occurrence of amide functions in these natural environments, thus suggesting that N is engaged in polar building blocks. As a result, pyrolysis in the presence of tetramethyl ammonium hydroxide (TMAH) appears as a powerful tool for the study of nitrogen-containing moieties. Indeed, the addition of TMAH was shown to (i) considerably increase pyrolysis efficiency and (ii) improve the detection of the pyrolysis products. TMAH which is a base reactant and a methylating agent, allows for the detection of non-GC amenable compounds as their methylated derivatives.

For a few years, TMAH-Py/GC/MS has been applied to the study of refractory OM from different sources, and focused on nitrogen-containing macromolecules (Garcette-Lepeck *et al.*, 2001; del Rio *et al.*, 2004; Zang *et al.*, 2001; Knicker *et al.*, 2001). In these works, many amino acids have been detected as their direct methylated derivatives (N,N-dimethyl methyl esters), and it appears that glycine (Gly) and alanine (Ala) were quasi-systematically reported within the identified amino acids, in higher proportion than expected from their natural distribution. The characterization of such compounds of low molecular weight, based on the MS features (58, 117) and (72, 131) for Gly and Ala, respectively, and hereafter referred to as A and B compounds, led to question the specificity of these derivatives as markers of their amino acid precursors.

To address this question, we pyrolysed amino acids, some peptides and Bovin Serum Albumin (BSA) in the presence of TMAH. TMAH-pyrolysis of free amino acids yielded the A and B compounds not only from Gly and Ala but also from other free amino acids such as serine, threonine (Fig. 1), tyrosine and tryptophan, besides the direct derivatives of the considered amino acids. An extensive study of TMAH-pyrolysis of the twenty proteinaceous

free amino acids led to distinguish different pathways depending on the considered amino acid and to explain the origin of the A and B compounds.

TMAH-pyrolysis of dipeptides revealed that they do not behave as the mixture of the corresponding amino acids but the A and B compounds were still observed for some dipeptides that do not contain either Gly or Ala (Val-Thr for instance). TMAH-pyrolysis of BSA also showed the A and B compounds in higher amount than expected based on the contribution of Gly and Ala.

So this study unambiguously establishes that other sources than Gly and Ala must be considered for their methylated derivatives in TMAH-pyrolysates and that these compounds released under Py-GC-MS in the presence of TMAH do not constitute specific markers for their amino acid precursor. However, the detection of these compounds still indicates the presence of amino acid-containing material. Macromolecules of higher molecular weight are now studied on the basis of these results.

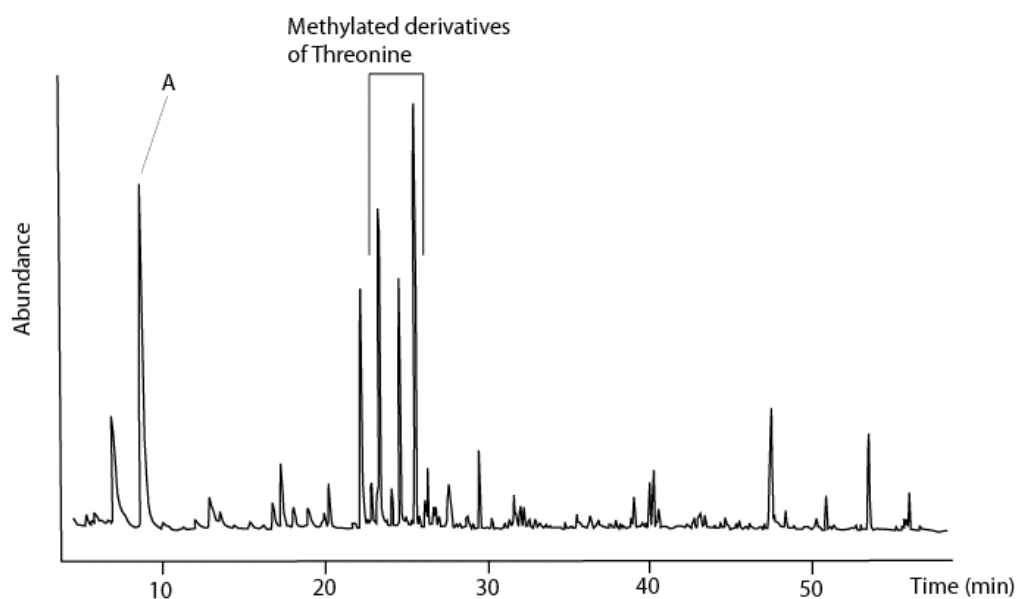


Fig.1. TIC chromatogram of the TMAH pyrochemolysis products released from threonine

References

- del Rio, J.C., *et al.*, (2004) *Organic Geochemistry*, 35, 993-999.
Garcette-Lepeck, A., *et al.*, (2001) *Journal of Analytical and Applied Pyrolysis*, 61, 147-164.
Knicker, H., *et al.*, (2001) *Organic Geochemistry*, 32, 733-744.
Knicker, H., *et al.*, (2001) *Organic Geochemistry*, 32, 397-409.
Schulten, H.R., *et al.*, (1998) *Biol Fertil Soils*, 26, 1-15.
Zang, X., *et al.*, (2001) *Journal of Analytical and Applied Pyrolysis*, 61, 181-193.

PM-3: Haloalkanes in polar geomacromolecules: myth or reality ?

V. Grossi¹, R. De Mesmay^{1,2}, A. Galtayries³, D. Raphel¹,
C. Largeau², S. Derenne²

1) Laboratoire de Microbiologie, Géochimie et Ecologie Marines (UMR CNRS 6117), Centre d'Océanologie de Marseille (OSU), Campus de Luminy - case 901, 13288 Marseille cedex 09, France

2) Laboratoire de Chimie Bioorganique et Organique Physique (UMR CNRS 7573), Ecole Nationale Supérieure de Chimie de Paris, 11 rue Pierre et Marie Curie, 75231 Paris cedex 05, France

3) Laboratoire de Physico-chimie des surfaces (UMR CNRS 7045), Ecole Nationale Supérieure de Chimie de Paris, 11 rue Pierre et Marie Curie, 75231 Paris cedex 05, France

During the last IMOG meeting in Krakow, we reported on the presence of series of C₁₂-C₃₀ 1-chloro-, 1-bromo-, and 1-iodo-*n*-alkanes in the pyrolysates of polar fractions of various sediment extracts (Grossi et al., 2003). The distribution of these compounds showed a strong even-over-odd carbon-chain lengths predominance (Fig. 1A), which strongly resembled that of some classical lipids such as fatty acids. These series of halogenated alkanes were present along with alkane/alkene doublets, alkylketones and alkylnitriles commonly observed upon pyrolysis of aliphatic geomacromolecules. At this time, the origin and/or mode of formation of these haloalkanes was not clearly understood. The absence of these compounds in the apolar hydrocarbon fractions of the same sediment extracts suggested one of the following origins: (i) haloalkanes are natural compounds of living organisms that, when reaching the sea-floor, can bind polar macromolecules; (ii) these compounds are formed *in situ* by halogenation (e.g. substitution of a functional group by halides) of sedimentary organic (macro)molecules; (iii) they can be formed artificially during pyrolysis.

The last hypothesis was tested by pyrolysing off-line individual model compounds (*n*-alkenes, linear alcohols and ketones, fatty acids, wax esters) in the presence of inorganic halides under the same conditions used for the analysis of sediment extracts (300°C, 20 min.). No halogenation reaction was observed during the treatment of heptadec-1-ene, tetradecan-1-ol, hexadecane-2-ol and hexadecane-3-one, whereas the pyrolysis of stearic acid or stearyl stearate in the presence of chlorinated salts both yield the formation of *ca.* 3-5% of 1-chlorooctadecane, in addition to other non-halogenated by-products.

The possible presence of inorganic halogenated salts in the aforementioned polar fractions of sediments extracts was thus investigated. Elemental and XPS analyses revealed that *ca.* 30-40% by weight of the fractions were composed of chlorine, which was present essentially under inorganic forms. In order to get rid of these salts, the organic fractions were intensively washed before being pyrolysed again. Haloalkanes were still detected in the obtained pyrolysates but their qualitative and quantitative distributions appeared

tremendously different from those observed without washing (Fig. 1). Since selective losses during washing are unlikely to be responsible for these differences, the preponderance of long-chain ($>C_{18}$) homologues before washing was due to artificial thermally-induced reactions. The detection of mid-chain homologues in the pyrolysate of the washed fraction remains questionable.

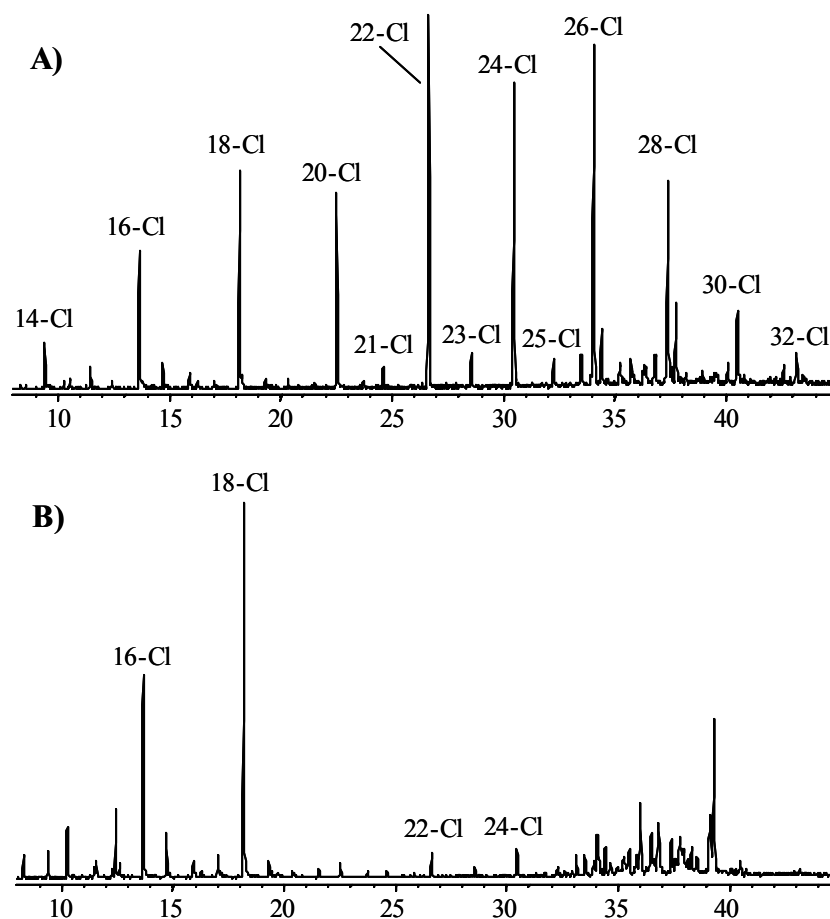


Fig.1. Mass chromatograms (m/z 91) showing the presence of 1-chloro- n -alkanes in the off-line pyrolysates of **A)** unwashed and **B)** washed polar fraction of a marine sediment extract

Although we cannot completely rule out the natural presence/formation of 1-halo- n -alkanes in marine sediments, our results indicate that these compounds can be at least partly formed artificially during pyrolysis of recent organic matter.

References

Grossi V., Derenne S., Raphel D., Largeau C., 2003. Haloalkanes in polar geomacromolecules: towards new pathways of organic matter diagenesis ? Oral presentation at the XXth IMOG meeting, Krakow 4-7 September.

**PM-4: Analysis of lignin phenols and alkanolic acids in lake and marine sediments
by on-line TMAH/thermochemolysis GC-MS:
comparison with alkaline CuO oxidation method**

S. Yamamoto¹, R. Ishiwatari²

1) Faculty of Education, Soka University, Tangicho 1-236, Hachioji, Tokyo 192-8577, Japan

2) Geotec Inc., Takaido-nishi 3-16-11, Suginami, Tokyo 168-0071, Japan

A high time-resolution analysis of organic matter in sediments is needed in order to obtain detailed information for paleoenvironment. Conventional organic matter analyses, however, are often time-consuming, because they need solvent extraction, chemolysis, fractionation, and a large amount of sediment sample for analysis. On-line TMAH/thermochemolysis GC-MS analysis consists of thermally-assisted hydrolysis and *in situ* methylation with tetramethyl ammonium hydroxide (TMAH) reagent. This method can analyze organic matter rapidly, and therefore, is expected to break down a drawback of the conventional organic matter analysis. Although the TMAH method has been applied to numerous natural samples, such as waxes, resins, woods and soil humic substances (Challinor, 2001), on-line TMAH analysis of organic matter in sediment samples is scarce. Furthermore, comparison of this method with the CuO oxidation method (e.g. Hatcher et al., 1995) is important for better use of the lignin data obtained by the CuO method for interpretation of the TMAH results. In this study, we examine reproducibility and an effect of reaction temperature at on-line TMAH/thermochemolysis of lignin and alkanolic acids in marine (offshore California) and lake (Lake Baikal) sediments using a Curie point pyrolyzer-GC-MS instrument, and compare the TMAH results with the CuO oxidation method. Typically, 5-7mg of dry fine powdered whole sediment sample was placed in a foil for pyrolysis (a pyrofoil) and 20 μ l of a methanol solution containing 25% TMAH and internal standard (e.g. *n*-C₁₉ alkanolic acid) was added. After methanol was evaporated to dryness, the pyrofoil was set into the pyrolyzer and heated at various temperatures (315–670°C) for 20 second. The TMAH products were introduced into a GC column and analyzed by MS.

Major TMAH-reaction products from sediment samples are lignin phenols and *n*-C₁₄-C₃₀ alkanolic acids. Lignin phenols are composed of aldehydes (vanillin: Vh, syringaldehyde: Sh), ketones (acetovanillone: Vo, acetosyringone: So), carboxylic acids (vanillic acid: Va, syringic acid: Sa) and cinnamyls (*p*-coumaric acid: Pc, ferulic acid: Vc). These products are the same as those obtained by the CuO method. Generally, a good linear correlation exists in terms of contents of lignin phenols between the on-line TMAH method (e.g. at 358°C and 590°C) and the CuO method, as shown in Figure 1. Correlation coefficients r^2 for lignin phenols between

the two methods range from 0.70 to 0.91, except for Pc and Vc.

The slope of the line plotted for the contents of lignin phenols and of alkanolic acids obtained by the TMAH method and the CuO method is different among different compounds. The slope (TMAH method against CuO method) is nearly 1 for ketones (Vo, So) and carboxylic acids (Va, Sa). The slope for cinnamyl phenols (Pc, Vc) is extremely high (14, 15), whereas those for lignin aldehydes (Vh, Sh) are low (0.38, 0.45). The high slope for Pc and Vc by the TMAH method might be caused by an efficient cleavage from non-woody tissue which is different from the CuO oxidation condition.

The slope for n-alkanoic acids is dependent on TMAH reaction temperatures. The slope for n-C₁₄-C₁₈ alkanolic acids which are probably mainly derived from glyceride of phytoplankton is generally nearly 1 (0.73) at 590°C, but it becomes 1.6 at a lower TMAH temperature (358°C). The slope for n-C₂₀-C₃₀ alkanolic acids, which are derived from wax, is nearly 1 (0.75, 0.78) at 358°C and 590°C. The differences in slope (TMAH method against CuO method) are probably associated with the differences in existence forms of compounds in sediments and/or thermal stability during TMAH reaction.

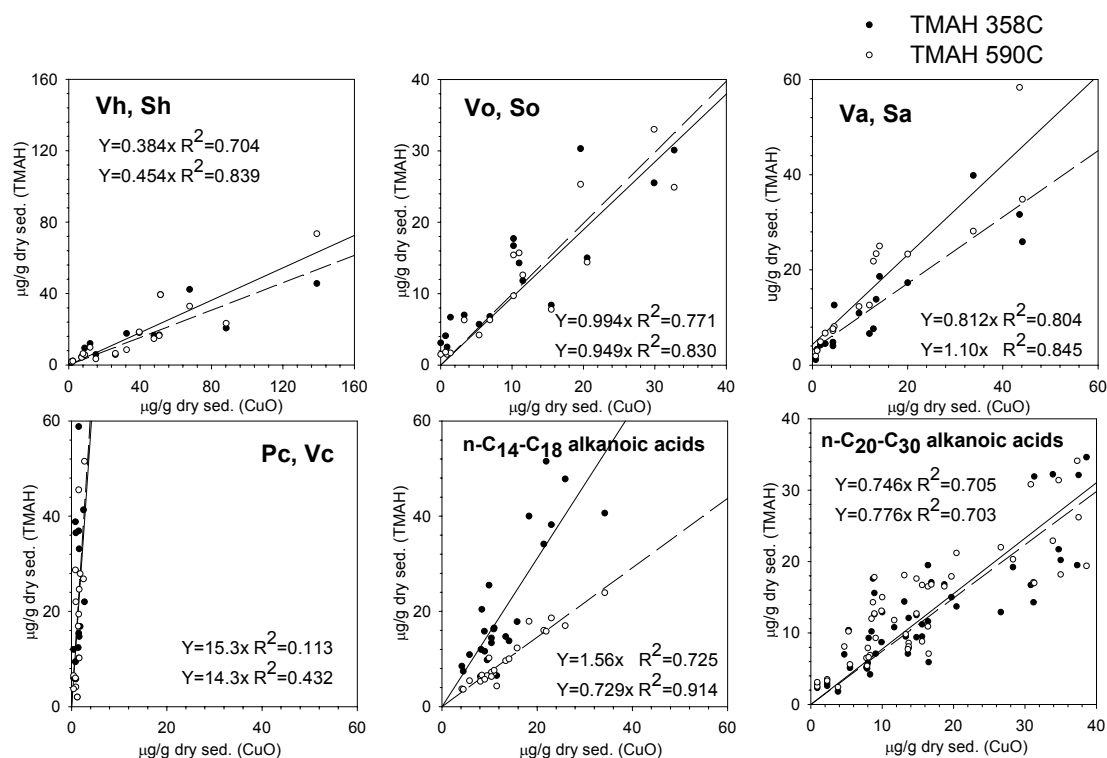


Fig.1. Relationship between products obtained by the on-line TMAH method and the CuO method. The upper equations and the correlation coefficients, and the lower ones are the results for TMAH reactions at 358°C and at 590°C, respectively

References

- Challinor, J.M. (2001) *J. Anal. Appl. Pyrolysis*, 61, 3-34.
 Hatcher, P.G., Nanny, M.A., Minard, R.D., Dible, S.D. and Carson, D.M. (1995) *Org. Geochem.*, 23, 881-888.

PM-5: Lignin and fatty acid records in Lake Baikal sediments over the last 130 kyrs: comparison with pollen analysis

R. Ishiwatari¹, S. Yamamoto², S. Shinoyama¹

1) Graduate School of Science, Tokyo Metropolitan University, Hachioji, Tokyo 192-03, Japan

2) Faculty of Education, Soka University, Hachioji 192, Japan

Lake Baikal is one of the largest and deepest freshwater lake in the world. This lake is located in high latitude and has not been glaciated throughout the late Cenozoic era. Therefore, its sediment is one of the best samples for investigating the records of biological responses to climatic changes in the past. Since 1990s, extensive studies including organic geochemical ones have been conducted to decipher a continental record of environmental changes in the northern hemisphere (e.g. Kashiwaya, 2003; Brincat, et al., 2000; Orem et al., 1997; Ishiwatari et al. 2005).

We present here analytical results of lignin phenols and fatty acids in a 10-m long sediment core Ver 98-1, St.6 (Academician Ridge) in Lake Baikal, the characteristics of organic matter compositions and environmental changes over the last 130 kyrs, including comparison with fossil pollen data (Oda et al., 2000). The sediment core covers marine isotope stages of 1-7. Lignin phenols and fatty acids were analyzed using an on-line TMAH thermochemolysis method (Yamamoto and Ishiwatari, 2005). Briefly, approximately 20 mg of dry fine powdered whole sediment sample with TMAH reagent and internal standard (e.g. *n*-C₁₉ alkanic acid) was added. After methanol was evaporated to dryness were wrapped in a pyrofoil (a foil for pyrolysis) and heated at 590°C for 20 second in a Curie point pyrolyzer (JHP-3). The methylation products were introduced into a HP-5 GC column and analyzed by MS (INCOS 50).

By this analytical procedure, we obtain lignin phenols (methylated derivatives) consisting of vanillyl phenols (vanillin: Vh, acetovanillone: Vo, vanillic acid: Va., total: V), syringyl phenols (syringaldehyde: Sh, acetosyringone: So, syringic acid: Sa, total: S), and cinnamyl phenols (*p*-coumaric acid: Pc, ferulic acid: Vc), and *n*-C₁₄-C₃₀ alkanic acids from our sediment samples. The results indicate that lignin phenols are abundant in sediments in interglacial periods (MIS 5e and 1) and extremely low in the MIS 4-2 period (Fig. 1). A palynological study indicates an expansion of coniferous forests in MIS 5e and 1 (Oda et al., 2000). Thus, an essential agreement exists between the temporal variations of the concentrations of lignin phenols (mg per g-dry sediment) with those (number of pollen grains per g-dry sediment) of fossil pollen. Comparison of lignin phenols with different types of fossil pollen suggests that Pc is associated with gymnosperm pollen.

Temporal variations of n -C₂₄-C₃₀ alkanolic acids are significantly different from those of lignin phenols. Significant amounts of these alkanolic acids are observed throughout the core in contrast to low values for lignin phenols in the glacial period. A considerable portion of n -C₂₄-C₃₀ alkanolic acids in these glacial sediments might have been derived from grasses and/or aquatic higher plants.

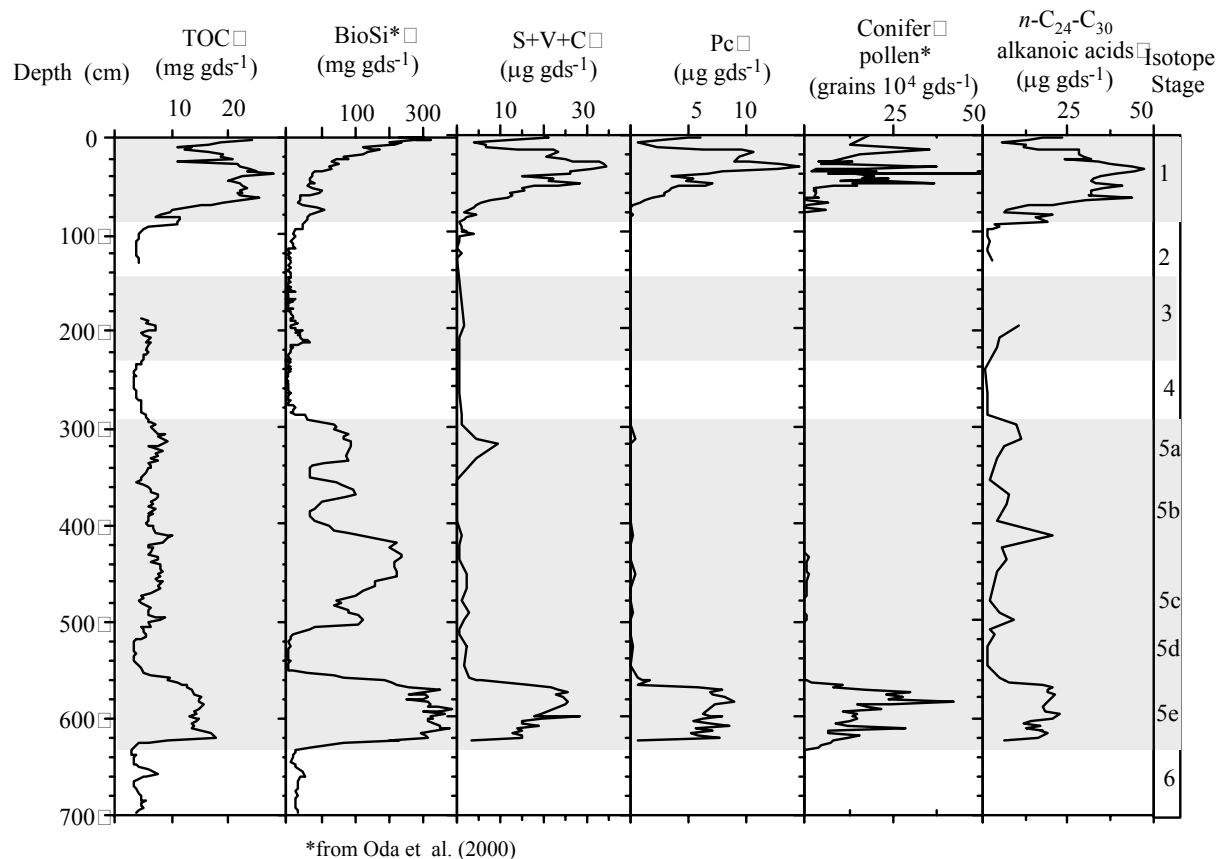


Fig.1. Vertical profiles of lignin phenols, fatty acids and fossil pollen in a Lake Baikal sediments

References

- Kashiwaya, K. (Ed.) Long continental records from Lake Baikal, Springer, Tokyo, pp.370 (2003).
 Brincat, D., Yamada, K., Ishiwatari, R., Uemura, H. & Naraoka, H. *Org. Geochem.*, **31**(4), 287-294 (2000).
 Orem, W.H., Colman, S.M. & Lerch, H.E. *Org. Geochem.*, **27**(3/4), 153-172 (1997).
 Ishiwatari, R., Yamamoto, S. & Uemura, H. *Org. Geochem.* (in press).
 Oda, T., Minoura, K., Fujimura, C., Nakamura, T. & Kawai, T. *Jpn. J. Palynol.*, **46** (2), 81-92 (2000).
 Yamamoto, S. & Ishiwatari, R. (this conference)

PM-6: Refractory organic matter from recent sediments: all melanoidins ?

A. Riboulleau¹, N. Tribovillard¹, F. Baudin²

1) CNRS UMR PBDS 8110- Université de Lille1, Bâtiment SN5, 59655 Villeneuve d'Ascq cedex, France
(e-mail: armelle.riboulleau@univ-lille1.fr)

2) CNRS UMR 5143, case 117, Université P. et M. Curie, 4 place Jussieu, 75252 Paris Cedex 05, France

Organic matter preservation processes have been studied for long in numerous settings and on sediments of various ages. Organic matter has gained the interests of several communities: soil science, geology, oceanography, among others, and this for various reasons. Due to the very different nature and age of studied samples, studying techniques are numerous and may differ considerably from one field to the other. Geologists deal with old refractory material called “kerogen” while oceanographers and soil scientists face relatively low weight and labile molecules and seldom care about the refractory “humin”. From these discrepancies it is relatively difficult to reconcile data from old and from recent sediments.

Regarding sediments deposited in marine setting, which is the case for most petroleum source rocks, the discrepancy between recent and ancient organic matter is particularly obvious. In ancient organic-rich sediments, preservation processes often call upon sulfurization of lipids or sugars and selective preservation while degradation-recondensation rarely accounts for very organic-rich samples. In contrast, in recent relatively organic-rich marine sediments, several studies of humin or protokerogens have emphasized the role of the degradation-recondensation pathway, indicated by the “melanoidin-like” characteristics of refractory material [1], [2], [3]. In the case of Cariaco Basin sediments where sulfurization was rather expected, such results have been assigned to the slow kinetics of sulfur incorporation into OM [3]. The above cited studies involved proto-kerogen isolation through the “classical” HF-HCl treatment [4], which is generally employed for “old” kerogen isolation. Applied on recent material, such strong acid hydrolyses have consequence on the OM [4]. In particular, melanoidins have been shown to form during hydrolyses used for algaenan extraction from fresh algal cultures [5]. It is therefore worth questioning to which extant melanoidins can be formed during extraction of proto-kerogen from recent sediments.

The present study explores the possibility of artifactual melanoidin formation during proto-kerogen isolation. To this end “melanoidin-rich” recent sediments from Cariaco Basin were chosen for re-examination. The studied sediment core was collected during P.I.C.A.S.S.O.-IMAGES11 campaign (May-June 2003). Refractory material obtained via the “classical” kerogen isolation treatment is compared with the one obtained via sequential extractions such as those used for fresh algal material [6].

References

- [1] Zegouagh, Y., Derenne, S., Largeau, C., Bertrand, P., Sicre, M.-A., Saliot, A., Rousseau, B., 1999. Refractory organic matter in sediments from the North-West African upwelling system: abundance, chemical structure and origin. *Organic Geochemistry* 30, 101-118.
- [2] Garcette-Lepecq, A., Derenne, S., Largeau, C., Bouloubassi, I., Saliot, A., 2000. Origin and formation pathways of kerogen-like organic matter in Recent sediments off the Danube Delta (northwestern Black Sea). *Organic Geochemistry* 31, 1663-1683.
- [3] Aycard, M., Derenne, S., Largeau, C., Mongenot, T., Tribovillard, N., Baudin, F., 2003. Formation pathways of proto-kerogens in Holocene sediments of the upwelling influenced Cariaco Trench, Venezuela. *Organic Geochemistry* 34, 701-718.
- [4] Durand, B., Nicaise, G., 1980. Procedures for kerogen isolation. In: Durand B. (Ed). *Kerogen*, Technip Paris, 33-53.
- [5] Allard, B., Templier, J., Largeau, C., 1997. Artifactual origin of mycobacterial bacteran. Formation of melanoidin-like artifact macromolecular material during the usual isolation process. *Organic Geochemistry* 26, 691-703.
- [6] Allard, B., Templier, J., Largeau, C., 1998. An improved method for the isolation of artifact-free algaenans from microalgae. *Organic Geochemistry* 28, 543-548.

PM-7: Organic matter fate in externally and internally buffered contact metamorphism processes in the Dębnik Anticline, South PolandA. Lewandowska¹, M.J. Rospondek¹, L. Marynowski²

1) Institute of Geological Sciences, Jagiellonian University, Kraków, ul. Oleandry 2a, Poland
(e-mail: ros@ing.uj.edu.pl)

2) Department of Earth Sciences, University of Silesia, Sosnowiec, ul. Będzińska60, Poland

Dębnik anticline is situated northwest of Kraków in the Southern Poland. It is build of the Devonian carbonates and marls, often containing organic matter, and underlain by the late Palaeozoic intrusion. Emplacement of the rhyodacite intrusion caused thermal metamorphism of dolomites resulting in the formation of ca. 300 m thick contact aureole [1, 3], and in the organic matter catagenesis accompanied by hydrocarbon generation. This metamorphism is marked by the distinct rock colour changes due to different organic matter preservation. The rocks distant to the contact are grey or brown and have R_o ca. 1.4 %. Towards the contact the dolomites are getting black, and vitrinite reflectance reaches $R_o=3.2$ %. At the contact rocks are white and are represented by predazzite build of the dolomite decomposition products: calcite and brucite [3]. The wide transitional zone between this black and white coloured rocks is build of layered rocks having appearance of stockwerks or breccias, where black dolomite is neighbouring white predazzite in the distance of centimetres. This study aims to explain differences of organic matter fate in co-existing black dolomite and white calcite-brucite marble (predazzite) in the same distance from the igneous rock intrusion.

The brown and black rocks contain 0.1-0.25 wt. % TOC. Organic matter is preserved, although in the strongly coalified form. Pyrolysis (Py(610°C)-GC-MS analysis) of the rock after extraction has not generated significant amounts of products, what is attributed to the organic compounds generation in the process of the thermal metamorphism. The natural pyrolisates were expelled from the source rock and some of them were trapped in the late generation of black calcite veins. The extractable organic matter reveals strong oxidation. The amounts of apolar fractions are minor with *n*-alkanes in the range C₁₃-C₃₆ having CPI ~1, and the extracts are rich in aromatic fractions. The aromatic fractions are composed of naphthalene, phenanthrene and their alkyl derivatives, anthracene, pyrene, dibenzo[*b*]furan, and often predominating dibenzo[*b*]thiophene. These fractions contain also some phenylphenanthrenes, polyphenyls and minor amounts of phenyldibenzo[*b*]thiophenes. Phenyl-naphthalenes and terphenyls show reversed distribution caused by overmaturation, with dominance of 1- and *o*- isomers, respectively (Fig. 1).

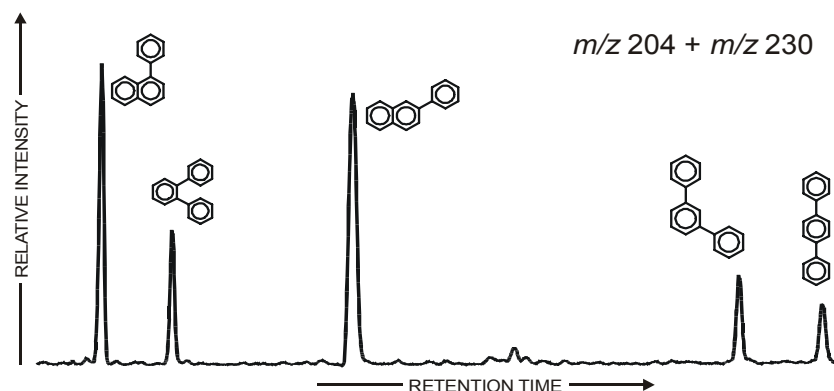
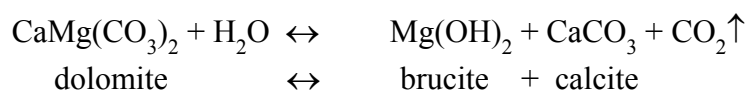


Fig.1. Partial mass chromatogram showing reversed distribution of phenylnaphthalenes (m/z 204) and terphenyls (m/z 230) in the overmature ($R_o=3.15\%$) sample from the black marly dolomite (the DB-35 column)

The studies of the white predazzites reveal the absence of detectable organic matter.

The formation of these black-white rocks can be explained in terms of internal and external buffering of metamorphic fluids resulting in the different organic matter alteration. The fate of the organic matter was controlled by the reaction of thermal decomposition and hydration of dolomite. This process led to the formation of calcite-brucite marble (predazzite) and carbon dioxide [2].



The metamorphic fluids circulated more vigorously along fissures. The fluid composition was externally buffered, and the CO_2 derived in this reaction was removed. The reaction was completed, and white predazzite composed of calcite and brucite formed. Brucite $\text{Mg}(\text{OH})_2$ strongly alkalized ($\text{pH} \sim 10.6$) the pore fluids enhancing organic matter removal, leading to the rocks whitening. The efficiency of the external buffering decreased away from the fissures. There, the reaction of dolomite decomposition internally buffered composition of metamorphic fluids. This process increased X_{CO_2} , and dolomite decomposition was restrained. Thus, this mineral is still the most important component of the rock. Organic matter was matured due to elevated temperatures and aromatic hydrocarbons formed.

Acknowledgements

This study was partially supported by grant PB0354/P04/2003/25 and DS/V/ING/12/2004.

References

- [1] Kozłowski, S., 1955. Intruzje porfirowe w grzbiecie Dębickim. *Biuletyn Instytutu Geologicznego* 97, 39-86.
- [2] Lewandowska, A., 2000. Contact metamorphism induced by the late Palaeozoic igneous activity in the Dębnik anticline. *Polskie Towarzystwo Mineralogiczne, Pr. Spec.*, 17, 41-46.
- [3] Lewandowska, A., 1998. Mineralogia skarnów magnezowych grzbieta Dębniaka. *Ph.D. thesis*, Jagiellonian University, Institute of Geological Sciences, Kraków, 173 p.

PM-8: Nitrogen functionality in various fractions of riverine dissolved organic matterJ. Templier¹, S. Derenne¹, F. Mercier², N. Barré², F. Miserque³, C. Largeau¹

1) LCBOP, CNRS UMR 7618, ENSC Paris, France (e-mail: joelle-templier@enscp.fr)

2) LAE, CEA/CNRS/Evry University, CE-Saclay France,

3) LRSI, CEA, CE-Saclay, France

Natural organic matter (NOM) is an ubiquitous component of natural waters with concentration up to 60 mg/l. Organic substances are transported from the continent to coastal marine environments via river discharge and contribute significantly to offshore water. River systems thus play a major role in the global biogeochemical cycles of carbon and nitrogen. Rivers are dynamic ecosystems, which integrate different inputs related to drainage basin and autochthonous production. Thus riverine dissolved OM (DOM) exhibits a large diversity in composition involving different reactivity in environmental processes such as solubilization, speciation and toxicity of xenobiotics. However, in spite of its importance and likely due to its refractory character, the precise chemical structure and origin of NOM is still partly unidentified. Characterization of organic nitrogen in terrestrial systems, which occurs primarily in the aquatic pool, is still incomplete, the chemical structure and origin of nitrogen compounds remaining widely unknown.

The purpose of this study was to investigate the forms of organic nitrogen in different fractions of riverine DOM. In a previous work, five fractions of DOM from two French rivers (Gartempe, Loire), termed hydrophobic (Gartempe: HPOA, Loire: HPO), transphilic (Gartempe: TPIA, Loire: TPI) and colloids (Loire) according to the fractionation procedure, were analysed by spectroscopic methods (FTIR, ¹³C NMR) and Curie point pyrolysis/GC/MS (1). Pyrolysis aimed at determining the chemical structure at the molecular level and hence the sources of these DOM fractions. A number of pyrolysis products were identified for each fraction, some of them being specific of macromolecular source. The results obtained established that hydrophobic fractions mainly originate from lignin-derived units, whereas the transphilic fractions mostly contain cellulose units with lignin derived ones and substantial amount of nitrogen-containing moieties. Characterization of colloidal fraction indicates the presence of compounds from bacterial origin, especially nitrogen-containing molecules that are characteristic pyrolysis products of peptidoglycans, along with lignin-derived units. Comparison of N-containing pyrolysis products detected in the five fractions reveals conspicuous differences in the detection of these compounds, though the contribution of nitrogen in these fractions does not vary in a range which can account for such a discrepancy (from 1.85% in HPO to 3.72% in TPI). Such pyrolysis products are noticeable in the HPO

fraction (N: 1.85%) while they are virtually absent in the HPOA one (N: 1.9%). Moreover the molecular structure of these compounds, which are mainly nitrogen- and oxygen- containing molecules, does not allow ascertaining their origin. These observations led to question, i) the occurrence of possible different nitrogen-macromolecule sources for the fractions, ii) the relative efficiency of pyrolysis according to the nature of the original macromolecule. The major biological sources of organic nitrogen such as proteins, amino sugars or tetrapyrrole pigments involving differences in the main nitrogen functionality, the aim of the present work was to determine the nitrogen functional groups present in the DOM fractions by including additional analytical approach, using two spectroscopic methods: X-ray photoelectron spectroscopy (XPS) and solid state ^{15}N NMR. The use of XPS to derive information on the chemical environment of one atom has not been applied to a large extent to the chemical analysis of organic matter (2,3). In the same way, due to its sensitivity approximately 50 times lower than ^{13}C NMR, ^{15}N NMR has not widely been used for study of natural biopolymers. However this method has clearly demonstrated the large dominance of amide nitrogen in soil OM (c.a. 80% of the total observable signal intensity) (4,5). Combination of these two methods reveals the presence of different functionality of nitrogen (amide, amine, and N-heterocycle), with variation in relative contribution depending on the considered fraction. Moreover it appears that Curie point pyrolysis does not account for the presence of the nitrogen in macromolecules with the same efficiency depending on the functional group involved. No detection of nitrogen pyrolysis products is observed in fraction where only amide groups are identified.

References

- (1) Templier, J., *et al.*, Organic Geochemistry, submitted for publication
- (2) Monteil-Rivera, F., *et al.*, (2000) *Analytica Chimica Acta*, 424, 243-255.
- (3) Mercier, F., *et al.*, (2002) *Organic Geochemistry*, 33, 247-255
- (4) Knicker, H., and Kögel-Knabner, I., (1998) In: Stankiewicz, B. A., Van Bergen, P. F., (Eds) *Nitrogen-containing macromolecules in the bio- and geosphere*. ACS, Oxford University Press, 339-356
- (5) Almendros, G., *et al.*, (2003) *Organic Geochemistry*, 34, 1559-1568

PM-9: Formation of alkylphenols during flash pyrolysisL.R. Boyd¹, B.G.K. van Aarssen¹, T.P. Bastow^{1,2}

1) Centre for Applied Organic Geochemistry, Curtin University, GPO Box U1987, Perth 6845, Western Australia

2) CSIRO Land and Water, Private Bag No 5, PO Wembley, Perth WA 6913, Australia

Alkylphenols can often be found amongst the products obtained from flash pyrolysis of kerogen, sometimes in very high relative abundances. As this analytical method is considered to minimize the occurrence of secondary reactions during the pyrolysis, the presence of alkylphenols in the pyrolysate is commonly inferred to reflect the presence of phenolic moieties in the kerogen.

Recently, a formation pathway for phenols present in crude oils has been suggested. This involves hydroxylation of alkylbenzenes *via* an electrophilic aromatic substitution, most likely during petroleum formation (Bastow et al., 2005). A typical distribution of alkylphenols in crude oils thus reflects the distribution of the alkylbenzenes present in the same oils. These distributions however, are quite different from those generally observed in pyrolysates of kerogen. In addition, the relative abundance of alkylphenols in crude oils is usually very low. This suggests that during pyrolysis alkylphenols may in fact be formed alkylbenzenes as secondary reaction products.

In order to facilitate the analysis of phenols present in pyrolysates of kerogen samples, an offline flash pyrolysis technique (OFP) was developed. Because the technique is offline, the resulting pyrolysates can be separated into less complex fractions and analysed in great detail. With the technique the sample was placed in the bottom end of a sealed, evacuated glass tube (~30cm x ~15mm i.d.). This end was then placed into a furnace. Upon release, volatile pyrolysis products immediately moved to the cooler part of the tube and condense. OFP of kerogens yielded compatible results to those obtained with online flash pyrolysis.

Using this new technique, alkylphenols were measured in the pyrolysates of two oil shales of different maturities and compared to the levels of alkylbenzenes released. For both shales, increasing the amount of sample used for pyrolysis dramatically increased the total abundance of alkylphenols formed relative to the alkylbenzenes (Figure 1). Interestingly, although the distribution of methylbenzenes changed, as shown by the relative decrease of xylenes, the distribution of methylphenols remained virtually the same.

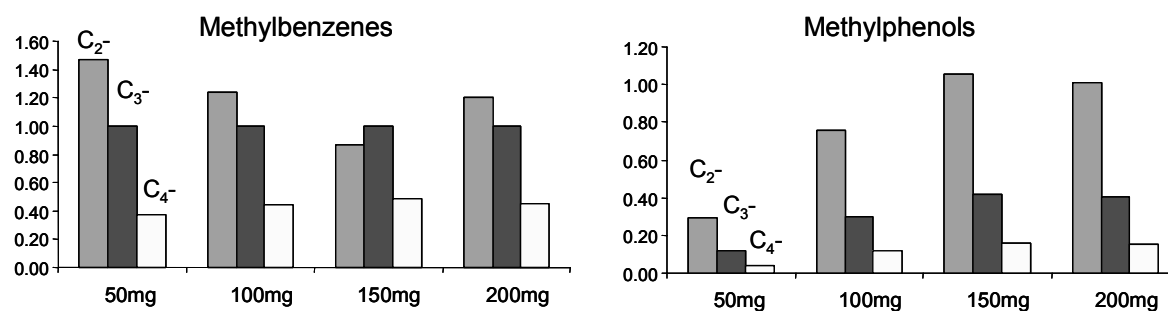


Fig.1. The change in abundance of the classes of methylbenzenes and methylphenols with an increase in sample volume. All abundances are relative to trimethylbenzenes

The correlation between the alkylphenols and alkylbenzenes suggests that formation of these compounds during pyrolysis is related. It is proposed that during pyrolysis the alkylbenzenes may be converted to alkylphenols by a hydroxylation reaction involving free radicals, possibly by reaction with water. Increasing the amount of sample may lead to more secondary reactions taking place, leading to an increased abundance of phenols.

The results strongly suggest that secondary reactions may play a larger role in flash pyrolysis than previously assumed. The amount of sample pyrolysed appears to have a large effect on the abundance and distribution of products formed, particularly the alkylphenols and alkylbenzenes, and interpretations of pyrolysis results should be carried out with this in mind.

References

Bastow, T.P., van Aarssen, B.G.K., Alexander, R., Kagi, R.I. (2005) Origins of alkylphenols in crude oils: Hydroxylation of alkylbenzenes. *Organic Geochemistry*, in press.

PM-10: Micromorphological and (bio)chemical organic matter changes in a formerly cutover peat bog : Le Russey, Jura Mountains, France

L. Comont, F. Laggoun-Défarge, J.-R. Disnar

ISTO, UMR 6113 CNRS/University of Orleans, BP 6759 45067 Orleans, France
(e-mail: laure.comont@univ-orleans.fr)

Peatlands have been exploited since the Middle Ages for diverse uses, including fuel, animal bedding and growth substrate in horticulture and agriculture. In many countries, these traditional peatland uses are now redundant, but the sites are being reappraised for their specific biodiversity and suitability for long-term carbon storage.

In order to monitor peat reaccumulation and hence long-term carbon sequestration in peatlands which have been abandoned or designated for restoration, it is essential to consider a wide range of indicators [1]. Among these indicators, it has previously been shown that physico-chemical properties of peat organic matter (OM) provide clues for the understanding of bog restoration processes [2].

Accordingly, the aim of the present study was to comprehend the processes of spontaneous peat regeneration in a cutover peatland through elemental, micromorphological and biochemical composition of the peat OM.

Le Russey is a *Sphagnum*-dominated cutover peatbog in the French Jura Mountains where peat cutting was stopped in 1984 (surface area: 27 ha; elevation: 864 m; precipitation: 1349 mm). The area that had been exploited comprises a range of natural regeneration stages from bare peat (FRA) to advanced regeneration stage (FRC) with mixed vegetation (*Sphagnum* spp., *Polytrichum strictum*, *P. commune*, *Eriophorum vaginatum* and *E. angustifolium*). The uppermost 50 cm of the peat were cored in zones FRA and FRC, respectively, and compared to a reference profile (FRD) taken from an un-exploited zone of the peatbog.

All core sections were wet-sieved at 200 µm. Bulk samples and fine-grained fractions were subjected to elemental (C, N), and micromorphological analyses. The cellulosic and hemicellulosic sugars of the fine-grained fractions were identified and quantified by gas chromatography.

Results show contrasting chemical and micromorphological OM compositions. In the bare peat (FRA) section, C/N values remain consistently high (~40). The peat is mainly composed of amorphous OM and structureless tissues, with rather high proportions of microbial secretions (namely mucilage), in the lower levels. In the advanced regeneration

stage (FRC), the C/N ratio decreases downcore with a clear threshold between the regenerating litter and the “old” catotelm peat. The “young” peat is also characterised by the presence of well-preserved tissues of *Sphagnum*, *Polytrichum* and *Cyperaceae*. In contrast, the underlying “old” peat shows characteristic features of intensive OM degradation (low C/N ratios and high proportions of amorphous OM and mucilage). In the un-exploited area (FRD), C/N ratios decrease progressively with depth, indicating progressive diagenesis. The uppermost peat OM is mainly composed of well-preserved *Sphagnum* tissues being gradually replaced by mucilage downcore.

Sugar analyses were performed on some specific peatland plants (*Cyperaceae*, *Sphagna* and *Polytrichum*) as well as on peat samples to identify biological sources and to ascertain the degree of plant material degradation. These analyses were carried out on the fine-grained peat fraction (<200 μ m) supposedly typical of humified material, i.e. with little or no unworked plant remains and relatively high proportions of products of microbial syntheses. Globally, the results of the molecular approach support and complement those obtained by elemental analysis and micromorphological studies. In particular, in the advanced regeneration stage (FRC), the evolution with depth of total, cellulosic and hemicellulosic sugars confirm the subdivision of the profile into two distinct stages: the “young” peat section (0- 25 cm) presenting higher sugar content than the « old » peat (below 25 cm depth).

In summary, contrary to commonly perceived ideas, amorphisation does not correspond to “chemical” degradation. Even in the fine-grained fraction supposedly representing the most humified material, high proportions of sugars (around 180-250 mg.g⁻¹ of sample) are still present. Even these compounds that are usually considered to be highly biodegradable, are well preserved both in intact and disturbed zones of the peatbog. The high sugar preservation allows use of such compounds both as indicators of humification and as tracers of plant sources.

References

- [1] Chapman S., Buttler A., Francez A.-J., Laggoun-Défarge F., Vasander H., Schloter M., Combe J., Grosvernier P., Harms H., Epron D., Gilbert D. & Mitchell E. (2003). Exploitation of northern peatlands and biodiversity maintenance: a conflict between economy and ecology. *Front. Ecol. Environ.*, 1(10): 525-532.
- [2] Grosvernier P., Matthey Y and Buttler A 1995 Microclimat and physical properties of peat :new clues to the understanding of bog restoration processes. In Restoration of temperate wetlands, Eds B D Wheeler, S C Shaw, W S Fojt and R A Robertson.pp 437-450. John Wiley & Sons, Chichester, UK.

**PM-11: Sorption of organic matter on clay minerals in aquatic system and influence on sedimentary organic preservation.
An example of lacustrine environment (Lac Pavin, France)**

S. Drouin, M. Boussafir, J.-L. Robert, P. Albéric

ISTO (UMR 6113, CNRS - Université d'Orléans), Bâtiment Géosciences, Rue de Saint Amand, BP. 6759, 45067 Orléans Cedex 2, France (e-mail : Sylvain.Drouin@univ-orleans.fr)

Sorption of organic molecules on clay surfaces in aquatic environment influence organic sedimentation fluxes. It is well known that mineral sorption affects transport of natural organic matter to bottom water and to sediments. These physical and chemical interactions produce a flocculation of organo-mineral complexes and then increase weight of sedimentary fractions. The resulting sedimentation rate reduces risks of bacterial recycling and/or oxidation. Other studies revealed that sorption also influences the fate of organic matters in sediments ([1]). Direct contacts between clay minerals and organic molecules allow creation of organo-mineral assemblages in sediments, and influence organic molecules availability to benthic fauna and bacteria ([2]). Many studies concluded that mineral sorption and chemical linkage created can be considered as one of preservation mechanism, leading incorporation of organic matter in sediments.

Many questions in this topic remain unresolved. Does sorption of organic molecules on clay minerals can occur in the water column (before sedimentation)? What is the behaviour of clay/organic matter complexes in the deep water? Does this sorption really protect organic molecules from bacteria recycling and oxidation in the water column?

The aims of this work are to test the possible *in situ* sorption of natural organic molecules in lacustrine environment, in different fresh and bottom water and for various interaction times. In this respect, the behaviour of natural organic matter in presence of synthetic saponites (high and low charge Na-smectites) has been studied in oxic and anoxic levels of an oligotrophic meromictic crater lake (Lac Pavin, Massif Central, France). Six clay samples positioned in the oxic layer and four clay samples in the anoxic deep layer have interacted with lake water during 3, 10 and 21 days. Clays were positioned in traps, closed by two hydrophilic 0.45µm Durapore[®] membranes, allowing only circulation of dissolved organic matters and there interaction with clays. After runs, interactions were interrupted on the spot by centrifugation, and clays were separated from water immediately.

Rock-Eval analysis shows the presence of organic carbon associated with clays after interaction in Lac Pavin. Failure of extractions by classical organic solvents suggests a very stable bonding between organic matters and clay particles. The molecular Pyro-GC/MS

investigation, performed on these clays, reveals the presence of n- and iso- alcohols, n-alkanes, iso-alkanes and fatty acids, in significant amounts (Fig. 1).

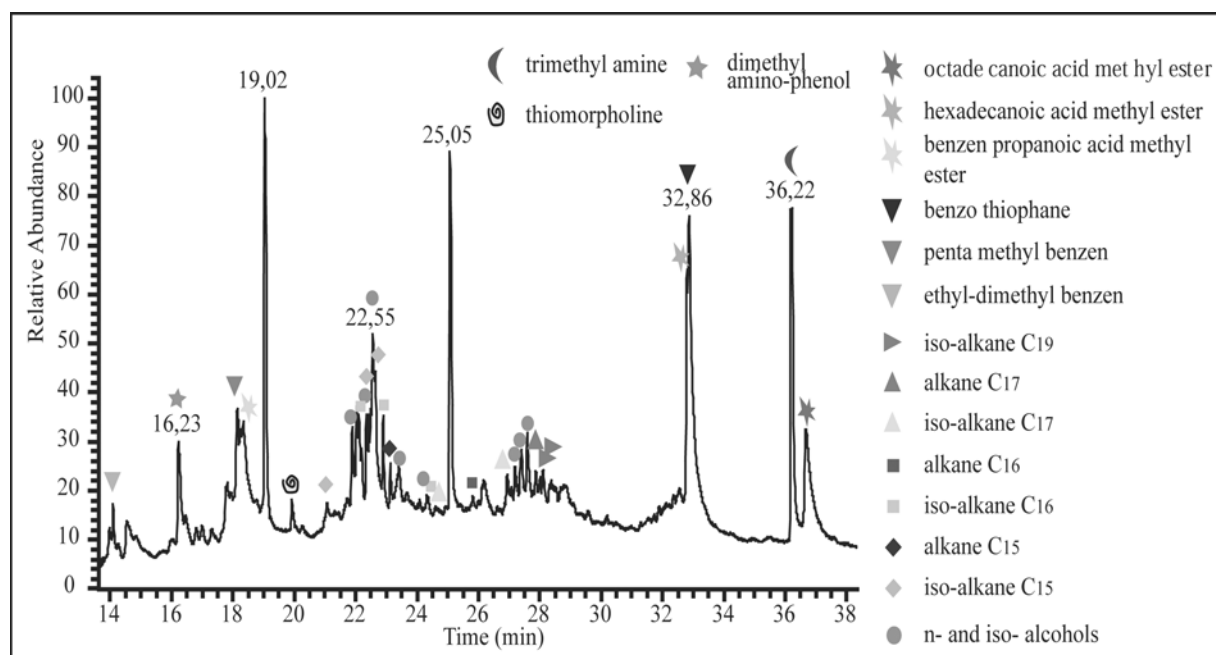


Fig.1. Spectral response of molecular analysis on low charge saponite by pyro-GC/MS (21 interaction days at 65 meters, in anoxic deep layer)

The same molecular GC/MS analysis of organic extracts carried out on waters, macrophytes algae (developed in the border between 2 and 7m depth), and phytoplanktonic fractions developed in the water column were performed in order to characterise the type and origin of organic clay-adsorbed fractions (see Boussafir et al., this meeting). These molecular investigations revealed that the same molecular fractions are present in macrophytes and phytoplankton lipid extracts.

ESCA analysis reveal a lost of sodium in the interlayer space of the two saponites, and its possible substitution by divalent iron in anoxic deep layer. This suggests the predominance of cation bridge mechanism, involving divalent iron, to explain the adsorption of organic molecules on clays.

References

- [1] Keil R.G., Montluçon D.B., Prahl F.G., Hedges J.I., 1994 - Sorption preservation of labile organic matter in marine sediments - *Nature*, Vol. 370, 549-551.
- [2] Sugai S.F., Henrichs S.M., 1992 - Rates of amino-acid uptake and mineralization on Resurrection Bay sediments - *Ecol. Prog. Ser.*, 88, 129-141.

PM-12: Source organisms and preservation pathways of the organic matter from Negev Phosphorite samples with contrasting quality (Israel, Upper Cretaceous)I. Franquin¹, A. Riboulleau¹, L. Bodineau², N. Tribovillard¹, E. Tannenbaum³

1) Laboratoire des Processus et Bilans Sédimentaires, Lille1, 59655 Villeneuve d'Ascq, France
(e-mail: isabelle.franquin@ed.univ-lille1.fr)

2) Laboratoire de Chimie Analytique et Marine, Lille1, 59655 Villeneuve d'Ascq, France

3) Kimron Oil and Minerals, Hod-Hasharon 45270, Israël

Negev phosphorites (South Israel) belong to the South Tethyan Phosphogenic Province, a Cretaceous-Eocene Tethyan Phosphorite belt which extends from Central America through North Africa and to Middle East. The problematic of phosphorites genesis have been previously discussed: according to Baturin model [1], sealevel highstands are thought to promote phosphogenesis. Productive surface waters and the export of organic matter (OM) to the sediment-water interface lead to a suboxic seafloor and the requisite solution and surface chemistries for phosphogenesis [2]. A lowering of wave base during a sealevel fall or low stand is suggested to allow the reworking and concentration of phosphatic strata into economic phosphorite [1]. During this phase, the environmental conditions are supposed to be more oxidative. But many phosphorite deposits contain OM.

A bulk study by Rock-Eval pyrolysis of samples of Negev phosphorites was performed, showing substantial TOC from 2 to 12%, and HI values between 298 and 773 mg HC/g TOC. Such a wide range of HI values reveals important differences in the quality of the OM. The relative low T_{max} (ranging from 400 to 420°C) reflect the immaturity of the OM, and, in a HI vs T_{max} diagram, the OM plot in Type I and Type II materials.

The presented results are devoted to the investigation of the OM present in three samples of Negev phosphorites with contrasting bulk characteristics. They were examined in order to specify the source organisms of the OM and its preservation pathways. To this end, their kerogens were examined by microscopy, spectroscopy and off-line pyrolysis, and their bitumens were submitted to chemical degradation by ether bond cleavage.

The first sample studied, termed *Phos-I*, is characterized by a kerogen enriched in oxygen and organic sulphur, which classifies as a Type II-S kerogen. In the extract, the sharp predominance of *n*-alkyl chains with linear skeletons (*n*-alkanes, alcohols, ketones and fatty acids) and their distribution centred at C₁₇ are consistent with a major algal or cyanobacterial origin of *Phos-I* OM. A low bacterial contribution is shown by the occurrence of a few branched hydrocarbons and of the hopanoids. The presence of 4-methyl steranes can indicate a low contribution of dinoflagellates, in agreement with palynological studies. A weak

contribution of higher plant debris is reflected by the occurrence of C₂₀₊ alkanes and fatty acids and by the observation of wood debris under light microscopy.

N-alkane/alkene doublets which are observed in *Phos-1* kerogen pyrolysate are often associated with the selective preservation of algaenans and cutans. However, when this type of pathway is dominant, some particular pyrolysis products, like alkylnitriles and alkan-18-one, which are not observed in this sample, are released upon pyrolysis, and some morphological features of the source organisms are retained in the kerogen [3]. The few lamellar structures and thick cell walls, and the abundance of nanoscopically-amorphous particles observed by TEM in *Phos-1* kerogen, suggest that selective preservation only plays a more minor role in the preservation of OM, and that chemical processes are dominant. The abundance of OSC released upon pyrolysis and the high Sorg content indicate that natural sulphurisation played a significant role, suggesting anoxic depositional environments. Conversely the high oxygen content and the variety of oxygenated compounds (mid-chain ketones) testify for an oxidative incorporation of lipids [4]. Such process should require relatively oxic depositional or diagenetic conditions.

The comparison of *Phos-1* with two other samples, one enriched in humic substances and one classified in Type I material, will allow to determine the differences in source organisms and depositional conditions of these three samples.

References

- [1] Baturin, G.N., 1971. Stages of phosphorite formation on the sea floor. *Nature* 232, 61-62.
- [2] Trappe, J., 1998. Phanerozoic Phosphorite Depositional Systems. A dynamic model for a sedimentary resource system. Springer, Berlin.
- [3] Derenne, S., Largeau, C., Casadevall, E., Berkaloff, C., Rousseau, B., 1991. Chemical evidence of kerogen formation in source rocks and oil shales via selective preservation of thin resistant outer walls of microalgae: Origin of ultralaminae. *Geochimica et Cosmochimica Acta* 55, 1041-1050.
- [4] Riboulleau, A., Derenne, S., Largeau, C., Baudin, F., 2001. Origin of contrasting features and preservation pathways in kerogens from the Kashpir oil shales (Upper Jurassic, Russian Platform). *Organic Geochemistry* 32, 647-665.

PM-13: Extraction of natural organic matter from marine waters - Fluorometric characterisation of the isolated fractions

A. Huguet, S. Relexans, E. Parlanti

Laboratoire de Physico-Toxicochimie des Systèmes Naturels - LPTC UMR 5472 CNRS - Université Bordeaux 1 - 351 cours de la Libération - 33405 Talence Cedex - France (e-mail: e.parlanti@lptc.u-bordeaux1.fr)

Natural organic matter (NOM), whose main components are humic substances (HS), is a complex mixture of polyfunctional macromolecules. These macromolecules are products of chemical and biological degradation and condensation reactions of plant and/or animal residues.

NOM composition is often very heterogeneous and depends on geographical, climatic, physical and biological conditions. It plays a dominant role in photochemical processes and physical, chemical or biological reactions. It is also of great importance in contaminant binding, transport and transformations in aquatic environments. An improvement in characterisation of these natural materials will provide a better understanding of their properties.

The aim of this investigation was to combine spectrofluorometry (three-dimensional excitation-emission-matrix (EEM) spectroscopy) and XAD resin extraction.

Significant differences are observed when analysing samples from different geographic origins using EEM spectroscopy. The interpretation of the spectroscopic analyses of NOM is however often complicated by severe overlapping of characteristic spectral features due to the complexity and polyfunctionality of the colloids.

The adsorption on XAD resins is the most popular technique of NOM extraction, due to chemical stability and high efficiency of these resins. Thus, between 70% and 80% of the DOC of surface natural waters is isolated using XAD-8 and XAD-4 resins in tandem. The organic matter from different marine environments was extracted on XAD-8 and XAD-4 resins according to the protocol recommended by the International Humic Substances Society (IHSS).

Three fractions were obtained following this procedure:

- an hydrophobic fraction (the compounds retained on the XAD-8 resin), mostly humic substances
- a transphilic fraction (the molecules retained on the XAD-4 resin)
- hydrophilic organic molecules, which do not adsorb on XAD-8 or XAD-4

The organic fractions isolated from seawaters and estuarine samples were then analysed using EEM spectroscopy, which is a very powerful analytical tool. Firstly, fluorescence is a non destructive method, sensitive to low concentrations of fluorescent compounds – as it is the case for humic substances in seawater. Secondly, it permits notably to characterise the source of the NOM (terrestrial or marine) and to follow its degradation and transformation.

To our knowledge, most of the previous work on extraction of aquatic NOM has been carried out with freshwater or brackish water samples. Therefore, the originality of our study is to isolate and analyse humic substances from both marine and estuarine environments, which is a real challenge.

In fact, in seawater, dissolved organic matter is a very dilute (~1 mg/l) and complex mixture. The presence of inorganic ions at high concentrations complicates considerably the concentration and analysis of marine NOM. That is certainly why so few studies were performed in marine environments. We wanted to fill the gap existing in this field. Our preliminary results allowed us to isolate fractions of marine and estuarine waters with specific spectral signatures.

PM-14: Analysis of kerogens from Jurassic-Cretaceous boundary in the Sierra de Aralar (Navarra, Spain) by Curie point pyrolysis-gas chromatography-mass spectrometry and pyrolysis Rock Eval

M. Iriondo¹, C. Dorronsoro¹, A. Permanyer², B. Hermosín³

1) Departamento de Geología. Facultad de Químicas. Universidad del País Vasco. P.O. Box 1072, 20080 Donostia-San Sebastián. Spain (e-mail: qppdoure@sq.ehu.es)

2) Dept. de Geoquímica. Universitat de Barcelona, Catalonia. Spain

3) Instituto de Recursos Naturales y Agrobiología, CSIC, Apartado 1052, 41080 Sevilla, Spain

The present work is a previous study of the composition of the kerogen of different samples. Four kerogens from Jurassic-Cretaceous boundary in the Sierra de Aralar (Navarra, Spain) were selected. The Jurassic-Cretaceous boundary is characterized by a marine carbonate platform (Kimmeridgian) up to 100 m thick, formed by limestones partially karstified and dolomitized. This change progressively to coastal and brackish facies represented by dark limestones and marls. These sediments are one hundred meters thick and they belong to the Purbeckian Facies (Portlandian-Berriasian). In the Kimmeridgian rocks the organic content is present as solid bitumen located in the karst porosity, whereas in the Purbeckian Facies the greater organic richness corresponds to the marl beds [1].

Rock samples were successively treated using conventional demineralization with HCl and HF in order to isolate the kerogen fraction. These samples were studied using a Rock-Eval II which yielded Tmax values between 438-441°C and rich values of S2, which places the samples in the beginning of the oil window, (Table 1).

Table 1. Results of Rock Eval pyrolysis of kerogens (P.F.: Purbeckian Facies)

Age	Sample	S2	TOC	IH	Tmax
P.F./Berriasian	K ₃	200.2	36.47	549	441
P.F./Berriasian	K ₄	133.5	36.68	364	439
P.F./Portlandian	K ₁	372	64.56	576	441
Kimmeridgian	K ₂	238.1	38.54	404	438

Thermally assisted hydrolysis and methylation was performed in a Fisons instrument GC 8000/MD 800 coupled to Fisher 0316 Curie-point pyrolyzer, using a 30 m x 0.25 mm SGL-5 column (film thickness 1.0 µm). The isolated kerogens were methylated with TMAH ([2], [3]) in order to see the fatty acids because in non methylated kerogens they were not detected. Kerogen thermochemolysates showed a unimodal distribution of n-alk-1-ene/n-alkane doublets extending up to C₃₂, with maximum around n-C₁₄ (Fig.1) and abundant homologues typical of marine kerogens ([4], [5]). CPI values was close to 1 (1.01-1.05) and Pr/Phy is approximately 0.7 indicating a reducing environment.

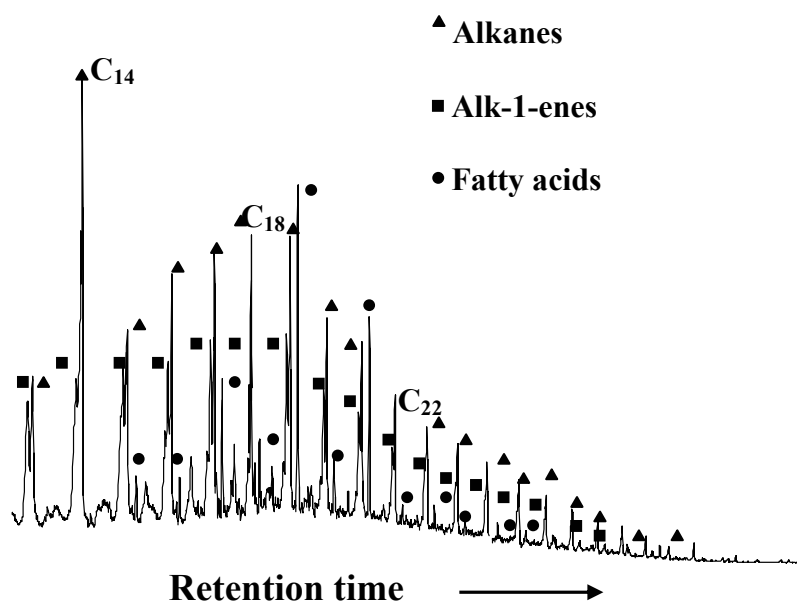


Fig.1. Chromatogram of K_1 from m/z : 85+83+74, illustrating the proportion of alkanes, alk-1-enes and fatty acids. C_{14} indicates the number of carbon atoms

The fatty acids (as methyl esters) series consists mainly of n - C_{10} - C_{26} monocarboxylic acids with an even over odd carbon atom number predominance with maxima at C_{16} . Also it was possible to observe aromatic compounds placed between the peaks of fatty acids and alk-1-enes. We could also identify a great number of aromatic compounds as the series of alkylbenzenes, alkyltoluenes, etc.

Acknowledgement

This research was funded by the MCYT under project BTE2003-06915

References

- [1] Villalobos L., 1971. Corte de dos Hermanas y Sección del Nacedero de Iribas. *Cuadernos Geología Ibérica* 2, pp. 625-630.
- [2] Kossa, W.C., MacGee, J., Ramadrandram, S. and Webber, A.J., 1979. Pyrolytic methylation /gas chromatography: a short review. *J. Chromatogr. Sci.* 17, 177-187.
- [3] Abraham, S.J. and Criddle, W.J. (1985) Quantitative studies on the pyrolytic methylation of simple carboxylic acids and phenols. *J. Anal. Appl. Pyrol.* 9, 53-64.
- [4] Horsfield, B., 1989. Practical criteria for classifying kerogens: Some observations from pyrolysis-gas chromatography. *Geochimica et Cosmochimica Acta*, 53(4), 891-901.
- [5] Flaviano C., Le Berre F., Derenne S., Largeau C. and Connan J., 1994. First indications of the formation of kerogen amorphous fractions by Selective Preservation Role of non-hydrolysable macromolecular constituents of Eubacterial cell walls. *Organic Geochemisstry.* 22, 759-771.

**PM-15: Properties of natural dissolved organic matter
in the Seine Estuary (France)**

E. Parlanti¹, L. Vacher¹, C. Garnier², S. Mounier², D. Fevrier², S. Relexans¹,
A. Ficht³, M. Olivier³

1) Laboratoire de Physico-Toxicochimie des Systèmes Naturels - LPTC UMR CNRS 5472, Université Bordeaux 1 - 351 cours de la Libération - 33405 Talence Cedex – France (e-mail: e.parlanti@lptc.u-bordeaux1.fr)

2) Laboratoire PROTEE-CAPTE, Université du Sud Toulon Var, BP20132, 83957 La Garde cedex

3) Cellule Antipollution - Service de la Navigation de la Seine 4^{ème} section 66 av. J. hastellain - Ile Lacroix - 76000 Rouen - France

The processes affecting natural dissolved organic matter (NDOM) through estuaries are of major importance in order to understand its role and behaviour during the mixing of river and marine waters. NDOM consists of a heterogeneous mixture of compounds with wide ranging chemical properties and diverse origins. It is well known to interact with organic and inorganic pollutants and to affect their transport and fate in the environment but these interactions strongly depend on the properties of the organic macromolecules (nature, size, structure, conformation...). To study the spatiotemporal changes of NDOM, water samples were collected at different sites from the Seine estuary every month between March 2002 and July 2003, and during NUTS01 and NUTS02 Cruises in August 2001 and September 2002 (French National Program: SEINE AVAL 2). Particulate and dissolved organic carbon measurements, fluorescence spectroscopy and acidic titration of filtered samples without any treatment or pre-concentration, were carried out in order to monitor the variation of the physico-chemical properties of the natural organic matter concerning its ability to transport pollutants like heavy metals. The optical characteristics of NDOM in the French Seine estuary were investigated using three-dimensional spectrofluorometry which provides Excitation-Emission-Matrices (EEM). The EEM spectra of the samples showed a variety of fluorescent organic matter and a decrease in concentration due to dilution along the estuary. In order to discuss the results of the fluorescence analyses, we considered the ratios of the intensities of the main observed fluorescent bands. Different trends in composition as well as in behaviour or production of NDOM were then observed along the estuary.

Fluorescence analysis allows the determination of the degree of maturation of NDOM whereas the acid-base micro-titration allows following the changing properties of samples and gives therefore an idea of the NOM environment. The influence of the city of Rouen concerning the samples quality is expressed by a significant increase of phenolic-range acid sites. In the 2002 summer period the weakest concentrations of dissolved organic carbon were measured during the year of investigation. At the same period the results of pH titration

treated with an optimisation and a speciation program show an increase of carboxylic sites. Furthermore, in the corresponding time, NDOM was characterised by a juvenile fluorescent organic matter probably due to a biological activity that produces very reactive compounds. The concerned samples are showing the highest density of acidic sites.

The influence of tides in macrotidal estuaries increases the residence times of waters and is responsible for the variations of environmental parameters (pH, salinity, temperature) and for the formation of the maximum turbidity zone (MTZ) which is characterised by intense cycles of settling and resuspension of anoxic mud fluid into the oxic water column. The variations of these physico-chemical parameters modify the structure and the size distribution of dissolved organic macromolecules by flocculation or deflocculation, thus changing the complexation properties of NDOM towards pollutants during the transit of organic material to the marine medium.

The precise characterisation of NDOM is very difficult because of the complexity of an estuarine system. In order to gain more information on its composition and properties, this highly complex material was fractionated according to molecular size by using tangential ultrafiltration as NDOM is a mixture of organic macromolecules with a broad range of molecular size and weight. Samples of water were collected in the MTZ and at the downstream and upstream MTZ limits of Seine Estuary. Each fraction was then further characterised by 3D-spectrofluorometry.

This study showed the modifications of NDOM properties along the Seine Estuary and that the size distribution of NDOM was different between samples collected in the Maximum Turbidity Zone and at its downstream and upstream.

PM-16: Ruthenium tetroxide oxidation of Orgueil and Murchison insoluble organic matter: assessment on aliphatic moieties

L. Remusat^{1,2}, S. Derenne², F. Robert¹

1) LEME, MNHN, 61 rue Buffon, 75231 Paris, France (e-mail: laurent-remusat@enscp.fr)

2) LCBOP, ENSCP, 11 rue Pierre et Marie Curie, 75231 Paris, France

Carbonaceous chondrites are the most primitive objects of the solar system. They exhibit significant carbon contents and most of this carbon occurs as insoluble organic matter (IOM) and this organic matter might be the first organic matter available on early Earth for life. IOM has been studied by various spectroscopic techniques, pyrolyses and chemical degradations [1, 2]. These analyses revealed that the macromolecular network of IOM is based on polyaromatic units cross-linked by aliphatic chains. Contrary to aromatic moieties that are quite well constrained, little is known about the aliphatic chains. Ruthenium tetroxide oxidation is a suitable technique for studying aliphatic chains linked to aromatic units since, as shown for terrestrial samples [3, 4], it oxidised aromatic units and converts ether and ester into carboxylic acids. We have thus chosen this technique to investigate the aliphatic linkages in the IOM of Orgueil and Murchison meteorites.

IOM of Orgueil and Murchison carbonaceous chondrites were isolated by classical HF/HCl treatment and subsequent solvent extractions [2]. It was then submitted to ruthenium tetroxide oxidation for 4 hours, at room temperature. Products were recovered by filtration with methanol and dichloromethane. They were derivatized by silylation and methylation, and further analysed by GC-FID and GC-MS.

In both samples, the products mainly consist of short aliphatic di- and tri-acids and polycarboxylic aromatic acids (fig 1). α,ω -Aliphatic diacids are related to aliphatic chains between two aromatic units, the two acid functions corresponding to the aromatic carbons bearing the aliphatic linkage. The methyl and ethyl substituted counterparts of the linear diacids also contribute to the oxidation products. In Orgueil IOM, the carbon number of these diacids range from 3 to 9, with a maximum at 4 and 5 carbon atoms, hence quite short chains, with at most 7 carbon atoms and mainly with 2 to 3 carbons. Aliphatic triacids are related to aliphatic links between 3 aromatic units. Their occurrence confirms the high level of substitution of the aliphatic chains, previously inferred from ^{13}C NMR [2], which shows that aliphatic part is highly substituted. Polycarboxylic aromatic acids are related to the fusion of aromatic units. They are less abundant than in oxidation products of terrestrial coals, thus indicating that chondritic IOM is less condensed (smaller aromatic units), in agreement with recent HRTEM observations [5]. Some short (3 and 4 carbons) hydroxy acids and diacids are

detected. They are related to incomplete oxidation of ether and ester functions in the aliphatic chains. Aliphatic long chain monocarboxylic acids in Orgueil IOM are related to terrestrial contamination, no monocarboxylic acid shorter than C₁₄ is detected.

The main difference between Orgueil and Murchison IOM is the length of the aliphatic chains (shorter in Murchison), along with the number of acid functions in the aromatic polycarboxylic acids (two in Murchison, and five in Orgueil) which points to less condensed polyaromatic units in Murchison.

This study provides, for the first time, precise information on the chemical structure of the aliphatic linkages in the chondritic IOM. Aromatic units are linked by short aliphatic chains (mainly two and three carbon atoms), with methyl and ethyl substitutions, and comprising ester and ether functions. This structure is highly cross-linked as one aliphatic chain can link several aromatic units. When compared to terrestrial samples, chondritic IOM is constituted of shorter aliphatic chains, smaller aromatic units and is more substituted.

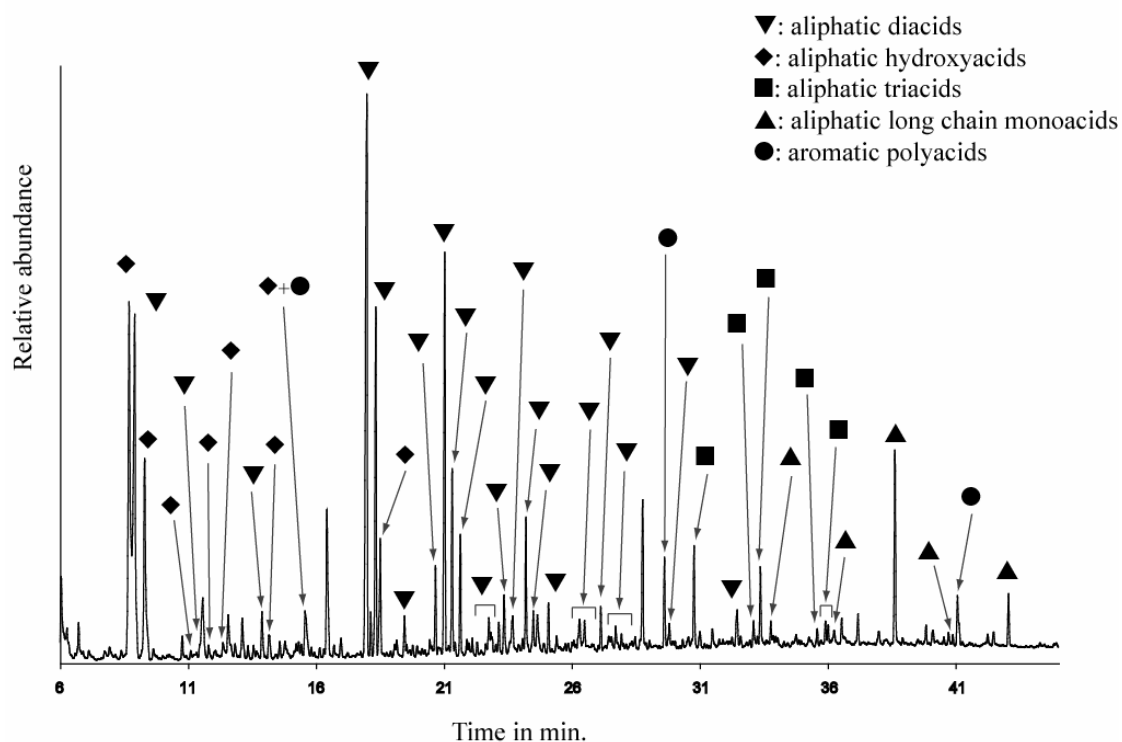


Fig.1. TIC chromatogram of ruthenium tetroxide oxidation products of Orgueil IOM, products were detected as trimethylsilyl esters

References

- [1].M. A. Sephton (2002) *Natural Products Report*, 19, pp. 292-311.
- [2].A. Gardinier, et al. (2000) *Earth and Planetary Science Letters*, 184, pp. 9-21.
- [3].L. M. Stock and S.-H. Wang (1986) *Fuel*, 65, pp. 1552-1562.
- [4].W. H. Ilsley, et al. (1986) *Fuel*, 65, pp. 1216-1220.
- [5].S. Derenne, et al. (2003) *34th Lunar and Planetary Science Conference*.

PM-17: Time dependent changes during the degradation of lignin by the white-rot fungus *Pleurotus ostreatus*: linking the biological and geochemicalS.A. Robertson¹, E. Hack², S. Mason², G.D. Abbott¹

1) School of Civil Engineering and Geosciences, Drummond Building, University of Newcastle upon Tyne, NE1 7RU, United Kingdom

2) School of Biology, Agriculture Building, University of Newcastle upon Tyne, NE1 7RU, United Kingdom

White-rot fungal degradation of lignin is researched internationally because of its significance and potential application in the carbon cycle, palaeoclimate modelling, land remediation and biopulping. We focus on the geochemical aspects of the fungal degradation process since the modifications occurring to a lignocellulosic substrate are the first stages of early diagenesis and occur at the interface between the terrestrial and atmospheric carbon reservoirs. Previous work in our laboratory (Vane *et al.*, 2001a,b) identified time-dependent chemical changes imparted to the lignin during the incubation of white rot fungi with wheat straw. These and other studies of white-rot degradation have generally centred on either enzymatic activity or the characterization of the degraded lignin's molecular structure but relatively little work has been done to link the two. The present study correlates these biological and geochemical aspects by comparing the time-dependent profiles of the lignin oxidation products, identified from our previous studies, with the enzymatic activity of the fungus.

Pleurotus ostreatus was grown from grain spawn inoculum under solid state fermentation conditions on wheat straw stem as well as leaf material and sampled every seven days. Extracellular enzymes were extracted from the samples and manganese peroxidase activity assayed. Proteins in the extract were profiled by SDS-polyacrylamide gel electrophoresis. Levels of lipophilic extractives including the fungal biomarker ergosterol were determined by GCMS analysis of the derivatised lipid fraction following alkaline hydrolysis. The extent of lignin degradation in the wheat straw substrate was determined by thermochemolysis in the presence of tetramethylammonium hydroxide (TMAH), followed by product analysis using GCMS.

The culture conditions chosen represent the early stages in the colonisation of a substrate by *Pleurotus ostreatus* during the phase of rapid expansion of the hyphal network, as indicated by an increase in ergosterol content from 0.35 to 0.55 mg ergosterol/g straw. Significant increases in both guaiacyl and syringyl acid to aldehyde ratios (0.325 to 0.812 and 1.179 to 1.581 respectively) as well as increasing extents of side chain scission were observed: these confirm the increasing oxidation of lignin with incubation time (Figure 1a,b). Manganese peroxidase activity might be expected to increase in proportion to the increased hyphal abundance but instead peak activity is reached after 3 weeks, followed by subsequent

decline (Figure 1c). A similar activity profile was observed by Boer *et al.* (2004) in the early stages of growth of *Lentinula edodes*. The results in our experiments demonstrate that indicators of lignin degradation (G6/G4, S6/S4, G6/G14+15, and S6/S14+S15 ratios) appear to increase in a linear fashion whilst enzymatic activity reaches a peak then falls and fungal biomass increases slowly at first before rising more rapidly as incubation time increases. These suggest the possibility of a time-lag between the degradation of the lignin and mycelial growth.

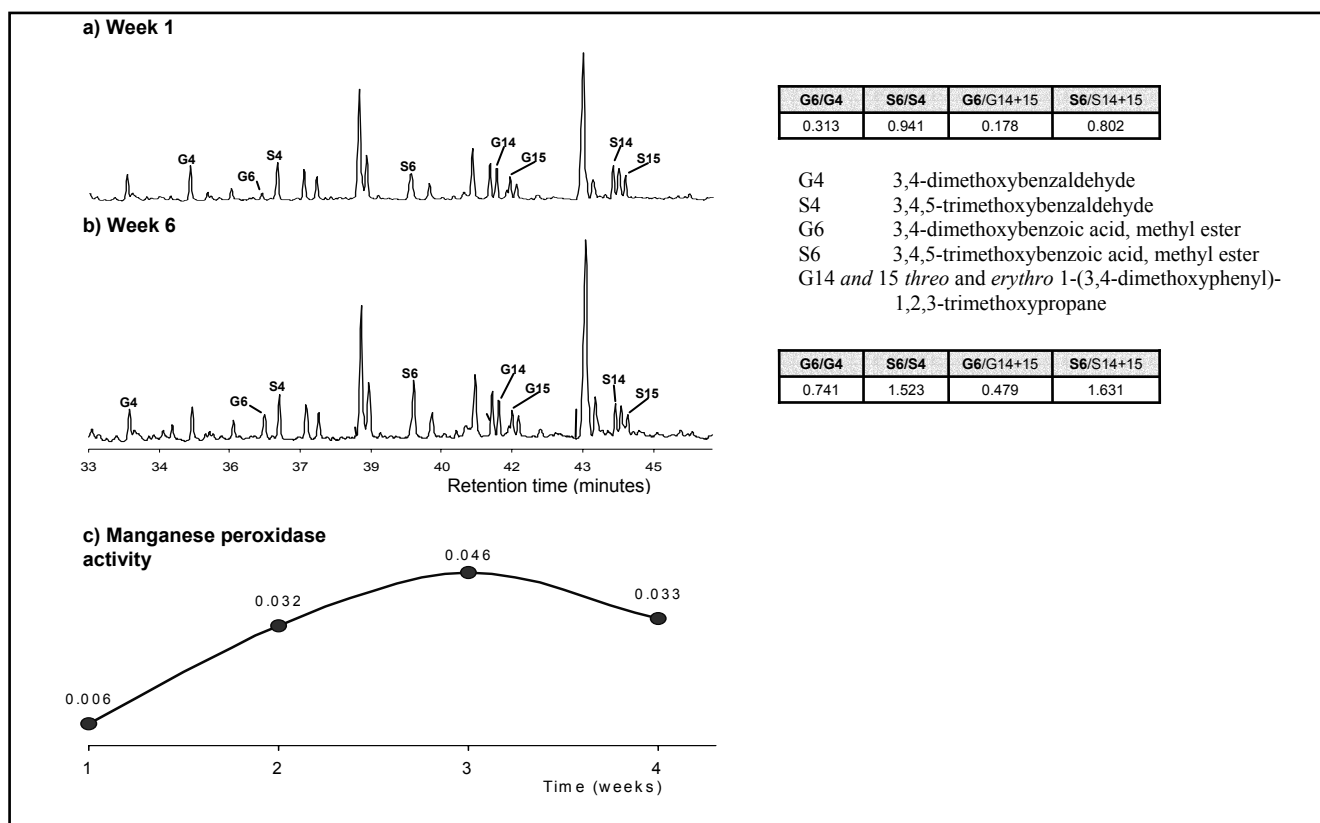


Fig. 1.

- Partial trace for the total Ion current (TIC) of the TMAH thermochemolysis products of wheat straw degraded for 1 week by *Pleurotus ostreatus*. Table shows ratios of peak areas indicative of the state of degradation.
- Partial trace for the total Ion current (TIC) of the TMAH thermochemolysis products of wheat straw degraded for 6 weeks by *Pleurotus ostreatus*. Table shows ratios of peak areas indicative of the state of degradation.
- Plot of manganese peroxidase activity (in activity units) measured in samples over a 4 week period.

References

- Boer, C.G., Obici, L., de Souza, C.G.M., & Peralta, R.M., 2004. Decolorization of synthetic dyes by solid state cultures of *Lentinula (Lentinus) edodes* producing manganese peroxidase as the main ligninolytic enzyme. *Bioresource Technology*, 94, 107-112.
- Vane, C.H., Abbott, G.D., & Head, I.M., 2001a. The effect of fungal decay (*Agaricus bisporus*) on wheat straw lignin using pyrolysis-GC-MS in the presence of tetramethylammonium hydroxide (TMAH). *Journal of Analytical and Applied Pyrolysis*, 60, 69-78.
- Vane, C.H., Martin, S.C., Snape, C.E., and Abbott G.D., 2001b. Degradation of lignin in wheat straw during growth of the oyster mushroom (*Pleurotus ostreatus*) using off-line thermochemolysis with tetramethylammonium hydroxide and solid-state ^{13}C NMR. *Journal of Agricultural and Food Chemistry*, 49, 2709-2716

PM-18: Syngeneity and biogenicity of organic matter in a 3.5 billion year old chert as revealed by Electron Paramagnetic Resonance and pyrolysis GCMS

A. Skrzypczak^{1,2}, S. Derenne¹, L. Binet², D. Gourier², F. Robert³

1) Laboratoire de Chimie Bioorganique et Organique Physique, ENSCP, UMR7618
(e-mail: audrey-skrzypczak@enscp.fr)

2) Laboratoire de Chimie Appliquée de l'Etat Solide ENSCP, UMR7574, 11 rue Pierre et Marie Curie, 75231 Paris cedex 05, France

3) LEME, Museum National d'Histoire Naturelle, 61 rue Buffon, 75005 Paris, France

The question of the origin of life is one of the most debated scientific questions to date. The discovery of microstructures in cherts from the Warrawoona Group, considered as the oldest microfossils on Earth (3.465 billion years old) created a considerable interest in the organic matter (OM) contained in this deposit [1]. However, their biogenicity has been recently debated since it was shown that similar structures can be formed through abiotic reactions to such a point that these microstructures were even considered as secondary artefacts, formed under hydrothermal conditions [2, 3, 4]. Moreover, even if the biogenicity can be proved, a contamination of archaean rocks by younger biological material (non syngenetic material) must not be underestimated [5]. These results point to the necessity of identifying fingerprints of the syngeneity and reliable biomarkers for this ancient organic matter. In the present study, the Insoluble Organic Matter (IOM) from a chert of the Towers Formation in the Warrawoona Group was analysed using a combination of analytical and spectroscopic techniques.

In a preliminary study, the OM was analysed in situ by Electron Paramagnetic Resonance (EPR) which aims at studying free radicals. The ageing of an organic matter creates radicals whose concentration and distribution evolve with maturation. So, the EPR signal evolves in a same way and EPR parameters (linewidth and lineshape) can be used as genuine markers of the evolution of the IOM in ancient cherts, providing that these cherts are not metamorphized. By comparing the EPR parameters of the Warrawoona chert with those of younger organic matter and organic matter artificially aged by heat treatment, we could ascertain that the carbonaceous matter in the 3.5-billion-year-old chert was not due to a contamination by younger organic matter but that it was unambiguously contemporaneous with the formation of the rock.

Then, the IOM was isolated from two pieces of the same bulk sample using the classical demineralization procedure via HF/HCl. This was carried out separately by our lab and by a team of the Institut Français du pétrole, to check that no contamination was

introduced during isolation. The same analyses were performed on both fractions of IOM and the same main results were obtained, which enables us to rule out any human contamination.

Solid state ^{13}C NMR provides information on the environment of the carbons and allows to distinguish the different types of carbons. It is, here, performed for the first time on such a sample. Because of the low amount of material, we used a cross polarization sequence and magic angle spinning at 20 kHz. This sequence results in an enhancement of the signal thanks to magnetization transfer from hydrogens to carbons. Three main types of carbons can be identified (figure 1) : aromatic and/or olefinic ones (100-140 ppm), carbons linked to oxygen and/or nitrogen atom through a single bond (70-80 ppm) and aliphatic carbons (10-30 ppm). The most important result is that the spectrum is sharply different from the one of mature kerogens which is strongly dominated by the aromatic signal. Moreover, it suggests a highly brached structure comprising unsaturations and heteroelements.

To derive information at the molecular level, the IOM of the Warrawoona chert was analysed by py-GC-MS. The pyrochromatogram shows a number of series of hydrocarbons (mainly alkenes and alkylated benzenes), extending up to C_{30} , contrary to what is observed upon thermal decomposition of abiotic materials. Moreover, some series exhibit an unusual distribution, consistent with an original biosynthetic pathway.

The combination of spectroscopic and analytical techniques proves that the organic matter trapped in the Warrawoona chert is unambiguously of archean age and that it is highly likely of biological origin. Consequently, these results strongly support the occurrence of life as far back as 3.5 billion years.

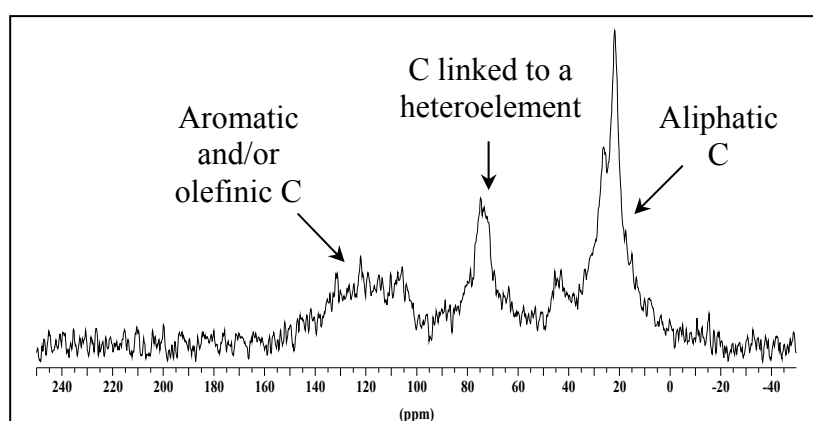


Fig.1. Solid State ^{13}C NMR of the OM isolated from the Warrawoona chert

References

- [1] Schopf J. W. (1993) *Science*, 260, 460, [2] Brasier M. D. et al. (2002) *Nature*, 416, 76-81, [3] Pasteris J. D. and Wopencka B. (2002) *Nature*, 420, 476.[4] Garcia-Ruiz J. M. et al. (2003) *Science*, 302, 1194-1197.[5] Westall F., and Folk R.L. (2003) *Precambrian Research*, 126, 313-330.

PM-19: Catalytic hydropyrolysis of Neoproterozoic kerogens from the South Oman Salt Basin

C. Stalvies¹, G.D. Love², E. Grosjean², W. Meredith³, P. Farrimond^{1,4}, J.P. Grotzinger²,
C.E. Snape³, R.E. Summons²

1) School of Civil Engineering and Geosciences, University of Newcastle upon Tyne, NE1 7RU, U.K.
(e-mail: charlotte.stalvies@ncl.ac.uk)

2) Department of Earth, Atmospheric & Planetary Sciences, Massachusetts Institute of Technology, MA 02139, USA.

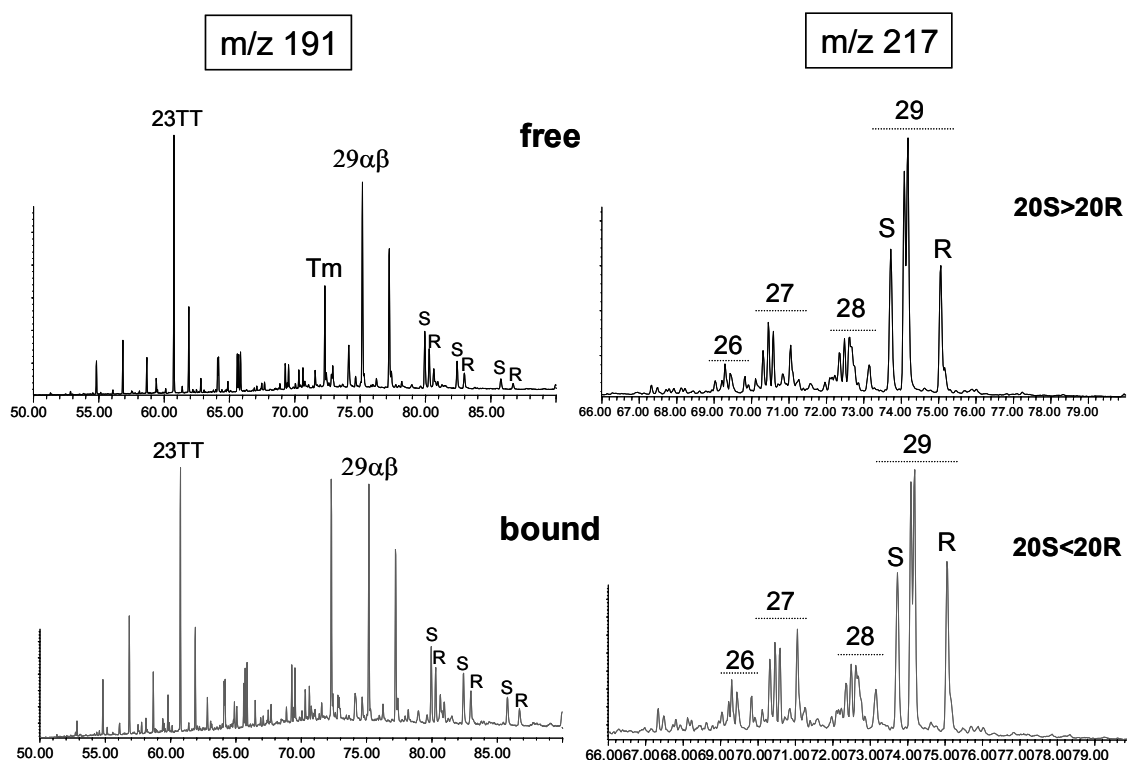
3) Nottingham Fuel & Energy Centre, SChEME, University of Nottingham, NG7 2RD, U.K.

4) Integrated Geochemical Interpretation Ltd., Hallsannery, Bideford, Devon, EX39 5HE, UK

The South Oman Salt Basin (SOSB) forms part of a belt of related sedimentary basins in the Middle East and Asia, and is filled with unmetamorphosed strata of the Huqf Supergroup ([1], [2]) which range in age from mid-Neoproterozoic to early Cambrian. Due to their organic-rich nature and exceptional preservation, these offer a rare opportunity to investigate both the biomarker content and the stable carbon ($\delta^{13}\text{C}$) isotopic ordering prevailing in sedimentary organic matter from the Proterozoic Eon. The terminal Neoproterozoic was a time of significant biogeochemical and environmental change but until recent years, the study of such ancient rocks was hampered by uncertainties due to the high maturities of organic matter, the possibility of migration contamination and the graphitic nature of many Precambrian kerogens.

15 samples were selected from various formations and lithologies within the SOSB to assess the composition of the free hydrocarbon and associated kerogen phases. All samples were solvent extracted and subjected to catalytic hydropyrolysis to determine the degree to which extractable bitumens and kerogen pyrolysates were similar or distinct. Catalytic hydropyrolysis (HyPy) involves open-system, temperature-programmed pyrolysis in stream of high pressure hydrogen gas (15 MPa) using a dispersed sulphided molybdenum catalyst.

Initial screening of free and kerogen-bound biomarker data were performed using conventional GC-MS, followed by further analyses of all fractions using MRM-GC-MS to probe the distribution of trace biomarkers such as methyl hopanes and methyl steranes. Since biomarkers bound into kerogen are protected from alteration by the host matrix, this explains why the bound triterpenoid hydrocarbons released by HyPy exhibit a less mature profile than the free hopane and sterane hydrocarbons found in the corresponding bitumens (Fig. 1). This is one of a number of biomarker ratio relationships formulated that indicate that bitumens are indeed co-eval with the host kerogens and have not migrated, from elsewhere, into the host rocks.



Typical free vs. bound trends are observed- HyPy products are genuine bound biomarkers

Fig.1. Comparison of free versus kerogen-bound hopanes and steranes from a Neoproterozoic carbonate source rock from the SOSB

Neoproterozoic rocks often exhibit distinctive biomarker patterns with a predominance of a single-sterane homolog, usually either C_{27} or C_{29} ([3]). The m/z 217 chromatograms for all Oman sediments investigated thus far show a clear pattern with a much higher abundance of C_{29} steranes over C_{27} and C_{28} steranes in both bitumen and kerogen phases. This sterane profile indicates that Chlorophyceae were prominent constituents of the ancient phytoplankton communities in the SOSB as observed before by Hold et al. (1999, [4]) for Huqf oils and source rocks. The combination of HyPy and MRM-GC-MS in particular is found to be a powerful combination for differentiating subtle changes in organic facies of source rocks using kerogen-bound biomarker profiles.

References

- [1] Gorin, G.E., Racz, L.G., Walter, M.R., 1982. Late Precambrian-Cambrian Sediments of Huqf Group, Sultanate of Oman. *The American Association of Petroleum Geologists Bulletin* 66, 2609-2627.
- [2] Amthor, J.E., Grotzinger, J.P., Schröder, S., Bowring, S.A., Ramezani, J., Martin, M.W., Matter, A., 2003. Extinction of *Cloudina* and *Namacalathus* at the Precambrian-Cambrian boundary in Oman. *Geology* 31, 431-434.
- [3] Brocks, J.J., Summons, R.E., 2003. Sedimentary Hydrocarbons, Biomarkers for Early Life. In: *Treatise on Geochemistry*, Elsevier, 63-115.
- [4] Höld, I.M., Schouten, S., Jellema, J., Sinninghe Damsté J.S., 1999. Origin of free and bound mid-chain methyl alkanes in oils, bitumens and kerogens of the marine, Infracambrian Huqf Formation (Oman). *Organic Geochemistry* 30, 1411-1428.

PM-20: Modifications of dissolved organic matter along the Gironde Estuary (France) - Impact on binding properties

L. Vacher¹, E. Parlanti¹, J. Schaefer², G. Blanc²

1) Laboratoire de Physico-Toxicochimie des Systèmes Naturels - LPTC UMR 5472 CNRS - Université Bordeaux 1 - 351 cours de la Libération - 33405 Talence Cedex - France (e-mail:e.parlanti@lptc.u-bordeaux1.fr)

2) Département de Géologie et Océanographie – EPOC-DGO UMR 5805 CNRS - Université Bordeaux 1 - Avenue des Facultés - 33405 Talence Cedex - France

Dissolved organic matter (DOM) in aquatic systems plays a dominant role in the carbon cycle and participates in many physical, chemical and biological reactions. It has been reported to interact with inorganic and organic pollutants and to affect their transport and fate in the environment.

DOM consists in a heterogeneous mixture of compounds with wide ranging chemical properties and diverse origins. This is particularly the case in estuaries where significant differences are observed when analysing water along a salinity gradient. These differences may result from the mixing of two very distinctive organic materials specifically produced in each type of aquatic medium or could be produced by chemical modifications of the organic material during the mixing of two water masses which have different physicochemical properties such as salinity and pH.

The maximum turbidity zone (MTZ) of an estuary is characterised by intense cycles of settling and resuspension of anoxic mud fluid. Moreover DOM accumulates in the MTZ where it has a longer residence time and is then submitted to flocculation and sedimentation processes that modify the size distribution of the macromolecules during the transit of organic material to the marine medium.

Because of its complexity, the precise characterisation of DOM is very difficult and it is necessary to separate this highly complex material in order to gain more information on its composition and properties. As DOM is a mixture of organic macromolecules with a broad range of molecular size and weight, we fractionated it according to molecular size by using tangential-flow ultrafiltration and then characterised the fractions using three-dimensional spectrofluorometry.

Samples of water were collected in the maximum turbidity zone (MTZ) and at the downstream and upstream MTZ limits in the Gironde Estuary during several cruises from 2001 to 2003. After a filtration (Whatman GF/F 0.70µm glass fibre filters) in order to obtain the colloidal and dissolved materials, these samples were fractionated using tangential-flow ultrafiltration systems. MILLIPORE ultrafiltration membranes and cartridges with different

molecular weight cut-off sizes were used in order to obtain different fractions characterised by different molecular weights. Each fraction was then further characterised by 3D-spectrofluorometry. This technique provides Excitation-Emission-Matrices (EEM).

The EEM spectra of the Gironde water samples were similar as expected for estuarine samples in and near the MTZ. They were characterised by a typical fluorescence signature mainly due to humic substances ($\lambda_{em} \approx 460\text{nm}$).

The spectra obtained for the fractions after ultrafiltration presented similar trends characterised again by the major presence of humic substances in each fraction. Thus, fluorophores mainly responsible for the fluorescence of DOM were present in every size class. Nevertheless, many differences were observed between the fractions for a same sample with the presence of another type of fluorophore at Ex./Em. 280nm/330nm (γ peak) in some fractions. It didn't appear on the EEM spectra of the different initial samples because of the very high fluorescence intensity of humic substances that hampered the observation of this peak. This fluorophore is due to protein-like compounds. It is interesting to notice that the molecules responsible for this γ fluorescence band were only present in some of the molecular weight fractions.

These results show that the size distribution of the molecules responsible for the fluorescence of DOM is different between samples collected in the MTZ and at its downstream or upstream limits. This implies a modification of the organic material and of its size distribution during the mixing of waters along the estuary.

The effects of the interaction between DOM and the Cu^{2+} cation have been determined by fluorescence quenching in each molecular size class. The results were compared with measurements of concentrations of trace metals in each fraction. This was done in order to estimate the influence of the colloidal and dissolved fractions on the complexation and transport of metal ions from the river to the coastal marine waters and especially in the maximum turbidity zone where organic matter is subject to particular environmental conditions.

PM-21: Spore chemistry as a proxy for UV-B flux

J.S. Watson¹, M.A. Sephton^{1,4}, S.V. Sephton², D.J. Beerling³, S. Self², I. Gilmour¹,
C.H. Wellman³

1) Planetary and Space Sciences Research Institute, Open University, Milton Keynes, MK7 6AA, UK (e-mail: j.watson@open.ac.uk)

2) Department of Earth Sciences, Open University, Milton Keynes, Buckinghamshire, MK7 6AA, UK

3) Department of Animal and Plant Sciences, University of Sheffield, Sheffield S10 2TN, UK

4) Department of Earth Science and Engineering, Royal School of Mines, Imperial College, London, SW7 2BP, UK

Placing current increased terrestrial UV-B fluxes, due to the seasonal depletion of the stratospheric ozone layer, in a historical context is difficult due to a lack of long-term (century or more) instrumental records and necessitates developing proxy indicators. One promising line of enquiry derives from the response of plants to increased near-surface solar fluxes of harmful ultraviolet radiation in the 280 – 315 nm wavelength (UV-B) (Rozema et al. 2001, 2002). Plants exposed to increased UV-B radiation typically experience a number of detrimental effects, including damage to proteins, membrane lipids and DNA. To reduce this damage, many plants, animals and microbes accumulate UV-B protecting pigments (Cockell & Knowland 1999; Rozema et al. 2001, 2002).

Here, we evaluate the potential of a promising candidate for such a proxy, which is based on changes in the chemical composition of spores in response to variations in near-surface UV-B fluxes, in a field setting. We obtained spores from five populations of the tropical lycopsid *Lycopodium cernuum* growing across an altitudinal gradient (650-1981 m a.s.l.) in S.E. Asia with the assumption that they experienced a range of UV-B radiation doses. Spores from each population were analyzed for UV-B protecting compounds using micro-Fourier transform infrared spectroscopy (micro-FTIR) and thermochemolysis-GC-MS.

The data reveal the presence of various functional groups associated with UV-B protecting pigments including OH, C=O and C=C. Thermochemolysis and subsequent pyrolysis liberated UV-B pigments (ferulic and *para*-coumaric acid) from the spores. All of the aromatic compounds liberated from spores by thermochemolysis and pyrolysis were active in UV-B protection. We show systematic increases in micro-FTIR aromatic absorption (1520 cm⁻¹) and olefinic or aromatic absorption (829 cm⁻¹) with altitude that reflect a chemical response to higher UV-B flux. Our results indicate that detailed chemical analyses of historical spore samples could provide a proxy for stratospheric O₃ layer variability and UV-B flux over historical (century to millennia) timescales.

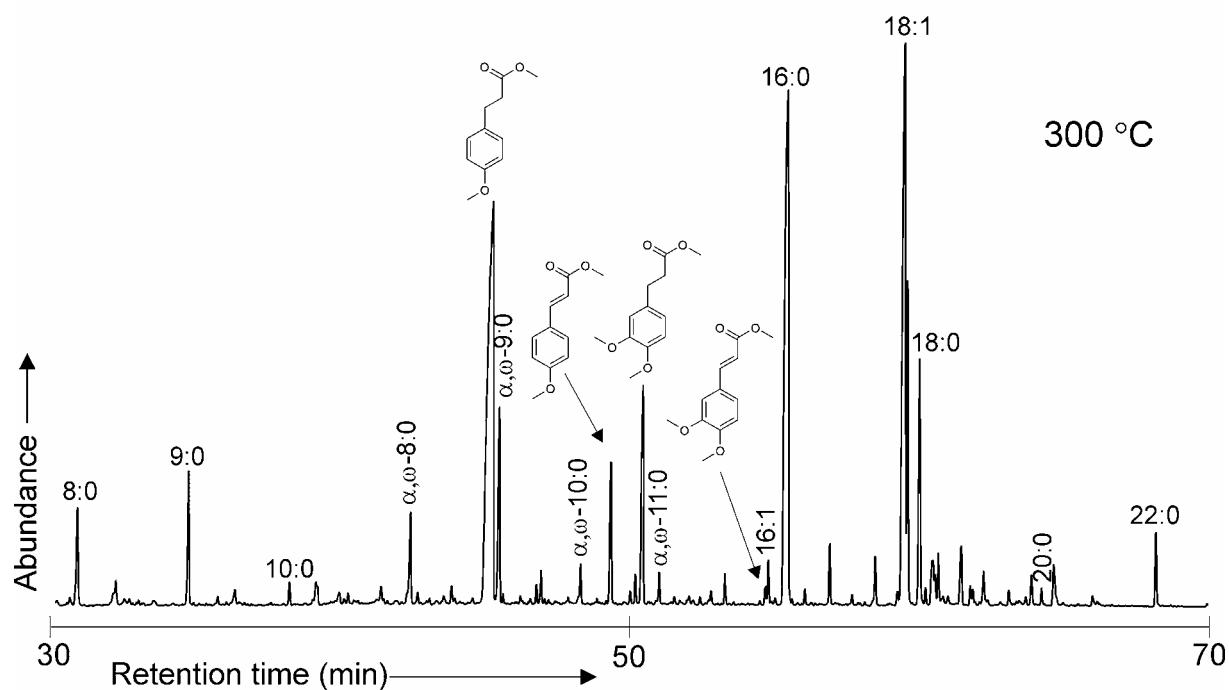


Fig.1. Total ion chromatogram of products from a typical *Lycopodium cernuum* sample liberated at 300 °C in the presence of TMAH

References

- Cockell, C. S., Knowland, J., 1999. Ultraviolet radiation screening compounds. *Biological Reviews*. 74, 311-345.
- Rozema, J., Broekman, R.A., Blokker, P., Meijkamp, B.B., de Bakker, N., van de Staij, J., van Beem, A., Ariese, F., Kars, S.M., 2001. UV-B absorbance and UV-B absorbing compounds (para-coumaric acid) in pollen and sporopollenin: the perspective to track historic UV-B levels. *Journal of Photochemistry and Photobiology B* 62, 108-117.
- Rozema, J., van Geel, B., Björn L.O., Lean, J., Madronich, S., 2002. Towards solving the UV puzzle. *Science* 296, 1621-1622.

PM-22: Biogeochemical comparison of modern and fossil woods

A.O. Baki, M.L. White, E. López-Capel, D.A.C. Manning, G.D. Abbott

School of Civil Engineering and Geosciences, Drummond Building, University of Newcastle upon Tyne, NE1 7RU, UK

Lignin is one of the most important and abundant aromatic biopolymers on earth; it acts as a vehicle for transporting carbon to the geological cycle from the atmospheric cycle. Vascular tissues such as wood can constitute as much as 33% lignin by weight (Higuchi, 1981). Lignin is formed by the dehydrogenative polymerisation of the three cinnamyl alcohols (monolignols) *p*-coumaryl (4-hydroxycinnamyl), coniferyl (4-hydroxy-3-methoxycinnamyl) and sinapyl (4-hydroxy-3,5-dimethoxycinnamyl), which are the precursors of *p*-hydroxyphenyl (*H*), guaiacyl (*G*) and syringyl (*S*) lignin units (Adler, 1977). Identification of these structural sub-units help us to characterize the molecular structure of lignin. The primary degradation processes decomposing lignin back to atmospheric carbon dioxide will either be biological (primarily mediated by white-rot fungi) or abiotic in nature. A unique opportunity to identify the molecular characteristics of abiotic deterioration exists in that there is a unique set of exquisitely preserved gymnosperms from a fossil forest in the Canadian High Arctic where no white-rot degradation has taken place (Blanchette et al., 1991).

This work focuses on the differences between the molecular composition of fossil and modern woods taken from two specific genera of gymnosperms. Twelve modern woods and eleven fossil samples (Axel Heiberg Island, northern Canada) of both the *Larix* and *Metasequoia* taxa have been studied. These were analysed using flash pyrolysis-gas chromatography-mass spectrometry (Py-GC/MS) in the presence and absence of tetramethylammonium hydroxide (TMAH). Lignin from these two sample sets is dominated by the guaiacyl units characteristic of lignin biosynthesized by gymnosperms (Fig 1). Comparison of the modern and fossil Py-GC/MS traces reveal some similarities with many of the *G* sub-units being present in both although there are also clear differences primarily in that the high molecular weight fraction is depleted in the fossil *Larix* (Fig. 1).

The two sample sets were also analysed using thermogravimetry (TG) and differential scanning calorimetry (DSC) TG-DSC-QMS. Furthermore, the coupling of the thermal analyser to a quadrupole mass spectrometer (MS) can also provide continuous identification of evolved gas species during thermal decomposition. The difference in thermal behaviour between recent and fossil woods is clear with the use of TG-DSC-QMS. Two discrete peaks

are present in the modern samples' DSC traces; the first can be attributed to the thermal decomposition of cellulose and hemicellulose, and the second to monomeric structural subunits of lignin. In contrast, fossil samples show only one broad peak, which is due to the partial degradation of lignin to other aromatic components and the absence of cellulose.

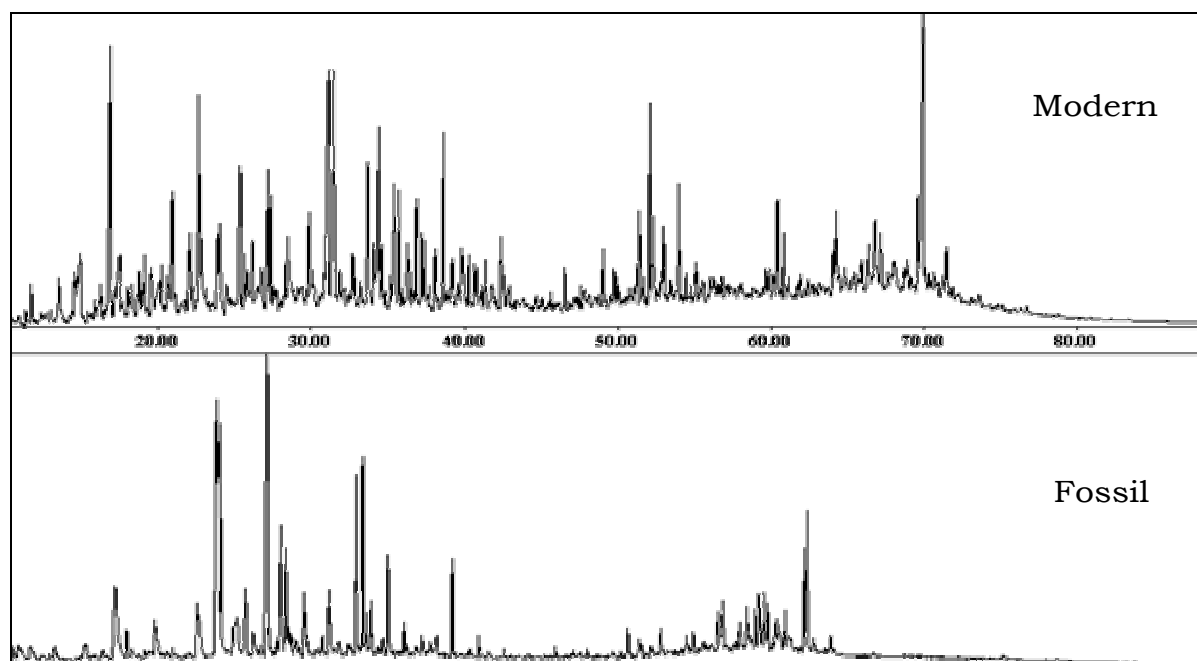


Fig.1. Py-GC/MS traces of TMAH-treated modern and fossil *Larix*

References

- BLANCHETTE, R.A., CEASE, K.R., ABAD, A.R., BURNES T.A. and OBST, J.R. (1991) Ultrastructural characterization of wood from Tertiary fossil forests in the Canadian Arctic. *Canadian Journal of Botany*, **69**, 560-568.
- ADLER, E., 1977. Lignin past, present and future. *Wood Science and Technology*, **11**, 169-218.
- HIGUCHI, T., 1981. Lignin structure and morphological distribution in plant cell walls. In: KIRK, T., HIGUCHI, T. & CHANG, H. (Eds), 2nd ed., *Lignin biodegradation: microbiology, chemistry, and applications*, 1. CRC Press, Boca Raton, p. 1.

PM-23: The chemical structure of cutan revisited: reinterpretation of the TMAH/thermochemolysis data

J.C. del Río

Instituto de Recursos Naturales y Agrobiología de Sevilla, Consejo Superior de Investigaciones Científicas, Apartado 1052, E-41080 Seville, Spain

Insoluble, non-hydrolyzable and highly aliphatic biopolymers have been detected in plant cuticles (cutan, suberan) and in cell walls of several freshwater and marine microalgae (algaenan). These biopolymers are highly resistant to microbial and chemical degradation and hence are selectively preserved in sediments. In past years, several structural models have been depicted for the different biopolymers. With respect to the cutan biopolymer, the current proposed structural models (McKinney et al., 1996; Schouten et al., 1998) consider an aromatic moiety in its structure, which was obtained from TMAH/thermochemolysis data. TMAH/thermochemolysis of cutan released high amounts of 1,3,5-trimethoxybenzene structures (shown in Figure 1a), along with a series of long chain fatty acid methyl esters (extending up to C₃₁). Based on this, McKinney et al. (1996) proposed an structural model for cutan (Figure 1b) in which the backbone of the structure consisted of long chain fatty acids that are ester bound to tetrasubstituted benzene rings linked together, probably via C-C-bonds, by an undetermined cross-link group. The nature of that cross-link group was uncertain but it was believed to consist of a carbonyl-type linkage, which would be consistent with ¹³C NMR and TMAH/thermochemolysis data.

It is well known that TMAH/thermochemolysis results in methylation of polar carboxylic acids, which have poor chromatographic behaviour or undergo decarboxylation in conventional pyrolysis. However, recent studies have shown that some *ortho*- and/or *para*-substituted aromatic carboxylic acids undergo decarboxylation during TMAH/thermochemolysis (Joll et al. 2003). Decarboxylation of hydroxybenzoic acids occurs when the ring has one or more hydroxy substituents in the positions *ortho*- (C-2 and C-6) and/or *para*- (C-4) to the carboxylic group. The 2,4,6-trihydroxybenzoic acid, with the substituents occupying all the *ortho*- and *para*- positions, is highly susceptible to decarboxylation. After TMAH/thermochemolysis this compound yields only 1,3,5-trimethoxybenzene, 2,4,6-trimethoxytoluene and 2,4,6-trimethoxybenzaldehyde, whereas the corresponding non-decarboxylated product 2,4,6-trimethoxy benzoic acid methyl ester, was not produced (Joll et al. 2003).

This important finding led us to reinterpret the TMAH/thermochemolysis data of cutan. As shown before, the cutan biopolymer released high amounts of aromatic moieties (mainly 1,3,5-trimethoxybenzene, 2,4,6-trimethoxytoluene and 2,4,6-trimethoxybenzaldehyde), which are the same as those released from 2,4,6-trihydroxybenzoic acid. Therefore, it is rather possible that the carbonyl-type cross-link group devised by McKinney et al. (1996) is composed by a carboxylate group, as depicted in Figure 1c.

In this case, a different structural model can be envisaged (and will be presented in this work) in which the aromatic units are ester linked in a head-to-tail (1-O4' ester link) position and with possibilities for extension to form a polymeric network. In the model previously proposed by McKinney et al (1996), the two aromatic rings are 1,1'-linked (head-head linked) with no possibilities for further linkages between the different aromatic moieties in order to produce a polymer. This new structural model proposed for the cutan biopolymer is consistent with the Py-GC/MS, TMAH/thermochemolysis, RuO₄ oxidation and ¹³C NMR data. The highly aliphatic character of the cutan biopolymer will encapsulate and protect the ester bonds (alkyl-aryl and aryl-aryl esters) from chemical and enzymatic degradation.

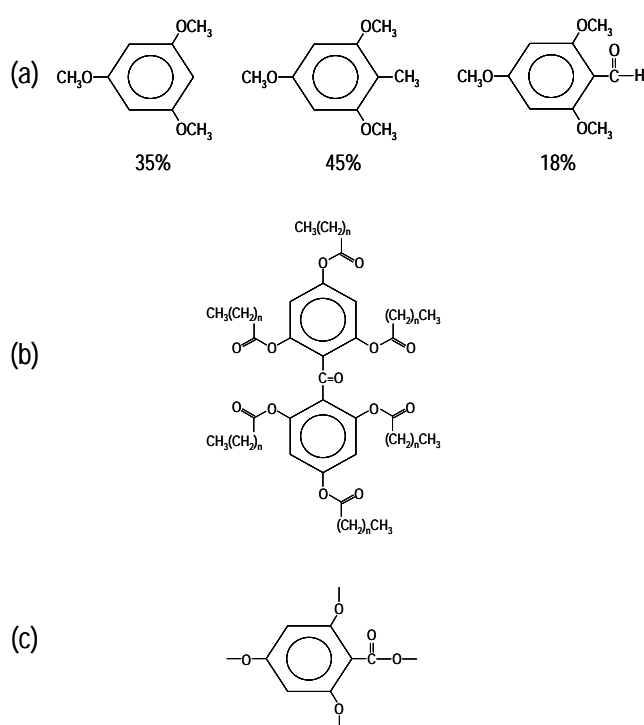


Fig.1. (a) Main aromatic constituents released after TMAH/thermochemolysis of cutan, (b) Structural model for the cutan proposed by McKinney et al. (1996), (c) New proposed aromatic unit in the cutan biopolymer

References

- Joll, C.A. Huynh, T. and Heitz, A. 2003. *Journal of Analytical and Applied Pyrolysis* 70, 151-167.
- McKinney, D.E., Bortiatynski, J.M., Carson, D.M., Clifford, D.J., de Leeuw, J.W. and Hatcher, P.G. 1996. *Organic Geochemistry* 24, 641-650.
- Schouten, S., Moerkerken, P., Gelin F., Baas, M., de Leeuw, J.W. and Sinninghe Damsté, J.S. 1998. *Phytochemistry* 49, 987-993.

PM-24: Detection of protein remnants in different types of kerogens upon pyrolysis in the presence of TMAH

J.C. del Río¹, F.J. González-Vila¹, A. Amblès², H. Knicker³

1) Instituto de Recursos Naturales y Agrobiología de Sevilla, CSIC, P.O.Box 1052, E-41080 Seville, Spain

2) Faculté des Sciences, Université de Poitiers, 40, Avenue du Recteur Pineau, 86022 Poitiers Cedex, France

3) Lehrstuhl für Bodenkunde, Technische Universität München, 85350 Freising-Weihenstephan, Germany

In recent years, amino acids have been released from several sulphur-rich kerogens after pyrolysis in the presence of tetramethylammonium hydroxide (TMAH) indicating that protein remnants could be preserved in a kerogen over geological time (Mongenot et al., 2001; Ribolleau et al. 2002; del Río et al., 2004). Since amino acids were only released from S-rich kerogens, it was suggested that sulphur might have a role in the amino acid preservation in kerogens. In this paper, however, we report for the first time the release of amino acids from different types of kerogens that are not characterized by a high content of organic sulphur. The samples selected for this study included the type I kerogens from Aleksinac and Irati (Brasil), the type II kerogens from Mesnil/Vair and Donnemarie (Paris Basin) and the type III kerogen from Mannville. Pyrolysis in the presence of TMAH and solid-state ¹⁵N NMR were used for the characterization of proteinaceous materials in these kerogens.

The solid state ¹⁵N NMR spectra of the kerogens showed intensity in the chemical shift region between -250 and -285 ppm, indicating that a part of the refractory nitrogen in the kerogens correspond to amide groups. Moreover, Py/TMAH demonstrated that this amide-N is mostly proteinaceous. The chromatograms are dominated by peaks corresponding to fatty acids (as methyl esters) and amino acid derivatives. The amino acids released are dominated by glycine and alanine (as N,N-dimethyl, methyl esters), which are especially abundant in Donnemarie and Manville kerogens. Additionally, minor amounts of aspartic acid and serine; a non-protein amino acid, tentatively identified as α -amino-*n*-butyric acid and two compounds with a base peak at *m/z* 116, probably α -amino acid derivatives, were also detected in the Mesnil/Vair and Donnemarie kerogens. It is interesting to note that the composition of amino acids released from these kerogens is very similar to that released from the S-rich kerogens previously studied (Mongenot et al., 2001; Riboulleau *et al.* 2002; del Río *et al.*, 2004) that also showed glycine and alanine as the most abundant amino acids. As far as we know, this is the first time that proteinaceous moieties are released from different types of kerogens that are not enriched in organic sulphur. Therefore, it seems that the occurrence of

protein remnants may be widespread in all types of kerogens, regardless of the sulphur content.

Several mechanisms have been proposed to explain the survival of peptide-like moieties in geological materials: a) absorption to clay minerals (Hedges and Keil, 1995); b) hydrophobic and hydrogen-bond interactions with other refractory organic materials in the sediment (Knicker *et al.*, 2001; del Rio *et al.*, 2004).

In S-rich kerogens, the preservation of proteinaceous moieties were assumed to be due to an encapsulation mechanism into the kerogen network, that is indeed favored by the presence of S-links (Mongenot *et al.*, 2001; Riboulleau *et al.*, 2002; del Río *et al.*, 2004). The present work supports those previous studies that also suggested that the survival of amino acids within an organic matrix is probably rather common in kerogens, especially glycine and alanine. Then, it is likely that these non-polar aliphatic amino acid components have stronger hydrophobic interactions with the paraffinic network than the fragments that have a higher content on polar amino acids. During kerogen formation, the paraffinic hydrocarbon moieties of the kerogen network may encapsulate the already closely associated aliphatic amino acid fragments and subsequently protect them from chemical and/or microbiological degradation.

In conclusion, it seems that the presence of protein remnants may be widespread in all types of kerogens, which may survive the geological time through an encapsulation mechanism.

References

- Knicker, H., del Río, J.C., Hatcher, P.G., Minard, R.D., 2001. *Organic Geochemistry* 32, 397-409.
- Hedges, J.I., Keil, R.G. 1995. *Marine Chemistry* 49, 81-115.
- Mongenot, Th., Riboulleau, A., Garcette-Lepecq, A., Derenne, S., Pouet, Y., Baudin, F., Largeau, C., 2001. *Organic Geochemistry* 32, 199-203.
- Riboulleau, A., Mongenot, Th., Baudin, F. Derenne, S., Largeau, C., 2002. *Organic Geochemistry* 33, 1127-1130.
- del Río, J.C., Olivella, M.A., Knicker, H., de las Heras, F.X.C. 2004. *Organic Geochemistry*, 35, 993-999.

PM-25: Aliphatic biopolymers and lignin signatures in resilient humic materials from an estuarine sedimentary sequence (Guadiana Valley, SW Iberian Peninsula)

F.J. González-Vila¹, T. Boski², O. Polvillo¹, A. Teran¹, J.A. González-Pérez¹, M.E. Arias³

1) IRNAS-CSIC, Avda. Reina Mercedes, 10, 41012-Sevilla, Spain (e-mail: fjon@irnase.csic.es)

2) CIMA – Centro de Investigação Marinha e Ambiental, Universidade do Algarve, Campus de Gambelas, 8000 FARO, Portugal.

3) Dept. Microbiología y Parasitología. Universidad de Alcalá. 28871 Alcalá de Henares, Madrid, Spain

The formation of refractory macromolecular organic materials is considered in general terms the end of diagenesis in recent and fossil deposits of organic matter (OM). These materials resembles not only in operative terms to the soil humic substances (HS), but also in their functionality and reactivity. It is sought that an important part of organic compounds are continuously deposited in sediments during long periods of time (in particular lipids) that could be incorporated and preserved within the poorly defined structures of this macromolecular material. Therefore this macromolecular material may preserve valuable information about the evolutionary history of particular sediments in response to climatic and/or environmental factors.

This communication is part of a wider study on diagenetic processes in sediments from Guadiana river estuary (SW Portugal/Spain border) representing a record of the last 13 kyr. As a continuation of the research done on the vertical distribution of terrestrial and phytoplankton biogeochemical markers identified along a 45 m depth core (1), we present here the results of the analyses of humic acids (AH) isolated at different depths aiming to get complementary information on the sources and alterations of the depositional OM.

The chemical structural features of humic acids (HA) were approached by a combination of spectroscopic techniques (FT-IR and ¹³C-NMR), wet chemical degradation methods and analytical pyrolysis (Py)-GC-MS) both in the presence and absence of tetramethylammonium hydroxyde (TMAH).

Both spectroscopic techniques (FT-IR and ¹³C-NMR) showed close similarities between the structural characteristics of the HA isolated at different depth along the core. Specific spectral features pointed at the presence of an important aliphatic domain in the structure of the HA and to the presence of methoxyphenols from lignin. This observation was also confirmed by Py-GC/MS analysis of the different HA. The pyrograms obtained by conventional pyrolysis exhibited a series of n-alkene/n-alkane doublets, which may be released from resistant aliphatic macromolecular precursors, such as cutan- and suberan-like materials. In addition, the main TMAH thermochemolysis products detected were series of

long-chain fatty acids methyl esters and typical lignin derived methoxyphenols, with both guaiacyl and syringyl nuclei. The detection of C₆-C₃ units suggest that lignins is only partially degraded in this environment. Different compounds arising from proteins and polysaccharides were also detected, although in lesser and varying amounts.

Chemical degradations involved potassium persulfate (a mild oxidant) oxidation, followed by potassium permanganate oxidation. The study of the sequential degradation products were specially informative with respect to elucidate bound strength and molecular structural organization of the studied HA's. A perborate oxidation, known for its efficiency in macromolecular depolymerisation, and a ruthenium tetroxide oxidation, especially suitable for investigating the structure of resistant aliphatic macromolecules like algaenans, cutans or suberans, were also performed.

The major products release after HA's persulfate oxidation were series of *n*-alkanes (C₁₆-C₃₃ with a clear odd-over-even carbon number predominance) and *n*-fatty acids, both saturated (C₁₀-C₂₆ with strong even-over-odd predominance) and unsaturated. The major products after degradation with permanganate of the persulfate residues were aromatic compounds (phenols, methoxi-dimethoxi-benzenecarboxylic acid and di, tri, tetra and pentacarboxylic benzenecarboxylic acids) derived from the aromatic backbone of the HA's, including lignin moieties and others poliphenols (flavonoids and tannins). The high proportion of diacids may originate from the oxidation of the ether bounds linking the building blocs that conforms the core of the HS's structure.

In general, the different approaches used shows that the humic materials isolated from the studied sedimentary sequence contains valuable information on the signature of aliphatic and aromatic biopolymers originally contributing to the depositional OM. Our data shows the presence of lignin-derived residues that suggest a large input from terrestrial carbon throughout the core.

References

- 1) González -Vila, F.J., Polvillo, O., Boski, T., de Andrés, J.R. (2003). *Org. Geochem.* 34,1601

PM-26: Organic matter preservation patterns in marine sediments from Celtic Sea & NW Iberian Margin. A contribution from the adsorption study of hydrolysable amino acids on mineral surfaces

P. Pedro¹, T. Boski¹, J.C. Pessoa², J. Thorez³

1) CIMA, Universidade do Algarve, Campus de Gambelas, 8000-139 Faro, Portugal

2) C. Química Estrutural, Instituto Superior Técnico, Av. Rovisco Pais 1, 1160 Lisboa, Portugal

3) Geologie des Argiles, Université de Liège, B18 Sart Tilman, 4000 Liège, Belgique

Association with mineral surfaces, mainly clay minerals, has been suggested as a form of preservation of organic matter in marine sediments though the precise nature of the controls on the burial of organic material in marine sediments are not fully understood by paleoceanographers and organic geochemists (1, 2, 3). Nine sediment cores, sampled on three transects on the NW Iberian margin from the shelf to the abyssal plain, and 6 cores from 2 transects of Celtic Sea were quantitatively analyzed for total hydrolysable amino acids (THAA), clay minerals, total carbon, total organic carbon, total nitrogen and grain size. Analysis on extractable silica, aluminium and iron were also performed on samples from the Iberian Margin. Sediment cores were collected during Discovery 216, Charles Darwin CD110 cruise and Pelagia 121 cruise using multicorer and boxcorer. THAA were determined by reverse phase HPLC after acid hydrolysis. For the NW Iberian Margin, the most abundant amino acids among the 12 quantified were, aspartic acid, glycine, serine, alanine and glutamic acid, representing between 60 to 80 % of the total, depending on the sample. A decreasing trend in concentration with depth was observed in the studied cores. Organic carbon, total carbon and total nitrogen were measured on a Carlo Erba C/N analyser, with nitrogen contents ranging from 0,1 to 0,03 % dw, decreasing from the shelf to the abyssal plain. Total organic carbon contents were between 2,77 and 0,20 % dw showing a decrease in depth on each analysed core. Illite was found to be the predominant clay mineral in all the sediment samples. Most of the samples in the NW Iberian Margin revealed important quantities of amorphous material. Given the abundance of gibbsite in the soils of neighbouring continental area, the presence of alofan was checked through chemical analyses of extractable aluminium silica and iron that can explain the lack of affinity between chlorites and amino acids in opposition to what was observed in the Celtic Sea samples. The concentrations of organic carbon in the NW Iberian margin are much higher than the ones found in Goban Spur – Meriadzek terrace sector, and may be attributed to seasonal up welling and to the geographic proximity of the rias (predominantly during the winter) and the river mouths, supplying the terrigenous organic matter during the winter. The faster burial rates and the refractory

characteristics of the organic carbon may in part account for the observed differences between NW Iberian margin and Goban Spur area, though high contribution of terrigenous material to the buried organic carbon reservoir seems to be much greater in some areas of the NW Iberian margin than in Goban Spur. For the Iberian Margin samples an alternative way of organic matter entrapment is proposed, i.e. mainly through adsorption, by amorphous SiO₂ and Fe & Al, oxy/hydroxides, leading to the maintenance of the high TOC yields.

References

- (1) Hedges, J.I., Keil, R.G., 1999 Organic geochemical perspectives on estuarine processes: sorption reaction and consequences. *Marine Chemistry*, 65, 55 - 65
- (2) Kennedy, M.J., Pevear, D.R., Hill, R.J., 2002. Mineral surface control of organic carbon in black shale. *Science* 259, 657–660..
- (3) Zimmerman A. R., Goyneb K. W., Chorover J., Komarneni S., Brantley S. L., 2004. Mineral mesopore effects on nitrogenous organic matter adsorption. *Organic Geochemistry* 35, 355–375

PM-27: Characterization of the organic constituents of aqueous and sediment phases of the Cébron reservoir

M. Poulain¹, C. Rodier¹, J.-P. Croue², A. Ambles¹

1) Laboratoire de Chimie XII -UMR 6514- « Synthèse et réactivité des substances naturelles », Faculté des Sciences, 40 avenue du Recteur Pineau, 86022 Poitiers Cedex

2) Laboratoire de Chimie de l'Eau et de l'Environnement – UMR 6008, ESIP Poitiers
(e-mail : andre.ambles@univ-poitiers.fr)

In natural aquatic systems such as wetlands, strong interactions between the sediments and the aqueous phase exist. The objective of our work is to develop a better knowledge of the quantity and the quality of the organic matter present in these two phases. The nature of the organic matter was investigated at low and high molecular levels by different extraction and degradation techniques.

Sample was collected from a wetland rich in organic matter connected to the Cébron reservoir (Deux-Sèvres, Western part of France). After sampling, the dissolved organic matter (OM) was isolated (dialysis, XAD resins) in three fractions: colloidal OM, hydrophobic OM and transphilic OM. The sediment (sludge) was fractionated following the IHSS protocol; the lipid, fulvic acid, humic acid and humine fractions were obtained.

The first part of the work has been focused on the analysis of small molecules as polycyclic aromatic hydrocarbons (PAH), sterols, known as excellent biomarkers and saturated linear hydrocarbons. These compounds were analysed in the aqueous and sediment phases. PAH were extracted from water using stir bar sorptive extraction technique and a quantitative method based on MS/MS has been developed for quantification. Sterols were extracted (solid phase extraction), silylated and then analysed by GC/MS. In the sediment, lipids were analysed by GC/MS. Results obtained for sterols and hydrocarbons showed similar distributions in both water and sediment, whereas for PAH, the major compound found in water (i.e. naphthalene) is not necessarily the most abundant in sediment. Most of the molecules isolated are mainly issue from vegetals or are natural compounds and can not be associated with pollution.

The different humic fractions of OM were submitted to flash pyrolysis and thermochemiolysis (pyrolysis in presence of an alkylating agent: tetramethylammonium hydroxyde). Using these methods, complex structures are reduced into small alkylated molecules which reveals the natural origin of organic matter in the sample. Distributions of fatty acids are similar in the OM from the aqueous and sediments fractions but aromatic compounds are more concentrated in the sediment. The determination of sterols and PAH distributions in the isolated dissolved OM is under progress.

PM-28: On the macromolecular structure of algal cell walls, notably dinoflagellate walls

G.J.M. Versteegh¹, P. Blokker²

1) Hanse Wissenschaftskolleg, Lehmkuhlenbusch 4, 27753 Delmenhorst, Germany (e-mail: gerardv@nioz.nl)

2) Institute of Ecological Science, Faculty of Earth and Life Sciences, Vrije Universiteit, De Boelelaan 1085, NL-1081 HV Amsterdam, the Netherlands

Sedimentary organic matter is by far the largest sink in the global carbon cycle, but its chemical composition due to its predominantly (95%) macromolecular nature is poorly understood. Over the last decades some resistant bio- and geopolymers from terrestrial and freshwater biota have been identified and transformation pathways proposed. In contrast, the composition of macromolecular marine organic matter entering the geological organic carbon cycle is still largely unknown. Without this vital information, our understanding of organic matter formation and preservation is severely incomplete. Since an important part of the macromolecular marine sedimentary organic matter is produced by microalgae we focus on these organisms, notably the chemical structure of their recent and fossil walls, in an attempt to obtain a better insight in the nature of the ‘marine gap’

Our current knowledge on the occurrence and composition of macromolecular resistant walls of microalgae and their fossil macromolecular counterparts is almost entirely restricted to the walls of Chlorophyta. Since for only very few members of other algal groups (e.g. Eustigmatophyta and Dinophyta) the wall composition has been investigated mainly the results on recent and fossil non-Chlorophyte algae will be presented. Only two biosynthetic pathways seem to be in use to produce resistant walls. The acetate/malate pathway, used by Chlorophyta, Eustigmatophyta and Dinophyta is considered to lead to a series of closely related resistant biomacromolecules; algaenans which consist of a network of predominantly linear carbon chains. A different, as yet unidentified, pathway is used by the Dinophyta to produce the aromatic walls of their cysts. The polyketide or acetogenic pathway may have been responsible for resorcinol-based algae or bacteria-derived microfossils of the acritarch *Gloeocapsomorpha prisca*, either through synthesis of the biomacromolecule or through a third pathway, the post-mortem polymerization of its resorcinol lipids. The post-mortem polymerization of lipids also appears to be responsible for the formation of fatty acid-based macromolecules in Eocene dinoflagellate-shaped remains from Pakistan. Finally, there is a clear need for elucidating the chemical differences between the biomacromolecules produced by the algae and their fossil analogs in the sediments. This notably applies to the release and condensation of aliphatic and aromatic moieties both at normal and at elevated temperature and pressure conditions.

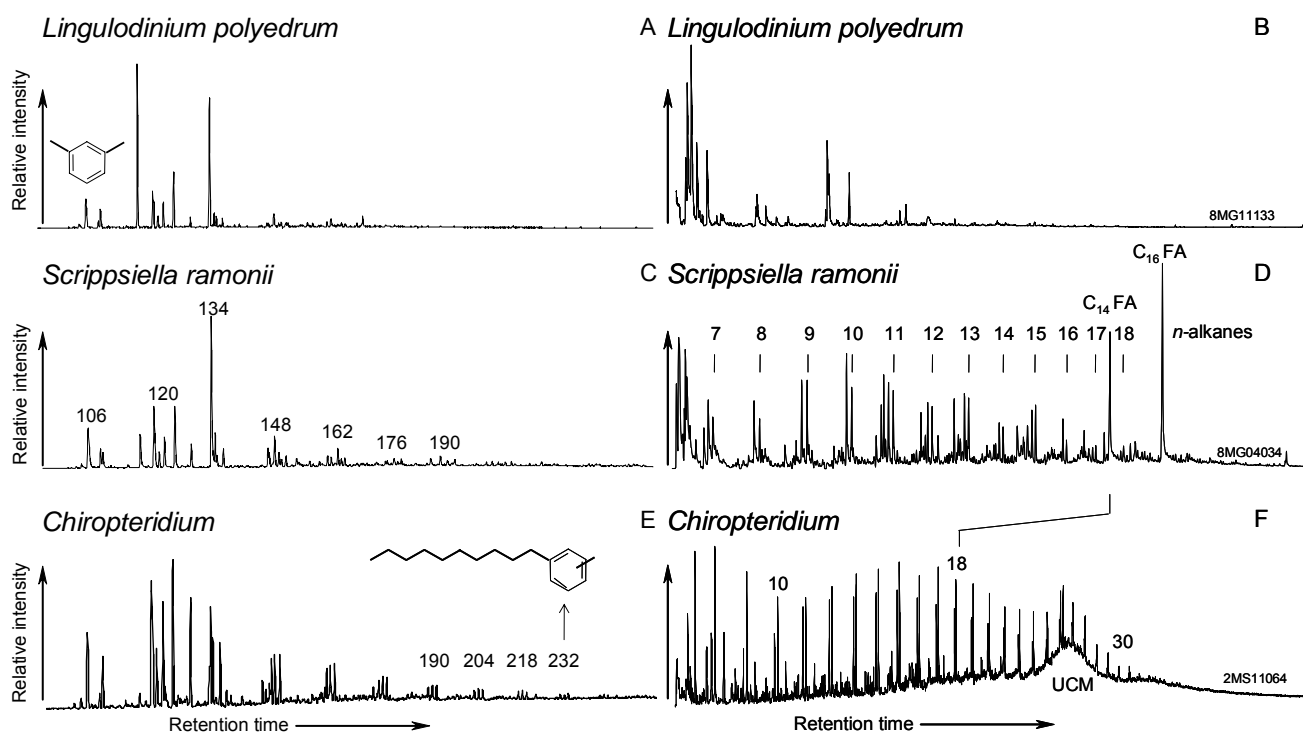


Fig.1. Examples of Pyrolysate mass chromatograms of dinoflagellate cyst walls. A,B. *Lingulodinium polyedrum* cysts from cultures, C,D. *Scrippsiella ramonii* cysts from cultures, E,F. *Chiropteridium* cysts from Oligocene sediments.

m/z 105 (A,C,E) showing the methyl-,alkyl-benzenes and m/z 55 + 57 (B,D,F) showing the aliphatic moieties, notably alkene/alkane doublets. Numbers in panels C, E refer to the M^+ of the corresponding components. FA= fatty acid, UCM = unresolved complex mixture

PSB-1: Complexation Properties of Esterified Soil Humic Acids

T. Andjelkovic¹, J. Perovic¹, M. Purenovic¹, S. Blagojevic², D. Andjelkovic³

1) Faculty of Natural Sciences, University of Nis, Visegradska 33, 18000 Nis, Serbia
(e-mail: darkoa@bankerinter.net)

2) Faculty of Agriculture, Nemanjina 16, 11081 Belgrade, Serbia

3) Water Work Association "Naissus", Kneginje Ljubice 1/1, 18000 Nis, Serbia

The environmental behavior of humic acids (HA) depends on its functionality. Stable complexes with heavy metals are formed mainly by carboxylic, phenolic hydroxylic and alcoholic groups. The aim of this work is to quantify the complexation of Cd by carboxylic groups in HA, by its selective blocking.

HAs was obtained following the procedure suggested by the International Humic Substances Society (IHSS) (Sparks, 1996) from a well-humified organic horizon of old beech-forest soil (10 cm depth), in autumn 2003, using standard grinding equipment. The soil was air-dried and sieved to pass a 2.0 mm sieve. Stock suspensions containing 1 g l⁻¹ HA were prepared as required and stored in the dark at 4°C. Complexometric titrations were made with two Hach sension3 pH/ion-meters; one of them was used for pH measurements and the other was used with an ion selective electrode (ISE-Metrohm, 6.0502.110) for Cd(II) against an double junction Ag/AgCl reference electrode (Metrohm, 6.0726.100). For pH monitoring a Hach gel-filled combination glass electrode (51935-00) was used. Throughout the titrations a N₂ gas was initially bubbled through the solution and then a constant atmosphere was maintained above the solution which was thermostat in a water bath at 25.0 ± 0.1°C. The pH of the solution was adjusted to 6.50 ± 0.05, by addition of minute amounts of diluted KOH or HNO₃. Titrations were performed with 40.00 ml of humic acid suspension, titrated with 5.19·10⁻⁴ M Cd²⁺ in ionic medium of 0.1M KNO₃.

Selective blocking of carboxyl functional groups was achieved by esterification, by isolation of esterified HA derivative (EHA). Esterification was performed by methanol-thionyl chloride procedure suggested by Schnitzer and Skinner (1965) and Hosangadi and Dave (1996). To a stirred solution of 500 mg of HA in 20 ml of methanol, under ice-cooling (approximately -5°C), was added thionyl chloride (5 ml) dropwise from the dropping funnel, over 2 hours. The reaction mixture was then heated on the water bath for 5 minutes to decompose excess thionyl chloride. The suspension was then centrifuged at 2000 rpm and washed with distilled water until free of chlorides. The EHA was dried in a rotary evaporator and finally in a vacuum desiccator over P₂O₅. Stock EHA suspension contained 1 g l⁻¹ EHA. IR-spectra were recorded on a Bomem Hartman & Braun MB-Series FT-IR

spectrometer from 4000 to 1000 cm^{-1} , using KBr pellet (1 mg of sample + 200 mg of dry KBr). The increased intensity of band at 1730 cm^{-1} (CO of carboxylic acid) confirms the carboxyl group esterification.

The Scatchard method (1949) was used for data evaluation. Scatchard plot is shown in figure, where $c(\text{CdA})$ is the concentration of the complexed metal and $c(\text{Cd}^{2+})$ is free metal concentration. Obtained values for conditional stability constant ($\log K$) were 3.57 for HA and 3.35 for EHA. The total concentration of binding sites was 0.980 mmol g^{-1} for HA and 0.425 mmol g^{-1} for EHA.

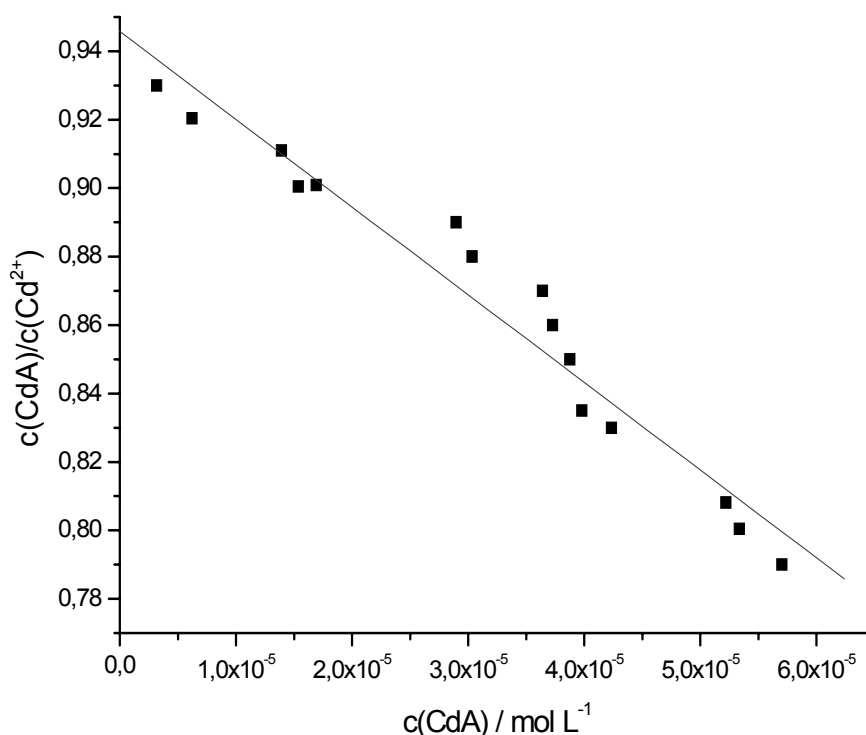


Fig.1. Scatchard plot for EHA (40.00 ml of 80 mg l^{-1} EHA suspension, $\text{pH} = 6.50 \pm 0.05$, 0.1M KNO_3 titrated with $5.19 \cdot 10^{-4}$ M Cd^{2+})

The differences in the total concentration of binding sites and conditional stability constants were directly related to availability of carboxylic groups for interaction with ions, indicating their importance in complexation.

References

- Hosangadi B. D. and Dave R. H. (1996) Tetrahedron letters 37: 6375-6378
 Scatchard, G. (1949) Ann. New York Acad. Sci. 51: 660
 Schnitzer, M. and Skinner S. I. M. (1965) Soil Sci. 99: 278-284
 Sparks, D. L. (Ed.) (1996) Methods of Soil Analysis, Part 3, Chemical Methods. Soil Sci. Soc. Am. Book Series 5, Soil Sci. Soc. Am., Madison WI, USA, pp. 1018

PSB-2: Physical-chemical characterization of humic acids isolated from Chilean Andisols

J. Canales¹, M. de la Luz Mora¹, M.J. Aguirre², M. González-Ibarra³, R. Gaviño⁴,
B. King-Díaz⁴, B. Lotina-Hennsen⁴

1) Departamento de Ciencias Químicas, Facultad de Ingeniería, Ciencias y Administración, Univ. de La Frontera, Casilla 54-D, Temuco, Chile

2) Dept. de Química de los Materiales, Facultad de Química y Biología, Univ. de Santiago de Chile, Casilla 40, Correo 33, Santiago, Chile

3) Dept. El Hombre y su Ambiente, Univ. Autónoma Metropolitana, Calzada del Hueso 1100, C.P. 04960, México City, México

4) Inst. y Facultad de Química, Univ. Nac. Autónoma de México, C.P. 04510, México D.F., México

Introduction

Humic acids are high molecular weight polymer whose structure presents several functional groups which have chelating capacities and immobilize nutrients temporarily to gradually liberate them to the plant. The purpose of our work was to obtain data on the biological influence of Humic acids (HA) from Andisols (Barros Arana and Gorbea series) and a commercial humic acid (Aldrich, AHA) on seed germination and root-shoot development in the following seeds: *Triticum vulgare*, *Lolium perenne* and *Physalis ixocarpa*.

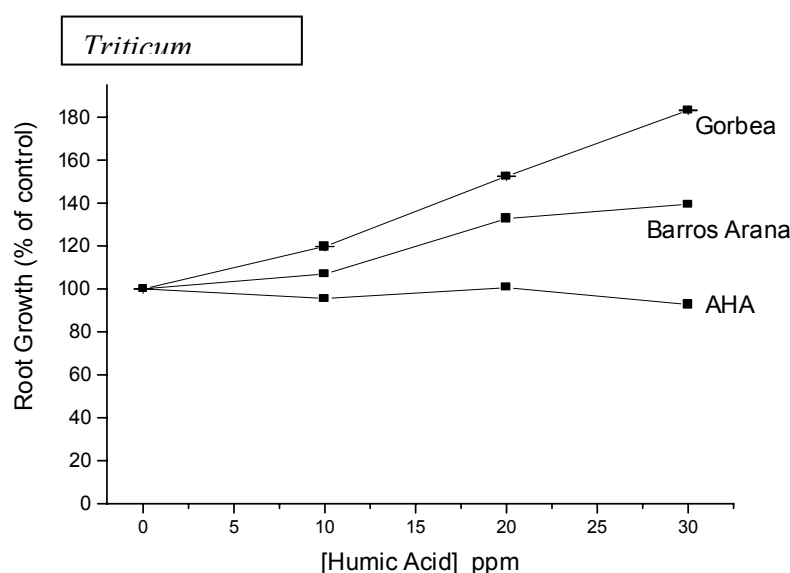
Materials and methods

The studied soils belong to the Barros Arana (B.A) and Gorbea (G) series characterized as Andisols located in the 9^a Region of Chile. Samples were taken between 0-20 cm deep and screened in a 2 mm sieve. Organic Matter (O.M) content was determined by the Walkley and Black method (1947). Germination bioassays were made in triplicate employing the following seeds: *Triticum vulgare*, *Lolium perenne* and *Physalis ixocarpa*. Seeds were set at 28 °C in Petri dishes (Hasegawa K. et al., 1982) on Whatman N°1 filter paper (85 mm diameter) under different concentrations of Humic Acids (0 to 30 ppm) in an incubator Indere Model 94006.

Results and discussion

The FT-IR spectra from the three varieties of humic acids can be interpreted under the studies of Stevenson and Goh (1971). A strong band is seen for Barros Arana and Gorbea, but none for Aldrich in the 1710-1750 cm⁻¹ zone attributed to the presence of -C=O groups, as part of -COOH groups. A greater difference between Humic (Barros Arana and Gorbea) acids and the Aldrich variety is the lack of bands at the 1720 and 1630 representing -C=O- groups from carboxylic functions zones and at 1200 cm⁻¹ zone, representing OH groups from carboxylic functions (Francioso *et al.*, 1998). The most important difference is the low amount of N in the commercial humic acid, which makes the relation C/N the highest. Even

though total acidity is similar between the humic acids from Barros Arana and the commercial HA, in the commercial humic acid, acidity is exclusively due to phenolic groups. The humic acid of Gorbea, as well as the HA of Barros Arana, has relatively equivalent quantities of both groups, carboxylic and phenolic. The H-NMR spectra show only on the aromatic zone a difference between the Aldrich commercial humic acid type and both local varieties. The HA P-NMR shows that both phosphates (ester and inorganic) are in greater proportion at the Barros Arana HA. The humic acid from Barros Arana soil has greater activity due to the presence of mono- and diester phosphates attributed to plant and microorganism activity. The commercial Aldrich HA does not present chemical shifts from this type. On the other hand, the reactivity toward the growing and development of roots and shoot with the content of HA Gorbea and Barros Arana depends on the seed. For *Triticum vulgare* root growing the activity is shown in Figure 1.



Acknowledgements

Authors acknowledge financial support from Universidad de La Frontera, Fondecyt project 1950773, 1010695 and Sagu Fischer Scientific.

References

- Wakley A., Black I.A., 1947, *Soil Sci.*, 37, 29-39.
 Hasegawa K., Shihara S., Iwagawa T., and Hase T., 1982, *J. Plant Physiol.* 70, 626-628.
 Stevenson, F.J. y Goh, M.K. 1971 "Geochim. Cosmochim"
 Francioso O., Sánchez Cortés S., Tugnoli V., Ciavatta C, and Gessa C., *Applied Spectroscopy*, 52, (2), 270-277, (1998).

PSB-3: Characterization of humic acid from Pahokee peat using Electrospray Ionization Tandem Mass Spectrometry

R.-H. Feng^{1,2}, P.-A. Peng¹, J.-Z. Song¹, W.-B. Zhang¹

1) State Key Laboratory of Organic Geochemistry, Guangzhou Institute of Geochemistry, Chinese Academy of Sciences, Guangzhou 510640, China (e-mail: pinganp@gig.ac.cn)

2) Graduate School of Chinese Academy of Sciences, Beijing 100039, China

Electrospray ionization (ESI) is a “soft ionization” technique. McIntyre et al. (1997) applied electrospray mass spectrometer to the study of humic substances for the first time^[1]. ESI can provide some component-specific structural information of aqueous humic acid (HA) in combination with MS/MS techniques. Pahokee peat HA (PHA) was recommend as the standard sample by International Humic Substances Society. Many studies of this sample have focused on solid-state HA. However, knowledge on the properties and structures of aqueous HA is also important even though few works in this area was done. In this study, the aqueous PHA was analysed using ESI-MS/MS technique, and then in combination with ESI-MS/MS data of 17 model compounds of lignin, the structural characteristics of aqueous PHA are discussed.

The ESI-MS spectra of aqueous PHA showed that distribution of its ion peaks was continuous with the mass charge ratios (m/z), ion peaks ranged from m/z 65 to 2000 and most of the peaks were under m/z 1500 (Fig. 1). The strength of ion peaks was characterized by “wave pattern” maxims at m/z 250, 350, 500 and 700, representing the dimeric, trimeric and tetrameric structures of lignin degraded products.

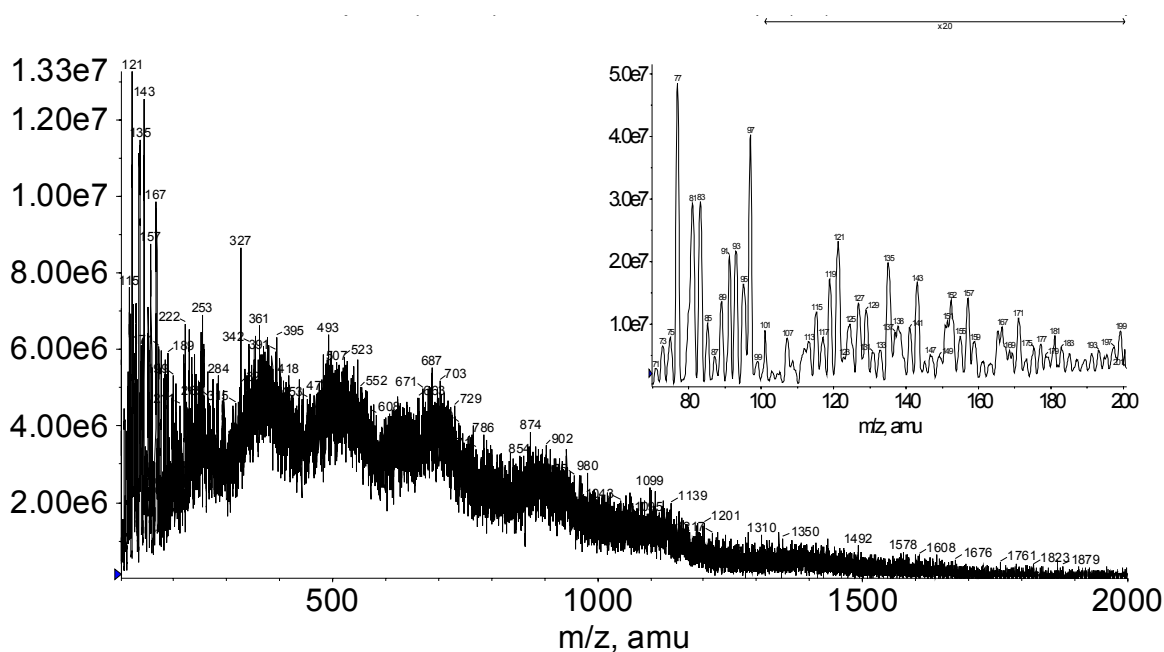
The most strong ion fragments in the range m/z 65 to 110 possibly belonged to the “building blocks” of PHA. The m/z 67, 81 and 77 assigned as ion of furan, pyrane and phenyl. The high abundance of m/z 77 showed that phenyl takes a large proportion in the structures of PHA. The m/z 83, 85, 91 are fragment ions of naphthene, straight chain alkyl and alkyl benzyl, while m/z 92 and 93 are ion of phenyl with an oxygen free radical. The m/z 95, 97, 107, 108, 109, and 111 are ions of carbonyl furan, methoxyl furan or pyrane, methoxyl phenyl, phenyl with two hydroxyls, carbonyl pyrane, and furan carboxylic acid respectively. Although assignments of ions still are tentative, the existence of furan, pyrane, substituted phenyl, cyclanes, and normal alkane structures in the PHA molecules may suggest that PHA partly derived from lignin, polysaccharide and their derivatives.

The ion fragments in the range m/z 110 to 200 were mainly the monomer of *p*-hydroxy phenols, vanillyl phenols, syringyl phenols and their derivations. These monomers mainly derived from the degraded lignin^[2]. The m/z 121, 135, and 137 are ion fragments of

benzoic acid or p-hydroxyphenyl lignin. The m/z 123 is ion degraded from guaiacyl lignin and syringyl lignin. The m/z 153 is ion fragment of 3,4-dihydroxy benzoic acid or 2,6-dimethoxy phenol. The m/z 165 and 167 are ions of acetovanillone and vanillic acid, while the m/z 169, 181, 195 and 197 are ions of 3,4,5-trihydroxy benzoic acid, syringaldehyde, acetosyringone and syringic acid, respectively. These ESI-MS/MS data indicated that PHA is mainly derived from grass and wood plants.

Neutral mass loss of 44(CO₂) can be found in the m/z 109, 121, 123, 137, 153, 165, 167, 169, 181 and 197 by analysis of MS-MS, implying that high amount of carboxyl existed in the humic acid. The homologue ions m/z 87, 101, 115, 129, 143, 157 and 171 may be alkyl tetrahydrothiophene compounds.

Results showed that ESI-MS/MS method was reduplicative and can be used to study the structures of humic acid. The “core structures” was viewed by “Building blocks” in range m/z 65-110, while linkage of molecules in the entity may interpreted from “wave pattern” from m/z 110-2000.



References

- [1] McIntyre C, Batts B D, Jardine D R. 1997. *Journal of Mass Spectrometry* 32: 328~330.
- [2] Saiz-Jimenez C, de Leeuw J W. 1986. *Organic Geochemistry* 10: 869~876.

PSB-4: Study of some structural features related to the humic nature of different organic materials through the complementary use of fluorescence and UV-Visible spectroscopy

M. Fuentes Ramírez¹, G. González-Gaitano¹, J.M^a. García-Mina^{1,2}

1) Department of Chemistry and Soil Chemistry, University of Navarra, 31080, Pamplona, Spain

2) R&D Department, Inabonos-Roullier Group, Polígono Arazuri-Orcoyen, 31160, Orcoyen, Spain
(e-mail: jgmina@inabonos.com)

An adequate knowledge on the chemical structure of humic substances (HS) is of major importance in order to better understand a great number of natural processes occurring in natural ecosystems. However, the chemical nature of those chemical characteristics and structural features related to the so-called “humic nature” remains still open for discussion.

Previous studies have shown that both fluorescence spectroscopy and UV-Visible spectroscopy are adequate tools to analyse the presence of specific functional groups in HS. In this context, the aim of our work is to characterize some of the structural features that could define the so-called “humic-nature” in different molecular systems by means of the complementary use of fluorescence and UV-Visible spectroscopy, in a comparative study including molecular systems obtained from different sources and humification stage: 5 HS samples obtained from natural ecosystems, 5 anthropogenic HS obtained from composted organic materials and the 5 original uncomposted organic materials.

The different organic systems were extracted using 0.1M sodium hydroxide under N₂ atmosphere, and the organic carbon content in the humic alkaline extracts was analyzed. For the fluorescence study, solutions of 10 ppm of organic carbon (C_{org}) of each system in 0.05 M NaHCO₃ were prepared. Emission spectra ($\lambda_{exc} = 240$ nm) were collected between 350-650 nm. The following parameters have been used to characterize the humification degree of the samples: As proposed by Zsolnay et al. (1999) emission spectra were divided into four regions, and the ratio of the last quarter's area and first quarter's area was used as an index of humification degree. Kalbitz et al. (1999) proposed as humification indices the ratio of fluorescence intensity at 470 and 360 nm, or 400 and 360 nm obtained in synchronous spectra. We have also used the ratio of fluorescence intensity at 350 and 480 nm to differentiate between different humification states.

UV/VIS spectra were recorded in solutions of HS in 0.05 M NaHCO₃ and 0.1M NaOH. E400/E600, E465/E665 (E₄/E₆) ratios, and absorption coefficients at 600 nm (E600/C_{org}) were calculated from these spectra.

In conclusion, among the parameters studied, the graphical representation of ratios I350/I480 versus E400/E600 obtained by fluorescence and UV/VIS spectroscopy came out to best distribute the different systems according to their humification degree. Our results confirm that humification degree is probably related to the conjugation of double bonds C=C, C=O and other functional groups in both aliphatic and aromatic structures, which implies a reduction in the difference between electronic level energies and its translation into a shift of spectra toward longer wavelengths.

References

- Zsolnay, A., E. Baigar, M. Jimenez, B. Steinweg, F. Saccomandi. 1999. Differentiating with fluorescence spectroscopy the sources of dissolved organic matter in soils subjected to drying. *Chemosphere*, 38: 45-50.
- Kalbitz, K., W. Geyer, S. Geyer. Spectroscopic properties of dissolved humic substances - a reflection of land use history in a fen area. *Biogeochemistry*, 47: 219-238.

PSB-5: Stability, solubility and maximum metal binding capacity in metal-organic complexes formed by humic substances with different origins and physico-chemical properties

J.M^a. García-Mina

Department of Chemistry and Soil Chemistry, University of Navarra, 31080, Pamplona, Spain
R&D Department, Inabonos-Roullier Group, Polígono Arazuri-Orcoyen, 31160, Orcoyen, Spain
(e-mail: jgmina@inabonos.com)

A number of studies have shown the ability of humic substances (HS) to affect the dynamics of different metals in either terrestrial or aquatic ecosystems. In some cases, these effects were expressed in an enhancement of metal bioavailability whereas in other cases significant decreases in this property were observed. These effects, which depended on soil characteristics and metal concentration in soil solution, could be explained if it is assumed that they are related to the formation of metal-humic complexes whose stability and solubility depend on certain soil properties such as pH and the soil solution chemical composition. Unfortunately, there are few studies in the literature dealing with the effects of these types of organic complexes on plant development and mineral nutrition that include a characterization of complex stability and solubility.

In this context, the aim of this work is to study the variation of the stability, solubility and the maximum metal binding capacity (MBA) as a function of pH and the HS : metal ratio, in molecular systems formed by organo-mineral complexes including HS with different genesis and physico-chemical characteristics.

Four different HS were used in the experiments: a humic acid and an unfractionated humic extract both obtained from black peat; and a fulvic acid and an unfractionated humic extract both obtained from a compost of solid wastes from wineries. The metals considered in the experiments were Cu (II), Zn (II) and Fe (II). The different physicochemical properties of metal-humic complexes were studied in the pH range of 5-12, and the HS (mg) : metal (mg) ratios in the reactions were: 2:0.1, 2:0.25, 2:0.40, 2:0.55, 2:0.70, 2:0.85, 2:1.00, 2:1.50, and 2:2.00.

The pH-dependent apparent stability of the humic complexes in solution was estimated using an apparent stability constant (K_0) calculated using the Scatchard method: $\theta / \text{MFT} = K_0 - \theta K_0$; MFT being the total free metal in the equilibrium; MCT the total complexed metal; and θ the Sites bound / MBA (MCT / MBA) ratio, where K_0 (K_{01} for low metal ion saturation and K_{02} for high metal ion saturation) was obtained from the plot θ / MFT vs θ .

MBA was obtained from experimental data using the double-surface Langmuir equation:

$MCT = [b_1 - MCT / K_1 MFT] + [b_2 - MCT / K_2 MFT]$. Results corresponding to HS:metal reaction ratios without precipitation of HS were only considered in the calculation of K_0 . The relative solubility of metal-humic complexes was evaluated studying the variation of bound metal concentration in solution as a function of pH and the HS:metal ratio.

In order to summarize the different results obtained in the experiments, the main conclusions are outlined below:

1. Regarding the variation of MBA as a function of pH, our results clearly indicated that it varied significantly depending on the pH value. Taking into account that the variation of pH is normally accompanied by significant conformational changes in macromolecules and molecular aggregates, this result shows the major influence of these conformational changes on the functionality of the binding sites present in HS. This influence can be associated with changes in either the stability or the integrity of binding sites, or even in both. However, the fact that the variation of MBA did not always correlate with that of apparent stability suggests that the effective concentration of binding sites could really be affected by the conformational changes that HS undergo with pH variation.

2. As for the apparent stability, this varied according to the complexed metal. In the case of Cu, the maximum apparent stability corresponded to a pH range of 5-7, thus suggesting that amino groups could play an important role in this process. With respect to Zn, the maximum apparent stability coincides with the maximum MBA in the pH range of 9-10. This result suggests the involvement of phenol groups, together with carboxylic groups, in the binding process. The results concerning Fe complexation were similar to those of Zn but the optimum pH in this case was of 8, thus suggesting the involvement of very acidic phenols, in addition to carboxylic groups, in the binding process.

3. As far as complex solubility is concerned, our results indicated that it decreased in line with the pH and HS:metal ratio.

In conclusion, these results suggest that the formation of metal-humic complexes in acid conditions and in the presence of high concentrations of soluble metal (a common situation in acid soils) is associated with the precipitation on HS-bound metal, thereby decreasing metal concentration in soil solution; whereas the formation of these same types of organic complexes in alkaline conditions and in the presence of low concentrations of soluble metal (a common situation in alkaline and calcareous soils) is associated with enhanced metal concentration in soil solution.

PSB-6: Lignin in soils turns over faster than bulk carbon

A. Heim, M.W.I. Schmidt

University of Zurich, Dept. of Geography, Winterthurerstr. 190, 8057 Zürich, Switzerland
(e-mail: alexheim@geo.unizh.ch)

The shift in stable carbon isotope ratios in soils after introduction of isotopically labeled biomass can be used to assess soil organic matter turnover. While studies on bulk soil turnover rates have been established during the past years, only little work has been done on the turnover times of specific compounds due to the analytical difficulties involved in determining isotope ratios of single compounds within a complex mixture. Lignin is a major plant constituent and is considered to be relatively resistant to decomposition, thus contributing to the slowly mineralising pool of soil organic matter (SOM). We analysed bulk soil and particle size fractions of various agricultural plots that had been isotopically labeled either by conversion from C3 to C4 crops or by fumigation with ^{13}C -depleted CO_2 . Using the microwave CuO oxidation method, the lignin macromolecule was converted into its monomer units (acids, aldehydes and ketones of vanillyl, syringyl, and cinnamyl units). These were identified by GC/MS and compound specific $^{13}\text{C}/^{12}\text{C}$ isotope ratios were determined by GC-C-IRMS.

The samples studied so far indicate a faster turnover time for lignin-derived monomers than for bulk SOM. This is in contrast to the existing assumption that the lignin macromolecule is selectively preserved within SOM. Among the structural units, cinnamyl units turn over faster than syringyl and vanillyl units. Under pasture, lignin turnover appears to be faster than in arable soil. First lignin analyses in particle size fractions support the view of relatively fast lignin turnover. We observed relatively small differences in lignin turnover times between the particle size fractions, while the proportion of lignin oxidation products to total organic carbon decreases from fine sand to clay fractions. The clay fraction is usually considered to contain the oldest and most stable carbon. Thus, the low percentage of lignin oxidation products in this fraction suggests that lignin molecules do not contribute significantly to this selectively preserved carbon pool. Current work aims at extending the available dataset by comparing different management practices (pasture versus arable soil) and different sites with similar management.

PSB-7: Organic geochemical studies of soil from a temperate-zone marsh

M. Hetényi¹, C. Sajgó², T. Nyilas¹, A. Brukner-Wein²

1) University of Szeged, H-6701 Szeged PO Box 651, Hungary

2) Inst. for Geochemical Research, Hung. Acad of Sci., H-1112 Budapest Budaörsi út 45, Hungary

(e-mail: hetenyi@geo.u-szeged.hu)

The terrestrial ecosystem contains three times more carbon than the atmosphere. This carbon plays an important role in the global carbon cycle and in modulating temperatures at the surface of the globe. In the last decade the largest surficial pool of organic carbon in continents, the soil organic matter, has received increasing attention. However, despite the large amount of carbon known to be stored in this ecosystem, the organic matter in wetland soils has been less investigated.

The aim of this work is to study different fractions of the organic matter occurring in a marsh environment. The surface horizon of a slightly acid (pH: 6.3), permanently water-covered (water depth ranges between 30 and 150 cm) marsh soil from East Hungary was sampled. The studied marsh is a remnant of the Ecsed Swamp which formed 9000 years BP and was drained in 1799. The present vegetation in this area is predominated by reeds (*Phragmites communis*) and sedges (*Carex*). The whole soil sample, as evidenced by XRD, is composed mainly of quartz, montmorillonite and organic matter. Bulk organic geochemical data (TOC=17.1%, S₂=33.7mg/g HI=197mgHC/gTOC, OI=163mgO₂/gTOC) point to predominantly higher-plant-derived sources. The mathematical deconvolution of the pyrogram - recorded by Rock-Eval pyrolysis, carried out at 180°C for 4 min, followed by programmed pyrolysis at 5°C/min to 600°C – reveals highly heterogeneous OM comprising of a mixture of original biomolecules, remnants of biopolymers with different decomposition rates and humic substances (Fig. 1). The relative proportion of biomolecules (about 40%), estimated by modified Rock-Eval pyrolysis (Hetényi et al., 2004), together with the HI/OI ratio (1.2) reflect relatively slow transformation of the biopolymers.

Isolation of the organic fractions - such as lipids, fulvic and humic acids, humin, as well as refractory organic matter (ROM) - was performed using a protocol reported by Poirier et al. (2002). After the extraction of lipids with CHCl₃/CH₃OH (3/1, v/v), humin was separated from fulvic and humic acids by alkaline extractions. Thereafter humin was submitted to stepwise acid hydrolyses (trifluoroacetic acid and HCl) so as to remove proteins and polysaccharides (to avoid any artifactual formation of insoluble melanoidins by random condensation of amino acids and sugars). The ROM was obtained after HCl and HF treatments. The whole soil sample, lipid-free sample, humin and ROM were investigated by

standard and modified Rock-Eval pyrolyses. Pyrolysis-GC analyses of these fractions are in progress. Lipids were separated and hydrocarbon fractions were analysed using GC and GC/MS. The lipid content of the whole sample is 0.78 % and its carbon-normalized value is 45.6 mg/g. The relative abundances of different fractions in the extract are as follows: HC_{nonar}: 1.2%, HC_{ar}: 2.6% and NSO: 96.2%. The gas-chromatogram of the HC_{nonar} is predominated (about 75%) by a series of *n*-alkanes ranging from *n*-C₁₆ to *n*-C₄₄ with odd-over-even carbon number predominance (CPI: 4.76). This distribution, in accordance with HI and OI values, reflects higher-plant-derived OM. The other GC-data (pr/ph: 0.56, pr/nC₁₇: 1.90, ph/nC₁₈: 0.68, nC₂₂/nC₂₃₊: 0.05) together with the relatively slow transformation of OM suggest that the great plant-derived input resulted in oxygen depleted conditions in this permanently water-covered environment.

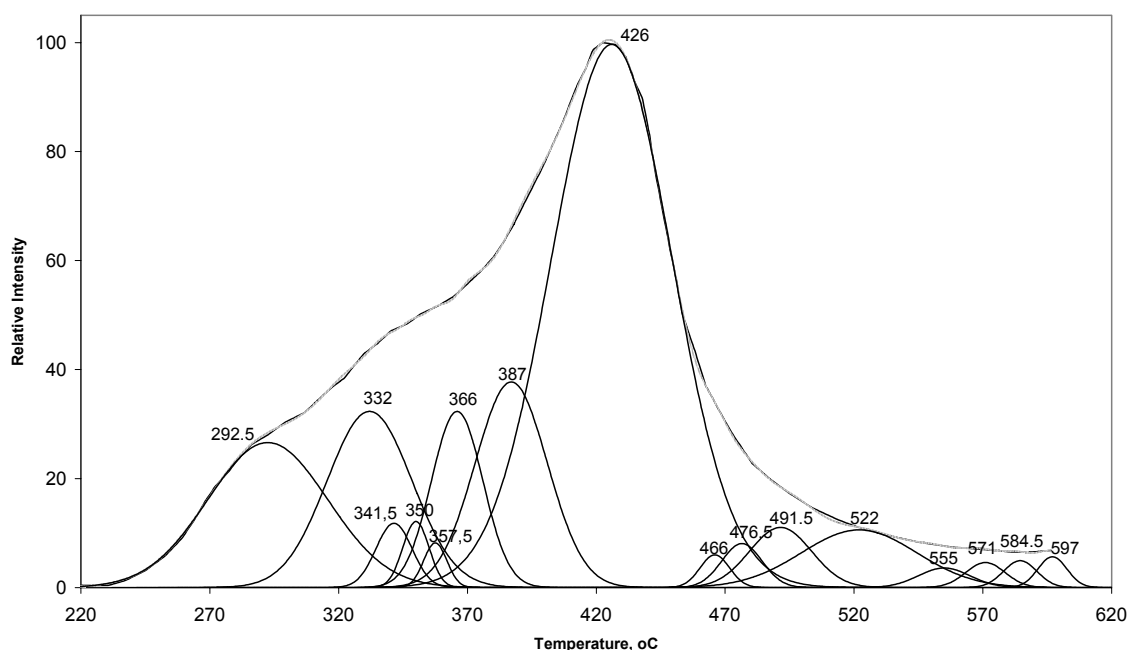


Fig.1 Mathematical deconvolution of the pyrogram obtained for the studied marsh soil. (Peaks with T_{\max} ranging from 280 to 340°C, from 340 to 380°C and from 380 to 430°C represent original biomolecules, partially decomposed biopolymers and humic substances, respectively.)

Acknowledgements

We thank the Hungarian National Science Foundation for grant T-048325.

References

- Hetényi, M., Nyilas, T., M Tóth, T., 2005. Stepwise Rock-Eval pyrolysis as a tool for typing heterogeneous organic matter in soils. *J. Anal. Appl. Pyrolysis* 73, 153-162.
- Poirier, N., Derenne, S., Balesdent, J., Rouzaud, J., Mariotti, A., Largeau, C., 2002. Abundance and composition of the refractory organic fraction of an ancient, tropical soil (Pointe Noire, Congo). *Organic Geochemistry* 33, 383-391.

PSB-8: Characterization of sulphur species in oxic and anoxic soils and soil particles using spectromicroscopy

N. Tyufekchieva¹, J. Prietzel¹, J. Thieme², I. Kögel-Knabner¹

1) Lehrstuhl für Bodenkunde, Department für Ökologie, Technische Universität München, 85350 Freising-Weißenstephan, Germany

2) Institut für Röntgenphysik, Georg-August-Universität, 37073 Göttingen, Germany

Different sulphur species in humic topsoil horizons of a forest soil toposequence with a hydrological gradient (Cambisol – Planosol – Histosol) different sulphur species were identified and quantified using X-ray spectromicroscopy (Sulfur K edge Near Edge X Ray Absorption Fine Structure Spectroscopy; NEXAFS, XANES) and wet chemical methods.

The study was conducted on four different soils in the Lehstenbach catchment in the Fichtelgebirge (Germany). The soils differ in the degree of groundwater influence on the topsoil and the abundance of Fe²⁺ in the soil water.

Conventional methods of sulphur speciation in soil allow only an unsatisfactory assessment of different S species in soil. The discrimination of different organic and inorganic S species is often based on methods yielding only operationally-defined fractions rather than precisely defined S species of distinct chemical composition. Thus, organic soils S cannot be assessed directly, but has to be calculated by difference from the total S concentration in a soil and the concentration of inorganic S. Consequently, error propagation results in considerable uncertainty of the determination of S org with conventional techniques (Prietzel and Hirsch, 2000). In anoxic soils, inorganic S may exist in a variety of oxidation states ranging from –II to +VI (Giblin and Wieder, 1992). In our study, in addition to the SO₄²⁻ concentration, the fractions of Cr²⁺-reducible S (Total Reduced Inorganic Sulfur; TRIS; including elemental S, FeS, FeS₂; Zhabina and Volkov, 1978) and the fraction of Sn/HCl-reducible S (Acid-volatile S – AVS; including amorphous FeS; Pruden and Bloomfield, 1968).

Using new methods of X-ray spectromicroscopy, the effects of different groundwater influence and different abundance of Fe²⁺ in the soil water on the S speciation of humic topsoil horizons were studied. The applied X-ray microscopy technique offers a unique possibility to investigate the S speciation of soil colloids and soil micro-aggregates with a spatial resolution of less than 1 µm in addition to a quantification of different S species in the bulk soil.

All obtained spectra showed a very good reproducibility when repeated and showed peaks, representing reduced and oxidised inorganic and organic S species (Prietzel et al., 2003). With increasing soil depth will extend the height of the reduced peak and will lessen the height of the oxidized peak, respectively.

References

- Giblin, A.E. and R.K. Wieder. 1992. Sulfur cycling in saline and freshwater wetlands in R.W. Howarth, J.W.B. Stewart, and M.V. Ivanov, eds. *Sulfur Cycling on the Continents; SCOPE 1992 (Scientific Committee on Problems of the Environment)*, John Wiley & Sons, New York. 85-117
- Prietzl, J. and Hirsch, C., 2000. Ammonium fluoride extraction for determining inorganic sulphur in acid forest soils; *European Journal of Soil Science*, June 2000, 323-333
- Prietzl, J., J. Thieme, U. Neuhäusler, J. Susini, I. Kögel-Knabner. 2003. Speciation of sulphur in soils and soil particles by X-ray spectromicroscopy. *European Journal of Soil Science* 54:423-43.
- Pruden, G. & Bloomfield, C. 1968. The determination of Fe(II) sulphide in soils in the presence of Fe(III) oxide. *Analyst*, **93**, 532–534.
- Zhabina, N.N. & Volkov, I.I. 1978. A method for determination of various sulfur compounds in sea sediments and rocks. In: *Environmental Biogeochemistry and Geomicrobiology: Methods, Metals, and Assessment*, Volume 3 (ed. W.E. Krumbein), pp. 735–746. Ann Arbor Science, Ann Arbor, MI.

PSB-9: Vegetation changes in the Sheng-Guang Area using $\delta^{13}\text{C}$ values of soil organic matterW. Wang¹, Y.N. Wang¹, M.K. Wang², P.N. Chiang², S.Y. Zhuang², S.T. Lin³

1) School of Forestry and Resource Conservation, National Taiwan University, Taipei, Taiwan, 106

2) Department of Agricultural Chemistry, National Taiwan University, Taipei, Taiwan, 106

3) Department of Natural Resources, National I-Lan University, I-Lan, Taiwan, 260

There was established artificial forest since 1968 by Taiwan Forest Bureau in Da-Jia Creek Working Circle. The major artificial forests were *Pinus taiwanensis* Hayata (PT), the other forests mixed with *Miscanthus transmorrisonensis* (MT), *Quercus variabilis* Blume (QV), *Myrica rubra* Sieb, *Zucc. var. acuminata* Nakai (MZ), *Rhododendron noriakianum* (RN), etc. Frequency forest fires at this study site (Sheng-Guang, SG), particular the historic record at *Pinus taiwanensis* Hayata (PT) have been reported several times of the Tungshih Forest District Office, but environmental factors that influenced the change of plant communities were not clear known. The aims of this study were evaluated why PT and MT forests were so easily to get fires, and to investigate forest fires disturbed factors influenced the plant vegetation changes at SG area using $\delta^{13}\text{C}_{\text{PDW}}$ values of soil organic matter. The fresh plant tissues and four pedons of unburned and burned soils were subjected to soil physical, chemical and mineralogical analyses, cross-polarization and magic angle spinning ^{13}C nuclear magnetic resonance (CPMAS ^{13}C NMR) and $\delta^{13}\text{C}_{\text{PDW}}$ values of soil organic matter (SOM). The texture of four pedons ranged from clay to silty loam. Soil pH ranged from 3.68 to 5.28 and increased with increasing soil depth. Illite, kaolinite and vermiculite were the major clay minerals. These high volatile oil contents should cause high frequency of forest fires, particular in PT and MT forests. The organic functional groups of MT showed the similar trend as PT, and contained high hemi-cellulose and lignin materials. These results indicate that PT and MT plant materials decompose easier than the other forests. In this study site, comparison with the $\delta^{13}\text{C}_{\text{PDW}}$ values of unburned and burned PT of pedons I and II, and mixed forest of pedons III and IV, respectively. The recent forest fires did not seriously disturb the $\delta^{13}\text{C}_{\text{PDW}}$ values and plant communities (C_3 and C_4 plants) in unburned and burned pedons under similar vegetations. Thus, the major environmental factor in this SG study area influenced the changes of $\delta^{13}\text{C}_{\text{PDW}}$ values and plant vegetations merit further study.

Pedon	Depth	$\delta^{13}\text{C}$ value	Estimated compositions of C_3 and C_4 plants	
			C_3 (%)	C_4 (%)
I. Pine forest (unburned)	(cm)	(‰)		
	0~10	-21.87±0.44	57	43
	10~20	-18.02±0.29	32	68
	20~30	-18.27±0.16	33	67
II. Pine forest (burned)	30~40	-18.27±0.22	33	67
	0~10	-24.19±0.61	72	28
	10~20	-23.89±0.60	70	30
	20~30	-23.75±0.33	69	31
	30~40	-24.32±0.11	72	28
	40~50	-24.28±0.17	72	28
	50~60	-23.91±0.23	70	30
	60~70	-23.92±0.25	70	30
70~80	-24.23±0.24	72	28	
>80	-23.96±0.48	70	30	
III. Mixed forest (unburned)	0~10	-26.96±1.41	89	11
	10~20	-24.34±0.49	72	28
	20~30	-23.61±0.48	68	32
	30~40	-24.13±0.09	71	29
	40~50	-23.84±0.26	69	31
	50~60	-24.11±0.09	71	29
IV. Mixed forest (burned)	0~10	-23.46±0.67	67	33
	10~20	-23.03±0.12	64	36
	20~30	-22.23±0.05	59	41
	30~40	-20.98±0.25	51	49
	40~50	-19.81±0.15	43	57
50~60	-22.35±0.25	60	40	

Table 1. $\delta^{13}\text{C}$ values of four pedons and estimated composition the compositions of C_3 and C_4 plants in study area (calculated from equations 3 and 4)

PSB-10: Impact of particulate organic matter (POM) biodegradation on selenium solid partition

C. Chabroulet¹, F. Coppin¹, A. Martin-Garin¹, J.P. Gaudet²

1) Laboratory of Radioecology and Ecotoxicology (LRE), IRSN/DEI/SECRE, bldg 186, Cadarache, B.P.3, 13115 Saint Paul-lez-Durance Cedex, France

2) Laboratoire d'Étude des Transferts en Hydrologie et Environnement (LTHE) CNRS/INPG/IRD/UJF, University of Grenoble I - B. P. 53, 38041 Grenoble Cedex 9, France

Size-density fractionation was largely used in order to evaluate the soil organic matter (SOM) quality and its biodegradation within carbon turnover studies. Size-density fractionation allowed, specially, to separate the fastest decomposable organic compounds (few years) from the other soil components. The study presented here originally used the size-density fractionation to determine the short and medium term behaviour of trace elements in soils by combining two crucial informations : the solid partition of a contaminant, selenium, among the different organic and inorganic fractions of the soil and its evolution with time due to carbon degradation by mineralisation and humification processes. The protocol used (based on Balesdent *et al.* (1991)) consisted in dispersion and wet sieving steps, followed by a density separation step. All these steps were conducted in water solution allowing to limit Se desorption and/or redistribution from/within the soil components. Finally, four different kinds of fractions were separated and followed in time : organic fractions bigger than 50 μm (define as the particulate organic matter, POM), mineral fractions bigger than 50 μm , mixed organic and mineral fractions smaller than 50 μm and an aqueous fraction. To realise this study, three different soils with contrasted organic matter quality and content but with a very similar mineralogical compositions were incubated at a constant temperature and moisture optimised to accelerate the carbon turnover. Size-density fractionations were performed at different times of incubation, corresponding to different degradation-states of the SOM. The characterisations of the different isolated fractions specifically aimed at determining selenium and organic carbon concentrations. The first results obtained at the beginning of incubation showed that up to 11 % of the total sorbed selenium were associated with the POM whereas only 4 % and 3 % were associated with the particulate mineral and the aqueous fractions respectively. Then, the evolution of the selenium partition and the POM degradation, followed during one year of controlled incubation, will be presented in order to estimate the redistribution of selenium within the different soil fractions. Finally, the experimental results of the POM degradation will be compared to the modelling of the carbon turnover using the RothC model (Jenkinson and Rayner, 1977).

References

Balesdent, J., Pétraud, J.P. and Feller, C. (1991). Effets des ultrasons sur la distribution granulométrique des matières organiques des sols. *Science du Sol*, 29 (2) : 95-106.

Jenkinson D.S. and Rayner J.H. (1977). The turnover of soil organic matter in some of the Rothamsted classical experiments. *Soil Science*, 123 : 298-305.

PSB-11: The role of lipids and other biogenic compounds in the development of soil water repellency

S.H. Doerr¹, P. Douglas², C.P. Morley², C.T. Llewellyn², K.A. Mainwaring², J. Schabauer²

1) Department of Geography, University of Wales Swansea, Singleton Park, Swansea, SA2 8PP, U.K.
(e-mail: s.doerr@swan.ac.uk)

2) Department of Chemistry, University of Wales Swansea, Singleton Park, Swansea, SA2 8PP, U.K.

Water repellent behaviour (hydrophobicity) is a common of many soils, which has wide ranging implications for soil fertility, hydrology, and stability. It is thought to be caused by naturally occurring hydrophobic organic compounds, although the presence of such compounds does not always lead to water repellency and it has remained unclear what determines its expression. Our approach to understanding this phenomenon has been two-fold: a) the measurement and chemical characterisation of the organic content of soils; and b) modelling of soil water repellency by studies of acid washed sand (AWS) coated with organic compounds found in soils. Here we bring together data from both types of experimental work, and discuss the results in the light of current ideas on how naturally occurring organic compounds may cause water repellency in soils in some, but not in other conditions.

Quantitative measurements and chemical characterisation of organics found on wettable and non-wettable sandy soils are presented. Techniques used include: TOC and DRIFT analyses, extractions, and GC and GC-MS analyses. These experiments show what is on the soil and in what quantity; they do not show which compounds, or what chemical properties or interactions, are important. To investigate the effect of functional group, molecular shape and packing efficiency on soil wettability we have studied the effect of applying organic compounds, such as found on soils, to AWS at different loadings, separately and as mixtures. Compounds used included: linear and branched alkanes and esters, long chain saturated and unsaturated (*cis* and *trans*) acids, long chain amides, and sterols. Compounds with strongly polar group caused repellency, those bearing non-polar or weakly polar groups did not. Addition of alkanes to acids generated higher repellency than acids alone. Studies with *cis* and *trans* unsaturated acids suggest that molecules which “pack” well are more effective in causing repellency than those that do not.

The results suggest that the chemical factors which influence whether soil water repellency is actually expressed are similar to those which control the stability of interfacial films formed by organics at liquid/liquid, and air/liquid, interfaces.

PSB-12: Composition of mineral associated soil organic matter in a Podzol profile

K. Eusterhues¹, C. Rumpel², I. Kögel-Knabner¹

1) Lehrstuhl für Bodenkunde, Technische Universität München, D-85350 Freising-Weihenstephan, Germany

2) CNRS, Laboratoire de Biogéochimie des Milieux Continentaux, Centre INRA de Versailles-Grignon, F-78850 Thiverval-Grignon, France

The association of organic matter with minerals affects many soil forming processes and is known as a major mechanism to protect soil organic matter from microbial degradation. To better understand the nature of this association we aim to characterize the composition of mineral bound organic matter in comparison to the free particulate organic matter. Bulk soil samples and fine particle size fractions < 6.3 µm were taken from surface and subsurface horizons of a Haplic Podzol and exposed to demineralisation by 10 % hydrofluoric acid (HF). Organic matter composition was analysed by ¹³C CPMAS NMR spectroscopy before and after demineralisation. A density fractionation at 2 g cm⁻³ was carried out to quantify the OC content in organo-mineral associations.

HF reacts with silicates and oxides by forming soluble fluoride complexes, but is expected to leave organic material relatively unharmed. It is widely used to enrich soils and sediments in organic matter (Gélinas et al., 2001). In our study we observed OC losses of only 5 - 10 % in mineral free forest floor layers and of 20 % in the A horizon, but we lost 30 - 90 % of the total OC after HF treatment in subsoil horizons. Moreover, we observed a correlation between the F-soluble OC and the amount of the OC in organo-mineral associations (OC in fraction > 2 g cm⁻³). We conclude that HF dissolves soil minerals and the mineral-associated organic matter, while the non-associated soil organic matter remains unaffected. This lead us to analyse the untreated and HF-treated samples by ¹³C CPMAS NMR and to calculate the composition of the HF-dissolved fraction by mass balance. Assuming that NMR signal loss due to paramagnetic materials is of minor importance we suppose that the calculated spectra of the HF-dissolved fraction represent the mineral-associated fraction of the organic matter. The chemical composition as seen by ¹³C CPMAS NMR spectroscopy did not change significantly after HF treatment. This indicates that the sorption of organic matter onto minerals does not involve major chemical fractionation of the organic matter. However, smaller systematic changes were observed (Figure 1). With depth or age of soil horizons the mineral-associated organic matter becomes enriched in O-alkyl C, aryl C and carbonyl C compared to the non mineral-associated organic matter. The smaller alkyl C/carboxyl C ratio in the mineral associated organic matter of subsoil samples points to a shorter chain length of the aliphatic material in deeper soil horizons.

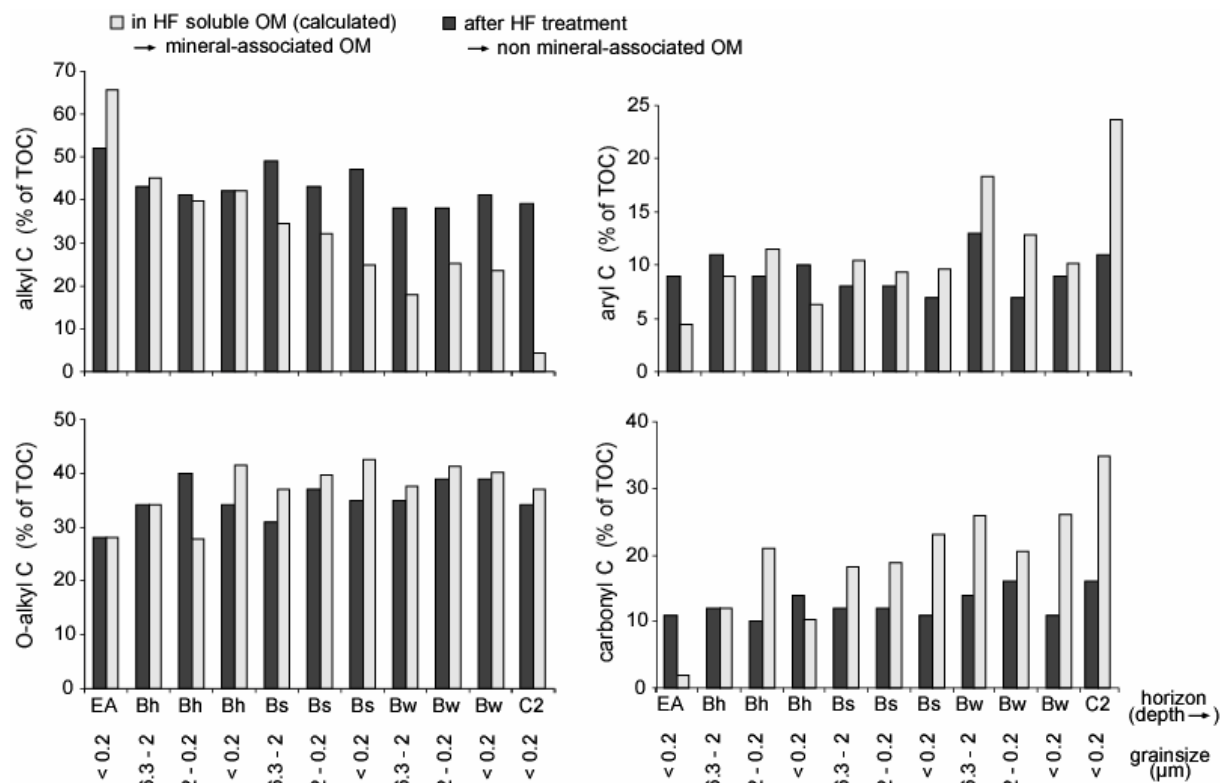


Fig.1. Results from ^{13}C CPMAS NMR spectroscopy on untreated and HF-treated particle size fractions. The composition of the HF soluble fraction was calculated by mass balance

Conclusions

Hydrofluoric acid selectively removes the mineral-bound organic matter. Loosing its bond to the mineral surface seems to (re-) solubilize this organic matter fraction. The composition of the mineral associated organic matter changes with soil depth: alkyl C concentrations decrease, whereas O-alkyl C, aryl C and carbonyl C contents increase. In subsoils of the Podzol up to 90 % of the organic matter is associated with minerals.

References

Gélinas, Y., Baldock, J.A., Hedges, J.I., 2001. Demineralisation of marine and freshwater sediments for CP/MAS ^{13}C NMR analysis. *Organic Geochemistry* 32, 677-693.

PSB-13: Characterization of humic acids in Tropical Spodosols by ^{13}C NMR spectroscopy

M. González Pérez^{1,2}, P. Vidal Torrado¹, L. Martin Neto², L.A. Colnago², D.M.P.B. Milori²,
F. Haenel Gomes¹

1) Escola Superior de Agricultura “Luiz de Queiroz” (ESALQ-USP). Departamento de Solos e Nutrição de Plantas. C.P. 09, CEP 13418-900. Piracicaba-SP, Brasil.

2) Embrapa Instrumentação Agropecuária. C.P.741, CEP: 13560-970. São Carlos, SP, Brasil
(e-mail: marta@cnpdia.embrapa.br)

Spodosols or Podzols occur worldwide from temperate to tropical climate. They are most commonly formed from quartz sandy parent materials. Spodosols are characterized by a peculiar horizon sequence: an organic surface horizon O, a weathered grey eluvial E horizon, and a dark brownish–reddish illuvial B horizon, which is enriched by Al and Fe (can be Bh, Bhs or Bs). Their main genesis process, called podzolization, is still researched. Nowadays, it has been generally accepted that transport of Al and Fe through the profile as organic complexes is the dominant mechanism of eluviation and podzolization (Lundström et al., 2000).

There are several papers showing the characterization of the organic matter (OM) in spodosols from temperate countries (Schmidt et al., 2000; Nierop et al., 1999), but there are not many papers neither explaining the podzolization process, nor showing characterization of the OM in tropical climate. Thus, the aim of the present work was to characterize the humic acids (HAs) from Brazilian spodosols by ^{13}C NMR spectroscopy to obtain evidences about the mechanism of podzolization process in Brazil.

It were studied two profiles from sandy coastal soils in Ilha do Cardoso, State of Sao Paulo, Southeast - Brazil. The first soil was an Histic Alaquod that we named profile H13 divided in Ho, Hd, A, Bhs1, Bhs2 and Bs horizons. The second was a Typic Alorthod that we named profile C14 divided in A, Bhs1, Bhs2, Bhs3 and Bs1 horizons.

Humic acids were extracted from every horizon of the two profiles, using the IHSS method (extraction with 0.1 mol.L^{-1} NaOH and precipitation with 6 mol.L^{-1} HCl).

^{13}C NMR spectra of HAs were obtained at the ^{13}C resonance frequency of 100.58 MHz on a Varian (Unity 400) spectrometer, equipped with a solid Doty probe. Spectra were measured using the technique of variable amplitude cross polarization magic angle spinning (VACP/MAS) and also using the technique of dipolar dephasing (DD).

The spectra showed signals for alkyl C indicative of methyl (25 ppm) and methylene (33 ppm) carbons. Furthermore, it were observed signals of O-alkyl C (72 and 105 ppm) ascribed to polysaccharides, bands of aromatic C (153 and 130 ppm) associated to lignin and

lignin-modified components and also a peak at around 172 ppm derived from carboxylic acids. For both profiles the spectra of HAs showed that aliphatic bands were more intense than aromatics, thus indicating a major contribution of aliphatic biopolymers to HAs composition and its aliphatic character.

Profile C14 above the 35cm E horizon, showed an increase of alkyl C, decrease of acetal and ketal carbon (carbohydrates, 90 – 110 ppm) and aromatic C (153 ppm) as depths increased, suggesting an increasing degree of decomposition of polysaccharides and lignin from plants, and an enrichment of methylene structures by the microbial biomass (Schmidt et al., 2000). The DD spectra showed that the band at 55 ppm could be associated mainly to aminoacids. The HAs had a high content of carbohydrates (di- O- alkyl band at 105 ppm) in the DD spectra that decreased with depth and also the decrease of intensities of aromatic C at 130 ppm can be associated with increment of humification process due to modification of aromatic rings of lignin (Preston, 1996).

The Ho, Hd and A, horizons from profile H13 showed a decrease of O-alkyl band (65 – 90 ppm) up to 30 cm depth and passing 8 cm E horizon, for horizons Bhs1, Bhs2 and Bs intensities increased again. The last three horizons showed very similar characteristics. The horizon A showed a significant increment of alkyl C, but analyzing the intensities of this band through the profile there is a tendency to decrease.

Analyzing VACP/MAS NMR spectra, were found similarities between A horizon of profile C14 and Ho horizons of profile H13. Above E horizon, spectra of Bhs1, Bhs2 and Bs horizons of profile H13 closely resembled spectra of Bhs3 and Bs1 horizons of profile C14.

Our results showed evidences of OM decomposition by microbial biomass and translocation through the profile, having similar composition without incorporation of OM components from other sources.

Acknowledgements

Financial Support: EMBRAPA and CNPq/PACDT (Brazilian Institutions).

References

1. Lundström, U.S.; Van Breemen, N.; Bain, D. *Geoderma*, 2000, 94, 91-107.
2. Nierop, K.G.J.; Buurman, P.; Leeuw, J.W. *Geoderma*, 1999, 90, 111-129.
3. Preston, C.M. *Soil Sci.*, 1996, 161(3), 145.
4. Schmidt, M. W. I.; Knicker, H.; Kögel-Knabner, I. *Org. Geochem.*, 2000, 31, 727-734.

PSB-14: Labelling of humic substances with ^{14}C and their use for sorption studies with different geomatrices

A. Mansel, H. Kupsch

Department of Georadiochemistry, Institute of Interdisciplinary Isotope Research, Permoserstr. 15, D-04318 Leipzig (e-mail: Mansel@iif-leipzig.de)

The reactive carbon compounds (humic substances, HS) of the dissolved organic matter (DOC) dominate the spreading of inorganic and organic pollutants in the biogeosphere. The classical analytical methods such as TOC-detection and UV-spectroscopy are of limited use in the lower concentration range (< 1 mg/l), usually found in environmental samples. By using radiolabelled HS, scenarios near to nature in the $\mu\text{g/l}$ -HS-concentration range can be studied. Based on our promising results of the HS radiolabelling with [^{14}C]phenyldiazonium ions, we applied these radiolabelled substances first time to sorption studies under conditions, usually found in subterranean waste repositories.

The natural HS (humic acid HA, fulvic acid FA) were purified by the IHSS-procedure. Aldrich-HA (AHA), Gorleben-HA (GoHy-532), an aquatic HA (HS3), a terrestrial HA (HS4), a lignite HA (HAL) and an aquatic FA (FS3) were used for our investigations. A synthetic HA (M42) was provided by the Forschungszentrum Rossendorf / Germany.

The radiolabelled HS were contacted in aqueous solution with a sandy soil, granite, diabase and kaolinite in batch experiments under conditions near to nature (figure). Adsorption isotherms of various radiolabelled humic acids were determined depending on geomaterial, pH, HS concentration, contact time and heavy metal content. The behaviour of the radiolabelled HS was not influenced by the labelling procedure. With the use of radiolabelled humic substances a concentration range below mg/l can be studied.

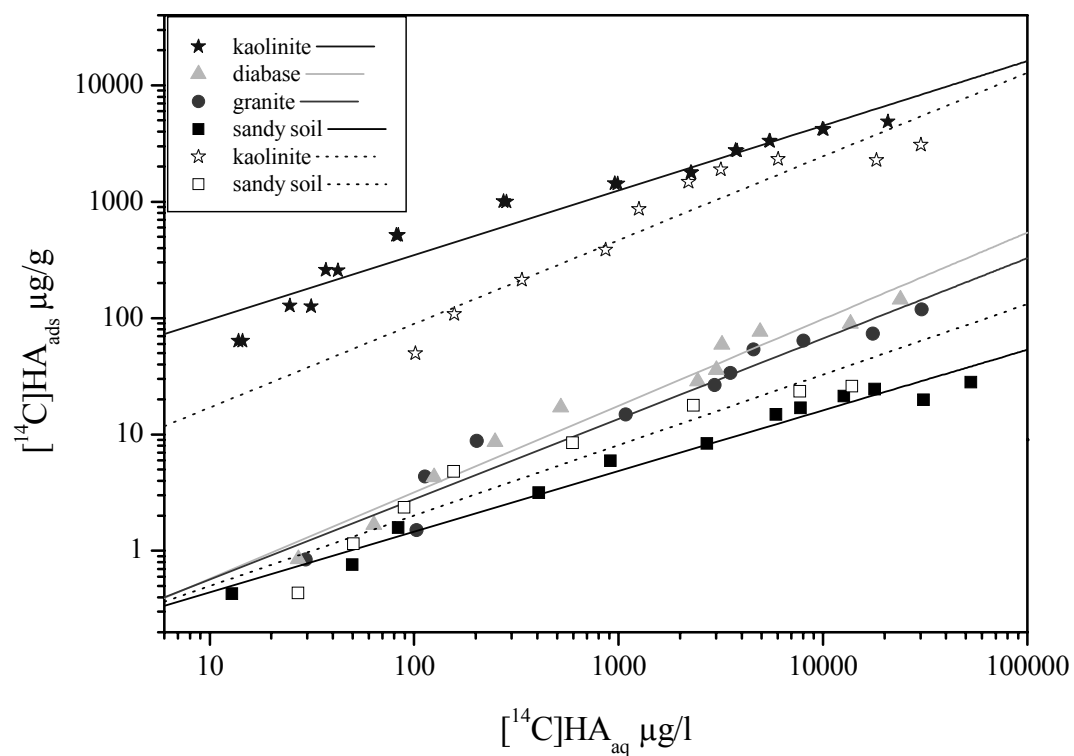


Fig.1. Adsorption isotherms of ^{14}C -radiolabelled HA on various geomaterials; M42 (full symbols); AHA (open symbols); 0.1 M NaClO_4 ; Equilibrium pH: kaolinite (4.7), sandy soil (5.0), granite (6.0), diabase (8.0)

PSB-15: Assessment of high affinity methane oxidising bacterial biomass and growth kinetics in upland and forest mineral soils by time-series $^{13}\text{CH}_4$ PLFA labelling

P. Maxfield¹, E. Hornibrook², R. Evershed¹

1) OGU, Bristol Biogeochemistry Research Centre, School of Chemistry, University of Bristol, Cantock's Close, Bristol BS8 1TS UK

2) Bristol Biogeochemistry Research Centre, Department of Earth Sciences, University of Bristol, Wills Memorial Building, Queens Road, Bristol BS8 1RJ UK

One of the most important methane removal processes is CH_4 oxidation in terrestrial environments by methane oxidising bacteria (MOB). The bacteria involved in the oxidation of atmospheric methane are referred to as high affinity methanotrophs as they exhibit much higher enzymatic affinities for CH_4 than low affinity methanotrophs, which are active in methane-rich environments. Unfortunately, as they have yet to be cultured successfully, obtaining detailed information about high affinity methanotrophs is more difficult than studying low affinity methanotrophic bacteria. Indirect techniques that have been generally used to investigate high affinity methanotrophs include: monitoring methane oxidation rates and molecular biological methods.

An additional approach we have developed for the study of high affinity methane oxidising bacteria involves $^{13}\text{CH}_4$ pulse chasing (Bull *et al.*, 2000; Crossman *et al.*, 2001). In this study we discuss the results of time series incubation experiments involving exposure of selected mineral soils to $^{13}\text{CH}_4$, in order to monitor carbon incorporation by high affinity methanotrophs at atmospheric concentrations with time. Using this technique we are also able to: (i) determine carbon recycling within the soil, (ii) study the mechanisms operating on the MOB under different soil treatment regimes, (iii) analyse methanotroph growth kinetics, and (iv) assess the methanotrophic biomass.

Two separate field sites have been studied, Bronydd Mawr and Alice Holt Forest. Bronydd Mawr is located in the Brecon Beacons national park and is the Institute for Grassland and Environmental Research (IGER) upland research station. Alice Holt Forest is the main UK Forestry Commission research station and it is located in Hampshire, England. At Bronydd Mawr the Inceptisol soils studied were from a low input farming study, which compares different fertiliser and grazing regimes within an upland grassland soil. At Alice Holt the soils studied included a coniferous spodosol and an oak alfisol.

Soil samples were incubated at 2 ppmv $^{13}\text{CH}_4$ over a range of time periods using a through-flow incubation technique where pre-mixed $^{13}\text{CH}_4$ in synthetic air is continuously flushed through the chamber, renewing the atmosphere and limiting accumulation of metabolically derived gases. Methanotrophic phospholipid fatty acids (PLFAs) were identified by gas chromatography-combustion-isotope ratio mass spectrometry (GC-C-IRMS), and methanotrophic biomass calculated by converting the amount of ^{13}C -labelled

PLFAs to numbers of active methanotrophic cells (Frostegård and Bååth, 1996). In-situ and in-vitro methane oxidation rates have been measured by GC and the kinetic isotope effect (KIE), has been calculated from soil gas CH₄ δ¹³C values, analysed using a gas pre-concentrator linked to an IRMS.

Initial incubations were run up to 11 weeks on the Bronydd Mawr untreated soils. We observed steadily increasing ¹³C-labelling of selected PLFAs with time. Slow labelling of certain PLFAs and absence of label in others indicate recycling of the ¹³C label is much slower than carbon incorporation by methanotrophs. The culture independent time-course study displayed methanotrophic growth that followed a typical microbial growth curve (Fig. 1) where 18:1ω7c is the predominantly labelled PLFA.

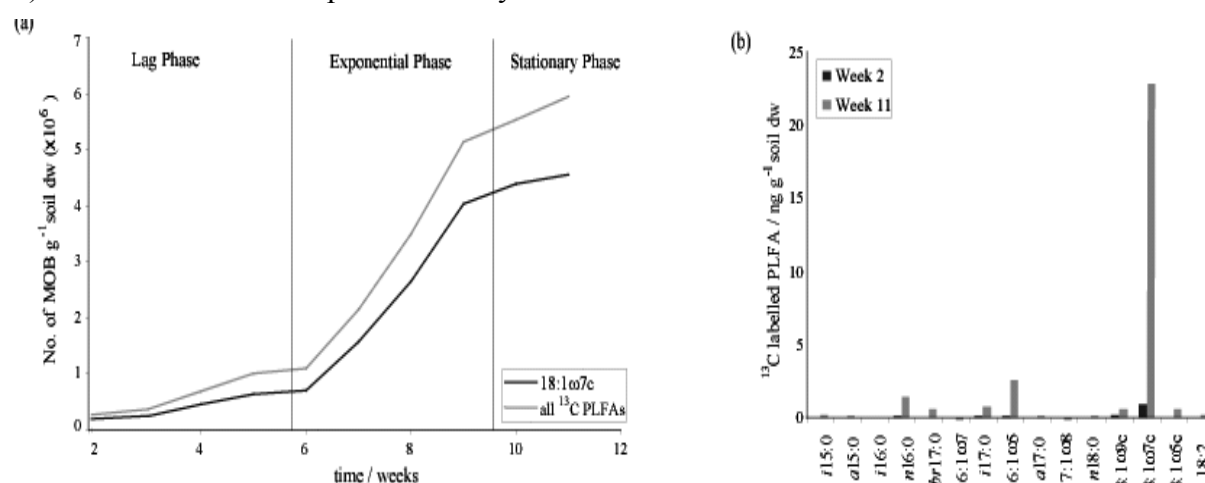


Fig.1. (a) Culture independent growth curve of high affinity methane oxidising bacteria in an upland mineral soil established by ¹³CH₄ time-series PLFA labelling. (b) Comparison of ¹³C label incorporation into PLFAs after 2 and 11 weeks of incubation

From the PLFA profile a novel species of methanotroph was observed that is similar to known type 2 methanotrophs *Methylosinus sporium* and *Methylocystis parvus*. We calculated an initial methanotrophic biomass estimate of 2.03 - 2.71 million MOB cells g⁻¹soil dry weight. Longer time-course ¹³C-labelling studies of the Alice Holt and treated Bronydd Mawr soils were then conducted enabling more accurate biomass calculations to be made. These experiments took the experiment further through the bacterial growth stages and into the death phase. The application of these new approaches to the elucidation of the impacts of various environmental variables, e.g. soil type and land use, on the active high affinity methanotrophic biomass will be discussed.

References

- Frostegård, Å. and E. Bååth (1996). *Biology and Fertility of Soils* **22**: 59-65
 Bull, I. D. *et al.* (2000). *Nature* **405**: 175-178
 Crossman, Z. M. *et al.* (2001). *Organic Geochemistry* **32**(2): 359-364

PSB-16: Characterisation of physically extracted soil fractions in the course of decomposition of ^{14}C -labelled maize straw

F. Schnitzler, A. Gierschner, A. Berns, P. Burauel

Institute Agrosphere, ICG IV, Forschungszentrum Jülich GmbH, 52425 Jülich, Germany
(e-mail: f.schnitzler@fz-juelich.de)

A classical procedure for separating and characterising organic carbon (Corg) compounds from soil is based on chemical fractionation approaches. However, these extraction methods can substantially modify the Corg compounds themselves and the nature of their association with the soil's mineral components. Therefore, the use of physical fractionations in studies of organic matter (OM) turnover in soil has increased steadily over the past two decades. Physical fractionation of soil according to the size and the density of particles is thus a useful approach to analyse soil organic matter (SOM) pools and related humification processes in soil.

The present work discusses the characterisation of physically extracted SOM pools of an orthic luvisol in the course of decomposition of fresh radiolabelled (^{14}C) crop residue. ^{14}C -labelled maize straw is incorporated into the first 10 cm of disturbed cropped soil from Merzenhausen (Germany). After 1, 2, 4, 6, 8 and 12 weeks the topsoil samples are submitted to a particle-size fractionation that obeys Stokes law. A soil/water mixture (1:2 w/v) is first shaken for six hours. Afterwards, four different soil phases are separated after sedimentation and centrifugation steps: sediment phase (2000-20 μm), microaggregate phase (20-2 μm), colloidal phase (< 2 μm) and electrolyte phase (< 0.5 μm) containing the dissolved organic carbon (DOC) [1, 2].

The quantitative analysis of the radiolabelled compounds shows that the organic carbon in the microaggregate (20-2 μm) and colloidal (< 2 μm) fraction is turned over more slowly than that associated with the sediment phase (2000-20 μm). With increasing decomposition of the fresh organic matter especially the colloid fraction becomes more important as stable and residual organic carbon pool.

The different pools of organic matter in soil phases are characterised by a variety of physicochemical techniques. Results of the electrophoretic mobility (particle surface electrokinetic) and photon correlation spectroscopy (particle hydrodynamic diameter) of the colloidal fraction lead to the conclusion that the incorporated fresh organic matter temporary increases the stability of the soil.

A variety of spectroscopic methods are applied to investigate DOC or the organic carbon pool in the electrolyte phase: UV-visible absorption, sensitive synchronous and

emission fluorescence and excitation-emission matrix (EEM), a three dimensional fingerprint of DOC, spectroscopy. After one week of incorporation of the crop residue a dilution of the aromatic content of the organic matter in the electrolyte phase is measured. Proteinlike or tryptophan-like fluorophores are sensitively detected. The polycondensation and humification degree of dissolved organic carbon increases steadily after two weeks of the incorporation of the fresh organic material.

Least-invasive physical particle-size fractionation, spectroscopic and wet-chemical techniques are essential tools to characterise the structure of soil organic matter and its turnover mechanisms. An understanding of the SOM fate would allow to better manage the filter and buffer functions of soil.

References

- [1] J.-M. Séquaris, H. Lewandowski, Physicochemical characterisation of potential colloids from agricultural topsoils, *Colloids and Surfaces A: Physicochem. Eng. Aspects* 217 (2003) 93-99
- [2] P. Bureau, F. Schnitzler, Soils as filter and buffer for pesticides – experimental concepts to understand soil functions, *Environmental Pollution* 133 (2005) 11-16

PSB-17: Is the atmospheric Suess-effect reflected in arable soils of urban areas?

G.L.B. Wiesenberg¹, M.W.I. Schmidt², L. Schwark¹

1) University of Cologne, Dep. of Geology and Mineralogy, Zulpicher Str. 49a, D-50674 Cologne, Germany (e-mail: guido.wiesenberg@uni-koeln.de)

2) University of Zurich-Irchel, Department of Geography, Winterthurer Str. 190, CH-8057 Zurich, Switzerland

Fossil fuel burning led to an increase in atmospheric CO₂ and a depletion in atmospheric stable carbon isotopic composition ($\delta^{13}\text{C}$) since the beginning of the industrial revolution [1], the so-called Suess-effect. Plants and especially annual crop plants have been strongly affected by the atmospheric Suess-effect with respect to their biomass production and stable carbon isotopic composition [2]. Within larger cities massive local increases in CO₂-concentrations are observed [3] producing a so-called “urban dome effect”. This urban dome effect should lead to enhanced carbon isotopic fraction in (crop) plants. Long-term increase of atmospheric CO₂ and associated stable carbon isotopic depletion of plant biomass have been detected in tree-rings. These effects have, however, not been documented in time-series of archived soil samples. In this study, we present a time-series of isotopic composition of archived arable soil samples covering four decades. We then discuss, how the atmospheric Suess-effect may influence the stable carbon isotopic composition of arable soils.

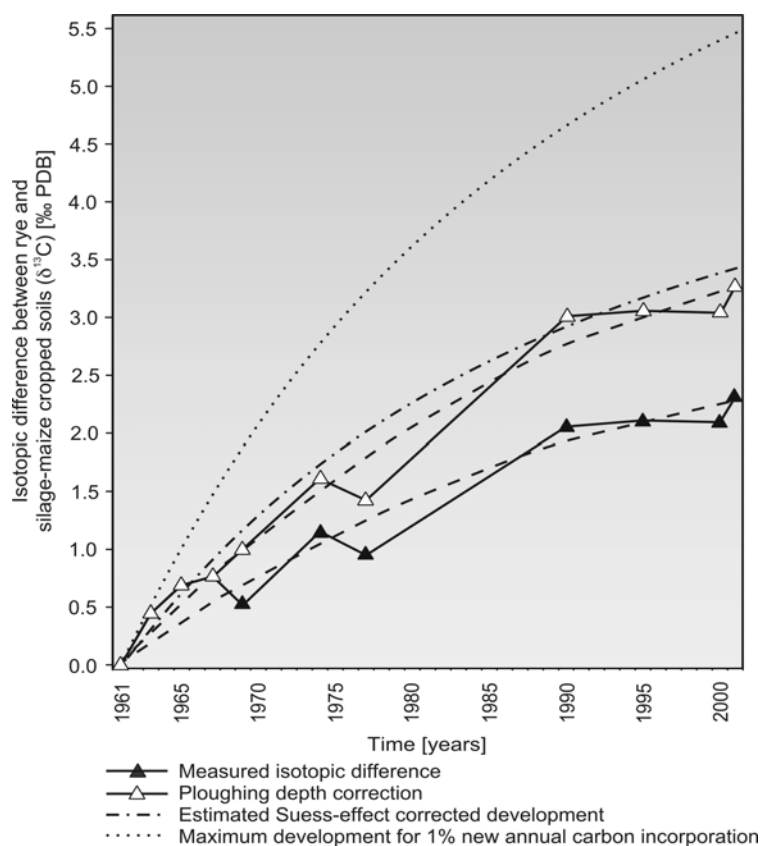
Arable soil samples were derived from the ‘Eternal Rye’ trial in the urban area of the city of Halle/Saale (Germany). Archived soil samples were available since 1958 for rye cropped soil. After introduction of silage-maize monoculture cropping on a part of the trial parallel samples of rye and silage-maize cropped soils were taken at twelve times since 1961 until 2004. Wheat straw grown on the ‘Eternal Rye’ trial showed a large carbon isotopic depletion of 2‰ V-PDB in comparison to wheat straw of the same year, which was grown in a rural area near Passau (Germany). This could be related to the enhanced Suess-effect in the urban Halle area. During the last four decades an isotopic depletion of wheat plant biomass of approximately 2.5‰ V-PDB could be expected, according to [2]. This isotopic development must result in an isotopic depletion of approximately 0.5‰ V-PDB in monoculture rye cropped soil, assuming an annual turnover of 0.5% of the total soil organic carbon. This depletion was observable although several plowing modifications led to a significant admixture of isotopically enriched carbon from the subsoil.

Maize and other C₄ plants are less influenced by the atmospheric Suess-effect than C₃-plants [4]. C₄ plants directly reflect the atmospheric isotopic composition with minor photosynthetic fractionation depending on the internal versus external CO₂-concentration. The maize cropped soil became successively isotopically enriched since introduction of maize monoculture cropping. Several plowing modifications caused isotopic depletions in maize cropped soil.

After four decades of parallel silage-maize and rye cropping an isotopic difference of 2.0‰ V-PDB occurs (see figure). Increases in plowing depth will dilute the Ap-horizon with

^{13}C -enriched soil organic matter. If plowing depth had not been increased during the last 40 years, we would expect an isotopic difference of 3.0‰ V-PDB. Calculations assuming an annual turnover of 0.5% of total soil organic carbon indicate a reduction of 0.2‰ V-PDB in isotopic difference of both soils due the atmospheric Suess-effect. When assuming higher turnover rates, the atmospheric Suess-effect will lead to an underestimation of the isotopic difference of up to 1.0‰ V-PDB between both soils.

In contrast to previous observations in rural areas [5] (without time-series of archived soils) this study detects a stable carbon isotopic changes in arable soils of urban areas caused by the atmospheric Suess-effect. For assessment of soil organic matter turnover rates it is thus recommended to correct for the effects of plowing modifications and atmospheric Suess-effect.



References

- [1] Friedli, H., Lötscher, H., Oeschger, H., Siegenthaler, U., Stauffer, B., 1986. Ice record of the $^{13}\text{C}/^{12}\text{C}$ ratio of atmospheric CO_2 in the past two centuries. *Nature* 324, 237-238.
- [2] Zhao, F.-J., Spiro, B., McGrath, S.P., 2001. Trends in $^{13}\text{C}/^{12}\text{C}$ ratios and C isotope discrimination of wheat since 1845. *Oecologia* 128, 336-342.
- [3] Idso, C.D., Idso, S.B., Balling, R.C. Jr., 2001. An intensive two-week study of an urban CO_2 dome in Phoenix, Arizona, USA. *Atmospheric Environment* 35, 995-1000.
- [4] Marino, B.D., McElroy, M.B., 1991. Isotopic composition of atmospheric CO_2 inferred from carbon in C4 plant cellulose. *Nature* 349, 127-131.
- [5] Torn, M.S., Lapenis, A.G., Timofeev, A., Fischer, M.L., Babikov, B.V., Harden, J.W., 2002. Organic carbon and carbon isotopes in modern and 100-year-old-soil archives of the Russian steppe. *Global Change Biology* 8, 941-953.

PSB-18: Tentatively quantifying fire impact, organic carbon balance and thermal structural rearrangements by ^{13}C CPMAS NMR of whole soil samples from Continental Mediterranean forests

G. Almendros¹, F.J. González-Vila², J.A. González-Pérez², H. Knicker³,
M.C. Zancada¹, O. Polvillo²

1) Centro de Ciencias Medioambientales, Serrano 115B, 28006 Madrid, Spain (e-mail: humus@ccma.csic.es)

2) Instituto de Recursos Naturales y Agrobiología, Av. Reina Mercedes 10, 41012 Sevilla, Spain

3) Lehrstuhl für Bodenkunde. Technische Universität München, 85350 Freising-Weihenstephan, Germany

Soils from ten Mediterranean pine and oak forests were studied by ^{13}C CPMAS NMR by comparing samples from neighbouring ecosystems affected or not by wildfires. Sample sites differ in fire intensity, duration and propagation models ranging from high intensity fires (in dense pine forest on flat semiarid site) to medium-intensity fires (where most effects on soil organic matter are tentatively attributed to allochthonous C forms from charred litter after a fire event affecting mainly forest canopy).

The soils (mainly Cambisols and Umbrisols) were thoroughly characterized by standard agrobiological analyses (C, N, macro- and microelements and laboratory incubation experiments) and detailed quantification of the humus fractions including lipids, particulate fractions, extractable humic substances and different types of humin.

The aim of the present study was: i) to estimate the balance for several C-types as seen in the ^{13}C NMR spectra (carbonyl, aromatic, *O*-alkyl and alkyl and their subranges) taking into account the C concentration in undisturbed and fire-affected soils, in an attempt to assess how changes in different structures could be related with fire type, ii) to make a tentative classification of forest fires according to their selective impact on the different C-types, and iii) to calculate an impact index in the whole soil organic matter considering the statistical dissimilarity between the spectral profile from undisturbed and fire-affected soils.

In order to distinguish recalcitrant structures and—as negative signals—any positive balance of soil C forms from allochthonous organic matter and/or thermal conversion of e.g., aliphatic structures into aromatic ones, subtraction spectra were obtained from paired (undisturbed minus fire-affected) soil samples after full-scale normalization based on total C content. Correspondence analysis and Euclidean distances between soils defined by variables consisting of relative fire-induced changes in eight C-types calculated from signal area values were also considered. The results pointed to an unexpectedly high variety in the transformation patterns of the organic matter depending on the intensity and type of wildfire. In the soil showing the greatest transformation as regards its corresponding control (*Pinus halepensis* forest on Calcaric Cambisol in Central Spain) it was evident that fire caused intense depletion of aliphatic structures (0–110 ppm) and carbonyl/amino groups (172 ppm signal), with the concomitant increase in aromatic/unsaturated constituents. That evolution is explained mainly from selective depletion in all C-types, the ratios between them suggesting that alkyl structures were found to be comparatively more recalcitrant than *O*-alkyl ones.

After a medium-intensity fire (mountain pine forest) a considerable enrichment in aromatic C forms was found to some extent higher than that calculated from the negligible variation in the total

soil C (69 and 64 g kg⁻¹ in undisturbed and fire-affected soil, respectively): this secondary C forms are interpreted as from the conversion of aliphatic structures into aromatic ones in addition to a compensating effect of the fall of burning litter.

In the extreme situation according to fires impact on soil (Dystric Xerochrept under *Quercus rotundifolia* forest) the spectra clearly showed enrichment in lignin not explained as an effect concomitant to the depletion of comparatively thermolabile compounds. The spectra suggested non-altered methoxyl substitution patterns in lignin, fairly intact alkyl- and *O*-alkyl structures and no effective decarboxylation. These patterns could define a signature for low self-combustibility of evergreen oak leaves incorporating into soil as not totally charred litter.

Once the above conditions are fixed to define a virtual gradient for the progressive thermal impact estimated as the extent to which the NMR profile has changed in the post fire soil, a series of collateral, intermediate situations were recognized: the NMR spectrum of a Dystric Xerochrept under pine forest suggested a scenario in which most of the organic matter was allochthonous material not only consisting of black-carbon particles but also of aliphatic and N- and O-containing aromatic structures indicating thermal reworking of plant biomacromolecules. In fact, after the passage of the fire this soil showed enhanced signal intensity in the carbonyl/amide and alkyl (0–45 ppm) spectral regions and a defined methoxyl/ α -amino peak (56 ppm). The striking enhancement of the alkyl/*O*-alkyl ratio after fire suggests accumulation and/or fixation of litter-derived water repellent substances, which coincides with the hydrophobic properties observed in the post-fire soil. Nevertheless, considering that fire increased both C and N levels in this soil, the contribution of melanoidins or other N-containing structures in the 0–45 ppm spectral region (and probably in the 56 and 175 ppm signals) should not be ruled out.

A different situation is observed in a Cambisol under *Pinus pinaster* forest, where not only the whole aromatic domain increased but also the ratios between O- or N-substituted/H-substituted aromatic Cs and the alkyl/*O*-alkyl ratio. This is interpreted as an intense modification in the stoichiometry of the original plant biomacromolecules; the C and N balances suggest prevalence of rearrangement processes of autochthonous organic matter with incorporation of thermally altered N forms into the surviving organic matter.

In conclusion the NMR profiles have led to discriminate a series of wildfire-induced patterns at first sight based on a common background irrespective of soil and forest type (aromatic enhancement, accumulation of O- or N-linked aromatic structures, systematically more recalcitrant than the *O*-alkyl (mainly carbohydrate) moiety. This common pattern overlaps with specific changes clearly distinguishing the different fire scenarios. These local differences include features such as the relative alkyl enhancement in soils developing hydrophobic properties, the possible oxidation and/or accumulation of melanoidins in heavily rearranged pyromorphic humus, external inputs of slightly altered lignin and carbohydrate, or the unspecific mineralization leading to black carbon-like residue. It is presumed that the above described variety of thermal rearrangement processes are perhaps causally associated with the specific soil physical and chemical properties (including N balance) observed in the post-fire soils.

PSB-19: Can $\delta^{13}\text{C}$ and ^{14}C from organic matter in soils complement records of Mid-Holocene palaeoclimate change in lacustrine sediments?

D.M. McKirdy¹, E.S. Krull², A.C. Mee¹, A.J. Brenchley³, B. Spiro⁴

1) Organic Geochemistry in Basin Analysis Group and CRC for Landscapes, Environment & Mineral Exploration, School of Earth & Environmental Sciences, University of Adelaide, SA 5005, Australia (e-mail: david.mckirdy@adelaide.edu.au)

2) CSIRO Land & Water and CRC for Greenhouse Accounting, PMB 2, Glen Osmond, SA 5064, Australia

3) Geoscience Department, Onkaparinga Institute of TAFE, O'Halloran Hill, SA 5158, Australia

4) Department of Mineralogy, The Natural History Museum, Cromwell Road, London SW7 5BD, UK

In this report we document and consider the possible significance of the similar changes from relatively ^{13}C -depleted to appreciably heavier organic matter observed in two ^{14}C -dated cores, one of a flood-plain Vertisol in southeastern Queensland (Krull & Skjemstad, 2003) and the other of calcareous sediments deposited in a small, presently hypersaline lake in southeastern South Australia (Mee et al., 2004). This positive shift of $\delta^{13}\text{C}_{\text{org}}$ in the Vertisol at Paget Creek occurred between 8 and 5 Ka BP, corresponding to the change from a widely reported effective precipitation (EP) maximum to drier conditions throughout southern, eastern and northern Australia (Dodson & Ono, 1997). Given that the Holocene EP maximum affected much of Australia, it is likely that under ideal conditions both soils (when influenced by vertical accretion processes) and lacustrine sediments (high sedimentation rate) will have recorded such a distinct palaeo-climatic deterioration. The observed $\delta^{13}\text{C}$ excursion in soil organic matter, which lies entirely within the C3 isotopic window, coincides with an abrupt “jump” in ^{14}C data, indicating marked changes in the soil-forming environment (e.g. increased erosion or less carbon accumulation). We suggest that the EP optimum allowed for maximum fractionation by terrestrial plants, resulting in relatively light plant and soil organic carbon ($\delta^{13}\text{C} = -25$ to -26‰). The $\sim 1.5\text{‰}$ offset towards less ^{13}C -depleted values during the ensuing drier conditions reflects a lower degree of fractionation in the water-stressed C3 vegetation after 5 Ka BP.

A similar, albeit smoother and more pronounced, isotopic shift is recorded in sapropelic organic matter preserved within mid-Holocene lacustrine calcareous muds at perennial Lake Amy. Here $\delta^{13}\text{C}_{\text{org}}$ values change from -23 to -20‰ in the lower part of the sequence to -18 to -16‰ in its upper part, presumably in response to increasing water temperature and salinity. The latter inference is supported by up-section changes in the affinity of the fossil ostracod assemblages (from fresh to saline). There are broadly parallel upward trends of decreasing total organic carbon contents (21–1%) and C/N ratios (13–10). ^{13}C -NMR analysis of the bulk organic matter (in progress) will help determine the extent to

which secular variation of an allochthonous (principally aeolian) terrestrial input was a contributing factor. These changes took place between 7.3 and 3.1 Ka BP, a period that spans the abrupt shift in the isotopic signature of soil organic matter at Paget Creek.

By further exploring the correlative use of $\delta^{13}\text{C}_{\text{org}}$ data from suitable ^{14}C -dated soils and lacustrine sediments, it might be possible to trace otherwise poorly resolved climatic changes across areas where a lack of lacustrine sediments hampers their detection.

References

- Dodson, J.R. & Ono, Y., 1997. Timing of Late Quaternary vegetation response in the 30-50° latitude bands in southeastern Australia and northeastern Asia. *Quaternary International* **37**, 89-104.
- Krull, E.S. & Skjemstad, J.O., 2003. $\delta^{13}\text{C}$ and $\delta^{15}\text{N}$ profiles in ^{14}C -dated Oxisol and Vertisols as a function of soil chemistry and mineralogy. *Geoderma* **80**, 243-270.
- Mee, A.C., McKirdy, D.M., Krull, E.S. & Williams, M.A.J., 2004. Geochemical analysis of organic-rich lacustrine sediments as a tool for reconstructing Holocene environmental conditions along the Coorong coastal plain, southeastern Australia. In: Roach, I.C. (ed.), *Regolith 2004*, CRC LEME, pp. 247-251.

PSB-20: Stabilization of nitrogen during humification. Study by acid hydrolysis

M. Toribio¹, P. Rovira¹, M.-M. Coûteaux², V.R. Vallejo^{1,3}

1) Dept de Biologia Vegetal, Facultat de Biologia, Univ. Barcelona, Av. Diagonal 645, 08028 Barcelona (Spain) (e-mail: mtoribio@ub.edu)

2) Centre d'Écologie Fonctionnelle et Évolutive, CNRS, Montpellier, France

3) CEAM, Ch. Darwin 14, 46980 Paterna, València (Spain)

The conversion of nitrogen into resistant forms is among the most important processes occurring during organic matter (OM) biodegradation and humification. In this paper, we use acid hydrolysis to quantify the degree of OM biochemical, as a simple method to separate labile and recalcitrant fractions. Acid hydrolysis has been applied to samples from the PROFILE experiment (see details in Bottner et al., 2000), in which ¹³C- ¹⁵N-labelled wheat straw was incubated in situ in a latitudinal gradient of forest soils: Umea and Jdraas (Sweden), Haldon and Friston (UK), Thézan and La Clape (France), Maials and Desert de les Palmes (Spain). The changes in the hydrolyzability of C and N after three years have been studied; only the results for N will be shown here.

Acid hydrolysis was done following González-Prieto & Carballas (1988), which involves: (i) boiling with HCl 1M, 3 h; (ii) with HCl 3M, 3 hours; (iii) with HCl 6M, 4 h; and (iv) with HCl 6M, 24 h. The unhydrolyzed residues were dried at 60°C; a subsample was analyzed for C, N, ¹³C and ¹⁵N by dry combustion-mass spectrometry.

Changes in the recalcitrancy of total N (not shown here) were less clear than those observed for straw-derived N, probably because the former is more stabilized against microbial activity. The recalcitrance of the straw-derived N (Fig. 1) usually increased slightly, with a few exceptions (H horizon of Thézan, A1 horizon of Maials). The changes in the recalcitrance of N were never too relevant: after three years of field exposure, the most of straw-derived remaining N is quite labile, for about 50% is hydrolyzed in the first step (HCl 1M, 3h).

We hypothesized that the higher the resistance to acid hydrolysis, the higher the resistance to biodegradation. Thus, the least hydrolyzable fractions were expected to increase in relative amount after three years. In contrast, our results suggest that the recalcitrance of N was roughly maintained. Actually, in some cases we observed a decrease in hydrolyzability (i.e., an increase in N quality). This result does not agree with the working hypothesis, and can be explained in two main ways. First, the resistance to acid hydrolysis could be not a good indicator of the resistance to decomposition. Against this explanation, however, there are evidences of a much slower turnover of the unhydrolyzable organic fractions (Stout et al.,

1981). A second explanation could be a continuous apport of both C and N to the labile pools, from the most recalcitrant ones. The several fractions (more or less labile/recalcitrant) are not closed compartments, but dynamic pools submitted to inputs and outputs of organic matter – including nitrogenous compounds.

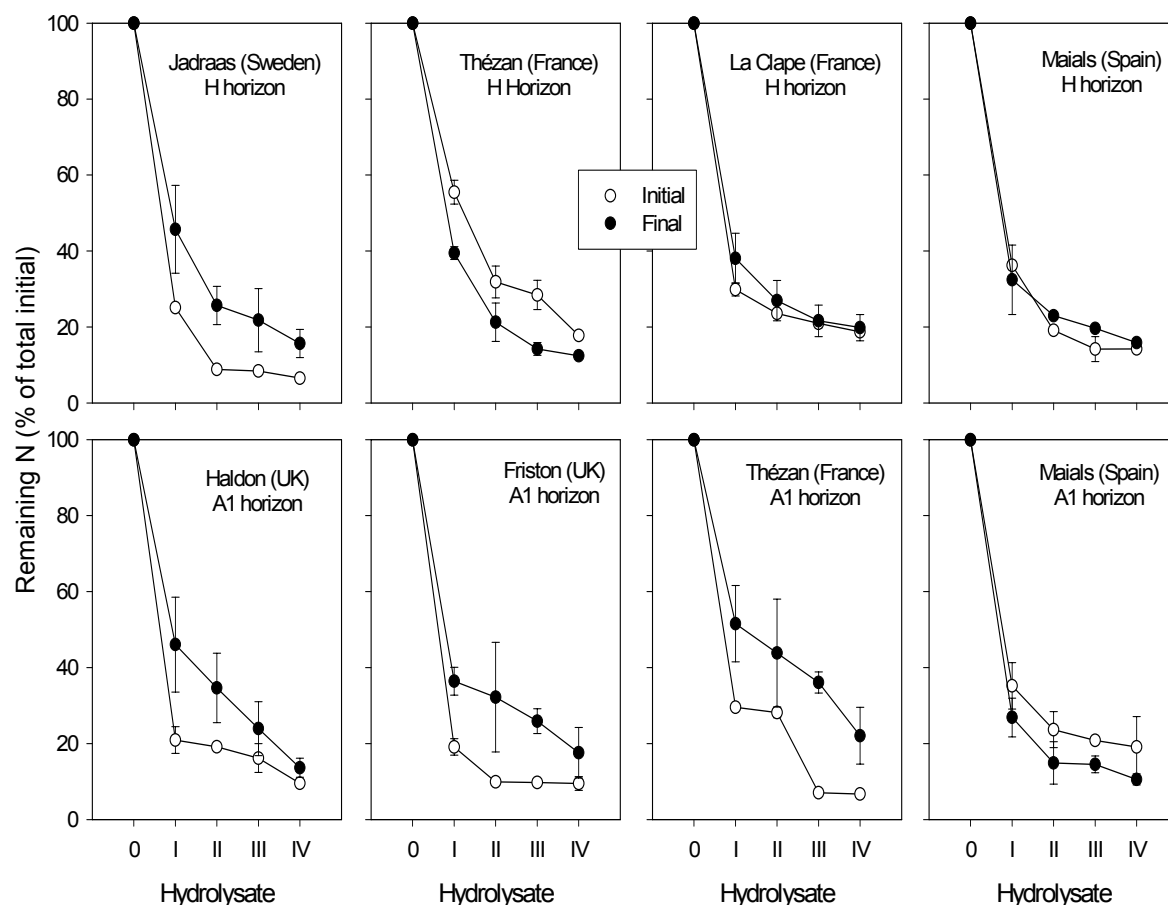


Fig.1. Remaining straw-derived N after each hydrolysis step (in % of the total), for some selected sites. Data are means of 4 replicates (2 replicates for initials)

References

- Bottner P., Coûteaux M.M., Anderson J.M., Berg B., Billès G., Bolger T., Casabianca H., Romanyà J. & Rovira P. (2000). *Soil Biology & Biochemistry* 32, 527-543.
- González-Prieto S.J. & Carballas T. (1988). *Soil Biology & Biochemistry* 20: 1-6.
- Stout J.D., Goh K.M. & Rafter T.A. (1981). Chemistry and turnover of naturally occurring resistant organic compounds in soil. In: E.A. Paul and J.N. Ladd (Editors), *Soil Biochemistry*, vol 5. Marcel Dekker, N.Y. pp. 1-73.

PSB-21: Distribution of C and N in fractions of cultivated volcanic soil

S. Covalada¹, S. Pajares¹, J.F. Gallardo¹, J.D. Etchevers²

1) Consejo Superior de Investigaciones Científicas, IRNA, Salamanca 37071 (España) (e-mail: jgallard@usal.es)
2) Colegio de Postgraduados, Campus Montecillo, Texcoco 56230, Etdo. de México (México)

The effect of management practices on the characteristics of the soil organic carbon (SOC) of an Oxisol (Atécuaro, Michoacán, México; 101° 08' W, 19° 35' N) was studied. The soil is the product of an intense weathering of volcanic material and is deep and rich in clay and sesquioxides.

During 2 years (2002-03) the experimental plots were submitted to four different soil managements: Traditional (Tt) as reference; improved traditional (Tm), organic (To), and intercalating farrow (Tb). Each treatment was replicate twice. Soil samples were taken at 0-10 and 10-20 cm depths, the layers most affected by management. These samples were air dried and subjected to physical fractionation (shaking and sieving during 20 min) to obtain three fractions: Very coarse (2.0-0.2 mm), coarse (0.2-0.05 mm), and fine (< 0.05 mm) aggregates.

The organic C of the fine fraction was fractionated according Moyano & Gallardo (1985, modified), obtaining fulvic (FA) and humic (HA) acids. The C of these fractions and the SOC were determined by dry combustion (TOCA) and the total N (Nt) using a semi-micro Kjeldahl apparatus.

Table 1 shows the C and N distribution in the different fractions obtained.

After 2 years of cultivation the SOC increased with To and Tb. Nevertheless, the Nt decreased with Tt and Tm.

The C content of the coarse fraction increased with Tb and the C content of the fine fraction increased with To. The N content of the very-coarse fraction increased with Tb.

The fractionation of the SOC associated to the fine fraction showed that 79 and 70 % of the C and N, respectively, were concentrated in the humins, which means that this C is stable and has a low mineralization risk. As a consequence, only a small decrease of C was observed in the humins after 2 years of cultivation under Tt and Tb. However, the N of the humins decreased significantly with Tt.

The C/N ratio of the soil and of the soil fractions increased with all the soil managements, indicating a loss of humus quality, mostly in Tt and To. This could indicate that the organic residues incorporated to soil were poor in N.

The humin C/N ratio was lower than the soil C/N in 2003 in all the soil managements, except with Tb. This fact could be a consequence of the intensification of the humification in the humin fractions on time.

Table 1. C and N distribution in the three fractions of aggregates.

Soil management	C (mg/g); year 2002				C (mg/g); year 2003			
	Organic C	> 0.2 mm	0.2-0.05 mm	< 0.05 mm	Organic C	> 0.2 mm	0.2-0.05 mm	< 0.05 mm
	Sample 0-10 cm				Sample 0-10 cm			
Traditional	19,1	11,6	5,5	2,1	16,3	7,8	5,3	3,1
Improved	17,5	10,8	4,7	2,1	18,5	11,2	5,1	2,2
Organic	20,4	12,1	6,5	1,7	22,1	11,6	7,1	3,4
Farrow	14,0	7,3	4,8	2,0	20,1	10,7	6,8	2,6
Mean 0-10 cm	17,8	10,4	5,4	2,0	19,3	10,3	6,1	2,8
	Sample 10-20 cm				Sample 10-20 cm			
Traditional	13,7	8,6	4,0	1,2	16,6	8,5	5,8	2,4
Improved	13,0	7,4	4,0	1,6	18,4	12,3	4,2	1,9
Organic	13,8	8,1	4,2	1,5	19,2	12,3	4,6	2,3
Farrow	14,8	8,3	4,7	1,8	19,4	10,8	6,0	2,6
Mean 10-20 cm	13,8	8,1	4,2	1,5	18,4	11,0	5,1	2,3
	N (mg/g) 2002				N (mg/g) 2003			
Soil management	Total N	> 0.2 mm	0.2-0.05 mm	< 0.05 mm	Total N	> 0.2 mm	0.2-0.05 mm	< 0.05 mm
	Sample 0-10 cm				Sample 0-10 cm			
Traditional	1,6	0,9	0,5	0,2	1,2	0,6	0,4	0,2
Improved	1,4	0,9	0,4	0,2	1,3	0,7	0,4	0,2
Organic	1,6	0,9	0,5	0,1	1,6	0,8	0,5	0,2
Farrow	1,1	0,5	0,4	0,2	1,4	0,7	0,5	0,2
Mean 0-10 cm	1,4	0,8	0,4	0,2	1,4	0,7	0,5	0,2
	Sample 10-20 cm				Sample 10-20 cm			
Traditional	1,2	0,7	0,4	0,1	1,2	0,6	0,4	0,2
Improved	1,1	0,6	0,3	0,1	1,4	1,0	0,3	0,1
Organic	1,1	0,6	0,3	0,1	1,4	0,9	0,3	0,2
Farrow	1,2	0,6	0,4	0,2	1,3	0,7	0,4	0,2
Mean 10-20 cm	1,1	0,6	0,4	0,1	1,3	0,8	0,4	0,2

PCS-1: Preliminary data on carbon sequestration in soils and biomass in some ecosystems of the Canary Islands

C.M. Armas, J.L. Mora, C.D. Arbelo, A. Rodríguez Rodríguez, J.S. Notario

Department of Soil Science and Geology, Faculty of Biology, University of La Laguna, Avda. Astrofísico Francisco Sánchez s/n, 38204 La Laguna, Tenerife, Canary Islands, Spain (e-mail: antororo@ull.es)

Soils are regarded as one of the most important CO₂ sinks all over the planet, accumulating more than 2300 Pg. Such a capability has been recognized worldwide, especially since the declaration of Kyoto Protocol. It is also known that plants contribute to capture atmospheric CO₂ via photosynthesis.

In this regard, it is important to determine the nature of the organic matter occurring in soils, so as to determine what types of compounds are most capable to sequester carbon. Three different fractions are usually considered: active (labile) organic matter, slowly oxidizable organic matter and passive (recalcitrant) organic matter. This latter fraction appears in association with soil minerals, forming organo-mineral complexes, which makes it hardly available to soil microorganisms (chemical sequestration). In the Canary Islands, organo-mineral complexes are generally formed with short-range ordered minerals, characteristic of volcanic soils that have been recognized as highly efficient to sequester CO₂.

Natural ecosystems in the Canary Islands are set in altitudinal levels, following the different climates that vary with height and with the exposure to the wet trade winds coming from the NE. Aridisols predominate in coastal areas and support xerophytic scrub communities. Laurel forests (a subtropical plant formation) appear on Andosols in mountainous humid areas, whereas in mountainous dry areas grow Canarian pine (*Pinus canariensis*) forests.

In this paper, a study on the performance of different ecosystems in the islands (both forests and scrubs), to sequester carbon has been made. With this purpose, ten study areas having different soils and plant communities (both, natural or degraded) were selected. An estimation of aerial total biomass was made in each zone from biometric measurements of the vegetation and using regression equations for each species that relate such measurements with biomass. In addition, representative samples of phytomass were taken to analyze total carbon in an elemental autoanalyzer.

Soil profiles were described and sampled in each area, so as to determine the total carbon content in the horizons, as well as the carbon content in the form of organo-mineral complexes (0.1 M sodium pyrophosphate-extractable organic carbon).

The areas with the highest carbon content in the biomass corresponded to the potential dominion of laurel forests (135-165 tm ha^{-1}). As far as soil types are concerned, those having andic properties show the highest total carbon contents (100 – 250 tm ha^{-1}), whereas Aridisols and Inceptisols are much poorer in total carbon (10 – 70 tm ha^{-1}). The complexed carbon forms are in general more important in andic soils, especially in surficial horizons, where most of the organic matter accumulates. However, the complexed-to-total carbon ratio usually increase with depth, due to a higher evolution degree of the organic matter, so that a higher proportion of stable organic carbon compounds scarcely available to soil microorganisms can be found with regard to the soil surface.

Finally, the proportion of carbon stored in the soil with regard to that in vegetation ranges from 1-7 tm ha^{-1} in forest ecosystems, whereas in the arid scrub communities and in degraded forests is much higher (12-20 tm ha^{-1}).

PCS-2: Carbon sequestration in Swedish boreal forests

J. Routh¹, T.S. Bianchi², L. Wysocki²

1) Department of Geology and Geochemistry, Stockholm University, 10691 Stockholm, Sweden
(e-mail: joyanto.routh@geo.su.se)

2) Department of Earth and Environmental Sciences, Tulane University, New Orleans, LA 70118, USA

During photosynthesis, plants take up a large amount of CO₂. This results in transformation of atmospheric CO₂ to carbon, which is sequestered within the vegetation. Hence, forests are believed to be as important sinks for atmospheric CO₂. However, there is active degradation of forest litter, which is affected by seasonal variations, the age of trees, albedo effects, and turnover rates among other parameters. This potentially dilutes the net effect of carbon sequestration by vegetative matter. In Sweden, where more than 50% of the area is covered by boreal forests, it is very important to know the actual potential of these forests in sequestering atmospheric CO₂. Hence, we have focused on studying the potential of these boreal forests as long-term sinks for atmospheric CO₂. We used variation in bulk organic C and N, specific biomarkers (lignin and long chained *n*-alkanes) and stable isotopes (C and N) as geochemical proxies for processes affecting sequestration of atmospheric CO₂ in coniferous and deciduous forests.

Materials and methods

The forests were sampled along a north-south transect across the country and included beech, oak, and pine forests. These forests are < 200 years old and managed by the national forest services - logging occurs, but it is regulated. Sampling involved taking six cores through the soil zone, each 25-30 cm long. Two cores were taken from each spot across a 6 m long profile, sectioned into 5 cm layers, and homogenized. The different layers from each core were pooled together leaving behind three composite cores from each site. The sub-sections were freeze-dried and sieved. Bulk C and N were analyzed with an elemental analyzer and stable isotopes were analyzed with a continuous flow mass spectrometer. Lignin was analyzed by the tetra-methyl ammonium hydroxide (TMAH) method (Filley et al. 1999). Long chained *n*-alkanes are being analyzed by gas chromatography mass spectrometry.

Results and Discussion

The analyses indicate a sharp decrease in organic C and N content with depth. The lignin content reflects the same trend too. Between the different forest types sampled (oak, beech, pine, fertilized and non-fertilized mixed vegetation), there is a difference in the lignin monomer signals and the ratios of syringyl, guaiacyl, and cinnamyl components. The most abundant guaiacyl units were represented by 1-(3,4-dimethoxyphenyl)-2-propanone and 3,4-dimethoxybenzoic acid, methyl ester. The most abundant syringyl markers used as indicators of hardwood were represented by 3,4,5-trimethoxybenzoic acid, methyl ester and *trans*-1-methoxy-2-(3,4,5-trimethoxyphenyl) ethylene. In the upper parts of the sediment core *trans*-4-(4-methoxyphenyl) acrylic acid, methyl ester was abundant indicating the presence of grass. The acid/aldehyde ratio for guaiacyl and syringyl components increased with depth suggesting greater degradation of lignin monomers. Likewise, stable C and N isotopes become heavier by 1 to 1.5‰ with depth, and imply degradation of organic matter. Presently, the analyses of long chained *n*-alkanes are in progress.

Conclusions

The preliminary results indicate an overall decrease in the organic matter content in terms of the bulk material and specific compounds (e.g., lignin and *n*-alkanes) with depth in the soil. The stable isotope signals also support greater degradation with depth as they become heavier. The study questions the effectiveness of atmospheric CO₂ sequestration process by forests to warrant CO₂ production concessions sought by specific countries under the Kyoto protocol.

Acknowledgement

The study is funded by the Swedish Research Council. Gunnar Jacks, Magnus Mörth, and Bryan Grace helped with fieldwork.

References

Filley et al. 1999. Org. Geochem. 30:607-621.

PCS-3: Stabilization and turnover of fatty acids in soils of long-term experiments

G. Jandl, P. Leinweber

University of Rostock, Institute for Land Use, Justus-von-Liebig-Weg 6, D-18051 Rostock, Germany
(e-mail: gerald.jandl@uni-rostock.de)

Soil samples, particle-size fractions and primary matter from long-term experiments are valuable tools to get more insight into the chemical composition and changes of soil organic matter according to different sample origin and soil management such as cultivation and fertilization. Fatty acids, which are the most abundant class of lipids, were chosen as indicator substances for the evaluation of these changes. Therefore, the diagnostic value of fatty acids in soils is used to trace the origin and turnover of soil organic matter in long-term field experiments as well as their importance for the stabilization of soil aggregates.

The total concentrations of the analyzed saturated *n*-alkyl fatty acids from Ap horizons of the long-term experiment at Halle, Germany (Phaeozem) and Bad Lauchstädt, Germany (Chernozem) were higher in the fertilized variants of Phaeozem 'farmyard manure' ($57.7 \mu\text{g g}^{-1}$) and Chernozem 'NPK + farmyard manure' ($25.8 \mu\text{g g}^{-1}$) than in the unfertilized variants of Phaeozem ($48.1 \mu\text{g g}^{-1}$) and Chernozem ($22.0 \mu\text{g g}^{-1}$) ([1], [2]). A striking feature of the fatty acids (*n*-C_{10:0} to *n*-C_{34:0}) in soils of different origin and fertilization was the bimodal distribution based on the C-chain length with maxima at *n*-C_{16:0} and at *n*-C_{28:0}. Both experiments showed a similar concentration level for *n*-C_{16:0}. The maxima at *n*-C_{28:0} were higher for the Phaeozem and lower for the Chernozem compared to *n*-C_{16:0}. The concentrations of *n*-C_{10:0} to *n*-C_{34:0} fatty acids in the organic-mineral particle-size fractions of the Chernozem Ap horizon increased from the coarse silt to the clay fraction (except for fine silt of the unfertilized variant). Fertilization with NPK and farmyard manure resulted in enrichments of *n*-C_{21:0} to *n*-C_{34:0} fatty acids with a maximum at *n*-C_{28:0} in clay (x2.2), medium silt (x2.0), coarse silt (x1.8) and sand (x2.9) compared with the unfertilized treatment (the factors of enrichment are given in parentheses). New evidence for the aggregate stabilizing function of *n*-C_{21:0} to *n*-C_{34:0} fatty acids was derived from the characteristic pattern of disaggregated and aggregated samples (Fig. 1). Highly significant correlations of fatty acid concentrations with organic C concentrations ($r^2 = 0.87^{***}$, $n = 12$) and specific surface areas ($r^2 = 0.72^{***}$, $n = 12$) were interpreted as indicators of (i) trapping of fatty acids in organic matter macromolecules and (ii) direct bonding to mineral surfaces. This was supported by the thermal volatilization and determination of fatty acids by pyrolysis-field ionization mass spectrometry (Py-FIMS) [2].

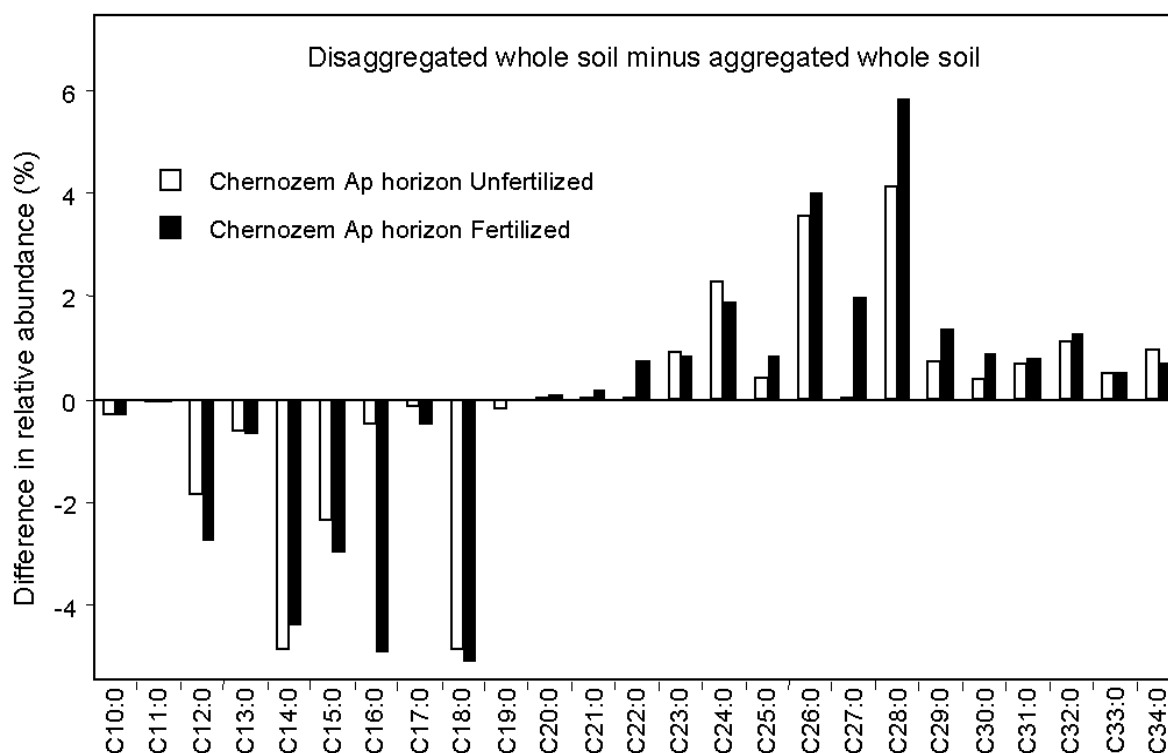


Fig.1. Difference of the relative abundance (%) of the single fatty acids of the disaggregated (ultrasonic treated) and the aggregated (air-dried) whole soil samples of the Chernozem Ap horizon, treatments 'Unfertilized' and 'NPK and farmyard manure'

Investigations of the fatty acid pattern of primary matter, such as plant materials, soil organisms and farmyard manure, proved the influence of these sources on the distribution pattern of C-chain length in cultivated soils. A change in mono-culture from rye to maize, 38 years prior to sampling, led to a decrease in fatty acid concentrations by factors of about 2.8 (unfertilized) and 2.5 (farmyard manure). Therefore, rye-derived fatty acids and soil tillage had a larger impact on fatty acid pools than the input of primary organic matter [3]. Currently, time series of fatty acid concentrations are studied in archived samples to record the kinetics of fatty acid decomposition or enrichment in differently managed soils.

References

- [1] Jandl, G., Schulten, H.-R., Leinweber, P., 2002. Quantification of long-chain fatty acids in dissolved organic matter and soils. *Journal of Plant Nutrition and Soil Science* 165, 133-139.
- [2] Jandl, G., Leinweber, P., Schulten, H.-R., Eusterhues, K., 2004. The concentrations of fatty acids in organo-mineral particle-size fractions of a Chernozem. *European Journal of Soil Science* 55, 459-469.
- [3] Jandl, G., Leinweber, P., Schulten, H.-R., Ekschmitt, K., 2005. Contribution of primary organic matter to the fatty acid pool in agricultural soils. *Soil Biology & Biochemistry* 37, 1033-1041.

PCS-4: Detection of differences between soil organic matter storage in topsoil and subsoil samples

I. Schöning, I. Kögel-Knabner

Lehrstuhl für Bodenkunde, Department für Ökologie, Technische Universität München, 85350 Freising-Weihenstephan, Germany (e-mail: Ingo.Schoening@wzw.tum.de)

Though the concentration of organic carbon (OC) in soils decreases with increasing soil depth, a large proportion of the terrestrial carbon is stored in subsoils (Davis et al. 2004). Little is known about the chemical composition and the age of this carbon reservoir (Eusterhues et al. 2003), whereas many studies were conducted with topsoil samples. Our objective was to compare age and composition of soil organic matter (SOM) in topsoil and subsoil samples from Luvisols and Cambisols under European beech (*Fagus Sylvatica L.*) and spruce (*Picea Abies*) forest. Particle size fractionation was employed to separate physical fractions of SOM (2000-200 μm , 200-20 μm , 20-2 μm and <2 μm) with contrasting turnover and composition. The radiocarbon age of the particle size fractions was measured by accelerator mass spectroscopy (AMS). ^{13}C CPMAS NMR spectroscopy after treatment of samples with 10% HF and analysis of lignin derived phenols after CuO oxidation were applied to characterise the chemical composition of SOM.

The percentage of modern carbon (pMC) of all profiles and physical fractions is decreasing with increasing soil depth (Fig.1a). Highest percentages of modern carbon were always found in the 2000-200 μm fractions. SOM in fine fractions (<20 μm) of topsoils and subsoils was significantly older than SOM in coarse fractions (2000-200 μm). The highest radiocarbon age was measured in the clay fraction from a B-horizon of a Luvisol (4745 yrs before present). The decrease of pMC with increasing soil depth is more pronounced in the 2-20 μm and <2 μm fractions compared to the 2000-200 μm fraction. This indicates that root litter contributes predominantly to the coarse fractions of the subsoil, but not to the fine fractions.

More than 50% of the total carbon stock was stored in the subsoil. The contribution of SOM stored in clay fractions to the total OC pools of the horizons is increasing with increasing soil depth. The soil organic matter in topsoils and subsoils is dominated by alkyl C and O-alkyl C. O-alkyl and alkyl C in particle size fractions of A and E/B horizons appeared to show similar trends. However, in subsoils an increasing proportion of OC was lost during HF treatment.

A correlation was evident between the OC loss during HF treatment and the proportion of OC stored in clay fractions ($n = 15$, Spearman correlation coefficient = 0.91). This indicates that the OC loss during HF treatment is attributed to the OC of the clay fraction, suggesting that HF mainly dissolves OC that was previously bound to soil minerals. The proportion of soil organic matter stabilized by interactions with soil minerals seems to be much higher in the subsoil (Fig.1b). The OC that is lost during HF treatment remains to be studied. In contrast to OC only low amounts of lignin (less than 37% of the total lignin) were found in the subsoil. This supports results from topsoils that showed that lignin is predominantly found in the younger coarse fractions (Schöning et al. 2005)

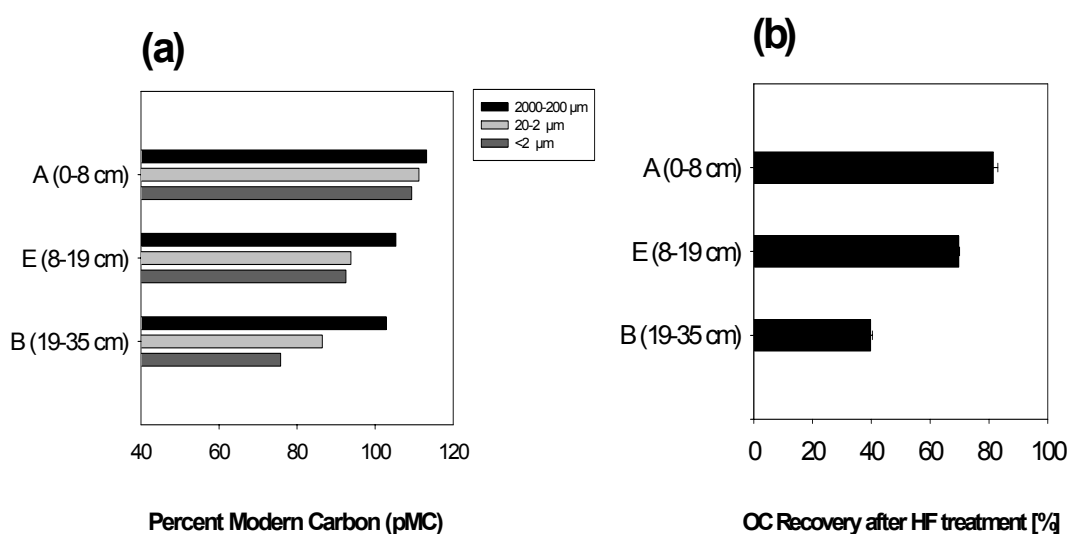


Fig.1. (a) Percent Modern Carbon (pMC) in the particle size fractions of the A, E and B horizon of a Luvisol from Leinefelde/Germany (b) Recovery of OC after HF treatment of bulk soil samples from the Leinefelde soil profile

References

- Davis AA, Stolt MH & Compton JE (2004) Spatial distribution of soil carbon in southern new England hardwood forest landscapes. *Soil Science Society of America Journal* 68: 895-903
- Eusterhues K, Rumpel C, Kleber M & Kögel-Knabner I (2003) Stabilisation of soil organic matter by interactions with minerals as revealed by mineral dissolution and oxidative degradation. *Organic Geochemistry* 34: 1591-1600
- Schöning I, Morgenroth G & Kögel-Knabner I (2005) O-alkyl C and alkyl C are stabilised in fine particle size fractions of forest soils. *Biogeochemistry* (in press).

PCS-5: Incorporation of elevated radiocarbon from roots or litter into protected and unprotected soil organic matter: evidence for a root-dominated soil carbon cycle

C.W. Swanston¹, M.E. Torn², P.J. Hanson³

1) Center for Accelerator Mass Spectrometry, Lawrence Livermore National Laboratory, PO Box 808 L-397, Livermore, California 94551, USA (e-mail: SWANSTON@LLNL.GOV)

2) Center for Isotope Geochemistry, Lawrence Berkeley National Laboratory, Berkeley, California, USA

3) Environmental Sciences Division, Oak Ridge National Laboratory, Oak Ridge, Tennessee, USA

Carbon stabilization in soil organic matter (SOM) occurs concurrently with destabilization, and large changes in the resident carbon in SOM may appear as only small net changes in bulk carbon values. Using carbon isotopes as tracers is an effective way to reveal the subtleties of SOM carbon dynamics, especially if combined with organic matter fractionation techniques. A large release of radiocarbon-labeled CO₂ from an incinerator at Oak Ridge Reservation (Oak Ridge, Tennessee, USA) in 1999 provided the opportunity to trace the elevated ¹⁴C through the forest vegetation and into SOM on an unprecedented scale. Senescent leaves were collected from ¹⁴C-labeled and near-background trees, and then plots were established alternatively in labeled and near-background stands in a factorial design. Thus, the primary source of elevated ¹⁴C could be traced from roots or litter. Soils from these plots were collected and physically separated into carbon reservoirs of differing stability. 'Free' light fractions (free LF) contain organic matter with high C turnover rates and typically found in macropores. Occluded light fractions (occluded LF) are chemically similar to the free LF, but are isolated inside soil aggregates and have correspondingly slower C turnover rates. Heavy fractions (HF) are primarily organo-mineral complexes forming the matrix of soil microaggregates, and have the longest overall mean residence time of C in most soils. Bulk soil carbon varied little between plots in first two years of the study. Also, Δ¹⁴C in the bulk soil showed no significant radiocarbon input to the mineral soil from labeled litter or roots in the first two years. Yet, there was clear input of elevated ¹⁴C into the soil fractions. The greatest incorporation of elevated ¹⁴C was into the free LF. There appears to be a significant gap in time before the occluded LF incorporates the elevated ¹⁴C. Although principally composed of more stable C, the HF appears to also contain a fast-turnover pool that reflects rapid incorporation and loss of the elevated ¹⁴C during the first two years. The occluded and heavy fractions below 15 cm were generally quite similar in Δ¹⁴C, and incorporated much less of the elevated ¹⁴C than the free LF. Considering ¹⁴C-elevated inputs from different sources, the initial results indicate that the SOM in this system may be dominated by root inputs and largely insensitive to or uncoupled from litter inputs.

PCS-6: Is Arctic climate warming causing remobilization of the huge reservoir of Tundra/Taiga soil carbon?

B.E. van Dongen¹, L. Guo², I. Semiletov^{2,3}, Ö. Gustafsson¹

1) Stockholm University, Department of Applied Environmental Science, Stockholm, Sweden
(e-mail: Bart.vanDongen@itm.su.se)

2) International Arctic Research Center, University of Alaska Fairbanks, Fairbanks, Alaska, USA

3) Pacific Oceanological Institute, Russian Academy of Science, Vladivostok, Russia

It is estimated that about one third of the world's surface soil organic carbon is accumulated in the pan-Arctic tundra/taiga ecosystems; alone nearly equalling the total amount held in the atmosphere as carbon dioxide. Further, the underlying Russian-Siberian permafrost zone contains an additional 15 times more carbon. This vast amount of old organic matter could re-enter "active" biogeochemical cycles if liberated by global-warming induced thermokarst, coastal erosion and an increase in the seasonal thaw depth of permafrost. Numerical climate models forecast an amplified warming in arctic continental region (e.g., Zwiers, 2002). Hence, it is reasonable to expect that the global warming effects will first be observed in the arctic and this will involve effects on the huge carbon inventory in Siberian soils. This may have profound influences on both the terrestrial and marine Arctic ecosystems with implications for the global carbon cycle and climate. However, existing studies are inconclusive of whether there is currently a release of "new" old carbon from the land.

A recent pilot study of estuarine surface sediments from a number of the major Russian Arctic rivers show that the average ¹⁴C ages of the bulk organic carbon (OC) was between 2600 and 13000 years "old" (Fig. 1). In addition, a climatologically-consistent increasing age trend from rivers which flow through non-permafrost regions in the west to those that flow through permafrost regions in the Eastern Siberian region can be observed, suggesting that old carbon is released through permafrost thawing and erosion (Guo et al., 2004). However, such bulk OC may contain material from both land and riverine/marine organisms.

As part of our ongoing pan-Arctic collaboration/study, larger amounts of surface sediments of major North American and Russian rivers have been sampled in 2004 and results will be presented on the patterns of their terrestrial biomarker molecules and their inherent isotopic signatures. Further, Russian Arctic River plumes will be sampled during the spring flood in 2005, which will provide information on a "pure" terrestrial component. River plume samples have the advantage over coastal surface sediment samples in that ice rafting and other resuspension processes can cause a substantial uncertainty in the chronology of coastal

surface sediments. Terrestrial biomarkers, such as n -C₂₃-C₃₃ alkanes, retene, triterpenoids and n -20:0-30:0 alkenols will be isolated using preparative capillary GC and dated using compound-specific radiocarbon analysis. This innovative approach is at the forefront of environmental geochemistry research since this study will contribute toward increased understanding of whether old carbon is released from the Russian-Siberian permafrost; a scenario which would have major implications for the global carbon cycle and climate.

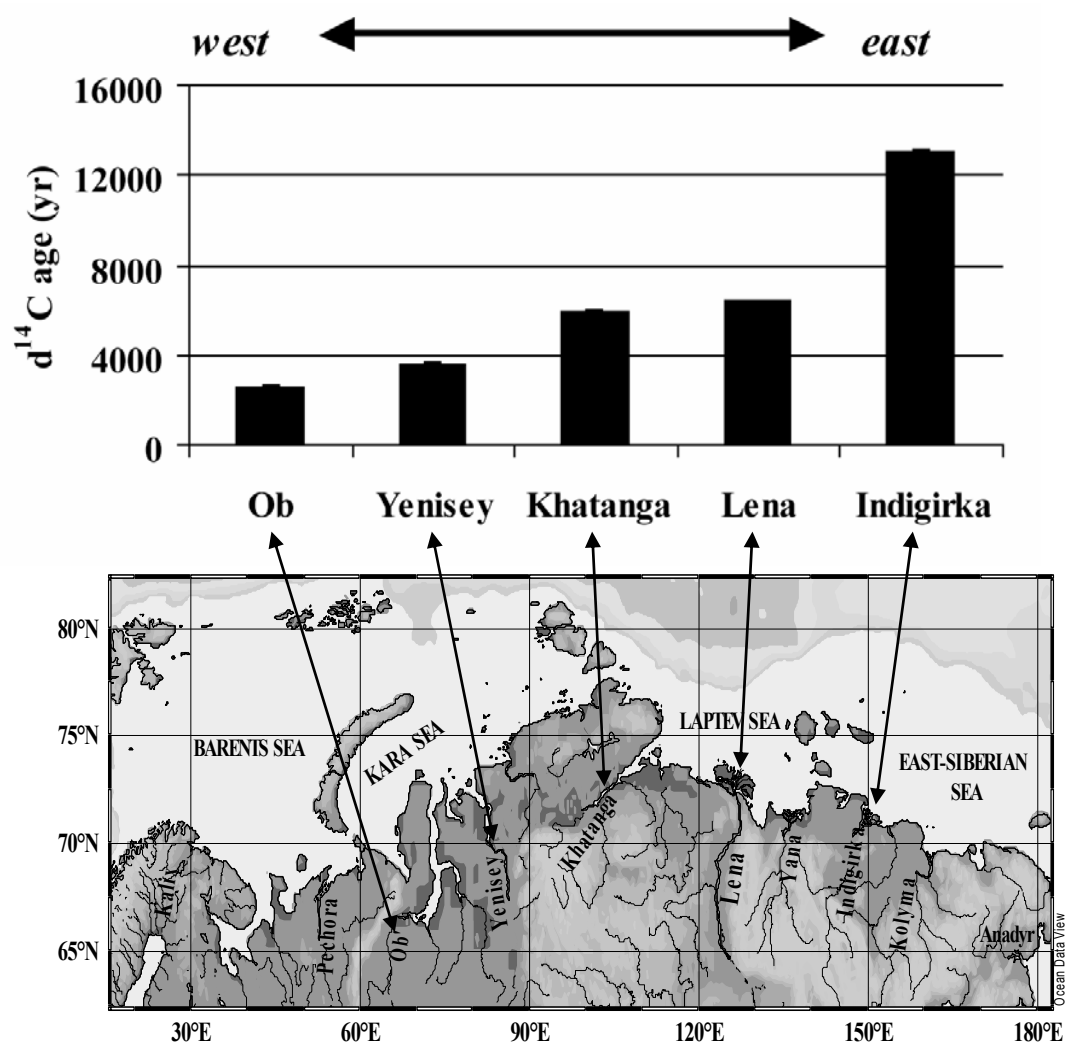


Fig.1. The average age of bulk organic carbon in surface sediments collected from the mouths of Russian Arctic Rivers along the entire continental stretch (after Guo et al., 2004)

References

- Guo, L., Semiletov, I., Gustafsson, Ö., Ingri, J., Andersson, P., Dudarev, O., White, D. (2004) *Global Biogeochem. Cycles*, **18**, GB1036, doi:10.1029/2003GB002087.
- Zwiers, F.W. (2002) *Nature*. **416**, 690.

PCS-7: Sequestration of bulk carbon, lipids and lignin in arable soils

G.L.B. Wiesenberg¹, M.W.I. Schmidt², A. Heim², J. Schwarzbauer³, L. Schwark¹

1) University of Cologne, Dep. of Geology and Mineralogy, Zuelpicher Str. 49a, D-50674 Cologne, Germany (e-mail: guido.wiesenberg@uni-koeln.de)

2) University of Zurich-Irchel, Department of Geography, Winterthurer Str. 190, CH-8057 Zurich, Switzerland

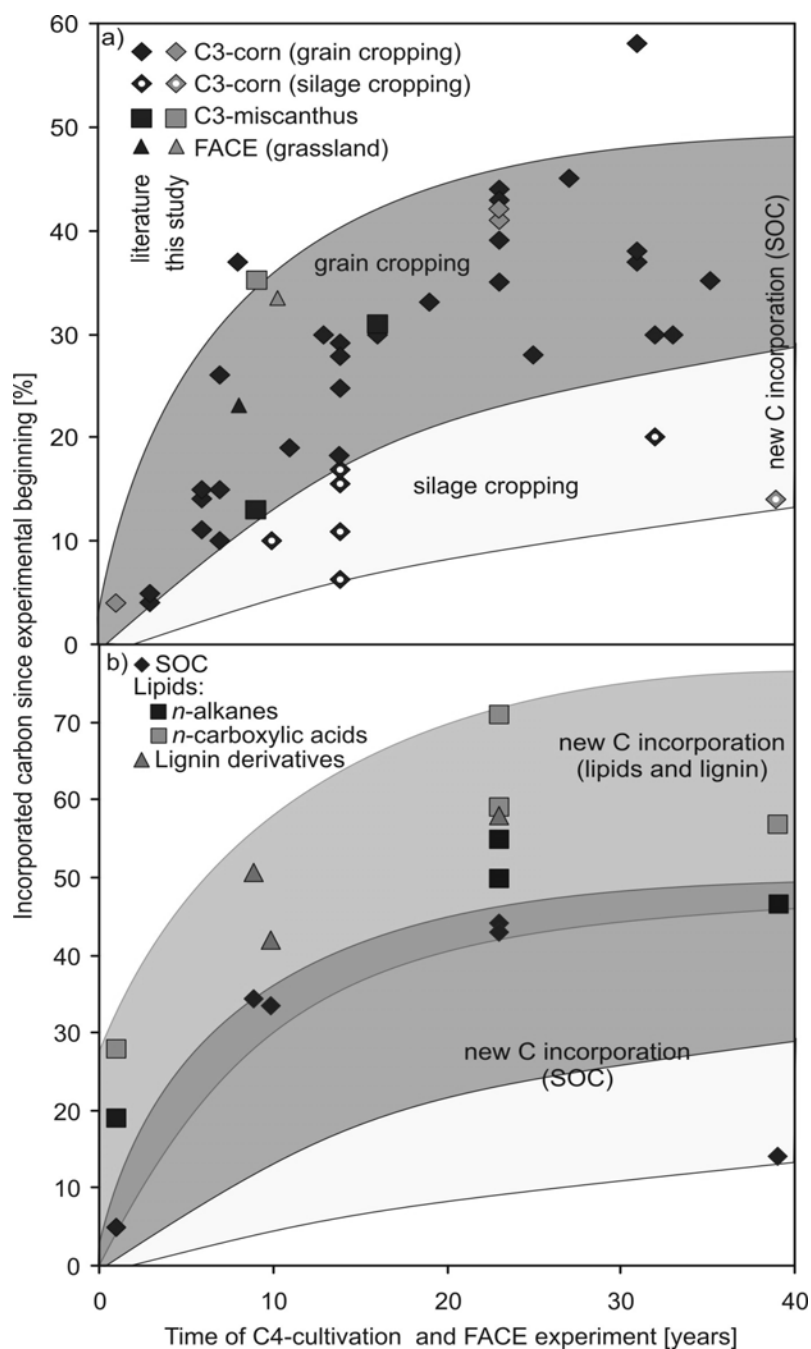
3) RWTH Aachen, LEK, Lochner Str. 4-20, D-52056, Germany

Sequestration of organic matter into soils plays an important role in global CO₂ dynamics. Models describing CO₂ budgets therefore assume different rates of soil organic carbon (SOC) turnover depending on the reactivity of plant-derived components. Lipids and lignin are assumed to represent a relatively stable fraction of soil organic matter (SOM) ([1], [2]). In contrast to macromolecular SOM-fractions these compounds are suitable for detailed structural and compound-specific $\delta^{13}\text{C}$ -isotope characterization. A standard approach for assessment of SOM turnover rates uses natural isotopic labeling after monoculture crop switching. Replacing isotopically light C₃-plants (e.g. rye) with isotopically heavier C₄-plants (e.g. corn) incorporates biomass with heavier C-isotopic signature into SOM, allowing calculation of proportions of C₄-plant derived carbon [3]. In this study, we simultaneously applied isotopic and biomarker analysis to obtain information on turnover times and sources for different fractions of SOM. We will compare results obtained by this approach with literature data of SOC turnover times determined by similar or alternative methods.

Soil and plant samples originate from experimental agricultural plots in Germany, Switzerland and France. Samples were taken up to 40 years after introduction of a C₄-monoculture, with reference sites kept under C₃-monoculture. Total lipids were recovered by accelerated solvent extraction and separated into eight fractions of different polarity by automated liquid chromatography [4]. Lignin derivatives were obtained via CuO-Oxidation followed by chromatographic clean-up. Fractions of aliphatic hydrocarbons, carboxylic acids and lignin derivatives were analyzed by GC-MS and GC-irmMS. Bulk SOC was analyzed by EA-IRMS after decarbonatization.

Incorporation of plant biomass into SOM follows an exponential increase for the first years. Establishment of steady state conditions on average is reached after 15–20 years (see figure 1a) for soils with high biomass input (i.e. grain cropping and conventional tillage). The proportion of newly fixed carbon by then has reached 30 to 50 % of total carbon. In contrast, sites with low biomass input (silage cropping, no-till) do not reach equilibrium conditions during the first five decades and accumulate only up to 20 % new carbon (see figure 1a).

Lignin and lipids are incorporated into SOM at higher rates and reach steady state conditions similar to bulk organic carbon (see figure 1b). Under steady state conditions the proportions of newly fixed carbon amount to 55 - 75 % for *n*-carboxylic acids, 50 - 60 % for lignin and only 45 - 55% for *n*-alkanes. The data clearly demonstrate that lipids and lignin do not contribute to the long-term stable pool of SOM as previously suggested. This adds new perspectives to the still unanswered question, which components make up the long-term stable pool of SOM.



References

- [1] van Bergen, P.F., Bull, I.D., Poulton, P.R., Evershed, R.P., 1997. *Organic Geochemistry* 26, 117-135.
- [2] Kögel-Knabner, I., 2002. The macromolecular organic composition of plant and microbial residues as inputs to soil organic matter. *Soil Biology and Biochemistry* 34, 139-162.
- [3] Lichtfouse, E., Wehrung, P., Albrecht, P., 1998. Plant wax *n*-alkanes trapped in soil humin by noncovalent bonds. *Naturwissenschaften* 85, 449-452.
- [4] Wiesenberg, G.L.B., Schwark, L., Schmidt, M.W.I., 2004. Improved automated extraction and separation procedure for soil lipids. *European Journal of Soil Science* 55, 349-356.

PCS-8: A dynamic model of the carbohydrates component of soil organic matter

D. Derrien, J. Balesdent, C. Marol

Laboratoire d'Ecologie Microbienne de la Rhizosphère, UMR CNRS/CEA/Univ. Aix-Marseille II n°6191, CEA de Cadarache, 13108 Saint Paul lez Durance, France (e-mail: derrien_delphine@yahoo.fr)

The chemical composition of soil organic matter (SOM) is the result of a dynamic system established between several fluxes: incorporation of vegetal molecules, biosyntheses, biotransformations, degradation, preservation processes (adsorption, humification). Reciprocally, the dynamics of SOM partly depend on the chemical nature of SOM. The dynamics of SOM are currently simulated quantitatively models, but have been poorly related to the chemical composition. Such a coupling would ideally reproduce the dynamics of both total carbon and individual sugars in soil.

To couple dynamics and chemical nature, we propose a model of one class of SOM components, the neutral carbohydrates, as a part of the whole carbon dynamics. We chose the Rothamsted carbon model as a frame-model and a cereal-cultivated cambisol as reference soil.

Natural and artificial carbon isotope labellings were used to calibrate the inputs and the fluxes of the model on various time scales. On a short time scale the input by root-exsudation was investigated through ^{13}C pulse chase of photoassimilates [1]. The microbial biosyntheses and the fate of microbial saccharides were evaluated after incubations with ^{13}C labelled substrates such as glucose or wheat straw. Long-term residence of carbohydrates was studied through natural ^{13}C and ^{14}C labellings in the field.

After transforming the sugars into their trimethylsilyl derivatives we used compound specific GC-C-IRMS analysis to identify ^{13}C -monosaccharides (glucose, xylose, arabinose, mannose, galactose, rhamnose and fucose) in various soil fractions [2].

The Rothamsted carbon model contains plant-derived material, microbial and humified compartments. It describes the mean residence time of each pool and the carbon fluxes between the compartments. We introduced sub-compartments of sugar carbon, and fluxes between sugars and non-sugars. Our model successfully described the amount of soil sugars, their signature and their life-time. The model properly reproduced the complex evolution of carbon chemistry starting with more than 50% of carbohydrates in the vegetal inputs towards finally about 12% in the bulk SOM pool, with an increasing signature of microbial sugars.

A perspective of this work is to extend the molecular approach of carbon dynamics (e.g. lignins [3]) in collaboration with other groups working on the same reference soil.

References

- [1] Derrien, D *et al.*; *Rapid Communications in Mass Spectrometry*; 2003.
- [2] Derrien, D *et al.*; *Plant and Soil*; 2004
- [3] Dignac *et al.*; *Geoderma*; *in press*.

PCS-9: Organic matter structure in the A horizons of Andosols from the Canary Islands

J.A. González-Pérez¹, C.D. Arbelo², A. Rodríguez-Rodríguez², H. Knicker³, C.M. Armas²,
O.P. Polvillo¹, T. Verdejo¹, F.J. González-Vila¹

1) Instituto de Recursos Naturales y Agrobiología de Sevilla, CSIC. Reina Mercedes 10, 41012-Sevilla, Spain
(e-mail: jag@irnase.csic.es)

2) Universidad de La Laguna, Avda. Astrofísico Fco. Sánchez, 38204 La Laguna, Tenerife, Spain

3) Lehrstuhl für Bodenkunde, TU München, 85350 Freising-Weihenstephan, Germany

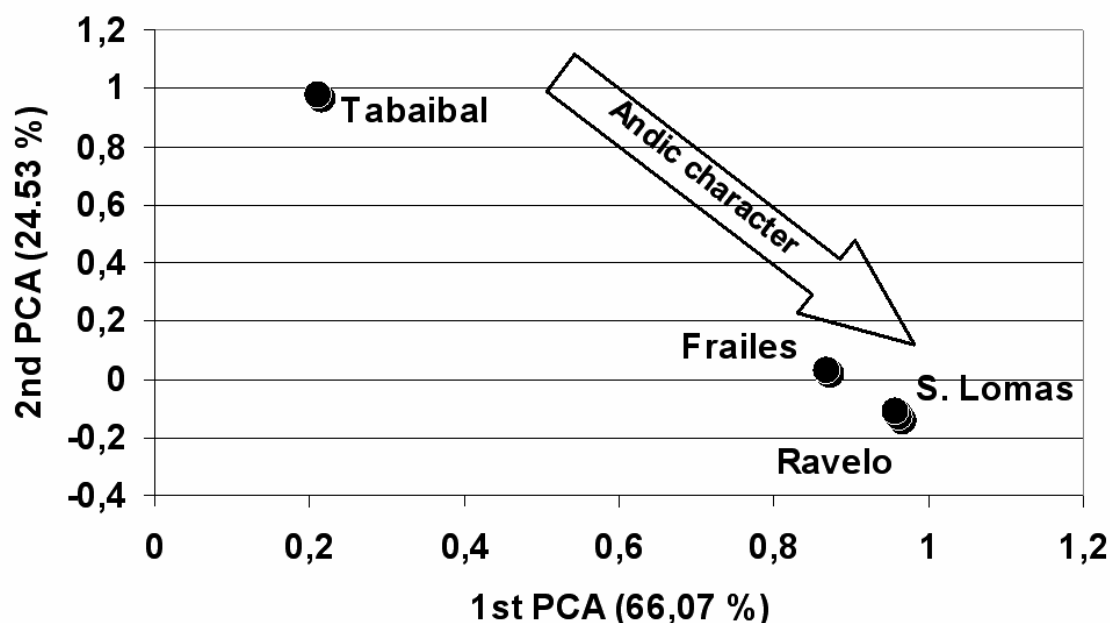
Andosols are soils usually formed from volcanic substrates, with thick dark A horizons rich in organic carbon content mainly in the form of stabilized humic fractions. The peculiar properties of these variable-charge soils are due, to large extent, to the occurrence of poorly crystalline materials like allophanes, imogolite and other Fe and Al oxyhydroxides. Such materials are prone to form organo-mineral structures with a high degree of stability. Consequently, Andosols store much more organic matter (OM) than other soils under similar conditions. There are few studies about the molecular composition of this stabilized OM (centennial to millennia timescale) in a soil scenario often considered as an efficient C-sink in terms of C sequestration processes.

In this work a series of structural features of whole soil and humic materials extracted from the organic A horizons of three soils with andic properties (*Ravelo*, *Siete Lomas*, *Frailles*) and a non-andic mineral soil (Sodic Cambisol, *Tabaibal*) from a nearby area from the island of Tenerife (Canary Islands) were analyzed by spectroscopic methods (FT-IR and ¹³C NMR) and by double shot pyrolysis-gas chromatography-mass spectrometry (Py-GC/MS).

Spectral characteristics (FT-IR and ¹³C NMR spectra) of the whole soils and isolated fulvic (AF) and humic acid (HA) fractions were of discriminant value to differentiate soils with andic properties from the mineral soil. Differences were also found by direct thermal desorption (250°C) and pyrolysis (610°C) of soil fine earth fractions of organic Andosols and the control mineral soil; higher preservation of long chain alkyl compounds (alkanes & alkenes) is observed in the Andic soils (C₁₁-C₃₃), showing a bimodal distribution with maxima at C₁₅ and C₂₀. The distribution of alkyl compounds in the Cambisol was close to normal with maximum at C₁₃ and a lower amount and range of saturated (C₁₁-C₂₇) and unsaturated chains (C₁₁-C₁₇) than the Andosols. Pyrolysis at 610°C of the HA fraction show a very well resolved lignin signature (methoxyphenol series) (Table 1), as well as of fatty acids with signs of bacterial activity (FAMES). Principal components analysis (PCA) of pyrolysis compounds released at 610°C from the FA fractions was particularly informative in differentiating the andic character of the soils (Fig. 1).

Table 1. Relative abundance* of methoxyphenols released by pyrolysis at 610 °C. *) % of the cumulative chromatographic area for total methoxyphenols; **) Non Andic soil; ---) No detected.

Compound*	RAVELO			SIETE LOMAS			FRAILES			TABAIBAL**		
	Soil	HA	FA	Soil	HA	FA	Soil	HA	FA	Soil	HA	FA
Guaiacol (G)	26.0	49.4	100.0	21.4	41.2	82.1	30.4	54.6	90.7	---	35.7	---
Syringol (S)	---	6.3	---	2.4	14.3	---	---	3.4	---	---	9.2	---
Methyl guaiacol	9.1	11.3	---	8.1	8.6	---	---	10.2	---	---	6.2	---
Methyl syringol	---	2.9	---	---	---	---	---	---	---	---	---	---
Ethyl guaiacol	---	4.2	---	3.3	3.5	---	---	3.9	---	---	2.4	---
Ethyl syringol	---	0.8	---	---	---	---	---	1.4	---	---	3.2	---
Vinyl guaiacol	27.6	8.4	---	28.6	15.2	---	26.1	11.1	2.6	---	18.4	---
Vinyl syringol	2.2	1.9	---	1.2	0.9	17.9	43.5	2.7	6.7	---	3.8	50.0
Propenyl guaiacol	5.6	1.9	---	4.8	2.3	---	---	2.4	---	---	3.2	50.0
Propenyl syringol	5.6	2.6	---	6.0	3.7	---	---	1.7	---	---	6.8	---
Acetoguaiacone	23.8	8.7	---	24.3	6.9	---	---	6.8	---	---	8.6	---
Acetosyringone	---	1.6	---	---	3.4	---	---	1.7	---	---	2.4	---
ΣG	92.2	75.5	100.0	83.8	70.7	82.1	56.5	81.2	93.3	---	69.7	50.0
ΣS	7.8	14.5	---	9.5	22.3	17.9	43.5	8.2	6.7	---	18.9	50.0
G/S	11.8	5.2	---	8.8	3.2	4.6	1.3	9.9	13.8	---	3.7	1.0

**Fig.1.** PCA based in the percentages of compounds released after pyrolysis from FA's

PCS-10: Land use change and carbon storage in soils from Galicia (Spain)

L. López-Sangil¹, M. Toribio¹, J. Torras¹, E. Bertran¹,
P. Rovira¹, V.R. Vallejo²

1) Dept de Biologia Vegetal, Facultat de Biologia, Univ. de Barcelona, Diagonal 645, 08028 Barcelona (Spain)

2) CEAM, Ch Darwin 14, 46980 Paterna, València (Spain)

The study of the storage of organic carbon (OC) in soils has become a relevant question due to its capacity for acting, within the global biogeochemical carbon cycle, as a sink for atmospheric CO₂. For these reasons, a considerable scientific effort is being made worldwide in order to quantify the OC soil storage and the way the different land uses can affect its dynamics.

In this study, we wanted to check the effect on OC storage of some land uses developed in an agricultural land in the NW part of Spain (Galicia). The human conversion into grasslands or its natural secondary evolution into shrublands (commonly dominated by *Sarothamnus* or *Ulex*) after crop abandonment are supposed to increase the amount of the total OC in the profile, as a result of several factors (or a combination of them): the high quantity, growth rate and renovation of fine roots (in grasslands) and the higher amount of total biomass present at the shrublands, and also because of the lack of tillage, which in agricultural lands accelerates organic matter decomposition by the increased aeration.

We studied a set of plots of a land chronosequence located in the district of Lugo (NW of Spain), with an atlantic-type climate, that was not affected by wildfires for the last 40 years. The soil is developed on acid parent material (basically schists). The zone has held historically *Secale* and *Hordeum* crop fields, which nowadays have been mostly replaced by grasslands or - after abandonment - by secondary shrublands. We focused our study on 2 types of shrublands (either dominated by *Sarothamnus* or by *Ulex*), and the evolution of different aged grasslands. All the plots were almost stuck together in space. The influence of different inclinations among plots were considered as non-significant (always less than 15%).

Six soil cores of 30 cm were taken in each plot. All were divided into 3 layers (0-10, 10-20, 20-30 cm). To quantify properly the organic layers, and/or the necromass (conceptually similar to an L-F horizon), they were removed and dried separately when found. OC was quantified by dichromate oxidation in soil samples, or with a CARLO ERBA analyzer in the necromass.

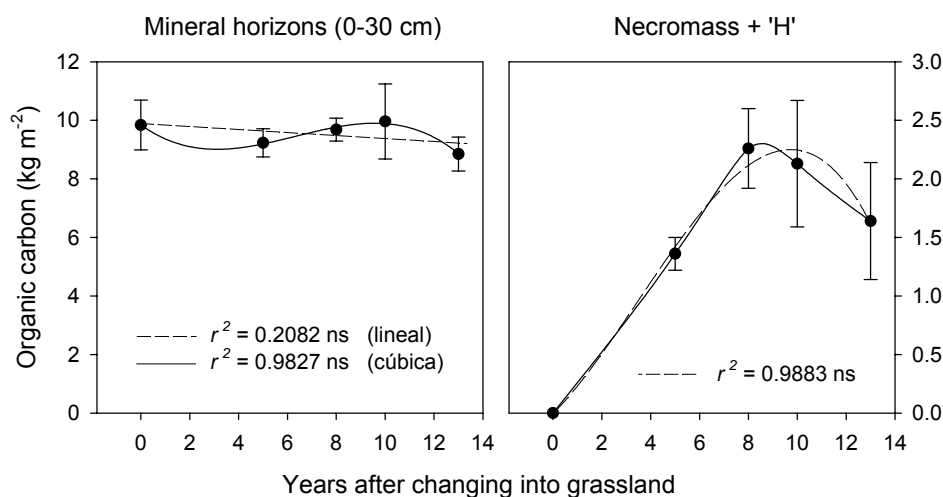


Fig.1. Changes in organic carbon accumulated in the plots, after conversion of arable land into grassland. Left: mineral soil; right: organic horizons and necromass

The conversion of an agricultural land (assumed to be the initial state) into grassland does not always result in a significant increase in total OC content in the mineral soil. Our data show a variable response in the different layers, but overall they suggest a small (non-significant) decrease. This could be explained by the high levels of OC found in the first layers of the agricultural soil (table 1), maybe related with the high amount of dead roots from cultivated plants, incorporated and mixed with the first layers due to ploughing. As a result, all the net sequestration in soils occurs in the organic horizons and/or the necromass (Fig. 1).

For other types of vegetation (shrublands, including ferns), the accumulation of necromass is also a substantial portion of the net C sequestration, even though the total sequestration did never reach 1 kg C m⁻² (not shown in this abstract). Unlike in grasslands, a net sequestration in the mineral soil is detected in some cases, due to an increased accumulation in the first 10 cm of the mineral soil (table 1).

Table 1. Organic carbon (% w/w) in the mineral soil. Data are means of 6 points, \pm standard deviation.

Use	Years	0 - 10 cm	10 - 20 cm	20 - 30 cm
Crop (<i>Avena</i> sp.)	0	3.29 \pm 0.18	3.02 \pm 0.43	1.92 \pm 0.87
	(initial)			
<i>Ulex europaeus</i>	17	4.95 \pm 0.52	2.47 \pm 0.14	1.87 \pm 0.18
<i>Ulex europaeus</i>	20	3.99 \pm 0.57	2.30 \pm 0.14	1.89 \pm 0.35
Ferns	20	4.62 \pm 1.32	2.21 \pm 0.31	1.62 \pm 0.56
<i>Sarothamnus</i> sp.	15	4.54 \pm 0.58	2.55 \pm 0.15	1.92 \pm 0.71

PCS-11: Decoupled mechanisms of C and N stabilization in soil: evidence from sequential density fractionation of three soils of contrasting mineralogy

P. Sollins¹, C. Swanston², S. Crow¹, B. Caldwell¹, T. Filley³, K. Lajtha¹

1) Oregon State University, Corvallis, Oregon, USA

2) Lawrence Livermore National Laboratory, Livermore, California, USA

3) Purdue University, West Lafayette, Indiana, USA

C:N ratio of soil particles drops consistently with increasing particle density across all soils studied to date. The variation in particle density is explained in large part by variation in the mass ratio of organic to mineral phase of these particles, which suggests that the thinner organic coatings are more N rich. In fact, considerable empirical and theoretical data show that proteins and other amino compounds sorb especially stably to mineral surface cation exchange sites. To explore mechanisms underlying this trend in C:N ratio, we sequentially fractionated an Oregon Andisol (mainly variable-charge), a Michigan Mollisol and a Puerto Rico Oxisol at a series of densities from 1.65 to 2.80 g cm⁻³ and analyzed the fractions for measures of organic matter composition: C, N, ¹⁴C, lignin, lignin oxidation products, and protein.

C and N results fit well with published results for other soils. $\Delta^{14}\text{C}$ concentrations for the Andisol decreased with particle density, except for the two lightest fractions which were rich in charcoal from a fire ca. 1500. Total lignin concentration decreased along the density sequence while the ratio of oxidized to non-oxidized monomers increased.

The decrease in $\Delta^{14}\text{C}$ with increasing density for the Andisol supports our hypothesis that the thinner, more N-rich coatings are more stable. The decrease in lignin with decreasing ¹⁴C concentration confirms findings that lignin is not especially long-lived in soil. The increase in oxidation state of the lignin with increasing density suggests increased ability of the monomers to ligand exchange with mineral surface hydroxyl sites due to more numerous carboxyl groups in the monomers. Published theory and empirical data suggest that stable bonding of the N-containing organics is due mainly to cation exchange, whereas stable bonding of the non-N-containing organics occurs mainly by ligand exchange. The two sorption processes can respond very differently to soil chemical parameters, especially pH, thus this decoupling of mechanisms for C and N stabilization deserves further attention.

**PCS-12: Moving from conventional to ecological farming in Mediterranean countries:
any effect on carbon sequestration in soil?**

J. Torras¹, M. Toribio¹, E. Bertran¹, P. Rovira¹, J. Romanyà²,
V.R. Vallejo^{1,3}

1) Dept de Biologia Vegetal, Facultat de Biologia, Univ. Barcelona. Diagonal 645, 08028 Barcelona (Spain)
(e-mail: jtorraba7@bio.ub.edu)

2) Dept de Productes Naturals i Edafologia, Facultat de Farmàcia, Universitat de Barcelona, (Spain)

3) CEAM, Ch Darwin 14, 46980 Paterna, València (Spain)

The conversion of forest soils to agricultural soils results in a massive loss of organic matter. Agricultural soils are usually the poorest in organic carbon, whatever the climatic conditions we consider. The adoption of ecological farming practices (manure or compost apports, partial or total suppression of the use of pesticides, replacing single-crop farming by crop rotation systems, reduction of tillage, including no-tillage as an extreme case, etc.) can result in a recovery of the levels of organic matter in soil, hence in a net sequestration of carbon in soil. Since the so-called ecological agriculture is progressively spreading in Spain, it is important to know how these practices affect net carbon accumulation.

For this study we took pairs (or groups) of adjacent plots: in all, at least one of the plots was submitted to conventional agricultural practices, while the other(s) were submitted to ecological farming. Three groups of plots, located in contrasted climates, were studied:

- A first zone, in a mediterranean, horticultural crop area (L'Horta, Valencia). This group includes irrigated plots only.

- A second zone, in a dry mediterranean, cerealistic area (La Conca de Barberà, Catalonia). This group includes only dryland farming, without any irrigation.

- A third zone, in a cerealistic area under a continental climate (Pirla, Huesca, Aragón). This group includes both dryland farming and irrigated plots.

All plots were sampled using a prismatic core sampler; 6 cores were taken from each plot. All cores were divided in 3 levels (0-10, 10-20, 20-30 cm). Once in the laboratory, samples were air-dried and sieved (2 mm) to discard gravel and gross organic fragments. A subsample of the sieved soil material was ground in an agatha mortar for chemical analyses. The samples were analyzed for total organic carbon, total N, texture, carbonates, and pH. Only results for total OC will be mentioned in this summary.

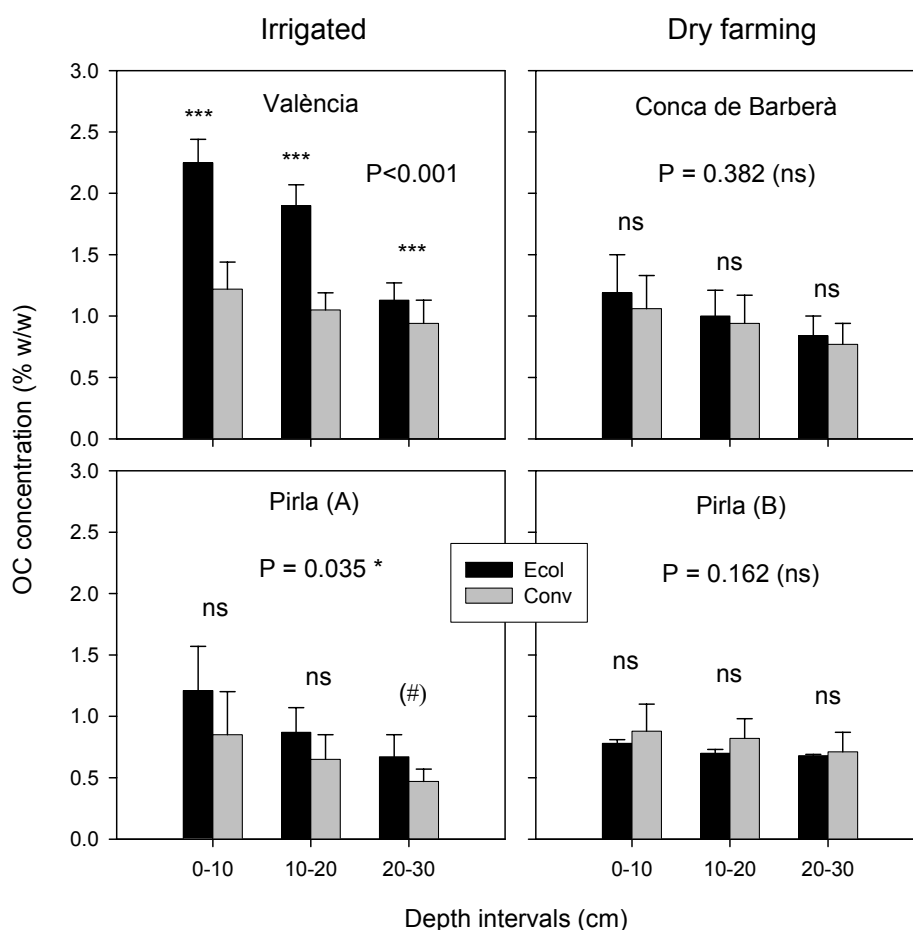


Fig.1. Carbon concentration at different depths. All pairs of plots have been pooled, for a given zone. Both the overall significance of the treatment (ecological vs conventional) and the significance of the differences for each depth are given. (#): in the limit of signification ($P < 0.100$ and $P > 0.05$)

The behaviour of carbon was very consistent with depth: when an increase (or a decrease) occurs, it occurs at all layers (down to 30 cm, at least). No specific effects on the uppermost of the soil have been detected.

Our results show that the substitution of conventional agricultural practices by ecological ones, by its own, does not necessarily result in a net sequestration of carbon in soil. A net sequestration seems to occur in irrigated lands, but under dryland farming the effects are not significant; even a slight decrease is detected in the drylands of Pirla – although not significant. Under irrigation, the net increase in carbon content may be very substantial, as evidenced in the soils of Valencia.

PCS-13: Organic carbon mineralization and CO₂ evolution of paddy topsoil and the temperature dependence

X. Zhang, G. Pan, L. Li

Institute of Resources, Ecosystem and Environment of Agriculture, Nanjing Agricultural University, Nanjing 210095 China (e-mail: gxpan@njau.edu.cn)

C mineralization and its response to climatic warming have received global attention for the last decade. Temperature effect on C mineralization and CO₂ evolution in soils have been heavily studied both by laboratory incubation and field experiments, however, the virtual influence is still in great debt. Little is known on mineralization of organic carbon (SOC) of paddy soils of China although they had been shown to have significant C sequestration potential. Here the authors report a study on SOC mineralization of selected four major types of China paddy soils by laboratory incubation for 120 days under soil moisture regime of 70% WHC at 20° and 25° respectively. C mineralized as CO₂ evolved was measured every day in the first 38-day and every two days in the following days. The results showed that C mineralized during 120-d incubation ranged from 241.5 mg CO₂-C to 353.0 mg CO₂-C at 20° and from 291.7 mg CO₂-C to 453.1 mg CO₂-C at 25° respectively; and a mineralizable C pool in range of 0.24 gC.kg⁻¹ to 0.59 gC.kg⁻¹, varying with the soils. The C mineralization in the whole course of 120d incubation could be divided into 4 stages, which represented 4 sub-pools of the total mineralizable C: very fast mineralized C at the first 0-6d, actively mineralized C at 7-29d, slowly mineralized C. The C mineralization rate varied both with the different soils and the different stages. The calculated Q₁₀ values ranged from 1.0 to 2.4, varying with the soil types and N status. Our data indicated that not the total SOC pool but the labile C pool and, to a lesser degree, C/N ratio controls C mineralization and the temperature dependence. The relatively small mineralization rate may support the C enhancement in paddy soils reported in our previous paper.

PCS-14: Is substrate availability a major limiting factor for the degradation of soil organic matter?

B. Marschner¹, U. Hamer²

1) Dept. of Soil Science/Soil Ecology, Geographical Institute, Ruhr-University, 44780 Bochum, Germany
(e-mail: bernd.Marschner@rub.de)

2) Institute of Soil Science and Site Ecology, TU Dresden, Piennner Str. 19, 01737 Tharandt, Germany

It is generally acknowledged that the protection of soil organic matter against microbial degradation may be due to one or several of the following mechanisms: (1) recalcitrance of OM, including charred OM, (2) stabilisation by spatial inaccessibility of OM to decomposer organisms due to occlusion, entrapment, intercalation or hydrophobicity, (3) stabilisation by interaction with mineral surfaces and metal ions (von Lützow et al., 2005). In the field, microbial activity is furthermore controlled by environmental factors such as temperature and moisture and by soil chemical and physical properties. In most soils, microbial catabolic activity can be greatly stimulated by the addition of easily degradable substrates, such as carbohydrates or amino acids. Numerous studies have shown that this substrate input may additionally induce so-called priming effects, leading to an enhanced breakdown of the native soil organic matter.

We have conducted a suite of laboratory experiments with various ¹⁴C-labelled substrate additions to soil samples from different depths, land use systems and climatic zones, to physical soil fractions and to model substances such as lignin and charred plant materials (Hamer & Marschner 2002, 2005a, 2005b, Hamer et al. 2004). In most cases, priming effects were induced, reaching up to a 2-fold increase in OM mineralization compared to an unamended control. When substrates were added repeatedly over periods of up to 4 months, priming effects did not always subside, indicating that the pool of potentially degradable OM was not easily depleted. With charred plant materials, a second glucose addition after 8 weeks of incubation even caused larger priming effects than the first dose. The magnitude of priming effects is not related to any soil chemical or physical property or to structural characteristics of the OM. However, priming effects are generally more pronounced in samples containing OM of low degradability, such as in podzol subsurface horizons or in charred plant materials (black carbon). These results indicate that in such cases, OM degradation is not primarily low due to structural recalcitrance, spatial inaccessibility or sorptive protection to minerals, but due to the non-availability of simple energy substrates for the microbial population.

We also have evidence that this may be relevant in the field, since OM pools in a Mediterranean soil under long-term effluent irrigation were greatly reduced compared to an adjacent plot that had been irrigated with freshwater. In the laboratory, priming effects could only be induced in a soil under freshwater irrigation. The mineralization rate in the effluent irrigated soil was already about 30% higher without substrate additions and could not be stimulated further.

These results and other data from the literature indicate that the observed effects of management practices and land use on soil organic matter turn-over may partly be due to the differential inputs of easily degradable organic compounds originating from crop residues, root exudates or manure additions.

References

- von Lützow, M., I. Kögel-Knabner, K. Ekschmitt, E. Matzner, G. Guggenberger, B. Marschner, B. & H. Flessa (2005): Mechanisms for organic matter stabilisation in temperate soils - a synthesis. *Geoderma* (in press)
- Hamer, U.; Marschner, B. (2002): Priming effects of sugars, amino acids, organic acids and catechol on the mineralisation of lignin and peat. *J. Plant Nutr. Soil Sci.* **165**, 261-268.
- Hamer, U.; Marschner, B.; Amelung, W.; Brodowski, S. (2004): Interactive priming of black carbon and glucose mineralization. *Organic Geochemistry* **35**, 823-830.
- Hamer, U.; Marschner, B. (2005a): Priming effects in different soil types after addition of fructose, alanine, oxalic acid or catechol. *Soil Biol. Biochem.* **37**, 445-454.
- Hamer, U.; Marschner, B. (2005b): Priming effects in soils due to combined and repeated substrate additions. *Geoderma* (in press).

PBC-1: Slash-and-burn in Neolithic agriculture - Conversion of biomass to charred organic carbon and its fate in soil

E. Eckmeier¹, R. Gerlach², M. Roesch³, O. Ehrmann⁴, W. Schier⁵, M.W.I. Schmidt¹

1) University of Zurich, Dept. of Geography, Winterthurerstr. 190, 8057 Zurich, Switzerland (eckmeier@geo.unizh.ch)

2) Rheinisches Amt für Bodendenkmalpflege, Endenicher Str. 133, 53115 Bonn, Germany

3) Landesdenkmalamt Baden-Wuerttemberg, Fischersteig 9, D-78343 Gaienhofen-Hemmenhofen

4) otto.ehrmann@gmx.de

5) University of Wuerzburg, Institut für Altertumswissenschaften, Residenzplatz 2, D-97070 Wuerzburg

Vegetation fire is an important factor in the global carbon cycle. Charred organic matter could act as an extremely slow carbon pool. In soils, residues of biomass combustion can resist degradation longer than most soil organic matter. The conversion rate of biomass to charred organic matter, however, is still poorly examined for many ecosystems, especially for mixed deciduous forests (Czimczik et al., 2003).

Natural fires are rare in temperate deciduous forests. Holocene vegetation fires in Central Europe have mainly anthropogenic causes (Tinner et al., 1999), e.g. as a tool to clear land for agriculture use. Archaeobotanical evidence for the early use of fire comes from the northern pre-alpine lowlands. Late Neolithic (4300-3500 BC) settlers used slash-and-burn to change forest into arable land, as inferred from archaeobotanical proxy-data (pollen and plant macrofossils). We took advantage of a long-term experimental burning experiment (Southwest Germany; Forchtenberg), which started in 1998. It was designed to mimic Neolithic agricultural slash-and-burn in a deciduous forest and assess the effects on vegetation, crop yields and soil properties (Rösch et al., 2002).

Here, we focused on the conversion rate of biomass-to-charred organic matter. We measured the amount of initial biomass and after the fire the amount of produced charred organic matter, accompanied by temperature data in different soil depths. Charcoal particles were analyzed gravimetrically and black carbon was detected using benzenepolycarboxylic acids (BPCA) as molecular markers in the topsoil. Additionally, we examined how charred organic matter was stored or transported in the soil matrix in a chronosequence (1998-2004).

References

- Czimczik, C.I., Preston, C.M., Schmidt, M.W.I. & Schulze, E.D. 2003. How surface fire in Siberian Scots pine forests affects soil organic carbon in the forest floor: Stocks, molecular structure, and conversion to black carbon (charcoal). *Global Biogeochemical Cycles*, **17**, art. no.-1020.
- Rösch, M., Ehrmann, O., Herrmann, L., Schulz, E., Bogenrieder, A., Goldammer, J.P., Hall, M., Page, H. & Schier, W. 2002. An experimental approach to Neolithic shifting cultivation. *Vegetation History and Archaeobotany*, **11**, 143-154.
- Tinner, W., Hubschmid, P., Wehrli, M., Ammann, B. & Conedera, M. 1999. Long-term forest fire ecology and dynamics in southern Switzerland. *Journal of Ecology*, **87**, 273-289.

PBC-2: Characterisation and evaluation of reference materials for black carbon analyses using elemental composition, $\delta^{13}\text{C}$ and ^{13}C NMR

K. Hammes¹, R. Smernik², M.W.I. Schmidt¹

1) Department of Geography, University of Zurich, Winterthurerstrasse 190, CH-8057 Zurich, Switzerland (e-mail: hammes@geo.unizh.ch)

2) Department of Soil and Water, University of Adelaide, PMB2, Glen Osmond, SA 5064, Australia

Black carbon (BC) is globally present as an inert residue resulting from vegetation and fossil fuel burning. BC has a diverse nature, and there are various methods with which to measure it (thermal, chemical, optical, indirect). An international ring trial was initiated to compare these different methods of analysis. Twelve reference materials were chosen as standard reference materials for BC measurement.

To validate if the reference materials were chosen appropriately to be representative of natural materials, we chemically characterised the twelve reference materials using elemental analysis, ^{13}C CP and BD NMR and $\delta^{13}\text{C}$. The materials are the following: (i) pure BC materials (soot, two chars), (ii) environmental BC matrices (aerosol, marine sediment, two soils, shale, natural organic matter, two coals) and (iii) a specific negative control (melanoidin), which is not supposed to contain any BC.

Most of the reference materials were obtained through (standard material) suppliers. The wood char, rice char and melanoidin were produced by us. No commercial standards for these materials are available. The wood and grass char was produced by pyrolysis to simulate natural conditions in a burning log. The starting materials for the wood and rice char were also chemically analysed.

The reference materials come from diverse environments, with large variations in C values, ranging from 2 % for the Chernozem to 90 % for the soot. The standard materials had H/C and O/C ratios within the typical range for these materials given in literature. This elemental data is supported by the CP and BD NMR analysis done on the materials. The ^{13}C CP and BD MAS spectra for the Vertisol and Chernozem are dominated by signals in the aryl C region, typical for charred organic matter.

Not all reference materials were specifically representative of natural samples (soot and char materials). Diesel soot could be considered for future study concerning methodological constraints with highly impure samples containing BC.

The char material lack at least two characteristics common for chars produced under natural conditions, e.g. large ^{13}C isotopic changes during charring and presence of levoglucosan, formed from partly combusted biomass. However, they conformed to other criteria including homogeneity, long-term availability and ease of preparation, which are also important when calibrating methods for BC analysis.

PBC-3: Particulate organic matter as a means for transport of black carbon in fire-affected Arenosols

A. Hilscher¹, H. Knicker¹, F.J. González-Vila², J.A. González²

1) Lehrstuhl für Bodenkunde, TU München, 85350 Freising-Weihenstephan, Germany
(e-mail: hilscher@wzw.tum.de)

2) Instituto de Recursos Naturales y Agrobiología, CSIC. P.O. Box 1052, E-41080 Sevilla, Spain

Introduction

In Mediterranean ecosystems, forest fires occur frequently during the hot and dry summers. From 1992 to 1997, 91% of all forest fires in the European Union occurred in the Mediterranean countries. Wildfires yield large amounts of CO₂ and NO_x to the atmosphere whereas considerable amounts of severely or partly charred necromass are incorporated into the soil. Due to the highly refractory nature of such thermally-condensed products, they are assumed to increase the passive SOM pool. At first sight, this could be considered as a benefit from the viewpoint of mitigating the effects of greenhouse gases from the atmosphere. However, elucidating the role of black carbon on geobiochemical cycles, the impact on the long-term availability of C and N for biomass production as well as possible alterations of the humification processes and their transport within the soil column need to be considered. Therefore, in the present study, the chemical compositions of organic matter in the potentially mobile (dissolved organic matter; DOM, and particulate organic matter; POM) and immobilized fractions (mineral associated organic matter of the silt and clay fractions) of burnt and unburnt Arenosols from Faro, Portugal, were compared by means of solid-state NMR spectroscopy.

Material and Methods

Sample material derived from Arenosols under *Pinus pinaster* located at Faro (Southern Portugal). Soil F1 experienced a first fire two years and a second fire one year before sampling. The blackish Ah horizon (F1S2; 0-1 cm) was sampled after removal of the litter layer. The litter (F1S1) consisted of dried needles (2 cm thickness) derived from the fire affected trees. Additionally, two samples were obtained from the B horizon at depths of 2-7 cm and 7 to 12 cm (F1S3, F1S4).

The control soil F3 is located approximately 1 km from site F1. Samples were taken from the O/Ah horizon (2 cm), the Ah horizon (2-7 cm) and the B horizon (7-12 cm). The density fractions were yielded after addition of Na₆(H₂W₁₂O₄₀) solution (density=1.8 Mg m⁻³). Subsequently, the mineral residue was fractionated into the sand (2 mm to 63 μm) and coarse

silt (63 to 20 μm) by wet sieving. The finer fractions were separated in Atterberg cylinders into medium silt (20 to 6 μm), fine silt (6 to 2 μm) and clay (< 2 μm).

Total carbon (C_t) and nitrogen (N_t) were determined by dry combustion (975°C) using an Elemental Vario EL analyser. The chemical composition of the fractions were and solid-state ^{13}C NMR spectroscopy with a Bruker DSX 200.

Results

Whereas the control site had no expressed Oh horizon, the fire events resulted in the development of a litter layer consisting of poorly degraded pine needles and a blackish A layer. Elemental analysis of the chemical composition of this material indicated enrichment factors (EF) caused by the fire events of 2.5 and 3.2 for C and N. In the B horizon no enrichment in C and N was observed.

In both the burnt and control soil, most of the organic matter was recovered in the POM fractions. EF of 1.4 and 1.3 caused by the fire were found for C and N content of the POM (> 2 μm) of the Ah horizons. Solid-state- ^{13}C -NMR spectroscopy unveiled that this is mostly due to the accumulation of aromatic C (EF = 7) and alkyl C (EF = 2) whereas the amounts of O-alkyl and carboxyl C were only slightly affected. The aromatic C content in the POM (> 2 μm) of the B horizon showed an EF = 2 indicating that some of the charred residues was transferred to the deeper horizon. Their accumulation occurred concomitantly with an enrichment of carboxyl C (EF = 2).

Our results show that one year after the second fire event, a considerable amount of charred residues were already incorporated into the Ah horizon, whereas the litter layer predominantly consisted of fresh plant litter lost from the decaying trees. The sandy texture of the studied soils offers only few reaction sites for organic matter adsorption which could contribute to the stabilization of the charred residues. This may explain why most of the charred residues was recovered with the POM fraction. After rain fall, this fraction can easily be translocated with the infiltrating water and thus contribute to a relative enrichment of aromatic structures from charred residues in the deeper horizons. Oxidation of those compounds prior to transportation increases the solubility and the formation of colloids which could facilitate this process. Such transport may also be responsible for the higher aromatic C found in layers at 30 cm depths of some Brazilian soils. Laboratory experiments are presently performed to disclose the impact of POM on the transportation of black carbon within the soil column.

PBC-4: Characterisation and quantification of black carbon in the refractory organic macromolecular fraction of forest and cultivated sandy soils

K. Quénéa^{1,2}, S. Derenne¹, C. Largeau¹, C. Rumpel², J.-N. Rouzaud³,
O. Gustafsson⁴, C. Carcaillet⁵

1) LBCOP, UMR CNRS 7573, ENSCP, 11 rue P. et M. Curie 75231 Paris 05, France

(e-mail: katell-quenea@enscp.fr),

2) BiomCO, INRA-CNRS-UPMC, bât EGER, 78850 Thiverval-grignon, France

3) Lab Géologie, ENS Paris, 24 rue Lhomond 75231 Paris cedex 05, France

4) Institute of Applied Environmental Research, Stockholm University, Stockholm, Sweden

5) Institut de Botanique, Université de Montpellier, France

Black carbon (BC), formed by incomplete combustion of biomass, is increasingly thought to be of importance for numerous environmental processes, especially the global carbon cycle and pollutant fate. BC formation via vegetation fires may partly convert a potentially active C pool into a more inert one and thus be a way for long-term stabilisation of organic C in soil. BC may also largely influence the degradation and transport of hydrophobic organic pollutants via adsorption. However, the degree of stability of BC in soil and its contribution to soil organic matter are still largely unknown. These uncertainties are related, for a large part, to the fact that BC encompasses a broad continuum of products, with varying compositions and levels of condensation, ranging from char to charcoal and to soot.

In the present study we examined the BC fraction in the refractory (i.e. resistant to drastic laboratory hydrolyses) organic macromolecular materials (ROMs) of two sandy spodosols from Cestas (“Landes de Gascogne”, south-west France). These ROMs were isolated from the soil of two adjacent plots: a reference plot where the natural vegetation of the area (pine forest) was preserved and a plot cleared 22 years ago and since then continuously used for intensive maize cropping.

Direct evidence for the occurrence of BC in both ROMs was obtained by high resolution transmission electron microscopy (HRTEM) observations using the lattice fringe mode (Figure). These observations also revealed the presence of two types of BC particles. The first (predominant) type corresponds to irregularly shaped particles where the basic polyaromatic units are randomly orientated and the second one to small spherical particles with a concentric “onion-like” microtexture and a much higher organisation of the basic units. Such components are thought to derive from the incomplete combustion of ligno-cellulosic materials (char formation) and of highly aliphatic materials like higher plant waxes (soot-like nanoparticle formation), respectively.

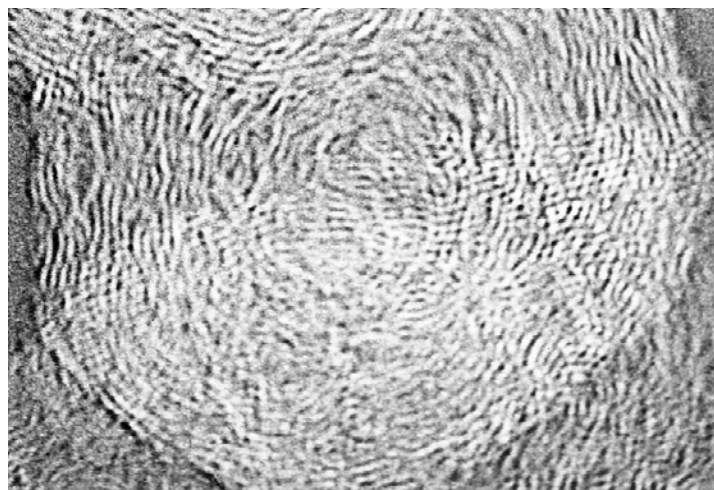


Fig.1. Typical highly ordered “onion-like” BC particle (diameter ca. 20 nm) as observed by HRTEM in the ROMs of the Cestas soils

BC was isolated for quantification using two different methods: chemothermal oxidation (CTO) of the ROMs under previously designed conditions considered to ensure a complete elimination of all non-BC components (Gustafsson et al., 2001) and direct hand-picking with binocular lens from the whole soils. The BC fractions thus obtained were weighed and their carbon contents determined via elemental analysis. It thus appeared that BC, as isolated through CTO, accounts for a very low proportion of the carbon of the ROMs (ca. 0.05 and. 0.04 % by weight for the forest and cultivated soils, respectively). On the contrary, much higher BC contents (ca. x 300 in both cases) were inferred from the direct method. Such differences illustrate the problems encountered for BC quantification. This is due to the occurrence of the BC continuum and hence, to the difficulties for finding a method (if any), suitable for complex matrices as soils, that would ensure a complete removal of all the non-BC products while avoiding elimination of the most sensitive BC components. The conspicuous differences observed in the present study probably reflect large underestimation for the values obtained, from the ROMs, using the CTO method. The causes of this will be discussed based on (i) parallel studies we are performing in relation with a “BC ring trial” where over 20 laboratories worldwide are implicated and (ii) HRTEM examination of the CTO-isolated BCs.

References

O. Gustafsson, T.D. Bucheli, Z. Kukulska, M. Anderson, C. Largeau, J-N Rouzaud, C.M. Reddy, T.I. Eglinton. Evaluation of a protocol for the quantification of black carbon in sediments. *Global Biogeochemical Cycles* **15**, 881-890 (2001)

PBC-5: Comparative analysis of reference materials for organic geochemical studies of black carbon – Results

M.W.I. Schmidt¹, J.O. Skjemstad², C. Masiello³, W.P. Ball⁴, L. Currie⁵, D.M. Smith⁶,
Contributing parties to the comparative analysis⁷

1) University of Zurich, Dept. of Geography, Zurich, Switzerland

2) CSIRO Land and Water, Adelaide, Australia

3) Rice University, Houston USA

4) Johns Hopkins University, Ort, USA

5) NIST, Gaithersburg, USA

6) University of Denver, Denver USA

7) Reference materials were distributed to 24 laboratories worldwide early 2003/4 for analysis. The final list of contributing parties will become clear after January 2005

Black carbon (BC) is a collective term used to describe recalcitrant organic, produced by incomplete combustion of fossil fuels and vegetation. It occurs ubiquitously in soils and sediments. BC exists as a continuum from partly charred material to highly graphitized soot particles, with no general agreement on clear-cut boundaries of definition or analysis (Hedges et al. 2000). The individual analytical BC methods rely on operational definitions with clear-cut but different boundaries and are developed for specific scientific questions whereas BC represents a continuum of materials with widely contrasting physicochemical properties. Thus, different methods may be inherently designed to analytically determine different parts of the continuum, and it is crucial to know how measurements made by different techniques relate to each other. The inherent difference can be illustrated by the results of a first comparative analysis on eight soil samples by six established methods (Schmidt et al., 2001). All methods involved removal of the non-BC components from the sample by thermal or chemical means, or a combination of both. The remaining carbon, operationally defined as BC, was quantified via mass balance, elemental composition or by exploiting benzene carboxylic acids as molecular markers or applying ¹³C MAS NMR spectroscopy. BC concentrations measured for individual samples vary over two orders of magnitude.

The need for intercomparison of BC methods is obvious. To address this need, a committee was formed during the 1999 Geochemical Society Meeting Goldschmidt Conference to develop representative and accessible BC reference materials for the entire environmental sciences community. It was clear from the preliminary comparative analysis that a collection of BC reference materials should be established as soon as possible i) to ensure long-term intra- and inter-laboratory data quality, and ii) to facilitate comparative analyses between different analytical techniques and scientific approaches. The final recommendations of the steering committee for Black Carbon Reference Materials included (i) five matrices containing BC (soot, charcoal, aerosol, soil, and sediment); and (ii) five

materials potentially creating BC during analysis (shale, melanoidin, natural organic matter, and coal), for use in detecting methodological artifacts Schmidt et al. (2003). Further details can be found at the Web site: <http://www.geo.unizh.ch/phys/bc>.

Early 2003/4, these reference materials were produced and distributed and analyzed in a comparative analysis project using these reference materials to gauge how different methods can be used to interpret BC components in aerosol, soils, and sediments. The intention of the study is not to advocate a single technique; rather, such a comparative analysis will help immensely to better understand what is actually being determined by the different methods and how these results relate to one another. Reference materials were requested by 24 research groups of many disciplines, including atmospheric, environmental, marine and soil sciences. Participating research groups are currently analyzing the materials and expected to make available all results and details of their methodology after January 2005 for discussion and eventual group publication. Summarizing, the aim of this contribution will be to present results of the comparative analysis of reference materials for organic geochemical analysis of black carbon and to stimulate discussion.

References

- Hedges, J.I., Eglinton, G., Hatcher, P.G., Kirchman, D.L., Arnosti, C., Derenne, S., Evershed, R.P., Kögel-Knabner, I., de Leeuw, J.W., Littke, R., Michaelis, W., Rullkötter, J. 2000. The molecularly-uncharacterized component of nonliving organic matter in natural environments. *Organic Geochemistry*, 31, 945-958.
- Schmidt M. W. I., Masiello C. A., Skjemstad J. O. 2003. Final recommendations for reference materials in black carbon analysis. *EOS* **84** (52), 582-583.
- Schmidt M. W. I., Skjemstad J. O., Czimeczik C. I., Glaser B., Prentice K. M., Gelin Y., Kuhlbusch T. A. J. 2001. Comparative analysis of black carbon in soils. *Global Biogeochemical Cycles* **15**, 163-167.

PBC-6: Insight into the structural features of various forms of refractory organic matter from marine sediments

J.M. de la Rosa¹, F.J. González-Vila¹, H. Knicker², E. López-Capel³, O. Polvillo¹,
J.A. González-Pérez¹, M.E. Arias⁴

1) IRNAS, C.S.I.C, Avda. Reina Mercedes, 10, P.O. Box 1052, 41080-Sevilla, Spain
(e-mail: jmrosa@irnase.csic.es)

2) Lehrstuhl für Bodenkunde, Technische Universität München, 85350 Freising-Weihenstephan, Germany

3) School of Civil Engineering & Geosciences, University of Newcastle, Newcastle upon Tyne, UK, NE1 7RU

4) Dept. Microbiología y Parasitología. Universidad de Alcalá. 28871 Alcalá de Henares, Madrid, Spain

Black carbon (BC) is a highly refractory material remaining after uncomplete biomass combustion. This material has an extremely long environmental lifetime, potentially contributing significantly to the Earth's slow-cycling carbon pools [1].

A wide set of analytical approaches have been proposed for the isolation and quantification of BC and other forms or Refractory organic matter (ROM) from different matrices. However, there are discrepancies concerning the obtained results; with natural BC concentrations varying with more than a factor of 500 for the same sample measured via different methods [2]. This is due to the fact that BC is not a pure substance but rather a continuum of materials with different physicochemical properties [3,4]. Therefore BC structural characterization presents serious experimental constraints.

A study of the structural features of BC and others forms or ROM isolated from marine sediments was done. The samples were collected in the continental platform, estuaries and rivers in the Southwest Atlantic Coast of Spain. Refractory organic matter was isolated by a progressive chemical removal of the more labile organic matter (lipids and humic materials). The ROM forms were finally subjected to different chemical and thermal treatments to obtain the BC forms. Both isolated ROM and BC forms were characterized using destructive (Pyrolysis-GC/MS and wet chemical degradations) and non destructive (FT-IR, solid-state ¹³C MAS NMR) techniques. For comparative purposes a set of BC-reference materials [5] including soots of various origins, lignocellulosic chars, melanoidins and humic materials was used.

The molecular structure of BC and ROM forms showed noticeable differences. ¹³C NMR revealed a very apparent loss of signal intensity in the alkyl C-O region of the spectra of the BC forms compared with those of ROM (fig. 1).

Although NMR data showed that the molecular structure of ROM and BC forms are mainly aromatic and comparable to that of the lignocellulosic char, an important contribution of certain aliphatic series were also detected by pyrolysis GC-MS in most of the samples. In

particular, several samples from marine sources revealed high contribution of aliphatic compounds suggesting the relevance of these alkylic moieties in the stabilization of carbonous materials in this environment.

The Pyr-GC-MS analysis performed on the same samples (data not shown) confirmed this behaviour.

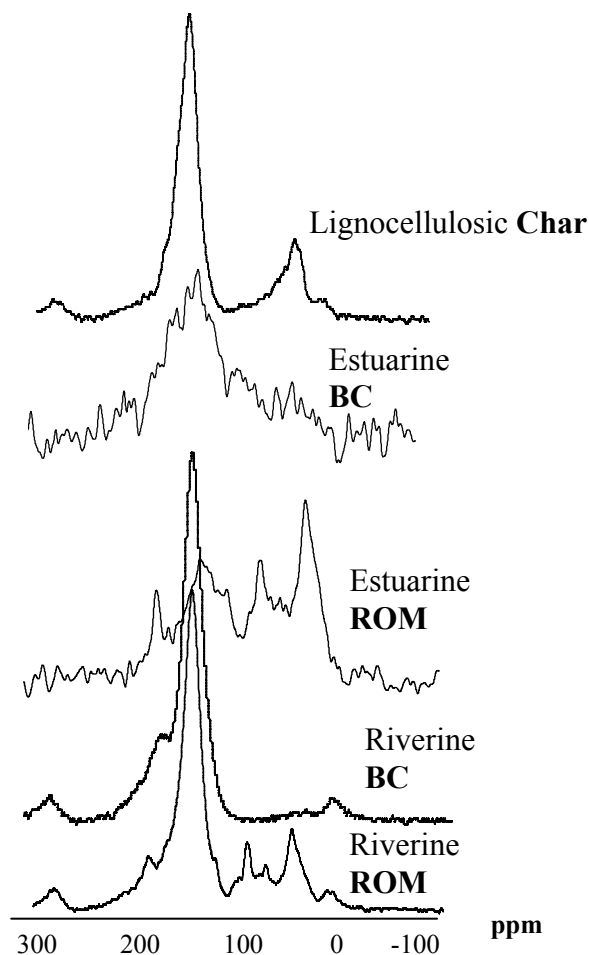


Fig.1. Solid state ^{13}C NMR spectra of ROM and BC forms isolated from different estuarine and riverine sediments, as well as the spectrum of a standard lignocellulosic char

References

- [1] Goldberg, E.D. (1985). *Black Carbon in the Environment*. John Wiley and Sons, NY.
- [2] Masiello, C.A. and Druffel E.R.M. (1998). Black Carbon in deep sea sediments. *Science* 280: 1911-1913.
- [3] Masiello, C.A. (2004). New directions in black carbon organic geochemistry. *Marine Chemistry* 92: 201-213.
- [4] Schmidt, M.W.I., et al. (2001). Comparative analysis of black carbon in soils. *Global Biogeochemical Cycles* 15: 163-167.
- [5] Schmidt, M.W.I., et al. The BC Ring Trial. <http://www.geo.unizh.ch/phys/bc/>

PBC-7: Thermal characterisation of refractory organic matter from marine sediments

E. López-Capel¹, J.M. de la Rosa², J.A. González-Perez², F.J. González-Vila²,
D.A.C. Manning¹

1) School of Civil Engineering & Geosciences, University of Newcastle, Newcastle upon Tyne, UK, NE1 7RU

2) Dpt. Biogeoquímica y Dinámica de Contaminantes, Instituto de Recursos Naturales y Agrobiología de Sevilla (IRNAS-CSIC), 41012 Sevilla, Spain

Due to their well known important geochemical and environmental implications, there is an increased interest in the study of the different forms of refractory organic matter (ROM) widely spread in soils, water and sediments. Among these materials are kerogen, humic-like materials as well as the so called “black carbon” (BC). As part of the BACH-BC project, samples from the internal continental platform and estuaries of the Atlantic side of Cadiz Gulf (Spain) were studied. The aim of this work was to thermally characterise and quantify the various types of carbon in these marine sediments (labile, recalcitrant and black carbon) and assess their source (terrestrial or marine).

Thermogravimetry (TG) and differential scanning calorimetry (DSC) analysis provided rapid bulk characterisation of the chemical transformations of refractory organic matter (ROM) (e.g. Figure 1). By coupling an isotope ratio mass spectrometer (IRMS) and a quadrupole mass spectrometer (MS) to a thermal analysis system, we have been able to continuously measure $\delta^{13}\text{C}$ and identify the evolved gases during the thermal decomposition of whole sediments and their corresponding humic acid (HA) fractions.

A set of samples were selected on the basis of organic matter (OM) total content and the distance from the coast. TG-DSC showed clear differences between the humic acid fraction (up to 90% total weight loss; simple DSC trace with predominant weight loss at approx 500°C; Figure 1a) and the bulk sample (1% weight loss; complex DSC trace losing water at 100°C and an exotherm at 340°C as well as 500°C, indicating presence of other organic components; Figure 1b). Observed weight losses show little change in the proportions of more refractory material in terms of distance from the coast, but there is a decrease in less stable organic matter, and the relative proportion of refractory organic matter increases.

TG-DSC-MS analysis showed changes in the distribution patterns of the different C and N forms. H₂O and CO₂ were the main degradation species observed during the combustion of whole sediments and the humic acid fractions. Relative yields of NO (*m/z* 30) and CO₂ (*m/z* 44) increased with increasing temperature. This suggested an increasing

proportion of C and N incorporated into more recalcitrant structures as distance from the coast increases.

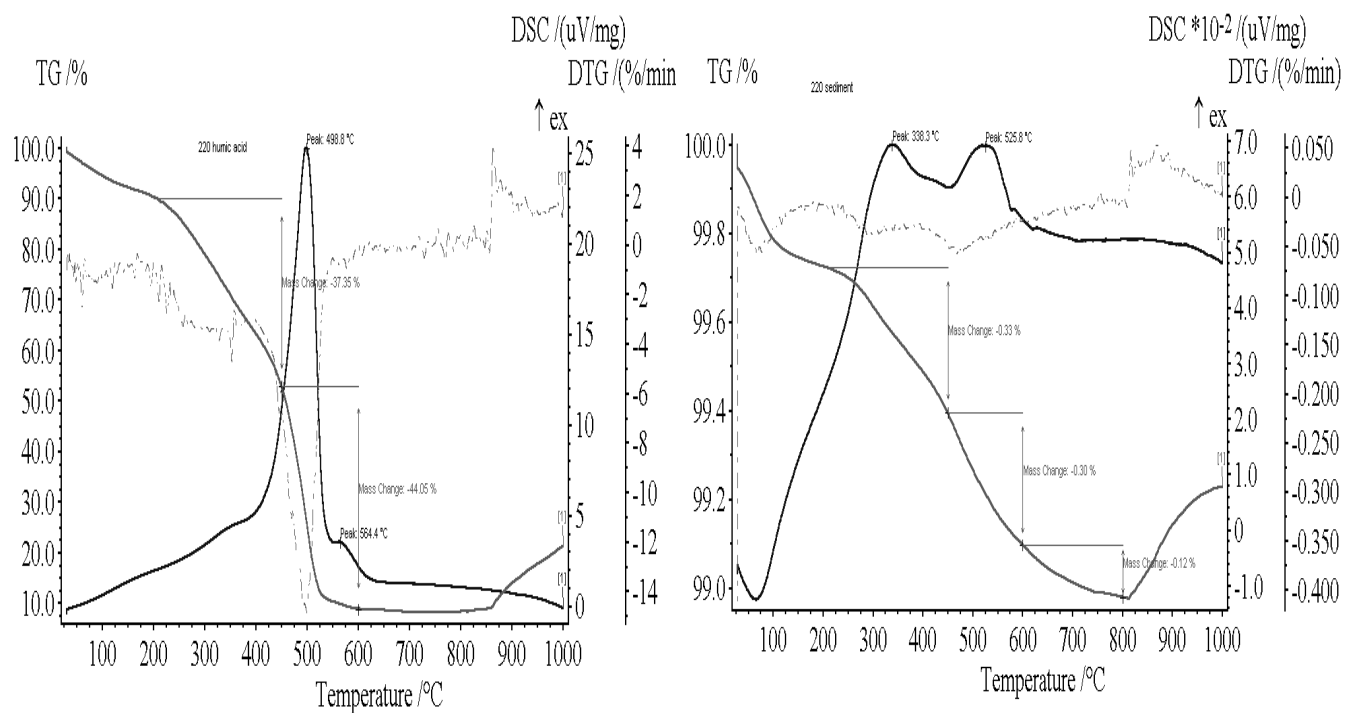


Fig.1. TG-DTG-DSC Thermograms of (a) humic acid and (b) sediment (sample 220)

PBC-8: Characterisation of charred materials left after slash-and-burn practices in agricultural tropical soils

C. Rumpel¹, J.A. González-Pérez², C. Largeau³, C. Valentin⁴, A. Mariotti¹

1) CNRS, BIOMCO, Centre INRA Versailles-Grignon, Thiverval-Grignon, France

2) CSIC, Instituto de Recursos Naturales (IRNAS), Seville, Spain

3) CNRS, LCBOP, UMR CNRS 7573, ENSCP, 11 rue P. & M. Curie, 75321, Paris 05, France

4) IRD, UR049, érosion et changement d'usages des terres BP 06, Vientiane, Laos

Studies carried out in laboratory controlled conditions as well as under field condition in forest soils indicate that heat-induced changes on organic matter mainly consists in the removal of functional groups, dehydration and cyclization reactions (González-Pérez et al., 2004). This pyrogenic material, enriched in condensed aromatic carbon forms and with nitrogen bound into heterocyclic structures (Knicker et al., 2004), is resistant to degradation.

In the tropical countries of South-East Asia slash-and-burn is a common agricultural practice, leading each year to an abundant production of charred materials that are deposited on the bare soil and on steep sites. Under these conditions black carbon (BC) forms were found to be eroded and transported preferentially with regards to other types of organic materials (Rumpel et al., 2005). Because SOM degrades quickly in soils with high temperature and water content the formation and accumulation of recalcitrant SOM is of particular importance in the humid tropics. Molecular features of size fractions of charred materials from a tropical forest soil are analyzed and their possible contribution to soil stable OM pool after deposition are discussed.

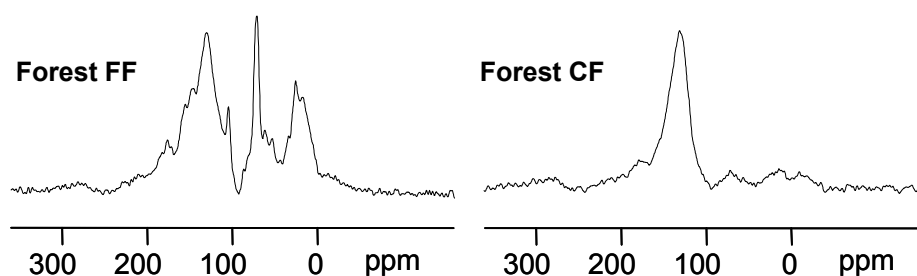
Samples were collected in the Howay Pano watershed (Laos) from an agricultural soil and an adjacent forested site. Particulate charred organic matter was hand picked and separated in a coarse fine fraction (FF < 1cm) and a coal-like fraction (CF > 1 cm). The two fractions were analysed for elemental and isotopic composition and chemical structure studied using ¹³C CPMAS NMR spectroscopy and Pyr-GC/MS.

The carbon content of the charred materials was in most cases higher than in the original plant material. The C:N ratio of BC ranges between 36 and 124. Higher C:N ratios than those of the plant material were only noticed in the CF fractions. The fine fraction has C:N ratios similar to the plant litter. At the forest site, the $\delta^{13}\text{C}$ and $\delta^{15}\text{N}$ ratios were in the same range to those found for charred and plant material whereas at the field site C4 plant input seems to be the cause for the $\delta^{13}\text{C}$ ratio increase (Table 1.).

Table.1. Elemental and isotopic composition of plant material and black carbon

	Carbon mg g ⁻¹	Nitrogen mg g ⁻¹	C:N	δ¹³C ‰	δ¹⁵N ‰
BC field FF	225	6.2	36	-21.9	1.8
BC field CF	663	5.9	112	-29.7	0.7
Plant material	443	8.6	51	-12.6	1.8
BC forest FF	529	13.6	39	-28.4	0.7
BC forest CF	686	5.5	124	-31.6	-1.4
Forest litter	414	10.5	39	-30.4	0.0

The chemical composition of the two charred fractions sampled from the forest site showed a highly aromatic structure for the CF. Contribution of O-alkyl C as well as alkyl C was evident in the FF fractions (Fig. 1).

**Fig.1.** ¹³C CPMAS NMR spectra of the different fractions sampled from both sites

We conclude that the differences observed in the chemical structure of the charred material fractions may be related to its morphology, with smaller charred particles being preferentially eroded and transported.

References

- González-Pérez J.A., González-Vila F.J., Almendros G., Knicker H. (2004). The effect of fire on soil organic matter—a review. *Environment International* 30: 855-870.
- Knicker H., González-Vila F.J., Polvillo O, González-Pérez J.A., Almendros G. (2005). *Soil Biology and Biochemistry*, in press.
- Rumpel, C., Chaplot, V., Planchon, O., Bernadou, J., Valentin, C., Mariotti, A. (2005). *Catena*, in press.

PBC-9: Cultivation-induced alterations recognized in the structural characteristics of resilient humic acids from a sequence of Southern African Soils with different maturity degree

G. Almendros¹, F.J. González-Vila², M.C. Zancada¹, M.T. Pardo¹,
J.M. de la Rosa², H. Knicker³

1) Centro de Ciencias Medioambientales, Serrano 115B, 28006 Madrid, Spain (e-mail: humus@ccma.csic.es)

2) Instituto de Recursos Naturales y Agrobiología, Av. Reina Mercedes 10, 41012 Sevilla, Spain,

3) Lehrstuhl für Bodenkunde, Technische Universität München, 85350 Freising-Weihenstephan, Germany

Extreme aromatisation found in the humic acids from some Southern African virgin soils is an unusual feature when humic substances are not affected by geological diagenetic processes. Apart from the depletion of aliphatic structures ascribed to intense soil biogeochemical activity, a series of ¹³C-NMR spectral patterns such as the low carboxyl/aryl ratio and the weak signals for O- and N-substituted aromatic structures could be pointing to deep abiotic processes as sunlight irradiation, periodic dehydration of the soil matrix, or accumulation of black-carbon related structures ascribed to the effect of soil-affecting fires in the past.

In order to establish the effect of clearing and continuous cultivation on soil organic matter characteristics, six surface soil samples (0–15 cm) from South Africa (Hertzog and Guquka), Zimbabwe (Chikwaka and Domboshawa) and Tanzania (Mafiga and Mkindo) were studied by Curie-point analytical pyrolysis and the corresponding extracted, purified humic acid fractions were analysed by ¹³C NMR under quantitative acquisition conditions.

On the whole, cultivation has led to considerable declining of total organic matter levels, although a relative increase in the percentage of colloidal fractions tightly bonded to the mineral fraction (i.e., humic acid and insolubilized humin) was observed at expenses of the percentage of the other fractions, of which fulvic acids behaved as most responsive for the effect of cultivation.

The results obtained by analytical pyrolysis of the whole soils suggested intense lignin alteration in the sites studied, hence methoxyphenolic patterns had a limited value in illustrating the stages through which lignin is transformed into humic acid-like macromolecules. Alkyl pyrolysis compounds (except fatty acids) suggested different biogeochemical trends in the sites studied. Mainly alkadienes and alkanes revealed microbial metabolism and selective preservation of alkyl biomacromolecules (cutans, suberans).

For instance, in Chikwaka and Domboshawa soils (Zimbabwe) a cultivation-induced “alkyl depletion” was observed after pyrolysis of the whole soils. In Guquka, Hertzog (South Africa) and Mafiga (Tanzania) there were less significant changes; whereas in Mkindo

(Tanzania) an intense cultivation-induced “alkyl enhancement” was observed. These differences are being interpreted as regards the extent to which pre-existent organic matter is degraded and substituted by microbial products and compounds from crop residues.

^{13}C NMR was used to obtain an insight on the quantitative changes in the different C types of the humic acids (Fig. 1). In general, most of the South African soils studied displayed intense peaks in the 110–160 ppm range suggesting dominant aromatic character. In the case of temperate soils, the ^{13}C NMR spectra often proved lignin as the major macromolecule contributing to aromatic structures (marked peaks occurring at 153 ppm and 58 ppm for methoxy/amino structures). In the tropical soils studied, however, this situation occurred only in Domboshawa and to a lesser extent in Guquka and Hertzog soils whereas in the other soils a extremely high maturity, aromatisation and demethoxylation of the soil organic matter suggested the above-indicated intense diagenetic transformations and/or accumulation of black carbon type C-forms.

With regard to the effect of cultivation, a progressive pattern between two extreme situations was observed: some soils, Domboshawa and less Hertzog and Guquka, showed comparatively raw organic matter composed of altered lignocellulose from fresh plant biomass. After cultivation, a small aliphatic depletion could be observed, mainly in the *O*-alkyl domain, which is frequent in soils from temperate countries.

Conversely, humic acids from Mafiga uncultivated soil showed extreme aromatisation, demethoxylation and dealkylation. The major effects of cultivation were oxidation and accumulation of aliphatic structures. In particular, before cultivation Mkindo showed the lowest signal intensity for aliphatic structures and the lowest concentration of carboxyl groups. In this soil, cultivation caused the most dramatic aliphatic enhancement in the humic acid fraction.

Guquka uncultivated soil showed similar characteristics to Hertzog: the important aromatic domain coexisted with major aliphatic structures, but the shape of the aromatic region indicated that typical lignin units were not present in high proportions. The humic acids displayed intermediate NMR profiles in terms of the above conditions, and the organic matter characteristics were not significantly affected by cultivation. This situation is similar to that in humic acids from Chikwaka, which behaved resilient with regard to cultivation effects: the prevailing aromatic domain coexisted with aliphatic structures including carbohydrate and alkyl compounds.

In summary, the results suggested contrasting conditions for humic acid formation and also a differential response to clearing and cultivation. The cultivation induced “aliphatic

enhancement” was observed to concur in exceptionally aromatic humic acids, whereas aromatisation after cultivation was noted in humic acids where structural modifications as regards biomacromolecules was less pronounced. From the agronomical viewpoint it is interesting to point out that several soils in the wide area studied show some virtual resilience attributable either to presence of matured organic matter in biogeochemically active scenarios (e.g. Chikwaka soil) or to selective preservation of lignocelluloses biomass (e.g. Domboshawa soil), where cultivation had some effect more similar to those soils in temperate countries with a preferential degradation of aliphatic structures in soil organic matter.

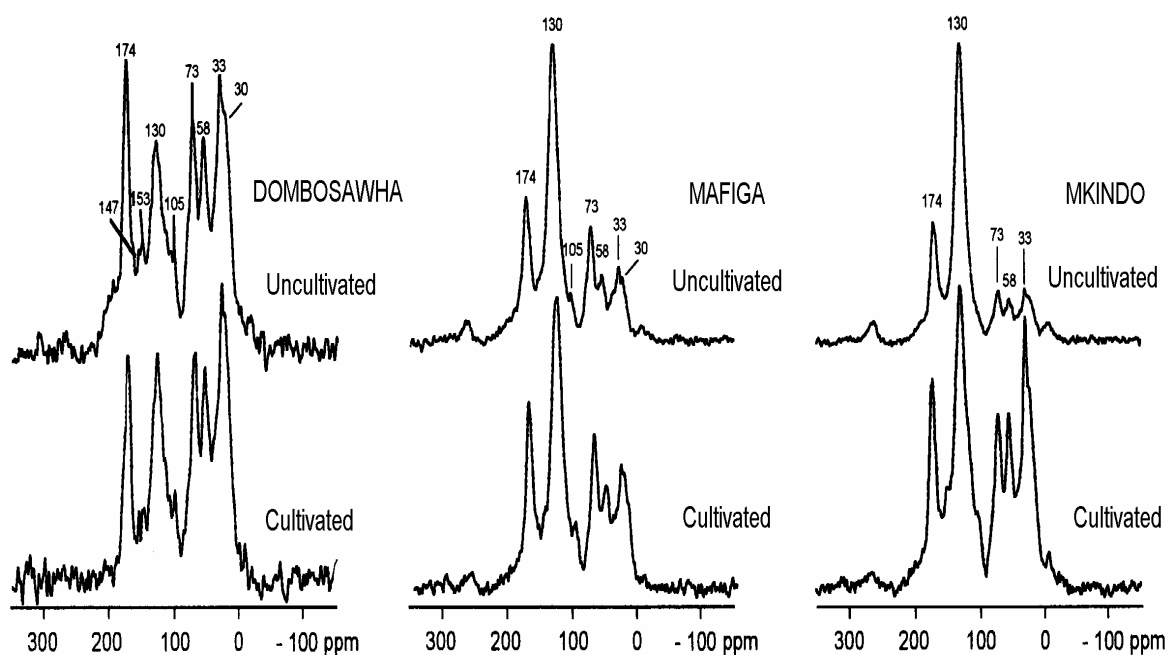


Fig.1. ^{13}C NMR spectra of humic acids from some selected Southern Africa soils

PBC-10: The chemical structure of a polar fraction obtained from diesel soot

B. Hermosin, M. Gaviño, C. Saiz-Jimenez

Instituto de Recursos Naturales y Agrobiología, CSIC, Apartado 1052, 41080 Sevilla, Spain
(e-mail: hermosin@irnase.csic.es)

In this paper we studied the composition of the organic compounds present in the soot obtained from the exhaust of a municipal bus. We were able to separate the components in different fractions by column fractionation. We focused our efforts in the characterisation of the most polar fraction. This yellow fraction was composed of aliphatic and aromatic carboxylic acids and phenols, and was found either in the black crusts from different European cathedrals, and analogously in diesel soot.

Recently, the finding of water soluble organic compounds, formed by soot oxidation, has been reported (Decesari et al. 2002). This water soluble fraction contains polycarboxylic acids and it was suggested that the structure of these compounds is analogous to that of naturally occurring macromolecular polyacidic compounds, humic and/or fulvic acids (Decesari et al. 2002). These results were considered consistent with previous findings concerning the presence of water soluble macromolecular humic-like substances in atmospheric aerosol samples (Havers et al. 1998).

References

- Decesari, S., Facchini, M.C., Matta, E., Mircea, M., Fuzzi, S., Chughtai, A.R. & Smith, D.M. 2002. Water soluble organic compounds formed by oxidation of soot. *Atmospheric Environment* 36: 1827-1832.
- Havers, N., Burba, P., Lambert, J. & Klockow, D. 1998. Spectroscopic characterization of humic acid-like substances in airborne particulate matter. *Journal of Atmospheric Chemistry* 29: 45-54.

PBC-11: Condensed aromatic ring structures in DOM detected with electrospray ionization and ultrahigh resolution MS: Insight to the cycling of black carbonW.C. Hockaday¹, A.M. Grannas¹, S. Kim², P.G. Hatcher¹

1) Department of Chemistry, The Ohio State University, Columbus, OH 43210, USA

2) Florida State University, National High Magnetic Field Lab, Tallahassee, FL 32310, USA

Because our understanding of the global cycling and reactivity of natural organic matter (NOM) draws heavily upon molecular information, biogeochemists are severely constrained by the fact that over half of the organic carbon in Earth's terrestrial and marine environments remains uncharacterized at the molecular level (Hedges et al., 2000). Moreover, a rapidly accumulating body of evidence suggests that refractory organic products of incomplete combustion, namely, soot and charcoal black carbon (BC), account for a substantial portion of uncharacterized NOM (Schmidt et al., 1999). Though lacking direct measurement of dissolved BC, Masiello and Druffel (1998) suggested that BC could also be a significant contributor to the dissolved organic matter (DOM) pool, substantiated recently by Mannino and Harvey (2004). Environmentally relevant oxidation processes can generate water-soluble products from BC. Hexane soot exposed to ozone produces water-soluble aromatic polyacids (Decessari et al., 2002) consistent with those detected in combustion aerosols, fog, and cloud water (Capiello et al., 2003). The only published measurements of dissolved BC employ the operational definition of BC based on thermal oxidation at 375°C (Mannino and Harvey, 2004). Using molecular information revealed by ultra high-resolution mass spectrometry, we establish criteria for molecular definitions of condensed aromatic ring structures (CARS) in DOM and substantiate the concept of a dissolved BC transport pathway by showing that many of the CARS identified in the DOM of a fire-impacted watershed can be extracted from the charcoal in those soils using C₁₈ solid-phase extraction.

Ultrahigh-resolution Fourier-transform ion cyclotron resonance mass spectrometry with electrospray ionization (ESI-FTICR-MS) provides sufficient mass accuracy (<0.5ppm) and resolving power to assign unique empirical formulae to 94-98% of the 4,000 ionizable species in each sample, without *a priori* physical separation. Figure 1 shows the ESI-FTICR-MS of C₁₈ DOM isolated from the Maple River, Michigan U.S.A. and an expansion of a single mass unit containing 30 well resolved peaks. Each peak represents a molecular species having a single unique empirical formula.

It is well known that BC-derived compounds have a condensed aromatic structure where the carbon-normalized double bond equivalent (DBE/C) is greater than 0.7. Applying this criterion to the empirical formulae assignments from the ESI-FTICR analysis, the water-

soluble portion of charcoal BC contains 1200 molecular species with DBE > 0.7—representing 47% of the total number of species identified. The remaining 53% of the molecular species in charcoal from our burn site are likely to be humic and microbial organics that have sorbed to the charcoal during its 100-year residence in the soil. We identify these species having DBE > 0.7 as CARS. In the samples examined in this study, CARS have low molecular weight (<1000Da), 1-14 oxygen atoms, and occasionally nitrogen and/or sulfur atoms. Therefore, we argue that the DBE/C threshold for describing CARS is a useful proxy for identifying combustion-derived species in NOM.

Though the quantitative abundance of CARS in DOM samples is not yet known, their discovery verifies the existence of a new pathway within the carbon cycle - the export of terrestrial BC to the DOC pool. The oxidation of charcoal BC to small (molecular weight <1000 Da) water-soluble molecules on a 100-year time scale implies that a fraction of BC in soils cycles rapidly, and does not act as a long-term carbon sink unless selectively preserved.

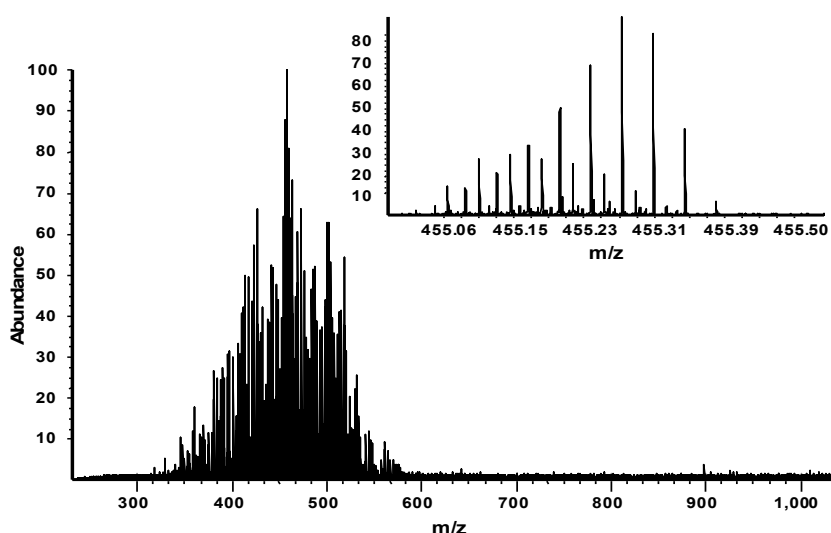


Fig.1. The ESI-FTICR mass spectrum of Maple River DOM containing 4,000 peaks. The inset expansion of the 455 m/z nominal mass shows 30 well-resolved peaks; each representing molecular species with unique empirical formulae

References

- M.W. Schmidt, Skjemstad, J.O., Gehrt, E., and Kögel-Knabner, I, 1999. Charred organic carbon in German chernozemic soils. *European Journal of Soil Science* 50, 351-365.
- C.A. Masiello, E.R.M. Druffel, 1998. Black carbon in deep-sea sediments. *Science* 280, 1911-1913.
- J.I. Hedges, G. Eglinton, P.G. Hatcher, et al. 2000. The molecularly uncharacterised component of nonliving organic matter in natural environments. *Organic Geochemistry* 31, 945-958.
- S. Decessari, M.C. Facchini, E. Matta, M. Mircea, S. Fuzzi, A.R. Chughtai, D.M. Smith, 2002. Water soluble organic compounds formed by the oxidation of soot. *Atmospheric Environment* 36, 1827-1832.
- A. Capiello, E. De Simoni, C. Fiorucci, F. Mangani, P. Palma, C. Facchini, S. Fuzzi, S., 2003. Molecular characterization of water-soluble organic compounds in fogwater by ESIMS/MS. *Environmental Science & Technology* 37, 1231-1240.
- A. Mannino, H.R. Harvey, 2004. Black carbon in estuarine and coastal ocean dissolved organic matter. *Limnology and Oceanography* 49, 261-266.

PBC-12: Soot/Graphitic black carbon in Mediterranean forest soils

P. Rovira¹, V.R. Vallejo²

1) Dept de Biología Vegetal, Facultat de Biología, Univ. de Barcelona. Diagonal 645, 08028 Barcelona (Spain)

2) CEAM, Ch Darwin 14, 46980 Paterna, València (Spain)

The importance of black carbon (BC) in the global biogeochemical carbon cycle has become increasingly evident in the last years. BC, mostly generated during wildfires, represents a pool of highly stable organic matter, that can become a substantial part of total organic matter in some environments. In mediterranean terrestrial ecosystems, often affected by wildfires, its relative importance can be hypothesized to be high.

To verify this, a set of forest profiles have been studied, all them located in Catalonia (NE of Spain) and over calcareous parent materials (limestones, marls, and calcareous sandstones). Profiles were mostly under native *Quercus rotundifolia* stands, but some were under subspontaneous *Pinus halepensis* stands or under shrublands or garrigues (*Quercus coccifera*). Both H, A and B horizons were studied. Organic layers (L and F horizons) were excluded from this study. The study of black carbon (BC) includes both charcoal and the soot-graphitic fraction of black carbon, which is chemically the most stabilized. Only the results for the soot-graphitic BC will be mentioned in this abstract.

The analysis of soot-graphitic BC was done by the method of Gelinás et al. (2001), slightly simplified. Essentially, the method involves the following steps: (i) pretreatment with diluted HCl, to destroy carbonates; (ii) treatment at room temperature with a mixture of 6M HCl and 37% HF, to destroy the mineral matrix that could occlude the organic matter in the organomineral complexes; (iii) two consecutive hydrolysis, first with 1M HCl, then with 6M HCl, both at 105°C, to release amino acids and carbohydrates which could give Maillard-type recalcitrant polymers that could be included in the BC pool; (iv) low-temperature combustion (375°C) in a muffle furnace, enough to destroy most organic compounds but not soot-graphitic carbon. The remaining solid material was analyzed for total carbon and nitrogen in a CARLO ERBA analyzer.

In contrast with the expected results, in our profiles the soot-graphitic BC represents a small proportion of total OC, less than 1 % in most cases (Fig. 1). This proportion tends to increase with decreasing total OC, but it is maintained below 5 % almost always (slightly more than 25 %, in an extreme case).

Black nitrogen was not detected in most cases (% N in the calcinated residue below the detection limit), but it could be quantified in some samples. The ratio BN / total N is always

higher than the ratio BC / total OC. The presence of 'black nitrogen' indicates that black carbon could act as a receiver of highly stable forms of N, probably originated by condensation of N-containing organic compounds during wildfires.

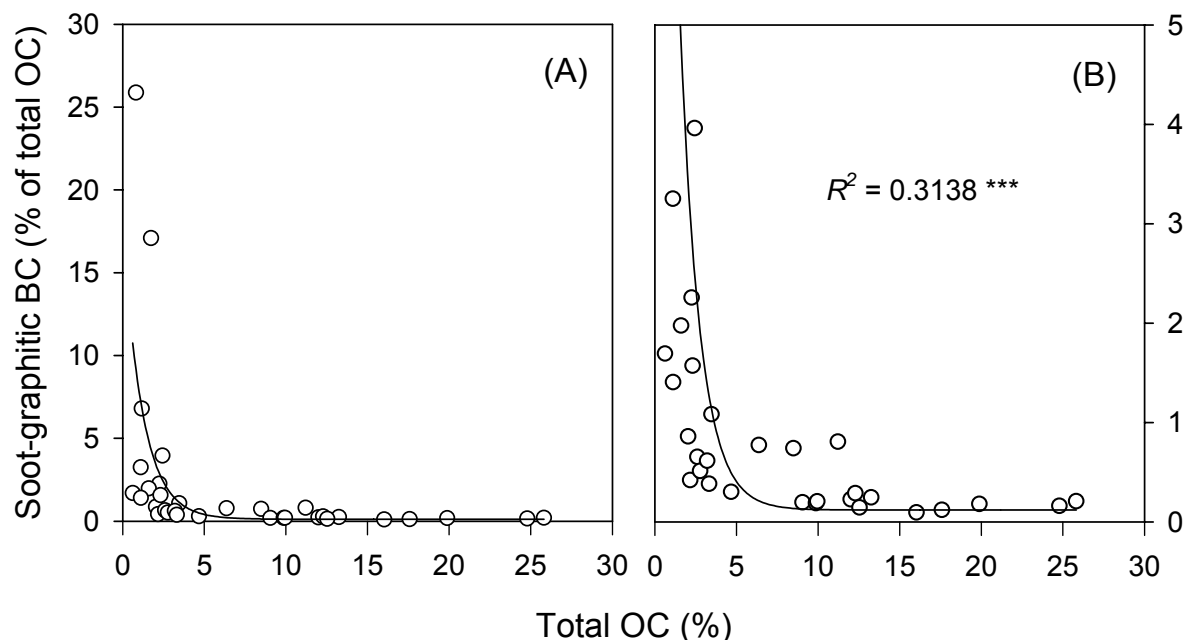


Fig.1. Proportion of soot-graphitic black carbon (as % of total organic carbon) in the studied soil horizons. Points have been tentatively fitted to a single-exponential equation. (A): all points included. (B): only points with < 5% of BC (as % of total OC), to improve the clearness.

Overall, the soot-graphitic BC is a pool less relevant than expected. Reasons for the low amounts obtained can be two (or a combination of both): either because in these forests the generation of soot-graphitic BC is small, or simply because black carbon could be much more biodegradable than often assumed (Bird et al., 1999). For soil samples, the results given by Gelinas et al. (2001) are also very low (< 1 % of total OC), in agreement with ours.

The higher relative BC content in the OC-poorest horizons – usually, B horizons – can be explained in several ways. The combustion of the roots of burned trees can last for several days, and result in an introduction of BC in deep horizons. Soil fauna can also introduce BC in deep horizons, where it can persist owing to the lower oxygen availability.

References

- Bird M.I., Moyo C., Veenendaal E.M., Lloyd J. & Frost P. (1999). Stability of elemental carbon in a savanna soil. *Global Biogeochemical Cycles* 13: 923-932.
- Gelinas Y., Prentice K.M., Baldock J.A. & Hedges J.I. (2001). An improved thermal oxidation method for the quantification of soot-graphitic black carbon in sediments and soils. *Environmental Science and Technology* 35, 3519-3525.

PBC-13: Biogeochemical characterization of sedimentary organic matter in marine sediments. Black carbon isolation discussion

L. Sánchez-García¹, J.R. de Andrés¹, J.A. Martín Rubí¹, A. Terán², J.M. de la Rosa²,
F.J. González-Vila²

1) IGME, C/Ríos Rosas, 1, 28003- Madrid, Spain (e-mail: l.sanchez@igme.es)

2) IRNAS, CSIC, Avda. Reina Mercedes, 10, 41012-Sevilla, Spain

Black carbon (BC) is usually defined as the highly condensed carbonaceous residue from incomplete combustion of fossil fuels and vegetation [1]. It is an ubiquitous form of refractory organic matter widely distributed in the environment [2], which exists as a continuum from partly charred material to highly graphitized soot particles. Due to the no general agreement on clear-cut boundaries of definition, there are a few different methods to identify and quantify the refractory organic matter from different matrices.

In this communication we present a complete geochemical study of marine sediments sampled in the Southwestern Atlantic continental shelf of Spain. It comprises inorganic characterization and deeply organic fraction study. The latter have been achieved with both, the more labile material (lipids and humic substances) and the most refractory one (BC). It is also presented a comparison of the results obtained in the BC isolation from the sediments carried out on with two different approaches.

Global characterization of the samples included standard physico-chemical analysis, as well as determination of heavy metals content, granulometry and XRD. Afterwards, the samples were subjected to a progressive chemical removal of the lipids and humic substances, to get finally intermediate refractory organic material and BC samples.

BC isolation and quantification was carried out by two different methods: i) a chemical method based on the measurement of benzenopolycarboxylic acids (BPCA), considered as specific markers for black carbon, [3]. The analytical procedure includes acid digestion for the elimination of polyvalent cations, oxidation with hot HNO₃ to degrade the less resistant materials, sample cleanup, derivatization and GC analysis of the released BPCA. ii) A thermal method based on weight loss determination after the treatment of the sample at 375°C for 24h [4, 5 and 1]. Previously, the samples were subjected to an acid treatment, dried at 60°C and converted into a fine powder. BC samples obtained by both procedures were characterized at molecular level using Pyrolysis-GC/MS and spectroscopic techniques (FT-IR and solid state ¹³C-NMR).

The marine sediments studied were neutral or slightly alkaline (pH: 7.5-8.2) and have OM contents between 0.87 % and 3.16 %. The total S contents were under 0.32 %. Specially

relevants are the Al (6-8 %) and Fe (3.5-5 %) high values, because of their influence on the formation of artefacts during the oxidation step in the chemical BC estimation. The data on BC/TOC were very variable (0.04-10.02 %) depending on the BC isolation procedure used.

As seen by pyrolysis and NMR data (Fig. 1), some samples shows an important refractory aliphatic moiety, this unsuspected feature will be discussed in terms of sample origin and isolation method used.

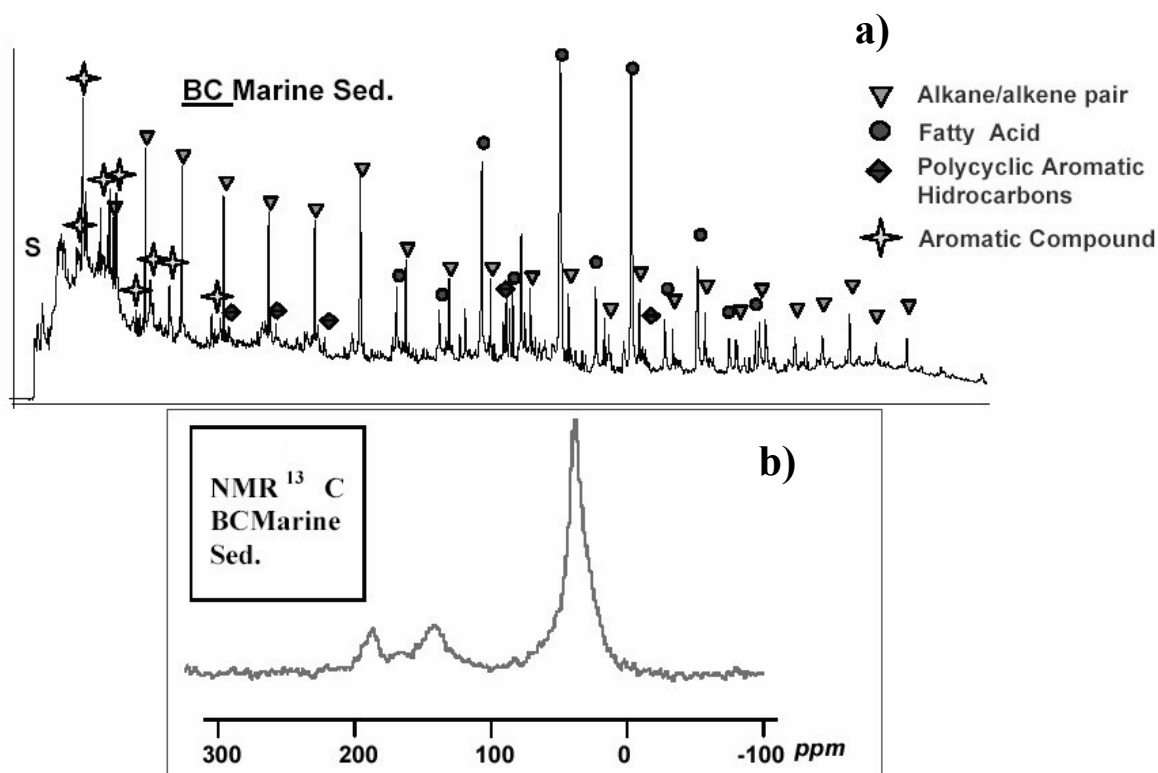


Fig.1. BC from a marine sediment: a) Pyr-GC/MS chromatogram and b) ¹³C NMR spectra from the same sample

References

- [1] Schmidt, M.W. I.; Skjemstad, J.O.; Czimezik, C.I.; Glaser, B.; Prentice, K.M.; Yelinas, Y. and Kuhlbusch, T.A.J. (2001). Comparative analysis of black carbon in soils. *Global Biogeochemical Cycles*, Vol.15, No.1, pp 163-167.
- [2] Kuhlbusch, T.A.J. (1998). Black carbon and the carbon cycle. *Science*, Vol.280.
- [3] Glaser, B.; Haumaier, L.; Guggenberger, G. and Zech, W. (1998). Black carbon in soils: the use of benzenecarboxylic acids as specific markers. *Org. geochem.* Vol.29, No.4, pp. 811-819.
- [4] Gustafsson, Ö.; Haghseta, F.; Chang C.; Macfarlane, J. and Gschwend, P.M. (1997). Quantification of the dilute sedimentary soot-phase: Implications for PAH speciation and bioavailability. *Environ. Sci. Technol.* **31**, 203-209.
- [5] Yelinas, Y.; Prentice, K.M.; Baldock, J.A. and Hedges, J.I. (2001). An improved thermal oxidation method for the quantification of soot/graphitic black carbon in sediments and soils. *Environ. Sci. Technol.* **35**, 3519-3525.

PBC-14: Molecular level descriptors of the effect of fire on soils under pine forest in continental Mediterranean soils

P. Tinoco¹, G. Almendros¹, J. Sanz², R. González-Vázquez³, F.J. González-Vila³

1) Centro de Ciencias Medioambientales, CSIC, Serrano 115B, 28006-Madrid, Spain
(e-mail: humus@ccma.csic.es)

2) Instituto de Química Orgánica General, CSIC, 28006-Madrid, Spain

3) Instituto de Recursos Naturales y Agrobiología, CSIC, P.O. Box 1052, 41080-Seville, Spain

The relatively frequent occurrence of wildfires in Mediterranean ecosystems is favoured by hot summer temperatures in addition to the historical reforestation with pyrophytic forest species such as most types of rapid growing conifers used in the second half of the past century. Concerning soil organic matter, it has been demonstrated that fire leads to progressive decarboxylation, dehydration and dealkylation of the humic and fulvic acids which, in turn, lead to insoluble polyaromatic macromolecular substances (humin-like). This material has been generically referred to as black carbon, a recalcitrant soil fraction which is considered of large interest by their possible effect in the biogeochemical balance with a significant impact on the global change through the soil C sequestration processes.

Although fire is considered to be one out of the abiotic factors with most significant bearing on the organic matter characteristics, assessing the occurrence of forest fires in the past is not a trivial problem since several studies have shown that fire-induced changes in soil properties cannot be easily distinguished from the effects of the biochemical humification process despite the latter may take hundred of years in undisturbed soils. In particular no sufficient information is currently available on important issues such as: **a)** the analytical descriptors betraying the effects of fires in soils with unknown history of external perturbations, **b)** those molecular features of black carbon and charred biomass that could be used to quantify these soil components and **c)** the organic matter descriptors most suitable to monitor the intensity-dependant effects of the different types of wildfires.

In this work a series soil organic matter fractions (lipids and humic acids) from two pine forests and from the corresponding neighbor plots affected by high- and medium-intensity wildfires (in the latter case fire mainly affected forest canopy) were characterized aiming to select significant parameters responsive for the effect of fire on the soil. In the case of humic acids visible, infrared and ¹³C NMR spectroscopy (Bloch-decay and dipolar dephasing), in addition to degradation methods (perborate degradation and Curie-point pyrolysis) were used, whereas the soil lipid fraction was methylated and studied directly by gas chromatography-mass spectrometry.

Microscopic examination of particulate soil fractions isolated by flotation in dense liquids suggests that qualitative and quantitative changes after medium-intensity fire could mainly be attributed to the fall of charred plant material from the forest canopy, whereas the

high intensity fire turn most of the plant biomass into black carbon-like material and ash, and leads to severe transformation of the preexisting organic matter.

Several of the variables determined in the humic acid fraction could be considered as possible descriptors of wildfire impact. This was mainly the case with the yield of benzenecarboxylic acids after perborate degradation, which increased to different extent depending on the intensity of the wildfire (x3 in the most intense forest fire), whereas the amount of fatty acids released after degradation increased only in the humic acids from the soil under the forest affected by the medium-intensity fire. The ^{13}C NMR spectra confirm the substantial increase in the total amount of aromatic structures, but other spectral characteristics such as the intensity of the infrared and NMR bands produced by oxygen-containing functional groups showed significant variations in terms of the type of fire (e.g., some oxidation may occur in medium-intensity fires). On the other hand, there was a series of molecular descriptors showing progressive trends hence being more suitable for the quantitative assessment of the fire intensity. For instance, there was a highly significant increase in the N content of the humic acids in terms of the effect of fire. The atomic H/C ratio (elemental analysis) showed a decrease in the postfire soils, to an extent depending on the intensity of the wildfire, as correspond to the above-indicated enhancement of the aromatic domain. The optical density of the humic acid paralleled the above patterns and reinforces the conclusion about removal (or transformation) of the whole aliphatic moieties.

Compounds behaving as biomarkers of the contribution of the fungal metabolism to the humic acid synthesis, such as the perylenequinonic pigment recognized by intense valleys at 455, 530, 570 and 665 nm in the second derivative spectra of the humic acids from soils under burnt forest were also significantly depleted (a phenomenon that could be tentatively attributed to a reductive insolubilization of humic acid fraction leading to the accumulation of these polynuclear pigments in the alkali-insoluble humin-like fractions).

Results from Curie-point analytical pyrolysis indicated that methoxyphenols are the pyrolytic products most responsive to fires' effects whereas the amount of fatty acids behaves as in the perborate digests: they increased to some extent after the medium-intensity fire. This conspicuous behavior of the fatty acid associated to humic acid structure could be pointing out to translocation and further fixation of hydrophobic compounds.

There was an also very significant change in the molecular assemblages of soil lipids extracted from soil with petroleum ether and analyzed by gas chromatography. The alkane concentration increased after both types of fires. In the soil subjected to the most intense fire there was depletion in the relative amounts of monoterpenes, sesquiterpenes and diterpenes and increases in the relative amounts or aromatic diterpenoid hydrocarbons. On the other hand, in soil where fire was less intense and mainly affected forest canopy there was a increase in the relative proportion of diterpene hydrocarbons.

PFA-1: Biomarkers in archaeology: the degradation of botanical remains and loss/preservation of chemical information

J. Kool^{1,2}, M.M. van den Berg¹, H. Huisman³, H. van Haaster⁴, R. van Heeringen³,
O. Brinkkemper³, H. Kars¹, P. Buurman²

1) Institute for Geo- and Bioarchaeology, Vrije Universiteit, De Boelelaan 1085, 1081 HV Amsterdam, the Netherlands (e-mail: johan.kool@falw.vu.nl)

2) Laboratory of Soil Science and Geology, Wageningen University, P.O. Box 37, 6700 AA Wageningen, the Netherlands

3) ROB, P.O. Box 1600, 3800 BP Amersfoort, the Netherlands

4) BIAx, Hogendijk 134, 1506 AL Zaandam, the Netherlands

All over Europe there is discussion concerning the degradation of the archaeological record with subsequent loss of information. This discussion has to lead to a uniform approach to preserve our archaeological heritage *in situ*, because the heritage is neither regenerable nor replaceable. Whilst legislation and planning policies differ from country to country, basic knowledge needed for the physical protection of sites and landscapes is still scarce and needs to be developed.

The study presented here concentrates on the preservation of botanical remains, an important component of many archaeological sites. The objective is to develop an assessment system for the preservation potential of sites in wetland areas. To find a correlation between soil conditions and loss/preservation of chemical information constitutes the first step in creating a model that predicts whether the preservation of archaeological resources is threatened by anthropogenic activities.

During the first step various botanical species and remnants of archaeological interest originating from several sources are analyzed to obtain insight in the diagenetic chemical pathway and natural variations in resistance to degradation. The selection of species is based upon high frequency findings in wetlands by archaeologists at excavations. This ensures that the resulting model can be used at a maximum number of sites.

The analyses are performed using Py-GC/MS. By identification and quantification of components that react upon decomposition, it will be possible to derive a decomposition scale using newly defined biomarkers. This more pragmatic approach to tackle the problem is an empirical investigation: differences in chemistry, degradation state, species and soil conditions are related using statistics. The main variables are the presence or absence of water and oxygen, pH and the buffer capacity of the soil. The large number of soil parameters and wide variety of soil conditions combined with the sheer complexity of the degradation processes occurring in the soil makes that studying the exact workings of the processes will

not result in usable results for the archaeologists any time soon, conversely the pragmatic approach will.

The next step in creating the model is determining the empirical relation between soil conditions and the biomarkers defined. With this model guidelines can be established with regard to strategies for the *in situ* preservation of sites; and to develop techniques and methods to monitor protected sites; as well as to contribute to a theoretical basis for the sustainable management of our archaeological heritage.

Furthermore, some organic remains of a species have very specific chemical components, which allow recognition even when macroscopic identification is no longer possible. The development of this knowledge by organic geochemists provides archaeologists with an extra technique in their toolbox to obtain more information from a site than is possible nowadays.

PFA-2: Mumie - the 'Blood of Mountains': an analytical approach

B.M. Scholz-Böttcher¹, A. Nissenbaum², J. Rullkötter¹

1) Institute of Chemistry and Biology of the Marine Environment (ICBM), Carl von Ossietzky University of Oldenburg, P.O. Box 2503, D-26111 Oldenburg, Germany (e-mail: bsb@icbm.de)

2) Department of Environmental Sciences, The Weizmann Institute of Science, 76100 Rehovot, Israel

Mumie (in Russian Mumiyo, and also called mumia) is described as sticky, brown to blackish, physiologically active organic matter exuded from rocks in mountainous regions of Central Asia (Pamir, Himalaya, Tien Shan, Karakorum, Caucasus and Altai). The deposits are found at high altitudes on the walls of caves, embedded in rocks or as rock exudates. The mumie material can exceed 500 kg in weight and is of unclear age. Since more than 3000 years mumie plays an important role with high economic value in the folk medicine of the former Soviet Union and also in Indian Ayurvedic and Tibetan pharmacology in indications comprising rejuvenator and immunomodulator functions. It is also used for healing bone fractures and diabetes, applied as growth promoter even for plants, and it is a traditional version of Viagra. There are several regional synonyms for mumie, the second most common one being shilajit (in Sanskrit "destroyer of weakness"), a term used in Indian Ayurvedic medicine. The main contents of mumie according to previous studies are humus-like organic matter (60-80%) and mineral matter (20-40%). However, the nature of this material is not well known and it is often described as asphalt, pitch or bitumen, particularly when referring to shilajit. Typical for mumie is a strong smell suggesting animal excrements as a significant component. Its possible pure vegetable origin is discussed controversially.

Two mumie (Altai Mountains, Siberia, and Yemen) and two shilajit (Pakistan, Nepal) samples were analysed by GC/MS of organic extracts and online-Curie-Point pyrolysates (590°C) of the extraction residues with and without TMAH. Between 1 and 5% of the samples are extractable with DCM/MeOH (99:1). The extracts are dominated by polar compounds. Long-chain *n*-alkanes in the aliphatic hydrocarbon fractions point to the presence of Recent higher plant material, although an admixture of more mature fossil material was recognized in the Yemen sample. All aromatic fractions are dominated by squalene, in three fractions traces of tocopheryl acetate were detected. Potential sources for squalene are oil seeds whereas the presence of tocopherol acetate may be an artificial substitute. The polar fractions are more heterogeneous. The major compound class are *n*-fatty acids (C₉-C₃₀), with palmitic and stearic acids being the most prominent ones. The major *n*-alcohols are the C₂₄, C₂₆ and C₂₈ homologues. All samples contain C₂₇ and C₂₉ steroid alcohols and glycerol. The mumie sample from the Altai mountains is dominated by a compound tentatively identified as

nonadecan-10-ol. Both shilajit samples contain small amounts of dehydroabiatic acid, an indicator of the presence of conifer resin, and triterpenoids such as amyryns and friedelin. The faecal indicator coprostanol is present in all samples, albeit in trace amount in the Yemen mumie sample. The major compound of the hydrolysates is benzoic acid in all cases.

In the absence of TMAH the pyrolysates of both mumie samples contain benzonitrile as the major compound followed by acetophenone, toluene, *p*-methylphenol, benzoic acid methyl ester, benzamide and several other alkylphenolic compounds. The pyrolysates of both shilajit samples are much more complex. Here, phenol, *p*-methylphenol and *p*-methoxyphenol are dominant. Furanone and pyranone derivatives as well as several methoxyphenols were detected. Homologues of aromatic nitriles are present as well.

The major pyrolytic cleavage and simultaneous TMAH methylation products of both mumie samples is benzoic acid methyl ester followed by a variety of methoxyphenols, methoxybenzoic and methoxyphenolic acid derivatives, often with 3,4-substitution related to the lignin component of the humic material. Both samples yield significant amounts of hippuric acid dimethyl ester and its derivatives. The main compound of the shilajit pyrolysates is methoxybenzoic acid methyl ester. Lignin- and tannin-derived components are also present together with traces of hippuric acid dimethyl ester.

All samples analysed represent a complex and heterogeneous mixture of humic material, possibly fulvic substances. Higher plant material is assumed to form the basis. Whereas lipids are mainly found in the extracts, the pyrolysates show indications of proteins, carbohydrates and lignin. Both mumie samples have abundant N-containing compounds, e.g. purins or proteins. This is indicated by the formation of benzonitrile and other N-aromatic compounds during pyrolysis. In contrast to this, the shilajit samples are characterised by abundant methoxybenzoic acid derivatives from lignin and tannins in their TMAH pyrolysates. Hippuric acid and coprostanol are urine/faecal indicators and suggest that animals excrements play a role in mumie formation. Animal excrements appear to be much less important in the shilajit samples. All samples show molecular differences and exclude a common source. Nevertheless, mumie and shilajit samples can be grouped into separate categories.

PFA-3: A shallow grave: using lipid and stable isotopic evidence in a murder case

R. Berstan¹, I.D. Bull¹, A. Vass², R.P. Evershed¹

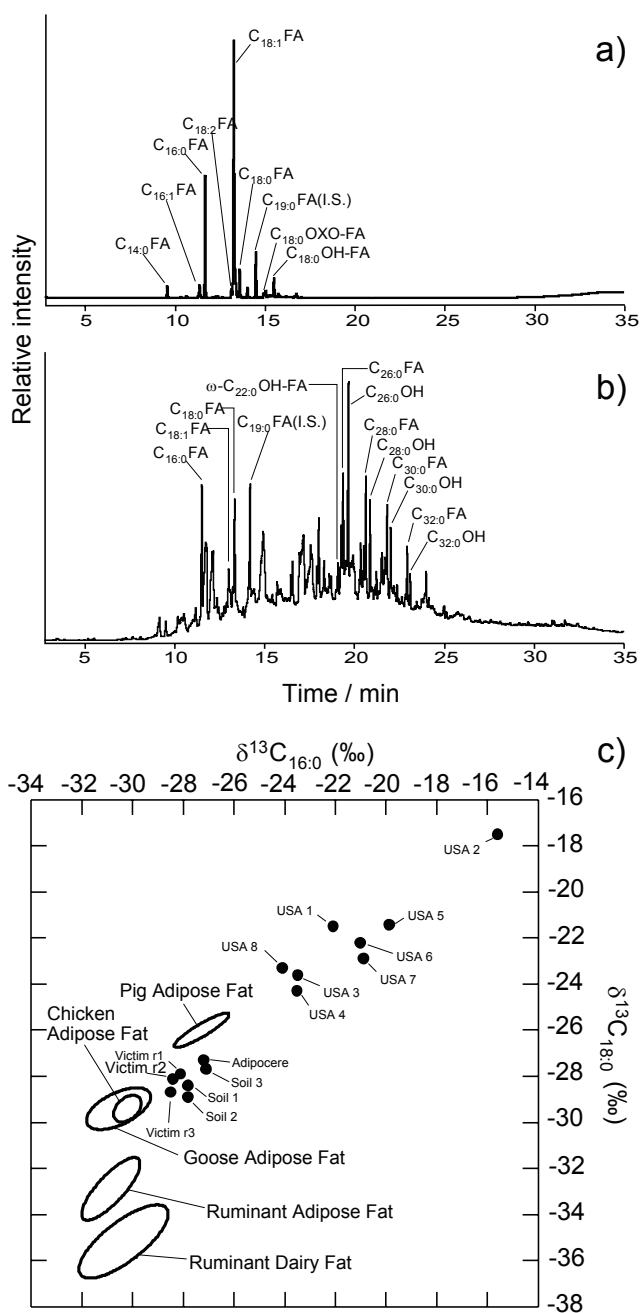
1) Organic Geochemistry Unit, Bristol Biogeochemistry Research Centre, School of Chemistry, University of Bristol, Cantock's Close, Bristol BS8 1TS, UK

2) Oak Ridge National Laboratory, P.O. Box 2008, Oak Ridge, TN 37831, USA

In November 1998, a property-holder in the London, UK was reported missing. Following investigation, Police suspected an occupant of murdering the missing landlord and disposing of the body in the back garden of his rented property. A subsequent search and excavation of the garden exposed an area of disturbance that was hypothesised to be the remains of a shallow grave. Whilst closer examination failed to reveal any obvious morphological remains, e.g. hair or tissue, a limited quantity of white/grey millimetre-sized particles were observed and identified as putative adipocere (degraded fatty tissue). mtDNA analyses established the particles as having originated from a person maternally related to the murder victim. However, as with previous cases, the high sensitivity of the PCR technique meant that additional chemical evidence was required in order to confirm, unambiguously, that a human body had been associated with the suspected grave.

GC and GC/MS analyses of the isolated particles and intimately mixed soils revealed a relatively simple lipid profile comprising predominantly fatty acids dominated by the C_{16:0} and C_{18:0} homologues with lower relative abundances of the corresponding unsaturated components (C_{16:1}, C_{18:1}, C_{18:2}) and associated oxidation products (Fig. 1a). The distribution is entirely consistent with the deposition of fatty tissue, the oxidation of octadec-9-enoic acid to 10-hydroxy-octadecanoic and 10-oxo-octadecanoic acid having been previously reported during the formation of adipocere (Takatori, 1996). This distribution contrasted markedly with that of the control soil which exhibited a lipid profile typical of that found in grassland soils (Fig. 1b). Additional analyses of adipose fat sampled from eight cadavers of North American origin revealed distributions of fatty acids similar to those observed for the putative adipocere although decomposition had not proceeded to the extent where the corresponding oxidation products were detectable.

Fig.1. Partial gas chromatograms of the solvent extractable lipid fractions obtained from: (a) soil intimately associated with the putative adipocere, and (b) a control soil sampled away from the suspected grave. Peak identities are: C_{14:0}FA to C_{34:0}FA, saturated normal-chain fatty acids with 14 to 34 carbon atoms; C_{16:1} and C_{18:1}, mono-unsaturated fatty acids with 16 and 18 carbon atoms, respectively; C_{18:2}, di-unsaturated fatty acid with 18 carbon atoms; C_{18:0}OH-FA and C_{18:0}OXO-FA, hydroxyl and oxo-fatty acids, respectively, with 18 carbon atoms; C_{26:0}OH to C_{32:0}OH, saturated normal-chain alcohols with 26 to 32 carbons; I.S., internal standard (*n*-C_{19:0} fatty acid). (c) depicts a cross-plot of $\delta^{13}\text{C}$ values obtained for the palmitic and stearic acid components derived from the suspect grave soil, putative adipocere, victim body fat, body fat from eight American cadavers and 95% confidence ellipses for non-human reference fats.



Fatty acids isolated from the samples showing evidence of adipocere formation were also analysed by GC/C/IRMS in an attempt to utilise $\delta^{13}\text{C}$ values thus obtained as a second level of characterisation in order to confirm the source of the adipocere. By using a cross-plot of $\delta^{13}\text{C}_{16:0}$ against $\delta^{13}\text{C}_{18:0}$ values it was demonstrated that the values obtained for the fatty acids from the putative adipocere were consistent with values of those derived from the victim's fatty tissue (obtained following a confession by

the accused; Fig. 1c). Moreover, use of $\Delta^{13}\text{C}$ ($\delta^{13}\text{C}_{18:0} - \delta^{13}\text{C}_{16:0}$) values removed dietary effects thus enabling a positive correlation between the suspect grave soil, putative adipocere, American body fat samples and those obtained from the victim to be made. Combined with the mtDNA evidence, these data were instrumental in securing a life sentence for the accused.

References

Takatori, T. (1996) Investigations on the mechanism of adipocere formation and its relation to other biochemical reactions. *Forensic Science International* **80**, 49-61.

PFA-4: Detection, use and occurrence of petroleum bitumen in Egyptian embalming

K.A. Clark, R.P. Evershed

Organic Geochemistry Unit, Bristol Biogeochemistry Research Centre, School of Chemistry, University of Bristol, Cantock's Close, Bristol, BS8 1TS. UK. (e-mail: k.a.clark@bris.ac.uk)

The blackened appearance of many mummies has frequently been attributed to the application of bitumen in the mummification processes. The origin for the term 'mummy' is often understood to have derived from *mummiya*, the Persian word for bitumen. The mistaken belief that mummies contained *mummiya* (ie. bitumen) resulted in powdered mummy being sold as a pharmaceutical treatment for a number of ailments in the 16th and 17th centuries. Furthermore, there has been speculation as to whether the use of black substances (such as bitumen or pitch) was deliberate (perhaps to represent the black silt which covers the soil after the annual inundation of the Nile, resulting in a perceived death and rebirth of the fertile flood plains) or whether the colour is due to the chemical alteration, over time, of other treatments applied, such as, fats or waxes. The confusion arising from *mummiya* and the misuse of the term bitumen has lead scholars to assume that bitumen was of importance in the mummification process.

However, of the relatively few investigations performed of mummy balms, those that have been undertaken, indicate that bitumen may not be a ubiquitous component of ancient Egyptian balms, with fat/oil beeswax and tree resins being the major constituents [1,2]. Where bitumen has been found, the amounts used varies widely and generally only mummies dating to the Graeco-Roman period have been studied [3-6]. This paper presents the results of the widest survey of Egyptian mummies to date, comprising *ca* 200 samples of balms, bandaging and tissues taken from 75 individuals, dating from 3200 BC to 395 AD. A number of the mummies examined here are among the oldest subjected to chemical investigation for the presence of balms.

GC and GC/MS of the total lipid extracts (TLE) of balms generally fails to detect bitumen biomarkers reflecting the low abundance of bitumen, even if present. The detection of biomarker steranes and terpanes relies on the analysis of the hydrocarbon fraction using the mass spectrometer in selected ion monitoring (SIM) mode, giving detection limits of 0.05 ng of steranes and 0.5 ng of terpanes. Our results show that the use of bitumen is not ubiquitous and generally only being detected in mummies dating from the Ptolemaic and Graeco-Roman Periods. The concentrations of bitumen biomarkers are typically 1000 times lower than the biomarkers derived from other embalming ingredients (such as oil/fat, beeswax) suggesting

that the use of bitumen is less significant than has been assumed. No bitumen has been found in the earliest mummies examined. Bitumen found in mummy balms can be sourced, using ratios of biomarkers to different seeps around accessible to the ancient Egyptians, however the majority of bitumens detected have been identified as originating from the Dead Sea.

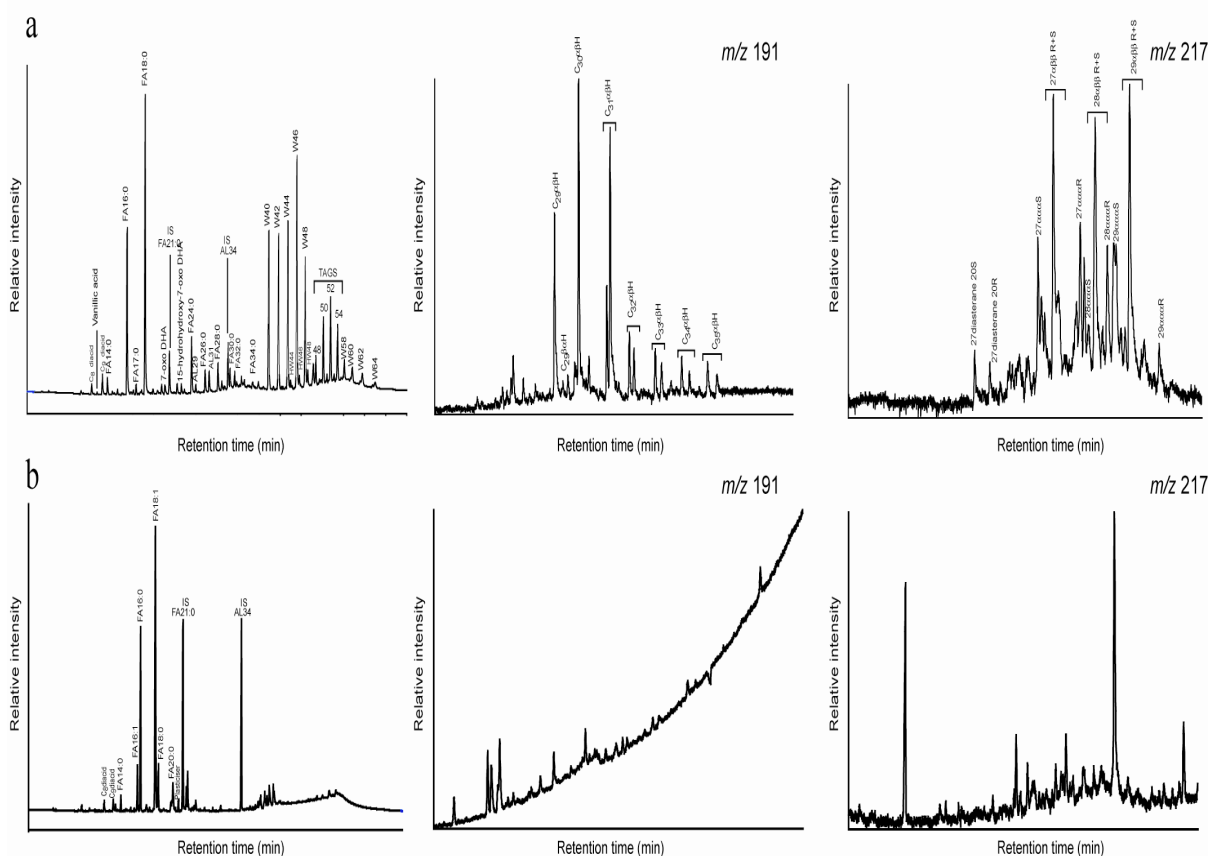


Fig.3. Partial gas chromatograms of the total lipid extract (left) and m/z 191 (centre) and 217 (right) mass chromatograms of hydrocarbon fractions taken from (a) resin coated outer bandages of a young male adult (323-30 BC) and (b) tissue from a female mummy (2410-2195 BC)

References

- [1] Buckley, S.A., Evershed, R.P., 2001. Organic chemistry of embalming agents in Pharaonic and Graeco-Roman mummies. *Nature* 413, 837-841.
- [2] Tchaplal, A., Mejanelle, P., Bleton, J., Goursaud, S., 2004. Characterisation of embalming materials of a mummy of the Ptolemaic era. Comparison with balms from mummies of different eras. *Journal of Separation Science* 27, 217-234.
- [3] Connan, J., Dessort, D., 1989. Du bitume de la Mer Morte dans les baumes d'une momie égyptienne: identification par critères moléculaires. *Comptes Rendus de l'Académie des Sciences (Ser II)* 309, 1665-1672.
- [4] Connan, J., Dessort, D., 1991. Du bitumen dans les baumes des momies égyptiennes (1295 av JC-300 ap JC): détermination de son origine et évaluation de sa quantité. *Comptes Rendus de l'Académie des Sciences (Ser II)* 312, 1445-1452.
- [5] Nissenbaum, A., 1992. Molecular Archaeology - Organic Geochemistry of Egyptian Mummies. *Journal of Archaeological Science* 19, 1-6.
- [6] Connan, J., 2002. Étude des baumes utilisés pour traiter les momies. In: Macke, A., Macke-Ribet, C., and Connan, J. (Ed.), *Ta Set Nefrou: Une nécropole de Thebes-Ouest et son histoire*. Dar Namatallah Press: Cairo. pp. 129-187.

PFA-5: Asphalt in the Iron Age excavations (12th-7th century BC) of the Philistine Tel Mique-Ekron city: origin and trade routes

J. Connan¹, A. Nissenbaum², K. Imbus³, J. Zumberge³, S. Brown³

1) Laboratoire de Géochimie Bioorganique, E.C.M.P., UMR 7059 CNRS, 25 rue Becquerel, 67087 Strasbourg Cedex 2, France (e-mail: connan.jacques@wanadoo.fr)

2) Department of Environmental Sciences and Energy Research, Weizmann Institute of Science, 76100, Rehovot, Israel

3) GeoMark Research, Ltd., 9748 Whithorn Drive, Houston Texas 77095, USA

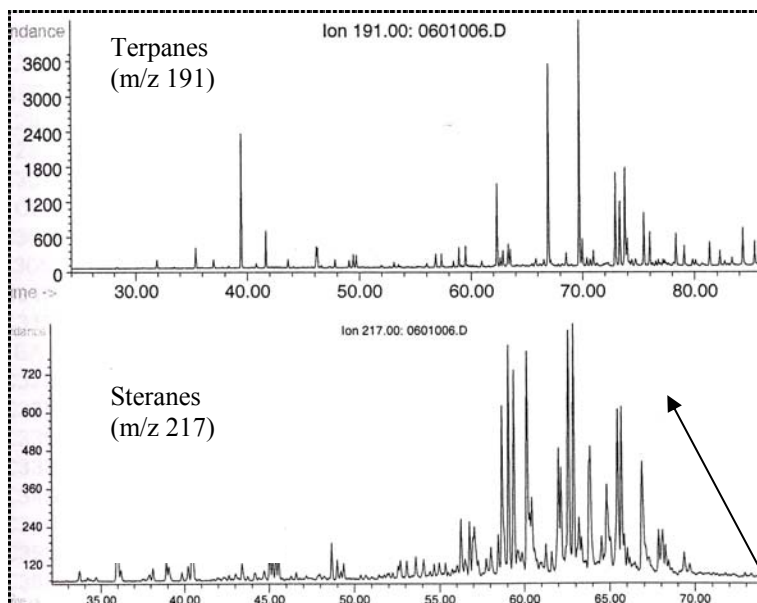
Lumps of pure asphalt as well as coatings of bitumen on potsherds were discovered during the excavations of Ekron, a Philistine capital city, located at Tel Mique in Israel. Ekron was one of the five Philistine capital cities, the others being Ashdod, Ashkelon, Gath and Gaza. The Philistine presence in Ekron covers a 600 year period, which ended in 604 BC, when the Babylonians, on their way to conquer Egypt, burned the Egyptian-allied cities to the ground.

Samples from two age periods were analysed. Three samples (4, 6 and 20) are from the Iron age I (4th quarter of the 12th century BC), i.e., immediately following the period when the Philistine founded the city of Ekron, and three samples (11,16 and 19) are from the Late Iron II period (7th century BC), i.e., the time just before the final destruction of the city. The sample set selected for analysis included lumps of pure asphalt with a typical conchoidal fracture similar to the asphalt of the Dead Sea floating blocks and coating of black shiny asphalt on potsherds (Fig.1). The potsherds are thought to come from jars used to store either olive oil or wine. The 7th century city of Ekron was the largest center for olive oil production yet uncovered in antiquity, as indicated by the 115 oil presses unearthed there.

Geochemical analysis, including carbon isotope measurements on bulk liquid chromatographic fractions as well as GC-MS analysis of both C₁₅₊saturates and C₁₅₊aromatics, were carried out on the archaeological samples and on a lump of asphalt from the Dead Sea floating blocks that was used as a reference.

$\delta^{13}\text{C}$ values of chromatographic fractions as well as sterane and terpanes parameters of archaeological samples (Fig.1) are in good agreement with the data obtained on the Dead Sea reference. Consequently, the bitumen from the Dead Sea had been imported to Ekron.

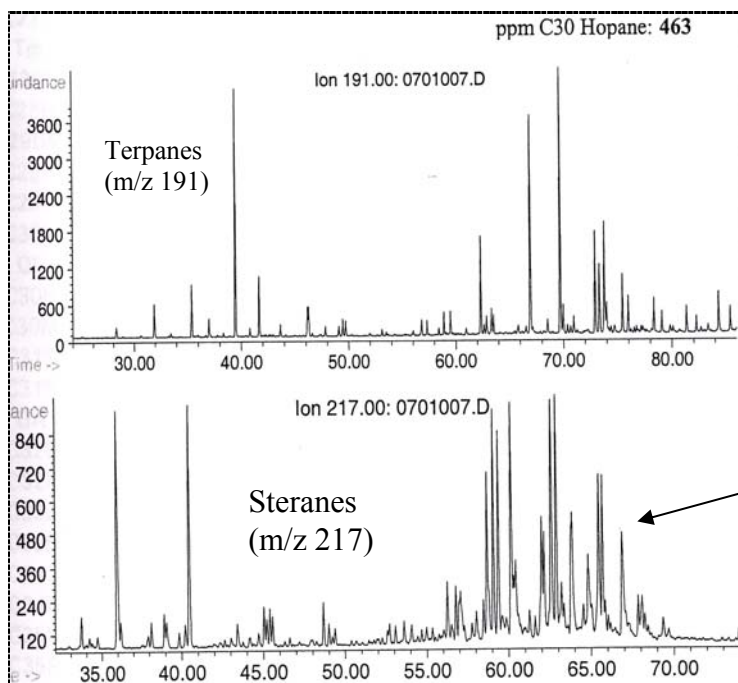
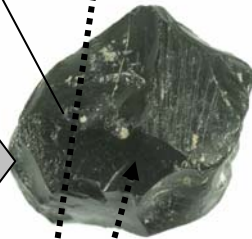
In addition to basalt used for grinding querns, asphalt was traded between Philistia and Israelite tribes through at least 5 centuries. In the 7th century BC, this trade posed no particular difficulties, since Philistia, Israel and Judah were then at peace as part of the Neo-Assyrian Empire. It raises, however, an issue for the Iron Age I period, when Philistia and Israelite tribes were constantly in conflict (as described in the Old Testament, e.g., the narrative of David and Goliath). Therefore, it appears that economies of trade and profit had superseded geopolitical and ethnic considerations.



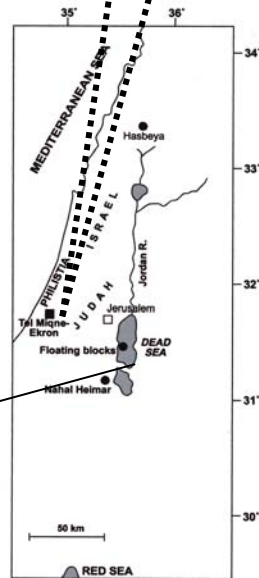
Ekron –sample 20- 12th century BC

Sample 20
12th century BC

Sample 11
Ekron
7th century BC



Dead Sea Floating blocks



**PFA-6: Recognition and evaluation of alteration of
antique vegetal resins by the use of biomarkers**

A. Charrié-Duhaut¹, J. Connan¹, M. Girard², B.T. Mai²,
C. Lampert³, P. Albrecht¹

1) Laboratoire de Géochimie Bioorganique, UMR 7509., C.N.R.S., Université Louis Pasteur, E.C.P.M., 25 rue Becquerel, 67087 Strasbourg Cedex 02, France (e-mail: acharrie@chimie.u-strasbg.fr)

2) Laboratoire de Palynologie, UMR 6130, C.E.P.A.M., 250 rue Albert Einstein, Sophia Antipolis, 06560 Valbonne, France

3) Department of Archaeological Sciences, University of Bradford, Richmond Road, Bradford, W.Yorks, BD7 1DP, UK

The study of resins from varied vegetal origin (*Pinus*, *Dipterocarpaceae*, *Pistacia*) is investigated since these substances have been widely used for example in Egypt or in Europe during the Gallo-Roman period (100BC-250AD), in particular for the manufacture of adhesives. Many samples are available in archaeological jars or on potsherds. The aim of the study is to determine their origin (botanical sources, geographical origin) by the identification of diagnostic biomarkers. Sometimes, resins are rather well preserved in particular in shipwrecks where the environment is often anoxic. In this case, the specific molecules can be directly recognized. In most situations, however, the molecular fingerprints have considerably changed because of alteration undergone by the materials due to aging processes such as oxidation and/or biodegradation. Consequently, identification of degradation products and understanding of the alteration mechanisms are necessary for a precise characterisation of the resin.

To analyse these complex mixtures, the investigation has been carried out by applying the flow chart currently used for the geochemical study of source rocks and crude oils. The resins were extracted by dichloromethane/methanol and the extract subsequently fractionated into saturated and aromatic hydrocarbons, ketones, alcohols and acids. The selected analytical approach, based on GC-MS analysis, offers the advantage to give access to polar, as well as non polar compounds, even if they are in very low amounts.

Stable isotope data ($\delta^{13}\text{C}$) and pollen analysis were recorded and correlated to the molecular informations.

In each series, several samples with different degrees of alteration were analysed (see Table 1).

Table 1	<i>Pinus</i>	<i>Dipterocarpaceae</i>	<i>Pistacia</i>
Origin of the archaeological samples	Resins found in jars originated from Pampelone and Saqqara	Resins from the famous Brunei shipwreck	Resins from Ulu Burun shipwreck, Deir el Medineh jars and Guimet Museum
Diagnostic biomarkers	Abietic acid related compounds	Dammarane-type compounds	Oleanonic, moronic, isomasticadienonic and masticadienonic acids

In the less degraded samples, the original specific biomarkers were detected. With alteration, severe modifications in the molecular fingerprints were observed in each series. For example, in the particular case of *Pistacia*, a series of aromatic triterpenes was identified in a slightly degraded resin from Ulu Burun shipwreck as a result of microbially induced processes (e.g. cleavage and degradation of ring A, followed by progressive aromatisation of the remaining tetracyclic skeleton). In a very altered *Pistacia* resin (embalming material from Guimet Museum) part of the diagnostic biomarker series was even lost as no isomasticadienonic nor masticadienonic acids related compounds could be detected. Furthermore the appearance of oxidative transformation products could be observed.

In addition, these results would allow to better identify resins in complex organic mixtures even degraded as, for example, in balms of mummies.

References

- Noble R.A., Alexander R., Kagi R.I., Knox J. (1985) Tetracyclic diterpenoid hydrocarbons in some Australian coals, sediments and crude oils, *Geochim. Cosmochim. Acta*, **49**, 2141-2147.
- Papageorgiou, V.P., Bakola-Christianopoulou M.N., Apazidou K.K., Psarros E.E. (1997) Gas chromatographic-mass spectroscopic analysis of the acidic triterpenic fraction of mastic gum, *J. of Chromatogr. A*, **769**, 263-273.
- Van der Doelen, G.A., van den Berg, K.J., Boon, J.J. (1998) Comparative Chromatographic and Mass-Spectrometric Studies of Triterpenoid Varnishes: Fresh Materials and aged samples from Paintings, *Studies in Conservation* **43**, 249-264.

PFA-7: Identification and origin of bitumen in the Neolithic artefacts (8100 BC) of Demirköy Höyük in Eastern Turkey

O. Kavak¹, J. Connan², E. Akin³, M.N. Yalcin⁴, K. Imbus⁵, J. Zumberge⁵, S. Brown⁵

- 1) Dicle Universitesi Muhendislik-Mimarlik Fakultesi, Maden Mühendisligi Bölümü, 21280-Diyarbakir, Turkey
- 2) Laboratoire de Géochimie Biorganique, Université Louis Pasteur, 25 rue Becquerel, 67087-Strasbourg Cedex 02, France
- 3) Dicle Universitesi Fen-Edebiyat Fakultesi Arkeoloji Bolumu, 21280 Diyarbakir, Turkey
- 4) Istanbul Universitesi, Muhendislik Fakultesi, 34850 Avcilar, Istanbul, Turkey
- 5) GeoMark Research Ltd., 9748 Whithorn Drive, Houston, TX 77095, USA

Two-ring like objects with a diameter of a few centimeters have been discovered among the artefacts made by the inhabitants of Demirköy Höyük, an aceramic Neolithic site (8100 BC) located on the west bank of the Batman Cayi, a tributary of the Tigris river (Fig.1). These ring fragments, ascribed to be made of a bituminous mixture represent, with clay baked figurines, the innovative use of plastic materials to prepare artefacts. The goals of the study were primarily to establish that the ring-shaped objects were indeed prepared with a bituminous mixture and subsequently, if this feature was confirmed, to try to determine the bitumen origin by analysing oil seeps outcropping in the vicinity of the excavations.

Two archaeological samples from the Diyarbakir Museum have been compared to oil seeps collected at two locations, south of Demirköy Höyük, namely at Boğazköy in the Germav (Middle Maestrichtian/Upper Palaeocene)-Gercus formation (Eocene) and Yeşilli in the Germav formation.

Geochemical analysis including carbon isotope measurements on bulk liquid chromatographic fractions as well as GC-MS analyses of both C₁₅+saturate and C₁₅+aromatic hydrocarbon fractions were carried out on archaeological samples and reference oil seeps.

First of all, the archaeological samples do show the properties of bituminous mixtures analysed elsewhere (Fig.1). As usual the bitumen is extensively oxidised. Comparison of the geochemical data (isotopes, sterane and terpane patterns) of Demirköy Höyük and oil seeps reveals that the bitumen came from the Boğazköy oil seep, i.e., from the closest oil seep. An extended study, using a data bank (especially the following genetic parameters: isotopic values of C₁₅+saturates and C₁₅+aromatics, Ts/Tm, Gammacerane/C₃₁αβHopane, rearranged steranes/regular steranes, tetracyclic terpane/tricyclic terpanes, etc.) and the data from this study, allowed the identification of the source rocks of the bitumen from the two oil seeps: Boğazköy originated from Silurian-Devonian shales whereas Yeşilli was derived from Cretaceous carbonates.

To conclude, the ring-shaped objects (and probably the cigar-shape artefacts not analysed) from the Demirköy Höyük aceramic site dated 8100 BC, are bituminous amalgams, prepared with bitumen which was likely collected at Boğazköy oil seep. This bitumen, outcropping at the surface in a Middle Maestrichtian to Eocene formation, has been identified to have been sourced at depth by Silurian-Devonian shales.

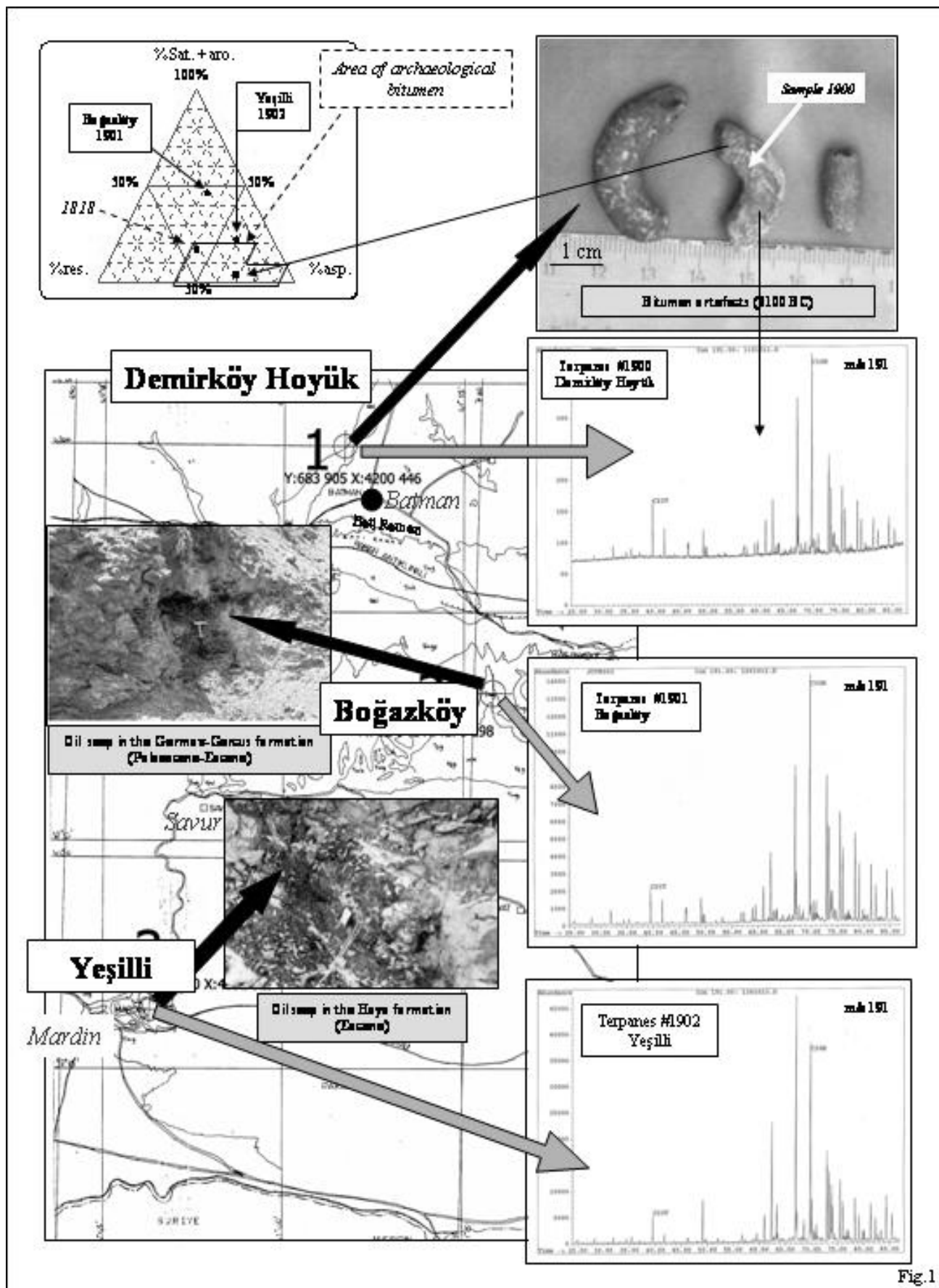


Fig.1

**PFA-8: Molecular archaeology: geochemical analysis of balms from
« Osiris Mummies »**

J. Maurer¹, A. Charrié-Duhaut¹, J. Connan¹,
M. Etienne², P. Albrecht¹

1) Laboratoire de Géochimie Bioorganique, UMR 7509, C.N.R.S., Université Louis Pasteur, E.C.P.M., 25 rue Becquerel, 67087 Strasbourg Cedex 02, France (e-mail: acharrie@chimie.u-strasbg.fr)

2) Département des Antiquités Égyptiennes, Musée du Louvre, 34-36 quai du Louvre, 75058 Paris, France

Within this study, a series of four mummy-like small statuettes of Osiris (two figurines and two mummies, ca. 30-40 cm) has been analysed. The preparation of these statuettes, symbol of fertility and rebirth, was an important part of the festivity of “choiak”, which was celebrated each year at the end of the Nile river flood. A mixture of mud and grains was put into a mould with the shape of Osiris and after drying, it was wrapped in linen treated with embalming material. Due to the ritualistic importance of these statuettes, it was the aim of this study to compare the ingredients used for embalming with those having been identified in human mummies (e.g. Buckley and Evershed, 2001; Macke et al., 2002; Maurer et al., 2002).

To analyse these complex mixtures, an organic geochemistry approach was used with success: the organic extract resulting from extraction with dichloromethane/methanol was fractionated to isolate saturated and aromatic hydrocarbons, ketones, alcohols and acids. Each fraction was then analysed by GC-MS. The identification of diagnostic compounds (biomarkers) and characteristic distribution patterns allowed to identify different components. The presence of *animal fats* was indicated by detection of triacylglycerols and fatty acids. Stable isotope data ($\delta^{13}\text{C}$) and relative concentrations of fatty acids was used to find the origin of fats. Identification of palmitic acid wax esters ranging from 40 to 50 carbon atoms coupled to specific distribution of *n*-alkanes and alkenes (C_{27} predominant for example) indicate the presence of *beeswax*. *Bitumen* is also clearly present as shown by the distribution of steranes and terpanes. Due to similarities in values of several biomarker parameters, bitumen in samples was identified as likely originating from the Dead Sea area. The detection of triterpenoids like moronic acid leads to the assumption of a *higher land plant* contribution but due to their widespreadness, the origin of the resin used could not be determined. The quantitative analysis of the three identified materials (animal fats, beeswax, bitumen) seems to indicate differences among sample composition.

In conclusion, the geochemical analysis of these four balms suggests that they were prepared with the same major constituents. Apparently these mixtures are as sophisticated as those used for human mummies.

References

- Bucley, S.A., Evershed, R.P. (2001) Organic chemistry of embalming agents in Pharaonic and Graeco-Roman mummies, *Nature*, **413**, 837-841.
- Macke, A., Macke-Ribet, C., Connan, J. (2002) Ta Set Neferou – Une Nécropole de Thébès-Ouest et son Histoire : momification, chimie des baumes, anthropologie, paléopathologie. Dar Namatallah Press, Giza, Le Caire, République Arabe d’Egypte.
- Maurer, J., Möhring, T., Rullkötter, J., Nissenbaum, A. (2002) Plant lipids and fossil hydrocarbons in embalming material from Roman Period mummies from the Dakhleh Oasis, Western Desert, Egypt, *J. of Archaeological Society*, **29**, 751-762.

PFA-9: Resin artefacts from a Bronze Age royal tomb in Syria

A.J. Mukherjee¹, M.A. James¹, P. Pfälzner², R.P. Evershed¹

1) Organic Geochemistry Unit, Bristol Biogeochemistry research Centre, School of Chemistry, University of Bristol, BS8 1TS, UK (e-mail: r.p.evershed@bristol.ac.uk)

2) Altorientalisches Seminar, Schloß Hohentübingen, 72070 Tübingen, Germany

During the Bronze Age the ancient city of Qatna flourished due to its commercial and political importance ([1]). During the 2002 excavation season a major discovery was made of an underground tomb beneath the Royal Palace. This tomb had been sealed since the destruction of the palace by fire in the Bronze Age and is the first to be found in an unlooted state. The tomb is thought to have been in continuous use for 300-400 years for the burial of elite individuals and ritual ceremonies. The contents of the tomb which were found *in situ* have never been buried or come into significant contact with groundwater and so are in a remarkable state of preservation. Almost 2000 finds have been recorded including jewellery and various carved objects, basalt statues, sarcophagi, human and animal bones, and *ca.* 200 pottery and stone vessels. The finds include objects of Egyptian, Mesopotamian and Aegean origin, evidence that long-distance trade/exchange was occurring.

Among the many finds were a series of artefacts made from a resin-like substance, these included an intricately carved lion's head (Fig. 1a), which was hollow and also had a circular 'lid', and several beads (Fig. 1b). As well as carved objects, traces of a reddish resinous substance were observed on a number of decorative gold and jewelled artefacts (Fig. 1c) suggesting that resins may also have been used as adhesives (e.g. [2]). Resins are sticky, water-insoluble metabolic by-products exuded by plants and are composed of complex mixtures of mono-, sesqui-, di- and triterpenoids, possessing structures based on the linking together of isoprene (C₅H₈) units ([3]). Under natural forest conditions, the volatile fractions of most resins evaporate while the remaining non-volatile dienic functions can polymerise over geological time and become fossilised ([4], [5]). Resins have been attractive materials for use as adhesives, coatings, pigments and incense since antiquity and have occasionally also been used to make jewellery and small sculptures, particularly in the case of fossil resins, such as amber or the various hard copals ([3]).

The diverse origins, chemical complexity and diagenetic alteration of aged resins has required the application of a wide range of organic geochemical techniques for their characterisation. One of the most useful techniques to emerge is pyGC-MS due to the polymeric nature of these materials, especially where only small samples (submilligram) are available. The use of pyGC-MS is enhanced by using simultaneous thermally assisted hydrolysis and methylation (THM) with tetramethylammonium hydroxide (TMAH; [6]). We report the use of GC-MS and pyGC-MS to investigate: (i) the nature of the resinous materials

used to produce the finds from the royal tomb at Qatna; (ii) whether the same materials were used for the adhesives as for the carved objects thus indicating different technologies being applied to the same raw material; (iii) whether the raw materials were locally produced or traded over long distances and, (iv) whether the resins used to make the carved lion's head and bead were of archaeological or geological origin, i.e. resins or fossil resins. Analyses have revealed a range of terpenoid biomarkers and succinic acid (fig. 1d,e). The presence of diterpenoids, such as methyl dehydroabietate, point to a coniferous origin for the resin used to produce these artefacts. The presence of a high abundance of succinic acid is a characteristic of some fossil ambers.

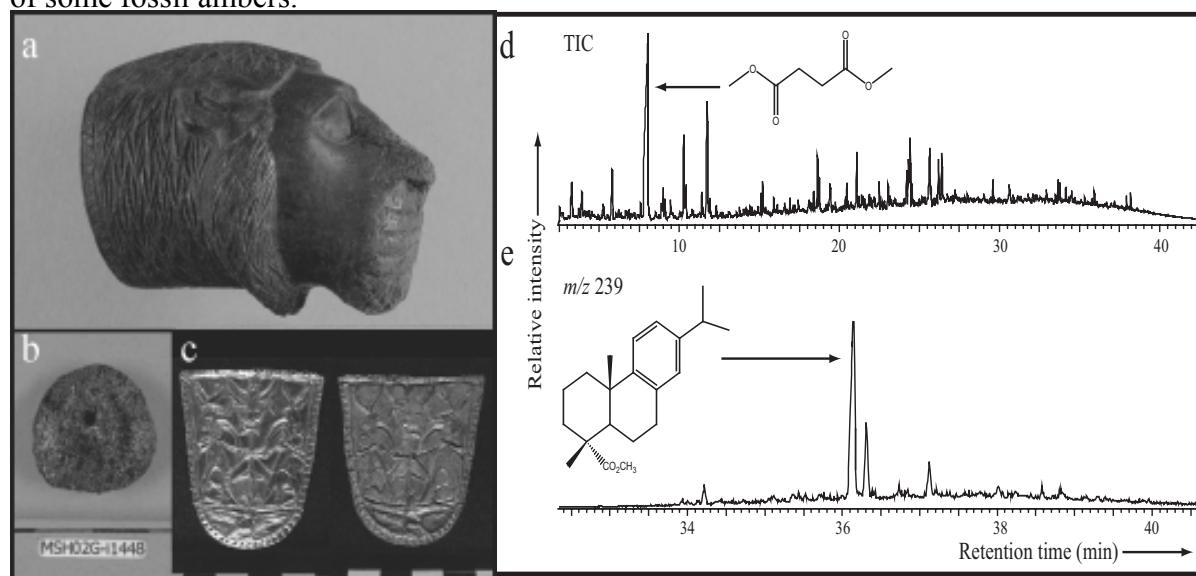


Fig.1. Resin artefacts from the royal tomb at Qatna: (a) lion's head, (b) bead (c) front and reverse of a decorative gold object indicating the possible use of resin as an adhesive; and PyGC-MS analyses of a resin bead: (d) Total ion current showing the peak corresponding to methyl succinic acid and, (e) m/z 239 indicating the presence of methyl dehydroabietate

References

- [1] Al-Maqdissi, M., Luciani, M., Morandi Bonacossi, D., Novák, M. and Pfälzner, P. 2002. Introduction. In Al-Maqdissi, M., Luciani, M., Morandi Bonacossi, D., Novák, M. and Pfälzner, P (Eds.) Excavating Qatna Volume 1 Preliminary report on the 1999 and 2000 campaigns of the joint Syrian-Italian-German archaeological research project at Tell Mishrifeh. pp. 7-16.
- [2] Regert, M. 2004 Investigating the history of prehistoric glues by gas-chromatography-mass spectrometry *Journal of Separation Science*, 27, 244-254.
- [3] Mills, J.S. and White, R. 1994 Natural resins and lacquers. In *The Organic Chemistry of Museum Objects* Butterworth-Heinemann, Oxford., pp. 95-128.
- [4] Langenheim, J.H. 1969 Amber: a botanical enquiry *Science*, 163, 1157-1169.
- [5] Lambert, J.B. and Poinar Jr., G.O. 2002 Amber: the organic gemstone *Accounts of Chemical Research*, 35, 628-636.
- [6] Anderson K.B. and Winans, R.A. 1991 Nature and fate of natural resins in the geosphere. 1. Evaluation of pyrolysis-gas chromatography/mass spectrometry for the analysis of natural resins and resinates *Analytical Chemistry*, 63, 2901-2908.

METHODS & NEW TRENDS

PMN1-1: Analysis of organic matter by Flash Pyrolysis - Gas Chromatography – Mass Spectrometry in the presence of Na-smectite: when clay minerals lead to identical molecular signature

P. Faure, L. Jeanneau, F. Lannuzel

UMR 7566 CNRS G2R, Université Nancy I, BP 239, 54506 Vandoeuvre Lès Nancy Cedex, France
(e-mail: Pierre.Faure@g2r.uhp-nancy.fr)

Different studies have already pointed out the influence of clays during the analysis of pure organic compounds (especially alkanols, alkanolic acids) as well as macromolecules (humic acids) by flash pyrolysis - gas chromatography – mass spectrometry (Nierop and Van Bergen, 2002, Faure et al., 2005). Especially, occurrence of clay minerals favors generation of aromatic units such as alkyl-benzene and polycyclic aromatic hydrocarbons.

So as to better identify the nature of the organic compounds which are sensitive to the presence of clays during analysis, a humic acid (Aldrich ref: H 1,675-2) mixed in variable proportions with a Na-homoionic clay was analyzed by PyGC-MS. The smectite/humic acid mixtures containing from 10% to 100% of humic acid allowed us to identify the progressive disappearance or appearance of specific compounds.

n-alk-1-enes disappear when clay proportion is higher than 67%. For higher content of Na-smectite, n-alkanes becomes less and less abundant with a preferential consumption of high molecular mass n-alkanes. In parallel, the aromatic hydrocarbons proportion increases (figure 1). For 90% of clay mineral, the proportion of aromatic hydrocarbons is higher than 80% whereas this proportion is less than 10% for pure humic acid.

Moreover, the distribution of each aromatic hydrocarbon family (alkyl-benzene and alkyl-naphthalene) has been investigated. Pure humic acid exhibit a specific distribution for these different families. With the increase in clay proportion, these distributions are modified and lead to other distributions controlled by the Na-smectite. As example, 1,2,5-trimethyl-naphthalene which is predominant in the C₃-naphthalene distribution of the pure humic acid, becomes less and less abundant with increasing clay content whereas 1,3,7 and 1,3,6-trimethyl-naphthalenes increase and dominate the C₃-naphthalene distribution when clay proportion is equal to 90%.

The comparison between the pyrograms obtained for 90% Na-smectite / 10% Humic acid mixture and a 90% Na-smectite / 10% undecanoic acid one is quite surprising. Indeed, pyrograms are similar and especially the alkyl-benzene and alkyl-naphthalene distributions. As a matter of fact, clays (Na-smectite in our experiment) in high proportion associated with humic acid modifies the initial product by recombination reactions and leads to the generation of new compounds whatever the initial organic matter nature (simple compounds such as alkanolic acids or macromolecules such as humic acid).

The association of clay minerals and organic matter containing free or bound alkanolic acids or alkanols favors recombination processes during PyGC-MS and the

generation of aromatic units to the expense of aliphatic chains, especially n-alk-1-ene and n-alkanes. Moreover, these recombinations lead to a new distribution independently of the initial organic matter and can induce major analytical artifacts and erroneous interpretations.

Thermally assisted hydrolysis and methylation was already suggested in order to limited recombination processes induce by clay minerals (Faure et al., 2005). However, such results underline the very important catalytic properties of clay minerals on functionalized organic matter during thermal stress. Especially, consequences on industrial treatments (polluted soils depollution by pyrolytic treatments, sewage sludges and waste incineration) and geochemical studies (fossilization) should be evaluated.

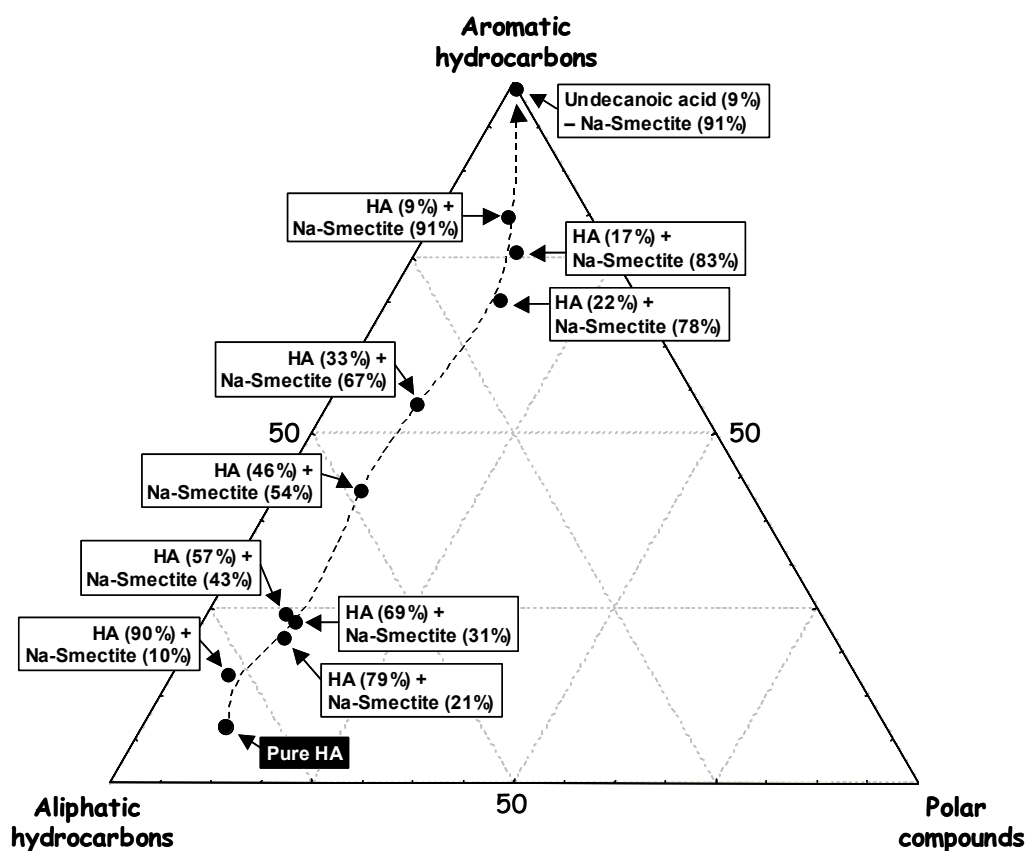


Fig.1. Evolution of the aliphatic hydrocarbons, aromatic hydrocarbons and polar compounds proportion deduce from pyrograms obtained for different Na-smectite/humic acid ratios (HA : Acide Humic) and for 90% Na-smectite / 10% undecanoic acid mixture

References

- Nierop K.J. and Van Bergen P.F. (2002) Clay and ammonium catalyzed reactions of alkanols, alkanolic acids and esters under flash pyrolytic conditions. *J. Anal. Appl. Pyrol.*, **63**, 197-208.
- Faure P., Schlepp L., Mansuy-Huault L., Elie M., Jarde E. and Pelletier M. (2005) Aromatization of organic matter during flash-pyrolysis – gas chromatography – mass spectrometry (PyGC-MS) induced by the presence of clays minerals. A major analytical artifact. *J. Anal. Appl. Pyrol. (in press)*.

PMN1-2: Enhancement of the capability of the laser micropyrolysis GC-MS technique

S.C. George¹, S. Barcikowski², C. McIntyre¹, D. Fuentes¹, R. Sattari², S. Sestak³

1) CSIRO Petroleum, PO Box 136, North Ryde, NSW 1670, Australia (e-mail: Simon.George@csiro.au)

2) Laser Zentrum Hannover e.V., Hollerithallee 8, 30419 Hannover, Germany

3) Planetary and Space Science Research Institute, The Open University, Walton Hall, Milton Keynes, MK7 6AA, United Kingdom

On-line laser micropyrolysis-GC-MS (LaPy-GC-MS) is a technique whereby a laser pulse is used to pyrolyse organic matter or organic materials, and then the resultant pyrolysates are analysed by GC-MS. There are no commercial instruments available, so the few existing instruments have been constructed by laboratories for specific purposes. Typical geochemical applications include chemical analysis of petrographically distinct entities within geological materials, such as macerals, microfossils and solid bitumens (e.g. Stout, 1993; Greenwood *et al.*, 1993, 1998; Yoshioka and Ishiwatari, 2002). Other applications include by-product prediction during laser materials processing (Barcikowski *et al.*, 2000), quality control in petrochemistry as well as in laser-assisted production (Barcikowski *et al.*, 2001), and tissue analysis in laser medicine (Maats *et al.*, 2000). Thus far, however, World-wide efforts to develop LaPy-GC-MS have been dispersed and isolated, and have not led to many significant instrumental break-throughs.

This paper reports on the initial outcomes of collaboration between two of the most active labs doing LaPy-GC-MS, which has resulted in the pooling of resources and ideas, mutual testing of concepts and much quicker advancement and development of the technique (Figure). A set of polymers that were originally analysed on the CO₂ LaPy-GC-MS system have been re-analysed on the Nd:YAG system. For most of these polymers remarkably similar results were obtained, showing that for this application the selection of laser type is not a key constraint. A set of oil shales that were originally analysed by Greenwood *et al.* (1998) will be repeated on the CO₂ LaPy-GC-MS system, and this instrument will also be used to analyse a set of sandstone samples containing oil-bearing fluid inclusions. It is envisaged that the CO₂ laser will be a better method for decrepitating the quartz grains to release oil from the inclusions, because the wavelength of the Nd:YAG laser is rather unsuitable for this application (Greenwood *et al.*, 1998). The advantage of the LaPy-GC-MS approach compared to conventional off-line and on-line methods of oil inclusion analysis are that individual or co-genetic populations of oil inclusions can be analysed selectively.

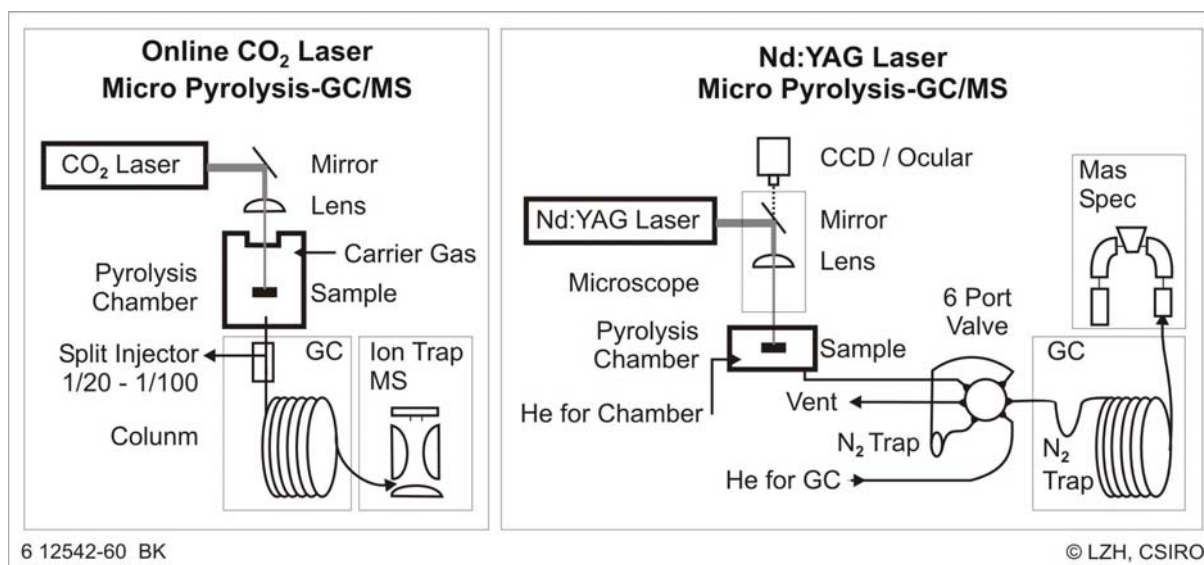


Fig. 1. Schematic setup of CO₂ (LZH) and Nd:YAG (CSIRO) LaPy-GC-MS systems

References

- Barcikowski, S., Feld, A., Goede, M. and Haferkamp, H. (2000) Laser Material Processing in Electronics: Control of Its Environmental Impacts. In: Joint International Congress and Exhibition "Electronics Goes Green 2000+", Berlin, 11-13 September 2000, Proceedings Volume 1, Technical Lectures, VDE Verlag Berlin, 613-617.
- Barcikowski, S., Goede, M., and Haferkamp, H. (2001) Incorporating environmental aspects in quality control of laser material processing. *Laser Opto 04*, pp. 68-71. AT-Fv. GmbH, Stuttgart, Germany
- Greenwood, P. F., Zhang, E., Vastola, F. J. and Hatcher, P. G. (1993) Laser micropyrolysis gas chromatography/mass spectrometry of coal. *Analytical Chemistry* **65**, 1937-1946.
- Greenwood, P. F., George, S. C., Wilson, M. A. and Hall, K. J. (1996) A new apparatus for laser micropyrolysis-gas chromatography/mass spectrometry. *Journal of Analytical and Applied Pyrolysis* **38**, 101-118.
- Greenwood, P. F., George, S. C. and Hall, K. (1998) Applications of laser micropyrolysis-gas chromatography-mass spectrometry. *Organic Geochemistry* **29**, 1075-1089.
- Maats, G., Heisterkamp, A., Lubatschowski, H., Barcikowski, S., Welling, H. (2000) Chemical and physical side effects at application of ultrashort laser pulses for intrastromal refractive surgery. *Journal of Optics A: Pure and Applied Optics* **2**, 59-64.
- Stout, S. A. (1993) Lasers in organic petrology and organic geochemistry, II. In-situ laser micropyrolysis-GCMS of coal macerals. *International Journal of Coal Geology* **24**, 309-331.
- Yoshioka, H. and Ishiwatari, R. (2002) Characterization of organic matter generated from Green River shale by infrared laser pyrolysis. *Geochemical Journal* **36**, 73-82.

PMN1-3: Analysis of ladderane lipids in cultures, water samples, and sediments using HPLC/MS/MS

E.C. Hopmans, M.V.M. Kienhuis, J.E. Rattray, A. Jaeschke, S. Schouten,
J.S. Sinninghe-Damsté

Royal Netherlands Institute for Sea Research, P.O. Box 59, 1790 AB Den Burg, Texel, The Netherlands

Recently, organisms capable of anaerobic ammonium oxidation ('anammox') in waste waters were discovered (Strous et al., 1999). These bacteria of the order Planctomycetales combine ammonium and nitrite directly into N₂. The anammox process takes place in a special compartment ('anammoxosome') of the cell surrounded by a dense bacterial membrane comprised of unique linearly concatenated cyclobutane (ladderane) lipids (Fig. 1) to protect the remainder of the cell from the toxic anammox intermediates and to maintain concentration gradients (Sinninghe Damsté et al., 2002). These lipids give rise to an exceptionally dense membrane, a tight barrier against diffusion, required to maintain concentration gradients during the exceptionally slow anammox metabolism and to protect the remainder of the cell from the toxic anammox intermediates (e.g. hydrazine). Although initial studies have focussed on anammox bacteria from waste water treatment plants, recent findings (Kuypers et al, 2003), using the ladderane lipids as unique tracer lipids, have indicated that anammox also occurs in the marine environment and may represent a quantitative important process for the loss of nitrogen from anaerobic systems.

Ladderane lipids are heat labile and are therefore difficult to analyze by GC/MS, giving poor chromatography and high detection limits. To circumvent these problems, a novel method for analysis of the methylated ladderane fatty acids, using HPLC/MS/MS, was developed. Appropriate sample fractions (either a total lipid extract or fatty acid fraction) were dissolved in acetone. Up to 20 µl was injected onto two Zorbax Eclipse XDB-C₈ columns (4.6 x 150 mm, 5 µm, Agilent), coupled in series. Ladderanes were eluted with 0.4 ml/min methanol. Detection was achieved on a triple quadrupole MS using atmospheric pressure positive ion chemical ionization (APCI) and Selective Reaction Monitoring (SRM). For each target compound, the first quadrupole selects only its protonated molecule ([M+H]⁺). Collision induced dissociation, with argon as collision gas, takes place in the second quadrupole. The third quadrupole then selects several diagnostic daughter ions. In case of the ladderane lipids, daughter ions were chosen that are characteristic fragments of the concatenated cyclobutane moieties of the ladderane molecules. This results in a highly selective method where a response only occurs when collision of a protonated molecule of a

PMN1-4: Hydropyrolysis as a preparative method for the compound specific carbon isotope analysis of fatty acids

W. Meredith¹, C.E. Snape¹, M.A. Sephton², G.D. Love³

1) Nottingham Fuel and Energy Centre, School of Chemical, Environmental and Mining Engineering, University of Nottingham, NG7 2RD, UK.

2) Centre for Earth, Planetary, Space and Astronomical Research, Open University, Milton Keynes, UK.

3) Department of Earth, Atmospheric and Planetary Sciences, Massachusetts Institute of Technology, USA.

The ability to accurately determine the carbon isotopic composition of fatty acids by standard gas chromatography-combustion-isotope ratio mass spectrometry (GC-C-IRMS) techniques would be of great benefit for a variety of geochemical, environmental and biological science applications. Unfortunately, in their natural form, fatty acids display excessive peak tailing and consequent peak overlap, making them unsuitable for accurate compound specific isotope analysis¹. This problem is avoided by derivatisation, but this approach adds extra carbon atoms that can corrupt the original carbon isotope signal of the target molecules².

This study describes the application of the hydropyrolysis technique to the defunctionalisation of individual fatty acids to yield their corresponding *n*-alkanes, thus retaining the carbon skeleton intact and improving chromatography, allowing for the faithful measurement of carbon isotope ratios. Hydropyrolysis, which involves the catalytic addition of hydrogen to the carbon skeleton under a high hydrogen gas pressure (15 MPa), has been developed as a method for liberating covalently bound biomarkers from macromolecular organic fractions in coals, source rocks and crude oils^(3,4).

The carbon isotopic composition (as determined by combustion-IRMS) and chromatographic performance of *n*-octadecanoic acid (stearic acid), was compared to that of the product from the hydropyrolysis at 520°C of the acid adsorbed to silica and impregnated with sulphided Mo catalyst. GC-MS and GC-C-IRMS analyses confirmed a highly selective conversion of the acid to the alkane, with >95% of the product consisting of *n*-octadecane (Fig. 1), indicating the lack of carbon-carbon bond disruption and rearrangement associated with the technique. Such rearrangement would result in the generation of more than one compound, leading to isotopic fractionation and products which do not reflect the isotopic ratio of the original fatty acid.

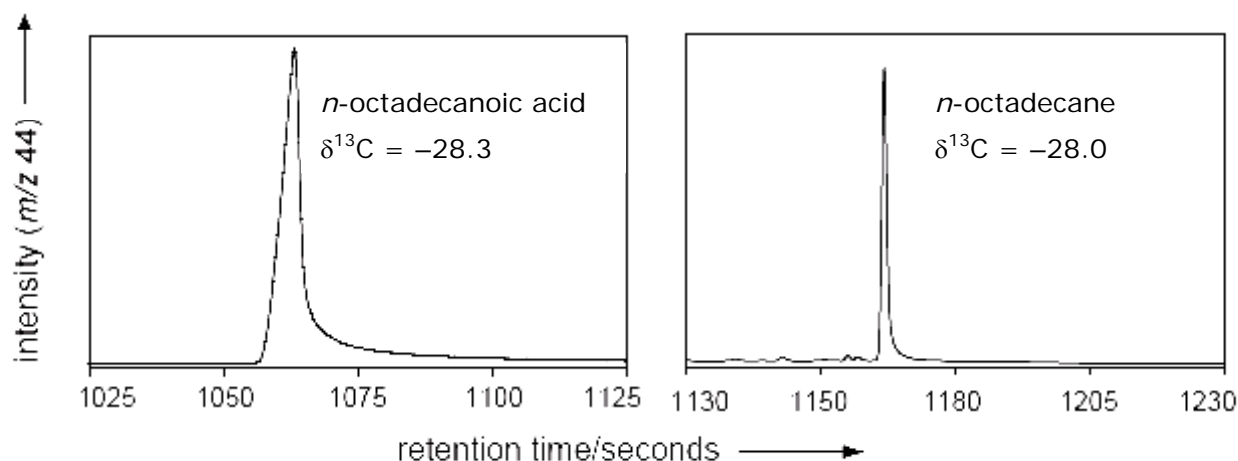


Fig.1. GC-C-IRMS traces of *n*-octadecanoic acid and its hydrolysis product, *n*-octadecane, displaying the expected marked increase in chromatographic performance

Comparison of carbon isotopic determinations for the untreated *n*-octadecanoic acid and the products from hydrolysis by GC-C-IRMS (Fig. 1), indicate that the isotopic composition of the processed sample is consistent with that of the starting material. The difference between the two measurements is within the error of the instruments and it appears that no isotopic effects are associated with the conversion from acid to alkane.

Results from tests with the naphthenic acid, 5 β -cholanic acid generated a similarly highly selective and isotopically consistent product, which demonstrates that the technique clearly allows for the effective determination of carbon isotopic compositions of individual fatty acids without the use of derivatising agents. Further experiments with saturated and unsaturated alcohols and steroids also show that hydrolysis has the potential to defunctionalise structurally more complex compounds as a preparative method prior to analysis by GC-C-IRMS.

References

- [1] Meier-Augenstein, W., 1999. *Journal of Chromatography A* 842, 351-371.
- [2] Ferchaud, V., LeBizec, B., Monteau, F. and Andre, F., 1998. *Analyst* 123, 2617-2620.
- [3] Love, G.D., Snape, C.E., Carr, A.D. and Houghton, R.C., 1995. *Organic Geochemistry* 23, 981-986.
- [4] Love, G.D., Snape, C.E., Carr, A.D. and Houghton, R.C., 1996. *Energy and Fuels* 10, 149-157.

PMN1-5: Removal of olefin based drilling fluids from geologic materials

R.K. Olson¹, H. Dembicki, Jr.², N. Hung¹

1) Baseline Resolution, Inc. 8701 New Trails Drive, The Woodlands, TX USA 77381
(e-mail: bolson@baselinedgsi.com)

2) Anadarko Petroleum Corporation P.O. Box 1330, Houston, TX 77251-1330 USA

Nova Plus is an olefin based ‘synthetic’ drilling fluid. It is widely used in the offshore Gulf of Mexico and use is spreading to other regions of the world. The growing popularity is, at least in part, due to the ever expanding environmental prohibitions on the used of diesel and mineral oil as the base oil for synthetic drilling fluids. The problem with this material (and all hydrocarbon-based mud systems) is that it often represents the majority of the extractable hydrocarbons in cutting and sidewall core samples and it can be the principle hydrocarbon liquid recovered during formation testing.

Baseline, with Anadarko, has developed a procedure that effectively removes approximately 95% of the Nova Plus contaminants from the saturate, aromatic and resin fractions of samples containing this material. Laboratory blends composed of 50:50, 75:25, 95:5 and 99:1 mixtures of Nova Plus and a Gulf of Mexico crude oil were decontaminated using this procedure. The resulting saturate and aromatic fractions of all but the most severely contaminated sample were suitable for all routine geochemical characterization procedures including biomarkers and carbon isotope analyses. In the most severely contaminated samples, the carbon isotope composition was altered by that portion of the Nova Plus which could not be removed.

PMN1-6: An improved method for micro-separation of straight chain and branched/cyclic-alkanes: urea inclusion paper layer chromatography

S. Xu, Y. Sun, X. Mo, P. Chai

SKLOG, Guanzhou Institute of Geochemistry, Chinese Academy of Sciences, Wushan, Guanzhou, 510640, P. R.China (e-mail: shiping@gig.ac.cn)

Separation of straight chain alkanes from branched/cyclic alkanes of a saturated hydrocarbon fraction is a routine work in an organic geochemistry laboratory. A clean sub-fraction is needed in most circumstances for the stable carbon/hydrogen isotopic measurements of individual alkanes and analyses of biomarker assemblages. The well-known methods include 5A molecular sieve and traditional urea adduction. However, the 5A molecular sieving method needs hydrofluoric acid (HF), which is hazardous, to recover the *n*-alkanes from the sieve, whereas using traditional urea adduction, the straight chain fraction usually contains branched material in small but significant amounts and vice versa. Another problem is the quantities of the sample separated. Normally, the abovementioned methods need a certain amount of starting material, at least several milligrams, if you want to get a good result. In many cases, for example: the recent sedimentary samples, environmental samples, high mature source rocks and severely biodegraded oils, this quantity are scarcely available.

In this paper, we describe a convenient paper layer chromatographic method involving urea inclusions for the separation of straight chain and branched/cyclic-alkanes. The result shows a clear separation of straight chain and branched/cyclic-alkanes. The quantity of a sample to be separated in a single operation ranges from 0.05 milligrams up to 100 milligrams and the recovery of material is reasonably good.

Severely biodegraded oil was comparatively separated into straight chain alkane and branched/cyclic alkane fractions by both urea paper layer chromatography and the traditional urea adduction method. As showed in Figure 1, the “*n*-alkane” fraction of traditional urea adduction method contained none of any normal alkane. In fact, this fraction was the original mixture retained in the networks of urea crystals, though in a tiny amount. But a relatively pure normal alkane fraction was still obtained by urea paper layer chromatography, even the sample quantity used was only one third (10 mg) of that used in traditional urea adduction method (30mg). The further GC/MS measurements showed that a clear separation of normal and branched/cyclic alkanes could be achieved by the urea paper layer chromatography because it indeed runs in a chromatography manner.

We also noted that, at room temperatures about 25°C, 10 minutes of standing is sufficient for the completion of inclusion compound formation. The whole procedure is much faster and easier than that of traditional urea adduction method or 5A molecular sieving method. However, the separation was poor at room temperatures below 15°C even the experiment was conducted for 48 hours. It suggested that the high room temperature could accelerate the formation of inclusion compounds. The problem is the high room temperature results in the loss of lighter components. Experimental data showed that the losses of C₁₂ to C₁₅ alkanes were significant and the peak apex shifted two carbon numbers higher compared to the original saturated fraction. To minimize the loss of lighter components, the other operation steps should be carried out in a cooler environment.

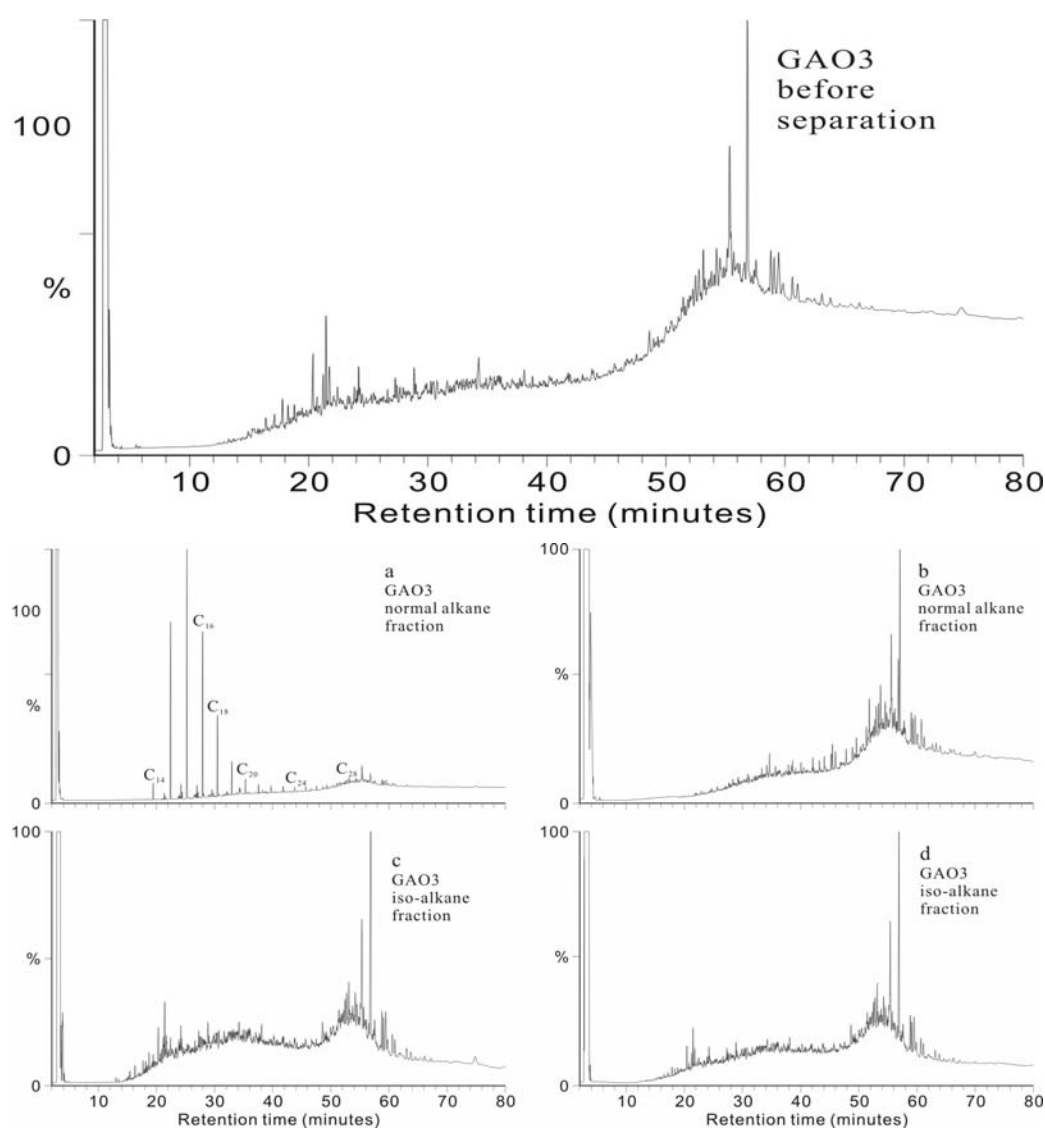


Fig.1. Gas chromatograms of the whole saturated hydrocarbons (above) of sample GAO3, the normal (below, a) and isomeric alkane (below, b) fractions separated by urea paper layer chromatography, the normal (below, c) and isomeric alkane (below, d) fractions separated by traditional urea adduction method

PMN1-7: Development of thermal extraction and thermal extraction-GC instruments for analysis of hydrocarbon pollutants in environmental studies

M. BJORØY, I.L. FERRIDAY, B.B. OLSEN

Geolab Nor AS, Hornebergveien 5, P.O. Box 5740, 7437 Trondheim Norway

The determination of the amount of organic pollutants in sediments has traditionally been undertaken by solvent extraction (dichloromethane or hexane) and weighing of the extract, or by undertaking GC analysis of the extract. Destruction of the used solvent is in itself polluting the environment to a certain degree. Undertaking the analyses in this way is also fairly time consuming since the samples have to be brought back to the laboratory before they can be extracted. Determinations of organic pollutants in sediments have been tried on thermal extraction systems such as Rock-Eval but these systems can only handle small amounts of sample material, up to 100 mg, and it is therefore difficult to get polluted sediment samples sufficiently homogenized such that the analyses can be reproduced.

To avoid such problems two new systems have been developed. The systems are based on the thermal extraction pyrolysis system Geofina Total Hydrocarbon Analyzer (GTHA), Bharati et al, 1993 and the Geofina Hydrocarbon Meter (GHM), BJORØY et al (1992). The injector systems on these are identical and can handle samples up to 2 g. Schematic diagrams of the two systems are shown in Figures 1a and b.

Both systems have been tested extensively with standards made up by mixing various types of oil samples in sand and glacial clay, with standards used for accreditation tests of different laboratories, and real samples from different areas with known pollution and some from non-polluted areas. The results from these tests are summarized below.

The thermal extraction system (EnviroCheck system) give values of the amount of pollutants in samples similar to that found when these were extracted with solvent and the extract weighed. The quantitative determination was undertaken by using external standards and constructing calibration curves. In general there is less than 5 % variation in the amounts determined by the solvent extraction and weighing of extract and those from the EnviroCheck system. The total analytical time for the EnviroCheck system is less than 15 minutes. By installing the system in a road vehicle. e.g. a van, the EnviroCheck system can be used in the field, allowing the samples to be analyzed while they are being collected.

The thermal extraction GC system (EnviroCheck-GC system) gives quantitative results similar to that found when extracting the samples with solvent and undertaking quantitative GC analyses of the extract when using external standards with the EnviroCheck-

GC system. The gas chromatograms show the same patterns for the two methods. In general there is less than 5 % variation in the total amount of pollution between what is determined using the EnviroCheck-GC system and that determined by solvent extraction and GC analysis of the extract. The system has been tested with a number of different pollutants. It is possible to determine not only the amount of pollutants but also to identify different pollutants based on retention time etc.

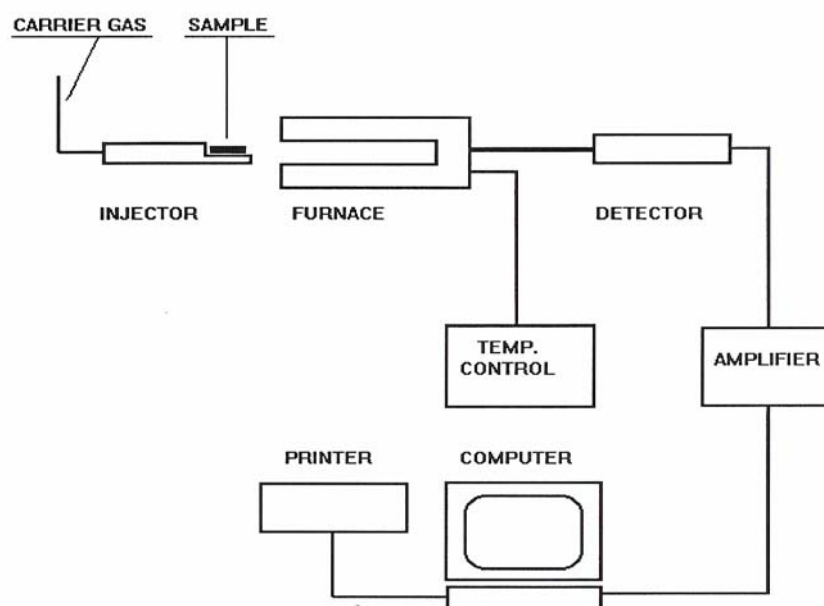


Fig.1.a. Schematic diagram of the EnviroCheck system

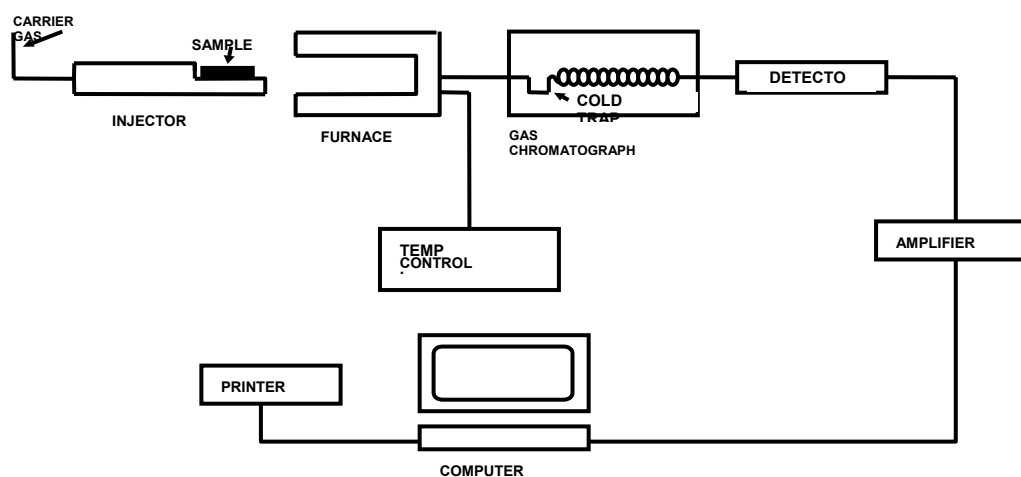


Fig.1.b. Schematic diagram of the EnviroCheck-GC system

References

- Bharati, S., Hall, K., Bjorøy, M. and Leplat, P. 1993. Geofina Total Carbon Analyser (GTHA): Its application, use and scope in the Petroleum industry. Organic Geochemistry Poster Session, 1993 (Ed. Kjell Øygard, Falch Hurtigtrykk, Oslo. pp 781 - 784
- Bjorøy, M., Hall, K., Hall, P.B. and Leplat, P. 1992. Detailed hydrocarbon analyser for well site and laboratory use. Marine and Petroleum Geology, 1992, vol 9, pp. 648 – 665.

PMN1-8: Analysis and characterisation of dissolved organic nitrogen in aquatic environment

H. Gallard, S. Ambonguilat, Y. Touchard, B. Parinet, J.-P. Croué

Laboratoire de Chimie de l'Eau et de l'Environnement UMR CNRS 6008, 40 avenue du Recteur Pineau 86022 Poitiers cedex, France (e-mail: herve.gallard@univ-poitiers.fr)

Quantification and characterization of dissolved organic nitrogen (DON) in aquatic environment is a crucial issue for environmental sciences and water treatment engineering. In the environment, DON plays a major role in nutrient cycles, participates in metal complexation by natural organic matter (NOM) and can be an indicator of NOM origin. In drinking water treatment, DON would contribute to membrane fouling and N-containing organic compounds are disinfection by-products precursor when chlorine is used.

Actually, DON is quantified by the difference between TDN (total dissolved nitrogen) minus DIN (dissolved inorganic nitrogen). Because DIN, essentially nitrate, can represent more than 95% of the TDN for human-impacted waters, samples should be pre-treated to eliminate DIN before DON determination. The objective of this study was first to propose and validate a pre-treatment technique for DON determination.

TDN and dissolved organic carbon (DOC) were analysed using a Shimadzu TOC-V_{CSH} analyser with the TNM-1 TN unit (high temperature combustion of NOM and chemiluminescent detection of NO_x). Nitrate and nitrite were analysed using ion-pair chromatography and ammonium ion using ion chromatography. Catalytic reduction of nitrate into nitrogen gas using bimetallic palladium-based catalysts was first investigated. Experiments performed in ultra-pure water showed a rapid reduction of nitrate with about 80% conversion into nitrogen gas. For nitrate solutions containing 20 mg/L DOC, nitrate was totally reduced within 1 hour but DIN was not decreased significantly (~100% conversion into ammonium). Also, DON adsorbed onto catalysts, which probably explained the lower conversion of nitrate into nitrogen. Therefore, this technique was not further investigated and dialysis pre-treatment, proposed by Lee and Westerhoff (2005), was tested.

Dialysis was conducted with cellulose ester dialysis tube (nominal molecular weight cut-off = 100 daltons) using synthetic solutions prepared with nitrate and NOM isolates. Results showed 50% elimination of nitrate within 24 hours of dialysis from MilliQ water. Nitrate was almost totally eliminated after 120 hours of dialysis and DOC remained constant. For high DIN content surface waters dialysis pre-treatment allowed DON determination with good accuracy whereas subtracting DIN from TDN led to negative values before dialysis. DON from different French surface waters ranged from 0.2 to 2.9 mgN/L and were affected by algae growth and discharge of waste water supporting that DON is a microbial waste product.

DON characterization was performed on 34 isolates extracted from surface waters (NOM isolates) and waste water treatment plant effluents (EfOM isolates) using dialysis (colloid fractions: > 3500 daltons) and the combination of XAD-4 and XAD-8 non-ionic resins. Isolates were dissolved in ultra pure water (20 mg/L). Both DOC and DON contents were found similar to the values expected from elemental analysis. Amino sugars and amino acids content were determined after acid hydrolysis (6 N HCl, 6 hours) using HPLC and precolumn derivatization (AccQ.Tag Waters method). Neutral amino acids were dominant in all isolates. Hydrophobic fractions were enriched in aromatic amino acids compared to hydrophilic fractions. Amino acids and amino sugars represent 1.5 to 34% and 0.02 to 10% of DON, respectively. Colloid fractions from WWTP were enriched in amino sugars and amino acids compared to colloid fractions from surface waters (“natural colloids”). Isolates were also characterized using UV₂₅₄ absorbance, fluorescence excitation-emission matrix mapping and size exclusion chromatography (SEC) coupled with UV ($\lambda = 260$ nm) and fluorescence detection. Fluorophore specific to soluble microbial by-product-like ($\lambda_{\text{excitation}} = 278$ nm and $\lambda_{\text{emission}} = 315$ nm) was monitored. Nitrogen detection (Antek 8060 analyser) coupled with SEC was also evaluated. All experimental data were interpreted using principal component analysis (PCA) and NOM and EfOM isolates were represented in PC1-PC2 plane. The first component was determined by the abundance of amino acids and amino sugars reflecting biologically active material and logically discriminated EfOM isolates. The second component represented the gradient in the humic character and discriminated different clusters corresponding successively to humic, non humic fractions and finally natural colloids that lied in the negative region. Nitrogen content was not correctly represented in the PC1-PC2 plane (i.e. no correlation with specific amino compounds and humic parameters). Non humic fractions and the natural colloids were characterized by high nitrogen content and the presence of fluorophores specific to soluble microbial products, confirming that DON would be associated with microbial activity, amino acids and amino sugars being probably degraded into unknown nitrogen containing compounds in aquatic environment.

Acknowledgments

This research was supported by a grant from the American Water Works Association Research Foundation (project 2900).

References

Lee W., Westerhoff P. Dissolved organic nitrogen measurement using dialysis pre-treatment. Environmental Science and Technology. In press

PMN1-9: Total Scanning Fluorescence (TSF) as an effective screening tool for delineating oil families

K. Liu¹, S.C. George², S. Li³, X. Pang³, S. Fenton¹, H. Volk², M. Ahmed²

1) CSIRO Petroleum, P.O. Box 1130, Bentley, WA 6102, Australia (e-mail: Keyu.Liu@csiro.au)

2) CSIRO Petroleum, P.O. Box 136, North Ryde, NSW 1670, Australia

3) University of Petroleum, China, Changping, 102249, China

Crude oils and fluid inclusion oils (FIOs) from two oil producing basins in China and Australia were investigated using the Total Scanning Fluorescence (TSF) technique in conjunction with biomarker and isotope geochemical analysis. The oils differ in their API gravities and SARA compositions, with the Chinese oils having low to medium gravities (15-30°) and high polar contents (30-40%), and the Australian oils having high gravities (35-55°) and high saturated hydrocarbon contents (~80%). The aromatic hydrocarbon contents for both groups of oils are similar. These oils have been derived from a wide range of marine, lacustrine and terrestrial source rocks. This study shows that TSF spectra are able to differentiate oil families of different source origins and maturities.

Edwards et al. (2004) defined three oil families in the Vulcan Sub-basin (Timor Sea, NW Australia), and TSF spectral signatures of these three oil families (Table 1) are different, in particular the parameter TSF R_1 of Brook et al. (1986).

The oils from multiple oil fields in the Jiyang Basin (east China) have TSF parameters which correlate well with biomarker parameters. The parameter R_1 correlates with $Ts/(Ts+Tm)$ ($R^2 > 0.75$), and there is also a correlation between TSF and some source-dependent biomarker parameters (e.g. Gammacerane/ C_{30} $\alpha\beta$ hopane, $C_{29}Ts/C_{30}$ $\alpha\beta$ hopane, Σ steranes/ Σ hopanes) ($R^2 > 0.6$). For sample sets from single fields, the correlation coefficients were as high as 0.93 (R^2), and there is a very strong correlation between the thermally-controlled biomarker ratio $Ts/(Ts+Tm)$ and the TSF parameter R_1 (Fig. 1). The Vulcan Sub-basin oils and FIOs have relatively high $Ts/(Ts+Tm)$ ratios and low TSF parameter R_1 but show a similar correlation as the Jiyang Basin oils except for the Group B oil, which exhibits distinct TSF spectral signature.

This study demonstrates that TSF can be used as a rapid and cost-effective screening technique for analysing crude oils and FIOs for thermal maturity and possibly source relationships prior to committing to detailed biomarker and isotopic analysis. Once calibrated for a particular basin, TSF signatures can be used to estimate the characteristics of reservoired and fluid inclusion oils.

Table.1. TSF parameters for three oil families identified by biomarkers and stable isotope geochemical data (Edwards et al., 2004). Two TSF peaks (1st and 2nd) were selected to characterise the spectra using the Excitation/Emission pairs

Oil Family	1 st λ_{\max} (nm) (Excitation)	1 st λ_{\max} (nm) (Emission)	2 nd λ_{\max} (nm) (Excitation)	2 nd λ_{\max} (nm) (Emission)	TSF R ₁ [#]
Group A	236	346	268	363-368	1.4-1.9
Group B	236	341-346	280-282	327-330	0.7-0.8
Mixed oil*	234; 258-260	344, 365-368	268, 280	335, 368	0.9; 2.0-2.2

* mixed with Group A and B and an unknown oil; #R₁=ratio of emission intensity at 360 nm to emission at 320 nm when excitation at 270 nm is used (after Brook et al., 1986)

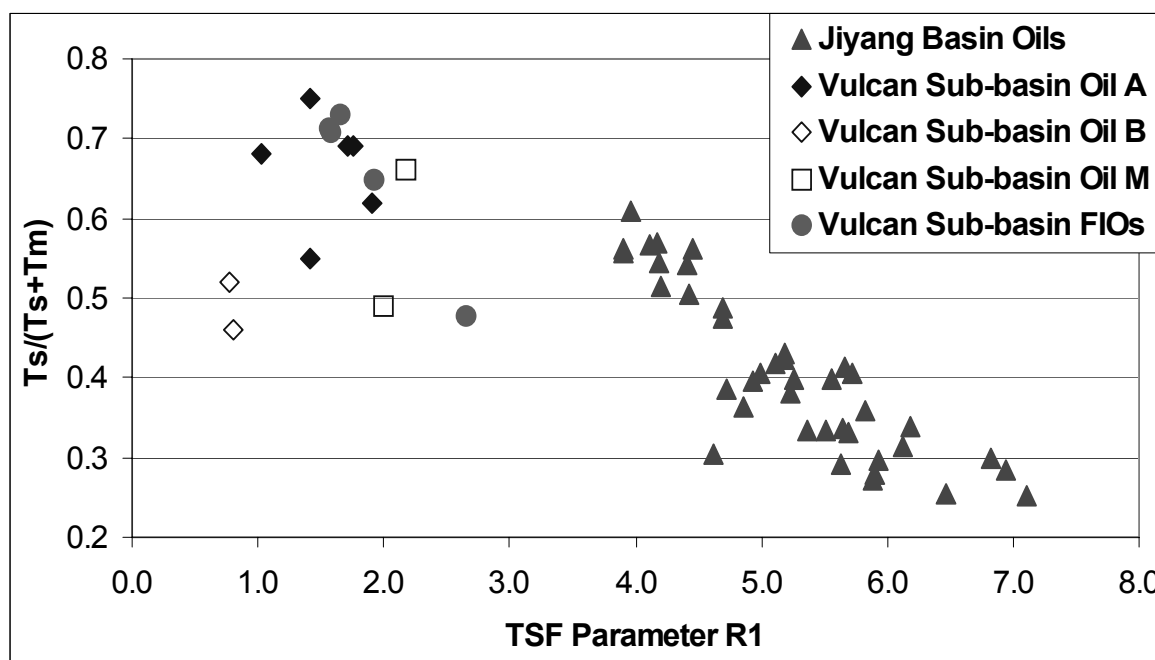


Fig.1. Maturity dependent biomarker, Ts/(Ts+Tm), plotted against TSF parameter R₁ for reservoir and fluid inclusion oils from the Vulcan Sub-basin, northwest Australia and Jiyang Basin, east China. Oil A, B and M refer to Group A, B and Mixed oil families

References

- Brooks, J. M., Kennicutt, M. C. and Carey, B. D., 1986. Offshore surface geochemical exploration: Oil and Gas Journal, October, 66-72.
- Edwards, D.S., Preston, J.C., Kennard, J.M., van Aarssen, B.G.K., Boreham, C.J. and Zumberge, J.E., 2004. Geochemical characteristics of hydrocarbons from the Vulcan Sub-basin, Bonaparte Basin, Australia, In: Ellis, G., Baillie, P.W. and Munson, T.J. (eds), 2004, Timor Sea Petroleum geoscience, Proceedings of the Timor Sea Symposium, Darwin, NT, June, 2003, 169-201.

**PMN1-10: Monofluorinated polycyclic aromatic hydrocarbons and dibenzothiophenes as internal standards.
Introduction of a new method of PAH analysis**

G.M. Luthe^{1,2}, H. Liu¹, G. Reijerink^{1,2}, J.E. Johansen¹

1) CHIRON AS, Stiklestadveien 1, 7041 Trondheim, Norway

2) The Norwegian University of Technology, Trondheim, Norway

We have recently synthesized a series of monofluorinated polycyclic aromatic hydrocarbons (F-PAHs[®]) and benzothiophenes, dibenzothiophenes (F-PASHs) and found that they provide a promising set of internal standards for geochemical and petroleum analysis. Fluorine substitution has two antagonistic effects: the creation of a dipole moment and the reduction of the London forces. As a result, F-PAHs[®] are largely similar to the corresponding non-fluorinated PAHs and PASHs in terms of physico-chemical properties

PAH analysis is routinely carried out in various types of samples because of their carcinogenic properties and their use as biomarkers in the geochemical field. In this presentation we address the suitability of F-PAH[®] as internal standards in PAH analysis during sample preparation and for liquid and gas chromatography. Because of the strength of the fluorine-carbon bond F-PAHs are highly resistant to scrambling. Additionally, there is no known occurrence in nature.

Our investigations with F-PAH[®] showed a high similarity to the corresponding parent PAHs in physico-chemical properties and retention times in both GC and LC analysis. This prompted us to study in greater detail their usefulness as internal standards in analytical chemistry. In this presentation we will demonstrate that F-PAH[®] are suitable as internal standards for a broad range of analytical applications including clean-up procedures for PAHs in waste-water using solid-phase extraction (SPE), for soil samples using pressurized liquid extraction (PLE) and for the use in PAHs and PASHs analysis in the petroleum industry.

Our experiments confirm the applicability of a mixture of 1-fluoronaphthalene, 3-fluorophenanthrene and 2-fluorodibenzothiophene as a suitable internal standard mixture for the analysis of NPD (naphthalene, phenanthrene and dibenzothiophenes) in water and in petroleum/source rock samples. The advantages of monofluorinated compounds over more commonly used standards like the deuterated and C13 labelled will be discussed.

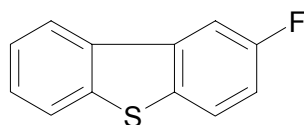


Fig.1. 2-Fluorodibenzothiophene, a useful internal standard for dibenzothiophene analysis

PMN1-11: Enhanced SARA compositional analysis of whole oil

S.R. Palmer, P. Walker, B. Olson

Baseline Resolution, 8701 New Trails Drive, The Woodlands, TX 77381 (e-mail: SPalmer@brilabs.com)

The determination of the weight percent saturates, aromatics, resins and asphaltenes in petroleum samples is used to monitor gross compositional relationships between samples and to help predict the flow and fouling characteristics of those samples, both as individual samples and as mixtures.

The traditional separation of a crude oil into its saturate, aromatic, resin and asphaltene fractions involves a precipitation of asphaltenes with a low molecular weight n-alkane (typically pentane or heptane) and then the open column chromatography of the deasphalted oil into saturates, aromatics and resins using a series of solvents of increasing polarity. To quantify the various fractions the solvent has to be removed. Unfortunately, this process also evaporates any indigenous volatile components of the crude oil resulting in an overall low recovery. To address this problem, the initial step in the SARA process is to top the oil for several hours to days at an elevated temperature prior to analysis so as to give a more stable initial sample. Unfortunately, it is not uncommon for crude oils and condensates to lose 50% or more of their weight during the topping procedure and this significant amount of material escapes characterization with the traditional SARA method. This can be clearly observed by gas chromatography of a typical oil before and after this topping. (see Figure 1). The result is a SARA compositional analysis that does not reflect the composition of the whole oil.

In this paper a technique that allows us to recalculate the SARA composition by proportionally adding back the saturate and aromatic components lost to evaporation is discussed. The technique uses a combination of gas chromatography, an abbreviated topping procedure and a modified SARA process to better characterize the composition of the whole oil samples. The resulting SARA composition more accurately reflect the relative abundances of saturate, aromatic, resin and asphaltene components in the original oil being produced at the wellhead and this should lead to better predictions of flow and fouling behavior.

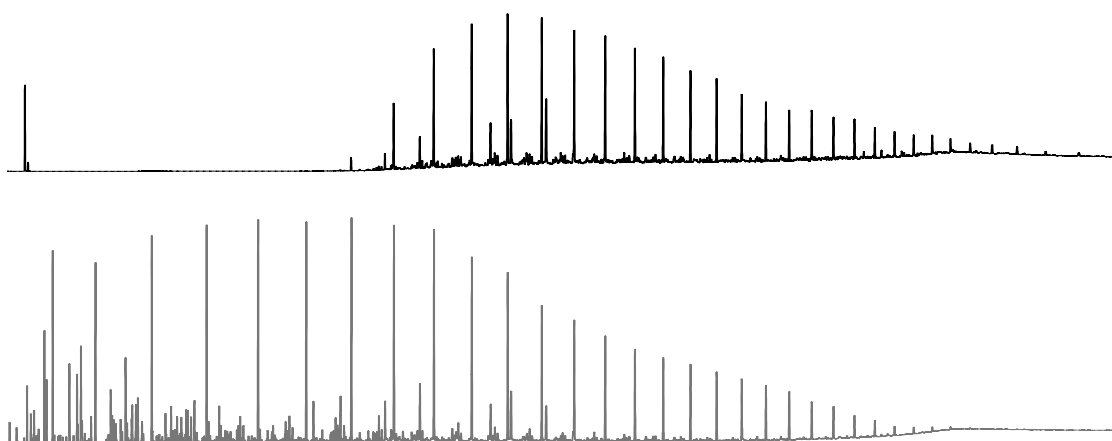


Fig.1. Gas chromatographs of a typical crude oil, before (bottom) and after (top), normal topping procedure adopted as part of traditional SARA compositional analysis

PMN2-1: Fluorescence indexes: new criteria for the characterisation of dissolved organic matter in aquatic environments

E. Parlanti, L. Vacher

Laboratoire de Physico-Toxicochimie des Systèmes Naturels - LPTC UMR 5472 CNRS - Université Bordeaux 1 - 351 cours de la Libération - 33405 Talence Cedex - France (e-mail: e.parlanti@lptc.u-bordeaux1.fr)

Dissolved organic matter (DOM) consists of a mixture of macromolecular compounds with wide ranging chemical properties and diverse origins. It participates in many physical, chemical and biological reactions in aquatic systems and has been reported to affect the transport and fate of pollutants in the environment. The processes affecting DOM through estuaries are of major importance for a better understanding of its influence on regulating the estuarine behaviour of contaminants.

The aim of this work was to apply fluorescence spectroscopy for the study of different aquatic environments in order to investigate the evolution of DOM properties during estuarine mixing. Aquatic ecosystems such as freshwaters, seawaters and estuaries were studied.

Fluorescence spectroscopy enables to distinguish humic substances from recent biological organic compounds in water samples. In order to discuss the results of the fluorescence analysis of the different samples, we considered the ratios of the intensities of the main fluorescence bands ($I_{\alpha'}/I_{\alpha}$, I_{β}/I_{α} and I_{γ}/I_{α}).

Peak	Excitation max. (nm)	Emission max. (nm)	Component type
α	330-350	420-480	Humic-like
α'	250-260	380-480	Humic-like
β	310-320	380-420	Marine humic-like
γ	270-280	300-320	Tyrosine / Tryptophane -like, protein-like or phenol-like

Zsolnay et al. introduced in 1999 a humification index (HIX) in order to estimate the maturation of DOM in soils. This index is the ratio H/L of two spectral region areas from the emission spectrum scanned for an excitation at 254 nm. These two areas are calculated between emission wavelengths 300 and 345 nm for L and between 435 and 480 nm for H. We applied for the first time this index to aquatic environments. Referring to this humification index HIX proposed by Zsolnay et al., we built another parameter BIX (biological index) to characterize the autochthonous inputs (biological origin) to DOM. This new index is the ratio of emission fluorescence intensities $I_{em=380nm} / I_{em=430nm}$ for an excitation at 310nm.

Spatial and temporal variations of DOM spectroscopic properties were investigated. Fluorescent DOM exhibited specific trends in the studied estuaries (especially Gironde, Loire and Seine estuaries in France) depending on environmental conditions (salinity, maximum turbidity zone MTZ, seasons) and in marine waters (especially in Atlantic Ocean). Seasonal variations of DOM were observed in the Seine estuary where higher contents of humic substances and dissolved organic carbon (DOC) were found during the winter season while fluorescent biological organic material was produced upstream and downstream of the MTZ during the summer. Humic substances represented the major fraction of DOM in the very turbid Gironde estuary although biological production was very important for salinities higher than 25 all year long. Seasonal variations of the HIX parameter were observed with lower values in winter and the highest one obtained in summer. The HIX maxima were determined in the Loire estuary and in the Gironde MTZ. We can then conclude that the DOM was more humified in this particular zone of the Gironde estuary. The seasonal variation of BIX along this estuary was less significant than for HIX. However the highest values were obtained in summer. The more marine waters (Salinity>30) were characterized by similar values of this parameter independently of the season.

This work showed that the use of fluorescence intensity ratios, and especially I_{γ}/I_{α} ratio, HIX and BIX parameters, was particularly well adapted to the characterisation of DOM in marine and coastal environments. The number of samples studied from different environments (freshwaters to pure marine waters, under various conditions) allowed us to draw up a scale of values for each index. These new criteria for the characterisation of DOM in aquatic environments will be very useful and can be proposed as an easy way to define DOM characteristics in such ecosystems.

References

Zsolnay A et al., 1999. Differentiating with fluorescence spectroscopy the sources of dissolved organic matter in soils subjected to drying. *Chemosphere*, 38 (1), 45-50.

PMN2-2: Nanogram-scale stable isotope analyses by “nano-EA-IRMS”P. Polissar, C.H. Turich, K.H. Freeman

Department of Geosciences, The Pennsylvania State University, University Park, PA

Continuous flow (CF) analyses of the C, N, H and O isotopic composition of bulk organic materials are routinely accomplished using an elemental analyzer (EA) coupled to an isotope-ratio mass spectrometer (IRMS). Elemental analyzers typically employ helium flow rates of 50 to 150 cm³/minute, and yet only ~0.2 cm³/min of this flow is transferred to the ion source of the IRMS. The minimum sample size required for acceptable analytical precision is ultimately a function of the ionization efficiency of the instrument and the relative abundance of the rare isotope. In current practice, sample requirements are artificially high because of the high carrier gas split ratios. Although typically some adjustment can be made to the relative flow rate of gas through the EA and into the ion source, in most instrument configurations, the lower limit on sample size is constrained by the minimum acceptable helium flow in the EA and the maximum flow rate that ion source pumps can accommodate.

In order to reduce dramatically the minimum sample size for EA-IRMS analyses, we have designed a system that traps sample gas (CO₂, N₂, H, and CO) from a high-flow EA effluent; the trapped gas is then introduced into a low-flow helium stream (1 cm³/min). The sample gas is focused into a narrow band by trapping it at the head of a 0.25mm i.d. silica capillary column. It is then released into the low-flow helium stream, separated from other gases by the capillary column and 0.2 cm³/min of this flow directed to the mass spectrometer. This system significantly reduces the minimum sample size required for EA analysis by both increasing the height/width ratio of the analyte peak (taller peaks for an equivalent sample size) and decreasing the EA/IRMS split ratio from between 250:1-750:1 to ~5:1. The lower split ratio increases the peak area by 50-150x while the improved peak shape increases peak height by ~2x. The net effect is a 100- to 300-fold decrease in sample size.

Our primary motivation for the development of the nano-EA is to facilitate isotopic analyses of trace quantities of large compounds extracted from natural samples such as intact membrane lipids and pigment-derived tetrapyrrole compounds. We have focused on large lipids δ D analyses because of our interest in reconstructing past signatures of environmental waters. Archaeal tetraether lipids are an excellent target for past δ D composition because Archaea are ubiquitous in the world's oceans and lakes and surface-dwelling organisms appear to be the dominant source of sedimentary ether lipids. The lipids are too large ($m/z =$

1292-1302) for volatilization by conventional GC, and methods that cleave ether-linked isoprenoid cores from the lipids can cause significant hydrogen exchange. The nano-EA-IRMS allows us to analyze small amounts of individual lipids separated and collected using liquid chromatography. Other applications for δD analysis using this system potentially include atmospheric water vapor, VOCs, and other trace materials.

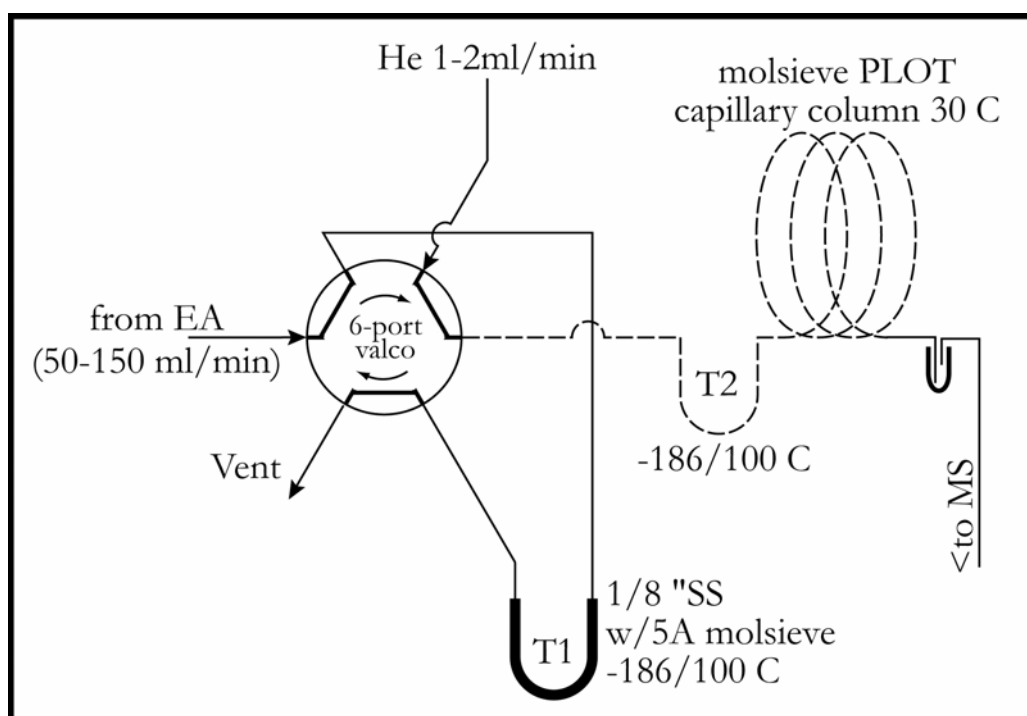


Fig.1. Schematic diagram of the nano-EA continuous-flow inlet system. Note that the analyte is trapped in a 1/8" stainless steel tube cooled to liquid nitrogen temperatures (-186 °C). For hydrogen gas, the trap is filled with 5A molecular sieve powder. Nitrogen and CO₂ are trapped on silica gel. On the low-flow side, we use a 5A molecular sieve PLOT column to trap and separate H₂ gas. For CO₂ or N₂, a HP-PLOT Q column is the best choice to trap and separate these gases

PMN2-3: Comparative study of results in Mexican samples of rock using the Rockeval II and Rockeval 6

L. Ramírez G., R. Martínez A., N. Cañipa M.

Instituto Mexicano del Petróleo, Parque Industrial Canacintra, Mineral de la Reforma, Hgo., México, C.P. 42083

The technology is developing very quickly nowadays in an amazing race, and the tools for oil exploration are developing simultaneously too. Rock Eval 6 determinations about organic matter type, source rock potential, maturity and depositional environment have been used for years

In the beginning the Rock Eval I it was a quickly technique for the determination of the petroleum potential, but it was less practice to use, due to manually flow controls. Later a new Rock Eval appeared in the market: the Rock Eval II + TOC, an automated version where the apparatus was easy to use, the time of analysis of this instrument was relatively faster in about 30 min. and the results were obtained. During many years this apparatus was used like a needed powerful tool for oil exploration.

In the last years the new version of this instrument is the Rock Eval 6, it has IR cells for the determination of the S3 peak and TOC content, besides it has some significant improvements like: the temperature for oxidation reaches the 850°C unlike the Rock Eval II, which it just reached to 650°C, this means a more complete oxidation in the Rock Eval 6.

Due to this improvements the Rock Eval 6 is a more fine, precise apparatus, and it has the option for programming multi heating ramps, this situation was not possible with Rock Eval II.

In this work a comparison study between the results obtained from Rock Eval II and 6 for mexican samples is made, in order to evaluate the advantages and limitations in the integration of the results on both instruments in the study of petroleum systems and plays. For this purpose a serial o real samples were analyzed for Rock Eval II and the same for Rock Eval 6, finding certain minimal differences in some cases S1, S2 S3 peaks, Tmax, PI, and PC parameters. For the TOC important differences were found, a 20 to 30 % more in the case of the Rock Eval 6. This is because Rock Eval 6 performs a more complete oxidation, and for the calculation of the Total Organic Carbon IR cells for CO and CO₂ are used, unlike the Rock Eval II use a TCD detector.

Minimal differences exists in the value of Tmax for pyrolysis between the 2 instruments, in spite of the temperature detectors in the case of the Rock Eval 6 are better positioned on it, giving a very precise temperature of pyrolysis. Some differences in the S2 value were found (petroleum potential), for the S1 peak there is no significant variation.

By these reasons, it is very important to bear in mind the results before integrating directly the data obtained from Rock Eval II and Rock Eval 6 models.

PMN2-4: A novel method for the determination of the acidity of crude oils using ^{13}C -labelled iodomethaneN. Rouquette¹, P. Schaeffer¹, I. Kowalewski, A. Fafet², D. Levaché³, P. Albrecht¹

1) Laboratoire de Géochimie Bio-organique, UMR 7509 du CNRS, Ecole de Chimie, Polymères et Matériaux, Université Louis Pasteur, 25 rue Becquerel, 67200 Strasbourg, France (e-mail: pschaeffer@chimie.u-strasbg.fr)

2) Direction Géologie – Géochimie, Institut Français du Pétrole, 1 et 4, Avenue de Bois Préau, 92852 Rueil-Malmaison Cedex, France

3) Total Exploration Production, avenue Larribau, 64018 Pau Cedex, France

Nowadays, the majority of the petroleum reservoirs under exploitation contains conventional crude oils. However, because of the constant increase of petroleum consumption, oil companies are more and more looking for alternative sources of fossil energy, such as extra heavy oils, heavily biodegraded oils, tar sands or bituminous shales. Exploitation of such oils is more difficult than conventional petroleum, due to their corrosive properties which results in the premature aging of the pipelines and the implementation of specific and expensive postprocessing procedures. Corrosion is notably thought to be associated with the presence of acidic organic compounds occurring in crude oils, and a standard method, called TAN (for Total Acid Number), based on potentiometric titration was established to quantify the acidity of the crude oils (ASTM D 664-95). TAN values typically found in the literature range from 0.1 to 8.0 mg KOH.g⁻¹ crude oil, the values higher than 0.5 being generally characteristic of acidic crude oils. Since 1 to 20 grams of crude oil are required for titration using this method, it is not possible to evaluate the acidity of samples present in low amounts such as, for instance, organic extracts from drilled cores. Furthermore, this method is not very well adapted in the case of very heavy oils which are difficult to render soluble in toluene and propanol as described in the ASTM-D 664-95 method. Thus, we have developed a new method based on the methylation of carboxylic acids using ^{13}C -labelled methyl iodide. This method, which is easy to handle and which can be carried out on small amounts of crude oil -as low as 20 mg of material-, is based on the fact that incorporation of ^{13}C -labelled methyl groups will be accompanied by an increase of the value of the $^{13}\text{C}/^{12}\text{C}$ ratio as compared to the non-methylated oil. The relative difference between the stable carbon isotopic composition of the reacted and unreacted oils can thus be determined by isotope ratio mass spectrometry (IRMS) and is expected to be proportional to the number of acidic functionalities which underwent methylation.

We have initially tested this method on one series of crude oils from the same source rock (oils A-F ; Table 1) but which are biodegraded to different extents and which exhibit different TAN values (the lowest TAN values being associated with the less biodegraded oils). It can be clearly seen from figure 1 that there is a good linear correlation ($R^2=0.992$) between the TAN values and the isotopic enrichment ($\Delta\delta^{13}\text{C}$) of these oils (filled squares in fig. 1), suggesting that the extent of ^{13}C -labelling is indeed proportional to the number of acidic functionalities. In order to further confirm these results, we have analysed additional

oils from various types and origins (Table 1). On average, there is also a relatively good linear correlation between the isotopic enrichment of the majority of the oils investigated and the TAN values, notably in the case of oils originating from the same source rocks (e.g., oils G-I ; black triangle in fig. 1). There are, however, a few exceptions, like, for instance, the oil Q which is a heavy and immature oil rich in heteroatoms. In this case, it is possible that other functionalities than carboxylic acids reacted with ^{13}C -labelled iodomethane, and contributed therefore to the abnormalous isotopic enrichment measured. This new approach based on ^{13}C enrichment and using low amount of material (few mg of oil) could be used at an early stage of reservoir characterization using core samples to assess the acidity of the C_{14+} fluid in place in order to optimize the production facilities.

Table 1. Main characteristics of the different oils investigated

<u>Crude oil</u>	<u>Type</u>	<u>TAN value</u>	<u>Crude oil</u>	<u>Type</u>	<u>TAN value</u>
A ¹	II	0.38	M	I	0.15
B ¹	II	1.24	N	?	1.20
C ¹	II	1.59	O	?	2.08
D ¹	II	1.90	P	?	1.01
E ¹	II	2.37	Q	II	1.50
F ¹	II	3.73	R	?	1.18
G ²	II	1.20	S	?	4.10
H ²	II	1.10	T	II	2.60
I ²	II	1.50	U	?	2.80
J	II	0.26	V	?	0.87
K	III	0.17	W	?	1.80
L	I	0.90			

^{1,2} genetically-related oils

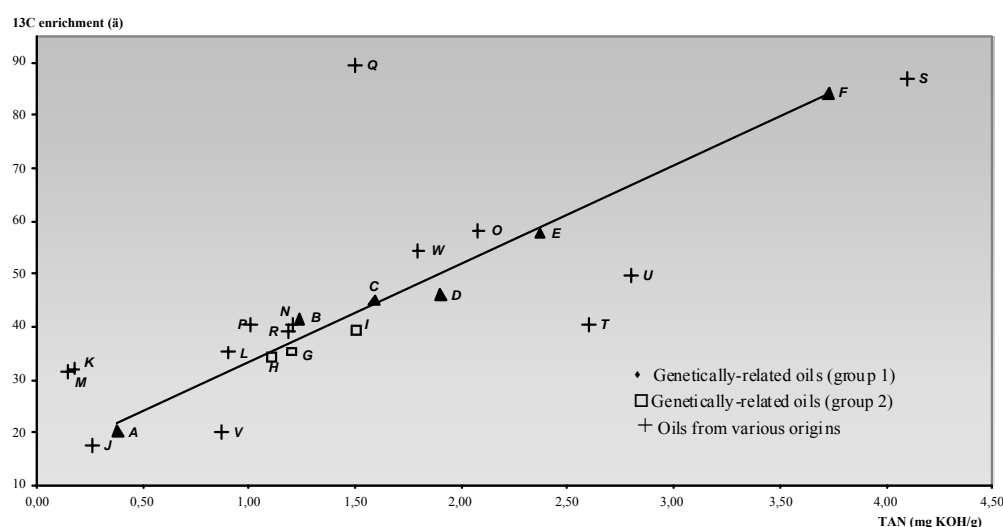


Fig.1. Graph showing the correlation between isotopic enrichment and TAN values for various oils

PMN2-5: Systematic Statistical Effects of Sample Collection Method on Geochemistry of Petroleum Compounds

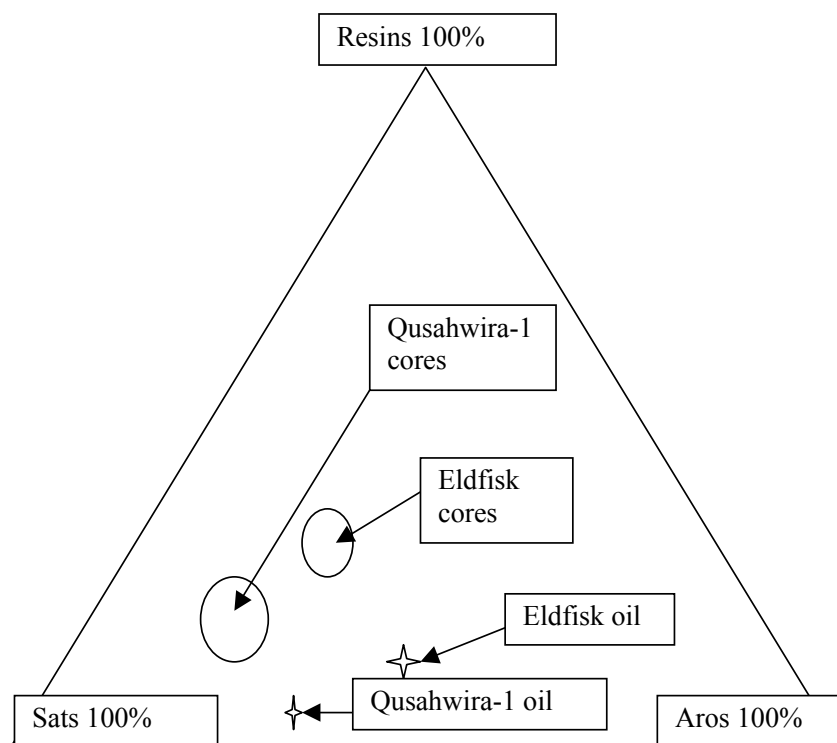
S.A. Baylis

University of Newcastle upon Tyne, Wishmoor House, 147 Hales Road, Cheltenham, GL52 6TD, UK (e-mail: sarahbaylis2000@hotmail.com)

Many geochemical parameters are biased, or at least influenced, by the type of sample from which they are derived. Geochemical analysis of reservoir core extract fluid is often used for characterisation in exploration when no produced or test sample is available. Samples of tested or produced petroleum and samples recovered by solvent extraction from cores obviously have broadly similar geochemical characteristics, but consistent differences have been observed between them (Baylis, 1998). These differences include the relative enrichment of non-hydrocarbons in samples extracted from cores with a polar solvent such as dichloromethane, compared with samples of well test fluids.

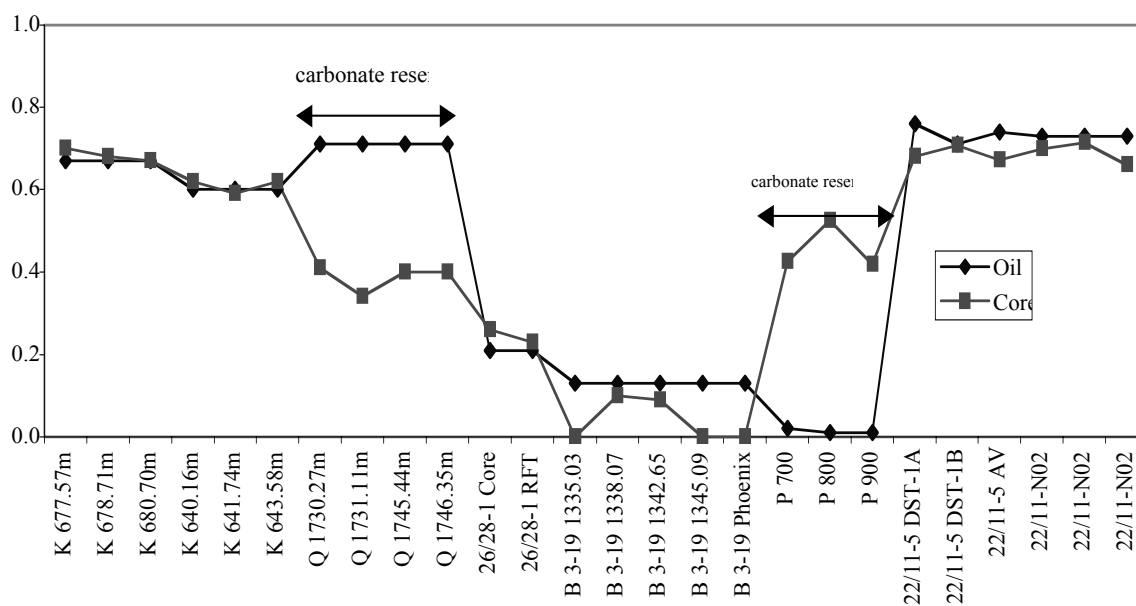
Simple statistical analysis was undertaken on the geochemical data generated during this study: a Pearson's χ^2 calculation was performed on the two sample sets (oils and core extract samples from six different reservoirs ranging from North sea clastic regimes to Middle Eastern carbonate systems) and the equation for the least squares line of regression was calculated. The gradient and the y intercept indicate any proportional relationship between the data sets and any offset or bias in the data arising from different sample types. The values calculated for χ^2 show that the content of both the aromatic hydrocarbon compounds and the resins of the core extract samples are statistically significantly different from those of the crude oils.

Particular differences were identified, for example, in the compound class distributions, especially in samples from carbonate reservoirs such as those plotted on the ternary diagram below (Eldfisk from the Norwegian North Sea and Qusahwira-1 from the Middle East):



Polar compounds adsorb on to mineral surfaces during secondary migration affecting the bulk petroleum composition: these data indicate that this is more pronounced in carbonate reservoir systems. Other parameters are discussed, some of which also show greater variation in carbonate reservoirs, for example, the extent of cracking of aromatic steranes used as a maturity indicator as defined by the ratio:

$$\frac{C_{20} \text{ triaromatic sterane}}{C_{20} \text{ triaromatic sterane} + C_{28} \text{ 20R triaromatic sterane}}$$



PMN2-6: The Optimization of Amino acid Derivatisation for GC-C-IRMS for Biogeochemical Applications

L.T. Corr, R.P. Evershed

Organic Geochemistry Unit, Bristol Biogeochemistry Research Centre, School of Chemistry, University of Bristol, BS8 1TS, UK

Stable carbon and nitrogen isotope analysis of bulk organic compounds (e.g. proteins) represents a highly sensitive technique for tracing the sources and fate of organic matter in biogeochemical processes. By adopting a compound-specific isotope approach, via GC-C-IRMS (gas chromatography-combustion-isotope ratio mass spectrometry) analysis, we can elucidate the various biosynthetic and diagenetic pathways of protein amino acids which were previously obscured by bulk isotope measurements. However, amino acids are non-volatile polyfunctional molecules which require derivatisation prior to GC-C-IRMS analysis. Until recently, trifluoroacetyl-*i*-propyl (TFA-IP) esters were the derivative of choice for $\delta^{13}\text{C}$ measurements in the Bristol laboratory. However, in our experience, and that of others¹, the gaseous HF generated on combustion of these fluorinated derivatives results in irreversible poisoning of the combustion catalyst. In an attempt to surmount this problem, we investigated the performance of 7 alternative derivatisation techniques with respect to (i) reaction yield, (ii) sample-to-derivative carbon ratio, (iii) chromatographic resolution, (iv) errors associated with $\delta^{13}\text{C}$ measurements as a result of kinetic isotope effects and (v) stability.

We derivatised a mixture of 17 amino acid standards as acetyl methyl esters (ACME), trifluoroacetyl-*i*-propyl esters (TFA-IP), *n*-acetyl *i*-propyl esters (NAIP), *n*-acetyl *n*-propyl esters (NANP), *n*-pivaloyl methyl esters (NPME), *n*-pivaloyl *i*-propyl esters (NPIP), *n*-pivaloyl *n*-propyl esters (NPNP) and *tert*-butyldimethylsilyl esters (*t*BDMS) and subjected them to GC and GC-C-IRMS analysis. Since amino acids are medium polarity compounds our approach was to investigate whether baseline resolution (which is imperative for reliable isotope measurements) could be enhanced on more polar GC columns. For this purpose the 8 amino acid derivatives were analysed on a range of commercially available GC columns, ranging from non-polar to medium and high-polarity stationary phases (cp-sil 5CB, ZB-5, ULTRA-2, VF-23ms, ZB-WAX, ZB-FFAP), in addition to a chiral column (Chirasil-Val). The 7 derivatisation techniques exhibited various advantages and disadvantages. For example, high reaction yields and superior chromatographic resolution for 17 amino acids was observed for NPNP and NPIP esters; however, these derivatives exhibited a low sample-to-derivative carbon ratio, because the sample carbon comprises a mean of only 34.2% of the derivatised

amino acid. Contrarily, while only 12 amino acid peaks were observed for ACME esters, the error associated with their $\delta^{13}\text{C}$ measurements was low because of their high sample-to-derivative carbon ratio (mean 56.6%). For all derivatives enhanced chromatographic resolution was observed on the more polar stationary phases, with optimal chromatography achieved using the VF-23ms column (see Figure 1). Ultimately, it was concluded that the NAIPs represented the optimal derivative because of their relatively high sample-to-derivative carbon ratio, well-resolved peaks, stability and low errors associated with their $\delta^{13}\text{C}$ measurements. Importantly, precise isotope measurements were achieved for the NAIP derivatisation of between 5 and 1000 μg of amino acid; for example, a standard deviation of 0.7‰ across the weight range was observed for glycine.

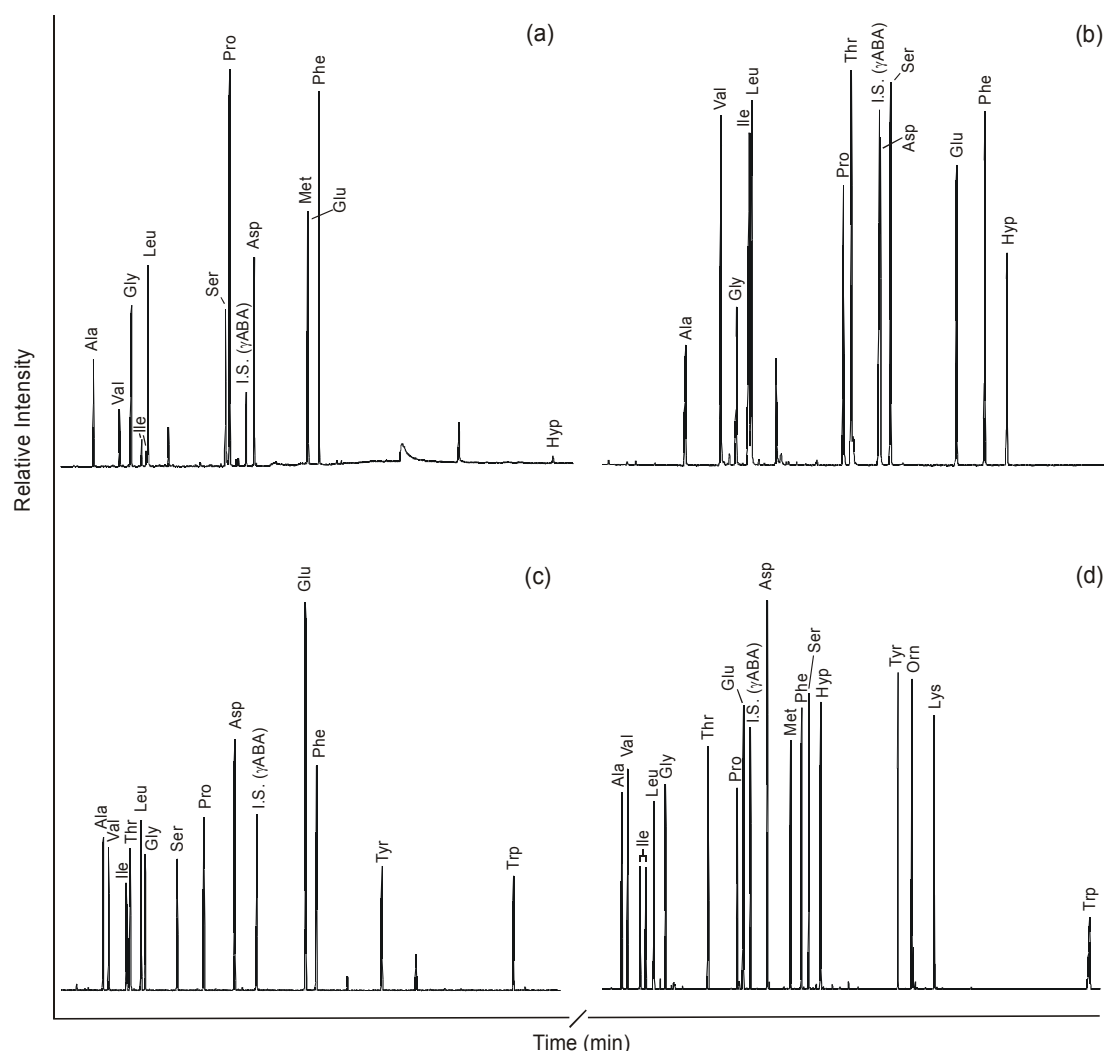


Fig.1. Total ion currents of amino acid standard mixtures derivatised as (a) acetyl methyl esters (ACME), (b) *n*-acetyl *i*-propyl esters (NAIP), (c) trifluoroacetyl *i*-propyl esters (TFA-IP) and (d) *n*-pivaloyl-*n*-propyl esters (NPNP)

References

- ¹Hofmann, D. *et al.*, *Isot. Environ. Healt. S.* **2003**, 3 (39), 233-244.

PMN2-7: Use of thermogravimetric-isotope ratio mass spectrometry to investigate C isotopic homogenisation of wheatstraw during growth of the oyster mushroom (*Pleurotus ostreatus*)

E. Lopez-Capel, G.D. Abbott, D.A.C. Manning

School of Civil Engineering & Geosciences, University of Newcastle, Newcastle upon Tyne, UK, NE1 7RU

Systematic changes in the composition of wheatstraw used as a substrate for the growth of the oyster mushroom (*Pleurotus ostreatus*) have been reported previously¹. In this paper, we report the results of an investigation of the carbon isotope composition of the same sample suite, using thermogravimetric analysis coupled to an isotope ratio mass spectrometer (TG-IRMS²). The weight loss observed for specific temperature intervals allows the relative proportions of different bulk constituents to be estimated, with simultaneous determination of carbon isotope ratios.

Using C/N ratios, increases in fungal biomass (C/N = 8) in wheatstraw (initial C/N = 57) compost are shown in Figure 1a, and changes with time in the ratio of carboxyl/carbonyl C determined by NMR¹ in Figure 1b. There is a corresponding decrease in the weight loss attributable to cellulosic material, and an increase in that attributed to lignin (Figure 1c). Absolute weight losses are dominated by the loss of cellulosic material, from 50% at time = 0, and 25% at 63 days. The absolute weight loss for components decomposing at higher temperatures is constant (30%).

C isotope data (Figure 1d) show clearly that the wheatstraw is isotopically heterogeneous at 0 and 28 days. The cellulosic component (230-330°C) has $\delta^{13}\text{C}$ values of -24 ‰, and the lignin component (450°C) is approximately 2 ‰ more negative, as seen in fresh plant material³. After 28 days, all $\delta^{13}\text{C}$ values are at least 1 ‰ less negative, reflecting loss from the substrate of ¹²C, and show similar internal heterogeneity. After 63 days, the substrate is isotopically homogeneous (with respect to C), with $\delta^{13}\text{C}$ values of -21 ‰.

The observed increases in $\delta^{13}\text{C}$ for cellulosic components can be accounted for by degradation of half the cellulose with associated loss of ¹²C from the system; lignin contents remain constant¹. The observed increase in $\delta^{13}\text{C}$ for lignin (up to 5 ‰, compared to 3 ‰ for cellulosic material) cannot be explained as loss of ¹²C using Rayleigh distillation models (fractionation factors would have to differ for the two fractions, or much more lignin would have to have decomposed). Thus the isotopic homogeneity of the wheatstraw after 63 days relates to the formation of new material that preserves a ¹³C-enriched isotopic signature. As shown in Figure 1a, new mycelial matter has been formed in the compost, and the observed

$\delta^{13}\text{C}$ values reflect the composition of this newly-formed material, consistent with other work on plant degradation products⁴.

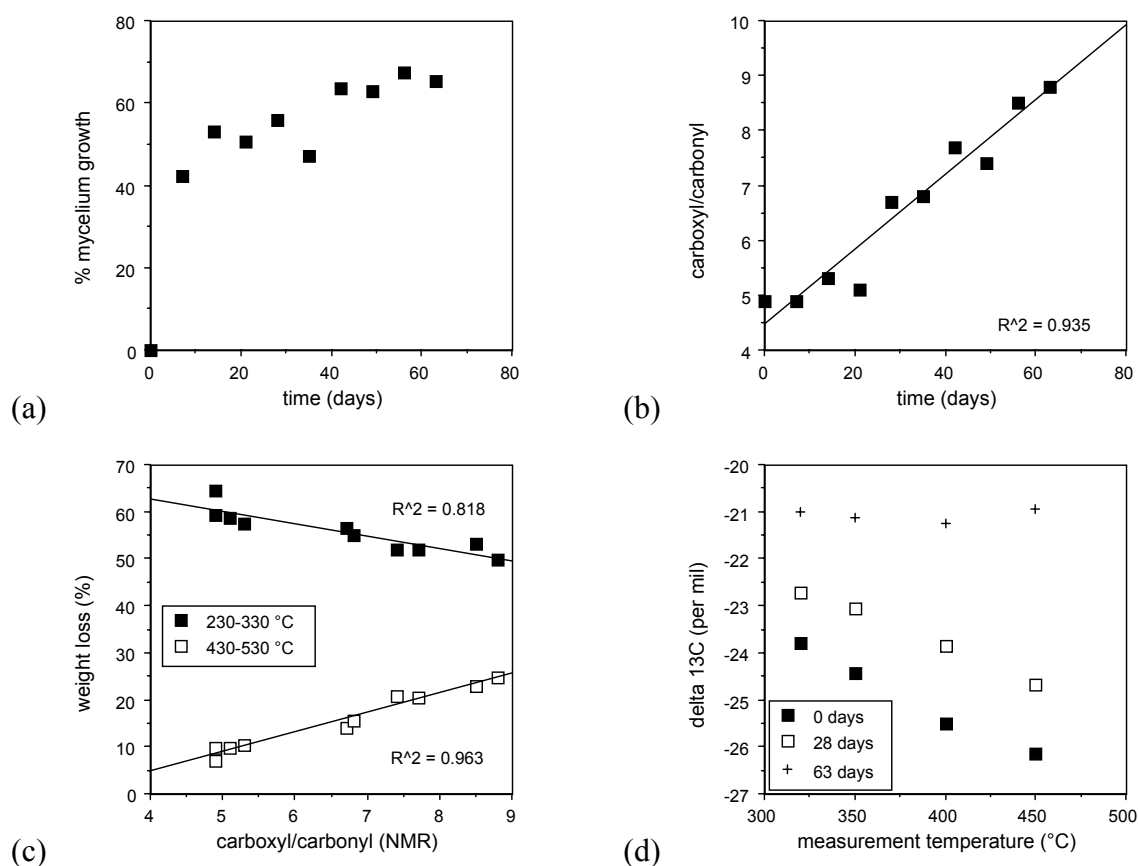


Fig.1. Changes with time observed for (a) fungal biomass¹ and (b) carboxyl/carbonyl ratio, compared with (c) weight loss due to degradation of 'cellulose' (230-330°C) and 'lignin' (430-530°C) components and (d) observed carbon isotope ratios at different degradation temperatures

References

- 1) Vane, C. H., Martin, S. C., Snape, C. E. & Abbott, G. D. 2001. *J. Agric. Food Chem.*, 49, 2709-16.
- 2) Lopez-Capel, E., Abbott, G. D., Thomas, K. M. & Manning, D. A. C. *J. Anal. App. Pyrolysis*, in press.
- 3) Marshall, J. D. & Monserud, R. A. 1996 *Oecologia*, 105, 13-21.
- 4) Gleixner, G., Danier, H. J., Werner, R. A. & Schmidt, H. L. 1993 *Plant Physiology*, 102, 1287-1290.

PMN2-8: Optimization of the programmable pyrolysis method in Rockeval 6

R. Martínez A., L. Ramírez G., N. Cañipa M.

Instituto Mexicano del Petróleo, Parque Industrial Canacintra, Mineral de la Reforma, Hgo., México, C.P. 42083
(e-mail: rayala@imp.mx)

There is a great demand of oil all over the world, due this situation the chances of discoveries in petroleum exploration relies on a good analytical tools for helping oil exploration, using a detailed characterization of the possible source rocks to locate oil and/or gas fields. The determination of the petroleum potential from the source rocks, maturity and the determination of kinetics parameters in core and cutting samples is one of those powerful analytical tools, performed by Rock Eval 6 apparatus.

Pyrolysis technique consist in an artificial thermal maturation of rock using heating cycles. This technique have been used for around 20 years, it has become a standard in the hydrocarbon exploration, and the Rock Eval 6 is the latest version of this kind of instruments.

The Rock Eval 6 has new important improvements and innovations like: quantification of the pure organic matter and mineral carbon, a better precision in the measurement of the temperature, it allows the acquisition of data for the calculation of kinetics, and it permits a good characterization of the TOC and Tmax (specially pure organic matter and coal). The Rock Eval 6 has infrared cells of CO and CO₂ for the calculation of the S3 peak, TOC and mineral carbon content.

An important quantity of samples (core, cuttings and outcrops) are analyzed every year in the Pyrolysis Lab at the IMP, using a basic heating cycle for pyrolysis phase from 300 °C to 650 °C, with a heating rate of 25 °C/min. On the other hand, for the oxidation phase a heating rate of 20°C/min is used, with a heating cycle of 300 °C to 850 °C allowing a better combustion of the sample.

The time of analysis takes about 1 hr approximately, and with the goal to optimize time and resources, a series of tests have been made between three Rock Eval 6 instruments modifying the heating rate for oxidation.

Multiple analysis of Standard IFP 160000 were done for validating the study, and to make a comparison between real samples and the standards, using the basic cycle and the modified cycle for oxidation phase.

According to the results obtained from these tests, the optimum value for the heating rate is 30 °C/min, with this modification equivalent results are obtained like in the original basic cycle. The significant contribution of this work is the reduction of analysis time in about 10 minutes, obtaining satisfying reproducible and repetitive results for the three Rock Eval 6 instruments.

PMN2-9: SARA Fractionation of poor bitumen extracts by solid phase extraction

J. Téllez¹, S. Capella², L. Castro³, N.K. Cañipa¹, C.R. Aldana¹, C.A. Zuñiga¹

1) Laboratorio de Geoquímica Orgánica, Instituto Mexicano del Petróleo, carretera Pachuca – Cd. Sahagún kilómetro 7.5, Parque Industrial “La Reforma”, Pachuca, Hgo., C.P. 42083, México

(e--mail: jmarquez@imp.mx)

2) Facultad de Química, Universidad Nacional Autónoma de México, Av. Universidad 3000, C.P. 04510, Col. Universitaria, México, D.F

3) Instituto Mexicano del Petróleo, Eje Central Lázaro Cárdenas Nte. No. 152, Col. San Bartolo Atepehuacan, Del. Gustavo A. Madero, C.P. 07730, México D.F

Analysis by CGC-FID and CGC-MS of the principal families of compounds obtained from SARA fractionation of rock extracts give important information about maturity, original matter and depositional environment and also it allows correlating with oils and other bitumens. However, traditional fractionation process employs deasphalted sample previous to the HPLC separation into saturated, aromatic and polar compounds, and requires at least hundred miligrams of rock extract for complete process. Poor rock extracts (less than 1.4 mg/g rock) of low quantity of sample available are not candidate for SARA fractionation with this traditional process, reducing the information needed for interpretative purposes.

An easy and rapid methodology (time analysis is approximately 2 ½ hours) was developed for SARA fractionation, using NH₂ and Silica phase impregnated with AgNO₃. The Solid Phase Extraction (SPE) methodology has been tested with oils (heavy, light, and very light oil) and rock extracts, showing that it can be use successfully for both kind of samples with comparable results to those obtained with HPLC techniques.

Minimum sample requirement (less than 20 mg of rock extract) makes this SPE method an important alternative to get CGC-FID and CGC-MS information of the principal families obtained from SARA fractionation, where deasphalting and HPLC can not be used. Besides, the sample preparation time is shorter, less solvent is wasted and simultaneous sample processing is possible.

PMN2-10: Separation of methane from gas mixtures as a technique of preparation for hydrogen isotopic analysis

H. Yoshioka, S. Sakata

Institute for Geo-Resources and Environment, National Institute of Advanced Industrial Science and Technology, 1-1-1 Higashi, Tsukuba 305-8567, Japan

We developed a line system for separation of methane from gas mixtures in order to determine stable isotopic compositions of methane. Carbon and hydrogen isotopic compositions of methane in natural environments provide important information about the origin of methane: values of the isotopic compositions help us interpret not only whether it is microbial or thermogenic, but also what kind of pathways methanogens employed to produce methane. Especially, hydrogen isotopic composition of methane is believed effective to discriminate two primary pathways in natural environments: CO₂ reduction and acetate fermentation (Whiticar et al., 1986). Although many hydrogen isotopic values of methane collected from fields and experiments were reported in previous studies, there has been some technical difficulty yet to be overcome: appropriate amount of purified methane, i.e., several ml STP, is necessary to obtain a reliable hydrogen isotopic value. It would be very difficult to collect appropriate amount of methane from fields or experiments if gas is diluted with atmosphere and concentration of methane is very low. Separation and collection of methane from coexisting gas components is, therefore, an essential technique for determining hydrogen isotopic composition of methane.

A line system that we developed for this purpose is shown schematically in Fig. 1. Gas mixture (including N₂, CO₂, H₂, and CH₄) in a glass bottle with stop valves at both ends is admitted with carrier gas (He) into the line system. With manual operation of one 2-way-valve I and two 6-way-valves I and II, the gas phase is allowed to pass first through a H₂O trap filled with magnesium perchlorate and a CO₂ trap filled with ascarite, and then collected in a trap filled with activated charcoal cooled down to -80 °C. The released methane is carried through a Porapak Q column in a GC, and passed through a 2-way-valve II, and admitted selectively to a combustion tube filled with CuO heated at 900 °C. The products of CO₂ and H₂O were separated by the method of cryogenic distillation using liquid nitrogen and dry ice, and collected for analysis of carbon and hydrogen isotopic composition, respectively. We could successfully separate and collect methane from headspace gas in which the concentration of methane was below 1%, and determine the carbon and hydrogen isotopic compositions.

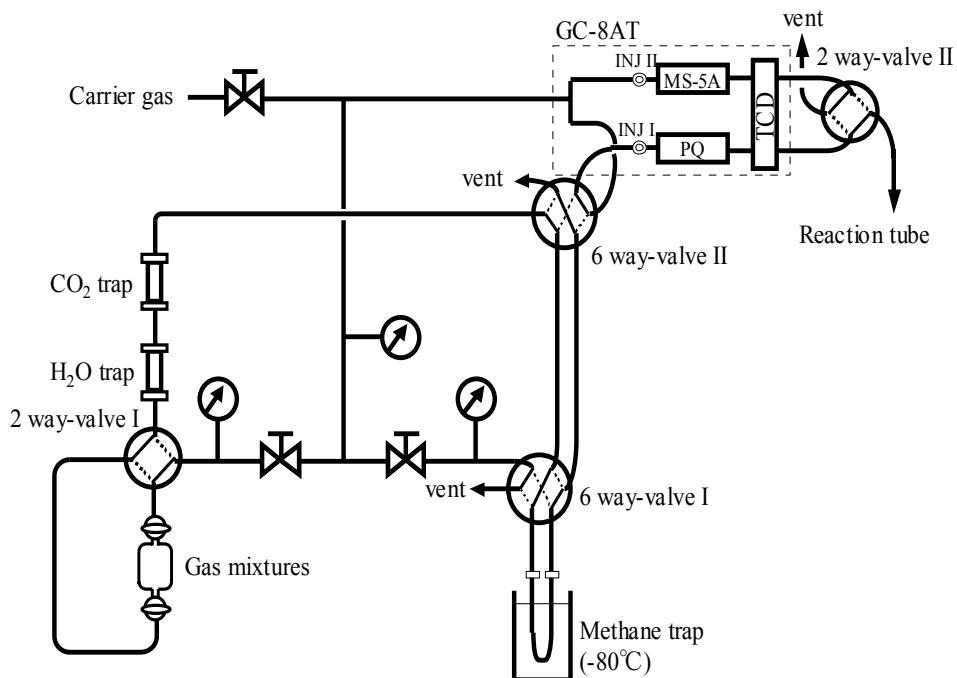


Figure 1

References

Whiticar M. J., Faber E. F., Schoell M., (1986) *Geochim. Cosmochim. Acta* **50**, 693-709.

PMN2-11: Direct analysis of polar fractions of heavy crude oils using a Finnigan LTQ FT hybrid mass spectrometerV. Zabrouskov¹, M. Senko¹, T. Moehring², H. Muenster²

1) Thermo Electron Corporation, 355 River Oaks Parkway San Jose, Ca, USA

2) Thermo Electron Corporation, Hanna Kunath-Str. 11 28199 Bremen, Germany

(e-mail: thomas.moehring@thermo.com)

Biodegraded oils are dominating the world petroleum inventory in form of heavy oils and tar sands. Therefore effective production and processing of heavy petroleum becomes increasingly important. The properties of heavy oils (API gravity, acidity, viscosity etc.) are strongly related to their molecular composition, especially to the composition of the polar fraction containing a complex mixture of heterocomponents (NSO-compounds). The characterization of these components is mainly based on chromatographic separation followed by mass spectrometric analysis (GC-MS, LC-MS)¹. Recent work by Marshall and co-authors demonstrated the unique utility of high field (9.4 Tesla) ESI-FTICR mass spectrometry for direct analysis of crude oil. Determination of the elemental composition of more than 3000 compounds in a single experiment became possible due to ultra-high resolving power of the FTITCR MS and its high detection limits². Here we used a Finnigan LTQ FT with a 7 Tesla magnet to directly analyze polar compounds in heavy petroleum.

The analysis of a South American heavy crude oil sample using a resolving power of 200,000 (FWHM at m/z 400) in positive and negative mode reveal the presence of more than 5,000 ion signals belonging to chemically different compositions. Figure 1a shows the positive ESI spectra containing singly charged ions distributed from m/z 200 to 800 with a maximum around m/z 462. The spectrum is dominated by series of signals with a clear 14.016 amu repeat unit attributed to $-CH_2$ -periodicity. The combination of the excellent mass accuracy (better than 2 ppm with external calibration) and high resolving power allows for determination of the elemental formulas of multiple isobaric signals which is exemplarily show for a narrow segment of the spectrum (Figure 1b, Table 1).

Besides the direct analysis the LTQ FT is also capable for LC-MS analysis providing the same mass accuracy and resolving power on chromatographic time scales which makes it an ideal tool for petrochemical analysis.

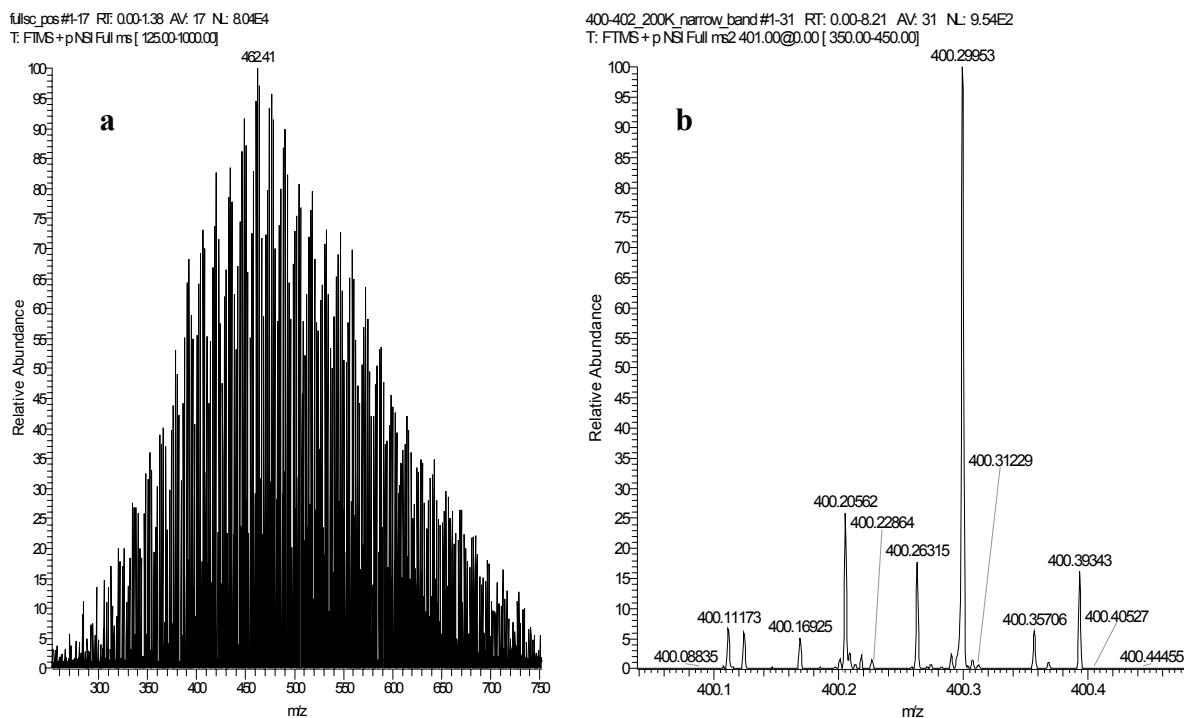


Fig.1. (a) Positive ESI Spectrum of a South American heavy crude oil sample acquired with a resolving power of 200,000; (b) narrow segment of the spectrum around m/z 400

Table 1. Table of the suggestion for the elemental composition of signals shown in Figure 1b

m/z	Elemental composition	Theoretical mass	Error (ppm)
400.11173	$C_{31}H_{14}N$	400.11208	-0.9
400.16925	$C_{29}H_{22}NO$	400.16959	-0.9
400.20562	$C_{30}H_{26}N$	400.20598	-0.9
400.22863	$C_{27}H_{30}O_2N$	400.22711	-0.7
400.26315	$C_{28}H_{34}NO$	400.26349	-0.9
400.29053	$C_{29}^{13}C_2H_{36}N$	400.29094	-1.1
400.29953	$C_{29}H_{38}N$	400.29988	-0.9
400.35706	$C_{27}H_{46}NO$	400.35739	-0.8
400.39343	$C_{28}H_{50}N$	400.39378	-0.9

References

- Willsch, H., Clegg, H., Horsefield, B., Radke, M., Wilkes, H. 1997. Liquid chromatographic separation of sediment, rock and coal extracts and crude oil into compound classes. *Analytical Chemistry* 69, 4203-4209.
- Qian, K., Robbins, W.K., Hughey, C.A., Cooper, H.J., Rodgers, R.P., Marshall, A.G. 2001. Resolution and identification of elemental compositions for more than 3000 crude acids in heavy petroleum by negative-ion microelectrospray high-field Fourier Transform Ion Cyclotron Resonance Mass Spectrometry. *Energy & Fuels*, 15, 1505-1511.

AUTHOR INDEX**A**

Abbas: OP2-1, PB1-10, PB1-11, PMP-1
 Abbott: PM-17, PM-22, PMN2-7
 Abdullah(F.H): PRG2-1
 Abdullah(W.H): POS2-10, POS2-8
 Abliia: PGG2-10, PGG2-11, PGG2-12
 Abolins: PBS-14, POS2-8
 Abrajano: PEB1-14
 Adam: OGPR-1, OP6-3, PB2-6
 Adams: PG-18
 Afanasenkov: PPM-4
 Affouri: POS2-14
 Agogu  : PMP-20
 Aguiar: PBS-13, PRG1-14
 Aguirre: PSB-2
 Ahmad: PM-1
 Ahmed(A.S): PEB1-18
 Ahmed(M): OP5-2, PMN1-9, PRG2-20
 Aitken: PRG2-2
 Aizenshtat: PM-1, POS1-1, POS1-2, POS1-3
 Akalin: PRG1-19
 Akin: PFA-7
 Al Darouich: OPG-1
 Albaig  s: PEB2-4, PEB2-5
 Albardeiro: OPE1-3
 Alb  ric: PB1-19, PBG1-9, PM-11
 Albrecht: OGPR-1, OP6-3, PB2-6, PC2-11, PFA-6, PFA-8, PGG2-7, PMN2-4
 Aldana: PMN2-9
 Alexander: PB1-5, POS1-4
 Alexeev: PGG1-6
 Alimi: POS1-10
 Almendros: OSB1-3, PBC-14, PBC-9, PSB-18
 Alsaab: PC-7
 Allen: PEB2-7
 Ambl  s: PM-24, PM-27
 Ambonguilat: PMN1-8
 Amijaya: PC-8
 Amrani: PM-1, POS1-1, POS1-2, POS1-3
 Andersen: PBS-22
 Anderson(B): PBG1-3
 Anderson(R): OB2-3
 Andersson: PBG2-12
 Andjelkovic(D): PSB-1
 Andjelkovic(T): PSB-1
 Andreeva: PEB1-11
 Aneke: OP4-3
 Anischenko: PBG1-7
 Anowai: OP4-3
 Antipenko: PRG1-1

Antonias: OOS-2
 Anuar: PBS-14
 Araujo: POS1-7
 Arbelo: PCS-1, PCS-9
 Arias: PBC-6, PM-25
 Armas: PCS-1, PCS-9
 Arnaboldi: PPC1-11
 Arouri: PBS-16, PPM-13, PRG2-16
 Arzayus: OB1-3
 Askvik: OPG-3
 Asuquo: PGG2-1
 Atkin: PC2-10
 Avery: PBS-23
 Avsejs: OPC2-2
 Azevedo: PGG1-5

B

Bahri: OSB2-1
 Baker: PPC1-22
 Baki: PM-22
 Balesdent: PCS-8, PSB-10
 Ball: PBC-5
 Bandeira de Mello: PPM-1
 Banning: OB3-1
 Barabanova: PEB1-11
 Baran: PG-26
 Barbanti: OBD1-2, OOS-3
 Barber: OP3-4, PB1-5
 Barcikowski: PMN1-2
 Bardoux: OSB2-1
 Baric: PPC1-1
 Barnes: PEB1-2
 Barr  : PM-8
 Barth: OPG-3, PGG2-14, PRG2-11, PRG2-14
 Bastow: PB2-5, PM-9
 Batova: PBG1-14
 Batts: PGG2-2
 Baudin: PM-6
 Baylis: PMN2-5
 Bayona: PEB2-4
 Bazhenova: PBS-8, POS2-9
 Bazhnova: PBS-2
 Bazylinski: PMP-19
 Beaucaire: OBD2-2
 Bechtel: PPC1-14
 Beerling: PM-21
 B  gu  ristain: PEB2-13
 Behar: OBD2-2, OPG-1, PG-21, PGG1-8
 Belicka: PPC1-21

- Belitskaja: OB3-2, PGG2-5
 Ben Hassen: PBG2-11
 Bence: OP5-4, OPS2-1, PPM-2
 Bendle: OPC1-1
 Benedict: PEB1-14
 Bennett: PG-18
 Benthien: PPC1-16
 Beramendi-Orosco: OM-3
 Bernasconi: PPC1-11, PPC1-9
 Berns: PSB-16
 Berstan: PFA-3
 Bertran: PCS-10, PCS-12
 Biache: PBG1-15
 Bian: PB1-16, POS2-7
 Bianchi: PB2-20, PCS-2
 Bice: PPC1-26
 Bickers: PB1-17
 Biddle: OB2-3
 Bijma: PBG2-1
 Billeck: PC2-22
 Binet: PM-18
 Birgel: PB1-18
 Bishop: OP3-4
 Bissada: OGC-4
 Bjørøy: PBS-15, PMN1-7, PPM-11
 Blagojevic: PSB-1
 Blanc: PM-20
 Blanco: PBS-4
 Blokker: OP3-1, PM-28
 Blumenberg: OP6-2, PMP-16
 Blyth: PPC1-22
 Bodineau: PM-12
 Boere: PMP-1
 Bohaty: OPC2-4
 Bojakowska: PEB1-17, PEB2-1
 Bojesen-Koefoed: PBS-3, PGG1-10, POS2-13
 Boles: OPG-2
 Boot: OB3-1, PPC1-23
 Bopp: PEB1-14
 Boreham: PB2-12
 Borgund: OPG-3
 Bornemann: PPM-12
 Borrego: PBS-4
 Boski: OPE1-3, PB2-13, PBC-3, PM-25, PM-26
 Böttcher: PPC1-4
 Botta: PBG2-3
 Bouchnev: PBG1-7, PG-14, POS1-11
 Bouloubassi: OB3-1
 Boulton: PRG2-16
 Bourdon: PPC1-25
 Bourrin: PBG2-14
 Boussafir: PB1-19, PC2-7, PM-11
 Bowring: OGPR-3
 Boyd: PM-9
 Bradley: OP5-1
 Bradshaw: PB2-12
 Brandsma: PMP-9
 Brassell: PB2-14, PPC1-27
 Brenchley: OB2-3, PSB-19
 Brennand: OP2-2
 Briggs: OP3-2, PC2-10, PPC1-24
 Brinkhoff: OP6-1
 Brinkkemper: PFA-1
 Brinkman: PEB1-2
 Brinzer: PRG1-2
 Brock: OB3-1
 Brocke: PB1-1, PBG1-10
 Brocks: OP4-4
 Brouwer: PPC1-16, PPC1-2
 Brown: PFA-5, PFA-7, PPM-15
 Brukner-Wein: POS2-6, PSB-7
 Budzinski: PEB1-1
 Bühring: PMP-10
 Bull: PFA-3
 Burauel: PSB-16
 Burdelnaya: POS1-11
 Burgess: OP7-4, POS1-10
 Burhan: POS1-12
 Burkova: PB2-4, PBG1-8B
 Burns: PEB1-2
 Buscail: PBG2-14
 Buurman: PFA-1
- C**
- Cabrera: PBS-4
 Cachada: PEB2-2
 Cadez: PG-1
 Cai: PRG1-20
 Caldiero: PGG1-2
 Caldwell: PCS-11
 Camacho: OPG-2
 Campbell: PB1-10, PB1-18
 Canales: PSB-2
 Cañipa-Morales: PMN2-3, PMN2-8, PMN2-9,
 PRG2-13, PRG2-3
 Cao: OPE2-3
 Capella: PMN2-9
 Carcaillet: PBC-4
 Carleer: PC-1
 Carmignani: PEB2-3
 Carr: OUM-3, PRG2-4
 Carrillo-Hernández: PG-15
 Carruthers: PPM-4
 Castañeda: OPC1-3, PB1-20, PPC1-3
 Castelo: PRG2-8
 Castro: PMN2-9
 Ceccanti: PEB2-3
 Cerqueira: PC2-21, PRG1-3
 Clark: PFA-4
 Clayton: PG-3
 Clemens: OPE2-2
 Cody: OPE2-1, PRG2-6
 Coelho: PEB1-4
 Coleman: OB3-1, PB1-14
 Colnago: PSB-13
 Collinson: OP3-2
 Comont: PM-10
 Condon: OGPR-3
 Connan: PFA-5, PFA-6, PFA-7, PFA-8
 Conte: PBG2-5, PBG2-6

Contreras-Santiago: PRG2-13
 Cooke: OP4-2
 Coolen: OP2-1, PMP-1
 Cooper(M): PPC1-24
 Cooper(W.T): OMN-2
 Coppin: PSB-10
 Coppola: PBG2-12
 Corbett: PPM-4
 Cornford: OP7-4
 Corr: PMN2-6
 Courty: PBG2-7
 Coûteaux: PSB-20
 Covaleda: PSB-21
 Cragg: OB3-1, OP7-3, PMP-13
 Cramer: PG-16, PG-23, PPM-12
 Creux: PRG1-12
 Crossman: OP2-2
 Croué: PM-27, PMN1-8
 Crovisier: PBG1-15
 Crow: PCS-11
 Culjak: PBS-11, PG-1
 Curiale: OP1-2
 Currie: PBC-5
 Curry: OP5-4, OPS2-1, PPM-2
 Curtis: POS2-11
 Cvetkovic: PC-12
 Czechowski: OB3-2

CH

Chabbi: OBD2-3
 Chabroulet: PSB-10
 Chai: OGC-1, PMN1-6
 Chalaya: PGG1-6, PGG1-7
 Chan: PMP-19
 Chang: PMP-3
 Chanton: OMN-2
 Chao: PPM-6
 Charrié-Duhaut: PFA-6, PFA-8
 Chen(D): PBS-9
 Chen(J): OGC-1
 Chen(Z): PRG1-20
 Chenghua: PG-4
 Chenu: OSB2-1
 Cheong: PBS-5, PG-19
 Chiang: PSB-9
 Chikaraishi: OP6-4, PPC1-6
 Chinwong: PB1-4
 Christiansen: PBS-3, PGG1-10

D

Da Silva: PGG2-13
 Dahl(B): OPS2-2, PBS-22, PRG2-15
 Dahl(J): OPS2-3, PGG2-3, PRG2-7
 Dahlgren: POS1-6
 Dai: PBS-12
 Dalgarno: PEB1-10
 Dashwood: PRG2-6
 David: PB1-14
 Davies: PEB1-18

Dawson(D): PB1-5, PEB1-15, POS1-4
 Dawson(M.N): PC2-19
 De Andrés: PBC-13
 De la Luz Mora: PSB-2
 De la Rosa: PBC-13, PBC-6, PBC-7, PBC-9
 De las Heras: PC-11
 De Mesmay: PM-3
 De Penteadó: OP6-3
 De Souza: PEB1-4
 De Torres: OP1-1
 Decker: OP1-2
 Del Monte: PRG2-8
 Del Río: PM-23, PM-24
 Delean: PEB1-2
 Deleeuw: OP3-1
 Delgado: PPC1-13
 Dembicki: PMN1-5
 Deng: PEB1-3
 Deniau: OBD2-2
 Denisevich: PB2-21
 Derenne: OSB1-2, PB1-13, PBC-4, PM-16, PM-18,
 PM-2, PM-3, PM-8
 Derksen: OP5-3
 Derrien: PCS-8
 Des Marais: OGPR-2
 Desaunay: PEB1-1
 Di Primio: OGC-3, OP7-3, PBS-18
 Dieckmann: OP2-3, OP7-3, PBG2-4, PC-6, POS2-5
 Diez: PEB2-4
 Dignac: OSB2-1
 Ding: PG-12
 Disnar: PBG1-9, PC2-18, PC2-6, PC2-7, PM-10,
 PPC1-25
 Distanova: POS2-9
 Dittmar: OMN-2
 Djajadihardja: PBG2-10
 Doerr: PSB-11
 Dong: PPM-7
 Dorronsoro: PM-14
 Douglas: PSB-11
 Drage: OM-3
 Drenzek: OPE1-2, PPC1-26
 Driancourt: PGG2-7
 Drouin: PB1-19, PM-11
 Drozd: POS1-10
 Duarte: PEB2-2
 Dubant: OGPR-1
 Duerto: PPM-8
 Dumitrescu: PPC1-27
 Dunning: PPC1-4
 Durringer: PC2-11
 Dutta: PB1-1
 Dyda-Rearick: PMP-11
 Dzou: OBD1-3, PRG1-15

E

Eble: OGC-2
 Eby: PRG1-21
 Ecim: PEB2-6
 Eckmeier: PBC-1

Edazawa: PMP-23
 Edwards: PB2-12
 Eglinton: OP4-1, OPE1-1, OPE1-2, PBG1-13,
 PBG2-10, PBG2-12, PBG2-13,
 PC2-24, PPC1-26
 Ehrenfreund: PBG2-3
 Ehrmann: PBC-1
 Eigenbrode: OPE2-1
 Ejedawe: OP4-3
 Elias: PRG1-4
 Elie: PB1-21, PBG1-12, PC-7, PC2-4
 Elmore: POS1-13
 Elordui-Zapatarietxe: PEB2-5
 Elsinger: OP3-4
 Elvert: OB2-3, OMN-3, PB1-18, PMP-10
 Engel: POS1-13
 England: PBS-6
 Erdmann: PGG2-14
 Erhuma: PBS-6
 Erstad: PRG2-14
 Ertas: OPS2-1
 Escala: PPC1-28
 Escudero: PG-15
 Esemé: POS1-14
 Espitalie: OOS-2
 Etchevers: PSB-21
 Etienne: PFA-8
 Eusterhues: PSB-12
 Evershed: OP2-2, OP3-2, OPC2-2, OSB1-1,
 PFA-3, PFA-4, PFA-9, PMN2-6, PMP-15, PSB-15
 Evseev: OB3-2, PBG2-2

F

Fadeeva: PBS-2
 Fafet: OP6-3, PMN2-4
 Faganeli: PMP-2
 Fang: PMP-19
 Farmer: PB1-18
 Farquhar: PB1-4
 Farrimond: OOS-1, OP4-2, PB2-22,
 PBS-6, PGG2-4, PM-19, PPC1-22
 Fasola: PRG2-8
 Faure: PBG1-12, PC2-14, PC2-2, PEB1-7,
 PEB2-13, PEB2-14, PMN1-1
 Fawley(K.P): PMP-4
 Fawley(M.W): PMP-4
 Fedoroff: PBG2-7
 Fehling: PB1-10
 Feng: PSB-3
 Fenton: PMN1-9
 Ferrer: PC2-23
 Ferriday: PBS-15, PMN1-7, PPM-11
 Fevrier: PM-15
 Ficken: PC2-1
 Ficht: PM-15
 Fichtel: PB1-2
 Fike: OOS-1
 Filareto: PEB2-3
 Filhine-Tresarrieu: PBG1-15
 Filimonova: PGG2-6

Filippova: OB3-2
 Filley: OMN-2, PB2-20, PC2-1, PCS-11
 Fischer: PPC1-17
 Forster: OPC2-3, PPC1-10
 Foster: PB1-5
 Fotland: OPG-3
 Fowler(B.R): PC2-22
 Fowler(M): PBS-23, PRG2-5, PRG2-6
 France-Lanord: PC2-14, PC2-2
 Franco: POS1-15, POS2-3
 Francolin: PPM-1
 Franiatte: PBG1-15
 Franquin: PM-12
 Freeman: PMN2-2
 Freund: OP5-4, OPS2-1, PPM-2
 Fry: OB3-1, OP7-3, PMP-15
 Fryer: PEB1-18
 Frysinger: OP2-4, PB2-14, PB2-3
 Fuentes-Pacheco: POS2-15
 Fuentes-Ramírez: PSB-4
 Fuentes: PMN1-2
 Fuhrmann: OGC-3, PBG2-4, PC2-9, PGG1-1
 Fukushima: PB2-1

G

Gagarin: PPM-4
 Gaidies: PC-6
 Gaines: OP2-4, PB2-14
 Galimberti: PGG1-2
 Galishev: PBG1-14
 Galtayries: PM-3
 Galy: PC2-14, PC2-2
 Gallard: PMN1-8
 Gallardo: PSB-21
 Gallego: OP1-1
 Gallois: PM-2
 Gammon: PPC1-7
 Ganz: OP3-4, OP4-3
 Gao: PRG2-19
 García-Martínez: OP1-1
 García-Mina: PSB-4, PSB-5
 García: PEB2-3
 Garnier: PM-15
 Gaudet: PSB-10
 Gautier: OP3-3
 Gaviño: PBC-10, PSB-2
 Gebhardt: PPC1-20
 Genevasen: PB1-14
 Geng(A): OPS1-3, PG-25, POS1-5, PPM-5,
 PRG1-12
 Geng(X): POS1-5
 George: OBD2-1, OP5-2, PGG2-2, PMN1-2,
 PMN1-9, PRG2-20
 Gerisch: PB1-3
 Gerlach: PBC-1
 Gerling: PG-23, PPM-12
 Gerrez: PEB1-5
 Gibbons: PC2-3
 Gierschner: PSB-16
 Gigantiello: PGG1-2

Gilmour: PBG2-3, PM-21
 Girard: PFA-6
 Giraudeau: PC2-13
 Gize: POS2-12
 Gladenkov(A.Y): PB2-18
 Gladenkov(Y.B): PB2-18
 Gleixner: PC2-15
 Gliddon: OP7-4
 Golovko(A): PGG1-11, PGG1-15, PGG2-6,
 POS2-2, PPM-3, PRG1-6
 Golovko(J): PGG1-11, PGG1-15, PPM-3, PRG1-5,
 PRG1-6
 Golubina: PRG1-1
 Gonçalves(F.T.T): PGG1-5
 Gonçalves(R.C.S): PPM-1
 Goncharov: OPS1-2, PG-2, PGG1-3, PPM-4,
 PRG1-1
 Gonsalvesh: PC-1
 González-Gaitano: PSB-4
 González-Ibarra: PSB-2
 González-Pérez: OBD2-3, PB2-13, PBC-3, PBC-6,
 PBC-7, PBC-8, PCS-9, PM-25, PSB-13, PSB-18
 González-Vázquez: PBC-14
 González-Vila: OBD2-3, OSB1-3, PB2-13,
 PBC-13, PBC-14, PBC-3, PBC-6, PBC-7, PBC-9,
 PCS-9, PM-24, PM-25, PSB-18
 Goozjaeva: PEB2-17, PEB2-18
 Góra: PB1-12, PB1-8
 Gorbaty: OP5-4
 Gorbunova: PGG2-6
 Gorchs: PC-11
 Gorringer: PC2-10
 Gourier: PM-18
 Goutx: PMP-20
 Graciaa: PRG1-12
 Grannas: PBC-11
 Graven: OGC-4
 Green: PB2-21
 Greenwood: OB1-1, PB1-1, PB1-5, PBG2-7
 Grelowski: PBG1-2
 Grice: OPE2-3, PB1-4, PB1-5, PBG2-7, PEB1-15,
 POS1-4, PPC1-4
 Grimalt: OP7-2, OPC2-1, PC2-23
 Grippo: PPC1-17
 Grootes: OP4-1
 Grøver: PC-4
 Grosjean: OGPR-3, OOS-1, OPE2-3, PB2-19,
 PB2-3, PM-19, PPC1-4
 Grossi: PM-3
 Grotzinger: OGPR-3, OOS-1, PM-19
 Grover: OP5-1
 Gržetic: PC-12
 Gui-Jian: PEB1-6
 Guillen: PBG2-14
 Güntner: PPC1-20
 Guo: PCS-6
 Guoyi: PG-4
 Gupta: OP3-2
 Gürgey: PG-3
 Gustafsson: PBC-4, PBG2-12, PCS-6

Gutiérrez-Mejía: POS2-15, POS2-4, PRG2-3
 Guzmán-Vega: PG-15
 Guzzo: PRG1-14, PRG1-3

H

Hack: PM-17
 Haddad: PEB2-10, PEB2-11
 Haenel-Gomes: PSB-13
 Hage: PMP-12
 Hai: PPM-7
 Hall(K): POS2-12
 Hall(P.A): POS2-12
 Hall(P.B): PBS-15
 Hallmann: PBS-16, PPM-13
 Hamer: PCS-14
 Hammes: PBC-2
 Handley: PB1-17
 Hanson: PCS-5
 Hao-Yuan: PEB1-6
 Hara: OPS2-3
 Harald: PBS-18
 Hartkopf-Fröder: PB1-1
 Harvey(H.R): PMP-11, PPC1-21
 Harvey(P): OBD2-1
 Hasegawa: PB2-18
 Hatcher: OM-2, PBC-11
 Hatlør: PGG2-14, PGG2-9
 Haug: PC2-9
 Hauteville: OB1-2, PC2-4, PC2-5
 Havertz: PPC1-5
 Hayes: OMN-3, OP4-1, OP5-1, PBG2-12, PBG2-9
 Hayward: PPC1-7
 He: PBS-21
 Head: OMN-1
 Hebbing: OOS-1, PB2-2, PB2-3
 Hedges: OM-1
 Heim(A): PCS-7, PSB-6
 Heim(S): OEB-3
 Herlec: PC2-20
 Hermosin: PBC-10, PEB2-15, PM-14
 Hernes: OM-1
 Herrle: PPC1-18
 Herrmann: PMP-6
 Herten: PBG1-10, PBG2-8
 Hetényi: POS2-6, PSB-7
 Heuer: OMN-3
 Hguoyi: PG-6
 Hicks,Jr: ORP-1
 Hilscher: OSB1-3, PBC-3
 Hiltmann: PC-12
 Hill: ORP-2, POS1-10, PRG2-7
 Hindle: PBS-6
 Hinrichs: OB2-3, OMN-1, OMN-3, PB1-18,
 PMP-10
 Hmelo: OMN-3
 Hockaday: PBC-11
 Hodneland: PGG2-9
 Hoernes: PPC1-14
 Hoffmann-Jähnicke: OSB2-3
 Hofmann: PC2-16, PPC1-18

Hoiland: PPM-6
 Høiland: OPG-3
 Holba: OBD1-3
 Holtvoeth: PC2-24
 Hong: PPM-6
 Honghan: PG-6
 Hoogakker: OPC2-1
 Hopmans: OB1-3, OPC1-3, OPC2-4, PB1-14,
 PB1-7, PMN1-3, PMP-9, PPC1-19
 Hornibrook: OB3-1, OP2-2, PSB-15
 Horsfield: OGC-3, OP2-3, OP7-3, PBG2-4, PC-6,
 PC2-9, PGG1-1, PMP-13, POS2-5
 Hosgörmez: PBG2-8, PG-17
 House: OB2-3
 Hsieh: PB1-6
 Hsu: OM-2
 Hu: PGG1-1
 Huang(H): OMN-1, PBS-1, PG-18, PG-9, PPM-10
 Huang(Y): OPE2-2, PC2-6, PMP-19, PPC1-3
 Hubred: POS1-6
 Huc: PG-15, PRG2-18
 Hughen: OPE1-2, PPC1-26
 Huguet: OPC2-4, PM-13
 Huguoyi: PG-7, PMP-7
 Huisman: PFA-1
 Hung: PMN1-5
 Hunter: PBG1-3, PBG1-4, PBG1-5
 Hwang: PGG2-15, PRG1-8

I

Ichikawa: PC2-27
 Idiz: OP3-4
 Ilyin: PB2-22
 Illich: PPM-15
 Imbus: PFA-5, PFA-7, POS1-13
 Ineson: OP2-2
 Inoubli: PBS-7
 Ione: PBG1-6, PGG1-4
 Ioppolo-Armanios: PEB1-15
 Iriondo: PM-14
 Isaksen: OPS2-2
 Ishiwatari: PC2-12, PM-4, PM-5
 Isono: PC2-27
 Issler: OUM-1, PRG1-13
 Ivanova(E): PBS-10, PGG1-11, PPM-3
 Ivanova(I.K.): PGG1-6, PGG1-7
 Izart: PC-7

J

Jacob: PC2-6, PC2-7
 Jaeschke: PB1-7, PMN1-3
 Jalfin: OPS1-1
 James: PFA-9
 Jandl: PCS-3
 Jardé: PEB2-14
 Jarvie(B.M): POS1-10
 Jarvie(D.M): ORP-2, POS1-10, PRG2-7
 Jeanneau: PEB1-7, PMN1-1
 Jeanty: PBG2-14

Jedrysek: PBG1-2
 Jesuino: PGG1-5
 Jetten: OP5-3, PMP-9
 Jian(L): PG-5
 Jian(X): PEB1-6
 Jiang: ORP-2, POS1-10
 Jin(Y): OPE2-3
 Jin(Z): PB1-16, PPM-9
 Jodlowski: PG-26, PG-27
 Joeckel: PMP-19
 Johansen(H): POS1-16
 Johansen(J.E): PMN1-10
 Johansen(P.E): PC-5
 Johnson: OPC1-3, PPC1-3
 Jones(M): PEB1-15
 Jones(M.D): PPC1-22, PRG2-2
 Jones(T.F): PC2-10
 Jovancicevic: PC-12, PGG1-14, PGG1-15
 Jovanovic: PEB2-6
 Juggins: PB2-22
 Jurisch: POS2-1
 Justwan: OPS2-2

K

Kalkreuth: POS1-15, POS2-3
 Kallmeyer: OP7-3, PMP-13
 Kammer: PBG1-15
 Kamyarov: PGG2-6, POS2-2
 Kanduc: PMP-2
 Kardamakis: PPM-14
 Karlsen: PBS-18, PG-20, POS1-6
 Kárpáti: PB2-16
 Kars: PFA-1
 Kashirtsev: PGG1-6, PGG1-7
 Kashiyama: PPC1-6
 Kaster: OMN-1
 Kästner: OSB2-3
 Kato: PB2-1
 Kaur: OB3-1
 Kavak: PFA-7
 Kawamura: OEB-1
 Keely: PB2-10, PB2-7
 Kelemen: OP5-4, OPS2-1, PPM-2
 Kelly: OB3-1
 Kenig: OP2-4, PB1-20, PB2-14, PB2-19, PC2-25,
 PC2-8
 Kern: POS2-3
 Kienhuis: PBG2-1, PMN1-3
 Kim(D): PRG1-9
 Kim(J.H): PG-19, PMP-3
 Kim(J.P): PBG1-3
 Kim(S): PBC-11
 Kindler: OSB2-3
 King-Díaz: PSB-2
 Kirjukhina: PBS-2
 Kitazato: OP6-4, PC2-12, PPC1-6
 Klimenko: PBG1-7
 Klock: PMP-14
 Kloppisch: PC2-8

- Knicker: OSB1-3, PBC-3, PBC-6, PBC-9, PCS-9, PB2-13, PM-24, PSB-18
 Kobayashi: OEB-1, PMP-23
 Kögel-Knabner: OSB2-2, PCS-4, PSB-12, PSB-8
 Koike: PGG2-13
 Kontorovich: PGG1-6
 Kool: PFA-1
 Kopinke: OSB2-3
 Korobochkina: PG-2
 Koschinsky: PBG1-4
 Köster: OP6-1, PB1-2
 Kostyreva: PBG1-14
 Kotarba: POS2-11
 Kovaleva: PRG1-10
 Kowalewski: OP6-3, PGG2-7, PMN2-4, PRG1-11, PRG2-18
 Kramer: PRG2-16
 Kranendonck: PBG1-10
 Krein: PM-1
 Kristen: PC2-9
 Kronimus: PGG1-14
 Krooss: POS1-14
 Krüge: PEB2-12
 Krüger: OP6-2
 Krull: PPC1-8, PSB-19
 Krummen: OMN-3
 Kuburovic: PEB2-6
 Kuder: PEB2-7
 Kupsch: PEB2-9, PSB-14
 Kurakolova: PB2-4, PBG1-8
 Kéravis: PC2-7
 Kuroda: PPC1-6
 Kursheva: PBG1-14
 Kvenvolden: PBG1-1
 Kwiatek: OPS2-1
- L
- Labayén: PRG2-8
 Ladipo: OP4-3
 Laggoun-Défarage: PM-10, PPC1-25, PRG2-18
 Lajtha: PCS-11
 Lalevic: PEB2-6
 Lallier-Vergès: PBG1-9, PC2-18
 Lamers: OP5-3
 Lamoureux-Var: PRG1-11
 Lampert: PFA-6
 Lana: POS1-7
 Landau: PGG1-5, PRG2-10
 Lang: PB2-5
 Langezaal: PMP-9
 Lannuzel: PC-7, PC2-5, PMN1-1
 Laporte-Chrostowska: PRG1-12
 Large: OM-3, PC2-10, PPC1-24
 Largeau: OBD2-2, OPG-1, OSB1-2, PBC-4, PBC-8, PM-2, PM-3, PM-8
 Larter: OMN-1, PG-18, PRG2-2, PRG2-5
 Laurence: PMP-20
 Le Du: PEB1-1
 Le Métayer: PC2-11
 Le Milbeau: PB2-6
- Le Solleuz: PBG1-12
 Lebaron: PMP-20
 Lee: PBS-5, PG-19, PMP-3
 Lehdorff: PEB2-8
 Lehner: OP4-3
 Leininger: PGG1-8
 Leinweber: PCS-3
 Leistner: POS2-1
 Leith(D.A): PRG2-17
 Leith(T.L): PRG2-17
 Levaché: PMN2-4
 Lewan: PG-21, POS1-1, POS1-2, POS1-3, POS2-11
 Lewandowska: PM-7
 Lewis(A.N): OGPR-3, OOS-1
 Lewis(C.A): PEB1-12
 Leythaeuser: PRG2-16
 Leyval: PEB2-13
 Li(J): PBS-12
 Li(M): OUM-1, PBS-12, PBS-8, PBS-9, PPM-9, PRG1-13
 Li(S): PG-12, PMN1-9, PPM-9, PRG2-19
 Li(L): PCS-13
 Liang: PBS-1
 Liao(Y): PPM-5
 Liao(Z): PRG1-12
 Lie: PBS-18
 Liebezeit: PB1-15
 Lifshits: PGG1-7
 Lijian: PG-6, PG-7, PMP-7
 Lima-Neto: PRG2-10
 Lima(A.L): OPE1-2
 Lima(S.G): PGG2-13
 Lin(R): OP1-2
 Lin(S.T): PSB-9
 Lin(X): OB1-3
 Linsley: PBG2-10
 Lipp: OB2-3, OMN-1
 Lippold: PEB2-9
 Littke: OEB-3, PC-8, PC-9, POS1-14
 Liu(D): OGC-1, OPS1-3, POS2-7
 Liu(H): PMN1-10
 Liu(H.-X): PC2-26
 Liu(J): OPS1-3, PG-25, POS1-5
 Liu(K): PMN1-9
 Liu(W): OPE2-2
 Liu(Y.-M): PC2-26
 Liuchenglin: PG-7
 Liurenhe: PG-7
 Lixin: PPM-6
 Lizhisheng: PG-7, PMP-7
 Logan: PB2-12
 Londry: OP5-1
 Lopes(J.A.D): PGG2-13
 Lopes(J.P): OBD1-2, PGG1-9, PRG1-14
 Lopes(L.V): PEB2-2
 Lopez: OP7-2, PGG1-1
 López-Capel: PBC-6, PBC-7, PM-22, PMN2-7
 López-López: POS2-15, POS2-4, PRG2-3
 López-Martínez: OPC2-1

López-Sangil: PCS-10
 Lorant: OOS-2, PG-21, PGG1-8, PRG1-11
 Lotina-Hennsen: PSB-2
 Lough: PEB1-2
 Love: OGPR-3, OOS-1, OPE2-3, OUM-3, PM-19, PMN1-4
 Lovrinevich: PRG2-8
 Lu(J): OPS1-3
 Lu(S.-T): PEB2-11
 Lucini: PPC1-13
 Lüders: PBG2-4
 Luofu: PPM-6
 Luong: PPM-7, PRG1-16
 Luoxia: PG-6, PG-7
 Luthé: PMN1-10

LL

Llamas: OP1-1, PPC1-13
 Llewellyn: PSB-11
 Lloyd: PC2-13

M

Macci: PEB2-3
 Macdonald: PC2-22
 Mackie: PEB1-16
 Macquaker: PC2-10
 Machado: POS1-15
 Machenghua: PG-6, PG-7
 Magos-Carmona: PRG2-13
 Mai: PFA-6
 Mainwaring: PSB-11
 Maizatto: POS1-7
 Makrygina: POS2-12
 Malartre: OB1-2, PC2-4, PC2-5
 Mandujano-Velázquez: PRG2-3
 Mangelsdorf: OB2-1, OP7-3, PC-6, PMP-13
 Mango: ORP-2
 Mann: PB1-1, PB1-3, PBG1-10, PBG2-8, PC2-8, PG-11, POS2-1, PPC1-5
 Manning: PBC-7, PM-22, PMN2-7
 Mansel: PSB-14
 Mansuy-Huault: PEB1-7, PEB2-13, PEB2-14
 Manzano-Kareah: OUM-2
 Marchand: PBG1-9
 Maricic: PBS-11
 Marinov: PC-1
 Mariotti: OSB1-2, OSB2-1, PBC-8
 Marol: PCS-8
 Marsaioli: PEB2-19
 Marschner: PCS-14
 Marshall: PC2-3
 Martikhaeva: POS2-12
 Martin-Garin: PSB-10
 Martin-Neto: PSB-13
 Martin: PC2-18
 Martins(H): OPE1-3
 Martins(Z): PBG2-3
 Martín-Rubí: PBC-13
 Martínez: PB1-21, PBG1-12, PC-7

Martínez(A): PMN2-3, PMN2-8
 Martínez-García: OPC1-1
 Marumo: PMP-22, PMP-23
 Marynowski: PB1-12, PB1-8, PBG1-2, PM-7
 Masciandaro: PEB2-3
 Masiello: PBC-5
 Maslin: PPC1-23
 Mason: PM-17
 Masqué: PEB2-5
 Mastalerz: OGC-2
 Mathiasen: PRG2-15
 Matsumoto: OP6-4, PC2-12, PPC1-6
 Matyasik: PBS-17
 Maurer: PFA-8
 Mawson: PB2-7
 Maxfield: OP2-2, PSB-15
 Maxwell: PBS-8
 Mazéas: PEB1-1
 Mazurov: PBG1-6
 McCave: OPC2-1
 McClymont: OPC2-2, PC2-13
 McIntosh: PEB1-10, PEB1-16
 McIntyre: OBD2-1, PGG2-2, PMN1-2
 McKirdy: PBS-16, PPC1-7, PPC1-8, PPM-13, PRG2-16, PSB-19
 McLaughlin: PC2-22
 McManus: PC2-24
 Medeiros: PBG1-11, PBG2-6
 Mee: PPC1-8, PSB-19
 Méhay: OP6-3
 Meier: PC-9
 Meisingset: OPS2-2, PRG2-15
 Mejri: PEB2-20
 Menetrier: PC-7
 Ménétrier: PBG1-12
 Menezes: POS1-7
 Mercier: PM-8
 Meredith: OUM-3, PM-19, PMN1-4, PRG2-4
 Mermoux: PBG2-7
 Metzger: PMP-4
 Meyers: PC2-18, PPC1-10, PPC1-11, PPC1-9
 Micklich: PB1-3
 Michael: PB2-21
 Michaelis: OP6-2, PMP-14, PMP-16
 Michels: OB1-2, OP3-2, PC2-4, PC2-5
 Milewska: PG-27
 Milkov: OP7-1, PRG1-15
 Milori: PSB-13
 Miltner: OSB2-3
 Miller: PPM-1
 Mills: PRG2-11
 Minot: PGG1-8
 Miserque: PM-8
 Mo: PMN1-6
 Mochida: OEB-1
 Moehring: PMN2-11
 Moffat: PEB1-10, PEB1-16, PEB1-18
 Moldowan: OGPR-2, OOS-3, OPS2-3, PB2-21, PGG2-3, PRG2-7
 Moldrheim: PGG2-9

Mollenhauer: OPE1-1, PC2-24
 Monnier: PBS-8
 Montacer: POS2-14
 Montluçon: PBG1-13, PBG2-10, PC2-24
 Moorman: PMP-19
 Mora(C): PBS-19
 Mora(J.L): PCS-1
 Morley: PSB-11
 Mort: PRG2-18
 Mosely: PBG1-5
 Motoyama: PB2-18
 Mottram: OSB1-1
 Mounier: PM-15
 Moura: OPE1-3
 Muehlenbachs: PG-10
 Mueller: PG-8, PRG1-2
 Muenster: PMN2-11
 Mukherjee(A): PEB1-8
 Mukherjee(A.J): PFA-9
 Mukherjee(S): PEB1-8
 Muller: PRG2-18
 Müller: PRG1-4
 Muri: PB1-9, PPC1-12
 Murray: OP3-4
 Muyzer: OP2-1, PB1-10, PB1-11
 Mysov: PBG1-6, PGG1-4
 Mytych: PEB1-9

N

Nakajo: OB2-2
 Nali: PGG1-2
 Negash: PRG2-14
 Nelson: OP2-4, PB2-14, PB2-3, PC2-25
 Nemerov: PBG2-2
 Neto: PGG2-13
 Neumann: PBS-4
 Newall: OOS-1
 Nissenbaum: PFA-2, PFA-5
 Nodzinski: PG-26
 Noke: PG-18
 Nosova: OPS1-2, PG-2, PGG1-3, PRG1-1
 Notario: PCS-1
 Nott: OPC2-2
 Noya: PPM-8
 Nyilas: PSB-7
 Nylén: PB2-21
 Nytoft: PBS-3, PC-3, PGG1-10

O

Oba(M): PMP-21
 Oba(T): PC2-27
 Oberhänsli: PC2-9
 Obermajer: PPM-14, PRG2-5, PRG2-6
 Obilaja: OP4-3
 Oblasov: OPS1-2, PG-2, PGG1-3
 O'Brien: POS1-13
 Ocampo: PB2-15
 Oda: PC-10
 Ogasawara: PB2-18

Ogawa: OP6-4, PPC1-6
 Ogihara: PMP-5
 Ogrinc: PMP-2, PPC1-12
 Ohkouchi: OP6-4, PBG1-13, PC2-12, PPC1-6
 Ohm: PG-20
 Okui: PBS-24
 Oldenburg: OMN-1, PG-18
 Olivares: PPM-8
 Oliveira: PEB2-19
 Olivella: PC-11
 Olivier: PM-15
 Olmstead: OP5-4
 Olsen: PMN1-7
 Olson(B): PMN1-11
 Olson(R.K): PMN1-5
 Ondrak: OP7-3
 Op den Camp: OP5-3
 Oppo: PBG2-10, PC2-24
 Ortega-Calvo: PEB2-16
 Ortiz: OP1-1, PPC1-13
 Osadetz: PPM-14
 Ossebaar: PBG2-1
 Ostertag-Henning: OPE2-1
 Otoghile: OP4-3
 Overmann: OP2-1

P

Packer: PEB1-10
 Pacheco: POS2-3
 Pajares: PSB-21
 Palhol: PC2-14, PC2-2
 Palmer: OBD1-3, PMN1-11, PRG2-9
 Pan(G): PCS-13
 Pan(X): PGG2-8
 Pancost: OB3-1, OP3-2, OPC2-2, PB1-14, PB1-17, PMP-18, PPC1-23
 Pang: PBS-9, PMN1-9, PPM-9, PRG2-19
 Panoto: PB1-10
 Pape: PMP-14
 Pardo: PBC-9
 Parente: PRG2-10
 Parfenova: PBS-10
 Parinet: PMN1-8
 Park(M.H): PMP-3
 Park(S.J): PBS-5
 Parker: PEB1-18
 Parkes: OB3-1, OP7-3, PMP-15
 Parlanti: PM-13, PM-15, PM-20, PMN2-1
 Pasadakis: PPM-14
 Paterson: PBS-6
 Patience: OGC-4
 Pearson(E.J): PB2-22
 Pearson(K.D): PB1-20
 Peckmann: PB1-18
 Pedersen(B.S): PRG2-11
 Pedersen(J.H): PBS-18
 Pedro: PM-26
 Peng(D): PBS-1
 Peng(P): PEB1-13, PEB1-3, PG-13, PSB-3

- Penteado: OBD1-2, PBS-13, PGG1-9, POS1-15, PRG1-14
 Pérez-Ortiz: POS2-15, POS2-4, PRG2-3
 Permyner: PBS-19, PEB2-12, PM-14, PRG2-12
 Perovic: PSB-1
 Pessoa: PM-26
 Pestman: OPS2-3
 Peters: OP3-3
 Petersen: PC-3
 Petrova: PBG1-14
 Pevneva: PGG1-11, PGG1-15, PPM-3, PRG1-5, PRG1-6
 Pfälzner: PFA-9
 Philp: PB1-6, PEB1-5, PEB2-7, PG-3, PGG2-8, PRG1-5, PRG1-9
 Piedad-Sánchez: PC-7
 Pierre: PC2-13
 Pignoc: PGG2-7
 Pintado-Moscoso: PRG2-3
 Pinturier: PMP-20
 Pitsch: OBD2-2
 Podolskaya: PGG2-11, PGG2-12
 Polissar: PMN2-2
 Polozov: POS2-12
 Poludetkina: PBS-2, POS2-13
 Polvillo: PB2-13, PBC-6, PCS-9, PM-25, PSB-18
 Pollard: PEB1-18
 Poole: OP3-1
 Posada-Baquero: PEB2-16
 Poulain: PM-27
 Poulsen: PEB1-2
 Poussart: OPE1-2
 Powers: OPC1-3, PPC1-3
 Powlson: OP2-2
 Prell: OPE2-2
 Prieto-Mollar: OMN-3
 Prietzel: OSB2-2, PSB-8
 Prinzhofer: PG-15
 Punanova: PGG1-12
 Purenovic: PSB-1
 Putnam: OB1-3
 Putra: POS1-12
 Püttmann: PPC1-14
- Q**
 Qiu: PRG2-19
 Quénéa: OSB1-2, PBC-4
- R**
 Radke: PC2-15
 Raghoebarsing: OP5-3
 Raichevic: PEB2-6
 Ramelli: PEB1-7
 Ramos: OP3-3, OUM-2
 Rampen: PB1-10, PB1-11
 Ramírez-G: PMN2-3, PMN2-8
 Rangel: PGG1-9, PRG1-14
 Raphel: PM-3
 Rasse: OSB2-1
 Rattray: PMN1-3
 Reddy: OP2-4, OPE1-2, PB2-14, PB2-3, PBG2-13, PC2-25
 Regier: PEB2-13, PEB2-14
 Reijerink: PMN1-10
 Rein: PGG2-9
 Reineke: OEB-2
 Reis: PGG2-13
 Relexans: PM-13, PM-15
 Remusat: PM-16
 Reyes: PEB2-15
 Riandra: POS1-12
 Riboulleau: PM-12, PM-6
 Richnow: OSB2-3
 Ridlo: PBG2-10
 Rigollet: PBG1-12
 Rijnstra: OP5-3
 Rinna: PMP-15
 Ritter: PC-4
 Riva: PRG1-4
 Robert(F): PM-16, PM-18
 Robert(J.L.): PB1-19, PM-11
 Roberts(A.P.): PMP-18
 Roberts(Z.E.): OPC2-2
 Robertson: PM-17
 Rocher: PB2-8, PRG2-9
 Rodier: PM-27
 Rodrigues(R): PB1-22
 Rodrigues(S.M.): PEB2-2
 Rodríguez-Rodríguez: PCS-1, PCS-9
 Rodríguez: PPM-8
 Roelofs: OP5-3
 Roesch: PBC-1
 Rojas: PPM-8
 Rokosov: PRG1-1
 Romanov: PPM-4
 Romanyà: PCS-12
 Rosell-Melé: OPC1-1, PC2-13, PEB2-5, PPC1-28
 Rosenthal: PBG2-10
 Rospondek: PB1-12, PB1-8, PM-7
 Rothman: PBG2-9
 Rouquette: PGG2-7, PMN2-4
 Roussé: PC2-11
 Routh: PCS-2
 Rouzard: PBC-4, PRG2-18
 Rovira: PBC-12, PCS-10, PCS-12, PSB-20
 Rowan: OMN-1
 Rowland: OEB-2, PEB1-12
 Rühlemann: PPC1-2
 Rullkötter: OEB-2, OP4-1, OP6-1, PB1-2, PFA-2, PMP-6, PPC1-2, PPC1-20, PRG1-17
 Rumenjak: PBS-11
 Rumpel: OBD2-3, OSB2-1, PBC-4, PBC-8, PSB-12
 Rushdi: PBG1-16
 Russell: PEB1-10, PEB1-16, PEB1-18
 Ryu: PG-19, PMP-3

S

- Sabaté: PEB2-4
 Sabel: PPC1-14
 Sachs: PC2-19
 Sachse: PC2-15
 Sadaoui: PBS-26
 Saenger: PC2-19
 Sáenz: PBG2-10
 Sánchez: PRG2-12
 Sánchez-García: PBC-13
 Safi: OP6-1
 Safronov: PGG1-7
 Sagachenko: POS1-9
 Sagon: PBG2-7
 Saidi: PEB2-20
 Saison: POS2-5
 Saito: PB2-9
 Saiz-Jiménez: PBC-10, PEB2-15
 Sajgó: PB2-16, POS2-6, PSB-7
 Sakamoto: PPC1-6
 Sakata: PB2-17, PMN2-10, PMP-21
 Saliot: PB1-13
 Samoilenko: OPS1-2, PG-2, PGG1-3
 Sander: PBG1-3, PBG1-4, PBG1-5
 Santos-Neto: PEB2-19
 Sanz: PBC-14
 Sarragoni: PBG2-14
 Sass: PB1-2, PMP-6
 Sattari: PMN1-2
 Savinikh(N): PPM-3
 Savinykh(Y.V): PRG1-16
 Sawada: PB2-9, PPC1-15
 Sayili: PRG1-18, PRG1-19
 Schabauer: PSB-11
 Schaefer(J): PM-20
 Schaefer(R.G): PB1-1, PB1-3, PBG2-8, PG-11, POS2-1, PPC1-5
 Schaeffer: PB2-6, PC2-11, PGG2-7, PMN2-4
 Scheeder: PC-12
 Schefuß: OP4-1, PPC1-19
 Scherf: PRG1-17
 Schier: PBC-1
 Schile: OGC-4
 Schimmelmann: OGC-2
 Schmid: OP5-3, PMP-9
 Schmidt(C): PC2-16
 Schmidt(M.W.I): PBC-1, PBC-2, PBC-5, PCS-7, PSB-17, PSB-6
 Schneider: OP4-1
 Schnetger: PPC1-2
 Schnitzler: PSB-16
 Schoell: PG-22
 Schöning: PCS-4
 Scholz-Böttcher: PFA-2
 Scholz: PG-8
 Schouten: OB1-3, OP2-1, OP4-1, OP5-3, OPC1-3, OPC2-3, OPC2-4, PB1-10, PB1-11, PB1-14, PB1-4, PB1-7, PBG2-1, PC2-16, PMN1-3, PMP-9, PPC1-18, PPC1-19
 Schulte: PPC1-16, PPC1-2
 Schuneman: OPC1-2
 Schwab: PC2-17
 Schwark: PB2-11, PBS-16, PCS-7, PEB2-8, PPM-13, PRG2-16, PSB-17
 Schwarzbauer: OEB-3, PB2-11, PC-8, PC-9, PCS-7, PGG1-14, POS1-14
 Scotchman: OUM-3, PRG2-4
 Scotese: PPM-15
 Seidel: PMP-6
 Seifert: OP6-2, PMP-16
 Self: PM-21
 Semiletov: PCS-6
 Senko: PMN2-11
 Sephton(M.A): PBG2-3, PM-21, PMN1-4
 Sephton(S.V): PM-21
 Serebrennikova: OB3-2, PBG2-2, PEB1-11, PGG2-5, POS1-9
 Serra: PEB2-12
 Sestak: PMN1-2
 Shackleton: OPC2-1
 Shanina: PG-14, PGG1-13
 Shanxiuqing: PG-6
 Sharapov: PBG1-6
 Shi: PBS-9
 Shiine: OB2-2, PB2-18
 Shimamune: PC2-27
 Shinoyama: PM-5
 Sholevic: PEB2-6
 Shuai: PG-13, PG-9
 Shuangwen: PPM-6
 Sievert: PMP-10
 Sifeddine: PC2-18, PC2-6, PC2-7
 Simioni: PEB2-19
 Simoneit: OEB-1, PBG1-11, PBG1-16, PBG2-6
 Sinninghe-Damsté: OB1-3, OP2-1, OP5-3, OPC1-3, OPC2-3, OPC2-4, PB1-10, PB1-11, PB1-14, PB1-7, PC2-16, PMN1-3, PMP-1, PMP-17, PMP-9, PPC1-18, PPC1-19
 Siskin: OP5-4
 Sizova: PEB1-11
 Skjemstad: PBC-5
 Skrzypczak: PM-18
 Slivko: PGG2-10, PGG2-11, PGG2-12
 Smernik: PBC-2
 Smith(B.E): PEB1-12
 Smith(D): PBG2-7
 Smith(D.M): PBC-5
 Smith(E.L): OEB-2
 Smith(H.D): PPC1-7
 Smith(J.N): PB2-22
 Smittenberg: PC2-19
 Smolders: OP5-3
 Snape(C.E): OGPR-3, OM-3, OUM-3, PM-19, PMN1-4, PPC1-24, PRG2-4
 Snape(I): OBD2-1
 Snowdon: OUM-1, PC-5, PC2-22, POS1-8, PRG1-13
 Sokolova: PGG2-10, PGG2-11, PGG2-12
 Solanas: PEB2-4

Sollins: PCS-11
 Somerfield: PC2-10
 Song(F): PB1-16
 Song(J): PEB1-13, PEB1-14, PEB1-3
 Song(J.-Z): PSB-3
 Sonter: PPC1-7
 Souza: PB1-22
 Soyhan: PRG1-18, PRG1-19
 Soyly: PG-17, PRG1-18
 Spadano-Albuquerque: PC2-6, PC2-7
 Spangenberg: PC2-17, PC2-20
 Spanic: PG-1
 Spielvogel: OSB2-2
 Spiro: PC2-10, PSB-19
 Stadnitskaia: PMP-17
 Stakhina: PEB1-11
 Stalvies: OGPR-3, OOS-1, PM-19
 Stamenova: PC-1
 Stankovic: PBS-11, PG-1
 Stansbury: OBD1-3
 Stasicka: PEB1-9
 Stasiuk: PBS-23, PBS-8, POS1-8
 Steczko: PBS-17
 Steele: OPE2-1
 Stefanova: PC-1, PC-2, PPC1-25
 Stojanovic: PGG1-14, PGG1-15
 Strapoc: OGC-2
 Strauß: PC-9
 Street-Perrott: PC2-1
 Strohschoenj: POS1-7
 Strous: OP5-3
 Stuart-Williams: PB1-4
 Sturt: OB2-3
 Stüsser: PPC1-18
 Su: PBS-1, PG-9
 Suárez-Luiz: PB1-21
 Suárez-Ruiz: PC-7
 Suemune: PC2-27
 Suga: OP6-4, PPC1-6
 Sugden: OP4-2
 Summons: OGPR-3, OOS-1, OP5-1, OPE2-3,
 PB1-5, PB2-12, PB2-19, PB2-2, PB2-3, PBG2-9,
 PC2-25, PM-19, PPC1-4
 Sun: OGC-1, PG-16, PMN1-6, PRG1-20
 Suping: PPM-6
 Süß: PMP-6
 Suzuki(M): PMP-11
 Suzuki(N): OB2-2, PB2-18, PB2-9
 Suzuki(Y): PGG2-16
 Swanston: PCS-11, PCS-5
 Syamsudin: PBG2-10
 Sykes: PC-5, PRG2-20
 Sylva: OP5-1

Š

Šajnovic: PC-12
 Šolevic: PGG1-14
 Španic: PBS-11

T

Tañeza: PEB1-5
 Tada: PPC1-6
 Takamatsu: PB2-1
 Takano: PMP-22, PMP-23
 Talbot: OP4-2, OP6-2
 Tamanqueira: PGG1-5
 Tang: PG-22, PG-28
 Tannenbaum: PM-12, POS1-1
 Tari: PPC1-1
 Taylor(G.T): OB1-3
 Taylor(P): OP3-4
 Taylor(P.N): OOS-1
 Teerman: PPC1-17
 Templier: PM-2, PM-8
 Téllez: PMN2-9
 Terán: PBC-13, PM-25
 Tharp: OBD1-3, PRG2-9
 Thiel: PB1-18
 Thielemann: OMN-1
 Thieme: PSB-8
 Thiemens: PBG2-7
 Thompson: ORP-2
 Thomsen: PBS-22
 Thorez: PM-26
 Thorpe: PC2-9
 Tilley: PG-10
 Timmermans: PB1-11
 Tinoco: PBC-14
 Todorovic: PEB2-6
 Toffin: OB2-1
 Tolosa: PPC1-12
 Toporski: OPE2-1
 Toribio: PCS-10, PCS-12, PSB-20
 Torn: PCS-5
 Torras: PCS-10, PCS-12
 Torres(M): PBS-19
 Torres(T): PPC1-13
 Totten: POS1-13
 Touchard: PMN1-8
 Treignier: PB1-13
 Tremblay: OMN-2
 Tribouvillard: PM-12, PM-6
 Trichet: PBG2-11
 Trigüis: PB1-22, PEB1-4
 Trindade: PPM-13
 Tronczynski: PEB1-1
 Troskot-Corbic: PBS-11
 Trouiller: OB1-2, PC2-4, PC2-5
 Tsukawaki: PC2-12
 Tsunogai: PMP-21, PMP-3
 Tu: POS2-7
 Turcq: PC2-7
 Turgeon: PPC1-4
 Turich: PMN2-2
 Turner: PEB1-15
 Turov: PEB2-17, PEB2-18
 Twitchett: PB1-5, PPC1-4
 Tyufekchieva: PSB-8

U

Uchida: PBG2-12
 Ueshima: PC2-27
 Ugama: OUM-3
 Uhle: OPC1-2, PMP-12
 Ukpabio: PGG2-1
 Urabe: PMP-23
 Utoplennikov: PRG1-16

V

Vacher: PM-15, PM-20, PMN2-1
 Vairavarmurthy: POS1-1
 Valentin: PBC-8
 Valyaeva: PBS-20
 Valle: PPC1-13
 Vallejo: PBC-12, PCS-10, PCS-12, PSB-20
 Van Aarssen: OP3-4, PB2-5, PM-9
 Van Bergen: OP3-1
 Van den Berg: PFA-1
 Van der Zwaan: PMP-9
 Van Dongen: PCS-6, PMP-18
 Van Haaster: PFA-1
 Van Heeringen: PFA-1
 Van Zuilen: PBG1-15
 Vandr e: PG-23
 Vane: OM-3
 Vars anyi: PB2-16
 Vasconcellos: PEB2-19
 Vasiljev: PEB2-17
 Vass: PFA-3
 Vautravers: OPC2-1
 Vaz dos Santos Neto: PC2-21, PRG1-3
 Veiga-Pires: OPE1-3
 Vekulenkova: PBG2-2
 Ventura: OP2-4, PB2-19, PC2-25
 Verdejo: PCS-9
 Versteegh: PM-28
 Veto: PG-24
 Vidal Torrado: PSB-13
 Vidal: PC-12
 Vieira: PGG1-9
 Vieth: OBD1-1, PRG1-4
 Vi nas: PEB2-4
 Villar: OPS1-1
 Vitorovic: PGG1-15
 Vogel: OGPR-2
 Volders: OPC2-2
 Volk: OP5-2, PGG2-2, PMN1-9, PRG2-20
 Volkman(J.K): OP2-1
 Volkman(N): PB1-3, POS2-1
 Voordouw: OMN-1B
 Vreca: PMP-2
 Vu: PC-6
 Vyacheslav: PPM-7

W

Wadham: OB3-1
 Wagner: PC2-16, PC2-24, PPC1-18, PPC1-19
 Wakeham: OB1-3, OPC2-4, PB1-11, PB1-9

Walker(J.S): PB2-10
 Walker(P): OBD1-3, PMN1-11, PRG2-9
 Walsham: PEB1-10, PEB1-16, PEB1-18
 Walters: OP5-4, OPS2-1, PPM-2
 Walls: PBG2-7
 Wang(C.G): PBS-21
 Wang(C.J): PBS-21, PC2-26
 Wang(D): PB1-16
 Wang(F): OPS1-3
 Wang(H): OPS1-3
 Wang(M.K): PSB-9
 Wang(S.X): PB1-4
 Wang(T.G): PBS-21
 Wang(W): PSB-9
 Wang(Y): OPE2-2, OPS1-3, PBS-9, PMP-19, PPM-10
 Wang(Y.N): PSB-9
 Wang(Z): OPS1-3
 Ward: POS1-3
 Watson: PBG2-3, PM-21
 Weber(J.C): PBG2-5, PBG2-6
 Weber(S): PMP-16
 Webster: PEB1-10, PEB1-16, PEB1-18, PMP-15
 Wehner: PC-12
 Wei: PGG2-3, PRG2-7
 Weightman: OB3-1, PMP-15
 Weijers: PB1-14, PPC1-19
 Wellman: PM-21
 Weniger: PC-9
 Wenzel: PPC1-20
 Werne: OPC1-3, PB1-20, PPC1-3
 White(H.K): PBG2-13
 White(M.L): PM-22
 Whitar: PRG1-21
 Wieclaw: POS2-11
 Wieland: PMP-14
 Wiesenberg: PB2-11, PCS-7, PSB-17
 Wilkes: OBD1-1, OP7-3, PB1-1, PBG2-4, PC2-8, PC2-9, PGG1-1, PRG1-17, PRG1-4, PRG2-11
 Wilkins: PG-28
 Wilson: PEB2-7
 Williams: PPC1-8
 Winsemann: PG-23
 Wirmann: PC2-18
 Witte: PMP-10
 W ojcik: PG-26, PG-27
 Wolff: PC2-3
 Wolters-Arts: OP5-3
 W ostmann: PB1-15
 Wuchter: OPC2-4
 Wysocki: PB2-20, PCS-2

X

Xia: PG-4, PG-5
 Xianming: PRG2-21
 Xiao(X.M): PG-28
 Xiao(Y): OP5-4
 Xiaojuan: PG-5, PG-6, PG-7
 Xinming: PEB1-6
 Xiong: PB1-16, PG-25, POS1-5, PRG1-13

Xu(G): PRG1-7

Xu(S): OGC-1, PMN1-6, PRG1-20

Y

Yalçın: PBG2-8, PFA-7, PG-11, PG-17, POS2-1

Yamamoto(M): PC2-27

Yamamoto(S): PM-4, PM-5

Yamamuro: PB2-17

Yan: PEB1-14

Yanovskaya: POS1-9

Yasuo: OB2-2

Yesiladali: PBG2-8

Yi: PBS-5

Yim: PB1-6

Ying: PG-4, PG-5

Yoda: PB2-1

Yoshioka: PMN2-10

Yperman: PC-1

Yuanzhuang: PPM-6

Yue: PG-12

Yum: PPC1-9

Yunker: PB2-12, PC2-22

Yunxia: PRG2-21

Yurdokök: OP4-2

Yuri: PPM-7

Z

Zabrouskov: PMN2-11

Zachos: OPC2-4

Zancada: PBC-9, PSB-18

Zaton: PBG1-2

Zdanaviciute: PBS-25

Zecchinello: PGG1-2

Zengye: PG-4

Zetra: POS1-12

Zhang(B): PB1-16

Zhang(H): PG-25, POS1-5

Zhang(S): OGC-1, OPS1-3, PB1-16, PBS-1, PBS-12, PBS-9, PG-9, POS2-7

Zhang(W.-B): PSB-3

Zhang(X): PCS-13

Zhangying: PMP-7

Zhao(C): OPS1-3

Zhao(Q): POS1-5

Zheng(Q.H): PG-28

Zheng(Y): PPM-10

Zhihuang: PRG2-21

Zhisheng: PG-4, PG-5

Zhong: PG-12

Zhongyao: PRG2-21

Zhou(H): PRG1-12

Zhou(S): PGG2-4

Zhou(Y): PB1-4

Zhu(G): PBS-12

Zhu(Y): PBS-1

Zhuang: PSB-9

Zink: OB2-1, OP7-3, PC-6, PMP-13, PMP-8

Zinniker: OGPR-2, OPS2-3, PB2-21

Zou(H): PGG2-4

Zou(Y.-R): PG-13

Zubova: PBS-10

Zueva: PGG1-6, PGG1-7

Zumberge: OP3-3, PB2-12, PFA-5, PFA-7,

POS1-13, PPM-15

Zuñiga: PMN2-9

Zuñiga-Santillán: PRG2-13

Ž

Žagar: PMP-2

Životić: PC-12

KEYWORDS

1

1-34-Dimethoxyphenyl-2-Propanone: PCS-2
 1-Alkyl-236-Trimethylbenzenes: PBS-21
 1-Chloro-*n*-alkanes: PM-3
 1-Chloro-octadecane: PM-3
 1-Fluoronaphthalene: PMN1-10
 1-Halo-*n*-Alkanes: PM-3
 1-Iodo-*n*-Alkanes: PM-3
 1-Methyldibenzothiophen: PGG1-3
 1-Methyldibenzothiophene: PRG1-16
 1-Methylnaphthalene: PGG1-8, POS2-1
 1-Methylnaphthalene: POS2-1
 1-Methylnaphthalene+2-Methylnaphthalene:
 POS2-1
 1-Methylphenanthrene: PPM-13
 1-Phenylnaphthalene: PB1-8
 10-Oxo-octadecanoic: PFA-3
 111333-Hexafluoroisopropanol: PRG2-2
 114-Diols: PB1-11
 12-Di-O-Alkyl-Sn-Glycerol: PB1-14
 1234-Tetramethylbenzene: PBG2-4
 125-Trimethyl-naphthalene: PMN1-1
 127-Trimethylnaphthalene: PGG2-2
 1314-Dimethyloctacosane: PB1-14
 1316-Dimethyloctacosane: PB1-14
 1317-Diasterenes: PBG1-2
 135-Trimethoxybenzene: PM-23
 136-Trimethyl-Naphthalenes: PMN1-1
 13a-H-*n*-Alkylated: PB1-16
 13Chopanoids: PC2-21
 13Cisoprenoids: PC2-21
 13Ckero: PC2-26
 13Cmethane: PG-24
 13Cmole: PC2-26
 13Cn-Alk: PC2-26
 13CPDB: PC2-21
 13CPMAS: PSB-18
 13Cpristane: PC2-21
 14-Dicyclo-Hexylbenzene: OEB-3
 14C Phenyldiazonium: PSB-14
 1516-Dimethyltriacontane: PB1-14
 16H-Phyllocladane: PC-12
 17-Dimethylphenanthrene: PEB1-14
 1721-Secohopanes: PGG2-8
 1721-Secohopanoic: PGG2-8
 17ah-diahopane: PB1-16, PPM-3
 17ah β h-Hopanes: PGG2-4
 17ah β h-hopanoic: PGG2-4
 17ahhopanes: PBG1-10
 18-Hydroxy: PB1-11
 18H-Oleanane: PRG1-13

2

2-2-Methylbutyl-35-di-2-16-
 Methylheptylthiophene: PB2-18
 2-Alkyl-134-trimethyl: PEB2-17

2-Ethyl-4-N-Alkylthiophenes: PB2-1
 2-Fluorodibenzothiophene: PMN1-10
 2-Methyl-4-n-Alkyl: PB2-1
 2-Methylanthracene: PRG1-1
 2-Methylbacteriohopanetetrol: OP4-2
 2-Methylguanossylhopane: OP4-2
 2-Methylhopane: OPE2-3
 2-Methylnaphthalene: PGG1-8, POS2-1
 2-Methylthiophene/toluene: POS2-6
 2-Naphthoic: PRG2-2
 2-Phenantrenes: PGG2-5
 2-Phenylnaphthalene: PB1-8
 2-Phenylnaphtho-Thiophenes: PB1-12
 2-Phenylphenanthrenes: PB1-8
 2-Syrkharatinskaya: PBS-20
 2-Yanemdeyskaya: PBS-20
 2 β -Methylhopanes: PC2-17
 21-Secohopanoic: PGG2-8
 22-Dimethylalkanes: PB1-20, PB2-21
 23-Di-*o*-alkyl-Sn-glycerol: PB1-14
 2324-Dimethylcholesteroids: OOS-3
 24-/23-Dimethylpentane: PGG2-2
 24-Ethylcholest-5-En-3-Ol: PPC1-12
 24-Ethylcholest-5-En-3 β -Ol: OB2-2
 24-Ethylcholest-5-En-3 β -Ol: PPC1-21
 24-Isopropylcholestanes: OGPR-3
 24-Isopropylcholesterols: OGPR-3
 24-Methylcholesta-5,22(E)-Dien-3 β -Ol: OB2-2
 24-Methylcholesta-5,24(28)-Dien-3 β -Ol: OB2-2
 24-N-Propylcholestane: OGPR-3
 24-N-Propylcholestanes: PRG1-6
 24-N-Propylcholesteroles: PRG1-6
 24-Norcholesta-522-Dien-3 β -Ol: PB1-10
 24-Norcholestane: OB2-2, PB1-10
 24-Norcholestanes: PB1-10
 24-Norcholesterol: OB2-2
 24-Nordiacholestane: OB2-2, PBS-3
 24-Norlupane: OP1-2
 24-Norsterane: PB1-10
 24-Norsterol: PB1-10
 24-Norsterols: PB1-10
 24/27+24-Nordiacholestane: PBS-5
 2428-Bisnorlupanes: OP1-2
 246-Trihydroxybenzoic: PM-23
 246-Trimethoxy-Benzaldehyde: PM-23
 246-Trimethoxy: PM-23
 246-Trimethoxybenzaldehyde: PM-23
 246-Trimethoxytoluene: PM-23
 25-DMT/2-ET+23-DMT+24-DMT: PG-14, POS1-
 11
 25-Norhopane: OGC-1, PRG1-6
 25-Norhopanes: PRG1-5, PRG2-19
 26-DMBA: PBG2-3
 26101519-Pentamethyleicosane: PMP-5
 26101519-Pentamethylcosane: PMP-21, PPC1-18
 2610151923-Hexamethyltetracosane: PMP-5
 261115-Tetramethylhexadecane: PMP-5

27-Nor-24-Methyl-5 α : OB2-2
 27-Nor-24-Methylcholestane: OB2-2
 27-Nor-24-Methylcholesterol: OB2-2
 27-Nor-Methylcholesta-: OB2-2
 27-Nor-Methylcholesta-5,22(E)-Dien-3 β -Ol:
 OB2-2
 27-Norcholestanes: OGPR-3

3

3-+4-Methyldiamantanes: PGG2-3
 3-2-Naphthyl-Benzo[B]Thiophene: PB1-12
 3-34-Dimethoxyphenyl-Propanoic: PC-2
 3-Fluorophenanthrene: PMN1-10
 3-Methyl-Alkane: PSB-4
 3-Methylheptane: PPM-14
 3-Phdbt: PB1-8
 3-Phenantrenes: PGG2-5
 3-Phenylnaphtho[21-B]Thiophene: PB1-12
 3 β -Methylhopanoids: OP4-4
 3 β -Methylhopanes: PC2-25
 30-2-5-Methylenethienylhopane: PC-11
 30-2-Methylenethienyl: PC-11
 3,4-Dihydroxy: PSB-3
 3,4-Dimethoxybenzoic: PC-2, PCS-2
 3,4-Dimethoxyphenylacetic: PC-2
 3,4-Dimethyl: OB1-1
 3,4-Dimethylbenzoic: PBG2-3
 3,4-Substitution: PFA-2
 3,4,5-Trihydroxy: PSB-3
 3,4,5-Trimethoxybenzoic: PCS-2
 3D-Spectrofluorometry: PM-15, PM-20

4

4-Hydroxy-3-methoxycinnamyl: PM-22
 4-Hydroxy-3,5-dimethoxycinnamyl: PM-22
 4-Hydroxycinnamyl: PM-22
 4-Isopropenylphenol: OPC2-2
 4-Me-Osterane: PPM-7
 4-Methyldibenzothiophen: PGG1-3
 4-Methyl-steranes: PC2-26
 4-Methylsteroids: PPC1-14
 4MDBT/1MDBT: OPS1-2, PGG1-3
 4Sorg/C: POS2-6
 4SPA: PB2-16

5

5-*n*-Alkylresorcinol: OPC2-2
 5 β -Cholanic: PMN1-4
 55-Diethylalkanes: PB1-20, PB2-21

8

8-Benzyloxy-26-Dimethyloctan-1-Ol: PB2-2
 8-Methylheptadecane: PC2-17
 814-Secohopanoids: PGG1-1

9

9-Methylphenanthrene: PGG1-8

A

A-Horizons: OSB2-2
 A-Ring: OM-1
 Aberdeen: PEB1-16
 Abies: PCS-4
 Abietane: OB1-2, PC-12
 Abietanes: OB1-2
 Abietic: PFA-6
 Abiogenic: PBG1-15, PG-17, PG-7
 Abiogenous: PGG1-4
 Abiotic: OGPR-1, OP7-3, PBC-14, PBC-9, PBG1-16, PBG1-4, PBG1-6, PC-6, PM-18, PM-22, PMP-16, PRG1-11
 Abscission: OSB1-1
 Absorbance: PMN1-8, PMP-23
 Absorption bands: PRG1-10
 Absorption: OPS2-1, PC-4, PEB1-1, PEB2-12, PG-26, PG-27, PM-21, PM-24, PSB-16, PSB-4, PSB-8
 Abyssal: PB1-13, PBG1-6, PGG1-4, PM-26
 Ac/Ad: PC-2
 Ac/Al: PC-2
 Ac/Als: OSB2-2
 Ac/Alv: OSB2-2
 Accreting: PBG1-9
 Accretion: OP7-3, PSB-19
 Accretionary: PB1-18, PB2-9
 Accumulation/Preservation: PSB-4
 Acenaphthene: PEB1-17
 Acer: OP3-2, OP6-4
 Aceramic: PFA-7
 Acetal: PSB-13
 Acetaldehyde: PEB1-15
 Acetate/Malate: PM-28
 Acetate: OB3-1, OMN-3, OP7-3, PB2-17, PB2-3, PC-6, PFA-2, PG-9, PMN2-10, PMP-13, PMP-15
 Acetic: OP4-3, POS1-9
 Acetoclastic: OMN-3
 Acetogenesis: PMP-13
 Acetogenic: PM-28
 Acetoguaiacone: PCS-9
 Acetone: PB2-15, PEB1-15, PMN1-3
 Acetophenone: PFA-2
 Acetosyringone: PCS-9, PM-4, PM-5, PSB-3
 Acetovanillone: PM-4, PM-5, PSB-3
 Acetyl: PMN2-6
 Acetylated: PB2-9
 Acid-acidified: PMP-21
 Acid-base: PGG1-4, PM-15
 Acid-based: PM-28
 Acid-catalysed: PBG1-2
 Acid-containing: PC-2, PM-2
 Acid-crude: PGG2-15
 Acid-free: PGG2-15
 Acid-like: PBC-9
 Acid-tolerant: PB2-1
 Acid-volatile: PSB-8
 Acid/aldehyde: PB2-20, PC2-1, PCS-2
 Acid/oil: PGG2-15

- Acidic: OBD2-3, OP5-3, OSB2-1, OSB2-2, PB2-1, PB2-4, PB2-7, PBG1-16, PBG1-4, PBG1-5, PEB1-12, PEB2-9, PGG2-13, PGG2-7, PM-15, PMN2-4, PPC1-15, PRG2-14, PRG2-2, PSB-5
- Acidification: OBD2-2, PC2-26
- Acidified: PB2-20
- Acidity: PGG2-7, PMN2-11, PMN2-4, PSB-2
- Acidophilic: OP5-3, PBG1-4
- ACL: PPC1-26
- ACP: PMP-23
- Acritarch: PBG1-10, PM-28, POS2-7
- Acritarchs: PB1-22, PBG1-10
- Acrylic: PB2-7, PCS-2
- Actinides: PEB2-9
- Actinobacteria: PMP-20
- Acuminate: PSB-9
- Acyclic: OBD2-1, PB1-18, PB2-19, PBS-12, PC-12, PC-9, PC2-17, PC2-25, PEB2-4, PMP-5, POS2-6, PSB-4
- Acyl: OB2-1, PMP-13, PMP-6, PMP-8
- Acylphosphatidylglycerols: PMP-8
- Ad/Al: PC2-1
- Ad/Alv: PBG1-9
- Adamantane: PGG1-5
- ADCP: PBG2-14
- Additives: OEB-3, POS2-15
- Adduction: PMN1-6, PRG1-7
- Adducts: OM-2
- Adelaide: PPC1-7
- Adenosylhopane: OP4-2
- Adipocere: PFA-3
- Adipose: PFA-3
- Adiyaman: PRG1-18
- Admixed: OUM-1, PGG1-9, PRG1-14
- Admixture: PBG1-7, PFA-2, PGG1-12, POS2-13, PSB-17
- Admixtures: PBS-17, POS2-1
- Adriatic-dinaridic: PPC1-1
- Adriatic/dinaridic: PPC1-1
- Adriatic: PPC1-1
- Adsorption-desorption: PPM-5
- Adsorption: OGC-2, OP7-3, OPG-3, PBC-3, PBC-4, PBG1-5, PC-4, PC-5, PC-7, PCS-8, PEB1-3, PEB2-9, PG-26, PG-27, PGG2-6, PM-11, PM-13, PM-26, PMP-20, POS1-9, PPM-13, PRG2-16, PSB-14
- Adsorptive: PPM-5, PRG1-5
- Advection: OPE1-1, PC2-24
- Advective: OPE1-1, PC2-24
- AED: PRG1-8
- Aegean: PBG2-7, PFA-9
- Aeolian: OPE1-2, OPE2-2, PPC1-15, PPC1-8, PSB-19
- Aerated: OP6-1
- Aeration: OP6-1, PBS-10, PCS-10
- Aerial: PCS-1
- Aerobes: OP6-2
- Aerobic: OB1-3, OBD2-1, OBD2-3, OP6-2, OPE2-3, OSB1-3, PB1-18, PB2-9, PC2-17, PC2-25, PEB1-12, PEB2-18, PEB2-19, PEB2-7, PMP-15, PMP-17, PRG1-17, PRG1-4, PRG2-10
- Aerobically: OB1-3
- Aerosol-based: PBG2-5
- Aerosol: OEB-1, PBC-10, PBC-2, PBC-5, PBG2-5, PBG2-6, PEB1-15, PEB2-15
- Aerosols: OB1-2, OEB-1, PBC-11, PBG2-5, PBG2-6, PC2-22, PC2-24, PEB2-15
- AF: PCS-9
- Affinities: OGPR-2, PBS-9, PC-4, PSB-15
- Affinity: OB2-1, OM-1, OM-2, OP2-2, OPG-3, PBS-16, PC-4, PGG2-10, PM-26, PRG2-16, PSB-15, PSB-19
- AFM: PBG1-5
- Africa: OP4-1, OPC1-3, PB1-20, PBC-9, PBG2-7, PC2-9, PG-23, PM-12, PPC1-1, PPC1-19, PPC1-28, PPC1-3, OP4-1, PBC-9, PC2-13, PC2-9, POS2-12, PPC1-20
- Ag/AgCl: PSB-1
- Ag: PBG2-2, PEB2-12
- Ag₂S: PM-1
- Agatha: PCS-12
- Agave: OP3-2
- Age-corresponding: OGC-2
- Age-diagnostic: PB1-10
- Age-range: OOS-3
- Age-related: OP3-3, OPS2-3
- Age-specific: PBS-3
- Ageing: PGG2-7, PM-18
- Agglomerate: OPG-3
- Agglomerating: OPG-3
- Aggregate: PBG1-6, PCS-3
- Aggregates: OMN-2, PBG1-6, PBG2-7, PCS-3, PCS-5, PEB2-9, PGG2-6, PSB-21, PSB-5
- Aggregation: OM-2, OMN-2, PEB2-9
- Agilis: PMP-20
- Aging: PFA-6, PMN2-4
- AgNO₃: PMN2-9
- Agricultural: OEB-1, OP2-2, OP4-2, PBC-1, PBC-8, PCS-10, PCS-12, PCS-7, PEB1-5, PEB2-1, PEB2-9, PSB-6
- Agriculture: OEB-1, PBC-1, PCS-12, PEB1-3, PEB2-2, PM-10
- Agrobiological: PSB-18
- Agronomical: PBC-9
- Air-dried: PCS-12, PCS-3, PSB-1
- Air-sea: PPC1-16
- Air-soil: PEB2-2
- Air/liquid: PSB-11
- Air: OEB-1, OP4-1, PBG2-5, PBG2-6, PC2-27, PEB1-13, PEB1-15, PEB1-3, PEB1-5, PEB2-15, PEB2-2, PEB2-8, PPM-3, PRG1-1, PSB-15, PSB-21
- Airborne: PEB1-15, PEB2-8
- Aircraft: OEB-1
- Airsheds: OEB-1
- AK-1: PG-28
- Akar: PBS-8
- Akata: OP4-3
- Aklak: POS2-5

- Al₂O₃: PB2-18
Ala: PM-2
Alanine: PB1-17, PM-2, PM-24, PM-26
Alaquod: PSB-13
Alaska: OP1-1, PBG2-5, PBG2-6
Albedo: PCS-2
Alberta: OP6-3, PG-10
Albian: OPC2-3, PC-11, PGG1-10, PPC1-10, PPC1-18
Albumin: PM-2
Alcaline: PBC-13
Alcohol-Benzol: PGG1-13
Alcohol-Toluene: POS1-9
Alcohol: OP4-2, PB1-14, PB2-17, PB2-9, PEB2-7, PMP-4
Alcoholic: PSB-1
Alcohols: PB1-15, PB1-19, PB1-9, PB2-2, PFA-2, PFA-3, PFA-6, PFA-8, PM-11, PM-12, PM-22, PM-3, PMN1-4, PMP-14, PMP-4, PPC1-12, PPC1-15
Aldehyde-containing: PC-2
Aldehyde: OSB2-1, OSB2-2, PB2-3, Aldehydes: PM-4, PSB-6
Aldehydic: OSB2-1
Aldrich-HA: PSB-14
Aldrin: PEB2-1
Aleksinac: PM-24
Alemanic: PC2-17
Aleurite: PBS-25
Aleutian: PC2-27
Alfisol: PSB-15
Alga: PB1-10, PB2-8
Algae-rich: PPM-9
Algae: OGPR-3, OOS-3, OP2-1, OP4-4, OP5-1, OP7-2, OPE2-3, PB1-1, PB1-10, PB1-11, PB1-16, PB1-19, PB1-22, PB2-5, PB2-8, PBG1-10, PBG1-11, PBG2-1, PC-10, PC2-17, PC2-19, PC2-20, PC2-21, PC2-6, PC2-8, PGG1-12, PGG2-10, PM-28, PMN1-8, PMP-11, PMP-12, PMP-4, POS2-7, POS2-9, PPC1-11, PPC1-14, PPC1-8, PPC1-9, PRG1-6
Algaenan: OP3-1, PB1-1, PM-23, PM-6
Algaenans: PM-12, PM-25, PM-28
Algae: PM-11
Algal-amorphous: PB1-5, PPC1-4
Algal-bacterial: PC2-8
Algal-derived: PBG2-7, PC2-6, PPC1-14, PPC1-17
Algal-dominated: PPC1-17
Algal-laminated: POS2-15
Algal/Bacterial: PSB-4
Algal: OB2-2, OOS-3, OP3-1, OPE1-1, PB1-1, PB1-16, PB1-22, PB1-5, PB1-6, PB2-10, PB2-4, PB2-5, PBG1-10, PBG1-9, PBG2-1, PBG2-7, PBG2-8, PC2-15, PC2-17, PC2-20, PC2-6, PC2-8, PGG2-10, PM-12, PM-28, PM-6, PMP-10, PMP-11, PMP-12, PMP-14, PMP-4, POS1-12, POS2-12, POS2-15, PPC1-1, PPC1-10, PPC1-14, PPC1-21, PPC1-5, PPC1-7, PRG1-13
Algarve: OPE1-3, PB2-13
Algerian: PBS-26
Alginate: POS2-4
Alginite: PBG2-4
Algorithms: PBS-22, PPM-14
Alicyclic: OP2-3
Aliphatic-rich: PPC1-17
Aliphatic/aromatic/Polar: PC2-4
Aliphatic/aromatic: PEB2-13
Aliphatichydrocarbons: PEB1-11
Aliphaticity: PRG1-10
Alk-1-enes: PM-14
Alkadienes: PB2-13, PBC-9
Alkali-insoluble: PBC-14
Alkaline: OB2-1, OBD2-3, PB1-21, PBG1-8, PC-2, PC-9, PC2-25, PM-17, PM-4, PPC1-8, PSB-4, PSB-5, PSB-7
Alkalinity: PMP-3
Alkalized: PM-7
Alkan-18-one: PM-12
Alkanamides: PBG1-16
Alkane/alkene: PB2-13, PM-3
Alkane/hopane: OP1-1
Alkanes: OEB-1, OUM-2, PB2-18, PB2-3, PBC-14, PBS-1, PBS-2, PBS-5, PC-12, PC2-15, PC2-22, PGG2-14, PMN1-4, PMN1-6, POS1-12, POS2-2, PRG1-13, PSB-3OB1-1, OBD1-2, OBD2-1, OGPR-2, OP6-1, PB1-16, PB1-20, PB2-11, PB2-19, PB2-21, PBC-9, PBG1-8, PBG2-2, PBS-12, PC-12, PC2-22, PC2-25, PC2-3, PCS-6, PCS-9, PEB1-11, PEB1-13, PEB2-18, PGG1-7, PGG2-2, PGG2-4, PM-12, PM-14, PM-3, PMN1-6, PMP-12, PMP-19, POS2-12, POS2-9, PPC1-15, PPM-14, PPM-3, PPM-7, PRG1-1, PRG1-12, PRG1-5, PRG1-6, PRG2-11, PSB-11
Alkanes+alkenes: POS2-1
Alkanoates: PB1-11
Alkanoic: OEB-1, PB1-6, PEB1-7, PM-4, PM-5, PMN1-1
Alkanol: OEB-1
Alkanols: PBG2-13, PEB1-7, PMN1-1, PMP-18, PMP-19
Alkene/alkane: PB1-1, PM-28
Alkene: OP2-1
Alkenes/alkanes: PEB1-13
Alkenes: OP2-1, PB2-18, PCS-9, PEB1-13, PFA-8, PGG2-3, PM-1, PM-18, PMP-19, PRG1-1
Alkenoate-biosynthesizing: PMP-1
Alkenoates: PMP-1
Alkenols: PCS-6
Alkenone-biosynthesizing: PMP-1
Alkenone-derived: PPC1-20
Alkenone-unsaturation: PMP-1
Alkenones: OP2-1, OP7-2, OPC1-1, OPC2-1, OPC2-4, OPE1-1, PBG1-13, PBG2-1, PC2-13, PC2-24, PMP-1, PMP-14, PPC1-16, PPC1-2, PPC1-20, PPC1-23, PPC1-28
Alkyl-aryl: PM-23
Alkyl-benzene: PMN1-1
Alkyl-benzenes: PC2-25

- Alkyl-cyclohexanes: PC2-25
 Alkyl-cyclopentanes: PC2-25
 Alkyl-metalloporphyrins: PPC1-6
 Alkyl-Naphthalene: PMN1-1
 Alkyl-steranes: PGG2-13
 Alkyl/*o*-alkyl: PSB-18
 Alkylamides: PEB2-12
 Alkylarene: PGG1-15
 Alkylaromatic: PGG2-6, PRG1-5 OPG-1
 Alkylated: OEB-2, PB2-1, PBS-17, PC-1, PEB1-1, PEB2-10, PEB2-11, PEB2-13, PEB2-14, PGG1-2, PM-18, PM-27, PPM-10
 Alkylating: PM-27
 Alkylation-dealkylation: PGG1-15
 Alkylation: OP4-4, PEB2-12, PEB2-4, PG-25, PGG1-15
 Alkylations: PB2-7
 Alkylbenzene: OBD2-3, OP3-4, PRG2-9
 Alkylbenzenes: OBD1-1, OPG-1, PB1-1, PB2-16, PB2-5, PC-11, PEB2-12, PEB2-17, PEB2-18, PEB2-4, PGG1-7, PM-14, PM-9, PRG2-9
 Alkylbenzenes: C1-C4: PB2-16
 Alkylbenzens: PRG1-1
 Alkylbiphenyl: OP5-2
 Alkylbiphenyls: PB2-5
 Alkylcarbazoles: PPM-13
 Alkylcycloalkanes: PRG1-5, PRG1-6
 Alkylcyclohexanes: PB2-3, PEB2-4, PGG1-7 PB1-5
 Alkylcyclopentanes: PB2-3, PRG1-6 PRG1-5
 Alkylcyclopentenes: PB2-3
 Alkylether: PMP-6
 Alkylethers: PMP-6
 Alkyllic: PBC-6
 Alkylketones: PM-3
 Alkyl-naphthalenes: PB1-1, PB2-5, PBG2-2 OP3-4, PGG2-2
 Alkyl nitriles: PEB2-12, PM-12, PM-3
 Alkylphenanthrene: OP3-4, PGG2-2
 Alkylphenanthrenes: PB1-1
 Alkylphenolic: PBG2-7, PFA-2
 Alkylphenols: PM-9
 Alkylphernols: PB2-16
 Alkylsteranes: PGG2-13
 Alkylthiols: OGPR-1
 Alkyltoluenes: PM-14
 Alkyltriaromatic: PGG1-6
 Alkylphenols: PM-9
 Allophanes: PCS-9, PM-26
 Almandine: PGG1-4
 Alorthod: PSB-13
 Alpha-cleavage: OP2-3
 Alpha-proteobacteria: PMP-11
 Alpine: PBG1-3, POS2-9
 Alps: PC2-11
 ALS: OUM-2
 Alsace: PC2-11
 Alterniflora: PBG2-13
 Altispira: OGC-4
 Alum: PBS-18
 Alumina: PBG1-5, PEB2-2
 Aluminium: PB2-4, PBG1-5, PEB2-2, PM-26
 Aluminum: PBG1-8
 Amalgams: PFA-7
 Amazon: OB3-1, PB1-13, PB1-22
 Amazone: PBG1-9
 Amber: PC-10, PFA-9 PC2-5
 Ambient: OB2-1, OP2-2, OP6-4, OPC2-4, PBG1-4, PBG2-6, PEB1-11, PEB1-15, PGG2-15, PPC1-2
 Amerasian: PBG1-14
 America: PBG1-1, PC2-1, PC2-6, PGG1-12, PM-12, PMP-4, POS1-13, PPC1-26
 American: PC2-7, PCS-6, PEB2-3, PFA-3, PMN1-8, PMN2-11, PRG1-13, PRG2-6
 Amide-/ether-Bound: PB1-6
 Amide-N: PM-24
 Amide: OM-2, PBG1-16, PM-2, PM-24, PM-8
 Amides: OP3-2, PBG1-16, POS1-9, PSB-11
 Amido-acid: PBG1-16
 Amines: PBG1-16 PM-8
 Amino-*n*-butyric: PM-24
 Amino: OM-1, OM-2, OSB1-1, OSB2-3, PB1-17, PBC-12, PBG2-14, PCS-11, PCS-14, PM-2, PM-24, PM-26, PM-8, PMN1-8, PMN2-6, PMP-22, PMP-23, PSB-5, PSB-7
 Aminoacids: PSB-13
 Ammonia-oxidiser: OP4-2
 Ammonite: OB1-2
 Ammonium: OP6-1, OSB1-1, PB1-7, PBG1-16, PC-2, PCS-2, PM-2, PM-4, PMN1-3, PMN1-8, POS1-3
 AMO: PMP-21, PMP-3
 Amoebae: OPC2-2
 Amon: PMP-17
 Amorphinite: POS2-7
 Amorphisation: PM-10
 Amorphogen: POS2-7
 Amphibolite: POS2-12
 Amphicephala: PB2-1
 Amphiphilic: OGPR-1, PEB2-9
 Amplicons: PMP-11
 Amyrins: PFA-2, PPC1-21 PB2-17, PPC1-20
 Amyrone: PB2-17
 Anadarko: PMN1-5, PRG1-9
 Anadyr: PBS-2
 Anaerobes: OP6-2
 Anammox: PB1-7, PMN1-3
 Anammoxosome: PB1-7, PMN1-3
 Anaplerotic: OSB2-3
 Anastomosing: PBS-4
 Anatolia: PBG1-10, POS2-1
 Anau: PBG1-3
 Ancestors: PB1-14
 Ancient: OB1-1, OGPR-2, OOS-3, OP2-1, OP4-1, OP7-2, OPC1-3, PB1-18, PBG1-15, PBG2-1, PBG2-13, PBG2-3, PBG2-9, PBS-1, PBS-12, PC2-14, PC2-5, PEB1-1, PEB2-17, PFA-4, PFA-9, PGG2-10, PGG2-6, PM-18, PM-19, PM-6, PMP-1, PMP-12, PMP-13, PMP-14, PMP-22, PMP-4, PRG1-13

- Andes: PC2-1, PC2-18
 Andesitic: PC-8
 Andosols: PCS-1, PCS-9 PCS-11 PSB-2
 Andra: OB1-2 PB1-21 PC2-4
 Androstane: PC2-4
 Angeles: OPG-2, PEB1-14
 Angiosperm-derived: OP1-2, PGG1-10
 Angiosperm-dominated: PPC1-14
 Angiosperm: OOS-3, OP1-2, PGG1-10, PGG2-2, PPC1-15, PRG2-20 PC2-27, PGG1-10
 Angola: PPC1-20, PRG2-18
 Anhydride: PB2-10
 Anhydrite-bearing: PBS-12, PG-24
 Anhydrite: PBS-12, PGG1-2, PGG2-3
 Anhydrous: PG-25, PGG2-3, POS1-5
 Animal: OPE2-3, PC2-26, PFA-2, PFA-8, PFA-9, PM-10, PM-13
 Animalia: PB2-11
 Animals: OGPR-3, PC2-26, PFA-2, PM-21
 Anion: PBS-1, PRG2-2
 Anionic: PEB2-9
 Anions: PEB2-3, PMP-3, PRG2-14
 Anisian-Ladinian: PBS-15
 Anisian: OB3-2, PC2-20
 Anisotropic: PRG2-18
 Anisotropy: PC-7
 Ankara: PBG1-10
 ANME-2: PMP-21
 Anmmox: PB1-7
 Anophagefferens: PB2-8
 ANOVA: PEB1-18
 Anoxia/Euxinia: PC2-16
 Anoxia: OOS-3, OPE2-3, OPS2-2, PB1-5, PBG2-4, PC2-17, PC2-26, PC2-8, PMP-1, PPC1-4
 Anoxic-Dysoxic: PBS-21
 Anoxic: OB1-3, OBD1-1, OGPR-1, OGPR-2, OP2-1, OP6-2, OPE1-1, OPE2-3, OPS1-1, PB1-19, PB1-7, PB1-9, PB2-4, PBG2-9, PC2-11, PC2-12, PC2-16, PC2-17, PC2-19, PC2-20, PC2-21, PC2-26, PFA-6, PGG2-1, PGG2-8, PM-11, PM-12, PM-15, PM-20, PMP-1, PMP-10, PMP-12, PMP-2, PMP-6, POS1-11, POS2-14, POS2-15, PPC1-1, PPC1-14, PPC1-18, PPC1-27, PPM-11, PRG1-4, PRG2-12, PRG2-2, PRG2-6, PSB-4, PSB-8
 Anoxity: PB2-4
 Anoxygenic: OP2-1, PPC1-4
 OPE2-3, PB2-13, PB2-9, PBG2-4, PC2-15, PC2-9, PEB1-1, PEB1-5, PM-11, PM-13, PM-2, PM-20, PM-27, PM-5, PM-8, PMN1-8, PMN2-1, PPC1-8, PSB-14, PSB-5
 Aquifer: OBD1-1, PB2-16, PEB1-8, PRG1-15, PRG2-10
 Aquifers: OBD1-1, PEB1-9, PG-24, POS1-16, PRG2-2
 Arabia: PEB1-2
 Arabian: OPC2-4, OPE2-2, PB1-11, PBG1-10, PEB1-2
 Arabinose: PBG2-6, PCS-8
 Arable: OP4-2, PBC-1, PCS-10, PCS-7, PSB-17, PSB-6
 Arade: OPE1-3
 Aragón: PCS-12
 Arana: PSB-2
 Araripe: PBS-4
 Araucariaceae: PBS-16
 Araucariaceae: OB1-2, PC2-5
 Araucariacean: PBS-16, PRG2-16
 Arborane: PPC1-14
 Arbuckle: PB1-1
 Arc: PB2-9, PBG1-4, PBS-8, PC2-25, ARCH: OB1-3
 Arch: PB2-14, PG-10, POS1-9, PPM-4
 Archaea-related: OMN-1
 Archaea: OB1-3, OB2-3, OGPR-3, OMN-1, OP2-1, OP2-4, OP5-1, OP6-2, OPC1-3, PB1-14, PB1-18, PB1-20, PB2-2, PBG1-4, PC2-19, PC2-25, PMN2-2, PMP-17, PMP-18, PMP-21, PMP-5
 Archaeal: OB2-3, OB3-1, OGPR-2, OMN-1, OP2-4, OP5-1, PB1-14, PB1-18, PC2-19, PC2-25, PMN2-2, PMP-17, PMP-18, PMP-5
 Archaeal: OP2-4, PC2-25, PMP-22, PMP-23
 Archaeobacterias: PB1-22
 Archaeobotanical: PBC-1
Archaeoglobus: OMN-1
 Archaeol: OB3-1, PB2-2, PMP-17, PMP-18, PMP-21, PPC1-23
 Archaeological: PB2-6, PBG2-7, PFA-1, PFA-5, PFA-6, PFA-7, PFA-9
 Archaeologists: PFA-1
 Archaeology: PFA-1, PFA-8
 Archean: PBG1-15, PM-18
 Archetypical: PPC1-7
Archobacter: PMP-15
 Arctic: OP1-2, OPC2-3, OUM-1, PB1-7, PBG1-14, PBS-3, PC2-22, PCS-6, PGG1-10, PM-22, PMP-11, PPC1-21
 Arenosols: PBC-3
 Argentina: OPS1-1, PRG2-8
 Argentous: PB2-1
 Argillaceous-siliceous: PBS-10
 Argillaceous: PBG1-12, PBS-10, PBS-12, PBS-21
 Argillite: PGG2-12, PSB-25
 Argillites: OP2-4, PGG2-5, PGG2-6, POS2-2
 Argillitic: OP2-4
 Argillutites: POS2-7
 Argon: PBG1-12, PC2-5, PMN1-3, POS1-5
 Argutum: OP6-4
 Aridification: OP4-1
 Aridisols: PCS-1
 Aridity: OP4-1, OPE2-2, PBG2-10, PPC1-15, PPC1-26 PPC1-3
 Arizona: OPC1-2
 Aromates: PC-12
 Aromatic-asphaltic: POS2-15, PRG2-3
 Aromatic-saturate: PPC1-17
 aromatic rings: PRG1-10
 Aromatic/unsaturated: PSB-18

Aromaticity: ORP-2, PC-8, PGG2-14, POS1-10
 PRG1-10
 Aromatisation/polycondensation: OP2-3
 Aromatisation: OP2-3, PB2-5, PB2-6, PBC-9, PC2-11, PFA-6
 Aromatised: PGG1-1
 Aromatization: PC-7, PG-25, PM-1, PMP-13
 Aromatized: OUM-1, PC2-17
 Arrabury: PRG2-16
 Arrhenius: POS1-10
 Artefacts: PBC-13, PFA-7, PFA-9, PM-18, PPC1-7
Artemia: PB2-4, PBG1-8
 Artesian: PRG2-10
 Arthrobacter: PMP-20
 Arthropod: OP3-2
 Arthropods: OP3-2
 Artifact: OB1-1, OP4-4
 Artifacts: PBC-5, PMN1-1, PMP-10
 Artifactual: PM-6, PSB-7
 Aryl-Alkanes: OGPR-2
 Aryl-Aryl: PM-23
 Aryl-Isoprenoids: PC2-25
 Aryl-Isoprenoids: PC2-25
 Aryl: OPE2-3, PBC-2, PBG2-4, PC2-17, PC2-8, PEB2-17, PSB-12
 Ascarite: PMN2-10
 Ashkelon: PFA-5
 Asia: OP3-4, ORP-2, PBC-8, PBG2-7, PBS-24, PEB1-5, PFA-2, PGG1-10, PGG1-12, PGG2-2, PM-19, PM-21, POS2-8, PPC1-15
 Asian: OEB-1, PBS-2, PGG2-2, PPC1-15
 Asphaltene: OUM-3
 Asparagine: OSB2-3
 Aspartate: OSB2-3
 Aspartic: PM-24, PM-26
 Asphalt: PEB2-14, PFA-2, PFA-5, PGG2-1 PRG1-10
 Asphaltene-Bonded: PRG1-7
 Asphaltene-Rich: PGG2-15, PRG1-9
 Asphaltene: OP1-1, OP4-3, OUM-3, PB2-14, PC-6, PG-16, PGG2-11, PGG2-6, PMN1-11, PRG1-12, PRG1-5, PRG1-7, PRG1-9, PRG2-14
 OBD1-3, OP1-1, OP5-4, OP6-3, OPG-3, ORP-2, OUM-3, PBG1-12, PBG2-4, PC-12, PC-4, PEB1-11, PEB2-18, PG-22, PGG1-12, PGG2-11, PGG2-15, PGG2-6, PMN1-11, PPC1-1, PPM-2, PRG1-1, PRG1-12, PRG1-20, PRG1-6, PRG1-7, PRG1-9, PRG2-13, PRG2-3, PRG2-4, PSB-25 PEB2-19 POS2-15, PRG2-19
 Asphaltenic: PGG2-6
 Asphaltic: PGG1-12, PGG2-15, POS1-1, PPM-6
 Asphaltite: PRG1-1
 asphaltite: PRG1-10
 asphaltites: PRG1-10
 Asphalts: POS1-1, POS1-3, PPM-6, PRG1-10
 asphalt-asphaltite-kerite-anthraxolite: PRG1-10
 Assynt: PPC1-22
 Asteroids: PBG2-3
 ASTM-D: PMN2-4
 ASTM: PMN2-4, PRG2-14

ASTM664-89: PRG2-14
 Astrobiologists: PBG1-16
 Astronomical: PPC1-19
 Astronomically: PMP-1
 Asturian: PC-7
 Asturias: PC-7
 Athel: OOS-1
 Atlantic-Type: PCS-10
 Atlantic: OM-3, OP1-1, OP4-1, OP7-2, OP7-3, OPC1-1, OPC2-1, PB1-13, PBC-13, PBC-6, PBC-7, PBG1-13, PBG1-14, PBS-23, PC2-13, PC2-16, PC2-24, PEB1-1, PEB2-5, PMN2-1, POS1-6, PPC1-10, PPC1-16, PPC1-18, PPC1-20, PPC1-26, PPM-11, PRG1-3
 Atmospheric: OPE1-3
 Atmosphere-Ocean: PPC1-18
 Atmosphere: OEB-1, OP5-3, OPC1-2, OPE1-2, OPE1-3, OPG-1, OSB2-3, PB1-7, PB2-20, PB2-5, PBC-3, PBG1-12, PBG2-5, PC2-5, PCS-6, PEB1-5, PEB2-8, PGG1-4, PMN2-10, PPC1-16, PPC1-18, PPC1-4, PSB-1, PSB-15, PSB-4, PSB-7, PPC1-3, OB2-1, OEB-1, OP2-2, OP5-3, OPC1-2, OPC2-1, OPE1-2, OPE1-3, OPE2-2, OSB1-1, OSB1-2, PB1-5, PB2-18, PBC-10, PBC-5, PBG1-3, PBG1-8, PBG2-5, PBG2-6, PC-1, PC2-1, PC2-15, PC2-22, PC2-23, PC2-24, PC2-27, PC2-6, PCS-1, PCS-10, PCS-2, PEB1-13, PEB1-15, PEB1-17, PEB1-3, PEB2-16, PEB2-8, PM-17, PM-22, PMN1-3, PMN2-2, POS1-16, PPC1-15, PPC1-16, PPC1-18, PPC1-19, PPC1-2, PP

B

Bacteria: PBG1-3
 Bacterial-Foraminiferal: PMP-9
 bacterial,: PB2-22
 Bacterial/Microbial: PB1-22
 Bacterial: OB1-1, OB2-2, OB3-1, OBD1-2, OGPR-2, OOS-2, OP4-2, OP4-4, OP5-1, OP5-3, OP6-1, OP6-3, OP7-3, OPE2-1, OSB1-1, PB1-14, PB1-16, PB1-2, PB1-22, PB1-6, PB1-7, PB1-8, PB1-9, PB2-13, PB2-21, PB2-4, PB2-6, PBG1-10, PBG1-7, PBG2-11, PC-12, PC-5, PC2-12, PC2-17, PC2-20, PC2-8, PCS-9, PEB1-12, PEB2-11, PEB2-12, PEB2-19, PG-22, PG-24, PGG2-4, PM-11, PM-12, PM-8, PMN1-3, PMP-10, PMP-11, PMP-13, PMP-14, PMP-15, PMP-17, PMP-2, PMP-20, PMP-3, PMP-8, PMP-9, POS1-12, POS1-16, POS2-14, POS2-2, PPC1-1, PPC1-12, PPC1-17, PPC1-22, PPC1-4, PPC1-5, PPC1-7, PRG1-4, PRG2-11, PSB-15, PBS-20, PSB-4
 Bacterially-Mediated: OB1-3
 Bacterially: PB2-4, PBS-2
 Bacteriochlorophylls: PB2-4
 Bacteriodetes: OP6-1
 Bacteriogenic: PG-3
 Bacteriohopanepolyols: OP4-2, OP6-2, PB2-9
 Bacteriohopanetetrol: OP4-2, OP6-2
 Bacteriohopanoids: OP2-2

- Bacterium: OB2-1, OP4-2, PMP-6
 Bacterivorous: PMP-19
 Bacteroides: PMP-11
 Bacteroidetes: OP6-1
 Badenian: PG-1
 Badenien: POS2-6
 Baffin: PBS-23, PBS-3
 Baffles: PRG1-15
 Bahia: PBS-13
 Bahloul: PBS-7, POS2-14
 Baikai: PB2-10, PM-4, PM-5, PMP-8, POS2-12, PPC1-28
 Bajocian: PBG1-2
 Balcony: PEB1-13
 Balingian: POS2-8
 Balms: PFA-4, PFA-6, PFA-8
 Balophiles: PMP-23
 Balthica: OGC-4
 Baltic: PBS-18, PSB-25
 Bamiange: PPM-9
 Bamianhe: PPM-9
 Banat: PGG1-15
 Bangladesh: PGG1-10
 Banja: PC-12
 Banyoles: PPC1-28
 Barato: PGG2-16
 Barbeque: OSB1-3
 Barberà: PCS-12
 Barcelona: PEB2-12, PPM-8
 Bare: PBC-8, PM-10
 Barents: PBS-15, PC2-22, PPM-11
 Barisan: POS1-12
 Bark: PPC1-14, PPC1-15
 Barkeri: OP5-1
 Barney: OP4-4
 Barreirinha: PB1-22
 Basal: PB1-22, PBS-14, PBS-3, PC2-18, PPC1-17, PPC1-8, PPM-12
 Basalt: PBG1-6, PFA-5, PFA-9, PGG1-4
 Basaltic: OB3-2, POS1-6
 Basalts: PBG1-6, PEB2-17, POS2-13
 Basement-Related: PBS-9
 Basement: PB1-8, PBS-16, PBS-9, PG-24, PG-7, PGG2-13, PRG1-16, PSB-25
 Basin-Wide: OGC-2
 Basin: OB1-2, OB1-3, OBD1-2, OEB-2, OGC-1, OGC-2, OGC-3, OGPR-3, OP1-2, OP2-3, OP3-3, OP4-1, OP4-4, OP5-2, OP6-3, OP7-4, OPC1-3, OPE1-1, OPE1-2, OPE2-3, OPG-2, OPS1-1, OPS1-3, OPS2-1, OPS2-2, OPS2-3, ORP-1, ORP-2, OUM-1, OUM-2, OOS-1, PB1-22, PB1-5, PB1-7, PB1-8, PB2-12, PB2-13, PB2-14, PB2-16, PB2-19, PB2-4, PB2-7, PB2-9, PBG1-10, PBG1-12, PBG1-13, PBG1-2, PBG1-7, PBG2-11, PBG2-12, PBG2-8, PBS-1, PBS-12, PBS-13, PBS-14, PBS-16, PBS-17, PBS-19, PBS-2, PBS-21, PBS-22, PBS-24, PBS-26, PBS-3, PBS-5, PBS-6, PBS-7, PBS-8, PBS-9, PC-1, PC-11, PC-12, PC-5, PC-7, PC-8, PC2-10, PC2-11, PC2-14, PC2-2, PC2-21, PC2-22, PC2-4, PC2-8, PC2-9, PEB1-10, PEB1-14, PEB1-16, PEB2-19, PG-1, PG-10, PG-13, PG-15, PG-16, PG-18, PG-19, PG-21, PG-22, PG-23, PG-24, PG-28, PG-3, PG-4, PG-5, PG-6, PG-7, PG-9, PGG1-1, PGG1-11, PGG1-12, PGG1-14, PGG1-15, PGG1-5, PGG1-7, PGG2-10, PGG2-11, PGG2-12, PGG2-13, PGG2-15, PGG2-4, PGG2-8, PM-19, PM-24, PM-6, PM-8, PMN1-9, PMP-1, PMP-13, PMP-17, PMP-19, PMP-3, PMP-9, POS1-1, POS1-10, POS1-11, POS1-12, POS1-15, POS1-4, POS1-5, POS1-7, POS1-9, POS2-12, POS2-15, POS2-3, POS2-4, POS2-7, POS2-8, POS2-9, PPC1-11, PPC1-13, PPC1-20, PPC1-21, PPC1-26, PPC1-4, PPC1-7, PPM-1, PPM-11, PPM-12, PPM-13, PPM-14, PPM-2, PPM-4, PPM-6, PPM-7, PPM-8, PPM-9, PRG1-13, PRG1-17, PRG1-2, PRG1-20, PRG1-21, PRG1-5, PRG1-7, PRG1-9, PRG2-10, PRG2-12, PRG2-16, PRG2-19, PRG2-20, PRG2-21, PRG2-4, PRG2-5, PRG2-6, PRG2-7, PRG2-8, PBS-20, PSB-25, PSB-4
 Basinal: OP4-4, OP5-4, POS1-16, POS2-7, PPC1-1
 Bathometry: PPM-15
 Bathonian: PBG1-2
 Bathyal: PBS-14, POS1-7
 Baturin Model: PM-12
 Bay: OB2-2, PBS-12, PBS-3, PBS-6, PBS-9, PEB1-1, PEB1-14, PEB2-10, POS1-11, POS2-5, PPM-9, PRG2-19, PB2-8
 BC-Derived: PBC-11
 BC-Reference: PBC-6
 BC/TOC: PBC-13
 BC: PBC-11, PBC-12, PBC-13, PBC-2, PBC-4, PBC-5, PBC-6, PBC-7, PBC-8, PFA-4, PFA-5, PFA-7
 BCF: OGC-4, OUM-2
 Bcm: PBS-12
 BCR: PBS-16
 BCs: PBC-4
 BD: PBC-2, PEB2-17, PGG2-2
 Bead: PFA-9
 Beads: PFA-9
 Beaufort-Mackenzie: OP1-2, OUM-1, PGG1-10, PRG1-13
 Beaufort: PBG1-14, PC2-22
 Bed: OGC-2, OGPR-3, OPE2-3, PB1-22, PB2-17, PBG1-6, PBG2-7, PBS-26, PC2-26, PG-2, PG-5, PG-6
 Bedding: PBG1-10, PM-10
 Beds: OGC-2, OGPR-3, OP7-1, OPE1-2, OPE2-3, OUM-1, PB1-22, PB2-17, PC-10, PC2-16, PC2-26, PM-14, POS2-2, PPC1-17, PPM-3, PPM-6, PSB-25
 Beech-forest: PSB-1
 Beech: PC2-15, PCS-2, PCS-4
 Beehive: OP5-1
 BEEP: PEB1-1
 Beeswax: PFA-4, PFA-8
 Belgium: OBD2-2

- Belt: OP4-1, PB2-14, PBS-2, PC2-25, PEB2-15, PG-10, PG-13, PM-12, PM-19, POS1-13, PPC1-7, PRG2-12
- Belts: PG-13, POS1-13, PPM-6
- Belém: PGG2-13
- Bengal: OPE2-2, PC2-14, PC2-2
- Benguela: OB3-1, PB1-17, PBG1-13, PPC1-23
- Benthamidia: OP6-4
- Benthic: PB1-13, PB1-16, PB2-1, PB2-21, PB2-8, PC2-13, PC2-23, PC2-27, PEB1-5, PM-11, PMP-10, PMP-12, PMP-2, PMP-9, POS2-7, PPC1-7
- Benthos: PB2-4, PEB1-10
- Benton: OPE2-3
- Bentonite:
- Benz[A]anthracene/triphenylene:
- Benz[A]anthracene: PC2-22
- Benzamide: PFA-2
- Benzamines: PEB2-11
- Benzanthracene-Like: OSB1-3
- Benzcphenanthrene: OB3-2
- Benzene-methanol: PB2-1
- Benzene-soluble: PRG1-1
- Benzene: OEB-2, OP3-2, PB2-16, PBC-5, PBS-17, PBS-2, PC-4, PEB1-15, PEB1-6, PEB2-12, PEB2-6, PG-27, PGG1-11, PGG2-2, PM-23, POS2-1, PPM-14, PRG1-1
- Benzenecarboxylic: PBC-14, PM-25
- Benzenepolycarboxylic: PBC-1
- Benzenes: OP3-4, PB2-16, PEB2-17, PEB2-18, PGG1-11, PM-18
- Benzenopolycarboxylic: PBC-13
- Benzghi fluoranthene: OB3-2
- Benzo[A]anthracene: PEB1-17
- Benzo[A]carbazole: PPM-13
- Benzo[A]pyrene/benzo[e]pyrene:
- Benzo[A]pyrene: PC2-22, PEB1-17, PEB1-3, PEB2-14, PEB2-8
- Benzo[B]carbazole: PRG1-1
- Benzo[B]fluoranthene: PEB1-17, PEB2-14
- Benzo[B]thiophenes: PC-1
- Benzo[C]carbazole: PPM-13
- Benzo[E]pyrene: PEB1-17
- Benzo[Ghi]perylene: PEB1-17
- Benzo[GHI]perylene: PEB1-3
- Benzo[Ghi]perylene: PEB2-8
- Benzo[K]fluoranthene: PEB1-17
- Benzoanthracene: PGG2-5
- Benzobfluoranthene: PEB1-17
- Benzocarbazole: PBS-16, PPM-13, PPM-6
- Benzocarbazoles: PGG1-1, PPM-13, PRG1-1
- Benzofluoranthenes: PGG2-5
- Benzofurans: PEB2-11
- Benzohopane: PGG1-1
- Benzohopanes: PC2-11, PC2-4
- Benzohopanoids: PGG1-1
- Benzoic: PBG2-3, PFA-2, PM-23, PSB-3
- Benzologues: POS1-9
- Benzonitrile: PFA-2
- Benzopyrenes: PGG2-5, POS2-12
- Benzothiophene: PC-1
- Benzothiophenes/Dibenzothiophenes: PRG1-1
- Benzothiophenes: OEB-2, PEB2-11, PMN1-10, PRG1-1
- Benzyl: OP6-1, PSB-3
- Benzylsuccinic: PRG2-2
- Berge: PGG1-7
- Bering: OB2-2, PB2-18, PBS-2
- Bermuda: PBG1-13, PBG2-6
- Besòs: PEB2-12
- Beta-alanine: PMP-22
- Beyerane: OB1-2
- BF3/methanol: PB2-1
- BH: PGG1-1
- Bh: PSB-13
- BHP: OP4-2
- BHPs: OP4-2
- Bhs: OSB2-2, PSB-13
- Bhs1: PSB-13
- Bhs2: PSB-13
- Bhs3: PSB-13
- Bi-Functional: PGG1-4
- Bi-oxygen: PG-14
- Bicadinane/hopane: PGG1-10
- Bicadinane: OOS-3, PGG1-10, PGG2-2
- Bicadinanes: PGG1-10, PGG2-2
- Bicadinoids: OP1-2
- Bicarbonate: OBD2-2, PB1-18, PB2-16, PBG1-16, PMP-10, PPC1-7
- Bicardinanes: POS2-8
- Bicyclic: OB3-2, OBD2-1, OP2-4
- Bicyclohexyl: PGG1-7
- Bidigare: OP6-4
- Bighorn: PC2-10
- Bight: PMP-10
- Bile: PEB1-1
- Bimetallic: PMN1-8
- Bio-available: OSB1-1
- Bio-degradation: PPM-6
- Bio-events: PC2-8
- Bio-geochemical: PBG1-9
- Bio-synthetic: OP7-2
- Bioaccessibility: PEB2-16
- Bioaccessible: PEB2-16
- Bioaccumulate: PEB1-5
- Bioaccumulated: PEB1-1
- Bioaccumulation: PEB1-1, PEB2-10
- Bioaccumulative: PEB2-2
- Bioassay: OEB-2, PEB1-12
- Bioassays: PSB-2
- Bioaugmentation: PEB2-3
- Bioavailability: PBG1-3, PEB1-1, PRG1-17, PRG2-5, PSB-5
- Biocenosis: PEB1-11
- Biochemical: OM-1, OP6-4, PB1-4, PBC-14, PC2-5, PEB2-3, PGG1-11, PM-10, PMP-22, PPM-14, PPM-3, PSB-20
- Bioclastic: PBG1-10
- Biodegradability: OP1-1, PEB2-18
- Biodegradable: OSB2-1, PBC-12, PM-10

- Biodegraded: PG-10
 Biodegradation: OB2-2, OBD1-1, OBD1-2, OBD2-1, OEB-2, OGC-1, OMN-1, OOS-1, OOS-2, OP1-1, OP3-4, OP4-3, OP5-2, OP6-1, OP6-3, OPS1-1, OPS1-3, ORP-2, OSB2-1, OUM-1, OUM-3, PB2-14, PBS-12, PBS-17, PBS-6, PBS-9, PC2-25, PEB1-11, PEB1-12, PEB1-4, PEB2-13, PEB2-16, PEB2-18, PEB2-19, PEB2-4, PEB2-7, PEB2-9, PFA-6, PG-18, PG-23, PGG1-1, PGG1-12, PGG1-14, PGG2-13, PGG2-4, PGG2-7, POS1-15, POS1-16, POS2-12, POS2-13, POS2-2, PPM-10, PRG1-13, PRG1-15, PRG1-17, PRG1-2, PRG1-20, PRG1-4, PRG1-5, PRG1-6, PRG1-8, PRG1-9, PRG2-1, PRG2-10, PRG2-11, PRG2-12, PRG2-14, PRG2-17, PRG2-19, PRG2-2, PRG2-3, PRG2-5, PRG2-6, PSB-10, PSB-20, PSB-25, OB2-2, OBD1-2, OBD1-3, OBD2-1, OEB-2, OMN-1, OP4-3, OP6-3, OPG-3, PB2-14, PBS-23, PBS-3, PBS-6, PC2-25, PC2-26, PEB1-11, PEB1-12, PG-18, PGG1-7, PGG1-9, PGG2-4, PGG2-8, PMN1-6, PMN2-11, PMN2-4, POS2-12, PPM-11, PRG1-11, PRG1-17, PRG1-20, PRG1-4, PRG1-5, PRG1-6, PRG1-7, PRG1-8, PRG2-11, PRG2-12, PRG2-14, PRG2-15, PRG2-17, PRG2-5, PRG2-6, PRG2-8
- Biodegrading: PEB2-19, PRG1-17
 Bioditerpenoids: OB1-2
 Biodiversity: OP2-1, OPE2-3, PC2-5, PEB1-4, PM-10, PMP-1, PPC1-4
 Biostructured: POS1-7
 Biofilm: OPE2-1
 Biogenetic: OPS1-3
 Biogenic/diagenetic: PG-1
 Biogenic: OGC-2, OGC-4, OP4-3, PB2-4, PBG1-15, PBG2-6, PC-9, PC2-19, PC2-20, PG-1, PG-10, PG-18, PG-19, PG-9, PGG1-4, PMP-23, PMP-7, POS1-16, PPM-3, PSB-11
- Biogenicity: PM-18
 Biogeochemical: OB1-3, OM-1, OMN-3, OP5-3, OPE1-2, PB1-7, PB2-13, PBC-12, PBC-13, PBC-14, PBC-9, PBG1-13, PBG1-4, PBG2-10, PBG2-12, PBG2-14, PBG2-9, PC2-11, PC2-12, PC2-9, PCS-10, PCS-6, PM-19, PM-22, PM-25, PM-8, PMN2-6, PMP-10, PMP-11, PMP-14, PMP-15, PMP-17
- Biogeochemically: PBC-9
 Biogeochemistry: OB2-3, PMP-12, PMP-22, PPC1-12, PPC1-7, PSB-11
 Biogeochemists: PBC-11, PBG1-16
 Biogeosphere: PSB-14
 Biohopanoids: OP6-2, PB2-9
 Biological: OOS-1, OB1-1, OB2-3, OEB-2, OGPR-2, OMN-3, OP2-1, OP2-2, OP3-1, OP4-4, OPC1-1, OPE1-3, PB1-1, PB1-10, PB1-20, PB2-1, PBG1-2, PBG1-3, PBG1-4, PBG2-1, PBS-3, PC2-11, PC2-4, PC2-5, PEB1-11, PEB1-2, PEB2-10, PEB2-3, PEB2-5, PEB2-9, PGG1-10, PGG1-5, PGG2-7, PM-10, PM-13, PM-15, PM-17, PM-18, PM-20, PM-22, PM-5, PM-8, PMN1-4, PMN2-1, PMP-16, PMP-5, PMP-8, POS2-14, POS2-15, POS2-2, PPC1-15, PPC1-6, PPM-14, PPM-3, PSB-15, PSB-2
- Biologically: OOS-2, PBG1-3, PG-22, PMN1-8
 Biology: OP5-3, PBG1-4, PMP-23
 Biomacromolecule: PM-28
 Biomacromolecules: OP3-1, OSB1-2, PBC-9, PM-28, PSB-18
 Biomarker-based: OP2-2, PC2-16, PPM-14
 Biomarker: PBS-17, PG-5, PGG2-13, OB1-3, OB3-1, OBD1-2, OBD1-3, OGPR-2, OGPR-3, OOS-1, OOS-3, OP2-1, OP2-4, OP3-3, OP3-4, OP4-2, OP4-4, OP5-2, OP5-3, OP7-4, OPC2-2, OPE2-3, OPG-2, OPS2-2, OPS2-3, OUM-1, OUM-2, PB1-10, PB1-15, PB1-16, PB1-18, PB1-2, PB1-22, PB1-5, PB1-7, PB2-11, PB2-12, PB2-13, PB2-14, PB2-18, PB2-19, PB2-20, PB2-22, PB2-8, PBG1-10, PBG1-11, PBG1-12, PBG1-13, PBG1-14, PBG2-1, PBG2-12, PBG2-5, PBG2-6, PBG2-9, PBS-1, PBS-10, PBS-17, PBS-19, PBS-20, PBS-6, PBS-8, PBS-9, PC-2, PC-8, PC-9, PC2-11, PC2-12, PC2-19, PC2-20, PC2-22, PC2-23, PC2-24, PC2-25, PC2-5, PC2-6, PCS-6, PCS-7, PEB1-18, PEB1-2, PEB1-5, PFA-4, PFA-6, PFA-8, PG-3, PG-5, PGG1-1, PGG1-10, PGG1-5, PGG1-7, PGG2-1, PGG2-13, PGG2-16, PM-17, PM-19, PMN1-6, PMN1-9, PMP-10, PMP-13, PMP-14, PMP-17, PMP-18, PMP-19, PMP-5, POS1-10, POS1-13, POS1-4, POS1-6, POS2-8, PPC1-1, PPC1-12, PPC1-14, PPC1-20, PPC1-21, PPC1-22, PPC1-23, PPC1-4, PPM-7, PPM-9, PRG1-13, PRG1-14, PRG1-16, PRG1-19, PRG1-2, PRG1-3, PRG1-8, PRG1-9, PRG2-4, PRG2-7, PSB-25, PSB-4, OB1-1, OB1-2, OB1-3, OB2-2, OB3-1, OBD1-2, OBD1-3, OEB-1, OGPR-3, OOS-1, OP1-1, OP2-1, OP2-2, OP2-4, OP3-3, OP3-4, OP4-1, OP4-4, OP5-1, OP5-2, OP5-3, OP6-2, OP6-4, OP7-4, OPC2-1, OPE1-1, OPE1-2, OPE2-1, OPE2-2, OPE2-3, OPS2-3, ORP-2, OSB1-1, OUM-1, OUM-3, PB1-1, PB1-10, PB1-11, PB1-13, PB1-15, PB1-18, PB1-19, PB1-20, PB1-22, PB1-4, PB1-5, PB2-12, PB2-13, PB2-14, PB2-17, PB2-18, PB2-19, PB2-2, PB2-20, PB2-22, PB2-9, PBC-14, PBG1-1, PBG1-11, PBG1-12, PBG1-13, PBG1-14, PBG1-2, PBG1-7, PBG2-1, PBG2-10, PBG2-13, PBG2-4, PBG2-6, PBG2-9, PBS-13, PBS-16, PBS-17, PBS-2, PBS-23, PBS-8, PBS-9, PC-11, PC-2, PC-9, PC2-11, PC2-12, PC2-15, PC2-17, PC2-19, PC2-20, PC2-23, PC2-24, PC2-25, PC2-3, PC2-4, PC2-5, PC2-6, PC2-8, PC2-9, PCS-2, PCS-6, PEB1-10, PEB1-2, PEB1-7, PEB2-19, PEB2-5, PFA-1, PFA-4, PFA-6, PFA-8, PFA-9, PGG1-14, PGG1-5, PGG1-6, PGG2-10, PGG2-11, PGG2-12, PGG2-13, PGG2-16, PM-18, PM-19, PM-27, PMN1-10, PMN1-4, PMN1-5, PMN1-9, PMP-1, PMP-13,

- PMP-14, PMP-15, PMP-17, PMP-18, PMP-20, PMP-21, PMP-22, PMP-4, PMP-5, PMP-6, POS1-1, POS1-15, POS1-6, POS2-14, POS2-15, POS2-8, PPC1-12, PPC1-13, PPC1-15, PPC1-18, PPC1-20, PPC1-21, PPC1-22, PPC1-23, PPC1-26, PPC1-28, PPC1-3, PPC1-4, PPC1-6, PPM-11, PPM-15, PPM-3, PRG1-14, PRG1-15, PRG1-3, PRG1-7, PRG2-12, PRG2-20, PRG2-7, PSB-4
- Biomass-To-Charred: PBC-1
- Biomass: OB2-3, OEB-1, OGPR-2, OGPR-3, OM-1, OMN-1, OP2-2, OP5-1, OPC1-2, OPE1-2, OSB1-1, OSB2-3, PB1-2, PB1-4, PB1-7, PB2-11, PB2-9, PBC-1, PBC-14, PBC-2, PBC-3, PBC-4, PBC-6, PBC-9, PBG1-4, PBG1-8, PBG2-13, PBG2-6, PBG2-7, PBG2-9, PC-12, PC2-1, PC2-19, PC2-8, PCS-1, PCS-10, PCS-7, PEB2-11, PEB2-12, PEB2-8, PM-17, PMN2-7, PMP-17, PMP-20, PMP-21, PMP-4, PMP-6, PMP-8, POS1-12, PPC1-14, PPC1-17, PPC1-18, PPC1-3, PPC1-7, PRG2-20, PSB-13, PSB-15, PSB-17, PSB-6
- Biomembranes: PMP-21
- Biometric: PCS-1
- Biomolecules: OP6-4, OSB2-3, PBG1-1, PGG1-11, PMP-20, PSB-7
- Biomonitoring: PEB2-8
- Biomorphic: PBG1-6
- Biophile: PMP-22
- Biophysical: PEB2-3
- Biopolymer: PB1-1, PC-2, PC2-1, PM-23, OP3-1, OSB2-1, PB2-13, PC-10, PM-22, PM-23, PM-25, PM-8, PSB-13, PSB-7
- Bioproducers: PBG1-8
- Bioproductivity: PB1-22, PBG1-10, POS1-11, POS2-9
- Biopulping: PM-17
- Bioremediated: PEB1-4
- Bioremediation: OBD2-1, OP1-1, PEB1-4, PEB2-16, PEB2-3
- Biosesquiterpenoids: PC2-5
- Biosphere: OB2-1, OB2-3, OMN-1, OP6-2, OP7-3, OPE1-2, OPE2-3, OSB1-1, PB1-2, PC-6, PMP-13, PMP-20, PMP-22, PMP-23, PMP-6
- Biostimulation: PEB2-3
- Biostratigraphic: PBG1-10, PC2-13
- Biostratigraphical: PC2-16
- Biostratigraphy: PC-10, PPC1-27
- Biosurfactant: OPG-3
- Biosurfactants: OPG-3
- Biosyntheses: OP6-4, PCS-8
- Biosynthesis: OP6-2, OP6-4, OPE1-2, OSB2-3, PB1-4, PB2-11, PC2-15
- Biosynthesise: PB1-14
- Biosynthesised: OP3-1
- Biosynthesising: OP6-2, PMP-1
- Biosynthesize: OP2-1, OPE2-1
- Biosynthesized: OP5-3, OPC2-4, PB2-11, PM-22
- Biosynthesizing: OP2-1, PMP-1, PMP-17
- Biosynthesys: PMP-5
- Biosynthetic: OP3-1, OP6-4, PB2-8, PBG2-1, PBG2-5, PC2-14, PC2-15, PM-18, PM-28, PMN2-6
- Biota: PBG1-14, PC2-9, PM-28, PPC1-20, PPC1-27, PPC1-8
- Biotechnology: PEB2-19
- Bioterpenoids: OB1-2
- Biotic: OPE2-3, PB2-18, PB2-3, PBG1-4, PC-6, PC2-26, PEB1-5, PPC1-8
- Biotically: PC2-19
- Biotransformation: PB2-4, PEB1-1, PEB2-19, PCS-8, PEB1-1
- Bioturbated: PC-10
- Bioturbation: OPE1-1, PBG1-9
- Bioturbational: OPE1-1
- Bioturbative/diffusive: PB2-21
- BIOZAIRE: PB1-13
- Biphenyl: OB3-2, PGG2-5
- Biphenyls: OPG-1, PEB1-5, PEB2-12, PEB2-2, PGG2-5
- Biphytane: OP2-4, PC2-25, PPC1-23
- Biphytanes: OB2-3, PC2-25, PMP-5
- Bireflectance: PRG2-18
- Birkhead: PRG2-16
- Birth: PEB2-15
- Bishomohopanoic: OP5-3, PB2-9
- Bishomohopanol: PB2-9
- Bisnorhopane: PGG2-1
- Bisnorhopanes: PGG2-1
- Bisnorlupanes: OP1-2, OUM-1, PRG1-13
- BIT-Index: PPC1-19
- BIT-Indices: PPC1-19
- BIT: PPC1-19
- Bitumen-stained: PRG2-4
- Bitumen: OP4-4, OP5-4, OPS2-1, PB1-16, PB2-14, PBG1-7, PBG2-4, PBS-1, PBS-10, PBS-11, PBS-13, PBS-18, PBS-2, PBS-20, PC2-20, PEB2-13, PEB2-17, PEB2-18, PFA-2, PFA-4, PFA-5, PFA-7, PFA-8, PG-22, PGG1-13, PM-14, PM-19, PMN2-9, POS1-1, POS1-11, POS1-14, POS1-2, POS2-15, POS2-9, PPC1-1, PPC1-17, PRG1-14, PRG2-18, PRG2-4, OOS-1, OGPR-3, OP4-4, PB1-16, PBG2-4, PBS-10, PBS-11, PBS-18, PC2-20, PC2-22, PEB1-11, PFA-4, PGG2-1, PM-12, PM-19, PMN1-2, PMN2-9, POS2-11, PRG1-10, PRG2-18, PRG2-4
- Bituminosity: PBG1-14
- Bituminite: PC-12, POS2-10, PPC1-17
- Bituminological: POS2-13
- Bituminous-Rich: PB1-21
- Bituminous: OGC-2, OP2-3, PBG1-8, PC-11, PC-4, PC-8, PFA-7, PGG2-12, PMN2-4, POS1-1, POS1-11, POS1-2, POS2-9, PPC1-1, PRG1-6, PRG2-20
- Bitumoid: PBS-2, POS2-13, PGG1-12, PGG1-13, PGG1-6, POS1-9, PPM-3
- Bivalve: OPE2-3
- Bivariance: PEB2-8
- BIX: PMN2-1

- BL: PBS-9
 Black-carbon: PBC-9, PSB-18
 Black-shale: PC2-16
 Black-white: PM-7
 Blackback-2: OP5-2
 Blackish: PBC-3, PFA-2
 Blackleaf: POS1-13
 Blake: OPC2-1
 Bligh-dyer: PMP-9
 Bligh: PMP-21
 Bloch-decay: OSB1-3, PBC-14
 Bloom: PB2-8, PBG1-10, PBG1-11, PC2-8, PMP-10, PPC1-21 OPE2-3, PB1-10, PB2-8
 Bloomed: PB1-5
 Bloomfield: PSB-8
 Blowout: OGC-4, PBS-12
 BMI-1: PGG1-10
 Bog: OMN-2, OP5-3, OPC2-2, PM-10, PPC1-13
 OMN-2, OP5-3, OPC2-2, PB1-14, PPC1-19
 Bohai: PBS-12, PBS-9, PPM-9, PRG2-19
 Bohaiwan: PRG1-7
 Bohemian: PBG1-2, PC2-17
 Boina-Arade: PB2-13 OPE1-3, PB2-13
 Bolide: OPE2-3
 Bolivia: PC2-18, PC2-7
 Bolton: OPC2-2
 Bomb-Spike: OPE1-1
 Bomem: PSB-1
 Bonan-Gubei: PBS-9
 Bonded-Sterane: PRG1-7
 Bonds: PRG1-10
 Bone: PFA-2
 Bones: PFA-9
 Book-Sheets: PB1-22
 Bore: PGG2-15
 Boreal: PBG2-5, PBG2-6, PCS-2
 Borehole: OPE2-3, PB1-1, PB1-22, PB1-8, PB2-13,
 PBG1-10, PBG1-12, PC-10, PC-6, PG-13,
 PPC1-13, PPC1-4
 Boreholes: OPE1-3, PB1-8, PBG1-12, PBG1-2,
 PBS-7, POS2-3
 Boride: PB2-14
 Borneo: OP1-2, POS2-10, POS2-8
 Boron: PBS-1
 Botanical: PB1-15, PFA-1, PFA-6
 Botneheia: POS1-6
Botryococcus: PSB-4
 Bou: PBS-7
 Boulders: PBG1-7
 Bovin: PM-2
 Boxcorer: PM-26
 Bozhong: PRG1-7
 BPCA: PBC-1, PBC-13
 Br15:0: PMP-8
 Br17:0: PMP-8
 Brackish/Saline: PPC1-17
 Brackish: OP2-1, OPS1-1, PBG1-9, PBS-13, PBS-9,
 PC-5, PM-13, PM-14, PPM-9, PRG2-20
 Bradarac-Maljurevac: PGG1-15
 Bradarats: POS2-2
 Brahmaputra: PC2-14
 Branched/cyclic-Alkanes: PMN1-6
 Branched/cyclic: PMN1-6
 Brassicasterol: PBG1-11
 Braunii: PB2-1
 Brazil: OMN-2, OP6-3, PB1-22, PBG1-11, PBS-13,
 PC-10, PC2-21, PC2-6, PC2-7, PEB2-19,
 PGG2-13, PGG2-3, POS1-15, POS1-7, POS2-3,
 PPM-1, PPM-13, PRG1-14, PRG2-10, PSB-13,
 PSB-4
 Brazilian: OBD1-2, PBC-3, PBG1-11, PEB1-4,
 PGG1-5, PGG2-13, POS1-15, PPM-1, PRG1-14,
 PRG2-10, PSB-13
 Break-Through: PPM-12
 Break-Throughs: PMN1-2
 Breccias: PBG2-4, PM-7
 Brecciated: PC2-25
 Brecciates: POS2-10
 Bremen: PBG1-4
 Brent: PG-20
Brevundimonas: PMP-20
 Brick-Pits: PBG1-2
 Bridport: PBS-6
 Brine: PB2-4, PGG1-13, PMP-17, PMP-19
 Brines: PMP-17
 Bristol: PMN2-6, PMP-15
 British: PG-10
 Bronydd Mawr: PSB-15
 Bronze: PFA-9
 Brucite: PM-7
 Brukner-Wein: POS2-6
 Brunei: PFA-6, POS2-10, PPM-11
 Bug river: PEB2-1
 Bulgaria: PC-1
 Bulgarian: PC-1, PC-2
 Buqu formation: POS2-7
 Burgan: PRG2-1
 Burnt: PBC-11, PBG2-6, PEB2-8
 PBC-12, PFA-5, PSB-9 OEB-1, OPC1-2, PBC-1,
 PBC-2, PBG2-6, PEB1-14, PEB2-8, PSB-17,
 PSB-18 OSB1-3, PBC-14, PBC-3, PBG2-7,
 PEB1-15
 Butane: PG-18, PG-20, PG-8, PPM-1, PG-14, PG-20
 Butterburn: OPC2-2
 Butyl-: OGPR-2
 Byarenes: PGG2-5
 Bydgoszcz: PEB2-1
 Bypass: PRG2-17
 BYRD: OPC1-3
 Bystrzyca: PEB2-1
- C
 C-Isotope: PB2-11, PC2-26, OPE2-3, PC2-26,
 PCS-7, PPC1-7, C-Pool: OSB1-3
 C-Sequestration: OSB1-3
 C-Sink: PCS-9
 C-Types: PSB-18
 C/Carboxyl: PSB-12
 C/G: OP5-3

- C/N: PB2-18, PB2-20, PB2-9, PBG2-14, PC2-18, PC2-3, PC2-9, PCS-13, PM-10, PM-26, PMN2-7, PPC1-10, PPC1-13, PPC1-14, PPC1-3, PPC1-8, PPC1-9, PSB-19, PSB-2, PSB-21
- C/O-Alkyl: OSB2-2
- C/T: POS2-14
- C/V: PC2-27
- C:N: PBC-8, PBG1-9, PCS-11
- C13-Isoprenoid: PMP-5
- C2-Benzenes2: POS2-1
- C20-Isoprenoid: PMP-5
- C23-N-Alkane: OPC2-2
- C23/C31-N-Alkane: OPC2-2
- C23-Heilantane/C30-hopane: PPM-7
- C25-Homologue: PMP-5
- C27-Steranes: PEB2-4
- C27/C29-sterane: PGG2-1
- C27-S-diasterane/: PGG1-14
- C28 *n*-alkanol: PPC1-3
- C29-Diasterane/Regular: PGG1-1
- C29-Sterane: PGG1-1
- C29-Hopane/C30hopane: PGG1-14
- C29-Moretane/C30hopane: PGG1-14
- C29-R-Sterane: PGG1-14
- C3-Monoculture: PCS-7
- C3-Naphthalene: PMN1-1
- C3-Naphthalenes: PGG2-5
- C3-Plants: PB2-11, PCS-7, PSB-17
- C30-Diahopanes: PB1-16
- C30-Homologue: PMP-5
- C31 *n*-alkane: PPC1-3
- C37-Alkenones: PPC1-16, PPC1-2
- C37:2-Alkenone: PPC1-16
- C4-Crop: PB2-11
- C4-Derived: OSB2-1
- C4-Monoculture: PCS-7
- C4-Naphthalenes: PGG2-5
- C4-Plant-derived: OP4-1
- C4-Plant: PCS-7 PB2-11, PCS-7
- Ca: OBD2-2, OGPR-3, OP4-1, OP6-1, OP7-3, OPC2-2, OPC2-4, OPE1-3, OPE2-1, OPE2-2, OSB1-2, PB1-16, PB1-5, PB1-8, PB2-13, PBC-4, PBG2-1, PBG2-11, PBS-6, PC-5, PC2-1, PC2-13, PC2-15, PC2-18, PC2-7, PCS-11, PEB1-16 PEB2-10 PEB2-12, PFA-4, PFA-8, PFA-9, PG-27, PM-3, PM-7 PM-8, PMN2-9, PMP-13, PMP-23, PPC1-13, PPC1-23, PPC1-25, PPC1-6, PPC1-7, PPC1-8, PPM-8, PRG1-21, PRG2-17 PBG1-5, PGG2-9
- CAA: PEB1-5
- CaCO₃: PBG1-14, PC2-16, PG-17, PGG2-3, PM-7, PPC1-22
- Cadalene: OB1-2, PBG1-2, PBS-17, PC2-17, PC2-5, PGG2-2
- Cadavers: PFA-3
- Cadinane-Type: OB1-2, PC2-5
- Cainozoic: PGG2-6
- Cake-shaped: PB1-16
- Calcareous: OPC2-3, PBC-12, PBS-9, PMP-1, PMP-6, PMP-9, PPC1-10, PPC1-8, PRG1-8, PSB-19, PSB-5
- Calcaric: PSB-18
- Calcification: PEB1-2, PPC1-2
- Calcified: OPC1-1
- Calcinated: PBC-12
- Calcite-Brucite: PM-7
- Calcite: PBG1-15, PBG1-6, PBS-10, PBS-12, PG-17, PM-7, PMP-2, PPC1-2, PPC1-22
- Calcites: PBG2-4
- Calcium: PB2-8, PEB2-12, PG-12, PGG1-2, PGG2-3
- Caldarchaeols: PB2-2
- Calditol: OB2-3
- Caledonian: PPM-6
- California: OEB-2, OGPR-2, OPE1-1, OPG-2, PB1-18, PB2-21, PC2-27, PEB2-10, PM-4
- Callovian: OB1-2, PBG1-2, PC2-4
- Callovo-Oxfordian: OB1-2, PBG1-12, PC2-4
- Calorimetry: PBC-7, PM-22
- Calyptogena: PMP-5 Cambisol: OSB2-2, PCS-8, PCS-9, PSB-18, PSB-8
- Cambisols: OSB2-2, PCS-4, PSB-18
- Cambrian-Ordovician: PG-4
- Cambrian: OOS-1, OGPR-3, OPS1-3, PBG2-2, PBS-10, PBS-16, PBS-18, PBS-21, PG-4, PGG1-6, PM-19, PPM-6, PSB-25
- Campanian: PC-10, PGG1-10
- Campeche: POS2-4
- Campesterol: PB2-17, PBG1-11
- Campos: PEB2-19
- Canada: OP1-2, OP2-4, OP3-3, OP6-3, OUM-1, PBS-23, PBS-3, PC2-25, PG-10, PGG1-10, PM-22, POS2-5, PPM-2, PRG1-12, PRG1-21, PRG2-5
- Canadian: OP1-2, PBS-3, PC2-22, PC2-25, PM-22, PRG1-13
- Canarian: PCS-1
- Canary: PCS-1, PCS-9
- Candeias: PBS-13
- Canfield: OPC1-2, PC2-20
- Canister: OGC-2
- Canisters: OGC-2
- Canned: PG-9
- Canning: OMN-1
- Canopy: PBC-14, PBG2-5, PSB-18
- Cans: PPM-11
- Cansona: PRG2-12
- Cantabric: OP1-1
- Canterbury: PC-5
- Cantoxantine: PB2-4
- Canyon: PB1-13, PB2-19
- Canyons: PB1-13
- Cap: PBS-15, PC2-21, PPC1-7, PRG2-15, PRG2-17, PRG2-19
- Cape: PEB2-5, PGG2-2
- Capiello: PBC-11
- Capiricual: PPM-8
- Capital: PFA-5

- CARB: POS1-10
 Carbargilite: PBS-8
 Carbazole-Type: PPM-6
 Carbazole/Alkyl: PPM-6
 Carbazole: PPM-6
 Carbazole+benzocbazole: PPM-6
 Carbazoles: PBS-16, PEB2-11, PPM-10, PPM-13, PRG1-1
 Carbide: PBG2-7
 Carbohydrate: PB2-13, PBC-9, PG-14, PSB-18
 OM-1, PB1-4, PBC-12, PBG1-9, PBG2-2, PCS-14, PCS-8, PFA-2, PG-14, PSB-13
 Carbon-carbon: OBD1-3, PMN1-4
 Carbon-chain: PB2-1, PB2-16, PM-3
 Carbon-containing: PB1-17
 Carbon-fixing: OP5-1
 Carbon-isotope: PGG1-7
 Carbon-osotopic: PBG2-9
 Carbon-like: PBC-14, PSB-18
 Carbon-normalized: PBC-11, PSB-7
 Carbon-number: PB2-1
 Carbon-numbered: PB2-11
 Carbon-related: OP7-3
 Carbon-rich: OPE2-1, PBG2-7
 Carbon-transforming: OMN-3
 Carbon/hydrogen: PMN1-6
 Carbon/nitrogen: PPC1-3
 Carbonate: OB1-2, OOS-3, OP3-3, OP3-4, OP4-1, OP5-1, OPC2-3, OPE2-3, OPS1-1, ORP-2, PB1-18, PB2-14, PB2-18, PB2-21, PB2-8, PBG1-10, PBG1-13, PBG1-2, PBG1-8, PBG2-11, PBG2-4, PBG2-9, PBS-10, PC-1, PC2-16, PC2-20, PC2-24, PC2-3, PG-1, PG-12, PG-17, PG-24, PG-28, PG-4, PGG1-2, PGG2-3, PGG2-6, PM-14, PM-19, PMN2-5, PMP-17, PMP-18, PMP-5, POS1-10, POS1-11, POS1-13, POS1-2, POS1-5, POS1-8, POS2-1, POS2-13, POS2-2, POS2-9, PPC1-1, PPC1-16, PPC1-17, PPC1-5, PPC1-7, PPM-11, PPM-15, PRG1-8, PRG2-1, PRG2-18, PRG2-21, PRG2-3, PRG2-5, PRG2-7, PSB-4 POS2-15, PRG2-12 OGC-1, OGPR-2, OPC2-3, ORP-2, PB1-18, PB1-5, PBC-12, PBG2-4, PBG2-7, PBS-10, PBS-18, PBS-20, PBS-21, PC2-9, PCS-12, PFA-7, PG-17, PG-24, PM-7, PMP-17, PMP-5, POS1-6, POS2-2, POS2-7, PPC1-7, PRG1-11, PRG1-8
 Carbondioxide: PG-17
 Carboniferous: OPC1-2, PB2-12, PBS-15, PBS-26, PC-3, PG-28, PG-8, PRG2-21
 Carbonilhalogenic: PGG1-13
 Carbonisation: PBG1-6
 Carbonium-ion: PGG2-3
 Carbonium: OB1-1, PGG2-3
 carbonization series: PRG1-10
 Carbonous: PBC-6
 Carbons: OB3-2, OGPR-2, PFA-3, PG-26, PM-16, PM-18, PSB-13
 Carbonyl-type: PM-23
 Carbonyl/amide: PSB-18
 Carbonyl/amino: PSB-18
 Carbonyl: OP7-2, PSB-12, PSB-18, PSB-3 OGPR-1
 Carboxyalkyl: PGG2-13
 Carboxyalkylsteranes: PGG2-13
 Carboxyl/Aryl: PBC-9
 Carboxyl/Carbonyl: PMN2-7
 Carboxyl: OSB1-3, PBC-3, PBC-9, PBG1-5, PCS-11, PSB-1, PSB-3
 Carboxylase/Oxygenase: OSB1-1
 Carboxylate: PM-23, PRG2-2
 Carboxylation: OSB2-3
 Carbyne: PBG2-7
 Carcinogenic: PEB1-1, PEB2-2, PEB2-8, PMN1-10
 Cardiff-1: PC-5, PRG2-20
 Carex: PSB-7
 Cariaco: PM-6, PPC1-26
 Caribbean: PPC1-2, PPC1-26, PPM-8
 Carlsberg: PC-3
 Carnallite: PGG1-13
 Carnarvon: OP5-2, PB2-12
 Carotane: PC2-21, PGG1-1
 Carotenoid: OP2-1, OPE2-3, PB2-7, PC2-11, PEB2-17 OP2-1, PB2-15, PB2-8, PEB2-17
 Carpathian: PB1-8, PBS-17
 Carpathians: POS2-11
 CARS: PBC-11
 Casercocha: PC2-1
 CaSO₄: PG-17, PGG2-3
 Caspian: PGG1-12
 Castanea: OP3-2
 Casting: PEB2-3
 Casts: PB1-14
 Cat: PGG2-9
 Catabolic: PCS-14
 Cataclastic: PG-8
 Catagenesis: OGC-1, OPS1-2, PB2-4, PBG1-14, PBS-11, PBS-5, PG-2, PG-21, PGG1-11, PGG1-12, PM-7, POS1-2, POS2-2 POS1-2 PBC-9, PEB1-1, PG-24, PGG1-12, PGG1-15, PM-1, POS1-3, POS2-2
 Catagenic: OPS1-2
 Catalogue: PC2-5
 Catalonia: PBC-12, PCS-12, PEB2-12
 Catalonian: PBS-19, PRG2-12
 Catalysed: OGPR-1, PC-3
 Catalysis: ORP-2, PC2-4
 Catalyst-Equipped: PEB1-14
 Catalyst: OUM-3, PB2-5, PM-19, PMN1-4, PMN2-6, PRG2-14
 Catalysts: OGPR-1, PBG1-4, PEB2-16, PGG1-4, PGG2-3, PMN1-8
 Catalytic: OGPR-1, ORP-2, OUM-3, PBG1-6, PGG1-4, PGG2-3, PM-19, PMN1-1, PMN1-4, PMN1-8, POS1-5, PRG2-4
 Catalyzed: OGPR-1, PB2-2, PG-22
 Catches: PEB1-10, PEB1-16
 Catchment: OP4-1, OP4-2, PC2-18, PC2-9, PSB-8 PBG1-11, PC-11
 Cathedral: PEB2-15 PBC-10

- Cathodic: PBG1-3
 Catotelm: PM-10
 Caucasian-Scythian: POS2-9
 Caucasus: PFA-2
 Caustobioliths: PGG1-11
 Caverns: PGG2-15
 Caves: PFA-2, PPC1-22
 Cayenne: PBG1-9
 Cayi: PFA-7
 Cell: OB2-1, OB2-3, OP2-2, OP3-1, OP4-3, OP4-4, OP5-3, OPC2-4, OPE2-1, PB1-2, PB1-6, PB1-7, PBG1-8, PBG2-11, PBG2-12, PC-10, PM-12, PM-23, PM-28, PMN1-3, PMP-13, PMP-20, PMP-21, PMP-22, PMP-4, PMP-6, PMP-8, PPC1-20, PRG2-16 PMP-8 OB1-3, OB2-3, OP2-1, OP5-3, OSB1-1, OSB2-3, PB1-2, PB2-10, PBG1-8, PC-7, PC2-23, PMN2-3, PMN2-8, PPM-4, PSB-15
 Cellular: OB2-1, OGPR-1, OP2-1, PB2-9, PBG1-4, PMP-20
 Cellulose: OM-3, OP3-2, PBG1-9, PBG2-6, PC2-14, PM-22, PM-8, PMN1-8, PMN2-7 PM-10, PMN2-7, POS2-15
 Celtic: PM-26
 Cendere: PRG1-18
 Cenomanian-Coniacian: PBS-19
 Cenomanian-Turonian: PB1-20, PBG2-9, PBS-3, POS2-14
 Cenomanian: OPC2-3, POS2-14, PPC1-9, PRG1-6
 Cenozoic: OB2-2, OGC-1, OP7-3, OUM-1, PB1-18, PB2-18, PBG1-14, PC-3, PGG1-1, PGG1-12, PM-5, PMP-13
 CENPES: PC2-21, PPM-1
 CH₄: OP2-2, OP5-3, PC-7, PG-14, PG-17, PG-24, PG-26, PG-8, PG-9, PMN2-10, PMP-16, PMP-2, PMP-7, PPM-3, PSB-15
 Chaetoceros: OB2-2
 Charred: OSB1-3, PBC-1, PBC-13, PBC-14, PBC-2, PBC-3, PBC-5, PBC-8, PCS-14, PSB-18, PSB-25
 Charring: OSB1-3, PBC-2
 Chars: OSB1-3, PBC-2, PBC-6
 Chart: PFA-6
 Chase: PCS-8
 Chasing: PSB-15
 Chattanooga: PB1-1
 Cheirolepidiacea: PSB-4
 Cheirolepidiacea: OB1-2
 Chelates: PB1-2
 Chelating: PSB-2
 Chelmek: PEB2-1
 Chemiluminescent: PMN1-8
 Chemo-Taxonomically: OP2-2
 Chemoautotrophic: OGPR-2, OSB2-3
 Chemoautotrophs: PC2-21
 Chemocline: OB1-3, OP2-1, PC2-19, PMP-19
 Chemolithotrophic: OGPR-2
 Chemolysis: PM-4
 Chemometric: OP3-3
 Chemoorganotrophic: PB2-21
 Chemostratigraphic: OB1-2
 Chemostratigraphy: OOS-1 OB1-2, PPC1-7
 Chemosynthesis-Based: PB1-18
 Chemosynthetic: PMP-17, PMP-5 PMP-5
 Chemosystematic: PC2-5
 Chemotaxonomic: OB1-2, OMN-1, PC2-5, PMP-4, PMP-6 PB1-7
 Chemothermal: PBC-4
 Chemotrophic: PB2-21
 Cherkey-HPS: POS2-9
 Chernozem: PBC-2, PCS-3
 Chert: PM-18
 Cherts: PBS-10, PM-18
 Chevron: POS1-10
 Chiapas: POS2-15
 Chicago: PB2-14
 Chicxulub: PBG2-4
 Chihuido: PRG2-8
 Chikaraishi: OP6-4, PC2-14
 Chikwaka: PBC-9
 Chile: PC2-1, PSB-2
 Chilean: PSB-2
 Chillrud: PEB1-14
 China: OGC-1, OGPR-3, OPE2-3, OPS1-3, PB1-16, PB2-14, PBG2-7, PBS-1, PBS-12, PBS-21, PBS-9, PC2-23, PC2-26, PCS-13, PEB1-13, PEB1-3, PEB1-6, PG-13, PG-18, PG-28, PG-4, PG-6, PG-7, PG-9, PGG1-1, PGG1-10, PGG2-4, PMN1-9, POS1-5, POS2-7, PPC1-4, PPM-10, PPM-11, PPM-6, PPM-9, PRG1-20, PRG1-7, PRG2-19
 Chinese: PBS-12, PMN1-9, PPC1-15, PPM-6
 Chinle: OPC1-2
 Chiral: PMN2-6, PMP-22, PMP-23
 Chirasil-Val: PMN2-6
 Chironomid: PC2-3
Chironomus: PB2-1
Chiropteridium: PM-28
 Chitin: OP3-2
 Chitinozoans: PBG1-10
Chlorella-like: PMP-4
 Chloride: PB1-2, PSB-1
 Chlorin: PB2-7
 Chlorinated: PEB1-3 PEB1-5, PEB2-1, PEB2-7, PEB2-8, PM-3
 Chlorination: PEB2-8
 Chlorine: PBS-1, PM-3, PMN1-8
 Chlorins: PB2-7
 Chlorite: PBG1-6 PM-26
 Chlorobactene: PC2-19
 Chlorobenzene: PEB1-15
 Chlorobiaceae: OPE2-3, PBS-21, PC2-17, PC2-19, PEB2-17
Chlorobium: OP2-1
 Chlorophenols: PEB1-9
 Chlorophyceae: PM-19
 Chlorophyll: OP6-4, PB2-10, PB2-15, PB2-20, PB2-4, PB2-7, PBG1-1, POS2-6, PPC1-21
 Chlorophyllide: OP6-4
 Chlorophyllides: OP6-4

- Chlorophylls: OP6-4, PB2-4, PB2-7
 Chlorophyta: PM-28
 Chloropigments: PPC1-6
 Chloroplasts: OSB1-1
 Chocholów: PB1-8
 Choiak: PFA-8
 Cholestane: OB2-2, PEB2-19
 Cholestanes: PBS-10
 Cholesterol: PBG1-11, PMP-4, PPC1-22
 Chondrites: PBG2-3, PM-16
 Chongqing: PBS-12
 Choose: PRG2-10
 Choricystis: PMP-4
 Chorine: PBS-1
 Christiansen: OP1-2
 Christine: PEB2-2
 Chromatiaceae: PC2-19
 Chromatography-combustion-ion: PC2-21
 Chromatography-combustion-isotope: PMN1-4,
 PMN2-6, PSB-15
 Chromatography-Isotope-Ratio: PEB1-15
 PB1-6, PEB1-5
 Chromatography-pyrolysis-isotope: PC2-14
 Chromatography/combustion/isotope: OSB1-1
 Chromatography/time-of-flight: PC2-24
 Chrome-diopside: PGG1-4
 Chromite: PGG1-4
 Chromium: PEB1-9
 Chrono-stratigraphical: POS2-3
 Chronosequence: OSB2-1, PBC-1, PCS-10
 Chrysene: PBG1-14, PEB1-17, PGG2-5
 Chrysenes: PEB2-4
 Chrysophanol: OB3-2
 Chrysophyte: OGPR-3
 Chuar: PB2-19
 Chukchi: PC2-22
 Ciliate: PC2-21 OP6-2 PMP-17, PMP-19
 Cinnamyl: OSB2-2 OSB2-1, PC2-27, PCS-2, PM-
 22, PM-4, PM-5, PSB-6, PM-4
 Circle=Mono-Methylalkane: PSB-4
 Circum-Arctic: OP3-3
 Cismon: PPC1-27
 Citric: OSB2-3
 Citronellol: PB2-2
 Ciénaga: PRG2-12
 Clarkforkian: PC2-10
 Classopollis: POS2-7
 Clastic-Influenced: PRG2-6
 Clastic-Stratigraphic: PG-3
 Clastic/Carbonate: PEB2-17
 Clastic: OP3-4, PBG2-4, PBS-21, PBS-22, PEB2-
 17, PMN2-5, PPM-13, PRG2-1, PRG2-5
 Clastics: OP4-3, PBS-12, PG-1
 Clasts: PBS-6, POS2-10
 Clathrated: POS2-5
 Clathrates: PBG1-8
 Clay-adsorbed: PM-11
 Clay-anhydrite: PGG1-13
 Clay-catalyzed: PB1-16
 Clay-free: PBG2-4
 Clay-mediated: PB2-19
 Clay/fulmar: OP4-3
 Clay/organic: PM-11
 Clay/silt: PPM-11
 Clayey-limestone: POS2-13
 Clayey-silty: POS2-13
 Clayey: PBG2-2, PC2-16, POS1-11, POS2-13,
 POS2-15, POS2-9, PPM-1, PSB-25
 Clayeyshale: POS1-11
 Clayriver: PEB1-17
 Claystone/limestone: PC2-4
 Claystone/shale: PBS-11
 Claystone: PC2-16
 Claystones: OB1-2, PC2-4, PMP-13, POS2-11,
 PPC1-10, PPC1-5
 Clear-Cut: OPG-1, PBC-13, PBC-5
 Cleavage: OB1-1, OB2-3, OBD2-3, OP4-2, PBG2-
 13, PBG2-3, PEB2-7, PFA-2, PFA-6, PM-12,
 PM-4, POS1-2 PBG2-13, PMN2-2 PC-4, PC2-
 25, PGG2-8
 Clement: PC2-27
 Climate-controlled: PC2-24
 Climate-induced: OP2-1
 Climate-proxies: PMP-1
 Climate-reconstruction: PB2-13
 Climate-related: PC2-24
 climate change: PPC1-3
 Climate: OB1-2, OB3-2, OEB-1, OM-3, OP4-1,
 OP5-3, OP7-2, OPC1-3, OPC2-2, OPC2-3,
 OPE1-2, PB1-20, PB1-22, PB2-19, PBG1-9,
 PBG2-10, PBG2-7, PC2-13, PC2-15, PC2-16,
 PC2-19, PC2-21, PC2-24, PC2-27, PC2-3,
 PC2-6, PC2-7, PC2-9, PCS-10, PCS-12, PCS-
 6, PEB2-2, PMP-1, POS2-9, PPC1-11, PPC1-
 14, PPC1-15, PPC1-18, PPC1-19, PPC1-2,
 PPC1-23, PPC1-26, PPC1-27 PPC1-3 PPC1-8,
 PSB-13 OPC2-2, PC2-15, PC2-5, PCS-1, PCS-
 12 OB1-2, OM-3, OP4-1, OP4-2, OPC2-1,
 OPE1-2, OPE1-3, PB1-4, PB2-13, PB2-18,
 PBG1-11, PC2-15, PC2-17, PC2-18, PC2-22,
 PC2-23, PC2-24, PC2-27, PC2-3, PC2-4, PC2-
 9, PCS-12, PCS-13, PCS-14, PM-13, PM-25,
 PM-5, PPC1-13, PPC1-15, PPC1-17, PPC1-2,
 PPC1-21, PPC1-22, PPC1-23, PPC1-8, PSB-19
 Climatically: OPC1-3, OPC2-4
 Climatologically-Consistent: PCS-6
 Clinochlore: PBG1-15
 Clogs: PRG2-13
 Clone: OP5-3, PMP-11
 Closeaux: OSB2-1
 Closed-System: OGC-3
 Clostridia: OP6-1
 Cluster-Size: OSB1-3
 Cluster: OOS-1 OP5-3, OSB1-3, PEB2-12, PGG1-
 14 OB1-3 OB1-1, OPG-3, OSB1-3, PBG1-6,
 PBG2-7, PC-1, PMN1-8
 Cmethyl-Oxygen: PEB2-7
 CO₂-C: OBD2-3, PCS-13
 CO₂-concentration: PSB-17
 CO₂-formation: PG-17

- CO₂-generating: OBD2-2 PG-17
CO₂/CH₄: PPM-3
CO₂/G: POS1-7
CO₂/H₂: OB3-1
CO₂: OBD2-2, OBD2-3, OGC-2, OGPR-1, OOS-2, OP2-2, OP4-3, OP5-1, OP5-3, OP6-2, OP7-1, OPE1-3, OSB1-1, OSB1-2, OSB2-3, PB1-4, PB1-5, PB2-20, PBC-3, PBC-7, PBG1-16, PBG2-11, PBG2-5, PBS-12, PC-6, PC2-17, PC2-26, PCS-1, PCS-10, PCS-13, PCS-2, PCS-5, PCS-7, PEB2-13, PEB2-3, PG-1, PG-14, PG-17, PG-18, PG-21, PG-24, PG-26, PG-28, PG-7, PG-8, PG-9, PGG1-2, PM-7, PMN1-2, PMN2-10, PMN2-2, PMN2-3, PMN2-8, PMP-10, PMP-12, PMP-16, PMP-2, PMP-3, PMP-7, POS1-16, POS1-8, PPC1-16, PPC1-2, PPC1-23, PPM-3, PRG1-11, PSB-17, PSB-6
- Coal-bearing: PC-1, PGG2-16
Coal-derived: PG-13
Coal-field: PGG2-16
Coal-formed: PG-7
Coal-forming: PC-3
Coal-genetic: OGC-1
Coal-like: PBC-8
Coal-sourced: PC-3
Coal/kerogen: OP2-3
Coal: OBD2-3, OGC-1, OGC-2, OMN-1, OP2-3, OUM-1, PBC-5, PBG1-1, PBS-16, PBS-2, PBS-24, PBS-8, PC-1, PC-10, PC-11, PC-12, PC-3, PC-4, PC-5, PC-6, PC-7, PC-8, PC-9, PC2-10, PEB1-17, PEB1-6, PEB1-7, PEB2-13, PG-13, PG-16, PG-20, PG-21, PG-26, PG-27, PG-28, PG-3, PG-4, PG-5, PG-6, PG-7, PGG2-12, PGG2-16, PGG2-3, PMN2-8, PMP-13, POS1-10, POS1-12, POS1-8, POS2-1, POS2-10, POS2-4, POS2-5, POS2-6, POS2-8, PPC1-14, PPC1-24, PPM-2, PPM-5, PRG2-20, OGC-2, OMN-1, OP2-3, OP5-4, OSB1-3, OUM-1, OUM-3, PB2-12, PB2-16, PBC-2, PBS-23, PBS-8, PC-1, PC-10, PC-11, PC-2, PC-3, PC-4, PC-5, PC-6, PC-7, PC-8, PC-9, PC2-22, PEB1-6, PG-10, PG-11, PG-20, PG-21, PG-26, PG-27, PG-8, PGG2-16, PM-16, PMN1-4, PMP-13, POS1-8, POS2-1, POS2-10, POS2-8, PPM-5, PRG2-16, PRG2-18, PRG2-20
- Coalbed: OGC-2 PC-10
Coalfield: PC-10, PEB1-6
Coalification: OP2-3, PC-2, PC-6, PC-8, PEB1-6
Coalified: PM-7
Coaly: OUM-2, PBS-23, PBS-5, PC-10, PC-3, PC-5, PG-16, PG-20, PG-24, PGG2-12, POS1-8, POS2-10, POS2-8, PPM-13
Coast: OB2-3, OP1-1, OP1-2, OP7-3, OPC2-1, OUM-2, PB2-17, PBC-6, PBC-7, PBG2-12, PC-10, PEB1-1, PEB1-4, PEB2-12, PEB2-4, PEB2-5, PG-19, PGG2-13, PGG2-16, PMP-12, POS2-12, PPC1-19, PRG1-2, OMN-2, OMN-3, OP1-1, OP1-2, OP7-2, OPC1-1, OPC2-4, OPE1-3, PB1-15, PB1-17, PB1-6, PB2-20, PBG1-9, PBG2-13, PBS-6, PBS-8, PC-5, PC2-22, PCS-1, PCS-6, PEB2-10, PM-14, PM-20, PM-8, PMN2-1, PMP-12, PMP-14, PMP-18, POS1-11, POS2-15, POS2-4, POS2-8, POS2-9, PPC1-23, PPC1-8, PRG2-20, PSB-13, PB2-21, POS2-8, OP1-1, PEB2-5
- Cobalt: OGPR-1
Coccolith: PMP-4
Coccolith: PC2-13, PPC1-16, PPC1-2
Coccolithophore: PC2-13
Coccolithophores: PC2-13
Coccolithophorid: OP2-1, PMP-1, PPC1-2, PBS-8, OPC1-1
Coccus: PEB2-19
Cockell: PM-21
Coelom: PB1-16
Cohenite: PBG1-6
Coido: OP1-1
Coiling: PBG1-5
Coke: OP5-4, PG-25, PRG2-18
Coking: OSB1-3
Colarusso: PC2-14, PC2-2
Cold-dry: PPC1-13
Cold-humid: PPC1-13
Cold-seep: OP5-1, PB1-18, PMP-5
Cold-seeps: PB1-18
Cold-water: PB1-10
Colloidal: PM-27, PBG1-5, PMN1-8, PSB-16, OSB1-3, PBC-9, PBG1-5, PM-20, PM-8, PSB-16, PBC-3, PBG1-5, PEB2-9, PM-13, PM-8, PMN1-8, PSB-8
Cologne: PEB2-8
Colombia: PBS-19, PC-10, PRG2-12
Colombian: PGG1-5
Colton: POS1-10
Columbia: PBG2-12, PG-10
Column: PM-11
Colwell: PMP-8
Combusted: OPC1-2, PBC-2, PBG2-7
Combustion-derived: OPC1-2, PBC-11, PC2-22, PEB1-13, PEB1-14
Combustion-IRMS: PMN1-4
Combustion: OEB-1, OPC1-2, OSB2-1, PB1-21, PBC-1, PBC-11, PBC-12, PBC-13, PBC-3, PBC-4, PBC-5, PBC-6, PBC-7, PBG2-6, PBG2-7, PC2-22, PEB1-1, PEB1-10, PEB1-14, PEB1-15, PEB1-16, PEB1-17, PEB1-3, PEB1-6, PEB2-13, PEB2-14, PEB2-8, PMN1-8, PMN2-10, PMN2-6, PMN2-8, PMP-15, PSB-20, PSB-21
Commingle: PG-8, PRG2-8
Commingle: OGC-4
Compartmentalization: PB2-11, PG-8, PRG1-15, PRG1-19, PRG1-8, PRG1-18, OP6-1, OP7-4, PB2-11, PCS-8, PG-8, PGG2-9, PRG1-15, PRG1-19, PRG2-15, PRG2-5, PB1-7, PEB2-2, PG-8, PGG2-9, PMN1-3, OGPR-1
Complexes: OB1-1, OB2-1, OBD1-1, OBD1-3, OEB-2, OEB-3, OGC-1, OMN-2, OMN-3, OP1-1, OP2-4, OP3-4, OP5-4, OP6-1, OPE1-3, OPG-1, OPG-2, OPS2-3, OUM-1, PB1-17,

- PB1-19, PB2-1, PB2-13, PB2-14, PBC-4, PBC-7, PBG1-2, PBG2-14, PBS-16, PBS-21, PBS-24, PC-5, PC2-11, PC2-17, PC2-25, PC2-4, PCS-8, PEB1-10, PEB1-11, PEB1-14, PEB1-15, PEB1-7, PEB2-18, PFA-2, PFA-6, PFA-8, PFA-9, PG-10, PG-12, PG-27, PG-8, PGG2-11, PGG2-14, PGG2-3, PGG2-9, PM-13, PM-15, PM-20, PM-27, PM-28, PM-9, PMN1-4, PMN2-11, PMP-12, PMP-9, POS1-13, POS1-9, POS2-3, PPC1-1, PPC1-12, PPC1-2, PPC1-23, PPM-2, PPM-4, PPM-8, PRG1-17, PRG1-5, PRG2-15, PRG2-19, PRG2-2, PRG2-4, PSB-25, PSB-5, PSB-6
- Complexation: OBD2-2, OSB1-3, PBG1-8, PEB2-9, PM-15, PM-20, PMN1-8, PSB-1, PSB-5 PCS-1 PBG1-4, PCS-1, PSB-1, PSB-5 OB3-2, OM-1, PBC-12, PBG1-3, PCS-1, PCS-5, PGG1-12, PGG2-6, PM-11, PPM-3, PSB-1, PSB-12, PSB-13, PSB-25, PSB-5
- Complexing: PB2-3
- Complexities: OPS1-1
- Complexity: OMN-2, OPE1-3, OPG-3, OPS2-1, PB2-2, PBG1-5, PC2-21, PFA-1, PFA-9, PGG1-11, PGG2-6, PM-13, PM-15, PM-20, PMP-10
- Complexometric: PSB-1
- Composite: PC2-10, PC2-3, PC2-9, PCS-2
- Compost: PCS-12, PEB2-3, PMN2-7, PSB-5 PSB-4
- Condensate-gas-ratio: OP4-3
- Condensate: OP3-4, OPS2-2, OUM-1, PBS-15, PBS-23, PBS-24, PBS-5, PBS-8, PC-4, PG-1, PG-13, PG-15, PG-2, PG-3, PG-8, PGG2-16, POS2-9, PPM-11, PRG2-4, PRG2-7 POS2-4 OGC-1, OPG-3, PB2-4, PBS-15, PBS-24, PBS-5, PC-4, PG-15, PG-23, PG-3, PG-8, PGG1-5, PGG2-2, PMN1-11, POS2-8, PPM-12, PRG1-13, PRG2-4, PRG2-7
- Condensation: OGC-1, OM-1, OSB1-3, PB2-16, PBC-12, PBC-4, PBG1-16, PBG1-6, PC-7, PG-16, PG-25, PM-13, PM-28, PPM-2 PRG1-10 PRG2-18, PSB-7
- Condor: POS1-14
- Conducive: PBS-3, PMP-16
- Conduct: PEB1-10
- Conductance: PB1-4
- Conductivity: PEB1-8, PEB2-3, PMP-12
- Congo-Angola: PB1-13
- Congo: OP4-1, PPC1-19, PPC1-20, PRG1-12
- Congruent: OEB-3, POS2-15
- Coniacian-Santonian: PC2-16
- Conifer-specific: PBS-16
- Conifer: OB1-2, PC2-5, PEB2-8, PFA-2
- Coniferales: OB1-2
- Coniferous: PBG2-5, PCS-2, PFA-9, PM-5, PSB-15
- Conifers: OB1-2, PBC-14, PBG1-11, PC2-5
- Coniferyl: PM-22
- Conodonts: PBG1-10
- Constant-pressure: PGG1-8, PPC1-21, PPM-15
- Contaminants: OB1-1, OM-1, PM-13, PSB-10 OBD2-1, OEB-3, OP6-1, PEB1-1, PEB1-12, PEB1-14, PEB1-5, PEB1-9, PEB2-2, PEB2-7, PMN1-5, PMN2-1, PMP-18, POS2-15
- Contaminated: OBD1-1, OBD1-3, PEB1-1, PEB1-10, PEB1-14, PEB1-9, PEB2-13, PEB2-6, PEB2-8, PG-8, PGG1-9, PMN1-5, PMP-13, PRG1-14, PRG1-8, PRG2-2
- Contaminating: PBS-16
- Contamination: OBD1-3, OBD2-1, OEB-3, OMN-1, OP5-2, OP6-1, OPE1-2, OPE2-1, OUM-1, PBS-13, PBS-15, PEB1-1, PEB1-10, PEB2-10, PEB2-11, PEB2-2, PGG1-9, PM-16, PM-18, PM-19, PMP-13, PMP-8, POS2-12, PPC1-22, PRG1-14 PGG2-4, PRG1-14
- Continent: OP4-1, PBG2-13, PBS-2, PM-8, POS2-3, PPC1-15, PPC1-19, PPC1-7
- Continental/marine: PC2-4
- Continental: OB3-1, OP4-1, OP4-3, OP7-3, OPC1-3, OPC2-1, OPE1-2, OPE1-3, OPE2-2, OPE2-3, OPG-3, OUM-3, PB1-13, PB1-17, PB1-18, PB1-22, PB1-7, PB2-13, PB2-18, PBC-13, PBC-14, PBC-6, PBC-7, PBG1-11, PBG1-14, PBG2-10, PBG2-12, PBG2-14, PBG2-6, PBS-2, PC2-11, PC2-14, PC2-16, PC2-23, PC2-24, PC2-4, PC2-5, PC2-6, PC2-9, PCS-12, PCS-6, PG-20, PGG2-10, PGG2-12, PGG2-13, PGG2-5, PGG2-9, PM-26, PM-5, POS1-11, POS2-13, POS2-7, POS2-9, PPC1-1, PPC1-11, PPC1-15, PPC1-20, PPC1-28, PRG2-11, PRG2-14, PSB-18
- Continentality: PC2-21
- Continents: OB1-2, OPE1-2, OSB1-2, PGG1-12, POS1-13, PSB-7
- Cooper: PB-12, PBS-16, PPM-13, PRG2-16
- Coorong: PPC1-8
- Copals: PFA-9
- Cope: PBG1-4
- Copper-binding: PBG1-4
- Copper: PBG1-4
- Coprostanol: PB1-6, PEB1-7, PFA-2
- Coral: PB2-17, PEB1-2
- Cordatum: OB1-2
- Cordillera: PBS-3, POS1-13
- Core: OB3-2, OBD2-2, OEB-3, OP4-1, OP5-4, OPC1-3, OPC2-1, OPC2-4, OPE1-2, OPE2-3, OSB1-3, PB1-14, PB1-19, PB1-22, PB1-6, PB2-13, PB2-2, PB2-4, PB2-7, PBG1-12, PBG1-8, PBG2-10, PBG2-4, PBS-6, PC2-12, PC2-18, PC2-22, PC2-23, PC2-25, PC2-27, PC2-3, PC2-6, PC2-7, PC2-9, PCS-12, PCS-2, PEB1-14, PEB1-2, PEB1-7, PEB2-12, PG-19, PG-20, PGG1-1, PM-10, PM-25, PM-26, PM-5, PM-6, PMN1-5, PMN2-4, PMN2-5, PMN2-8, PMP-13, PMP-17, PMP-21, PMP-22, PMP-23, PMP-3, PMP-8, POS1-10, POS2-15, POS2-3, POS2-4, PPC1-14, PPC1-15, PPC1-16, PPC1-19, PPC1-25, PPC1-27, PPC1-4, PPC1-5, PPM-1, PPM-11, PRG1-9, PRG2-1, PRG2-16, PRG2-18, PRG2-4, PSB-3 OPE1-3,

- OPE2-3, PM-10, PPM-11 PB2-4 PEB1-2, PPM-11, OBD2-1, OOS-2, OP5-4, OPC1-1, OPC2-2, OPE1-1, OUM-3, PB1-20, PB1-9, PB2-13, PB2-2, PBG1-8, PBG1-9, PBG2-10, PBG2-14, PBS-11, PBS-12, PBS-16, PBS-8, PC2-11, PC2-14, PC2-19, PC2-2, PC2-22, PC2-23, PC2-24, PC2-3, PC2-7, PC2-8, PCS-10, PCS-12, PCS-2, PEB1-2, PEB1-7, PEB2-12, PG-19, PM-26, PMN2-2, PMN2-4, PMN2-5, PMP-3, PMP-8, PPC1-15, PPC1-19, PPC1-22, PPC1-26, PPC1-8, PPM-11, PRG2-18, PRG2-3, PSB-19 PEB1-2, PEB2-12, PMP-8
- Corn: PCS-7
 Coronene: POS2-12
 Counter-acting: OP4-1
 Counter-intuitive: PRG2-5
 Counteract: OB2-1
 Counterpart: PRG1-7
 Counterparts: OP3-1, OP3-2, PBG1-8, PBS-13, PC2-5, PEB2-8, PM-16, PM-28, PMP-14, PPC1-7
 Counting: PMP-20, POS2-3
 CPMAS: OSB1-3, OSB2-2, PBC-8, PCS-4, PSB-12, PSB-18, PSB-9
 CPRM: POS2-3
 Cr-Containing: PGG1-4
 Cr: PBG2-2, PGG1-4
 CR: PMN2-9, PPM-15
 Cr₂⁺-Reducible: PSB-8
 Cracking: OBD1-3, OGC-1, OP2-3, OP5-4, OPG-1, OPS1-3, OPS2-3, ORP-1, ORP-2, PB2-4, PBG2-11, PBS-26, PBS-5, PG-10, PG-15, PG-16, PG-21, PG-22, PG-23, PG-25, PG-3, PGG1-5, PMN2-5, POS2-5, PPC1-1, PPM-2, PPM-5, PRG1-1, PRG1-11, PRG2-18, PRG2-4, PRG2-7
 Cracks: PC2-19, PG-19, PG-25
 Cracky: PGG2-6
 Crater: PBG2-4, PC2-9, PM-11
 Craters: POS2-6
 Crato: PSB-4
 Craton: PBG1-15, PC2-25
 CREN: OB1-3
 Crenarchaeal: OB2-3, OPC2-3
 Crenarchaeol: OB2-3, OPC2-4, PPC1-19
 Crenarchaeota: OPC1-3, OPC2-3, OPC2-4, PBG2-10, PC2-3, PPC1-19
 Crenarchaeotal: PPC1-28
 Creosote: PEB2-10, PEB2-13
 Crest: PRG2-17
 Cretaceous-aged: PRG1-18
 Cretaceous-Eocene: PM-12
 Cretaceous-Paleogene: PG-24
 Cretaceous-Sourced: PBS-23
 Cretaceous-Tertiary: PBG2-4, PGG2-1
 Cretaceous: OGC-1, OOS-3, OP2-3, OP4-3, OPC2-3, OPS2-3, OUM-1, OUM-2, PB1-10, PB1-18, PB1-21, PB1-7, PB2-12, PBG2-4, PBS-15, PBS-2, PBS-23, PBS-3, PBS-6, PBS-8, PC-10, PC-11, PC-5, PC-6, PC2-26, PFA-7, PG-10, PG-2, PG-6, PGG1-10, PGG1-11, PGG2-1, PGG2-5, PM-12, PMP-5, POS1-13, POS1-15, POS2-11, POS2-13, POS2-15, POS2-4, POS2-5, PPC1-1, PPC1-18, PPC1-27, PPC1-9, PPM-8, PRG1-13, PRG1-2, PRG1-3, PRG2-1, PRG2-12, PRG2-16, PRG2-4, PRG2-5, PRG2-6, PSB-4
 Cretan: PMP-10
 Crew: PBG1-4
 Crimea: POS2-9
 Crimean-Caucasian: POS2-9
 Croatia: PG-1
 Croce: PPM-8
 Crocetane: PB1-18, PMP-13, PMP-21, PMP-5
 Crocetanes: PMP-21
 Crocker: PBS-14
 Crossman: OP2-2, OP4-2, PSB-15
 Crude: OBD1-1, OBD1-2, OBD2-1, OEB-2, OP1-2, OP3-3, OP3-4, OP5-2, OP6-3, OPG-1, OPG-3, OUM-1, OUM-3, PB1-10, PB1-16, PB2-14, PB2-3, PB2-4, PBG1-1, PBG2-4, PBS-12, PBS-15, PBS-24, PBS-9, PC-5, PEB1-1, PEB1-11, PEB1-12, PEB1-16, PEB1-18, PEB1-2, PEB1-4, PEB2-18, PEB2-19, PEB2-5, PFA-6, PG-25, PG-5, PGG1-1, PGG1-14, PGG1-15, PGG1-6, PGG1-7, PGG1-9, PGG2-11, PGG2-15, PGG2-16, PGG2-2, PGG2-4, PGG2-5, PGG2-6, PGG2-7, PGG2-8, PM-9, PMN1-11, PMN1-4, PMN1-5, PMN1-9, PMN2-11, PMN2-4, PMN2-5, POS1-4, POS2-15, PPC1-4, PPM-15, PPM-9, PRG1-12, PRG1-13, PRG1-16, PRG1-17, PRG1-2, PRG1-20, PRG1-3, PRG1-4, PRG1-5, PRG1-6, PRG1-7, PRG1-8, PRG1-9, PRG2-11, PRG2-12, PRG2-13, PRG2-14, PRG2-18, PRG2-2, PRG2-3, PRG2-9, PSB-25
 Crudes: PGG1-11, PGG2-15, PGG2-7
 Cruise: OB1-3, OB2-2, PB1-13, PBG1-14, PBG1-4, PC2-2, PM-26, PMP-17, PMP-23, PMP-6, POS2-13
 Crust: PBG1-6, PBS-3, PG-24, PGG1-4, PMP-16, PRG2-19 PBC-10, PEB2-15, PMP-18
 Cu-Complexes: PPC1-6
 Cu: PB2-1, PBG1-3, PBG2-2, PEB2-12, PSB-5
 Cu₂⁺-binding: PBG1-3
 Cu₂⁺-ligand: PBG1-3
 Cu₂⁺-NOM: PBG1-3
 Cu₂⁺: PBG1-3, PBG1-4, PM-20
 Cuo-oxidation: PCS-7 OSB2-1, OSB2-2, PB2-20, PC-2, PC2-1, PCS-4, PM-4, PMN2-10, PSB-6
 Cuparane-Type: OB1-2, PC2-5
 Cupressaceae: OB1-2, PC2-5
 Curde: PGG2-15
 Curie-point: PBC-14, PBC-9, PM-14
 Curie: OSB1-2, PB1-1, PM-14, PM-4, PM-5, PM-8
 Curiri: PB1-22
 Current-Driven: PC2-24
 Currently-held: PMP-12
 Curtailed: PC2-22
 Cut-off: PEB1-14, PM-20, PMN1-8

- Cutan: PM-25 OP3-1, OP3-2, PM-23 OSB1-2, PBC-9, PM-12, PM-25
 Cuticle/Internal: OP3-2
 Cuticle: OP3-2, POS2-7, PRG2-1
 Cuticles: OP3-1, OP3-2, OSB1-2, PM-23
 Cuticular: OP3-2
 Cutin: OP3-2
 Cutinite: PBS-23, PBS-8, PC-5, POS2-4
 Cyanobacteria: OP2-1, OP4-2, OP6-1, OPE2-3, PB2-4, PB2-8, PC2-17, PC2-20, PC2-21, PMP-10, PMP-12, PMP-14, PMP-19, PPC1-11, PPC1-8, PRG1-5 OGPR-2, OP4-2, OPE2-3, PC2-17, PC2-20, PM-12, PMP-14, PPC1-27 PB1-22 PB2-8
 Cycadales: OB1-2, PC2-5
 Cycads: PC2-5
 Cyclanes: PSB-3
 Cyclo-alkanes: PC2-4
 Cycloalkane: PB2-3, PRG1-5
 Cycloalkanes: PB2-3, PG-4
 Cycloalkyl: PRG2-2
 Cycloaromatic: PRG1-6
 Cyclobutane: PB1-7, PMN1-3
 Cyclohexane: ORP-2, PG-27, PPM-14
 Cyclohexanes: OGPR-2, PB2-3
 Cyclohexylbenzenes: PGG1-7
 Cyclopentane: OPC2-3, OPC2-4, ORP-2, PB1-14, PMP-18
 Cyclopentanebromide: PB2-3
 Cyclopentanes: OGPR-2, PB2-3
 Cyclopentanone: PB2-3
 Cyclopentyl: PB2-3
 Cyperaceae: PM-10
 Cyst: PM-28
 Cysts: PC-5, PM-28
Cytophaga: PMP-11, PMP-20
 Cytoskeletal: OP4-4
 Czech: PBG1-10
 Czimeczik: PBC-1
- D**
- D6-Benzene: PC-1
 Dabbous: PBS-7
 DAC: PBC-7, PM-22, PMN2-7
 Dacian: PC-1
 Dadas: PBG1-10
 Dagestan: POS2-9
 Dahl: OPS2-2, PBS-22, PGG2-3
 Dalkenones: PBG2-1
 Dammarane-type: PFA-6
 Damon: PEB1-14
 Danish: PBS-22
 Danismen: PG-3
 Danube: PG-24, PGG1-15
 DAPI-Stained: OB1-3
 Daqing: PG-7
 Darc: PBS-3
 Darmstadt: PB1-22
 Darussalam: POS2-10
 Darwin: PM-26
 Database: OP6-1, OP7-4, PEB1-14, PPM-4, PRG2-11
 Dating: OP6-2, OPC2-2, PBG1-13, PBG2-7, PFA-4, PPC1-21
 Dealkylation: PBC-9, PG-25, PGG1-15
 Deasphalted: PGG1-2, PMN2-9
 Deasphaltened: PMN1-11
 Deasphaltenized: PGG2-6
 Deasphalting: PMN2-9
 Debnik: PM-7
 Debris: OP1-2, OPE2-3, PB1-21, PB1-22, PBG1-9, PBS-14, PM-12, PMP-11, PSB-4
 Debye: PBG1-5
 Decarbonation: PC2-25, PG-17, PCS-7
 Decarboxylation: PB2-5, PBC-14, PGG2-4, PGG2-8, PM-23, PSB-18
 Deck: PPM-11
 Decontaminated: PMN1-5
 Decontamination: PEB2-20, PEB2-3
 Deep-drilled: PGG2-16
 Deep-drillings: PB1-22
 Deep-Lake: PPC1-8
 Deep-occurred: POS2-2
 Deep-sea: OP2-1, OPE2-2, PB1-20, PMP-10, PMP-17, PMP-23
 Deep-seated: PG-3
 Deep-water: PG-19, PRG1-15 PPM-15 OPC1-1, PBS-14
 Deepening: PC2-27
 Deeply-buried: OB2-3, OMN-3
 Degassed: PG-27
 Degassing: OGC-1, PBG1-6
 Deglacial: PC2-24
 Deglaciation: OGC-2, OP4-1, PC2-23, PC2-7
 Degliai: PSB-25
 Degradinite: PC-10
 Dehydroabietal: OB1-2
 Dehydroabietane: OB1-2, PBG1-2, PC-12
 Dehydroabietate: PFA-9
 Dehydroabietic: OB1-2, OEB-1, PBG1-11, PFA-2
 Dehydroabietins: OB1-2
 Dehydroaromatization: POS2-2
 Dehydrogenation: PB2-16
 Dehydrogenative: PM-22
 Deir: PFA-6
 Deltaic: OP1-2, OUM-1, PB2-12, PBS-19, PC-10, PG-15, PG-3, POS1-10, POS2-5, PRG1-13, PRG2-12
 Deltaproteobacteria: PMP-15
 Deltas: OPE1-3
 Deluvial: PBG1-14
 Demerara: OPC2-3, PC2-16, PPC1-10, PPC1-9
 Demersal: PEB1-10, PEB1-16
 Demethoxylation: PBC-9
 Demethylated: OBD1-2
 Demethylation: OB2-2
 Demineralisation: OSB2-2, PSB-12
 Demineralization: PM-14, PM-18
 Demospongiae: OGPR-3
 Dendrites: PBG1-6

- Denitrification: OPE2-3, PB1-7, PMP-9
 Denitrifying: PB2-4
 Densinite: PC-12
 Density-gradient: PMP-15
 Denudation: PPM-6
 Depands: PSB-1
 Dephasing: OSB1-3, PBC-14, PSB-13
 Deploys: PRG1-15
 Depocenters: OPE1-1, PBS-13, PPM-8, PPC1-8
 Depolymerization: OBD2-3
 Depollution: PMN1-1
 Depolymerisation: PM-25
 Depolymerization: OEB-1
 Deposit: OEB-3, PB1-18, PBG1-10, PBG2-14, PBG2-2, PBS-7, PEB1-17, PEB2-12, PGG1-13, PGG2-11, PGG2-12, PGG2-6, PM-18, PMP-16, POS1-1, POS1-4, PRG1-1 OGPR-3, OP1-2, OP4-4, OP7-3, OPC2-4, OPE1-1, OPE1-2, OPS1-1, PB1-13, PB1-15, PB1-22, PB1-6, PB2-13, PB2-4, PB2-8, PBC-8, PBG1-13, PBG1-6, PBG1-8, PBG2-14, PBG2-4, PBS-12, PBS-13, PBS-18, PBS-19, PBS-21, PBS-23, PBS-9, PC-10, PC-11, PC2-11, PC2-17, PC2-18, PC2-21, PC2-22, PC2-24, PC2-26, PEB2-14, PG-14, PG-2, PG-3, PGG1-1, PGG1-7, PGG2-1, PGG2-16, PGG2-6, PM-25, PMP-2, POS1-11, POS1-12, POS2-10, POS2-14, POS2-6, POS2-8, PPC1-1, PPC1-17, PPC1-5, PPC1-7, PPM-15, PRG1-3, PRG1-9, PRG2-1, PRG2-12, PRG2-20, PRG2-6, PSB-19, PSB-4, PBG1-8, PBS-20, PBS-21, PC2-26 OOS-1 OOS-2, OPC2-2, PB1-20, PB1-22, PB1-8, PBG1-14, PBG1-6, PBG1-8, PBG1-9, PBS-10, PBS-2, PBS-22, PBS-3, PC2-10, PC2-11, PC2-20, PC2-4, PC2-9, PEB1-11, PEB1-16, PEB2-12, PEB2-14, PFA-2, PG-12, PG-2, PGG1-11, PGG1-4, PGG2-10, PGG2-11, PGG2-12, PGG2-6, PM-12, PM-25, POS1-11, POS1-9, POS2-1, POS2-13, POS2-6, POS2-9, PPC1-22, PPC1-4, PPC1-7, PPM-3, PRG1-5, PSB-25
 Deposition: OOS-1 OB1-2, OEB-3, OOS-2, OP2-1, OP4-1, OP4-4, OPE2-2, ORP-2, OSB1-2, PB1-15, PB1-19, PB1-22, PB2-13, PB2-14, PB2-19, PB2-20, PB2-5, PB2-8, PBC-8, PBG1-6, PBG2-1, PBG2-4, PBG2-8, PBS-12, PBS-14, PBS-3, PBS-9, PC2-11, PC2-12, PC2-17, PC2-21, PC2-25, PC2-4, PEB1-13, PEB1-14, PEB1-8, PEB2-16, PFA-3, PGG1-1, PGG1-11, PGG2-7, PGG2-8, PMP-1, POS1-11, POS2-8, PPC1-11, PPC1-18, PPC1-26, PPC1-4, PPC1-8, PPM-15, PRG1-11, PRG1-5, PRG1-9 OOS-3, OP3-3, OP4-1, OP4-2, OP5-2, OPC1-1, OPE2-2, PB1-9, PB2-21 PB2-22 PB2-8, PBG1-13, PBG2-12, PBG2-13, PBG2-4, PBG2-8, PBS-1, PBS-11, PBS-14, PBS-17, PBS-21, PBS-22, PBS-9, PC-11, PC2-17, PC2-21, PC2-24, PC2-25, PC2-4, PC2-8, PEB2-17, PG-2, PGG1-11, PGG2-4, PGG2-8, PM-12, PM-25, PMN2-3, PMN2-9, PMP-18, POS1-1, POS1-10, POS1-12, POS1-4, POS1-7, POS2-1, POS2-13, POS2-14, POS2-5, POS2-7, POS2-8, PPC1-5, PPM-10, PPM-15, PPM-7, PRG1-5, PRG1-6, PRG2-1, PSB-4 PPC1-6
 Depression: OGC-1, PBS-21, PBS-9, PC2-18, PEB2-17, PG-1, PG-13, PG-28, PG-7, PGG1-1, PGG1-13, PGG1-15, PGG2-10, POS1-11, PPM-10, PPM-4, PPM-9, PRG1-7, PRG2-19, PBS-20 PBS-12, PG-1, PGG2-5, POS1-9, PPC1-1, PPM-4
 Depth-distributions: OB1-3
 Depth-independent: PMP-8
 Depth-related: PPC1-25
 Depyritization: PC-1
 Derivatisation: PB1-17, PEB1-12, PMN1-4, PMN2-6, PRG2-14 PB1-14, PEB1-12, PM-17, PMN2-6 PMN1-4, OMN-3, PBC-13, PMN1-8, PRG2-2
 OEB-1, OPG-3, PB2-13, PGG2-8, PM-16, PRG2-2
Des-A-Lupanes: OP1-2
 Descriptors: PBC-14
 Desert: OEB-1, PMP-12, PSB-20
 Desmethylsteranes: PBS-8
 Desorption-Gas: PEB1-15
 Desorption: OGC-2, PC-1, PCS-9, PEB1-15, PEB2-20, PG-20, PSB-10 POS1-9
Desulfobacter: OP6-2
Desulfobacterium: OP6-2
Desulfosporosinus: PMP-6
Desulfovibrio: OP6-2
 Desulfurization: OGPR-1, PB2-14
 Desulphurisation: PC-2
 Detergent: PEB2-12 PEB1-9
 Deterioration: PB1-19, PB2-18, PEB2-15, PM-22, PSB-19
 Detoxification: PBG1-4
 Detoxify: PBG1-4
 Detoxifying: PBG1-4
 Detrohuminite: PC-12
 Detroit: PRG2-5
 Deuterated: PEB2-5, PGG2-3, PMN1-10, PPM-5
 Deuterium/hydrogen: PC2-6
 Deuterium: PBG2-1, PC2-15, PG-8, PG-9, POS1-4 PPC1-3 PRG1-13, PRG1-20
 Devonian: OP3-3, PB1-1, PB1-12, PB1-22, PB2-12, PBG1-10, PBS-15, PBS-20, PC2-26, PC2-8, PEB2-17, PG-14, PM-7, POS1-13, PPM-6, PRG1-9, PRG2-5, PSB-25
 Dewaxing: POS2-2
 DHA=Dehydroabietic: OEB-1
 Di-acylglycerol: PMP-20
 Di-esters: PB1-14
 Di-ether: PB1-14
 Di-iso-propylnaphthalenes: OEB-3
 Di-O-alkyl-Sn-glycerol: PB1-14
 Di-unsaturated: PFA-3
 Di/triterpenoids: PB2-16
 Diabase: PC2-25, PSB-14
 Diacholestenes: PC-11

- Diacids: PM-16, PM-25, PPC1-25
 Diacyl: PBG1-16, PMP-6
 Diagenesis: OM-1, OM-2, OPC2-3, PB1-17, PB1-19, PB1-21, PB1-7, PB1-8, PB2-1, PB2-18, PB2-19, PB2-4, PB2-5, PB2-6, PB2-7, PB2-8, PB2-9, PBG1-14, PBG1-2, PBG1-8, PBG1-9, PBG2-11, PBG2-12, PC-11, PG-14, PGG1-2, PGG2-8, PM-10, PM-17, PM-25, POS1-13, POS1-2, POS2-6, PPC1-15, PPC1-25, PRG2-1, PRG2-20, PBS-20
 Diagenetic: OGC-1, OM-1, OP2-1, OP3-1, OP6-2, PB1-17, PB1-19, PB1-7, PB1-8, PB2-15, PB2-16, PB2-8, PB2-9, PBC-9, PBG1-2, PBG1-8, PBG1-9, PBG2-11, PBG2-13, PC-10, PC-12, PC-6, PC2-11, PC2-20, PC2-22, PC2-4, PEB1-1, PFA-1, PFA-9, PG-8, PGG1-12, PM-12, PM-25, PMN2-6, PMP-18, POS1-11, POS1-13, POS1-2, POS1-4, POS2-15, POS2-9, PPC1-12, PPC1-23, PPC1-7, PRG2-1, PRG2-20, PRG2-4 PMP-18 OP3-1, PC-2
 Diahopane/hopane: OOS-3
 Diahopanes/hopanes: OP5-2
 Diahopanes: PB2-19
 Dialkyl: OB3-1, OPC2-3, PB1-14, PC2-25, PMP-18, PMP-21, PPC1-19
 Dialphanaphthylethane: PGG1-8
 Dialysis: PM-27, PMN1-8
 Diamantane: PGG1-5
 Diamond-Like: PGG1-5
 Diamond-Rich: PBG2-7
 Diamondoid-Biomarker: OPS2-3
 Diamondoid: OGC-1, OPS2-3, PGG1-5, PGG2-3, PRG2-7
 Diamondoids-Derived: PGG1-5
 Diamondoids: OBD2-1, OPS2-3, PBS-24, PGG1-5, PGG2-3
 Diamonds: PBG2-7
 Diapir-Related: PB1-18
 Diapir: PPM-12
 Diaromatic: PEB2-17
 Diaromatics: OPG-1
 Diaryl: PC2-17
 DiaS/RegS: PBS-20
 Diasterane/: PBS-20
 Diasterane/C₂₉: PBS-8
 Diasterane/sterane: OOS-3
 Diasterane: OOS-3, ORP-2, POS2-12
 Diasteranes/steranes: OP5-2
 Diasteranes: OBD2-1, PBS-13, PBS-8, PBS-20, PEB2-4, PGG1-1, POS2-12, PRG2-12
 Diasterenes: PBG1-2, PC2-4
 Diastereoisomers: OB1-1
 Diatom-rich: OB2-2
 Diatom: OB2-2, OP2-1, PB1-10, PB2-18, PGG2-10 PPC1-3
 Diatomaceous: OB2-2, PB1-10, POS2-6
 Diatomite: PBS-8
 Dibenz[AJ]anthracene: PC2-22
 Dibenz[Ah]anthracene: PEB1-17
 Dibenzofuran: PM-7
 Dibenzofuran: PGG2-5 PEB2-11, PGG2-5
 Dibenzothiophene: OP6-1, PB1-12, PGG2-5, PMN1-10 PBS-21, PEB2-11, PEB2-4, PGG2-5, PMN1-10, PRG1-1
 Dibiphytanyl: PMP-17
 DIC: OB2-3, OPE1-1, PMP-2, PMP-3, PPC1-8
 Dicarboxylic: OBD2-2, OEB-1, PBG2-3, PRG2-2
 Dichloromethane-methanol: PB2-13 PFA-6, PFA-8 PGG1-5
 Dichloromethane: OPE2-1, PB1-1, PB1-21, PBG1-12, PC2-5, PEB1-7, PM-16, PMN1-7, PMN2-5, PPC1-5, PRG1-11, PRG1-9, PRG2-16, PRG2-18, PSB-4
 Dichromate: PCS-10
 Dieldrin: PEB2-1
 Dienes: PB2-1
 Dienic: PFA-9
 Diesel-Oil: PGG1-9
 Diesel-Powered: PEB2-15
 Diesel: OBD2-1, PBC-10, PBC-2, PEB1-13, PEB1-14, PEB1-16, PEB1-18, PEB2-13, PEB2-15, PGG1-9, PMN1-5
 Diester: PRG2-2, PSB-2
 Dietary: PFA-3
 Diether: OP5-1, PPC1-23
 Diethers: OB3-1, OP5-1, PB1-18, PMP-18, PPC1-23
 Diethylalkane: OPE2-1
 Diethylalkanes: OGPR-2
 Diffraction: PBG2-11, PBG2-7
 Dihydrophenanthrene: PEB2-19
 Dihydroxy: PB2-2
 Dihydroxyarchaeol: OP5-1, PB2-2
 Dihydroxyarchaeols: PB2-2
 Dimeric: PSB-3
 Dimethylalkanes: OGPR-2
 Dimethylalkanes: OGPR-2
 Dimethylalknes: OGPR-2
 Dimethylcarbazoles: PPM-10
 Dimethylcyclopentane: ORP-2
 Dimethyldisulphide: PC-1
 Dimethylfluorenes: PB1-8
 Dimethylnaphthalene: PC2-22
 OB3-2, OPG-1, PBG2-2, PGG1-8
 Dimethylphenanthrene: PEB1-14 PGG1-15
 Dimethylpyrenes: PB1-8
 Dimethylsulfone: PBG2-3
 Dinaphthylmethane: PGG1-8
 Dinarides: PPC1-1
 Dinaridic: PPC1-1
 Dinitrile: PBG1-16
 Dinitrogen: PB1-7
 Dinoflagellate-Shaped: PM-28
 Dinoflagellate: PB1-10, PC-5, PM-28, POS2-7
 Dinoflagellates: PB1-10, PC2-19, PC2-26, POS1-7
 Dinophyta: PM-28
 Dinostanol: PPC1-23
 Dinosteranes: PBS-3, PC2-17
 Dinosteroids: OOS-3

- Dinosterol: PC2-19
 Diol: PB2-2, PC2-11
 Diols: PB1-11, PC2-24, PPC1-23
 Dioxygenase-Initiated: OP6-1
 Dip: PBS-13, PRG2-10
 Dipeptides: PM-2
 Diphosphatidylglycerides: PMP-20
 Diphosphatidylglycerol: PMP-6
 Dipicolinic: PB1-2
 Diploptene: OP6-2, PB2-9, PC2-12, PPC1-12
 Diplopterol: OP6-2, PMP-17
 Dipterocarp: PGG2-2
 Dipterocarpaceae: PFA-6, PGG1-10
 Distal-Deltaic: OP3-3
 Distal: OP3-3, OPS2-3, PC2-14, PC2-2, POS1-10, PPM-15
 Disulfide: PB2-1, PBG1-16
 Disulphides: PC-1
 Diterpane: OOS-3, PGG2-16
 Diterpanes: OB1-2, PC-12
 Diterpanoid: PGG2-16
 Diterpene: PBC-14
 Diterpenes: PB2-17, PBC-14
 Diterpenoid: PBC-14
 Diterpenoids: OB1-2, OP6-4, PC2-4, PFA-9
 Diterpnoid: PGG2-16
 Dithionite-extractable: PPC1-4
 Diunsaturated: PB1-1
 Diyarbakir: PFA-7
 DNA: OP2-1, OP2-2, OP3-1, OP5-3, PB1-14, PM-21, PMP-1, PMP-15, PMP-6
 DOC: OBD2-3, OM-1, OSB2-2, PBC-11, PM-13, PMN1-8, PMN2-1, PSB-14, PSB-16
 Docosaehaenoic: PB2-5
 Dodan: PG-17
 Dodecyl- β -D-glucopyranoside: PEB2-9
 Dodecylsulfate: PEB2-9
 Dodecyltrimethylammoniumbromide: PEB2-9
 Dolgorae: PBS-5
 Dolomite: PB2-14, PBS-11, PC2-20, PM-7, PPC1-7
 Dolomites: PM-7, PPC1-7
 Dolomitic: PBS-10, PPC1-7
 Dolomitisation: PPC1-7
 Dolomitized: PM-14
 Dolostone: PPC1-7
 Dolostones: PC2-20
 DOM: OMN-2, PBC-11, PBC-3, PEB2-17, PGG1-11, PM-2, PM-20, PM-8, PMN2-1, POS1-9
 Domanic: PBS-20
 Domanik: PBS-15
 Domboshawa: PBC-9
 Dome: PBS-16, PC2-23, PPC1-20, PPM-12, PRG2-16, PSB-17
 Domen: POS1-6
 Domes: PPM-12
 DON: PMN1-8
 Donets: PC-7
 Dongying: PBS-9, PPM-9, PRG1-7, PRG2-19
 Donnemarie: PM-24
 Dorset: PBS-6
 Double-Peaks: PPM-10
 Double-Surface: PSB-5
 Doushantuo: OGPR-3
 Downcore: OPC1-1, PB1-17, PB2-13, PBG2-10, PC2-19, PM-10, PPC1-21, OPC2-2, PB1-13, PB2-22, PC2-24
 Downdip: ORP-1
 Downstream: PB2-17, PBG1-11, PEB1-14, PEB1-7, PM-15, PM-20, PMN2-1
 Drainage: OP7-4, OPE1-2, ORP-1, PB1-15, PB2-13, PBG1-11, PEB1-5, PM-8, PPM-9
 Drained: PSB-7
 Draining: OP4-1, PBG1-11, PEB1-7, PPC1-20
 Draugen: PRG2-11
 Draupne: OPS2-2, PGG2-14
 Drava: PG-1, PG-24
 Dredging: PEB1-5
 Drenzek: OPE1-2
 Drift: PBG1-14, PC2-22, PC2-24
 DRIFT: PSB-11
 Drill-Stem-Test: PBS-8
 Drill: OGC-2, OP4-4, OPS1-3, PBG2-4, PEB1-10, PMP-13, PPC1-14, PPC1-4, PRG2-4
 Drilled: OB1-2, OPE2-3, OUM-2, PB1-22, PB1-8, PBG1-12, PBG1-2, PBG2-4, PBS-11, PBS-23, PBS-3, PBS-5, PBS-6, PC-10, PC-6, PC2-4, PG-4, PG-8, PG-9, PGG1-6, PGG1-9, PMN2-4, PMP-13, POS1-10, POS2-5, PPC1-10, PPC1-13, PPC1-9, PPM-11, PRG1-2
 Drilling: OEB-3, OGC-4, OMN-1, PBS-12, PC-6, PEB1-10, PEB1-16, PEB2-20, PG-23, PG-8, PGG1-9, PGG2-9, PMN1-5, PMP-13, PMP-23, POS2-7, PPC1-10, PPC1-20, PPM-11, PRG2-4, PC2-2, PMP-21
 Drinking: PMN1-8
 Drip: PPC1-22
 Drought: PBG2-7, PC2-19, PRG2-10, PC2-19
 Drovenik: PC2-20
 Druffel: PBC-11
 Drums: PGG2-2
 Dryas: OPC1-3, PC2-3, PC2-6, PPC1-26
 Dryasholocene: PC2-3
 Drylands: PCS-12
 Dujiatai: PGG1-1
 Dunaliella-Like: PC2-21
 Dundee: PRG2-5
 Duplessy: PC2-2
 Duraporer: PM-11
 Durkay: OB1-1
 DURSI: PBS-19, PRG2-12
 Dutch: PGG2-2
 Dwarfism: PC2-10
 Dwat-Alg: PC2-6
 Dynoflagellates: PM-12
 Dysaerobic: PPC1-9
 Dysoxic/anoxic: PC2-8
 Dystric: OSB2-2, PSB-18

E

- E4/E6: PSB-4
 EA-IRMS: PCS-7, PMN2-2, PPC1-6, PMN2-2
 EA: OB3-2 OPS1-3 PB2-4, PBG1-8, PBS-10, PGG2-5, PMN2-2 PB2-17
 Early-cleaved: POS1-3
 Early-mature: OGC-3, PG-3
 Early-trapped: OGC-1
 Earth-based: PBG2-3
 Earth: OGPR-1, OP2-4, OP3-3, OPC2-3, OPE1-3, PB1-16, PB2-19, PB2-9, PBG1-15, PBG1-6, PBG2-3, PC2-2, PC2-9, PCS-9, PEB1-13, PGG1-12, PGG1-4, PGG2-6, PM-16, PM-18, PM-2, PM-22, PMP-12, PMP-13, PMP-23, PPC1-2, PPC1-7 OB2-3, OPE1-2, OPE2-3, PB2-18, PBC-11, PBG1-6, PC2-10, PC2-27, PGG1-4, PPC1-23
 Earthworms: PEB2-3
 EC: OPC1-3, PB1-14, PB1-7, PMN1-3, PMP-9, PPC1-19
 Echinone: PB2-4
 Eclipse: PMN1-3
 Ecological: OB3-1, OP4-4, PB1-14, PB1-5, PC2-1, PC2-10, PCS-12, PEB1-11, PMP-15, PMP-17, PMP-23
 Ecologically: PB1-14
 Ecologists: PBG1-9, PMP-15
 Ecology: OB1-3, OB2-3, PMP-17
 Ecophysiological: PC2-1
 Ecosystem: PB1-5, PB2-17, PBG2-6, PMP-10, PMP-12, PMP-19, PPC1-14, PPC1-16, PSB-7 OP4-4, OP5-3, OP7-3, OPE2-3, OSB1-1, PB1-13, PB2-17, PBC-1, PBC-12, PBC-14, PBC-3, PBG1-9, PBG2-5, PC2-15, PC2-20, PCS-1, PCS-6, PEB2-3, PM-8, PMN2-1, PMP-10, PMP-14, PMP-17, PMP-20, PPC1-12, PSB-18, PSB-4, PSB-5
 Ecotoxicity: OEB-2
 Ecsed: PSB-7
 Ectosymbiotic: OP6-2
 Ecuador: PRG2-5, PRG2-6
 Ediacaran: OGPR-3
 Edodes: PM-17
 EDS: PRG2-18
 EDTA: PEB1-9
 Edulis: OEB-2, PEB2-10
 EDX: PBG1-6
 EEM: PM-13, PM-15, PM-20, PSB-16
 Eemian: PMP-6
 EF: PBC-3, PM-28
 Eggs: PB2-4
 Egypt: PBG2-7, PFA-5, PFA-6, PG-23
 Egyptian-Allied: PFA-5
 Egyptian: PFA-4, PFA-9
 Eh-Ph: PGG1-12
 Eh: ORP-2, PGG1-12
 EHA: PSB-1
Eichornia: PB1-15
 Eicosapentaenoic: PB2-5
Eisenia: PEB2-3
 Ekron: PFA-5
 Eksinite: PBG1-7
 Electrokinetic: PSB-16
 Electrolyte: PBG1-5, PSB-16
 Electrophilic: PM-9
 Electrophoresis: OSB1-1, PC-2, PM-17, PSB-16
 Electrospray: OMN-2, PBC-11, PMP-6, PSB-3
 Electrostatic: PBG1-5
 Elie: PC2-4
 Ellesmere: PBS-3
 Ellis: OP2-1, OSB1-1, POS1-13
 Eluvial: PSB-13
 Eluviation: PSB-13
 Emanations: PMP-17, PRG2-12
 Embalming: PFA-4, PFA-6, PFA-8
 Embayment: PB2-21
 Embryo: PEB1-12
 Emigrated: PGG2-6
 Emigration: POS2-2, POS2-9
Emiliana: OP2-1, OPC1-1, PBG2-1, PC2-13, PMP-1
 Emsquarzit: PPC1-5
 Emulsion: PGG2-15, PGG2-7, PRG2-14
 Emulsions: PEB2-5
 Enantiomers: PB1-17
 Enantiomeric: PMP-23
 Encapsulate: PM-23, PM-24
 Encapsulation: OM-2, PM-24
 Encrusted: PBG1-6
 End-member: PB2-20, PGG2-14, PRG1-3
 End-members: PBS-22, PGG2-14, PRG1-3
 End-Permian: PB1-5, PC2-26
 Endmembers: PMP-16
 Endorheic: PPC1-28
 Endospore: PB1-2
 Endosulfanii: PEB2-1
 Endosymbiotic: OP6-2
 Endrin: PEB2-1
 England: PB1-14, PBS-6, PC2-3, PGG2-14, PSB-15
 Enim: PC-8
 ENSO-related: PBG2-10
 ENSO: OM-3, PBG2-10, PC2-19, PC2-27
 Enspel: OPE2-1
 Entic: OSB2-2
 Entrapment: OGC-3, OP1-2, PCS-14, PM-26, PPM-8 PBG2-11
 Entrepreneurs: PBG1-1
 Environment: PBG1-4 OP2-2 PMN2-9, PMN1-7OB2-2, OBD2-3, OEB-2, OEB-3, OGPR-1, OM-1, OM-2, OOS-2, OOS-3, OP3-3, OP4-4, OPE1-2, OPS1-1, OSB1-1, PB1-10, PB1-13, PB1-4, PB2-10, PB2-14, PB2-19, PB2-4, PB2-5, PB2-9, PBC-13, PBC-6, PBG1-1, PBG1-4, PBG1-9, PBG2-4, PBG2-8, PBS-17, PBS-19, PBS-5, PBS-7, PC-11, PC2-11, PC2-12, PC2-17, PC2-20, PC2-21, PC2-24, PC2-25, PC2-8, PEB1-1, PEB1-10, PEB1-11, PEB1-12, PEB1-13, PEB1-14, PEB1-16, PEB1-4, PEB1-6, PEB1-9, PEB2-10, PEB2-11, PEB2-13, PEB2-

- 14, PEB2-17, PEB2-18, PEB2-20, PEB2-5, PEB2-8, PFA-6, PG-2, PG-3, PGG1-11, PGG1-12, PGG2-1, PGG2-4, PGG2-7, PM-11, PM-14, PM-15, PM-18, PM-20, PM-25, PM-8, PMN1-3, PMN1-6, PMN1-7, PMN1-8, PMN2-1, PMN2-3, PMP-1, PMP-12, PMP-15, PMP-18, PMP-19, PMP-20, PMP-22, PMP-3, PMP-6, PMP-8, PMP-9, POS1-10, POS1-12, POS1-16, POS1-3, POS1-4, POS2-1, POS2-5, POS2-6, POS2-7, POS2-8, PPC1-19, PPC1-22, PPC1-28, PPC1-8, PPM-7, PRG1-16, PRG1-5, PRG1-6, PRG2-1, PRG2-20, PSB-19, PSB-7
- Environmental-driven: PPC1-17
- Environmental/climate: OP4-2
- Environmental: OB2-1, OB2-3, OBD2-1, OBD2-3, OEB-2, OEB-3, OGPR-3, OM-1, OP1-1, OP2-1, OP4-1, OP4-4, OP6-1, OPC2-2, OPE1-2, OPE1-3, OPE2-3, OSB1-2, PB1-15, PB1-19, PB1-20, PB1-6, PB2-13, PB2-19, PB2-22, PB2-7, PBC-2, PBC-4, PBC-5, PBC-6, PBC-7, PBG1-9, PBG2-1, PBG2-14, PBS-11, PC2-11, PC2-14, PC2-15, PC2-18, PC2-2, PC2-26, PC2-3, PCS-14, PCS-6, PEB1-1, PEB1-10, PEB1-11, PEB1-12, PEB1-2, PEB1-4, PEB1-6, PEB2-12, PEB2-14, PEB2-16, PEB2-18, PEB2-2, PEB2-3, PEB2-4, PEB2-5, PEB2-7, PEB2-8, PEB2-9, PGG2-2, PM-12, PM-15, PM-19, PM-2, PM-20, PM-25, PM-5, PM-8, PMN1-4, PMN1-5, PMN1-6, PMN1-7, PMN1-8, PMN2-1, PMN2-2, PMP-12, PMP-13, PMP-15, PMP-18, PMP-6, PMP-9, POS2-1, POS2-5, PPC1-17, PPC1-20, PPC1-22, PPC1-27, PPC1-28, PPC1-5, PPC1-8, PRG1-13, PSB-1, PSB-14, PSB-15, PSB-9, PB2-21, PBC-11, PEB1-12, PEB2-7, OB1-1, OB1-2, OB1-3, OB2-3, OGPR-2, OM-2, OMN-1, OMN-3, OOS-3, OP1-1, OP1-2, OP2-1, OP4-2, OP4-4, OP5-1, OP6-2, OP7-2, OP7-3, OPC1-1, OPE1-2, OPE2-1, OPE2-2, OPE2-3, OSB1-1, PB1-17, PB1-18, PB1-19, PB1-20, PB1-7, PB1-8, PB1-9, PB2-1, PB2-10, PB2-12, PB2-13, PB2-21, PB2-22, PB2-8, PBC-11, PBC-12, PBC-2, PBG1-4, PBG1-9, PBG2-1, PBG2-8, PBG2-9, PBS-10, PBS-13, PBS-21, PBS-3, PBS-9, PC-12, PC2-12, PC2-17, PC2-20, PC2-25, PEB1-1, PEB1-2, PEB2-3, PG-15, PGG1-12, PGG2-4, PGG2-5, PGG2-8, PM-12, PM-13, PM-2, PM-8, PMN2-1, PMN2-10, PMP-10, PMP-17, PMP-18, PMP-22, PMP-23, PMP-7, PMP-8, PMP-9, POS1-1, POS1-10, POS1-16, POS1-3, POS2-13, POS2-14, POS2-15, POS2-4, POS2-5, PPC1-1, PPC1-20, PPC1-21, PPC1-28, PPM-10, PPM-15, PRG1-5, PRG2-12, PSB-15
- Enzymatic: PM-17, PM-23, PMP-22, PMP-23, PSB-15
- Enzymes: OBD2-3, PBG1-4, PM-17, PMP-23, OSB1-1, PBG1-4, PEB2-3
- Eocene-Oligocene: PB2-18, PBS-12, PBS-9, PGG1-1, PPM-9, PRG2-17
- Eocene/Oligocene: PC-6
- Eocene: OUM-1, OUM-2, PB1-22, PB2-18, PBS-2, PBS-23, PC-5, PC2-10, PC2-11, PFA-7, PG-3, PM-28, POS1-10, POS1-7, POS2-4, POS2-9, PPC1-14, PPC1-17, PPM-8, PRG2-20
- Eolian: OP4-1, PC2-23, PC2-24, PG-8, PMP-12
- EOM/TOC: PBS-11
- EPA: OPC1-2, PB2-5, PEB1-1, PEB1-6, PEB2-11
- Epicontinental: PBG1-2, PC2-17, PPC1-1
- Epicuticular: OB1-2, OPE1-2, PBG1-11, PBG2-6, PC-12, PEB2-8, PPC1-26
- Epidermis: POS2-7
- Epifluorescence: PB1-2
- Epimers: PGG2-8
- Epoxide: PEB2-1
- EPR: PBG1-6, PC-2, PM-18
- EPS: OB1-3
- Epsilonproteobacterium: PMP-15
- Equator: OP1-2, PB2-19, PPM-15
- Equatorial: OP1-2, PC2-16, PGG2-13, PPC1-10, PPC1-16
- Era: OGC-1, PM-5
- Eras: PC2-22
- Erbacher: PC2-16
- ERC: OB3-1
- Ergosterol/G: PM-17
- Ergosterol: PM-17
- Erika: PEB1-1
- Eriophorum*: PM-10
- EROD: PEB1-1
- Eromanga: PBS-16, PPM-13, PRG2-16
- Erosion/accretion: PBG2-14
- Erosion: OEB-1, PB1-22, PBG1-12, PBG2-13, PBG2-14, PBG2-7, PBS-15, PC2-2, PC2-3, PCS-6, PPC1-19, PPM-8, PRG1-9, PRG2-4, PSB-19, PBS-26
- Erosional: OGC-2
- ESCA: PM-11
- Escaping-structure: PMP-17
- Escherichia*: PMP-20
- ESI-FTICR-MS: PBC-11, PBC-11, PMN2-11
- ESI-MS/MS: PSB-3
- ESI-MS: OB2-1, OMN-2, PSB-7
- ESI: OMN-2, PMN2-11, PSB-3
- EST: PC2-4
- Ester-bound: PB1-6
- Ester-linked: PBG2-13, PMP-20, PMP-8
- Ester: PB1-14, PB1-7, PB2-2, PB2-5, PBG1-16, PC-2, PCS-2, PFA-2, PM-16, PM-23, PMN1-8, PMP-21, PRG2-2
- Esterification: PC-3, PSB-1
- Esterified: PC-3, PSB-1
- Esterifying: PRG2-2
- Esters: OEB-3, PB1-17, PB2-5, PBG1-16, PBG2-3, PC-2, PFA-8, PM-14, PM-16, PM-2, PM-23, PM-24, PM-25, PM-3, PMN2-6, PMP-20, PPC1-25, PRG1-7, PRG2-2, PSB-11
- Estuaries: OMN-2, OPE1-3, PB2-8, PBC-6, PBC-7, PM-15, PM-20, PMN2-1
- Estuarine: OPE1-2, OPE1-3, PB1-15, PB1-7, PB2-13, PB2-20, PBC-6, PCS-6, PM-13, PM-15,

PM-20, PM-25, PMN2-1, PMP-15, POS1-11, POS2-10, PRG1-16
 Estuary: OM-1, OMN-2, PB1-13, PB1-15, PB2-13, PC-11, PM-15, PM-20, PM-25, PMN2-1
 Ethane: PBS-5, PG-13, PG-18, PG-2, PG-20, PG-22, PG-23, PG-25, PG-8, PPM-1, PPM-3
 Ethanolamine: PMP-6
 Ethene: PPM-1 PEB2-7
 Ether-linked: PMN2-2
 Ether: OB2-3, OB3-1, PB1-14, PB1-7, PB2-2, PBC-14, PBG1-16, PBG2-13, PG-14, PM-12, PM-16, PM-25, PMN2-2, PMP-21, PMP-8, POS1-9 OB3-2, PMP-8
 Ethyl: OP7-2, PB2-3, PB2-5, PBG2-3, PCS-9, PM-16
 Ethylacetate: PB1-2
 Ethylalkanes: OGPR-2
 Ethylalkyl: PB2-1, PGG1-11
 Ethylbenzene: PEB1-15, PGG2-2, POS2-1
 Ethylbenzothiophenes: OPG-1
 Ethylcholestane: PBS-10, PBS-2, POS2-9 PBS-10
 Ethylene: PBG1-16, PCS-2
 Ethylnaphthalenes: OPG-1
 Eu-ulminite: PC-12
 Eubacteria: OP6-2, PB2-9 PC-11
 Eukaryote: OP2-4 OP4-4, OP6-2, PBG1-4, PMP-14 OP4-4, PC2-20, PPC1-17, PPC1-18
 Euphotic: OB1-3
 Eurasian: OP7-3, PBG1-14, PC2-22, PGG2-6, PPC1-15
 Europe: OPC2-2, PBC-1, PBS-17, PBS-18, PBS-6, PFA-1, PFA-6, PMP-4, POS2-11, PPC1-1
 European: OPC2-2, PBC-10, PBC-3, PBG1-1, PC2-15, PCS-4, PEB1-1, PEB2-2
 Eustigmatophyceae: PB1-11
 Eustigmatophyta: PM-28
 Eutrophic: PMP-2
 Eutrophication: PB2-17, PPC1-17
 Euxinia: OPE2-3, PBS-21, PC2-19, PPC1-4 OPE2-3, PBS-21, PC2-19, PC2-8, PPC1-4
 EV: PEB1-11, PEB2-19, PRG1-3
 Eval: OOS-2, PBG1-2, PBS-11, PC2-7, PEB2-20, PG-11, PM-14, PMN2-3, PMN2-8, POS1-6, POS2-13, POS2-3, PRG2-18
 Evaporite-Carbonate: PPC1-1
 Evaporite: PBS-12 OOS-1 OGC-1, PBG2-4, PBS-12, PG-24
 Evaporitic: PBS-12, PC2-11, PPM-12
 Even-numbered: PBG1-8
 Even-over-odd: PB1-6, PB2-3, PM-25, PM-3
 Eventdominated: PBG2-14
 Evergreen: PEB2-8, PSB-18
 EVS: PGG2-13
 Ex/Em: PM-20
 Excavation: PC2-17, PFA-3, PFA-9
 Excavations: PFA-1, PFA-5, PFA-7
 Excitation-Emission-Matrices: PM-15, PM-20 PM-13 PMN1-8, PSB-16 PMN1-9
 Excitation: PMN1-8, PMN1-9, PMN2-1
 Exocyclic: PB2-7

Exogenic: PPC1-24
 Exogenous: OM-1, PBG2-7
 Exotherm: PBC-7
 Exothermic: OP5-1, PGG1-4
 Expulsion/retention: PPM-2
 Exsudatinitite: PBS-23, POS2-10, POS2-7
 Extra-heavy: PGG1-1
 Extra-Tropical: PBG2-10
 Extracellular: PM-17
 Extremophilic: PMP-22
 Exudates: PCS-14, PFA-2
 Exuded: PFA-2, PFA-9
 Exuding: PPM-11

F

Fabric: PC2-25
 Facies-dependence: PRG2-20
 Facies-indicative: PBG2-4
 Facies: OOS-1 OGC-3, OP4-4, OPS2-2, ORP-2, OUM-1, PBG1-10, PBS-13, PBS-14, PBS-15, PBS-16, PBS-17, PBS-19, PBS-2, PBS-21, PBS-6, PBS-9, PC-10, PC-11, PC-12, PC2-20, PC2-25, PC2-26, PG-1, PG-8, PGG1-1, PGG1-12, PM-14, PM-19, POS1-10, POS1-11, POS1-2, POS1-4, POS2-12, POS2-14, POS2-15, POS2-4, POS2-5, POS2-6, POS2-8, PPC1-1, PPC1-14, PPC1-17, PPC1-4, PPC1-8, PRG1-13, PRG1-2, PRG2-12, PRG2-20, PRG2-3, PRG2-7, PSB-25, PSB-4
 Faecal: PFA-2
Fagus: PCS-4
 Falmouth: PBG2-13
 FAM: PGG2-13
 Famennian: PB1-1, PB1-22
 Fames: PCS-9, PPC1-21
 Families/fields: OP4-3
 Fangst: PRG2-17
 Far-Field: PEB1-18
 Farm: PBS-6
 Farming: PCS-12, PSB-15
 Farmyard: OSB2-3, PCS-3
 Farnesane: PB2-4, PC2-21, POS2-12
 Farnesol: PC2-12
 Farnezane: OB3-2
 Faro: PBC-3
 Farrow: PSB-21
 Farsund: PBS-22
 Fast-Turnover: PCS-5
 Fat/Oil: PFA-4
 Façades: PEB2-15
 Fats: PFA-3 PBG1-16, PFA-3, PFA-4, PFA-8
 Fatty: OB1-3, OB2-1, OB3-1, OB3-2, OMN-3, OP2-2, OP3-2, OP6-1, OPE1-1, OPE1-2, OSB1-1, OSB1-2, OSB2-3, PB1-15, PB1-9, PB2-1, PB2-11, PB2-16, PB2-5, PBC-14, PBC-9, PBG1-11, PBG1-13, PBG1-16, PBG1-8, PBG2-13, PC-2, PC-3, PC-9, PC2-12, PC2-19, PC2-6, PCS-3, PCS-9, PEB1-13, PFA-3, PFA-8, PGG1-11, PGG2-13, PGG2-4, PM-11, PM-12, PM-14, PM-23, PM-24, PM-25, PM-

- 27, PM-28, PM-3, PM-5, PMN1-3, PMN1-4, PMP-10, PMP-11, PMP-12, PMP-14, PMP-15, PMP-19, PMP-20, PMP-4, PMP-6, PMP-8, PPC1-22, PPC1-25, PPC1-26, PSB-15
- Fauna: PB1-13, PB2-8, PBC-12, PC2-17, PC2-8, PM-11, PMP-16, PPC1-14, PSB-25, OPC2-1, PC2-3, PC2-8
- Fayalite: PBG1-15
- Fazenda: PGG2-13
- Fe-: PPC1-4
- Fe-Binding: PBG1-4
- Fe-S: PG-12
- Fe: OGPR-1, OGPR-2
- FE: PB1-10
- Fe: PBC-13, PBG1-6, PCS-9, PG-12, PGG1-12, PGG1-4
- FE: PGG2-1
- Fe: PM-26, PSB-13, PSB-5
- Fe₂⁺: PSB-8
- Fe₂O₃: PG-12
- Fe₃S₄: PMP-18
- Feed: ORP-1, OSB2-1, PC2-20, PMP-16
- Feeder-carrier: PMP-13
- Feixianguan: PBS-12
- Fennoscandian: PBG1-2
- Fernane: PB2-6
- Fernene: PB2-6
- Fernenenes: PB2-6
- Ferns: OP6-2, PC2-11, PCS-10
- Ferric: PC-1, PGG2-15
- Ferriday: PPM-11
- Ferromagnetic: PMP-18
- Fertile: OPE1-3, PFA-4
- Fertiliser: PSB-15
- Fertility: PFA-8, PSB-11 OP4-2, PCS-3 PCS-2, PCS-3
- Fertilizer: OPE1-3, PEB1-4, PEB2-4 PEB1-5
- Ferulic: PM-21, PM-4, PM-5
- Fetlika-1: PB1-1, PBG1-10
- Fibres: OP3-2, PBG2-7 PM-20
- Fichtelite: OB1-2, PBG1-2
- FID: OP2-4, PG-14, PGG1-15, PM-1, PMP-20, POS1-8
- Field: OBD1-1, OBD2-2, OGC-1, OGC-4, OMN-3, OP4-3, OP5-1, OP5-3, OPE2-1, OSB2-1, OUM-3, PB2-1, PB2-2, PBC-8, PBG1-1, PBG1-4, PBG1-9, PBG2-1, PBS-12, PBS-14, PBS-16, PBS-8, PC2-7, PCS-13, PCS-14, PCS-3, PCS-8, PEB1-1, PEB1-10, PEB1-18, PEB2-18, PEB2-20, PEB2-4, PEB2-7, PG-13, PG-17, PG-3, PG-6, PG-7, PG-8, PGG1-14, PGG1-3, PGG1-7, PGG1-9, PGG2-13, PGG2-2, PGG2-9, PM-13, PM-21, PM-6, PMN1-10, PMN1-7, PMN2-11, PMP-10, PMP-16, POS1-16, POS2-2, POS2-9, PPM-7, PPM-9, PRG1-14, PRG1-15, PRG1-16, PRG1-19, PRG1-2, PRG1-5, PRG1-8, PRG1-9, PRG2-1, PRG2-11, PRG2-13, PRG2-15, PRG2-16, PRG2-17, PRG2-2, PRG2-3, PRG2-5, PRG2-6, PRG2-8, PSB-15, PSB-20 OBD1-2, OMN-1, OOS-2, OP4-3, OPG-2, OPS1-1, OPS1-2, OPS2-3, PBS-16, PBS-18, PBS-2, PBS-6, PC-4, PCS-10, PEB1-11, PEB1-16, PG-1, PG-13, PG-17, PG-2, PG-24, PG-3, PG-4, PG-6, PG-7, PGG1-3, PGG2-13, PGG2-15, PGG2-2, PGG2-4, PGG2-9, PMN1-9, PMN2-10, PMN2-8, POS1-16, POS2-2, POS2-8, POS2-9, PPM-4, PPM-9, PRG1-14, PRG1-15, PRG1-18, PRG1-19, PRG1-5, PRG1-8, PRG1-9, PRG2-1, PRG2-10, PRG2-11, PRG2-15, PRG2-16, PRG2-5, PRG2-6, PSB-25
- Fieldwork: PCS-2
- Filicales: OB1-2
- Fill-Spill: OP7-4, PPM-4
- Filling: OBD1-2, OEB-3, OGC-1, OP4-3, OP7-4, OPS1-1, OUM-3, PB1-16, PBS-6, PG-20, PGG1-3, PGG2-14, PPM-4, PRG1-19, PRG1-2, PRG1-7, PRG1-9, PRG2-15, PRG2-9
- Fills: PB1-18, PGG1-3
- Filter-Feeding: PB2-8
- Filter: OB2-2, PB1-19, PBG1-3, PSB-16, PSB-2 PM-15, PPM-13 OPC1-1, PEB1-3, PM-20, PMP-12
- Filtration: OSB1-1, PB1-1, PM-16, PM-20, PMP-23, PRG1-11
- Fine-Cut: PC2-5
- Fine-grained: OP6-1, PBG1-9, PBS-9, PM-10
- Fine-laminated: PC2-9
- Fingerprint: OP2-2, PB1-14, PBS-11, PBS-21, PEB1-17, PEB1-8, PRG1-14, PRG1-16, PRG1-8, PSB-16, PSB-4
- Fingerprinted: POS1-10 OP4-3, PBS-8, PEB1-5, PRG1-16, PRG1-21, PRG1-8 OP4-3, PEB1-7, PEB2-13, PFA-6, PM-18, PMP-6, POS2-8, PRG1-14, PRG1-15, PRG1-8, PSB-4
- Finisterre: PEB2-5
- Finland: OPC2-2, PC2-15
- Fire-affected: OSB1-3, PBC-3, PSB-18
- Fire-impacted: PBC-11
- Fire-induced: PBC-14, PSB-18
- Fire: OPC1-2, PBC-1, PBC-14, PBC-3, PCS-11, PFA-9, PSB-18, OEB-1, OPC1-2, PBC-1, PBC-14, PBC-3, PBC-4, PBC-9, PBG2-10, PBG2-5, PC2-17, PEB1-1, PSB-18, PSB-9
- Firmicutes: PB1-2, PMP-20
- FISH-SIMS: OB2-3
- Fission: PBG1-12
- Fjord: OP2-1
- Fjords: OP2-1
- Flavonoids: PM-25
- Flinty-carbonaceous: PGG2-12
- Flinty: PBG2-2
- Floating: PC2-3, PFA-5
- Flocculation: PM-11, PM-15, PM-20
- Flocculents: PEB2-12
- Flood-plain: PSB-19 PC2-2
- Flooding: PC-5, PC2-11, PEB1-5, PRG1-11
- Floods: PBG2-14 PBG2-14, PCS-6, PFA-4, PFA-8
- Florida: PBG2-6

- Fluid-Rock: PBG1-15
 Fluid: OGC-1, OGC-3, OMN-3, OP3-4, OP4-3, OP5-2, OPG-2, OPG-3, ORP-1, OUM-1, PB1-21, PBG1-12, PBG1-15, PBG1-4, PBG1-6, PBG2-4, PBG2-7, PBS-16, PC2-25, PEB2-17, PEB2-18, PG-2, PG-20, PG-28, PG-4, PG-6, PGG2-12, PGG2-14, PM-15, PM-20, PM-7, PMN1-2, PMN1-5, PMN1-9, PMN2-4, PMN2-5, PMP-16, PMP-17, POS1-13, POS1-16, POS1-8, POS2-2, POS2-7, PPM-2, PPM-4, PRG1-15, PRG1-2, PRG1-9, PRG2-21, PRG2-4, PRG2-9 OB2-1 OOS-1 OGC-3, OGPR-1, OP3-4, OP5-1, OP7-3, OPG-2, OPS2-1, OPS2-3, OUM-1, PBG1-4, PBG1-6, PBS-12, PBS-24, PBS-8, PBS-9, PC-4, PC2-20, PG-15, PGG2-11, PGG2-12, PGG2-14, PM-7, PMN1-5, PMN2-5, PMP-16, PMP-17, PMP-23, POS1-13, POS1-16, POS1-9, POS2-12, POS2-13, POS2-15, POS2-2, PPM-2, PRG1-15
 Fluo/Py-Ratio: PEB2-8
 Fluo/Py-Ratios: PEB2-8
 Fluorane: PBG2-3
 Fluoranthene: PEB1-17, PEB2-14, PEB2-8, PGG2-5
 Fluorapatite: PBG2-11
 Fluorene: PEB1-17, PGG2-5
 Fluorescence: PB1-21, PC-5, PEB1-10, PEB1-16, PEB1-18, PEB2-5, PG-6, PM-13, PM-15, PM-20, PMN1-8, PMN1-9, PMN2-1, PMP-13, POS1-16, PSB-16, PSB-4
 Fluorescent: OB1-3, PM-13, PM-15, PMN2-1, POS2-15, POS2-4, PRG2-3
 Fluorescing: PB1-2, PSB-4
 Fluoride: PSB-12
 Fluorimetric: PB1-2
 Fluorinated: PMN2-6
 Fluorine-carbon: PMN1-10
 Fluorine: PGG2-5, PMN1-10
 Fluorometric: PM-13
 Fluorophore: PM-20, PMN1-8
 Fluorophores: PM-20, PMN1-8, PSB-16
 Fluvial/deltaic: PC2-11
 Fluvial: OP3-3, OP4-1, OPE1-2, PB2-13, PBS-8, PC2-23, PPC1-11, PPC1-19, PPC1-20, PPC1-8
 Fluvially: PPC1-19
 Fluviatile: PBS-16
 Fluvio-Deltaic: POS2-13, PRG1-13
 Fluvio: PG-3
 Flysch: PB1-8, PG-24, POS2-11
 Foinaven: PRG1-17
 Fold-thrust: PPC1-7
 Fondecyt: PSB-2
 Food: PBG2-9, PC2-21, PMP-10, PMP-9
 Foote: PEB2-11
 Foraminiferal: PPC1-23
 Foraminifera: OPC2-1, OPE1-1, PB2-21, PBG1-13, PBG2-1, PC2-13, PC2-2, PC2-23, PC2-24, PC2-27, PMP-9, POS1-7
 Foraminiferal: PB2-21, PBG1-13, PBG2-10, PC2-24, PMP-9
 Forchtenberg: PBC-1
 Fore-Caucasus: PGG1-12
 Forensic: PEB2-10
 Forest: OP4-1, OPC1-2, OPE1-2, OSB1-2, OSB2-1, OSB2-2, PB2-17, PBC-1, PBC-12, PBC-14, PBC-3, PBC-4, PBC-8, PBG1-9, PBG2-10, PBG2-5, PBG2-6, PBG2-7, PC2-15, PC2-17, PC2-18, PCS-1, PCS-12, PCS-2, PCS-4, PCS-5, PEB1-1, PFA-9, PM-22, PSB-12, PSB-15, PSB-18, PSB-20, PSB-8, PSB-9
 Forested: PBC-8, PBG1-11
 Forestry: PSB-15
 Forests: OP2-2, OPC1-2, PBC-1, PBC-12, PBC-14, PBG1-11, PBG1-9, PBG2-5, PCS-1, PCS-2, PM-5, PSB-18, PSB-9
 Formaldehyde: PEB1-15
 Formic: PGG2-8
 Fossil: OB1-2, OEB-1, OGPR-3, OMN-1, OP2-1, OP3-1, OP3-2, OP4-4, OP6-2, OPC1-2, OPC2-3, OPE1-2, OPE2-1, PB1-10, PB1-16, PB1-22, PB1-5, PB1-7, PB2-18, PB2-21, PB2-8, PB2-9, PBC-13, PBC-2, PBC-5, PBG2-1, PBG2-13, PBG2-7, PC-10, PC2-13, PC2-5, PEB1-14, PEB1-17, PEB1-3, PEB1-6, PEB1-7, PEB2-13, PEB2-14, PFA-2, PFA-9, PG-5, PM-22, PM-25, PM-28, PM-5, PMN2-4, PMP-1, PMP-14, PMP-5, PMP-9, POS2-15, PPC1-14, PSB-17, PSB-19
 Fossilisation: OP3-1, OSB1-2 PC2-5, PMN1-1
 Fossilised: OB1-1, PFA-9 OP2-1, PGG1-13
 Fossils: OGPR-3, OP3-1, OP3-2, OP4-4, OPE2-1, PB1-22, PB1-5, PB2-18, PB2-21, PB2-7, PBG1-10, PBG2-9, PC2-17, PC2-5, POS1-12
 Fouling: PMN1-11, PMN1-8
 Fourier-Transform: PBC-11
 Fourier: OMN-2, PC-3, PC-8
 Frailes: PCS-9
 Framboids: PBG1-9
 Frame-Model: PCS-8
 Franc: PEB2-2
 France-Lanord: PC2-14, PC2-2
 France: OB1-2, OSB1-2, OSB2-1, PB1-18, PBC-4, PBG1-12, PBG1-9, PC2-11, PC2-4, PCS-7, PEB1-1, PEB2-13, PEB2-14, PG-21, PM-10, PM-11, PM-15, PM-20, PM-27, PMN2-1, PSB-20
 Francolite: PBG2-11
 Français: PB1-19, PEB1-1, PM-18
 Frasnian/Famennian: PC2-8
 Frasnian: PB1-22
 Free-radical: PG-14, PGG1-8
 Free+sorbed/pyrolyzed: PBG1-7
 French: PBG1-9, PC2-4, PEB1-1, PM-10, PM-15, PM-8, PMN1-8
 Fresh-water: OPS1-1, PGG2-10, PRG1-6
 PB1-17 OB3-1, OP2-1, OP6-2, OP7-2, OPC1-1, OSB1-1, PB1-20, PB2-6, PBG1-5, PBS-8, PBS-9, PCS-14, PGG1-1, PM-13, PM-23, PM-28, PM-5, PMP-1, PMP-12, PMP-4, PMP-8,

PPC1-12, PPC1-17, PRG1-13, PRG1-5 PMN2-1
 Frick: PC2-17
 Friedelin: PB2-17, PFA-2, PPC1-15
 Fringe: OP4-1, PBC-4
 Frozen: OPE2-1, PEB2-2, PMP-22, PPM-11
 FT-ICR: OMN-2
 FT-IR: PB2-13, PBC-13, PBC-6, PCS-9, PG-12, PM-25, POS1-14, PSB-1, PSB-2 PMN2-11 OPG-3, OSB1-2, PC-3, PC-8, PM-8, PRG2-18
 FTITCR: PMN2-11
 FTT: PGG1-5
 Fucose: PBG1-9, PCS-8
 Fuel-oil: PEB2-4
 Fuel-specific: OEB-1
 Fuel/water: PEB2-11
 Fuel: OBD2-1, OEB-1, OMN-1, OP1-1, OPC1-2, OPE1-3, PBC-2, PEB1-14, PEB1-15, PEB2-11, PEB2-13, PEB2-4, PEB2-5, PGG1-9, PGG2-2, PM-10, PPC1-21, PSB-17 PEB2-8 OP6-2 OBD2-1, OEB-1, OPC1-2, PBC-13, PBC-5, PEB1-3, PEB1-6, PEB2-11, PEB2-13, PEB2-14, PGG2-2
 Fukushima: PB2-1
 Fulvic: OMN-2, PBC-10, PBC-14, PBC-9, PBG1-5, PCS-9, PFA-2, PM-27, PSB-14, PSB-21, PSB-5, PSB-7
 Fumaroles: PB2-1
 Fumigation: PSB-6
 Fungal: OSB1-1, PBC-14, PBG1-11, PM-17, PMN2-7, POS1-7
 Fungi: OGPR-3, OP6-2, PB2-11, PM-17, PM-22
 Fungicides: PEB1-9
 Fungus: OMN-2, PM-17
 Furan: PEB1-13, PSB-3
 Furanone: PFA-2
 Fusain: PC-1
 Fusinite: PBS-11, PPM-5
 FWHM: PMN2-11
 FXC: PC-11

G

G=Galactosan: OEB-1
 G1-/9-Methylphenanthrene: PPM-13
 Galactose: PBG2-6, PCS-8
 Galapagos: PMP-23
 Galbana: PMP-1
 Galicia: OP1-1, PCS-10
 Gamma-aminobutyric: PMP-22
 Gamma-Proteobacteria: PMP-11
 Gammacerane/C30: PMN1-9, PPC1-17
 Gammacerane/C30-hopane: PGG1-14
 Gammacerane/C₃₁αβ Hopane: PFA-7
 Gammacerane/Hopane: PBS-12
 Gammacerane: OOS-3, PB2-19, PBS-10, PBS-13, PBS-19, PC2-21, PGG1-1, PGG2-1, PGG2-10, POS2-12, PPM-3, PRG1-6
 Gammon: PPC1-7
 Ganga-Brahmaputra: PC2-14, PC2-2
 Ganga: PC2-14

Gaosheng: PGG1-1
 Gaoyao: PEB1-3
 Gaoyou: PPM-10
 Garbage: OEB-1, PEB1-5
 Garden: OP4-2, PFA-3
 Gartempe: PM-8
 Gary: PBG1-4
 Garzan: PG-17, PRG1-19
 Gas-: PBS-23, PC-4, PEB1-14, PG-3
 Gas-bearing: PBS-26, PPM-3
 Gas-condensate: PBS-16, PG-1, PGG1-4
 PBS-16 PC-5, PG-23
 Gas-field: PGG2-16 PG-9
 Gas-fired: PEB1-14
 Gas-generating: OP2-3, PG-25, POS2-13
 Gas-generation: PG-25
 Gas-hydrate: OPG-3
 Gas-liquid: PGG2-10, PPM-3, PBS-20
 Gas-oil-Ratio: ORP-1
 Gas-oil: PPM-8, PRG2-10
 Gas-phase: PBG2-7, PEB2-8
 Gas-prone: OPS2-2, PBS-22, PG-16, PG-21, POS2-13
 Gas-Proneness: PC-3
 Gas-rich: PBG2-7, PMP-16
 Gas-well: PBS-12
 Gas/liter: PG-19
 Gas/oil: OP7-4, OUM-1
 Gas: OBD1-2, OBD1-3, OBD2-2, OEB-2, OGC-1, OGC-2, OGC-3, OGC-4, OGPR-3, OOS-3, OP2-2, OP2-3, OP2-4, OP3-4, OP4-3, OP5-2, OP5-3, OP5-4, OP7-1, OP7-3, OPE2-1, OPG-1, OPG-3, OPS1-2, OPS1-3, OPS2-1, OPS2-2, OPS2-3, ORP-1, OSB1-1, OSB2-1, OUM-1, OUM-2, OUM-3, PB1-21, PB1-5, PB1-6, PB1-7, PB2-1, PB2-14, PB2-17, PB2-19, PB2-2, PB2-3, PBC-14, PBG1-11, PBG1-12, PBG1-16, PBG1-6, PBG2-13, PBG2-4, PBS-1, PBS-11, PBS-12, PBS-14, PBS-17, PBS-18, PBS-19, PBS-2, PBS-22, PBS-23, PBS-24, PBS-26, PBS-5, PBS-6, PBS-7, PBS-8, PC-10, PC-3, PC-4, PC-7, PC-8, PC2-14, PC2-21, PC2-24, PCS-2, PEB1-10, PEB1-11, PEB1-14, PEB1-15, PEB1-16, PEB1-18, PEB1-4, PEB1-5, PEB1-7, PEB2-11, PEB2-18, PEB2-2, PEB2-20, PFA-3, PFA-4, PG-1, PG-10, PG-11, PG-12, PG-13, PG-15, PG-17, PG-18, PG-19, PG-2, PG-20, PG-21, PG-22, PG-23, PG-24, PG-25, PG-26, PG-28, PG-3, PG-4, PG-5, PG-6, PG-7, PG-8, PG-9, PGG1-1, PGG1-13, PGG1-14, PGG1-2, PGG1-5, PGG1-8, PGG1-9, PGG2-5, PGG2-9, PM-10, PM-19, PM-22, PMN1-1, PMN1-10, PMN1-11, PMN1-3, PMN1-4, PMN1-6, PMN1-7, PMN1-8, PMN2-10, PMN2-2, PMN2-6, PMN2-8, PMP-14, PMP-17, PMP-21, PMP-3, PMP-7, POS1-1, POS1-10, POS1-16, POS1-5, POS2-14, POS2-15, POS2-5, POS2-8, POS2-9, PPC1-18, PPC1-27, PPC1-5, PPM-1, PPM-10, PPM-11, PPM-12, PPM-2, PPM-3, PPM-5, PPM-6,

- PPM-8, PRG1-1, PRG1-11, PRG1-14, PRG1-15, PRG1-16, PRG1-3, PRG1-8, PRG1-9, PRG2-16, PRG2-17, PRG2-2, PRG2-3, PRG2-4, PRG2-6, PRG2-9, PSB-1, PSB-15, PSB-25, PSB-40GC-2, OGC-4, OGPR-1, OP2-2, OP4-3, OP7-1, OP7-3, OPS1-3, OSB1-1, PB2-16, PBC-3, PBC-7, PBS-11, PBS-12, PBS-16, PBS-5, PC-1, PC-10, PEB2-15, PG-1, PG-10, PG-11, PG-13, PG-14, PG-15, PG-17, PG-18, PG-2, PG-20, PG-22, PG-23, PG-24, PG-25, PG-26, PG-3, PG-4, PG-5, PG-7, PG-8, PG-9, PGG1-13, PGG1-4, PMN2-2, PMP-16, POS1-1, POS1-16, PPC1-2, PPM-11, PPM-2, PPM-3, PRG1-11, PSB-15 PG-1
- Gasoline-Range: PBS-20
- Gasoline: PBS-8, PEB2-14, PEB2-6, PGG2-2, POS2-2, PPM-14, PRG1-21, PRG2-6 PEB2-15
- gass savannah: PPC1-3
- Gastropods: PC2-19
- Gaza: OP6-1, PFA-5
- GC-AED: PRG1-8
- GC-amenable: PC-5
- GC-C-IRMS: PB1-17, PCS-8, PMN1-4, PB2-11, PCS-7PMN2-6, PMP-21, PPM-5, PSB-15, PSB-6 PB2-20, PBG2-3, PG-13, PG-9, PMP-18, PPM-11 PPC1-15 PEB1-15
- GC-CF-IRMS: PB1-17 OSB2-1 OSB1-1, PFA-3 PC-9 PG-8
- GC-chromatogram: PB1-10
- GC-Combustion-Isotope: OP2-2
- GC-data: PSB-7
- GC-FID: OPG-1, OUM-2, PB2-3, PEB1-18, PM-16, PMP-21, POS1-6 PPC1-15
- GC-GC-MS: PB2-3
- GC-MC: PBS-20
- GC-MS-MS: OP4-4, PBS-24, PC2-22, PGG1-10
- GC-MS/FID: PB2-17
- GC-MS: OB1-1, OPE2-1, PEB2-5, PG-5, PM-17, PM-18, PRG1-2 OB1-2, OB2-1, OBD1-2, OBD2-3, OEB-1, OEB-2, OGPR-3, OOS-3, OP2-4, OP4-2, OPG-3, PB1-12, PB1-21, PB1-7, PB2-1, PB2-11, PB2-13, PB2-14, PB2-3, PBC-6, PBG1-14, PBG1-16, PBG2-3, PBS-15, PBS-16, PBS-17, PBS-19, PC-1, PC-11, PC-2, PC-3, PC2-2, PC2-5, PCS-7, PEB1-12, PEB1-13, PEB1-18, PEB1-6, PEB1-7, PEB2-13, PEB2-14, PEB2-19, PFA-5, PFA-6, PFA-7, PFA-8, PFA-9, PGG1-13, PGG1-14, PGG1-2, PGG1-6, PGG2-11, PGG2-14, PM-16, PM-19, PM-4, PMN1-2, PMN1-4, PMN2-11, PMP-11, PMP-20, PMP-21, PMP-8, POS1-12, POS1-6, PPM-11, PRG1-16, PRG1-7, PRG2-14, PRG2-15, PRG2-4, PSB-11 OEB-3, OGC-1, OP1-1, OP2-2, OPG-1, PB1-17, PB1-19, PBG2-13, PC-1, PC-9, PEB1-4, PEB2-17, PEB2-18, PFA-2, PFA-3, PFA-4, PGG1-3, PGG2-8, PM-11, PM-27, PMN1-3, PMN1-6, PMP-15, PMP-18, POS1-13, PPC1-15, PRG1-1, PRG2-12, PSB-4, PSB-6, PSB-7, GC: OB1-1, OBD1-2, OBD2-2, PB1-17, PB1-22, PB2-1, PB2-3, PBC-13, PBG1-14, PBS-15, PBS-17, PBS-19, PCS-6, PEB1-11, PEB2-12, PEB2-5, PFA-3, PFA-4, PG-13, PG-14, PG-5, PG-9, PGG1-13, PGG1-15, PGG1-9, PGG2-14, PGG2-8, PM-1, PM-14, PM-4, PM-5, PMN1-10, PMN1-7, PMN2-10, PMN2-2, PMN2-6, PMP-11, PMP-18, POS2-13, POS2-9, PPM-1, PPM-11, PPM-3, PRG1-2, PRG1-6, PRG2-11, PRG2-12, PRG2-15, PRG2-18, PSB-11,
- GC-Pyr-IRMS: PC2-14
- GC-TOF-MS: PC2-24
- GC-Traces: PPM-10
- GC/MS-MS: PGG1-2
- GC/MS-QP5050A: PEB2-2
- PSB-15, PSB-7
- GCFA: PRG1-16
- GC×GC-FID: PB2-14
- GC×GC-Mass: OP2-4
- GC×GC-Time: OP2-4, PB2-14
- GC×GC: OP2-4, PB2-14
- GCMS-QP5050: PEB1-14
- GCMS-SIR: OGPR-2
- GCxGC-TOF-MS: OEB-2
- Gdrforpro: PB1-21
- Gearing: PB1-6
- Geet: OBD2-2
- Geiseltal: PPC1-14
- Gem-dialkylalkanes: OGPR-2, PB2-21
- Gemerden: PMP-12
- Genesis: OGC-2, OPS1-2, PB2-16, PBG1-14, PBG1-6, PBG2-7, PC2-26, PG-13, PG-14, PG-25, PGG1-11, PGG2-5, PM-12, POS2-7, PRG1-1, PRG1-5, PRG1-6, PSB-13, PSB-5
- Genetic: OB1-3, OGC-1, OGC-2, OP4-3, OUM-1, PB1-14, PBG1-14, PBS-12, PBS-2, PBS-9, PBS-20, PC2-5, PFA-7, PG-1, PG-15, PG-17, PG-22, PG-23, PGG1-12, PGG1-6, PGG1-7, PGG2-11, PMP-11, POS2-13, POS2-9, PPC1-1, PPM-14, PRG1-7, PRG2-19, PRG2-7
- Genetically-related: PMN2-4 OOS-1, OP3-3, OP6-3, OPS1-2, PG-3
- Genomic: OP5-3
- Genotoxic: OEB-2
- Genotypes: PGG2-11
- Gentle: OPE2-1, PG-20, PPM-10
- Geo-chemical: PGG2-6
- Geo-environment: PMP-22, PMP-23
- Geobacter*: OP6-2
- Geochromatography: PPM-13
- Geochronology: OOS-1
- Geochronology: OGPR-3
- Geofina: PMN1-7
- Geogenic: OBD2-3
- Geohazard: OP7-1
- Geomacromolecules: OP3-1, PM-3
- Geomark: PB2-12, POS1-13
- Geomaterial: PSB-14
- Geomaterials: PSB-14
- Geomatrices: PSB-14
- Geometry: OP7-4, POS1-8, PPM-13

- Geomolecules: PBG1-1
 Geophysical: PBS-3, PEB2-12, PG-19, PPC1-1, PPM-3, PRG1-15, PRG2-9
 Geophysics: PBS-3, POS1-13
 Geopolitical: PFA-5
 Geopolymer: PG-14
 Geopolymers: OP3-1, PM-28
 Geoscience: PB2-12, PBG1-1, PG-19, PGG1-5
 Geosynclinal: PGG1-12, PGG2-6
 Geosynthesis: OGPR-1
 Geoterpenoids: OB1-2
 Geothermal: OPG-2, OPS1-3, PB2-1, PG-4, PMP-13, PPC1-1
 Gephyrocapsa: PBG2-1, PC2-13
 Geraniol: PB2-2
 Geranylgeraniol: PB2-2
 German: PBG1-4, PC2-9, PMP-10, PMP-16
 Germany: OBD2-3, OP2-3, OPE2-1, OPS1-2, PB1-1, PB1-22, PB2-11, PBC-1, PBG1-1, PCS-3, PCS-7, PEB2-8, PG-8, POS1-10, POS1-14, PPC1-14, PPC1-5, PPM-12, PRG1-2, PSB-14, PSB-16, PSB-17, PSB-8 PRG1-2 PFA-7
 Germinans: PBG1-9
 Gething: PG-10
 Ghadir: OGPR-3
 Ghareb: POS1-1, POS1-2
 Gibbsite: PM-26
 Gibraltar: PEB2-16
 Gidgealpa: PBS-16
 Gill: POS1-13
Ginkgo: OP3-2, PC2-5
 Ginkgoales: OB1-2
 Gippsland: OP5-2, PB2-12
 Gipslend: PBS-2
 Girkaliai: PSB-25
 Gironde: PM-20, PMN2-1
 Giunta: PMP-1
 Glacial-Age: PG-24
 Glacial-Bolling: PPC1-26
 Glacial-Interglacial: OPE1-3, PB1-17, PB2-21, PC2-23, PC2-27, PPC1-20, PPC1-23 PPC1-3 PC2-23 PC2-1, PC2-9, PPC1-23
 Glacial: OP4-1, OPC2-4, OPE1-3, PB1-6, PB2-13, PBG1-7, PC2-1, PC2-14, PC2-18, PC2-2, PC2-22, PC2-23, PC2-24, PC2-3, PC2-6, PC2-7, PM-5, PMN1-7, PMP-12, PPC1-15, PPC1-16, PPC1-20, PPC1-23, PPC1-3, PPC1-7 PPC1-20, PPC1-7
 Glaciated: PM-5
 Glaciation: OGPR-3, PB1-17, PBG1-7, PPC1-23 PPC1-23, PPC1-7
 Glacigenic: PPC1-7
 Glasgow: PEB2-2
 Glass-incorporated: PBG2-7
 Glassy: PPM-5
 Glauconitic: PRG2-1
 Global-scale: PPC1-18
 Global-warming: PCS-6
 Globe: PB1-5, PSB-7
Globoquadrina: OGC-4
Globorotalia: OGC-4
Gloeocapsamorpha: PM-28
 Glucopyranose: PBG2-6
 Glucose: OEB-1, PBG1-11, PBG2-6, PCS-14, PCS-8, PMP-15
 Glucosidase: PEB2-3
 Glutamic: PM-26
 Gly: PM-2
 Glyceride: PM-4
 Glycerol: OB3-1, OP5-1, OPC2-3, PB1-14, PB2-2, PBG1-16, PC2-25, PFA-2, PMP-17, PMP-18, PMP-21, PMP-6, PPC1-19, PPC1-23
 Glyceroldialkylglyceroltetraethers: OB2-3
 Glycerols: PMP-6
 Glycerophosphate: PB1-14
 Glycine-Glycine-Glycine-Arginine: OM-2
 Glycine: PM-2, PM-24, PM-26, PMN2-6
 Glycol: PBG1-16
 Glycolipid: PMP-19 PMP-20
 Glycolyl: PBG1-16
 Glycophospholipid: PMP-8
 Glycosidic: OB2-3
 Glycovorans: OB2-1
 Goban: PM-26
 Goethite: PGG1-4
 Gohy-532: PSB-14
 Gold-tube: OPS1-3
 Gold: OP2-4, OP3-2, OPG-1, PBG1-12, PBG2-2, PC-7, PC2-25, PC2-5, PFA-9, PG-21, PG-25, PGG1-13, POS1-5
 Golfo: OPS1-1
 Goliath: PFA-5
 Gondwana: POS2-3 PB2-12
 Gorae: PBS-5
 Gorbea: PSB-2
 Gorgosterol: PB2-17
 Gorleben-HA: PSB-14
 Gorleben: PPM-12
 Gors: OGC-3, PRG1-2
 Gosan: OEB-1
 Gosiute: PPC1-17
 Gosp-4: PEB1-2
 Goynuk: PBG2-8
 GPC: OPG-3, PRG2-14
 Grab: PEB1-18 PC2-22
 Graben: OPS2-2, OPS2-3, PBS-13, PBS-22, PG-8, PPC1-1, PRG2-4
 Grabens: OP7-4
 Grace: PCS-2
 Graeco-Roman: PFA-4
 Gram-negative: PEB2-19
 Gram-positive: PEB2-19
 Graminoids: PC2-1
 Granada: PPC1-13
 Granatic: PB1-2
 Granite: OP1-1, PC-10, PRG1-16, PSB-14
 Graphite-like: OSB1-3
 Graphite crystal: PRG1-10
 Graphite: PBG1-6
 Graphitic: OSB1-3, PBG2-7, PM-19

Graphitized: PBC-13, PBC-5
 Graptolites: PBG1-10
 Grass: OP5-2, PBC-2, PCS-2, PEB1-13, PSB-3
 Grasses: OP4-1, PC2-27, PM-5, PPC1-13
 Grassland: OP4-1, OP4-2, OSB1-1, PCS-10, PFA-3, PPC1-22, PSB-15
 Grasslands: OP2-2, OP4-1, PCS-10 PPC1-3
 Grave: PFA-3
 Gravel: PCS-12
 Gravelly: PC2-9
 Gravitates: PGG1-15
 Gravitational: PEB1-13, PRG2-18
 Gravities/Highest: OP4-3
 Gravities: OBD1-2, OP4-3, OPS1-1, PBS-13, PGG1-9, PMN1-9, PRG1-14, PRG2-13, PRG2-6 OBD1-2, OGC-3, OP4-3, ORP-1, PBS-15, PBS-23, PBS-3, PGG1-1, PGG1-9, PGG2-7, PMN2-11, PPM-11, PPM-2, PPM-4, PRG1-11, PRG1-15, PRG1-2, PRG1-8, PRG2-12, PRG2-6
 Grazing: PSB-15
 Greenhouse: OP2-2, OP5-3, OPC2-3, PB1-4, PBC-3, PC2-16, PC2-26, PPC1-2
 Greenland: OP1-2, OPC1-1, OPC2-1, PB1-5, PBS-23, PBS-3, PC2-22, PC2-7, PGG1-10, POS2-13
 Greenschist: PC2-25
 Greenstone: PC2-25
 Greigite: PMP-18
 Greywackes: PC2-25
 Griesbachian: PPC1-4
 Grinding: PFA-5, PSB-1
 Groundwater-Fed: PPC1-8
 Groundwater-Related: PMP-19
 Groundwater: OEB-3, PEB1-8, PEB1-9, PEB2-11, PEB2-7, PFA-9, PSB-8
 Groundwaters: OB1-1, PB1-21
 Grup: PBS-19, PRG2-12
 Grushevoe: PGG1-3
 Guacamaya-1: POS2-4
 Guadiana: OPE1-3, PM-25
 Guaiacol: PCS-9
 Guaiacyl: OM-3, OSB2-1, PM-17, PM-22, PSB-3, PM-25 OSB2-1, PB2-20, PCS-2
 Guangzhou: PEB1-13, PEB1-6
 Guanosylhopane: OP4-2
 Guantao: PBS-9
 Guarico: OPS2-3
 Guaymas: PMP-17
 Gudrid: PBS-23
 Guiana: PBG1-9
 Guianas: PBG1-9
 Guilds: OB1-3
 Guimet: PFA-6
 Guinea: PGG1-10
 Gullfaks: OBD1-1, OEB-2
 Guquka: PBC-9
Gymnodinium: PB1-10
 Gymnospermous: PC-2, PPC1-15

Gymnosperms: PC-12, PC2-27, PM-22, PM-5
 PRG2-20
 Gypsum: PC-11, PGG1-9
 Gyre: OPC2-1, PBG1-14, PC2-22

H

H-NMR: PSB-2
 H-X: PC2-26
 H/C: OSB1-3, PBC-14, PBC-2, PC-5, PM-1, POS1-11, POS2-6, PPC1-13, PRG2-18
 H₂: OGPR-1, OP5-1, ORP-2, PBG1-6, PG-14, PG-9, PMN2-10, PMN2-2, PMP-16
 H₂S-Fe₂O₃-H₂O: PG-12
 H₂S-Fe₂O₃: PG-12
 H₂S-MeO: PG-12
 H₂S-Rich: PBS-12, PC2-20
 H₂S-Saturated: PB2-1
 H₂S: OB1-3, OGPR-1, OOS-2, OP2-1, PB2-1, PBS-12, PC2-17, PC2-20, PG-1, PG-14, PG-17, PG-24, PGG1-2, PM-1, POS1-1, POS1-16, POS1-2, POS1-3, PRG1-11
 Habaro: PGG2-16
 Hach: PSB-1
 Hachinohe: PC-10
 Haematite: PGG1-4
 Hakuho: OB2-2
 Haldon: PSB-20
 Halides: PM-3
 Halite: PBG1-6, PC2-11, PGG1-13
 Halle/Saale: PSB-17
 Halle: PCS-3, PSB-17
 Haloalkanes: PM-3
 Halocline: PPC1-21
 Halogenated: PM-3, PRG2-2
 Halogenation: PEB2-9, PM-3
 Halokinetic: PPM-12
 Halowax: PEB2-8
 Halpern: PRG1-18, PRG1-19
 Hamitabat-Eocene-Oligocene: PG-3
 Hamitabat: PG-3
 Hampshire: PBG1-1, PSB-15
 Hanba: PPC1-15
 Hanin: PGG1-2
 Hansonii: PMP-17
 Haplic: OSB2-2, PSB-12
 Harada: OPC1-1
 Hardwood: PBG2-5, PCS-2, PGG2-2
 Hawaiian: PEB1-5
 Hawea: PBG1-3
 HC-Gases: PG-24
 HC-Generation: PG-11
 HC/G: OPS1-2, PB1-22, PBG2-8, PBS-17, PBS-8, PC-5, PC2-8, PG-11, PM-12, POS1-8, POS2-1, POS2-11, POS2-13, POS2-9
 HC/Odd: POS2-9
 HC/T: PBS-7, POS2-13, POS2-9
 HC/TOC: POS2-13
 HC: PB1-9, PB2-16, PB2-4, PBG1-14, PBG1-7, PBS-10, PBS-22, PG-17, PG-19, PG-24, PGG2-11, POS1-12, PPM-3, PSB-25

- Heat-induced: PBC-8
 Heat fluxes: PPC1-3
 Hebei: PB1-16
 Heiberg: PM-22
 Heidrun: PRG2-11, PRG2-17
 Hemi-cellulose: PSB-9
 Hemicellulose: PM-22
 Hemicellulosic: PM-10
 Hemin: PBG1-1
 Hemipelagic: OP7-3
 Hemisphere: OP5-3, OPC2-1, OPE1-2, PB1-17, PC2-23, PC2-7, PC2-9, PM-5, PPC1-23
 Hennes: PBG1-16
 Henry: PG-21
 Hepperle: PMP-4
 Heptachlor: PEB2-1
 Heptachlorinated: PEB2-8
 Heptadec-1-Ene: PM-3
 Heptane: OP5-2, PBS-17, PG-27, PMN1-11
 Herbaceous: PBS-7
 Herbicides: PEB1-9
 Herbs: PPC1-13
 Hercynian: PPM-6
 Hetero-organic: PGG2-6
 Hetero-phase: PBG1-6
 Heteroaromatic: PB2-16
 Heteroatomic: PGG2-6 PMN2-4
 Heterocomponents: PMN2-11
 Heterocompounds: PC-6
 Heterocyclic: PBC-8
 Heteroelements: PM-18
 Heteronuclear: OM-2
 Heterorganic: PGG2-6, PRG1-1
 Heterotrophic: OB2-3, OBD2-3, OP6-1, OSB2-3, PMP-14 PB1-5 PPC1-7
 Hettangian: PC2-17
 Hexachlorinated: PEB2-2 PEB2-8
 Hexadecanamide: PBG1-16
 Hexadecane-2-ol: PM-3
 Hexadecane-3-one: PM-3
 Hexadecane: OGPR-2, OPS2-1
 Hexadecanedioic: PBG1-16
 Hexadecanoic: PMP-15
 Hexane-toluene: POS1-9
 Hexane/acetone: PEB2-2
 Hexane/ethyl: PB2-17
 Hexane: OP2-3, PBC-11, PG-27, PMN1-7, PG-20
 Hexavalent: PEB1-9
 HF-Dissolved: PSB-12
 HF-Treated: PSB-12
 HF/Hcl: PM-6 PBG2-3, PM-16, PM-18
 HF: OB2-3, OSB2-2, PB1-1, PBC-12, PCS-4, PCS-5, PM-14, PMN1-6, PMN2-6, PRG2-1, PSB-12, PSB-7
 Hg-porosimetry: POS1-14
 Hg: PG-1
 HI-OI: PB1-21
 HI/LiAlH₄: PB1-10
 HI/OI: PSB-7
 HI: OPS1-2, PB1-22, PBG1-7, PBG1-9, PBG2-11, PBG2-8, PC-10, PC-3, PC-5, PC-6, PC2-7, PC2-8, PG-11, PM-12, POS1-12, POS1-15, POS2-10, POS2-13, POS2-3, POS2-6, POS2-8, POS2-9, PPC1-14, PPC1-8, PRG2-6, PSB-7
 Hicks: PEB1-13
 High-resolution: OPC1-3, OPC2-2, OPE2-2, PBC-11, PBG2-10, PBG2-7, PC2-10, PC2-24, PC2-27, PPC1-11, PPC1-27, PPC1-3
 High-temperature: OP5-1, PBG1-15, PGG1-4, PGG1-9, PRG1-1
 High-throughput: PPC1-6
 High-wax: PGG1-10
 Higher-chlorinated: PEB2-2
 Higher-plant-Derived: PSB-7
 Higher-plant: OP4-1, POS1-4
 Highly-mature: POS1-4
 Highstands: PM-12
 Hildebrand: OPS2-1
 Hills-boundary: OUM-1
 Himalaya: PC2-2, PFA-2
 Himalayan: PC2-2
 Himax: PC-3
 Himmetoglu: PBG2-8, POS1-14
 Hindeodus: PB1-5
 Hint: PBS-3
 Hinterland: PEB1-8
 Hippuric: PFA-2
 Histic: PSB-13
 Histosol: PSB-8
 Holocene-Pleistocene: PBG1-14
 Holocene: OP2-1, OP4-1, OPC1-3, OPC2-2, OPE1-3, PB1-20, PB1-6, PB2-13, PBC-1, PC2-1, PC2-12, PC2-18, PC2-19, PC2-2, PC2-22, PC2-24, PC2-3, PC2-6, PMP-1, PMP-6, PPC1-28, PPC1-8, PSB-19
 Holonucleus: PBG1-14
 Homohapanes: PBS-10 OOS-3, PB2-8 PBS-10, PC2-21, PEB2-4, PGG1-7
 Homopregnane/C27-C29: PBS-12
 Hop-1318-enes: PBG1-2
 Hop-1721-ene: PB2-9, PGG2-8
 Hop-1721-enes: PBG1-2
 Hop/Ste: POS1-15
 Hop/Sterane: PGG2-1
 Hopane-type: OPE2-1
 Hopane/moretane: PRG2-20
 Hopane/sterane: OPE2-3, PC2-17, PGG1-10, PPM-7, PRG1-16
 Hopane/steranes: PC2-20
 Hopane C30: PGG2-11
 Hopanediols: PB2-9
 Hopanepolyols: PB2-9
 Hopanes/steranes: PB1-22, POS2-14
 Hopanes: OB3-2, OBD1-2, OBD2-1, OP1-1, OPE2-1, PB1-18, PB1-21, PB2-14, PB2-19, PB2-4, PB2-9, PBG1-12, PBG1-2, PBS-10, PBS-13, PBS-17, PBS-20, PC-12, PC2-17, PC2-20, PC2-22, PC2-25, PC2-4, PGG1-10, PGG2-1, PGG2-13, PGG2-2, PGG2-4, PGG2-

- 8, PM-19, POS1-1, POS1-13, PRG2-12, PSB-25 OOS-3, OP1-1, OP4-4, OP6-2, OPC2-3, OPE2-1, PB2-12, PB2-19, PB2-8, PBG1-14, PBS-10, PBS-19, PC-12, PC2-17, PC2-20, PC2-21, PC2-22, PEB1-5, PG-5, PGG2-1, PGG2-11, PGG2-8, PM-19, PMN1-9, POS1-12, POS2-15, PPC1-17, PPM-3, PRG1-6, PRG2-20, PSB-25
- Hopanetetrol: OP5-3
Hopanetetrols: PB2-9
Hopanetriols: PB2-9
Hopanic: PGG2-13
Hopanoic: OP4-2, PB2-9, PC2-12, PGG2-4, PGG2-8, PRG1-7
POS1-12
Hopanoids: OB3-1, OP4-2, OP6-2, PB1-18, PB2-1, PB2-14, PB2-9, PC-9, PC2-21, PC2-4, PGG1-1, PM-12, PMP-13, PMP-19, PRG1-7 OP2-2, OP6-2, OPE2-1, PB1-16, PB2-1, PB2-9, PBS-16, PBS-9, PGG2-4, PGG2-8,
Hopanols: OP4-2, PB2-9, PMP-19, PPC1-23 PB2-9
Hopenes: OPE2-1, PC-11, PC2-4, PPC1-18
Hopenoic: PGG2-8
Hopmans: PPC1-19
Hordeum: PCS-10
Hornblende: PGG1-4
Horticulture: PM-10 PCS-12
Hosangadi: PSB-1
Host-rocks: OP4-4
Hot-shales: PG-20
Houston: OGC-4, OPE2-2, POS1-13
Hovea-3: OPE2-3, PPC1-4
Hoyle: OP2-4, PC2-25
HPLC-ESI-MS: OB2-1, PMP-6
HPLC-ESI-Msn: OB2-3
HPLC-ESI/MS: PMP-9
HPLC-Electrospray: PMP-8
HPLC-MS: PB1-7
HPLC-separation: PGG1-10
HPLC/MS/MS: PMN1-3
HPLC/MS: OPC2-3
HPLC: OB2-3, OEB-2, OMN-3, PB2-15, PB2-20, PBG1-14, PEB1-11, PEB2-16, PEB2-5, PM-26, PMN1-8, PMN2-9, PPC1-6
HPLCMS: PEB2-5
HRTEM: PBC-4, PM-16, POS1-15
HTGC: PRG1-6
Hudson: PEB1-14
Huesca: PCS-12
Hull: PEB2-5
Humate: PEB2-9 OBD2-3
Humic-like: PBC-10, PBC-7, PMN2-1
Humic-nature: PSB-4
Humic: OM-2, OMN-2, OSB1-3, OUM-1, PB1-22, PB2-13, PB2-16, PBC-10, PBC-11, PBC-13, PBC-14, PBC-6, PBC-7, PBC-9, PBG1-5, PBG1-7, PBG1-8, PBG2-11, PBS-17, PBS-8, PC-12, PC-5, PCS-9, PEB2-9, PFA-2, PG-11, PG-15, PG-5, PG-7, PGG1-12, PM-12, PM-13, PM-2, PM-20, PM-25, PM-27, PM-4, PMN1-1, PMN1-8, PMN2-1, POS1-11, POS2-1, POS2-7, PRG2-16, PSB-1, PSB-13, PSB-14, PSB-18, PSB-2, PSB-21, PSB-3, PSB-4, PSB-5, PSB-7, PSB-8
Humic coal: POS2-1
Humics: OMN-2
Humification: OM-2, OPC2-2, PBC-14, PBC-3, PCS-8, PM-10, PMN2-1, PSB-10, PSB-13, PSB-16, PSB-20, PSB-21, PSB-4
Humified: PCS-8, PMN2-1
Humin-like: PBC-14
Humin: PBC-9, PM-6, PSB-18, PSB-21, PSB-7 PSB-21
Humine: PM-27
Huminite: PB1-21, PC-12, PSB-4
Hummocks: OP5-3
Hummocky: PC-10
Humoclarain: PC-1, PC-2
Humovitrain: PC-1, PC-2
Humus-like: PFA-2
Humus: PBG1-4, POS1-9, PSB-18, PSB-21
Hungarian: PB2-16, POS2-6, PSB-7
Hungary: PB2-16, POS2-6, PSB-7
Hyaline: OP5-3 OGC-4
Hyden: PGG1-12
Hydratation: PM-7
Hydrate-bearing: OP7-1
Hydrate-bound: OP7-1
Hydrate: OP7-1, OPG-3, POS2-5
Hydrated: OP7-1
Hydrates: OP7-1, OP7-3, OPE2-3, OPG-3, PB1-5, PG-19, PMP-21, PPC1-18, PPM-11
Hydrazine: PB1-7, PMN1-3
Hydridization: OB1-3
Hydrobiontic: PBG1-14
Hydrocarbon-Based: PMN1-5
Hydrocarbon-Biomarkers: PGG1-11
Hydrocarbon-Caso4: PG-12
Hydrocarbon-Degrading: PBS-6
Hydrocarbon-Dominated: PB1-18
Hydrocarbon-Generated: OGC-1
Hydrocarbon-Generating: POS2-7
Hydrocarbon-Generative: PBS-17
Hydrocarbon-Rich: OPS2-1, PB1-19
Hydrocarbon-Seep: PB1-18
Hydrocarbonquaternary: PEB1-17
Hydrocarbons: OB1-1, OBD1-1, OBD1-3, OEB-2, OGC-1, OGC-3, OGPR-3, OMN-1, OP1-1, OP2-4, OP4-3, OP7-1, OP7-3, OP7-4, OPG-2, OPS1-1, OPS2-1, OPS2-2, OPS2-3, ORP-1, ORP-2, OUM-1, OUM-3, PB1-16, PB1-21, PB1-22, PB2-1, PB2-11, PB2-12, PB2-14, PB2-16, PB2-19, PB2-6, PBG1-14, PBG2-4, PBS-1, PBS-11, PBS-12, PBS-14, PBS-15, PBS-16, PBS-17, PBS-19, PBS-2, PBS-21, PBS-22, PBS-5, PBS-6, PBS-9, PC-12, PC-3, PC-7, PC2-11, PC2-22, PC2-25, PEB1-10, PEB1-11, PEB1-14, PEB1-17, PEB1-18, PEB1-5, PEB2-10, PEB2-11, PEB2-18, PEB2-20, PEB2-3, PEB2-4, PFA-2, PFA-4, PFA-7,

- PG-1, PG-11, PG-13, PG-17, PG-19, PG-2, PG-20, PG-21, PG-25, PG-28, PG-3, PG-5, PG-7, PG-8, PGG1-13, PGG1-15, PGG1-4, PGG1-5, PGG1-7, PGG2-11, PGG2-14, PGG2-16, PGG2-6, PGG2-8, PM-19, PM-24, PM-3, PM-7, PMN1-1, PMN1-5, PMN1-6, PMN1-7, PMN1-9, PMN2-5, PMN2-8, PMP-18, PMP-4, PMP-5, POS1-1, POS1-10, POS1-11, POS1-12, POS1-13, OB1-2, OB3-2, OBD1-1, OBD2-1, OEB-2, OGC-1, OGC-2, OGPR-1, OP1-1, OP1-2, OP2-3, OP2-4, OP3-4, OP4-3, OP5-2, OP6-1, OP6-3, OP7-3, OP7-4, OPC1-2, OPG-1, OPG-2, OPS1-2, OPS2-1, OPS2-2, OPS2-3, ORP-1, ORP-2, OUM-1, OUM-2, PB1-1, PB1-21, PB1-5, PB1-9, PB2-11, PB2-16, PB2-19, PB2-3, PB2-4, PB2-6, PBC-14, PBG1-14, PBG1-15, PBG1-6, PBG1-8, PBG2-10, PBG2-13, PBG2-3, PBG2-4, PBG2-7, PBS-10, PBS-11, PBS-12, PBS-17, PBS-2, PBS-23, PBS-26, PBS-5, PBS-8, PC-12, PC-3, PC-4, PC-7, PC-8, PC2-11, PC2-17, PC2-20, PC2-21, PC2-22, PC2-25, PC2-4, PCS-7, PEB1-1, PEB1-10, PEB1-11, PEB1-13, PEB1-14, PEB1-15, PEB1-16, PEB1-17, PEB1-18, PEB1-2, PEB1-3, PEB1-5, PEB1-6, PEB1-7, PEB2-10, PEB2-11, PEB2-13, PEB2-14, PEB2-16, PEB2-17, PEB2-18, PEB2-19, PEB2-20, PEB2-3, PEB2-4, PEB2-5, PFA-6, PFA-8, PG-15, PG-19, PG-21, PG-23, PG-25, PG-3, PG-4, PGG1-10, PGG1-11, PGG1-13, PGG1-4, PGG1-5, PGG1-6, PGG1-7, PGG1-8, PGG2-10, PGG2-11, PGG2-12, PGG2-14, PGG2-15, PGG2-4, PGG2-5, PGG2-6, PGG2-8, PM-12, PM-18, PM-19, PM-27, PM-7, PMN1-1, PMN1-10, PMN1-5, PMN1-6, PMP-13, PMP-14, PMP-17, PMP-20, PMP-21, PMP-4, PMP-5, POS1-10, POS1-15, POS1-16, POS1-4, POS1-5, POS1-6, POS1-8, POS2-1, POS2-10, POS2-12, POS2-13, POS2-15, POS2-2, POS2-3, POS2-4, POS2-5, PPC1-1, PPC1-12, PPC1-15, PPC1-5, PPM-1, PPM-10, PPM-11, PPM-12, PPM-14, PPM-3, PPM-5, PPM-6, PPM-8, PPM-9 PRG1-10 PRG1-11, PRG1-12, PRG1-17, PRG1-21, PRG1-4, PRG1-5, PRG1-6, PRG1-9, PRG2-11, PRG2-12, PRG2-16, PRG2-18, PRG2-19, PRG2-2, PRG2-20, PRG2-4, PRG2-6
- Hydrochemical: PB2-22
 Hydrodynamic: PSB-16
 Hydrodynamically: PBG2-12
 Hydrofluoric: OSB2-2, PMN1-6, PSB-12
 Hydrogen-bond: PM-24
 Hydrogen-bonding: OB2-1
 Hydrogen-rich: PC-6
 Hydrogen: OBD1-1, OBD1-2, OGC-1, OGPR-1, OGPR-3, OM-3, OP4-1, OP6-4, OP7-3, OPC2-2, OPE1-2, OPE2-2, OPE2-3, OPS1-2, ORP-2, OUM-1, OUM-3, PB1-21, PB1-4, PB2-1, PBG1-15, PBG2-1, PBG2-10, PBG2-8, PBS-11, PBS-17, PBS-22, PBS-8, PC-10, PC-3, PC-5, PC-6, PC2-14, PC2-15, PC2-19, PC2-21, PC2-6, PC2-7, PEB2-7, PG-1, PG-11, PG-12, PG-14, PG-16, PG-20, PG-8, PG-9, PGG1-8, PM-1, PM-19, PMN1-4, PMN2-10, PMN2-2, PMP-13, PMP-14, PMP-16, POS1-10, POS1-12, POS1-4, POS1-7, POS2-1, POS2-10, POS2-11, POS2-3, POS2-9, PPC1-1, PPC1-10, PPC1-14, PPC1-4, PPC1-5, PPM-13, PPM-3 PRG1-10
 PRG1-13, PRG1-20, PRG1-21, PRG1-3, PRG2-18
 Hydrogenated: OEB-3, PB1-6, PB2-3
 Hydrogenation: OP6-4, OUM-3, PB1-10, PB2-5, PB2-8, PC2-25, PEB1-12, PRG2-4
 Hydrogenised: POS2-4
 Hydrogeologic: OGC-2
 Hydrogeological: PGG1-6, PPC1-13
 Hydrologic: PEB1-7, PMP-12
 Hydrological: OP4-1 PB2-22
 Hydrological: PC2-10, PC2-24, PC2-6, PC2-9, PEB1-3, PPC1-18, PSB-8
 Hydrology: OPC2-2, PC2-6, PPC1-24 PSB-11
 Hydrophilic-lipophilic: PEB2-9
 Hydrophilic: PEB2-9, PM-11, PM-13, PMN1-8
 Hydrophobic: OP6-1, PBC-14, PBC-4, PEB1-3, PEB1-5, PEB2-9, PM-13, PM-24, PM-27, PM-8, PMN1-8, PSB-11, PSB-18
 Hydrophobicity: PCS-14, PSB-11
 Hydropyrolysis: OGPR-3, OM-3, OUM-3, PM-19, PMN1-4, PRG1-1, PRG2-4
 Hydrostatic: OB2-1, OGC-1, POS2-2
 Hydrothermal: OGPR-1, OP5-1, PB1-20, PB1-8, PB2-2, PBG1-15, PBG1-16, PBG1-4, PBG2-4, PC2-20, PC2-25, PM-18, PMP-16, PMP-18, PMP-23, POS1-4, PRG1-1 PMP-17
 Hydroxyacids: OSB1-2
 Hydroxyarchaeol: OB3-1, OP5-1, PB2-2, PMP-17, PMP-5 OP5-1, PB2-2
 Hydroxybenzoic: PM-23
 Hydroxycarboxylic: OEB-1
 Hydroxylamine: PB1-7
 Hyne: PRG1-11
 Hyper-Alkaline: PB1-21
 Hypergenesis: PEB1-11, PGG1-12
 Hypersaline: PB2-22 OGPR-2, OOS-3, PB2-4, PBG1-8, PBG1-9, PBS-12, PC2-20, PC2-9, PGG2-1, PMP-7, PSB-19
 Hypersalty: PGG2-10
 Hyperthermophiles: PMP-23
 Hyperthermophilic: OPC2-4
 Hyphal: PM-17
 Hyphenated: PEB2-5
 Hypsithermal: PC2-2
 Hypthesis: PBG1-3
 Hypy: OM-3, OUM-3, PM-19, PRG2-4
- I**
 Iapetus: PBS-18
 Iatrosan: PMP-20, POS1-6
 Iberian: PM-25, PM-26, PPC1-28
 Iceland-Scotland: PC2-24

- Ices: PBG2-3 PPC1-3 OPC2-1, OPC2-2, OPC2-4, OPE2-1, OPG-3, PB1-7, PB2-18, PBG1-14, PBG2-7, PC2-14, PC2-21, PC2-22, PC2-7, PCS-6, PGG2-2, PMN2-10, PMP-11, POS2-12, PPC1-19, PPC1-21, PPC1-26, PPC1-7, PPM-11
- Ichnofossils: PB2-21
- Iferous: OGC-1
- IHSS-Procedure: PSB-14
- IHSS: PM-13, PM-27, PSB-1, PSB-13
- Iberian: PM-26
- Illite: PM-26
- Illinois: OGC-2, PB2-14
- Illite: PRG2-4, PSB-9
- Illitization: POS1-13
- Illuvial: PSB-13
- Immature: OP2-3, OPC2-3, OUM-1, PB1-12, PB1-21, PB1-22, PB2-4, PBG1-12, PBG1-2, PBS-17, PBS-19, PBS-6, PBS-7, PBS-9, PC-1, PC-10, PC-12, PC-2, PC-6, PG-11, PG-20, PG-21, PG-24, PGG1-1, PGG2-4, PGG2-8, PM-1, PMN2-4, POS1-1, POS1-15, POS1-3, POS1-4, POS1-9, POS2-11, POS2-3, POS2-5, POS2-9, PPC1-1, PPC1-10, PPC1-18, PPM-9, PRG1-1, PRG1-14, PRG2-1, PRG2-12, PRG2-18, PRG2-4
- Immaturity: PC-1, PGG2-7, PM-12, POS2-15, PPC1-1
- Imogolite: PCS-9
- In-gauge: PGG1-9
- In-house: PPM-9, PRG1-8
- In-reservoir-Biodegradation: PRG1-17
- In-reservoir: OBD1-1, OP3-4, OPS2-2, ORP-1, PEB1-12, PRG2-11, PRG2-14
- In-vitro: PG-20, PSB-15
- Inceptisols: PCS-1 PSB-15
- Indane: OPG-1
- Indanes: OPG-1
- Indene: OPG-1
- Indenes: OP3-2, OPG-1, PEB2-12
- Indeno[123-Cd]Piren: PEB1-17
- Indeno[123-Cd]Pyrene: PC2-22
- Indeno[7123-Cdef]Chrysene: PC2-22
- Indere: PSB-2
- India: OPE2-2, PGG1-10
- Indian: OPE2-2, PBG1-13, PC2-23, PEB1-5, PFA-2
- Indiana: OGC-2
- Indica: PB1-11
- Indochina: PBS-24
- Indole-: OP3-2
- Indole: PEB2-12
- Indoles: PEB2-11, PEB2-12
- Indonesia: OP1-2, PBG2-10, PBS-8, PC-10, PC-8, PGG1-10, POS1-12
- Indonesian-German: PB1-15
- Indonesian: PBG2-10
- Indus: OPE2-2, PBG2-7
- Inertinite-: PC-5
- Inertinite: PB1-21, PC-12
- Inertinitic: PG-20
- Inertodetrinite: PC-12
- Infill: OPE1-3, PC2-7, PGG2-9
- Infilling: PB2-13
- Infiltrating: OGC-2, PBC-3, PG-24
- Infra-Red: PBG2-11, POS1-14 OOS-2, PB1-21, PBC-14, PC-3, PC-8, PEB1-8, PM-21, PMN2-8, POS1-8, PRG2-14
- Inkaba: PC2-9
- Inositol: PBG1-11 PMP-6
- Inoxic: OBD2-3
- Interglacial: PC2-21, PC2-3, PM-5, PPC1-23 OPE1-3
- Intertidal-Supertidal: PB2-19
- Intertidal: PBG1-9, PC2-20, POS2-10
- intertropical convergence zone: PPC1-3
- Intertropical: PPC1-26
- Intra-Jurassic: PRG2-16
- Intra-mountain: PB1-8
- Intra-reef: PB2-14
- Intra-shelf: PPM-15
- Intracellular: PMP-18
- Intracontinental: POS2-3
- Intracratonic: PB2-19, POS1-15
- Intramolecular: OP3-1,
- Intrapelletal: PBG2-11
- Inventory: OB2-1, PCS-6, PMN2-11
- Invertebrate: PC2-8, PPC1-4 PB1-10, PB2-8, PRG1-6
- Iodogen: PEB2-9
- Iodomethane: PMN2-4
- Ion-Chromatograms: PGG2-16
- Ion-Pair: PMN1-8
- Ionisation-MS-MS: PMP-8
- Iosprenoids: OPE2-3
- IR-spectra: PSB-1 OP2-3, PEB1-11, POS1-9 PRG1-10 PRG1-10 PBG1-6, PBG2-11, PEB1-12, PMN2-3
- Iraq-Iran: PEB1-2
- Irati: PC2-21, PGG2-3, PM-24, POS1-15, POS2-3
- IRM-EA-MS: OMN-3
- IRM-LC/MS: OMN-3
- IRM-MS-Systems: OMN-3
- IRMS: PBC-7, PM-1, PMN2-2, PMN2-4, PSB-15
- Iron-Free: PGG2-15
- Iron-Laden: PGG2-15
- Iron: OB1-3, OGPR-1, OOS-2, OPE2-3, PB2-13, PBG1-15, PBG1-5, PBG2-8, PEB2-8, PFA-5, PGG1-13, PGG2-15, PM-11, PM-26, PMP-18, POS1-2, PPC1-4, PRG2-2
- Iso-C¹⁵*: PC2-12
- Iso-C₁₇*: PC2-12
- Iso-Configurations*: PG-8
- Iso-Hydrocabons*: PPM-3
- Iso-Methylalkyl*: PGG1-11
- Iso-Paraffins*: PGG1-4
- Iso-Pentadecanoic*: OP6-1
- Isoalkanes: ORP-2, PB2-3 OPE2-1 ORP-2, POS2-2 PM-11, PRG1-1, PRG1-5, PRG1-6
- Isobutane/*n*-butane: PG-18

- Isochrysidales: OP2-1
 Isochrysis: PMP-1
 Isolink: OMN-3
 Isomasticdienonic: PFA-6
 Isomorphitic: PBG2-11
 Isooctane: PEB2-2
 Isopach: PBS-22
 Isopranyl glycerol: PMP-21
 Isoprene: PFA-9
 Isoprenoid/cyclic: PBS-12
 Isoprenoid: OB3-2, OOS-3, OP2-1, OPS2-3, PB1-14, PB2-1, PB2-2, PB2-4, PBG1-7, PBG2-2, PBS-1, PBS-9, PC-12, PC2-26, PEB1-11, PEB2-17, PMN2-2, PMP-5, POS2-12, PPC1-19, PRG1-17
 Isoprenoidal: OP5-1, PMP-18
 Isoprenoides: PSB-25
 Isoprenoids/N-Alkanes: OP5-2
 Isoprenoids: OB1-1, OBD1-2, OBD2-1, OP1-1, OP2-4, OP6-2, OPE2-3, PB1-18, PB1-5, PB2-18, PB2-19, PB2-4, PBG2-2, PBS-10, PC-9, PC2-17, PC2-21, PC2-25, PC2-8, PEB2-17, PEB2-4, PGG1-14, PGG1-7, PMP-5, POS1-4, POS2-12, POS2-6, PRG1-17, PRG2-12, PRG2-19, PSB-4
 Isoprenoid: PGG2-4
 Isoprime: PEB1-15
 Isopropyl: OB3-2, PB1-17
 Isorank: PRG2-20
 Isorenieratane: OPE2-3
 Isorenieratene: OP2-1, OPE2-3, PB2-7, PBS-21, PC2-11, PC2-12, PC2-19, PC2-8, POS1-11
 Isorenieretane: PC2-17
 Isorenieretene: PC2-17
 Isotactic: OB1-1
 Isotherm: PG-26, PG-27
 Isothermal: OBD2-2, PBG1-12, PEB2-12, PPM-5, PRG2-20
 Isotherms: PG-26, PG-27, PSB-14
 Isotope-mixing: POS1-3
 Isotope-ratio: PB2-17, PMN2-2
 Isotope-ratio-monitoring: OMN-3
 Isotope: OB1-3, OBD1-1, OM-3, OMN-3, OP2-2, OP3-1, OP3-4, OP4-1, OP5-1, OP6-3, OP6-4, OPC1-3, OPC2-1, OPE1-1, OPE2-2, OPE2-3, OPG-2, OPS2-2, OPS2-3, OSB1-1, OSB2-1, OSB2-3, OUM-1, PB1-17, PB1-18, PB1-4, PB1-5, PB1-6, PB2-20, PBC-7, PBG1-10, PBG1-8, PBG1-9, PBG2-1, PBG2-8, PBG2-9, PBS-12, PBS-15, PBS-17, PBS-5, PC-9, PC2-1, PC2-10, PC2-15, PC2-17, PC2-3, PC2-6, PCS-2, PCS-8, PEB1-15, PEB2-5, PEB2-7, PFA-5, PFA-6, PFA-7, PFA-8, PG-1, PG-10, PG-13, PG-16, PG-18, PG-19, PG-2, PG-20, PG-22, PG-23, PG-25, PG-3, PG-5, PG-8, PG-9, PM-5, PMN1-4, PMN1-5, PMN1-9, PMN2-2, PMN2-4, PMN2-6, PMN2-7, PMP-10, PMP-13, PMP-14, PMP-15, PMP-16, PMP-2, PMP-22, PMP-5, PMP-7, PMP-9, POS1-15, POS1-16, POS1-2, POS1-3, POS1-4, POS2-11, PPC1-1, PPC1-11, PPC1-12, PPC1-14, PPC1-15, PPC1-16, PPC1-2, PPC1-20, PPC1-21, PPC1-23, PPC1-24, PPC1-26, PPC1-27, PPC1-4, PPC1-6, PPC1-7, PPC1-8, PPM-3, PPM-5, PRG1-13, PRG1-20, PRG1-3, PRG1-9, PSB-17, PSB-19
 Isotopically-depleted: PB1-18, PG-18
 Isotopically-labelled: OSB1-1
 Isotopically: OGC-2, OGC-4, OP4-3, OPC2-1, PB1-17, PB2-11, PBG2-7, PBS-2, PC2-12, PC2-17, PC2-21, PCS-7, PG-13, PG-18, PG-20, PG-3, PM-1, PMN1-4, PMN2-7, PMP-5, POS1-2, POS1-3, PPC1-11, PPC1-14, PPC1-18, PPC1-7, PSB-17, PSB-6 PG-17
 Isotopograms: PRG1-21
 Isotopy: PBG1-8
 Israel: PFA-5, PM-12, POS1-1, POS1-2
 Israelite: PFA-5
 Italy: OP3-4, PB2-7, PBG1-1, PC2-15, PEB2-2, PPC1-1, PPC1-6
 Itasca: PMP-4
 ITCZ: PPC1-26, PPC1-3
 Izu-Bonin: PMP-23

J

Japan: OB2-1, OP7-3, PB2-1, PB2-17, PB2-9, PC-10, PC2-12, PC2-27, PGG2-16, PMP-22, PMP-23, PMP-3, PMP-5, PPC1-15
 Japanese: PB2-9, PC-10
 Japonica: OP6-4
 Jarosite: POS2-10
 Javaux: OP4-4
 Jersey: PEB1-14
 Jurassic-Cretaceous: PBS-16, PGG2-12, PM-14, PRG2-16
 Jurassic-Lowermost: PPC1-1
 Jurassic/Cretaceous: PPC1-1
 Jurassic/Lower: PPC1-1
 Jurassic: OB1-2, OGC-1, OOS-3, OP3-3, OP5-2, OPC2-3, OPS2-2, OPS2-3, OUM-1, OUM-3, PB1-10, PB1-18, PB1-7, PB2-12, PBG1-2, PBS-15, PBS-16, PBS-22, PBS-3, PBS-6, PC-3, PC2-26, PC2-4, PG-13, PG-15, PG-16, PG-2, PG-20, PG-24, PG-28, PG-4, PG-6, PGG1-11, PGG1-7, PGG2-12, PGG2-5, PGG2-9, POS1-11, POS1-13, POS1-4, POS1-6, POS1-9, POS2-15, POS2-4, POS2-6, POS2-7, PPC1-1, PPM-12, PPM-15, PPM-4, PRG1-13, PRG1-2, PRG2-16, PRG2-18, PRG2-4
 Jurayd: PEB1-2

K

K37/K38: PC2-13
 Kachergatska: PBG2-2
 Kaijiang-Liangping: PBS-12
 Kakwa: PG-10
 Kalaat: POS2-14
 Kalbitz: PSB-4
 Kama: PGG2-10
 Kamchatka: PB2-18, PBS-2, PBS-8
 Kamik: OUM-1, PRG1-13
 Kandleri: PB2-2
 Kanguk: PBS-3
 Kaniów: PEB2-1
 Kankakee: PB2-14
 Kansas: PRG1-9
 KANSO: PG-22
 Kaolinite: PEB2-9, PSB-14, PSB-9
 Kara: PC2-22
 Karababa: PRG1-18
 Karacali: PG-3
 Karachi: PB2-4, PBG1-8
 Karakorum: PFA-2
 Karakus: PRG1-18
 Karan: PEB1-2
 Karavanke/Drau: PC2-20
 Karen: PEB1-2
 Kargh: PEB1-2
 Karst: PM-14
 Karstic: PC2-19
 Karstified: PM-14
 Kashi: PG-28
 Kashmir-Tibet: PB1-5

Kasx: PMP-22
 Kata-Numa: PB2-1
 Katangli: PGG2-16
 Katzs: OGC-2
 Kaur-16-Ene: PB2-17
 Kaurane-: OB1-2
 Kaw: PBG1-9
 Kazantash: POS2-9
 Keigwin: OPC2-1
 Keil: OM-2, PB2-20, PM-24
 Kela: OGC-1, PG-13
 Kelasu-Yiqikelik: PG-13
 Kelasu: PG-13
 Kellwasser: PC2-8
 Kentucky: OGC-2
 Kerite: PRG1-10
 Kermadec: PBG1-4
 Kerogen-bitumen-Oil: POS1-2
 Kerogen-bound: OGPR-3, PM-19
 Kerogen-like: PB2-1
 Kerogen-oil-H₂S-Pyrite: POS1-2
 Kerogen/bitumen/Oil: OPS2-1
 Kerogen/bitumen: PBG2-4
 Kerogen/solvent: OPS2-1
 Kerogen: OBD2-2, OGPR-3, OP2-4, OP3-2, OP5-4, OP7-4, OPE2-3, OPS1-3, OPS2-1, ORP-2, PB1-22, PB1-5, PB2-16, PB2-5, PBC-7, PBG2-11, PBG2-4, PBG2-7, PBG2-8, PBS-11, PBS-12, PBS-14, PBS-23, PBS-26, PBS-5, PBS-8, PBS-9, PC-4, PC-6, PC2-20, PC2-5, PG-1, PG-10, PG-11, PG-14, PG-20, PG-21, PG-22, PG-23, PG-24, PG-25, PG-3, PGG2-3, PGG2-4, PM-1, PM-12, PM-14, PM-19, PM-24, PM-6, PM-9, POS1-1, POS1-11, POS1-14, POS1-15, POS1-2, POS1-5, POS1-6, POS1-8, POS2-1, POS2-11, POS2-13, POS2-3, POS2-9, PPC1-1, PPC1-17, PPC1-4, PPC1-7, PPM-11, PPM-14, PPM-2, PPM-9, PRG1-12, PRG1-3, PRG2-1, PSB-25 OOS-1 OGPR-3, OOS-2, OP5-4, OPS2-1, PB1-21, PBG2-8, PBS-22, PBS-23, PBS-7, PC2-20, PG-14, PG-21, PG-22, PG-28, PGG2-3, PM-1, PM-12, PM-14, PM-18, PM-19, PM-24, PM-9, POS1-1, POS1-2, POS1-3, POS1-5, POS2-1, POS2-11, POS2-3, POS2-6, PPM-2, PPM-9, PRG2-18, PRG2-4
 Kerogen+H₂O: PGG2-3
 Kerogen+H₂O+Anhydrite: PGG2-3
 Kerogen+H₂O+Caco₃: PGG2-3
 Kerogen+H₂O+Caco₃+S₀: PGG2-3
 Kerogen+H₂O+Montmorillonite: PGG2-3
 Kerogen+H₂O+Montmorillonite+Caco₃: PGG2-3
 Kerogen+H₂O+Montmorillonite+Caco₃+S₀: PGG2-3
 Kerogen+H₂O+Montmorillonite+S₀: PGG2-3
 Kerogene: PBS-17
 Kerosene: PEB2-6
 Ketal: PSB-13
 Keto-ols: PB1-11
 Ketone/ester: PMP-5
 Ketones: OSB2-1, PB2-6, PMP-5

OP7-2, PB1-15, PB2-6, PFA-6, PFA-8, PM-12,
 PM-3, PM-4, PMP-5, PPC1-15, PSB-6 PG-14
 Ketophenolic: OB1-2
 Khakasia: PEB2-17, PEB2-18 PEB1-11
 Khomolkinska: PBG2-2
 Khoreyver: PBS-20
 Khushaym: PB1-21
 Kimmeridge: OP4-3, OP7-4, OUM-3, PBS-6 PM-
 14
 Kinabalu: PBS-14
 Komatiite: PBG1-15
 Komatitic-Tholeiitic: PC2-25
 Korea: OEB-1, PBS-5, PG-19
 Kraków: PM-7 PM-3
 Krefthberget: POS1-6
 Kugmallit: POS2-5
 Kukersite: ORP-2, PRG2-7
 Kupferschiefer: PB1-8, PPM-12
 Kuwait: PRG2-1
 Kyoto: OP2-2, PCS-1, PCS-2

L

Labdane: OB1-2
 Labrador: PBS-23, PBS-3, POS2-13
 Lactate: OP6-2
 Lactic: PB2-2
 Lactones: PMP-20
 Lacustrine: OGC-1, OOS-3, OP3-3, OPC1-3,
 OPE2-1, OPS1-1, ORP-2, OUM-3, PB1-19,
 PB2-1, PB2-12, PB2-21, PB2-9, PBG2-8,
 PBS-1, PBS-12, PBS-13, PBS-24, PBS-8,
 PBS-9, PC2-11, PC2-6, PC2-9, PG-11, PG-13,
 PGG1-1, PGG2-13, PGG2-4, PM-11, PMN1-9,
 PMP-1, PMP-8, POS1-10, POS1-12, POS1-14,
 POS2-1, PPC1-13, PPC1-17, PPC1-26, PPC1-
 28, PPC1-8, PPM-15, PPM-9, PRG1-14,
 PRG1-3, PRG1-5, PRG1-6, PSB-19, PSB-4
 Ladderane: PB1-7, PMN1-3
 Ladderanes: PB1-7, PMN1-3
 Ladinian: PC2-20
 Lagoonal-Marine: POS2-4
 Lagoonal: POS2-6, POS2-7
 Lagoons: OPE1-3, PC2-20 PC2-7 PC2-17
 Laguna: PC2-1
 Lake-level: PC2-1
 Lake Malawi: PPC1-3
 Lake: OP2-1, OP4-2, OPC1-3, OPE1-2, OPE2-1,
 OPE2-2, PB1-19, PB1-20, PB1-22, PB1-9,
 PB2-1, PB2-10 PB2-22, PB2-4, PBG1-3,
 PBG1-8, PBG2-5, PBG2-6, PBG2-7, PC2-1,
 PC2-15, PC2-18, PC2-19, PC2-3, PC2-6, PC2-
 9, PEB1-14, PEB1-17, PEB1-9, PG-2, PGG1-
 1, PM-11, PM-4, PM-5, PMP-1, PMP-2, PMP-
 8, POS1-12, POS2-12, PPC1-12, PPC1-14,
 PPC1-17, PPC1-25, PPC1-28, PPC1-8, PSB-19
 PB2-22 OBD2-3, OP2-1, OP4-2, OPC1-3,
 OPE2-2, PB1-20, PB1-9, PB2-10, PB2-22
 PBG1-3, PC2-1, PC2-15, PC2-19, PC2-3, PG-
 11, PMN2-2, PMP-12, PMP-4, PPC1-17,
 PPC1-28, PPC1-8

Lakeside: PB2-4
 Lamalginite-Dominated: PPC1-17
 Lamalginite: PB1-21, PBG2-4, PPC1-17, PSB-4
 Lancaster: PMP-19
 Land-derived: PB1-21, PPC1-10
 Land-ocean: PC2-16
 Land-plant: PPC1-9 PC2-5
 Land-use: OPE1-2
 Landa: PGG2-3
 Landfill: OEB-3, OP2-2, PEB2-8
 Langezaal: PMP-9
 Langworthy: PB1-14
 Laos: PBC-8
 Lapy-GC-MS: PMN1-2
 Larapintine: PB2-12
Larix: PM-22
 Larvae: OGPR-3
 Laser-Assisted: PMN1-2
 Laser-Raman: PG-6
 Laser: PMN1-2
 Last-interglacial: PB1-6
 Lateglacial: PC2-6, PC2-7
 Latrobe Valley: PPC1-24
 Latvia: PBS-18
 Laurentia: PC2-8
 LC-MS: OMN-1, PMN2-11, PMP-11, PRG2-14
 PMN2-11 PB2-10, PB2-7, PEB1-12
 LC-Multistage: PEB1-12
 LC/MSD: OPC2-4
 LC/Tripleqms: OPC2-4
 LC: OMN-3, OPC2-4, PMN1-10
 LCHF: OP5-1
 LD: PEB1-11, POS1-8
 Lead: OM-3, OP7-4, OPE2-1, PB2-13, PB2-6,
 PBC-14, PC2-11, PC2-2, PC2-20, PC2-26,
 PEB1-9, PFA-1, PFA-4, PG-25, PG-27, PGG1-
 2, PGG2-14, PM-12, PM-28, PM-9, PMN1-1,
 PMN1-11, PMP-14, POS1-15, POS1-6, PPC1-
 1, PPC1-6, PPM-13, PRG1-11, PSB-11, PSB-
 12, PSB-16, PSB-17
 Leaf-derived: PC-5
 Leaf-wax: PC2-15
 Leaf: OP3-2, OP4-1, OPE1-2, OPE2-2, OSB1-1,
 PB1-4, PB2-11, PBG2-5, PBG2-6, PC2-15,
 PC2-23, PM-17, PPC1-14, PPC1-26
 Leafy: PBS-8
 Leaves: PSB-12, OB1-2, OM-1, OP3-2, OP5-3,
 OP6-4, PB2-11, PB2-15, PC2-15, PC2-5, PCS-
 5, PEB1-11, PSB-18
 Leg: OB2-1, OB2-3, OP7-3, OPC2-3, PB1-17,
 PB2-9, PC2-16, PC2-24, PMP-8, POS2-13,
 PPC1-10, PPC1-20 PPC1-20 PPC1-27, PPC1-
 9, PRG2-5 PEB1-16, PMP-8, PRG2-15
 Leif: PBS-23
 Leinefelde/Germany: PCS-4
 Leiosphaeridia: PB1-1
 Lena: PBS-10
 Lengjiapu: PGG1-1
 Leonardite: PC-11
 Levantine: PPC1-11

- Levoglucosan: OEB-1, PBC-2, PBG2-6, PPC1-23
 Lherzolite: PGG1-4
 Lhorta: PCS-12
 Light-hydrocarbon: OBD1-1
 Light: OBD1-1, OGC-1, OGC-2, OGC-4, OP3-4, OP4-1, OP4-3, OP6-3, OPE2-1, OPG-1, OPG-2, OPG-3, ORP-2, OUM-1, PB1-4, PB2-11, PB2-16, PB2-4, PBG1-8, PBG2-12, PBG2-7, PBS-10, PBS-17, PBS-2, PBS-23, PBS-8, PC-4, PC2-17, PCS-5, PCS-7, PEB1-4, PEB2-18, PEB2-6, PG-13, PG-16, PG-18, PG-2, PG-20, PG-4, PG-5, PG-9, PGG1-5, PGG2-11, PGG2-14, PGG2-15, PM-12, PMN2-9, PMP-10, POS1-10, POS1-6, POS2-15, POS2-4, PPC1-11, PPC1-18, PPC1-8, PPM-10, PPM-13, PPM-2, PPM-3, PPM-7, PRG1-10, PRG1-13, PRG1-19, PRG1-9, PRG2-1, PRG2-10, PRG2-11, PRG2-18, PRG2-21, PRG2-3, PRG2-7, PSB-11, PSB-19
 Lignin-derived: OM-2, PEB1-13, PM-25, PM-8, PSB-6
 Lignin-modified: PSB-13
 Lignin-phenol: PC2-1
 Lignin: PFA-2 OM-1, OM-2, OM-3, OMN-2, OP3-1, OP3-2, OSB1-2, OSB2-1, OSB2-2, PB2-13, PB2-20, PBC-9, PBG1-8, PBG1-9, PC-2, PC2-1, PC2-27, PCS-11, PCS-14, PCS-2, PCS-4, PCS-7, PCS-9, PFA-2, PM-17, PM-22, PM-25, PM-4, PM-5, PM-8, PMN2-7, PSB-13, PSB-18, PSB-3, PSB-6, PSB-9 PSB-3 OSB2-1, PCS-8, PM-17, PM-25
 Lignite-containing: OBD2-3
 Lignite/coal: PC-6
 Lignite: OBD2-3, PC-1, PC-11, PC-2, PEB2-8 PPC1-24 PSB-14 PC-1, PG-24
 Ligno-cellulosic: PBC-4, PBG1-9, PBS-7 PBC-9 PBC-9 PB1-21, PBC-6, PM-17, POS2-15 POS2-4
 Lima: PGG2-13
 Limestone: PB2-14 PBS-19, PC2-16, PC2-19, PG-5, PGG2-3, PMP-5, POS1-2, PPC1-1, PRG2-1, PSB-25, PSB-4 PBC-12, PBG1-10, PBS-10, PC2-17, PC2-20, PC2-4, PG-17, PM-14, POS2-1, POS2-13
 Limnic: PPC1-28
 Limnology: PPC1-17
 Limon-1: POS2-4
 Lindane: PEB2-1
 Lingulodinium: PM-28
 Linoleic: PB2-1
 Liophobic: PBG1-8
 Lipid-Derived: PB2-11
 Lipid-environment: PB2-22
 Lipid-extracted: OP3-2, OPC2-2
 Lipid-free: PSB-7
 lipid-inferred: PB2-22
 Lipid-rich: PPC1-14
 Lipid-specific: OP4-1
 Lipid: OB2-1, OEB-1, OGPR-2, OGPR-3, OP2-1, OP2-2, OP3-2, OP4-1, OP4-2, OP5-1, OP5-3, OP6-2, OPC2-4, OPE1-1, PB1-14, PB1-15, PB1-18, PB1-19, PB1-22, PB1-4, PB1-6, PB1-7, PB1-9, PB2-1, PB2-11, PB2-13, PB2-14, PB2-17, PB2-22
 Lipid: PB2-22 PBC-14, PBG1-8, PBG2-13, PBS-8, PC2-24, PC2-25, PC2-6, PC2-8, PC2-9, PEB2-10, PFA-3, PFA-4, PM-11, PM-17, PM-27, PMN1-3, PMP-1, PMP-11, PMP-12, PMP-14, PMP-17, PMP-18, PMP-20, PMP-21, PMP-4, PMP-6, PMP-8, POS1-11, PPC1-1, PPC1-12, PPC1-19, PPC1-20, PPC1-21, PPC1-22, PPC1-25, PPC1-26, PPC1-28, PPC1-5, PSB-7 OGPR-1 OB2-1, OB2-3, OB3-1, OEB-1, OGPR-1, OMN-1, OP2-1, OP2-2, OP3-1, OP3-2, OP4-1, OP5-1, OP6-2, OP7-2, OPC1-3, OPC2-3, OPC2-4, PB1-11, PB1-14, PB1-18, PB1-19, PB1-4, PB1-6, PB1-7, PB1-9, PB2-11, PB2-13, PB2-17, PB2-2, PB2-5, PBC-13, PBC-14, PBC-6, PBG1-11, PBG1-16, PBG1-8, PBG2-1, PBG2-10, PBG2-14, PC2-1, PC2-19, PC2-24, PC2-25, PC2-26, PC2-3, PC2-6, PCS-3, PCS-7, PEB1-13, PEB1-5, PFA-2, PG-14, PM-12, PM-21, PM-25, PM-27, PM-28, PM-3, PM-6, PMN1-3, PMN2-2, PMP-11, PMP-14, PMP-17, PMP-18, PMP-19, PMP-20, PMP-21, PMP-4, PMP-5, PMP-6, PMP-8, PMP-9, PPC1-1, PPC1-12, PPC1-14, PPC1-15, PPC1-19, PPC1-20, PPC1-22, PPC1-28, PSB-11, PSB-18, PSB-7
 Lipophilic: PEB2-2, PM-17
 Lipopolysaccharide: PMP-19
 Liptain: PC-2
 Liptinite: PB1-22
 Liptinite: PBS-23, PC-12, PC-5, PC-7, POS2-8 PC-4, POS2-10, POS2-15, POS2-4, PB1-22
 Liptodetrinite: PBS-11, PC-5
 Liquefied: OP4-3
 Liquidambar: PB2-15
 LiquidRovsamples: PMP-16
 Lithification: PGG1-12, PGG2-6
 Lithified: PB1-16
 Lithological: PC-10
 Litho-facies: PBS-14
 Litho-geochemical: POS2-13
 Lithofacies: ORP-2, PMP-13, POS1-10, POS2-8, PPC1-5
 Lithology: OOS-3, OP3-3, OP3-4, PB1-22, PBS-10, PC2-16, PC2-4, PRG2-7 PBS-12, PC2-21 OPS2-1, PB1-22, PBS-9, PC-10, PC2-18, PMP-13, POS2-13, POS2-9, PPM-4, PRG1-16, PRG2-17 PPC1-17
 Lithosphere: PBG1-6, PMP-16 PC-6, PC2-16, PM-19, POS2-1 POS1-11
 Lithostratigraphic: PBS-7 PB1-22
 Lithostructural: PC2-25
 Lithotypes: PC-1, PC-2, PG-20
 Lithuania: PBS-18 PSB-25
 Litter-derived: PSB-18

- Litter: OBD2-3, OPE1-2, OSB2-2, PBC-3, PBC-8, PCS-2, PCS-4, PCS-5, PM-10, POS1-5, PSB-18 PBG1-9
 Littoral: OBD2-3, PBG1-9, PGG1-11
 Livermore: POS1-10
 Liverpool: PEB1-8
 Livingston: PC2-7
 Ljubljana: PEB2-2
 Llandovery-Ludlow: PSB-25
 Loam: PSB-9 PBG1-7
 Lobnik: PEB2-2
 Loboziak: PB1-22
 Loch: OP4-2
 Lochkovian: PBG1-10
 Loci: PB2-3
 Loire: PM-8, PMN2-1
 Loliolide: PPC1-23
Lolium: OSB1-1, PSB-2
 London-Brabant: OB1-2
 London: PFA-3, PMN1-10
 Long-chain: OP3-2, OPE1-2, PB1-11, PB1-16, PB2-11, PBG1-14, PBG2-13, PC-3, PC2-1, PC2-15, PC2-24, PEB2-12, PFA-2, PM-25, PM-3, POS2-9, PPC1-15, PPC1-18, PPC1-20, PPC1-22, PRG1-17
 Lorraine: PEB2-14
 Louisiana: PB2-20
 Lowland: PBG1-2 PBC-1
 Lupane: OP1-2, PPC1-14 PGG1-10
 Lupanoid: OP1-2
 Lupenone: PBG1-11
 Lupeol: PB2-17
 Lupeone: PB2-17
 Lusatian: OBD2-3
 Lutea: PEB1-2
 Luther: OGPR-1
 Luvisol: PCS-4, PSB-16
 Lybian: PBS-7
 Lycopane: PPC1-18
Lycopodium: PC2-11, PM-21
 Lycopsid: PM-21
 Lysophosphatidylglycerol: PMP-8
 Lysophospholipids: PMP-20
- M**
- Maastrichtian: OPC2-3
 Maceral: PBS-1, PBS-7, PC-10, PC-12, PC-7, PC2-9, PG-20, POS2-10, POS2-7, PPC1-17 PBG2-4, PBS-1, PC-12, PC-4, PC-5, PC-7, PG-20, PMN1-2, POS2-10, POS2-4, POS2-8, PSB-25
 Macrofossil: OPC2-2, PB2-21, PC2-5, OP3-1, OPE2-1, PB2-21, PBC-1, PC2-19, PC2-5
 Macromolecules: PBC-9, PBG2-3, PM-8, PSB-6 OBD1-3, OBD2-3, OP3-2, OP5-4, PBC-9, PCS-3, PM-13, PM-15, PM-2, PM-20, PM-25, PM-28, PM-3, PM-8, PMN1-1, PSB-5
 Macroorganisms: OPE2-1
 Macrophytes: PB1-19, PC2-3, PM-11
 Macropores: PCS-5
 Macrotidal: PM-15
 Madagascar: PPC1-25
 Madrid: PEB2-2
 Maestrazgo: PC-11
 Maestrichtian/Upper: PFA-7
 Magdalena: PBS-19
 Magic-angle: OSB1-3
 Magma: PBG1-6 PBS-12, POS1-6
 Magnesium: PMN2-10
 Magnetite: PBG1-15, PBG1-6, PGG1-4, POS1-13
 Magnetite+silicoaluminophosphate: PGG1-4
 Magnetite+zeolite: PGG1-4
 Magnetostratigraphy: PMP-18
 Mahakam: OP1-2, PC-7
 Maials: PSB-20
 Maillard-type: PBC-12
 Malaysia: PBS-14, PBS-24, PGG1-10, POS2-8
 Maltene: PRG2-14 PRG2-13
 Mammal: PB1-22 PC2-10
 Mandong: PG-4
 Manganese: OB1-3, OGPR-2, PM-17
 Mangrove-Derived: OMN-2, POS2-8
 Mangrove-Fringed: OMN-2
 Mangrove: OM-1, OMN-2, PB2-17, PBG1-9, PC-5, POS2-10, PPC1-20 PBG1-9, PC2-19
 Manhattan: PEB1-14
 Manji-Shikoroza: PMP-5
 Manjaer: PBS-21, PPM-6
 Mannose: PCS-8
 Mannville: PM-24
 Manure: OSB2-3, PCS-12, PCS-14, PCS-3
 Manville: PM-24
 Manzanal-1: POS2-4
 Maracaibo: PGG1-12
 Marais: PC2-20
 Marble/cement: PB1-21 PM-7 PB1-21
 Marine-algal: OPS2-3
 Marine-carbonate: PBS-19
 Marine-derived: PB1-22, PBS-3
 Marine-evaporitic: PGG2-13
 Marine-influenced: PC-5, POS2-10, POS2-8, PRG2-20
 Marine/brackish: OPC1-1
 Marine: OB1-3, OB2-1, OB2-2, OB3-1, OEB-1, OGC-1, OGPR-3, OMN-3, OOS-3, OP3-3, OP4-1, OP4-2, OP4-3, OP4-4, OP5-1, OP6-2, OP7-2, OPC1-1, OPC1-3, OPC2-1, OPC2-3, OPC2-4, OPE1-2, OPE2-2, OPE2-3, OPS1-2, ORP-2, OSB1-1, OUM-1, OUM-2, PB1-10, PB1-11, PB1-13, PB1-15, PB1-16, PB1-17, PB1-20, PB1-21, PB1-22, PB1-5, PB1-6, PB1-7, PB2-12, PB2-13, PB2-15, PB2-18, PB2-19, PB2-20, PB2-21, PB2-8, PBC-11, PBC-13, PBC-2, PBC-5, PBC-6, PBC-7, PBG1-13, PBG1-14, PBG1-16, PBG1-4, PBG1-5, PBG1-8, PBG2-1, PBG2-10, PBG2-11, PBG2-12, PBG2-13, PBS-16, PBS-18, PBS-19, PBS-2, PBS-3, PBS-5, PBS-6, PBS-7, PBS-8, PC-5, PC2-10, PC2-11, PC2-12, PC2-14, PC2-16, PC2-17, PC2-19, PC2-20, PC2-21, PC2-23, PC2-24, PC2-26, PC2-4, PCS-6, PEB1-1,

- PEB1-10, PEB1-16, PEB1-18, PEB1-4, PEB2-12, PEB2-17, PEB2-5, PG-16, PG-17, PG-2, PG-20, PG-21, PG-3, PGG1-11, PGG1-12, PGG2-1, PGG2-10, PGG2-11, PGG2-12, PGG2-5, PM-13, PM-14, PM-15, PM-20, PM-23, PM-26, PM-28, PM-3, PM-4, PM-5, PM-6, PM-8, PMN1-3, PMN1-9, PMN2-1, PMP-1, PMP-14, PMP-18, PMP-20, PMP-21, PMP-4, PMP-8, PMP-9, POS1-11, POS1-14, POS1-5, POS1-6, POS1-7, POS2-10, POS2-13, POS2-14, POS2-15, POS2-4, POS2-5, POS2-6, POS2-7, POS2-8, POS2-9, PPC1-1, PPC1-11, PPC1-16, PPC1-18, PPC1-19, PPC1-20, PPC1-21, PPC1-23, PPC1-24, PPC1-26, PPC1-27, PPC1-28, PPC1-4, PPC1-8, PPC1-9, PPM-12, PPM-15, PPM-8, PRG1-13, PRG1-14, PRG1-16, PRG1-3, PRG1-5, PRG1-6, PRG1-9, PRG2-1, PRG2-12, PRG2-20, PRG2-3, PSB-25
- Marinoan: OGPR-3, PPC1-7
- Maritime: PEB1-16
- Maritza-Iztok: PC-2
- Marker: OOS-3, OP4-2, OP5-1, PB1-22, PB1-6, PBS-3, PC2-15, PC2-4, PGG1-2, PPM-14, OGPR-3, OP1-2, OP3-1, OP4-2, OP5-2, OUM-1, PB1-16, PB1-18, PB1-21, PB1-6, PBC-1, PBC-13, PBC-5, PBG1-13, PBG1-9, PBS-3, PC2-11, PC2-23, PC2-4, PC2-5, PC2-6, PCS-2, PEB2-12, PEB2-4, PGG1-1, PGG1-10, PGG1-2, PGG2-2, PM-18, PM-2, PM-25, PMP-11, PMP-13, PMP-20, PMP-23, PMP-8, POS2-14, PPC1-21
- Marl: OP3-3, PB2-7, PM-14, POS1-11, PPM-15, PB1-21, PBC-12, PG-11, PM-14, PM-7, POS2-7, POS2-9
- Marly: ORP-2, PBS-7, PC-12, PC2-17, PM-7, PMP-5
- Marne: PC2-4, PC2-11
- Marraat: PGG1-10
- Marsh: PB2-20, PB2-21, PBG2-13, PSB-7
- Marshy-Swamp: PG-3, PC2-18
- Marsing: POS1-10
- MAS: OSB1-3, PBC-2, PBC-5, PBC-6
- Maslinic: PB2-6
- Massoth: PBG1-4
- Masticadienonic: PFA-6
- Mats: OGPR-2, OOS-2, OP6-1, OP6-2, PB1-20, PB2-4, PBG1-9, PMP-12, PMP-14
- Maturated: PM-7
- Maturation: OGC-1, OP3-2, OP5-4, OPG-2, OPS1-3, OPS2-1, PB1-21, PB1-8, PB2-5, PBG1-12, PBS-12, PBS-13, PBS-15, PBS-26, PBS-5, PBS-6, PBS-9, PC-3, PC-7, PC2-5, PC2-8, PG-10, PG-21, PG-24, PG-3, PGG1-10, PGG1-11, PGG1-14, PGG1-15, PGG2-14, PGG2-8, PM-1, PM-15, PM-18, PMN2-1, PMN2-8, PMP-13, POS1-1, POS1-10, POS1-13, POS1-15, POS1-4, POS2-11, POS2-5, POS2-6, POS2-7, PPC1-1, PPM-10, PPM-4, PPM-5, PPM-9, PRG1-1
- PRG1-10, PRG1-13, PRG1-19
- Maturity-Dependence: PC-4
- Maturity-Levels: OPS1-3
- Maturity-Related: POS2-5
- Maturity: PBS-14, OBD2-2, OGC-1, OGC-2, OGC-3, OOS-3, OP2-3, OP3-4, OP4-3, OP5-2, OP5-4, OP7-3, OP7-4, OPS1-1, OPS1-2, OPS1-3, OPS2-1, ORP-2, OUM-1, OUM-3, PB1-12, PB1-16, PB1-18, PB1-22, PB1-8, PB2-16, PB2-18, PB2-4, PBC-9, PBG1-12, PBG1-14, PBG2-4, PBS-1, PBS-11, PBS-15, PBS-16, PBS-17, PBS-19, PBS-20, PBS-21, PBS-23, PBS-5, PBS-6, PBS-8, PBS-9, PC-1, PC-11, PC-5, PC-6, PC-9, PC2-20, PC2-22, PC2-25, PC2-4, PG-13, PG-15, PG-18, PG-2, PG-20, PG-21, PG-25, PG-3, PG-4, PG-7, PG-8, PGG1-1, PGG1-10, PGG1-15, PGG1-3, PGG1-5, PGG2-11, PGG2-12, PGG2-14, PGG2-16, PGG2-2, PGG2-4, PGG2-5, PGG2-8, PMN1-9, PMN2-3, PMN2-5, PMN2-8, PMN2-9, PMP-13, POS1-10, POS1-12, POS1-13, POS1-15, POS1-16, POS1-4, POS1-5, POS1-6, POS1-8, POS1-9, POS2-10, POS2-13, POS2-14, POS2-15, POS2-4, POS2-5, POS2-6, POS2-8, PPC1-1, PPC1-17, PPM-10, PPM-11, PPM-12, PPM-13, PPM-2, PPM-7, PPM-9, PRG1-1, PRG1-13, PRG1-14, PRG1-16, PRG1-2, PRG1-20, PRG1-6, PRG1-7, PRG2-16, PRG2-18, PRG2-20, PRG2-3, PRG2-4, PRG2-5, PRG2-6, PRG2-7, PSB-25, PSB-4
- Mauddud: PRG2-1
- Melanoidin-like: PM-6
- Melanoidin-rich: PM-6
- Melanoidin-type: OSB1-2
- Melanoidin: PBC-2, PBC-5, PM-6
- PBC-6, PM-6, PSB-18, PSB-7
- Meli/Mei: PM-1
- Mello: PGG2-13, PRG1-3
- Melt-Incorporated: PBG2-7, PBG1-6, PBG2-7
- Membrane-spanning: PB1-14
- Menilite: POS2-11
- Mercury: PBG1-3, PEB1-15
- Meromictic: PM-11, PPC1-14
- Merseyside: PEB1-8
- Merzenhausen: PSB-16
- Mesh: PBS-9, PPM-5
- Mesnil/Vair: PM-24
- Meso-Cenozoic: PPM-8
- Meso-Paleozoic: PGG1-11
- Mesocosm: OPC2-4, PEB1-4, OPC2-4
- Mesopotamia: PBG2-7, PFA-9
- Mesozoic-Cenozoic: PBS-12, PGG1-12
- Mesozoic: OUM-1, PB1-16, PB1-18, PB1-8, PBG1-14, PBS-15, PBS-26, PBS-3, PBS-8, PGG1-12, PGG2-11, PGG2-6, POS2-7, PPC1-1, PRG2-16
- Messel: PB1-22, POS1-14, PPC1-14
- Meta-Anthracite: PC-8
- Metabolic: OB2-3, OGPR-2, OP7-3, PB1-2, PBG1-11, PEB1-4, PEB2-3, PFA-9, PMP-13

- Metabolically: PB1-2, PMP-12, PSB-15
 Metabolised/catabolised: OSB1-1
 Metabolism: OB2-3, OMN-3, OP6-1, OSB2-3, PB1-2, PB1-7, PBC-14, PBC-9, PBG2-9, PMN1-3, PMP-14
 Metabolite: OSB2-3, PBG1-11, PEB1-1, PEB2-1, PRG2-2 OEB-3, OMN-3, OP6-1, PEB1-1, PEB1-12, PEB2-1, PRG2-2
 Metabolizable: PMP-2, PMP-6
 Metabolized: PEB1-1 PMP-2
 Metagenesis: OGC-1
 Metagenetic: PC-6, PG-24
 Metal-bearing: PBG2-2
 Metal-binding: PBG1-4
 Metal-containing: PGG1-4
 Metal-free: PPC1-6
 Metal-halogen: PEB2-6
 Metal-humate: PEB2-9
 Metal-humic: PSB-5
 Metal-organic: PSB-5
 Metal: OGPR-1, OGPR-2, PB1-8, PB2-21, PBG1-3, PBG1-4, PBG2-7, PC2-8, PCS-14, PG-12, PG-14, PGG1-12, PGG1-4, PM-20, PMN1-8, PMP-16, PPC1-4, PSB-1, PSB-14, PSB-5 OGPR-1 OGPR-1, PBC-13, PBG1-4, PC2-8, PEB1-14, PEB2-12, PGG1-12, PGG1-13, PM-15, PM-20, PSB-1, PSB-5 PBG1-4
 Metallogenic: PGG1-12
 Metalloporphyrins: OB3-2, PPC1-4
 Metamorphic: PB1-21, PB2-21, PBG2-2, PM-7, POS1-6, POS2-12
 Metamorphism: PC2-25, PM-7
 Metamorphized: PM-18 PB1-21, PC-8
 Metasedimentary: PC2-25
Metasequoia: PM-22
 Metastable: OBD1-2, OOS-3, PB2-19
 Metazoa: OGPR-3 OGPR-3 PB2-8
 Meteorite: PBG2-3, PBG2-4, PC2-9 PBG1-16, PBG2-3, PM-16
 Meteoritic: PBG2-3, PBG2-4
 Methane-consuming: PMP-21
 Methane-cycling: OP5-1
 Methane-enriched: OMN-1
 Methane-rich: PBS-17, PSB-15
 Methane/G: PG-11
 Methane/Sum: OGC-4
 Methane: OB2-3, OB3-1, OGC-1, OGC-2, OGC-4, OMN-3, OP2-1, OP2-2, OP2-3, OP5-1, OP5-3, OP6-2, OP7-1, OP7-3, OPE2-3, PB1-18, PBS-12, PBS-17, PBS-2, PBS-5, PC-6, PC-7, PC2-12, PC2-21, PC2-26, PEB1-15, PG-1, PG-11, PG-13, PG-16, PG-17, PG-18, PG-19, PG-2, PG-20, PG-21, PG-22, PG-23, PG-25, PG-26, PG-28, PG-3, PG-4, PG-5, PG-6, PG-8, PG-9, PGG1-4, PGG1-8, PMN2-10, PMP-16, PMP-17, PMP-18, PMP-2, PMP-21, PMP-3, PMP-5, POS1-5, PPC1-18, PPM-1, PPM-2, PPM-3, PSB-15 PG-16, PG-18 POS2-2
 Methanethiol: OGPR-1
 Methanization: PGG2-6
Methanococcus: PB2-2
 Methanogenesis: OB3-1, OGPR-2, OMN-3, OP2-2, OP7-3, PB1-14, PG-18, PG-24, PG-9, PMP-13, PMP-2, PMP-3, PPC1-14, PPC1-7 OGC-2, OMN-1, OMN-3, OP4-3, OP5-1, OP6-2, OPC1-3, PB2-2, PEB2-7, PMP-15, PPC1-14, PPC1-7, PRG2-2
 Methanogens: OB3-1, OP2-4, OP5-1, PB1-14, PB2-2, PMN2-10, PMP-21, PPC1-23, PPC1-7 OB3-1, PB2-2, PC2-12
 Methanol-thionyl: PSB-1
 Methanol/water: PB2-17
 Methanol: OPE2-1, PB2-15, PBG1-8, PC-1, PM-16, PM-4, PM-5, PMN1-3, PMP-13, PRG1-9, PSB-1
Methanopyrus: PB2-2
Methanosarcina: OP5-1, PMP-5
 Methanosarcinales: OB3-1, OP5-1
 Methanotrophic: OP2-1, OP2-2, OP4-2, OP4-4, OP5-3, PB1-18, PB2-2, PC2-12, PMP-17, POS1-12, PPC1-12, PPC1-17, PPC1-23, PSB-15
 Methanotrophs: OB3-1, OP2-2, OP2-4, OP5-3, PB1-18, PB2-2, PMP-19, PPC1-23, PPC1-25, PSB-15 OB3-1, OP2-2, PSB-15 PMP-17 OP5-3 OP2-2
 Methoxy-Dimethoxy-Benzenecarboxylic: PM-25
 Methoxybenzenes: OSB1-2
 Methoxybenzoic: PFA-2
 Methoxychlor: PEB2-1
 Methoxyl/□-Amino: PSB-18
 Methoxyl: PSB-18, PSB-3
 Methoxyphenolic: PBC-9, PFA-2
 Methoxyphenols: PBC-14, PCS-9, PFA-2, PM-25 PCS-9
 Methyl-alkyl-benzenes: PM-28
 Methyl-dibenzothiophenes: PEB1-4
 Methyl-phenanthrenes: PEB1-4
 Methyl-phenantrenes: PEB1-4
 Methyl-sterane: POS2-14
 Methyl-tertiary-butyl-ether: PEB2-6
 Methylalkanes: PC2-20 PGG2-10
 Methylenaromatics: OPG-1
 Methylation: OP4-4, OSB1-2, PFA-2, PFA-9, PM-14, PM-16, PM-23, PM-4, PM-5, PMN1-1, PMN2-4
 Methylbenzenes: OP3-4, PM-9
 Methylbicadinanes: PGG2-2
 Methylcholest-5-en-3β-ol: OB2-2
 Methylcholesta-5,24(28)-Dien-3a-Ol: OB2-2
 Methylcholestane: PBS-10
 Methylcholesterol: OB2-2
 Methylcyclohexane: OP5-2, ORP-2, PPM-14
 Methyldehydroabietate: OB1-2
 Methyladamantanes: OGC-1, PGG1-5
 Methylerythritol: OP6-4
 Methylindole: PEB2-12
 Methyliodide: PMN2-4
 Methylnaphtalenes: PBG2-2 PGG1-15, OB3-2, OBD2-1, OPG-1, POS2-1

- Methylococcus*: PMP-17
Methylocystis: PSB-15
Methylosinus: PSB-15
Methylosphaera: PMP-17
 Methylotrophic: OP4-2
 Methylphenanthrenes: OB3-2, PBG2-4, PGG1-1, PGG1-15 OP5-2, PB1-21, PC-11, PGG1-15, PRG2-20
 Methylphenols: PM-9
 Methylretenes: OB1-2
 Methylsteranes: PC2-17
 Methylsteroids: PPC1-14
 Methylthiol: PC-1
 Methylthiophene: PC-1
 Metoxyl/amino: PBC-9
 Mexican: PMN2-3
 Mexico: OGC-4, OGPR-2, OP3-4, PBG1-13, PBG2-4, PC-7, PG-15, PMN1-5, POS2-15, POS2-4, PRG1-15, PRG2-9
 Mg: OBD2-3, OP6-1, OP7-3, OPE2-1, OPS1-2, PB1-22, PB2-20, PBC-3, PBG2-11, PBS-17, PBS-8, PC-2, PC-5, PCS-13, PEB1-13, PEB2-9, PG-11, PG-14, PGG2-7, PM-12, PM-17, PM-5, PMN1-6, PMN1-7, PMN2-4, PMN2-9, POS1-12, POS1-7, POS1-8, POS2-11, POS2-13, POS2-9, PPC1-8, PPM-5, PSB-1, PSB-5 PGG2-9
 Michigan: PB2-14, PBC-11, PC2-8, PCS-11, PRG2-5
 Michoacán: PSB-21
 Micrinite: POS2-7
 Micrite: PPC1-7
 Micritic: PMP-5, PPC1-1
 Micro-aggregates: PSB-8
 Micro-analysis: PBG1-6
 Micro-breccias: PBG2-7
 Micro-charcoal: PC2-18
 Micro-crystals: PBG1-6
 Micro-Fourier: PM-21
 Micro-fracture: POS1-14
 Micro-fractures: PBG1-6
 Micro-FTIR: PM-21
 Micro-petrographically: POS2-1
 Micro-seeps: PPM-11
 Micro-separation: PMN1-6
 Micro-spheres: PBG1-6
 Micro-titration: PM-15
 Micro-xenoliths: PBG1-6
 Microaerophilic: OB1-3, OGPR-2
 Microaggregates: PSB-16 PCS-5
 Microalgae: PMP-19 OGPR-3, PB1-21, PM-23, PM-28, PMP-19, PMP-4 PMP-4
 Microbacterium: PEB2-19
 Microbeads: PMP-13
 Microbes: OB1-1, OP2-2, OP7-3, PB2-11, PB2-9, PM-21, PMP-10, PMP-12, PPC1-22, PPC1-23, PRG1-17
 Microbial-derived: PPC1-14
 Microbiocoenosis: PB2-4
 Microbiota: PEB2-19
Micrococcus: PEB2-19
 Microcosm: PEB2-7, PRG2-2 PEB2-7 OBD2-3, OMN-1, PEB1-1, PEB2-3, PEB2-7, PMP-20
 Microcoulometry: PG-12
 Microcrystals: PBG2-11
 Microcystis: PB2-4, PBG1-8
 Microdroplets: PGG1-13
 Microelements: PSB-18
 Microflora: OSB2-3
 Microfossil: OP4-4 OP4-1, OP4-4, OPC2-3, PB1-1, PBG1-6, PM-18, PM-28, PMN1-2, POS1-7, PRG2-1
 Microinclusions: PGG1-13
 Microlayer: PMP-20
 Micromorphological: PM-10
 Microoil: POS2-9
 Microorganisms: OP2-2 PEB2-19, PMP-20, PSB-8 OB2-1, OB3-1, OBD2-3, OGPR-3, OMN-1, OMN-3, OP6-2, OSB1-1, OSB2-3, PB1-2, PB1-7, PBS-10, PC-6, PC2-20, PCS-1, PEB1-11, PEB1-4, PEB2-16, PEB2-18, PEB2-19, PEB2-3, PMP-13, PMP-14, PMP-17, PMP-19, PMP-20, PMP-22, PMP-4, PMP-6, POS2-2, PPC1-14, PRG2-5 OP7-3, OSB1-1, PBG1-4 PBG2-1
 Micropetroleum: PGG1-13
 Microplankton: PB1-22
 Micropores: PC-4
 Microporosity: PRG2-4
 Micropyrolysis-GC-MS: PMN1-2
 Microorganisms-Enzymes-Nutrients: PEB2-3
 Microscopy: PB1-2, PB1-21, PBC-4, PBG1-10, PBG2-11, PGG1-13, PM-12, POS1-14, POS1-15, PPC1-1, PRG2-18, PSB-8
 Microsensors: PMP-14
 Microspectroscopy: PB1-21, PBG2-7
 Microstructures: PM-18
 Microtexture: PBC-4 PRG2-18
 Microwave: PSB-6
 Mid-Atlantic-Ridge: PBG1-4, PMP-16
 Mid-Atlantic: OP5-1, PB2-2, PBG1-6
 Mid-chain: OP6-1, PB1-11, PB1-15, PM-12, PM-3
 Mid-Cretaceous: OPC2-3, PC2-16, PPC1-27, PPC1-6, PPC1-9
 Mid-Devonian: OPC1-2
 Mid-European: PBG1-2
 Mid-Holocene: PSB-19
 Mid-Miocene: PC-6
 Mid-Neoproterozoic: PM-19
 Mid-oil-window: PG-20
 Mid-Pleistocene: PC2-13, PPC1-19
 Mid-Proterozoic: OGPR-3, OP4-4
 Middelburg: PMP-10
 Middle-Jurassic: POS2-7
 Migration-accumulation: PPM-10
 Migration-contamination: OP1-2
 Migration-fractionation: PBS-17
 Migration: OBD2-1, OGC-1, OGC-3, OP1-2, OP4-3, OP5-2, OPG-2, OPS1-1, OPS2-1, OPS2-3, ORP-1, OUM-1, OUM-3, PBS-1, PBS-11,

- PBS-13, PBS-15, PBS-17, PBS-2, PBS-24,
 PBS-6, PBS-9, PC-7, PG-10, PG-15, PG-24,
 PG-5, PGG1-12, PGG1-14, PGG1-3, PGG1-5,
 PGG2-14, PGG2-4, PGG2-5, PM-19, PMN2-5,
 PMP-18, PMP-9, POS1-13, POS1-14, POS1-
 15, POS1-16, POS1-2, POS1-3, POS1-9,
 POS2-13, PPC1-1, PPC1-26, PPM-10, PPM-
 12, PPM-13, PPM-4, PPM-5, PPM-6, PPM-8,
 PRG1-13, PRG1-14, PRG1-19, PRG1-2,
 PRG1-5, PRG2-7, PEB1-8 OP7-1, ORP-1,
 OUM-1, PBS-6, PBS-20, PGG2-4, PPM-4,
 PPM-5, PPM-6 OGC-1, OGPR-3, OP7-3, PB1-
 1, PB1-22, PBG2-4, PBS-11, PBS-12, PBS-16,
 PG-1, PG-24, PGG2-16, PM-19, POS2-13,
 PPM-12, PPM-6, PRG1-14, PRG1-2, PRG2-1,
 PRG2-21 PPM-10, PPM-4 OP7-3, OPG-2,
 PB1-8, PC2-26, PGG2-12, PPM-13, PRG1-19,
 PRG2-16
- PBS-2 POS1-9 PGG2-12
 Migwa: PRG2-1
 Mikerinos: PMP-17
 Milan: PBG1-1
 Milani: POS2-3
 Mineral-associated: PSB-12
 Mineral-bituminous: PC-12
 Mineral-bound: PSB-12
 Mineralisation: PBG2-3, PMP-14, PSB-10 PB2-5
 PSB-6 PCS-13 OBD2-3, OSB1-1, OSB2-3,
 PB1-17, PB2-16, PBG1-6, PC2-25, PCS-13,
 PCS-14, PEB2-16, PSB-18, PSB-21
 Mineralized: OBD2-3, OSB1-3, PC2-20, PCS-13
 Mineralogical: OB1-2, PBG1-15, PBG2-11, POS1-
 10, PSB-10, PSB-9
 Mineralogy: OBD2-2, ORP-2, PC2-11, PC2-4,
 PCS-11, POS1-10
 Minerals: OGPR-1, OM-1, OOS-2, OPE2-3, OSB2-
 2, PB1-19, PB1-8, PB2-13, PB2-8, PBG1-6,
 PBG1-8, PBG1-9, PBG2-11, PC-12, PC2-4,
 PCS-1, PCS-14, PCS-4, PGG1-13, PGG1-2,
 PGG2-3, PGG2-9, PM-11, PM-24, PM-26,
 PMN1-1, POS1-14, POS1-8, POS2-2, PPM-13,
 PSB-12, PSB-9 OM-1, OM-2, OOS-2, OP6-1,
 OPE2-1, ORP-2, OSB2-2, PB1-21, PB2-4,
 PBC-12, PBC-3, PBC-9, PBG1-5, PBG1-6,
 PBG1-8, PBG2-11, PBS-1, PC-5, PC2-4, PCS-
 10, PCS-11, PCS-14, PCS-3, PCS-5, PCS-9,
 PEB1-11, PEB1-16, PEB1-7, PFA-2, PG-19,
 PGG2-3, PM-11, PM-26, PM-7, PMN1-1,
 PMN1-5, PMN2-5, PMN2-8, PMP-16, POS1-
 13, POS1-16, POS1-2, POS1-5, POS1-9,
 POS2-10, POS2-3, POS2-4, POS2-8, PPM-10,
 PPM-11, PPM-13, PRG1-11, PSB-10, PSB-12,
 PSB-15, PSB-16, PSB-5
- Mines: PC2-25, PG-26, POS2-3
 Mining: OBD2-3, POS1-12, PPM-12
 Minnesota: OMN-2, PB1-20, PMP-4
 Minusinsk: PEB2-17
 Miocene-Aged: PC-2
 Miocene: OB2-2, OOS-3, OP4-3, OPC2-4, OPE2-
 2, OPG-2, PB2-7, PBG2-8, PBS-17, PBS-24,
 PBS-8, PC-12, PC2-14, PG-1, PG-11, PG-15,
 PG-23, PG-24, PGG1-10, PGG2-16, POS1-14,
 POS2-10, POS2-11, POS2-8, PPC1-24, PPC1-
 6, PPM-8, PRG1-16, PRG2-12 OGC-4
- Miospores: PB1-22
 Miqne-Ekron: PFA-5
 Miqne: PFA-5
 Miscanthus: PSB-9
 Mississippi: PB2-20, PEB1-3
 Mississippian: PG-10, POS1-13, PRG1-9, PRG2-5
 Molecular-isotope: PC2-1 OP4-1 PC2-26
 Mollisol: PCS-11
 Molybdenum: PM-19
 Mono-aromatic:
 Mono-methylalkanes: PSB-4
 Mono-oxygen: PG-14
 Mono-unsaturated: OB2-1, PFA-3
 Monoaromatic: OEB-2, PB1-1, PB2-6, PC2-11,
 PGG1-1, PGG1-11, POS1-11 PEB2-4 OPG-1
 Monoaxonal: OGPR-3
 Monocarboxylic: PGG2-4, PM-14, PM-16, PRG2-2
 Monocline: PB1-12
 Monoculture: PCS-7, PSB-17
 Monocyclic: OP2-4, PEB1-12
 Monoene: OB1-2
 Monofluorinated: PMN1-10
 Monogalactosyldiglycerides: PMP-20
 Monolignols: OP3-1, PM-22
 Monomethyl: PB2-19, PRG1-5, PRG1-6
 Monomethylalkane: PRG1-6 PC2-20, PRG1-6
 Monomethylphenanthrene: PC2-22
 Monosaccharides: PBG2-6
 Monosemantic: PBS-2
 Monospecific: PMP-20
 Monoterpenes: PBC-14
 Monounsaturated: PB1-1, PMP-20, PMP-4
 Monsoon: OPE2-2, PC2-1, PC2-2
 Montenegro: PC-12
 Monterey: OEB-2, PGG2-3
 Montmorillonite: OP6-1, PGG2-3, PSB-7
 Moretane/C₃₀: PRG1-6
 Moretane: PRG2-20, PSB-4
 Moretane C₃₀/: PGG2-11
 Moretanes: PB2-14
 Moronic: PFA-6, PFA-8
 Morrowan: PRG1-9
 Moscow: PGG2-10
 Moselle: PEB1-7
 Moss: OPC2-2 PSB-25 OP5-3, OP6-2
 Mould: PFA-8
 Mounds: PPC1-22
 Mountevans: PGG2-2
 Mourguiart: PC2-18
 MRM-GC-MS: OBD1-2, OGPR-3, OOS-3, PM-19
 PB2-19
 MRM: PGG2-2
 MS: OMN-2, OP2-2, PB2-15, PB2-6, PBC-11,
 PBC-7, PEB1-12, PEB2-12, PM-1, PM-2, PM-
 22, PM-4, PM-5, PMN1-3, PMN2-11, PMP-6,
 POS2-13, PRG2-3 PSB-3

- PB1-12 OB2-1, PM-27, PSB-3
 MTBE-Contaminated: PEB2-7 PEB2-6,
 Mucilage: PM-10
 Muddy-Silt: PBG2-14 PBG2-14 PBG2-14, PEB1-18
 Mudflow: PC2-9
 Mudgas: PG-8
 Muds: OP7-3, PEB1-10, PGG1-9, PRG1-8, PRG2-4, PSB-19 OMN-1, OP7-1, PBG1-9, PBG2-14, PFA-8, PG-10, PGG1-9, PM-15, PM-20, PMN1-5, PMP-13, PMP-17, PMP-19, POS1-10, PRG1-15, PRG1-8, PRG2-12
 Mudstone: PB1-22, PC-10, PC-6, PG-28, PG-4, PG-7, POS2-10, PPC1-8, PPM-5
 PB1-16, PB2-18, PBS-18, PBS-9, PC-5, PGG1-1, POS2-10, POS2-11, POS2-7, PPC1-6, PPM-5, PPM-9, PRG1-8
 Muehlenbachs: PG-22
 Muffle: PBC-12
 Mummies: PFA-4, PFA-6, PFA-8
 Mummification: PFA-4
 Mummiya: PFA-4
 Mummy-Like: PFA-8
 Murchison: PBG2-3, PM-16
 Mushroom: PMN2-7
 Mussel: OEB-2, PEB2-10, PMP-16, OEB-2, PEB2-10
 Mutagenic: PEB1-1, PEB2-2
 Mxico: POS2-4, PSB-21
 Mycelial: PM-17, PMN2-7
 Mycobacteria: OP3-3 PEB2-16
 Mycose: PBG1-11
 Myrica: PSB-9
 Mytilus: OEB-2, PEB2-10
 Myxoxanthophylls: PB2-4
- N**
n-Acetyl: PMN2-6
n-Acids: PGG2-4
n-Alcohols: PB1-13, PB1-15, PFA-2, PMP-4, PPC1-12, PPC1-20, PPC1-22 PB1-13, PPC1-22
n-Alk-1-ene/*n*-alkane: PM-14
n-Alk-1-enes: PEB2-12, PMN1-1 PMN1-1
n-Alkan-1-ols: OPC2-1, PC2-23
n-Alkan-2-ones: PB1-15, PBG1-16
n-Alkane-isoprenoid: POS1-4
n-Alkane/*n*-alkene: OP3-2 OP3-2, PM-12, POS2-10 PBG2-7 PG-14
n-Alkanes: OBD1-1, OBD1-1, OBD1-2, OBD1-3, OBD2-1, OEB-1, OGC-1, OGPR-2, OP3-2, OP5-2, OPC2-1, OPE2-1, OSB1-2, OUM-1, OUM-3, PB1-20, PB1-21, PB1-22, PB2-11, PB2-13, PB2-14, PB2-17, PB2-19, PB2-3, PB2-4, PB2-5, PB2-9, PBG1-11, PBG1-14, PBG1-16, PBG1-7, PBG1-8, PBG2-13, PBG2-2, PBG2-6, PBS-1, PBS-10, PBS-11, PBS-12, PBS-17, PBS-2, PC-3, PC-9, PC2-14, PC2-15, PC2-17, PC2-2, PC2-21, PC2-22, PC2-23, PC2-3, PC2-4, PC2-8, PCS-2, PCS-7, PEB1-10, PEB1-11, PEB1-13, PEB1-16, PEB1-4, PEB1-7, PEB2-12, PEB2-4, PFA-2, PFA-8, PG-23, PG-25, PGG1-11, PGG1-14, PGG1-4, PGG1-7, PGG1-9, PGG2-2, PGG2-4, PM-11, PM-12, PM-25, PM-7, PMN1-1, PMN1-4, PMN1-6, PMP-18, PMP-4, POS1-11, POS1-12, POS1-15, POS1-4, POS2-1, POS2-2, POS2-9, PPC1-12, PPC1-13, PPC1-15, PPC1-18, PPC1-20, PPC1-23, PPC1-5, PPC1-8, PPM-13, PPM-3, PPM-5, PRG1-12, PRG1-13, PRG1-17, PRG1-20, PRG1-21, PRG1-3, PRG1-4, PRG1-5, PRG1-6, PRG2-11, PRG2-12, PRG2-19, PSB-25, PSB-7 OBD1-1, OGPR-2, OPC2-2, OPE2-1, OPE2-2, ORP-2, OUM-3, PB1-15, PBG1-11, PBS-17, PBS-2, PC2-14, PC2-15, PC2-22, PC2-8, PEB1-16, PEB1-18, PEB2-18, PG-3, PGG1-11, PGG2-4, PMN1-11, PMN1-6, POS1-12, POS2-13, PPC1-13, PPC1-22, PPC1-5, PRG1-13, PRG1-17, PRG1-20, PRG1-5, PSB-4
n-Alkanoic: OEB-1, PB1-6, PB2-9, PBG1-16, PBG2-6, PGG2-4, PM-4, PRG1-7
n-Alkanols: OEB-1, PB1-6, PB2-9, PBG1-11, PBG1-16, PBG2-6, PMP-18, PPC1-20, PPC1-23, PBG1-11
n-Alkene/*n*-Alkane: PM-25
n-Alkenes: PB2-13, PB2-4, PBG1-16, PM-3, PMP-4, POS2-1
n-Alkylthiophenes: POS1-11
n-Aromatic: PFA-2
n-Heterocycle: PM-8
n-Linked: PSB-18
n-Paraffins: PEB2-18 POS1-10
n-Pentadecylcyclopentane: PC2-20
n-Pivaloyl-*n*-Propyl: PMN2-6 PMN2-6
n-Propylcholestane: OGPR-3
N₂: OPE2-3, OSB1-3, PB1-7, PBG1-6, PG-1, PG-14, PG-24, PG-28, PG-4, PG-8, PMN1-3, PMN2-10, PMN2-2, PPC1-27, PPM-3, PSB-1, PSB-4
Na-Acetate: OMN-3
Na-Homoionic: PMN1-1
Na-Smectite/Humic: PMN1-1
Na-Smectites: PM-11
Na: PBG2-11 PEB1-12 PEB2-12, PMP-2 PGG2-9
Naftaplin: PBS-11
Namibian: PPC1-20
Namur: PRG2-16
Nankai: OB2-1, OP7-3, PB2-9, PMP-21
Nannochloris-Like: PMP-4
Nannochloropsis: PB1-11
Nannofossil: OPE2-2, PPC1-27 PC2-16
Nano-: PC-4
Nano-EA-IRMS: PMN2-2
Nano-Tubes: PBG2-7
Nanofibers: PBG2-7
Nanopores: PC-4
Nanoscopically-Amorphous: PM-12
Napanskaya: PBS-8
Naphtenoaromatics: OPG-1

- Naphthalene/Phenanthrene: PGG2-5 PMN1-10
 Naphthalenes: OP3-4, PC2-22, PEB2-12, PEB2-4, PGG2-5, PRG1-1 PBS-17 PM-27 OB3-2, PB1-12, PEB2-12, PEB2-13, PEB2-8, PGG1-15, PGG1-8, PGG2-5, PGG2-6, PM-7, PMN1-10, PRG2-2 POS2-1 PBG1-7, PBS-10, PSB-3 PGG2-5 PBS-10, POS2-2 PB2-4, PEB1-12, PGG2-6, PMN1-4, POS2-2, PPM-3 PRG1-10 PRG1-6
 Naphthides: PGG1-12
 Naphtho[12-B]thiophene: PB1-12
 Naphtho[21-B]thiophene: PB1-12
 Naphtho[23-B]thiophene: PB1-12
 Naphtho[B]thiophenes: PB1-12
 Naphthoic: PBG2-3, PRG2-2
 Naphthylbenzo[B]thiophenes: PB1-12
 Napo: PRG2-5, PRG2-6
 Nappes: POS2-11
 Natural-gas: PBG1-1
 Nausodis: PSB-25
 Navarra: PM-14
Navicula-Species: OP2-1 PB2-18
 Nebraska: PMP-19
 Necromass: PBC-3, PCS-10
 Negev: PM-12, POS1-1, POS1-2
 Negra-Lomitas: PRG2-8
 Neo-Assyrian: PFA-5
 Neocomiano: OPS1-1
 Neof ormation: OP2-3
 Neogene: PB2-1, PBS-2, PBS-9, PC-10, PC-2, PG-23, PG-24, PG-4, POS2-1, PPM-8
 Neolithic: PBC-1, PFA-7
 Neoproter oic: OGPR-3
 Neoproterozoic-Early: OGPR-3
 Neoproterozoic: OB1-1, OGPR-3, OP4-4, PB1-20, PB2-19, PB2-3, PBG2-2, PBG2-9, PM-19, PPC1-7 OOS-1
 Nepal: PFA-2
 Neritic: PB2-21
 Ness: OP4-2, PGG2-9, PRG2-15
 Net-To-Gross: ORP-1
 Netherlands: OP5-3
 Neunlist: OP4-2
 Neuquina: PRG2-8
 Newfoundland: PBS-3
 Niño: OM-3, PBG2-10, PC2-19 PBG2-10 PC2-19, PC2-27
 Niagaran: PB2-14
 Niaqornaarsuk: PGG1-10
 Nickel-Iron-Ore: PGG1-4
 Nickel: OB3-2, OGPR-1, PB2-14, PGG1-12, PRG2-8 OGPR-1, PBG2-2, PEB2-12, PGG1-12, PGG1-4
 Niger: OP4-3, PGG2-1, PPC1-19
 Nigeria: OP3-4, OP4-3, PGG2-1
 Nigerian: OP4-3, PGG2-1
 Nile: PFA-4, PFA-8, PG-23, PMP-17
Nipponothracia: PMP-5
 Nishishichitou: PPC1-15
 Nitracline: OB1-3
 Nitrate: OB1-3, OPE2-3, OSB1-1, PB1-7, PGG1-2, PMN1-8, PPC1-9
 Nitrification: PMP-9
 Nitrile: PBG1-16 PFA-2
 Nitrite: pb1-7, PMN1-3, PMN1-8
 Nitrogen-bearing: PPM-10
 Nitrogen-containing: OM-2, PB1-17, PM-2, PM-8, POS1-9
 Nitrogen-exposed: PPM-13
 Nitrogen-fixing: PPC1-11, PPC1-9
 Nitrogen-macromolecule: PM-8
 Nitrogen-proton: OM-2
 Nitrogen-rich: PPC1-10
 Nitrogen-shielded: PPM-13
 Nitrogen: OM-1, OM-2, OP4-2, OP6-4, OPE2-3, PM-8 OPG-1, OSB1-1, OSB2-2, PB1-17, PB1-6, PB1-7, PB2-8, PBC-11, PBC-12, PBC-3, PBC-8, PBG1-5, PBS-1, PBS-5, PC-6, PC2-9, PEB1-4, PEB2-11, PEB2-3, PG-14, PG-23, PM-18, PM-2, PM-24, PM-26, PM-8, PMN1-3, PMN1-8, PMN2-10, PMN2-2, PMN2-6, PMP-12, POS1-10, POS1-9, PPC1-11, PPC1-27, PPC1-9, PPM-10, PPM-11, PPM-13, PPM-3, PPM-6, PRG1-1, PRG2-14, PSB-20 OM-2
 Nitrogenous: PPC1-9, PSB-20
 Niuzhuang: PPM-9
 NMR: OM-2, OM-3, OP5-4, OSB1-2, OSB1-3, OSB2-2, PB1-14, PB2-15, PB2-2, PB2-6, PBC-13, PBC-14, PBC-2, PBC-3, PBC-5, PBC-6, PBC-8, PBC-9, PBG2-3, PC2-11, PCS-4, PCS-9, PEB1-12, PGG2-14, PM-1, PM-16, PM-18, PM-2, PM-23, PM-24, PM-8, PRG2-4, PSB-12, PSB-13, PSB-18, PSB-9 PMN2-7
n,n-Dimethyl: PBG1-16
N,N-Dimethyl: PM-2, PM-24
 No-Till: PCS-7 PCS-12
 Nonacosanol: PBG2-6
 Nonadecan-10-Ol: PFA-2
 Nonadecanoic: PEB2-19
 Nor-Sterols: PB1-10
 Norabietane: OB1-2
 Norfarnesane: OB3-2
 Norhopane: PBS-10, PC2-21, PRG2-12 PBS-10, PEB2-19
 Noriakianum: PSB-9
 Norian-Rhaetian: POS2-6
 Norlupanes: OPI-2
 Norpristane: PC-9, PC2-21 PSB-4
 Norway: OBD1-1, OPS2-2, OSB2-2, PBS-18, POS1-6
 Norwegian: OPG-3, OPS2-2, PBS-15, PBS-18, PG-20, PGG2-9, PMN2-5, POS1-16, PRG2-11, PRG2-14
 NSO-Compounds: PEB2-13, PEB2-14, PMN2-11, PPC1-5
 NSO-Rich: PRG2-18
 NSO: OBD1-2, OBD1-3, PBS-5, PC-4, PC2-21, PEB2-11, PG-22, PGG1-5, POS1-15, PRG1-11, PRG2-18, PRG2-19, PRG2-6, PSB-7

- Nuccaleena: PPC1-7
 Nutrient: OP4-3, OP5-3, OPE2-3, PB1-11, PB2-17, PB2-8, PC2-24, PC2-3, PEB1-4, PMN1-8, PMP-1, PMP-12, PPC1-18, PPC1-17, PPC1-3, PPC1-8, PRG2-5
- O**
- OM-1, OP1-1, OP4-3, PB1-7, PB2-8, PEB1-4, PMP-13, POS1-16, PPC1-2, PSB-2
o-Alkyl: OSB2-2, PBC-3, PBC-8, PBC-9, PCS-4, PMP-6, PSB-12, PSB-13, PSB-18
o-Containing: PGG2-6, PSB-18
o-Methylterphenyl: PB2-5
o-Terphenyl: PB2-5
o-Tolylalkanes: PGG1-11
o-Xylene: POS2-1
 Oak: OM-3, PB2-6, PCS-2, PCS-5, PSB-15, PSB-18
 Oasis: PMP-23
 Ocean-Atmosphere: PC2-26, PPC1-6
 Ocean-Climat: PC2-19
 Ocean: OP7-2, OPC2-3, PB1-5, PB1-7, PB2-20, PC2-24, PMN2-2, PMP-1, PPC1-16, PPC1-2, PPC1-4, OBD2-1, OGPR-3, OMN-2, OP4-1, OPC1-1, OPC2-3, OPE1-3, OPE2-3, OUM-1, PB1-15, PB1-5, PB1-7, PB2-20, PBG1-13, PBG1-14, PBG1-4, PBG1-6, PBG2-5, PBS-18, PBS-3, PC-10, PC2-22, PC2-23, PC2-24, PC2-27, PGG2-1, PMN2-1, PMP-11, PMP-16, PMP-21, PMP-23, PPC1-1, PPC1-10, PPC1-15, PPC1-16, PPC1-18, PPC1-19, PPC1-2, PPC1-20, PPC1-21, PPC1-27, PPC1-4, PPC1-7, PPC1-9
 Oceanic: OM-2, OPC2-4, OPE2-3, PB1-5, PB1-7, PB2-18, PB2-9, PBG1-13, PBG2-1, PBG2-6, PBG2-9, PBS-12, PBS-3, PC2-12, PC2-16, PC2-19, PC2-21, PC2-27, PC2-6, PMP-16, PPC1-16, PPC1-18, PPC1-2, PPC1-27, PPC1-6, PPC1-7
 PBG2-1, PC2-13
 Oceanography: PM-6, PM-6, PEB2-5, PPC1-20
 Octadec-9-Enoic: PFA-3
 Octadeca-9,12-Dienoic: PB2-1
 Octanol-Water: PEB2-9
 Octatriaconta-9E16E23E-Trien-3-One: OP7-2
 Offshore: OB2-1, OBD1-1, OBD1-2, OGC-4, OP1-2, OP4-2, OP4-4, OUM-1, PB2-20, PBS-14, PBS-18, PBS-23, PBS-3, PBS-5, PBS-6, PBS-9, PC-10, PC2-22, PEB1-10, PEB1-16, PEB1-2, PEB2-12, PEB2-5, PG-23, PGG2-7, PM-4, PM-8, PMN1-5, POS2-13, POS2-4, POS2-8, PPC1-1, PPC1-21, PPM-1, PPM-11, PRG1-14, PRG2-10, PRG2-18
 Oil-and-Gas: OPS1-2, PGG1-4, POS1-9, PPM-3, PRG1-5, PRG1-6, PPM-3, POS2-13
 Oil-associated: PPM-11
 Oil-based: PEB1-10, PRG2-4
 Oil-bearing: OPS1-3, PGG2-6, PMN1-2, POS2-13, POS2-2, POS2-9, PRG2-16, PSB-25
 Oil-cemented: PBS-6
 Oil-charging: PBS-16
 Oil-condensate: PRG2-7
 Oil-cracking: OGC-1, OPS1-3
 Oil-degrading: PEB1-4
 Oil-derived: PG-25
 Oil-fired: PEB1-14
 Oil-gas: PBS-2, PG-1, PG-2, PGG1-4, PPM-6, POS2-13
 Oil-generation: PGG2-16, POS2-9, PPM-6, POS2-13, POS2-2, POS2-7, POS2-9, PPC1-1, PB1-21, POS1-4
 Oil-like: OBD1-3, PPM-3
 Oil-mineral: PRG2-18
 Oil-mixing: PRG1-9
 Oil-oil: OP3-3, PG-2, PRG1-13
 Oil-polluted: PEB1-11
 Oil-producing: PBS-10, PGG2-9, POS2-2, PRG1-14
 Oil-prone: OPS2-2, PBS-22, PG-1, PG-21, POS2-10, PPM-2
 Oil-proneness: PC-3
 Oil-rich: POS2-10
 Oil-seep-Source: PPM-8
 Oil-shale: POS1-10
 Oil-show: PGG2-10
 Oil-source: OOS-1, OP1-2, OP3-3, OPS2-2, OUM-1, PBS-1, PBS-20, PBS-21, PBS-9, PG-2, PGG2-5, PPM-4, PRG1-13, OUM-1, PRG1-20
 Oil-spills: PEB1-14
 Oil-to-oil: PRG1-3
 Oil-to-source: PPM-9, PRG1-3
 Oil-water: OP6-3, PGG2-9, POS1-16, PRG1-17, PRG1-2, PRG2-15
 Oil-window: PBS-8, PG-20
 Oil-yieldS: PPC1-17
 Oil/condensate: OUM-2
 Oil/fat: PFA-4
 Oil/gas: POS1-16
 Oil/oil: OUM-1, PRG1-20
 Oil: OOS-1, OBD1-1, OBD1-2, OBD1-3, OBD2-1, OEB-2, OGC-1, OGC-3, OGC-4, OMN-1, OOS-2, OOS-3, OP1-1, OP1-2, OP2-3, OP3-3, OP3-4, OP4-3, OP5-2, OP5-4, OP6-3, OP7-4, OPG-1, OPG-2, OPG-3, OPS1-1, OPS1-2, OPS1-3, OPS2-1, OPS2-2, OPS2-3, ORP-1, ORP-2, OUM-1, OUM-2, OUM-3, PB1-12, PB1-16, PB1-22, PB2-12, PB2-14, PB2-4, PBG1-1, PBG1-12, PBG2-4, PBS-1, PBS-12, PBS-13, PBS-14, PBS-15, PBS-16, PBS-17, PBS-18, PBS-19, PBS-2, PBS-20, PBS-21, PBS-22, PBS-23, PBS-24, PBS-26, PBS-3, PBS-5, PBS-6, PBS-7, PBS-8, PBS-9, PC-10, PC-3, PC-5, PC-7, PC2-25, PEB1-1, PEB1-10, PEB1-11, PEB1-16, PEB1-18, PEB1-2, PEB1-4, PEB2-11, PEB2-13, PEB2-14, PEB2-17, PEB2-18, PEB2-19, PEB2-20, PEB2-4, PEB2-5, PFA-2, PFA-5, PFA-7, PG-1, PG-11, PG-13, PG-14, PG-15, PG-16, PG-17, PG-18, PG-2, PG-21, PG-22, PG-23, PG-24, PG-25, PG-3, PG-5, PG-7, PGG1-1, PGG1-10, PGG1-11,

- PGG1-12, PGG1-13, PGG1-14, PGG1-15, PGG1-2, PGG1-3, PGG1-5, PGG1-6, PGG1-9, PGG2-1, PGG2-10, PGG2-11, PGG2-12, PGG2-14, PGG2-15, PGG2-16, PGG2-2, PGG2-3, PGG2-4, PGG2-5, PGG2-7, PGG2-8, PGG2-9, PM-1, PM-14, PM-9, PMN1-11, PMN1-2, PMN1-5, PMN1-6, PMN1-7, PMN1-9, PMN2-11, PMN2-3, PMN2-4, PMN2-8, PMN2-9, PMP-17, POS1-1, POS1-10, POS1-11, POS1-12, POS1-14, POS1-15, POS1-16, POS1-2, POS1-5, POS1-9, POS2-1, POS2-10, POS2-11, POS2-12, POS2-13, POS2-14, POS2-15, POS2-2, POS2-6, POS2-7, POS2-8, POS2-9, PPC1-1, PPC1-14, PPC1-17, PPM-1, PPM-10, PPM-11, PPM-12, PPM-13, PPM-14, PPM-15, PPM-2, PPM-3, PPM-4, PPM-5, PPM-7, PPM-8, PPM-9, PRG1-11, PRG1-12, PRG1-13, PRG1-14, PRG1-15, PRG1-16, PRG1-17, PRG1-18, PRG1-19, PRG1-2, PRG1-20, PRG1-21, PRG1-3, PRG1-4, PRG1-5, PRG1-6, PRG1-7, PRG1-8, PRG1-9, PRG2-1, PRG2-10, PRG2-11, PRG2-12, PRG2-13, PRG2-14, PRG2-15, PRG2-16, PRG2-17, PRG2-18, PRG2-19, PRG2-2, PRG2-3, PRG2-4, PRG2-5, PRG2-6, PRG2-7, PRG2-8, PRG2-9, PSB-25, PSB-4, PSB-9, PBS-17, PRG2-5, OB2-2, OBD1-2, OBD1-3, OBD2-1, OEB-2, OGC-1, OGPR-3, OOS-2, OOS-3, OP1-2, OP3-3, OP3-4, OP4-3, OP5-2, OP6-3, OP7-4, OPG-1, OPG-2, OPG-3, OPS1-1, OPS1-2, OPS1-3, OPS2-1, OPS2-3, ORP-2, OUM-1, OUM-2, OUM-3, PB1-10, PB1-16, PB1-5, PB2-12, PB2-14, PB2-16, PB2-3, PB2-4, PBS-1, PBS-12, PBS-13, PBS-14, PBS-15, PBS-16, PBS-17, PBS-18, PBS-19, PBS-2, PBS-21, PBS-23, PBS-24, PBS-3, PBS-6, PBS-8, PBS-9, PC-10, PC-4, PC-5, PEB1-1, PEB1-11, PEB1-12, PEB1-2, PEB2-17, PEB2-4, PFA-6, PG-17, PG-2, PG-22, PG-25, PG-3, PGG1-1, PGG1-10, PGG1-11, PGG1-12, PGG1-14, PGG1-15, PGG1-2, PGG1-3, PGG1-5, PGG1-6, PGG1-7, PGG1-8, PGG1-9, PGG2-1, PGG2-10, PGG2-11, PGG2-12, PGG2-13, PGG2-14, PGG2-15, PGG2-16, PGG2-2, PGG2-4, PGG2-5, PGG2-6, PGG2-7, PGG2-8, PM-1, PM-19, PM-9, PMN1-11, PMN1-4, PMN1-6, PMN1-9, PMN2-11, PMN2-4, PMN2-5, PMN2-9, POS1-1, POS1-12, POS1-15, POS1-2, POS1-3, POS1-4, POS1-9, POS2-11, POS2-13, POS2-15, POS2-2, POS2-6, POS2-8, POS2-9, PPC1-4, PPM-10, PPM-13, PPM-14, PPM-15, PPM-7, PPM-9, PRG1-1, PRG1-11, PRG1-13, PRG1-14, PRG1-16, PRG1-17, PRG1-18, PRG1-19, PRG1-2, PRG1-20, PRG1-21, PRG1-3, PRG1-4, PRG1-5, PRG1-6, PRG1-7, PRG1-8, PRG1-9, PRG2-10, PRG2-11, PRG2-12, PRG2-14, PRG2-15, PRG2-16, PRG2-18, PRG2-19, PRG2-2, PRG2-20, PRG2-21, PRG2-3, PRG2-4, PRG2-5, PRG2-6, PRG2-7, PRG2-8, PRG2-9, PSB-25
- Oilfield: OBD1-2, OEB-2, PBS-12, PBS-21, PBS-6, PGG1-3, PGG2-9, PRG1-14, PRG1-7, PRG2-11, PGG2-16, PGG2-6, POS2-2, OBD1-2, OPS1-2, PBS-21, PBS-9, PGG2-9, PRG1-5, PRG1-7
- Oils/biogenic: OP4-3
- Oils/condensates: PRG1-21
- Oily-resin: PGG1-13
- Ojay: PG-10
- Okenone: PC2-19
- Okha: PGG2-16
- Okhotsk-chukotsk: PBS-2, PBS-8
- Okhouchi: PB1-15
- Oki-trough: PC2-12
- Okinawa: PB2-17
- Oklahoma: PMP-10, PB1-1, POS1-13
- Okonek: PBG1-2
- Okruznoe: PGG2-11
- Olah: PGG2-3
- Oleanane/C₃₀-hopane: PGG1-14
- Oleanane/hopane: OOS-3, PPM-7
- Oleanane: OOS-3, OPS2-3, PBS-17, PBS-5, PC2-11, PGG2-1, PGG2-2, POS2-8, PPC1-14, PRG1-13, PRG1-16, PRG2-12
- OOS-3, OP1-2, PGG1-10, PGG2-1
- Oleananes/Lupanes: PGG1-10
- Oleandienes: PPC1-15
- Oleanenes: PPC1-15, PB2-6
- Oleanoidal: PPC1-15
- Oleanoids: OP1-2
- Oleanonic: PFA-6
- Olefins: PB2-4, PGG1-4, PMP-4, OP1-2, PM-18, PM-21, PMN1-5
- Oleic: PB2-1, PMP-4
- Oleophilic: PEB2-4
- Oligocaenica: PB2-18
- Oligocene-Eocene: POS1-7
- Oligocene-Miocene: PBS-7, PB1-10
- Oligocene: OB2-2, OBD2-2, OPE2-1, PB1-10, PB2-18, PBS-24, PC-10, PC-6, PC2-11, PG-3, PM-28, POS1-7, POS2-11, POS2-12, POS2-15, POS2-5, POS2-8, PPM-8, PRG2-12, PRG1-16
- Oligomers: OB1-1
- Oligotrophic: PM-11, PMP-10, PPC1-11, PPC1-28
- Olive: PFA-5
- Oliver: POS1-13
- Olivine: PBG1-15
- Olivinite: PGG1-4
- OM Organic-Matter: PBG1-1, PC2-1, OB3-2, OBD2-2, OPE1-3, OPS1-2, OSB1-2, PB1-19, PB1-22, PB2-13, PB2-4, PBC-13, PBC-7, PBC-8, PBG1-14, PBG1-2, PBG1-7, PBG1-8, PBG1-9, PBG2-13, PBG2-14, PBG2-4, PBS-10, PBS-20, PBS-2, PC-12, PC2-24, PC2-3, PC2-8, PCS-14, PCS-9, PEB2-18, PG-14, PGG1-11, PGG1-12, PGG2-11, PM-1, PM-10, PM-12, PM-18, PM-2, PM-25, PM-27, PM-6,

- PM-8, POS1-11, POS2-13, POS2-9, PPC1-18, PPC1-25, PPC1-27, PPC1-7, PPC1-8, PPM-3, PRG1-6, PSB-13, PSB-16, PSB-2, PSB-20, PSB-7
- Omalley: PEB1-14
- Oman: OOS-1 OGPR-3, OP3-4, PB2-3, PM-19
- Ombilin: POS1-12
- Ombrotrophic: OPC2-2
- Onnagawa: PPC1-6
- Onshore: OP4-3, PBS-18, PBS-6, PBS-9, POS2-12, POS2-8, PPC1-4, PRG1-14, PRG2-10, PRG2-20
- Ontario: OP2-4, PC2-25, PRG2-5
- OOIP: PRG1-2
- Oolitic: PBS-12
- Ophiolites: PBG1-16
- Ophiomorpha*: PC-5
- Ordos: PG-5, PG-6
- Ordovician-Silurian: OP3-3
- Ordovician: OPS1-3, PBS-18, PBS-21, PC2-26, PEB2-17, PG-4, PG-6, POS2-13, PPM-6, PRG1-9, PRG2-19, PRG2-21, PSB-25
- Ore-bearing: PBG1-2
- Ore: PC2-20 PGG2-9 POS1-4 PBG2-11, PGG1-4
- Oregon: OP1-2, PBG1-11, PCS-11
- Organic-Sulfur: PG-14 OEB-2
- Organo-mineral: OM-2, OSB1-3, PBG2-11, PCS-1, PCS-5, PCS-9, PM-11, PSB-12, PSB-5 PCS-3 PBC-12
- Organochlorine: PEB1-5
- Organofacies: OGC-3, ORP-2, PC-6, POS1-10
- Organogenic: PPC1-7
- Organonitrogen: PEB2-12
- Organosulfur: PB2-1
- Organosulphur: PC-11, PRG1-11
- Orgueil: PM-16
- Orogen: PBS-17
- Orogenic: POS1-13
- Orphan: OB2-3
- Ostreatus: PM-17, PMN2-7
- Oswiecim: PEB2-1
- Otabbong: PEB2-2
- Otago: PBG1-4
- Outcrop: OPE2-3, PBS-6, PBS-8, POS2-3, POS2-7, POS2-9, PRG2-6 OPE2-3, PC2-17, PEB2-18, PFA-7, PPC1-4 PC2-11, PMN2-8, POS1-11, POS1-13, POS2-13, POS2-14
- Overmaturation: PB1-21, PM-7 OPS2-1, PB1-22, PG-24, PM-7, PRG2-4
- Oxalic: PBG1-16
- Oxaloacetate: OSB2-3
- Oxaphosphetane: PB2-3
- Oxford: PBS-6
- Oxfordian-Kimmeridgian: PPC1-1
- Oxfordian: OB1-2, PC2-4, PPM-4
- Oxide/hydroxides: PB2-13
- Oxide: OGPR-1, OGPR-2, PB2-3, PBG1-5, PGG1-13, PSB-12
- Oxisol: PCS-11, PSB-21
- Oxo-fatty: PFA-3
- Oxy/hydroxides: PM-26
- Oxycline: OB1-3, PC2-8
- Oxygenation: PB2-10
- Oxyhydroxides: PCS-9
- Oyster: PEB1-12, PMN2-7
- Ozone: PBC-11, PM-21

P

- p*-Methoxyphenol: PFA-2
- p*-Methylphenol: PFA-2
- p*-Methyphenol: PFA-2
- p*-Nitrophenol: PMP-23
- p*-Nitrophenyl: PMP-23
- p*-Terphenyls: PB1-8
- p*-Tr: OPE2-3, PB1-5, PPC1-4
- p*-Xylene: POS2-1
- p*-Xylene+: POS2-1
- Pacific: OB2-2, OEB-1, OPC2-4, PB2-18, PB2-9, PBG1-14, PBG1-4, PBG2-10, PBG2-12, PC-10, PC2-19, PC2-27, PMP-23, PPC1-15, PPC1-27
- Packstone: PRG2-1 PRG2-1
- Paddy: PCS-13
- Padul: PPC1-13
- Paget: PSB-19
- PAH-Analysis: PEB2-8
- PAH-Degrading: PEB2-16
- PAH-Loaded: PEB2-8
- PAH-Ratio: PEB2-14
- PAH/hopane: OP1-1
- PAH/PCN: PEB2-8
- PAH: OB3-2, OEB-1, OPC1-2, PC2-17, PC2-22, PEB1-1, PEB1-10, PEB1-14, PEB1-16, PEB1-17, PEB1-18, PEB1-5, PEB1-7, PEB2-10, PEB2-13, PEB2-14, PEB2-16, PEB2-8, PM-27, PMN1-10 OEB-2, OGC-1, PB2-16, PB2-5, PBG2-10, PBG2-7, PC2-22, PEB1-1, PEB1-10, PEB1-13, PEB1-14, PEB1-16, PEB1-17, PEB1-18, PEB1-3, PEB1-5, PEB1-6, PEB2-10, PEB2-13, PEB2-14, PEB2-16, PEB2-4, PMN1-10, PRG2-4
- Pahoee: PSB-3
- Pakistan: OPE2-2, PFA-2, PM-28
- Palace: PFA-9
- Palaeo-CO₂: PPC1-2
- Palaeo-evaporation: PC2-15
- Palaeo-indicators: PPC1-2
- Palaeo-oil: PBS-16
- Palaeo-petroleum: PBS-16
- Palaeo-reservoirs: OPS1-3
- Palaeo-sea: PPC1-20
- Palaeo-SSS: OPC1-1
- Palaeo-temperature: PGG2-2
- Palaeobasin: POS1-11
- Palaeoceanic: PPC1-2
- Palaeoceanographic: PPC1-20
- Palaeocene-Eocene: PC2-10 PB1-21, PC2-10
- Palaeocene-Gercus: PFA-7
- Palaeochannels: PEB1-8

- Palaeoclimate: PC2-15, PC2-9, PM-17, PSB-19
 PPC1-7 PB1-4, PC-9, PC2-1, PC2-11, PPC1-20, PPC1-22 OP4-1, PC2-14, PC2-19, PPC1-26 OB1-2, OPC2-1, PC2-14, PC2-16, PC2-5, PPC1-15, PPC1-17, PPC1-26, PPM-15 PC-9
 Palaeodepositional: OP2-1, PC-11
 Palaeoenvironmental: OB3-1, OP3-1, OPC2-2, OPE2-3, PB1-11, PB1-4, PB2-10, PC2-11, PC2-17, PC2-18, PC2-20, POS1-12, PPC1-13, PPC1-22, PPC1-25, PPC1-6, PPC1-8 PPC1-5 PB1-19, PB1-20, PB2-13, PC-9, PC2-14, PC2-2, PC2-7, PMP-9 POS1-7
 Palaeoenvironments: PC-11, PC2-11, PC2-20, PPC1-14, PPC1-25, OP2-1, PC2-11, PPC1-6 POS2-3, PRG1-3 PC2-21, PM-4, POS1-7, PRG1-3, PRG2-6
 Palaeogene: PGG1-10
 Palaeogeography: POS2-8
 Palaeohydrology: PC2-15
 Palaeolatitute: PB1-5
 Palaeopasteurisation: PBS-6 PRG2-5 PC-6, PMP-13
 Palaeotopographic: PPM-4
 Palaeozoic: PBS-15, PBS-16, PBS-18, PBS-26, PC-3, PC-9, PG-2, PM-7, PSB-25
 Paleo-carbon: PMP-12
 Paleo-davis: PBS-3
 Paleo-environmental:
 Paleo-erosion: PBG1-12
 Paleo-geographic: PBS-22
 Paleo-indicators: PPC1-16
 Paleo-lake: PPC1-17
 Paleo-latitudes: OP3-3 OPC2-4
 Paleo-longitudes: OP3-3
 Paleo-pools: PPM-6
 Paleo-pressure: ORP-1, PG-6
 Paleo-redox: PBG2-8
 Paleo-salinity: OPC1-1
 Paleo-shoreline: PBS-22
 Paleo-SST-Reconstructions: OPC2-3
 Paleo-SST: PBG2-10
 Paleo-Ssts: OPC2-3
 Paleo-topographic: PBS-9 PBS-22
 Paleo-tropics: OPC2-3
 Paleoatmospheric: OPC1-2
 Paleobathymetric: POS1-7
 Paleobiodiversity: PC2-5
 Paleobiological: OP2-4
 Paleobotanical: OB1-2, PC2-5
 Paleocceanography: OP7-2 PPC1-16 OPC1-1, PM-26 OPC2-1, PC2-16, PPC1-16
 Paleocene-eocene: PBS-8, POS2-4 OPC2-4
 Paleocene-oligocene: POS2-4
 Paleocene: OP3-3, PBS-23, PBS-8, PC2-10, PGG1-10, POS1-12, POS1-7, POS2-13, POS2-4, PPC1-18
 Paleochemotaxonomy: OB1-2, PC2-5 PB1-15
 Paleodensities: OPC1-1
 Paleodiversity: OB1-2
 Paleoecology: PB2-21, PPC1-5 OP3-1 PC2-11 PMP-1
 Paleoequator: OPC2-3
 Paleofacies: POS2-3
 Paleofires: PC2-18
 Paleoflora: OB1-2
 Paleogene-retaceous: PC2-16
 Paleogene: OPS2-2, PB1-8, PBS-2, PBS-8, PC-10, PGG2-16, POS1-7, PPM-8
 Paleogeography: PB2-12, PBS-3, POS2-8 OP3-3, PBS-26, PBS-3, POS2-8, PPC1-17, PPC1-18
 Paleohydrology: PC2-6 PBG2-1
 Paleolake: PGG1-1
 Paleolimnology: PPC1-17
 Paleomagnetic: PMP-18, POS1-13
 Paleomap: OP3-3
 Paleontological: OB1-2, PC2-21, PPC1-14
 Paleoproterozoic: PC2-25
 Paleoreconstruction: PPC1-28
 Paleoredox: POS2-1
 Paleosalinities: PBG2-1
 Paleosea: PBS-10
 Paleosoils: PC2-2 OPE2-2
 Paleostuctural: PBS-26
 Palaeothermometry: PMP-1, OP7-2, OPC1-3, PBG1-12, PC-8, PPC1-28, PRG2-19
 Paleotemperatures: PC2-3OP7-2, OPC2-3, PBG1-12, PC-8, PPC1-28
 Paleothermometer: OPC1-3, POS2-15 PC2-13 POS2-15 OPC2-3, OPC2-4
 Paleovalley: PB2-13
 Paleovegetation: OB1-2, PC2-5
 Paleowater: PPC1-4
 Paleozoic-Age: PEB2-17
 Paleozoic-Mesozoic: PGG1-7
 Paleozoic: OPS1-3, PB1-1, PB2-8, PBG1-14, PBS-21, PBS-3, PBS-9, PC-9, PG-6, PGG1-11, PGG1-12, PGG2-6, PPM-6, PRG1-5, PRG1-6, PRG2-5, PSB-25
 Palestine: OP6-1, PBG2-7
 Palhol: PC2-2
 Palladium-based: PMN1-8
 Pallasser: OGC-2
 Palmes: PSB-20
 Palmitamide: PBG1-16
 Palmitic: PBG1-16, PFA-2, PFA-3, PFA-8, PMP-4
 Palmyride: PBS-11
 Palynofacies: PB1-5, PBG1-9, POS1-7, POS2-3, PPC1-4
 Palynology: PBS-3, PC2-5, PC2-6, PPC1-13 OB1-2, PBS-3, PM-12, PM-5, POS1-7, POS2-3 PB1-1
 Palynomorphous: PBS-7 POS1-7, POS2-8
 Palynomorphs: PB1-1, PBG1-10, PBS-3, POS1-7, POS2-3
 Pamir: PFA-2
 Pampelone: PFA-6
 Pan-Arctic: PCS-6
 Pangaea: OPE2-3

- Pannonian: PB2-16, PG-1, PG-24, PGG1-14, PGG1-15, PGG2-6
- Papaloapan-Veracruz: POS2-4
- Papillosum: OP5-3
- Papua: PGG1-10
- Para-coumaric: PM-21
- Paraffin-naphthenic: PRG2-12
- Paraffinic: ORP-2
- Paraffinless: POS2-2
- Paraffins: OBD1-2, PBS-2, PC2-21, PEB2-18, PRG1-6, PRG2-3 PB2-4, PGG2-6, POS1-10, POS2-2, PRG2-12 PC-5, PGG2-15, PGG2-6, PM-24, POS2-2 PRG1-10 PRG1-9, PRG2-12
- Paragenesis: PPC1-7
- Paralic-Deltaic: OP3-3
- Paralic: PC-5, POS2-8
- Paramagnetic: PM-18, PSB-12
- Paraná: PC2-21, POS1-15, POS2-3
- Paris: OB1-2, PBG1-12, PC2-4, PEB1-16, PM-24
- Passau: PSB-17
- Pasteurised: PBS-6
- Pasture: OP4-2, PSB-6
- Patchawarra: PBS-16, PRG2-16
- PCB: PEB2-2 PEB1-5, PEB2-8
- PCN: PEB2-8
- Peat-Mineral: PEB1-11
- Peatlands: OP5-3, PM-10 OMN-2, PC2-10, PM-10, PPC1-24 PPC1-24 PM-10
- Peats: OMN-2, OP4-2, OPC2-2, PB1-15, PC-3, PC-6, PMP-13 Peat: OP5-3, OPC2-2, OSB1-3, PB1-14, PC-10, PC-12, PC-3, PC-6, PC2-17, PC2-18, PEB1-11, PEB2-18, PM-10, PMP-11, PPC1-13, PPC1-19, PPC1-22, PPC1-25, PSB-3, PSB-5
- Peaty: PC2-18
- Pedogenesis: OSB2-2
- Pedons: PSB-9
- Pelagic: PBS-14, PEB1-10, PEB1-16, PPC1-1, PPC1-19, PPC1-27, PPC1-7, PRG2-12
- Pelagophyte: PB2-8
- Pennsylvanian-Age: OGC-2
- Pennsylvanian: OGC-2, PRG1-9
- Penta-Chlorinated: PEB2-8
- Pentaaromatic: PB2-16
- Pentacarboxylic: PM-25
- Pentafluorobenzyl: PRG2-2
- Pentafluorobenzylbromide: PRG2-2
- Pentamethylcosane: PMP-17
- Pentamethylnaphthalenes: OP3-4
- Peptide-Like: PM-24
- Peptide/HA: OM-2
- Peptides: OM-2, PM-2 OM-2, OSB1-1
- Peptidoglycans: PM-8
- Per: OPE2-3, OSB1-1, OSB2-2, PB1-13, PB1-2, PC-2, PC2-10, PC2-20, PEB1-16, PEB1-18, PG-9, PGG1-7, PM-5, POS1-10, POS1-12
- Perborate: PBC-14, PM-25
- Perchlorate: PMN2-10
- Perialpine: PC2-11
- Permafrost: PCS-6, PMP-22
- Permian-Late: POS1-4
- Permian-Triassic: OPE2-3, PBS-16, PC2-26, PPC1-4 PB1-5
- Permian: OPE2-3, PB1-12, PB1-5, PB2-8, PBS-12, PBS-15, PBS-16, PC-3, PC-5, PC2-21, PGG1-7, PGG2-15, POS1-14, POS1-15, POS1-5, PPC1-4, PPM-12, PPM-6, PRG2-16
- Permo-Carboniferous: PG-6
- Permutation: OB1-1
- Peroxidase: PM-17
- Persian: PFA-4
- Persulfate: PM-25
- Perturbation: PC2-19
- Perturbations: OGPR-3, OPE2-3, PBC-14, PC2-19, PPC1-18, PPC1-27
- Peru: OB2-3
- Perylen: PEB1-17
- Perylene: PBG1-14, PBG1-2, PC2-17, PEB1-17, PGG2-5
- Perylenequinonic: PBC-14
- Pesticide: PEB2-1
- Pesticides: PCS-12, PEB1-3, PEB1-5, PEB2-1, PEB2-9
- Petrified: OPC1-2
- Petrochemical: PEB2-6, PMN2-11
- Petrochemistry: PMN1-2
- Petrogenesis: PB2-4
- Petrogenic: PBG2-13, PC2-22, PEB1-10, PEB1-14, PEB1-5, PPM-11
- Petrographic: PB1-16, PB1-21, PBS-7, PC-7, PC2-18, POS1-13, POS2-10, PPC1-7, PRG2-1, PRG2-18, PSB-4
- Petrographical: PC2-18, POS1-6, POS2-3, PPC1-25
- Petrographically: PMN1-2
- Petrography: PB1-22, PBS-7, PBS-8, POS2-5, PRG2-18
- Petrol: PGG1-13, PGG2-2
- Petroleum-Associated: PG-1
- Petroleum-Derived: PC2-22, PEB1-14
- Petroleum-Impacted: PEB2-11
- Petroleum-Petroleum: PPM-14
- Petroleum-Producing: OOS-1
- Petroleum/Source: PMN1-10
- Petroleum: OBD1-1, OBD1-2, OBD1-3, OBD2-1, OEB-1, OGC-1, OGC-3, OGPR-3, OMN-1, OOS-1, OOS-2, OOS-3, OP2-3, OP3-3, OP3-4, OP4-3, OP5-2, OP5-4, OP6-1, OP6-3, OP7-1, OP7-3, OP7-4, OPE2-1, OPG-1, OPG-2, OPG-3, OPS1-1, OPS1-3, OPS2-1, OPS2-2, ORP-2, OUM-1, OUM-2, OUM-3, PB1-10, PB2-12, PB2-14, PB2-5, PBC-14, PBG1-1, PBG1-10, PBG1-12, PBG2-4, PBS-1, PBS-11, PBS-12, PBS-15, PBS-16, PBS-17, PBS-18, PBS-22, PBS-23, PBS-24, PBS-3, PBS-6, PBS-7, PBS-8, PBS-9, PC-10, PC-3, PC-4, PC2-22, PC2-7, PEB1-1, PEB1-14, PEB1-4, PEB1-7, PEB2-10, PEB2-11, PEB2-17, PEB2-18, PEB2-19, PEB2-20, PEB2-4, PFA-4, PG-17, PG-2, PG-23, PGG1-1, PGG1-11, PGG1-12, PGG1-13, PGG1-2, PGG1-5, PGG2-1, PGG2-11, PGG2-

- 14, PGG2-3, PGG2-4, PGG2-6, PM-1, PM-6, PM-9, PMN1-10, PMN1-11, PMN2-11, PMN2-3, PMN2-4, PMN2-5, PMN2-8, POS1-1, POS1-10, POS1-14, POS1-16, POS1-2, POS1-3, POS1-4, POS1-8, POS2-10, POS2-11, POS2-12, POS2-13, POS2-4, POS2-5, POS2-7, PPC1-1, PPC1-4, PPM-10, PPM-11, PPM-12, PPM-13, PPM-14, PPM-15, PPM-2, PPM-4, PPM-5, PPM-8, PPM-9, PRG1-1, PRG1-11, PRG1-13, PRG1-14, PRG1-15, PRG1-17, PRG1-20, PRG1-21, PRG1-3, PRG1-4, PRG1-7, PRG2-10, PRG2-11, PRG2-13, PRG2-14, PRG2-15, PRG2-16, PRG2-18, PRG2-2, PRG2-20, PRG2-21, PRG2-3, PRG2-4, PRG2-7, PRG2-8, PRG2-9, PSB-25
- Petroleums: PBG2-4, PBS-18, PGG1-1, PGG2-6, PRG1-1, PRG2-13
- Petroliferous: OP6-3, PBG2-4, PGG1-12
- Petrologic: POS1-14
- Petrological: PBS-23, PC-12, POS2-10, POS2-8
- Petrologically: PBS-23
- Petrology: PBG2-4, PC-12, POS1-6, POS2-7
- Petromod: PBG1-12, PPM-12
- Petrophysical: PPM-4
- Phaeophyta: POS2-7
- Phaeovibrioides: OP2-1
- Phaeozem: PCS-3
- Phanerozoic: OOS-1
- Phanerozoic: OGPR-3, OP4-4, OPC1-2, PB1-16, PB1-5, PBS-9, PC2-25, PC2-8, POS1-13, PPM-15
- Pharmaceutical: PFA-4
- Pharmacology: PFA-2
- Phenanthrene/Anthracene: PB2-16
- Phenanthrene: OB3-2, OP6-1, PB1-12, PB1-21, PB2-16, PB2-5, PBG1-14, PBG2-4, PEB1-17, PEB2-16, PEB2-8, PGG1-15, PM-7, PMN1-10, PRG1-16
- Phenanthrenes: OP3-4, PC2-22, PEB2-4, PGG2-5, PRG1-1
- Phenantrene: PEB2-16, PGG2-5
- Phenantrenes: PGG2-5
- Phenantrenic: PGG2-5
- Phenathrene: PGG1-15
- Phenol-Like: PMN2-1
- Phenol: PB2-16, PBG2-7, PC2-1, PEB2-12, PFA-2, POS2-6, PPM-10, PSB-3, PSB-5
- Phenolic-Range: PM-15
- Phenolic: OB1-2, OP2-3, OSB2-1, PB2-6, PBG1-5, PBG2-7, PEB1-13, PEB1-9, PM-9, PRG2-14, PSB-1, PSB-2
- Phenols: OBD2-2, OP3-2, OSB2-1, PB2-16, PBC-10, PBG1-9, PC-2, PC2-1, PCS-4, PEB1-13, PEB1-9, PEB2-11, PEB2-12, PM-25, PM-4, PM-5, PM-9, PPM-10, PPM-13, PSB-3, PSB-5
- Phenyl: PB1-12, PB1-8, PC-2, PSB-3
- Phenylacetic: PBG2-3
- Phenylalkanes: PGG1-11
- Phenylamine: OP7-2
- Phenyldibenzo[B]Thiophenes: PM-7
- Phenyldibenzofurans: PB1-8
- Phenyldibenzothiophenes: PB1-12, PB1-8
- Phenylnaphthalenes: PB1-8, PM-7
- Phenylnaphtho[21-B]Thiophene: PB1-12
- Phenylnaphtho[23-B]Thiophenes: PB1-12
- Phenylnaphtho[B]Thiophenes: PB1-12
- Phenylphenanthrenes: PB1-8, PM-7
- Philippine: OP7-3, PB2-9
- Philippines: PEB1-5
- Philistia: PFA-5
- Philistine: PFA-5
- Phitane: PGG1-3
- Phodophyta: POS2-7
- Phoenix: OPE2-2
- Phos-1: PM-12
- Phosphatase: PMP-23
- Phosphatase: PMP-23
- Phosphate: OP6-4, PMP-21, PMP-23, PPC1-16, PPC1-2
- Phosphates: PSB-2
- Phosphatic: PBG2-11, PM-12
- Phosphatidyl: PMP-6
- Phosphatidylethanolamine: PMP-20
- Phosphatidylethanolamines: OB2-1
- Phosphatidylglycerides: PMP-20
- Phosphatidylglycerols: OB2-1
- Phosphatidylinositol-Archaeol: OB2-1
- Phosphatidylinositol-Glycosaminyl-Archaeol: OB2-1
- Phospho: PMP-20
- Phosphoenolpyruvate: OSB2-3
- Phosphogenesis: PM-12
- Phosphogenic: PM-12
- Phospholipid: OB2-1, OB3-1, OP2-2, OSB2-3, PMP-15, PMP-19, PMP-20, PMP-6, PMP-8, PSB-15
- Phospholipids: OB2-1, OMN-1, OP7-3, OSB1-1, PMP-13, PMP-20, PMP-21, PMP-6, PMP-8, PMP-9
- Phosphoric: PMP-23
- Phosphorite: OGPR-3, PM-12
- Phosphorites: PM-12
- Phosphorous: PEB1-4
- Phosphorus-Based: PB2-3
- Phosphorus: PB1-7, PEB2-3, PPC1-11
- Photic-Zone: PMP-1
- Photic: OP2-1, OPE2-3, PB2-8, PBG2-4, PBS-21, PC2-12, PC2-17, PC2-19, PC2-8, PMP-1, POS1-11, PPC1-11, PPC1-4, PPC1-7, PPC1-9
- Photoassimilates: PCS-8
- Photoautotroph: PPC1-23
- Photoautotrophic: PMP-12
- Photoautotrophs: OP5-1, OP6-4
- Photobacteria: PB2-4
- Photobacterium: PMP-6
- Photochemical: PEB1-9, PM-13
- Photodegradation: PEB1-9
- Photodiode: PB2-15
- Photoelectron: OP5-4, PM-8
- Photograph: PBG2-4, PPC1-27

- Photoinhibition: PB2-8
 Photolithotrophic: OP2-1
 Photolytic: PBG2-7, PEB2-6
 Photomicrograph: PBG1-10
 Photon: PSB-16
 Photonic: PBG2-11, PRG2-18
 Photooxidation: PEB1-9
 Photoprotective: PB2-8
 Photoreactions: PEB1-9
 Photoredox: PEB1-9
 Photoreduction: PEB1-9
 Photosynthate: PBG2-1
 Photosynthates: PB2-11
 Photosynthesis: OP5-3, PBG2-5, PCS-1, PCS-2, PMP-12, PPC1-21, PPC1-8
 Photosynthetic: OP4-1, PBG2-5, PBS-21, PC2-11, PC2-17, PC2-19, PEB2-17, PMP-12, PMP-19, PPC1-11, PPC1-4, PPC1-9, PSB-17
 Photosynthetically: OP5-1, PBG2-9, PMP-12
 Phototrophic: OGPR-2, OSB2-3, PC2-17, PC2-20, PMP-10, PMP-19, PPC1-6
 Phototrophs: PBG1-8
Phragmites: PSB-7
 Phthalate: OEB-1
 Phthalic: OEB-3, PBG2-3
 Phycmata: PBG1-10
 Phydophyta: POS2-7
 Phyllocladane-type: OB1-2
 Phyllocladanes: PGG2-16
 Phyllocladene: PB2-17
 Phylogenetic: OP2-1, OP5-1, PB1-14, PEB2-19, PMP-11, PMP-4, PMP-6
 Phylogenetically: OP5-3
 Phylogeny: PB1-10, PB2-2
 Phylotypes: PMP-1, PMP-11
 Phylum: PB1-2, PMP-11
 Physalis: PSB-2
 Phytadienes: PBG1-11
 Phytadiens: PMP-19
 Phytan-11-Ol: PB2-2
 Phytane/N-Octadecane: PRG1-4
 Phytane/Nc18: PBS-5
 Phytane: OB3-2, OP1-1, PB1-5, PB2-2, PBS-17, PBS-2, PC-9, PC2-17, PC2-20, PC2-21, PC2-4, PEB2-19, PGG1-11, PGG1-7, POS1-4, POS2-12, PRG1-4, PSB-25, PSB-4
 Phytanediol: PB2-2
 Phytanes: PB2-2
 Phytanol: PB2-2
 Phytanols: PB2-2
 Phytene: PB2-4, PMP-19
 Phytoclasts: POS1-7, POS2-3
 Phytol: OP6-4, PC2-17, PEB1-7, PEB2-19, PMP-19
 Phytomass: PCS-1
 Phytoplankton: PM-11
 Phytoplanktonic: PM-11
 Phytoplankton: PB1-5
 Phytoplankton-Blackout: PC2-8
 Phytoplankton: OM-2, OP2-1, OPE1-1, OPE2-3, PB1-22, PB1-5, PB1-7, PB2-15, PB2-8, PBG1-3, PC2-24, PC2-6, PC2-8, PM-19, PM-25, PM-4, PMP-10, PMP-19, PPC1-12, PPC1-23, PPC1-4
 Phytoplanktonic: PB1-19, PB1-5, PC2-21
 Phyttoplankton: PGG1-13
 Picea: PC2-11, PCS-4
 Picenes: PC2-22
 Picinguaba: PBG1-11
 Picked: PBC-8, PC-1, PC-2
 Picoalgae: PMP-4
 Picoalgal: PB2-8
 Picophytoplankton: PMP-4
 Picophytoplanktonic: PMP-4
 Picoplankton: OPC2-3
 Picoplanktonic: PB2-8, PMP-4
 Piezotolerant: OB2-1
 Pigment-Derived: PMN2-2
 Pigment: PB2-10, PB2-20, PBC-14
 Pigments: OP2-1, PB2-15, PB2-20, PB2-4, PB2-7, PBC-14, PBG1-1, PBG1-8, PC2-19, PFA-9, PM-21, PM-8
 Pilbara: PBG1-15
 Pilings: PEB2-10
 Pillow: PPM-12
 Pimarane-type: OB1-2
 Pinaceae: OB1-2, PC2-5
 Pinaster: PBC-3, PSB-18
 Pine: OM-1, OSB1-2, PBC-14, PBC-3, PBC-4, PBG2-6, PCS-1, PCS-2, PEB1-14, PEB2-8, PSB-18
 Pinnacle: PB2-14
 Pinnularia: PB2-1
 Pinus: OP3-2, PBC-12, PBC-3, PCS-1, PEB2-8, PFA-6, PSB-18, PSB-9
 Pipe: PGG2-7, PRG2-13
 Pipeline: PRG2-14
 Pipelines: OPG-3, PEB1-11, PMN2-4
 Pipes: OGC-4, PEB2-12
 Pistacia: PFA-6
 Pit: PB1-22, PC2-21
 Pitch: PFA-2, PFA-4
 Pith-Cavity: PB1-16
 Planctomycetales: PB1-7, PMN1-3
 Planctomycetes: OP6-2
 Planktic: OPE1-1
 Plankton: OB2-2, PBG1-8, PMP-2, POS2-7, PPC1-18, PPC1-27
 Planktonic-bacterial: PBS-10
 Planktonic: OB1-3, OPE2-3, PB1-10, PB1-9, PB2-13, PB2-4, PBG1-13, PBG1-8, PBG2-11, PC2-18, PC2-24, PEB1-5, PMP-2, POS2-14, POS2-7, PPC1-12, PPC1-7
 Planktonogenic: POS2-9
 Planosol: PSB-8
 Plant-Derived: OP4-1, OSB2-1, PB2-9, PBG2-6, PC2-22, PCS-7, PCS-8, PSB-7
 Plant-Internal: PB2-11
 Plant-Internally: PB2-11

- Plant-Sourced: PC2-22
Plant: OB1-2, OBD2-3, OEB-1, OOS-3, OP3-1, OP3-2, OP4-1, OP5-3, OPC2-1, OPC2-2, OPE1-1, OPE1-2, OPE2-2, OSB1-1, OSB1-3, OSB2-1, PB1-15, PB1-22, PB1-4, PB1-5, PB1-6, PB2-11, PB2-22, PB2-6, PBC-1, PBC-14, PBC-3, PBC-4, PBC-8, PBC-9, PBG1-11, PBG1-13, PBG1-7, PBG2-10, PBG2-5, PBG2-6, PBG2-8, PC-10, PC-12, PC2-1, PC2-11, PC2-19, PC2-22, PC2-23, PC2-24, PC2-3, PC2-4, PC2-5, PC2-6, PC-3, PC-9, PCS-1, PCS-14, PCS-3, PCS-7, PEB1-14, PEB2-12, PEB2-8, PFA-2, PFA-8, PGG2-10, PGG2-11, PGG2-16, PGG2-2, PM-10, PM-12, PM-13, PM-23, PMN1-8, PMN2-7, POS2-7, PPC1-14, PPC1-15, PPC1-18, PPC1-24, PPC1-26, PPC1-4, PPC1-8, PRG1-13, PSB-17, PSB-18, PSB-19
Plants: OB1-2, OBD2-3, OM-1, OP3-1, OP3-2, OP4-1, OP5-3, OP6-2, OP6-4, OPC1-2, OPE1-2, OPE2-2, OSB1-1, OSB1-2, OSB2-1, PB1-13, PB1-15, PB1-4, PB2-11, PB2-17, PB2-4, PB2-9, PBG1-11, PBG1-2, PBG1-8, PBG1-9, PBG2-8, PC-12, PC-3, PC2-1, PC2-14, PC2-15, PC2-19, PC2-2, PC2-20, PC2-4, PC2-5, PC2-6, PCS-1, PCS-10, PCS-2, PEB1-13, PEB1-14, PEB1-6, PEB1-7, PEB2-14, PEB2-8, PFA-2, PFA-9, PGG1-12, PGG2-16, PM-10, PM-21, PM-5, PMN1-3, PMP-19, POS2-7, PPC1-14, PPC1-22, PPC1-23, PPC1-26
Plants: PPM-3, PSB-13, PSB-17, PSB-19, PSB-3, PSB-4, PSB-9
Plasma: PEB1-1, PRG1-8
Plastic: PFA-7, POS2-2
Plasticity: PB1-22
Plasticizers: OEB-3, PMP-18
Plate-Like: PG-27
Plate: OP7-3, PB1-18, PB2-9, PBG1-10, PBS-12, POS1-6, PPC1-1, PPM-15
Plateau: PEB2-16, PPC1-18
Plates: PBG1-6
Platform: OOS-1
Platform: OB1-2, OGC-4, OPG-3, PBC-6, PBC-7, PBG1-14, PBS-10, PBS-21, PGG1-6, PGG1-7, PGG2-10, PGG2-6, PM-14, POS2-6, POS2-7, PPC1-1, PPM-6, PRG1-21, PRG2-12
Platforms: OOS-1, PEB1-18, PPC1-1
Platinum: PB2-3, PGG1-13
Platte: OP7-4
Plausible: OGPR-1, OP4-4, PB1-8, PG-3, PMP-23, PPC1-18
PLE: PMN1-10
Pleistocene: OGC-2, OGC-4, OP2-1, PC-6, PC2-12, PC2-13, PC2-14, PPC1-13
Plenty: PC2-19
Pleurosigma: OP2-1, PB2-18
Pleurotus: PM-17, PMN2-7
PLFA: OB2-1, OP2-2, PMP-15, PMP-6, PSB-15
Pflas: OP2-2, PMP-15, PMP-8, PSB-15
Plio-Pleistocene: PB2-21, PG-23, PRG2-4
Pliocene: OGC-4, OPC2-4, OPG-2, PB2-16, PBS-23, PG-23, PG-24, PG-28, PMP-1, PMP-18, PPM-8
Pliocenic: PGG1-14
Ploughing: PCS-10
Plowing: PSB-17
Plume: OPE2-3, PB1-21, PB2-20, PBG2-5, PCS-6, PEB2-12, PMP-16, POS1-16
Plumes: PB1-21, PBG2-6, PCS-6, PMP-16
Pneumatic: PRG2-3
Podocarpaceae: OB1-2
Podzol: OSB2-2, PCS-14, PSB-12
Podzolization: OSB2-2, PSB-13
Podzols: OSB2-2, PSB-13
Poland: PB1-12, PBS-17, PB1-8, PBG1-2, PBS-17, PEB2-1, PM-7
Polar-rich: OPS2-1
Polar: OB1-2, OB2-1, OB2-3, OB3-1, OBD1-3, OBD2-2, OEB-1, OMN-1, OP6-3, OPC1-1, OPC2-1, OPC2-3, OPE2-1, OPG-3, PB1-10, PB1-12, PB2-14, PB2-2, PBC-10, PBG1-8, PBG2-3, PBG2-4, PBS-16, PC-6, PC-7, PC2-2, PC2-27, PC2-4, PEB1-7, PEB2-11, PEB2-13, PEB2-14, PFA-2, PFA-6, PGG2-2, PGG2-6, PM-2, PM-23, PM-24, PM-3, PMN1-1, PMN1-9, PMN2-11, PMN2-5, PMN2-6, PMN2-9, PMP-11, PMP-12, PMP-18, PMP-20, PMP-21, PMP-5, PMP-6, POS1-13, POS1-9, PPC1-15, PPC1-16, PPC1-19, PPM-13, PPM-2, PRG1-1, PRG2-18, PSB-11
Polarised: PRG2-18
Polarity: PB2-11, PB2-17, PB2-3, PB2-6, PCS-7, PM-1, PMN1-11, PMN2-6, PPM-6
Polarization: OSB1-3, PM-18, PSB-13
Polarized: PRG2-1
Polarizing: OSB1-3
Polars: PC-7
Pole: PC2-22, PGG2-2, POS1-13
Polycyclic: PC-12
Poliphenols: PM-25
Polish: PBG1-2, PG-26, POS2-11
Political: PB1-15, PFA-9
Pollen: OP3-1, OPC2-2, PB2-13, PBC-1, PBG1-7, PBS-8, PC-5, PC2-1, PC2-18, PC2-19, PC2-3, PC2-5, PFA-6, PM-5, POS1-7, POS2-10, PPC1-28, PRG2-1
Pollutant: OP6-1, PBC-4, PEB1-8, PEB2-16, PEB2-8
Pollutants: OP1-1, OP6-1, OSB2-3, PBC-4, PEB1-1, PEB1-3, PEB1-5, PEB1-8, PEB1-9, PEB2-13, PEB2-14, PEB2-16, PEB2-18, PEB2-2, PEB2-20, PEB2-6, PEB2-8, PEB2-9, PM-15, PM-20, PMN1-7, PMN2-1, PSB-14
Polluted: OP6-1, PEB1-11, PEB1-3, PEB2-16, PEB2-3, PMN1-1, PMN1-7
Polluter: PEB2-14
Polluting: PMN1-7
Pollution: OEB-1, OP1-1, OP6-1, PBG2-7, PEB1-1, PEB1-11, PEB1-13, PEB1-16, PEB1-2, PEB1-3, PEB1-7, PEB2-14, PEB2-15, PEB2-

- 16, PEB2-20, PEB2-6, PG-5, PGG2-1, PM-27, PMN1-7
- Poly-Ether: OP3-1
- Polyacidic: PBC-10
- Polyacids: PBC-11
- Polyalkyl: OB3-2
- Polyamide: PGG2-7
- Polyarene: PGG2-6
- Polyarenes: PGG2-5, POS2-2
- Polyarenic: PGG2-6
- Polyaromatic: OB3-2, OP2-3, PB1-8, PB2-6, PBC-14, PBC-4, PBG1-14, PM-16, PRG2-18
- Polyaromatics: PGG1-8
- Polycadinene: PGG1-10
- Polycarboxylic: PBC-10, PM-16
- Polychlorinated: PEB1-5, PEB2-2
- Polycondensation: POS2-6, PSB-16
- Polycondensed: OSB2-1
- Polycyclic aromatic: PRG1-10
- Polycyclic: OPC1-2, PB1-19, PB1-5, PB1-8, PB2-19, PBG2-10, PBG2-7, PBS-10, PBS-2, PC-1, PEB1-1, PEB1-10, PEB1-12, PEB1-14, PEB1-16, PEB1-17, PEB1-18, PEB1-3, PEB1-5, PEB1-6, PEB1-7, PEB2-10, PEB2-13, PEB2-14, PEB2-16, PEB2-18, PEB2-4, PGG1-13, PGG1-5, PGG2-3, PM-27, PMN1-1, PMN1-10, POS2-12, POS2-2, PPM-14
- Polycyclic: PEB1-5, PRG1-10, PRG1-12, PRG2-18, PRG2-2
- Polycycloalkane: PGG2-3
- Polydisperse: PGG2-6
- Polyedrum: PM-28
- Polyesters: OP3-1
- Polyfunctional: PEB2-9, PM-13, PMN2-6
- Polyfunctionalised: OP4-2, PB2-9
- Polyfunctionality: PM-13
- Polyketide: PM-28
- Polylayer: PG-26
- Polymer: OB1-1, OEB-3, OP3-2, OPS2-1, PC-4, PGG2-7, PM-1, PM-23, POS1-3, PSB-2
- Polymeric: OMN-2, PFA-9, PM-1, PM-23
- Polymerisation: OP3-2, PM-22, POS2-6
- Polymerise: PFA-9
- Polymerization: OB1-1, PEB1-6, PG-25, PM-1, PM-28
- Polymers: PBC-12, PM-1, PMN1-2, POS1-3
- Polymolecular: PGG2-6
- Polymorphs: PBG2-7
- polynuclear aromatic: PRG1-10
- Polynuclear: PBC-14
- Polyphenyls: PB1-8, PM-7
- Polyprenoids: PGG2-2
- Polypropylene: OB1-1
- Polysaccharide-Derived: PEB1-13
- Polysaccharide/Lignin: PB1-21
- Polysaccharide: OM-3, PB1-21, PSB-3
- Polysaccharides: OM-3, OP3-1, OSB1-2, PEB1-13, PM-25, PSB-13, PSB-7
- Polysulfide: PM-1, POS1-3
- Polysulfides: PBG1-16
- Polytopic: ORP-2
- Polytrichum*: PM-10
- Polyunsaturated: OP7-2, PB2-5, PMP-19
- Polyvalent: PBC-13
- POM: OPC1-1, OPC2-4, OPE1-3, PBC-3, PM-2, PSB-10
- Pond: PMP-12
- Ponds: OGPR-2, PC2-20, PMP-12
- Pool: OP5-3, OP7-3, OSB1-1, OSB1-2, OSB2-2, OSB2-3, PBC-1, PBC-11, PBC-12, PBC-3, PBC-4, PBC-8, PBG2-10, PC2-19, PCS-13, PCS-14, PCS-5, PCS-7, PCS-8, PG-13, PG-16, PG-28, PM-8, PPC1-21, PPC1-8, PPM-6, PRG2-19, PRG2-21, PSB-16, PSB-6, PSB-7
- Pooled: PCS-12, PCS-2, PRG2-16
- Pooling: PMN1-2
- Pools: OP5-3, OPE2-1, OPS1-1, OSB2-1, OSB2-2, PBC-6, PBG2-13, PBS-12, PBS-16, PC-9, PCS-14, PCS-3, PCS-4, PG-7, PG-8, PGG1-12, PM-2, PPC1-25, PPM-3, PPM-6, PRG2-16, PRG2-19, PRG2-21, PSB-16, PSB-20, PSB-25
- Porapack: PMN2-10
- Porcupine: OP2-4, PC2-25
- Pore-Fractured: POS2-9
- Pore-Water: OMN-3
- Pore-Waters: OMN-3, PBG1-9
- Pore: OMN-2, OP7-1, ORP-1, PBG1-9, PC-4, PC-5, PC2-20, PG-17, PG-26, PG-27, PGG2-15, PM-7, PMP-18, PMP-3, POS1-14, PPC1-7, PPM-13, PRG2-1, PRG2-16
- Pores: OP7-1, PB2-14, PBG1-6, PBG2-7, PBS-2, POS1-14, POS2-2, PRG2-16
- Porewaters: PMP-21
- Porifera: OGPR-3
- Porites*: PEB1-2
- Poroperm: PRG2-18
- Porosity-permeability: PG-10
- Porosity: ORP-1, PBG2-14, PC-4, PG-6, PM-14, POS1-14, PRG1-11, PRG2-1, PRG2-15, PRG2-19
- Porous: PBG1-6, PBS-9, PC-4, PG-26, PG-27, PRG1-8
- Porphyrin: PB2-7, PBG1-1, PBG2-2, PPC1-6
- Porphyritic: PPC1-6
- Porphyryns: OB3-2, OSB2-3, PB1-5, PB2-7, PPC1-6
- Portimao: PB2-13
- Portishead: PMP-15
- Portlandian-Berriasian: PM-14
- Portugal/Spain: PM-25
- Portugal: PB2-13, PBC-3, PEB2-2
- Posidonia*: POS1-14, PRG1-2
- Post-Accumulation: PRG1-15
- Post-Deposition: PPC1-22
- Post-Depositional: PG-10, PMP-3, POS1-13, PPC1-15, PPC1-7
- Post-Devensian: PC2-3
- Post-Fire: PSB-18
- Post-Generation: PRG1-13
- Post-Glacial: OPC1-3, PMP-1, PPC1-7

- Post-Laramide: PRG1-9
 Post-Mature: POS1-4
 Post-Sedimentation: PGG1-13
 Postfire: PBC-14
 Postglacial: OP2-1, OPE1-3
 Potash: PGG1-13
 Potassium-Magnesium: PGG1-13
 Potassium: PGG1-13, PM-25
 Potentiometric: PMN2-4, POS1-9
 Potiguar: OP6-3, PGG2-13, PRG2-10
 Potsherds: PFA-5, PFA-6
 Potteries: PEB1-8
 Pottery: PFA-9
 Pr/C₁₇: PBG1-7, POS2-6
 PBS-10, PEB2-18, POS1-15, PRG1-1
 PC2-26, PPM-7, PSB-7
 Pr/Ph: OPE2-3, PBG2-2, PBS-10, PBS-19, PBS-2,
 PBS-21, PBS-20, PC-12, PC2-26, PC2-4,
 PEB2-18, PG-5, PGG1-3, PGG1-7, POS1-12,
 POS1-15, POS1-9, POS2-9, PSB-7
 Pr: OB3-2, OP5-2, PB2-4, PC2-4, PEB1-13, PEB1-
 16, PEB2-12, PG-5, PGG1-1, POS1-4, POS2-13
 PPC1-7, PRG1-9, PSB-4,
 Prague: PBG1-10
 Prasinophyte: PB1-1, PB2-8
 Prasinophytes: PB1-1, PBG1-10
 Prasynophites: POS1-7
 Pre-Aged: OP4-1, OPE1-2, PBG2-13, PC2-24
 Pre-Alpine: PBC-1
 Pre-Anthropogenic: OPE1-2, PBG2-13
 Pre-Biotic: PBG2-3
 Pre-Cambrian: PGG2-10
 Pre-Cleaned: PPM-11
 Pre-Concentration: OMN-3, PGG1-2, PM-15
 Pre-Concentrator: PSB-15
 Pre-Cracking: PPM-2
 Pre-Cretaceous: OPS2-3, PG-10
 Pre-Crisis: PPC1-4
 Pre-Dated: PPC1-18
 Pre-Dating: PC2-13
 Pre-Devonian: POS1-4
 Pre-Drill: OP5-4, ORP-1, PBS-6
 Pre-Enriched: PB1-1
 Pre-Existent: PB1-22, PBC-9
 Pre-Exponential: PBG1-12, PG-11, PG-16, PPM-2
 Pre-Holocene: PB1-6, PC2-22
 Pre-Jurassic: PBS-16
 Pre-Miocene: OP4-3, PG-23
 Pre-Oil: OP5-2
 Pre-Permian: PBS-16, PRG2-16
 Pre-Quaternary: PB2-13
 Pre-Salt: OGPR-3, OOS-1
 Pre-Selected: PMN1-3
 Pre-Tertiary: OP3-2
 Pre-Treated: PMN1-8
 Pre-Treatment: OP3-2, PEB2-11, PMN1-8
 Pre-Zechstein: PPM-12
 Prebiotic: OGPR-1, PBG1-15, PBG1-16
 Precambrian-Cambrian: OOS-1
 Precambrian: OGPR-2, OOS-3, OP3-3, OP6-2,
 OPE2-1, PB2-3, PGG2-13, PM-19, POS1-13,
 POS2-12, PSB-25
 Precaucasus: POS2-9
 Precession: PC2-27, PPC1-17
 Precessional: PC2-9, PPC1-11, PPC1-17, PPC1-26
 Precious: PGG1-13, PRG1-11
 Precipitant: PRG2-13
 Precipitants: PMP-17
 Precipitate: PRG1-9
 Precipitated: OBD1-3, OGPR-1, PBG2-7, PRG1-9,
 PRG2-4
 Precipitates: PRG2-3
 Precipitation-Dissolution: PBG1-4
 Precipitation-Evaporation: PC2-6
 Precipitation: OP4-1, OPC1-1, OPC2-2, OPE2-2,
 PB1-4, PC-6, PC2-1, PC2-14, PC2-19, PC2-20,
 PC2-6, PEB1-5, PM-10, PMN1-11, PMP-18,
 POS1-13, PPC1-14, PPC1-19, PPC1-22,
 PPC1-26, PPC1-7, PRG1-1, PRG1-11, PRG1-
 5, PRG1-9, PRG2-13, PSB-13, PSB-19, PSB-5
 Precipitations: PC2-14
 Precipitous: PEB1-2
 Precolumn: PMN1-8
 Precursor-Biomarker: PPC1-6
 Predazzite: PM-7
 Predazzites: PM-7
 Pregnane: PBS-12, PC2-4
 Pregnanes: PBS-10
 Pressure-Dependent: OB2-1
 Pressure-High: OPG-1
 Pressure-Temperature: PC-1
 Pressure-Volume-Temperature: PPM-2
 Prestige: OP1-1, PEB2-4, PEB2-5
 Pretoria: PC2-9
 Priming: PCS-14
 Primitive: OGPR-3, PBG2-3, PM-16
 Prism: PB1-18, PB2-9
 Prist-1-Ene: PEB2-12, POS2-6
 Prist-2-Ene: POS2-6
 Pristan/N-C17: PBS-20
 Pristan/Phytan: PBS-20, POS1-11
 Pristan: PBG1-7
 Pristane-Phytane: POS1-9
 Pristane-to-phytane: POS1-10
 Pristane/N-Heptadecane: POS2-6
 Pristane/N-C17: PB1-22
 Pristane/Nc17: PBS-5
 Pristane/Phytane: OOS-3, PB1-22, PBS-12, PBS-
 17, PBS-19, PBS-23, PBS-5, PBS-8, PC-12,
 PGG1-1, PGG2-1, POS1-12, PRG1-13, PRG1-
 16, PSB-4
 Pristane: OB3-2, OP1-1, OP5-2, OP6-1, PB1-22,
 PB1-5, PBS-17, PBS-2, PC-9, PC2-17, PC2-
 20, PC2-21, PC2-26, PC2-4, PGG1-11, PGG1-
 3, PGG1-7, POS1-4, POS2-12, PSB-25, PSB-4
 Pristenes: PMP-19
 Pristine: OBD1-2, OBD2-1, ORP-2, PBG2-13,
 PEB2-10
 Pro-Deltaic: PG-3

- Proboscia: PB1-11
 Procrustes: PPM-14
 Prodelta: PB1-6, PBG2-14
 Prokaryote: PB2-9, PC2-17, PC2-21
 Prokaryotes: OB2-3, OP2-1, PB2-9, PMP-10, PMP-15, PMP-17, PPC1-18
 Prokaryotic: PB2-9, PC2-20, PC2-25, PMP-10, PMP-15, PMP-17, PPC1-17
 Propane: PG-18, PG-20, PG-23, PG-25, PG-8, PPM-1, PPM-3
 Propanoic: PC-2
 Propanol: PMN2-4
 Propene: PPM-1
 Propenyl: PCS-9
 Proper: PB1-7, PRG1-15
 Propylbenzene: PEB1-15
 Propylcholestane: PB2-8
 Propylcholestanes: PB2-8
 Propylcholesterols: PB2-8
 Propylene: PEB2-12
 Protease: PEB2-3
 Proteases: OSB1-1
 Protein-derived: PEB1-13
 Protein-like: PM-20, PMN2-1
 Protein: OM-2, OP3-2, OSB1-1, PB1-17, PB2-13, PBG1-4, PCS-11, PM-24, PMN2-6, PPC1-7
 Proteinaceous: OM-2, PM-2, PM-24
 Proteinlike: PSB-16
 Proteins: OGPR-3, OM-2, OP3-1, OSB1-1, PB1-17, PCS-11, PEB1-13, PEB2-12, PFA-2, PM-17, PM-21, PM-25, PM-8, PMN2-6, PSB-7
 Proteobacteria: OB1-3, OP6-1, PMP-11
 Proterozoic-Cambrian: PBG2-9
 Proterozoic: OP4-4, OP5-2, PB1-16, PB2-8, PBG2-9, PC2-25, PGG2-10, PM-19, POS1-4
 Proto-Antarctic: PB2-18
 Proto-Arctic: PBS-3
 Proto-Atlantic: PBS-3
 Proto-kerogen: PM-6
 Protobacteria: PMP-20
 Protokerogen: PB2-4, PBG1-8
 Protokerogen Eastin: PB2-4
 Protokerogens: PM-6
 Protonated: OP2-3, PMN1-3, PRG2-14
 Protoplast: PB1-2
 Prototurbostatal: PGG2-6
 Protozoa: PMP-9
 Protozoan: PC2-21
 Protozoans: OP6-2
 Proxies: OPC1-1, OPC2-1, OPC2-2, OPC2-4, OPE1-2, PB1-4, PB1-5, PB1-9, PB2-13, PB2-22, PC2-11, PC2-14, PC2-19, PC2-2, PC2-8, PC2-9, PCS-2, PMP-1, PMP-20, PMP-9, PPC1-13, PPC1-16, PPC1-19, PPC1-2, PPC1-22, PPC1-28
 Proxy-Data: PBC-1
 Proxy: OPC1-1, OPC1-3, OPC2-3, OPC2-4, PB2-10, PB2-13, PBC-11, PBG2-10, PBG2-8, PC2-14, PC2-15, PC2-16, PC2-19, PC2-21, PC2-24, PC2-3, PC2-6, PM-21, PMP-1, PMP-20, PMP-9, PPC1-16, PPC1-19, PPC1-2, PPC1-22, PPC1-28
 Prunus: OP6-4
 Pseudohomologous: PB1-20
 Pseudomonas: PEB2-19, PEB2-6
 Ptolemaic: PFA-4
 PUFA: PB2-5
 Pufas: PB2-5
 Purbeckian: PM-14
 Purine: OSB2-3
 Purins: PFA-2
 Putrefaciens: OGPR-2
 Py-FIMS: PCS-3
 Py-GC-IR-MS: PBG2-7
 Py-GC-MS: PB2-13, PBG2-7, PEB1-13, PM-18, PM-2, PM-25
 Py-GC/MS: PEB2-12, PFA-1, PM-22, PM-23, PM-25
 Py-GC: POS2-10
 Py/TMAH: PM-24
 PY: POS1-12
 Py610°C-GC-MS: PM-7
 Pygc-MS: PFA-9, PMN1-1
 Pyr-GC-MS: PBC-6
 Pyr-GC/MS: PBC-13, PBC-8
 Pyr: OBD2-3
 Pyrane: PSB-3
 Pyranone: PFA-2
 Pyrene: PEB1-1, PEB1-17, PEB2-8, PGG2-5, PM-7
 Pyrenes: PEB2-4
 Pyrenol: PEB1-1
 Pyridine-26-dicarboxylic: PB1-2
 Pyridine: POS1-9
 Pyridines: OP3-2
 Pyrimidine: OSB2-3
 Pyrite-kerogen: POS1-2
 Pyrite: OGPR-1, OOS-2, PB2-13, PBG1-9, PBG2-8, PG-14, POS1-2, PPC1-4, PRG2-1
 Pyritic: PPC1-7
 Pyritized: PSB-4
 Pyro-GC/MS: PM-11
 Pyro-Products: PM-1, POS1-3
 Pyrobitumen-bearing: PRG2-18
 Pyrobitumen: OGC-1, OOS-2, OPG-1, OPS2-3, PRG1-11, PRG2-18
 Pyrobitumens: PBS-12, PRG2-4
 Pyrochemolysis: PM-2
 Pyrochromatogram: PM-18
 Pyrococcus: OB2-1
 Pyrofoil: PM-4, PM-5
 Pyrogenic: OPC1-2, PBC-8, PBG2-4, PEB1-5, PEB1-7, PEB2-10
 Pyrogram: OPC2-2, PEB1-13, PEB2-12, POS2-10, PSB-7
 Pyrograms: PM-25, PMN1-1
 Pyrolitic-Derived: PC2-17
 Pyrolysable: PC-5
 Pyrolysate-GC: PC-5

Pyrolysate: OGC-3, OP3-2, OSB1-2, PB2-14, PC-5, PM-12, PM-28, PM-3, PM-9, POS1-11, POS2-1, POS2-6

Pyrolysates: OB1-1, OBD2-3, OP2-3, PB1-1, PC2-5, PEB1-13, PFA-2, PG-13, PG-25, PGG2-14, PGG2-3, PM-7, PM-19, PM-3, PM-9, PMN1-2, POS2-1, POS2-6

Pyrolyse: PMN1-2

Pyrolysed: PC2-5, PG-14, PM-2, PM-3, PM-9

Pyrolyses: OBD2-2, OPG-1, PBS-11, PG-21, PG-25, PM-1, PM-16, POS1-2, POS1-3, PSB-7

Pyrolysing: PM-3

Pyrolysis-field: PCS-3

Pyrolysis-gas-chromatography: PRG1-10

Pyrolysis-gas: OP3-2, PB1-1, PB1-22, PC-5, PCS-9, PEB1-13, PEB2-12, PM-14, PM-22, POS2-1

Pyrolysis-GC-MS: POS2-5

Pyrolysis-GC/MS: OBD2-3, PBC-13, PBC-6

Pyrolysis-GC: OP5-4, POS2-5, PSB-7

Pyrolysis/GC/MS: PM-8

Pyrolysis: OBD1-3, OGC-2, OGC-3, OGPR-3, OM-3, OOS-2, OP2-3, OP3-2, OP5-4, OP7-3, OP7-4, OPC2-2, OPG-1, OPS1-3, OPS2-2, OSB1-2, OUM-3, PB1-1, PB1-21, PB1-22, PB2-13, PB2-5, PBC-13, PBC-14, PBC-2, PBC-6, PBC-9, PBG1-1, PBG1-14, PBG1-16, PBG2-11, PBG2-4, PBS-19, PBS-7, PC-1, PC-10, PC-11, PC-2, PC-7, PC2-21, PC2-5, PC2-7, PCS-9, PEB2-12, PEB2-20, PFA-2, PG-11, PG-13, PG-14, PG-16, PG-20, PG-21, PG-25, PG-8, PGG1-8, PGG2-14, PGG2-3, PGG2-8, PM-1, PM-12, PM-14, PM-18, PM-19, PM-2, PM-21, PM-23, PM-24, PM-25, PM-27, PM-3, PM-4, PM-5, PM-7, PM-8, PM-9, PMN1-1, PMN1-7, PMN2-3, PMN2-8, POS1-1, POS1-11, POS1-12, POS1-13, POS1-14, POS1-15, POS1-2, POS1-3, POS1-5, POS1-7, POS1-8, POS2-1, POS2-11, POS2-13, POS2-14, POS2-15, POS2-3, POS2-5, POS2-6, PPC1-1, PPC1-10, PPC1-9, PPM-5, PRG1-1, PRG1-10, PRG1-11, PRG2-1, PRG2-18, PSB-7

Pyrolytic: OP2-3, OSB1-2, PB2-16, PBC-14, PBG1-9, PC-2, PEB1-1, PEB1-10, PEB1-18, PEB2-14, PFA-2, PG-14, PMN1-1, POS2-1, POS2-11

Pyrolyzate: OP5-4, PEB2-12

Pyrolyzates: PEB2-12

Pyrolyzed: POS1-8, POS2-5

Pyrolyzer-GC-MS: PM-4

Pyrolyzer: PM-14, PM-4, PM-5

Pyromorphic: OSB1-3, PSB-18

Pyrophosphate-extractable: PCS-1

Pyrophytic: PBC-14

Pyroprobe: PEB2-12

Pyrroles: OP3-2

Pyruvate: OSB2-3

Q

Quadrupole/time-of-flight: PMP-6

Quadrupole: PBC-7, PM-22, PMN1-3

Quantum: OM-2, PGG1-8

Quarried: PB2-14

Quarry: PB2-14

Quarrying: PEB1-8

Quartz: OGC-1, OPC1-2, PBG1-15, PG-14, PGG1-15, PMN1-2, PSB-13, PSB-7

Quartzitic: PPC1-5

Quasicrystalline: PGG2-6

Quaternary: OP2-1, OPE1-3, PB1-20, PB2-19, PB2-21, PBG1-14, PBG1-7, PC2-1, PC2-13, PC2-18, PC2-25, PEB1-17, PG-24, PG-28, PG-9, PMP-1, PMP-3, PPC1-23, PPC1-26

Queensland: PSB-19

Quenching: PB1-2, PM-20

Quercus: OP3-2, PBC-12, PSB-18, PSB-9

Quinolines: PEB2-11, PPM-13

Quinone-Like: OM-2

Quinone: OM-1, OM-2, PBG1-5

R

R-6-Benzyloxy-1-bromo-4-methylhexane: PB2-2

R-Isomer: PB1-18

R-Isomers: PB1-18

R-Mosher: PB1-14

R-Squared: OPC1-2

Racemisation: PB1-17

Racemization: PMP-22

Radiative: PB1-22

Radiated: PPC1-4

Radiation: OGPR-3, OOS-3, PB2-8, PBG1-3, PBG2-3, PEB1-9, PEB2-6, PM-21, PMP-12, PPC1-15

Radical: OGC-3, PG-14, PSB-3

Radically: PBS-2

Radicals: PM-18, PM-9

Radio: OSB2-2

Radioactive: OBD2-2, OSB2-3, PB1-22, PC2-4, PGG1-13

Radioactives: PB1-21

Radioactivity: OSB2-3

Radioanalytical: PEB2-9

Radiocarbon-Labeled: PCS-5

Radiocarbon: OP4-1, OPE1-1, OPE1-2, OSB2-2, PBG1-13, PBG2-10, PBG2-12, PBG2-13, PC2-12, PC2-18, PC2-19, PCS-4, PCS-5, PCS-6, PPC1-21, PPC1-8

Radioisotopes: PMP-10

Radiolabelled: OSB2-3, PEB2-9, PSB-14, PSB-16

Radiolabelling: PSB-14

Radionuclide: OBD2-2

Radionuclides: PEB1-14, PGG1-13

Railway: PEB2-8

Rain: OP4-1, OP5-3, PB1-22, PBC-3, PC2-19

Rainfall: OBD2-1, OP4-1, OSB1-1, PBG2-10, PC2-9, PEB1-5

Rainforest: OP4-1

Rains: PC2-21

Rainwater: OP4-1

Rainy: PEB1-13, PPC1-17

Raman: PBG1-6, PBG2-7

- Ray: PSB-8
 Re-Crystallized: PBG2-7
 Recalcitrance: PCS-14, PSB-20
 Recalcitrancy: PSB-20
 Recalcitrant: OP3-2, OP7-3, OPE1-1, OSB2-1, PB2-13, PBC-12, PBC-14, PBC-5, PBC-7, PBC-8, PCS-1, PEB2-18, PEB2-4, PMP-12, PPC1-21, PSB-18, PSB-20
 Recolonised: PBS-6
 Recrystallization: PRG2-1
 Recrystallized: PGG1-13, PRG2-1
 Recycled: OP5-3, PPC1-21
 Recycling: OP5-3, PB1-15, PB1-19, PB1-5, PM-11, PPC1-11, PSB-15
 Redeposition: PBG1-14
 Redistribution: PRG1-10
 Redox: OB1-3, OBD2-3, OGPR-2, OGPR-3, PB1-20, PB2-19, PB2-21, PBG1-11, PBG1-4, PBG1-9, PBG2-14, PBG2-8, PC2-20, PC2-8, PG-17, PGG1-11, PGG1-12, PGG2-8, PMP-17, PMP-9, POS1-16, POS1-9, PPC1-21, PPC1-23, PPC1-4, PRG2-7
 Reduce: OOS-2, OP1-1, PBS-20, PBS-22, PEB1-4, PEB2-13, PEB2-20, PEB2-3, PGG2-15, PM-21, PMN2-2, POS1-16, POS2-8
 Reduced: OBD2-3, OEB-1, OEB-2, OGPR-1, OP4-3, OP6-3, PB2-13, PBG1-6, PBS-15, PC-5, PC2-17, PC2-22, PC2-6, PC2-8, PCS-14, PEB1-11, PEB1-2, PEB2-16, PG-18, PGG1-12, PM-27, PMN1-8, POS1-16, POS1-3, PPC1-17, PPM-14, PRG2-2, PRG2-6, PSB-25, PSB-8
 Reducers: OB1-3, OB3-1, PB2-4, PC2-20, PPC1-7
 Reduces: OBD2-3, OMN-1, PBS-12, PM-11, PMN2-2, POS1-4
 Reduction-sulfurization: OGPR-1
 Reduction: OB3-1, OEB-2, OGC-2, OGPR-1, OGPR-2, OOS-2, OP6-3, ORP-2, PB1-8, PB2-1, PB2-3, PBG1-15, PBG1-9, PBG2-7, PBG2-8, PBS-12, PC-1, PC2-20, PCS-12, PEB1-9, PEB2-16, PEB2-3, PG-12, PG-17, PG-18, PG-9, PGG1-13, PGG1-2, PGG2-15, PMN1-10, PMN1-8, PMN2-10, PMN2-8, PMP-14, PMP-15, PMP-16, PMP-18, PMP-19, PMP-2, PMP-3, PMP-9, POS1-11, POS1-2, POS2-8, PPC1-23, PPC1-7, PPM-14, PRG1-11, PRG2-1, PRG2-18, PRG2-9, PSB-17, PSB-4
 Reductive: OGPR-1, PBC-14, PBG1-16, PBS-21, PC-1, PPC1-1
 Reduplicative: PSB-3
 Reef: PB2-14, PB2-17, PEB1-2
 Reefs: PB2-14, PEB1-2, PBS-20, PSB-25
 Refine: PMP-20
 Refined: OBD2-1, PBG1-13, PEB2-10, PGG1-5
 Refinement: PPM-14
 Refinery: OP5-4, PGG2-2
 Refining: OMN-1, OP5-4, PGG2-7, PRG1-5, PRG2-10
 Reflectance: OGC-1, OPS1-2, PB1-21, PB1-8, PBG1-12, PBG2-4, PBS-23, PBS-8, PC-10, PC-12, PC-5, PC-7, PC-8, PC2-8, PEB1-8, PG-13, PG-21, PGG2-2, PM-7, POS1-15, POS1-4, POS1-6, POS1-8, POS2-10, POS2-15, PPM-12, PRG2-18, PRG2-20, PSB-4
 Reflective: PRG2-18
 Reforestation: PBC-14
 Refractory: OBD2-1, OOS-2, OPE1-1, OSB1-2, PB1-9, PBC-11, PBC-13, PBC-3, PBC-4, PBC-6, PBC-7, PBG1-9, PBG2-14, PM-2, PM-24, PM-25, PM-26, PM-6, PM-8, PMP-22, POS1-7, PSB-7
 Regioisomer: OPC2-4
 Regressive: PBG1-2, PPC1-5
 Relatives: OP6-1, OP6-2, OPC2-4
 Relaxation: OSB1-3, PGG2-14
 Relicts: PGG1-13, PMP-17
 Relief: OPE1-2, PBS-26
 Relies: PB2-7, PC2-13, PFA-4, PMN2-8, PPC1-21
 Relieve: OGC-4
 Rely: PBC-5, PBS-3, PC2-5
 Relying: PEB2-16
 Remagnetisation: PMP-18
 Remagnetizations: PMP-18
 Remanent: POS1-13
 Remanents: PEB2-5
 Remediation: OM-1, OP1-1, PEB2-11, PEB2-12, PEB2-6, PEB2-9, PM-17
 Remedy: PC2-19, PEB2-20
 Remigration: PGG1-5
 Remineralisation: PB1-5, PPC1-23
 Remineralization: PB2-13
 Remineralized: OB1-3, OM-1, PMP-10, PMP-2, PPC1-21
 Remnant: PRG2-15, PSB-7
 Remnants: OP3-4, PB1-11, PB1-6, PB1-7, PFA-1, PM-24, PSB-7
 Repeatability: PC2-21, PRG2-13
 Repellency: PSB-11
 Repellent: PSB-11, PSB-18
 Resedimentation: PEB2-12
 Reservoir: OBD1-1, OBD1-2, OGC-1, OMN-1, OOS-1, OOS-2, OP4-3, OP6-3, OP7-4, OPS1-1, OPS1-3, OPS2-1, ORP-1, OUM-3, PB2-10, PBG1-6, PBG2-9, PBS-11, PBS-12, PBS-15, PBS-16, PBS-18, PBS-5, PBS-6, PCS-4, PCS-6, PG-15, PG-17, PG-18, PG-2, PG-25, PG-26, PG-28, PG-4, PG-6, PG-8, PGG1-9, PGG2-14, PGG2-15, PGG2-9, PM-2, PM-26, PM-27, PMN2-4, PMN2-5, POS1-16, POS1-2, POS1-3, POS2-8, PPM-2, PPM-3, PPM-4, PPM-6, PPM-8, PRG1-7, PRG1-11, PRG1-12, PRG1-14, PRG1-15, PRG1-16, PRG1-17, PRG1-18, PRG1-19, PRG1-2, PRG1-20, PRG1-5, PRG1-6, PRG1-7, PRG1-8, PRG1-9, PRG2-1, PRG2-15, PRG2-16, PRG2-17, PRG2-18, PRG2-19, PRG2-21, PRG2-5, PRG2-6, PRG2-9
 Reservoired: OP7-4, OPG-1, OPS2-2, PBS-13, PBS-16, PBS-17, PBS-21, PG-10, PG-17, PMN1-9, PMN2-5, PRG1-11, PRG1-14, PRG1-2

- Reservoirs/Depositional: PB2-12
 Reservoirs: OBD1-1, OMN-1, OOS-2, OP4-3, OP6-3, OP7-3, OPE1-2, OPE1-3, OPG-1, OPG-2, OPS1-1, OPS1-3, OPS2-2, OPS2-3, OOS-1, OUM-1, OUM-2, PB1-5, PB2-14, PBG2-4, PBG2-9, PBS-12, PBS-17, PBS-6, PBS-8, PBS-9, PC-10, PCS-5, PEB2-19, PG-1, PG-12, PG-15, PG-21, PG-24, PG-3, PG-4, PG-7, PGG1-11, PGG1-2, PGG1-6, PGG1-8, PGG2-10, PGG2-14, PM-17, PMN2-4, PMN2-5, POS1-16, POS1-2, POS2-2, POS2-8, POS2-9, PPM-10, PPM-2, PPM-3, PPM-6, PPM-8, PRG1-11, PRG1-12, PRG1-13, PRG1-16, PRG1-17, PRG1-18, PRG1-2, PRG1-20, PRG1-3, PRG1-4, PRG1-8, PRG1-9, PRG2-1, PRG2-10, PRG2-16, PRG2-17, PRG2-18, PRG2-2, PRG2-21, PRG2-4, PRG2-5, PRG2-6, PRG2-8, PSB-25
 Resilience: PBC-9
 Resilient: OBD2-3, PBC-9, PM-25
 Resin-like: PFA-9
 Resin-producing: PGG1-10
 Resin: OBD1-3, PBG1-11, PEB1-15, PFA-2, PFA-4, PFA-6, PFA-8, PFA-9, PGG2-11, PGG2-6, PM-13, PMN1-11, PMN1-5
 Resinite-rich: OUM-1
 Resinite: PBS-23, PC-12, POS2-10, POS2-4
 Resinous: PBS-2, PFA-9, PGG1-12, PGG2-6, PRG1-6
 Resins: OB1-2, OOS-3, OP1-1, OP6-3, PBG1-12, PC2-5, PEB1-11, PEB2-18, PFA-4, PFA-6, PFA-9, PGG1-10, PGG1-12, PGG2-15, PGG2-6, PM-13, PM-27, PM-4, PMN1-11, PMN1-8, PMN2-5, PPC1-1, PPC1-14, PRG1-1, PRG1-20
 Resinsasphaltenes: PEB1-11
 Resonance: OMN-2, PBC-11, PM-18, PSB-13, PSB-9
 Resorcinol-based: PM-28
 Resorcinol: PM-28
 Respiration: OP7-3
 Respiratory: PBG2-9
 Retene: OB1-2, PBG1-2, PBS-17, PCS-6, PGG2-5
 Retro-reactions: POS1-2
 Revolatisation: PEB2-8
 Rewetting: PMP-12
 Rhamnose: PBG1-9, PCS-8
Rhizosolenia: OB2-2, OP2-1, PB2-18
 Rhizosphere: OBD2-3
 Rhodochrosite: OGPR-2
 Rhodochrosites: OGPR-2
Rhododendron: PSB-9
 Rhodolith: PB1-16
 Rhomboids: OM-3
 Rhyodacite: PM-7
 Ribosomal: OP2-1, OP5-3, PB1-14, PMP-1, PMP-11
 Ribulose-15-bisphosphate: OSB1-1
 Rich-kerogen: PPC1-1
 Rift: PB2-19, PB2-2, PBS-12, PBS-9, PC2-11, PGG1-1, POS1-1, POS2-12
 Riparian: PBG1-11
 Riphean: PPC1-7
 River-Dominated: PB2-20
 River-Influenced: PB1-15
 River-Transported: PPC1-20
 River/Beaufort: PC2-22
 River/Estuarine: PBG1-11
 River: OP1-2, OP4-1, OPE1-2, OPE1-3, PB1-15, PB1-6, PB2-13, PB2-20, PB2-4, PBC-11, PBG1-11, PBG1-5, PBG1-7, PBG1-9, PBG2-12, PBG2-13, PBG2-14, PBS-10, PBS-8, PC-10, PC2-10, PC2-14, PCS-6, PEB1-14, PEB1-17, PEB1-3, PEB1-5, PEB1-7, PEB1-8, PEB1-9, PEB2-1, PEB2-12, PFA-7, PFA-8, PG-10, PGG1-15, PGG2-8, PM-15, PM-20, PM-25, PM-26, PM-8, POS1-10, POS1-13, PPC1-17, PPC1-19, PPC1-20, PPM-3, PRG2-5, PRG2-6
 Riverine/Marine: PCS-6
 Riverine: OMN-2, PB1-15, PB2-20, PBC-6, PBG1-11, PC2-27, PM-8
 Rivers: OP7-4, OPE1-3, PBC-6, PBG1-11, PC2-22, PCS-6, PEB1-5, PEB1-8, PEB2-1, PM-8, PPC1-20, PPC1-21, PPM-3
 RNA: OP2-1, OP5-3, PMP-11, PMP-15
 Rock-Eval/TOC: PBS-8
 Rock-Eval: OP5-4, OPS1-2, OPS2-2, PB1-21, PB1-22, PBG1-14, PBG1-7, PBG2-11, PBS-17, PBS-19, PBS-22, PBS-23, PBS-7, PC-10, PC-5, PC-6, PC2-21, PC2-7, PG-11, PM-11, PM-12, PM-14, PMN1-7, POS1-1, POS1-10, POS1-12, POS1-13, POS1-14, POS1-7, POS1-8, POS2-1, POS2-13, POS2-14, POS2-5, PPC1-10, PPC1-5, PPC1-9, PRG1-11, PSB-7
 Rock-Fluid: POS1-16
 Rock-Oil: PBS-19
 Rodinia: PB2-19
 Romania: PBS-17
 Rome: PMP-18
 Root-dominated: PCS-5
 Root-exsudation: PCS-8
 Root-shoot: PSB-2
 Root: OSB1-1, OSB2-2, PB2-11, PBG1-9, PCS-14, PCS-4, PCS-5, PSB-2
 Roots: OBD2-3, OSB1-1, PB2-11, PBC-12, PBG2-13, PCS-10, PCS-5, PSB-2
Roseobacter: PMP-11
 Rubber: OPS2-1
 Rubisco: OSB1-1
 Rural: OEB-1, PEB2-14, PSB-17
 Russia: OPS1-2, PB2-18, PEB2-17, PEB2-18, PG-2, PGG1-11, PGG1-3, PGG2-16, POS1-10, POS1-11, PPM-3, PRG1-5, PBS-20, PCS-6, PBS-8, PC2-22, PCS-6, PEB2-4, PFA-2, POS1-11, PRG1-5
 Ruthenium-ions-catalyzed-oxidation: PRG1-7
 Ruthenium: PC-3, PM-16, PM-25, PM-23
 Rye: PB2-11, PCS-3, PCS-7, PSB-17
 Ryegrass: OSB1-1

S

- S-2-Trifluoromethanesulfonyloxy-ethylpropanoate: PB2-2
- S-IRMS: OP6-3
- S-Isomers: PB1-18
- S-Links: PM-24
- S-Organic: PC-1
- S-R: PBG1-12
- S-Rich: PM-24, PRG2-5
- S/V: PBG1-9, PC2-27
- Saccharides: PCS-8
- Sahara: PBS-26
- Salicylaldehyde: PBG1-3
- Saline: PB1-20, PB2-22, PBS-1, PBS-9, PMP-1, PMP-19, PPC1-28, PPC1-8, PPM-9, PRG1-3, PSB-19
- Salinities: PBG2-1, PMN2-1
- Salinity: OP6-3, PB2-22, OGPR-2, OPC1-1, OPC2-3, PB2-19, PBG1-8, PBG1-9, PBG2-1, PBS-1, PBS-10, PEB2-17, PEB2-5, PM-15, PM-20, PMN2-1, PMP-1, PMP-12, PMP-7, PMN2-1, POS2-9, PPC1-8, PRG1-6, PRG2-10, PRG2-5, PRG2-7, PSB-19
- Salt-rich: PMP-16
- Salt: OOS-1, OGPR-2, OGPR-3, OMN-3, PB2-20, PB2-21, PBG2-13, PG-8, PGG1-13, PGG1-9, PM-19, PMP-19, POS1-1, PPM-12, PRG1-2
- Salts: PGG1-13, PM-3
- Salty: PGG2-10
- Sand-rich: OP4-3
- Sand-shale: PRG2-15
- Sand: OB3-2, OEB-1, OP1-1, OP4-3, PBC-3, PBS-9, PCS-3, PGG2-5, PMN1-7, POS1-10, PPM-4, PRG2-1, PRG2-19, PSB-11, PSB-6
- Sands: OGC-4, OP4-3, PBS-17, PBS-6, PEB1-10, PEB1-12, PG-24, PG-8, PMN2-11, PMN2-4, POS2-9, PRG1-8, PRG2-1, PRG2-15
- Sandstone: PBS-12, PBS-16, PBS-6, PBS-8, PC-10, PEB1-8, PG-3, PG-8, PGG2-12, PMN1-2, PRG1-9, PRG2-1, PRG2-10, PRG2-16, PRG2-21, PRG2-4, PSB-25
- Sandstones: OPS2-2, PBC-12, PBS-16, PBS-18, PG-10, PG-20, PGG2-12, PGG2-16, PGG2-9, PMP-13, POS2-10, POS2-11, POS2-13, PPC1-5, PPM-4, PPM-6, PRG1-2, PRG2-16, PRG2-4
- Sandwiched: OOS-1, PEB1-8
- Sandy-pebbles: PB2-13
- Sandy: OSB1-2, PB2-13, PBC-3, PBC-4, PC-10, PC2-9, PEB1-17, PMP-10, POS1-10, PPM-1, PSB-11, PSB-13, PSB-14
- Santonian: OPC2-3, PBS-3, PC2-16, PPC1-10, PPC1-9
- Saponification: OP3-2, PPC1-25, PBG1-8, PBG2-13, PPC1-25
- Saponified: PB2-1, PB2-17, PBG2-13
- Saponite: PM-11
- Saponites: PM-11
- Sapropel-humic: PGG1-12
- Sapropel-type: PGG1-12
- Sapropel: OP2-1, PBS-1, PG-5, PGG1-12, PMP-1, PMP-6, PPC1-11, PPC1-8, PSB-25
- Sapropelic: PG-11, PGG1-11, POS1-11, POS1-9, POS2-1, POS2-7, PRG2-1, PSB-19
- Sapropels: OP2-1, PMP-1, PMP-6, PPC1-11, PPC1-8
- Saprophytes: PB2-4
- Saprophytic: PBG1-8
- Sarcophagi: PFA-9
- Sarothamnus*: PCS-10
- Satellite: PEB1-8
- Satellites: PRG2-15
- Saturate: OB1-2, OBD1-2, OOS-3, OP1-1, OP3-4, OUM-3, PBG2-4, PBS-8, PEB2-18, PM-1, PMN1-11, PMN1-5, PPM-2, PRG1-20, PRG1-7, PRG1-9, PRG2-11, PRG2-12, PRG2-6
- Saturated/aromatic: PBS-17, PRG2-5
- Saturated/unsaturated: OP2-4, PB2-14, PC2-25
- Saturated: OB1-1, OB1-2, OB2-1, OBD2-1, OGPR-1, OP2-1, OP6-3, OPG-1, OPS2-1, OUM-3, PB1-14, PB2-3, PB2-4, PBG2-4, PBS-10, PBS-15, PBS-2, PBS-5, PC-12, PC2-2, PC2-21, PCS-3, PCS-9, PEB2-18, PFA-3, PFA-6, PFA-8, PG-25, PGG1-14, PGG1-5, PGG1-6, PGG1-7, PGG2-15, PGG2-16, PGG2-6, PM-25, PM-27, PMN1-4, PMN1-6, PMN1-9, PMN2-9, PMP-17, PMP-20, PMP-4, POS1-11, POS2-2, PPC1-25, PPC1-5, PPM-10, PPM-3, PRG1-11, PRG1-12, PRG1-16, PRG1-6, PRG2-10, PRG2-19, PSB-11, PSB-25
- Saturation: OGC-3, ORP-1, PB1-16, PBG2-7, PC-5, PC2-24, POS1-16, PPM-7, PRG1-15, PRG1-2, PSB-5
- Scandinavia: PBS-18
- Scatter: POS2-3, PPM-5
- Scattered: PBG2-7, PC-11
- Scattering: PBG2-8
- Schistes: PC2-11
- Schists: PCS-10
- Scotland: OP3-3, OPC1-1, PBS-18, PEB2-2, PPC1-22
- Scrippsella*: PM-28
- Sculptures: PEB2-15, PFA-9
- SDS-polyacrylamide: PM-17
- Sea-Floor: PM-3
- Sea-Ice: OPC1-1
- Sea-Land: PBG1-9
- Sea-Level: OPC1-1, OPE1-3
- Sea-Surface: OP4-1, OPC2-3, PC2-13, PMP-20
- Sea-Water: OPC2-3
- Sea: OB1-3, OB2-2, OEB-1, OGPR-1, OMN-1, OP2-1, OP4-3, OP5-2, OP6-1, OP6-2, OP7-2, OP7-3, OP7-4, OPC1-1, OPC2-1, OPC2-3, OPC2-4, OPE1-3, OPE2-2, OPE2-3, OPS1-2, PB1-11, PB1-13, PB1-15, PB1-2, PB1-7, PB2-13, PB2-18, PB2-9, PBG1-11, PBG1-14, PBG1-4, PBG1-9, PBG2-1, PBG2-10, PBG2-14, PBS-15, PBS-18, PBS-2, PBS-3, PBS-8, PC-10, PC2-11, PC2-12, PC2-16, PC2-21, PC2-22, PC2-23, PC2-24, PC2-27, PEB1-10,

- PEB1-16, PEB1-18, PEB2-12, PEB2-5, PFA-4, PFA-5, PFA-8, PG-19, PG-22, PGG2-14, PGG2-9, PM-1, PM-26, PMN1-9, PMN2-5, PMP-1, PMP-10, PMP-16, PMP-3, PMP-6, POS1-1, POS1-11, POS1-16, POS1-2, POS1-3, POS2-13, POS2-9, PPC1-1, PPC1-11, PPC1-15, PPC1-19, PPC1-2, PPC1-20, PPC1-23, PPC1-24, PPC1-26, PPM-11, PPM-2, PRG1-16, PRG1-6, PRG2-1, PRG2-4
- Seabed: PMP-17
- Seafloor: OB2-1, PBG2-14, PBS-17, PM-12, PMP-16, PMP-23, PMP-3, PPC1-7
- Seagrass: PB2-17
- Seagrasses: PB2-17
- Sealevel: PM-12
- Seas: OP4-4, OPC1-1, OPE1-3, PC2-22, PPC1-1
- Seaside: PBG1-9
- Seawater: OMN-3, PBG1-15, PBG1-3, PBG1-4, PBG2-1, PC2-11, PC2-19, PEB1-4, PEB2-5, PM-13, PMN1-3, PMP-11, PMP-15, PMP-16
- Seawaters: PM-13, PMN2-1
- Secale: PCS-10
- Secohopanoic: PGG2-8
- Secretions: PM-10
- Sediment-Based: PPC1-16, PPC1-2
- Sediment-Borne: PC2-22
- Sediment-Bound: PC2-22
- Sediment-Water: OMN-3, OP7-3, PB1-19, PBG2-14, PBS-14, PM-12
- Sediment/Pore-Water: OMN-3
- Sediment/Water: PPC1-5
- Sediment: OB1-2, OBD2-3, OGPR-2, OGPR-3, OMN-3, OP4-1, OP4-2, OP6-1, OP7-3, OPC1-1, OPE1-1, OPE1-2, OPE1-3, OPE2-1, OPE2-2, PB1-11, PB1-13, PB1-15, PB1-17, PB1-19, PB1-2, PB1-20, PB1-6, PB1-7, PB1-9, PB2-1, PB2-13, PB2-17, PB2-19, PB2-20, PB2-22, PB2-3, PB2-4, PB2-7, PB2-8, PB2-9, PBC-13, PBC-2, PBC-5, PBC-7, PBG1-11, PBG1-13, PBG1-8, PBG1-9, PBG2-1, PBG2-10, PBG2-12, PBG2-13, PBG2-14, PBS-22, PBS-9, PC-12, PC2-11, PC2-14, PC2-16, PC2-19, PC2-20, PC2-22, PC2-24, PC2-3, PC2-5, PC2-6, PC2-8, PC-6, PCS-2, PCS-6, PEB1-10, PEB1-14, PEB1-16, PEB1-17, PEB1-18, PEB1-7, PEB2-1, PEB2-12, PG-15, PM-24, PM-26, PM-27, PM-3, PM-4, PM-5, PM-6, PMN1-7, PMP-10, PMP-15, PMP-17, PMP-2, PMP-21, PMP-22, PMP-23, PMP-3, PMP-6, PMP-8, PMP-9, POS1-12, POS2-1, PPC1-11, PPC1-12, PPC1-15, PPC1-18, PPC1-2, PPC1-20, PPC1-22, PPC1-26, PPC1-7, PPC1-8, PSB-16
- Sedimentaria: PBS-19, PRG2-12
- Sedimentary-Oorganic: PBS-21
- Sedimentary: OB1-2, OB2-1, OB2-2, OB2-3, OB3-1, OBD2-2, OM-2, OMN-3, OOS-2, OP1-2, OP2-1, OP3-2, OP4-1, OP4-4, OP7-2, OPC1-3, OPE1-1, OPE1-2, OPE1-3, OPE2-1, OPS1-1, OSB1-2, PB1-1, PB1-12, PB1-13, PB1-16, PB1-17, PB1-19, PB1-20, PB1-21, PB1-22, PB1-6, PB1-7, PB1-8, PB1-9, PB2-10, PB2-13, PB2-15, PB2-18, PB2-21, PB2-4, PB2-5, PB2-7, PB2-8, PB2-9, PBC-13, PBG1-10, PBG1-12, PBG1-13, PBG1-14, PBG1-2, PBG1-8, PBG1-9, PBG2-1, PBG2-11, PBG2-13, PBG2-14, PBG2-4, PBG2-9, PBS-1, PBS-12, PBS-16, PBS-17, PBS-26, PBS-3, PBS-8, PC-10, PC-7, PC2-1, PC2-11, PC2-15, PC2-16, PC2-18, PC2-2, PC2-20, PC2-23, PC2-24, PC2-25, PC2-3, PC2-4, PC2-7, PC2-8, PEB1-7, PEB2-12, PG-10, PG-11, PG-15, PG-16, PG-17, PG-21, PG-22, PG-23, PGG1-1, PGG1-12, PGG1-5, PGG2-4, PGG2-5, PM-11, PM-19, PM-25, PM-28, PM-3, PMN1-6, PMN2-2, PMP-13, PMP-15, PMP-18, PMP-2, PMP-22, PMP-8, PMP-9, POS1-1, POS1-13, POS1-16, POS1-3, POS1-4, POS1-6, POS2-1, POS2-13, POS2-15, POS2-2, POS2-3, POS2-4, POS2-5, POS2-9, PPC1-14, PPC1-17, PPC1-23, PPC1-27, PPC1-3, PPC1-5, PPC1-6, PPC1-8, PPM-1, PPM-12, PRG1-13, PRG1-21, PRG2-5, PSB-25
- Sedimentated: PBS-20
- Sedimentation: OB3-2, PB2-16, PB2-20, PB2-8, PBG1-9, PBG2-10, PBS-10, PBS-22, PC-12, PC2-11, PC2-16, PC2-17, PC2-2, PC2-20, PC2-22, PC2-24, PEB1-14, PEB2-17, PGG1-12, PGG2-10, PM-11, PM-20, POS1-11, POS1-4, POS1-9, POS2-12, POS2-13, POS2-9, PPC1-8, PSB-16, PSB-19
- Sedimented: PC-11
- Sedimentologic: PC2-4
- Sedimentological: PBG1-13, PC-10, PC2-16, PC2-19, PC2-20, PPC1-8, PPM-14
- Sedimentologists: PC2-11
- Sedimentology: PPC1-5
- Sediments: OB1-1, OB1-2, OB2-1, OB2-3, OB3-1, OBD2-3, OGPR-2, OGPR-3, OM-1, OM-2, OMN-1, OMN-3, OOS-1, OOS-2, OP1-1, OP1-2, OP2-1, OP2-4, OP4-1, OP4-2, OP4-4, OP6-1, OP7-1, OP7-2, OP7-3, OPC1-1, OPC1-3, OPC2-3, OPC2-4, OPE1-1, OPE1-2, OPE2-1, OPE2-2, OPE2-3, OPG-2, OPS2-3, OSB1-2, PB1-1, PB1-10, PB1-11, PB1-13, PB1-15, PB1-16, PB1-17, PB1-19, PB1-2, PB1-20, PB1-4, PB1-5, PB1-6, PB1-7, PB1-9, PB2-1, PB2-10, PB2-13, PB2-14, PB2-17, PB2-20, PB2-21, PB2-22, PB2-3, PB2-4, PB2-5, PB2-6, PB2-7, PB2-8, PB2-9, PBC-13, PBC-5, PBC-6, PBC-7, PBG1-1, PBG1-11, PBG1-12, PBG1-13, PBG1-14, PBG1-7, PBG1-8, PBG1-9, PBG2-1, PBG2-10, PBG2-12, PBG2-13, PBG2-4, PBG2-6, PBG2-8, PBS-1, PBS-11, PBS-16, PBS-18, PBS-2, PBS-21, PBS-26, PBS-3, PBS-5, PBS-8, PBS-9, PC2-1, PC2-11, PC2-12, PC2-13, PC2-14, PC2-15, PC2-16, PC2-17, PC2-18, PC2-19, PC2-2, PC2-20, PC2-22, PC2-24, PC2-25, PC2-26, PC2-3, PC2-5, PC2-6, PC2-8, PC2-9, PC-6, PCS-6, PEB1-1, PEB1-10, PEB1-14, PEB1-16, PEB1-17, PEB1-18, PEB1-5, PEB1-7, PEB1-9,

- PEB2-1, PEB2-12, PEB2-16, PEB2-17, PEB2-18, PEB2-5, PEB2-8, PG-10, PG-11, PG-15, PG-19, PG-23, PG-24, PGG1-12, PGG1-13, PM-11, PM-14, PM-19, PM-23, PM-25, PM-26, PM-27, PM-28, PM-3, PM-4, PM-5, PM-6, PMN1-3, PMN1-7, PMP-1, PMP-13, PMP-14, PMP-15, PMP-17, PMP-18, PMP-19, PMP-20, PMP-21, PMP-22, PMP-3, PMP-4, PMP-6, PMP-8, PMP-9, POS1-11, POS1-12, POS1-13, POS1-4, POS1-6, POS1-9, POS2-1, POS2-10, POS2-12, POS2-13, POS2-14, POS2-15, POS2-2, POS2-4, POS2-5, POS2-9, PPC1-1, PPC1-11, PPC1-12, PPC1-13, PPC1-14, PPC1-15, PPC1-16, PPC1-17, PPC1-19, PPC1-20, PPC1-21, PPC1-22, PPC1-23, PPC1-25, PPC1-26, PPC1-27, PPC1-28, PPC1-4, PPC1-5, PPC1-6, PPC1-7, PPC1-8, PPM-1, PPM-11, PPM-12, PPM-9, PRG1-16, PRG2-20, PSB-12, PSB-19, PSB-25
- Seed: PSB-2
 Seeds: PFA-2, PSB-2
 Seep: OP3-3, PB1-18, PBS-23, PFA-7, PMP-18, PMP-19, PRG2-12
 Seepage: PB1-18, PB1-21, PEB2-17, PEB2-18, PMP-17, POS2-12, PPM-11
 Seepages: PBS-3, POS2-12, POS2-13
 Seeps: OB3-1, OP3-3, OP5-1, PB1-18, PBG1-16, PBS-23, PBS-6, PFA-4, PFA-7, PMP-18, PMP-19, PPM-11, PRG2-12
 Seismic: OP4-3, OPS2-3, PBS-22, PBS-3, PBS-6, PEB2-12, PG-19, PG-8, PMP-21, PPM-11, PPM-4, PRG1-15
 Seismics: PBS-3
 Seismology: PPM-3
 Skeleton: OB2-2
 Selenium: PSB-10
 Self-Combustibility: PSB-18
 Self-Similarity: PC2-10
 SEM-Analysis: PEB2-8
 SEM: PRG2-1, PRG2-18
 Semi-Anthracitic: PG-8
 Semi-Arid: PC2-6
 Semi-Coke: PRG2-18
 Semi-Permafrost: PMP-22
 Semi-Volatile: OP3-4
 Semiarid: PSB-18
 Semifusain: PC-1
 Senescence: OSB1-1, PB2-15
 Senescent: PB2-10, PCS-5
 Senescing: OSB1-1
 Senonian: POS1-1, POS1-2, POS1-3
 Sequence-Stratigraphic: PBS-22
 Sequestration: OBD2-1, OM-1, PB2-1, PBC-14, PCS-1, PCS-10, PCS-12, PCS-13, PCS-2, PCS-7, PCS-9, PG-26, PM-10, POS1-16, PPC1-27
 Serbia: PC-12, PGG1-14, PGG1-15, PGG2-6, POS2-2 PGG1-14
 Serine: PM-2, PM-24, PM-26
 Serines: PMP-6
- Serpentine: PB1-18, PGG1-4
 Serpentinities: PBG1-6
 Serpentinization: OGPR-1, OP5-1
 Serpentinization: PMP-16
 Serratane: PC2-11
 Serratene: PC2-11
 Serratenediol: PC2-11
 Serum: PM-2
 Sesquioxides: PSB-21
 Sesquiterpanes: PGG2-13
 Sesquiterpanes: OB3-2, PGG2-13
 Sesquiterpenes: PBC-14
 Sesquiterpenoids: OB1-2, PC2-5
 Sesterterpanylglycerol: PB1-18
 Sewage: PB1-6, PEB1-14, PEB1-5, PEB1-8, PEB2-1, PEB2-12, PEB2-13, PEB2-14, PEB2-9, PMN1-1
 Shale-Bearing: POS1-11
 Shale: OOS-1, OOS-3, OP3-3, OP4-3, OPC2-3, OPE2-3, OPS1-1, ORP-2, OUM-2, PB1-1, PB1-16, PB1-22, PB2-3, PB2-8, PBC-2, PBC-5, PBG1-1, PBS-18, PBS-3, PC-10, PC2-16, PC2-8, PEB2-20, PG-14, PG-21, PG-22, PGG1-6, PGG2-3, PGG2-8, POS1-10, POS1-11, POS1-12, POS1-13, POS1-14, POS1-5, POS1-6, POS2-10, POS2-6, PPC1-10, PPC1-14, PPC1-17, PPC1-18, PPC1-7, PPC1-9, PPM-12, PPM-15, PRG1-2, PRG1-9, PRG2-1, PRG2-7, PSB-4
 Shales: OOS-3, OPC2-3, OPS1-1, OPS2-2, ORP-2, OUM-3, PB1-16, PB1-20, PB2-12, PB2-4, PB2-8, PBG2-2, PBS-10, PBS-13, PBS-14, PBS-18, PBS-21, PBS-3, PBS-8, PBS-9, PC-10, PC-11, PC2-16, PC2-22, PC2-25, PFA-7, PG-14, PG-24, PG-3, PGG1-1, PGG1-6, PGG1-9, PM-9, PMN1-2, PMN2-4, POS1-11, POS1-12, POS1-13, POS1-14, POS1-6, POS2-1, POS2-10, POS2-11, POS2-3, POS2-5, POS2-6, POS2-7, POS2-8, PPC1-10, PPC1-6, PPC1-9, PPM-9, PRG2-16
 Shallow: OGC-4, OP2-1, OP4-3, OP6-3, OP7-1, OPE1-3, OPE2-3, PB1-22, PB2-19, PB2-22, PB2-8, PBG2-10, PBS-1, PBS-9, PC-10, PC2-20, PC2-22, PC2-25, PC2-9, PC-6, PFA-3, PG-10, PG-19, PG-23, PG-24, PG-9, PGG1-11, PGG2-16, PMP-22, POS1-14, POS1-6, POS2-10, POS2-2, POS2-5, POS2-6, PPC1-1, PPC1-20, PPC1-8, PPM-10, PPM-15, PPM-9, PRG1-11, PRG2-2, PRG2-5
 Shallower: OGC-4, OPC2-4, OPG-2, PBS-11, PBS-6, POS2-5, PRG1-2, PRG2-5, PRG2-6
 Shallowest: PB1-8, PRG1-2
 Shallowly: PRG2-19
 Shanina: PG-14
 Shelf: OB3-1, OP4-4, OPE1-3, OPG-3, OUM-3, PB1-17, PB1-20, PB1-7, PB2-13, PB2-20, PB2-21, PBC-13, PBG1-14, PBG2-12, PBG2-13, PBG2-14, PBS-2, PBS-23, PBS-3, PG-20, PGG2-13, PGG2-9, PM-26, PPC1-21, PPC1-7, PRG1-16, PRG1-9, PRG2-11, PRG2-14

- Shewanella*: OGPR-2
 Shipwrecks: PFA-6
 Shore: PG-2, POS2-12, PPM-11
 Shoreface: PB2-21
 Shoreland: PB1-15
 Shoreline: OP1-1, OP4-4, PBS-22, PEB1-4
 Shorelines: OP1-1
 Shrimps: PB2-4
 Shrublands: PBC-12, PCS-10
 Siberia: OB3-2, OP3-3, OPS1-2, PB2-4, PBG1-8, PBG2-2, PC2-18, PEB1-11, PEB2-17, PEB2-18, PFA-2, PG-2, PGG1-11, PGG1-12, PGG1-3, PGG2-5, PGG2-6, PGG2-8, POS1-9, POS2-12, PPM-3, PPM-4 OPE2-3, PBG1-14, PBG2-2, PBS-10, PC2-26, PCS-6, PG-2, PGG1-6, PGG1-7, PGG2-10, PGG2-8, PRG1-6
 Side-Chain: OB2-1, OP4-4, PMP-8
 Side-Chains: OB2-1, PB2-9, PG-16, PMP-13, PMP-6, PMP-8
 Siderite: PPC1-14
 Siderites: PBG1-2, PPC1-14
 Siderophores: PBG1-4
 Silesian: POS2-11
 Silica-Gel: PEB2-11
 Silica-Prone: OOS-1
 Silica: OPE2-1, PB1-21, PB2-1, PB2-17, PB2-18, PBG1-5, PEB2-11, PEB2-2, PGG1-2, PGG1-5, PGG2-8, PM-26, PMN1-4, PMN2-2, PMN2-9, PMP-21, PRG1-1
 Silicate: PB2-4, PBG1-8, PBG2-7, PC2-3
 Silicated: PB1-16
 Silicates: PSB-12
 Siliceous: OB2-2, OGPR-3, PB1-16, PBS-10, PPC1-6
 Silicic: POS1-9
 Siliciclastic: PRG2-12
 Siliciclastics: POS2-1
 Silicilyte: OOS-1
 Silicites: PBS-10
 Siliclastic: PB2-19
 Siliclastics: PBS-23
 Silicoflagellates: PBS-8
 Sill: PC2-17, POS1-6
 Sills: POS1-6
 Silt: PBC-3, PBG2-14, PC-6, PCS-3, PMP-13, PPC1-5, PFA-4
 Silts: PEB1-17
 Siltstone: PBS-12, PC-10
 Siltstones: PC2-25, PMP-13, POS2-13, POS2-9, PRG2-16
 Silty-Clay: PB2-13
 Silty-Clays: PB2-13
 Silty: PBG2-14, PC2-4, POS2-10, PSB-9
 Silurian-Devonian: PBG1-10, PFA-7
 Silurian: OPC1-2, OPS1-3, PB1-1, PB2-14, PBG1-10, PBS-18, PBS-26, PEB2-17, PPM-6, PRG2-5, PSB-25
 Silver: PGG1-2
 Silylated: PBG1-11, PM-27
 Silylation: PM-16
 SIM: OBD2-3, PC-1, PEB2-2, PFA-4
 Sinapyl: PM-22
 Sinemurian: PC2-17
 Singenetically: PBS-20
 Single-Crop: PCS-12
 Single-Sterane: PM-19
 Sink: OP2-2, OSB1-2, PB1-7, PB2-17, PB2-20, PBC-11, PCS-10, PEB1-13, PM-28, PPC1-23
 Sinking: OB1-3, PB1-13, PB2-20, PPC1-10, PPC1-21
 Sinks: PBG2-5, PCS-1, PCS-2, POS1-16, PPC1-16, PPC1-2
 SiO₂: PB2-18, PM-26, PRG1-6, PBG1-15
 SIR-GCMS: PGG2-3
 Sitosterol: OP5-3, PB2-17, PBG1-11
 Size-Density: PSB-10
 Size-Exclusion: OMN-2, PPM-13
 Size-Fractionated: PBG2-12
 Skeleton: PB1-10, PB2-6, PFA-6, PG-5, PMN1-4, PPC1-14
 Skeletonema: OB2-2
 Skeletons: PB2-6, PEB1-2, PM-12, PMP-1
 Slash-and-burn: PBC-1, PBC-8
 Sledges: PGG2-2
 Slickensides: PEB2-17
 Slope/Base: POS2-5
 Slope: OP3-3, OPC2-4, ORP-2, PB2-21, PBG1-14, PBG2-12, PBG2-14, PBS-21, PGG1-6, PM-4, POS1-16, POS2-5, POS2-6, PPC1-21, PPC1-7, PPM-10, PPM-9, PRG1-13, PRG2-19
 Slopes: PPC1-7
 Slow-Cycling: PBC-6
 Sludge: PEB2-12, PEB2-13, PEB2-14, PEB2-9, PGG2-15, PM-27
 Sludges: PEB2-13, PGG2-15, PMN1-1
 Sludging: PGG2-15
 Slump: PBS-22
 Slumps: PBS-14
 Slurries: PMP-15
 Slurry: PMP-15
 Smectite/humic: PMN1-1
 Sn-2-Hydroxyarchaeol: PMP-21
 Sn-3-Hydroxyarchaeol: PB2-2
 SN/SP: PGG2-5
 SO₂: OOS-2, PBG2-7
 SO₄²⁻: OB3-1, PSB-8, PG-17
 Soap: PEB1-8
 SOC: PCS-13, PCS-7, PSB-21
 Sodid: PCS-9
 Sodium: PCS-1, PEB2-6, PEB2-9, PM-11, PSB-4
 Soft-Bodied: OGPR-3
 Softwood: PEB1-14
 Soil-Affecting: PBC-9
 Soil-Derived: PPC1-11, PPC1-8
 Soil-Forming: PSB-19
 Soil/Groundwater: PEB2-7
 Soil/Peat: PPC1-22
 Soil/Sediment:
 Soil/Water: PSB-16

- Soil: OBD2-1, OBD2-3, OEB-1, OEB-3, OM-1, OMN-2, OP2-2, OP4-1, OP4-2, OPC1-3, OSB1-1, OSB1-2, OSB1-3, OSB2-1, OSB2-2, OSB2-3, PB1-4, PB2-11, PBC-1, PBC-11, PBC-12, PBC-14, PBC-3, PBC-4, PBC-5, PBC-8, PBC-9, PBG1-4, PBG1-9, PBG2-14, PBG2-7, PCS-1, PCS-10, PCS-11, PCS-12, PCS-13, PCS-14, PCS-2, PCS-3, PCS-4, PCS-5, PCS-6, PCS-7, PCS-8, PCS-9, PEB1-11, PEB1-13, PEB1-8, PEB1-9, PEB2-13, PEB2-16, PEB2-18, PEB2-2, PEB2-3, PEB2-9, PFA-1, PFA-3, PFA-4, PGG1-12, PM-2, PM-25, PM-4, PM-6, PM-8, PMN1-10, PMP-20, PPC1-19, PPC1-22, PPM-1, PSB-1, PSB-10, PSB-11, PSB-12, PSB-13, PSB-14, PSB-15, PSB-16, PSB-17, PSB-18, PSB-19, PSB-2, PSB-21, PSB-5, PSB-6, PSB-7, PSB-8, PSB-9
- Soils: OBD2-3, OP2-2, OP4-1, OP4-2, OP5-3, OPE1-2, OSB1-1, OSB1-2, OSB1-3, OSB2-1, OSB2-2, PB1-14, PB1-2, PBC-1, PBC-11, PBC-12, PBC-14, PBC-2, PBC-3, PBC-4, PBC-5, PBC-7, PBC-8, PBC-9, PBG1-9, PBG2-7, PC2-6, PCS-1, PCS-10, PCS-11, PCS-12, PCS-13, PCS-14, PCS-3, PCS-4, PCS-5, PCS-6, PCS-7, PCS-9, PEB1-1, PEB1-11, PEB1-9, PEB2-14, PEB2-16, PEB2-18, PEB2-2, PEB2-6, PEB2-8, PFA-3, PGG1-12, PM-26, PMN1-1, PMN2-1, PPC1-15, PPC1-19, PPC1-22, PPC1-25, PPC1-8, PPM-1, PSB-10, PSB-11, PSB-12, PSB-13, PSB-15, PSB-16, PSB-17, PSB-18, PSB-19, PSB-2, PSB-20, PSB-5, PSB-6, PSB-7, PSB-8, PSB-9
- Solar: PBG1-16, PEB1-9, PEB2-6, PM-16, PM-21, PPC1-15
- Solid-gel: OB2-1
- Solid-liquid: PEB2-9
- Solid-phase: PBC-11, PEB1-15, PEB2-16, PMN1-10
- Solid-state-¹³C-NMR: PBC-3
- Solid-state: OSB1-2, OSB1-3, PBC-3, PBC-6, PM-24, PSB-3, OM-3, OMN-3, OP5-4, OPC1-2, OPG-1, PB2-13, PBC-12, PBC-13, PBC-6, PBG1-5, PBG1-6, PBS-16, PC-1, PC-7, PC2-13, PEB1-11, PEB1-14, PEB2-14, PGG1-13, PGG2-15, PM-14, PM-17, PM-18, PM-24, PM-27, PM-8, PMN1-2, PMN2-9, PMP-9, POS1-1, POS1-16, PPM-13, PPM-2
- Solvent-extracted: PBG2-13
- Solvent-kerogen: OPS2-1
- Solvent-solvent: OPS2-1
- SOM-Fractions: PCS-7
- SOM: OM-2, OSB1-2, OSB2-1, OSB2-2, PB1-19, PBC-3, PBC-8, PCS-4, PCS-5, PCS-7, PCS-8, PM-2, PPM-9, PSB-10, PSB-16, PSB-6, PSB-9
- Sonication:
- Soot-graphitic: PBC-12
- Soot-like: PBC-4
- Soot/graphitic: PBC-12
- Soot: OEB-1, OSB1-3, PBC-10, PBC-11, PBC-13, PBC-2, PBC-4, PBC-5, PEB2-13
- Soots: PBC-6
- Sorb: PCS-11
- Sorbate: PG-27
- Sorbed: PBC-11, PEB2-16, PG-26, PSB-10
- Sorbent: PG-27
- Sorbents: PG-27
- Sorbitol: OEB-1
- Sorption-Desorption: PBG1-4
- Sorption/Desorption: OM-1
- Sorption: PBG1-8, PC-4, PCS-11, PG-26, PG-27, PGG2-12, PM-11, PSB-12, PSB-14
- Sorptive: PCS-14, PM-27
- Sour: PBS-12, PG-12, PG-24, PGG1-2, PRG1-11
- Source-Contributed: OP1-2
- Source-Dependent: PGG1-5, PMN1-9
- Source-Diagnostic:
- Source-Effects: POS1-4
- Source-Rock: OP3-3, PBG1-8, PBS-13, PGG2-16, POS2-13, PRG1-14
- Source-Rocks: PBG1-1, POS1-4
- Source-Specific: OP4-2, OUM-1, PC2-17
- Source-Vs-Migration: OP1-2
- Source/Maturity/Alteration: PBS-15
- Source/Maturity: OUM-1
- Source: OB1-2, OB2-3, OB3-1, OEB-1, OGC-1, OGC-3, OGC-4, OGPR-3, OM-1, OMN-3, OOS-2, OOS-3, OP1-2, OP2-1, OP2-3, OP3-2, OP3-3, OP3-4, OP4-1, OP4-3, OP4-4, OP5-1, OP5-2, OP5-3, OP6-2, OP7-3, OP7-4, OPE2-2, OPG-2, OPS1-1, OPS1-2, OPS1-3, OPS2-1, OPS2-2, OPS2-3, ORP-1, ORP-2, OSB1-2, OSB2-3, OOS-1, OUM-1, OUM-2, OUM-3, PB1-1, PB1-10, PB1-12, PB1-14, PB1-16, PB1-17, PB1-18, PB1-19, PB1-20, PB1-22, PB1-4, PB1-8, PB2-11, PB2-12, PB2-13, PB2-14, PB2-16, PB2-21, PB2-22, PB2-4, PB2-7, PB2-8, PBC-7, PBG1-1, PBG1-11, PBG1-2, PBG1-8, PBG1-9, PBG2-12, PBG2-13, PBG2-4, PBG2-5, PBG2-6, PBG2-7, PBS-1, PBS-11, PBS-12, PBS-13, PBS-14, PBS-15, PBS-16, PBS-17, PBS-18, PBS-19, PBS-21, PBS-22, PBS-23, PBS-24, PBS-26, PBS-3, PBS-5, PBS-6, PBS-7, PBS-8, PBS-9, PC-10, PC-3, PC-5, PC2-14, PC2-15, PC2-19, PC2-20, PC2-21, PC2-22, PC2-24, PC2-25, PC2-26, PC2-4, PC2-7, PCS-5, PEB1-1, PEB1-13, PEB1-14, PEB1-16, PEB1-2, PEB2-10, PEB2-11, PEB2-13, PEB2-14, PEB2-17, PEB2-4, PEB2-6, PEB2-8, PFA-2, PFA-3, PFA-6, PFA-7, PG-1, PG-11, PG-13, PG-14, PG-15, PG-16, PG-17, PG-18, PG-2, PG-21, PG-22, PG-23, PG-24, PG-25, PG-28, PG-4, PG-5, PG-7, PG-8, PG-9, PGG1-1, PGG1-10, PGG1-11, PGG1-12, PGG1-13, PGG1-14, PGG1-15, PGG1-3, PGG1-4, PGG1-5, PGG1-6, PGG1-7, PGG2-1, PGG2-12, PGG2-14, PGG2-16, PGG2-2, PGG2-4, PGG2-5, PGG2-8, PM-1, PM-12, PM-13, PM-19, PM-2, PM-6, PM-7, PM-8, PMN1-4, PMN1-6, PMN1-9, PMN2-2, PMN2-3, PMN2-4, PMN2-8, PMP-12, PMP-16, PMP-

- 17, PMP-19, PMP-4, PMP-6, PMP-9, POS1-1, POS1-10, POS1-11, POS1-12, POS1-13, POS1-14, POS1-15, POS1-16, POS1-2, POS1-3, POS1-4, POS1-5, POS1-6, POS1-7, POS1-8, POS1-9, POS2-11, POS2-12, POS2-13, POS2-14, POS2-2, POS2-3, POS2-4, POS2-5, POS2-7, POS2-8, POS2-9, PPC1-1, PPC1-12, PPC1-15, PPC1-25, PPC1-4, PPC1-8, PPM-10, PPM-11, PPM-12, PPM-13, PPM-14, PPM-15, PPM-2, PPM-3, PPM-4, PPM-5, PPM-6, PPM-7, PPM-8, PPM-9, PRG1-12, PRG1-13, PRG1-14, PRG1-19, PRG1-2, PRG1-20, PRG1-3, PRG1-5, PRG1-6, PRG1-7, PRG1-9, PRG2-1, PRG2-10, PRG2-12, PRG2-16, PRG2-20, PRG2-3, PRG2-5, PRG2-6, PRG2-7, PRG2-9, PSB-20, PSB-25
- Sourced: OP1-2, OP7-4, OPS2-2, OPS2-3, ORP-2, OUM-2, OUM-3, PB1-1, PBS-16, PBS-18, PBS-23, PC-5, PC2-24, PFA-4, PFA-7, PG-10, PG-16, PG-3, PGG2-1, PGG2-2, PGG2-8, PRG1-5, PRG2-16, PRG2-5, PRG2-7
- Sources: OB1-1, OB1-2, OB1-3, OB3-1, OEB-1, OGC-1, OGPR-2, OM-1, OM-2, OMN-2, OOS-3, OP1-1, OP2-2, OP3-4, OP4-1, OP6-2, OP6-3, OP7-1, OPC2-1, OPE1-2, OPE2-1, OPE2-2, OPS2-2, OPS2-3, ORP-2, OUM-2, OUM-3, PB1-1, PB1-11, PB1-15, PB1-17, PB1-19, PB1-6, PB2-11, PB2-20, PB2-5, PB2-9, PBC-6, PBG1-5, PBG1-13, PBG1-14, PBG1-8, PBG2-12, PBG2-7, PBS-21, PBS-3, PC2-1, PC2-24, PC2-4, PCS-3, PCS-5, PCS-7, PEB1-1, PEB1-12, PEB1-14, PEB1-15, PEB1-18, PEB1-5, PEB1-7, PEB2-10, PEB2-11, PEB2-13, PEB2-14, PEB2-2, PEB2-5, PEB2-6, PEB2-8, PFA-1, PFA-2, PFA-6, PG-22, PG-24, PG-28, PGG1-12, PGG2-1, PGG2-4, PGG2-8, PM-10, PM-2, PM-25, PM-8, PMN2-4, PMN2-6, PMP-11, PMP-23, PMP-4, POS1-11, POS1-15, POS1-16, POS2-12, PPC1-12, PPC1-16, PPC1-2, PPC1-21, PPC1-22, PPM-2, PPM-7, PRG1-3, PRG1-7, PSB-13, PSB-4, PSB-7
- Sourcing: OOS-1
- Sourcing: PPC1-1
- Sourcing: PBS-12
- Sources: PEB2-17
- South-American: POS2-3
- South-Caspian: PGG2-6
- South-Central:
- South-Chinese: PRG1-16
- Soxhlet: OPC2-4, PEB1-6, PEB2-2, PPM-5, PRG1-6, PRG1-9, PRG2-16
- Soya: PGG2-16
- Space: OP2-4, OP7-1, OP7-3, PBG1-16, PBG2-5, PCS-10, PEB1-14, PG-24, PM-11, POS1-16, PRG2-1
- Spaghnum*: OP5-3
- Spain: OSB1-3, PB2-1, PBC-12, PBC-13, PBC-6, PBC-7, PBG1-1, PC-11, PC-7, PCS-10, PCS-12, PEB2-12, PEB2-16, PEB2-2, PEB2-5, PM-14, PPC1-13, PSB-18, PSB-20
- Spartina*: PBG2-13
- Spatial: PBG2-5, PBS-1, PCS-14, PEB1-14, PEB1-18, PEB1-5, PEB1-7, PEB2-2, PMN2-1, PMP-12, PMP-14, PMP-9, PPC1-28, PPM-8, PSB-8
- Speciation: PBG1-3, PC-1, PM-15, PM-8, PSB-8
- Species-level: OP2-1
- Species-specific: PMP-1
- Spectra: OB1-1, OGPR-2, OM-2, OMN-2, OP4-2, OP7-2, OSB1-3, OSB2-2, PB1-12, PB1-2, PB2-13, PB2-3, PBC-13, PBC-14, PBC-2, PBC-6, PBC-8, PBC-9, PC-3, PC-8, PCS-9, PEB1-17, PGG1-10, PGG1-5, PGG2-14, PGG2-8, PM-15, PM-20, PM-24, PMN1-9, PMN2-11, PMP-15, POS1-14, PRG2-18, PRG2-2, PSB-12, PSB-13, PSB-18, PSB-2, PSB-3, PSB-4, PSB-8
- Spectral: OB1-1, OM-3, OMN-2, PB1-21, PB2-3, PBC-14, PBC-9, PC2-10, PCS-9, PEB1-8, PM-11, PM-13, PM-25, PMN1-9, PMN2-1, PRG1-15, PSB-18
- Spectrofluorometry: PM-13, PM-15, PM-20
- Spectrometer: OSB1-3, PB2-17, PBC-7, PBG1-6, PCS-2, PEB1-15, PFA-4, PG-12, PGG2-14, PM-22, PMN2-11, PMN2-2, PMN2-7, PMP-6, PSB-1, PSB-13, PSB-3, PSB-4
- Spectrometric: OP2-4, PMN2-11, PSB-4
- Spectrometry: OBD1-2, OBD1-3, OMN-2, OMN-3, OOS-3, OP2-2, OP2-4, OP3-2, OPC2-4, OPE2-1, OPG-1, OPG-3, OPS1-2, OSB1-1, OSB2-1, OSB2-2, PB1-1, PB1-21, PB1-6, PB2-10, PB2-14, PB2-19, PB2-2, PB2-6, PB2-7, PBC-11, PBC-14, PBG1-11, PBG1-12, PBG2-13, PBS-19, PBS-20, PBS-6, PC2-14, PC2-24, PCS-2, PCS-3, PCS-9, PEB1-13, PEB1-15, PEB1-4, PEB1-5, PEB1-7, PEB2-12, PGG1-1, PGG1-14, PGG1-2, PGG2-5, PM-14, PM-22, PMN1-1, PMN1-4, PMN2-11, PMN2-4, PMN2-6, PMN2-7, POS2-15, PPM-6, PRG1-3, PRG2-14, PRG2-2, PRG2-6, PSB-15, PSB-20, PSB-3
- Spectromicroscopy: PSB-8
- Spectroscopic: OM-2, OSB1-2, PB2-13, PB2-2, PBC-13, PCS-9, PEB1-12, PGG2-14, PM-13, PM-16, PM-18, PM-25, PM-8, PMN2-1, POS1-14, PSB-16
- Spectroscopy: OBD2-3, OM-2, OP5-4, OSB2-2, PB1-14, PB2-13, PB2-2, PBC-14, PBC-3, PBC-5, PBC-8, PBG1-6, PBG2-11, PBG2-7, PC-3, PC-8, PCS-4, PEB1-10, PEB1-16, PEB1-18, PEB2-18, PM-12, PM-13, PM-15, PM-2, PM-21, PM-8, PMN2-1, POS1-14, PRG2-14, PSB-12, PSB-13, PSB-16, PSB-4, PSB-8
- Spectrum: OM-2, OM-3, OP7-4, OPS1-1, PB1-8, PB2-6, PBC-11, PBC-6, PEB1-17, PEB1-8, PEB1-9, PGG2-8, PM-18, PMN2-1, PMN2-11, PPC1-17, PRG2-2, PSB-18
- Sphagna: PM-10

- Sphagnum*-derived: OP5-3
Sphagnum-dominated: PM-10
Sphagnum: OP5-3, OPC2-2, PM-10
 Sphenophyta: PC2-5
 Spinning: OSB1-3, PM-18, PSB-13, PSB-9
Spirulina: PMP-7
 SPME-GC-Reduction-IRMS: PRG1-21
 Spodosol: OSB1-2, PSB-15
 Spodosols: PBC-4, PSB-13
 Sponge: OGPR-3
 Sponges: OGPR-3
 Spore: PB1-2, PM-21, POS2-3
 Spores: OP3-1, PB1-2, PC2-5, PM-21, POS1-7, PRG2-1
 Sporinite: PBS-23, PC-12
 Sporinites: PBS-8
 Sporium: PSB-15
 Sporomorphs: POS1-7
 Sporomorphs: POS1-7
 Sporopollenin: OP3-1
 Sporopollens: POS2-7
 Spruce: OSB2-2, PCS-4
 Squalane: PC2-20, PMP-5
 Squalene: PFA-2
 Sr-Isotope: PPC1-7
 Sr/Ca-Ratio: PPC1-16, PPC1-2
 SST-Proxy: OPC2-3 OPC2-1 OP7-2, OPC1-1, OPC2-3, OPC2-4, OPE2-2, PBG2-10, PC2-16, PC2-24, PC2-27, PMP-1, PPC1-18, PPC1-19, PPM-15 OPC1-1, OPC2-3, PBG2-10, PC2-13, PC2-27, PPC1-19
 Stable-isotope: PMP-15
 Stages: OBD1-2, OBD2-1, OGC-1, OP1-1, PB2-6, PB2-7, PBC-9, PBG1-6, PCS-13, PG-18, PG-23, PGG1-4, PGG2-11, PGG2-8, PM-10, PM-17, PM-5, POS1-15, POS1-2, POS1-3, POS1-9, POS2-3, POS2-5, PPC1-20, PPC1-23, PRG1-15, PRG1-4, PRG2-1, PSB-15
 Stagnant: PB1-5, PBS-10
 Stalactites: PPC1-22
 Stalagmite: PPC1-22
 Stalagmites: PPC1-22
 Stanols: PB1-6
Staphylococcus: PMP-20
 Star: PRG2-9
 Stark: PPC1-7
 Startified: PEB1-16
 Starvation: OSB2-3
 Stassfurt-Carbonate: PPM-12
 Statues: PFA-9
 Statuettes: PFA-8
 Status: OEB-1, PBG1-12, PC2-3, PCS-13, PPC1-8
 Statute: PEB1-14
 Statutory: PG-27
 Steam: OEB-1, OOS-2, PBG2-6, PRG1-11, PRG2-10
 Steams: PB1-12
 Stearate: PM-3
 Stearic: PFA-2, PFA-3, PM-3, PMN1-4
 Stearyl: PM-3
 Stem: OP5-3, OPS1-3, PB2-11, PEB1-14, PM-17
 Stems: PB2-11
 Sterane/C20: PMN2-5
 Sterane/hopane: PBG1-10, PBS-2, PC2-8, PPC1-17
 Sterane/pregnane: PBS-10
 Sterane/sterane: PRG1-7
 Sterane: OB2-2, OGPR-3, OOS-1, OOS-3, OP7-4, OUM-1, PB1-10, PB1-16, PB1-22, PB2-12, PB2-18, PB2-19, PB2-8, PBG1-14, PBS-10, PBS-12, PBS-19, PBS-20, PBS-2, PBS-5, PBS-8, PC2-17, PC2-20, PC2-21, PC2-22, PEB1-2, PEB1-5, PEB2-19, PFA-5, PFA-7, PGG1-1, PGG1-14, PGG1-6, PGG2-10, PGG2-11, PGG2-13, PGG2-16, PGG2-2, PM-19, PMN2-5, POS1-15, POS2-12, POS2-14, PPC1-1, PPM-10, PPM-15, PPM-7, PRG1-13, PRG1-14, PRG1-16, PRG1-7, PRG2-20, PSB-25, PSB-4
 Steranes/Hopananes: PMN1-9
 Steranes/Regular: PFA-7
 Steranes: OB3-2, OBD1-2, OGPR-3, OOS-3, OP1-1, OP4-4, OP7-4, PB1-10, PB1-22, PB2-14, PB2-18, PB2-19, PB2-4, PB2-8, PBG1-10, PBG1-12, PBS-10, PBS-13, PBS-17, PBS-19, PBS-2, PBS-21, PBS-3, PBS-8, PC2-20, PC2-22, PC2-25, PC2-4, PEB1-10, PEB1-18, PEB1-2, PEB2-12, PEB2-4, PFA-4, PFA-5, PFA-7, PFA-8, PGG1-10, PGG1-14, PGG1-6, PGG2-11, PGG2-13, PM-12, PM-19, PMN2-5, POS1-1, POS1-11, POS1-13, POS1-15, POS2-12, POS2-14, POS2-8, POS2-9, PPC1-1, PPC1-17, PPM-3, PRG1-1, PRG1-12, PRG1-13, PRG1-14, PRG1-3, PRG1-6, PRG2-12, PSB-20
 Steranic: PGG2-13
 Steranoic: PRG1-7
 Sterene: PG-5
 Sterenes: PBG1-2, PEB2-12, PPC1-18
 Stereochemistry: PGG2-4
 Stereoconfiguration: PB1-14
 Stereoisomers: PB1-18, PBS-10
 Steroid: OGPR-3, OOS-3, PB1-15, PBS-16, PBS-9, PC2-4, PFA-2, PGG1-6
 Steroids: OBD2-1, OP4-4, PB2-16, PC2-4, PEB2-12, PGG1-6, PMN1-4, PRG1-7
 Sterol: OB2-2, OP5-3, PB1-10, PEB1-7, PMP-19, PMP-4, PPC1-12, PPC1-22
 Sterolethers: PPC1-18
 Sterols: OB2-2, OB3-2, OPE1-1, PB1-10, PB1-6, PB1-9, PB2-17, PBG1-11, PBG1-2, PC2-24, PM-27, PMP-17, PMP-19, PPC1-12, PPC1-20, PSB-11
 Stigmast-5-En-3 β -Ol: OB3-2
 Stigmastane: PGG1-5
 Stigmastanol: PEB1-7
 Stigmasterol: PB2-17, PEB1-7
 Stomata: OB1-2
 Stomatal: PB1-4
 Stone: PB2-14, PB2-2, PFA-9
 Storm-Wave: PC2-17

- Storm: PBG2-14
 Storms: OEB-1, PBG2-14
 Strain: OB2-1, PEB2-19, PEB2-6, PMP-20, PMP-4
 Strains: PMP-20, PMP-4, PMP-6
 Strait: PBG2-10, PBS-23, PBS-3
 Strand: PGG2-1
 Strata: OB2-3, OPS1-3, OPS2-2, PB1-18, PBG1-6, PBG2-7, PBS-12, PBS-17, PBS-2, PBS-21, PBS-23, PBS-3, PBS-8, PBS-9, PC-1, PC-6, PC2-26, PC2-8, PEB1-10, PG-13, PG-6, PGG1-4, PGG1-9, PGG2-16, PGG2-6, PM-12, PM-19, POS1-11, POS1-5, POS2-11, POS2-13, POS2-2, POS2-9, PPC1-1, PPM-10, PPM-12, PRG1-13, PRG2-5
 Stratification/Anoxia: OOS-3
 Stratification: OBD2-1, PB1-5, PBG1-9, PBS-21, PC2-19, PMP-1, PMP-14, PPC1-17
 Stratified: OB1-3, OP2-1, PC-10, PC2-25, PEB1-10, PEB1-18, PGG1-1, PMP-14, POS2-2, PPC1-11, PPC1-20
 Stratigraphic: OB1-2, OGC-4, OP2-1, OP3-1, OPC2-2, PB1-1, PB2-18, PB2-19, PB2-21, PB2-7, PBG1-13, PBG1-14, PBG2-10, PBS-8, PBS-9, PC-10, PC-5, PC2-24, PC2-3, PG-10, PG-15, POS1-12
 Stratigraphic: PPC1-24, PPC1-27, PPC1-5, PPM-8, PPM-9, PRG1-15, PRG1-2, PRG2-16, PRG2-6
 Stratigraphically: OOS-1, PB2-19, PBS-6, PG-15, PPM-4, PRG1-2, PRG2-5, PRG2-6
 Stratigraphy: OPE1-1, OPE2-2, PB1-22, PB2-18, PC2-3, PC2-4, PG-23, PMP-1, POS1-10, POS2-3, PPC1-13, PPC1-25
 Stratospheric: PM-21
 Stratotype: PPC1-4
 Stratum: PEB1-10
 Straw-Derived: PSB-20
 Straw: PCS-8, PM-17, PPC1-22, PSB-16, PSB-17, PSB-20
 Stream: OP7-4, OPC2-1, PM-19, PMN2-2, PPM-3
 Streambed: PEB1-5
 Streams: PMP-12, PPM-3
 Stringer: OOS-1
 Stringers: OOS-1
 Stromatolite: PPC1-8
 Stromatolites: PMP-14
 Strontium: PPC1-2
 Structural-Geological: PRG1-2
 Sturtian: OGPR-3, PB2-19, PPC1-7
 Styrene: PEB2-12, POS2-1
 Sub-bituminous: PC-8, PMP-13, POS2-10
 Sub-Boreal/Sub-Atlantic: OPC2-2
 Sub-fossil: OP3-1
 Sub-oxic/anoxic: OB1-3
 Sub-oxic: PB1-16
 Sub-polar: OPC1-1, PPC1-16
 Sub-pools: PCS-13
 Sub-seafloor: OB2-1, PPC1-7
 Subalpine: PB1-9
 Subantarctic: PC2-23
 Subaqueous: PC2-25
 Subboreal/subatlantic: OPC2-2
 Subcontinent: OPE2-2
 Subducted: OP7-3
 Subduction: PB2-9
 Suberan-like: PM-25
 Suberan: PM-23
 Suberans: OSB1-2, PBC-9, PM-25
 Suberin: OSB1-2
 Suberinite: POS2-10
 Suberinitic: POS2-8
 Suberized: OSB1-2
 Subfurcatum: PBG1-2
 Sublethal: OEB-2
 Submarine: PB1-13, PC2-17, PEB2-12, PMP-23, PPC1-18
 Submediterranean: PBG1-2
 Submerged: OP5-3, OPE1-3, PBG1-8, PC2-3
 Suboxic: OB1-3, OPS1-1, PBS-11, PC2-8, PM-12, POS2-15, PRG2-12
 Subseismic: PG-8
 Subsoil: OSB2-2, PCS-4, PSB-12, PSB-17
 Subsoils: OSB2-2, PCS-4, PSB-12
 Subsurface: OB2-1, OBD1-3, OMN-1, OMN-3, OPG-2, PB1-2, PB2-21, PB2-9, PBS-6, PC-6, PCS-14, PEB2-10, PMP-13, PMP-20, PMP-6, PMP-8, POS2-5, PPM-3, PRG1-4, PRG2-12, PRG2-5, PSB-12
 Subterranean: PMP-22, PMP-23, PSB-14
 Subterrestrial: PB1-2
 Subtidal: PB2-19
 Subtropical: OPC2-1, PB2-17, PC2-9, PCS-1, PPC1-18
 Suburb: PB2-14
 Succinate: PRG2-2
 Succinates: PRG2-2
 Succinic: PC-2, PFA-9, PRG2-2
 Sucrose: OEB-1
 Sudetic: PB1-12
 Suess-Effect: PSB-17
 Suez: OP1-2
 Sugar: PCS-8, PM-10, PMP-21
 Sugars: OEB-1, OSB1-1, OSB2-3, PBG1-11, PBG1-9, PBG2-14, PCS-8, PM-10, PM-6, PM-8, PMN1-8, PMP-22, PSB-7
 Sulfate-depleted: OP2-1
 Sulfate-methane: OB3-1, PMP-3
 Sulfate-reducers: PMP-12
 Sulfate-reducing: OMN-3, OP5-1, PC2-20, PMP-14
 Sulfate/methane: OB2-3
 Sulfate: OB1-3, OB3-1, OGPR-2, OMN-1, OOS-2, OP6-3, OPE2-3, ORP-2, PB2-21, PBG1-9, PBS-12, PC2-20, PG-12, PG-17, PG-19, PGG1-2, PMP-18, PMP-19, PMP-3, POS1-2
 Sulfates: OOS-2, OP6-3, PRG1-11
 Sulfide: OGPR-1, OOS-2, OPE2-3, PB1-20, PB1-5, PB2-1, PC2-25, PG-12, PG-14, PM-1, PMP-14, PMP-17, PMP-18, POS1-11, POS1-3, PPC1-4
 Sulfides: OGPR-1, PB2-21, PC2-20, PMP-18

- Sulfidic: OP2-1, OPE2-3, PMP-10, PMP-19, PPC1-4
 Sulfoxide: PRG1-10
 Sulfur-containing: OOS-2
 Sulfur-oxidizing: PMP-10
 Sulfur-rich: OGPR-1, OOS-2, PB2-1, PB2-14, PBG2-7, PBS-12, PG-17, PRG1-1
 Sulfur: OB1-3, OB3-2, OGPR-2, OOS-2, OP2-1, OP5-4, OP6-3, OPE2-3, ORP-2, PB2-1, PB2-14, PB2-21, PB2-4, PBC-11, PBG2-7, PBG2-8, PBS-12, PC2-11, PC2-12, PC2-17, PC2-19, PC2-21, PEB2-11, PEB2-17, PG-12, PG-14, PG-17, PGG1-12, PGG1-2, PGG1-7, PGG2-11, PGG2-3, PGG2-7, PM-1, PM-6, PMP-12, PMP-19, PMP-22, POS1-1, POS1-11, POS1-2, POS1-3, POS2-15, PPC1-1, PPC1-27, PPC1-4, PRG1-8, PRG2-3, PSB-8
 Sulfured: OOS-2
 Sulfurisation: PG-14, PGG1-2
 Sulfurization: OGPR-1, OP6-3, PB2-1, PM-6, POS1-11, PRG1-10
 Sulfurized: OP2-1, PG-14
 Sulfurous: POS1-11, PPM-7
 Sulphate-reducers: PRG2-5
 Sulphate-reducing: PB1-18, PB1-6, PPC1-23, PRG2-2
 Sulphate-reduction: PB2-13
 Sulphate/rethane: PMP-15
 Sulphate: OP6-2, PB1-8, PBG2-8, PC-1, PC-11, PMP-14, PMP-15, PMP-6, PMP-9, PPC1-23, PPC1-7, PRG1-11
 Sulphates: PBG2-4, PRG1-11
 Sulphide: PMP-18
 Sulphided: OUM-3, PM-19, PMN1-4
 Sulphides: PC-1
 Sulphur-carbon: POS2-11
 Sulphur-containing: OEB-2, OPG-1, PRG1-11
 Sulphur-rich: PM-24, PRG1-11, PRG1-2, PRG2-5
 Sulphur: OEB-2, OPE2-3, PB1-12, PB1-22, PB1-8, PB2-13, PBG2-4, PBG2-8, PBS-21, PC-1, PC-11, PC-5, PC2-17, PC2-8, PM-12, PM-24, POS2-1, POS2-11, PPC1-4, PRG1-11, PRG1-2, PRG2-12, PRG2-20, PRG2-5, PRG2-6, PRG2-8, PSB-25, PSB-8
 Sulphureous: PBS-2
 Sulphuric: POS1-9
 Sulphurisation: PM-12
 Sumatra: PB1-15, PBS-8, PC-8, POS1-12
 Sunlight: PBC-9, PEB1-9
 Super-acid: PGG2-3
 Super-continent: OPE2-3
 Superanoxic: PPC1-4
 Superbasin: OP5-2
 Superficial: PBG2-14, PG-15
 Supergene: PGG1-12
 Supergroup: OOS-1, PM-19
 supermolecular: PRG1-10
 Supersaturated: PPC1-16
 Superseded: PB2-10, PFA-5
 Supersequence: POS2-3
 Supersequences: POS2-3
 Supersystem: PB2-12
 Supersystems: PB2-12
 Supra-Tidal: PC2-20
 Supratidal: PC2-20
 Surfactant: PEB2-9
 Surfactants: PEB2-9
 Swamp: PC-10, PSB-7
 Swamps: PBG1-9, PPC1-20
 Swarms: PC2-25
 Sweden: OP3-3, PB1-14, PBS-18, PCS-2, PEB2-2, PSB-20
 Sweetgum: PB2-15
 Swelled: OPS2-1
 Swelling: OPS2-1, PC-4, PG-26, PG-27
 Swells: OPS2-1
 Sylvin: PGG1-13
 Sylvinite: PGG1-13
 Sylvins: PGG1-13
 Symbionts: OP5-3, PMP-17
 Symbiotic: OGPR-3, PMP-17, PMP-9
 Syncline: OPG-2, PPC1-5
 Synclines: PPM-12
Synechococcus: PB2-8
 Syneclise: PSB-25
 Syngeneity: PM-18
 Syngenetic: OP2-4, PB2-19, PBS-10, PC2-25, PGG1-13, PM-18, POS2-9, PSB-25
 Synsedimentary: PC-5, PC2-17
 Syntrophic: OB3-1, PMP-17
 Syringaldehyde: PM-4, PM-5, PSB-3
 Syringic: PM-4, PM-5, PSB-3
 Syringol: PCS-9
 Syringyl: OSB2-2
 Syringyl-Type: OSB2-1
 Syringyl: OSB2-1, OSB2-2, PC2-1, PC2-27, PCS-2, PM-17, PM-22, PM-25, PM-5, PSB-3, PSB-6
 Syryngyl: OM-3
- T**
 TA-Steroids: PGG1-6
 Talc: PBG1-15
 Tannin-: OMN-2
 Tannin-derived: PFA-2
 Tannin-mineral: OM-1
 Tannin: OM-1
 Tannins: PFA-2, PM-25
 Tanzania: PBC-9
 Taphonomic: PPC1-22
 Tar: OOS-2, PEB1-12, PEB2-13, PGG2-8, PMN2-11, PMN2-4
 Taraxerol: PB2-17, PC2-19, PPC1-20
 Tars: OOS-2, PGG2-1
 Tasmanite: PBS-8
 Tasmanites: PB1-1, PB1-22, PBG1-10
 Taxa: OPE2-3, PB1-1, PC2-5, PM-22
 Taxodiaceae: OB1-2, PC2-5
 Taxonomic: OP2-2, PMP-4
 Taxonomically: PB1-1

- TD-GC-Ir-MS: PEB1-15
 TD-GC-MS: PEB1-13
 TD-GC-MS: PEB1-15
 TD-GC: PEB1-15
 TD: PEB1-15, PEB2-4
 Tectonic: OGC-1, OGC-2, PC2-11, PC2-25, PEB2-17, PG-10, POS1-9, POS2-9, PPC1-1, PPC1-17, PPM-6, PPM-8, PRG2-4
 Tectonically: PC-10, PC2-25
 Tectonics: PPC1-1
 Tectonostratigraphic: POS2-8
 Teistberget: POS1-6
 Tektite-like: PBG2-7
 Tel: PFA-5
 Telalginite: PSB-4
 Telinite/collinite: PC-10
 Telinite: PC-10
 Telocollinite: PC-10
 TEM: PBG2-7, PM-12, PRG2-18
 Temperate-zone: PSB-7
 Temperate: PB2-17, PBC-1, PBC-9, PBG1-11, PC2-15, PMP-1, PSB-13
 Tempero-spatial: OMN-2
 Terbium: PB1-2
 Terephthalic: OEB-3
 Teriterpenoids: OP6-4
 Terpane: PB1-16, PB1-22, PB2-12, PBS-10, PBS-19, PC2-22, PFA-7, PGG1-6, PGG2-2, PGG2-8, PPM-15, PRG1-6, PFA-7
 Terpanes/steranes: PRG1-12
 Terpanes: OBD1-2, PB1-1, PB1-16, PB2-19, PBS-10, PBS-21, PBS-8, PC2-25, PFA-4, PFA-5, PFA-7, PFA-8, PGG1-7, PGG2-13, PGG2-8, POS1-12, POS2-14, PRG1-1, PRG1-12
 Terpanic: PGG2-13
 Terpanoid: PB1-16
 Terpene: OP1-1, PPC1-12
 Terpenes: PB1-1
 Terpenoid-Like: OMN-2
 Terpenoid: PB1-1, PFA-9, PPC1-14, PPC1-15
 Terpenoidal: PPC1-15
 Terpenoids: OB1-2, PB1-1, PC2-11, PC2-5, PPC1-15
 Terphenyls: PB1-8, PM-7
 Terrace: PM-26
 Terrains: OPE1-3
 Terrane: PG-24
 Terranes: PG-24
 Terrestrial-influenced: OPS1-1
 Terrestrial-plant: PBG2-5
 Terrestrial/deltaic: PPM-11
 Terrestrial/planktonic: PC2-18
 Terrestrial: OB2-1, OB3-1, OEB-1, OM-1, OP2-2, OP2-3, OP4-1, OPC1-3, OPC2-1, OPE1-2, OPE1-3, OPE2-2, OPE2-3, ORP-2, OSB1-1, OUM-1, OUM-2, PB1-13, PB1-15, PB1-22, PB1-4, PB1-5, PB1-6, PB1-9, PB2-12, PB2-17, PB2-18, PB2-20, PB2-4, PB2-9, PBC-11, PBC-12, PBC-7, PBG1-11, PBG1-13, PBG1-14, PBG1-2, PBG1-8, PBG2-10, PBG2-12, PBG2-13, PBG2-5, PBG2-6, PBG2-7, PBG2-8, PBS-16, PBS-17, PBS-19, PBS-23, PBS-5, PC2-10, PC2-15, PC2-17, PC2-18, PC2-19, PC2-2, PC2-27, PC2-3, PC2-6, PC2-8, PC2-9, PCS-4, PCS-6, PG-3, PGG2-1, PGG2-5, PGG2-16, PGG2-2, PGG2-5, PM-13, PM-16, PM-17, PM-2, PM-21, PM-25, PM-28, PM-8, PMN1-9, PMP-11, PMP-13, PMP-14, PMP-18, PMP-22, PMP-8, POS1-12, POS1-6, POS1-7, POS2-12, POS2-5, POS2-6, PPC1-12, PPC1-14, PPC1-15, PPC1-16, PPC1-18, PPC1-19, PPC1-20, PPC1-21, PPC1-24, PPC1-26, PPC1-3, PPC1-4, PPC1-5, PPC1-8, PPM-5, PRG1-16, PRG1-7, PRG2-1, PRG2-12, PRG2-20, PSB-14, PSB-15, PSB-19, PSB-5, PSB-7
 Terrestrially-derived: OPE1-1, PC2-6
 Terrestrially-influenced: PGG2-2
 Terrestrially-sourced: PBG2-7
 Terrestrially: OOS-3, ORP-2, PBS-22
 Terrigenous: PB1-16, PRG1-13
 Terrigenous/combustion:
 Terrigenous: OP4-1, OPC2-1, OPE1-2, ORP-2, PB1-13, PB1-6, PB2-12, PB2-13, PB2-9, PBG1-13, PBG1-14, PC2-14, PC2-16, PC2-19, PC2-2, PC2-23, PC2-24, PG-1, PGG1-10, PGG1-7, PGG2-6, PM-26, POS1-11, POS1-7, POS2-2, POS2-4, POS2-8, PPC1-14, PPC1-15, PPC1-20, PPC1-21, PRG2-7
 Tersko-Caspian: PGG2-11
 Tert-butylidimethylsilyl: PMN2-6
 Tertiary-terrestrial/marine: OPS2-3
 Tertiary-terrestrial: OPS2-3
 Tertiary: OBD1-3, OOS-3, OP1-2, OP2-3, OPS2-3, OUM-1, PB2-12, PBG2-11, PBS-1, PBS-15, PBS-2, PBS-6, PBS-8, PC-12, PC-6, PC-8, PG-15, PG-3, PG-9, PGG1-1, PGG2-1, PGG2-2, POS1-12, POS2-15, POS2-4, POS2-5, POS2-8, PRG1-13, PRG1-2, PRG1-3, PRG2-16, PRG2-19, PRG2-21
 Tethyan: PM-12, PPC1-27
 Tethys: OPE2-3, PC2-17, PPC1-1, PPC1-18, PPC1-4
 Tetra-alkylbenzenes: PEB2-17
 Tetra-chloronaphthalenes: PEB2-8
 Tetraaromatic: PB2-6, PC2-11
 Tetracyclanes: PBS-10
 Tetracyclic: OOS-3, PB1-16, PB2-6, PC-12, PFA-6, PFA-7, PGG2-8, PPM-15
 Tetracyclicpolyprenoid: OOS-3
 Tetracycloaromatic: PGG2-6
 Tetracyl: PMP-6
 Tetradecan-1-ol: PM-3
 Tetraethers: PB1-14
 Tetraether: OB2-3, OPC1-3, OPC2-3, OPC2-4, PB1-14, PBG2-10, PMN2-2, PPC1-19
 Tetraethers: OMN-1, OPC1-3, OPC2-3, OPC2-4, PB1-14, PC2-25, PMP-17, PMP-21, PPC1-19
 Tetrahydrochrysenes: PC2-22
 Tetrahydroretene: OB1-2
 Tetrahydrothiophene: PSB-3

- Tetrahymanol: OP6-2, PMP-17, PMP-19
 Tetrahymena: PC2-21
 Tetralins: OBD2-1, OPG-1
 Tetrameric: PSB-3
 Tetramethyl: PM-2, PM-4
 Tetramethylalkylbiphenyls: PC2-17
 Tetramethylammonium: PFA-9, PM-17, PM-22, PM-24, PM-25, PM-27
 Tetramethylbenzenes: OP3-4
 Tetramethylnaphthalene: OP5-2
 Tetramethylpentadecyl-Thiophene: PB2-18
 Tetramethylphenanthrenes: OB3-2
 Tetrapeptide: OM-2
 Tetrapyrrole: PM-8, PMN2-2, PPC1-6
 Tetrapyrroles: PB2-10, PB2-7
 Tetrasubstituted: PM-23
 Tetraunsaturated: OP7-2, OPC1-1
 Tetroxide: PC-3, PM-16, PM-25
 Texas: PGG2-15
 TG-DSC-MS: PBC-7
 TG-DSC-QMS: PM-22
 TG-DSC: PBC-7
 TG-DTG-DSC: PBC-7
 TG-IRMS2: PMN2-7
 TG: OP2-2, PBC-7, PM-22
Thalassiosira: OB2-2, PB1-10
 Thermal treatment: PRG1-10
 Thermal: OBD2-2, OGC-1, OOS-2, OP2-3, OP3-2, OP4-4, OP5-2, OP5-4, OP7-3, OPC1-3, OPC2-4, OPG-1, OPG-2, OPS1-1, OPS1-3, OPS2-1, OPS2-3, ORP-2, PB1-18, PB1-21, PB1-7, PB1-8, PB2-16, PB2-4, PBC-11, PBC-13, PBC-2, PBC-5, PBC-6, PBC-7, PBG1-12, PBG1-6, PBG2-11, PBG2-4, PBG2-7, PBS-11, PBS-12, PBS-13, PBS-17, PBS-19, PBS-5, PBS-9, PC-1, PC-3, PC-5, PC-7, PC-9, PC2-10, PC2-17, PC2-20, PC2-4, PC2-8, PCS-3, PCS-9, PEB1-15, PEB2-20, PG-1, PG-12, PG-14, PG-15, PG-17, PG-21, PG-24, PG-25, PG-28, PG-7, PGG1-1, PGG1-5, PGG1-8, PGG2-12, PGG2-14, PGG2-3, PGG2-5, PGG2-7, PGG2-8, PM-1, PM-18, PM-22, PM-4, PM-7, PMN1-1, PMN1-7, PMN1-9, PMN2-8, PMP-13, PMP-23, POS1-10, POS1-11, POS1-12, POS1-13, POS1-14, POS1-15, POS1-2, POS1-3, POS1-4, POS1-6, POS1-8, POS2-10, POS2-12, POS2-13, POS2-14, POS2-15, POS2-2, POS2-3, POS2-4, POS2-5, POS2-8, PPC1-1, PPC1-17, PPC1-18, PPM-10, PPM-12, PPM-14, PPM-4, PPM-6, PPM-7, PPM-8, PPM-9, PRG1-1, PRG1-10, PRG1-11, PRG1-13, PRG1-14, PRG1-16, PRG1-3, PRG1-6, PRG1-7, PRG1-9, PRG2-15, PRG2-16, PRG2-18, PRG2-20, PRG2-4, PRG2-7, PSB-18, PBS-20, PSB-25
 Thermally-assisted: PM-4
 Thermally-sondensed: PBC-3
 Thermally-controlled: PMN1-9
 Thermally-induced: PM-3
 Thermally: OGC-1, OOS-2, OP4-4, OPC2-3, OPG-2, OSB1-2, PB1-22, PB1-8, PB2-19, PBC-7, PBG2-7, PBS-9, PC-8, PFA-9, PG-15, PGG2-14, PM-14, PMN1-1, POS1-1, POS1-12, POS1-2, POS1-3, POS1-4, POS1-6, POS1-8, POS2-11, PPC1-10, PPM-14, PRG1-1, PRG2-18, PSB-18
 Thermicity: PBG1-12
 Thermo-reduction: PRG1-11
 Thermobaric: POS2-2
 Thermocatalytic: PBG1-16, POS2-2
 Thermochemical: ORP-2, PBS-12, PG-12, PGG1-2, POS1-2, PRG2-18
 Thermochemiolysis: PM-27
 Thermochemolysates: PM-14
 Thermochemolysis: OM-3, PBG2-3, PC-2, PM-17, PM-21, PM-25, PM-5
 Thermocline: PBG2-10, PPC1-20
 Thermodesorption: PEB1-13
 Thermodynamic: OP5-4, OPS2-1, PBG1-4, PBG1-6, PEB2-2, PG-1, PG-12, POS1-3
 Thermodynamical: PG-27
 thermodynamically stable structure: PRG1-10
 Thermodynamically: PB1-21, PB2-13, PC-12, PC2-22, PG-25, PGG1-4
 Thermodynamics: OP5-4, PG-12
 Thermogenetic: PC-9
 Thermogenic: OGC-2, OP7-1, OP7-3, PB2-16, PBS-12, PG-1, PG-13, PG-17, PG-18, PG-21, PG-23, PG-24, PG-25, PG-3, PG-8, PMN2-10, PMP-3
 Thermogeological: POS2-4
 Thermogram: PEB1-13
 Thermograms: PBC-7
 Thermogravimetric: PMN2-7
 Thermogravimetry: PBC-7, PM-22
 Thermohaline: PC2-24
 Thermokarst: PCS-6
 Thermolabile: PSB-18
 Thermochemolysis-GC-MS: PM-21
 Thermolysis: PB2-4, PBG1-16, PRG1-10
 Thermophilic: OB2-1, PB1-14, PB1-20, PB2-2
 Thermosynthesis: PBG1-16
 Thermovaporisation-Gas: PB1-22
 Thermovaporisation: POS2-5
 Thiaadamantane: PGG1-2
 Thiaadamantanes: PGG1-2
 Thiadiamondoids: PGG1-2
 Thienylhopanes: PC-11
 Thioacid: OGPR-1
 Thioacids: OGPR-1
 Thioalkanes: PBG1-16
 Thioester: OGPR-1
 Thioesters: PBG1-16
 Thiol: OGPR-1
 Thiols: OGPR-1, PC-1, PM-1
 Thionyl: PSB-1
 Thiophene: PB2-1, PG-14, PGG1-2, PM-1, POS1-11

- Thiophenes: OEB-2, PB2-1, PB2-18, PC-1, PEB2-11, PG-14, PM-1, POS1-11
 Thiophenic: PB2-1, PBG2-4
 Thiophenoles: PRG1-1
 Thiophens: PM-1
 Threonine: PM-2
 Tibet: POS2-7 PFA-2
 TIC: OEB-1, PBG1-16, PC2-9, PM-16, PM-17, PM-2, PMN1-3, PMP-4, POS1-16, PSB-4
 Tidal: PB1-2, PEB1-5, PMP-15, POS2-10, PRG1-2
 Tidally: POS2-10
 Tides: PBG1-9, PM-15
 Tigris: PFA-7
 Tillage: PCS-10, PCS-12, PCS-3, PCS-7
 Time-of-flight: PB2-3
 Time-Resolution: PM-4
 Time-Resolved:
 Tissue: OEB-2, OP3-2, OP5-3, OP6-4, PC2-1, PEB1-1, PEB2-10, PFA-3, PFA-4, PM-4, PMN1-2
 Tissues: OM-1, OP3-1, OP3-2, OPE2-1, OSB1-1, PB2-11, PEB1-1, PEB1-5, PEB2-10, PFA-4, PM-10, PM-22, PSB-9
 Tithonian: PB1-18, POS2-15, PRG2-3
 Titrated: PRG2-14, PSB-1
 Titration: PBG1-3, PGG2-7, PM-15, PMN2-4, POS1-9, PRG2-14
 Titrations: PSB-1
 TJ: OB3-2, PBS-5, PG-19
 TK: PMP-5
 TL-1: PC2-12
 TL-2: PC2-12
 TL: PC2-12, POS1-9, PPM-7, PRG1-16, PRG2-17
 TLC-FID: POS1-6
 TLC: PEB2-17
 TLE: PBG2-13, PFA-4
 Tm: PB1-16, PB2-19
 TM: PBS-10
 Tm: PBS-10, PCS-1, PSB-21
 TMAH-Py/GC/MS: PM-2
 TMAH-Pyrollysates: PM-2
 TMAH-Pyrolysis-GC/MS: PC2-27
 TMAH-Pyrolysis: PM-2
 TMAH-Reaction: PM-4
 TMAH-Treated: PM-22
 TMAH/Thermochemolysis: PM-23, PM-4
 TMAH: OM-3, OSB1-2, PC-2, PCS-2, PFA-2, PFA-9, PM-14, PM-17, PM-2, PM-21, PM-22, PM-24, PM-25, PM-4, PM-5
 Toarcian: OPE2-3, PBG1-12, PG-21, POS2-6
 Tobacco: PEB1-8
 TOC-detection: PSB-14
 TOC-normalized: PG-11
 TOC-plot: PC2-16
 TOC-profile: OEB-3
 TOC-VCSH: PMN1-8
 TOC%: PBG1-9
 TOC/TN: PB1-17
 TOC: OEB-3, OP5-1, OP7-3, OP7-4, OPC2-3, OPE2-1, OPS1-2, OPS1-3, PB1-16, PB1-17, PB1-22, PB2-17, PB2-19, PB2-20, PB2-9, PBG1-14, PBG1-7, PBG2-12, PBG2-2, PBG2-8, PBS-1, PBS-11, PBS-17, PBS-20, PBS-22, PBS-23, PBS-26, PBS-7, PBS-8, PC-10, PC-5, PC-6, PC2-16, PC2-18, PC2-20, PC2-25, PC2-27, PC2-3, PC2-7, PC2-8, PC2-9, PEB1-10, PEB1-17, PEB1-18, PEB2-20, PG-11, PG-14, PG-16, PG-19, PG-7, PM-12, PM-26, PM-7, PMN2-3, PMN2-8, PMP-6, POS1-10, POS1-11, POS1-12, POS1-15, POS1-5, POS1-6, POS1-7, POS1-8, POS2-1, POS2-10, POS2-11, POS2-13, POS2-3, POS2-9, PPC1-18, PPC1-20, PPC1-23, PPC1-3, PPC1-5, PPC1-7, PPC1-8, PPM-11, PPM-9, PRG2-6, PSB-11, PSB-4, PSB-7
 TOCA: PSB-21
 Tocopherol: PFA-2
 Tocopheryl: PFA-2
 TOF-SIMS: OPE2-1
 TOF: PMP-6
 Toluene-diethyl: POS1-9
 Toluene/N-C7: POS1-10
 Toluene: OEB-2, OGC-1, OP5-2, ORP-2, PBS-17, PEB1-15, PEB2-12, PFA-2, PGG2-2, PMN2-4, PMP-23, POS1-9, POS2-1, PPM-14, PRG2-13, PRG2-4
 Toluene+ethylbenzene+: POS2-1
 Tomato: OP3-2
 Tomb: PFA-9
 Topographic: PRG2-1
 Topographical: PBS-22
 Topography: PBG1-9, PPM-15
 Toposequence: PSB-8
 Topsoil: OSB2-2, PBC-1, PCS-13, PCS-4, PSB-16, PSB-8
 Topsoils: PCS-4, PEB1-11
 Torbanite: POS1-14
 Torino: PEB2-2
 Torres2: OP1-1
 Totaloc: PCS-10
 Touch: PPM-9
 Toulouse: PBG1-9
 Towers: OEB-1, PM-18
 Town: PB2-16, PEB2-10
 Towns: PB1-8
 Township: PEB1-8
 Toxic: OEB-2, OP1-1, OPE2-3, PB1-7, PBG1-4, PC2-26, PEB1-1, PEB1-12, PEB1-15, PEB1-5, PEB2-3, PEB2-6, PMN1-3, PRG1-11
 Toxicities: PEB1-12
 Toxicity: OEB-2, OP1-1, PB1-5, PBG1-3, PBG1-4, PEB1-1, PEB1-12, PEB1-4, PEB1-9, PEB2-8, PM-8
 Transgression: POS2-5
Trans-1-methoxy-2-3,4,5-trimethoxyphenyl: PCS-2
Trans-4-4-methoxyphenyl: PCS-2
Trans-trans-trans-Bicadinane: PGG1-10
 Transaminated: OSB2-3

- Transect: OPE2-2, PBG1-14, PBG1-9, PBG2-12, PC2-1, PC2-15, PCS-2, POS2-3, PPC1-15, PPC1-20, PPC1-28
- Transects: OPC1-1, PC2-4, PM-26, PMP-13
- Transesterified: PBG2-3
- Transgressing: PPC1-1
- Transgression/regression: OPE1-3
- Transgression: OPE1-3, PC2-26, PPC1-4, PRG2-1
- Transgressional: PC2-8
- Transgressive: PBG1-10, PBG1-2, PC-10
- Transphilic: PM-13, PM-27, PM-8
- Transpiration: OP4-1, PC2-6
- Transpolar: PBG1-14, PC2-22
- Transpressional: PG-8
- Tree savannah: PPC1-3
- Tree: OM-3, OP3-3, PB2-15, PC2-14, PFA-4, PPC1-15
- Trees: OP4-1, PB2-15, PBC-12, PBC-3, PC2-15, PCS-2, PCS-5, PGG1-10, PPC1-13
- Trenches: PB2-9
- Tri-acids: PM-16
- Tri-aromatic: PEB2-4
- Tri-unsaturated: OP7-2, OPC1-1
- Triacids: PM-16
- Triacylglycerols: PFA-8
- Triaromatic: OB3-2, OOS-3, OP4-4, PB2-6, PGG1-6, PMN2-5, POS1-11
- Triassic-late: PPC1-1
- Triassic-sourced: OGC-1
- Triassic: OB3-2, OGC-1, OOS-3, OP3-3, OPC1-2, OPE2-3, OPS2-2, PB1-5, PB2-12, PBS-11, PBS-12, PBS-15, PBS-6, PC-11, PG-10, PG-13, PG-24, PG-6, POS1-4, POS1-6, POS2-6, POS2-7, PPC1-4, PRG2-16, PRG2-21
- Tricarboxylic: OP6-4
- Trichloroacetic: PMP-21
- Trichome: PB1-16
- Tricyclanes: PBS-10
- Tricycle: PG-5
- Tricyclic: OOS-3, OP2-4, PB1-1, PB1-16, PBS-19, PBS-2, PBS-21, PBS-8, PC-12, PC2-25, PGG1-15, PGG1-7, PGG2-13, POS1-11, POS2-14, PSB-25
- Tricyclics/Hopanes: PB1-22
- Tricyclics/Pentacyclics: PBS-13
- Tricyclics: PBS-13
- Tricycloterpanes: PPM-3
- Trifluoroacetic: PSB-7
- Trifluoroacetyl-I-Propyl: PMN2-6
- Trifluoroacetyl: PB1-17, PMN2-6
- Triglycerides: PBG1-16
- Trihydroxylated: OM-1
- Trimeric: PSB-3
- Trimethyl: OP6-1, PBG2-7, PPM-6
- Trimethylalkanes: PRG1-5
- Trimethylbenzenes: PM-9
- Trimethylnaphthalene: OP5-2, PGG1-15, PRG2-20
- Trimethylnaphthalenes: OP5-2
- Trimethylsilyl: PCS-8, PM-16
- Trimethylsilylated: PMP-21
- Trimethylsilylation: PB2-17
- Trimethylsilyldiazomethane: PB2-13
- Trimosina*: OGC-4
- Triphenylene/chrysene:
- Triphenylene: PB2-5
- Triplets: PB2-13
- Tripoli: PB2-1
- Trisnorhopanes: PBS-10
- Trisulphides: PC-1
- Triterpane: PB1-16, PC-12, PEB1-2, POS2-12, PSB-25
- Triterpanes: PB1-16, PBS-19, PC-12, PEB1-10, PEB1-18, PEB1-4, PEB1-7, PGG1-14, POS2-12, POS2-8, PRG2-12, PSB-25
- Triterpene: PB2-6
- Triterpenes: PFA-6
- Triterpenoid: OUM-1, PB2-6, PM-19, PPC1-14
- Triterpenoids: OP6-2, PB1-15, PB2-6, PBG1-11, PC2-11, PC2-4, PCS-6, PFA-2, PFA-8, PFA-9, PMP-14, PPC1-14, PPC1-20
- Triterpenols: PB2-17
- Triterpenones: PB2-17
- Triticum*: PSB-2
- Trivalent: PEB2-9
- Tropical-subtropical: OP4-1
- Tropical/subtropical: PEB1-5
- Tropical: OM-1, OP4-1, OPC1-3, OPC2-3, PB1-15, PB2-12, PB2-17, PBC-8, PBC-9, PBG1-11, PBG2-10, PBG2-7, PC2-16, PC2-19, PC2-23, PC2-27, PC2-6, PEB1-4, PEB1-5, PGG1-10, PM-21, PPC1-3, PPC1-20, PPC1-26, PSB-13
- Tropics: PBC-8, PBG1-11, PC2-6, PC2-7, PPC1-26
- Troposphere: PEB1-13
- Tryarenes: PGG2-5
- Tryptophan-like: PSB-16
- Tryptophan: PM-2
- Tryptophane: PMN2-1
- Tube-worm: PMP-5
- Tundra/taiga: PCS-6
- Tundra: PBG2-5, PBG2-6
- Tunisia: PBG2-11, PBS-7, PEB2-20, POS2-14, PBS-7, PBG2-11, PBS-7
- Turbidite: OPE2-2, PB1-13, PB1-18, PC2-25
- Turbidites: OP7-3, PB1-13
- Turbiditic: PB1-13, PPC1-14
- Turbidity: PM-15, PM-20, PMN2-1
- Turbulence: PBG2-7
- Turkey: PB1-1, PBG1-10, PFA-7, PG-11, PG-17, PG-3, POS2-1, PRG1-18, PRG1-19, PBG1-10
- Turonian: PBS-7, PC2-16
- Turonien: POS2-14
- Tyrosine: PM-2, PMN2-1
- Tyrrhenian: PPC1-11

U

- Ulex*: PCS-10
- Ultrafiltration: PM-15, PM-20
- Ultramafic: PGG1-12, PMP-16
- Ultrasonic: OPC2-4, PCS-3
- Ultrasonically: PSB-4

- Ultraviolet: PEB1-10, PEB1-16, PEB1-18, PM-21
 Umberatana: PPC1-7
 Umbrisols: PSB-18
 Unbiodegraded: OEB-2, PBS-23, PGG2-2, PRG2-5, PRG2-6
 Undecanoic: PMN1-1
 Undecene: POS2-1
 Undegraded: OBD1-3, PBS-6, PEB2-7
 Undersaturated: PPC1-16
 Unhydrolyzable: PSB-20
 Unhydrolyzed: PSB-20
 Unicellular: PMP-9
 Unmetamorphosed: PM-19
 Unprecipitated: PRG1-9
 Unsaturated: OB1-1, OP3-1, OP7-2, PB2-1, PBG1-8, PC-11, PCS-9, PFA-3, PGG1-11, PM-25, PMN1-4, PMP-15, PMP-18, PMP-21, PMP-5, PPC1-12, PPC1-25
 unsaturated: PRG1-10
 Unsaturated: PSB-11
 Unsaturation: OP7-2, OPC1-1, PB2-3, PM-1
 Unsaturation: OP7-2, PM-18
 Ural: PGG1-11, PGG1-13, PBG1-7
 Uranium: PPC1-27
 Urban-industrial: PEB2-1
 Urban/industrial: OEB-1
 Urban: OEB-1, OP4-2, PB2-1, PEB1-13, PEB1-17, PEB1-8, PEB2-1, PEB2-15, PEB2-2, PEB2-8, PSB-17
 Urea: PMN1-6
 Urine/faecal: PFA-2
 Ursane: PPC1-14
 Ursanes: OP1-2
 Ursanoids: OP1-2
 Ursenes: PPC1-15
 USA/Canada: PB1-20
 USA: OP1-2, OPE1-2, OPG-2, PB1-1, PB2-14, PBC-11, PBG1-11, PBG2-13, PBG2-5, PBG2-6, PBS-3, PC2-10, PCS-5, PEB1-1, PEB2-7, PG-21, PMP-4, POS1-13, PPC1-17
 Utrillas: PC-11
 UV-Spectroscopy: PSB-14
 UV-Vis: PB2-15
 UV-Visible: PSB-16, PSB-4
 UV/VIS: PSB-4
 UV: PBG1-3, PBG2-3, PBG2-7, PEB1-18, PEB2-6, PMN1-8
 Uvigerina: PC2-27
- V**
 V-PDB: PMP-15, PPC1-20, PSB-17
 V-Phenols: PC2-27
 V-Pnenols: PC2-27
 V-Type: OSB2-1
 V/Ni: PGG1-12
 VA: POS2-12
 VACP/MAS: PSB-13
 Val-Thr: PM-2
 Valdez: OP1-1
 Vanadium: PGG1-12, PRG2-8
 Vanadyl: PBG2-2
 Vanadylporphyrins: OB3-2
 Vanillic: PM-4, PM-5, PSB-3
 Vanillin: PM-4, PM-5
 Vanillyl-: OSB2-2
 Vanillyl-type: OSB2-1
 Vanillyl: OSB2-1, OSB2-2, PC2-1, PC2-27, PM-5, PSB-3, PSB-6
 Vapor: PMN2-2, PMP-12
 Vaporisation: PC-4
 Vapour-liquid-solid: PBG2-7
 Vapour-rich: PBG2-7
 Vapour: PB1-4, PEB1-15, PMP-16
 Vascular: OB1-2, OP4-1, OPE1-1, PBG1-11, PBG1-13, PBG1-9, PBG2-10, PC2-1, PC2-22, PC2-24, PM-22, PPC1-26
 Vegetable: PFA-2
 Vegetal: PBG1-9, PCS-8, PEB1-7, PFA-6
 Vegetals: PM-27
 Vegetation: OB1-2, OEB-1, OP4-1, OPC1-2, OPC2-2, OPE1-2, OSB1-2, OSB1-3, OSB2-1, PB1-15, PB2-13, PBC-1, PBC-13, PBC-2, PBC-4, PBC-5, PBG1-11, PBG1-9, PBG2-10, PBG2-5, PC2-1, PC2-18, PC2-19, PC2-2, PC2-23, PC2-27, PC2-9, PCS-1, PCS-10, PCS-2, PCS-5, PEB1-8, PEB2-8, PM-10, PPC1-14, PPC1-19, PPC1-26, PPC1-3, PSB-19, PSB-7, PSB-9
 Vegetational: PC-3, PC2-9
 Vegetations: PC2-5, PSB-9
 Vegetative: PCS-2, PMP-6
 Vehicular: PEB1-13
 Venezuela: OPS2-3, PC2-1, PGG1-12, PRG1-12, PPM-8
 Vermiculite: PSB-9
 Verrucomicrobia: OP6-1
 Vertisol: PBC-2, PSB-19
 Vessel: PEB2-5, PGG2-2, POS1-10, PPM-2
 Vessels: PFA-9, PG-21, POS1-3
 Vietnam: PGG1-10, PPM-7, PRG1-16
 View-Basin: PPM-8
 Viking: OP7-4, OPS2-2, PRG2-5
 Vitreous: PBG1-6
 Vitrinite-like: PSB-25
 Vitrinite-rich: PC-5, PPM-5
 Vitrinite/huminite: POS2-4
 Vitrinite: OGC-1, OPS1-2, PB1-21, PB1-8, PBG1-12, PBG2-4, PBS-11, PBS-23, PBS-8, PC-10, PC-4, PC-5, PC-7, PC-8, PC2-8, PG-13, PG-16, PG-20, PG-21, PGG2-2, PM-7, POS1-15, POS1-4, POS1-6, POS1-8, POS2-10, POS2-15, POS2-8, PPM-12, PPM-5, PRG2-1, PRG2-18, PRG2-20
 Volatile: OB3-1, OGC-2, OMN-3, OP2-3, OP4-3, OP7-2, PBG2-6, PC-5, PC-8, PEB1-13, PEB1-15, PEB2-3, PFA-9, PM-9, PMN1-11, POS1-3, POS1-8, PRG1-10
 Volatile: PRG1-10, PRG2-20, PSB-9
 Volatiles: PC-1
 Volatilisation: PEB2-2

Volatility: OP1-1, OP3-4, PEB1-3
 Volatilization: PBG2-6, PCS-3, PMN2-2
 Volatilize: PRG1-10
 Volatilized: OSB1-3
 Volcanic: OB3-2, OGPR-1, OGPR-3, PBS-2, PCS-1, PCS-9, PMP-17, POS1-6, POS2-12, PPC1-18, PSB-21
 Volcaniclastic: PC2-25
 Volcanics: PBS-16
 Volcanism: OPE2-3
 Volcano-sedimentary: PB2-13
 Volcano: PBG1-4
 Volcanoclastic: OPE2-1
 Volcanoes: OP7-1, PBG1-16, PMP-17, PRG2-12
 Volga-Ural: PGG1-12, PRG1-5 PGG1-11
 Voltammetric: PBG1-4
 Voltammetry: PBG1-3
 Vulcan: PMN1-9

W

Waals: PC-4
 Washout: PBG1-14
 Waste-Water: PMN1-10
 Waste-Waters: PGG2-7
 Wastewater: PB1-7, PEB1-7, PEB2-6
 Water-Borne: PC2-22
 Water-Covered: PSB-7
 Water-Dissolved: PG-24
 Water-Gas: OGPR-1
 Water-In-Oil: PEB2-5, PGG2-15
 Water-Insoluble: PFA-9
 Water-Mineral: PGG2-9
 Water-Rich: POS1-6
 Water-Saturation: PBG1-9
 Water-Soluble: OBD2-3, OEB-1, OMN-3, PBC-11, PEB1-4, PRG2-6
 Water-Stressed: PSB-19
 Water-Washed: PRG2-6
 Water-washing: PRG1-2, PRG2-5, PRG2-6
 Water/gas: PG-20
 Water/rock: PMP-16
 Watercourse: PEB2-6
 Waterlogged: PBG1-9
 Watershed: PBC-11, PBC-8, PEB1-7
 Waterwashing: PBS-15
 Waterway: PEB1-14
 Wave-gauge: PBG2-14
 Wave-generated: PB2-8
 Wave: PBG2-14, PM-12, PSB-3
 Wavelength: PBG1-3, PEB1-9, PM-21, PMN1-2
 Wavelengths: PMN2-1, PSB-4
 Wax: OEB-1, OP4-1, OPE2-2, PB1-4, PBG1-11, PBG1-16, PBG2-6, PBG2-10, PBG2-5, PC2-23, PFA-8, PGG1-7, PM-3, PM-4, PPC1-15, PPC1-26, PRG1-5, PRG1-6, PRG1-9
 Waxes: OB1-2, OP3-2, OP4-1, OPC2-1, OPE1-2, OPE2-2, PB1-15, PBC-4, PBG2-5, PBG2-6, PC-12, PC2-24, PEB2-8, PFA-4, PM-4, PPC1-14, PPC1-18, PPC1-26, PRG1-6, PRG1-9, PSB-4

Waxy: OUM-3, PBS-23, PBS-8, PC-6, PPC1-14, PRG1-9, PRG2-5
 Weathered: OP4-1, PEB1-13, PEB2-18, PSB-13
 Weathering: OP1-1, PC-11, PEB2-18, PEB2-4, PRG2-19, PSB-21
 Well-humified: PSB-1
 Well-preserved: OPE2-1, PB1-20, PB1-21, PB1-22, PM-10, PSB-4
 Well-Resolved: PBC-11, PMN2-6
 Wenlockian: PBG1-10
 Westphalian: OP2-3, PG-8
 Wet-chemical: PSB-16
 Wet-gas: PB1-21
 Wet-sieved: PM-10
 Wet-sieving:
 Wetland: PFA-1, PM-27, PSB-7
 Wetlands: OP5-3, OPE1-2, PB1-14, PFA-1, PM-27, PPC1-19
 Wettability: PSB-11
 Wettable: PSB-11
 Wettening: PPC1-26
 WHC: PCS-13
 Wheat: OSB2-1, PB2-11, PCS-8, PM-17, PSB-17, PSB-20
 Wheatstraw: PMN2-7
 White-rot: PM-17, PM-22
 Wildfire-Induced: PSB-18
 Wildfire: OSB1-3, PBC-14, PBG2-6, PSB-18
 Wildfires: OEB-1, OPC1-2, OSB1-3, PB1-21, PBC-12, PBC-14, PBC-3, PBG2-6, PCS-10, PSB-18
 Wind-derived: PPC1-20
 Wind: OEB-1, OPC2-1, PC2-23, PC2-24, PPM-15
 Winds: PCS-1, PPC1-3
 Wine: PFA-5
 Wineries: PSB-5
 Winery: OB1-1
 Wood: OM-2, OM-3, OP3-1, PB2-6, PBC-2, PBG1-2, PEB1-13, PEB1-14, PGG1-13, PM-12, PM-22, PPC1-14, PSB-3
 Wooded: OP4-2
 Wooden: PEB2-10, PGG2-2
 Woods: OB1-2, PM-22, PM-4, POS1-13, PRG1-9
 Woody-plant: PC2-1
 Woody: PB1-21, PC2-1
 PPC1-3, PRG2-1
 Wustite: PBG1-6

X

X-Ray: OP5-4, PBG1-6, PBG2-11, PM-8, PSB-8
 XAD-4: PM-13, PMN1-8
 XAD-8: PM-13, PMN1-8
 XAD: PM-13, PM-27
 Xenobiotics: OEB-3, PM-8
 Xenolith: PGG1-4
 Xerochrept: PSB-18
 Xerophytic: PCS-1
 XPS: OP5-4, PM-3, PM-8
 XRD: PG-12, PRG2-18, PSB-7
 Xylain: PC-1, PC-2

Xylene: PRG2-9
Xylenes: OP3-4, PEB2-12, PGG2-2, PM-9
Xylite-rich: PC-12
Xylite: OBD2-3
Xylose: PCS-8

Y

Yemen: PFA-2
Yim: PB1-6
Yucatan: PBG2-4
Yuchi: PGG2-16

Z

Zeolites: PGG1-4
Zimbabwe: PBC-9
Zinc: PC2-20
Zircons: OGPR-3
Zn-Pb: PC2-20
Zn: PBG2-2, PC2-20, PEB2-12, PG-12, PGG1-4,
PSB-5
Zooclast: POS2-7